

Marine Structural Design

Second Edition

Yong Bai
Wei-Liang Jin



AMSTERDAM • BOSTON • HEIDELBERG • LONDON
NEW YORK • OXFORD • PARIS • SAN DIEGO
SAN FRANCISCO • SINGAPORE • SYDNEY • TOKYO

Butterworth-Heinemann is an imprint of Elsevier



Butterworth-Heinemann is an imprint of Elsevier
The Boulevard, Langford Lane, Kidlington, Oxford OX5 1GB, UK
225 Wyman Street, Waltham, MA 02451, USA

Copyright © 2016 Elsevier Ltd. All rights reserved.

No part of this publication may be reproduced or transmitted in any form or by any means, electronic or mechanical, including photocopying, recording, or any information storage and retrieval system, without permission in writing from the publisher. Details on how to seek permission, further information about the Publisher's permissions policies and our arrangements with organizations such as the Copyright Clearance Center and the Copyright Licensing Agency, can be found at our website: www.elsevier.com/permissions.

This book and the individual contributions contained in it are protected under copyright by the Publisher (other than as may be noted herein).

Notices

Knowledge and best practice in this field are constantly changing. As new research and experience broaden our understanding, changes in research methods, professional practices, or medical treatment may become necessary.

Practitioners and researchers must always rely on their own experience and knowledge in evaluating and using any information, methods, compounds, or experiments described herein. In using such information or methods they should be mindful of their own safety and the safety of others, including parties for whom they have a professional responsibility.

To the fullest extent of the law, neither the Publisher nor the authors, contributors, or editors, assume any liability for any injury and/or damage to persons or property as a matter of products liability, negligence or otherwise, or from any use or operation of any methods, products, instructions, or ideas contained in the material herein.

ISBN: 978-0-08-099997-5

British Library Cataloguing-in-Publication Data

A catalogue record for this book is available from the British Library

Library of Congress Cataloging-in-Publication Data

A catalog record for this book is available from the Library of Congress

For Information on all Butterworth-Heinemann publications
visit our website at <http://store.elsevier.com/>



Working together
to grow libraries in
developing countries

www.elsevier.com • www.bookaid.org

Publisher: Joe Hayton

Acquisition Editor: Carrie Bolger

Editorial Project Manager: Naomi Robertson

Production Project Manager: Jason Mitchell

Designer: Matthew Limbert

Typeset by TNQ Books and Journals

www.tnq.co.in

Printed and bound in the United States of America

Preface to First Edition

This book is written for marine structural engineers and naval architects, as well as mechanical engineers and civil engineers who work on structural design. The preparation of the book is motivated by the extensive use of finite element and dynamic/fatigue analyses, fast-paced advances in computer and information technologies, and the application of risk and reliability methods. As the professor of offshore structures at Stavanger University College, I developed this book for my teaching course TE 6076 “Offshore Structures” and TE6541 “Risk and Reliability Analysis of Offshore Structures” for MSc and PhD students. This book has also been used in IBC/Clarion industry training courses on the design and construction of floating production systems for engineers in the oil/gas industry.

As reliability-based limit-state design becomes popular in structural engineering, this book may also serve as a reference for structural engineers in other disciplines, such as the engineering of buildings, bridges, and spacecraft.

My former supervisors should be thanked for their guidance and inspiration. These include: Executive Vice President Dr Donald Liu at the American Bureau of Shipping (ABS), Prof. Torgeir Moan at the Norwegian University of Science and Technology, Profs. Robert Bea and Prof. Alaa Mansour at the University of California, Berkeley, Prof. Preben Terndrup Pedersen at the Technical University of Denmark, Prof. T. Yao at Osaka University, and Prof. M. Fujikubo at Hiroshima University. The friendship and technical advice from these great scientists and engineers have been very important for me in developing the materials used in this book.

As manager of the advanced engineering department at the JP Kenny Norway office (now a section of ABB) and manager of the offshore technology department at ABS, I was given opportunities to meet many industry leaders of oil companies, design/consulting offices, classification societies, and contractors. From ISSC, IBC, SNAME, OMAE, ISOPE, and OTC conferences, as well as industry (ISO/API/Deepstar) committees, I learned about recent developments in industry applications and research.

The collaboration with Dr Ruxin Song and Dr Tao Xu for a long period has been helpful in my development of research activities on structural reliability and fatigue, respectively. Sections of this book relating to extreme response, buckling of tubular members, FPSO hull girder strength, and reliability were based on my SNAME, OMAE, and ISOPE papers coauthored with Profs. Preben Terndrup Pedersen and T. Yao, and Drs Yung Shin, C.T. Zhao, and H.H. Sun.

Dr Qiang Bai and PhD student Gang Dong provided assistance in formatting the manuscript.

Prof. Rameswar Bhattacharyya, Elsevier Senior Publishing Editors James Sullivan and Nick Pinfield, and Senior Vice President James Card of ABS provided me continued encouragement in completing this book.

I appreciate my wife Hua Peng and children, Lihua and Carl, for creating an environment in which it has been possible to continue to write this book for more than five years in different cultures and working environments.

I wish to thank all of the organizations and individuals mentioned in the above (and many friends and authors who were not mentioned) for their support and encouragement.

Yong BAI
Houston, USA

Preface to Second Edition

It has been 12 years since the 1st edition of the book *Marine Structural Design* was published by Elsevier. The 2nd edition of this book reflects upon the new technologies developed by the oil & gas and shipbuilding industries and contains 50 chapters, 16 of which are new.

With the rapid development of marine structural engineering, researchers and engineers are constantly exploring and advancing new design and analysis methods in this field. More and more new materials are being applied to marine structures, and new types of these structures have appeared. In addition, considerable progress has been made in areas such as reliability theory, risk assessment, fixed platforms, and FPSOs. The newly added chapters of this book focus on all the aforementioned areas, and we'd like to introduce the new progress to our readers.

We hope that this book is a useful reference source for marine structural engineers and naval architects, as well as mechanical and civil engineers who work on structural design.

The authors would like to thank their graduate students, PhD students, and postdoctoral fellows who provided editing assistance (Mr Huibin Yan and Mr Alex Lam).

We appreciate the assistance of Elsevier in the editorial and publishing work.

We wish to thank all of the organizations and individuals mentioned above (and many friends and authors who were not mentioned) for their support and encouragement.

Prof. Yong Bai & Prof. Weiliang Jin

Introduction

1.1 Structural Design Principles

1.1.1 Introduction

This book is devoted to the modern theory for design and analysis of marine structures. The term “marine structures” refers to ships and offshore structures. The objective of this book is to summarize the latest developments of design codes, engineering practices, and research into the form of a book, focusing on applications of finite element analysis and risk/reliability methods.

Calculating wave loads and load combinations is the first step in marine structural design. For structural design and analysis, a structural engineer needs to understand the basic concepts of waves, motions, and design loads. Extreme value analysis for dynamic systems is another area that has had substantial advances from 1995 to 2015. It is an important subject for the determination of the design values for motions and strength analysis of floating structures, risers, mooring systems, and tendons for tension leg platforms.

Once the functional requirements and loads are determined, an initial scantling may be sized based on formulas and charts in classification rules and design codes. The basic scantling of the structural components is initially determined based on stress analysis of beams, plates, and shells under hydrostatic pressure, bending, and concentrated loads. Three levels of marine structural design have been developed:

- Level 1: Design by rules
- Level 2: Design by analysis
- Level 3: Design based on performance standards

Until the 1970s, structural design rules were based on the design by rules approach, which used experiences expressed in tables and formulas. These formula-based rules were followed by direct calculations of hydrodynamic loads and finite element stress analysis. The finite element methods (FEM) have now been extensively developed and applied to the design of ships and offshore structures. Structural analysis based on FEM has provided results that enable designers to optimize structural designs. The design by analysis approach is now applied throughout the design process.

The finite element analysis has been very popular for strength and fatigue analysis of marine structures. During the structural design process, the dimensions and sizing of the structure are optimized, and structural analysis is reconducted until the strength and fatigue requirements are met. The use of FEM technology has been supported both by the rapid development of computers and by information technologies. Information technology is widely used in structural analysis, data collection, processing, and interpretation, as well as in the design, operation, and maintenance of ships and offshore structures. The development of both computers and information technologies has made it possible to conduct complex structural analysis and process the results. To aid the FEM-based design, various types of computer-based tools have been developed, such as CAD (computer-aided design) for scantling, CAE (computer-aided engineering) for structural design and analysis, and CAM (computer-aided manufacturing) for fabrication.

Structural design may also be conducted based on performance requirements such as designing for accidental loads, where managing risks is of importance.

1.1.2 Limit-State Design

In a limit-state design, the design of structures is checked for all groups of limit states to ensure that the safety margin between the maximum loads and the weakest possible resistance of the structure is large enough and that fatigue damage is tolerable.

Based on the first principles, the limit-state design criteria cover various failure modes such as

- Serviceability limit state
- Ultimate limit state (including buckling/collapse and fracture)
- Fatigue limit state
- Accidental limit state (progressive collapse limit state).

Each failure mode may be controlled by a set of design criteria. Limit-state design criteria are developed based on ultimate strength and fatigue analysis, as well as the use of the risk/reliability methods.

The design criteria have traditionally been expressed in the format of working stress design (WSD) (or allowable stress design), where only one safety factor is used to define the allowable limit. However, in recent years, there is an increased use of the load and resistance factored design (LRFD) that comprises a number of load factors and resistance factors reflecting the uncertainties and the safety requirements.

A general safety format for LRFD design may be expressed as

$$S_d \leq R_d \quad (1.1)$$

where

$S_d = \sum S_k \cdot \gamma_f$, design load effect

$R_d = \sum R_k / \gamma_m$, design resistance (capacity)

S_k = Characteristic load effect

R_k = Characteristic resistance

γ_f = Load factor, reflecting the uncertainty in load

γ_m = Material factor, the inverse of the resistance factor.

Figure 1.1 illustrates the use of the load and resistance factors where only one load factor and one material factor are used, for the sake of simplicity. To account for the uncertainties in the strength parameters, the design resistance R_d is defined as characteristic resistance R_k divided by the material factor γ_m . The characteristic load effect S_k is also scaled up by multiplying by the load factor γ_f .

The values of the load factor γ_f and material factor γ_m are defined in design codes. They have been calibrated against the WSD criteria and the inherent safety levels in the design codes. The calibration may be conducted using structural reliability methods that allow us to correlate the reliability levels in the LRFD criteria with the WSD criteria and to ensure the reliability levels will be greater than or equal to the target reliability. An advantage of the LRFD approach is its simplicity (in comparison with direct usage of the structural

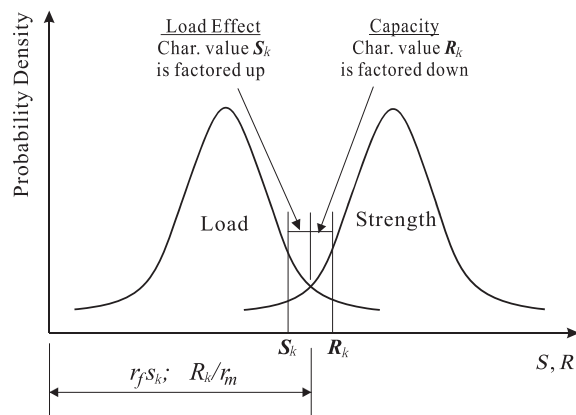


Figure 1.1

Use of load and resistance factors for strength design.

reliability methods) while it still accounts for the uncertainties in loads and structural capacities based on structural reliability methods. The LRFD is also called the partial safety factor design.

While the partial safety factors are calibrated using the structural reliability methods, the failure consequence may also be accounted for through the selection of the target reliability level. When the failure consequence is higher, the safety factors should also be higher. Use of the LRFD criteria may provide unified safety levels for the whole structures or a group of the structures that are designed according to the same code.

1.2 Strength and Fatigue Analysis

Major factors that should be considered in marine structural design include

- Still water and wave loads, and their possible combinations
- Ultimate strength of structural components and systems
- Fatigue/fracture in critical structural details.

Knowledge of hydrodynamics, buckling/collapsing, and fatigue/fracture is the key to understanding structural engineering.

1.2.1 Ultimate Strength Criteria

Ultimate strength criteria are usually advocated in design codes for various basic types of structural components such as

- columns and beam-columns
- plates and stiffened panels
- shells and stiffened shells
- structural connections
- hull girders.

An illustration of the Euler buckling strength is given in [Figure 1.2](#) for pinned columns under compression. Due to the combination of axial compression and initial deflection, the column may buckle when the axial compression approaches its critical value,

$$P_{CR} = \frac{\pi^2 EI}{l^2} \quad (1.2)$$

where l and EI are column length and sectional bending rigidity, respectively. Due to buckling, the lateral deflection δ will increase rapidly.

Initiation of yielding usually occurs in the most loaded portion of the structural members. As the yielding portion spreads, the bending rigidity of the structural component decreases

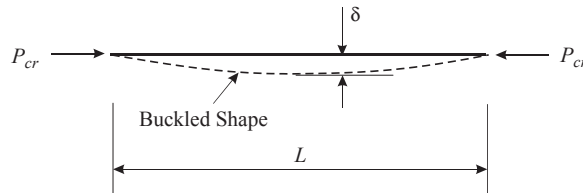


Figure 1.2
Buckling of pinned columns.

and consequently buckling occurs. For structural members other than unstiffened thin-walled shells, ultimate strength is reached when inelastic buckling occurs.

The design of the components in ships and offshore structures is mainly based on relevant classification rules as well as API and ISO codes. The classification rules are applicable to ocean-going ships, mobile offshore drilling units, and floating structures. For offshore structural designs, however, API and ISO codes are more frequently applied.

It should be pointed out that final fracture is also part of the ultimate strength analysis. The assessment of the final fracture has been based mainly on fracture mechanics criteria in British standard PD6493 (or BS7910) and American Petroleum Institute code API 579. In fact there is a similarity between buckling strength analysis and fracture strength analysis, as compared in [Table 1.1](#).

In general, the strength criteria for code development may be derived using the following approaches:

- Derive analytical equations based on plasticity, elasticity, and theory of elastic stability;
- Conduct nonlinear finite element analysis of component strength;
- Collect results of mechanical tests;
- Compare the analytical equations with the results of finite element analysis and mechanical testing;
- Modify the analytical equations based on finite element results;

Table 1.1: Comparisons of buckling strength analysis and fracture strength analysis

	Buckling Strength	Fracture Strength
Loads	Compressive/shear force	Tensile loads
Imperfection	Geometrical and residual stress due to welding, etc.	Defects due to fabrication and fatigue loads
Linear solution	Elastic buckling	Linear fracture mechanics
Design criteria	Curve fitting of theoretical equations to test results	Curve fitting of theoretical equations to test results

- Finalize the upgraded formulations through comparisons with numerical and mechanical tests;
- Further calibrate the derived strength equations on design projects.

From the above discussions, it is clear that the theoretical knowledge and practical design experience are vital for the successful development of ultimate strength criteria.

As an alternative to the criteria in rules and codes, mechanical testing and finite element analysis may be applied to determine the ultimate strength of structural components. For simple components, the prediction of finite element analysis and rule criteria is usually close to the results of mechanical testing. Therefore, mechanical testing is now mainly applied to subjects in which less experience and knowledge have been accumulated.

Subjects that warrant future research on ultimate strength analysis include

- Development of strength equations for combined loads
- Calibration of partial safety factors using risk assessment and structural reliability analysis
- Standardization of the finite element models and benchmark of the models
- Development of procedures for the determination of partial safety factors for finite element analysis and strength design based on testing.

1.2.2 Design for Accidental Loads

The accidental loads that should be considered in the design of ship and offshore structures are, for example,

- Ship collision and impacts from dropped objects offshore
- Ship grounding
- Fire/explosion
- Freak waves.

The term “accidental loads” refers to unexpected loads that may result in a catastrophe, causing negative economical, environmental, material consequences, and the loss of human life. Extreme and accidental loads differ in the sense that the magnitude and frequency of the extreme loads can be influenced to a small extent by the structural design, whereas active controls may influence both the frequency and the magnitude of accidental loads.

The design for accidental loads includes determining the design of the loads based on risk consideration, predicting the structural response using rigid-plastic analytical formulation and/or nonlinear FEM and selecting the risk-based acceptance criteria. Traditionally rigid-plastic analytical formulations have been popular for the designs against accidental loads because large plastic deformation is usually the mechanism for energy absorption in accidents. In recent years, the nonlinear finite element analysis has been used to simulate

the structural behavior in accidental scenarios and to design the structure for the performance standards. Use of the finite element analysis enables us to deal with complex accidental scenarios and to better predict the structural response.

1.2.3 Design for Fatigue

Fatigue damage and defects may threaten the integrity of marine structures. This concern is aggravated as the cost of repair and loss of production increases. Fatigue design is an important subject due to use of higher strength materials, severe environmental conditions, and optimized structural dimensions. In recent years there has been a rapid development in analysis technologies for predicting fatigue loading, cyclic stress, fatigue/fracture capacity, and damage tolerance criteria. The fatigue capacities are evaluated using the S–N curve approach or the fracture mechanics approach. The S–N curves are established by stress-controlled fatigue tests and may generally be expressed as

$$N = K \cdot S^{-m} \quad (1.3)$$

where

N = Number of cycles to failure

S = Stress range

m, K = Material constants depending on the environment, test conditions, etc.

The S–N curve approach is mainly applied in designs for fatigue strength, and it consists of two key components: determining a hot-spot stress and selecting appropriate S–N curves. A bilinear S–N curve is shown in Figure 1.3 where, on a log–log scale, the x -axis and y -axis are the number of cycles until failure and the stress range, respectively. The slope of the curve changes from m to r where the number of cycles is $N_R (=5 \cdot 10^6 \text{ for steel})$.

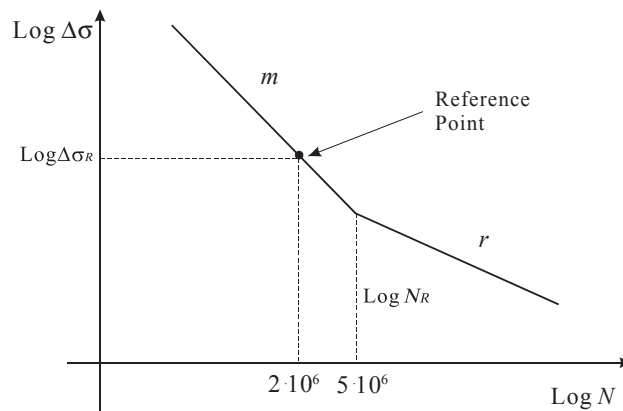


Figure 1.3
S–N curves for fatigue assessment.

Discrepancy has been observed between the hot-spot stresses predicted by different analysts or in different analyses. It is therefore important to derive an optimum procedure and standardize the analysis procedure as part of the rules/code development. In recent years, there has been a rapid development in the standardization of the S–N curves. The International Institute of Welding (IIW) has published new guidance documents on the selection of S–N curves and the determination of hot-spot stresses. In the IIW code, the S–N curves are named according to their reference stress range $\Delta\sigma_R$ that corresponds to $(2 \cdot 10^6)$ cycles.

With the increasing use of finite element analysis, a design approach based on the hot-spot stress will be increasingly popular. The fatigue uncertainties are due to several factors such as

- Selection of environmental conditions such as sea states and their combinations
- Extrapolation of fatigue stresses in the hot-spot points
- Selection of design codes such as the S–N curves and the stress calculations
- Combination of wave-induced fatigue with the fatigue damages due to vortex-induced vibrations and installation
- Selection of safety factors and inspection/repair methods.

The accumulative fatigue damage for a structural connection over its life cycle is usually estimated using Miners rule, which sums up the damage caused by individual stress range blocks.

$$D = \sum \frac{n_i}{N_i} \leq D_{\text{allow}} \quad (1.4)$$

where n_i and N_i denote the number of stress cycles in stress block i , and the number of cycles until failure at the i -th constant amplitude stress range block. D_{allow} is the allowable limit that is defined in design codes.

A simplified fatigue analysis may be conducted assuming that stress ranges follow Weibull distributions. This kind of analysis has been widely applied in classification rules for fatigue assessment of ship structures. The Weibull parameters for stress distribution have been calibrated against in-service fatigue data for ships and more refined fatigue analysis. The value of Weibull parameters may be found from classification rules, as a function of ship lengths and locations of interest. Alternatively, in offshore design codes API RP2A, a simplified fatigue analysis is proposed assuming the wave height follows Weibull distributions.

There are three approaches for predicting accumulated fatigue damages accounting for wave scatter diagrams, namely,

- Frequency domain (e.g., spectral fatigue analysis based on Rayleigh model or bimodel)
- Time domain (which could account for nonlinearities and contact/friction due to soil–structure interactions)

- A mixture of frequency-domain and time-domain approaches (e.g., using the stress range spectrum from frequency-domain fatigue analysis and the rain-flow counting approach to sum up the fatigue damages due to individual sea states).

As an alternative to the S–N curve approach, fracture mechanics is now used for evaluating the remaining strength of the cracked structural connections and in planning inspections of welded connections. There is an approximate linear relationship between the crack growth rate and the ΔK on a log–log scale. This is generally characterized by the Paris equation

$$\frac{da}{dN} = C(\Delta K)^m \quad (1.5)$$

where

$$\Delta K = K_{\max} - K_{\min} \quad (1.6)$$

K_{\max} and K_{\min} are the maximum and minimum values of the stress intensity factor at the upper and lower limit stresses during a cyclic loading. The values of material properties C and m may be found using design codes for typical materials that are used in marine structures and other types of steel structures. The stress intensity factors may be available from handbooks for simplified structural and defect geometries and loads.

1.3 Structural Reliability Applications

1.3.1 Structural Reliability Concepts

Component reliability is concerned with the failure probability modeled by a single limit-state function. It is a fundamental part of the structural reliability analysis since all marine structures are composed of their components.

The concept of structural reliability is illustrated in [Figure 1.4](#), where both the load and the strength are modeled as random variables. Failure occurs when the load exceeds the strength. Denoting the probability density function for load and strength as $F_S(x)$ and $F_R(x)$, respectively, the failure probability may be expressed as

$$P_f = P(S \geq R) = \int_0^{\infty} F_S(x)F_R(x)dx \quad (1.7)$$

System reliability deals with the evaluation of failure probability where more than one limit-state function must be considered. There are two types of basic systems: series systems and parallel systems. A system is called a series system if it is in a state of failure whenever any of its elements fails. Such systems are often referred to as weakest link

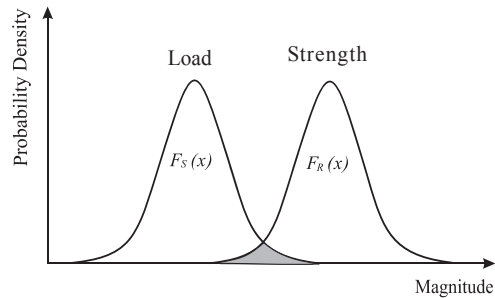


Figure 1.4
Structural reliability concepts.

systems. A typical example of this is marine pipelines and risers, where a parallel system fails only when all of its elements fail.

Structural reliability analysis has been used to determine load combinations, derive design criteria, and plan in-service inspections.

The life-cycle cost of a marine structure consists of

- Initial investment relating to the steel weight and manufacturing process
- Maintenance cost
- Loss caused by damage or failure—a risk resulted expenditure.

Degradation or failure of a structural system may lead to a reduction/shutdown of the operation and loss/damage of the structure. The owner and the builder want a structure with a low initial cost, the highest possible operating margin, and an extendable operating period. A life-cycle cost model based on probabilistic economics may be a useful tool for improving the design analysis, inspection, and maintenance.

This is further illustrated in [Figure 1.5](#) where the total cost is the sum of the initial investment and maintenance cost plus the loss caused by structural damage/failure. A target reliability level may then be estimated based on cost optimization, if it is higher than the value required by legislative requirements.

1.3.2 Reliability-Based Calibration of Design Factor

One of the structural reliability applications is the calibration of safety factors for structural design. The calibration process may help achieve a consistent safety level. The safety factors are determined so that the calibrated failure probability for various conditions is as close to the target safety level as possible. The following steps should be taken when conducting a reliability-based code calibration:

- Step 1: Identify potential failure modes for the given design case
- Step 2: Define design equations

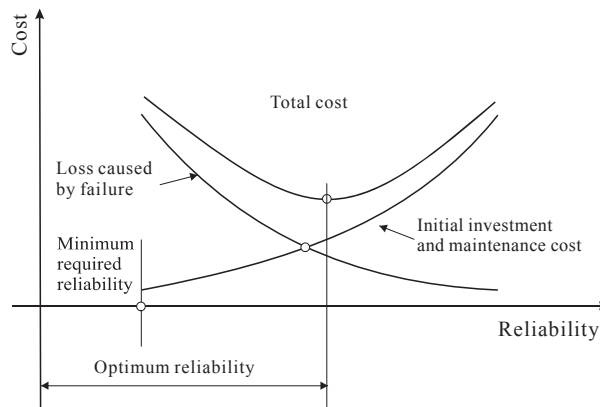


Figure 1.5

Target reliability and minimization of life-cycle cost.

- Step 3: Form limit-state functions
- Step 4: Measure uncertainties involved with random variables of the limit-state functions
- Step 5: Estimate failure probability
- Step 6: Determine the target safety level
- Step 7: Calibrate safety factors
- Step 8: Evaluate the design results.

The load and resistance factors (or safety factors) in the design criteria may be calibrated using risk/reliability methods.

1.3.3 Requalification of Existing Structures

Requalification of existing ship and offshore structures is one of the important subjects for structures in operation. The requalification is conducted when the environmental design conditions change, and the structure has degraded due to corrosion, fatigue, and possible impact loads.

Corrosion defects may significantly reduce the ultimate and fatigue strength of the structures. Various mathematical models have been developed to predict the future corrosion development in structures such as pipelines, risers, and platings. Various methods have been applied by the industry to measure the amount, locations, and shapes of corrosion defects, as all these are crucially important for strength and fatigue assessment.

In many cases, the use of nonlinear analysis of loads, structural response, and risk/reliability methods is required to fully utilize the design margins. The requalification may be conducted using the strength and fatigue formulations, and the risk/reliability methods discussed in this book.

1.4 Risk Assessment

1.4.1 Application of Risk Assessment

Risk assessment and management of safety, health, and environment protection (HSE) have become an important part of the design and construction activities.

Use of risk assessment in the offshore industry dates back to the second half of the 1970s when a few pioneer projects were conducted with an objective to develop analysis methodologies and collect incident data. At that time, the methodologies and the data employed were used for some years by the nuclear power and chemical industries.

The next step in the risk assessment development came in 1981 when the Norwegian Petroleum Directorate issued their guidelines for safety evaluations. These guidelines required that a quantitative risk assessment be carried out for all new offshore installations in the conceptual design phase. Another significant step was the official inquiry led by Lord Cullen in the United Kingdom following the severe accident of the Piper Alpha platform in 1988.

In 1991, the Norwegian Petroleum Directorate replaced the guidelines for safety evaluations issued in 1981 with regulations for risk analysis. In 1992, the safety case regulation in the United Kingdom was finalized and the offshore industry in the United Kingdom took up risk assessments as part of the safety cases for their existing and new installations. In 1997 formal safety assessments were adopted by IMO as a tool for evaluating new safety regulations for the shipping industry.

1.4.2 Risk-Based Inspection

Based on risk measures, the development of a system-level, risk-based inspection process involves the prioritization of systems, subsystems, and elements and the development of an inspection strategy (i.e., the frequency, method, and scope/sample size). The process also includes making decisions about the maintenance and repair. The risk-based inspection method, using inspection results, may also be applied for updating the inspection strategy for a given system, subsystem, or component/element.

The important features of the risk-based inspection method include

- The use of a multidisciplinary, top-down approach that starts at the system level before focusing the inspection on the element level;
- The use of a “living” process that is flexible, strives for completeness, and can be easily implemented;
- The use of qualitative and quantitative risk measurements;
- The use of effective and efficient analytical methods, which provide results that are sound and familiar to inspection personnel.

A risk-based inspection approach may be developed based on the evaluation of structural performance for fatigue/corrosion, fracture mechanics, corrosion engineering, structural reliability, and risk assessment.

1.4.3 Human and Organization Factors

Statistics show that over 80% of the failures are initially caused by the so-called human and organization factors. Figure 1.6 shows the interaction among the structure, human, and organization and management system. Human behavior, organizational culture, and management of HSE will all influence the structural safety.

1.5 Layout of This Book

Risk-based limit-state designs, combining probabilistic methods with FEM-based structural analysis, will be widely accepted and implemented by the industry for the cost-effective and safe design and operation of marine structures. The purpose of this book is to summarize these technological developments in order to promote advanced structural design. The emphasis on FEM, dynamic response, risk/reliability, and information technology differentiates this book from existing ones.

Figure 1.7 illustrates the process of a structural design based on finite element analysis and risk/reliability methods.

There are several well-known books on marine/offshore hydrodynamics, for example, Bhattacharyya (1978), Sarpkaya and Isaacson (1981), Chakrabarti (1987), Faltinsen (1990), CMPT (1998), Jensen (2001), and Coastal Engineering Manual (CEM, 2003). However, there is a lack of books on marine/offshore structural design, ultimate strength, fatigue

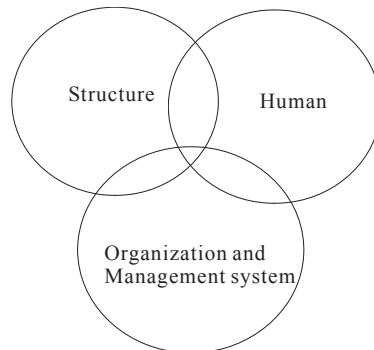


Figure 1.6
Human—organization factors in structural safety.

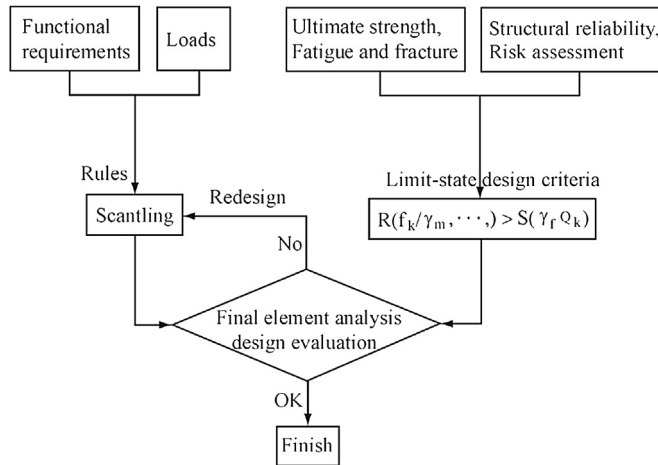


Figure 1.7

Modern theory for marine structural design.

assessment, and risk/reliability analysis. In an integrated manner, the current book will address modern theories for structural design/analysis and ultimate strength and fatigue criteria as well as the practical industry applications of the risk and reliability methods:

Part I—Structural Design Principles (Chapters 1–7): Summarizes the hydrodynamic loads for structural designs of ships and offshore structures, and scantling of ship hulls. It also addresses the applications of the finite element technologies in marine structural design. The design by analysis procedure is also called the direct design method. Applications to practical designs are discussed for ships, fixed platforms, FPSO, TLP, Spar, and semisubmersibles.

Part II—Ultimate Strength (Chapters 8–15): Presents applications of buckling and plasticity theories, as well as nonlinear finite element formulations. The nonlinear finite element analysis may also be applied to the design of structures under accidental loads such as ship collisions, groundings, fires, and explosions.

Part III—Fatigue and Fracture (Chapters 16–22): Explains fatigue mechanisms, fatigue resistance, fatigue loads and stresses, simplified fatigue analysis, spectral fatigue analysis, and fracture assessment. The basics of fatigue and fracture are provided for finite element analysts and structural engineers.

Part IV—Structural Reliability (Chapters 23–28): Provides simplified methods for the application of structural reliability theories for ships and offshore structures. The objective is to explain complex theories in simplified terms. An outline of the analysis software and tools is given for readers to find references or more information.

Part V—Risk Assessment (Chapters 29–34): Summarizes recent industrial developments to facilitate the use of risk analysis when applied to measure and reduce risks in marine structures and their mechanical components. Risk analysis and human reliability are applied to justify and reduce risks in the economy, the environment, and human life.

1.6 How to Use This Book

When this book was first drafted, the author’s intention was to use it to teach the course Marine Structural Design. However, the material presented in this book may be used for several MSc or PhD courses such as

- Ship Structural Design
- Design of Floating Production Systems
- Ultimate Strength of Marine Structures
- Fatigue and Fracture
- Risk and Reliability in Marine Structures

This book addresses the marine and offshore applications of steel structures. In addition to the topics that are normally covered by civil engineering books on the design of steel structures (e.g., [Salmon and Johnson, 1995](#)), this book also covers hydrodynamics, ship impacts, and fatigue/fractures. Compared to books on spacecraft structure designs (e.g., [Sarafin, 1995](#)), this book describes, in greater detail, applications of FEM and risk/reliability methods. Hence, it should also be of interest to engineers and researchers working on civil engineering (steel structures and coastal engineering) and spacecraft structures.

For more information on the use of risk/reliability-based limit-state design, reference is made to a separate book entitled “Pipelines and Risers” ([Bai, 2001](#)). Practical aspects for design and construction of floating production systems are addressed in [Bai et al. \(2001\)](#).

References

- Bai, Y., 2001. Pipelines and Risers. In: Elsevier Ocean Engineering Book Series, vol. 3. London, ISBN:0-08-043712-5.
- Bai, Y., Ayney, C., Huang, E., Maher, J., Parker, G., Song, R., Wang, M., 2001. Design and construction of floating production systems. In: Course Notes for an Industry Training Course Led by Yong Bai and Organised with Clarion Technical Conferences in Houston and IBC in London.
- Bhattacharyya, R., 1978. Dynamics of Marine Vehicles. John Wiley & Sons, Inc.
- Chakrabarti, S.K., 1987. Hydrodynamics of Offshore Structures. Computational Mechanics Publications.
- CMPT, 1998. In: Baltrop, N. (Ed.), Floating Structures: A Guide for Design and Analysis. Oilfield Publications, Inc.
- Faltinsen, O.M., 1990. Sea Loads on Ships and Offshore Structures. Cambridge Ocean Technology Series, Cambridge University Press.

- Jensen, J.J., 2001. Load and Global Response of Ships, vol. 4. Elsevier Ocean Engineering Series.
- Salmon, C.G., Johnson, J.E., 1995. Steel Structures, Design and Behavior, fourth ed. Harper Collins College Publishers.
- Sarafin, T.P., 1995. Spacecraft Structures and Mechanism. Space Technology Series, Microcosm & Kluwer Academic Publishers.
- Sarpkaya, T., Isaacson, M., 1981. Mechanics of Wave Forces on Offshore Structures. Van Nostrand Reinhold Co.
- US Army Corps of Engineers, 2003. Coastal Engineering Manual (CEM) [M]. Washington, D.C: U.S. Army Corps of Engineers.

Marine Composite Materials and Structure

2.1 Introduction

Composites are relatively new to the marine industry, having only come into use since 1965. The use of composites in the marine industry has become more prevalent in recent decades, and is now well established. Traditional shipbuilding materials have been wood, steel, and aluminum; although larger vessels are constructed mainly of steel, composites are sometimes used in part for ship superstructures and interior components. Applications range from pleasure boats and military vessels to helicopter decks on offshore platforms. One of the main reasons for using these materials is their good resistance to harsh environmental conditions (Hasson and Crowe, 1988). Table 2.1 shows the advantages of composites.

2.2 The Application of Composites in the Marine Industry

Glass-fiber reinforced plastics (GRP), one form of fiber-reinforced plastics (FRP), were first introduced in the 1940s for Navy personnel boats, as shown in Figure 2.1. The first major interest in commercial FRP vessels was in the fishing industry, starting in the late 1960s with the construction of FRP shrimp trawlers. Since that time, the use of FRP materials has become universally acceptable in yachts, pleasure crafts, performance crafts (i.e., racing boats), and small commercial vessels such as fishing trawlers. Today, approximately 50% of commercial fishing vessels are of FRP construction, and their use in the recreational boating industry is well recognized and established. Canoes, kayaks, sailboats, powerboats, and performance craft are all good examples of crafts made almost exclusively of composites (Andrew et al., 1998). As lightweight construction is an important feature, composites have proven to be very valuable to state-of-the-art vessels.

Other commercial uses include deep sea submersibles, navigational aids (buoys), and offshore engineering applications (i.e., offshore drilling platforms and pilings). In lifeboats and utility boats, where longevity and low maintenance are important (primarily for lifeboats, which may sit out of the water in the weather for many years), FRP construction has proven to be very effective and economical, as shown in Figure 2.2.

Table 2.1: The advantages of composites (Galanis, 2002)

Composite Property	Advantage to Marine Industry
Corrosion resistance	Longer life of component and reduced maintenance
Lightweight	Greater payload capacity, increased depth, higher speeds, easier handling/installation
Monolithic seamless construction of complex shapes	Easier manufacturing of complex shapes
Near net shape and good finish	Reduced need for secondary machining, reduced material waste, reduced painting needed
Tailor ability	Improved performance of component
Nonmagnetic	Signature reduction, reduced galvanic corrosion
Nonreflective	Reduced radar cross section
Inherently damping	Radiate noise reduction
Radar/acoustically transparent	Improved radar/sonar performance
Low thermal conductivity	Improved fire performance
Multiple domestic sources	Availability of raw materials
Design cascading effect	Improved performance of one component

2.2.1 Ocean Environment

As known, the environment in the ocean is very rough. Recent studies estimate that the direct cost of corrosion in the United States is nearly \$300 billion dollars per year. On the open sea, waves can commonly reach 7 m in height or even up to 15 m in extreme weather. As shown in [Figure 2.3](#) there are even some reports of rogue waves that have exceeded 30 m in height.

Applications of composite materials in the marine industry are extensive, ranging from pleasure boats and military vessels to helicopter decks on offshore platforms. How can composites be used in this extreme environment? One of the main reasons for using these materials is because of their good resistance to harsh environmental conditions.

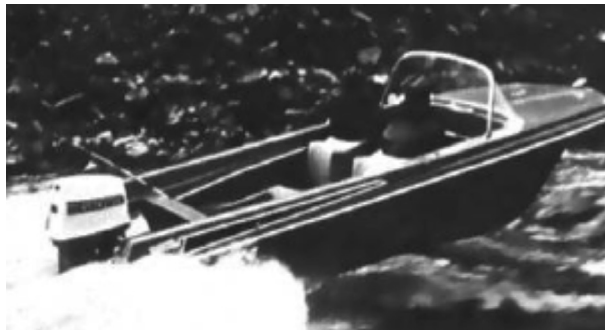


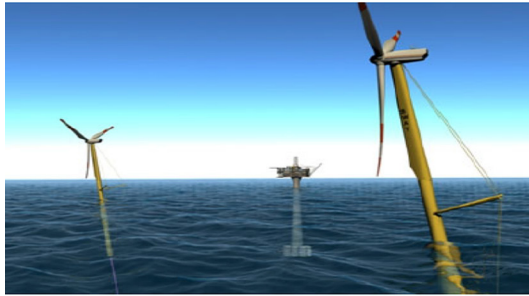
Figure 2.1
First boat constructed from composite.



Scandinavian performance marine vehicles



Large composite hull fabrication



Offshore wind energy



Ocean tidal energy

Figure 2.2

Composites in different commercial uses.



Figure 2.3

Corrosion and extreme waves.

FRP composites potentially offer significant weight savings in surface warships and fast ferries and may be considered at a number of levels:

- Superstructures
- Masts
- Secondary hull structures (internal decks and bulkheads, fairings)
- Primary hull structure.

FRP composites are now established as marine construction materials and their long-term behavior is well understood. By following a logical approach to analysis, testing, and trials as designs are developed, highly durable and cost-effective ship structures result.

2.2.2 Application in the Shipbuilding Industry

There is an increasing worldwide demand for small, low signature, long range/endurance, and low cost ships for close in-shore operations. The optimum size of such a ship is still evolving but ships in the range of 300 foot long and 1200 ton displacement would appear to be representative of the class.

As seen in [Figure 2.4](#), this 160 foot composite motor yacht is typical of infused hulls produced by Christensen. The company has plans to produce a 186 foot, 500+ GT (gross tonnage) yacht, which will be constructed in a purpose-designed facility in Tennessee.

Pleasure Boats Industry

Small pleasure boats have been built from composites since before 1965. The principal fabrication route is the hand lay-up method.

There is an increasing number of fast passenger vessels under construction and the design of such vessels will be used to illustrate the origins of safety factors in design. For large ships the hull and most bulkheads must be noninflammable, thus excluding polymeric composites. For smaller boats and fishing vessels the rules are less strict.



Figure 2.4
Composite motor yacht.

Recreational Applications

The development of composite material technology in recreational boats has come the closest to matching the advances made for aircraft. Composite use has soared in the recreational marine industry due to economic and operational factors that are different than those in commercial and naval shipbuilding.

Uses in the recreational boating industry are well recognized and established. Canoes, kayaks, sailboats, power boats, and performance craft are all good examples of craft made almost exclusively of composites. Where lightweight construction is an important feature, such as for racing powerboats and sailboats, composites have proven to be very valuable to the state of the art of these vessels. Another advantage of FRP or other composite construction, especially in recreational boats, is the ease of repair compared to wood or metal structures.

Commercial Applications

Cost is a major concern in commercial shipbuilding because of international competition. Composite usage has extended to fishing trawlers, lifeboats, passenger ferries, and larger ships such as cargo ships and tankers. Industrial submersibles for research and inspection have also been made with composites to help them achieve their requirements.

Military Applications

The most significant naval application of FRP has been in the construction of mine countermeasure vessels as shown in [Figure 2.5](#). The growth of composite use on naval vessels has been hinged by performance requirements and the need to keep cost to a minimum.

The Navy and Army have integrated several applications of composites into their vehicles, namely small boats, submarines, patrol craft, and minesweepers. As seen in [Figure 2.6](#) other components, ranging from small equipment brackets to propellers, have also proven effective. The development of passenger ferries from 1995 to 2015 has made great strides with regard to speed and economy due to the increased use of composite materials. Due to current regulations in the United States, the use of composites in the passenger ferry market is limited primarily to relatively small (up to 150 passengers) commuter-type vessels. In European countries, there exist some larger passenger and automobile ferries capable of very high speeds.

2.2.3 Marine Aviation Vehicles and Off-Shore Structure

Howard Hughes' Spruce Goose was 218 feet long with a 320 foot wingspan and designed to carry 700 soldiers. At 181 tons at takeoff, the flying boat flew only about one mile in



Figure 2.5
Mine countermeasure vessels.



Figure 2.6
Large naval composite marine structures.

1947. In 1984, the Dornier Company introduced an all-composite, 12 passenger amphibian transport as seen in [Figure 2.7](#).

StatoilHydro (Norway) is investing \$79M to build a 2.3 MW offshore windmill. The floating wind turbine can be anchored in water depths from 120 to 700 m.

2.3 Composite Material Structure

Composite materials are basically hybrid materials formed of multiple materials in order to utilize their individual structural advantages in a single structural material ([Civgin, 2005](#)). A composite material is defined as consisting of a resin matrix reinforced with a fibrous material (i.e., glass, carbon, or polymer), as shown in [Figure 2.8](#). The fibers are the part of the composite material that contributes to the strength while the matrix holds the fibers together ([Mohan and Gurit, 2008](#)).

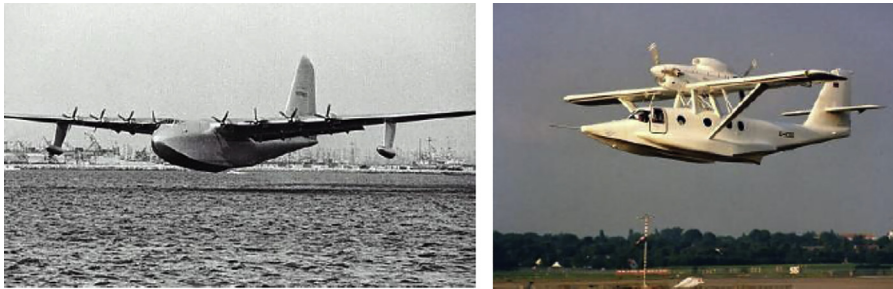


Figure 2.7
All-composite amphibian transport.

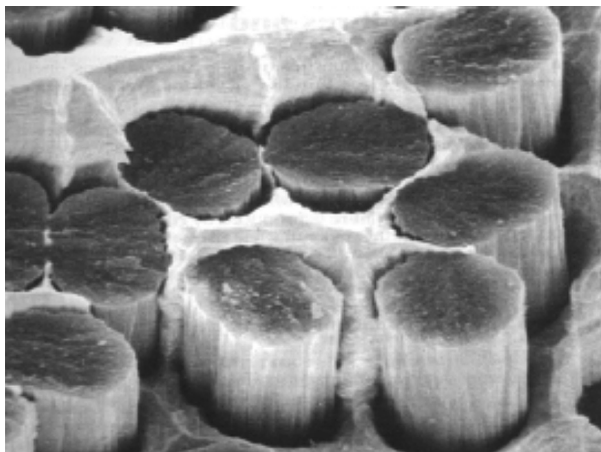


Figure 2.8
Composite laminates cross section.

A composite material consists of two or more constituent materials combined in such a way that the resulting material has more useful applications than the constituent materials alone. The constituent materials play an important role in the development of the final material properties. Advanced composite materials used in structural applications are obtained by reinforcing matrix material with continuous fibers, which have high strength and stiffness properties. The selection of a composite material for any application will involve the selection of the reinforcing fiber and matrix, and their fractional volume in the resulting material (Ratwani, 2002).

In practice, most composites consist of a bulk material (the matrix) and a reinforcement of some kind, added primarily to increase the strength and stiffness of the matrix. This reinforcement is usually in the form of fiber. Today, the most common man-made composites can be divided into three main groups: polymer matrix composites, metal matrix composites, and ceramic matrix composites, as seen in Figure 2.9.

In this section, polymer matrix composites are mainly introduced. These are the most common composites and will be the main area of discussion in this guide. FRP (or plastics) composites use a polymer-based resin as the matrix, and a variety of fibers such as glass, carbon, and aramid as the reinforcement.

2.3.1 Fiber Reinforcements

Fiber is an important constituent in composites. A great deal of research and development has been done with the fibers on the effects for the different types, volume fractions, architecture, and orientations. The fiber generally occupies 30–70% of the matrix volume. The fibers can be chopped, woven, stitched, and/or braided. Usually, they are treated with sizings such as starch, gelatin, oil, or wax to improve the bond, as well as binders to

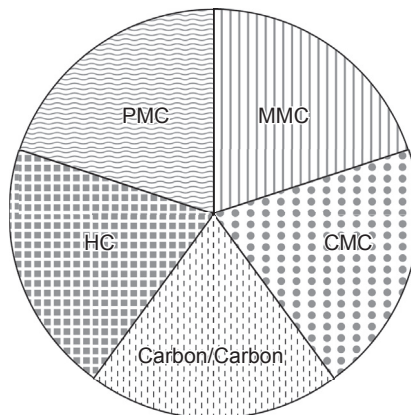


Figure 2.9

The most man-made composites (Vinson and Sierakowski, 2008).

improve the handling. The most common types of fibers used in advanced composites for structural applications are fiberglass, aramid, and carbon. Fiberglass is the least expensive while carbon is the most expensive. The cost of aramid fibers is about the same as that of the lower grades of carbon fiber. Other high-strength high-modulus fibers, such as boron, are also now considered to be economically prohibitive (Podolny, 1996).

Glass Fibers

Glass fibers can be divided into three classes: E-glass, S-glass, and C-glass. The E-glass is designed for electrical use and the S-glass for high strength. The C-glass is designed for high corrosion resistance, and is not in use for civil engineering applications. Of the three fibers, the E-glass is the most common reinforcement material used in civil structures. It is produced from lime–alumina–borosilicate, which can be easily obtained from an abundance of raw materials such as sand. The fibers are drawn into very fine filaments with diameters ranging from 2 to 13×10^{-6} m. The glass fiber strength and modulus can degrade with increasing temperature. Although the glass material creeps under a sustained load, it can be designed to perform satisfactorily. The fiber itself is regarded as an isotropic material and has a lower thermal expansion coefficient than that of steel. Depending on the glass type, filament diameter, sizing chemistry, and fiber form, a wide range of properties and performance can be achieved (Slater and Houlston, 1980), as shown in Table 2.2.

Aramid Fibers

Aramid fiber is a man-made organic polymer (an aromatic polyamide) produced by spinning a solid fiber from a liquid chemical blend. The bright golden yellow filaments produced can have a range of properties, but all have high strength and low density, which give very high specific strengths. All grades have good resistance to impact, and lower modulus grades are used extensively in ballistic applications. Compressive strength, however, is only similar to that of E-glass. The aramid fibers have excellent fatigue and creep resistance. Although there are several commercial grades of aramid fibers available, the two most common ones used in structural applications are Kevlar 29 and Kevlar 49. The Young's modulus curve for Kevlar 29 is linear to a value of 83 GPa, but then becomes slightly concave upward to a value of 100 GPa at rupture; whereas for Kevlar 49 the curve

Table 2.2: Properties of glass fibers (Zweben, 1989)

Typical Properties	E-glass	S-glass
Density (g/cm^3)	2.60	2.50
Young's modulus (GPa)	72	87
Tensile strength (GPa)	1.72	2.53
Tensile elongation (%)	2.4	2.9

is linear to a value of 124 GPa at rupture (see Table 2.3). As an anisotropic material, its transverse and shear modulus are an order of magnitude less than those in the longitudinal direction. The fibers can have difficulties achieving a chemical or mechanical bond with the resin.

Carbon Fibers

The graphite or carbon fiber is made from three types of polymer precursors: polyacrylonitrile fiber, rayon fiber, and pitch. The tensile stress–strain curve is linear to the point of rupture. Although there are many carbon fibers available on the open market, they can be arbitrarily divided into three grades, as shown in Table 2.4. They have lower thermal expansion coefficients than both the glass and the aramid fibers. The carbon fiber is an anisotropic material, and its transverse modulus is an order of magnitude less than its longitudinal modulus. The material has a very high fatigue and creep resistance. Since its tensile strength decreases with increasing modulus, its strain at rupture will also be much lower. Because of the material brittleness at higher modulus, it becomes critical in joint and connection details, which can have high stress concentrations. As a result of this phenomenon, carbon composite laminates are more effective with adhesive bondings that eliminate mechanical fasteners.

2.3.2 Resin Systems

Resin is another important constituent in composites. The two classes of resin are the thermoplastics and the thermosets. A thermoplastic resin remains a solid at room temperature. It melts when heated and solidifies when cooled. The long-chain polymers do not chemically cross-link, and because they do not cure permanently, they are undesirable

Table 2.3: Properties of aramid fibers (Zweben, 1989)

Typical Properties	Kevlar 29	Kevlar 49
Density (g/cm^3)	1.44	1.44
Young's modulus (GPa)	83/100	124
Tensile strength (GPa)	2.27	2.27
Tensile elongation (%)	2.8	1.8

Table 2.4: Properties of carbon fibers (Zweben, 1989)

Typical Properties	High Strength	High Modulus	Ultrahigh Modulus
Density (g/cm^3)	1.8	1.9	2.0–2.1
Young's modulus (GPa)	230	370	520–620
Tensile strength (GPa)	2.48	1.79	1.03–1.31
Tensile elongation (%)	1.1	0.5	0.2

for structural applications. Conversely, a thermosetting resin will cure permanently by irreversible cross-linking at elevated temperatures. The most common resins used in composites are the unsaturated polyesters, epoxies, and vinyl esters; the least common ones are the polyurethanes and the phenolics. [Table 2.5](#) shows some properties of the three main types of matrix resins.

2.4 Material Property

In fact, one of the main advantages of composites is the complementary nature of their components. For example, thin glass fibers exhibit relatively high tensile strength, but are susceptible to damage. By comparison, most polymer resins are weak in tensile strength but are extremely tough yet malleable. The combination of these materials is more useful than either of the individual components.

In this section, the stress and strain relationships for individual ply or lamina are examined. These relationships form the basic building blocks on which all subsequent analysis and design procedures are based. It is assumed that the material under consideration is orthotropic; that is, it has directional stiffness properties but certain symmetries will hold. In particular, an orthotropic material has planes of symmetry and principal material axes, such that loading along these principal axes in tension or compression does not induce shear stresses and strains; the applications of shear stresses do not produce normal strains. The individual layers of a composite, whether it is a layer in a laminate or a layer in a filament-wound structure, closely follow this assumption, with the principal material axes aligned transverse to the fibers.

A lamina is a single ply (unidirectional) in a laminate, which is made up of a series of layers, as shown in [Figure 2.10](#).

When a kind of composite is considered to be an orthotropic material, the individual constituents of the fiber and the matrix are no longer explicitly considered, but instead,

Table 2.5: Properties of typical matrix resins ([Galanis, 2002](#))

Material	Specific Gravity	Modulus (GPa)	Tensile Strength (MPa)	Strain to Fail (%)	Poisson Ratio	Shrinkage on Cure (%)	Max Use (°C)
Polyester	1.2	3	60	2	0.36	7	65
Vinyl ester	1.15	3.4	80	4	0.36	5	90
Epoxy low T	1.2	3.2	90	4	0.38	2	90
Epoxy high T	1.28	3.8	80	3	0.38	2	140
Phenolic	1.15	3	50	2	0.35	N/A	130

only averaged or smeared properties in the different directions are employed. Because many composite structures are thin in the through-the-thickness direction, the theory is essentially a two-dimensional stress theory.

The major point of this section is to develop the relationships between stress and strain for a thin lamina (layer) of aligned fibers in a matrix. These relationships are applicable to all continuous-fiber composites and to aligned short-fiber composites. Those short-fiber composites that have more random fiber orientations and other materials, such as continuous fibers in what is called a random mat, may be considerably less directional in stiffness; in many cases, they can be analyzed as if they were conventional isotropic materials.

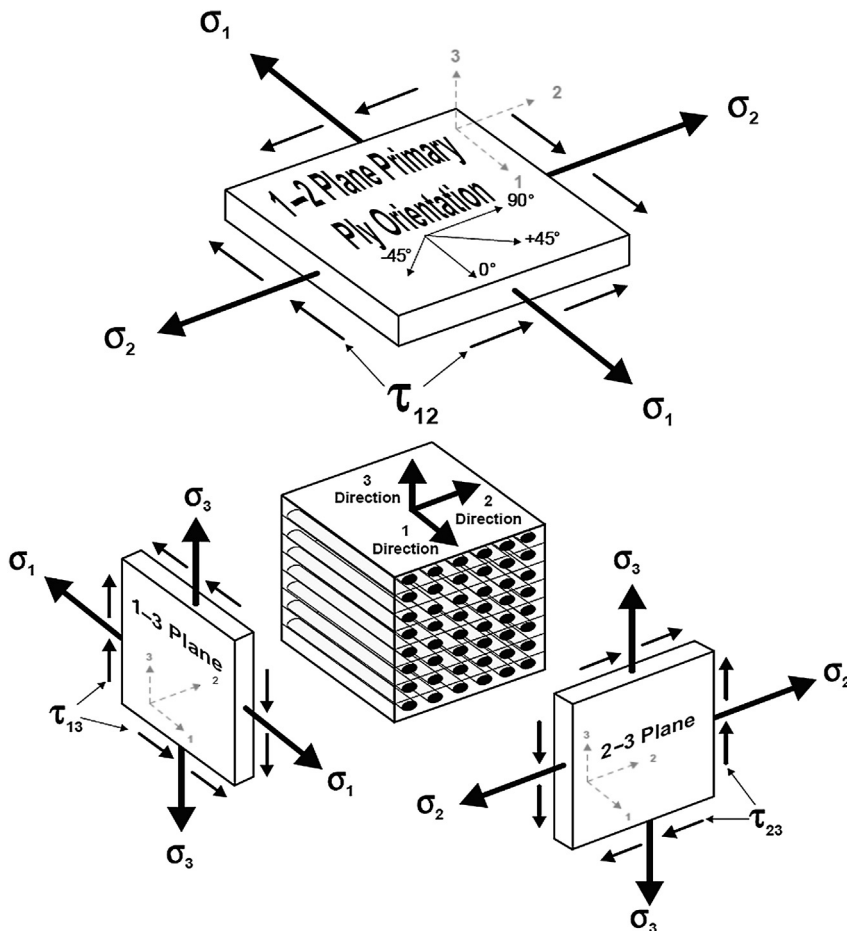


Figure 2.10
The lamina.

2.4.1 Orthotropic Properties

A unidirectional layer is shown below in Figure 2.11, along with the coordinate system used to establish notation. Here directions 1 and 2 refer to the fiber direction and transverse to the fibers in the plane of the ply, and direction 3 refers to the through-the-thickness direction. The modulus of the ply in the direction of the fibers is denoted by E_{11} , and the modulus of the ply in the transverse direction is denoted by E_{22} . The transverse to a uniaxial stress in the fiber direction is a strain given by

$$\varepsilon_1 = \frac{\sigma_1}{E_{11}} \quad (2.1)$$

The response to a uniaxial stress in (transverse) direction 2 is a strain given by

$$\varepsilon_2 = \frac{\sigma_2}{E_{22}} \quad (2.2)$$

It should be noted that the numbers 1 and 2 indicate directions and have nothing to do with the principal stresses. Similarly, in-plane shear modulus G_{12} can be defined so that the response to a shear stress is a shear strain given by

$$\gamma_{12} = \frac{\tau_{12}}{G_{12}} \quad (2.3)$$

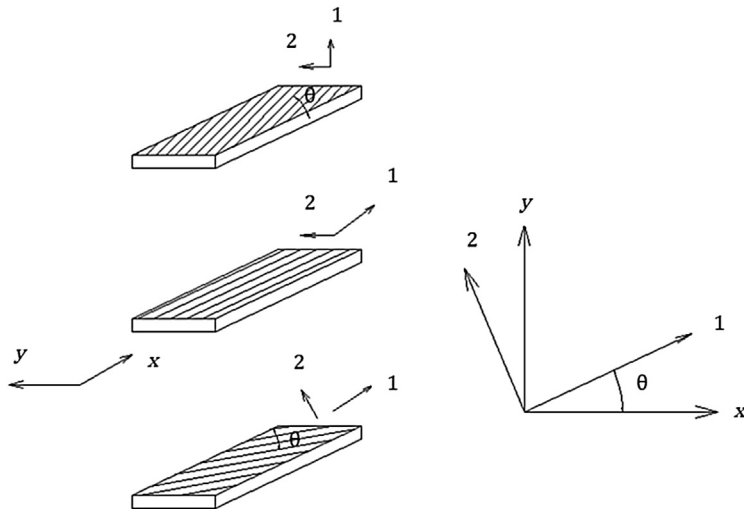


Figure 2.11
A unidirectional layer.

The Poisson ratio can also be defined in the same way. Considering a uniaxial stress in (fiber) directional, a strain in (transverse) direction 2 will occur due to the Poisson effect. The appropriate Poisson ratio can be defined as (for uniaxial stress in direction 1)

$$\varepsilon_2 = -\nu_{12}\varepsilon_1 \quad (2.4)$$

Conversely, if a uniaxial stress is applied in (transverse) direction 2, the strain in (fiber) direction 1 can be defined in terms of the appropriate Poisson ratio as (for uniaxial stress in direction 2)

$$\varepsilon_1 = -\nu_{21}\varepsilon_2 \quad (2.5)$$

The stress and strain in the through-the-thickness direction can be defined in a similar manner.

$$\varepsilon_3 = \frac{\sigma_3}{E_{33}} \quad (2.6)$$

$$\varepsilon_1 = -\nu_{31}\varepsilon_3 \quad (2.7)$$

For uniaxial stress in direction 2,

$$\varepsilon_2 = -\nu_{32}\varepsilon_3 \quad (2.8)$$

Finally, these straightforward notions can be combined using the idea of superposition. The strain in direction 1 results both from a stress σ_1 through the Poisson effect and from stresses σ_2 and σ_3 . Thus, stresses σ_1 and σ_2 and σ_3 are then applied. A strain in direction 1 results from each of these stresses, and is the sum of the strains that would result from these stresses applied separately. The strains in direction 1, for each load acting separately, are as follows.

σ_1 loading:

$$\varepsilon_1 = \frac{\sigma_1}{E_{11}} \quad (2.9)$$

σ_2 loading:

$$\varepsilon_1 = -\nu_{21}\varepsilon_2 = \frac{-\nu_{21}\sigma_2}{E_{22}} \quad (2.10)$$

σ_3 loading:

$$\varepsilon_1 = -\nu_{31}\varepsilon_3 = \frac{-\nu_{31}\sigma_3}{E_{33}} \quad (2.11)$$

Combining these loadings and adding the strains in direction 1 by superposition the following is obtained.

$$\varepsilon_1 = \frac{\sigma_1}{E_{11}} - \frac{\nu_{21}\sigma_2}{E_{22}} - \frac{\nu_{31}\sigma_3}{E_{33}} \quad (2.12)$$

Similarly,

$$\varepsilon_2 = -\nu_{12}\frac{\sigma_1}{E_{11}} + \frac{\sigma_2}{E_{22}} - \frac{\nu_{32}\sigma_3}{E_{33}} \quad (2.13)$$

It is convenient to arrange these in a matrix. Using the standard matrix notation and procedures, the following matrix can be obtained.

$$\begin{pmatrix} \varepsilon_1 \\ \varepsilon_2 \\ \varepsilon_3 \\ \gamma_{23} \\ \gamma_{31} \\ \gamma_{12} \end{pmatrix} = \begin{bmatrix} \frac{1}{E_{11}} & -\frac{\nu_{21}}{E_{22}} & -\frac{\nu_{31}}{E_{33}} & 0 & 0 & 0 \\ -\frac{\nu_{12}}{E_{11}} & \frac{1}{E_{22}} & -\frac{\nu_{32}}{E_{33}} & 0 & 0 & 0 \\ -\frac{\nu_{13}}{E_{11}} & -\frac{\nu_{23}}{E_{22}} & \frac{1}{E_{33}} & 0 & 0 & 0 \\ 0 & 0 & 0 & \frac{1}{G_{23}} & 0 & 0 \\ 0 & 0 & 0 & 0 & \frac{1}{G_{31}} & 0 \\ 0 & 0 & 0 & 0 & 0 & \frac{1}{G_{12}} \end{bmatrix} \cdot \begin{pmatrix} \sigma_1 \\ \sigma_2 \\ \sigma_3 \\ \tau_{23} \\ \tau_{31} \\ \tau_{12} \end{pmatrix} \quad (2.14)$$

or

$$\{\varepsilon\} = \{S\} \cdot \{\sigma\} \quad (2.15)$$

The S matrix is often referred to as the compliance matrix for the lamina, or the strain–stress form of material properties with the strains being the dependent variables. It can be shown that the matrices describing the stress–strain relationships of an elastic material must be symmetric. The relationship can be given as

$$E_{11}\nu_{21} = E_{22}\nu_{12} \quad (2.16)$$

$$\frac{\nu_{12}}{E_{11}} = \frac{\nu_{21}}{E_{22}} \quad (2.17)$$

The off-diagonal terms are held off so that only nine material properties are required in order to fully characterize the linear behavior of a lamina in 3-D stress and strain

states. The zeros in the compliance matrix reflect the fact that the stress–strain behavior of an orthotropic material is being described (rather than a generally anisotropic material), and that the description is made with respect to the principal material axes.

2.4.2 Orthotropic Properties in Plane Stress

Because many engineering structures made of laminates are thin in the thickness direction, the following two-dimensional subset is frequently used. This can be obtained by setting $\sigma_3 = \tau_{13} = \tau_{23} = 0$ (a plane-stress assumption).

$$\begin{pmatrix} \varepsilon_1 \\ \varepsilon_2 \\ \gamma_{12} \end{pmatrix} = \begin{pmatrix} \frac{1}{E_{11}} & \frac{-\nu_{21}}{E_{22}} & 0 \\ \frac{-\nu_{12}}{E_{11}} & \frac{1}{E_{22}} & 0 \\ 0 & 0 & \frac{1}{G_{12}} \end{pmatrix} \begin{pmatrix} \sigma_1 \\ \sigma_2 \\ \tau_{12} \end{pmatrix} \quad (2.18)$$

The matrix of Eqn (2.18) can be inverted to obtain the stress–strain stiffness matrix below.

$$\begin{pmatrix} \sigma_1 \\ \sigma_2 \\ \tau_{12} \end{pmatrix} = \begin{pmatrix} Q_{11} & Q_{12} & 0 \\ Q_{21} & Q_{22} & 0 \\ 0 & 0 & Q_{66} \end{pmatrix} \begin{pmatrix} \varepsilon_1 \\ \varepsilon_2 \\ \gamma_{12} \end{pmatrix} \quad (2.19)$$

or

$$\{\sigma\} = [Q]\{\varepsilon\} \quad (2.20)$$

where the individual terms of the matrix are given by

$$Q_{11} = \frac{E_{11}}{D} \quad (2.21)$$

$$Q_{12} = \frac{\nu_{21}E_{11}}{D} \quad (2.22)$$

$$Q_{21} = \frac{\nu_{12}E_{22}}{D} \quad (2.23)$$

$$Q_{22} = \frac{E_{22}}{D} \quad (2.24)$$

$$Q_{66} = G_{12} \quad (2.25)$$

$$D = 1 - \nu_{12}\nu_{21} \quad (2.26)$$

so that

$$Q = \begin{pmatrix} \frac{E_{11}}{1 - \nu_{12}\nu_{21}} & \frac{\nu_{21}E_{11}}{1 - \nu_{12}\nu_{21}} & 0 \\ \frac{\nu_{12}E_{22}}{1 - \nu_{12}\nu_{21}} & \frac{E_{22}}{1 - \nu_{12}\nu_{21}} & 0 \\ 0 & 0 & \frac{1}{G_{12}} \end{pmatrix} \quad (2.27)$$

It should be noted that it is conventional to identify the Q_{66} term from its location in the full six-by-six matrix before the plane-stress assumption is made. Although there are five independent constants needed to describe the stress–strain response of the lamina, the S and Q matrices must still be symmetric. As a result, there are only four independent properties considered, and the reciprocity relation below is used.

$$E_{11}\nu_{21} = E_{22}\nu_{12} \quad (2.28)$$

2.5 Key Challenges for the Future of Marine Composite Materials

The main disadvantages of marine composites:

- Flexibility as a design constraint for equivalent thickness; an FRP hull would deflect about 10–12 times as much as steel hull;
- General issues: jointing, compressive strength, creep, vibration, abrasion, fuel tanks, quality control, lay-up, assembly, secondary bonds, vulnerability to fire, installation of the system.

Although high cost is a major factor, a number of technical issues are holding back composites from becoming widely used in the large-structure marine market. [Table 2.6](#) and [Table 2.7](#) summarize these challenges and opportunities.

Table 2.6: Military and commercial issues (Slater and Houlston, 1980).

Thick sections	Ultraviolet radiations
Compressive load behavior	Impact resistance
High stress design	Scaling/modeling
Nondestructive evaluation	Reliability
Joints and joining	Residual stress effects
Repair	Smoke and toxicity
Fire performance	Creep/stress rupture

Table 2.7: Primarily military (Slater and Houlston, 1980).

Shock performance	Acoustic behavior
Electromagnetic radiation	Ballistic performance

There are two major challenges for composite use: First from an economic front, there is a need to ensure that the CAPEX (capital expenditure) and OPEX (operating costs) of ships, boats, and other artifacts are optimized and the material specification leads are satisfactory. Second, with an ever-growing concern for sustainability, it is important to appreciate and understand environmental issues. These economic and energy-based outcomes can lead to the following five technical challenges (Shenoi et al., 2009):

- An enhanced fundamental understanding of the load transfer mechanisms in layered orthotropic structures using empirical, physical means to ensure confidence in the theoretical modeling capabilities;
- Better appreciation of the modeling for safety concerns, which account for potential variability and uncertainties in both material and structural behaviors;
- Life-cycle assessment of composite structures, leading to cradle-to-grave design concepts that are better able to account for environmental impacts based on energy considerations;
- Development of concurrent engineering approaches that account for design—production interaction leading to the specification of optimal design choices from a cost viewpoint;
- Identification of suitable inspection, intervention, and repair strategies in order to ensure continued structural health of the artifact throughout its life.

References

- Civgin, F., 2005. Analysis of Composite Bars in Torsion, Graduate School of Natural and Applied Sciences. Dokuz Eylul University.
- Galanis, K., 2002. Hull construction with Composite Materials for Ships over 100m in Length. Massachusetts Institute of Technology. Dept. of Ocean Engineering.
- Hasson, D.F., Crowe, C.R., 1988. Materials for Marine Systems and Structures. Academic Press, Inc.
- Mohan, M., Gurit, 2008. In: The Advantages of Composite Material in Marine Renewable Energy Structures, RINA Marine Renewable Energy Conference.
- Podolny Jr., W., 1996. In: Winds of Change and Paradigms of Obsolescence; Proc., the National Steel Bridge Symposium, October 15–17. Illinois, Chicago.
- Ratwani, M.M., 2002. Ph.D, Composite Materials and Sandwich Structures — a Primer.
- Shenoi, R.A., Dulieu-Barton, J.M., Quinn, S., Blake, J.I.R., Boyd, S.W., 2009. Composite Materials for Marine Applications—key Challenges for the Future, Composite Materials.

- Slater, J.E., Houlston, R., 1980. Selection of GRP composites for naval ship structures. In: Sih, G.C., Pindera, J.T. (Eds.), *Development and Design with Advanced Materials*. Elsevier, Amsterdam, pp. 289–300.
- Vinson, J.R., Sierakowski, R.L., 2008. *The Behavior of Structures Composed of Composite Materials, Solid Mechanics and Its Applications*, vol. 105.
- Zweben, C., 1989. *Introduction to Mechanical Behavior and Properties of Composites Materials*, vol. 1. DCDE.

Green Ship Concepts

3.1 General

Green ship means a ship with advanced, environmentally friendly technologies that reduce greenhouse gases (GHGs) or air pollutants generated during voyage. The technologies are divided into three large parts: reducing emissions, improving energy efficiency, and developing propulsion power.

Current environmental regulation systems are making the shipping industry more competitive. Shipping manufacturers are now making an effort to develop more fuel-efficient ships to compete with other global companies. There is existing technology that helps to mitigate environmental impacts due to ships. Equipment manufacturers must maintain levels of investment for new technologies, especially in the present economy. Future regulations for the “greening” of ships are likely to be adopted on an international level in the near future. This could provide a benchmark for further innovation and would ensure high-level technical designs that result in better products.

Considering the staggering percentage of world trade vessels transported, it should be noted that shipping is presently the most environmentally friendly mode of transportation, because emissions from ships are relatively small. Operational pollution has been reduced to a negligible amount. The International Convention for the Prevention of Marine Pollution from Ships (MARPOL 73/78) is the most important set of international rules dealing with the environment and the mitigation of pollution from ships (EMEC, 2010).

In addition, the International Maritime Organization (IMO) has extensively discussed ways to reduce GHG emissions. The energy efficiency design index (EEDI), indicated by the quantity of CO₂ allowed during transportation, in units of freight per distance, was enforced in 2013. If the EEDI is not satisfied, transportation is forbidden.

The purpose of this chapter is to discuss a few green technologies, and specifically emissions technology, because it plays a large role in the greenhouse effect.

3.2 Emissions

Shipbuilding companies are focusing on some specific regulations, such as those pertaining to GHGs and air pollutants. Emissions regulations were created in order to try to reduce these effects.

3.2.1 Regulations on Air Pollution

Annex VI of MARPOL 73/78 sets regulations regarding air pollution from the operation of ships. The first convention took place on May 19, 2005. Nitrogen oxides (NO_x) and sulfur oxides (SO_x) represent air pollution in the regulations set up in Annex VI; however, there are still no detailed regulations for GHGs within Annex VI (Table 3.1 Annex VI NO_x Emission Control).

3.2.2 Regulations on GHGs

A GHG is air in the earth's atmosphere that creates a greenhouse effect by absorbing partial radiant energy. CO₂ is considered a GHG. Contents covered at the 57th meeting of the Marine Environment Protection Committee (MEPC) in 2008 included

- setting compulsive restrictions on the EEDI for the latest shipbuilding architectures
- compulsive/voluntary energy efficiency operational indicator (EEOI) report
- including a penalty for value that does not satisfy the established compulsive restriction EEOI value.

A plan to set market regulations and the progress of research previously done on GHG by IMO were discussed at the MEPC 58th meeting in 2009.

3.2.3 Effect of Design Variables on the EEDI

Shipping companies had to develop new methods to increase oil efficiency and reduce the amount of oil used, in response to increasing oil prices. IMO produced an EEDI that

Table 3.1: Annex VI NO_x emissions control

Year of Ship Construction	Range of Application			Emission Control
1990–1999	Size of engine >5000 kW			Tier I
2000–2010	Size of engine >130 kW			
2011–2015				Tier II
2016–	Ship >24 ML			
	Total propulsive power >750 kW			Tier III
Net Weight of NO ₂ Emission (g/kWh)				
RPM	<130	130–2000	>2000	Decrease in NO ₂ Relative to Tier I
Tier I	17.0	45.0*n ^(-0.2)	9.8	—
Tier II	14.36	44.0*n ^(-0.2)	7.66	15.5%–21.8%
Tier III	3.40	9*n ^(-0.2)	1.96	80%

would measure the efficiency of CO₂ from a new ship. The EEDI set up at the MEPC 57th–59th meetings is an equation that calculates carbon emission quantity per tonne-mile, given by

$$EEDI = \frac{\text{Engine Power} \times \text{SFC} \times \text{CF}}{\text{Capacity} \times \text{Speed}} \quad (3.1)$$

where,

SFC: Specific fuel consumption

CF: Conversion factors

and where the numerator is the carbon emission quantity and the denominator is the efficiency of shipping. A small EEDI means that the ship is more eco-friendly and efficient. The total formulation of the above equation is

$$EEDI = \frac{\left(\sum_{i=1}^{n_{ME}} P_{ME(i)} \cdot C_{FME(i)} \cdot SFC_{ME(i)} \right) + (P_{AE} \cdot C_{FAE} \cdot SFC_{AE*}) + \left(\left(\sum_{j=1}^M f_j \cdot \sum_{i=1}^{n_{PTI}} P_{PTI(i)} - \sum_{i=1}^{n_{eff}} f_{eff(i)} \cdot P_{AEeff(i)} \right) C_{FAE} \cdot SFC_{AE} \right) - \left(\sum_{i=1}^{n_{eff}} f_{eff(i)} \cdot P_{eff(i)} \cdot C_{FME} \cdot SFC_{ME} \right)}{f_i \cdot \text{Capacity} \cdot V_{ref} \cdot f_w} \quad (3.2)$$

where,

Power: P_{ME} and P_{AE}

Conversion factors: C_{FME} and C_{FAE}

Specific fuel consumption: SFC_{ME} and SFC_{AE}

Speed: V_{ref}

Capacity

Innovative energy efficiency technologies: P_{eff} , P_{AEeff} , and f_{eff}

Correction factors: f_i , f_j , and f_w

Power should be 75% of the maximum continuous rating (MCR) when calculating the above formula, because of the class and because IMO mostly assigned weights about fuel consumption measurement and NO_x emission control. The power of the auxiliary engine is calculated using an empirical formula. The influence of the development of innovative energy efficiency is also considered through the quantities P_{eff} and P_{AEeff} .

How design values are influenced by the EEDI is discussed in an experiment using assumptions shown in [Table 3.2](#) below.

Table 3.2: Container ship assumptions used for calculations

	Feeder	Panamax	Baby Neo-Panamax	Post-Panamax	Ultralarge
Slot (TEU)	1000	4500	4500	8000	12,500
Round trip distance (nm)	1317	11,665	11,665	11,380	11,380

CO₂, which is used to calculate the EEDI, is first calculated using

$$\text{CO}_2 \text{ Production} = \text{Time} \times \left\{ \begin{array}{l} (\text{ME}_{\text{LOAD}} \times \text{SFC}_{\text{ME}} \times \text{Cf}_{\text{ME}}) \\ + (\text{SSDG}_{\text{LOAD}} \times \text{SFC}_{\text{SSDG}} \times \text{Cf}_{\text{SSDG}}) \end{array} \right\} \quad (3.3)$$

where,

Time: Time to take round trip

ME_{LOAD}: Main engine average power consumption (kW)

SFC_{ME}: Main engine fuel consumption rate

Cf_{ME}: Carbon content conversion factor of consumed fuel at the main engine

SSDG_{LOAD}: Auxiliary engine average power consumption (kW)

SFC_{SSDG}: Auxiliary engine fuel consumption rate

Cf_{SSDG}: Carbon content conversion factor of consumed fuel at the auxiliary engine

The standard used for calculating the EEDI with regard to the carbon content conversion factor of fuel is given in Table 3.3 below.

The term Cf proposed above is the carbon content conversion factor, and is used for calculating CO₂ emission quantities. Emitted CO₂ is computed by multiplying Cf by the specific fuel consumption during a ship's operation.

The table below shows CO₂ emission quantities for post-Panamax ships of about 8000 TEU. Table 3.4 CO₂ Emission of 8000 TEU post Panamax.

Table 3.3: Carbon content of fuel and C_f

Kind of Fuel	Basis	Carbon Content	C _f
Diesel/Gas oil	ISO 8217	0.875	3.20600
Light fuel oil	ISO 8217	0.860	3.15104
Heavy fuel oil	ISO 8217	0.850	3.11440
LPG (propane)	2006 IPCC guidelines	0.819	3.00000
LPG (butane)	2006 IPCC guidelines	0.827	3.03000
Natural gas	2006 IPCC guidelines	0.750	2.75000

Table 3.4: CO₂ emissions of post-Panamax ships of about 8000 TEU

HFO Cons.	Time (Days)	Fuel Cons. (kg/h)	Fuel Cons. (t)	CO ₂ Emissions (t)
At sea—westbound	9.21	8824	1950.9	6076
At sea—eastbound	9.21	8824	1950.9	6076
Maneuvering—westbound	0.07	3026	5.3	16
Maneuvering—eastbound	0.07	3026	5.3	16
At anchor	0.00	1098	0.0	0
Port—cargo operations	1.58	1098	41.6	130
Port—waiting	0.04	1098	1.1	3
Total	20.19		3955.1	12,318

3.2.4 Influence of Speed on the EEDI

MAN Diesel & Turbo B&W and ME series engines, which are often used these days, are selected when considering a change in a container ship's speed. Each engine's power is controlled to achieve a designed speed. It is assumed that the main engine is operating at 15% of the sea margin and 90% of the MCR. The specific fuel consumption of each engine assumes that it is operating at 75% of the MCR and using marine diesel oil. This meets ISO conditions. The resulting EEDIs are given in Table 3.5.

3.2.5 Influence of Hull Steel Weight on the EEDI

Two situations were put to the test to determine how a 5% increase in the steel weight of the ship influences the EEDI. One is where the block coefficient (C_B) is constant at the

Table 3.5: Influence of speed on the EEDI

Design Speed Variation		−4 kn	−2 kn	Standard
4500 TEU (Panamax)	Service speed (design)	20.50	22.50	24.50
	DWT (t)	60,008	59,519	58,817
	MCR _{ME} (kW)	20,484	28,040	38,532
	EEDI	11.31	14.15	17.99
	Change vs standard design	−37%	−21%	—
4500 TEU (Baby Neo-Panamax)	Service speed (design)	20.50	22.50	24.50
	DWT (t)	62,079	61,539	60,747
	MCR _{ME} (kW)	21,279	29,575	41,330
	EEDI	11.34	14.39	18.64
	Change vs standard design	−39%	−23%	—
8000 TEU (post-Panamax)	Service speed (design)	21.00	23.00	25.00
	DWT (t)	97,857	97,089	96,068
	MCR _{ME} (kW)	31,982	43,341	57,843
	EEDI	10.53	13.07	16.17
	Change vs standard design	−35%	−19%	—

Table 3.6: Influence of 5% increase in hull steel weight on the EEDI (Youngsoo et al., 2010)

Standard Design			Hull Steel Weight Increased by 5%	
			C _B	Constant DWT
4500 TEU (Panamax)	DWT (t)	58,817	58,184	58,845
	EEDI	17.99	18.20	18.14
	Change vs standard design	—	1.1	0.8
4500 TEU (Baby Neo-Panamax)	DTW (t)	60,747	60,123	60,747
	EEDI	18.64	18.85	18.81
	Change vs standard design	—	1.1%	0.9%
8000 TEU (post-Panamax)	DTW (t)	96,068	94,991	96,068
	EEDI	16.17	16.36	16.33
	Change vs standard design	—	1.2%	1.0%

design draft—the efficiency of decreasing DWT can be obtained through this assumption. The other is where DWT is constant at the load line, through C_B. Results for each condition are given in Table 3.6 (Youngsoo et al., 2010).

3.3 Ballast Water Treatment

Ballast water is the water in a ballast tanker that balances out the ship when its weight is unevenly distributed during voyage. Usually in coastal regions, ballast water in the tanker is filled to equal 10–50% of the ship's tonnage; it is drained when the load changes. During this process, 10–12 billion metric tons of salt water is displaced.

Changing ballast water displaces many aquatic organisms. Displacing organisms can alter marine flora and fauna and cause damage to huge marine industries such as the fishing industry (EMEC, 2010).

The following are examples of marine plants, animals, and microbes that are carried around the world in ships' ballast water as shown in Figure 3.1.

1. Cholera—*Vibrio cholerae* (various strains)
 - a. Native to various strains with broad ranges
 - b. Introduced to South America, the Gulf of Mexico, and other areas
 - c. Some cholera epidemics appear to be directly associated with ballast water
2. Cladoceran water flea—*Cercopagis pengoi*
 - a. Native to the Black Sea and the Caspian Seas
 - b. Introduced to the Baltic Sea
 - c. Reproduces and forms very large populations that dominate the zooplankton community and clog fishing nets and trawls

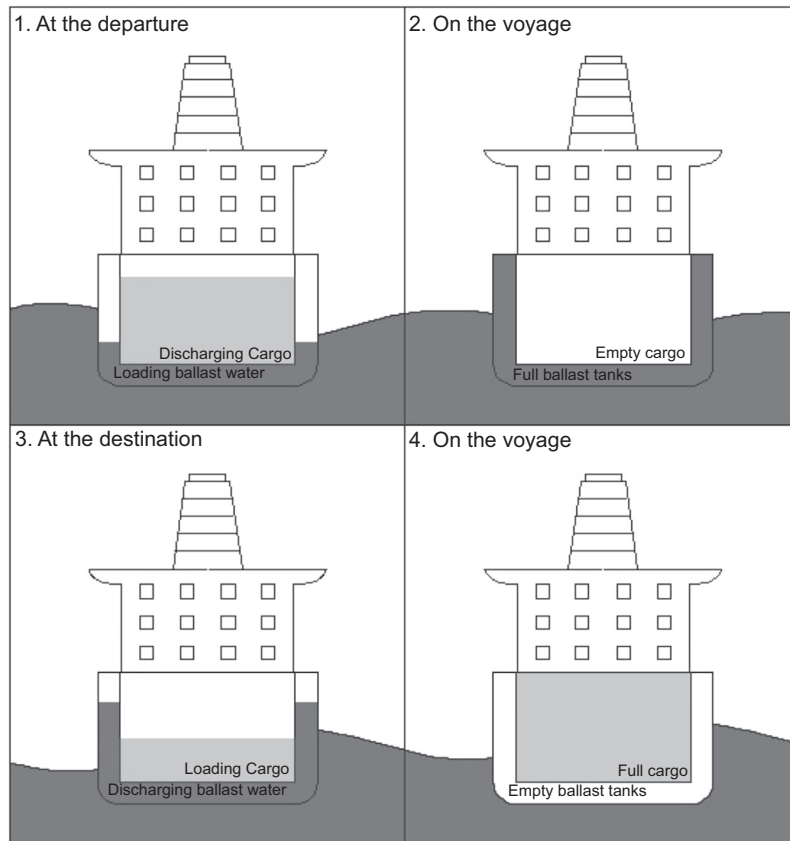


Figure 3.1

The circulation of ballast water during a ship's voyage.

3. Mitten crab—*Eriocheir sinensis*
 - a. Native to Northern Asia
 - b. Introduced to Western Europe, the Baltic Sea, and the West Coast of North America
 - c. Undergoes mass migrations for reproductive purposes; burrows into riverbanks and dykes, causing erosion and siltation; preys on native fish and invertebrate species, causing local extinctions to occur during population outbreaks; interferes with fishing activities
4. Toxic algae (red/brown/green tides)—various species
 - a. Native to various species with broad ranges
 - b. Several species have been transferred to new areas in the ballast water of ships
 - c. May form harmful algae blooms; much marine life is killed by toxins and/or mucus released by some species; can foul beaches and impact tourism and recreation; some species may contaminate filter-feeding shellfish and cause fisheries to close; consumption of contaminated shellfish may cause severe illness and death

5. Round goby—*Neogobius melanostomus*
 - a. Native to the Black Sea, the Sea of Asov, and the Caspian Seas
 - b. Introduced to the Baltic Sea and North America
 - c. Highly adaptable and invasive; increases in number and spreads quickly; competes for food and habitats with native fishes, including commercially important species, and preys on their eggs and young; spawns multiple times per season and can survive in poor water quality
6. North American comb jelly—*Mnemiopsis leidyi*
 - a. Native to the Eastern Seaboard of the Americas
 - b. Introduced to the Black Sea, the Sea of Azov, and the Caspian Seas
 - c. Reproduces rapidly (self-fertilizing hermaphrodite) under favorable conditions; it alters the food chain and ecosystem function by excessively feeding on zooplankton; contributed significantly to closure of fisheries in the Black Sea and Sea of Azov in the 1990s, resulting in massive economic and social impacts; now threatens similar impacts to the Caspian Sea
7. North Pacific sea star—*Asterias amurensis*
 - a. Native to the Northern Pacific
 - b. Introduced to Southern Australia
 - c. Reproduces in large numbers, rapidly reaching “plague” proportions, and invades environments; feeds on shellfish, including commercially valuable scallop, oyster, and clam species
8. Asian kelp—*Undaria pinnatifida*
 - a. Native to Northern Asia
 - b. Introduced to Southern Australia, New Zealand, the West Coast of the United States, Europe, and Argentina
 - c. Grows and spreads rapidly, both vegetatively and through the dispersal of spores; displaces native algae and marine life; alters its habitat, the ecosystem, and the food web; may affect commercial shellfish stocks through space competition and alteration of habitats
9. European green crab—*Carcinus maenas*
 - a. Native to the European Atlantic Coast
 - b. Introduced to Southern Australia, South Africa, the United States, and Japan
 - c. Highly adaptable and invasive; resistant to predation due to its hard shell; competes with and displaces native crabs, and becomes a dominant species in invaded areas; consumes and depletes a wide range of prey species; alters intertidal rocky shore ecosystems

All ships now have to be fitted with ballast water treatment systems. The various technologies/methods currently available are chemical treatment, heating, filtration, ultraviolet light, etc. The International Convention for the Control and Management of

Ships' Ballast Water and Sediments also allows for the adoption of prototype technologies in certain ships if agreed upon by the IMO. There are already effective technologies in existence, but those are open to further innovation and research. Removing organisms from ballast water goes a long way to ensuring that alien species do not invade fragile marine ecosystems (EMEC, 2010).

3.4 Underwater Coatings

Attached marine growth and serious corrosion affect the frictional resistance performance of any ship. Many ships are protected from marine growth and corrosion through different coatings, such as antifouling paints, that include hazardous toxic chemicals that can be harmful to marine organisms. Annex I of the IMO AFS Convention contains a list of harmful antifouling systems and the measures that need to be taken when they are applied.

Another possible solution to marine growth and corrosion is the marine growth prevention system (MGPS), which has the same effects as antifouling paint. The MGPS is equipment that uses sodium hypochlorite produced by electrodes used in electrolysis. Another possibility is the use of modern biocides, which have short life expectancies and a low risk of environmental accumulation. Biocides with low risks of biological accumulation also can be acceptable (EMEC, 2010).

References

- EMEC, 2010. Green Ship Technology Book 2nd Edition, second ed. European Marine Equipment Council.
Youngsoo, Y., Seongteak, K., Sinhyung, K., 2010. "Green Ship Design", Computational Structure Engineering, third ed., vol. 23 Planned Special Articles, pp. 55–60.

LNG Carrier

4.1 Introduction

An LNG carrier, or LNG ship, is a tank ship designed for transporting liquefied natural gas (LNG) under the temperature of $-162\text{ }^{\circ}\text{C}$. A typical modern LNG carrier is approximately 300 m long and 43 m wide and has a draft of about 12 m. LNG carriers vary in cargo capacity, from 1000 to 267,000 m^3 , but the majority of modern vessels are between 125,000 and 150,000 m^3 . Smaller LNG carriers (1000–25,000 m^3 capacity) also operate in some areas, such as Norway and Japan.

It is a product that is internationally known by its high technology, high difficulty, and high value. It has the honor of being called “the crown jewel,” and only 13 shipyards in the world are capable of building this LNG carrier.

LNG carriers provide the link in the LNG chain between where the natural gas is liquefied and where it can be turned into gas. LNG carriers enable large amounts of clean natural gas energy to be transported to the consumer long distances from the LNG Liquefaction Plant. The fleet of LNG carriers continues to experience tremendous growth as the LNG market grows. [Figure 4.1](#) is a picture of two typical LNG carriers.



Figure 4.1
Two typical LNG carriers.

4.2 Development

The first LNG carrier, Methane Pioneer, left the Calcasieu River on the Louisiana Gulf coast on January 25, 1959. It carried the world's first ocean cargo of LNG to the United Kingdom. Subsequent expansion of that trade has brought on a large expansion of the fleet to today where giant LNG ships carrying up to 266,000 m³ are sailing worldwide.

The success of the specially modified C1-M-AV1-type standard ship Normarti, renamed The Methane Pioneer, caused the Gas Council and Conch International Methane Ltd. to order two purpose-built LNG carriers to be constructed: the Methane Princess and the Methane Progress. The ships were fitted with Conch-independent aluminum cargo tanks and entered the Algerian LNG trade in 1964. These ships had a capacity of 27,000 m³. In the late 1960s opportunity arose to export LNG from Alaska to Japan, and in 1969 that trade was initiated. Two ships, each with a capacity of 71,500 m³, were built in Sweden. In the early 1970s, the United States Government encouraged United States shipyards to build LNG carriers, and a total of 16 LNG ships were built. The late 1970s and early 1980s brought the prospect of Arctic LNG ships with a number of projects being studied.

With the increase in cargo capacity to approximately 143,000 m³, new tank designs were developed, from Moss Rosenberg to Technigaz Mark III and Gaztransport No. 96.

The size and capacity of LNG carriers have increased greatly in recent years. Since 2005, Qatargas has pioneered the development of two new classes of LNG carriers, referred to as Q-Flex and Q-Max. Each ship has a cargo capacity of between 210,000 and 266,000 m³ and is equipped with a reliquefaction plant. The following figure gives a brief introduction of the number of LNG ships built from 1965 to 2006, and we can naturally see the increasing number of LNG ships in recent years as shown in [Figure 4.2](#).

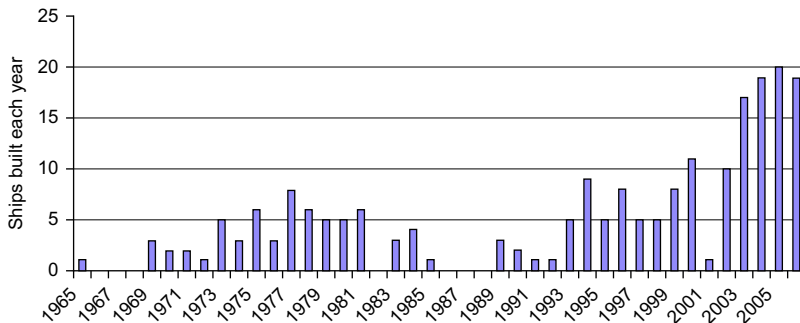


Figure 4.2
Number of LNG ships built 1965–2006.

According to a presentation by Golar LNG Partners, in June 2012 there were 72 new builds on order. Today the majority of the new ships under construction are in the size of 120,000–140,000 m³ but there are orders for ships with capacity up to 260,000 m³.

Since the 1980s, as Japan and South Korea became the first and second largest LNG import countries, the shipyards in Japan and South Korea imported the building technology and building patent of independent liquid cargo-type LNG carriers and membrane-type LNG carriers from the European shipyards, and separately started to build LNG carriers in the early 1980s and early 1990s. With the increasing number of LNG carriers built in the shipyards of Japan and South Korea, the shipyards of Europe got less and less market share of LNG carriers. From 2001 to October 2006, there were 89 LNG carriers completed, 55 of which were completed by South Korean shipyards, and 22 of them were completed by Japanese shipyards. Thus, the center of LNG carrier building has changed from Europe–America to Asia.

At the end of 2011, there were 359 LNG ships engaged in the ocean movement of LNG.

4.3 Typical Cargo Cycle

There are seven steps that should be followed for a typical cargo cycle of the LNG. The specific steps are as follows: Gas free → Inert → Gas up → Cool down → Bulk loading → Voyage → Discharge → Gas free. A simple introduction of the typical cargo cycle can be seen in [Figure 4.3](#).

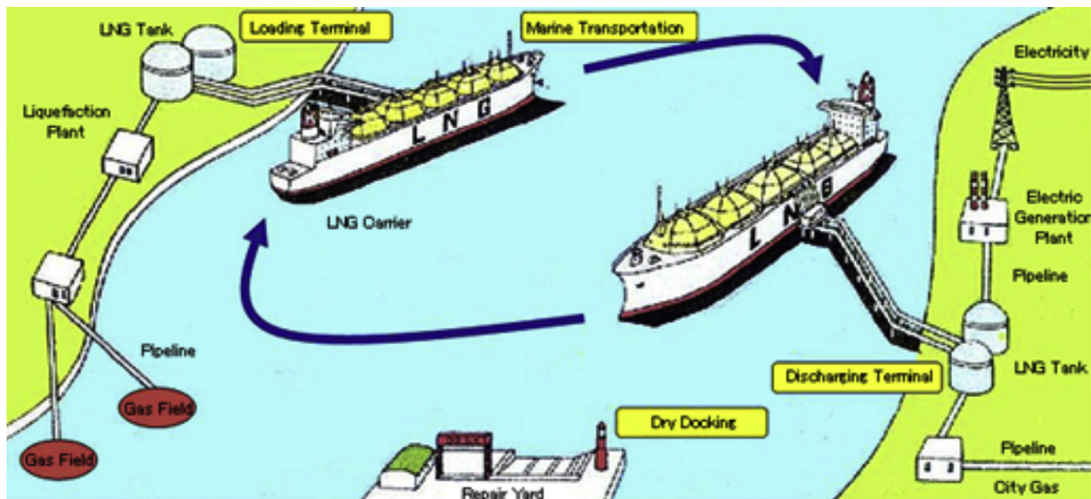


Figure 4.3
Typical cargo cycle.

4.3.1 Inert

A typical cargo cycle starts with the tanks in a “gas-free” condition, meaning the tanks are full of air, which allows for maintenance on the tank and pumps. Cargo cannot be loaded directly into the tank, as the presence of oxygen would create an explosive atmospheric condition within the tank, and the rapid temperature change caused by loading LNG at $-162\text{ }^{\circ}\text{C}$ could damage the tanks. So, the tank must be “inert” first to eliminate the risk of explosion. An inert gas plant burns diesel in air to produce carbon dioxide (CO_2); this is blown into the tanks until the oxygen level is below 4%. Then, the vessel goes into port to “gas up” and “cool down,” because it still cannot load directly into the tank. The CO_2 will freeze and damage the pumps and the cold shock could damage the tank’s pump column.

4.3.2 Gas Up

At this step, liquid LNG is brought onto the vessel and taken along the spray line to the main vaporizer, which boils off the liquid into gas. This is then warmed to roughly $20\text{ }^{\circ}\text{C}$ in the gas heaters and then blown into the tanks to displace the “inert gas.” This continues until all the CO_2 is removed from the tanks. Initially, the inert gas is vented to the atmosphere. Once the hydrocarbon content reaches 5% (lower flammability range of methane) the inert gas is redirected to shore via a pipeline and manifold connection by the HD (high duty) compressors. Shore terminal then burns this vapor to avoid the dangers of having large amounts of hydrocarbons around that may explode. Now the vessel is gassed up and warm. The tanks are still at ambient temperature and are full of methane. The next stage is cool down.

4.3.3 Cool Down

Liquid LNG is sprayed into the tanks via spray heads, which vaporizes and starts to cool the tank. The excess gas is again blown ashore to be reliquefied or burned at a flare stack. Once the tanks reach about $-140\text{ }^{\circ}\text{C}$ the tanks are ready to load bulk.

4.3.4 Bulk Loading

Bulk loading starts and LNG is pumped from the storage tanks ashore into the vessel tanks. Displaced gas is blown ashore by the HD compressors. Loading continues typically until 98.5% of the capacity is reached (the other 1.5% allows for thermal expansion/contraction of cargo).

4.3.5 Voyage

The vessel can now proceed to the discharge port. During passage various boil-off management strategies can be used. Depending on the design of the vessel, the boiled-off

gas can be burned in boilers to provide steam for propulsion, or it can be reliquefied and returned to the cargo tanks.

4.3.6 Discharge

Once in the discharge port, the cargo is pumped ashore using the cargo pumps. As the tank empties, the vapor space is filled by either gas from ashore or by vaporizing some cargo in the cargo vaporizer. Either the vessel can be pumped out as far as possible, with the last being pumped out with spray pumps, or some cargo can be retained on board as a “heel.” If all the cargo is pumped ashore, then on the ballast passage the tanks will warm up to ambient temperature, returning the vessel to a gassed up and warm state. The vessel can then be cooled again for loading.

4.3.7 Gas Free

If the vessel is to return to a gas free state, the tanks must be warmed up by using the gas heaters to circulate warm gas. Once the tanks are warmed up, the inert gas plant is used to remove the methane from the tanks. Once the tanks are methane free, the inert gas plant is switched to dry air production, which is used to remove all the inert gas from the tanks until they have a safe working atmosphere.

4.4 Containment Systems

Today, there are five containment systems in use for new-build vessels. Two of the designs are of the self-supporting type, while the other three are of the membrane type. The patents are owned by Gaz Transport & Technigaz (GTT).

Table 4.1 gives a brief comparison of the SPB-type, MOSS-type, and membrane-type LNG carriers. We can see from the table when compared to the MOSS type and the

Table 4.1: Comparison of SPB, MOSS, and membrane-type LNG carriers

Compared Contents	SPB	MOSS	Membrane
Size	Compact	Large	Compact
Ship weight	Light	The most weighted	Light
Number of tanks	The least	More	More
Rate of gasification	0.05%/day	0.08%/day	$GT \geq 0.1\%/day$
Space of the deck	Totally unlimited	Limited	Unlimited
Arbitrary loading	Possible	Possible	Impossible
Navigation	Easy	Hard	Easy
Pressure control	Easy	Complicated	Most complicated
Temperature control	Easy	Complicated	Complicated
Amount of liquid unpumped	3 m ³ /tank	6 m ³ /tank	200–400 m ³ /tank

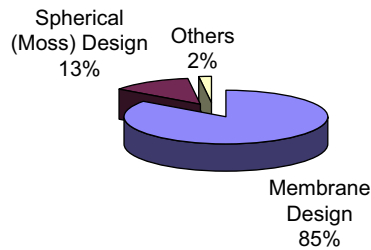


Figure 4.4

LNG fleet containment system order book (number of ships) (2005–2010).

membrane type, the SPB-type tanks have the advantages of easy operation, elimination of different pressure controls, and an easy handling method between the inner hull and the cargo hull.

There is a trend toward the use of the two different membrane types instead of the self-supporting storage systems. [Figure 4.4](#) gives a brief introduction of the LNG fleet containment system order book from years 2005–2010. From the figure we can see that the membrane-type tanks are in 85% of the fleet, and Moss-type tanks are in 13%, and other types are in 2%.

This is most likely due to the fact that the prismatic membrane tanks utilize the hull shape more efficiently and thus have less void space between the cargo tanks and the ballast tanks. As a result of this, the Moss-type design compared to a membrane design of equal capacity will be far more expensive to transit the Suez Canal. However, self-supporting tanks are more robust and have greater resistance to sloshing forces, and will possibly be considered in the future for offshore storage where bad weather will be a significant factor.

We will separately introduce the self-supporting-type and the membrane-type tanks in detail in the following paragraphs.

4.4.1 Self-Supporting Type

There are two types of LNG containment systems for the self-supporting-type containment system: Moss tanks (spherical IMO-type B LNG tanks) and IHI (prismatic IMO-type B LNG tanks).

Moss Tanks (Spherical IMO-Type B LNG Tanks)

This spherical tank design is owned by the Norwegian company Moss Maritime. Most Moss-type vessels have four or five tanks. The typical inner structures of the Moss tank and the typical Moss-type LNG carrier can be seen in [Figures 4.5 and 4.6](#).

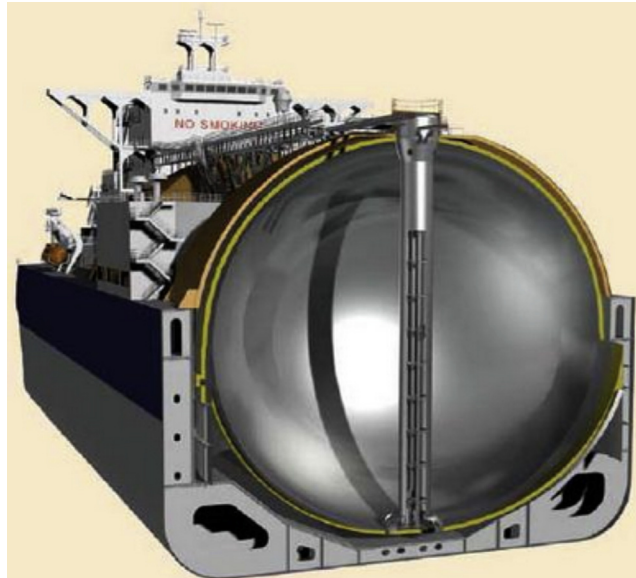


Figure 4.5
Typical inner structures of the Moss tank.

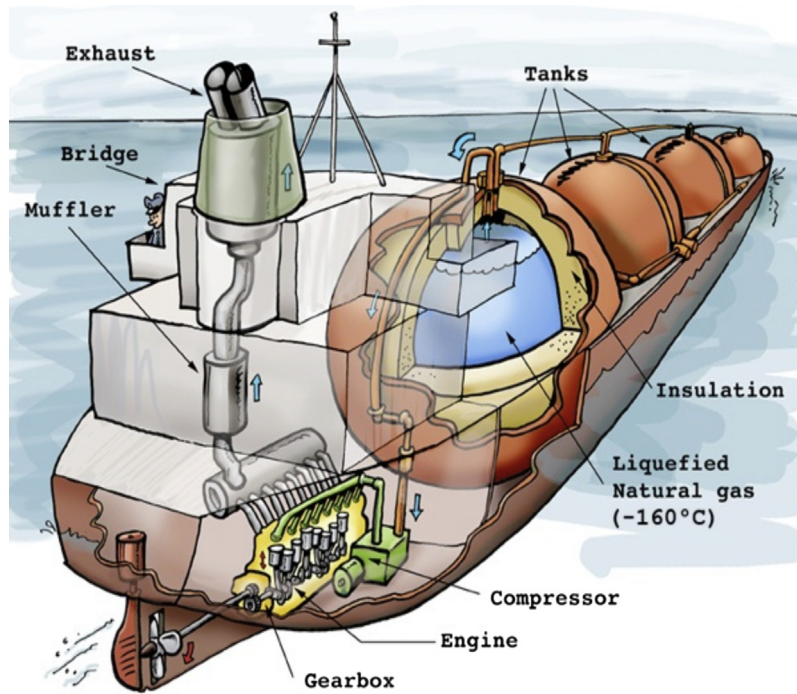


Figure 4.6
Typical Moss-type LNG carrier.

The outside of the tank has a thick layer of foam insulation that is fitted in panels. Over this insulation is a thin layer of “tin foil,” which allows the insulation to be kept dry with a nitrogen atmosphere. This atmosphere is constantly checked for any methane that would indicate a leak of the tank. Also the outside of the tank is regularly checked at a roughly 3 month interval for any cold spots that would indicate breakdown in the insulation.

The tank is supported around its circumference by the equatorial ring, which is supported by a large circular skirt that takes the weight of the tank down to the ship’s structure. This skirt allows the tank to expand and contract during cool-down and warm-up operations. During the cool-down or warm-up phase, the tank can expand or contract about 2 ft. Because of this expansion and contraction all piping into the tank comes in via the top and is connected to the ships lines via flexible bellows.

Inside each tank there is a set of spray heads. These heads are mounted around the equatorial ring and are used to spray liquid LNG onto the tank walls to reduce the temperature.

IHI (Prismatic IMO-Type B LNG Tanks)

The self-supporting prismatic type B (SPB) tank was developed by Ishikawajima—Harima Heavy Industries. Only two vessels currently have the SPB containment system.

The SPB-type LNG tanks use alloy-5083 (aluminum—4.5% magnesium) as the material because of its properties of high strength and capability for welding. The prismatic tank structure makes it easier to be installed in the ship hull, and makes the deck more flat.

The SPB LNG tanks also have an important advantage over membrane LNG carrier tanks, which may break due to sloshing impact and therefore destroy the ship’s hull. No sloshing problems have ever occurred on SPB LNG tanks. In addition, SPB LNG tanks can sustain internal accidental damage due, for example, to internal equipment releases. This is absolutely not the case for membrane LNG tanks, because several incidents have been recorded inside membrane LNG tanks.

4.4.2 Membrane Type

Gaz Transport & Technigaz (which were merged into one company named GTT) designed the two types of membrane systems, whose stiffness and stability were provided by the ship hull structure. Currently, a new system named CS1, which combines the advantages of the two membrane systems, has been developed. The common characteristics of the three systems are that they all use thin metal (0.7–1.5 mm) material as the inner plane of the tanks; they are used as insulation boards and secondary barrier membranes, and every layer is closely connected with the ship hull. But the construction material, construction method, and the connection method of the three systems are very different.

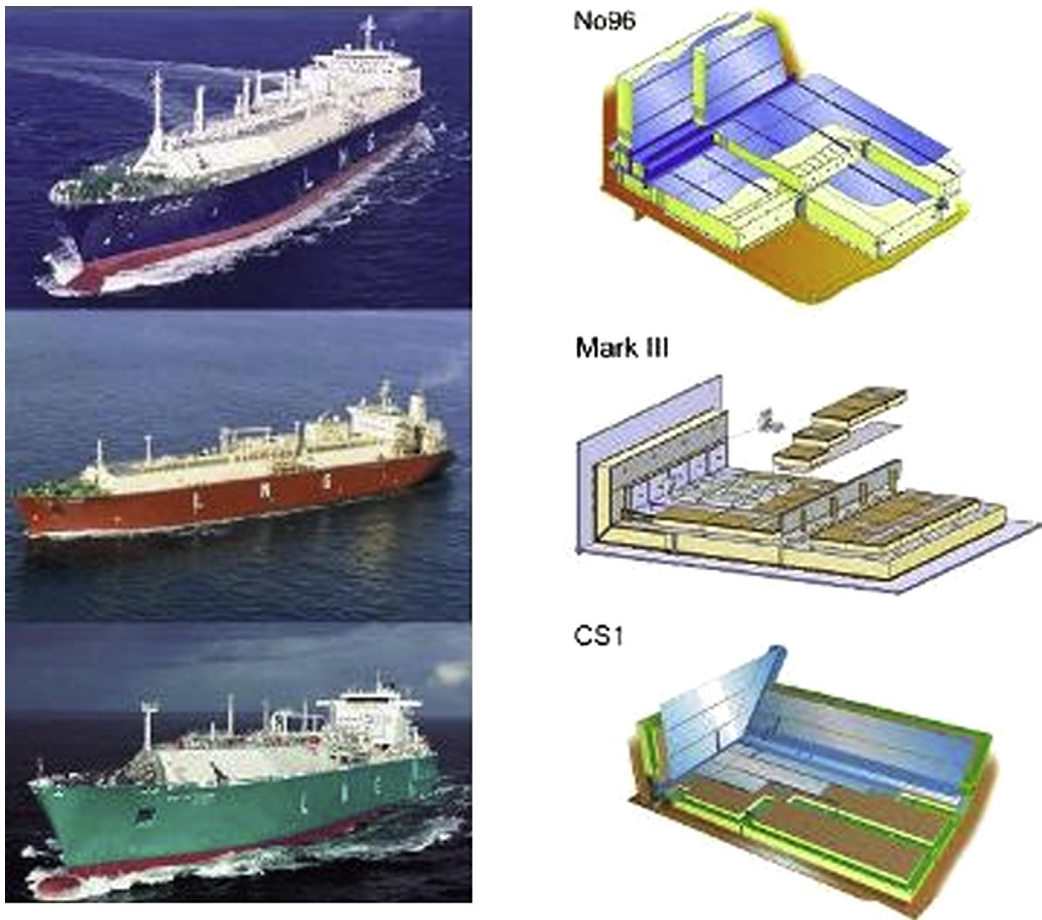


Figure 4.7
Three membrane systems.

Figure 4.7 shows a simple introduction of the three systems.

GT96

The GT96 is Gaz Transport's tank design.

The GT96 tanks consist of a primary and secondary thin membrane made of the material Invar, which has almost no thermal contraction. Thus, the pressure produced by contraction can be neglected. Invar is a kind of material that is very expensive, but its advantage in weight can make up its weakness. The 4000 ton Moss-type tank has the same volume as the 400 ton GT96.

Compared to the barriers, the insulation materials are cheaper and more common. The insulation is made out of plywood boxes ($200 \times 1000 \times 1200$ mm) filled with perlite and

continuously flushed with nitrogen gas. The outer insulation layer is connected with the ship hull by an adhesive resin rope, which is very important to the hull structure because the loads can be passed by the connections. For the hull shells that are not inflatable, different thicknesses of the adhesive resin rope should be used to ensure a complete bond between the hull and the tank.

The integrity of both membranes is permanently monitored by detection of hydrocarbon in the nitrogen. An evolution to replace the nitrogen with argon as the flushed inert and insulation gas is proposed by NG2. Argon has a better insulation power than nitrogen, which could save 10% of boil-off gas.

TGZ Mark III

The membrane TGZ Mark III is design by Technigaz.

The membrane consists of stainless steel, which is cheap and easy to buy. For a high thermal expansion rate, the stainless steel will have contraction when the temperature goes down, so the stainless steel is made to be corrugated and absorb the thermal contraction when the tank is cooled down.

The secondary barrier is a kind of composite material named “Triplex.” Just as the GT96 system, the design of the Mark III system also has two insulation layers: one between the ship hull and the secondary barrier and one between two barriers.

Going from the inside of the tank outward, there are five layers, which are introduced as follows:

- Primary barrier of 1.2-mm-thick corrugated stainless steel
- Primary insulation
- Secondary barrier of triplex membrane
- Secondary insulation
- Ship’s hull structure.

The size of the stainless steel plate is $1.2 \times 3000 \times 1000$ mm; the plates are welded by auto TIG. At first, the complicated areas are completed by manual welding, but in the development of the machine for a special mission, especially in Japan, nearly all of the welding processes are completed by machines.

During construction, the screw is first welded to the ship hull to fix the $300 \times 3000 \times 1000$ mm polyurethane foam board, then the polyurethane foam board is coated with adhesive resin rope, and finally the board is installed onto the ship hull, ensuring the close connection between the hull and the board. The hole of the screw on the board should be filled with polyurethane foam, and the gap between the boards should be filled with fiber insulating materials to ensure the smoothness of the insulating board

before the Triplex barrier is laid. A new polyurethane foam board with plywood welt will be bonded on the Triplex barrier, and then the corrugated stainless steel plate can be fixed on the new polyurethane foam board and welded to form a sealed tank.

CS1

CS1 stands for Combined System Number One, which was designed by the now merged Technigaz & Gaz Transport companies, and consists of the best components for both the MkIII and the No96 systems. The primary barrier is made from Invar 0.7 mm, and the secondary from Triplex. The primary and secondary insulation consists of polyurethane foam panels. Three vessels with CS1 technology have been built by one shipyard, but established shipyards have decided to maintain production of the MKIII and No96.

4.5 Structural Design of the LNG Carrier

4.5.1 ULS (Ultimate Limit State) Design of the LNG Carrier

Design of the LNG Carrier Hull Girder

Design Principles

The ULS capacity of the LNG carrier hull girder is primarily governed by the buckling and yield capacity of the top and bottom flanges of the hull girder, when the carrier experiences maximum longitudinal bending stresses. The buckling capacity of the stiffened panels in a considered section is dependent on:

- structural arrangement and dimensions of plates and stiffeners
- stresses parallel to the stiffener direction
- stresses normal to the stiffener direction (typically transverse stresses due to bending of transverse frames and vertical stresses from top side loads)
- shear stresses
- lateral pressure.

The hull girder bending capacity in the operating conditions must comply with

$$\gamma_s M_s + \gamma_w M_w \leq M_g / \gamma_m \quad (4.1)$$

The hull girder shear capacity in the operating conditions must comply with

$$\gamma_s Q_s + \gamma_w Q_w \leq Q_g / \gamma_m \quad (4.2)$$

where

M_g : bending moment resistance of the hull girder

M_s : still water bending moment based on actual cargo and ballast conditions

M_w : wave bending moment based on an annual probability of exceedance of 10^{-2}

Table 4.2: The partial load factors

Load Combination	Load Category	
	Still Water Loads	Environmental Loads
A	1.2	0.7
B	1.0	1.15

Q_g : shear resistance of the hull girder

Q_s : still water shear force based on actual cargo and ballast conditions

Q_w : wave shear force based on an annual probability of exceedance of 10^{-2}

γ_m : material factor

γ_s : load factor for still water loads (permanent + variable functional loads)

γ_w : environmental load factor.

According to DNV-RP-C102, the partial load factors to be used in the ULS hull girder capacity of the LNG carrier checks are given in [Table 4.2](#).

Design Wave

In order to establish the design loads for the LNG carrier hull girder section, a design wave approach may be used. The longitudinal stresses, both global and local, will be combined with transverse stresses and shear stress. Stresses due to lateral pressure on the panel will be included.

These stresses will be taken from consistent loads using actual internal and external pressures corresponding to the worst combination of still water loads and wave position. In order to obtain consistent loads, a design wave is defined.

The “equivalent” regular design wave is defined as the regular wave that gives the same response level as the long-term value for a specific response parameter. For the ULS of the LNG carrier, the critical long-term design response level is to be determined for North Atlantic environment at a 100 years return period. The design wave is found to be

$$H_D = \frac{\text{Long-term response}}{RAO} \quad (4.3)$$

where

H_D : design wave amplitude.

In general, the loads are transferred from the wave period and direction to where the transfer function has its maximum value. Under extreme “head sea conditions” the vertical bending moment at the middle of the ship with a return period of 100 years, M_{Wv100} , is the most important load effect.

The regular design of the wave is then chosen as the wave where the transfer function of the response, M_{Wv} , has its maximum value. The regular design of the wave amplitude H_D is chosen to give a value of response of M_{Wv} , where the design wave length is equal to the long-term extreme amplitude. The specified return period can be defined as

$$H_D = \frac{M_{Wv}}{RAO_{M_{Wv}}} \quad (4.4)$$

In some cases, this procedure may result in a regular wave design with a wave steepness that is too high:

$$S = 2 \cdot \frac{H_D}{\lambda_D} > \text{approx} \cdot 1/7 \quad (4.5)$$

This may occur in case of transfer function curves with somewhat blunt peaks. In that case it may be necessary to choose a slightly longer wave length than the wave length where the transfer function has its actual maximum. This should be repeated in the procedure for the new wave length. Still water loads are to be combined with the corresponding design hydrodynamic loads such that sets of simultaneously acting loads are obtained. These will then be the set of design loads to be used in the strength evaluation of the LNG carrier. This will ensure consistent loads in the design. Phase angles between the different responses are neglected and the maximum values are used as a conservative approach.

Global Load Conditions

The ULS–B combination is used for the global load conditions to conduct capacity checks of the LNG carrier hull girder. These load conditions are selected as they will result in the highest longitudinal hull girder bending compression stress in bottom and deck, respectively.

Load Condition 1—Maximum Hogging The purpose of the “maximum hogging” load condition is to combine the still water condition, normally a ballast condition, and a position of the design wave such that both will result in maximum longitudinal compression stress below the neutral axis of a transverse section. The extreme hogging condition is considered in a head sea situation, but may allow for some fluctuation. Typical values are 15 or 30 °C.

The extreme load conditions may be summarized as follows:

- Head sea condition (i.e., 180 °C)
- Speed: 0 knots
- Extreme still water hogging condition. Include the simultaneous global distribution of the topside that is most likely to occur for long crested waves

- 100 years return period for environmental loads
- Environmental loads based on the scatter diagram (North Atlantic).

Load Condition 2—Maximum Sagging The purpose of the “maximum sagging” load condition is to combine the still water condition, normally a fully loaded condition, and a position of the design wave such that both will result in maximum longitudinal compression stress above the neutral axis of a transverse section. The extreme sagging condition is considered in a head sea situation, but may allow for some fluctuation as in load condition 1.

The extreme load conditions may be summarized as follows:

- Head sea condition (i.e., 180 °C)
- Speed: 0 knots
- Extreme still water sagging condition. Include the simultaneous global distribution of the top side loads that is most likely to occur
- Long crested waves
- 100 years return period for environmental loads
- Environmental loads based on the scatter diagram (North Atlantic).

The wave-induced linear responses are normally:

- vertical bending moment
- global shear force
- external sea pressure distribution
- accelerations (induced internal tank pressure)
- global axial force
- torsional moment, if relevant.

Combination of Stresses

In order to carry out ULS moment capacity checks, both global and local stresses must be combined.

Generally the total longitudinal design stress may be derived as

$$\sigma_{x,total} = \sigma_{x,global} + \sigma_{x,local} \quad (4.6)$$

Total transverse design stress:

$$\sigma_{y,total} = \sigma_{y,global} + \sigma_{y,local} \quad (4.7)$$

Total design shear stress:

$$\tau_{total} = \tau_{global} + \tau_{local} \quad (4.8)$$

The global and local stresses must be calculated for static and dynamic loads separately in order to include the ULS partial load factors in the calculation of design stresses.

Longitudinal Stresses The following stress components for the total longitudinal design stress are discussed:

$$\sigma_{x,total} = (\sigma_v + \sigma_h + \sigma_t + \sigma_a + \sigma_{ve})_{x,global} + (\sigma_2 + \sigma_{v2} + \sigma_{a2})_{x,local} \quad (4.9)$$

where

σ_v : Nominal vertical hull girder bending stress

$$\sigma_v = \frac{\gamma_s \cdot M_s + \gamma_w \cdot M_w}{Z_i} \quad (4.10)$$

where

Z_i : Section modulus at the considered transverse section (i), other symbols are introduced in the above section.

σ_h : Nominal horizontal hull girder bending stress

$$\sigma_h = \frac{\gamma_w \cdot M_w}{Z_i} \quad (4.11)$$

where symbols are introduced in the above section.

σ_a : Nominal axial stresses due to hull girder end pressure

$$\sigma_a = \frac{\gamma_s \cdot F_{as} + \gamma_w \cdot F_{aw}}{A_i} \quad (4.12)$$

where

F_{as} : Still water axial force due to hull end pressure

F_{aw} : Wave axial force based on an annual probability of exceedance of 10^{-2} (100 years)

γ_s : Load factor for still water loads

γ_w : Environmental load factor

A_i : Cross-sectional area based on gross thickness at the considered transverse section (i)

σ_{ve} : Nominal vertical hull girder bending stress due to end pressure

σ_2 : Nominal secondary bending stress in double bottom or double side

σ_{v2} : Nominal secondary vertical hull girder bending stress due to lateral pressure on tank boundaries

σ_{a2} : Nominal secondary axial stress due to lateral pressure on tank boundaries.

Transverse Stresses The nominal transverse stresses in the hull girder panels are caused by the bending of the transverse frames and transverse axial force from external/internal pressure.

The bottom plate acts as a flange for the transverse frame and will be exposed to transverse compression stresses in the middle of the span. This will represent the transverse stresses due to bending of the transverse frames as applied in the ULS capacity checks.

Shear Stresses From experience the hull shear capacity at the “1/4 lengths” of the hull must be considered early in the design, and the effect of topside loads must be included. The main reasons for this are as follows:

- The still water shear forces and wave shear forces are usually maximum at the ends of the cargo area;
- The scantlings of the longitudinal bulkheads/sides are also often reduced in these regions or terminate completely;
- The hull girder wave bending moment and wave shear force are almost in phase;
- The shear stresses and vertical stresses from the topside loads are often higher than in the midship areas due to pitch accelerations.

In Eqn (4.8),

τ_{global} : Total nominal design shear stress from global shear force

τ_{local} : Total nominal design shear stress from local effects

$$\tau_{global} = \frac{\gamma_S \cdot Q_S + \gamma_W \cdot Q_W}{t} \cdot q(Fz1) \quad (4.13)$$

Q_S : Still water shear force based on actual cargo and ballast conditions;

Q_W : Wave shear force based on an annual probability of exceedance of 10^{-2} (100 years);

γ_S : Load factor for still water loads;

γ_W : Environmental load factor;

t : Plate thickness of considered panel;

$q(Fz1)$: Shear flow factor [N/mm] given by the shear flow analysis (e.g., in Nauticus) due to a unit vertical shear force ($Fz = 1$ N).

The nominal shear stresses from local effects are normally derived from the cargo hold FE analysis or the local FE analysis.

Capacity Checks

General Principles

The ULS capacity checks include both checks of yield and buckling resistance. The yield check reads:

$$\sigma_{ed} \leq \frac{1}{\gamma_m} f_y \quad (4.14)$$

σ_{ed} : Design Von Mises equivalent stress (including load factors)

γ_m : Material factor = 1.15

f_y : Characteristic yield strength of the material.

Stresses in areas with local concentrations such as bracket toes and other limited areas within brackets may significantly exceed the yield limit. This means that yielding will

occur, but if the extent of yielding is governed by the forced deformation from the surrounding structure, it is considered to be acceptable. Therefore, in general, it is assumed that local linear peak stresses in areas with pronounced geometrical changes may exceed the yield stress criterion given above, provided that plastic mechanisms are not developed in the adjacent structural parts and that local buckling is avoided.

The buckling resistance of the different plate panels can be calculated according to DNV Classification Notes 30.1—Buckling Strength Analysis. The stiffened plate panels should be checked for the effect of biaxial stresses and lateral pressure. Stiffened flat plates should be checked for buckling. The stiffeners are typically aligned in the longitudinal direction, which is the most dominant direction with respect to compressive loads. Heavier and more widely spaced transverse girders support the stiffeners. Large girder webs may also be considered and designed as a stiffened plate.

The longitudinal girders and bulkheads may also provide support for topside equipment, such as topside modules, etc. In such cases the structures will be exposed to both longitudinal and transverse compression stresses.

Stiffened panels shall be designed to resist the acting loads with required load and material factors. Stiffened panels that are asymmetric in geometry about the plate plane must be checked for both plate-induced failure and stiffener-induced failure.

Overall flexural buckling of girders may usually be disregarded. Otherwise, strength checks for orthogonal stiffened panels must be carried out. The girder strength can be assessed as a stiffened panel. Girders that are subjected to high stresses due to topside loads can be assessed as a stiffened panel.

Buckling capacity of large stiffened brackets can be calculated according to Classification Notes 30.1—Buckling Strength Analysis.

Nonlinear strength assessment methods using recognized programs may alternatively be used. In such cases, geometrical imperfections must be included; residual stresses and boundary conditions need careful evaluation. The model should be capable of capturing all relevant buckling modes and detrimental interactions between them.

Hull Girder Moment Capacity Checks

Hull girder capacity checks are carried out for load conditions 1 and 2 as defined in Section 5.1.1.4. In order to calculate the buckling capacity of each panel in the hull girder section, the stresses defined in Section 5.1.1.5 shall be used. This implies that the hull cross-section shall be based on stresses within the elastic range of the material. Each longitudinal panel in the cross-section shall be checked for permissible yield (von Mises equivalent stress) and buckling capacity.

Hull Girder Shear Capacity Check

The global shear capacity at any section is found from the following expression:

$$Q_g = \sum_j \tau_{crj} \cdot A_{pj} \quad (4.15)$$

where

A_{pj} : Area of panel in the shear element (plate area only)

τ_{cr} : The smaller of the:

Shear stress in the panel corresponding to critical buckling capacity or

Shear stress in the panel corresponding to the yield capacity of the panel

j : Includes all panels in the longitudinal shear element.

The global shear capacity is considered slightly different from the moment capacity checks. Each global shear element such as ship side, inner side, and longitudinal bulkheads is considered separately. No redistribution of shear forces between the global elements is assumed, but each global element may be fully utilized for the total shear force in the element. The total shear force taken by a global shear element can be derived from a shear flow analysis of the transverse section.

Note that the panels must be checked for both yield and buckling. The lower of the two values is used in the “Maximum shear stress associated with yield or critical buckling.” Most buckling codes (like Classification Notes 30.1) include both a yield check and a buckling check when both in-plane stress components are in compression. However, when only one stress component is in tension the yield check must be carried out separately and also a buckling check setting the tension component to zero.

4.6 Fatigue Design of an LNG Carrier

In terms of the fatigue design of an LNG carrier, a design cycle that consists of a preliminary design phase and a fatigue design phase is preferred.

A brief description of the different fatigue phases is given below.

4.6.1 Preliminary Design Phase

The aim of the preliminary design phase is to ensure that the main scantlings of the LNG carriers are adequately designed with respect to fatigue to allow confidence when ordering steel, therefore avoiding potentially costly modifications later in the construction phase.

The initial scantlings are often based on strength (structural capacity) considerations, with limited attention to fatigue capacity requirements. Hydrodynamic loads should, as a minimum, be based on the worldwide scatter diagram. Site-specific wave data should be

used if these conditions are more complicated than the worldwide distribution. The mass of LNG carrier-specific equipment/modules can change both global and local stress ranges and the mass should be included as early as possible in the analyses.

Simplified fatigue analysis can be performed to calculate initial scantlings for at least four sections outside the midship area.

The bulkhead/frame relative deflections and associated nominal stresses can be determined in several ways. It is recommended that nominal stresses are calculated using a beam or shell model because these models are required during the “fatigue design phase” and are also used for general strength analysis.

4.6.2 Fatigue Design Phase

The fatigue design phase is used to document the estimated fatigue capacity for a selection of structural details. A suitable selection of details will be analyzed to ensure that the worst of equal local details meets the fatigue requirements. Therefore, screening analysis is important for identifying areas prone to the most fatigue for further analysis. At the completion of this phase an overall understanding of the hull fatigue performance should be achieved.

Typical fatigue calculations to be performed in this phase are:

Load component-based fatigue analyses for a minimum of five sections along the vessel. Results from dynamic sea pressure calculations at waterline should be the basis for selection of cross-sections. At least one section at a transverse bulkhead shall be analyzed.

Fatigue screening, using global or part-ship models, in order to ensure that areas other than those analyzed have satisfactory fatigue lives.

Fatigue calculations using stress concentration models may be necessary for fatigue-sensitive areas where adequate geometric stress concentration factors, K , do not exist. Stiffener lugs connected to transverse frames/bulkheads are a typical case where such calculations are required.

The bulkhead/frame relative deflections and associated nominal stresses should be established from a beam or shell element model of the region under consideration.

In order to obtain a thorough overview of the fatigue performance for the LNG carrier hull, fatigue calculations need to be completed for many details. Analytical focus on screening is necessary. Several approaches are available to the fatigue designer that varies in the level of complexity and required information. At this stage it is anticipated that the hydrodynamic and cargo hold FE analyses (three holds) have been completed and should be used to establish a more comprehensive overview of the hull fatigue performance.

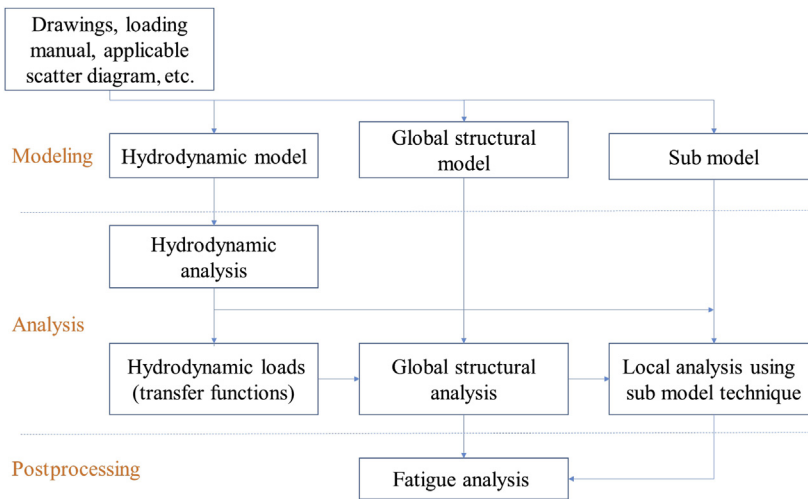


Figure 4.8

Full stochastic analysis procedure flowchart—global model.

Three primary fatigue approaches, depending on the detail type, may be used at this stage to identify where further calculations should be conducted. For transverse frame gussets, hopper knuckles, stringer connections, etc. a unit load applied to the cargo hold FE model may be used to identify the hot spot locations. Combining the results from both the unit load approach and the preliminary design phase the designer will be able to identify the details to be analyzed further.

Using the global FE model as shown in [Figure 4.8](#), the nominal global stresses in the hull girder may be more accurately obtained compared to a section scantlings approach since this will include effects such as shear lag.

Similarly the part-ship FE models as shown in [Figure 4.9](#) can be used for this purpose, although the shear lag effects may not be as accurately captured as for a global model. In addition these models provide more accurate relative deflection magnitudes for updating the nominal stresses for the longitudinal stiffeners that intersect a transverse bulkhead.

Load component stochastic method ([Figure 4.10](#)) is found to be sufficient for longitudinal hull members such as stiffeners, side shell, deck, and bottom. LNG carrier-specific details should be analyzed using an integrated model in order to capture all load effects, hence reducing uncertainties.

The revised nominal stresses can be combined with appropriate stress concentration factors to obtain the hot spot stress. These stresses may then be used for postprocessing with the hydrodynamic loads to determine revised fatigue damages.

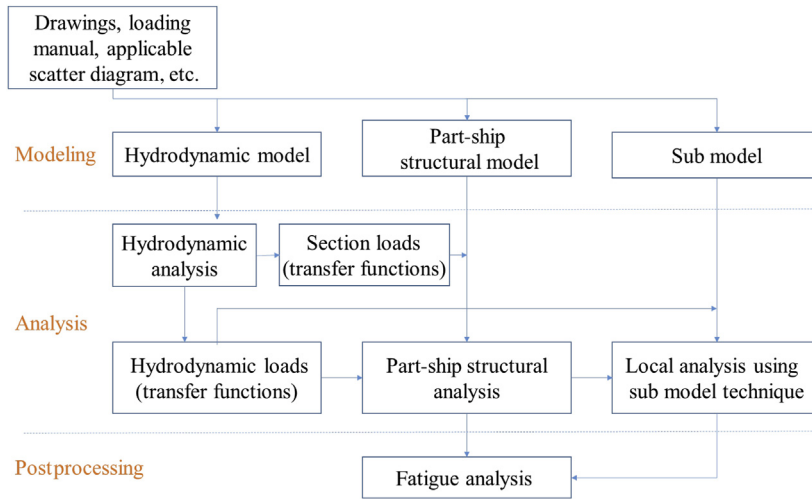


Figure 4.9

Full stochastic analysis procedure flowchart—part-ship model.

The stress concentration factor K is defined as

$$K = \frac{\sigma_{hot\ spot}}{\sigma_{nominal}} \tag{4.16}$$

The relation between the hot spot stress range to be used together with the S–N curve and the nominal stress range is

$$\Delta\sigma_{hot\ spot} = K \cdot \Delta\sigma_{nominal} \tag{4.17}$$

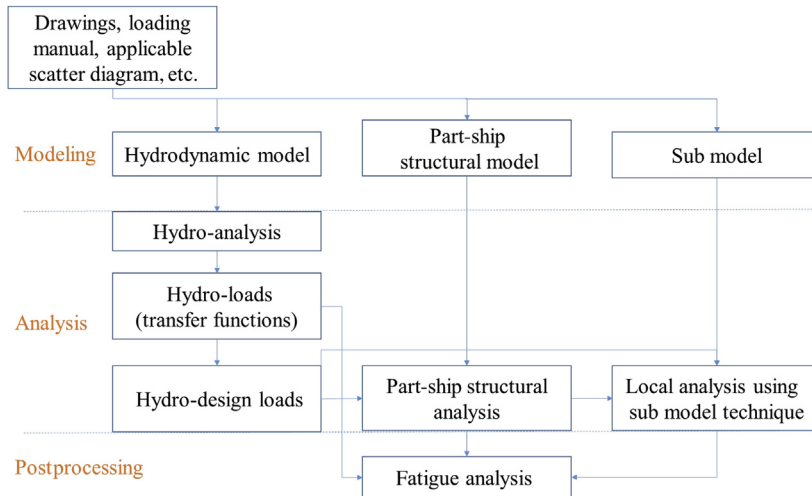


Figure 4.10

Load component stochastic fatigue analysis flowchart.

Many of the stress concentration models will be selected based on experience and/or lack of an available geometric stress concentration factor, K , for the detail. Development of stress concentration models on the basis of experience may commence at an earlier phase in the project.

The basic design S–N curve is given as

$$\log N = \log \bar{a} - m \log \Delta\sigma \quad (4.18)$$

where

N : predicted number of cycles to failure for stress range $\Delta\sigma$;

$\Delta\sigma$: stress range;

m : negative inverse slope of S–N curve;

$\log \bar{a}$: intercept of log N-axis by S–N curve.

$$\log \bar{a} = \log a - 2s \quad (4.19)$$

where

a : constant relating to mean S–N curve;

s : standard deviation of log N.

The specific values of these parameters can refer to DNV-RP-C204.3.

If sufficient fatigue life cannot be reached using load component stochastic analysis further refinement in analysis methodology using full stochastic analysis can be performed. Alternatively, redesign of the details should be considered.

References

http://en.wikipedia.org/wiki/LNG_carrier.

http://www.beg.utexas.edu/energyecon/lng/LNG_introduction_08.php.

<http://www.kline.co.jp/en/service/lng/>.

http://www.beg.utexas.edu/energyecon/lng/LNG_introduction_08.php.

http://www.veristar.com/wps/portal!/ut/pl/cmd/cs/ce/7_0_A/s/7_0_1C3M/_s.7_0_A/7_0_1C3M?content=veristarinfo,sloshhome.

Chun, M.S., Kim, M.H., Kim, W.S., Kim, S.H., Lee, J.M., 2009. Experimental investigation on the impact behavior of membrane-type LNG carrier insulation system. *Journal of Loss Prevention in the Process Industries* 22 (6), 901–907.

DNV-RP-C102, 2002.

DNV-RP-C203, 2005.

DNV-RP-C206, 2006.

DNV Classification Notes 30.1, 2004.

Han, H.Y., Lee, J., Kim, Y., Shipbuilding, D., January 2002. Design development of FSRU from LNG carrier and FPSO construction experiences. In: *Offshore Technology Conference*.

Kim, M.H., Lee, S.M., Lee, J.M., Noh, B.J., Kim, W.S., 2010. Fatigue strength assessment of MARK-III type LNG cargo containment system. *Ocean Engineering* 37 (14), 1243–1252.

- Mravak, Z., de Lauzon, J., Chung, Y.S., Diebold, L., Baudin, E., January 2009. Strength assessment of membrane LNG tank structure based on direct calculation of structural response. In: ASME 2009 28th International Conference on Ocean, Offshore and Arctic Engineering. American Society of Mechanical Engineers, pp. 767–774.
- Wang, B., Kim, J.W., January 2007. Strength evaluation of LNG containment system considering fluid-structure interaction under sloshing impact pressure. In: ASME 2007 26th International Conference on Offshore Mechanics and Arctic Engineering. American Society of Mechanical Engineers, pp. 545–552.

Wave Loads for Ship Design and Classification

5.1 Introduction

A major aspect of ship design is the calculation of wave-induced loads on the ship structure. The difficulty in calculating this load arises from the fact that the sea is highly irregular, and hence a number of techniques have been developed to tackle this problem. These techniques enable sea waves to be defined in a mathematical form that can then be used to calculate wave loads on the ship and ultimately the response of the ship to these loads.

When designing a ship, formulae provided by classification societies are used to calculate the wave loads and the ship's response. However, a ship designer must have some knowledge of the theory and techniques utilized for the statistical determination of wave loads. Novel ship designs also exist, and require that an extensive statistical estimation of wave loads be undertaken in addition to using rule-based formulae.

As a basis for marine structural design, the objectives of this chapter are threefold:

- Present various ocean wave spectra and wave statistics
- Discuss wave-induced loads, slamming, and green-water loads, and hence the response of the ship
- Outline design load calculations per ship classification rules.

More information on wave loads acting on ship structures can be found in the references by [Bhattacharyya \(1978\)](#), [Hughes \(1988\)](#), and [Jensen \(2001\)](#).

5.2 Ocean Waves and Wave Statistics

5.2.1 Basic Elements of Probability and Random Processes

Obtaining ocean wave data requires the use of different elements of statistics and probability. Therefore, an introductory reference to statistics and probability is given prior to dealing with wave loads.

In statistics, a random variable X is an event or an outcome among all possible outcomes. If all possible outcomes form a continuous space $-\infty < x < \infty$, and all possible events

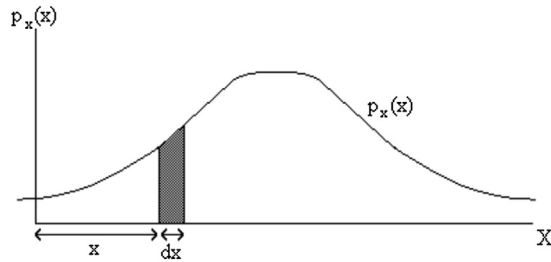


Figure 5.1
Probability density function.

are a part of this space, then the probability density function of an event occurring is the probability that X lies within that portion of x . The probability density function is written as $p_x(x)$. Thus in [Figure 5.1](#), the probability that X lies between x and $x + dx$ is $p_x(x)dx$. From this figure, the mean value μ_X is defined as

$$\mu_X = \int_{-\infty}^{\infty} xp_X(x)dx \quad (5.1)$$

$$\text{Var}[X] = (\sigma_X)^2 = E[(X - \mu_X)^2] \quad (5.2)$$

Another important aspect of statistics is random process distribution, which describes the likelihood of occurrence of a random process. One of the most common random process distributions is the normal or Gaussian distribution. Typical examples of a Gaussian distribution can be seen in [Figure 5.2](#). One of the most important features of the Gaussian distribution is that it may be described entirely in terms of two parameters: the mean value μ_X and the variance σ_X^2 .

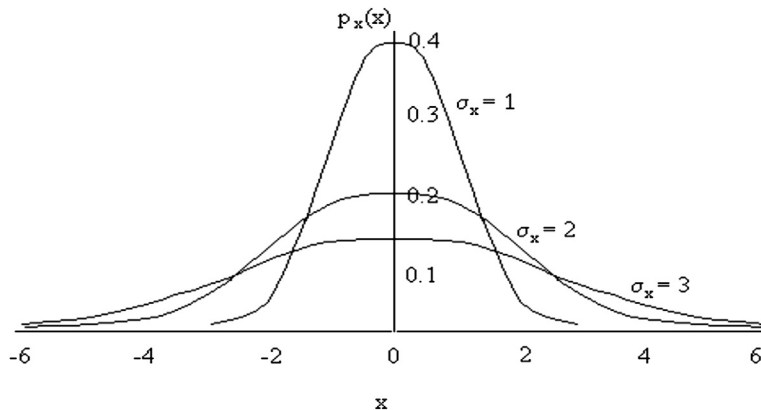


Figure 5.2
Gaussian probability density function (with $\sigma_x = 1, 2,$ and $3,$ and $\mu_x = 0$).

The waves that make up a sea state are normally described using two parameters: the significant wave height and the peak period. These two parameters follow a lognormal distribution, meaning that their natural logarithm $Z = \ln X$ follows a Gaussian distribution. The surface elevation at any point in the ocean is a random variable that follows a Gaussian distribution with zero mean.

The parameters used to describe ocean waves are stochastic processes and continuous functions of time. Thus, measurements of the same parameter taken at different times could result in very dissimilar readings. Data regarding parameters used to describe ocean waves are collected by taking different samples over a period. For the validity of these data, it is essential to ensure that each sample is collected under similar conditions. In the case of ocean waves, a parameter such as sea elevation is influenced by a number of different variables—for example, wind speed and wind direction. In order to be certain that these different variables remain relatively constant from sample to sample, the data are collected within a short observation period.

A random process is *stationary* if the statistical characteristics of the process do not change with time t . This means that averages and moments of the stationary process are invariant over time. Ocean data are usually collected from samples spanning from 30 min to 3 h, because during this period data are considered stationary.

The two methods for defining the average of samples for random processes are the ensemble and temporal methods. The ensemble average is the average taken over all samples at one instant in time. The temporal average is the average of a particular sample over time. In the case of random processes such as ocean waves, time averages that are formed from a single sample over a given time interval are equal to ensemble averages. This situation is known as an ergodic random process.

A random process may be characterized as narrowband or wideband. In simple terms, a narrowband process is made up of waves with frequencies lying within a narrow range, while a wideband process consists of waves with widely varying frequencies. Ocean wave data show that a fully developed, wind-generated, mid-ocean sea state (i.e., with no growth or decay, and no coastal effects) is essentially narrow banded. Of course, there are always wave components that differ by having high frequencies, but these waves tend to be small in both height and length and have little effect on the ship. It is also interesting to note that a ship acts as a filter, meaning that only a narrow band of wave frequencies has an effect on the ship's motion and hull girder loads. Thus, the ship's response is even more narrow banded than the sea itself, and this response is usually characterized as a Gaussian and stationary process, just like the ocean waves.

Chapter 31 of this book contains more information on random variable definitions.

5.2.2 Statistical Representation of the Sea Surface

This section deals with the representation of a complete sea surface. Of course, the sea surface is known to be highly irregular and random under all sorts of conditions. However, it has been found that this random process may be accurately represented by a series of different regular waves of varying heights, lengths, directions, and phases that are superimposed on each other.

Three papers paved the way for further work on statistical representations of the sea surface and were published by [Pierson \(1952\)](#), [St. Denis and Pierson \(1953\)](#), and [Pierson et al. \(1955\)](#). These papers proved that the sea surface could be represented by the superposition of a large number of regular sinusoidal waves of varying frequencies. The following represents a typical sinusoidal wave:

$$\zeta(x, t) = a \sin(-kx - \omega t + \theta) \quad (5.3)$$

where,

a = Wave amplitude

$k = 2\pi/\lambda$: wave number

λ = Wave length

$\omega = 2\pi/T$: wave frequency

T = Wave period

θ = Phase angle.

[Pierson et al. \(1955\)](#) also proposed that the surface elevation $h(x,t)$ of an irregular sea could be represented as

$$h(x, t) = \lim_{N \rightarrow \infty} \sum_{I=1}^N a_I \sin(-k_I x - \omega_I t + \theta_I) \quad (5.4)$$

A number of procedures exist for describing a sea surface. [Jensen \(2001\)](#) provides a detailed analysis of surface waves.

5.2.3 Ocean Wave Spectra

A vast amount of data regarding ocean waves has been collected and measured throughout the years. These data are needed in order to define the sea state where the ship is likely to sail. One of the most comprehensive collections of data regarding ocean waves was published by [Hogben et al. \(1986\)](#). It tabulates data from 104 ocean areas, known as the Marsden areas, covering all major shipping routes.

The representation of ocean data may be carried out in a number of ways. [Bretschneider \(1959\)](#) proposed that the wave spectrum for a given sea state could be described in terms

of two parameters: the significant wave height (H_s) and the modal wave frequency (ω_m). The modal wave frequency is the peak frequency at which the wave spectrum's maximum height occurs. One of the most popular spectra in use is given by [Pierson and Moskowitz \(1964\)](#). This spectrum assumes a deep sea and a fully developed sea state. For coastal waters, the Joint North Sea Wave Project (JONSWAP) spectrum is used as described by [Hasselman et al. \(1973\)](#) and [Ewing \(1976\)](#).

[Chakrabarti \(1987\)](#) gives mathematical descriptions for various wave spectra such as

- Phillips
- Neumann
- Pierson–Moskowitz
- Bretschneider
- ISSC
- ITTC
- Unified form
- JONSWAP
- Scott
- Liu
- Mitsuyasu
- Ochi–Hubble.

The Pierson–Moskowitz (P–M) spectra for fully developed seas may be analytically expressed as

$$S(\omega) = \frac{\alpha g^2}{\omega^5} \exp \left[-0.74 \left(\frac{\omega V_w}{g} \right)^{-4} \right] \quad (5.5)$$

where,

- $S(\omega)$ = spectral ordinate in cm^2s
- g = acceleration of gravity in cm/s^2
- ω = frequency in rad/s
- $\alpha = 0.00810$
- V_w = wind speed in cm/s (19.5 m above sea level).

The Bretschneider spectrum is a two-parameter family that permits period and wave height to be assigned separately, and has the form

$$S(\omega) = 0.1687 H_s^2 \frac{\omega_s^4}{\omega^5} \exp[-0.675(\omega_s/\omega^4)] \quad (5.6)$$

$$\omega_s = \frac{2\pi}{T_S} \quad (5.7)$$

$$T_S = 0.946T_0 \quad (5.8)$$

where T_S and T_0 are the significant wave period and peak period, respectively. Significant wave height is denoted by H_S . The JONSWAP spectrum can be written by modifying the P–M spectrum as

$$S(\omega) = \frac{\alpha g^2}{\omega^5} \exp\left[-1.25(\omega/\omega_m)^{-4}\right] \gamma^{\exp\left[-\frac{(\omega-\omega_m)^2}{2\sigma^2\omega_m^2}\right]} \quad (5.9)$$

where,

$$\gamma = 3.3$$

$$\sigma = 0.07 \text{ and } 0.09 \text{ for } \omega < \omega_m \text{ and } \omega > \omega_m, \text{ respectively}$$

$$\alpha = 0.076\bar{x}^{-0.22}$$

$$\omega_m = 2\pi \frac{3.5\bar{x}^{-0.33}g}{V_{W10}}$$

$$V_{W10} = \text{wind speed 10 m above sea level}$$

$$\bar{x} = \frac{gx}{V_{W10}^2}$$

x in the above equations denotes fetch.

However, the Ochi six-parameter spectrum provides a better method to represent all stages of development of a sea in a storm (Ochi, 1978). They start with the basic form

$$S(\omega) = \frac{\left(\frac{4\lambda+1}{4}\omega_m^4\right)^\lambda H_S^2}{4\Gamma(\lambda)\omega^{4\lambda+1}} \exp\left[-\frac{4\lambda+1}{4}(\omega_m/\omega)^4\right] \quad (5.10)$$

where $\Gamma(\lambda)$ is a gamma function, the parameter H_S is the significant wave height, λ is a shape parameter, and the Ochi six-parameter spectrum reduces to the Bretschneider form when $\lambda = 1$. By adding two of these forms, Ochi (1978) obtained a six-parameter spectral form

$$S(\omega) = \sum_j \frac{\left(\frac{4\lambda_j+1}{4}\omega_{mj}^4\right)^{\lambda_j} H_{Sj}^2}{4\Gamma(\lambda_j)\omega_j^{4\lambda_j+1}} \exp\left[-\frac{4\lambda_j+1}{4}(\omega_{mj}/\omega)^4\right] \quad (5.11)$$

where $j = 1, 2$ stands for the lower- and higher-frequency components respectively. The size parameters H_{S1} , H_{S2} , ω_{m1} , ω_{m2} , λ_1 , and λ_2 may be determined numerically to minimize the difference from a specific observed spectrum.

Figure 5.3 compares the Bretschneider wave spectrum with JONSWAP wave spectra of various sharpness parameters (H_S and T_P are unchanged). Bretschneider and JONSWAP ($\gamma = 3.3$) wave spectra are frequently used in calculations of extreme values and fatigue damage.

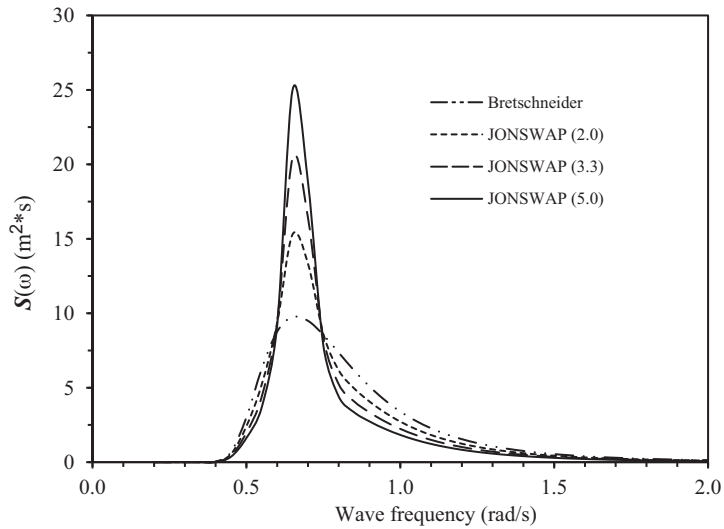


Figure 5.3

Wave spectral density functions ($H_S = 8.5$ m, $T_P = 9.5$ s, $m_0 \approx 4.4$).

Figure 5.4 shows the relationship between a time-domain solution of waves (Eqn (5.3)) and a frequency-domain representation of waves by a wave spectrum $S(\omega)$.

5.2.4 Moments of Spectral Density Function

The moments of a spectral density function $S(\omega)$ may be expressed as (Bhattacharyya, 1978)

$$m_n = \int_0^{\infty} \omega^n S(\omega) d\omega \quad (5.12)$$

where n is an integer. The zero moment m_0 is the area under the energy density spectrum curve

$$m_0 = \int_0^{\infty} S(f) df = \int_0^{\infty} S(\omega) d\omega \quad (5.13)$$

where f is the cyclic frequency equal to $2\pi\omega$. Hence the following relation may be derived as

$$S(f) = 2\pi S(\omega) \quad (5.14)$$

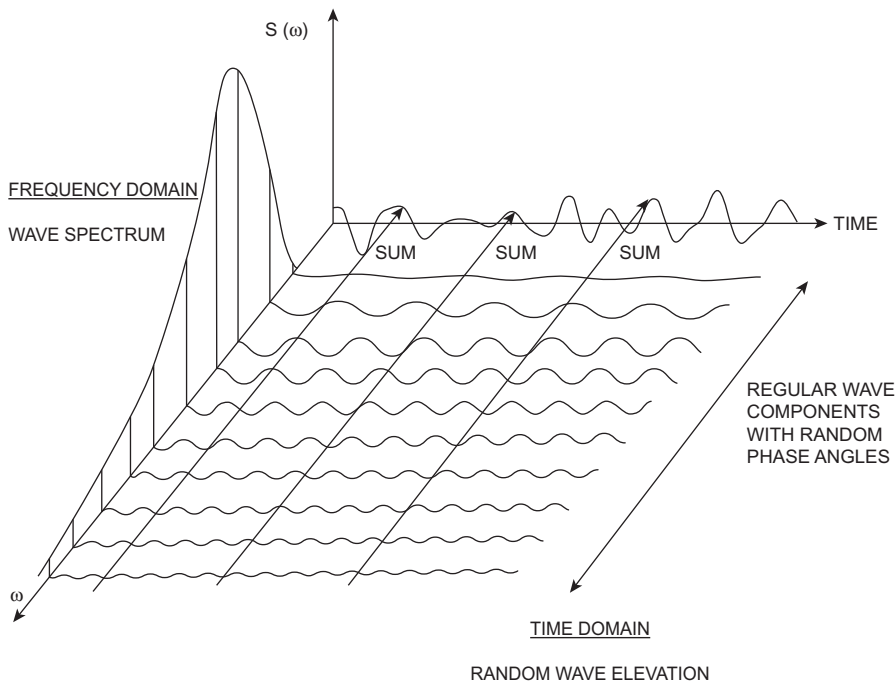


Figure 5.4

Relations between frequency-domain and time-domain representation of waves in a long-crested short-term sea state (Faltinsen, 1990).

$$m_n(f) = \int_0^{\infty} f^n S(f) df = (2\pi)^{-n} m_n \quad (5.15)$$

5.2.5 Statistical Determination of Wave Heights and Periods

In the time-domain analysis, the significant wave height H_S is defined as the average height of the highest one-third of all waves, and is denoted $H_{1/3}$ in

$$H_{1/3} = \frac{1}{N/3} \sum_{i=1}^{N/3} H_i \quad (5.16)$$

where N is the number of individual wave heights, and H_i is a series of wave heights ranked from highest to lowest. In frequency-domain analysis, the significant wave height H_S is defined based on the zero moment, m_0 , which is the area under the energy density spectrum curve

$$H_S = 4\sqrt{m_0} \quad (5.17)$$

In time-domain analysis, the root-mean-square wave height H_{rms} is defined as

$$H_{\text{rms}} = \sqrt{\frac{1}{N} \sum_{i=1}^N H_i^2} \quad (5.18)$$

In frequency-domain analysis, H_{rms} is defined as

$$H_{\text{rms}} = 2\sqrt{2m_0} \quad (5.19)$$

In time-domain analysis, the maximum wave height H_{max} is the largest value of the wave heights recorded. In frequency-domain analysis, the most probable maximum wave height H_{max} is defined by [Longuet-Higgins \(1952\)](#) for a narrow band of the wave spectrum as

$$H_{\text{max}} = \left(\sqrt{\ln N} + \frac{0.2886}{\sqrt{\ln N}} \right) H_{\text{rms}} \quad (5.20)$$

In time-domain analysis, the mean-zero upcrossing period $T_{0,2}$ is defined as the total length of time divided by the number of zero upcrossings recorded. The mean crest period $T_{0,1}$ is calculated as the total length of time divided by the number of crests in the record.

In frequency-domain analysis, the mean wave period is defined as

$$T_{0,1} = 2\pi \frac{m_0}{m_1} \quad (5.21)$$

$$T_{0,2} = 2\pi \sqrt{\frac{m_0}{m_2}} \quad (5.22)$$

5.3 Ship Response to a Random Sea

5.3.1 Introduction

The six degrees of freedom a ship is capable of are illustrated in [Figure 5.5](#).

Once the data describing the sea states encountered by a ship during its lifetime are available, wave-induced loads on the ship's structure, and the ship's response to such loads, may be calculated. It is useful to classify the different forces that act on a ship during its lifetime into four groups:

- Body forces such as weight and inertia
- Dynamic pressure on the ship's hull due to incident and diffracted waves

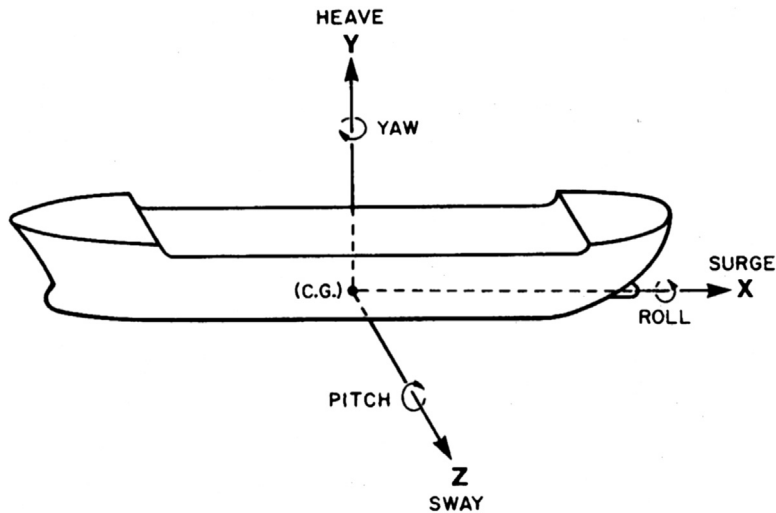


Figure 5.5

Six degrees of freedom of motion of ships and floating systems (Charkrabarti, 1987).

- Inertial forces arising from the acceleration of fluid (referring to both the sea and liquids carried in tanks on the ship)
- Inertial and damping forces arising because of wave radiation from the ship.

These forces are considered when building a ship–sea interaction model. This model comprises several equations describing the waves, motion of the ship, and interactions between the two. The equations used are nonlinear due to the random and irregular nature of the sea, which results in very expensive and time-consuming analysis. New methods are developed in order to simplify such analysis.

Bhattacharyya (1978) gives an easy-to-follow discussion of the wave loads such as vertical/horizontal bending moments, shear forces, and slamming loads. One of the most popular methods employed is a technique known as strip theory, which utilizes an assumption in order to simplify the ship–sea interaction model. The principal assumption made in strip theory is that the ship is slender. Forces acting on the ship are calculated separately on each segment using a two-dimensional flow theory, neglecting the longitudinal component of relative velocity and any type of interaction between different segments. The shear force and bending moment of the ship are then obtained by integrating the vertical forces of each segment along the length of the ship. The name “strip theory” arises from the fact that the ship’s hull is divided into a number of prismatic segments or strips. Strip theory originated from a linear theory of Korvin-Kroukovsky (1955) and Gerritsma and Beukelman (1964). Strip theory is still widely applied due to its efficiency. However, its weaknesses include the lack of three-dimensional effects, inability to account for the above-water hull form, need for forward speed corrections, and lack of

viscous effects. All of these methods assume the ship is a rigid beam. Bishop and Price (1979) developed a flexible-beam strip theory that accounts for bending and shear stiffness of the hull when solving for compatibility between strips. This kind of theory can estimate the distortional higher-frequency responses of a hull due to slamming and whipping excitations. It is still linear analysis, however, and an extreme response is not well modeled.

5.3.2 Wave-Induced Forces

Jensen and Pedersen (1979) proposed a second-order strip theory for hydroelastic analysis in a frequency domain. Their theory is based on a perturbational expression of the hydrodynamic and hydrostatic coefficients around the still-water line and includes the incident pressure field from second-order Stokes' waves. The equation is used to evaluate the forces acting on a ship, similar to

$$F(x, t) = F_H(x, t) + F_B(x, t) \quad (5.23)$$

Using the above equation is rather complicated due to the nonlinear nature of some parameters. The following explanation is only to give a basic understanding of the parameters present in Eqn (5.23).

The right-hand side of Eqn (5.23) consists of two parts. The second part is the buoyancy force known as the Froude–Krylov force

$$F_B(x, t) = - \int_{-T}^{-\eta} B(x, y) \left(\frac{\partial p}{\partial y} \right)_{y+V} dy \quad (5.24)$$

where,

B = Breadth of the ship

y = Distance along an axis starting from the bottom of the hull and moving vertically upward

V = Instantaneous vertical displacement of the hull

η = Distance from the calm water surface to the local elevation of the ocean wave

x = Distance along an axis starting from the aft of the ship and traveling forward along a horizontal axis

t = Time

T = Still-water draught

p = Pressure given by Bernoulli's equation below

$$p(y, x, t) = \rho \left(\frac{\partial \phi}{\partial t} + gy + \frac{1}{2} (\nabla \phi)^2 \right) \quad (5.25)$$

where,

ρ = Fluid density

ϕ = Velocity potential which is made up of first- and second-order terms. The derivation of ϕ is well described by [Jensen and Pedersen \(1979\)](#)

g = Acceleration due to gravity.

The first part of the right-hand side of [Eqn \(5.23\)](#) refers to the hydrodynamic forces acting on the ship

$$F_H(x, t) = -\frac{D}{Dt} \left(m(x, \eta) \frac{D\eta}{Dt} \right) - N(x, \eta) \frac{D\eta}{Dt} \quad (5.26)$$

where,

m = Added mass (due to hydrodynamic load) per unit length

N = Damping force per unit length

D/Dt = Total derivative with respect to time t .

In recent years, diffraction and radiation theories based on panel methods have become widely accepted ([Faltinsen, 1990](#)).

More recent advanced methods include fully nonlinear time-domain approaches. [Cao et al. \(1991\)](#) used a desingularized method in which the source panels were located outside the fluid domain, and thus the kernel in the governing integral equation is desingularized. This method was developed for more general boundary value problems of potential flows and was used in the time-domain computations of fully nonlinear waves. [Jensen et al. \(2000\)](#) gave a detailed discussion of the different theories and comparisons with experiments on extreme hull girder loads. [Beck and Reed \(2001\)](#) gave a precise account of all fundamental theoretical developments in the field of seakeeping over the past 50 years, as well as the computational methods currently in use.

The large amplitude motion programs FREDYN ([De Kat and Pauling, 1989](#)) and LAMP ([Lin et al., 1997](#)) may be used to calculate extreme loads, capsizing, habitability, and crew effectiveness. Other popular hydrodynamic codes include WAMIT ([WAMIT, 1999](#)) and SWAN ([Sclavounos et al., 1997](#)).

5.3.3 Structural Response

Once the forces (or loads) acting on a ship are calculated, the hull girder response of the ship can be determined. In most cases, hull girder analysis means calculating the longitudinal bending moment of the ship. It is performed by assuming the hull is rigid (e.g., no deformation). In a number of cases, however, the ship must be considered a flexible beam, thus resulting in a more complicated solution that must include hydroelastic

analysis of wave-induced loads. Examples of cases in which the ship is assumed flexible are

1. When the ship's natural vibration is low enough for significant vibrations to occur during its operational life
2. When the ship's response to slamming and green water on deck needs to be investigated.

The governing differential equation for the vertical deflection of a flexible beam subjected to a dynamic distributed load $F(x,t)$ is

$$EI \frac{\partial^4 v}{\partial x^4} + m_S \frac{\partial^2 v}{\partial t^2} - m_S r^2 \frac{\partial^4 v}{\partial t^2 \partial x^2} = F(x, t) \quad (5.27)$$

where,

E = Young's modulus

I = Moment of inertia for vertical bending

v = Hull girder deflection

m_S = Ship mass per unit length

r = Radius of gyration of the sectional mass m_S in rotation about a horizontal transverse axis through the section's center of mass.

The theories and equations described in this section are used to calculate the wave-induced bending moment. This bending moment, along with the still-water bending moment, can help determine the longitudinal strength of the ship. Refer to Chapter 8 to obtain a description of bending moments and scantling designs.

For stress analysis of types of ships (e.g., container ships), see [Pedersen \(1983\)](#).

5.3.4 Slamming and Green Water on Deck

So far, only loads occurring at wave-encounter frequencies have been discussed. However, waves can also cause loads at much higher frequencies due to impacts between the ship's hull and the water surface, such as slamming and green water on deck. Slamming occurs when the forward part of the ship hits the water surface after a bow emergence. If the slam takes place with a relatively high velocity, there is a probability of damage to the ship, because a high impulsive load is created in the ship's bow structure. Green water on deck takes place when the deck becomes submerged underwater. The water on the deck may cause structural damage to the deckhouse of the ship and to the deck facility and cargo. The ship's speed is usually reduced, or its heading changed, if such an action reduces the likelihood of slamming or green water on deck.

Loads from both slamming and green water on deck are functions of the relative motion of the ship with respect to the sea. Two conditions need to be satisfied for slamming to occur

at any section of the ship. First, the relative vertical motion, $\eta(x,t)$ should be larger than the draught at the section being considered. Also, the relative velocity, $D\eta/Dt$, must be larger than the threshold velocity v_0 in

$$\eta_T \equiv \frac{D\eta}{Dt} = \frac{\partial\eta}{\partial t} - V \frac{\partial\eta}{\partial x} \geq v_0 \quad (5.28)$$

In a stationary stochastic seaway, both η and η_T are normally distributed parameters with zero mean values. Thus, it is possible to determine the likelihood of slamming on the ship through the statistical probability of the occurrence of η and η_T . The resultant load can then be calculated and used in ship design. The sectional force $q_{SL}(x,t)$ associated with slamming has been found to be approximately proportional to the square of the relative velocity η_T in

$$q_{SL}(x,t) = \alpha\eta_T^2 \quad (5.29)$$

Equation (5.29) may be included in Eqn (5.23) to account for all wave loads experienced by a ship when performing global wave load analysis. Equation (5.29) is useful to describe what is known as bow flare slamming, which occurs when the bow flare of a ship hits the sea surface. Another type of slamming is bottom slamming, where the flat bottom of a ship hits the water. This type of slamming cannot be described by Eqn (5.29), because bottom slamming is not directly related to the relative vertical motion and velocity of the ship that are the starting points of the analysis leading to Eqn (5.29). In the case of bottom slamming, empirical formulae are used; see Zhao and Faltinsen (1993).

For green water to occur on deck, the relative immersion of the section of the ship must be larger than the distance between the water level and the deck (freeboard). The actual force green water exerts on the deck is difficult to assess because of the complicated water flow. Wang et al. (1998) derived the following equation to calculate the sectional force $q_{GW}(x,t)$ resulting from green water on deck

$$q_{GW}(x,t) = -gm_{GW}(x,t) - \frac{D}{Dt} \left[m_{GW}(x,t) \frac{DZ_E}{Dt} \right] \quad (5.30)$$

where,

m_{GW} = Sectional mass of water on the deck

Z_E = Modified relative vertical motion depending on z and a parameter known as the Smith correction factor κ .

The first term on the right-hand side of Eqn (5.30) represents the gravity force, while the second term is analogous to a momentum slamming force. Equation (5.30) may also be included in a global wave load equation such as Eqn (5.23).

Green water causes damage to the bow superstructure and floating production, storage, and offloading unit (FPSO) topsides along the length of the ship. A prediction theory for green

water on deck and the resulting green-water loading has been developed by [Zhou et al. \(1999\)](#). The greenwater or deck wetness slamming phenomena are highly nonlinear. [Wang et al. \(2001\)](#) proposed the following design procedures for green-water impact on FPSOs:

1. Estimate the possibility of green-water occurrence using past experience and approximate methods. Ideally, some preliminary analysis using computer software should be done to get a more reliable estimation.
2. If the estimation indicates that green water is likely to occur in a significant manner, model tests should be arranged and performed as part of a global performance model testing program. The critical parameters should be identified during planning stages of the model tests. If the green-water impact is judged serious, the height, occurrence frequencies, and impact pressure of green water should be carefully measured.
3. If the model tests do not or cannot cover a sufficient number of values of identified critical parameters, some complementary numerical simulations using benchmarked software should be performed to identify the critical value of each critical parameter for design considerations.
4. Analyze the results of model tests and numerical simulations to judge whether the green water needs to be dealt with in design and engineering. Risk analysis may be conducted to help make decisions, if judgment is too difficult to make directly from the results of model tests and numerical simulations.
5. If it is found that green water must be considered, model test results should be used for the design. In cases where no applicable model test results are available, impact pressure can be calculated using approximate formulas. For instance, the formulas summarized in Reference 1 may be used to estimate the horizontal pressure of green-water impact, while classification society rules may be used in the calculation of the pressure acting vertically on the vessel deck. Due to the complexity of green-water analysis and the limitations of those simple formulas, calculated results may be inaccurate.
6. If particular measures are required in order to prevent/reduce green-water impacts, past design experiences can be used, including increasing freeboard, using a better bow shape and flare, and increasing the number of protective measures.

It should be noted that steps 1 through 3 may be replaced by a single step (e.g, sophisticated numerical analysis) if a reliable prediction method becomes available in the future.

Although great effort has been made in recent years to develop such methods, no method is considered satisfactory. Therefore, use of model test results is recommended for any design.

A risk-based approach may be more helpful for design decision-making. The probability analysis presented in [Wang et al. \(2001\)](#) can be expanded and modified to form such a method. However, the likelihood of a vessel heading involves a considerable quantity of analysis work, and model tests may also be required. In addition, the probability of a vessel draft is difficult to accurately determine because it is a function of production rate, offloading rate (and frequency), ballast plan and rate, etc.

5.4 Ship Design for Classification

5.4.1 Design Value of Ship Response

The ultimate goal of determining wave loads and the ship's response to these loads is to obtain the design value of the ship's response. This involves making predictions under the worst conditions the ship may encounter within its lifetime. The four factors that influence the design value of the ship's response (Hughes, 1988) are

- Severity of the sea state as characterized by the significant wave height, the frequency of occurrence, and the duration of each level of severity; these data are used to determine the ship's exposure time to each sea state of different severity.
- Shapes of wave spectra for each sea state
- Ship heading (direction) in a given sea state
- Ship speed for a particular heading and sea state.

The overall goal is to determine the largest response value resulting from the worst combination of wave loads, which has a probability α of being exceeded during the ship's life. This design value α is a risk parameter determined by the ship designer, and is used to calculate the structural response of the ship. A typical value of α is 0.01.

Two methods are used to determine the design value. The first method assumes that the largest waves appear in the most severe stationary sea state that the ship is likely to encounter. This is called the "design wave method." Thus, this wave value is used as the design value of the ship, along with a couple less severe sea states. This method may not be considered accurate, because larger waves may be encountered in a less severe sea state. However, it is less time-consuming, and the preferred method unless a more accurate determination of the design value is required.

The second method requires that all possible sea states the ship is likely to encounter in its lifetime are evaluated. A complete analysis of all the sea states is carried out, and the different sea states are weighted according to the likelihood of being encountered by the ship. This method is a computationally more expensive but also more realistic analysis; see Chapter 8.

Once a method is chosen and the design wave load is determined, the ship's required structural strength can be evaluated.

5.4.2 Design Loads per Classification Rules

General

Structural analysis can be divided into three parts:

- establishing the design load;
- defining the acceptance criteria; and
- conducting the strength assessment.

It is relatively easy to establish acceptance criteria, thanks to many years of accumulated knowledge and expertise from owners, builders, class societies, and researchers; see Parts II and III of this book for more details. The strength assessment is also rather simple once the loads and acceptance criteria are defined. However, the most challenging task is calculating the different loads to which the ship may be subjected. This difficulty arises from the fact that the ship may be exposed to various sea and wave conditions, and different loading patterns of the cargo.

Classification societies have proven techniques for calculating the loads on a ship and evaluating the structural integrity of ship hulls.

Load Components

A detailed design consists of two steps:

- the nominal design for initial scantlings, and
- a more detailed analysis where finite element analysis is used to evaluate combinations of different load cases and their effects on the ship's structure.

In a ship's structural design, three load components are considered:

- hull girder load, which consists of the still-water/wave-induced bending moments and shear forces;
- external pressure, which consists of a static, hydrodynamic, and an impact slamming load; and
- internal pressure caused by the liquids carried in tanks onboard the ship. This pressure depends on the hydrostatic pressure, the changes in pressure head due to pitching and rolling motions, and the inertial force of the liquid column resulting from accelerations of the fluid.

The following subsections describe the evaluation process of these different loads.

Hull Girder Loads

Wave data measured from the North Atlantic are used to determine wave loads. Thus, the nominal design value of a ship represents the long-term extreme value for the North Atlantic Sea in 20 years, which corresponds to a probability of exceedance of 10^{-8} . Global spectral ocean wave models provide data about different wave spectra and heights.

The structural response to waves used in the global structural analysis of a ship is calculated based on the ship's response amplitude operations when exposed to regular sinusoidal waves, for different wave headings and frequencies.

The structural integrity of the ship is assured by implementing a number of different load combinations, wave periods, and heading angles. For each situation, a number of load

components are calculated, such as external wave pressure, acceleration of the liquid cargo and ballast tanks, accelerations at several stations along the ship's length, wave-induced bending and torsional moments together with the corresponding shear forces along the length of the ship, and the ship's motion in roll and pitch modes.

The short-term response of the ship is obtained through the evaluation of the seaway spectrum, which is assumed to become stationary in a period of a few hours. The long-term response and the probability of exceedance of the load are evaluated from the short-term prediction.

Hull girder loads are calculated from a number of components. The most significant of these are the still-water moments and shear forces resulting from the weight, cargo weight, and buoyancy of the ship. The second major component consists of dynamic-induced loads that include vertical and horizontal bending moments, shear forces, and torsional moments. These dynamic loads result from wave motions encountered by the ship.

Classification rules are used to determine still-water bending moments and shear forces, as these are mainly dependent on the loading conditions of the vessel. A more detailed analysis is required when determining the dynamic aspects of hull girder loads. Such analysis is based on the sea conditions that the vessel is bound to encounter over its lifetime. Normally, a 20-year service life is chosen and appropriate wave data are selected. The result from such an analysis determines the extreme values that are used to calculate a design value for the hull girder loads.

When determining hull girder loads, vertical bending moments and shear forces are calculated first. Then tables and other sources of data are used to calculate the ratio of vertical to horizontal bending moments and shear forces. These ratios are mainly dependent on the ship's dimensions and loading conditions.

External Pressure

Determining the external pressure acting on a ship is a more complicated process than the calculation of hull girder loads. This is because external pressure is influenced by a larger number of parameters such as hull form, wave motion characteristics, ship speed, and heading angles. The methods and theories used to determine the external pressure on a ship are usually based on a number of assumptions, such as having a wall-sided hull, small motions of the vessel, and being in an inviscid fluid. Thus, one has to be careful when predicting a value for the external pressure.

The external pressure on a vessel is determined by initially dividing the vessel into two parts. The pressures distributed over 40% of the length of the vessel centered around the amidships are normally very similar from ship to ship. Thus, the calculation of the pressure in these regions is relatively straightforward and is done by applying the results

of a complete seakeeping analysis for full form tankers and bulk carriers. Formulae are used for the pressure applied over the rest of the ship, since the pressure varies significantly from one ship to the next depending primarily on hull form.

In simplified form, the total external pressure P_E on a ship may be expressed as (ABS, 2002)

$$P_E = \rho g(h_s + k_U h_{DE}) \quad (5.31)$$

where,

ρg = Specific weight of sea water

h_s = Hydrostatic pressure head in still water

k_U = Load factor

h_{DE} = Hydrodynamic pressure head induced by the wave.

The pressure distribution may be predicted across a vessel in both lengthwise and girth-wise directions. Most data required to carry out such calculations are obtained from seakeeping analysis.

Internal Tank Pressure

The internal pressure in a tank that carries liquids onboard a ship is made up of three parts:

- hydrostatic pressure equivalent to ρgh ,
- changes in pressure head due to the pitching and rolling motions of the ship, and
- inertial force of the liquid column due to accelerations caused by the motion of the ship.

The internal pressure in a tank is calculated by a series of formulae specific to the shape of the tank being analyzed. A number of different tank shapes exist, such as J-shaped, rectangular, and U-shaped. Other factors that affect the internal pressure are the amount of liquid carried in the tank, and the location and number of air pipes in the tank.

For example, a simplified formula used to determine the internal pressure in a liquid-carrying tank is (ABS, 2002)

$$P_I = \rho g(\eta + k_U h_D) \quad (5.32)$$

where,

η = Local coordinate in vertical direction for tank boundaries measuring from the top of the tanks

k_U = Factor that considers the resultant acceleration of the liquid due to the ship's motion

h_D = wave-induced internal pressure head, including inertia force and added pressure head.

References

- ABS, 2002. Rules for Building and Classing Steel Vessels. American Bureau of Shipping.
- Bhattacharyya, R., 1978. Dynamics of Marine Vehicles. John Wiley & Sons, Inc.
- Bishop, R.E.D., Price, W.G., 1979. Hydroelasticity of Ships. Cambridge University Press.
- Bretschneider, C.L., 1959. Wave Variability and Wave Spectra for Wind-generated Gravity Waves. Beach Erosion Board, US Army Corps of Engineers. Technical Memorandum, No. 118.
- Beck, R., Reed, A.M., 2001. Modern computational methods for ships in a seaway. SNAME Transactions 109.
- Cao, Y., Schultz, W.W., Beck, R.F., 1991. A three-dimensional desingularized boundary integral method for potential problems. International Journal for Numerical Methods in Fluids 11, 785–803.
- Chakrabarti, S.K., 1987. Hydrodynamics of Offshore Structures. Computational Mechanics Publications.
- Ewing, J.A., 1976. Wave prediction: progress and applications. In: Proc. of 6th International Ship Structures Congress, Boston.
- Faltinsen, O.M., 1990. Sea Loads on Ships and Offshore Structures. In: Cambridge Ocean Technology Series. Cambridge University Press.
- Gerritsma, J., Beukelman, W., 1964. The distribution of the hydrodynamic forces on a heaving and pitching ship model in still water. In: Fifth Symposium on Naval Hydrodynamics, Washington.
- Hasselmann, K., et al., 1973. Measurements of wind-wave growth and swell decay during the Joint North Sea Wave Project (JONSWAP). Deutsche Hydrographischen Zeitschrift A8, 12.
- Hogben, N., Dacunha, N.M.C., Olliver, G.F., 1986. Global Wave Statistics. British Maritime Technology, Unwin Brothers Ltd., U.K.
- Hughes, O.F., 1988. Ship Structural Design: A Rationally-Based, Computer-Aided, Optimisation Approach. SNAME.
- Jensen, J.J., Pedersen, P.T., 1979. Wave-induced bending moments in ships — a Quadratic Theory. RINA, 121.
- Jensen, J.J., 2001. Load and Global Response of Ships. In: Elsevier Ocean Engineering Book Series.
- Jensen, J.J., Beck, R.F., Du, S., Faltinsen, O.M., Fonseca, B., Rizzuto, E., Stredulinsky, D., Watanabe, I., 2000. Extreme Hull Girder Loading. ISSC Committee Report.
- De Kat, J.O., Pauling, J.R., 1989. The simulation of ship motions and capsizing in severe seas. Transactions of SNAME 97, 139–168.
- Korvin-Kroukovsky, B.V., 1955. Investigation of ship motions in regular waves. Transactions of SNAME 63, 386–435.
- Lin, W.M., Shin, Y.S., Chung, J.S., Salvesen, N., 1997. Nonlinear Predictions of Ship Motions and Wave Loads for Structural Analysis. OMAE.
- Longuet-Higgins, M.S., 1952. On the statistical distribution of the heights of sea waves. Journal of Marine Research 11, 245–266.
- Ochi, M.K., 1978. Wave statistics for the design of ships and ocean structures. Transactions of SNAME 86.
- Pedersen, P.T., 1983. Beam model for torsional-bending response of ship hulls. Transactions of RINA 125, 171–182.
- Pierson, W.J., 1952. A Unified Mathematical Theory for the Analysis of Propagation and Refraction of Storm-generated Ocean Surface Waves, Part I and II. New York University.
- Pierson, W.J., Neumann, G., James, R.W., 1955. Practical Methods for Observing and Forecasting Ocean Waves by Means of Wave Spectra and Statistics. Hydrographic Office Publication.
- Pierson, W.J., Moskowitz, L., 1964. A proposed spectral form for fully developed wind seas based on the similarity of S. A. Kitaigorodskii. Journal of Geophysical Research 69 (24).
- St. Denis, M., Pierson, W.J., 1953. On the motions of ships in confused seas. Transactions of SNAME 61.
- Sclavounos, P.D., Kring, D.C., Huang, Y.F., Mantzaris, D.A., Kim, S.G., Kim, Y.W., 1997. A computational method as an advanced tool of ship hydrodynamic design. Transactions of SNAME 105, 375–392.
- WAMIT, 1999. WAMIT User Manual. www.wamit.com.

- Wang, Z., Jensen, J.J., Xia, J., 1998. Effects of bow flare shape to the wave loads of a container ship. *Journal of the Society of Naval Architects of Japan* 166.
- Wang, M., Leitch, J., Bai, Y., 2001. Analysis and Design Consideration of Greenwater Impact on Decks and Topsides of FPSO. OTC, 13208.
- Zhao, R., Faltinsen, O.M., 1993. Water entry of two-dimensional bodies. *Journal of Fluid Mechanics* 246.
- Zhou, Z., De Kat, J.O., Buchner, B., 1999. A non-linear 3-D approach to simulate green water on deck. In: *Seventh International Conference on Numerical Ship Hydrodynamics*, Nantes.

Wind Loads for Offshore Structures

6.1 Introduction

Wind loads are often considered secondary in terms of the overall loading of marine structures because average static forces and moments induced by wind are only fractions of total loads. However, for offshore offloading operations, helicopter landings, and cyclonic storms, wind loading is considered critical and should be accounted for in the design. Specifically, drag forces induced by winds are most important for the mooring, dynamic positioning, and maneuvering phases of compliant or floating structures. The stability of floating and fixed structures may be affected by overturning moments due to drag and lift forces (Walree and Willemssen, 1988). Figure 6.1 shows damage caused by Hurricanes Ivan, Katrina, Rita, Gustav/Ike during 2004–2008 in the Gulf of Mexico. More than 100 platforms were destroyed in 2005 by Hurricanes Katrina and Rita, and about 50 platforms were extensively damaged (Shen et al., 2010).

Wind loads exerted on the complex bluff bodies of vessels and platforms are not amenable to theoretical analysis. Wind coefficients used in simulations are often taken from literature (e.g., OCIMF (1994) and SIGTTO (2007)), empirical methods, or wind tunnel tests. Meanwhile, computational fluid dynamics (CFD) has become a cost-efficient alternative due to the significant increase in computational power and improvement of mathematical models (Koop et al., 2012). However, the review of related papers in recent years indicates that wind tunnel tests are still the best option for evaluating wind loads, and CFD methods are not yet mature enough to predict wind loads with confidence (ISSC2012-vol3).

For marine structural design, this chapter gives the basic classification rules (DNV) about the wind, and concludes the related research of wind effects on offshore structures.

6.2 Classification Rules for Design

6.2.1 Wind Data

Wind conditions for various offshore structures design are to be established from collected wind data, and should be consistent with other environmental parameters assumed to occur simultaneously. Wind data are normally to include information from the frequency of occurrence, duration, and direction of various wind speeds. Published data and data from nearby land and sea stations may be used if available. Wind speed measurements should

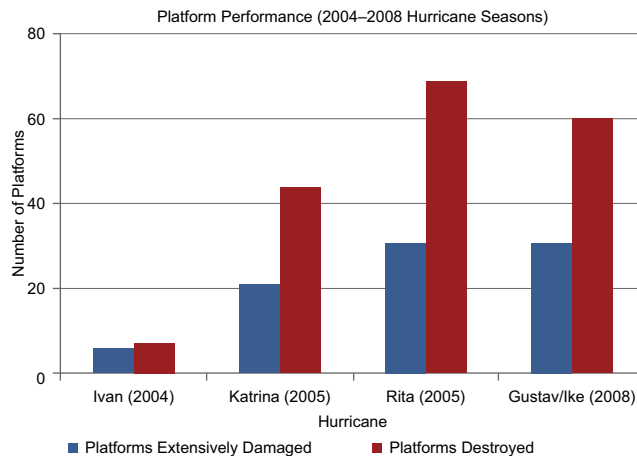


Figure 6.1

Number of platforms damaged or destroyed by hurricanes from 2004 to 2008 in the Gulf of Mexico ([Offshore platform brochure, Risk Management Solutions](#)).

be carried out at the location in question if the wind speed is of significant importance to the design and existing wind data are scarce and uncertain. The wind climate database for the design should preferably cover a 10-year period or continuous data with sufficient time resolution. Recently updated or newly developed meteocean databases are ERA-Interim, NORA10, HIPOCAS, ARGOSS, Fugro-OCEANOR, and SIMORC URL.

Local on-site measurements, traditionally at a height of 10 m, have been the standard way of recording wind characteristics for decades. [Jiménez et al. \(2010\)](#) have made great efforts to evaluate records of the data reports at 41 automated weather stations in northeast of the Iberian Peninsula. Besides traditional local measurements, the advent of remote measurement techniques (e.g., scatterometer) has allowed for much more detailed descriptions of wind in the offshore environment. The most recent developments about this measurement include improvement of high wind speed estimation and grid refinement of wind fields, using multiple mission observations; see [Ricciardulli and Wentz \(2011\)](#), [Quilfen et al. \(2011\)](#), [Bentamy and Croize-Fillon \(2011\)](#), etc. for more information. Still, numerically generated wind data are commonly used in design, and data are available for only some ocean areas ([ISSC2012-vol3](#)).

6.2.2 Wind Conditions

General

The main characteristics of wind speed in an atmospheric boundary layer are

1. wind speed that is made up of mean wind and fluctuating wind;
2. wind speed that varies with time and the height above the sea surface—mean wind speed increases with height, while the content of fluctuating wind decreases with height;

3. a very wide frequency range in the fluctuating wind; and
4. waves of fluctuating wind similar to the gust at any height, especially slow-changing or low-frequency ones.

The wind climate can be represented by the 10-min mean wind speed U_{10} at height 10 m and the standard deviation σ_U of the wind speed at height 10 m. This stationary and constant wind climate representation is intended to cover neither wind conditions experienced in tropical storms such as hurricanes, cyclones, and typhoons, nor those experienced during small-scale events such as fast-propagating arctic low pressures of limited extension or other nonstationary extreme wind conditions like wind gusts.

The short-term 10-minute stationary wind climate may be represented by a wind spectrum—that is, the power spectral density of the wind speed process, $S_U(f)$. $S_U(f)$ is a function of U_{10} and σ_U , and expresses how the energy of the wind speed in a specific point in space is distributed between various frequencies. The long-term probability distributions for wind climate parameters U_{10} and σ_U , derived from available data, can be represented in terms of generic distributions or scatter diagrams. An example of a generic distribution representation consists of a Weibull distribution for the arbitrary 10-minute mean wind speed U_{10} in conjunction with a lognormal distribution of σ_U conditional on U_{10} . Unless data indicate otherwise, a Weibull distribution can be assumed for the arbitrary 10-minute mean wind speed U_{10} at a given height z above the ground or above the seawater level as

$$F_{U_{10}}(u) = 1 - \exp\left(-\left(\frac{u}{A}\right)^k\right) \quad (6.1)$$

in which the scale parameter A and the shape parameter k are site and height dependent.

Wind Profile

The offshore wind speed profile represents the variation of the mean wind speed with height above the still-water level. If a different averaging period other than 10 min is used for the determination of loads, the wind data may be converted by the application of appropriate gust factors. Unless data indicate otherwise, conversions for calculation of mean wind speed U with averaging period T at height z above sea level may be carried out by means of the expressions below including

$$U(T, z) = U_{10} \left(1 + 0.137 \ln \frac{z}{H} - 0.047 \ln \frac{T}{T_{10}} \right) \quad (6.2)$$

where $H = 10$ m, $T_{10} = 10$ min, and U_{10} is the 10-min mean wind speed at height H . This expression converts mean wind speeds between different averaging periods. When given the original 10-min averaging period with stationary conditions for mean wind speed U_{10} and $T < T_{10}$, the expression provides the largest likely mean wind speed over the specified

Table 6.1: Mean wind speed $U(T,z)$ recommended in DNV-OS-C102

Elevation above Sea Level (z)	Average Time (s)					
	3 s	5 s	15 s	1 min	10 min	60 min
1 m	0.934	0.910	0.858	0.793	0.685	0.600
5 m	1.154	1.130	1.078	1.013	0.905	0.821
10 m	1.249	1.225	1.173	1.108	1.000	0.916
20 m	1.344	1.320	1.268	1.203	1.095	1.011
30 m	1.400	1.376	1.324	1.259	1.151	1.066
40 m	1.439	1.415	1.363	1.298	1.190	1.106
50 m	1.470	1.446	1.394	1.329	1.220	1.136
60 m	1.494	1.470	1.419	1.354	1.245	1.161
100 m	1.564	1.540	1.489	1.424	1.315	1.231

averaging period T . The conversion does not preserve the return period associated with U_{10} . The values in Table 6.1 are based on the expression above.

The Frøya wind speed profile is a special case of the logarithmic wind speed profile and is the best-documented wind speed profile for offshore locations and maritime conditions. For extreme mean wind speeds corresponding to specified return periods in excess of approximately 50 years, the Frøya model implies that the following expression can be used for conversion of the 1-h mean wind speed U_0 at height H above sea level, to the mean wind speed U with averaging period T at height z above sea level.

$$U_{(T,z)} = U_0 \cdot \left\{ 1 + C \cdot \ln \frac{z}{H} \right\} \cdot \left\{ 1 - 0.41 \cdot I_U(z) \cdot \ln \frac{T}{T_0} \right\} \quad (6.3)$$

where $H = 10$ m, $T_0 = 1$ h and $T < T_0$,

$$C = 5.73 \cdot 10^{-2} \sqrt{1 + 0.148 U_0} \quad (6.4)$$

and

$$I_U = 0.06 \cdot (1 + 0.043 U_0) \cdot \left(\frac{z}{H} \right)^{-0.22} \quad (6.5)$$

and U will have the same return period as U_0 .

The expressions above contain gust factors for conversion of wind speeds between different averaging periods. HSE (2002) gives an indication of the accuracy that can be expected when conversions of wind speeds between different averaging periods are carried out by means of gust factors. To account for uncertainty in such wind speed conversions, the addition of a wind speed increment to the wind speeds resulting from the conversions is recommended.

The wind profile also depends much on atmospheric stability conditions. The stability-corrected logarithmic wind profile reads

$$U(z) = \frac{u^*}{\kappa} \left(\ln \frac{z}{z_0} - \psi \right) \quad (6.6)$$

in which ψ is a stability-dependent function that is positive for unstable conditions, negative for stable conditions, and zero for neutral ones. Unstable conditions typically prevail when the surface is heated and the vertical mixing is increasing. Stable conditions prevail when the surface is cooled, such as during the night, and vertical mixing is suppressed.

Turbulence

The natural variability of the wind speed about the mean wind speed U_{10} in a 10-min period is known as turbulence and characterized by the standard deviation σ_U . For a given value of U_{10} , the standard deviation σ_U of the wind speed exhibits natural variability from one 10-min period to another. Measurements from several locations show that σ_U conditioned on U_{10} can often be well represented by a lognormal distribution.

$$F_{\sigma_U|U_{10}}(\sigma) = \Phi \left(\frac{\ln \sigma - b_0}{b_1} \right) \quad (6.7)$$

in which $\Phi ()$ denotes the standard Gaussian cumulative distribution function.

$$\Phi(x) = \frac{1}{\sqrt{2\pi}} \int_{-\infty}^x e^{-\xi^2/2} d\xi \quad (6.8)$$

The coefficients b_0 and b_1 are site-dependent coefficients dependent on U_{10} .

Wind Spectra

When site-specific spectral densities based on measured data are used, the following requirement to the energy content in the high frequency range should be fulfilled unless the data indicate otherwise: The spectral density $S_U(f)$ shall asymptotically approach the following form as the frequency f in the high-frequency range increases:

$$S_U(f) = 0.14 \cdot \sigma_U^2 \left(\frac{L_u}{U_{10}} \right)^{-\frac{2}{3}} f^{-\frac{5}{3}} \quad (6.9)$$

where L_u is the integral length scale of the wind speed process.

Unless data indicate otherwise, the spectral density of the wind speed process may be represented by a model spectrum. The most commonly used model spectra with length scales are Davenport, Kaimal, and Harris spectra. For design of offshore structures, the empirical Simiu and Leigh spectrum, and the empirical Ochi and Shin spectrum, may be applied.

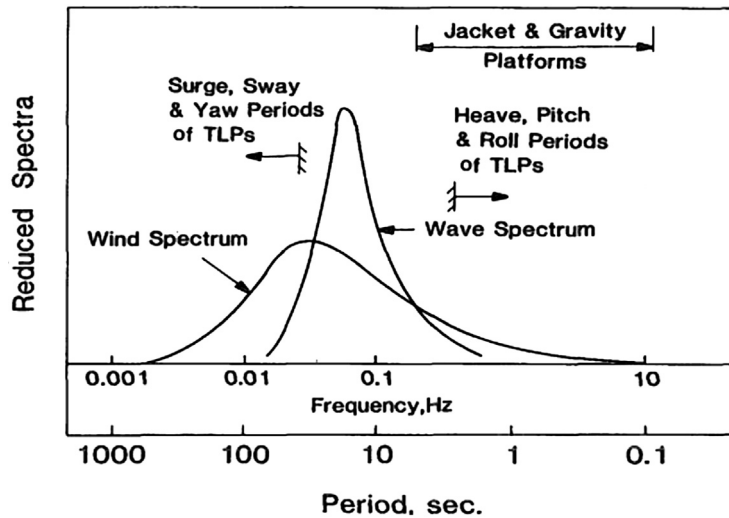


Figure 6.2

Excitation and frequency ranges of offshore platforms (Kareem, 1985).

For situations where excitation in the low-frequency range is important, the Frøya model spectral density proposed by Andersen and Løvseth (1992, 2006) is recommended for wind over water. Figure 6.2 gives excitation source spectra used in offshore design.

Hurricanes

In areas where hurricanes occur, the Weibull distribution determined from available 10-minute wind speed records may not provide adequate representation of the upper tail of the true distribution of U_{10} . In such areas, the upper tail of the distribution of U_{10} needs to be determined based on hurricane data.

Therefore, in areas where hurricanes occur, the distribution of the annual maximum 10-min mean wind speed $U_{10, \max}$ should be based on available hurricane data. This refers to hurricanes for which the 10-min mean wind speed forms a sufficient representation of the wind climate.

In the absence of information on tropical storm winds in the region of interest, the conversion expressions of wind profiles may also be applied to winds originating from tropical storms. This implies that expressions can be applied to winds from hurricanes.

6.2.3 Wind Loads

General

Wind-induced loads on structures are in general time-dependent loads due to fluctuations in wind velocity. Wind loads act on external surfaces of closed structures and may also act

on internal surfaces of open structures. Wind pressure loads act in a direction normal to the surface. Frictional forces due to tangential drag should be considered when a large surface is swept by wind. As discussed before, since wind speed varies with elevation, the height of the structure or component considered should be taken into account.

The response of an offshore structure to wind loading is a superposition of a static response and resonant response due to excitation close to natural frequencies. Dynamic effects can be

- resonant response due to turbulence in wind;
- response due to vortex shedding; and
- galloping/flutter.

Guidance on galloping and flutter can be found in [Blevins \(1990\)](#).

Global wind loads on structures shall be determined using a time-averaged design speed in the form of sustained wind speed. For design of individual components, a time-averaged wind speed is also adequate, but the averaging time interval should be reduced to allow for smaller turbulence scales. The time and spatial variation of the wind speed should be accounted for in the design of offshore structures that exhibit considerable dynamic response. When the wind field contains energy at frequencies near the natural frequencies of the structure, a dynamic analysis using a wind frequency spectrum should be carried out.

Wind Pressure

The basic wind pressure is defined by the following equation:

$$q = \frac{1}{2} \rho_a U_{T,z}^2 \quad (6.10)$$

where:

q = the basic wind pressure or suction

ρ_a = the mass density of air, which is to be taken as 1.226 kg/m³ for dry air at 15 °C

$U_{T,z} = U(T,z)$; see the “Wind Profile” subsection of [Section 6.2.2](#).

The external horizontal or vertical surfaces of closed structures that are not efficiently shielded should be checked for local wind pressure or suction using the following equation:

$$p = \pm C_p q \quad (6.11)$$

where:

p = wind pressure or suction

C_p = pressure coefficient.

The pressure coefficient may be chosen equal to 1.0 for horizontal and vertical surfaces. Also, The wind pressure acting on the surface of helidecks may be calculated using the pressure coefficient $C_p = 2.0$ at the leading edge, linearly reducing to $C_p = 0$ at the trailing edge, taken in the direction of the wind. The pressure may act both upward and downward.

Wind Forces

The wind force F_w on a structural member or surface acting normal to the member axis or surface may be calculated according to

$$F_w = CqS \sin \alpha \quad (6.12)$$

where:

q = as defined in [Eqn \(6.10\)](#)

S = projected area of the member normal to the direction of the force

α = angle between the direction of the wind and the axis of the exposed member or surface

C = shape coefficient.

The shape coefficients for different situations are recommended as follows. All shape coefficients below include the effect of suction on the leeward side of the member.

Circular Cylinders

The shape coefficient C_∞ for circular cylinders of infinite length may be chosen according to [Figure 6.3](#).

The Reynolds number (R_e) is then defined as

$$R_e = \frac{DU_{T,z}}{\nu_a} \quad (6.13)$$

where:

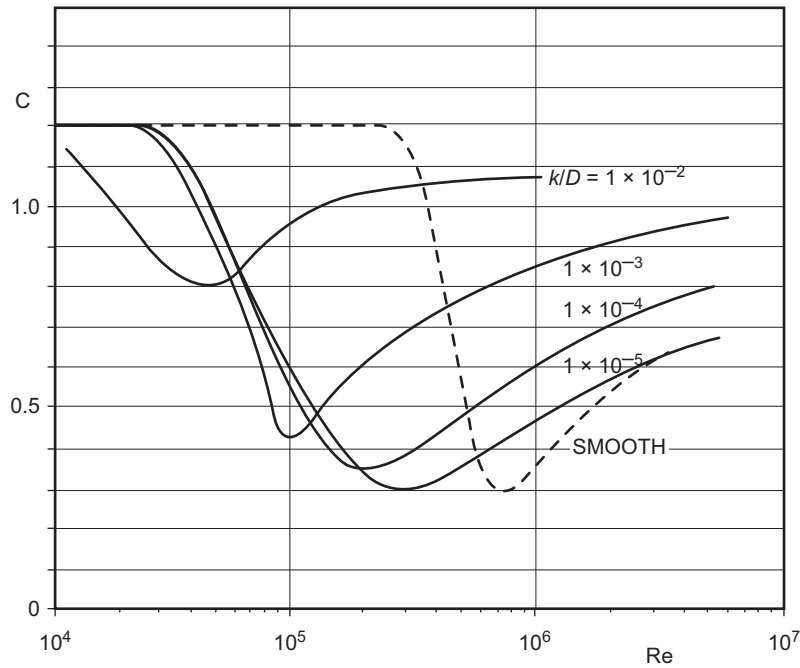
D = diameter of the member

ν_a = kinematic viscosity of air, which may be taken as $1.45 \times 10^{-5} \text{ m}^2/\text{s}$ at 15°C and standard atmospheric pressure.

Rectangular Cross Sections

The shape coefficients for smooth members with rectangular cross sections may be taken as

$$C_{s1} = 2K_R \sin \alpha \quad (6.14)$$


Figure 6.3

Drag coefficient for fixed circular cylinder for steady flow in a critical flow regime, for various roughnesses (DNV-RP-C205).

$$\begin{aligned}
 C_{s2} &= \left(1 + \frac{b_2}{b_1}\right) K_R \sin \alpha \quad \text{for } b_2 \leq b_1 \leq 2b_2 \\
 &= 1.5K_R \cos \alpha \\
 K_R &= 1.0 \quad \text{for } \frac{r}{b} \leq 0.10 \\
 &= \frac{1}{3} \left(4.3 - 13 \frac{r}{b}\right) \quad \text{for } 0.10 < \frac{r}{b} < 0.25 \\
 &= 0.35 \quad \text{for } \frac{r}{b} \geq 0.25
 \end{aligned} \tag{6.15}$$

where:

b_1 = longer side of rectangle

b_2 = shorter side of rectangle

r = corner radius of the section

α = angle between side b_1 of the rectangle and the flow component in the cross-sectional plane.

Parameters b_1 , b_2 , and α are also shown in [Figure 6.4](#).

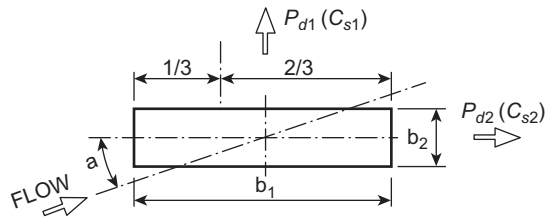


Figure 6.4
Drag forces on rectangular cross sections (DNV-RP-C205).

For wide rectangular cross sections, it may be necessary to take into account that the resultant drag force P_{d1} is assumed to be acting at a distance $b_1/3$ from the leading edge of the surface; see [Figure 6.4](#).

The shape coefficients and characteristic dimensions for various smooth members with irregular cross sections may be taken in accordance with Table 5.2 in [DNV-RP-C205](#) where dimensions perpendicular to P_{d1} and P_{d2} are to be understood as b_1 and b_2 respectively.

Finite Length Effects

The shape coefficient C for individual members of finite length may be obtained like:

$$C = \kappa C_{\infty}$$

Where κ is the reduction factor function of the ratio l/d where d is the cross-sectional dimension of a member normal to the wind direction and l is the length of the member.

For members with one end abutting another member or a wall in such a way that free flow around that end of the member is prevented, the ratio l/d should be doubled for the purpose of determining κ . When both ends are abutted as mentioned, the shape coefficient C should be taken equal to that for an infinite long member.

Other Structures

For spherical and parabolic structures like radar domes and antennas, the shape coefficient C may be taken from Table 5.3 in [DNV-RP-C205](#).

For three-dimensional bodies such as deck houses and similar structures placed on a horizontal surface, shape coefficients may be taken from Table 5.5 in [DNV-RP-C205](#).

More information about shape coefficients for various structures is given in Eurocode EN 1991-1-4: General actions—wind actions.

Two effects should be considered when defining wind force. On the basis of [Eqn \(6.12\)](#), if several members are located in a plane normal to the wind direction, as in the case of a

plane truss or a series of columns, the solidification effect ϕ must be taken into account. The wind force is

$$F_{W,SOL} = C_e q S \phi \sin \alpha \quad (6.16)$$

where:

C_e = the effective shape coefficient

q = as defined in Eqn (6.12)

S = as defined in Eqn (6.12), to be taken as the projected area enclosed by the boundaries of the frame

ϕ = solidity ratio, defined as the projected exposed solid area of the frame normal to the direction of the force, divided by the area enclosed by the boundary of the frame normal to the direction of the force

α = angle between the wind direction and the axis of the exposed member as defined before.

The other is the shielding effect. If two or more parallel frames are located behind each other in the wind direction, this effect may be taken into account. The wind force on the shielded frame $F_{W,SHI}$ may be calculated as

$$F_{W,SHI} = F_W \eta \text{ (if } F_w = C q S \sin \alpha \text{ is applicable)} \quad (6.17)$$

or as:

$$F_{W,SHI} = F_{W,SOL} \eta \text{ (if } F_{W,SOL} = C_e q S \phi \sin \alpha \text{ is applicable)} \quad (6.18)$$

where

η = shielding factor.

The shielding factor η depends on the solidity ratio ϕ of the windward frame, the type of member comprising the frame, and the spacing ratio of the frames. The shielding factor may be chosen according to Table 5.1 in [DNV-RP-C205](#).

If more than two members or frames are located in line after each other in the wind direction, the wind load on the rest of the members or frames should be taken equal to the wind load on the second member or frame.

Dynamic Wind Analysis

A detailed dynamic wind analysis considering the time variation of wind forces should be performed for wind-exposed equipment and objects sensitive to varying wind loads. Typically, high towers, flare booms, compliant platforms like tension leg platforms (TLP) and catenary anchored platforms, and similar equipment should be considered for such analysis. The time-varying component of wind force can induce low-frequency resonant

surge, sway, and yaw motion of floating catenary-anchored platforms. Low-frequency wind forces are computed from a wind energy spectrum. Structural analyses of semisubmersibles (Ochi and Bales, 1977), TLP (Kareem and Dalton, 1982), and jack-ups (Weaver and Briskman, 1995) have been carried out in either the time domain or the frequency domain for appropriate loading of wind and wave. A method for estimating wind forces on ships is given in OCIMF (1994).

The gust variation of the wind field can be described as the sum of a sustained wind component and a gust component. The fluctuating gust velocity can be described by the gust spectrum discussed before. The spatial correlation (or distribution) of the gust in a plane normal to the sustained wind direction can be described by a coherence function using a horizontal decay factor normal to the sustained wind direction, and a vertical decay factor.

The instantaneous wind force on a wind-exposed structure can be calculated by summation of the instantaneous force on each wind-exposed member. The instantaneous wind pressure q can be calculated by the formula

$$q = \frac{1}{2} \rho_a |U_{T,z} + u - \dot{x}| (U_{T,z} + u - \dot{x}) \quad (6.19)$$

where:

u = the gust speed and direction variation

\dot{x} = the instantaneous velocity of the structural member.

For time-domain calculations, time histories of wind velocities corresponding to spectra can be used in combination with the force calculations given above to establish time histories of wind forces.

When using a frequency-domain calculation, the instantaneous wind pressure can normally be made linear to

$$q = \frac{1}{2} \rho_a U_{T,z}^2 + \rho_a U_{T,z} u \quad (6.20)$$

for structures where the structural velocity is negligible compared with wind velocity. This means that the fluctuating wind force is linear in the fluctuating velocity.

In direct frequency-domain analysis, the solution can be obtained by multiplication of the cross-spectral densities for the dynamic wind load by the transfer function of response; a modal formulation could be applied. Modal responses may be combined with the square-root-of-sum-of-squares (SRSS) method if the modes are not too closely related. The SRSS method assumes that all maximum modal values are statistically independent of each other. In case of modes having periods close to each other, the complete-quadratic-combination method can be used instead. This method assumes that all maximum modal

values occur at the same point in time. The peak value of the load is estimated by the formula

$$F = \sqrt{\sum_n \sum_m f_n \rho_{nm} f_m} \quad (6.21)$$

where f_n is the modal force associated with mode n , and summation is over all modes. The cross-modal coefficients ρ_{nm} with constant damping ζ are

$$\rho_{nm} = \frac{8\zeta^2(1+r)r^{3/2}}{(1-r^2)^2} + 4\zeta^2r(1+r)^2 \quad (6.22)$$

where r is the ratio between modal frequencies $r = \omega_n/\omega_m \leq 1$.

All relevant effects such as structural, aerodynamic, and hydrodynamic damping should normally be considered in the analysis.

For the structural design, the extreme load effect due to static and dynamic wind can be assessed by

$$F_e = F_s + g\sigma(f) \quad (6.23)$$

where:

F_s = the static response due to the design average wind speed

$\sigma(f)$ = the standard deviation of dynamic structural responses

g = wind response peak factor.

Model Wind Tunnel Tests

Wind tunnel tests should be carried out when wind loads are significant for overall stability, offset, motion, or structural response, or there is the danger of dynamic instability. Wind tunnel tests may support or replace theoretical calculations when available theoretical methods are susceptible to large uncertainties (e.g., due to a new type of installation or an adjacent installation that influences the relevant installation).

Data obtained from reliable and adequate model tests are recommended for the determination of pressures and resulting loads on structures of complex shape.

Tests should be carried out on a properly scaled model of the full scale shape of the structure. The actual wind should be modeled to account for the variation of the mean wind speed with height above ground or seawater, and the turbulence level in the wind.

Computational Fluid Dynamics

As described before, wind loads on structures can be calculated using CFD, solving Navier–Stokes equations for the motion of air and taking into account compressibility and

turbulence effects. One should be aware of the following when applying CFD to calculate wind-induced forces on structures:

- results may depend strongly on the turbulence model used;
- the input wind velocity field should be properly modeled, including boundary layer effects;
- the exposed area of the structure(s) should be a small fraction of the computational domain outflow area;
- the grid resolution should be at least 10 cells per cubic foot of structure volume and at least 10 cells per separation distance between structures;
- grid convergence studies should be carried out; and
- results should be validated with results from wind tunnel tests.

6.3 Research of Wind Loads on Ships and Platforms

6.3.1 Wind Loads on Ships

For the ship design, wind loads will be accounted for in the design of topside structures subject to significant wind exposure (e.g., flare tower, derrick, and modules). The mean wind speed over a one-minute period at actual position above the sea level shall be used together with inertia loads from the waves. Wind loads should normally not be less than 2.5 kN/m^2 . For slender members (e.g., members in a flare tower structure), additional assessments of vortex shedding shall be carried out. Global wind loading acting on vessels (Figure 6.5) should be determined by appropriate calculation formulas using the drag coefficients C_X , C_Y in the X and Y directions, and yaw moment coefficient C_M as shown below.

$$R_X = \frac{1}{2} \rho_a U_{T,z}^2 A_T C_X, \quad R_Y = \frac{1}{2} \rho_a U_{T,z}^2 A_L C_Y, \quad M_M = \frac{1}{2} \rho_a U_{T,z}^2 A_L L C_M \quad (6.24)$$

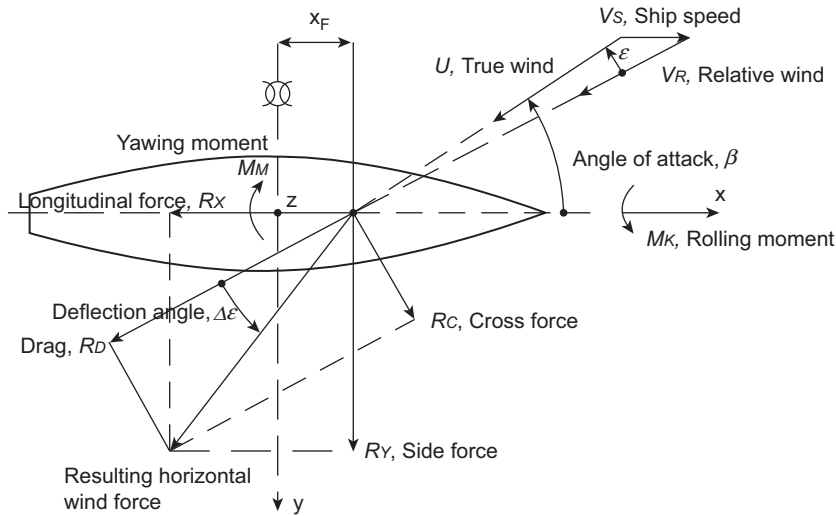
where R_X , R_Y , and M_M are components of wind forces in the X and Y directions, and the moment of the wind load about the midship. A_T and A_L are the frontal and side projected areas above the water surface, and L is the length overall.

As stated in DNV-RP-C205, Isherwood (1972) has just presented drag coefficients for passenger ships, ferries, cargo ships, tankers, ore carriers, stern trawlers, and tugs. The wind coefficients are given by the equations below.

$$C_X = A_0 + A_1 \frac{2A_L}{L^2} + A_2 \frac{2A_T}{B^2} + A_3 \frac{L}{B} + A_4 \frac{S}{L} + A_5 \frac{C}{L} + A_6 M \quad (6.25)$$

$$C_Y = B_0 + B_1 \frac{2A_L}{L^2} + B_2 \frac{2A_T}{B^2} + B_3 \frac{L}{B} + B_4 \frac{S}{L} + B_5 \frac{C}{L} + B_6 \frac{A_{SS}}{A_L} \quad (6.26)$$

$$C_M = C_0 + C_1 \frac{2A_L}{L^2} + C_2 \frac{2A_T}{B^2} + C_3 \frac{L}{B} + C_4 \frac{S}{L} + C_5 \frac{C}{L} \quad (6.27)$$


Figure 6.5

Coordinates; wind forces and moments acting on vessels (Anton et al., 2009).

where S represents the length of the lateral projection perimeter, C is the distance from bow to the centroid of the lateral projected area, A_{SS} is the lateral projected area of the superstructure, and M is the number of distinct groups of masts or king posts. Constants A_0 to A_6 , B_0 to B_6 , and C_0 to C_5 from the above equations are presented in tabular form along with residual standard errors and can be found in Isherwood (1972).

Additional numerical methods have been developed for the prediction of wind forces on floating structures without reverting to direct model testing. Haddara and Soares (1999) selected three methods available in the literature (see Isherwood (1972), Gould (1982), and OCIMF (1994)) to estimate wind loads on a 351.0 m tanker in the loaded and ballast conditions, and compared their results with the experimental data obtained by Blendermann (1993). This comparative study indicates that there is no general agreement between methods used for the estimation of wind forces on ships. Alternately, Haddara and Soares (1999) used a neural network technique to obtain a universal expression for the estimation of wind loads on any type of ship. The following expressions of this method are used to calculate coefficients of the wind forces:

$$C_k = \sum_{i=1}^m \gamma_{ki} H_{ki}, \quad k = 1, 2, 3 \quad (6.28)$$

where $k = 1, 2, 3$ refer to the longitudinal force, transverse force, and yaw moment, respectively, and

$$H_{ki} = \frac{[1 - e^{-G_{ki}}]}{[1 + e^{-G_{ki}}]}, \quad G_{ki} = \sum_{j=1}^5 w_{kij} x_j, \quad k = 1, 2, 3 \quad (6.29)$$

and

$$x_1 = \frac{A_L}{L^2}, x_2 = \frac{A_T}{B^2}, x_3 = \frac{L}{B}, x_4 = \frac{S}{L}, x_5 = \varepsilon, x_6 = 1,$$

where A_L is the lateral projected area, A_T is the transverse projected area, s is the distance between the center of the lateral projected area and the middle section of the ship, ε is the angle between the centerline of the ship and the wind velocity, L is the ship's length, and B is the ship's beam. Values for weights γ_{ki} and w_{kij} are calculated by the neural network. Table 6.2 shows a list of ships used in the training of the network. Figures 6.6–6.11 (Haddara and Soares (1999)) show the comparisons between the experimental and the predicted wind forces coefficients for the tanker. The predicted data agreed qualitatively with experimental data in all cases.

Computational wind engineering (CWE) is a branch of CFD, and has developed rapidly over the last three years to evaluate the interaction between wind and ships numerically. For example, Koop et al. (2010) investigated the applicability and accuracy of CFD analysis to derive wind loads for an FPSO tandem offloading configuration. This work was performed within the OO1 Joint Industry Project, and analyzed the wind load on a fully loaded barge-shaped FPSO with five square blocks on the deck and a ballast-loaded shuttle tanker at a distance of 450 m. A similar analysis was performed by Tannuri et al. (2010)

Table 6.2: Ships used in the training of the neural network
(Haddara and Soares, 1999)

Ship	Load (m)	B (m)	D (m)
Container ship (full)	210.75	30.50	11.6
Container ship (empty)	210.75	30.50	9.6
Container ship (loaded)	210.75	30.50	9.6
Container ship (empty)	216.40	23.77	6.94
Drill ship	150.1	21.35	7.00
Cruise ship	143.90	17.35	5.90
Cruise ship	161.00	29.00	6.05
Cutter	25.05	5.80	2.50
Cargo ship (loaded)	141.1	18.50	7.32
Cargo ship (empty)	141.1	18.50	4.43
Cargo ship (loaded)	155.45	23.10	8.69
Cargo ship (container on deck)	155.45	23.10	8.69
Research vessel: Wind from Port	55.00	12.50	3.95
Research vessel: Wind from Starboard	55.00	12.50	3.95
Speed boat	53.60	9.20	2.50
Offshore supply vessel	61.95	13.00	4.85
Offshore supply vessel	61.00	13.00	4.85
Gas tanker (loaded)	274.00	47.20	10.95
Gas tanker (ballast)	274.00	47.20	8.04

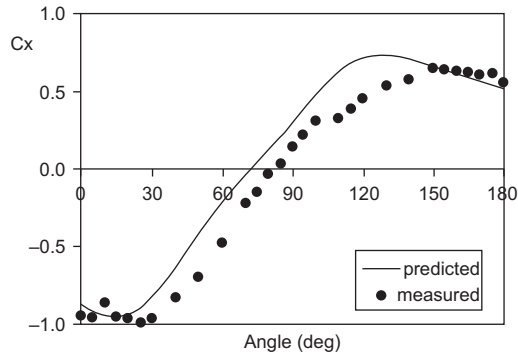


Figure 6.6

Predicted and measured longitudinal force coefficient (loaded tanker).

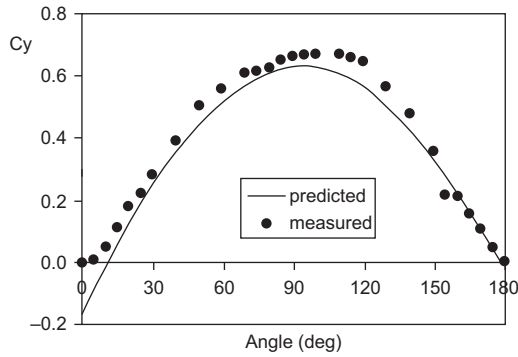


Figure 6.7

Predicted and measured side force coefficient (loaded tanker).

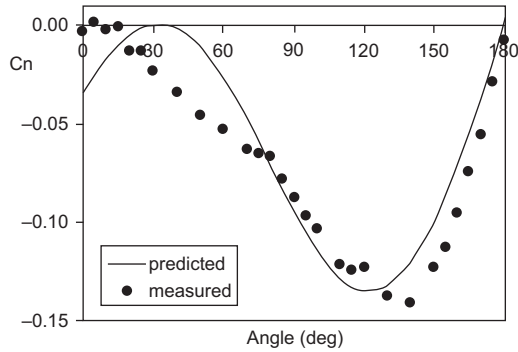


Figure 6.8

Predicted and measured yaw moment coefficient (loaded tanker).

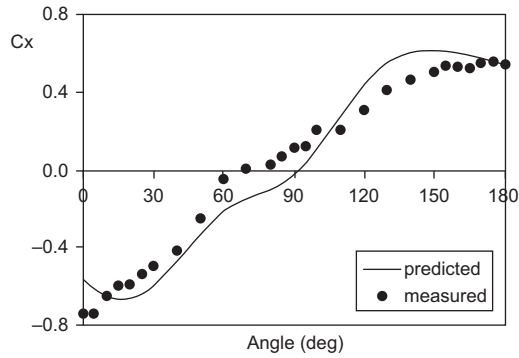


Figure 6.9

Predicted and measured longitudinal force coefficient (tanker in ballast).

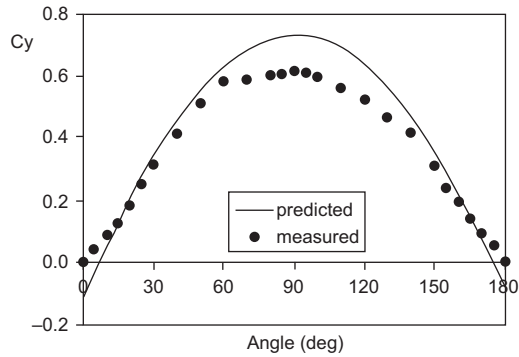


Figure 6.10

Predicted and measured side force coefficient (tanker in ballast).

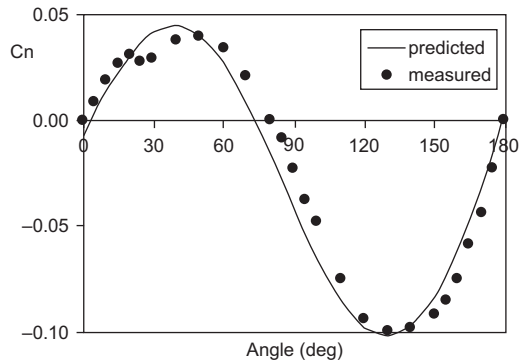


Figure 6.11

Predicted and measured yaw moment coefficient (tanker in ballast).

on a typical shuttle tanker when offloading an FPSO moored in a spread mooring system. In that work, shielding effects when the shuttle was shifted to a tandem position, aligned to the FPSO, were analyzed. Within the OO1 and OO2 “offloading operability” JIPs, [Koop et al. \(2012\)](#) investigated the development of the profile in the CFD calculations. Using the appropriate grid resolution and velocity profile, wind loads on five different vessels (see three of them in [Figure 6.12](#)) are calculated for the angles 0° – 180° in steps of 10° . Furthermore, the wind velocity distribution in the wake of the FPSO shows good agreement with velocity measurements. From the results it is concluded that with ReFRESKO, wind loads on typical offshore vessels can be predicted with reasonable accuracy in a cost-efficient manner.

6.3.2 Wind Loads on Platforms

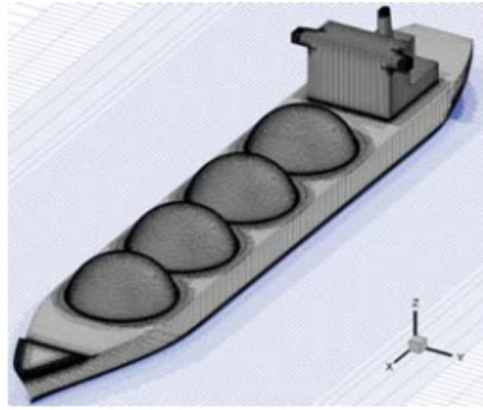
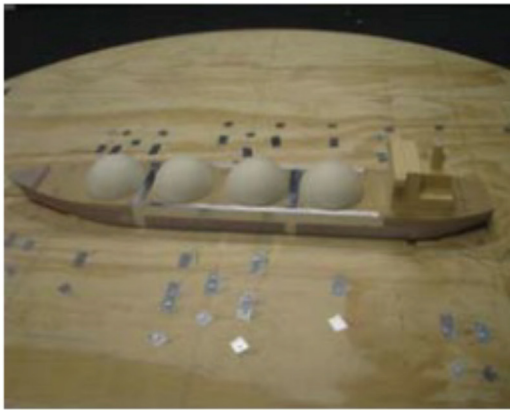
Wind effects on platforms can be categorized into two classes: integral and local. Integral loads are responsible for global effects such as overturning moments and base shear. As suggested in [DNV-OS-C105](#), lift and overturning moments generated on the TLP by wind loads shall be included in the tendon response calculations. At the global level, the lateral wind load in the design of fixed offshore structures is on the order of 10% of total lateral loads, and 25% in the case of compliant and floating platforms. In the event of cyclonic winds, these loads tend to increase to 20% and 40–50%, respectively, in jackets and complaints. The local effects concern the design of deck structures, deck components, and envelopes. A normal platform consists of different structures that can be approximately categorized into the four types shown in [Figure 6.13](#).

Type 1—Cylindrical members of small diameter consisting of drilling towers, hoist equipment, etc. As with water flow around a circular cylinder, airflow may separate and give rise to lift forces.

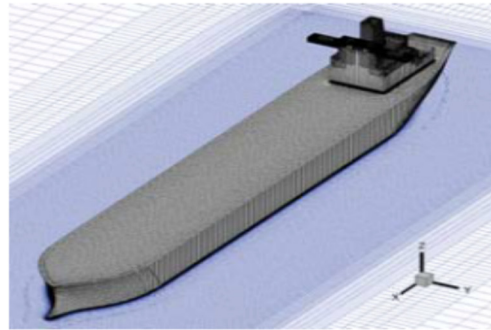
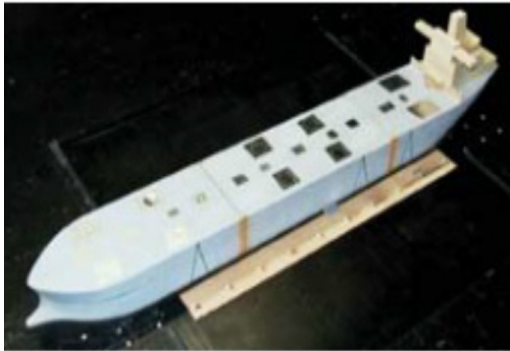
Type 2—Rectangular surfaces usually consisting of living quarters, offices, etc. The flow separates at sharp corners of objects; the resulting forces on a plane vertical wall facing the wind are calculated using Davenport’s gust factors. The flow separation that occurs may build up lateral forces as well.

Type 3—Decks and a helicopter landing platform consisting of flat horizontal surfaces. The wind flow is in line with surfaces that ultimately correspond to the main upward force trying to lift up this type of the structure.

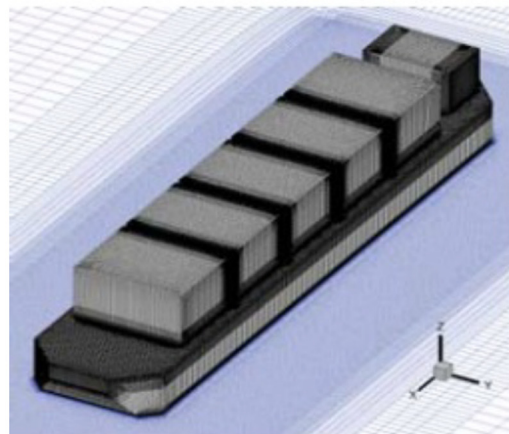
Type 4—Platform supporting columns. The main concern here is that during tow out the exposed length could be up to 130 m with a base diameter of 20 m. A full spectral analysis with certain cross-correlation assumptions must be done, since these are basically shell-like structures for which diffraction theory is not applicable.



Moss type LNG carrier



Shuttle tanker at 10 m draft



FPSO

Figure 6.12

Models used in the wind tunnel experiments of the OO1 and OO2 JIPs (left); computational grids for wind loads on offshore vessels (right) (Koop et al., 2012).

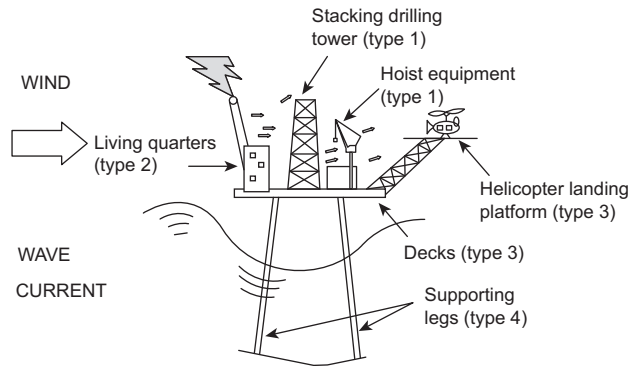


Figure 6.13

Schematic of wind action on offshore deck structures, showing geometric types (Anton et al., 2009).

Researchers had carried out the wind load studies on offshore platforms and some beneficial results were obtained. Aquiree and Boyce (1974) have estimated wind forces on offshore drilling platforms. Lee and Low (1993) obtained results of wind tunnel tests on models of rigid offshore platforms. Pressure transducers located at 141 locations on the 1:268 scale model were used to measure wind loads. Wind speed was measured using a hot wire anemometer. Wind tunnel results show an overriding influence of the legs. They accounted for about 70% of all drag and about 80% of all overturning moments in the floating mode (Haddara and Soares, 1999). Yang et al. (2009) analyzed loads on drilling rig tie-down systems during hurricane conditions. The authors allocated special effort to analyzing the dynamics of the structures. Wind force time series were calculated in a classic manner and applied as collinear to wave and current actions.

CWE on platforms is also developed. Wang et al. (2010) performed a wind load analysis for a semisubmersible platform using CFD analysis and compared the results with wind tunnel experiments. Wnęk and Guedes Soares (2011, 2012) presented an analysis of the aerodynamic forces acting on a floating LNG platform and an LNG carrier. Results have been obtained using the commercial CFD ANSYS CFX code and were compared with experimental measurements performed in a wind tunnel. The biggest discrepancy occurred at the lateral forces, where CFD underpredicts experimental results by about 50%.

Zhang et al. (2010) presented a numerical study of wind loads on a semisubmersible platform. Techniques of CFD such as the Reynolds-averaged Navier–Stokes equations model and large eddy simulation (LES) were adopted to predict wind loads on and wind flows around the platform. Among the concerned turbulence models, the LES with a dynamic SGS model (see Figure 6.14) can provide satisfactory predictions for mean pressure coefficients and reasonable results of fluctuating pressure coefficients, as well as power spectral densities of wind-induced forces for a typical rectangular tall structure.

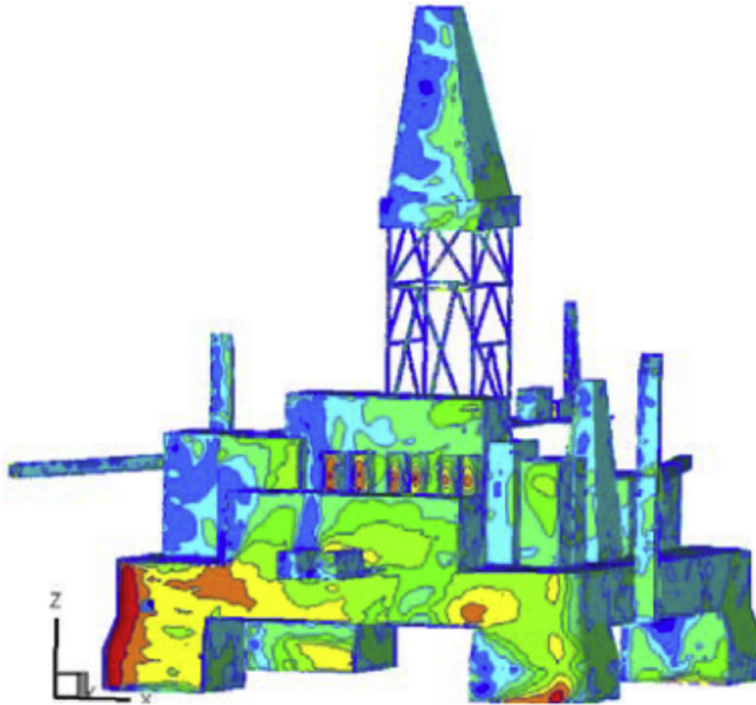


Figure 6.14

Les turbulence model (Zhang et al., 2010).

Accurate modeling of the boundary conditions of incident flows, such as the velocity profile and turbulence intensity profile in numerical simulations, is of great importance for getting good agreement between numerical results and experimental measurements. Different inflow boundary conditions in wind tunnel tests resulted in discrepancies of the mean pressure coefficients.

References

- Andersen, O.J., Løvseth, J., 1992. The Maritime Turbulent Wind Field. Measurements and Models. Norwegian Institute of Science and Technology, Trondheim, Norway. Final Report for Task 4 of the Statoil Joint Industry Project.
- Andersen, O.J., Løvseth, J., 2006. The Frøya database and maritime boundary layer wind description. *Marine Structures* 19, 173–192.
- Anton Turk, 2009. Brodo Gradnja. Jasna PRPIĆ-oršić, Estimation of Extreme Wind Loads on Marine Objects, 60, 2, pp. 147–156.
- Aquiree, J.E., Boyce, T.R., 1974. Estimation of wind forces on offshore drilling platforms. *Transactions Royal Institution of Naval Architects (RINA)* 116, 93–119.
- Blendermann, W., 1993. Schiffsforn und Windlast-Korrelations-und Regression analyse von Windkanalmesungen am Modell. Report No. 533. Institut fur Schiffbau der Universitat Hamburg, 99 pages plus Appendix.

- Bentamy, A., Croize-Fillon, D., 2011. Gridded surface wind fields from Metop/ASCAT measurements. *International Journal of Remote Sensing* 8, 1–26.
- Blevins, R.D., 1990. *Flow-Induced Vibrations*. Krieger Publishing Company, Malabar, 2001.
- DNV-RP-C205, April, 2014. Environmental Conditions and Environmental Loads.
- DNV-OS-C102, October, 2014. Structural Design of Offshore Ships.
- DNV-OS-C105, July, 2014. Structural Design of TLPs (LRFD Method).
- Gould, R.W.F., 1982. The estimation of wind loads on ship superstructures. *The Royal Institution of Naval Architects, Monograph* 8, 34.
- HSE(Health & Safety Executive), 2002. Environmental Considerations. HSE Books, Suffolk, England. Offshore Technology Report No. 2001/010.
- Haddara, M.R., Guedes Soares, C., 1999. Wind loads on Marine structures. *Marine Structures* 12, 199–209.
- ISSC2012-vol3, 2012. 18th International Ship and Offshore Structures Congress.
- Isherwood, R.M., 1972. Wind resistance of merchant ships. *Transactions Royal Institution of Naval Architects (RINA)* 114, 327–338.
- Jiménez, P.A., González-Rouco, J.F., Navarro, J., Montávez, J.P., García Bustamante, E., 2010. Quality assurance of surface wind observations from automated weather stations. *Journal of Atmospheric and Oceanic Technology* 27, 1101–1122.
- Kareem, A., Dalton, C., 1982. Dynamic effects of wind on tension leg platforms. In: *Offshore Technology Conference, USA, vol. I, pp. 746–757*. OTC Paper 4229.
- Kareem, A., 1985. Lateral-torsional motion of tall buildings to wind loads. *Journal of Structural Engineering* 111 (11), 2479–2496.
- Koop, A., Klaij, C.M., Vaz, G., June 2010. Predicting wind shielding for FPSO tandem Offloading using CFD. In: *Proceedings of OMAE2010, Shanghai, China*.
- Koop, A., Rossin, B., Vaz, G., July 2012. Predicting wind loads on typical offshore vessels using CFD. In: *Proceedings of OMAE2012, Rio de Janeiro, Brazil*.
- Lee, T.S., Low, H.T., 1993. Wind effects on offshore platforms: a wind tunnel model study. In: *Proceedings of the Third International Offshore and Polar Engineering Conference, Singapore, pp. 466–470*.
- Ochi, M.K., Bales, S.L., 1977. Effect of various formulations in predicting responses of marine vehicles and ocean structures. In: *Offshore Technology Conference, USA, vol. I, pp. 133–148*.
- Offshore platform brochure, Risk management solutions (RSM).
- OCIMF, 1994. *Prediction of Wind and Current Loads on VLCCs*, second ed. Oil Companies International Marine Forum.
- Quilfen, Y., Vandemark, D., Chapron, B., Feng, H., Sienkiewicz, J., 2011. Estimating gale to hurricane force winds using satellite altimeter. *Journal of Atmospheric and Oceanic Technology* 28, 453–458.
- Ricciardulli, L., Wentz, F., 2011. Reprocessed QuikSCAT (V04) Wind Vectors With Ku-2011 Geophysical Model Function, Remote Sensing Systems. Technical Report 043011.
- Shen, K., Wang, J., Dong, X., 2010. Fluid inclusions of the high pressure granulites from the Namche Barwa complex of the eastern Himalayan syntaxis, Tibet: fluid composition and evolution in the continental subduction-zone. *Journal of Asian Earth Sciences* 38, 44–56.
- SIGTTO, 2007. *Prediction of Wind Loads on Large Liquefied Gas Carriers*. Society of International Tanker & Terminal Operators, Ltd.. Technical report.
- Tannuri, E.A., Agostinho, A.C., Morishita, H.M., et al., 2010. Dynamic positioning systems: An experimental analysis of sliding mode control. *Control Engineering Practice* 18 (10), 1121–1132.
- Weaver, T.O., Briskman, C.R., 1995. Calibration of a Dynamic Analysis Procedure Based on Measurements from the North Sea Jack-up in Severe Storm, OTC Paper 7840, vol. 3. OTC, 333–342.
- Walree, F., Willemsen, E., 1988. *Wind Loads on Offshore Structures*, BOSS.
- Wang, L., Zhang, S., Yang, S., Yang, H., 2010. Numerical evaluation of wind loads on semi-submersible platform by CFD. In: *Proceedings of the 29th International Conf on Ocean, Offshore and Arctic Engineering, Shanghai, China*.

- Wnęk, A.D., Guedes Soares, C., 2012. Numerical analysis of the shadow effect of an LNG floating platform on an LNG carrier under wind conditions. In: Rizzuto, S., Guedes (Eds.), *Sustainable Maritime Transportation and Exploitation of Sea Resources*. Taylor & Francis Group, London, ISBN 978-0-415-62081-9.
- Wnęk, A.D., Guedes Soares, C., 2011. Numerical analysis of the shadow effect of LNG floating platform on a LNG carrier under wind condition. In: *Proceedings of 14th Congress of the International Maritime Association of Mediterranean*. Genoa, Italy.
- Yang, C.K., Bae, Y.H., Kim, M.H., Ward, E.G., 2009. Loads on tie-down systems for floating drilling rigs during hurricane conditions. In: *Proceedings of the 19th International Offshore and Polar Engineering Conference*, Osaka, Japan.
- Zhang, S., Wang, L., Yang, S-zhi, Yang, H., 2010. Numerical evaluation of wind loads on semi-submersible platform by CFD. In: *Proceedings of the ASME 2010 29th International Conference on Ocean, Offshore and Arctic Engineering*. OMAE2010–20209.

Loads and Dynamic Response for Offshore Structures

7.1 General

One of the key issues in the design of offshore structures is to define the environmental conditions for the transportation route and installation site, and to determine the environmental loads acting on the structure for conditions such as transit, installation, operational extremes, and survival. The parameters to be defined in the environmental conditions may be found from design codes such as API RP 2T, among several others.

Predicting extreme values is required for evaluating the structural strength. Various methods have been proposed for determining the extreme values (Ochi, 1981, 1990). In this chapter, approaches for both long- and short-term (surviving a storm) wave data are detailed.

The aim of this chapter is to give an overall picture of the environmental conditions and loads for offshore structural designs, and to detail the recent developments in the prediction of an extreme response. A systematic method for structural analysis of offshore structures has been developed to predict the extreme response and fatigue assessment under wave loads.

Vibrations and the associated dynamic effects are also important factors in both structural design and vibration control. Basics of vibration analysis will be covered in the Appendix of this chapter.

The contents related to extreme loads in this chapter were modified from Zhao et al. (2001).

7.2 Environmental Conditions

7.2.1 Environmental Criteria

The collection and selection of the environmental criteria for the design of offshore structures are the owner's responsibility. Statistical models are essential to adequately describe environmental conditions. In general, the following environmental conditions need to be considered in the design (API RP 2T, 1997):

- Wind
- Waves

- Currents
- Tide
- Ice
- Earthquake
- Marine growth

Some of the above-noted items are detailed below.

Wind

Wind is a significant design factor. The wind conditions used in a design should be appropriately determined from collected wind data and should be consistent with other associated environmental parameters. Two methods are generally used to assess the effects of wind on the design:

- Wind forces are treated as constants and calculated based on the 1-min average velocity.
- Fluctuating wind forces are calculated based on a steady component, the 1-h average velocity plus a time-varying component calculated from an empirical wind gust spectrum.

The choice of method depends on the system's parameters and the goals of the analysis. Either approach may give a more severe load than the other, depending on the system's mooring and the wind spectrum used. The design wind speed should refer to an elevation of 10 m above the still water level. Rapid changes of wind direction and resulting dynamic loads should also be considered in the design.

Waves

Wind-driven waves are a major component of environmental forces affecting offshore structures. Such waves are random, varying in wave height/length, and may approach an offshore structure from more than one direction simultaneously. Due to the random nature, the sea state is usually described in terms of a few statistical wave parameters such as significant wave height, spectral peak period, spectral shape, and directionality.

The calculation of extreme wave loads and their load effects may be based on selected short-term sea states. The overall objective of this approach is to estimate loads and load effects corresponding to a prescribed annual exceedance probability, for example, 10^{-2} or 10^{-4} , without having to carry out a full long-term response analysis. This is the so-called design storm concept.

An appropriate formulation of the design storm concept is to use combinations of significant wave height and peak period along a contour line in the H_{m0} and T_p plane. Such a contour line can be established in different ways. The simplest way to establish the contour line at a probability level of 10^{-2} is to first estimate the 10^{-2} value of H_{m0} along with the conditional mean value of T_p . The contour line is then estimated from the joint

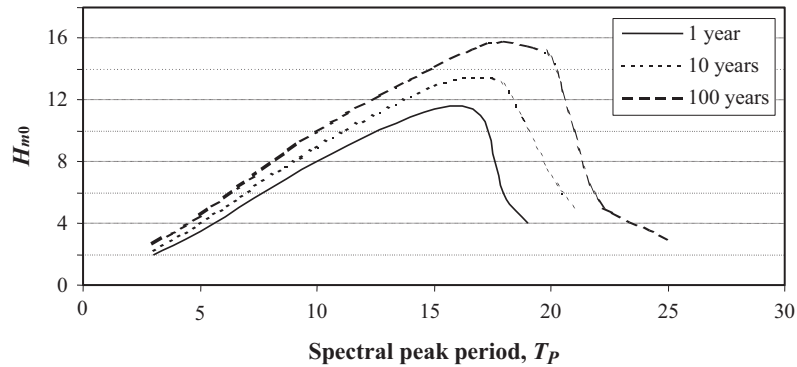


Figure 7.1
Example $H_{m0} - T_p$ contour lines.

probability model of H_{m0} and T_p with a constant probability density. An example of such a contour line is shown in [Figure 7.1](#). The estimation of the loads effect at the probability level of 10^{-2} is then obtained by determining a proper extreme value for all sea states along the contour line and then taking the maximum of these values.

Current

The most common categories of currents are

- Tidal currents, which are associated with astronomical tides
- Circulation currents, which are associated with oceanic-scale circulation patterns
- Storm generated currents
- Loop and eddy currents.

The vector sum of these currents is the total current. The variations of current speed and direction with elevations are represented by a current profile. The total current profile associated with an extreme storm sea state should be specified for the design. In certain geographic areas, the current force can be one of the governing design loads.

Consequently, selecting the appropriate current profile requires careful consideration.

Detailed descriptions of environmental conditions related to wind and current may be found from [Chakrabarti \(1987\)](#) and [CMPT \(1998\)](#).

7.2.2 Regular Waves

Regular wave theories may be applied to describe the velocity and acceleration of the water particles. Commonly used wave theories include ([Chakrabarti, 1987](#))

- Linear airy wave theory (The small amplitude wave theory is the simplest and most useful of all wave theories.)
- Stokes finite amplitude wave theory

- Cnoidal wave theory
- Stream function wave theory
- Standing wave theory.

7.2.3 Irregular Waves

A real sea does not possess the characteristics of a regular wave, but has an irregular form. The slowly varying local sea state can reasonably be assumed stationary in a “short” time interval, with an appropriate 3-h duration. A sea state is usually described by a wave spectrum with significant wave height (H_S), and a characteristic period (T), such as the peak period (T_P), or the zero-crossing period (T_Z). One wave spectrum describes only a short-term sea state. The statistical value based on a single short-term sea state is referred to as short term. When predicting extreme responses using the short-term methods, an “extreme” storm wave spectrum based on long-term wave statistics is usually used as a short-term sea state. [Bhattacharyya \(1978\)](#) gives a comprehensive discussion of the irregular waves and most probable large wave amplitude.

7.2.4 Wave Scatter Diagram

Long-term descriptions are required to describe the variation of sea states. The wave scatter diagram provides a joint probability table of significant wave heights and characteristic periods for a site. [Beck et al. \(1989\)](#) outlined methods of collecting ocean wave data:

1. Visual estimates of wave conditions (of heights and periods) by trained observers aboard weather ships: [Hogben and Lumb \(1967\)](#) collected log entries of some 500 British ships from 1953 to 1961 in oceans worldwide.
2. Point spectra from wave measurements using a shipborne meter: [Pierson and Moskowitz \(1964\)](#) evaluated the wave generation process and the fully developed spectra.
3. Directional spectra
4. US Naval hindcast wave climatology: An alternative to wave data is to calculate a set of spectra from the comprehensive wind data that have been collected for years over important trade routes worldwide; see, for example, [Bales et al. \(1982\)](#).

[Figure 7.2](#) compares contours of two wave scatter diagrams retrieved from a wave database for a site in the North Sea (W156) and a site in the Gulf of Mexico (W391). As observed, the wave environment at site W156 is much more severe than that at site W391. In order to obtain a wave scatter diagram, various short-term wave data that have accumulated over a long period of time (e.g., 10–20 years) and cover all sea states defined by different combinations of (H_S , T) are statistically averaged. The statistical value based

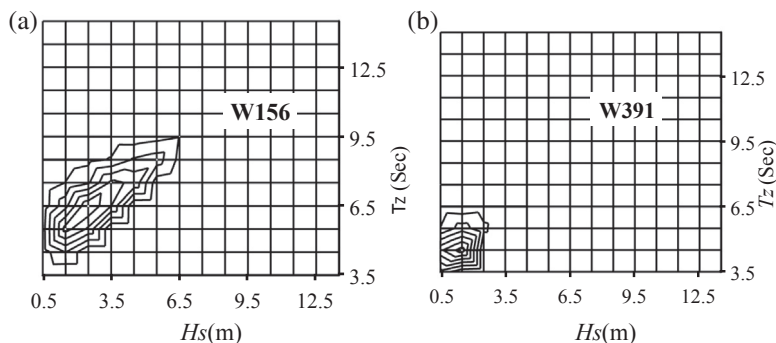


Figure 7.2

Graphic comparison of wave scatter diagrams for two locations (Zhao et al., 2001). (a) A site in the North Sea (W156). (b) A site in the Gulf of Mexico (W391).

on the long-term description of sea states is referred to as long term. The wave directional probability corresponding to each wave scatter diagram table should also be provided. Figure 7.3 shows the wave directional probability distributions at two grid zones, W156 and W391, with 24 equally divided directional divisions. The radius for each direction shown in Figure 7.3 describes the probability for that specific direction.

An example of a two-dimensional wave scatter diagram for the Northern North Sea is shown in Table 7.1.

A wave scatter diagram provides a long-term wave description for only one specific region. In order to assess the fatigue damage for a ship on past service, it is necessary to obtain additional wave information along the routes. For this purpose, a global wave

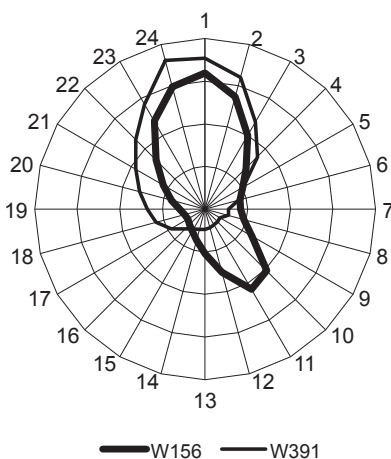


Figure 7.3

Wave directional probabilities (Zhao et al., 2001).

Table 7.1: Wave scatter diagram, representative data from the Northern North Sea (Faltinsen, 1990)

Significant Wave Height (m) (Upper Limit of Interval)	Spectral Peak Period (s)																		Sum	
	3	4	5	6	7	8	9	10	11	12	13	14	15	16	17	18	19	21		22
1	59	403	1061	1569	1634	1362	982	643	395	232	132	74	41	22	12	7	4	2	2	8636
2	9	212	1233	3223	5106	5814	5284	4102	2846	1821	1098	634	355	194	105	56	30	16	17	32 155
3	0	8	146	831	2295	3896	4707	4456	3531	2452	1543	901	497	263	135	67	33	16	15	25 792
4	0	0	6	85	481	1371	2406	2960	2796	2163	1437	849	458	231	110	50	22	10	7	15 442
5	0	0	0	4	57	315	898	1564	1879	1696	1228	748	398	191	84	35	13	5	3	9118
6	0	0	0	0	3	39	207	571	950	1069	885	575	309	142	58	21	7	2	1	4839
7	0	0	0	0	0	2	27	136	347	528	533	387	217	98	37	12	4	1	0	2329
8	0	0	0	0	0	0	2	20	88	197	261	226	138	64	23	7	2	0	0	1028
9	0	0	0	0	0	0	0	2	15	54	101	111	78	39	14	4	1	0	0	419
10	0	0	0	0	0	0	0	0	2	11	30	45	39	22	8	2	1	0	0	160
11	0	0	0	0	0	0	0	0	0	2	7	15	16	11	5	1	0	0	0	57
12	0	0	0	0	0	0	0	0	0	0	1	4	6	5	2	1	0	0	0	19
13	0	0	0	0	0	0	0	0	0	0	0	1	2	2	1	0	0	0	0	6
14	0	0	0	0	0	0	0	0	0	0	0	0	0	1	0	0	0	0	0	1
15	0	0	0	0	0	0	0	0	0	0	0	0	0	0	0	0	0	0	0	0
Sum	68	623	2446	5712	9576	12 799	14 513	14 454	12 849	10 225	7256	4570	2554	1285	594	263	117	52	45	100 001

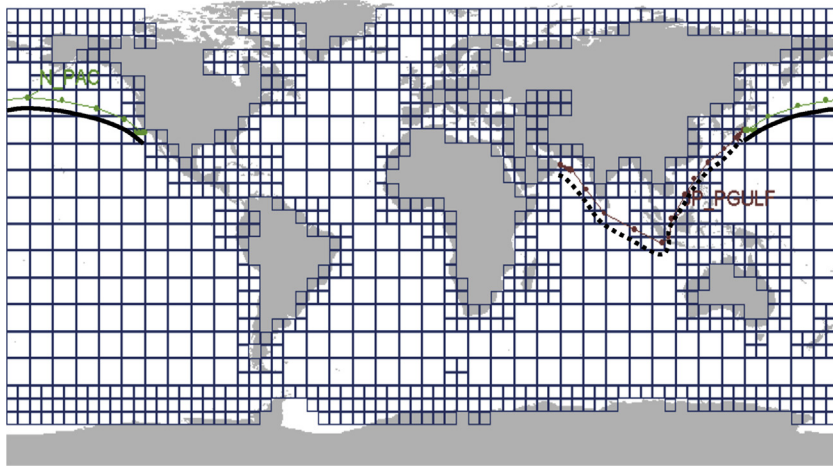


Figure 7.4

Wave grid of a wave database and two sample service routes (Zhao et al., 2001).

database can be used, from which wave data for any wave zone on the service route can be retrieved (Figure 7.4).

7.3 Environmental Loads and Floating Structure Dynamics

7.3.1 Environmental Loads

According to [API RP 2T \(1997\)](#), the environmental loads to be considered in the design of offshore structures include

- Wind forces
- Current forces
- Wave loads
- Ice loads
- Wave impact forces
- Earthquakes
- Accidental loads
- Fire and blast loading

7.3.2 Sea Loads on Slender Structures

For slender structures such as jackets, jack-ups, pipelines, risers, and mooring lines, viscous flow phenomena are of importance. Wave loads on slender structures may be predicted using the Morison equation; see [Sarpkaya and Isaacson \(1981\)](#) and [Chakrabarti \(1987\)](#). The Morison equation assumes that the force is the sum of the inertia and drag forces.

Vortex-induced vibration (VIV) occurs when the wave/current flow causes resonance with the natural frequency of the structure. When designing pipelines and risers, it is necessary to account for the wave-induced fatigue and VIV-induced fatigue (Bai, 2001).

7.3.3 Sea Loads on Large-Volume Structures

When the size of the structure is comparable to the length of a wave, the pressure on the structure may alter the wave field in the vicinity of the structure. In the calculation of wave forces, it is then necessary to account for the diffraction of the waves from the surface of the structure and the radiation of the wave (Charkrabarti, 1987).

First-Order Potential Forces: Panel methods (also called boundary element methods, integral equation methods, or sink-source methods) are the most common techniques used to analyze the linear steady state response of large-volume structures in regular waves (Faltinsen, 1990). They are based on potential theory. It is assumed that the oscillation amplitudes of the fluid and the body are small, relative to the cross-sectional dimension of the body. The methods can only predict damping due to radiation of surface waves and added mass. But they do not cover viscous effects. In linear analysis of response amplitude operator (RAO), forces and responses are proportional to wave amplitude and the response frequency is primarily at the wave frequency.

Second-Order Potential Forces: The second-order analysis determines additional forces and responses that are proportional to wave amplitude squared. The second-order forces include steady force, a wide range of low-frequency forces (which will excite surge, sway, and yaw of a moored floating system), and high-frequency forces (which will excite roll, pitch, and heave springing of a TLP). The most common way to solve nonlinear wave-structure problems is to use perturbation analysis with the wave amplitude as a small parameter. The nonlinear problem is solved in second order (Faltinsen, 1990).

In addition to boundary element methods, finite element methods or hybrid methods are available for developing commercial codes for a body of general geometries. Other special simplified methods have also been mathematically developed for specific geometries that are much more efficient. When viscous forces become important, a hybrid diffraction and Morison drag method is required in which the drag force, calculation based on the undisturbed flow but a more elaborate approach, is applied to account for the change in flow velocity due to diffraction.

In very deep seas various higher order wave loading effects also become important (CMPT, 1998):

- Higher order potential flow and drag forces coupled with highly nonsinusoidal waves lead to ringing;

- Impact of parts of the structure with water surface leads to bottom slamming and run up (on near-vertical surfaces). The duration of slamming pressure at a specific location is of the order of milliseconds and the location of the peak pressure moves with time.

Bhattacharyya (1978) gives a comprehensive and easy to follow discussion of the wave loads, deck wetness, and slamming, as well as the influence of slamming on the hull girder bending moment.

7.3.4 Floating Structure Dynamics

A dynamic response of an offshore structure includes the seakeeping motion of the vessel in waves, the vibration of the structure, and the response of the moored systems. The response of an offshore structure may be categorized by frequency—content as below:

- **Wave-frequency response:** Response with the period in the range of 5–15 s. This is the ordinary seakeeping motion of a vessel. It may be calculated using the first-order motion theory.
- **Slowly varying response:** Response with the period in the range of 100–200 s. This is the slow-drift motion of a vessel with its moorings. The slowly varying response is of equal importance as the linear first-order motions in design of mooring and riser systems. Wind can also result in slowly varying oscillations of marine structures with high natural periods. This is caused by wind gusts with significant energy at periods on the order of magnitude of a minute. Figure 7.5 shows wave frequency and slow-drift constituents for a floating system.
- **High-frequency response:** Response with the period substantially below the wave period. For ocean-going ships, high-frequency springing forces arise producing a high-frequency structural vibration that is termed whipping (Bhattacharyya, 1978). Owing to the high

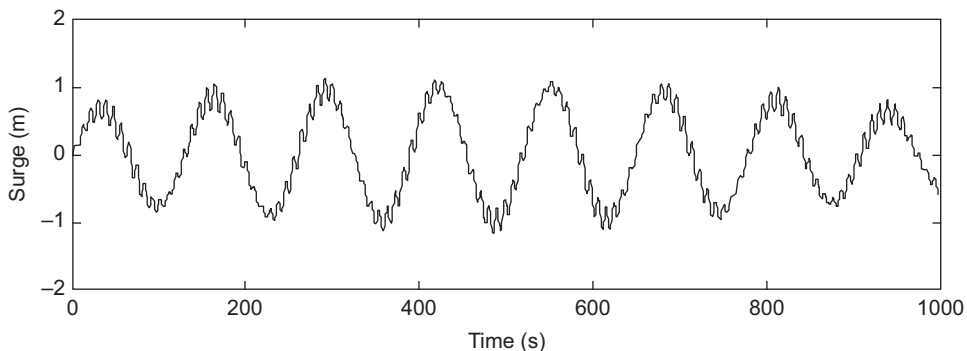


Figure 7.5

Surge time—history of a moored vessel showing wave frequency and slow-drift constituents (CMPT, 1998).

axial stiffness of the tethers, TLPs have natural periods of 2–4 s in heave, roll, and pitch. Springing is a kind of resonance response to a harmonic oscillation (CMPT, 1998).

- **Impulsive response:** Slamming occurs on the bottom of a ship/platform when impulse loads with high-pressure peaks are applied, as a result of the impact between an object and the water. Ringing of TLP tethers is a kind of transient response to an impulsive load. The high-frequency response and impulsive response cannot be considered independently of the structural response. Hydroelasticity is an important subject.

Damping forces are important when a system is under resonant loading, which is cyclically applied at one of the system's natural frequencies. They consist of hydrodynamic damping, structural damping, soil/foundation damping, etc.

The above is just a road map to floating structure dynamics as this book is devoted to structural design. Details of motion and load calculations can be found in Bhattacharyya (1978), Beck et al. (1989), Faltinsen (1990), and CMPT (1998).

7.4 Structural Response Analysis

7.4.1 Structural Analysis

For structural analysis of FPSO, Zhao et al. (2001) proposed the following general procedure:

1. Defining the major service profiles for an FPSO based on the operations that significantly affect the local deck and storage tank loads as well as the global motion responses. Typical operations include normal operations, storm survival conditions, loading conditions, and offloading conditions.
2. Determining a series of static deck and tank loading patterns Λ_l based on the major service profiles.
3. Calculating global motion of the FPSO with mooring and riser systems and the hydrodynamic forces on the FPSO for each Λ_l .
4. Loading the hull girder structure under each Λ_l , wave frequency, and wave heading. The following components should be included (Zhao, 1996; ABS, 1992):
 - Static deck and internal tank loads
 - Static structural loads
 - Hydrostatic forces
 - Hydrodynamic forces
 - Motion-induced hydrostatic restoring forces
 - Motion-induced structural inertial loads and internal tank sloshing loads
 - Mooring and riser forces
 - Shear forces, bending moments, and torsional moments like structural boundary conditions

5. Performing structural analysis to calculate stress frequency response function (FRF) $H(\omega, \alpha_k, \Lambda_l)$ for each wave frequency ω , wave heading α_k , and loading pattern Λ_l . Each combination $(\omega, \alpha_k, \Lambda_l)$ forms a different loading case in the structural analysis. The finite element method or other simplified structural analysis can be applied for the various levels of analysis (see Chapter 11). For example, to analyze the strength of the deck and bottom plating in the hull girder strength level, calculations using vertical bending moments and sectional modulus can provide satisfactory results.

Table 7.2 provides an example of tank loading patterns (ABS, 1992):

Hydrodynamic force components consist of incident wave forces, diffraction wave forces, and motion-induced radiation forces (added mass and damping forces). The potential theory of fluid mechanics based on boundary element methods using source distributions can be applied to numerically calculate the hydrodynamic forces. Currently, hydrodynamic analysis software, which uses three-dimensional models (preferred) or two-dimensional strip methods, is widely applied. A detailed discussion of numerical techniques and other load effects (such as bow flare impact, bottom slamming, green water, ice loads, and accident loads) are beyond the scope of this chapter, and may be found from, for example, Faltinsen (1990).

The wave heading α_k is defined with respect to an FPSO (see Figure 7.6). Depending on the mooring type, the wave probability at direction α_k needs to be converted into FPSO local coordinates. For example, if the turret-mooring system is adopted, the weather vaning system should be considered, and some of the wave headings can be removed.

7.4.2 Response Amplitude Operator

A wave scatter diagram provides a long-term wave description for only one specific site. Determining the stress FRF or RAO, $H(\omega; \alpha_k, \Lambda_l)$ is one of the major efforts in the strength assessment, because it allows the transfer of the exciting waves into the response of the structures. This concept of linear dynamic theory is applicable to any type of oscillatory “load” (wave, wind gust, mechanical excitation, etc.) and any type of “response” (motion, tension, bending moment, stress, strain, etc.).

Table 7.2: Tank loading patterns

No.	Tank Loading Description	
1	Homogeneous full	Design draft
2	Normal ballast load	Light draft
3	Partial load	33% Full
4	Partial load	50% Full
5	Partial load	67% Full

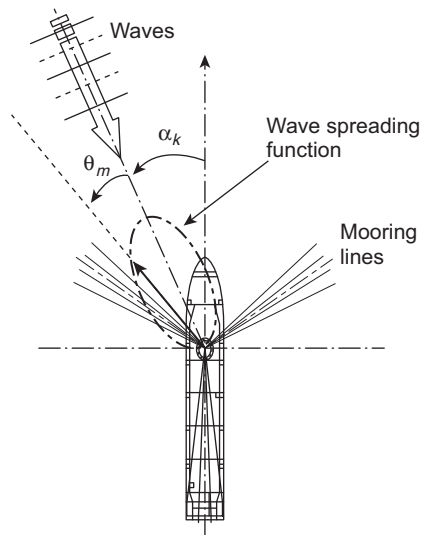


Figure 7.6

An FPSO system and coordinates for wave directionality and wave spreading.

For a linear system the response function at a wave frequency can be written as

$$\text{Response}(t) = \text{RAO} \cdot \eta(t)$$

where $\eta(t)$ denotes the wave profile as a function of time t . The RAO could be determined using theoretical computation or experimental measurements (Bhattacharyya, 1978).

Almost all of the theoretical computation have neglected viscosity and used potential flow.

The structure may be envisaged in general terms as a “black box” (see Figure 7.7). The input to the box is time history of loads and the output from the structural analysis is time history of the response. The basic assumption behind the RAO concept is linearity

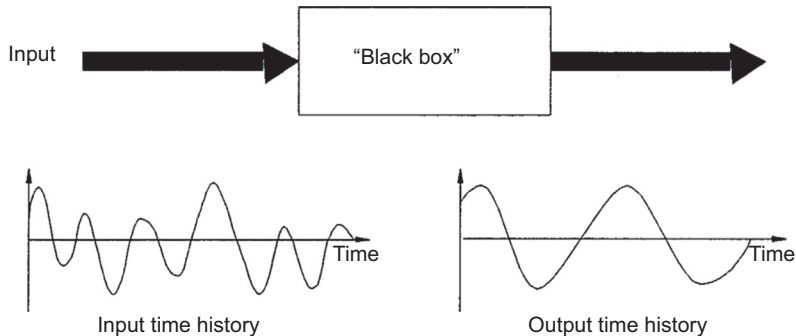


Figure 7.7

The concept of RAO for a structure (CMPT, 1998).

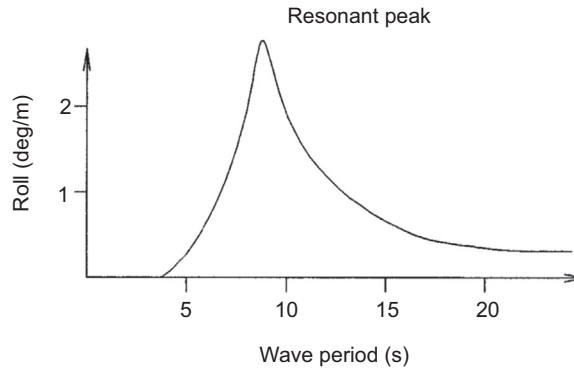


Figure 7.8

Typical RAO of barge roll motion in beam seas (CMPT, 1998).

that allows one to superimpose the output based on the superimposing of the input. In these situations, the response to regular oscillatory loadings of any waveform can be obtained by expressing the load as a Fourier series, and then estimating the corresponding Fourier series of the response for each of the components. A typical RAO is shown in Figure 7.8, that is, a roll RAO of a barge in beam seas. The RAO is given in degrees (or m/ft) of motion amplitude, per meter (or ft) of wave amplitude and expressed as a function of wave period (s). The RAO may be calculated using the first-order wave theory as the wave frequency response.

Another application of the RAO is to calculate loads in irregular waves. Bhattacharyya (1978) suggests that the total response of a vessel in an irregular seaway is the linear superposition of the response to the individual components that may be determined using RAO.

In the calculation of $H(\omega, \alpha_k, \Lambda_l)$, a suitable range for the wave frequency, the number of frequency points, and the wave headings should be used. The commonly used parameters for an FPSO analysis are

- Frequency range: $0.20 \leq \omega \leq 1.80$ rad/s
- Frequency increment: 0.05 rad/s
- Wave heading: 0° – 360° with 15° increment.

If a finite element method is used, the pressure distribution needs to be mapped from a hydrodynamic model onto a finite element model with $N_A \times N_F \times N_H$ loading cases, where:

N_A = Number of loading patterns

N_F = Number of frequency points

N_H = Number of wave headings.

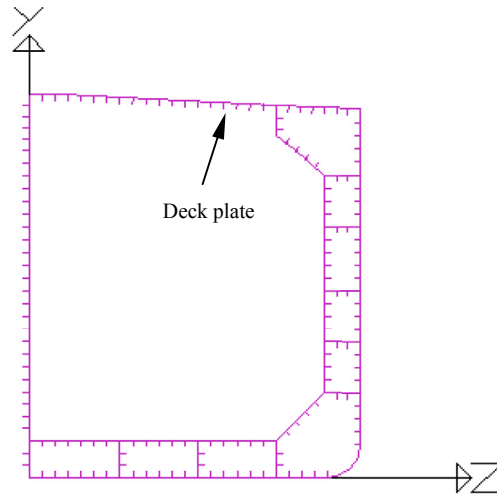


Figure 7.9

Deck plating at the mid cross section.

Figure 7.9 shows a deck plating at the midsection. The FRF stresses at 24 incident wave directions (refer to Figure 7.10) are calculated by using the 2D strip method. The 3D hydrodynamic and FE method can be used for the general structural details.

The spectral density function of the response (stresses or loads) to a wave spectrum using the wave scatter diagram and the FRF can be determined by

$$\mathbf{S}_x^{ijkl}(\omega) = \sum_m \bar{\mathbf{H}} \cdot \mathbf{H}(\omega; \alpha_k + \theta_m, \Lambda_l) \mathbf{S}_w^{ij}(\omega, \theta_m) \quad (7.1)$$

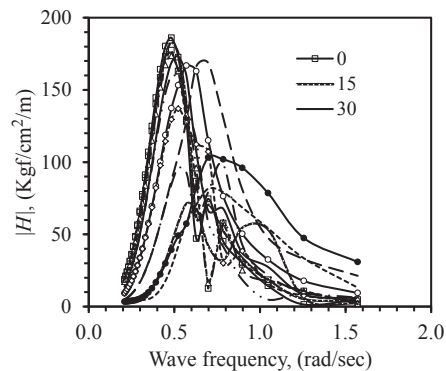


Figure 7.10

Comparison of stress frequency response functions at 13 wave directions (symmetric with respect to $\alpha = 0^\circ$ or $\alpha = 180^\circ$) (Zhao et al., 2001).

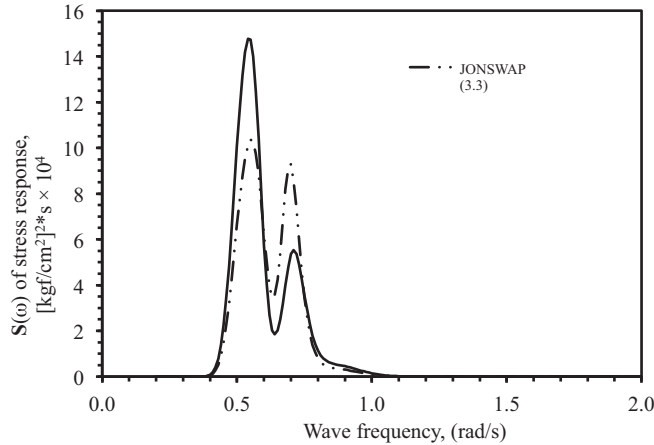


Figure 7.11

Stress spectral density functions using the JONSWAP spectrum ($\gamma = 7.3$) and using the Bretschneider spectrum (Zhao et al., 2001).

where

$\mathbf{S}_x^{ijkl}(\omega)$ = Spectral density function for response x
 $\mathbf{S}_w^{ij}(\omega, \theta_m)$ = Wave spectral density function with wave spreading
 $\Theta(\theta_m)$ = Spreading function.

$$\mathbf{S}_w^{ij}(\omega, \theta_m) = \mathbf{S}_w^{ij}(\omega)\Theta(\theta_m) \quad (7.2)$$

where

$\mathbf{S}_w^{ij}(\omega)$ = Wave spectral density function specified by (H_S, T) and $\Theta(\theta_m)$ is expressed as

$$\Theta(\theta_m) = C_n \cos^{2n}(\theta_m) \quad (|\theta_m| \leq \pi/2, n = 1, 2, \dots) \quad (7.3)$$

where

$$C_n = \frac{\Gamma(n+1)}{\sqrt{\pi}\Gamma(n+\frac{1}{2})} = \frac{2^{2n}(n!)^2}{\pi(2n)!} \text{ where } \Gamma() \text{ is the gamma function.}$$

Figure 7.11 demonstrates the stress spectral density functions at $\alpha_k = 0$. The bandwidth parameter ϵ of the response to JONSWAP and Bretschneider is shown in Table 7.7.

7.5 Extreme Values

7.5.1 General

Strength analysis generally involves assessing the yield, buckling, ultimate, and fatigue strengths (see Part II and Part III of this book). The yield, buckling, and ultimate strength

are directly related to the extreme values of stress response, which will be discussed in this section.

Figure 7.12 illustrates the extreme response and strength assessment procedure, which uses short-term and long-term approaches. Ochi and Wang (1979), showed that both long- and short-term approaches predict very close extreme values. It seems that applying one approach is good enough. This is true only for ideal situations. In fact, using either approach cannot guarantee a conservative design in practice, for the following reasons:

- It is impossible to predict the extreme storm spectrum defined with a set of (H_S, T) perfectly. Even with the same H_S , the characteristic wave period may be different depending on wave development stages or regions of a storm.
- Structural responses depend on both incident wave height and wave frequency. It is obvious that an extreme storm may not generate the largest structural response.
- The currently used wave scatter diagram may be incomplete to cover all severe storms due to the lack of data, while the long-term extreme value predicted is sensitive to those storms. Therefore, if possible, both short- and long-term approaches should be used to achieve a conservative design.

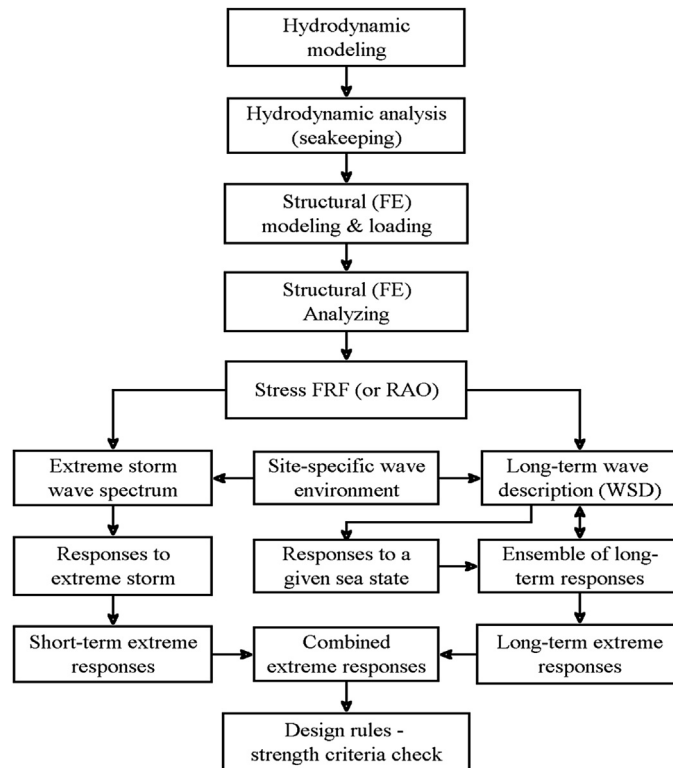


Figure 7.12

Extreme response and strength assessment procedure (Zhao et al., 2001).

7.5.2 Short-Term Extreme Approach

The short-term extreme values can be estimated based on a known initial probability distribution of the maxima. For a *Gaussian random response with zero mean*, the probability density function of the maxima (peak values) can be represented by the following Rayleigh distribution

$$p(x) = \frac{x}{m_0} \exp\left(-\frac{x^2}{2m_0}\right) \quad x \geq 0 \quad (7.4)$$

based on the assumption of a small bandwidth ε , where

$$\varepsilon = \sqrt{1 - \frac{m_2^2}{m_0 m_4}}$$

m_0 , m_2 , and m_4 are the moments of response spectral density functions of zeroth, second, and fourth order, respectively.

The cumulative probability distribution is

$$P(x) = \int_0^x p(\xi) d\xi = 1 - \exp\left(-\frac{x^2}{2m_0}\right) \quad (7.5)$$

The probable extreme value (PEV) can be determined by

$$x_{\text{PEV}} = \sqrt{2 \ln N} \sqrt{m_0} \quad (7.6)$$

Sometimes, the extreme response that is exceeded at a small possibility level α (risk parameter) can be expressed as (Bhattacharyya, 1978)

$$x_{\text{ext}}|_{\alpha} = \sqrt{2 \ln(N/\alpha)} \sqrt{m_0} \quad \text{for } \varepsilon \leq 0.9 \quad (7.7)$$

where N is the number of observations (or cycles) and x_{PEV} represents the value that may be exceeded once out of N observations. The chance for x_{PEV} to be exceeded is $1/\alpha$ times what it is for $x_{\text{ext}}|_{\alpha}$ to be exceeded. $\alpha (\leq 1)$ is chosen at the designer's discretion, depending on the condition of application.

For a response spectrum with a finite ε , the probability density function of maxima in Eqn (7.4) can be represented as (Zhao et al., 2001)

$$p(x) = \frac{2}{1 + \sqrt{1 - \varepsilon^2}} \left[\frac{\varepsilon}{\sqrt{2\pi m_0}} \exp\left(-\frac{x^2}{2\varepsilon^2 m_0}\right) + \sqrt{1 - \varepsilon^2} \frac{x}{m_0} \exp\left(-\frac{x^2}{2m_0}\right) \right. \\ \left. \times \phi\left(\frac{\sqrt{1 - \varepsilon^2}}{\varepsilon} \frac{x}{\sqrt{m_0}}\right) \right] \quad (x \geq 0) \quad (7.8)$$

in which $\phi(r) = \frac{1}{\sqrt{2\pi}} \int_{-\infty}^r \exp\left(-\frac{r^2}{2}\right) dr$.

Similar to Eqns (7.6) and (7.7), the PEV of responses is given by

$$x_{PEV} = \sqrt{2 \ln \left(\frac{2\sqrt{1-\epsilon^2}}{1+\sqrt{1-\epsilon^2}} N \right)} \sqrt{m_0} \quad \text{for } \epsilon \leq 0.9 \quad (7.9)$$

and the extreme response at the possibility level α is

$$x_{ext|\alpha} = \sqrt{2 \ln \left(\frac{2\sqrt{1-\epsilon^2}}{1+\sqrt{1-\epsilon^2}} \frac{N}{\alpha} \right)} \sqrt{m_0} \quad \text{for } \epsilon \leq 0.9 \quad (7.10)$$

Ochi (1981) has shown that the expected number of positive maxima (peak values) for a short-term random process can be expressed as

$$N = (60)^2 \frac{T_S}{4\pi} \cdot \frac{1 + \sqrt{1 - \epsilon^2}}{\sqrt{1 - \epsilon^2}} \sqrt{\frac{m_2}{m_0}} \quad (7.11)$$

where T_S is the time length of wave data, where the unit of time is in hours.

Figure 7.13 indicates the dependency of ϵ versus spectral peak periods in a wave scatter diagram and describes the range of ϵ where the stress response is mostly between

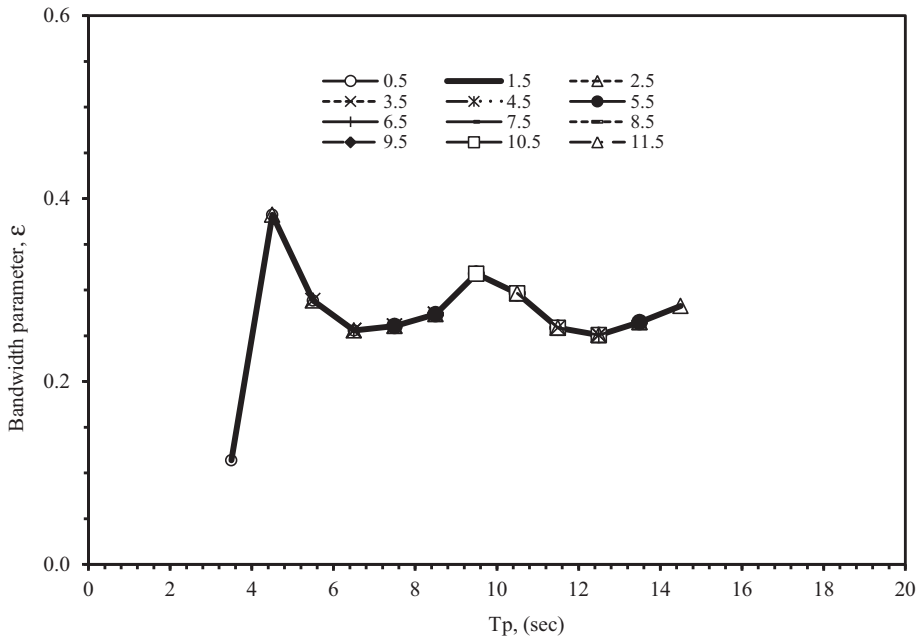


Figure 7.13

Variation of bandwidth parameters of stress responses versus T_p and H_S (wave spectrum used: JONSWAP; wave at W156) (Zhao et al., 2001).

Table 7.3: Comparison of different wave and response spectra (Zhao et al., 2001)

	Wave Spectrum				Response Spectrum	
	H_S (m)	T_P (s)	m_0 (m ²)	ϵ	m_0 [kgf/cm ²] ²	ϵ
JONSWAP ($\gamma = 7.3$)	8.5	9.5	4.4	0.59	2.17×10^5	0.32
Bretschneider	8.5	9.5	4.4	0.59	2.33×10^5	0.36

0.25 and 0.40. Based on Eqn (7.11), the relative counting error can be determined in case ϵ is ignored. For the wave conditions listed in Table 7.3, the relative counting errors are compared in Table 7.4. It is evident that ϵ can be easily close to 0.4, and an error of 5–10% could be introduced if ϵ is ignored. Therefore, it is suggested that a correction factor for ϵ be used.

Using Eqn (7.11), Eqns (7.9) and (7.10) can be rewritten as

$$x_{PEV} = \sqrt{2 \ln \left(\frac{(60)^2 T_S}{2\pi} \sqrt{\frac{m_2}{m_0}} \right)} \sqrt{m_0} \tag{7.12}$$

$$x_{ext|\alpha} = \sqrt{2 \ln \left(\frac{(60)^2 T_S}{2\pi\alpha} \sqrt{\frac{m_2}{m_0}} \right)} \sqrt{m_0} \tag{7.13}$$

Equations (7.12) and (7.13) are not directly dependent on ϵ .

When applying the short-term approach, a design wave spectrum of the extreme storm condition is usually combined with a long-term extreme value of H_S and T . Ochi's (1981) results indicate that the probability density function of (H_S, T) takes a bivariate lognormal distribution. A commonly used approach is to determine the long-term extreme value of H_S , and obtain T along with the conditional probability distribution $p(T|H_S)$, or using a simpler formula between H_S and T based on the wave steepness.

The long-term PEV of H_S with different return periods is listed in Table 7.5, where H_S is calculated by applying the long-term extreme approach discussed in the next section. T_P is required in order to determine the extreme wave environment used in the short-term approach (two-parameter wave spectra for this example). Table 7.6 lists the peak periods

Table 7.4: Comparison of relative counting errors (Zhao et al., 2001)

	Wave spectrum		Response spectrum	
	ϵ	Error	ϵ	Error
JONSWAP	0.59	11.8	0.32	2.7
Bretschneider	0.59	11.9	0.36	7.7

Table 7.5: Extreme significant wave height (Zhao et al., 2001)

Wave	H_S (m) with Return Period		
	20 years	50 years	100 years
W156	17.0	18.2	19.1
W391	10.2	11.6	12.6

Table 7.6: Wave spectral family with different H_S (Zhao et al., 2001)

	H_S (m)			Weighting Factor
	17.0	18.2	19.1	
T_P (s)	17.1	17.4	17.5	0.0500
	17.8	14.1	14.3	0.0500
	14.8	15.0	15.2	0.0875
	15.7	16.0	16.2	0.1875
	16.6	16.8	17.0	0.2500
	18.4	18.7	18.9	0.1875
	19.7	19.9	20.1	0.0875
	20.7	21.0	21.2	0.0500
	22.1	22.4	22.6	0.0500

associated with H_S . The values of T_P are calculated by using $p(T|H_S)$ for confidence levels of 0.5, 0.75, 0.85, and 0.95, separately (Ochi, 1978). All H_S and related T_P each form a wave spectral family and they are used to determine the response spectrum, and the short-term extreme values.

m_0 and m_2 need to be calculated properly when applying Eqns (7.12) and (7.13). Table 7.7 compares the short-term extreme values obtained by two different methods. Method I uses the weighting factors listed in Table 7.6 to calculate the mean values of m_0 and m_2 , while

Table 7.7: Short-term extreme values of dynamic stresses for deck plates (Zhao et al., 2001)

Method	Wave	Spectrum	Return Period (years)		
			20	50	100
I	W156	JONSWAP	2021.0	2135.4	2139.6
	W156	Bretsch.	1991.9	2121.4	2156.2
	W391	JONSWAP	1288.6	1446.9	1527.6
	W391	Bretsch.	1211.0	1372.7	1467.4
II	W156	JONSWAP	2304.1	2468.7	2565.7
	W156	Bretsch.	2081.3	2226.6	2334.0
	W391	JONSWAP	1381.3	1568.0	1714.7
	W391	Bretsch.	1248.9	1412.8	1547.2

Stress in unit: kgf/cm^2 .

method II uses each member of the spectral family in [Table 7.6](#), and takes the maximum, that is,

$$x_{\text{PEV}} = \max_j \{x_{\text{PEV}}(H_S, T_j)\} \quad (7.14)$$

The extreme values provided by the latter are up to 16% larger than those obtained using the former method. This is understandable, because the sample size (or exposure time) for the latter is relatively larger. In this example, extreme values for H_S with risk parameter $\alpha = 1$ are directly applied. Obviously, the final extreme values of responses are dependent on the designer's discretion and choice of H_S .

7.5.3 Long-Term Extreme Approach

A long-term initial cumulative probability distribution function $P(x)$ of responses is required when predicting a long-term extreme value. Although the function $P(x)$ cannot be predicted explicitly, due to the complications of the responses in various sea states, it can be built up approximately through accumulations of various short-term statistical analyses. Generally, $P(x)$ can be of the form

$$P(x) = 1 - \exp[-q(x)] \quad (q(x) \geq 0) \quad (7.15)$$

Weibull distributions or lognormal distributions are commonly used for $P(x)$. The Weibull cumulative probability distribution function can be represented as

$$P(x) = 1 - \exp\left[-\left(\frac{x - \gamma}{\beta}\right)^m\right] \quad (\beta, m > 0) \quad (7.16)$$

where parameters m , β , and γ can be determined from the observed data by the least-squares fitting method. [Ochi \(1981\)](#) also suggested using a generalized form to achieve higher accuracy in the curve fitting

$$q(x) = cx^m \exp(-\rho x^k) \quad (7.17)$$

where c , m , ρ , and k are four constant parameters to be determined by nonlinear least-squared fitting

$$Q = \ln[-\ln(1 - P(x))] = \ln c + m \ln x - \rho x^k \quad (7.18)$$

Once the mathematical expression of $P(x)$ in [Eqn \(7.15\)](#) is obtained, the long-term PEV can then be determined by

$$1 - P(x_{\text{PEV}}) = \frac{1}{N} \quad (7.19)$$

$$1 - P(x_{\text{ext}}|\alpha) = \frac{\alpha}{N} \quad (7.20)$$

Here α is the possibility level as in Eqns (7.7) and (7.10) and N is the number of observations or cycles related to the return period. In the design of offshore structures, a return period of 100 years is commonly used for estimating the long-term extreme values.

When the wave scatter diagram is applied, $P(x)$ from Eqn (7.15) can be obtained by using the definition of probability density function of the maxima.

$$\begin{aligned} p(x) &= \frac{\sum_{i,j,k,l} n_{ijkl} \Pr(w_{ij}) \Pr(\alpha_k) \Pr(\Lambda_l) p_{ijkl}(x)}{\sum_{i,j,k,l} n_{ijkl} \Pr(w_{ij}) \Pr(\alpha_k) \Pr(\Lambda_l)} = \frac{1}{\bar{N}_S} \sum_{i,j,k,l} n_{ijkl} \Pr(w_{ij}) \Pr(\alpha_k) \Pr(\Lambda_l) p_{ijkl}(x) \\ &= \frac{1}{\bar{f}_S} \sum_{i,j,k,l} f_{ijkl} \Pr(w_{ij}) \Pr(\alpha_k) \Pr(\Lambda_l) p_{ijkl}(x) \end{aligned} \quad (7.21)$$

where

$\Pr(w_{ij})$ = Normalized joint wave probability of $(H_S(i), T(j))$ or cell w_{ij} in wave scatter diagram, $\sum_{i,j} \Pr(w_{ij}) = 1$

$\Pr(\alpha_k)$ = Probability of wave in direction α_k , $\sum_k \Pr(\alpha_k) = 1$

$\Pr(\Lambda_l)$ = Probability (or percentage) of loading pattern Λ_l during service, $\sum_l \Pr(\Lambda_l) = 1$

n_{ijkl} = Average number of responses in T_S corresponding to cell w_{ij} of wave scatter diagram, wave direction α_k , and loading pattern Λ_l . n_{ijkl} can be computed by Eqn. (7.11)

f_{ijkl} = Average number of responses per unit of time of a short-term response corresponding to cell w_{ij} , wave direction α_k , and loading pattern Λ_l , unit in 1/h. $f_{ijkl} = n_{ijkl}/T_S$

$p_{ijkl}(x)$ = Probability density function of short-term response maxima corresponding to cell w_{ij} , wave direction α_k , and loading pattern Λ_l . If the wave spreading (short-crest sea) effect is considered, it should have been included in the responses as shown in Eqn (7.8).

\bar{N}_S = Long-term based, average number of observations of responses in T_S ,

$$\bar{N}_S = \sum_{i,j,k,l} n_{ijkl} \Pr(w_{ij}) \Pr(\alpha_k) \Pr(\Lambda_l) = T_S \sum_{i,j,k,l} f_{ijkl} \Pr(w_{ij}) \Pr(\alpha_k) \Pr(\Lambda_l) \quad (7.22)$$

Denoting the long-term based average number of observations of responses in T_D by \bar{N}_D ,

$$\bar{N}_D = \frac{T'_D}{T_S} \bar{N}_S = T'_D \bar{f}_S \quad (7.23)$$

T_D = Duration of service, unit of time in years

T'_D = Duration of service, unit of time in hours.

Figure 7.14 displays the long-term distribution $P(x)$ of stress responses to waves W156 and W391. It is obvious that the wave environment is the dominant factor affecting the long-term probability distribution, since the effects of spectral shape are not as significant.

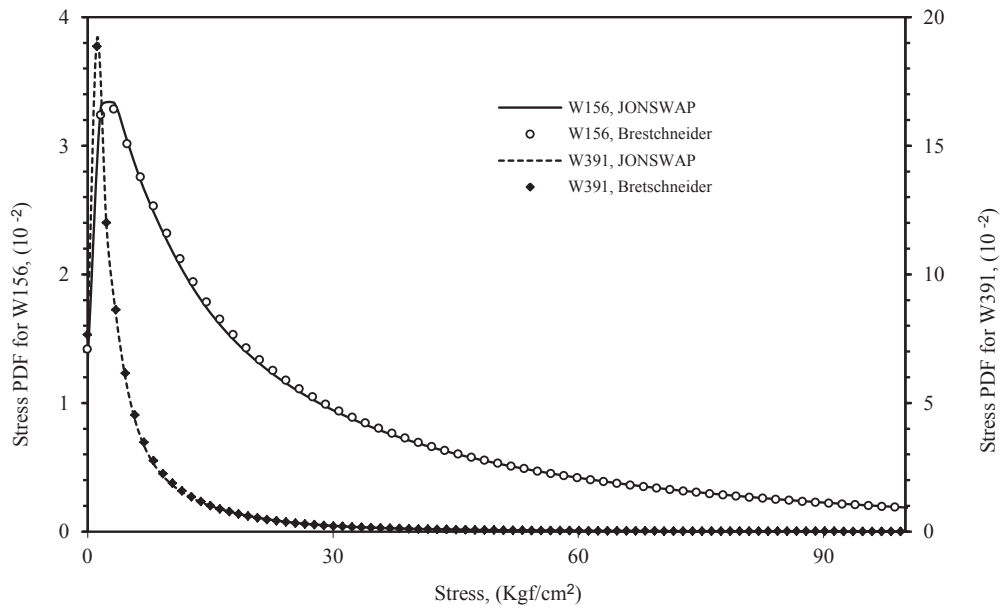


Figure 7.14

Long-term probability density function $P(x)$ of stress responses for deck plate (Zhao et al., 2001).

After the mathematical formula of $q(x)$ in Eqn (7.17) has been determined by curve fitting using Eqns (7.18) and (7.21), the extreme value can be calculated by Eqn (7.19) or Eqn (7.20). Figure 7.15 compares the long-term extreme values for waves W156 and W391, using the JONSWAP and Bretschneider spectra. The extreme values of stress dynamic components are listed in Table 7.8. The extreme values obtained by using the long-term approach are up to 9% larger than the short-term extreme values listed in Table 7.7. The long-term approach uses the probability distribution of responses, which may avoid the uncertainty caused by the choice of extreme H_S and associated wave spectral family (a series of T_p). Based on this point of view, the long-term approach is more reliable than the short-term approach under the given circumstances and with the same environmental information.

7.5.4 Prediction of Most Probable Maximum Extreme for Non-Gaussian Process

For a short-term Gaussian process, there are simple equations for estimating extremes. The most probable maximum value (MPM), of a zero-mean narrow-band Gaussian random process, may be obtained by Eqn (7.6), for a large number of observations, N . In this section, the prediction of the most probable maximum extremes (MPME) for a non-Gaussian process based on Lu et al. (2001, 2002) is discussed.

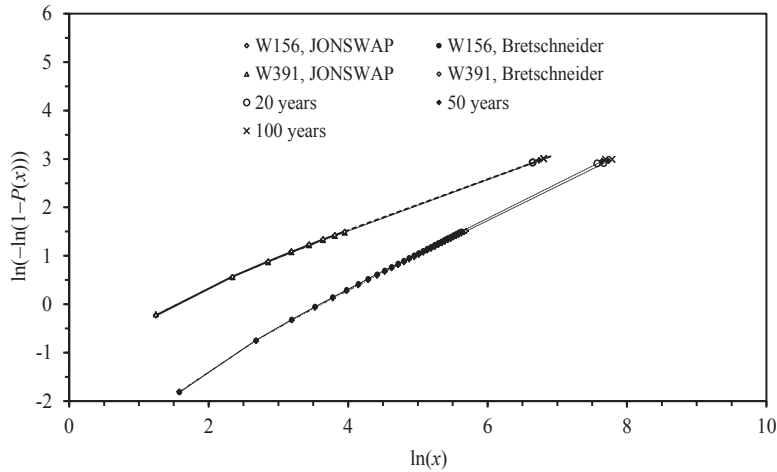


Figure 7.15

Long-term extremes of dynamic stress responses for deck plate (return period = 20, 50, and 100 years) (Zhao et al., 2001).

Wave- and current-induced loading is nonlinear due to the nonlinear drag force and free surface. Nonlinearity in response is also induced by second-order effects due to large structural motions and hydrodynamic damping caused by the relative velocity between the structure and the water particles. Moreover, the leg-to-hull connection and soil–structure interaction induce structural nonlinearity. As a result, although the random wave elevation can be considered as a Gaussian process, the response is nonlinear (e.g., with respect to wave height) and non-Gaussian.

Basically, the prediction procedure is to select a proper class of probabilistic models for the simulation in question and then to fit the probabilistic models to the sample distributions. For the design of jack-ups, the T&R Bulletin 5-5A (SNAME, 1994) recommends four methods to predict the MPME from time–domain simulations and dynamic amplification factors (DAFs) using statistical calculation.

Table 7.8: Long-term extreme values of dynamic stress for deck plates (Zhao et al., 2001)

Wave	Spectrum	Return Period (year)			Number of Cycles (1/h)
		20	50	100	
W156	JONSWAP	2476.9	2669.3	2818.2	509.2
W156	Bretsch.	2166.4	2328.0	2452.8	500.9
W391	JONSWAP	1751.6	1982.9	2169.9	694.0
W391	Bretsch.	1676.6	1899.1	2079.0	677.2

Stress in unit: kgf/cm².

Drag/Inertia Parameter Method

The drag/inertia parameter method is based on the assumption that the extreme value of a standardized process can be calculated by splitting the process into drag and inertia into two parts, evaluating the extreme values of each and the correlation coefficient between the two, and then combining as

$$(\text{mpm}_R)^2 = (\text{mpm}_{R1})^2 + (\text{mpm}_{R2})^2 + 2\rho_{R12}(\text{mpm}_{R1}) \cdot (\text{mpm}_{R2}) \quad (7.24)$$

The extreme values of the dynamic response can therefore be estimated from the extreme values of the quasi-static response and the so-called “inertia” response, which is in fact the difference between the dynamic response and the quasi-static response. The correlation coefficient of the quasi-static and inertia responses is calculated as

$$\rho_R = \frac{\sigma_{Rd}^2 - \sigma_{Rs}^2 - \sigma_{Ri}^2}{2\sigma_{Rs}\sigma_{Ri}} \quad (7.25)$$

The Bulletin recommends that the extreme value of the quasi-static response be calculated using one of the following three approaches:

Approach 1: The static extreme can be estimated by combining the extreme of quasi-static response to the drag term of Morison’s equation and the extreme of quasi-static response to the inertia term of Morison’s equation, using Eqn (7.25) as above.

Approach 2: Baar (1992) suggested that static extremes may be estimated using a non-Gaussian measure. The structural responses are nonlinear and non-Gaussian. The degree of nonlinearity and the deviation from a Gaussian process may be measured by the so-called drag–inertia parameter, K , which is a function of hydrodynamic properties and the sea state. This parameter is defined as the ratio of drag force to inertia force acting on a structural member of a unit length.

$$K = (2C_D\sigma_V^2)/(\pi C_M D\sigma_A) \quad (7.26)$$

As an engineering postulate, the probability density function of force per unit length may be used to predict other structural responses by obtaining an appropriate value of K from time–domain simulations. K can be estimated from the standard deviation of a response due to the drag force only and the inertia force only.

$$K = \sqrt{\frac{\pi}{8}} \frac{\sigma_R(C_M = 0)}{\sigma_R(C_D = 0)} \quad (7.27)$$

Approach 3: Alternatively K can be estimated from the kurtosis of structural response.

$$K = \left[\frac{(\kappa - 3) + \left\{ \frac{26(\kappa - 3)}{3} \right\}^{1/2}}{(35 - 3\kappa)} \right]^{1/2} \quad (7.28)$$

The third approach may be unreliable because the estimation is based solely on kurtosis without the consideration of lower order moments. As explained by Hagemeyer (1990), this approach ignores the effect of free-surface variations. The change in a submerged area with time will produce nonzero skewness in the probability density function of the structural response (say, base shear), which has not been accounted for in the equations for force on a submerged element of unit length. Hagemeyer (1990) also pointed out that the skewness and kurtosis estimated (as is the parameter K) from short simulations (say 1–2 h) are unreliable.

Weibull Fitting

Weibull fitting is based on the assumption that structural response can be fitted to a Weibull distribution.

$$F_R = 1 - \exp \left[- \left(\frac{R - \gamma}{\alpha} \right)^\beta \right] \quad (7.29)$$

The extreme value for a specified exceedance probability (say $1/N$) can therefore be calculated as

$$R = \gamma + \alpha [- \ln(1 - F_R)]^{1/\beta} \quad (7.30)$$

Using a uniform level of exceedance probability of $1/N$, Eqn (7.30) leads to

$$R_{MPME} = \gamma + \alpha [- \ln(1/N)]^{1/\beta} \quad (7.31)$$

The key for using this method is therefore to calculate the parameters α , β , and γ , which can be estimated by regression analysis, maximum likelihood estimations, or static moment fitting. For a 3-h storm simulation, N is approximately 1000. The time series record is first standardized $\left(R^* = \frac{R - \mu}{\sigma} \right)$, and all positive peaks are then sorted in ascending order.

Figure 7.16 shows a Weibull fitting to the static base shear for a jack-up platform.

As recommended in the SNAME Bulletin, only a small fraction (e.g., the top 20%) of the observed cycles is to be used in the curve fitting and least-square regression analysis is to be used for estimating Weibull parameters. It is true that for predicting extreme values, the upper tail data are far more important than lower tail data. What percentage of the top ranked data should be extracted for regression analysis is, however, very hard to establish.

Gumbel Fitting

Gumbel fitting is based on the assumption that for a wide class of parent distributions whose tail is of the form

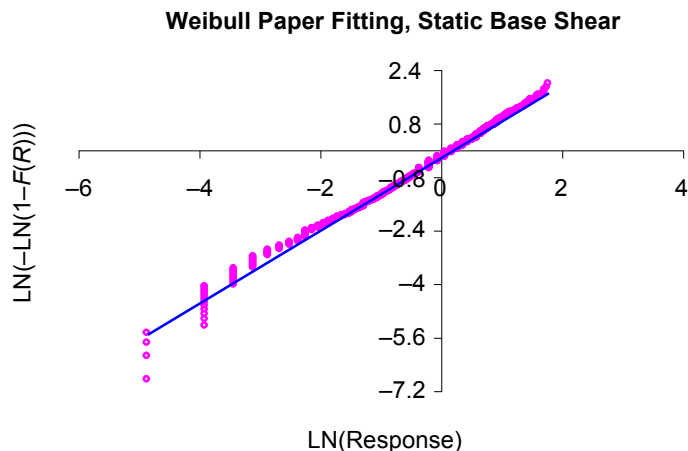


Figure 7.16

Weibull fitting of a static base shear for a jack-up.

$$F(X) = 1 - \exp(-g(x)) \quad (7.32)$$

where $g(x)$ is a monotonically increasing function of x . The distribution of extreme values is Gumbel (or type I, maximum) with the form

$$F(x_{\text{extreme}} \leq X_{\text{MPME}}) = \exp\left[-\exp\left(-\frac{1}{\kappa}(X_{\text{MPME}} - \psi)\right)\right] \quad (7.33)$$

The MPME typically corresponds to an exceedance probability of 1/1000 in a distribution function of individual peaks or to 0.63 in an extreme distribution function. The MPME of the response can therefore be calculated as

$$X_{\text{MPME}} = \psi - \kappa \cdot \ln(-\ln(F(X_{\text{MPME}}))) \quad (7.34)$$

Now the key is to estimate the parameters ψ and κ based on the response signal records obtained from time-domain simulations. The SNAME Bulletin recommends extracting the maximum simulated value for each of the 10, 3-h response signal records, and to compute the parameters by a maximum likelihood estimation. Similar calculations are also to be performed using the 10, 3-h minimum values. Although it is always possible to apply the maximum likelihood fit numerically, the method of moments (as explained below) may be preferred by designers for computing the Gumbel parameters, in light of the analytical difficulty involving the type I distribution in connection with the maximum likelihood procedure.

For the type I distribution, the mean and variance are given by

Mean: $\mu = \psi + \gamma \cdot \kappa$, where $\gamma = \text{Euler constant (0.5772...)}$

Variance: $\sigma^2 = \pi^2 \kappa^2 / 6$.

In which, the parameters ψ and κ can be directly obtained using the moment fitting method.

$$\kappa = \frac{\sqrt{6}\sigma}{\pi}, \quad \psi = \mu - 0.57722 \cdot \kappa \quad (7.35)$$

Winterstein/Jensen method

The basic premise of the analysis according to [Winterstein \(1988\)](#) or [Jensen \(1994\)](#) is that a non-Gaussian process can be expressed as a polynomial (e.g., a power series or an orthogonal polynomial) of a zero mean, narrow-banded Gaussian process (represented here by the symbol U). In particular, the orthogonal polynomial employed by Winterstein is the Hermite polynomial. In both cases, the series is truncated after the cubic terms:

Winterstein

$$R(U) = \mu_R + \sigma_R \cdot K [U + h_3(U^2 - 1) + h_4(U^3 - 3U)] \quad (7.36)$$

Jensen

$$R(U) = C_0 + C_1U + C_2U^2 + C_3U^3 \quad (7.37)$$

Within this framework, the solution is essentially separated into two phases. First, the coefficients of the expansions, that is, K , h_3 , and h_4 in Winterstein's formulation and C_0 to C_3 in Jensen's formulation, are obtained. Subsequently, on substituting the most PEV of U in [Eqn \(7.36\)](#) or [Eqn \(7.37\)](#), the MPME of the responses will be determined. The procedure of Jensen appears perfectly simple.

[Ochi \(1973\)](#) presented the expression for the most probable value of a random process that satisfies the generalized Rayleigh distribution (i.e., the wide-banded Rayleigh). The bandwidth, ε , of this random variable is determined from the zeroth, second, and fourth spectral moments. For ε less than 0.9, the short-term, most PEV of U is given by

$$U = \sqrt{2 \ln \left(\frac{2\sqrt{1-\varepsilon^2}}{1+\sqrt{1-\varepsilon^2}} N \right)} \quad (7.38)$$

For a narrow-banded process, ε approaches zero and reduces to the more well-known expression

$$U = \sqrt{2 \ln N} \quad (7.39)$$

Comparison of Eqns (7.38) and (7.39) clearly indicates that the consideration of the bandwidth effect for a Gaussian process, U , results in a reduction of the most probable value.

Lu et al. (2001, 2002) compared the above four methods recommended in the SNAME Bulletin, investigated the random seed effect on each method, and presented the impact on the dynamic response due to various parameters, for example, leg-to-hull flexibility, P-delta effect, and foundation fixity. The structural models employed in this investigation were constructed to reflect the behavior of two jack-up rigs in service. These rigs were purposely selected to represent two of the most widely used jack-up designs, which are of different leg types, different chord types, and designed for different water depths. Comparison of the four methods was presented in terms of the calculated extreme values and the respective DAFs. The Winterstein/Jensen method is considered preferable from a design viewpoint. The Gumbel fitting method is theoretically the most accurate, if enough simulations are generated. Ten simulations are minimally required, which may still not be sufficient for some cases.

7.6 Concluding Remarks

This chapter gave an overall picture of the environmental conditions and loads for offshore structural designs, and detailed the recent developments in the prediction of extreme responses. A systematic method for structural analysis of offshore structures has been developed to predict extreme responses and fatigue assessments under wave conditions. For the convenience of structural analysis, vibration frequency analysis was also briefly outlined. This chapter concludes the following:

- Design of offshore structures is highly dependent on wave conditions. Both the extreme response and the fatigue life can be affected significantly by site-specific wave environments. Collecting accurate wave data is an important part of the design.
- Wave spectral shapes have significant effects on the fatigue life. Choosing the best suitable spectrum based on the associated fetch and duration is required.
- The bandwidth parameter ϵ of responses is only dependent on the spectral (peak) period. The effect of H_S on ϵ is negligible.
- The long-term approach is preferred when predicting extreme responses, because it has less uncertainty. However, using the long-term approach is recommended along with the short-term approach for obtaining a conservative result.
- The short-term extreme approach depends on the long-term prediction of an extreme wave spectra and proper application of the derived wave spectral family. It is more complex than the long-term approach.

For a more detailed information on environmental conditions and loads for offshore structural analysis, readers may refer to [API RP 2T\(1997\)](#), [Sarpkaya and Isaacson \(1981\)](#),

Chakrabarti (1987), Ochi (1990), Faltinsen (1990), and CMPT (1998). On ship wave loads and structural analysis, reference is made to Bhattacharyya (1978), Beck et al. (1989), and Liu et al. (1992).

References

- ABS, 1992. Analysis Procedure Manual for the Dynamic Loading Approach (DLA) for Tankers. American Bureau of Shipping.
- API RP 2T, 1997. Recommended Practice for Planning, Designing, and Constructing Tension Leg Platforms. American Petroleum Institute.
- Baar, J.J.M., 1992. Extreme values of Morrison-type processes. *Applied Ocean Research* 14, 65–68.
- Bai, Y., 2001. Pipelines and Risers. In: Elsevier Ocean Engineering Book Series, vol. 7.
- Bales, S.L., Cumins, W.E., Comstock, E.N., 1982. Potential impact of twenty year hindcast wind and wave climatology in ship design. *Journal of Marine Technology* 19 (2) (April).
- Beck, R., Cummins, W.E., Dalzell, J.F., Mandel, P., Webster, W.C., 1989. Motions in waves. In: Principles of Naval Architecture, second ed. SNAME.
- Bhattacharyya, R., 1978. Dynamics of Marine Vehicles. John Wiley & Sons, Inc.
- Chakrabarti, S.K., 1987. Hydrodynamics of Offshore Structures. Computational Mechanics Publications.
- CMPT, 1998. In: Baltrop, N. (Ed.), Floating Structures: A Guide for Design and Analysis. Oilfield Publications, Inc.
- Faltinsen, O.M., 1990. Sea Loads on Ships and Offshore Structures. In: Cambridge Ocean Technology Series. Cambridge University Press.
- Hagemeyer, P.M., 1990. Estimation of drag/inertia parameters using time-domain simulations and the prediction of the extreme response. *Applied Ocean Research* 12, 134–140.
- Hogben, N., Lumb, F.E., 1967. Ocean Wave Statistics. Her Majesty's Stationery Office, London.
- Jensen, J.J., 1994. Dynamic amplification of offshore steel platform response due to non-Gaussian wave loads. *Marine Structures* 7, 91–105.
- Liu, D., Spencer, J., Itoh, T., Kawachi, S., Shigematsu, K., 1992. Dynamic load approach in Tanker design. SNAME Transactions, vol. 100.
- Lu, Y., Chen, Y.N., Tan, P.L., Bai, Y., 2001. Prediction of Jack-up Dynamic Response. OMAE. Paper No. 2171.
- Lu, Y., Chen, Y.N., Tan, P.L., Bai, Y., 2002. Prediction of most probable extreme values for Jack-up dynamic analysis. *Journal of Marine Structures* 15, 15–34.
- Ochi, M.K., 1973. On prediction of extreme values. *Journal of Ship Research* 17 (1).
- Ochi, M.K., 1978. Wave statistics for the design of ships and ocean structures. SNAME Transactions 86, 47–76.
- Ochi, M.K., Wang, S., 1979. The probabilistic approach for the design of ocean platforms. In: Proc. Conf. Reliability, Amer. Soc. Civil Eng, pp. 208–217.
- Ochi, M.K., 1981. Principles of extreme value statistics and their application. In: Extreme Loads Responses Symposium, Arlington, VA, October 19–20, 1981. SNAME.
- Ochi, M.K., 1990. Applied Probability and Stochastic Processes. John Wiley and Sons, New York.
- Pierson, W.J., Moskowitz, L., 1964. A proposed spectral form for fully developed wind seas based on the similarity of S. A. Kitaigorodskii. *Journal of Geophysical Research* 69 (24).
- Sarpkaya, T., Isaacson, M., 1981. Mechanics of Wave Forces on Offshore Structures. Van Nostrand Reinhold Co.
- SNAME Technical & Research Bulletin 5-5A, 1994. “Guideline for Site Specific Assessment of Mobile Jack-up Units”, “Recommended Practice for Site Specific Assessment of Mobile Jack-up Units”, “Commentaries to Recommended Practice for Site Specific Assessment of Mobile Jack-up Units”.

Winterstein, S.R., 1988. Non-linear vibration models for extremes and fatigue. *Journal of Engineering Mechanics* 114 (10).

Zhao, C.T., 1996. Theoretical Investigation of Springing-Ringing Problems in Tension-Leg-Platforms (dissertation). Texas A&M University.

Zhao, C.T., Bai, Y., Shin, Y., 2001. Extreme response and fatigue damages for FPSO structural analysis. In: Proc. of ISOPE'2001.

Appendix A: Elastic Vibrations of Beams

In order to conduct fatigue assessment and the control of vibrations and noises, it is typically necessary to estimate the natural frequency and vibration modes of a structure. In this section, basic dynamics for the vibration of beams and plates is described.

Vibration of a Spring/Mass System

Consider a system with a mass m , and spring constant k . When the system does not have damping and external forces, the equilibrium condition of the system may be expressed as

$$m\ddot{u} + ku = 0 \quad (7.40)$$

where u is the displacement of the mass. The free vibration may be expressed as the solution of Eqn (7.40),

$$u = u_0 \cos(\omega_1 t + \alpha) \quad (7.41)$$

where the natural frequency ω_1 may be expressed as

$$\omega_1 = \sqrt{\frac{k}{m}} \quad (7.42)$$

and where u_0 and α are determined by the initial conditions at time t_0 .

Assuming that a cyclic force, $F_0 \cos \omega t$, is applied to the mass, the equilibrium condition of the mass may be expressed as

$$m\ddot{u} + ku = F_0 \cos \omega t \quad (7.43)$$

and the above equation has a special solution as expressed in the following

$$u = \frac{F_0/k}{1 - (\omega/\omega_1)^2} \cos(\omega t - \phi) \quad (7.44)$$

where the value of ϕ may be taken as 0 (if $\omega \leq \omega_1$) or π (if $\omega > \omega_1$). The general solution is the sum of the special solution and the solution to the free vibration. When $\omega \rightarrow \omega_1$, the value of u will be far larger than that due to F_0 alone, that is, F_0/k . This phenomenon is called "resonance." In reality, the increase of vibration displacement, u , may take time,

and damping always exists. Assuming that the damping force is proportional to velocity, an equilibrium condition of the system is obtained.

$$m\ddot{u} + c\dot{u} + ku = F_0 \cos \omega t \quad (7.45)$$

The general solution to the above equation is

$$u = \frac{F_0/k}{\left(\left(1 - (\omega/\omega_1)^2 \right)^2 + 4\zeta^2 (\omega/\omega_1)^2 \right)^{1/2}} \cos(\omega t - \phi) \quad (7.46)$$

where

$$\zeta = \frac{c}{2m\omega_1} \quad (7.47)$$

$$\tan \phi = \frac{2\zeta(\omega/\omega_1)}{1 - (\omega/\omega_1)^2} \quad (7.48)$$

The displacement at resonance ($\omega = \omega_1$) is

$$u = \frac{F_0/k}{2\zeta} \cos(\omega t - \phi) \quad (7.49)$$

Elastic Vibration of Beams

The elastic vibration of a beam is an important subject for the fatigue analysis of pipelines, risers, and other structures such as global vibrations of ships. The natural frequency of the beam may be written as

$$\omega_i = a_i \sqrt{\frac{EI}{mL^4}} \quad (\text{rad/sec}) \quad (7.50)$$

Table 7.9: Coefficient for determination of natural frequency for beams

	Clamped-Free Beam	Pin-Pin Beam	Free-Free Beam	Clamped-Clamped Beam	Clamped-Pin Beam
First mode a_1	7.52	$\pi^2 = 9.87$	22	22	15.4
Second mode a_2	22	$4\pi^2 = 39.5$	61.7	61.7	50
Third mode a_3	61.7	$9\pi^2 = 88.9$	121	121	104
Fourth mode a_4	121	$16\pi^2 = 158$	200	200	178
Fifth mode a_5	200	$25\pi^2 = 247$	298.2	298.2	272

where

EI = bending stiffness of the beam cross section

L = length of the beam

m = mass per unit length of the beam including added mass

a_i = a coefficient that is a function of the vibration mode, i .

Table 7.9 gives the coefficient a_i for the determination of natural frequency for alternative boundary conditions.

Scantling of Ship's Hulls by Rules

8.1 General

In this chapter, the term “scantling” refers to the determination of geometrical dimensions (such as wall thickness and sectional modules) for a structural component/system. The initial scantling design is one of the most important and challenging tasks throughout the entire structural design process.

After signing the contract, the next step is scantling design, which continues throughout the design process until the owner, the shipyard, the classification society, and other maritime authorities approve the design. During the initial design phase, the hull form, design parameters for auxiliary systems, structural scantlings, and final compartmentation are decided on. Hull structural scantling itself is a complicated and iterative procedure.

In recent years, the procedure for dimensioning the hull structure is changing. First, the full benefit of modern information technology is applied to automate the routine scantling calculation based on the classification rules. Meanwhile, the application of rational stress analysis and the direct calculation approach, using finite element analysis, have gained increasing attention.

In order to develop a satisfactory ship structure, an initial scantling design is generally performed, to establish the dimensions of the various structural components. This will ensure that the structure can resist the hull girder loads in terms of longitudinal and transverse bending, torsion, and shear, both in still water and among the waves. This process involves combining the component parts effectively. Furthermore, each component part is to be designed to withstand the loads imposed on it from the weight of cargo, passengers, hydrodynamic pressure, impact forces, and other superimposed local loads, such as the deckhouse and heavy machinery.

Generally, this chapter introduces the design equations for tankers based on IACS (International Association of Classification Societies) requirements and classification rules (e.g., [ABS, 2002](#)).

8.2 Basic Concepts of Stability and Strength of Ships

8.2.1 Stability

Two resultant forces act on a free floating body, the force of weight acting downward and the force of buoyancy acting upward. The force of the weight (W) acts through a point known as the center of gravity (CG), and the force of buoyancy (B) acts through what is known as the center of buoyancy (CB). From Archimedes' principle it is known that the force of buoyancy equals the weight of the liquid displaced by the floating body, and thus the CB is the CG of the displaced liquid (Figure 8.1).

When a floating body is in equilibrium and is displaced slightly from its original position, three conditions may apply. As shown in Figure 8.2 (Pauling, 1988), the body may

1. return to its original position, a situation known as positive stability,
2. remain in its new position, a situation known as neutral stability, and
3. move further from its original position, a situation known as negative stability.

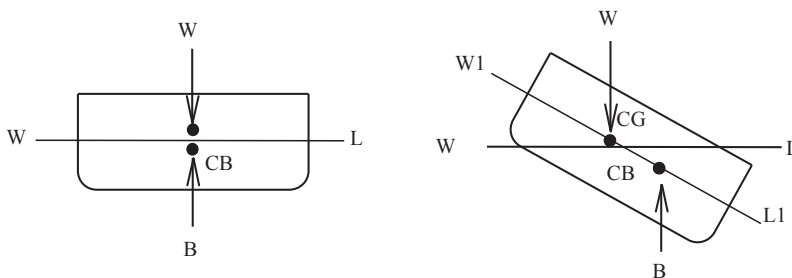


Figure 8.1
Interaction of weight and buoyancy.

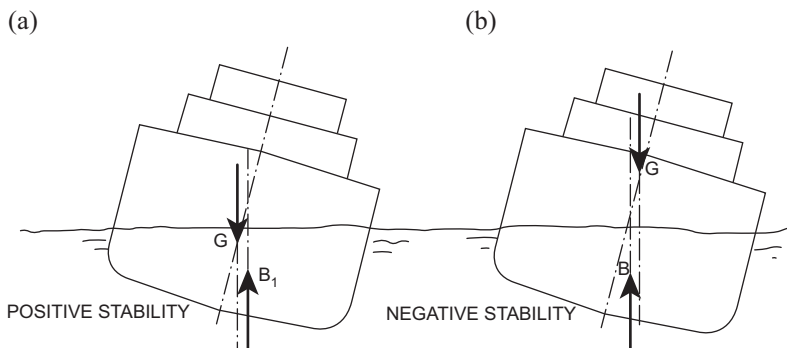


Figure 8.2
Positive and negative stability.

A ship should be positively stable, so that it can return to its original position without overturning when displaced from its original position.

The stability of a floating body such as a ship is determined by the interaction between the forces of weight, W , and buoyancy, B , as seen in [Figure 8.1](#). When in equilibrium, the two forces acting through the centers of gravity, CG , and buoyancy, CB , are aligned ([Figure 8.1\(a\)](#)). If the body rotates from WL to $W1L1$ ([Figures 8.1\(b\)](#) and [8.2\(a\)](#)), a righting moment is created by the interaction of the two forces and the body returns to its original equilibrium state, as shown in [Figure 8.1\(a\)](#). This is a case of positive stability. If the interaction between the weight and the buoyancy forces led to a moment that would have displaced the floating body further from its original position, it would have been a case of negative stability, as shown in [Figure 8.2\(b\)](#). Thus, when designing a ship, it is very important to ensure that the centers of gravity and buoyancy are placed in a position that results in positive stability for the ship.

8.2.2 Strength

Another essential aspect of ship design is the strength of the ship. This refers to the ability, of the ship structure, to withstand the loads imposed on it. One of the most important strength parameters is the longitudinal strength of the ship, which is estimated by using the maximum longitudinal stress that the hull may withstand. The shear stress is another relevant parameter.

The longitudinal strength of the ship's hull is evaluated based on the bending moments and shear forces acting on the ship. Considering a ship as a beam under a distributed load, the shear force at location X , $V(X)$, may be expressed as

$$V(X) = \int_0^X (b(x) - w(x))dx \quad (8.1)$$

where $b(x)$ and $w(x)$ denote the buoyancy force and weight at location x , respectively. The bending moment at location X , $M(X)$, is the integral of the shear curve,

$$M(X) = \int_0^X V(x)dx \quad (8.2)$$

This is further illustrated in [Figure 8.3](#) for a ship in still water (e.g., in harbors). As seen in [Figure 8.3\(a\)](#), an unloaded barge of constant cross section and density, floating in water, would have an equally distributed weight and buoyancy force over the length of the barge. This is represented by the weight and buoyancy curves, seen in [Figure 8.3\(b\)](#). If the barge were loaded in the middle ([Figure 8.3\(c\)](#)), the weight distribution would change and the resulting curve is shown in [Figure 8.3\(d\)](#). This difference between the weight and the

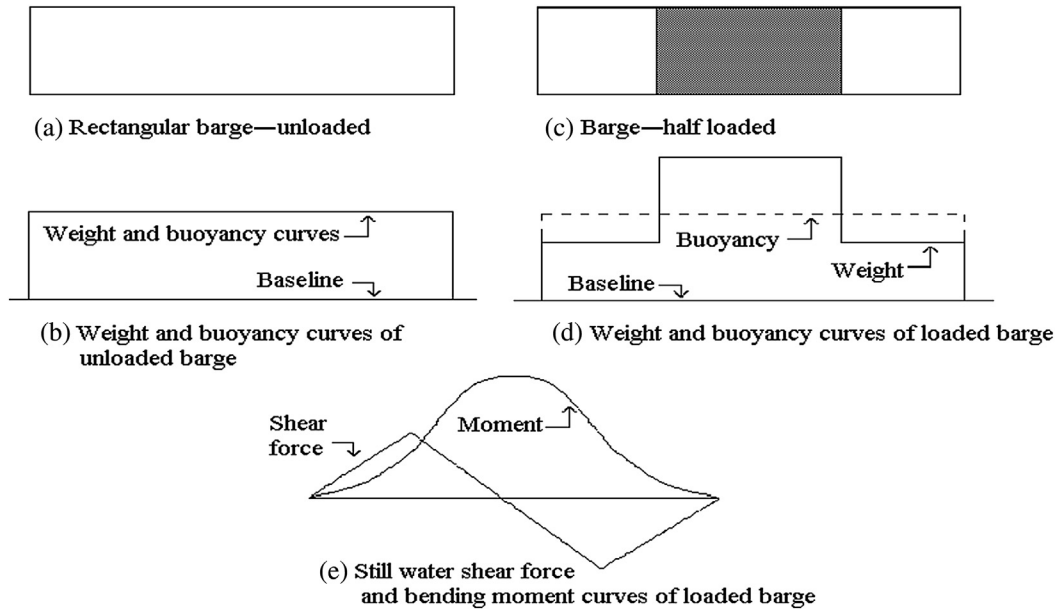


Figure 8.3

Bending moment development of a rectangular barge in still water.

buoyancy curves results in a bending moment distribution over the length of the ship. This bending moment is known as the still water bending moment, M_S , as seen for a loaded barge in [Figure 8.3\(e\)](#). For a ship in waves, the bending moment is further separated into two terms

$$M = M_S + M_W \quad (8.3)$$

where M_S and M_W denote still water and the wave bending moment, respectively. [Figure 8.4](#) illustrates a ship in a wave equal to its own length. [Figure 8.4\(a\)](#) shows the still water condition where the only bending moment acting on the ship is the still water bending moment. [Figure 8.4\(b\)](#) shows the condition when the wave hollow is amidships (i.e., in the middle of the ship). This results in a larger buoyancy distribution near the ends of the ship and thus the ship experiences a sagging condition. In a “sagging” condition, the deck of the ship is in compression while the bottom is in tension.

[Figure 8.4\(c\)](#) shows a wave crest amidships. In this case, the buoyancy force is more pronounced in the amidships section than at the ends of the ship, resulting in a hogging condition. “Hogging” means that the ship is arching up in the middle. Thus, the deck of the ship will be in tension while the bottom will be in compression.

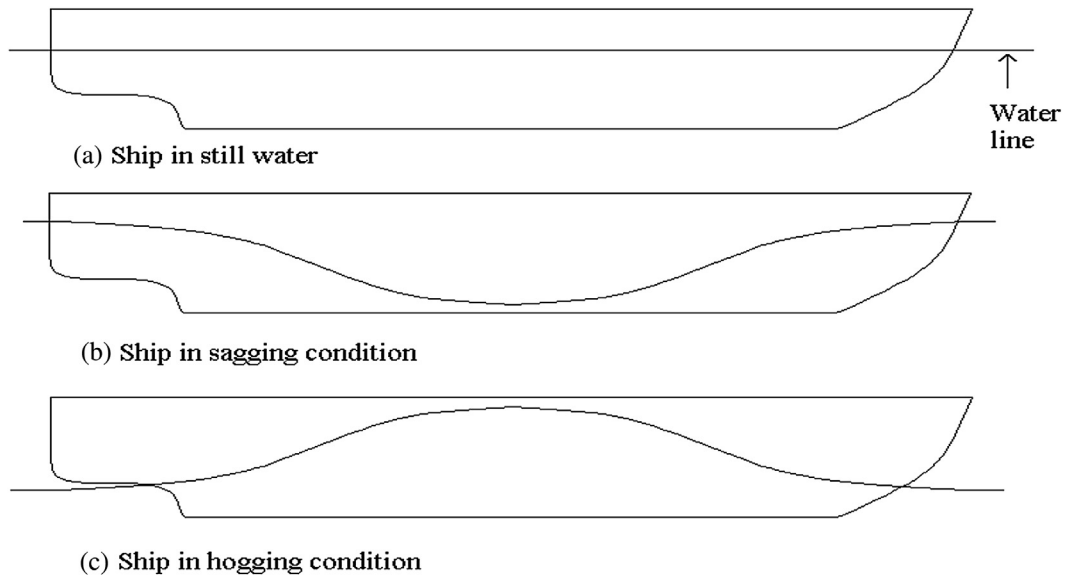


Figure 8.4

Wave bending moment in a regular wave.

In order to compute the primary stress or deflection due to vertical and horizontal bending moments, the elementary Bernoulli–Euler beam theory is used. When assessing the applicability of this beam theory to ship structures, it is useful to restate the following assumptions:

- The beam is prismatic, that is, all cross sections are uniform.
- Plane cross sections remain plane and merely rotate as the beam deflects.
- Transverse (Poisson) effects on the strain are neglected.
- The material behaves elastically.
- Shear effects can be separated from, and not influence, the bending stresses or strains.

The derivation of the equations for stress and deflection using the same assumptions as those used for elementary beam theory may be found in textbooks relative to material strength. This gives the following well-known formula

$$\sigma = \frac{M}{SM} = \frac{M_S + M_W}{SM} \quad (8.4)$$

where SM is the section modulus of the ship. The maximum stress obtained from Eqn (8.4) is compared to the maximum allowable stress that is defined in the rules provided by Classification Societies for ship design. If the maximum stress is larger than the maximum allowable stress, the ship's section modulus should be increased, and the drawing changed. The maximum bending moment is usually found in the midsection of the ship, and thus

the longitudinal strength at the midsection of the ship is usually the most critical. In general, the maximum shear stress is given by

$$\tau = \frac{F_T S}{tI} \quad (8.5)$$

where F_T is the total shear force. t and I denote the web thickness of the hull girder, and the moment of inertia of the hull. S is the first moment of effective longitudinal area above or below the horizontal neutral axis, taken about this axis.

8.2.3 Corrosion Allowance

The strength requirements in the ship design rules are based on a “net” ship approach. The nominal design corrosion allowance is to be accounted for, because the scantlings correspond to the minimum strength requirements acceptable for classification, regardless of the vessel’s design service life. Apart from coating protection for all ballast tanks, minimum corrosion allowance for plating and structural members is to be applied, as shown in [Figure 8.5](#).

For regions of structural members, where the corrosion rates might be higher, additional design margins should be considered for primary and critical structural members. This may minimize repairs and maintenance costs throughout the vessel’s life cycle.

8.3 Initial Scantling Criteria for Longitudinal Strength

8.3.1 Introduction

In order to assess the structural strength of the ship, the minimum basic scantlings, which depend on the expected loads, must be determined. The load effects acting on a ship may be categorized as primary and secondary stresses. The primary stresses, also termed hull girder stresses, refer to the global response induced by hull girder bending. In contrast, the secondary stresses are termed local stresses, and refer to the local response caused by local pressure or concentrated loads. The design rules require that the combined effect of primary and secondary stresses of structural members fall below the allowable strength limits of various failure modes.

Basic scantling is an iterative procedure, as shown in [Figure 8.6](#). The left part of the figure represents the scantling based on function requirements and engineering experience. The right part shows that these basic scantlings must be evaluated against applicable design rules. Alternatively, the structural strength may be evaluated by means of rational analysis, such as finite element methods (see Chapter 9).

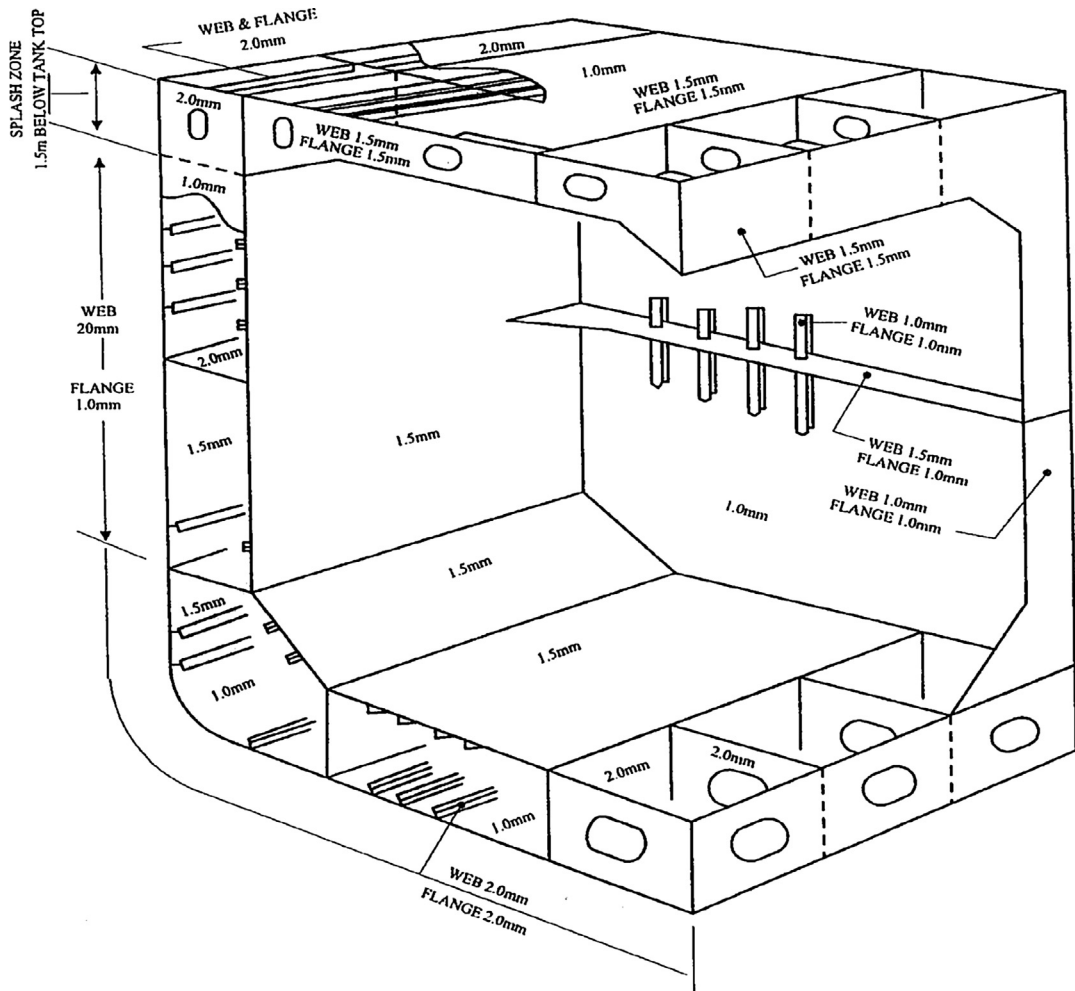


Figure 8.5
Design corrosion allowance for tankers (ABS, 2002).

8.3.2 Hull Girder Strength

The structural members involved in the primary stress calculations are, in most cases, the longitudinally continuous members, such as deck, side, bottom shell, longitudinal bulkheads, etc. and continuous or fully effective longitudinal stiffening members.

Most design rules control the hull girder strength by specifying the minimum required section properties of the hull girder cross sections. The required section properties are calculated based on hull girder loads, and maximum allowable hull girder stresses for the midship parallel body (region in which the cross sections are uniform).

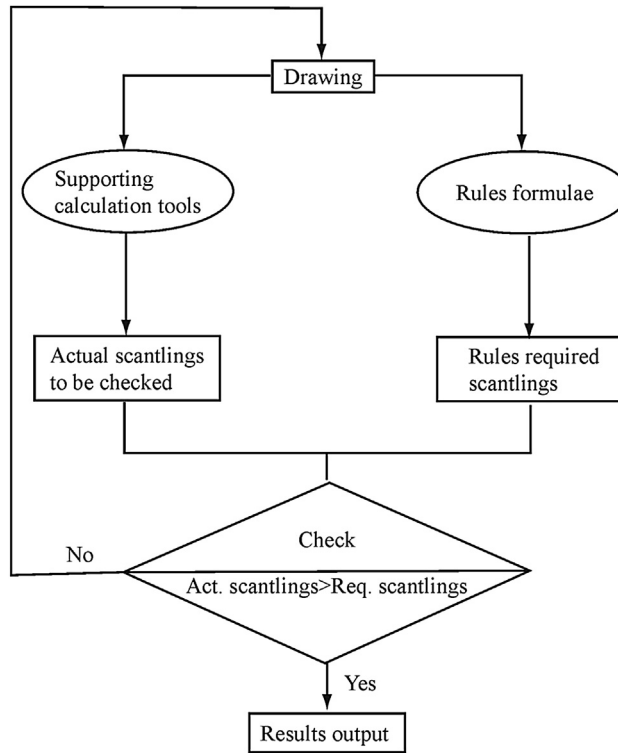


Figure 8.6

Data flow in the procedure of structural scantling.

Longitudinal stress

In order to determine the hull girder section modulus for 0.4L amidships, classification rules require that the greater value of the following equation be chosen,

$$SM = \frac{M_S + M_W}{\sigma_p} \quad (8.6)$$

$$SM = 0.01C_1L^2B(C_b + 0.7) \quad (8.7)$$

σ_p is the nominal permissible bending stress and it may be taken as 17.5 kN/cm². The second equation calculates the minimum required section modulus. The constant, C_1 , depends on the length, and the block coefficient, C_b . If the top and/or bottom flange consist of higher strength materials, the section modulus calculated above may be reduced by a factor Q , according to the following:

$$SM_{hts} = Q \cdot SM \quad (8.8)$$

Q depends on the yield strength and is 0.78 for grade H32 material or 0.72 for grade H36 material.

In the classification rules, equations and charts are available for calculating the still water bending moment, the wave bending moment amidships, and the wave shear force, as well as distribution factor for the wave bending moment.

Shear stress

The distribution of the shear force on the sides and on the bulkheads is very complicated, and hence the required thickness is not easily expressed with a simple formula. Each classification society has its own empirically based formulas for shear force and its distribution along the longitudinal direction. The general equation for the net thickness is

$$t = \frac{(F_S + F_W) \cdot S}{I \cdot \sigma_s} \quad (8.9)$$

where F_S is the still water shear force and F_W is the vertical wave shear force, which is zero for in-port conditions. The net thickness of the side shell plating is given by

$$t_s \geq \frac{F_t \cdot D_s \cdot S}{I \cdot \sigma_s} \quad (8.10)$$

and the thickness of the longitudinal bulkhead is given by

$$t_i \geq \frac{(F_t + R_i) \cdot D_i \cdot S}{I \cdot \sigma_s} \quad (8.11)$$

In these equations, I is the moment of inertia of the net hull girder section at the position considered. S is the first moment of the net hull girder section above the neutral axis of the area between the vertical level at which the shear stress is being determined and the vertical extremity of the section, which is being considered. As noted above, σ_s is the permissible shear stress, which is defined for either sea or in-port conditions. It is equal to 18.96 divided by Q for sea conditions and 10.87 divided by Q for in-port conditions. Q is the material conversion factor and depends consequently on the material. D is the shear distribution factor, which depends on the designs of the longitudinal bulkheads.

8.4 Initial Scantling Criteria for Transverse Strength

8.4.1 Introduction

The ship hull is subjected to static and dynamic hydrostatic pressure on its bottom, two sides, and under loads due to the weight of the cargo inside the hull, seen in [Figure 8.7](#). The transverse loads may cause cross-sectional deformation as depicted by the dotted lines, and may cause stresses in transverse bulkheads, floors, side frames, and deck beams. In general, hulls of the cargo ships are based on transverse systems where the transverse

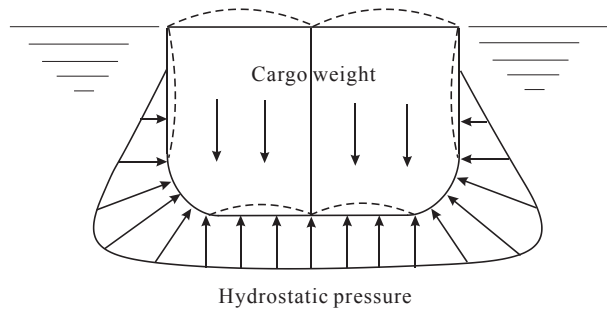


Figure 8.7
Transverse loads on ship hulls.

strength may be modeled as two-dimensional (2D) frames. The 2D frame is subjected to the hydrostatic pressure and cargo weight loads, as shown in [Figure 8.7](#), as well as the shear forces transferred from the longitudinal members.

8.4.2 Transverse Strength

Two-dimensional frame analysis may be applied to calculate the transverse strength. The frame analysis may be conducted using analytical equations that are available from typical books on structural analysis, or by the finite element methods.

In some cases, the frame analysis may be based on 2D plane stress analysis. The allowable stress for transverse strength is defined in classification rules with the methods for stress analysis. Typical arrangements for transverse frame may be found in the classification rules.

8.5 Initial Scantling Criteria for Local Strength

8.5.1 Local Bending of Beams

The local strength of primary and secondary structural members is evaluated by means of stresses due to local loads, such as lateral pressure or concentrated loads, etc. Again, the elementary Bernoulli–Euler beam theory is utilized when computing the stresses or deflections for stiffeners and girders, while the plate theory is used for plates. The derivation of the equations for stress and deflection, using the same assumptions as for elementary beam theory or plate theory, may be found in textbooks on material strength, such as [Timoshenko and Goodier \(1956\)](#).

Scantlings, of individual structured members, as shown in [Figure 8.8](#), with respect to local bending moments and shear strength, are presented in this section.

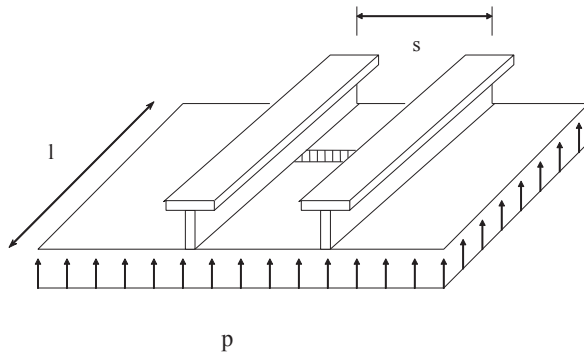


Figure 8.8
Individual structural members.

Stiffeners

The minimum required stiffener size is specified by the section modulus of the stiffener as a function of stiffener spacing, stiffener span, design pressure, and allowable stress (Figure 8.9).

From the beam theory, the required section modulus of a stiffener is

$$SM = \frac{M}{\sigma} \quad (8.12)$$

Considering a stiffener with fixed ends, the maximum bending moment is

$$M = \frac{ql^2}{12} \quad (8.13)$$

A stiffener is supposed to carry lateral pressure, which acts on the plate attached to the stiffener, with a loading breadth equal to the stiffener spacing. Therefore, the distributed load on the stiffener, q (in N/mm), can be calculated from the equation

$$q = p \cdot s \quad (8.14)$$

where s is the stiffener spacing and p is the design pressure in N/mm^2 .

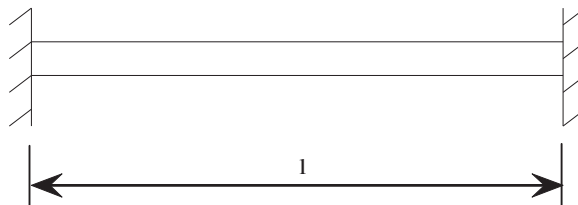


Figure 8.9
Stiffener.

By inserting Eqns (8.13) and (8.14) into Eqn (8.12), the following is obtained.

$$SM = \frac{p \cdot s \cdot l^2}{12 \sigma} \quad (8.15)$$

The classification rules contain this kind of equation for the design of beams under lateral pressure.

Girders

Girders are to comply with the same scantling criteria as stiffeners with respect to the section modulus. In addition, shear force should be considered, due to the height of the girder (Figure 8.10). The following equation represents the scantling criterion in terms of the cross-sectional area of the girders.

$$\tau = \frac{Q}{A} \quad (8.16)$$

where τ is the shear stress at the girder end in N/m^2 and A is the cross-sectional area at the girder end in m^2 . If the load is equally distributed, with each end of the girder carrying half the load, Q will be defined as

$$Q = 0.5 \cdot p \cdot b \cdot S \quad (8.17)$$

where p and b denote the design pressure acting on the girder (N/m^2), and the loading breadth (m). The girder span is denoted as S (m). Substituting Eqn (8.17) into Eqn (8.16), the following equation is obtained.

$$\tau = \frac{Q}{A} = \frac{0.5 \cdot p \cdot b \cdot S}{A} \quad (8.18)$$

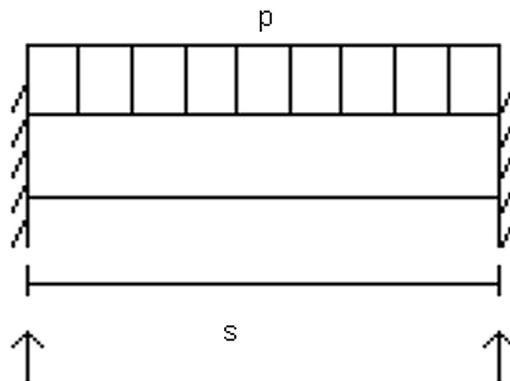


Figure 8.10
Girder.

From Eqn (8.18), the required sectional area is derived as the following

$$A \geq \frac{0.5 \cdot p \cdot b \cdot S}{\tau_{all}} \quad (8.19)$$

The allowable shear stress τ_{all} depends on the girder. In addition, girders are used to satisfy the requirements of the web plate thickness, the girder web area, and the ratio of the girder flange thickness to flange width.

8.5.2 Local Bending Strength of Plates

In the design rules, the minimum required plate thickness is defined as a function of stiffener spacing, design pressure, and allowable stress. This criterion may be derived from plate theory. A plate panel between two stiffeners and two girders can be simplified and considered as a rectangular plate under uniform lateral pressure p , with all edges fixed.

Based on the plate theory, the maximum stresses are given as

$$\text{Max } \{\sigma\} = \frac{-\beta_1 p \cdot s^2}{t^2} \text{ (at the center of the long edge)} \quad (8.20)$$

$$\sigma = \frac{\beta_2 p \cdot s^2}{t^2} \text{ (at the center)} \quad (8.21)$$

If the aspect ratio of the plate (l/s) is greater than 2, $\beta_1 = 0.5$ and $\beta_2 = 0.25$ are to be used as correction factors for the aspect ratio. For plates with an aspect ratio greater than 2, which are designed against the maximum stress at the center, the required minimum thickness is

$$t = \frac{0.5s\sqrt{p}}{\sqrt{\sigma}} = \frac{s\sqrt{p}}{\sqrt{4\sigma}} \quad (8.22)$$

where σ is the allowable local bending stress, p is the design pressure, and s is the spacing. In the actual design, a corrosion allowance should be added to the calculated thickness.

Allowable bending stresses should be determined by taking into account the plate location, the stiffening system, and the material strength. Each classification society has its own definition of allowable stresses.

In the classification rules, formulas are available for the design of plating under lateral pressure, and for the determination of plate thickness. Between classification rules, there is a certain difference in the way corrosion allowance is handled.

8.5.3 Structure Design of Bulkheads, Decks, and Bottom

For each individual longitudinal or vertical/horizontal stiffener on longitudinal and transverse bulkheads, along with the effective plating to which it is attached, the net section modulus must be larger than that obtained from

$$SM = \frac{M}{\sigma_b} \quad (\text{cm}^3) \quad (8.23)$$

where

$$M = \frac{1000}{12} c_1 c_2 p s l^2 \quad (\text{N cm}) \quad (8.24)$$

c_1 is different for longitudinal, horizontal, and vertical stiffeners, c_2 depends on the design and loading of the tank, l is the span of longitudinals or stiffeners between effective supports, p is defined above, and σ_b is the permissible bending stress, which depends on the type and position of the stiffener.

8.5.4 Buckling of Platings

General

Buckling is one of the main concerns in structural designs (Figure 8.12). Structural elements, which are exposed to high compressive stresses, may experience instability before reaching the yield stress.

Platings should be evaluated, so as to avoid local buckling of plates between stiffeners. This section discusses the scantling of longitudinal members with respect to buckling control by considering the total compressive stresses.

Elastic compressive buckling stress

The elastic buckling stress is the highest value of the compressive stress in the plane of the initially flat plate, in which a nonzero out-of-plane deflection of the middle portion of the plate can exist. The Bryan formula gives the theoretical solution for the compressive buckling stress in the elastic range. For a rectangular plate subject to a compressive in-plane stress in one direction, it may be expressed as

$$\sigma_{el} = k_c \frac{\pi^2 E}{12(1 - \nu^2)} \left(\frac{t}{s} \right)^2 \quad (8.25)$$

The plate nomenclature may be obtained from Figure 8.11, and t , the net thickness, is reduced by corrosion addition. The buckling coefficient k_c is a function of the plate aspect ratio $\alpha = l/s$, boundary conditions, and loading conditions. If the plate is assumed to have

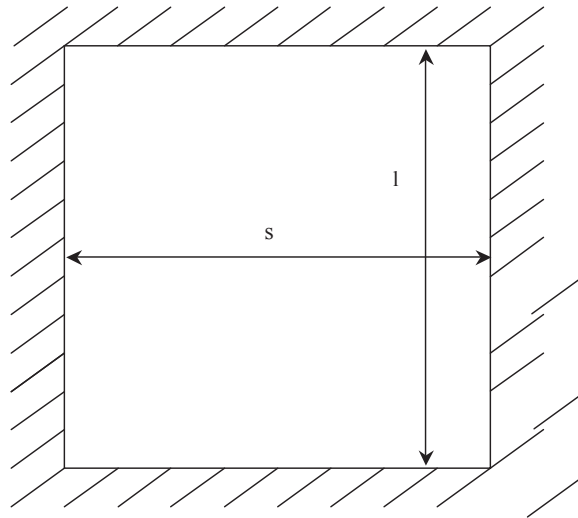


Figure 8.11
Plate.

the load applied uniformly to a pair of opposite edges only and if all four edges are simply supported, then k_c is

$$k_c = \left(\frac{n}{l} + \frac{l}{n} \right)^2 \quad (8.26)$$

Here, n is the number of half-waves of the deflected plate in the longitudinal direction (Figure 8.12).

For a transversely stiffened plate with an aspect ratio of $\alpha < 1$, as shown in Figure 8.13, the critical stress will correspond to $n = 1$, which leads to a more convenient expression for the elastic compressive buckling stress,

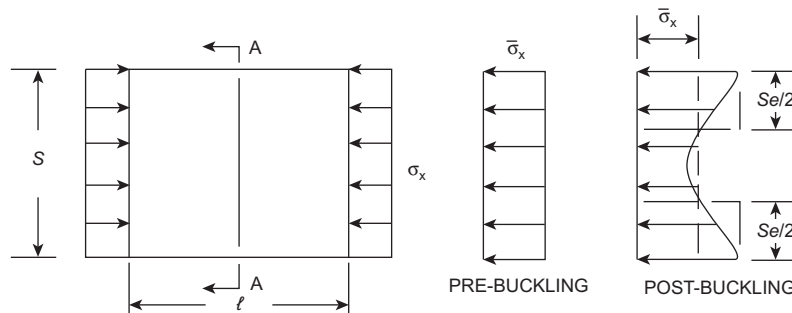


Figure 8.12
Plate buckling.

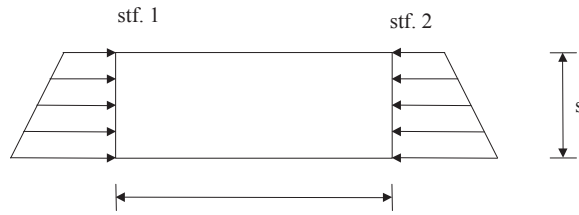


Figure 8.13
Transverse stiffened plate.

$$\sigma_{el} = \frac{\pi^2 E}{12(1-\nu^2)} \left(\frac{t}{s}\right)^2 (1 + \alpha^2)^2 \quad (8.27)$$

Figure 8.14 shows a longitudinal stiffened plate, for which k_c is approximately 4, and the elastic critical stress is given by

$$\sigma_{el} = \frac{\pi^2 E}{3(1-\nu^2)} \left(\frac{t}{s}\right)^2 \quad (8.28)$$

The critical compressive buckling stress, σ_c , is given by

$$\sigma_c = \sigma_{el} \quad \text{for } \sigma_{el} < \frac{\sigma_y}{2} \quad (8.29)$$

$$\sigma_c = \sigma_y \left(1 - \frac{\sigma_y}{4\sigma_{el}}\right) \quad \text{for } \sigma_{el} > \frac{\sigma_y}{2} \quad (8.30)$$

The elastic shear buckling stress, τ_e , is calculated similarly. The critical buckling shear stress is given by

$$\tau_c = \tau_{el} \quad \text{for } \tau_{el} < \frac{\tau_y}{2} \quad (8.31)$$

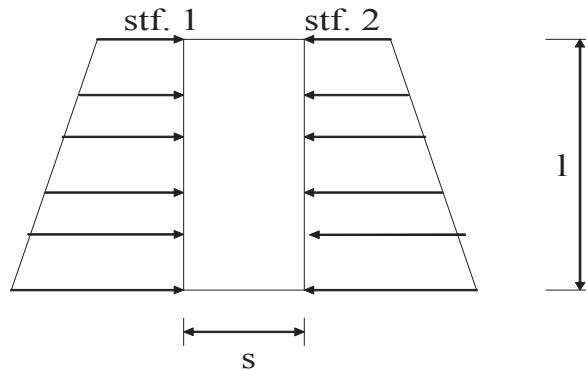


Figure 8.14
Longitudinal stiffened plate.

$$\tau_c = \left(1 - \frac{\tau_y}{4\tau_{el}}\right) \quad \text{for } \tau_{el} > \frac{\tau_y}{2} \quad (8.32)$$

where τ_{el} is the ideal elastic shear buckling stress and τ_y is the yield stress in shear of a material in N/mm^2 , which is given by $\tau_y = \sigma_y/\sqrt{3}$.

Buckling evaluation

Design codes, with respect to buckling strength, are developed based on the above-noted formulas. The following interaction formula may be used to calculate the buckling of plates under combined compression and shear stress (Bannerman and Jan, 1980)

$$\left(\frac{\sigma}{\sigma_c}\right)^2 + \left(\frac{\tau}{\tau_c}\right)^2 \leq 1.0/S.F. \quad (8.33)$$

where σ and τ denote the predicted maximum compressive stress (due to axial compression and bending), and the predicted average shear stress, respectively. σ_c and τ_c are the critical buckling stress that corresponds to axial compression/bending and to pure shear loading, respectively. *S.F.* is the safety factor.

8.5.5 Buckling of Profiles

Axially compressed profiles (longitudinal) should be evaluated to withstand the following buckling modes:

- Lateral buckling mode
- Torsional buckling mode
- Web and flange buckling mode

Transverse stiffeners and girders require special considerations.

The elastic buckling stress will be discussed below.

- Lateral buckling mode

The elastic buckling stress of lateral buckling may be derived from the column buckling theory and is given by

$$\sigma_{el} = n \cdot E \frac{I_A}{Al^2} \quad (\text{N/mm}^2) \quad (8.34)$$

where I_A is the moment of inertia of the longitudinal, including attached plate flange, in cm^4 , A is the cross-sectional area of the longitudinal, including the attached plate flange, in cm^2 , l is the span of the longitudinal, and n is a buckling coefficient, which depends on the end supports (for an ideal case, $n = 0.001$).

It should be noted that the section properties of the longitudinals used in the buckling evaluation should make up the deducted net properties, with a corrosion allowance.

- Torsional buckling mode

$$\sigma_{el} = \frac{\pi^2 EI_W}{10^4 I_p l^2} \left(m^2 + \frac{K}{m^2} \right) + 0.385E \frac{I_T}{I_P} \quad (\text{N/mm}^2) \quad (8.35)$$

where

$$K = \frac{Cl^4}{\pi^4 EI_W} 10^6 \quad (8.36)$$

where I_W is the warping constant of the longitudinal about the connection of the stiffener to the plate, in cm^6 , I_p is the polar moment of inertia of the longitudinal about the connection of the stiffener to the plate, in cm^4 , l is the span of the longitudinal, in m, I_T is the St. Venant's moment of inertia of the longitudinal (without the attached plate), in cm^4 , m is the number of half-waves (usually varying from 1 to 4), and C is the spring stiffness exerted by the supporting plate panel.

- Web and flange buckling

For the web plate of longitudinal, the elastic buckling stress is given by

$$\sigma_{el} = 3.8E \left(\frac{t_W}{h_W} \right)^2 \quad (\text{N/mm}^2) \quad (8.37)$$

where t_W is the web thickness, in mm, and h_W is the web height, in mm.

For flanges on angels and T-beams, the following requirement should be satisfied

$$\frac{b_f}{t_f} \leq 15 \quad (8.38)$$

where b_f is the flange breadth and t_f is the flange thickness.

Eqns (8.29)–(8.33) may also be applied to calculate the critical buckling stress for profiles and therefore, to conduct buckling evaluations. Refer to Part II of this book for further details of buckling evaluation and safety factors.

References

- ABS, 2002. Rules for Building and Classing Steel Vessels. American Bureau of Shipping.
- Bannerman, D.B., Jan, H.Y., 1980. Analysis and design of principal hull structure. In: Ship Design and Construction. SNAME.
- Paulling, J.R., 1988. Strength of ships. In: Principles of Naval Architecture, vol. I. SNAME.
- Timoshenko, S., Goodier, J.N., 1956. Strength of Materials, vol. I (vol. II).

Ship Hull Scantling Design by Analysis

9.1 General

Classification rules have traditionally been the mainstay of ship design practices. These rules are primarily semiempirical in nature and have been calibrated to ensure successful operational experience. They have obvious advantages—they are simple in format and familiar to most ship designers. Nevertheless, ship sizes have increased dramatically, and ship designs have changed remarkably in the past 20 years. The conventional design approach that relied on the “rule book” has been seriously challenged by the development of unconventional ship types and complex ship structures such as high-speed vessels, large-opening container ships with considerably increased capacity, large LNG carriers, drilling ships, and FPSOs. Conventional design rule formulae involve a number of simplifying assumptions and can only be used within certain limits. Moreover, scantlings based on rules are not necessarily the most cost-efficient designs. Hence, the application of rational stress analysis using the finite element method (FEM) has gained increasing attention in the shipbuilding industry. With the rapid growth of information technology, computational complexity is no longer a big issue, and numerical efficiency is not the main concern in the design process. The actual design approach includes overall strength analysis by accounting for both static and dynamic loads and the evaluation of the fatigue life for all critical structural details. This approach provides a well-designed and uniformly utilized structure that ensures a higher degree of reliability than past structures.

A rational analysis procedure is presented in this chapter starting from design loads, strength criteria, and FEM analysis, up to the assessment of obtained calculation results. FEM analysis is discussed in detail, including modeling, load application, application of boundary conditions, element selection, and postprocessing. The summarized procedure of strength analysis can be seen in [Figure 9.1](#).

9.2 Design Loads

Design loads acting on the overall ship structure consist of static and dynamic loads. Static loads include dead and live loads such as hydrostatic and wind loads. Dynamic loads include wave-induced hydrodynamic loads, inertia loads due to vessel motion, and impact loads. The various loading conditions and patterns likely to impose the most onerous local and global regimes are to be investigated to capture the maximum local and global loads in the structural

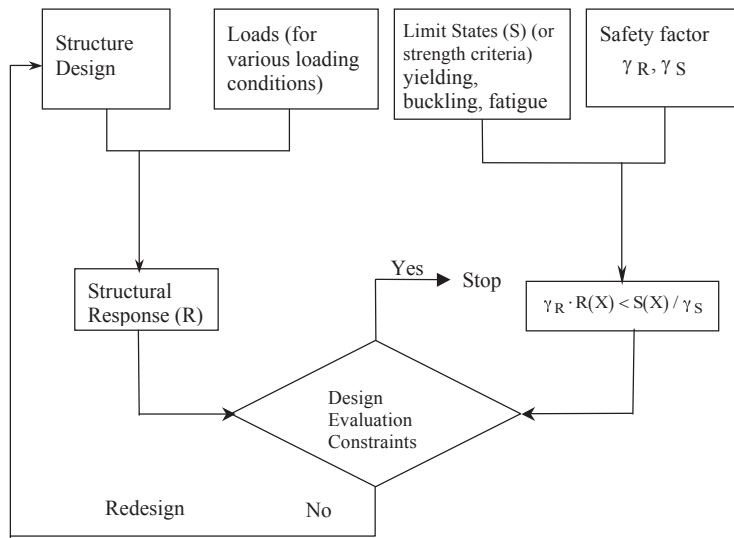


Figure 9.1
Stress analysis procedure.

analysis. Sloshing and slamming loads should also be taken into account where applicable. When designing oceangoing ships, environmental loads are usually based on the global sea state criteria because of their mobility, whereas for offshore structures, environmental loads are calculated in accordance with specifically designed routes and/or site data.

Liu et al. (1992) developed a dynamic load approach for ship designs, where the loads experienced by a tanker were calculated including ship motions and wave-induced, internal, structural, and cargo-inertial loads. Three loading conditions are analyzed, namely the full load, ballast load, and partial load conditions.

- **Static Loads**

The distribution of hull girder shear forces and bending moments is calculated by providing the vessel's hull geometry, lightship (i.e., the weight of the steel structure, outfitting, and machinery), and deadweight (i.e., cargoes and consumables such as fuel oil, water, and stores) as input for each loading condition. An analysis of a cross-sectional member along the length of the ship is required in order to account for discontinuities in weight distribution.

- **Hydrodynamic Coefficients**

Each loading condition requires hydrodynamic coefficients to determine the ship's motions and dynamic loads. It is important to consider a broad range of wave frequencies in this calculation.

- Ship Motion and Short-Term/Long-Term Response
Ship motion analysis should be carried out using a suitable method (e.g., linear seakeeping theory and strip theory). Frequency response functions are to be calculated for each load case. The short-term response is then obtained by multiplying the frequency response functions by the wave spectra. The long-term response is calculated by using the short-term response and wave statistics, which consist of wave scatter diagrams.

9.3 Strength Analysis Using Finite Element Methods

9.3.1 Modeling

In principle, strength analysis using the FEM should be performed with the following model levels:

Global Analysis

A global analysis models the whole structure with a relatively coarse mesh. For a huge structure like a ship, the global model mesh must be quite rough; otherwise, too many degrees of freedom may consume unnecessary labor hours and cause computational difficulties. The overall stiffness and global stresses of primary members of the hull should be reflected in the main features of the structure. Stiffeners may be lumped, as the mesh size is normally greater than the stiffener spacing. It is important to have a good representation of the overall membrane panel stiffness in the longitudinal and transverse directions. This model should be used to study the global response of the structure under the effects of functional and environmental loads, in order to calculate global stresses due to hull girder bending and provide boundary conditions for local finite element (FE) models. Design loads should reflect extreme sagging and hogging conditions imposed by relevant operation modes such as transit, operating, storm survival, and installation.

Local Structural Models

For instance, cargo-hold and ballast-tank models for ship-shaped structures may be analyzed based on the requirements of classification rules.

Cargo Hold and Ballast Tank Model

The local response of the primary hull's structural members in the cargo and the ballast area is analyzed for relevant internal and external load combinations. The extent of the structural model shall be decided by considering structural arrangements and load conditions. Normally, the extent covered is the tank itself and one-half the tank outside each end of the considered structure ([Figure 9.2](#)).

The mesh fineness shall be determined based on the method of load application. The model normally includes plating, stiffeners, girders, stringers, web-frames, and major

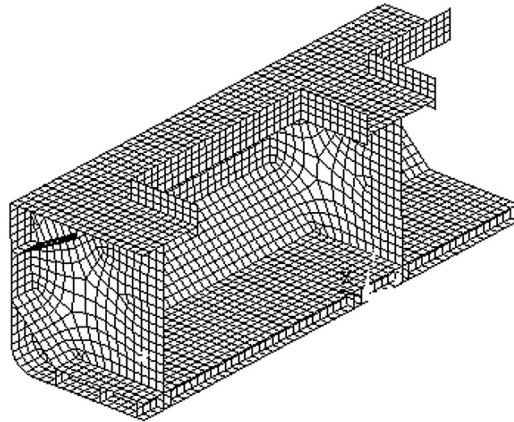


Figure 9.2
Tank model.

brackets. Additional stiffness may be employed in the structure for units with topsides, and should be considered in tank modeling.

From the results of the global analysis, the boundary conditions for the cargo hold and ballast model may be defined. Analytical results of the cargo hold/ballast model may be used as boundary conditions for the frame and girder models.

The following basic loads are to be considered in the model:

- static and dynamic loading from cargo and ballast,
- static and dynamic external sea pressure, and
- deadweight, topside loading, and inertia loads.

Frame and Girder Model

The frame and girder analysis is used to analyze the stresses and deformations in the main frame or girder system. The calculations should include results induced by bending, shear, and torsion. The minimum requirements are a function of the type of vessel being analyzed, but should include at least one transverse web in the forward cargo hold or tank (Figure 9.3).

The model may be included in the cargo hold and ballast tank models or run separately using the boundary conditions from that model analysis.

Stress Concentration Area

In the areas where high-stress concentrations may occur, local fine-mesh models are to be applied by using forces or forced deformations as boundary conditions, based on the results obtained in the global analysis. Alternatively, submodeling, superelement techniques, or direct mesh refinement may be introduced.

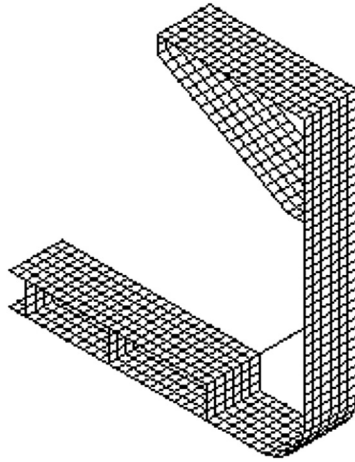


Figure 9.3
Frame model.

Attention should be paid particularly to the following areas:

- around large openings;
- longitudinal stiffeners between transverse bulkheads and the first frame at each side of the bulkhead;
- vertical stiffeners at transverse bulkheads with horizontal stringers in the way of the inner bottom and deck connections;
- horizontal stiffeners at transverse bulkheads with vertical stringers in the way of the inner side and longitudinal bulkhead connections (Figure 9.4); and
- corrugated bulkhead connections.

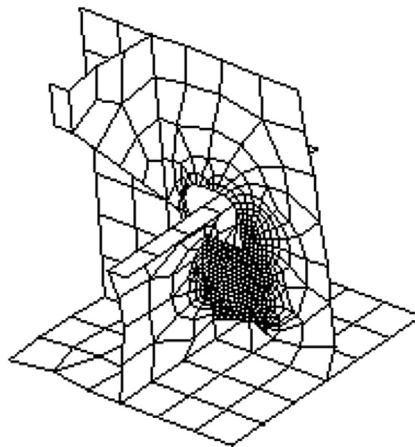


Figure 9.4
Stress concentration model.

Fatigue Model

If fatigue is of concern, analysis of critical structural details should be performed. Fine-mesh models shall be completed for critical structural details in areas such as:

- hopper knuckles in the way of web frames,
- topside support stools,
- details in the way of the moon pool,
- other large penetrations in longitudinal load-bearing elements,
- longitudinal bulkhead terminations,
- stiffener terminations,
- pontoon-to-column or column-to-deck connections, and
- other transition areas where large changes in stiffness occur.

The size of the model should be such that the calculated hot-spot stresses are not affected significantly by assumptions made for boundary conditions. Element sizes for stress concentration analysis should be of the same order of magnitude as the plate thickness. Normally, shell elements may be used for the analysis. Only dynamic loads are applied in the model, because only these affect the fatigue life of the structure. The correlation between different loads such as global bending, external and internal pressure, and acceleration of the topside should be considered in the fatigue assessment.

9.3.2 Boundary Conditions

Defining boundary conditions is one of the most important steps in FEM analysis. For local analysis models, the boundary conditions imposed by surrounding structures should be based on deformation or forces calculated from the global model.

The boundary conditions for a global model have no other purpose than to restrict rigid body motion. Fixing six degrees of freedom at both ends (and corners) of the model should be suitable. The total loading must be balanced so that the reaction forces at the boundaries approach zero.

When modeling, the length of the model ship structure should be sufficient to minimize the effects of boundary conditions over the analyzed area. [ABS \(2002\)](#) requires three cargo holds to be covered for models of tankers, bulk carriers, and container ships; LR's "Direct Calculation: Guidance Notes" (1996) require that two cargo holds be covered for the model of a bulk carrier. All continuous longitudinal elements should be restrained to remain plane under the effects of hull girder bending and must be rotationally fixed about the vertical axis if the calculated deformations or forces are not available at the free ends of the model. Conditions of symmetry should be applied at each end of the FEM. Rotation about the two axes in the plane of symmetry is to be constrained where symmetry is

imposed at the centerline or ends of the model. The model should be supported vertically by distributed springs with shiplines and longitudinal bulkheads at the intersections of the transverse bulkheads.

9.3.3 Types of Elements

The types of elements are chosen to provide a satisfactory representation of the deflections and stress distributions within the structure. Conventional frame analysis may be carried out with a beam model—it has significant advantages for its modeling simplicity and computational efficiency. However, thanks to the availability of powerful computers, computational efficiency is no longer a concern, and more refined and accurate element types can be used.

In research conducted by the ISSC (Zillotto et al., 1991), nine different FEMs were applied to different combinations of beams, trusses, rods, membranes, planes, and shell elements. A considerable scatter was observed in the results. The conclusion was that a detailed analysis of the deformations and stress levels in all elements of the transverse frames should be performed using a refined FEM for all the different types of structures and ships.

In “Direct Calculation: Guidance Notes,” LR (1996) suggests that modeling for all areas should consist of shell elements for plating, line elements (bars or rods) for secondary stiffeners, three or more plate elements over the depth of the members for double-bottom girders and floors, and plate or bar elements for side shells.

In general, if the structure is not subjected to lateral bending, membrane and rod elements may be applied. Otherwise, plate and beam elements, which have both bending and membrane resistance, should be employed. The selection of element types depends on many aspects, such as the type of structure, the load application approach, the type of analysis performed, the results generated, and the accuracy expected. There is no substitute for engineering judgment.

9.3.4 Postprocessing

The design is a complicated and iterative process in which building and solving an FE model is simply the first step. A more important step is that designers use their knowledge and judgment to analyze the results, and if necessary redesign or reinforce the structure.

First, the engineer must ensure that the results calculated by the FE program are reasonable, and that the model and the load application are correct. This can be achieved by plotting stress contour, deformation, reactions & applied load equilibrium, force & moment diagrams, etc. The next step is to check the strength of the structure against

relevant design criteria. Load and stress combinations are not always straightforward. Assumptions are usually made to certain degrees in both creating and solving the model. The designers must bear this in mind and be familiar with the FE program being used in order to account for the assumptions adopted, evaluate the calculated results, and if necessary modify the results.

Yielding Check

The yield check ensures that the stress level on each structural member is below the allowable stress. The allowable stress is defined as the yield limit of the material divided by a safety factor. Stresses calculated from different models are combined to derive the equivalent von Mises stress and evaluated against the yield criterion. Component stresses such as axial stress, bending stress, normal stress in the x-direction, normal stress in the y-direction, and shear stress and combined stress, are to be evaluated. The combination of global and local stresses should account for actual stress distributions and phases. If the phase information is limited or uncertain, the maximum design value for each component may be combined as the worst scenario. The possible load offset due to the simplified assumptions made in the FE analysis should be accounted for in stress combinations.

Buckling Check

Structural members subjected to compressive loads may normally buckle before reaching the yield limit. Various buckling modes should therefore be evaluated. Four different modes of buckling are usually recognized, as discussed in Sections 8.3.5 and 8.3.6:

- *Mode 1*: Simple buckling of the plate panel between stiffeners and girders
- *Mode 2*: Flexural buckling of the individual stiffener along with its effective width of plating, in a manner analogous to a simple column
- *Mode 3*: Lateral-torsion or tripping mode. The stiffener is relatively weak in torsion, and failure may be initiated by twisting the stiffener in such a way that the joint between the stiffener and the plate does not move laterally.
- *Mode 4*: Overall grillage buckling

See Part II of this book for more information. To ensure that the local bending stresses resulting from loads acting directly on stiffeners are included in the buckling code check, the lateral pressure should be explicitly included in the capacity check, and combined with membrane stresses calculated from the FE analysis. Relevant combinations of buckling load checks should include an evaluation of the capacity with relevant lateral pressure applied to either side of the plate. Compressive stresses calculated from global and local models are to be superimposed. Each structural member is to be designed to withstand the maximum combined buckling loads, of which the critical load cases and wave phases may be different from those pertaining to the yield check.

9.4 Fatigue Damage Evaluation

9.4.1 General

The fatigue strength of welded joints (structural details) in highly dynamically stressed areas needs to be assessed to ensure structural integrity and optimize the inspection effort. The analysis of fatigue strength should be based on the combined effects of loading, material properties, and flaw characteristics. At the global scantling design level, the fatigue strength check for hull girder members can be conducted for screening purposes. At the final design level, an analysis for structural notches, cutouts, bracket toes, and abrupt changes of structural sections need to be performed.

Stress types commonly used in fatigue analysis based on the S–N curves include nominal stress, hot-spot stress, and notch stress. Each of these methods has specific applicable conditions. Although only nominal stress is used in the examples, the analysis approach is not limited to any stress type.

Spectral fatigue analysis based on the S–N curve and the Palmgren–Miner cumulative damage hypothesis has been widely applied in the fatigue damage assessment of marine structures; see Part III of this book. [Figure 9.5](#) shows the procedure for SFA.

9.4.2 Fatigue Check

Only cyclic loads are relevant in the fatigue analysis. Static loads should therefore be subtracted from total design loads. Environmental loads for fatigue analysis may differ from those for yielding and buckling analysis. Either a stochastic or simplified fatigue analysis can be performed. When a simplified fatigue analysis is applied, the stress range corresponding to a return period equal to the design life is calculated, and the fatigue life is then computed based on S–N curves. If stochastic fatigue analysis is used, stress ranges corresponding to each sea state in the wave scatter diagram are calculated by FE analysis, and the fatigue life of each stress range is found using the S–N curves. The cumulative fatigue damage is then computed using the Palmgren–Miner hypothesis

$$D = \sum_i \frac{n_i}{N_i} \quad (9.1)$$

where,

n_i = Number of cycles in the i th stress range interval between the stress ranges $\Delta\sigma_i$ and

$\Delta\sigma_{i+1}$

N_i = Number of cycles to failure at the stress range $(\Delta\sigma_i + \Delta\sigma_{i+1})/2$ and can be read from S–N curves

D = Allowable cumulative damage, which varies for different structural members but normally should be less than 1.

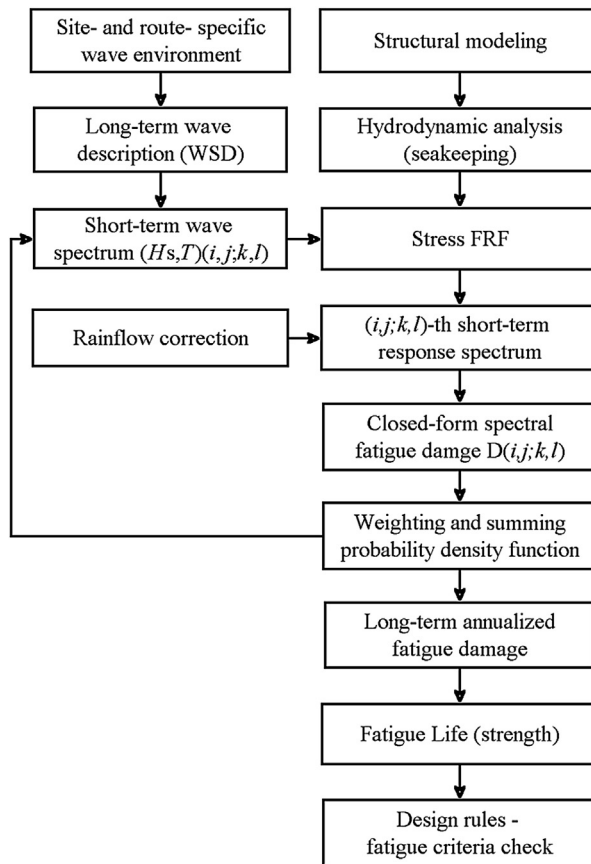


Figure 9.5
Procedure of spectral fatigue analysis.

However, a significant safety factor is usually employed with the Palmgren–Miner hypothesis, and D is often less than 0.1, 0.3, or 0.6, depending on the type of structure, the strength significance of the member, availability for inspection, etc. Reference is made to Part III of this book for more information on fatigue assessment.

References

- ABS, 2002. Rules for Building and Classing Steel Vessels. American Bureau of Shipping.
- Liu, D., Spencer, J., Itoh, T., Kawachi, S., Shigematsu, K., 1992. Dynamic load approach in tanker design. SNAME Transactions 100.
- Lloyd's Register, 1996. Structural Design Assessment Procedure, Direct Calculation-Guidance Notes.
- Ziliotto, F., et al., 1991. Comparison of different finite element analysis of transverse frame of a 350,000 TDW tanker. Marine Structures 4 (3).

Offshore Soil Geotechnics

10.1 Introduction

The world's sustained demands for energy, oil, and gas have resulted in offshore developments that move beyond the immediate continental shelf into deeper waters. The spatially distributed nature of pipelines and deepwater infrastructure have resulted in greater use of geophysical tools to define and assess associated geotechnical and geologic hazards (McCarron, 2011). The deepwater infrastructure comprises an integrated network of manifolds and wells, all of which are supported by foundations. Offshore engineers face challenging design requirements within deepwater geotechnical engineering, including the following:

- Characterizing soil in remote locations
- Mobile infrastructure
- Changing soil properties
- Fatigue-based design

The study of subsea soil, including the subsea survey, positioning, and soil investigation, is the main activity for subsea field development. This chapter provides the minimal functional and technical requirements for the subsea soil issue, but these guidelines can be used as a general reference to help subsea engineers make decisions [Figure 10.1](#).

As part of the planned field development, a detailed geophysical and geotechnical field development survey and a soil investigation, based on the survey results, are to be performed. The purpose of the survey is to identify potential human-made hazards, natural hazards, and engineering constraints when selecting a subsea field area and flow line construction; assess the potential impact on biological communities; and determine seabed and sub-bottom conditions.

10.2 Subsea Soil Investigation

Subsea soil investigations are performed by geotechnical engineers or engineering geologists to obtain information on the physical properties of soil and rock around the subsea field development for use in the design of subsea foundations for the proposed subsea structures. A soil investigation normally includes surface and subsurface exploration of the field development. Sometimes geophysical methods are used to

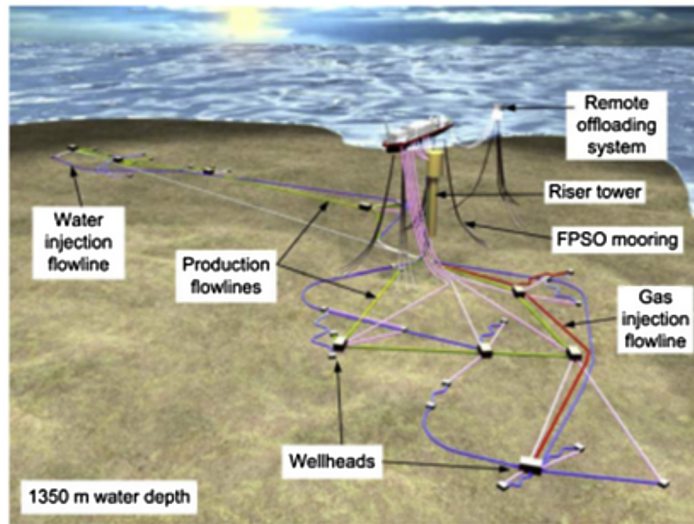


Figure 10.1

Example infield layout—the Greater Plutonio project offshore of Angola (Jayson et al., 2008).

obtain data about the field development. Subsurface exploration usually involves soil sampling and laboratory tests of the soil samples retrieved. Surface exploration can be as complex as geological mapping, geophysical methods, and photogrammetry, or as simple as a professional diver diving around to observe the physical conditions at the site.

To obtain information about soil conditions below the surface, some form of subsurface exploration is required. Methods of observing soils below the surface, obtaining samples, and determining the physical properties of soils and rocks include test pits, trenching (particularly for locating faults and slide planes), boring, and in situ tests.

10.2.1 Offshore Soil Investigation Equipment Requirements

General

The general requirements for soil investigations are as follows:

- Drilling, sampling, and testing a 120 m or deeper hole below the seabed.
- Carry out relevant seabed in situ testing; for example, performing a cone penetration test to a maximum of 10 m depending on soil conditions.
- The actual sampling and subsequent handling are carried out with minimum disturbance to the sediments. The choice of a sampler and sampling tubes reflects the actual sediment conditions and the requirements for the use of the sediment data. Therefore, different types of equipment are required.

- All equipment capable of electronic transmission is designed to sustain the water pressure expected in the field.
- Records of experience with the use of the equipment, and routines and procedures for interpretation of measurements for assessment of sediment parameters are documented and made available.

A detailed description of the sampling is provided, as is testing equipment, which includes the following:

- Geometry and weight in air and water of all sampling and testing equipment
- Handling of the seabed equipment over the side, over the stern, or through the moon pool as applicable
- Required crane or A-frame lifting force and arm length
- Any limitations as to crane and A-frame capacity, water depth, sediment type, penetration depth, and the like
- Zeroing of the PCPT before deployment
- During testing, recording of the zero readings of all sensors before and after each test

Calibration certificates for all cones are presented on the commencement of operations. Sufficient spare calibrated cone tips should be provided to ensure that work can be completed.

Seabed Corer Equipment

The coring equipment used should be well-proven types with documented histories of satisfactory operation for similar types of work. Seabed corers have a nonreturn valve at the top of the tube to avoid water ingress and sample washing-out when pulling the sampler back to the surface. Both penetration and recovery are measured and recorded.

The main operational requirements for the corers are as follows:

- The corer is capable of operating on the seabed.
- The corer is monitored continuously in the water column using a transponder.

Piezococone Penetration Test

The main operational requirements for the PCPT are as follows:

- PCP equipment is capable of operating on the seabed.
- All cones are of the electric type, and cone end point resistance, sleeve friction, and pore water pressure are continuously recorded with depth during penetration.
- The PCP rig is monitored continuously in the water column using a transponder.
- Typical penetration below the seabed is up to 5 m, pending soil conditions.

- During PCPT operations, prior to the start of the penetration of pushrods into the soil, the following data are recorded—water head, the resistance at the penetrating probe, the lateral friction, and the pore pressure starting from an elevation of 1 m above the seabed.
- The penetrometer is positioned in such a way as to provide perfect verticality of the pushrods.

A typical scheme for a PCPT is shown in [Figure 10.2](#).

Drill Rig

[Figure 10.3](#) illustrates a typical jack-up drilling rig. The drilling rig should be provided with all drill string components: drill pipe, drill bits, insert bits, subs, crossovers, and so on. The ability of the drill string on the drilling rig to be heave compensated, such that the drill bit has a minimum of movement while drilling and performing downhole sampling and testing, is very important.

Borings are drilled from the seabed to the target depth using rotary techniques with a prepared drilling mud. The objective of the borings is to obtain high-quality samples and perform in situ testing.

Downhole Equipment

Equipment for performing sampling and testing in a downhole operation mode through a drill string is relevant to the investigation:

- PCPT
- Push sampling
- Piston sampling
- Hammer sampling

An ample number of cones and sample tubes should be available. Push sampling is performed with thin-wall or thick-wall sample tubes, depending on the soil conditions. The main operational requirement for downhole equipment is that the equipment can be used in the maximum relevant water and drilling depths.

Laboratory Equipment

The vessel is provided with either a room or a container to act as an offshore soil-testing laboratory with sufficient equipment and personnel for 24 h per day operation. All necessary supplies and equipment for cutting liners and sealing and waxing samples, including transportation boxes for shipping of samples to the onshore laboratory, must be carefully provided.

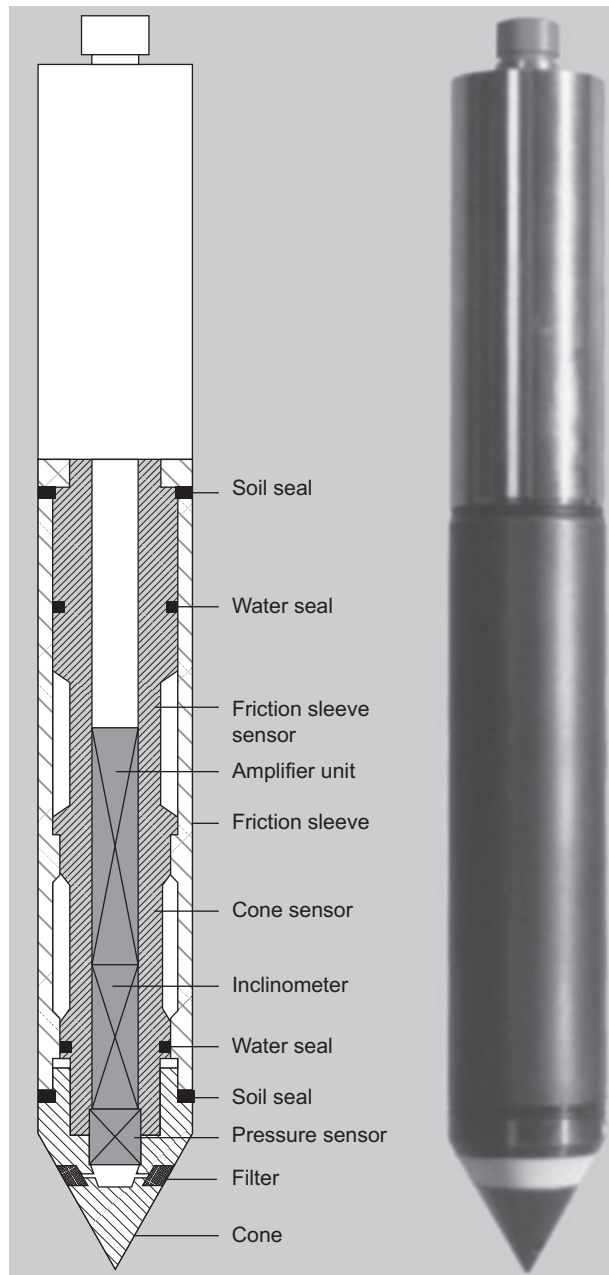


Figure 10.2
Piezocone penetration (3).

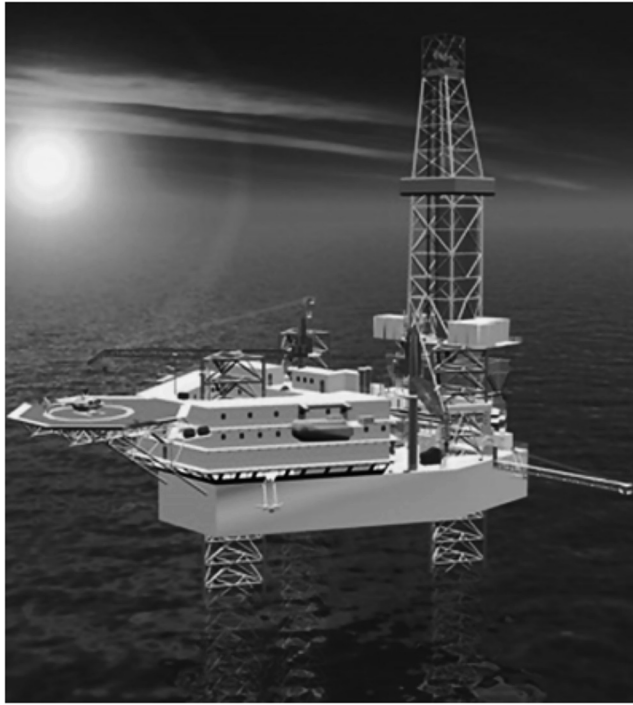


Figure 10.3
Jack-up drilling rig.

The offshore laboratory varies depending on the nature of the project. Equipment is required for performing the following types of standard laboratory tests:

- Extrusion of samples
- Description of samples
- Bulk density
- Specific gravity
- Water content
- Shear strength of cohesive sediment

10.2.2 Subsea Survey Equipment Interfaces

Onboard Laboratory Test

The cores are cut into sections no more than 1 m in length. Disturbance of the cores is avoided during cutting and at other times. The following tests are conducted at each end of the 1 m samples:

- Pocket penetrometer
- Torvane
- Motorized miniature vane

Sediment samples obtained by a Ponar or Van Veen grab sampler are described, bagged, and sealed for transportation with the cores. A motorized miniature vane measurement is conducted within the box core sample near the center of the core where the soils are undisturbed.

Core Preparation

Prior to sealing, a visual classification of the sediment types is performed. Pocket penetrometer and shear vane tests are undertaken at the top and bottom of each core section. All cores are then labeled and sample tubes are cut to minimize air space, sealed to prevent moisture loss, and stored vertically. Minimum labeling includes this information:

- Company
- Project name
- Core location reference number
- Date
- Water depth
- Clear indications of the top and bottom of the core (e.g., use different colored caps or mark the cores “Top” and “Bottom”)
- An “UP” mark indicates proper storage orientation

Onshore Laboratory Tests

The following tests, as applicable depending on soil types and locations, are carried out in a geotechnical laboratory on core samples sealed and undisturbed in the field as soon as possible after recovering the samples:

- Sample description
- Sieve analysis
- UU (unconsolidated, undrained) and triaxial (cohesive soil)
- Miniature vane (cohesive soil)
- Classification tests (Atterberg limits, water content, submerged unit weight)
- Carbonate content
- Ferrous content
- Thermal properties
- Organic matter content
- Hydrometer

The onshore laboratory program is approved prior to the commencement of testing.

Nearshore Geotechnical Investigations

To carry out geotechnical investigations in nearshore areas, a self-elevating jack-up is fully utilized—alternatively, an anchored barge for drilling operations can be used in water as

deep as 20 m and as shallow as 2 m. The general requirements for certification, integrity, and safe, efficient, working conditions described in preceding sections are applied. In addition, the acceptable sanitary conditions and messing conditions are guaranteed, which can reduce impacts on the environment in nearshore areas.

For support of the geotechnical drilling unit, any small boat operations should comply with the following guidelines:

- Small boats are equipped with spare fuel, basic tool kit, essential engine spares, radar reflector, portable radio, mobile telephone, potable water, first aid kit, and distress signals or flares (secure in a waterproof container).
- Small boats are driven only by members of the crew or other personnel who have undergone a specialized small boat handling course.

10.3 Deepwater Foundation

10.3.1 Foundations for Mooring

The type of mooring system used for floating drilling and production vessels has evolved with application into deepwater. [Table 10.1](#) shows foundation types used for mooring ([McCarron, 2011](#)).

10.3.2 Suction Caisson

The suction caisson is one of the most widely used anchor types for deeper mooring application. As shown in [Figure 10.4](#), a typical suction caisson consists of a steel cylindrical shell with a top plate and various fittings that allow water to be pumped into or out of the shell. It has an open bottom that allows soil to enter the internal volume of the caisson.

Table 10.1: Foundation used for mooring

Mooring Application	Foundation Loading Conditions			
	Vertical Compression	Vertical Tension	Horizontal	Oblique Lateral Tension
Suction caisson	Yes	Yes	Yes	Yes
Driven pile	Yes	Yes	Yes	Yes
Vertical-loaded plate anchors	No	Yes	Yes	Yes
Drag embedment	No	Some	Yes	Yes
Suction-embedded plate anchor	No	Yes	Yes	Yes
Dynamically penetrating anchor	No	Some	Yes	Yes

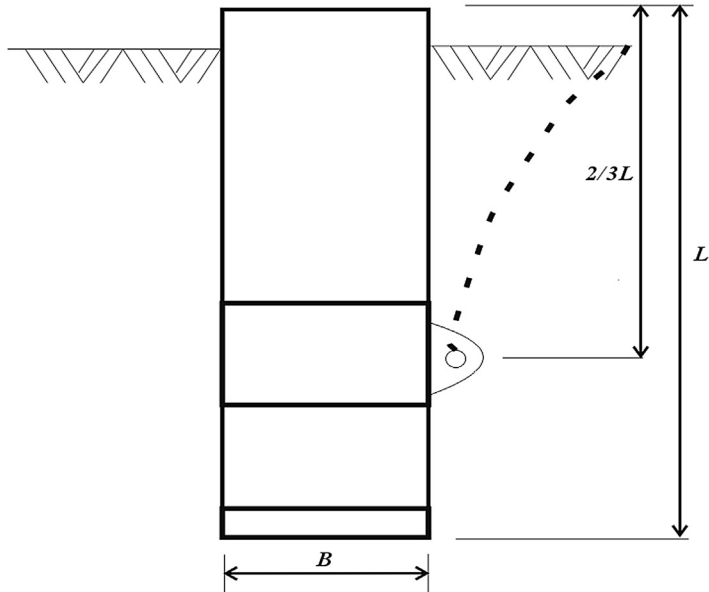


Figure 10.4

Typical suction caisson geometry (after McCarron, 2011).

The vertical holding capacity of a suction caisson is computed as the skin friction resistance on the external caisson surface and the end-bearing capacity computed over the total bottom area. The vertical holding capacity of the suction caisson in clay soil is:

$$Q_{\tau} = \pi D L S_u \alpha + N_c S_u \frac{\pi D^2}{4} \quad (10.1)$$

where D is the diameter of the suction caisson, L is the length of the suction caisson, S_u is the average DSS shear strength over the caisson embedment depth, α is the ratio of skin friction to undrained shear strength, and N_c is the bearing capacity factor.

Analytical methods for predicting holding capacity should account for the coupling effects of lateral and vertical resistance (Aubeny et al., 2005). As shown in Figure 10.5, the suction caisson under inclined load may have vertical and lateral components that are smaller than the pure vertical and horizontal failure load.

10.3.3 Spudcan Footings

Spudcan footings are usually assumed circular for the purpose of analysis, with an appropriate equivalent diameter (Martin, 1994). Solutions for the deflection of a rigid footing on the surface of a homogenous elastic half space are presented by Poulos and Davis (1974):

$$V = \left[\frac{4GR}{1-\nu} \right] z \quad (10.2)$$

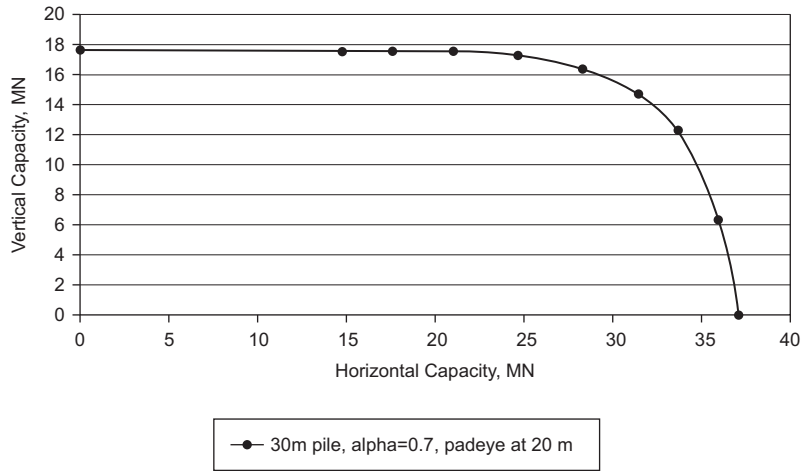


Figure 10.5
Interaction diagram of suction caisson loading.

$$H = \left[\frac{32GR(1-v)}{7-8v} \right] h \quad (10.3)$$

$$M = \left[\frac{8GR^3}{3(1-v)} \right] \theta \quad (10.4)$$

where G and ν are the elastic shear modulus and Poisson's ratio of the soil, and R is the equivalent diameter of footing.

- Central Vertical Loading

[Skempton \(1951\)](#) presented an empirical equation to predict jack-up footing penetration into clay soil, which is written as:

$$Q/A = 6s_u (1 + 0.2D/2R) + \gamma'D \quad (10.5)$$

For a partially penetrated spudcan $R = R_{equiv}$, A is the area of footing in contact with the soil.

For the case of a square footing under purely vertical loading on undrained clay, [Brinch Hansen \(1951\)](#) gives the following solution:

$$Q/A = (\pi + 2)s_u(1.2 + 0.4D/B) + \gamma'D, \quad D/B \leq 1 \quad (10.6)$$

$$Q/A = (\pi + 2)s_u(1.2 + 0.4 \tan^{-1}(D/B)) + \gamma'D, \quad D/B > 1 \quad (10.7)$$

For square footings on clay soil, [Vesic \(1975\)](#) gives:

$$Q/A = (\pi + 2)s_u \left(1 + \frac{1}{\pi + 2} \right) (1 + 0.4D/B) + \gamma'D, \quad D/B \leq 1 \quad (10.8)$$

$$Q/A = (\pi + 2)s_u \left(1 + \frac{1}{\pi + 2}\right) (1.2 + 0.4 \tan^{-1}(D/B)) + \gamma' D, \quad D/B > 1 \quad (10.9)$$

- Combined Loading: Vertical Load and Horizontal Load

Bolton (2013) presented an exact bearing capacity theory for the case of a rough strip footing on clay. The maximum load is calculated as:

$$H_0 = As_u = \left(\frac{1}{\pi + 2}\right) \cdot V_0 \quad (10.10)$$

The footing experiences sliding failure at this load if $V/V_0 \leq 0.5$. For a larger vertical load, the combined failure envelope is:

$$\frac{V}{V_0} = \frac{\pi + 1 + \sqrt{1 - (H/H_0)^2} - \sin^{-1}(H/H_0)}{\pi + 2} \quad (10.11)$$

Meyerhof (1963) carried out inclined loading tests for square and strip footings, finding that vertical-bearing capacity decreased as the angle of inclination α increased. Then, Meyerhof and Koumoto (1987) introduce inclination factors into the expression, which is written as:

$$\frac{V}{V_0} = \left(1 - \frac{\alpha^\circ}{90^\circ}\right)^2 \quad \alpha \leq \alpha_s = \tan^{-1}(H_0/V) \quad (10.12)$$

For larger inclinations, it is assumed that the footing fails by sliding at the maximum horizontal load.

- Combined Loading: Vertical, Horizontal, and Moment Loads

An inclined load of combined vertical and horizontal load is assumed to act centrally on a reduced foundation area determined by eccentricity $e = M/V$. For a surface circular footing on clay, Brinch Hansen (1951) presented the following $V : H : M$ failure envelope:

$$\frac{V}{V_0} = \frac{1 + 0.2B'/L' - 0.5 \left(1 - \sqrt{1 - H/A's_u}\right) (1 + 0.4B'/L') \frac{A'}{A}}{1.2}, \quad H \leq A's_u \quad (10.13)$$

where $V_0 = 1.2(\pi + 2)As_u$, $A = \pi R^2$, and A' , B' , and L' are functions of eccentricity defined as:

$$A' = B'L' = \pi R^2 - 2e\sqrt{R^2 - e^2} - 2R^2 \sin^{-1}(e/R) \quad (10.14)$$

$$L'/B' = \sqrt{\frac{R+e}{R-e}} \quad (10.15)$$

Vesic (1975) gives the failure model:

$$\frac{V}{V_0} = \left(1 - \frac{\left(\frac{2+B'/L'}{1+B'/L'} \right) H}{(\pi + 2)A's_u} \right) \left(\frac{\pi + 2 + B'/L'}{\pi + 3} \right) \cdot \frac{A'}{A}, \quad H \leq A's_u \quad (10.16)$$

10.3.4 Pipe Piles

The design practice for offshore pile foundation is mature. Generally, the design of piles for axial and lateral loading is considered an uncoupled problem. The two aspects of behavior will be discussed in this section.

Axial Capacity

Traditionally, the method to calculate the ultimate axial capacity in compression is adding the shaft resistance Q_f to the end-bearing capacity Q_p (McCarron, 2011). The shaft resistance is calculated by integrating unit skin friction f for each soil layer penetrated over the entire surface area of the pile. Q_p is calculated by integrating the unit end-bearing q over the total end area of the pile. Thus, the total axial capacity of the pile is obtained as:

$$Q_t = \pi D \int_0^L f(z) dz + \pi D^2 q / 4 \quad (10.17)$$

where

D = pile diameter

$f(z)$ = unit skin friction as a function of depth

q = unit end bearing

The method most widely used to calculate unit skin friction is the current API (2000) design guidelines. The friction has a correlation with α , the fraction of shear strength mobilized, and the strength ratio (s_u/σ'_v). RP2A then incorporated a simplified method to compute the friction:

$$f = \alpha s_u \quad (10.18)$$

where

α = a dimensionless factor

s_u = undrained shear strength of the soil at the point in question

The factor can be calculated as

$$\alpha = 0.5\psi^{-0.5} \text{ for } \psi \leq 1.0 \quad (10.19)$$

$$\alpha = 0.5\psi^{-0.25} \text{ for } \psi > 1.0 \quad (10.20)$$

where $\psi = s_u/\sigma'_v$

σ'_v = effective overburden pressure at the point

The unit end bearing Q_p in clay soils has traditionally been calculated based on the formula below:

$$q = N_c S_u \quad (10.21)$$

where

N_c = bearing capacity factor usually assumed equal to 9.0.

The most common method to calculate the shaft resistance Q_f and the bearing capacity Q_p in sand is described in the current API/ISO guidelines (API 2000). The unit skin friction f and unit end bearing q are calculated as:

$$f = k \sigma'_v \tan \delta \leq f_{max} \quad (10.22)$$

where

k = dimensionless earth pressure coefficient

δ = friction angle between the pile wall and the soil

f_{max} = limiting value for unit skin friction

- Lateral Capacity

For conventional design, the pile–soil interaction can be represented as shown in [Figure 10.6](#). The pile is modeled as a linearly elastic beam column, and the soil is assumed to comprise continuous, uncoupled, nonhomogeneous, and nonlinear soil springs. The characteristics of these springs are based on test data of the soil.

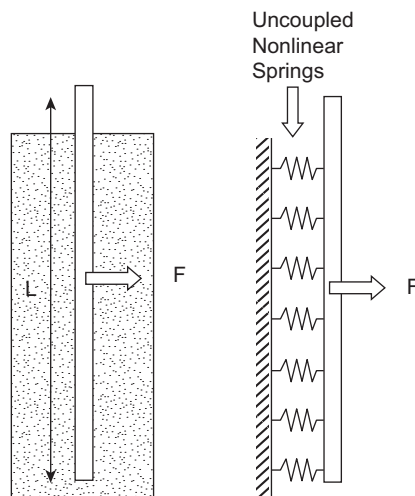


Figure 10.6
Pile–soil idealization.

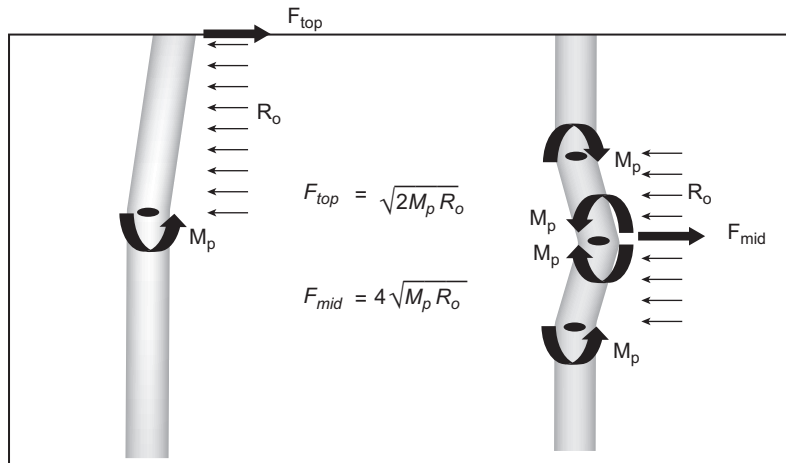


Figure 10.7

Pile failure modes under lateral loading.

The basic governing equation for the pile–soil system is similar to the form of the formula for a beam on elastic foundation:

$$EI \frac{d^4 y}{dx^4} + k(x, y)y = 0 \quad (10.23)$$

where

EI = bending stiffness of the pile

x = distance along the pile length

y = lateral displacement

k = soil spring stiffness, which is a nonlinear function of x and y

An exact solution can be obtained for some simple cases with different boundary conditions. [Figure 10.7](#) shows pile failure modes under lateral loading.

References

- Aubeny, C.P., Kim, B.M., Murff, J.D., 2005. Proposed upper bound analysis for drag embedment anchors. In: Proc. Int. Symp. On Frontiers in Offshore Geotechnics, ISFOG, pp. 179–184.
- Bolton, M.D., 2013. A Guide to Soil Mechanics. Universities Press.
- Hansen, J.B., 1951. A Revised and Extended Formula for Bearing Capacity.
- Jayson, D., Delaporte, P., Albert, J.-P., Prevost, M.E., Bruton, D., Sinclair, F., 2008. Greater Plutonio project—subsea flowline design and performance. In: Proceedings of the Conference on Offshore Pipeline Technology, OPT (Amsterdam).
- McCarron, W.O. (Ed.), 2011. Deepwater Foundations and Pipeline Geomechanics. J. Ross Publishing.
- Martin, C.M., 1994. Physical and Numerical Modelling of Offshore Foundations under Combined Loads. University of Oxford.
- Meyerof, G.G., 1963. Some recent research on the bearing capacity of foundations. Can. Geotech. J. 1, 77–87.

- Meyerhof, G.G., Koumoto, T., 1987. Inclination factors for bearing capacity of shallow footings. *J. Geotech. Engrg.* 113 (9), 1013–1018.
- Poulos, H.G., Davis, E.H., 1974. *Elastic Solutions for Soil and Rock Mechanics*. John Wiley.
- Skempton, A.W., 1951. *The Bearing Capacity of Clays*, 180.
- Vesic, A.S., 1975. Bearing Capacity of Shallow Foundations, *Foundation Engineering Hand Book*, 5, no. 4: 121–147.

Offshore Structural Analysis

11.1 Introduction

11.1.1 General

This chapter describes the primary considerations that the design engineer should keep in mind during the initial design and subsequent structural analysis. In this chapter, the notation “Structures” refers to all types of marine units ranging from floating ship-shaped vessels to bottom founded platforms. Emphasis has been placed on ship-shaped structures. However, consideration is also given to column-supported structures (e.g., semisubmersibles, tension leg platforms (TLPs), spars, and mooring buoys) as well as to steel bottom founded offshore structures, such as fixed steel jackets.

The UK HSE completed a study on offshore structures in the North Sea, which estimated that around 10–15% of failures were related to inadequate design, at either the initial design phase or a subsequent upgrade in the design. Inadequacy in design includes lack of operational considerations, failure to evaluate all structural elements, and incorrect use of the design formulas.

In the process of design, the primary concerns for the designer are risks to life, the structure, the environment, and project economy. Hence, the relevant design codes and standards will employ the appropriate safety factors in order to minimize these risks without being excessively conservative.

Throughout this chapter, emphasis is placed on the design process where the finite element analysis will be employed. Reference is made to the formulas used in the design of marine structures, although these are not reproduced within this chapter. These formulas may be found in Part II and Part III of this book, along with background information.

11.1.2 Design Codes

The designer is faced with a large number of rules, codes, standards, and specifications. All of which describe the general policy for structure systems and the detailed design of structural components. These documents are produced and distributed by:

- National Governments
- Certification Authorities

- Technical Standards Committees
- Companies, Universities, or Individual Expertise.

Chapters relating to loads and safety factors, which give a more detailed explanation of the different design methods employed in these codes, should be referenced, that is, the load and resistance factored design method, allowable stress design method, and design by testing or observation.

11.1.3 Government Requirements

Governments set legal requirements for when using their ports or territorial waters, which must be followed in the design of marine structures. Some of these laws, particularly those relating to vessel movements, are generally internationally consistent so as to avoid problems when passing through national waters during transit. However, most national laws, which relate to the design, construction, and operation of marine structures, differ from country to country, each reflecting local conditions and health and safety laws as well as expertise and experiences, including previous major incidents and accidents.

The government requirements, such as those published by

- Norwegian Petroleum Directorate (NPD),
- UK Health and Safety Executive (HSE),
- US Mineral Management Service (MMS),

are just legalities that need to be met rather than specific design methods and criteria to be employed. Such rules are mainly the concern of the project manager and the client representative, who should ensure that the relevant pieces of legislation are reflected in the Design Basis (see Section 17.2.2).

11.1.4 Certification/Classification Authorities

Historically, the Certification/Classification Authority (CA) acted as an independent body among the vessel's designer, builder, owner, operator, and the insurance company. The government's interest of reducing the risks to life and the environment from marine accidents has increased the need for CAs to also provide their expertise in government policies and legislation.

CAs include companies such as:

- American Bureau of Shipping (ABS),
- Bureau Veritas (BV),
- Det Norske Veritas (DNV),

- Lloyds Register of Shipping (LR),
- ClassNK (NK).

Ships and mobile offshore drilling units (MODU) travel from one location to another worldwide. Therefore, the use of the CA's service may avoid repetitive approvals from the many concerned national governments. The role of the CA has been questioned in recent years, concerning the fixed (bottomed supported) structures, which generally remain at one location within one nation's territorial waters throughout its life.

CA performs an independent third party assessment of the structure, throughout the design of the structure, to ensure that it fits for its purpose. This may include reviews of the design reports and independent structural analyses, particularly with the increasing use of the computer-aided finite element method (FEM). The CAs may be chosen based on their office location relative to the sites for structural design, fabrication, or operation, their specialist knowledge in regard to the type of structure, client recommendation, or their ability to meet cost and time budget requirements.

The rules published by CAs place emphasis on safety targets and consequently give precedence to safety factors and failure levels, along with general specifications of the design. Consequently, all design engineers should have access to the relevant CA rules to ensure that certification requirements are met.

11.1.5 Codes and Standards

Codes and standards provide details on how structures should be designed, built, and operated.

The difference between a code and a standard is that a code should be followed more rigorously, while a standard recommends practices that should be followed. This difference is largely ignored now with, for example, the Eurocode for steel design, which is classified as a national standard.

The range of worldwide codes and standards is substantial. However, the important aspect of these documents is that they both have national or in some cases international standings. Examples of these codes and standards, for the design of steel marine structures, include the following:

- ANSI/AWS D1.1, Structural Welding Code,
- API RP2A (Working Stress Design or Load Resistance Factored Design, Recommended Practice for Planning, Designing, and Constructing Fixed Offshore Platforms),
- Eurocode 3 (NS-ENV 1993 1-1 Eurocode 3),
- [ISO Codes for Design of Offshore Structures](#),
- NORSOK Standard N-004, Design of Steel Structures,
- NS3472,
- BS5750.

The design or reassessment of steel marine structures will be based on one or more of the above-noted documents. The software used will be an essential program for all members of the design team. However, with regard to the use of the FEMs during the design, none of these documents give a thorough assessment of the preferred or recommended techniques.

Standards such as NS3472 and BS5750 provide the fundamental equations needed to determine stresses in steel components, regardless of their area of application. Documents such as NORSOK N-004 and API RP2A apply the relevant fundamental equations, along with appropriate factors of safety that correspond to the design limit-states for particular marine structures. NORSOK N-004 (NTS, 1998) gives state-of-the art specifications for designing floating and fixed marine structures. It is based on the NS3472, Eurocode 3, oil company's specifications for the design of steel structures, and many of the best features taken from technical papers.

API RP 2A (2001a) has been widely applied for design and construction fixed platforms, and serve as a basic document for offshore structure design.

API RP 2T (1987) has been mainly used for tension leg platforms. It provides comprehensive guidance on design criteria, environmental forces, global design and analysis, structural designs of hulls and decks, tendon system designs, foundation design and analysis, riser systems, facility designs, fabrication, and installation and inspection, as well as structural materials.

Recently an API RP 2FPS (2001b) was issued for floating production systems. It gives a high-level specification for the design and analysis of floating production systems, such as semisubmersibles, spars, FPSO, and conversion/reuse of existing structures. The guide defines design environmental criteria, accident loads, and fire and blast loads and specifies design requirements with respect to design load cases, structural designs of the hull and deck, fatigue assessment, weight control, watertight and stability, transit conditions, and fabrication tolerances. The API RP 2FPS (2001b) also provides general guidance on a station keeping and anchoring system, well and production fluid control, a transportation system and export system, facilities, fabrication, installation and inspection, materials, and welding and corrosion protection, as well as risk management.

11.1.6 Other Technical Documents

When performing the design or reassessment of steel marine structures, reference may be made to specialized documents, which include:

- Company specifications and procedures that are based on specific expertise or test results developed in-house by the designer, a subcontractor, or the client manuals that give support to finite elements, risk and reliability, or other engineering tools.

- Reports, conference proceedings, or technical journals in the public domain covering a particular design aspect in-depth.
- Books on steel designs that allow fundamental stresses and strains to be estimated.

The above documents will need to be referenced in the Design Basis and made available to the design members, as required.

11.2 Project Planning

11.2.1 General

It is essential that adequate planning be undertaken at the initial stages of the design process in order to achieve a good design within the estimated cost and time schedule.

The main output of the planning process is a “Design Basis,” describing both the criteria and a “Design Brief,” which describes the procedure to be followed and software to be used. For smaller projects in particular, it may be preferable to gather all the information into one concise document.

Ideally, the Design Basis and Design Brief will be written to and agreed on by the client prior to the design phase. However, in practice this is not always possible. In such cases, it is strongly recommended that these documents be issued in draft format with as much detail as possible or with relevant items labeled as “Preliminary.” This will enable the project team to begin developing the design with some understanding of the criteria that will be the most critical throughout the design.

The Design Basis and Design Brief may be updated throughout the project as particular problems arise. It is important that all-relevant team members are aware of such changes.

11.2.2 Design Basis

The Design Basis document lists the basis criteria relevant to the structure and should include the following:

Unit Description and Main Dimensions

A summary, describing the structure, includes:

- A general description of the structure, including the main dimensions and draught/water depth
- Main structural drawings
- Service and design lives
- Location of the structure (if fixed)
- Specification of the system of units employed.

Rules, Regulations and Codes

A list of relevant, applicable references to the design codes and project-related documents include:

- Environmental design criteria, including all relevant conditions, such as wind, wave, current, snow, ice, and earthquake description with 10E-1, 10E-2, and 10E-4 annual probability occurrence.
- Soil/foundation criteria for design of fixed structures, mooring/anchoring, pipelines, and risers.
- Design temperatures.

Stability and Compartmentalization

Stability and compartmentalization design criteria for relevant conditions include:

- External and internal watertight integrity
- Boundary conditions including interfaces with other structures or foundation conditions
- Lightweight breakdown report
- Design load cases and global mass distribution
- Damage conditions.

Materials and Welding

Design criteria for materials and welding include:

- Yield and ultimate tensile strength
- Corrosion allowances to be taken
- Corrosion protection systems or coatings
- Material flexibility and avoidance of brittle fracture
- Crack growth properties
- Weld specifications and fatigue classifications
- Postweld heat treatment
- Minimum access for welding
- Marine growth type and thickness.

Temporary Phases

Design criteria for relevant temporary phases include:

- Limiting permanent, variable, environmental, and deformation action criteria
- Procedures associated with construction, including major lifting operations
- Essential design parameters associated with the temporary phase
- Relevant accidental limit-state.

Operational Design Criteria

Design criteria for relevant operational phases include:

- Limiting permanent, variable, environmental, and deformation action criteria
- Deck load description (maximum and minimum)
- Wave motion accelerations on appurtenances
- Mooring actions
- Tank loading criteria
- Fatigue and fracture criteria
- Air gap requirements
- Accidental event criteria.

In-service Inspection and Repair

Criteria for inspecting the structure postfabrication and in-service and criteria for allowing repairs to be efficiently carried out and recorded include:

- Description of the in-service inspection hierarchy and general philosophy
- Access for inspection and repair
- Redundancy and criticality of components.

Reassessment

The data needed for reassessment include:

- Inspection records
- Fabrication and welding records
- Details of cracked and damaged components
- Details of replaced or reinforced components
- Details of on-site measurements
- Details of corrosion protection methods and marine growth state.

11.2.3 Design Brief

A Design Brief document lists the procedures to be adopted in the initial stages of the design process, and include the following:

Analysis Models

A general description of models to be utilized, including the description of

- Global analysis model(s)
- Local analysis model(s)
- Load cases to be analyzed.

Analysis Procedures

A general description of analytical procedures to be utilized including a description of the procedures to be adopted with respect to:

- The evaluation of temporary conditions
- The consideration of accidental events
- The evaluation of fatigue actions
- Air gap evaluation
- The establishment of dynamic responses (including methodology, factors, and relevant parameters)
- The inclusion of “built-in” stresses
- The consideration of local responses (e.g., those resulting from mooring and riser actions, ballast distribution in tanks as given in the operating manual, etc.)
- Consideration of structural redundancy.

Structural Evaluation

A general description of the evaluation process including:

- Description of procedures to be completed when considering global and local responses
- Description of fatigue evaluation procedures (including the use of design fatigue factors, S–N curves, basis for stress concentration factors (SCFs), etc.)
- Description of procedures to be completed during the code check.

11.3 Use of Finite Element Analysis

11.3.1 Introduction

Basic Ideas behind FEM

The FEM is a powerful computational tool that has been widely used in the design of complex marine structures over the decades. The basic idea behind the FEM is to divide the structure into a large number of finite elements. These elements may be one, two, or three-dimensional. The finite element model may be in the form of a truss of members connected at nodal points, or a detailed assembly of elements representing an entire structure, or even a particularly complex and critical component of the structure.

Taking an irregularly shaped plate, for example, the displacements and consequently the stresses within the plate under a given load for a specified material and boundary conditions can be estimated. The field variable of interest here is the displacement. Instead of determining the displacement at every point in the plate, the FEM divides the plate into a finite number of elements and provides the displacements at the nodal points of each

element. Interpolation functions are used within each element to describe the variations of the field variable (e.g., displacement in this example) as a function of the local coordinates. Using nodal displacements and the interpolation function, the designer can compute the stress variation within any given region.

Computation Based on FEM

Commercial software has been developed based on the finite element theory. As input data for the software, the designer defines relevant coordinates of each node, element definitions, material properties, boundary conditions, etc. Generally, the accuracy of the solution improves as the number of elements increases, but the computational time and cost also increase. A high-speed computer is required to perform and solve the large amount of element assembling involved.

Different element types (rod, beam, membrane, solid, bending with 3-node, 4-node, 6-node, 8-node, etc.) are applied to various types of structures, which yield different accuracies and CPU times. However, there is no substitute for experience when trying to determine the element density and element type, when trying to achieve the required level of accuracy for the finite element analysis of a particular structure.

The computer program determines the displacements at each node and then the stresses acting through each element. One of the essential tasks in FE analysis is to analyze the results, which is known as postprocessing. The designer may view the results in a tabular or graphical form. A graphical view may be used initially to identify the regions and nodes of interest and subsequently tabulate the output specified for the chosen areas of interest. If this were not the case, the physical data of the whole structure may otherwise be too large to be structurally assessed.

Marine Applications of FEM

The analyst may then use the results from the finite element analysis to strengthen the structure via an increase in the material strength, an additional reinforcement, or by changing the load path or the boundary conditions.

The critical areas, where loads or stresses are concentrated, or where there are complex joint details, will generally need to have a more detailed finite element model or finer element mesh. The finite element analysis output will only be as good as the input data specified. Again, it is particularly important for the designer to consider the limits of the model and consequently the accuracy of the analysis results.

Probably the most serious problem affecting ocean-going vessels in recent years has been brittle fractures near bulkheads on very large bulk carriers. Such an effect could be easily missed in a finite element model. Local flexibility/rigidity and material behavior could be overlooked since the design emphasis is placed on increasing the stiffness of local details, in order to meet the requirements of the relevant codes.

Below, stiffness matrices are derived for 2D and 3D beam elements in order to illustrate the finite element methods for offshore structural analysis and to prepare a theoretical basis for Chapters 18–21.

11.3.2 Stiffness Matrix for 2D Beam Elements

Figure 11.1 shows a beam element. The neutral axis of the beam is defined as the x -axis, while one of the principal axes of inertia for a beam is defined as the y -axis. In this section, a bending problem is discussed in the x – y plane.

When the depth of the bend is very small compared to the length, the Bernoulli–Euler assumption, that the perpendicular cross section of neutral axis is kept perpendicular to the neutral axis after deformation, is valid (Figure 11.2). Under this assumption, the angle of clockwise rotation of cross section θ can be expressed as

$$\theta = -\frac{dv}{dx} \quad (11.1)$$

If the displacement in the y direction of a neutral axis is defined as $v(x)$, the point (x,y) before deformation varies in x,y directions as $u(x,y)$, and $v(x,y)$, which is expressed as

$$u(x,y) = -y\frac{dv(x)}{dx} \quad (11.2)$$

$$v(x,y) = v(x) \quad (11.3)$$

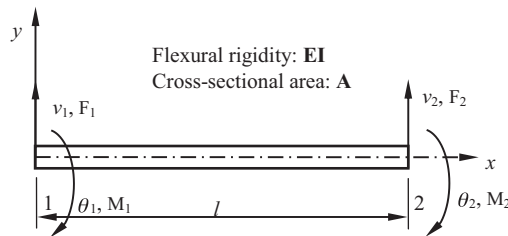


Figure 11.1
Beam element.

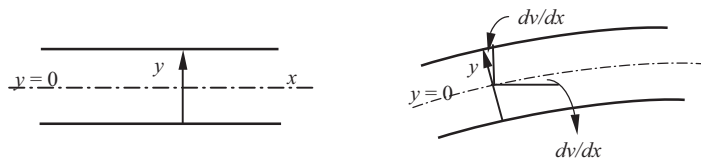


Figure 11.2
Assumption of Bernoulli–Euler.

The displacement v may be expressed as the following three-order polynomial formula,

$$v = a_1 + a_2x + a_3x^2 + a_4x^3 \quad (11.4)$$

When the two nodal points of the element are defined as 1 and 2, and the degree of freedom at the nodal point is set as the flexure and rotation angle, the displacement vector for the two nodal points of the beam have four degrees of freedom,

$$\{d\}_e = \begin{Bmatrix} v_1 \\ \theta_1 \\ v_2 \\ \theta_2 \end{Bmatrix} \quad (11.5)$$

where the subscript is the number of the nodal points. The undetermined coefficients for v in Eqn (11.4) can be expressed as the four deformations of nodal points, and expressed as

$$\begin{Bmatrix} v_1 \\ \theta_1 \\ v_2 \\ \theta_2 \end{Bmatrix} = \begin{bmatrix} 1 & 0 & 0 & 0 \\ 0 & -1 & 0 & 0 \\ 1 & 0 & l^2 & l^3 \\ 0 & -1 & -2l & -3l^2 \end{bmatrix} \begin{Bmatrix} a_1 \\ a_2 \\ a_3 \\ a_4 \end{Bmatrix} = [A]\{a\} \quad (11.6)$$

By solving Eqn (11.6), a solution for $\{a\}$ is obtained.

$$\{a\} = [A]^{-1}\{d\}_e$$

and the strain is expressed as

$$\varepsilon_x = \frac{du}{dx} = -y \frac{d^2u}{dx^2} \equiv y\kappa_x \quad (11.7)$$

where κ_x is the curvature and may be expressed as

$$\begin{aligned} \kappa_x &= -\frac{d^2v}{dx^2} = 2a_3 + 6a_4x = [0 \quad 0 \quad 2 \quad 6x] \{a\} \\ &= [0 \quad 0 \quad 2 \quad 6x] [A]^{-1} \{d\}_e \equiv [B] \{d\}_e \end{aligned}$$

The stress σ_x is then given as

$$\sigma_x = E\varepsilon_x = -Ey\kappa_x$$

The principle of virtual work for this beam element may be expressed as

$$E \int_0^l \int_A \delta\varepsilon_x \sigma_x dA dx = \{\delta d\}_e^T \{f\}_e \quad (11.8)$$

where A is the cross-sectional area, and $\{f\}_e$ is the nodal force vector corresponding to the nodal displacement,

$$\{f\}_e = \begin{Bmatrix} F_1 \\ M_1 \\ F_2 \\ M_2 \end{Bmatrix} \quad (11.9)$$

where $F_\alpha, M_\alpha (\alpha = 1, 2)$ is the shear force and bending moment for nodal point α . Eqn (11.8) may then be rewritten as

$$\{\delta d\}_e^T \int_0^l [B]^T EI [B] dx \{d\}_e = \{\delta d\}_e^T \{f\}_e$$

where I is the second-order inertia moment for the cross section and is expressed as

$$I = \int_A y^2 dA$$

where $\{\delta d\}_e$ is any value. The stiffness matrix equation for an element is

$$\{f\}_e = [K]_e \{d\}_e \quad (11.10)$$

where $[K]_e$ is a stiffness matrix

$$[K]_e = \int_0^l [B]^T EI [B] dx = \frac{EI}{l^3} \begin{bmatrix} 12 & 6l & -12 & 6l \\ 6l & 4l^2 & -6l & 2l^2 \\ -12 & -6l & 12 & -6l \\ 6l & 2l^2 & -6l & 4l^2 \end{bmatrix} \quad (11.11)$$

11.3.3 Stiffness Matrix for 3D Beam Elements

In Figure 11.3, \bar{x}, \bar{y} denote local member axes and x, y denote global system axes. The moments M_1 and M_2 can be considered as vectors normal to the x - y plane, corresponding to angles θ_1 and θ_2 . Hence, the transformation equations relating nodal force components in local axes and global axes may be written as

$$\begin{aligned} \{\bar{f}\} &= [T] \{f\} \\ \{f\} &= [T]^T \{\bar{f}\} \end{aligned} \quad (11.12)$$

where the nodal force vector in local axes $\{\bar{f}\}$ and the nodal force vector in a global system $\{f\}$ are defined by

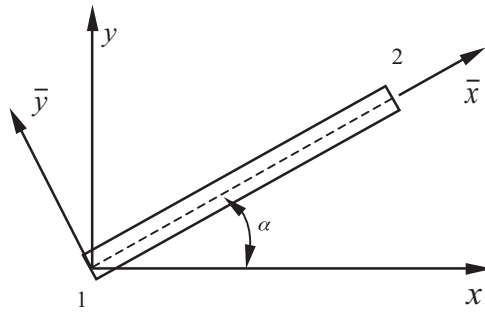


Figure 11.3
Inclined 2D beam element.

$$\{\bar{f}\} = \begin{Bmatrix} \bar{F}_{1x} \\ \bar{F}_{1y} \\ \bar{M}_1 \\ \bar{F}_{2x} \\ \bar{F}_{2y} \\ \bar{M}_2 \end{Bmatrix}, \quad \{f\} = \begin{Bmatrix} F_{1x} \\ F_{1y} \\ M_1 \\ F_{2x} \\ F_{2y} \\ M_2 \end{Bmatrix}$$

and the transformation matrix $[T]$ is given, from geometrical consideration, as

$$[T] = \begin{bmatrix} \lambda & \mu & 0 & 0 & 0 & 0 \\ -\mu & \lambda & 0 & 0 & 0 & 0 \\ 0 & 0 & 1 & 0 & 0 & 0 \\ 0 & 0 & 0 & \lambda & \mu & 0 \\ 0 & 0 & 0 & -\mu & \lambda & 0 \\ 0 & 0 & 0 & 0 & 0 & 1 \end{bmatrix} \quad (11.13)$$

with $\lambda = \cos \alpha$, $\mu = \sin \alpha$.

Similarly, the nodal displacement components are given as

$$\begin{aligned} \{\bar{U}\} &= [T]\{U\} \\ \{U\} &= [T]^T\{\bar{U}\} \end{aligned}$$

where $\{\bar{U}\}$ and $\{U\}$ are defined by

$$\{\bar{U}\} = \begin{Bmatrix} \bar{U}_1 \\ \bar{V}_1 \\ \bar{\theta}_1 \\ \bar{U}_2 \\ \bar{V}_2 \\ \bar{\theta}_2 \end{Bmatrix}, \quad \{U\} = \begin{Bmatrix} U_1 \\ V_1 \\ \theta_1 \\ U_2 \\ V_2 \\ \theta_2 \end{Bmatrix}$$

Based on the element stiffness equation in the local axes given as

$$\{\bar{f}\} = [\bar{K}]\{\bar{U}\} \quad (11.14)$$

the element stiffness equation in the global axes is easily obtained (Figure 11.4).

$$[K] = [T]^T [\bar{K}] [T] \quad (11.15)$$

If the force and corresponding displacement vectors are written as

$$\{\bar{f}\} = \begin{Bmatrix} \bar{F}_{1x} \\ \bar{F}_{1y} \\ \bar{F}_{1z} \\ \bar{M}_{1x} \\ \bar{M}_{1y} \\ \bar{M}_{1z} \\ \bar{F}_{2x} \\ \cdot \\ \cdot \end{Bmatrix}, \quad \{\bar{U}\} = \begin{Bmatrix} \bar{U}_1 \\ \bar{V}_1 \\ \bar{W}_1 \\ \bar{\theta}_{1x} \\ \bar{\theta}_{1y} \\ \bar{\theta}_{1z} \\ \bar{U}_{2x} \\ \cdot \\ \cdot \end{Bmatrix} \quad (11.16)$$

Having the stiffness matrix $[\bar{K}]$ defined in local axes for each beam element, the stiffness matrix $[K]$ in global axes for the beam element may be derived using the transformation matrix $[T]$,

$$[K] = [T]^T [\bar{K}] [T] \quad (11.17)$$

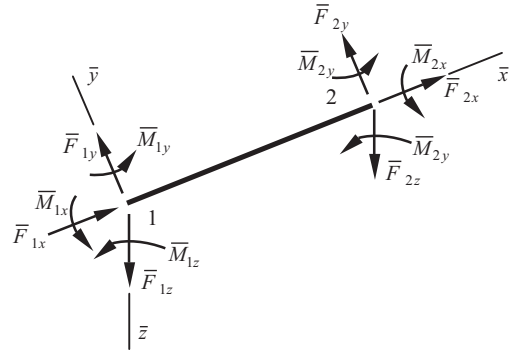


Figure 11.4
Nodal forces for 3D beam element in local axes.

$$[L] = \begin{bmatrix} \lambda_x & \mu_x & \nu_x \\ \lambda_y & \mu_y & \nu_y \\ \lambda_z & \mu_z & \nu_z \end{bmatrix}, \quad [0] = \begin{bmatrix} 0 & 0 & 0 \\ 0 & 0 & 0 \\ 0 & 0 & 0 \end{bmatrix} \quad (11.19)$$

where λ_x denotes the cosine of the angle between the x and \bar{x} axes, μ_x denotes the cosine of the angle between the y and \bar{x} axes, ν_x denotes the cosine of the angle between the z and \bar{x} axes, etc.

The stiffness matrix for the structural system may be established by assembling the stiffness matrices for individual elements of the structural system. Once the system stiffness matrix for the structure is established, boundary conditions can be applied to determine nodal displacements/forces. The element nodal forces in local axes may then be determined and nodal displacements and stresses in local axes can be estimated. For more information on the FEM, reference is made to [Zienkiewicz \(1977\)](#).

11.4 Design Loads and Load Application

Dead Loads

Structural weight can be calculated directly from the structural model based on the material density and volume input. These loads are generated automatically by the FEM program as nodal forces or uniform loads on members. Equipment and miscellaneous loads may be applied by means of surface loads or concentrated nodal forces at their actual locations.

Variable Loads

Within the design of structural members, the variable loads and weights must be analyzed for several cargo distributions in order to capture the extreme values of loads. The variable loads are usually included in the FEM model as surface pressure on relevant decks or tank boundaries.

Static Sea Pressure

Static sea pressure at each design draft is computed and applied in the FEM model as a surface load, which acts like a constant surface pressure on the bottom and as a linearly varying surface pressure on the side plates.

Wave-Induced Loads

The wave-induced hydrodynamic loads and inertia loads due to vessel motion are considered to be low-frequency dynamic loads and can be analyzed using a quasi-static approach. The solutions for these ship motions and hydrodynamic loadings are most frequently accomplished through the use of the strip theory.

For ships: A global extreme sea state is imposed on the structure. Inertia loads are calculated based on a conservatively assumed motion of the vessel.

For offshore structures: A different analysis is carried out and a sufficient number of periods should be analyzed for the following reasons:

- To adequately cover the site-specific wave conditions
- To satisfactorily describe transfer functions at and around the wave cancelation and amplification periods
- To satisfactorily describe transfer functions at and around the heave resonance period of the structure.

Global wave frequency: Structural responses should be established by an appropriate methodology. For example:

- A regular wave analysis
- A design wave analysis
- A stochastic wave analysis.

Once the extreme waves are selected for a design, wave-induced loads may be computed by commercial programs, such as AQUA and WAMIT. The phase angles of waves should be represented properly, and the structural members are therefore designed to withstand the maximum stresses resulting from various phases of waves.

Wind Loads

Wind loads are usually considered static loads and are calculated based on the actual area and wind pressure by simply using the following formula:

$$F_{wind} = P_{wind} \cdot A_{wind} \quad (11.20)$$

$$P_{wind} = V^2 \cdot C_h \cdot C_s \quad (11.21)$$

where

V = Wind velocity

C_h = Height coefficient

C_s = Shape coefficient

A_{wind} = Projected area perpendicular to the wind direction.

The height and shape coefficients are specified in classification rules. The quasi-static wind pressure in Eqn (11.21) was derived in accordance with Bernoulli's theorem for an ideal fluid striking an object, which states that the dynamic pressure may be expressed as

$$P_{wind,dynamic} = \frac{1}{2} \rho V^2 \quad (11.22)$$

where ρ denotes the mass density of air. Wind loads may be applied as surface loads if the projected areas are modeled. In most cases, they are applied as horizontal concentrated loads at appropriate elevations.

11.5 Structural Modeling

11.5.1 General

This section gives a general overview for the design of marine structures using a finite element modeling technique. Reference is made to recommendations described in NORSOK N-004 (NTS, 1998), which is one of a few codes that provides guidance on finite element modeling in marine structure designs. This section will address structural modeling defined by industry codes for fixed platforms and floating production installations.

11.5.2 Jacket Structures

A Jacket structure is a welded tubular space frame consisting of vertical or battered legs supported by a lateral bracing system. The function of the jacket is to support the topside facilities, provide supports for conductors, risers, and other appurtenances, and serve as a template for the foundation system. Graff (1981) and Dawson (1983) gave an introduction to the design and analysis of jacket structures, including basic formulations for environmental loads, modeling of the foundation, finite element analysis, dynamic response, and stress acceptance criteria. In general the design activities include:

- Identify the project needs.
- Evaluate environmental and soil conditions.
- Develop preliminary design proposals focusing on the methods of installation.
- Evaluate the installation methods in terms of technical and economical feasibility, construction and installation challenge, foundation requirements, cost, etc.
- Dimension the structure to resist the in-place load during operating conditions, for each mode of operation such as drilling, production, work over, or combinations thereof.
- Evaluate the design to ensure that it can resist actions due to transportation from the fabrication yard to the installation site, including load-out, sea transportation, installation, mating, and hook-up.
- Account for the abandonment of the structure after decommissioning.
- Meet quality and HSE requirements.

Analysis Models

The global analysis of platforms starts from defining the geometrical and material properties of the structural members, the foundation properties, and functional, environmental, and accidental loads.

Two types of structural analysis may be conducted.

- A linear analysis to check the ultimate strength and fatigue criteria that is based on industry codes (such as API RP 2A) using internal member forces.
- A nonlinear finite element analysis of structural responses to accidental loads (such as ship collision, dropped objects, fire, explosion, and earthquake) or an extreme response to wave load as part of the reassessment of existing platforms.

The basic formulation for linear finite element analysis is given in Section 17.3, and the nonlinear finite element analysis is detailed in Chapter 18.

The finite element model for analysis of jackets includes:

1. **Loads:** The loads include:
 - a. Functional loads such as gravity load
 - b. Environmental loads due to wind, waves, currents, and earthquakes, and
 - c. Accidental loads that may occur during its service life.

The increase in hydrodynamic and gravity actions, caused by marine growth, should be accounted for. The hydrodynamic model of the structure should include appurtenances such as conductors, I-tubes and risers, caissons, ladders and stairs, a launch box, boat landings, guides, and anodes. Depending on the type and number, appurtenances can significantly increase the global wave forces. In addition, forces on some appurtenances may be important for local member designs. Appurtenances not welded to the main structure are generally modeled as nonstructural members that only contribute as equivalent wave forces.

2. **Foundation:** The foundation system for the jacket, a temporary on-bottom condition prior to installation of the permanent foundation system, should be documented to have the required foundation stability for the specified environmental conditions, and for all relevant limit-states. Throughout the analysis, structure-to-ground connections should be selected in order to represent the response of the foundations. They may normally be simulated using linear stiffness matrices. The finite element analysis may explicitly model behavior of axial and lateral soil–foundation systems.
3. **Structures:** The stiffness of the deck structure shall be modeled in sufficient detail to ensure compatibility between the deck design and the jacket design. In a linear analysis normally it is sufficient to model one member using only one element. However, in order to account for member buckling and local dynamic response, one or more beam-column elements are required to model each member, depending on the element formulation and distribution of actions. Major eccentricities of load carrying members may be modeled as rigid ends.

Modeling for Ultimate Strength Analysis

The load cases include each mode of operation, such as drilling, production, workover, or a combination of operations. According to [NTS \(1998\)](#), it is necessary to perform analyses to establish the following.

- Maximum base shear of wave and current actions for dimensioning jacket bracings.
- Maximum overturning moments for dimensioning jacket legs and foundation systems.
- Maximum local member forces which may occur for wave positions other than that causing the maximum global force.

Modeling for Fatigue Analysis

Fatigue analysis should include all relevant actions contributing to the fatigue damage both in nonoperational and in operational design conditions. When calculating fatigue damage, local action effects due to wave slamming and vortex shedding should be included, if relevant.

While jackets in shallow water depths are normally insensitive to dynamic effects, nonlinearities associated with wave theory and free-surface effects may be important. A deterministic analysis is normally recommended for such jackets. For deepwater jackets where the dynamic effects are important, a fatigue analysis in the frequency domain (dynamic stochastic analysis) is recommended. In order to linearize the actual nonlinear soil response, the stiffness matrices for the structure–soil interaction should be developed based on a wave height, which contributes most significantly to the fatigue damage.

Assessment of Existing Platforms

An existing platform should be reassessed if the design conditions change. For example,

- If the original operating load is significantly exceeded due to the addition of facilities.
- If the structure is altered and degraded due to fatigue and corrosion damages.
- If the structure has an inadequate air gap, is operated under different environmental and operating conditions.
- When the life-safety level becomes more restrictive.

[API RP 2A \(1997a,b\)](#) gives comprehensive recommendations on the survey, metocean, seismic and ice load criteria, structural analysis methodologies, and evaluation criteria as well as mitigation alternatives.

Fire, Blast, and Accidental Loading

[API RP 2A \(1997a,b\)](#) proposes a risk-based structural assessment for fire, blast, and accidental loading. The assessment includes the following tasks:

- For the selected platform, a platform exposure category, based on the consequence of failure in terms of human life and cost, needs to be assigned.
- For a given event, assign risk levels Low, Medium, and High to the probability (frequency) of the event occurring.
- Determine the appropriate risk level for the selected platform and the event based on a risk matrix.

- Conduct further study or analysis to better understand frequency, consequence, and cost of mitigation and set acceptance criteria based on the (As Low As Reasonably Practicable) ALARP principle.
- Reassign a platform exposure category and/or mitigate the risk or the consequence of the event.

For those platforms considered as high risk for a defined event, a detailed structural integrity assessment is to be conducted for fire, blast, or an accidental loading, based on nonlinear finite element analyses or experimental tests.

For a comprehensive reference list and guidance on the design against fire and blast loads, reference is made to [ISSC \(1997\)](#). The panels V.2 report for [ISSC \(1997\)](#) summarized the design and assessment philosophy, preventive and protective measures for fires, analysis methods for fire loads and load effects, analysis methods for blast loads and load effects, probabilistic analysis, and design recommendations.

11.5.3 Floating Production and Offloading Systems (FPSO)

Structural Design General

The design of FPSO should comply with the classification requirements and industry standards, for example, NORSOK ([NTS, 1998](#)) and API RP 2FPS. In cases where the FPSO is registered in a specific country, the relevant requirements of the flag state authority shall also be followed.

The main difference between an ocean-going ship and a site-specific FPSO is:

- An FPSO is stationed in a specific site using mooring and anchoring systems, and subjected to site-specific environmental conditions.
- The operating life for an FPSO may be equal to or longer than 20 years.
- Risers are attached to the FPSO hulls through riser porches or I-tubes.
- Topside facilities may impose requirements such as motion/green water/safety and the standard of living is higher.
- An FPSO may have cyclic offshore offloading with a frequency of approximately once per week.
- An FPSO is designed to have no dry docking imposing stricter requirements for inspection/maintenance and repair.

Design and analysis of an FPSO include the following aspects ([Bai et al., 2001](#)):

- Vessel hull configuration selection
- Design load case definition
- Stability and compartmentalization
- Global performance
- Green water

- Intact strength covering transit, temporary conditions, extreme operating conditions, and survival conditions
- Structural strength under damaged conditions
- Mooring and riser systems
- Topside consideration.

The design load cases include:

- In-place operating conditions: environmental loads of up to 100 years return period, quartering/head seas (turret moored) or all headings (spread moored), and various loading conditions from topsides, risers, and mooring systems.
- Survival conditions: 100 years return environment/responses, worst loading conditions from topsides, and damaged conditions (for strength and stability).
- Transportation conditions: 10 years return period or less, ballast loading conditions, dry topside, and head seas.
- Installation and hoop up: selected weather window(s), ballast tanks, dry topsides, and heading of up to quarter seas.

In developing the design criteria, consideration should be given to site-specific services, including the following factors that may influence the hull actions:

- Site-specific environmental conditions
- Effect of a mooring system
- Long-term service at a fixed location
- Seas approaching predominantly from a narrow sector ahead
- Zero ship speed
- Range of operating loading conditions
- Tank inspection requirements
- Different return period requirements compared with normal trading tankers.

For ocean-going vessels, classification rules specify corrosion control, coating requirements, corrosion prevention equipment/operation, and wall-thickness allowance, all based on 20 years of operating life. For FPSOs, additional wall-thickness allowance may be required considering factors such as:

- An FPSO may have a longer operating life.
- An FPSO requires no dry docking inspection.
- The cost for coating repair and reduced production is high.

Analysis Models

Five typical levels of modeling may be developed for the finite element analysis of the hull structure including:

- Global Structural Model (Model level 1)
- Cargo Tank Model and Turret Model for FPSO (Model level 2)

- Frame and Girder Model (Model level 3)
- Local Structural Analysis (Model level 4)
- Stress Concentration Models (Model level 5).

The 3D FEM models are developed for the following:

- Cargo tank area at midship
- Fore end area including the structure supporting the flare boom
- Module supports and the supporting structure
- Main crane pedestals supporting structure
- Porches for production/injection risers and export risers including the supporting structures, and pull-in supports
- Spread mooring attachments.

The structural design considers the loads that are imposed by the topsides, risers, and mooring connection. This consideration should be reflected in the FEM model. The main stress contributions include:

- Primary stress due to global hull girder bending
- Secondary stress due to panel bending between bulkheads
- Tertiary stress due to local plate bending between web frames.

Modeling for Ultimate Strength Analysis

A finite element analysis may be conducted to calculate global longitudinal stresses and global shear stress. For turreted FPSOs, it is necessary to predict the stress distribution around the openings, in particular at the deck and bottom, and at the ends of the longitudinal strength elements.

All relevant variations in a tank filling should be considered in the analysis and reflected in the Operation Manual. The following stress components can be found from the FEM analysis:

- Local transverse and longitudinal stresses
- Transverse stresses in web frames
- Double shell and double bottom stresses
- Local shear stresses in panels.

The combination of global and local stresses should account for actual stress directions and phases. However, if phase information is limited or uncertain, the maximum design value for each component should be combined as a “worst-case” scenario. A combination of typical stress components is shown in [Figure 11.5](#).

Internal static and dynamic pressures can be calculated using simplified formulas.

In some cases, detailed element mesh models may be necessary in order to check the maximum peak stresses and the possibility of repeated yielding, during the ultimate limit-state assessment.

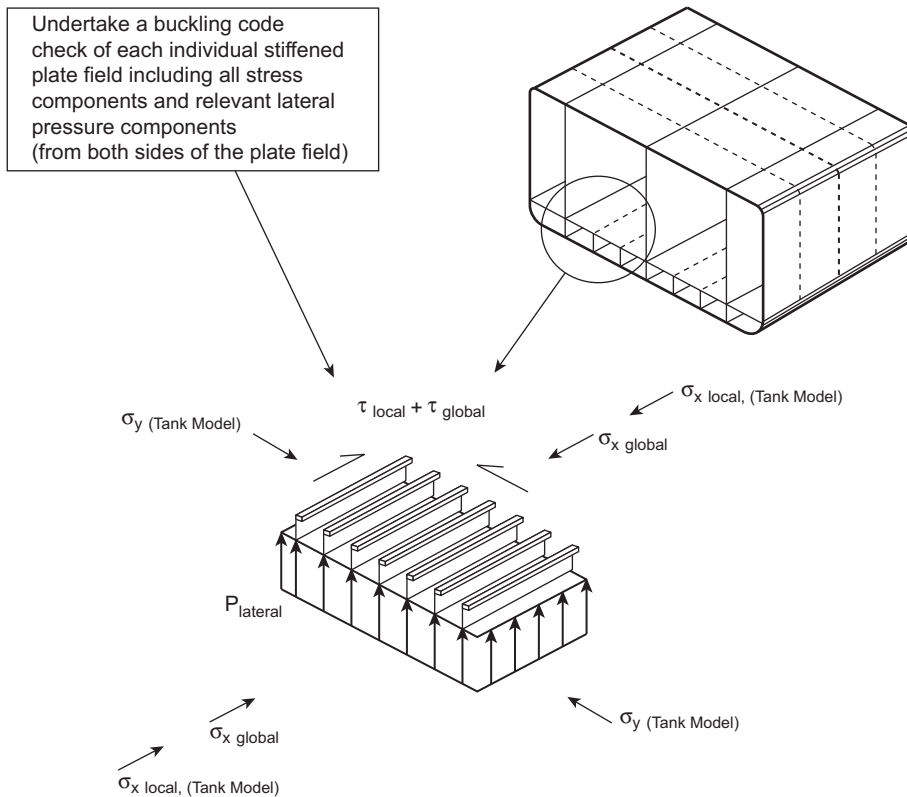


Figure 11.5
Typical stress components in the hull beam (NTS, 1998).

The hull girder strength should be evaluated to withstand relevant combinations of still water, wave-induced bending moments, and shear forces. The extreme hogging and sagging conditions are considered in the analysis. The appropriate site-specific environmental data should be applied in the analysis.

Transverse strength refers to the hull's ability to resist lateral pressure and racking actions in combination with longitudinal action effects. This resistance is provided by means of transverse bulkheads, web frames, girders, and stringers. Transverse strength should be evaluated using a finite element model of a specific portion of the hull, and the effects of deck equipment actions should be included.

Usually buckling and ultimate strength for plated members and stiffeners are checked based on NTS (1998) or API 2V or classification rules. Typical criteria for plated members and stiffeners are discussed in Chapter 16. The strength checks are carried out for main structures, secondary structures, and structures supporting hull appendages.

In some cases, the FPSO hull is also designed for collision, such that the collision, with supply vessels and shuttle tankers, does not cause penetration of the side or inner longitudinal bulkhead. Impacts from the bow, stern, and side of the supply vessels and shuttle tankers are all considered. Firefighting, explosion protection, and heat protection are all designed based on the risk assessment. See Part V for details.

[ABS \(2001\)](#) gives guidance on Safe Hull–Dynamic Loading Approach (DLA) for Floating Production Storage and Offloading Systems (FPSO). The DLA approach provides enhanced structural analysis to assess the capabilities and sufficiency of a structural design. A precondition to use DLA is that the initial scantling for hull structures is based on rule requirements. The results of a DLA analysis may not be used to reduce the dimension of the hull structures. However, if an increase of basic scantling is identified through the DLA analysis, such an increase is needed to meet the DLA requirement. The DLA analysis procedure consists of the following ([ABS, 2001](#)):

- Create sea-keeping analysis models
- Assemble hull loading scenarios and create still-water load file
- Obtain and verify environmental data
- Conduct analysis of ship motions and predict wave-induced loads and the extreme value for each DLP (Dominant Load Parameters, such as vertical hull girder bending moment amidships)
- Derive equivalent wave for each DLP
- Establish wave-induced load effects
- Create structural analysis for the defined load cases
- Conduct global and local structural analysis
- Check structural analysis results against acceptance criteria.

The benefits from conducting a finite element analysis like DLA analysis is the increased safety (by increasing scantling in the weak areas), reducing possible future renewals, and providing structural models that may be used immediately in the event of emergency situations.

Modeling for Compartmentalization and Stability

The relevant detrimental effects in the compartmentalization and stability assessment of an FPSO are:

- Environmental actions
- Relevant damage scenarios
- Rigid body motions
- The effects of free surface
- Boundary interactions (e.g., mooring and riser systems).

In order to determine the vessel's mass and the location of the center of gravity, an inclining test is conducted when the construction is near completion. In the Operational Manual, the vessel's center of gravity is recorded.

The number of openings in watertight structural elements should be kept to a minimum. Arrangements for access, piping, venting, cables, etc., should be made to ensure that the watertight integrity of the structure is maintained.

The stability of an FPSO should satisfy the requirements stated in relevant Codes. The requirements for stability are given in IMO regulations (resolution A167, A206, and A502, superseded by A749 (18)), IMO MODU Code (issued in 1989), and the classification rules. Adequate stability should be established for all relevant in-service and temporary phase conditions. The assessment of stability should consider both the intact and the damaged conditions.

Modeling for Fatigue Analysis

Fatigue-sensitive details and the materials selected should be documented to have sufficient fatigue strength for transportation and in-place conditions. Three levels of fatigue analysis may be conducted.

- A fatigue check based on simple stress formulas for scantling (primarily aimed at connections between longitudinal stiffeners and transverse web frames in the hull structure); see Section 27.11.
- A simplified fatigue assessment to check the allowable stress range assuming the long-term stress range follows the Weibull distribution; see Section 27.3.
- A spectral fatigue assessment based on the first principles; see Chapter 28.

The spectral fatigue assessment makes use of the wave scatter diagrams for the installation sites for in-place conditions and route-specific wave conditions for the transportation phase, which can be seen in Chapter 7. The wave scatter diagrams define the occurrence probability for various sea states defined by significant wave height and period. The analysis also takes into account the direction of the sea and swell conditions relative to the vessel heading.

Particular attention should be given to the connection details, which include:

- Integration of the mooring system with hull structure
- Main hull bottom, sides, and decks
- Main hull longitudinal stiffener connections to transverse frames and bulkheads
- Main hull attachments, seats, supports, etc.
- Openings in main hull
- Transverse frames
- Flare tower

- Riser porches
- Major process equipment seats.

Any turret structure will be exposed to high levels of dynamic action. The following actions should be considered throughout the fatigue design of turret structures:

- Dynamic fluctuations of mooring line tension
- Dynamic actions (tension and bending moment) from risers
- Local varying hydrodynamic pressure due to wave action and vessel motion
- Reactions in the bearing structure due to the other effects
- Inertia actions due to accelerations of vessel motions including variations in internal fluid pressure
- Fluctuating reactions in pipe supports due to thermal and pressure-induced pipe deflections.

Local stress ranges are determined from dynamic pressures acting on panels and accelerations acting on the equipment and topside. Other environmental actions also affect part of the structure as local stresses with a variety of ranges.

The transfer function for the dynamic pressure could be used directly to calculate local stress transfer functions and combined with the global stress transfer function, or a long-term pressure distribution could be calculated. At the least, the following dynamic pressure components should be considered:

- Double hull stresses due to bending of double hull sections between bulkheads
- Panel stresses due to bending of stiffened plate panels
- Plate bending stresses due to local plate bending.

Global and local stresses should be combined to give the total stress range for the details in question. The global and the local stress components differ in amplitude, phase, and location. The method of combining these stresses for the fatigue damage calculation will depend on the location of the structural detail.

Local, detailed FE analysis (e.g., unconventional details with insufficient knowledge about typical stress distribution) should be undertaken in order to identify local stress distributions, appropriate SCFs, and/or extrapolated stresses, which will be utilized in the fatigue evaluation. Dynamic stress variations through the plate thickness shall be documented and considered.

During the fatigue assessment, fine element mesh models will be developed for critical stress concentration details that do not comply with the stress concentration factors given in recognized standards. The size of the model should be such that the assumptions made for the boundary conditions do not significantly affect the calculated hot-spot stresses. Element sizes for stress concentration analysis should have the same order of magnitude as the plate thickness. Normally, shell elements may be used for the analysis.

The fatigue hot-spot stresses are obtained by combining stress components from the global hull girder bending, secondary and tertiary bending, and locally imposed loading. The stress concentration factors may be obtained using parametric equations or fine mesh finite element analysis of critical regions. Principal stresses are used in the evaluation of fatigue damage. The selection of S–N curves and methodologies for fatigue damage assessment are discussed in detail in Part III.

11.5.4 TLP, Spar, and Semisubmersible

A column-stabilized structure (semisubmersible or TLP) is defined as a floating installation, consisting of a deck structure with a number of widely spaced, large diameter, supporting columns that are attached to submerged pontoons.

Some special components of column-stabilized structures include:

- Ring (continuous) pontoons
- Twin pontoons
- Multifooting arrangements
- Tension legs (TLPs)

Such structures may be kept in position by a passive mooring system (e.g., anchor lines), an active mooring system (e.g., thrusters), or a combination of both.

In recent years Spar structures became a type of popular floating installations for use in the Gulf of Mexico, where the water depth is deeper than 1000 m. Air-filled buoyancy cans in the central moonpool of the hull support production risers. For truss spars, the bottom half of the spars consist of tubular truss and heave plate structures.

In the conceptual design phase, the design and analysis for TLP, Spar, and semisubmersible include:

- Establish design basis
- Select facilities and conduct system design
- Determine layout
- Size hulls and estimate global performance
- Design topside and hull structures
- Design risers and foundations such as piles for mooring/tethering
- Estimate weight, schedule, and costs for fabrication and installation
- Review HSE compliance and quality assurance.

Successful deepwater development depends on an experienced team using a system approach to select a concept, such for floating installations. [Dorgant et al. \(2001\)](#) presented

primary drivers for system selection for three major field development projects, and discussed technical/commercial/feasibility/regulatory issues for alternative facility systems (TLP, Spar, FPSO, and semisubmersible).

Demirbilek (1989) edited a couple of interesting articles on various design topics for TLP design and analysis, such as environmental criteria, hydrodynamic loads, structural analysis and criteria, foundation design and analysis, riser analysis, tendon analysis, fatigue design and fracture mechanics analysis, material selection, model tests, and measurement.

A floating installation may be designed to function in a number of modes, for example, transit, operational, and survival. The limiting design criteria include relevant considerations regarding the following:

- Structural strength under intact conditions
- Structural strength under damaged conditions
- Air gap
- Compartmentalization and stability.

For novel designs, where limited or no direct experience exists, relevant analysis and model testing should be conducted, in order to demonstrate that an acceptable level of safety is obtained.

The structure should be designed to resist relevant actions associated with conditions that may occur during all stages of the unit's life cycle, including:

- Fabrication
- Site moves
- Mating
- Sea transportation
- Installation
- Decommissioning.

It is generally more practical and efficient to analyze different action effects via a range of models, with the responses superimposed from each model, factored as relevant.

A simplified model may be applied for the preliminary design to establish approximate design responses and to get a feel of how the structure will behave.

The purpose of the global analysis model is to enable the assessment of the responses resulting from the global actions. An example of such a model is given in [Figure 11.6](#). Large, thin-walled structures, and three-dimensional finite element models created in a shell (or membrane), normally require finite elements. For space frame structures consisting of slender members, a three-dimensional space frame representation of the structure may be adequate.

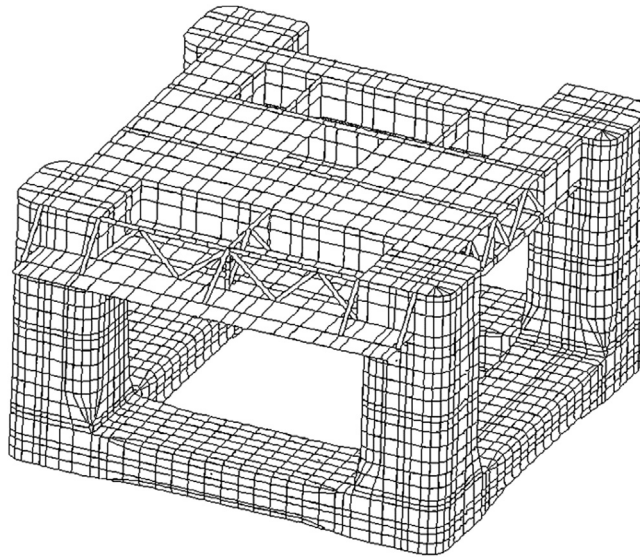


Figure 11.6
Example of global analysis model (NTS, 1998).

The stiffness of major structural connections (e.g., pontoon to column or column to deck) should be modeled in detail, in order to represent the stiffness of the connection. The hydrodynamic loading model may be mapped directly onto the structural model.

Typically, a simplified space–frame model of the structure may be created to obtain the maximum range of stresses in the tank for a range of tank loading conditions. These load conditions include both full and empty pontoons, which represent the maximum and minimum sagging and hogging conditions.

The simultaneity of the responses resulting from the global and local analysis models may normally be accounted for by a linear superposition with appropriate load factors.

In buckling and ultimate strength checks, relevant lateral pressure is applied together with in-plane forces. The criteria for plated members, stiffeners, and stiffened shells are available from classification rules, industry standards such as NORSOK N-004 (NTS, 1998), API 2U, and API 2V; see Chapters 16 and 17.

The ultimate strength criteria of TLP tethers under combined external pressure, tension, and bending may govern their design. These strength criteria may be modified using the formulation developed in the 1990s for strength design of deepwater pipelines and risers.

The fatigue assessment of TLP, Spar, and semisubmersibles is similar to that described for FPSO, see Part III.

References

- ABS, 2001. Guidance Notes on “SafeHull—Dynamic Loading Approach” for Floating Production, Storage and Offloading (FPSO) Systems. American Bureau of Shipping.
- API, 1987. Recommended practice for planning, designing, and constructing tension leg platforms, first ed.
- API, 1997a. Supplement 1 to the API RP 2A LRFD, first ed.
- API, 1997b. API RP 2T—Recommended Practice for Planning, Designing and Constructing Tension Leg Platforms, second ed.
- API, 2001a. API RP 2A WSD, Recommended Practice for Planning, Designing and Constructing Fixed Offshore Platforms—Working Stress Design, latest ed. American Petroleum Institute.
- API, 2001b. API RP 2FPS, Recommended Practice for Planning, Designing and Constructing Floating Production Systems, first ed.
- Bai, Y., Ayney, C., Huang, E., Maher, J., Parker, G., Song, R., Wang, M., 2001. Design and construction of floating production systems. In: Course Notes for an Industry Training Course Led by Yong Bai and Organised with Clarion Technical Conferences in Houston and IBC in London.
- Dawson, T.H., 1983. Offshore Structural Engineering. Prentice-Hall Inc.
- Demirbilek, Z., 1989. Tension Leg Platform—A State of the Art Review. American Society of Civil Engineers.
- Dorgant, P.L., Balint, S.W., Rodenbusch, G., Luyties, W.H., Rainey, R.M., 2001. System selection for deepwater production installations. In: Offshore Technology Conferences. OTC12966.
- Graff, W.J., 1981. Introduction to Offshore Structures—Design, Fabrication, Installation. Gulf Publishing Company, Houston, Texas.
- ISO Codes for Design of Offshore Structures (being drafted).
- ISSC, 1997. Design against Fire and Blast Loads. The Panel V.2 Report from International Ship and Offshore Structures Congress, Trondheim, Norway.
- NTS, 1998. NORSOK N-004, Design of Steel Structures. Norwegian Technology Standards Institution available from: www.nts.no/norsok.
- Zienkiewicz, O.C., 1977. The Finite Element Method. McGraw-Hill Book Company.

Development of Arctic Offshore Technology

12.1 Historical Background

Geographically, Arctic areas can be defined as lands to the north from the Arctic Circle, which is situated at latitude $66^{\circ}34'$. But from an engineering standpoint, this criterion is not so important, because geographic location does not solely influence the climate and other environmental conditions in this region. According to the definition commonly accepted in engineering practices, “Arctic” refers to those places where the average temperature for the warmest month of the year is less than 10°C (Freitag et al., 1997). From a construction point of view, Arctic region grounds can be divided into two areas: those with permanent or temporal permafrost, and those without any frozen ground. Figure 12.1 shows the circumpolar Arctic region, the countries it includes, the most significant oil reserves, and the location of the Arctic Circle. The red isothermal line borders areas where the average temperature for the warmest month is below 10°C (Brown et al., 1998); the yellow line shows the Arctic Circle; and gray areas indicate the largest oil fields located in the Arctic region (2011).

During the late 1970s and early 1980s, interest in Arctic research and development was very high due to anticipated resource development. In 1985, the Technology Development Center (TEKES) embarked on a five-year technology program intended to improve the competitiveness of Finnish industries (mainly shipbuilders and construction) on projects exploiting natural resources in Arctic areas. The program was one of 12 respected technology programs recommended in a 1984 statement by the Ministry of Trade and Industry’s “Technology Program Board.”

In the late 1980s, interest in Arctic development dropped, and consequentially the volume of related R&D declined to a minimum. This trend changed in the late 1990s and early 2000s when global warming became a global topic of interest. Evidence reveals that the ice cap in the Arctic has been shrinking year by year. The Northern Sea Route (NSR), which was historically impassable, has been opened for a small number of commercial ships during the summertime. Recently, the US government announced that it would permit further drilling in certain areas offshore Alaska. All of these events may imply the coming of another boom in Arctic development. These recent demands resulted from



Figure 12.1
Map of the Arctic region.

interest in exploring for oil and gas in the Arctic, and the potential of commercial shipping using Arctic routes. [Figure 12.2](#) shows the Arctic ice cap, which has been found to be retreating year by year. Accompanying this trend, as is shown in [Figure 12.3](#), research on ice-going ships and Arctic structures has been revived.

In fact, the original program proposal was for exploitation of the vast oil and natural gas deposits in Arctic areas (shown in [Figure 12.4](#)) for the near future. It was clearly necessary to obtain further information and carry out more research in order to gather basic data for structural designs that is suitable for the extreme climatic conditions found

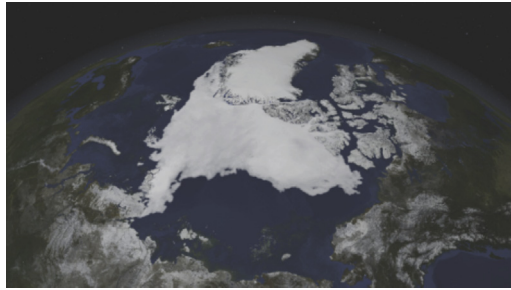


Figure 12.2
Arctic ice cap.

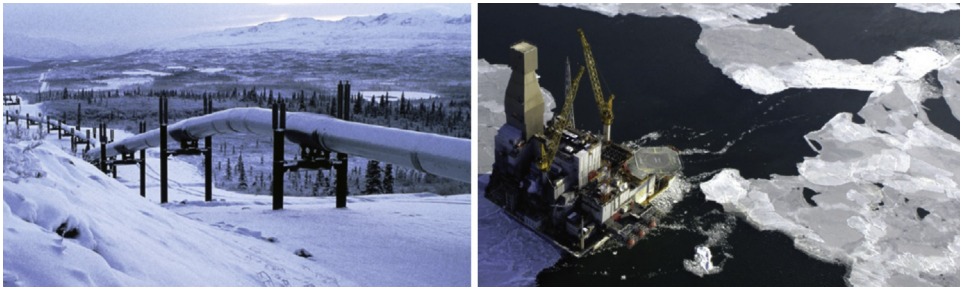


Figure 12.3
Research on arctic structures.

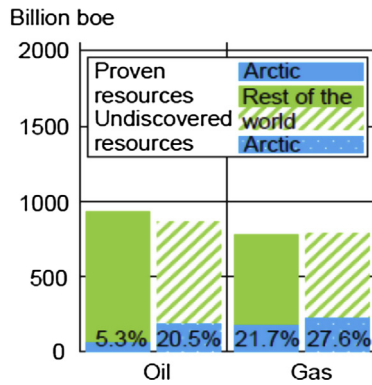


Figure 12.4
Percentage of Arctic oil and gas reserves, replotted from Kwak et al. (2010).

in Arctic offshore areas. Considerable research efforts went into materials technology, specifically for the application of concrete in Arctic structures. In addition, techniques related to ice model testing and measurements of ice forces were developed and discussed within the course of the program. Most of Finland lies north of the 60th

parallel; the mean annual temperature ranges from $+5\text{ }^{\circ}\text{C}$ to $-1\text{ }^{\circ}\text{C}$, and the mean length of winter is from 100 to 200 days. Temperatures below $-40\text{ }^{\circ}\text{C}$ are commonly recorded, and the freezing index may approach 300 days in the northernmost parts of the country. Yet, the relatively warm summers permit extensive agriculture and forestry.

In the subarctic environment, Finnish construction and materials industries have developed their own specialized technologies; midwinter construction is now commonplace. Modified and improved construction materials have been developed to meet rigorous environmental requirements, including extreme low temperatures where conventional materials are unusable. Special steel grades for Arctic applications are a well-known example.

12.2 *The Research Incentive*

Cold region engineering research in Finland has developed in response to urgent needs; however, most practical solutions in civil engineering and naval architecture were first achieved by trial and error. Research often started as troubleshooting. Furthermore, the basic incentive for research that comes from real life has been intensified by the demands of international competition, which require improvements in structural economy and safety.

The winter environment is certainly the first “laboratory” to be used in Arctic technology research. The frozen sea that surrounds Finland, and its thousands of icebound lakes, provided plentiful opportunities for ship trails and field ice tests. More than 100 ships have been full-scale tested since the 1960s to investigate ice resistance, propulsion, steering, and hull strength. A basic test with a small ship may be cheaper than an ice model test with a scale model in an instrumented model basin facility. For years, Finland’s engineers have been involved in the field study of ice and frost action on actual structures—bridges, piers, lighthouses, and lock facilities.

Rational model test technologies were not developed before the 1970s. From the beginning, the simultaneous fulfillment of geometric, kinematic, and dynamic similarities was a struggle. The difficulty lay in the proper scaling of ice properties. Today, all major projects rely on both field tests and physical and mathematical modeling.

Refrigerated cold rooms are commonly used for material and structural research. In addition to the study of basic mechanical and physical properties at low temperatures, cold rooms are used for dynamic strength and ductility testing, freeze–thaw resistance testing, abrasion testing, and building materials evaluations. Temperatures in some cold rooms can go down to $-60\text{ }^{\circ}\text{C}$, and the means to create rapid temperature fluctuations are available (Figure 12.5).



Figure 12.5
Model testing of ice–structure interaction.

12.3 Industrial Development in Cold Regions

Above latitude 60° north, well-developed industrial and civil infrastructures only exist in Scandinavia, the Soviet Kola area, and Southeast Alaska. Development elsewhere has been concentrated mainly around a few mineral and hydrocarbon deposits and on harbors along the Soviet NSR.

On the other hand, it has been estimated that perhaps 30% of the world's undiscovered hydrocarbon resources lie in Arctic or subarctic areas. Here the potential for strategic minerals, hydropower, and forest products is also very large. A significant portion of exports from southern Siberia must be transported via the NSR.

The growing need to exploit natural resources of northern regions is already apparent in the Soviet Union, and will become increasingly important in North America in coming years. Arctic industrial output will increase with the growing diversity of industrial infrastructures and transportation networks. It is likely that within the next century, development of industrial infrastructures above the 60th parallel will follow the evolutionary course seen in Scandinavia.

12.3.1 Arctic Ships

The diverse range of activities in the Arctic and Antarctic, like increased shipping and oil and gas developments, will require the operation of a wide range of vessel types and sizes. Operational experience to date has primarily been limited to escort and research icebreakers and relatively small cargo ships, coastal tankers, and bulk carriers (as it is shown in [Figure 12.6](#)). Recently built icebreaking tankers have deadweight capacities less than 100,000 metric tons, even though much larger sizes have been proposed for tankers, liquefied natural gas carriers, and bulk carriers since the early 1970s. Commercial resource developments will also require supply vessels, tugs, and dedicated icebreakers.



Figure 12.6
Some kinds of Arctic ships.

Finally, governments intending to enforce laws and provide emergency responses will need a year-round presence in all areas with commercial development and along proposed shipping routes. A variety of different vessels will be required to satisfy these needs. Because these vessels will be designed to operate in a wide range of ice conditions and climates, some operators will elect to operate year-round, while others will choose seasonal operations. Depending on the specific geographic area of operation and the season, the design ice conditions could include:

- open water with occasional small, thin ice floes,
- first-year ice with coverage from 5% to 100% and thicknesses from several centimeters to two meters,
- compact first-year ice with large pressure ridges and rafting,
- thick multiyear ice with weathered-consolidated pressure ridges,
- other possible operating conditions would include open water with occasional large ice features such as icebergs, bergy bits, growlers, or ice floes.

12.3.2 Offshore Structures

According to [Novitsky et al. \(2009\)](#), offshore structures are generally divided into fixed and mobile. Each group can then be split based on different criteria such as body material or type of stability support. Offshore platforms can be divided into four groups based on operating depth: shallow (≤ 30 m), average depth (30–150 m), deepwater (150–350 m), and ultra-deepwater (≥ 350 m). [Figure 12.7](#) shows various types of offshore structures and their operating depths. From a structural point of view, an offshore platform can be either fixed at the seabed or buoyant. Typically, buoyant platforms operate in deeper areas.

Extensive offshore exploration activities in Canada and Alaska from the 1960s into the 1980s were mostly land based. In 1983, specially designed drilling unit Kulluk was put into operation, drilling in limited level ice. Oil and gas has been produced in approximately 50 m water depths using jacket wellhead platforms and jack-up-based production.

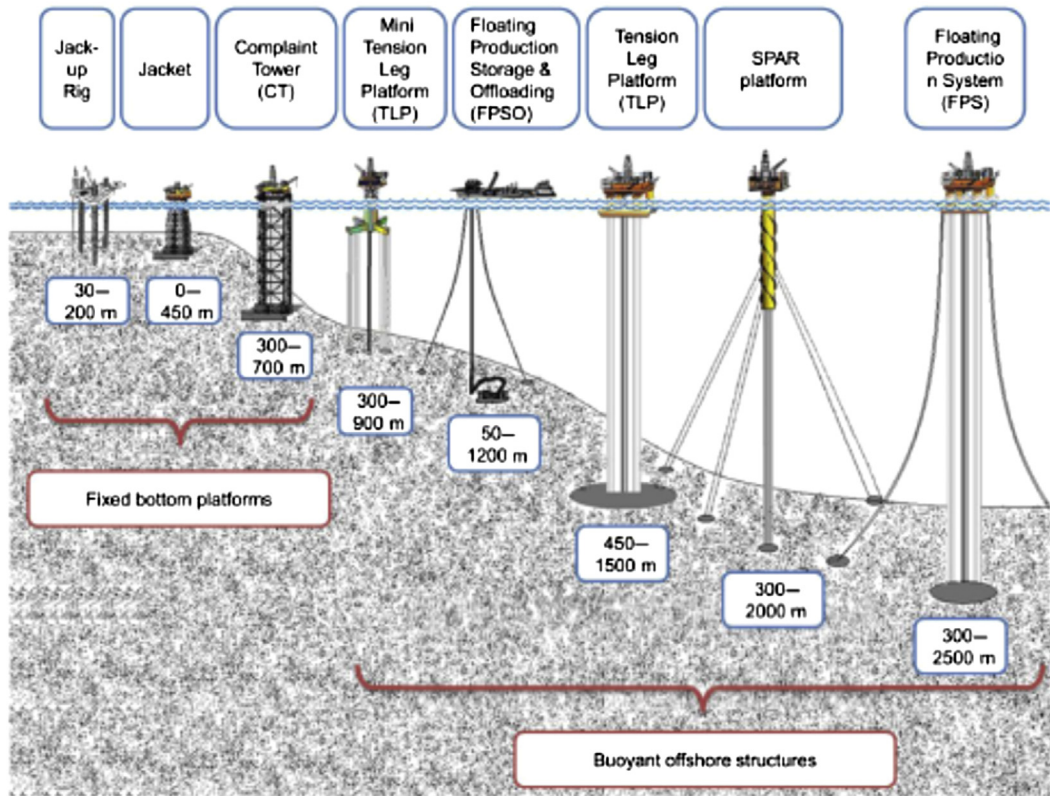
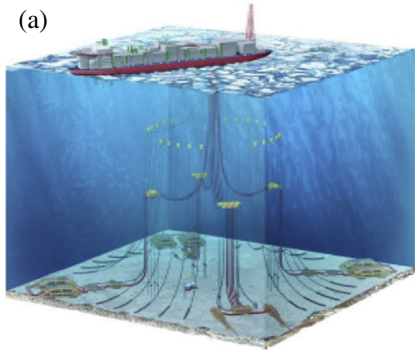


Figure 12.7

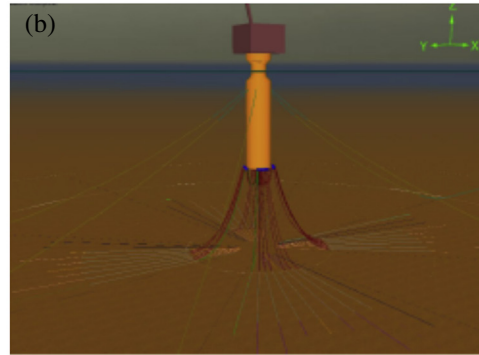
Different types of offshore structures based on sea depth, replotted from [Kobe \(2011\)](#).

Along the Canadian East Coast, the Hibernia, Terra Nova, and White Rose oil fields use bottom-founded, “iceberg-proof,” or disconnectable FPSO production facilities that can leave their locations when threatened by icebergs. In the Russian Arctic region, northern oil and gas activities are mainly onshore. The Varandey field includes an offshore loading facility approximately 21 km from shore at a water depth of 17.5 m. Oil is loaded onto shuttle tankers that have icebreaking capacities. The Prirazlomnoye oil field adopts a square ice-resistant gravity platform ([Velikhov et al., 2010](#)). This innovative platform is built by Sevmash in Severodvinsk, towed to the field, and ballasted down to sit on the seabed. It combines all aspects of drilling, production, storage, and offloading.

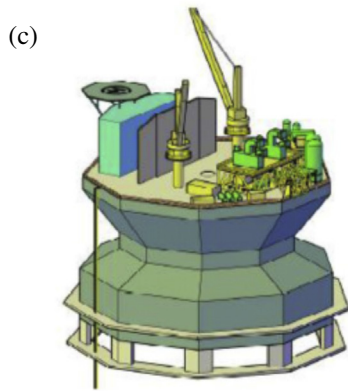
The ISO 19906 standard gives a general basis for the design of Arctic offshore structures. The design has to be further developed by following design standards from classification societies. It is also necessary to strike a balance between the requirements for ice-sea environments during the winter and open-sea environments during the summer, as shown in [Figure 12.8](#) ([Marechal et al., 2011](#); [Sablok et al., 2011](#); [Srinivasan et al., 2011](#); [Dalane et al., 2009](#); [Bereznitski et al., 2011](#)).



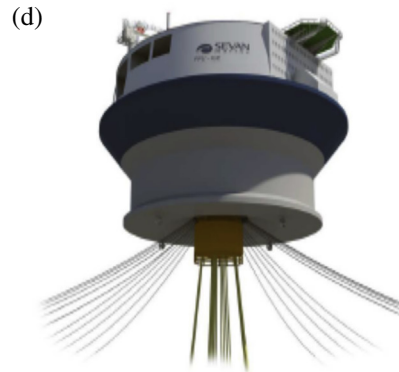
Shtokman field



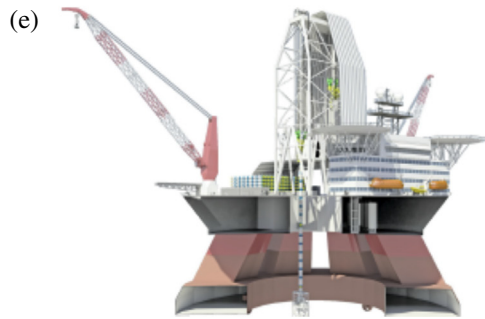
Disconnectable spar



Circular FPSO



Alternative circular FPSO



Circular MODU

Figure 12.8

Some proposed concepts for Arctic floating structures.

12.4 The Arctic Offshore Technology Program

When the Finnish Ministry of Trade and Industry began to develop technology programs as a component of industrial policy, the selection of Arctic offshore technology as a major research and development effort was quite natural. Finland had already established a formidable position in this highly specialized technology field. From a strategic point of view, industrial development of the northern regions was seen as inevitable. Since World War II, Finnish industries have established an impressive record as exporters of Arctic technology. The potential for further exports could in fact be predicted. During the past decade, the international development of Arctic technology has rapidly increased. A strong commitment to the improvement of Arctic offshore technologies was seen to be essential in assuring the continued competitiveness of Finnish industries.

12.4.1 Three Areas of Focus

The technology program titled “Development of Arctic Offshore Technology” consists of 18 research projects focusing on three basic themes:

- Interactions between structures (ships or fixed) and ice
- Construction materials technology
- Support functions for Arctic development

Some projects were initiated by academic and governmental research organizations, and some were initiated by industry. Research proposals underwent a strict review and selection process. Factors that characterized successful proposals include:

- The relevance and importance of the problem to be studied
- The likelihood of achieving significant results with the fixed funding allocation
- Evidence of interest and concern by industry
- Close relationships to wider national problems or historical challenges.

Quite often, product development work is a good guide to those areas where new basic research is needed. In this case, initial development work occurred mainly for the heavy metals, construction, building materials, and petroleum industries.

12.4.2 Environmental and Climatic Change

According to the National Snow and Ice Data Center, Arctic sea ice extent is declining at a rate of 3.5% per decade. Particularly, the Arctic ice cap in the summer of 2007 was 4.2e6 km², which marked the lowest record (23% less than the high record of September 2005). Some studies estimate that the Arctic could become ice-free during the summer months in a few decades (Wang et al., 2009). Reports also suggest increasing variability in ice extent.

In situ measurements have reported that Arctic ice has been thinning (Rothrock et al., 1999). Substantial amounts of older perennial ice have been observed drifting out of the Arctic through the Fram Strait (Rigor et al., 2004). These environmental changes may result in a need for reevaluation of ice loads that are the basis of structural design. So far, there is only very limited research on potential changes in ice loads based on the long-term decreasing trend in measured peak ice loads (Matsuzawa et al., 2010). Melting ice gives rise to the likelihood of iceberg collision (Hill B. T. 2006), which is not adequately addressed in existing design codes or safety regulations.

12.4.3 Materials for the Arctic

A wide variety of steel and concrete structures have been designed for the Arctic and subarctic; these structures are designed to resist high lateral forces from the ice and to transmit those forces down to foundation soils. The main challenge for conventional steels under Arctic conditions is brittle fracture behavior below a certain temperature. This phenomenon has already caused many serious accidents, as steels for Arctic operation must stay ductile at low temperatures. Therefore, this property of steels should be examined carefully and extensively before choosing a certain steel grade.

The success of engineering solutions largely depends on the materials selected. Under Arctic conditions, materials should meet different criteria, which typically include (Odessky, 2006; Gorynin et al., 2007):

- Low temperature toughness down to -60°C
- Yield strength requirements of 235–690 MPa
- Isotropy of properties across dimensions of material
- Resistance to forming brittle fracture
- Reasonable weld ability without preheat and postheat treatment (or with minimal preheat temperature required)
- Good corrosion resistance for marine applications
- Capability of withstanding static and dynamic wind and wave loads according to operational parameters
- High strength that allows for reduction in the weight of structures
- Reasonable elongation for construction work within a wide range of temperatures.

The three main trends in modern cold-resistant steel development (Gorynin et al., 2007) are:

- Improving the quality of already developed and used materials
- Creating new steel grades that include high strength, improved weld ability, and other useful properties
- Improving the steel manufacturing process in order to increase quality levels and lower costs.

Table 12.1: Some materials used in Arctic structures

Steel Grade	Operating Temperature, °C	Weldability	Applications	Yield Strength, MPa	KCU, J cm ⁻² , (-40 °C to 70 °C)
Ст3	-50	+	Constructions without significant loads	450	≥5
20	-30 to 40	++	Cases, vessels, pipes	400	n/a
45	-50	+/-	Pipes, nuts, bolts	400	n/a
09Г2С	-70	+	Steel structures	300	≥30
10Г2	-70	++	Sheet metal structures	420	150
16ГС	-70	+	Pipes, welded structures	480	≥25
14Г2АФ	-50	+/-	Vessels	530	n/a
18Г2Ф	-30 to 60	+/-	Steel structures	440	29
20Х	-50	+/-	Wearing applications, pipes	800	150
40ХН	-60	-	Heavy-loaded structures, gears	800	≥40
30ХН2МФА	-70 to 196	+/-	Critical parts	950	160
38ХН3МФА	-70	-	Critical parts, rotors	850	≥60
10ХСНД	-70	++	Shipbuilding, ship hulls	600	≥35
12ХН3А	-60 to 125	+/-	Shafts, pipes	800	≥70
12Х2Н4А	-60	n/a	Large parts	930	91

These trends are encouraged by increasing interest in the Arctic region by the oil and gas production industries. Moreover, as mentioned earlier, the Arctic region has satisfactory conditions for wind turbine operations that can be placed offshore (Table 12.1).

12.5 Highlights

The wide-ranging nature of the TEKES program resulted in few results with immediate applicability, yet the extensive body of new knowledge shown in project reports and publications represents a major addition to marine and mechanical engineering literature.

In some cases, data analysis will continue after the technology program has been completed. Hopefully the real value of some results will be demonstrated in future product developments and practical applications. Typical projects are described in the following.

12.5.1 Mechanical Resistance to Slip Movement in Level Ice

Mechanical friction was known to influence all ice-resistance components. Resistance predictions from ice model tests are sensitive to the friction coefficients assigned to the models. Yet, measured values of the friction coefficient depend on the testing

method and the normal force. There is a clear potential to reduce ship icebreaking resistance by improving the hull coating in order to reduce friction.

The numerical model includes edge crushing and the bending of a floating ice beam, and the potential flow due to the motion of ice sheets and vessel advances. Simulating a full potential flow with remote boundaries is a sophisticated way of including the entrained mass of water. Ventilation above the deflected ice sheet is considered. The cycle is numerically analyzed and then recomputed until the broken slab is turned flat against the bow. The rotation of the slab is described by the Euler–Lagrange formulation and time-dependent coordinate mapping. Time integration is done by means of the Adams–Moulton predictor-corrector method. Presently, an extension to the three-dimensional case does not seem feasible with conventional computer capacities.

A comparison between experimental and computed results confirms a satisfactory correlation. Maximum forces are strongly velocity dependent, but average forces are not.

12.5.2 Ice Forces on Fixed Structures

Numerous ice events have relevance in the design of fixed offshore structures. The most important are those that may endanger the overall stability or serviceability of the structure. The nature of these events depends on the local ice environment and the type of structure.

A conical shape has been proposed for offshore structures such as oil platforms in ice-covered sea areas. Theoretically, this shape reduces ice loads substantially, compared with vertical cylindrical shapes. However, experience with such structures in dynamic ice conditions was practically nonexistent. Model tests alone are not considered reliable because of problems associated with the added effects of rubble, freezing, and impacting ridges. Conservative design assumptions would wipe out the benefits believed to be inherent in the conical shape (Figure 12.9).

Ice features need horizontal forces to come into motion. The applied forces include two parts: wind stress (τ_w) and current stress (τ_c). Floating ice sheets can start drifting due to the wind and currents. The drift speed is in relation with the drag forces on the ice sheet during motion as indicated in Figure 12.10 (Bjerkås, 2006).

According to Bjerkås, M., there exist six methods to record ice actions:

- Interfacial methods
- Hinged beams
- Structural response
- Hindcast calculations
- Newton's second law
- Ice stress measurements



Figure 12.9
Ice forces on fixed structures.

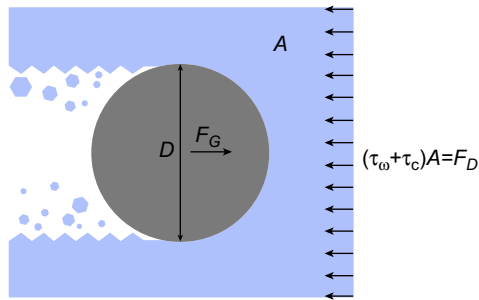


Figure 12.10
Cross-section of an offshore structure under wind and current stresses.

The recommended practice for ice load is to design for the crushing of ice. The following formula is from API Bulletin 2N:

$$F_h = IK\sigma_c Dh \quad (12.1)$$

where F_h = horizontal ice force, I = indentation factor, K = contact factor, σ_c = unconfined compressive strength of ice, D = diameter or width of the structure in contact with ice, and h = ice thickness.

The presented formula was first developed from plasticity limit analysis (Hill, 1950; Michel, 1978). The indentation factor has a relationship with the aspect ratio of the structure (D/h); the following values are based on the test data:

$$I = 4.5 \quad \text{for} \quad D/h = 0 \quad (12.2)$$

$$I = 3.3 \quad \text{for} \quad D/h > 2 \quad (12.3)$$

The basis of the limiting stress approach is the study of the penetration of an ice sheet by an offshore structure acting as a rigid indenter (Wong et al., 1988). Based on the work

done by Korzhavin (1962), Neil (1976) presented a semiempirical formula for ice action on bridge abutments:

$$\sigma_e = \frac{I}{(v/v_0)^{1/3}} mK\sigma_c \quad (12.4)$$

where σ_e = effective ice pressure (MPa), I = semiempirical indentation factor = 2.5 for $b/D > 15$, b = ice sheet width (m), D = structure width (m), m = shape factor = 1 for flat rectangular shapes, K = coefficient of contact = 0.4–1.0, σ_c = unconfined compressive strength (MPa), v = velocity of ice (ms^{-1}), and v_0 = reference velocity = 1.0 ms^{-1} .

A more common form is to include velocity effects in the definition of the compressive strength of the ice:

$$\sigma_e = ImK\sigma_c \quad (12.5)$$

12.5.3 Concrete Durability in Arctic Offshore Structures

Arctic offshore structures are subjected to severe combined mechanical, physical, and chemical attacks, especially near the waterline. A unique Arctic feature is ice abrasion, yet there is very little information about ice abrasion damage to concrete structures. Finnish lighthouses have stood for more than two decades in dynamic ice environments. Many have shown severe deterioration just below the mean water level. However, it is hard to distinguish the damage caused by ice abrasion arising from frost. Moreover, information on the magnitude and direction of ice movements in the vicinity of each lighthouse is nonexistent, making it impossible to extrapolate this fragmentary evidence to new ice environments and new structures built with greatly improved concrete technology. Significant differences were found in the abrasion resistance of different concretes after they were subjected to the combined effects of seawater exposure and freeze–thaw cycling.

12.6 Conclusion

When the industry confronts the increasing need to transport expensive and essential materials through severe ice conditions, the Finnish capacity to design a new generation of ships has proved ready. The results already achieved within this technology program promise that such ships will have lighter yet stronger structures, highly efficient propulsion systems, low-drag-resistance hulls, and superior maneuverability. Even for extrapolation to significantly greater tonnages, the solid technical background and improved modeling tools developed in this program will minimize prototype risks.

References

- Arctic Oil and Natural Gas Resources, 2011. United States Energy Information Administration (December). www.eia.doe.gov.
- Bereznitski, A., Roodenburg, D., 2011. In: JBF Arctic - a Mobile Offshore Drilling Unit with High Performance in Ice Covered Waters and in Open Seas, Offshore Technology Conference.
- Brown, J., Ferrians Jr., O.J., Heginbottom, J.A., Melnikov, E.S., 1998. Circum-Arctic Map of Permafrost and Ground-Ice Conditions. revised February 2001. National Snow and Ice Data Center/World Data Center for Glaciology. Digital Media, Boulder, CO.
- Bjerkås, M., 2006. Ice Actions on Offshore Structures[D] (Doctoral thesis). Norwegian University of Science and Technology, Trondheim, Norway (to be published).
- Dalane, O., Aksnes, V., Aarsnes, J.V., 2009. In: A Moored Arctic Floater in First-year Sea Ice Ridges, 28th International Conference on Ocean, Offshore and Arctic Engineering, Honolulu, HI, 31 May-5 June.
- Freitag, D.R., McFadden, T.T., 1997. Introduction to Cold Regions Engineering. ASCE Publications, p. 2, 110.
- Gorynin, V., Malushevskiy, P., 2007. Creating and introducing of new materials. *Morskoy Vestnik* 3 (6), 74–77 (in Russian).
- Hill, B.T., 2006. Ship Iceberg Collision Database. National Research Council of Canada.
- Hill, R., 1950. *The Mathematical Theory of Plasticity*. Oxford University Press, Oxford, United Kingdom.
- Kwak, M., Choi, J., Park, S., Kang, J., 2010. Strength assessment for bow structure of Arctic tanker (107K) under ship-ice interaction. *Journal of Offshore and Polar Engineering*, 28–29.
- Kobe steel, 2011. In: Meeting the Requirements of 610 MPa High Tensile Strength Steel and Low Temperature Service, *KOBELCO Welding Today*, No. 14, p. 1.
- Korzhasin, K.N., 1962. Action of Ice on Engineering Structures. Translated by United States Joint Publication Research Service for United States Army, Cold Regions Research & Engineering Laboratory, 1971.
- Matsuzawa, T., Takimoto, T., Shimoda, H., Wako, D., 2010. In: Five-Year Observations of Ship Hull Ice Load in the Southern Sea of Okhotsk, 20th IAHR International Symposium on Ice.
- Marechal, G. Le, Anslot, P., Mravak, Z., Liferov, P., Guennec, S. Le, 2011. In: Design of a Floating Platform Hull for Arctic Conditions in the Barents Sea, Arctic Technology Conference, Houston, TX, February.
- Michel, B., 1978. *Ice Mechanics*. Laval University Press, Quebec, Que.
- Novitsky, I.G., Portnoy, A.S., Razuvaev, V.N., 2009. Design of Offshore Platforms. Requirements of Standards (in Russian) *SPBGMTY*, pp. 8–10, 48–54, 72–75, 112–113.
- Neill, C.R., 1976. Dynamic ice forces on piers and piles. An assessment of design guidelines in the light of recent research. *Canadian Journal of Civil Engineering* 3, 304–341.
- Odessky, P.D., 2006. Microalloying of Steels for the North and Unique Metal Structures (in Russian). *Internet Engineering*, Moscow, p. 28.
- Rothrock, D.A., Yu, Y., Maykut, G.A., 1999. Thinning of the Arctic sea-ice cover. *Geo-physical Research Letters* 26 (23), 3469–3472.
- Rigor, I.G., Wallace, J.M., 2004. Variations in the age of Arctic sea ice and summer sea ice extent. *Geophysical Research Letters* 31.
- Sablok, A., Ramachandran, M., Kim, J.W., 2011. In: Disconnectable Arctic Spar, Arctic Technology Conference, Houston, TX, February.
- Srinivasan, N., Sreedhar, M.S., 2011. In: Circular FPSO for Arctic Deep Water, Arctic Technology Conference, Houston, TX, February.
- Velikhov, E.P., Kuznetsov, V.P., Makarov, V.I., Mikhailichenko, V.V., Lavkovskiy, S.A., Glumov, I.F., 2010. What's Going on in the Russian Arctic. *ICETECH*, Anchorage, Alaska, pp. 36–37.
- Wang, M., Overland, J.E., 2009. A sea ice free summer Arctic within 30 years. *Geo-physical Research Letters*.
- Wang, T.T., Sego, D.C., 1988. Design requirement for ice forces. *Canadian Geotechnical Journal* 26 (4), 524–535.

Limit-State Design of Offshore Structures

13.1 Limit-State Design

In this section, the concept of limit-state design is introduced to allow an assessment that considers the following limit states:

- ULS—Ultimate limit state—ultimate strength behavior
- FLS—Fatigue limit state—fatigue and fracture behavior
- SLS—Serviceability limit state—displacements and deflections
- ALS—Accidental limit state—collisions, fires, blasts, and dropped objects.

In general, the structure will need to be checked for all groups of limit states to ensure sufficient safety margins between the maximum likely loads and minimum resistance of the structure.

The general safety format for limit-state design is expressed as

$$S_d \leq R_d \quad (13.1)$$

where

$S_d = \sum S_k \cdot \gamma_f$ Design action effect

$R_d = \sum R_k / \gamma_m$ Design resistance

$S_k =$ Characteristic action effect

$R_k =$ Characteristic resistance

$\gamma_f =$ Action (load) factor

$\gamma_m =$ Material factor (equals the inverse of the resistance factor)

Both the load and the resistance factors may comprise subfactors that reflect the uncertainties and safety requirements of load effects and resistance.

Extreme care is required in the finite element analysis (FEA) to ensure that the correct load and resistance factors have been applied, particularly when several models are being used and the results are linearly superimposed.

In marine-specific FEA programs, the relevant code of practice can be selected by the analyst. This allows appropriate design formulae to be chosen and the material factor to be defined by the analyst prior to postprocessing the results. The user will generally have to

select the load factors prior to the definition of load combinations and ensure inclusion of the material factors.

When a fine mesh is modeled for a local detailed analysis, the loads and boundary conditions may be taken from a more simplified analysis, which may either include the load factors or be supplied unfactored. Therefore, it is recommended that all basic loads be tabulated along with the appropriate factors for the limit states considered. In this table, it should be clearly stated whether load factors are included in the basic loads.

13.2 ULS Design

The codes generally require that the ULS of the structure complies with two conditions: ULS-A reflecting extreme permanent loads with regular environmental conditions, and ULS-B reflecting large permanent loads with extreme environmental conditions.

The structural analysis may be carried out as linear elastic, simplified rigid-plastic, or elastic–plastic.

13.2.1 Ductility and Brittle Fracture Avoidance

Ductile failure modes will allow the structure to redistribute the forces in accordance with the structural model. However, regardless of the analysis method used, the model will not be able to fully represent the redistribution of forces. The redistribution of forces in the structure will avoid brittle fracture modes or at least verify their excess capacity in relation to the ductile failure modes.

Brittle fracture should be considered in the following areas:

- Unstable fracture caused by a combination of brittle material, high local stresses, and weld defects
- Details where ultimate capacity is reached with only limited plastic deformation, thus making the global behavior brittle

Unstable fracture may occur under unfavorable combinations of geometry, fracture toughness, welding defects, and stress levels, with the risk of such failures being the greatest in steels of high thickness (i.e., >40 mm) that are undergoing a deformation.

In general, the steel structure will meet requirements for adequate ductility when

- material toughness requirements are met;
- combinations of high local stresses and undetected weld defects are avoided;
- details are designed to develop plastic deformation;
- components do not exhibit a sudden drop in capacity when deformations continue beyond the maximum capacity;
- local and global buckling interactions are avoided.

The maximum allowable defect size can be calculated based on the total stress or strain and the design fracture toughness using a fracture mechanics approach. It should be shown that both the maximum undetected defect following fabrication and the maximum crack size following fatigue loading over the design life of the structures will be less than the maximum allowable defect size.

13.2.2 Plated Structures

The failure modes to be considered for plate structures are

- yielding of the plates;
- buckling of slender plates due to in-plane compressive stresses and lateral pressure;
- buckling of plates due to concentrated patch loads.

The plate panel may be part of a box girder, pontoon, hull, integrated plated deck, or merely a web or flange on a simple beam member. An example of a stiffened plate panel is shown below.

Ultimate strength capacity checks shall be performed, for all structural components, directly to the longitudinal and transverse strength of the structure. Checking of structural components must include all plates and continuous stiffeners, such as

- main deck, bottom, and inner bottom;
- ship side, inner ship side, and longitudinal bulkheads;
- stringers and longitudinal girders;
- foundations of turret and topside structures;
- transverse bulkheads;
- transverse web frames.

In FEA, the plated area will generally be formed as one unit of simple panel elements. If the panel is stiffened, this strengthening may be ignored in an initial assessment to avoid the need for inclusion of all structural components, with some or all of the stiffening included in subsequent analyses. While this is a valid approach, the effect of plate stiffening upon the ductility of the structure should not be overlooked. Furthermore, if detailed stiffening is added, the analyst should consider the fabrication and inspection consequences of stiffening. For example, questions could include: “Can the welder get sufficient access to the area?”; “Will the weld type be limited (e.g., is only a single-sided welding possible)?”; “Will the weld detail cause a local stress concentration?”; and “What are the possibilities for the inspection of the weld postfabrication and in-service, if required?”

Plated sections of beams (i.e., web and flange sections) or the walls of box sections will be defined as standard sections in the FEA program and will be checked against the appropriate code without the need for additional hand checks. However, for joints in

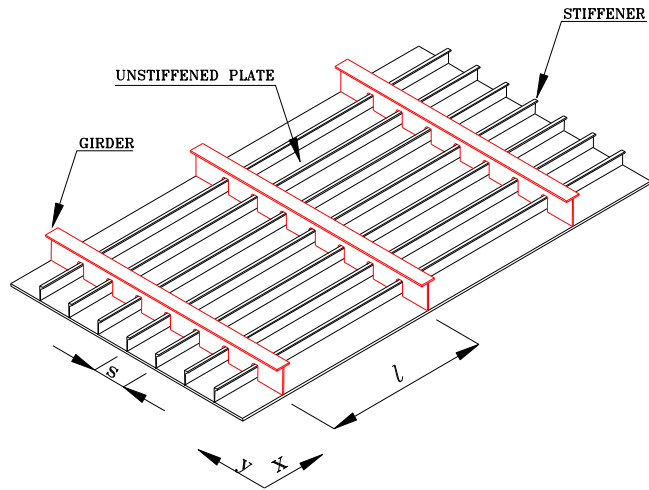


Figure 13.1
Stiffened panel (NTS, 1998).

particular, forces will often need to be taken using FEA and used in either hand or spreadsheet calculations to establish if sufficient strength exists.

The FEA program will generally center both the panel and the stiffeners on the nodal points for stiffened panels. Therefore, a horizontal deck panel's plate will appear to run through the center of the stiffeners, rather than being supported on the stiffener ends, see [Figure 13.1](#). There may also be a small inconsistency with the elevation, since the nodes may be based on the top-of-steel or bottom-of-steel coordinates rather than the centerline of the plate as it would be when modeled. In both cases, offsets can be modeled to give the correct visual appearance; however, this is generally unnecessary for the calculation of stresses in the model.

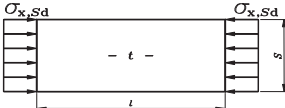
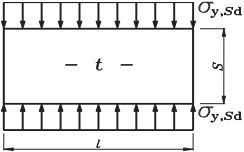
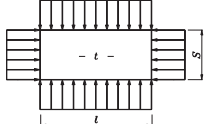
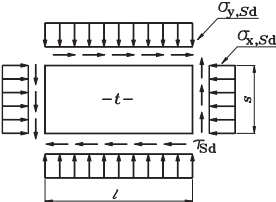
NORSOK N-004 gives a useful reference table for buckling checks of plate panels under different loading conditions. The recommended reference for the check is in NORSOK, NS 3472, or Eurocode 3. The most useful are the limiting values in the following section, which state where buckling checks are not necessary. These tables are reproduced in [Table 13.1](#).

13.2.3 Shell Structures

Unstiffened and ring-stiffened cylindrical shells subjected to axial forces, bending moments, and hydrostatic pressures may be designed as tubular members or, in a more refined analysis, as a shell structure.

A tubular section in air with a diameter-to-thickness ratio in excess of 60 is likely to fail by local buckling at an axial stress less than the material yield strength. The failure capacity of members that fail due to local buckling is more sensitive to geometric imperfections than it is for members that can sustain yielding over the thickness, which

Table 13.1: Limiting values for buckling checks of plate panels under different loading conditions

Description	Load	Sketch	Code Reference	Limiting Value
Unstiffened plate	Longitudinal compression		NORSOK	$s < l$ buckling check not necessary if $\frac{s}{t} \leq 42\epsilon$
Unstiffened plate	Transverse compression		NORSOK	$s < l$ buckling check not necessary if $\frac{s}{t} \leq 5.4\epsilon$
Unstiffened plate	Combined longitudinal and transverse compression		NORSOK	$s < l$ buckling check not necessary if $\frac{s}{t} \leq 5.4\epsilon$
$s < l$ buckling check not necessary if $\frac{s}{t} \leq 5.4\epsilon$	Combined longitudinal and transverse compression and shear		NORSOK	

Continued

Table 13.1: Limiting values for buckling checks of plate panels under different loading conditions—cont'd

Description	Load	Sketch	Code Reference	Limiting Value
Unstiffened plate	Pure bending and shear		NS 3472 or Eurocode 3	
Unstiffened plate	Concentrated loads		NS 3472 or Eurocode 3	
Unstiffened plate	Uniform lateral load and in-plane normal and shear stresses		NORSOK	$s < l$ buckling check not necessary if $\frac{s}{t} \leq 5.4\epsilon$
Unstiffened plate	Concentrated loads		NS 3472 or Eurocode 3	
Unstiffened plate	Uniform lateral load and in-plane normal and shear stresses		NORSOK	$s < l$ buckling check not necessary if $\frac{s}{t} \leq 5.4\epsilon$

$\epsilon = \sqrt{235/\sigma_Y}$ where σ_Y in (N/mm²) unit.

allows some redistribution of the local stress due to yielding. The failure of such members is normally associated with a descending postcritical behavior compared with that of a brittle structure. Structures with this behavior are known as shells.

Thin-walled shell structures might not be adequately covered by the formulations for tubular members and joints that are included in FEA programs that handle truss and beam models. Therefore, shells in general should not simply be defined as thin-walled tubulars and treated in the same manner. Rather, a more complex FEA mesh should be developed and analyzed, particularly where the shell includes the ring and/or longitudinal stiffening as shown in [Figure 13.2](#).

Stiffened cylindrical shells must be dimensioned against several buckling failure modes. The buckling modes for stiffened cylindrical shells are categorized below.

- Shell buckling—buckling of shell plating between rings and longitudinal stiffeners
- Panel stiffener buckling—buckling of shell plating including longitudinal stiffeners, rings are nodal lines
- Panel ring buckling—buckling of shell plating including rings. Longitudinal stiffeners act as nodal lines
- General buckling—buckling of shell plating, including longitudinal stiffeners and rings
- Column buckling—buckling of the cylinder as a column
- Local buckling of longitudinal stiffeners and rings

Buckling modes and their relevance for different cylinder geometries are illustrated in [Table 13.2](#) from NORSOK N-004. The strength equations for these failure modes are discussed in Part II, Chapter 17.

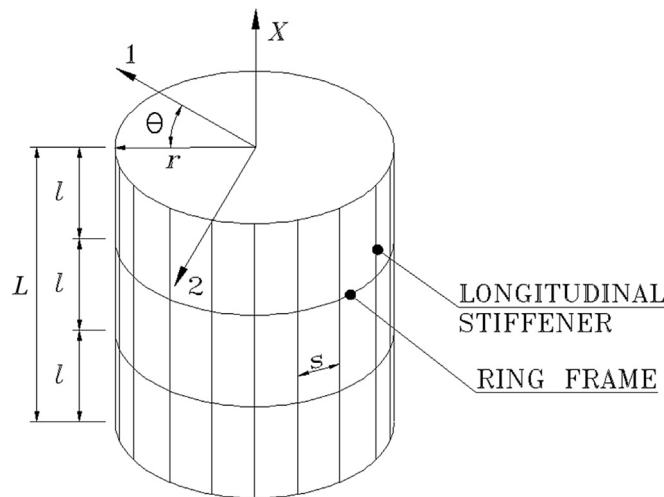


Figure 13.2
Example of a cylindrical shell.

Table 13.2: Reference table for buckling checks of plate panels

Flange outstand	Longitudinal compression		NS 3472 or Eurocode 3	Buckling check of flange outstand not necessary if $\frac{b}{t} \leq 15\epsilon$
Transversely stiffened plate panel	Bending moment and shear		NS 3472 or Eurocode 3	
Longitudinally stiffened plate panel	Longitudinal and transverse compression combined with shear and lateral load		NORSOK	

$\epsilon = \sqrt{235/\sigma_Y}$ where σ_Y in (N/mm²) unit.

Caution should be exercised when performing the FEA of a shell. It has been found through experience that semiempirical methods give a closer agreement to experimental results than theoretical methods provide. This is due to the effects of geometric imperfections, residual stresses, and inaccurately defined boundary conditions. Wherever possible, modeling should consider the real boundary conditions, prebuckling edge disturbances, actual geometric imperfections, nonlinear material behavior, residual welding stresses, and heat-effect zone. Note that relevant strength criteria may also be found from API codes (e.g., those listed in the references) (Table 13.3).

13.3 FLS Design

13.3.1 Introduction

Marine structures are subjected to a wide variety of loads that are cyclic in nature (e.g., storm winds, waves, and currents). These cyclic loadings develop cyclic strains in these structures. If the strains are large enough, the strength, stiffness, and capacity of the structural elements can be reduced due to fatigue degradation.

Most fatigue problems have been associated with flaws that come during design fabrication and construction (e.g., poor welding and misaligned members) or in the course of operation (e.g., corrosion damage and dropped-objects damage). Thus, a primary aspect of design for fatigue reliability includes quality assurance and control throughout the life cycle of the structure through inspection, maintenance, and repair (IMR).

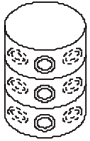

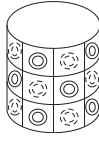
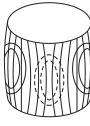

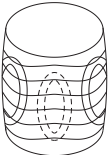
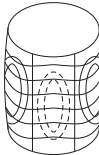

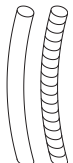

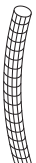
In general, the design for fatigue reliability is concentrated on details of elements, in particular joints. This is the first line of fatigue “defense.” It is in the local details and joints that the significant or major stress—strain raisers are developed. However, given the very large uncertainties associated with predictions of cyclic strain histories and fatigue strength, a high fatigue reliability of elements is rarely achieved.

Structure robustness, or the ability of the structure system to tolerate defects without significant reductions in its serviceability or ULS characteristics, is the second line of defense for fatigue. Effective structure redundancy, ductility, and capacity must be mobilized.

The third line of defense against fatigue is IMR. Inspections help disclose unanticipated flaws and defects, and confirm design objectives. Maintenance is intended to help preserve the structure so that it can fulfill its intended purposes. A repair strategy is intended to draw the engineer’s attention to the necessity for restoring the structure’s capacity after the future occurrence of damage and defects.

Present experience with the majority of marine structures indicates that although engineers have adequately designed for fatigue failure, notable exceptions exist—for example,

Table 13.3: Buckling modes for different types of cylinders (NTS, 1998)

Buckling Mode	Type of Structure Geometry		
	Ring-Stiffened (Unstiffened Circular)	Longitudinally Stiffened	Orthogonally Stiffened
Shell buckling			
Panel stiffener buckling			
Panel ring buckling			
General buckling			
Column buckling			

structures in which certain types of loadings and stress raisers are ignored where high-strength steels are used. It should not be expected that fatigue strength would increase proportionally with yield strength.

13.3.2 Fatigue Analysis

Fundamentally, the fatigue analysis approaches in engineering applications can be subdivided into the following categories:

- S–N-based fatigue analysis approach
- The local stress or strain approach, where the calculation includes the local notch effects in addition to the general stress concentration
- The fracture mechanics approach, which allows for the effects of cracks in the structure

These approaches have been well implemented in fatigue design and the assessment. However, FLS design is still one of the most difficult topics in structural design, assessment, or reassessment. For marine structures, additional complications arise because of the corrosive environment. The fundamental difficulties associated with fatigue problems are related to:

- lack of understanding of some underlying phenomena at both microscopic and macroscopic levels;
- lack of accurate information on parameters that affect the fatigue life of a structure.

The general explicit fatigue-design-by-analysis of marine structures involves a complex procedure. The dominant cause of cyclic stresses within a marine structure is the sea environment. Therefore, a fatigue assessment requires a description of the sea environment, or the sequence of sea states, that the structure is likely to meet over its planned operational life. Vessel motions, wave pressures, stress transfer functions, and resulting fatigue stresses (generally expressed in terms of the number of cycles of various stress ranges) at locations of potential crack sites (hot spots) are then calculated. In order to describe the fatigue durability of the joints of marine structures, experimental-data-based S–N curves are selected or fracture mechanics models are applied. This demand and capability information is then used to calculate fatigue lives via a damage summation process (typically the Palmgren–Miner hypothesis) or critical crack size. This procedure is summarized below:

- Characterization of the sea environment
- Hydrodynamic response analysis
- Structural analysis
- Stress transfer function
- Stress concentration factor

- Hot-spot stress transfer function
- Long-term stress range
- Selection of S–N curves
- Fatigue analysis and design
- Fatigue reliability analysis
- IMR plan

Characterization of the sea environment: The sea environment is represented by the number of occurrences of various sea states, each defined by a set of spectra. A two-parameter (significant wave height and zero upcrossing rate) wave-scatter diagram is used to characterize the sea states. All sea-state spectra are defined by, for example, the Pierson–Moskowitz relationship. Wave-direction probability is included in the sea environment characterization.

Hydrodynamic response analysis: Once waves with appropriate frequencies, heights, and directions are selected, the hydrodynamic response and loading of the structure are computed for each wave condition.

Structural analysis: A global structural analysis is performed to determine the applied loading for the local structure (load transfer function per unit wave amplitude as a function of frequency). The local structural analysis is carried out to determine the stress transfer function per unit load at each hot spot in the structural detail.

Stress transfer function: The load transfer function per unit wave amplitude as a function of wave frequency is multiplied by the stress transfer function per unit load.

Stress concentration factor (SCF): The geometric SCF is considered in the fatigue assessment. For the fatigue screening analysis, an upper bound SCF is assumed 3.0. For the detailed fatigue analysis, the SCF is determined using parametric equations or fine mesh FEA.

Hot-spot stress transfer function: The stress transfer function is multiplied by the SCF to determine the hot-spot stress transfer function.

Long-term stress range: Based on the wave spectrum, wave-scatter diagram, and hot-spot stress response per unit wave amplitude, the long-term stress range is determined. This is done by multiplying the ordinate of the wave amplitude spectrum for each sea state by the ordinate squared of the hot-spot stress transfer function, in order to determine the stress spectrum. The stress range distribution is assumed to follow a Rayleigh distribution. The long-term stress range is then defined through a short-term Rayleigh distribution within each sea state for all different wave directions.

Selection of S–N curve: For each critical location considered in the analysis, S–N curves are assigned based on structural geometry, applied loading, and welding quality.

Fatigue analysis and design: Several levels of fatigue analysis may be performed, including:

- fatigue screening;
- detailed analysis;
- reanalysis of welding improvements;
- reanalysis of design improvements.

Fatigue reliability: Each early step involves considerable uncertainty, with many sources of complex interrelated uncertainties and variations. The primary purpose of a fatigue reliability analysis is to logically organize these sources and then quantitatively evaluate them to determine what factors of safety (alternatively, levels of reliability) should be employed in a given design-analysis framework.

IMR: Given the time-dependent fatigue reliability analysis, a rational risk/reliability-based IMR plan should be developed to minimize the life cycle cost for the acceptable fatigue durability.

13.3.3 Fatigue Design

The fatigue resistance of critical structural details (joints) can be expressed in terms of S–N curves. S–N curves are obtained from laboratory testing in which a specimen is subjected to cyclic loading until the occurrence of final fracture.

The spectral method is the most important fatigue-design-by-analysis tool. The Weibull method is a simplified fatigue-analysis tool. These methods will be detailed in Part III of this book.

Fatigue durability is a life cycle problem. Fatigue durability can only be achieved under certain conditions:

- Stress–strain raisers (stress concentrations) and cyclic straining–stressing are minimized through good engineering of the structural system and its details. This requires a high level of engineering quality assurance (QA) at the concept-development-design stage.
- Flaws (misalignments, poor materials, porosity voids, etc.) are minimized through good, practical material and fabrication specifications and practices. This requires a high level of QA during the development of plans and specifications, and during construction (involving materials selection, fabrication, transportation, and installation). Furthermore, a similar QA program is required during operations to maintain the system properly.
- Degradation at the local element is minimized by selecting good materials, fabrication practices, and engineering designs (e.g., crack stoppers, damage localizers, and repairable elements). This requires recognition that when fatigue degradation occurs,

all reasonable precautions are taken to restrict its development and effects. Note that QA plays an essential role, particularly during operations to disclose the presence of fatigue degradation (early warning).

- Degradation at the system level is minimized so that when local fatigue degradation occurs, there are no significant effects on the system's ability to perform satisfactorily. Here, good fatigue design requires system robustness (redundancy, ductility, and capacity) and system QA. Inspections and monitoring to disclose global system degradation are another strategy to minimize potential fatigue effects.

Cyclic strains, material characteristics, engineering designs, specifications, and life cycle QA (inspections and monitoring) are all parts of the fatigue equation. This is the engineering equation of “fail-safe design”—fatigue may occur, but the structure can continue to function until the fatigue symptoms are detected and repairs are made.

The alternative is “safe life design”—no significant degradation will occur and no repairs will be necessary. Safe life designs are difficult to realize in many long-life marine structures or elements of these structures. This is because of the very large uncertainties that pervade fatigue design and analysis. Safe life design has been the traditional approach used in fatigue design for most ocean systems. The problems that have been experienced with fatigue cracking in marine structures, and the extreme difficulties associated with inspections of all types of marine structures, ensure that large factors of safety are needed to truly accomplish safe life designs. For this reason, the fail-safe design must be used whenever possible. Because of the extreme difficulties associated with inspections of marine structures and the high likelihood of undetected fatigue damage, it is not normally reasonable to expect that inspections will provide the backup or defenses needed to assure fatigue durability.

References

- NTS, 1998. NORSOK N-004, Design of Steel Structures. Norwegian Technology Standards Institution. Available from: www.nts.no/norsok.

Ship Vibrations and Noise Control

14.1 Introduction

When a ship is subjected to an impulsive load, such as when a descending anchor is suddenly arrested, it will execute elastic vibrations in addition to whatever rigid body motions are excited. Of these vibrations some are observed only locally and some are observed throughout the hull (Figure 14.1). The latter are generally the type that may exist in a beam free in space and are called “beam-like.” Although the surrounding water plays an important role in these vibrations, it does not destroy their beam-like characteristic and it is helpful to consider the vibrations of the ideal solid beam to be in free space. This is frequently spoken of as the free–free beam (both ends free).

As emphasized in standard works on mechanical vibration, the two terms “modes” and “nodes” are used repeatedly in the discussion of continuous systems and must not be confused with each other in spite of the similarity in spelling. Thus, the mode is the pattern of configuration that the body assumes periodically while in the vibratory condition, whereas the node is a point in the body that has no displacement when the vibration is confined to one particular mode. “Normal mode” of vibration is another very common term. The normal modes are the patterns in which the body can vibrate freely after the removal of external forces.

A beam free in space may undergo four principal types of elastic deformation designated as bending, twisting, shearing, and extensional deformations. These all can occur simultaneously. In a solid beam, these same types of deformation may exist with respect to any of the three principal directions, even though the relative magnitudes of bending, shearing, and torsion may be very different with respect to the different axes. In the case of the ship, the elastic deformation, which plays a significant role in its vibration, is

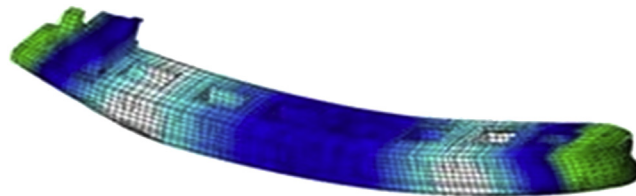


Figure 14.1
Ship vibrations.

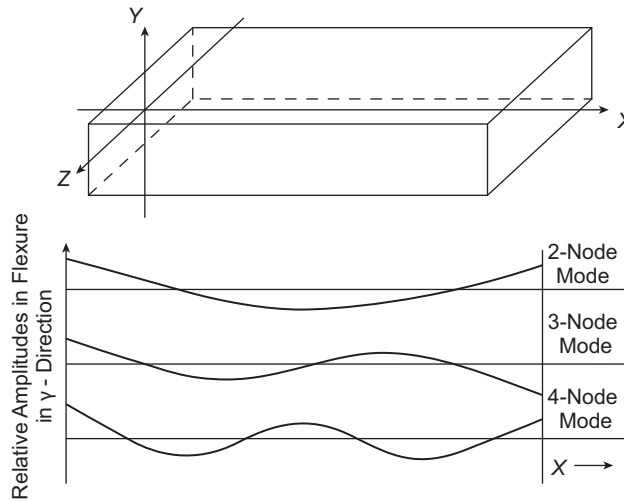


Figure 14.2
Flexural modes of a free-free uniform bar.

limited to bending and shearing in both the vertical and horizontal planes through its longitudinal axis, and to torsion about the longitudinal axis. The identification of extensional (longitudinal) beam-like vibrations of hulls has so far been inconclusive, and this type of vibration is ordinarily considered insignificant in ships, although it may be quite significant in the propulsion systems themselves.

In a symmetrical beam the bending and shearing effects combine to produce what are usually called the flexural modes, as illustrated in Figure 14.2. The curves plotted in Figure 14.2 indicate the displacements, in the Y -direction, of points falling on the A -axis when the bar is at rest. Similar modes exist for displacements in the Z -direction.

Figure 14.3 illustrates the torsional modes in which a uniform beam may vibrate, and the curves plotted show the angular displacement versus the distance from the end.

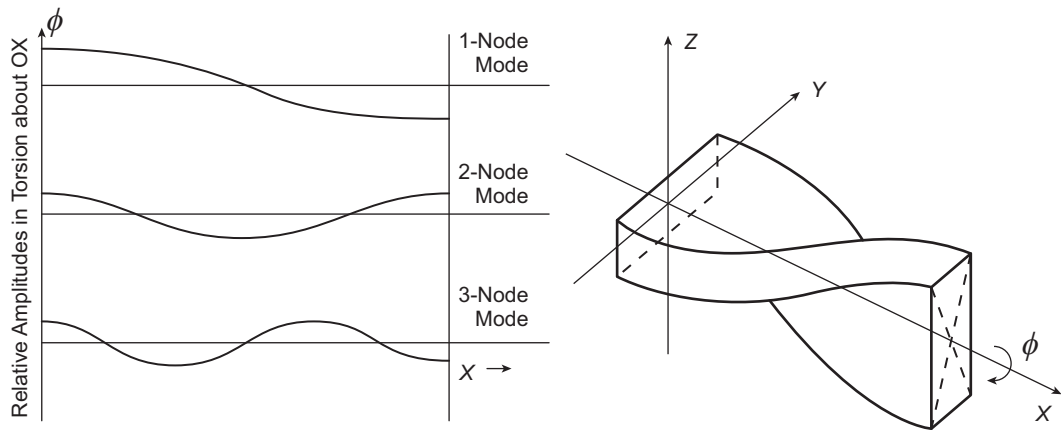
14.2 Basic Beam Theory of Ship Vibration

The fundamental system considered in all texts on mechanical vibration is the lumped mass-spring system for one degree of freedom, shown schematically in Figure 14.4.

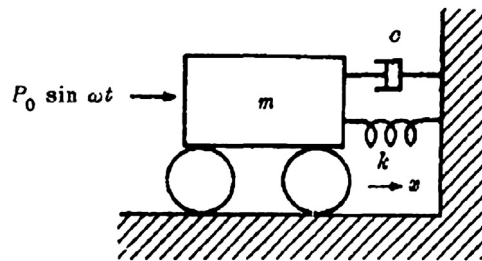
This system has mass m , spring constant k , viscous damping constant c , and in this case is acted upon by a simple harmonic driving force $P_0 \sin \omega t$ in the x -direction. The mass m is so restrained that it can move only in the x -direction.

The differential equation governing this case is given by

$$m\ddot{x} + c\dot{x} + kx = P_0 \sin \omega t$$


Figure 14.3

Torsional modes of a free–free uniform bar.


Figure 14.4

Rectilinear vibratory system of one degree of freedom.

14.3 Beam Theory of Steady-State Ship Vibration

As in previous chapters the treatment of hulls given here is based on the beam theory. However, at this point, the limitations of this theory must be taken into an account. This leads to what is known as the “rational” theory of ship vibrations. The methods presented in this chapter are thus essentially heuristic and “quasimathematical.” When there is an external forcing function applied to the ideal Euler–Bernoulli beam (otherwise free in space), the differential equation applicable to the system is

$$EI \frac{\partial^4 y}{\partial x^4} + \mu \frac{\partial^2 y}{\partial t^2} = P(x, t) \quad (14.1)$$

where $P(x, t)$ is the driving force in the Y -direction per unit length of the beam. It should be noted that, in general, P varies both with distance from the left end of the beam and with time. When the forcing function is specified mathematically, particular solutions of Eqn (14.1) can be given.

For the nonuniform Euler–Bernoulli beam the differential equation has the more general form of

$$\frac{\partial^2}{\partial x^2} \left(EI(x) \frac{\partial^2 y}{\partial x^2} \right) + \mu(x) \frac{\partial^2 y}{\partial t^2} = P(x, t) \quad (14.2)$$

where EI and μ now vary with x . Even if the ship were of such construction that $EI(x)$ and $\mu(x)$ could be expressed mathematically it can be appreciated that Eqn (14.2) would have severe limitations in indicating the manner in which the hull would vibrate under a given exciting force. In the first place, the inertia effect of the surrounding water is accounted for simply by the added mass component of g ; second, there is no dissipation or damping term in the equation; and third, there is no provision for deflection due to shearing. Last, but not least, there is nothing to indicate that the equation is not equally valid, regardless of the frequency of the driving force. Thus, whether the driving force has a frequency of 1 cps or 10,000 cps, the patterns of vibratory response should be expected to be beam-like.

14.4 Damping of Hull Vibration

The most widely used assumption in the analytical treatment of the damping of a mechanical system in vibration is that it is of the viscous type, as indicated in the previous section. As applied to the elementary system of one degree of freedom, this is the type of damping produced by a frictional force that is proportional to the velocity and has a direction opposite to that velocity.

In spite of the fact that mechanical damping is rarely of the true viscous type, an “equivalent viscous” constant is widely used because the solutions of the resulting linear differential equations are well known. The equivalent viscous constant is based on energy dissipation per cycle. If this is designated W , then

$$c = \frac{W}{\pi \omega Y^2}$$

where Y is the single amplitude and ω is the circular frequency. The viscous damping concept is also commonly retained in establishing damping constants from the logarithmic decrements deduced from observations of decaying free vibrations. Thus, in the elementary system of one degree of freedom, the critical viscous damping constant is given by

$$c_c = 2m\sqrt{\frac{k}{m}}$$

and the logarithmic decrement is

$$\delta = \frac{2\pi \frac{c}{c_c}}{\sqrt{1 - \left(\frac{c}{c_c}\right)^2}}$$

For small damping:

$$\delta = 2\pi \frac{c}{c_c}$$

A common criterion of the degree of damping is the resonance magnification factor. This is frequently designated by the symbol Q , and is widely used in electrical circuit theory as an index of dissipation for inductances. The lower the dissipation in the coil, the higher its Q is. For viscous damping:

$$Q = \frac{1}{2 \frac{c}{c_c}}$$

and for low damping:

$$Q = \frac{\pi}{\delta}$$

14.5 Vibration and Noise Control

There are a number of sources of vibration and noise present in a ship or marine vehicle. Typically these may include:

- The prime movers—typically diesel engines.
- Shaft-line dynamics.
- Propeller radiated pressures and bearing forces.
- Air conditioning systems.
- Maneuvering devices such as transverse propulsion units.
- Cargo handling and mooring machinery.
- Vortex shedding mechanisms.
- Intakes and exhausts.
- Slamming phenomena.

14.5.1 Propeller Radiated Signatures

The excitation from machinery is frequently, but not invariably, harmonic in content. As such, signatures from these items tend to more closely follow the mathematical basis for conventionally used analysis technique: typically Fourier' analysis. Propeller generated signatures, however, are the most commonly produced time series signatures with significant cyclic perturbations.

The development basis of the propeller-induced hull pressure signature is the acceleration of the cavity volumes with respect to time on the propeller blades, which is modified by

the self-induced component of pressure generation arising from the vibration of the ship structure at the point of interest. As such, the hydrodynamic excitation process is a time domain event whose physical processes can better be understood through the pressure time series.

In experimental studies the pressure time signature is most commonly analyzed using a Fourier-based technique, due largely to the need to relate excitation sources to ship hulls and structural response characteristics. Fourier techniques, which were originally developed as a curve fitting process, have as their underlying tenet the requirement of piecewise continuity of the function that is being analyzed; whether this is over a long or short timeframe. Given that this condition is satisfied, assuming a sufficient number of terms are taken in the series and the numerical stability of the algorithm is acceptable, then the method will satisfactorily curve fit the function as a sum of transcendental functions whose coefficients may then be input in finite element or other computational processes.

To gain a phenomenological understanding of cavitations behavior, sufficient to affect a proper cure to a technical problem rather more than a Fourier-based curve fitting algorithm, is necessary. This is for two reasons: first, a set of coefficients of transcendental functions tell little about the structure of the underlying cavitations causing the problem, and second, and perhaps more importantly, cavitations-based signatures are rarely uniform with respect to time. There are blade surface pressure changes, which vary from blade to blade in a single revolution and changes from one revolution to the next. These changes are random in nature and result from the interaction of the temporal changes in the flow; the flow field, this being the sum of the steady inflow field and the seaway induced velocities; and the blade-to-blade geometric variations due to the manufacturing tolerances of the propeller blades. These changes influence both the general form of the cavity volume variation and the higher frequencies, and the noise generated from the random perturbations of the topological form of the underlying cavity structure.

If a phenomenological approach is adopted for the analysis of propeller-induced hull pressure signatures so as to develop a solution to a practical problem and minimize sea trials or dry docking down times, then other analytical approaches are required. A number of candidate approaches offer themselves. Among these are short form Fourier transforms, joint time–frequency analysis, wavelet techniques, and a double integral analysis of the underlying pressure signature. Experience has shown that each of these methods has shortcomings due for the most part to the near adiabatic collapse of the cavity volumes in adverse wake gradients. Nevertheless, the wavelet methods and the double integral technique have been shown to have some advantages when considering different aspects of the problem. In the case of the wavelets most of Lloyd's Register's current work focuses on standard applications of Daubechies formulations, which allow some progress to be made.

Further discrimination is believed to be possible if purpose-designed wavelet forms are used to describe different cavity phenomena.

Notwithstanding the wavelet class of methods, the double integral approach has been shown to be the most successful at phenomenological discrimination. The pressure integration approach is essentially a time domain process, which together with visual observations of cavitations can link the dynamics of visual events with the dynamics of pressure pulses. It is clear from both ship- and model-scale analysis that the more severe excitation events are generated by cavitations that grow, collapse, and rebound in a small cylindrical sector of the propeller disc and slipstream that span the wake peak. It is the passage of the propeller blades through this slow-speed region that causes the flare-up and collapse of cavity volumes on the blade and in the tip vortex shed by the advancing blade.

14.5.2 Vortex Shedding Mechanisms

Vibration induced from the flow over sea chest openings has been a troublesome feature in some ships and has prevented the ships from meeting the localized comfort criteria. Such vibrations, which commonly manifest themselves in local structural resonant behaviors, are clearly not directly related to rotational machinery speeds. Rather, they are related to the vortex shedding over the sea chest hull opening grills and, therefore, are Strouhal and Froude number dependent, based on the speed of the ship.

Other examples of vortex shedding induced vibrations have recently been encountered. These have included A-brackets, extended centerline skegs and fin appendages fitted to ships to improve course keeping stability. The characteristics of these problems were high vibration levels in the ship structure or failure of the structural elements.

Vortex shedding occurs when the fluid flow around the after part of an appendage is separated from the structure at a given Reynolds number and the oscillating pressures cause the elastic structure to vibrate. The shedding frequency is given in terms of the Strouhal number, and for bodies with rough surfaces at scale, it is frequently acceptable for estimation purposes to use a value for the Strouhal number of 0.2. When structures vibrate in the transverse direction with a frequency at or near the vortex shedding frequency they tend to increase the strength of the shed vorticity, which, in turn, may increase the structural excitation. Furthermore, if the vortex shedding frequency is close to the natural frequency of the structure it will move to the frequency of the structure. Once the vortex shedding frequency is synchronized with the frequency of the structure it will often tend to remain at that frequency even when the flow speed changes over a limited range.

The following two examples illustrate this type of problem. In the first case two fins were installed aft of the rudder to improve the ship's course keeping, and the ship was propelled

by a four blade controllable pitch propeller. Installation of the fins resulted in increased vibration levels and subsequent failure of the fins. It was concluded that the fin's first response to vortex excitation started when the vortex shedding became coincident with the fin's natural frequency of 22 Hz in a bending-torsion mode. As a result of the resonance, the fin's vibration increased. The vortex frequency did not change with the ship speed but remained locked to the fin's natural frequency. The fin's next vibration mode of 25.4 Hz, a torsional mode, was excited when the vortex shedding frequency became coincident with that frequency. At the ship's maximum operating speed the only remaining frequency component was that of 25.4 Hz. The high stresses resulted in the fin failures.

In the second case the centerline skeg was extended to improve the ship's directional stability. This ship's propulsion system comprised two thruster units employing two contrarotating fixed pitch propellers on each unit: the propeller blade numbers being four and five. The skeg extension resulted in excessive vibrations in the ship structure and the investigation showed that the skeg's natural frequency of 18.3 Hz was excited by the five blade propeller at around 7 knots. As a result, the skeg's vibration amplitudes increased, initiating synchronization of the vortex shedding and the skeg natural frequencies. Higher up the speed range, when the four bladed propeller excitation became coincident with the skeg natural frequency, the vibration levels reached their first peak amplitude at 9.5 knots. A second vibration peak was then measured between 10 and 11 knots when the vortex shedding frequency became coincident with the skeg natural frequency.

The dynamic behavior of structures subjected to vortex shedding excitation depends on the ship speed, the structural profile and its trailing edge shape, the structural natural frequencies and damping, and the interaction between the fluid flow and structural vibrations. Reduction of the vibration amplitudes of the structure caused by vortex shedding may be achieved by:

- Avoiding resonance between the vortex-induced excitations and the structural natural frequency.
- Lowering the vortex excitation levels.
- Reducing response of the structure.

Resonance can be avoided by modifying either the vortex excitation frequency or the structural natural frequency. Ordinarily the structural natural frequency should be increased sufficiently to avoid resonances with vortex shedding mechanisms; this can be achieved by increasing the structure's stiffness or changing the aspect ratio. Other solutions can be to increase the vortex shedding excitation frequency by changing the structure's trailing edge shape. In all cases it is necessary to evaluate the structural natural frequencies and ensure that they are not coincident with the vortex shedding and propeller excitations.

14.5.3 After-Body Slamming

Shock impacts such as slamming also need consideration since, as well as generating structural tertiary stresses in the ship structure, these events can be disturbing to passengers. In particular after-body slamming can excite resonant conditions in the ship structure; most typically the 2-node vertical mode. The incidence of after-body slamming, in contrast to fore-body slamming, frequently reduces with increasing ship speed. This is because the ship's entrained wave system increases at higher speeds and gives a measure of protection to the hull after-body from the otherwise uninterrupted incidence of the environmental wave system. In addition to being a function of reducing ship speed, the slamming threshold speed is also dependent on the sea state, recognizing that the resultant sea state comprises both underlying swell and wind-induced wave components, which strongly influence the directional slamming threshold. Furthermore, a common characteristic possessed by ships that suffer from after-body slamming is a relatively flat after-body design coupled with relatively small immersions. In this latter context after-body slamming has been known to occur in sea conditions with wave heights less than 1 m. Consequently, the exploration, at an early design stage of hull forms that avoid this problem in association with the predicted sea and ship motions, is of particular importance.

14.6 Vibration Analysis

The design and construction of a ship free of excessive vibration continues to be a major concern and, as such, it is prudent to investigate, through analysis, the likelihood of vibration problems early in the design stage. Vibration analysis is aimed at the confirmation of the many design considerations associated with:

- Stern configuration.
- Main propulsion machinery.
- Propeller and shafting system.
- Location and configuration of major structural assemblies.

The ship hull structure includes the outer shell plating and all internal members, which collectively provide the necessary strength to satisfactorily perform the design functions in the expected sea environment. The hull structure responds as a free-free beam (both ends free) when subjected to dynamic loads. The vibration induced by the propulsion system is a common source of ship vibration. The vibration from this source manifests itself in several ways. Dynamic forces from the shafting system are transmitted to the hull through shaft bearings. The propeller induces fluctuating pressures on the surface of the hull, which induces vibration in the hull structure. The main and auxiliary engines can directly cause vibrations through dynamic forces transmitted through their supports and foundations. The response to this forcing can cause the vibration of the hull girder,

deckhouse, deck and other structures, local structures, and equipment. When attempting to determine the source of vibration, it is necessary to establish the frequency of excitation and to relate the frequency of excitation to the shaft rotational frequency by determining the number of oscillations per shaft revolution. The main engine-induced unbalanced excitations encountered with slow-speed diesel-driven ships are the primary and secondary free engine forces and moments. The engine manufacturer is to provide the magnitude of these forces and moments.

The response of the hull structure may be resonant or nonresonant. The hull structure will normally vibrate in the following modes:

- Vertical bending.
- Horizontal bending.
- Torsional (twist).
- Longitudinal.
- Coupling exists between horizontal and torsional modes, especially in containerships.

Typical major substructures include deckhouses, main deck structures, large propulsion machinery systems, etc., which because of the direct coupling with hull structure vibration can significantly influence the total or global pattern of ship vibration. In analyzing vibration patterns of such large complex structures, it is necessary to identify the principal reason for observed excessive vibration. Excessive vibration of a major substructure may be the result of structural resonance in the substructure or in the attachment detail for the substructure and hull structure.

Local structural components are the minor structural assemblies, relative to major substructures previously referred to. Local structures may be identified as panels, plates, girders, bulkheads, platforms, handrails, minor equipment foundations, etc., and are components of larger structures (major substructures) or of the entire hull structure. Most ship vibration problems occur in local structural components and are the result of either strong inputs received from the parent structure amplified by resonance effects in the local structure or are the response to vibratory forces generated by mechanical equipment attached to the local structure.

This section describes the analysis procedure for propeller and main engine-induced ship hull vibration using a three-dimensional finite element method. The objective of vibration analysis is to determine the overall vibration characteristics of the hull structure and major superstructures so that areas sensitive to vibratory forces may be identified and assessed relative to standard acceptance criteria on vibration level.

14.6.1 Procedure Outline of Ship Vibration Analysis

The flowchart of the procedure is shown in [Figure 14.5](#). The procedure recommended is to perform the vibration analysis using a three-dimensional finite element model representing

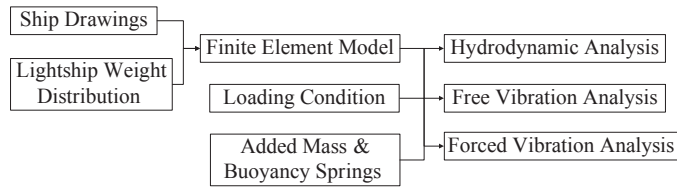


Figure 14.5

The flowchart of the procedure.

the entire ship including the deckhouse and main propulsion machinery system. Both free and forced vibration analyses are included.

14.6.2 Finite Element Modeling

Ship structures are complex and may be analyzed after idealization of the structure. Several simplifying assumptions are made in the finite element idealization of the hull structure. The modeling requirements are that all significant structural sections are to be captured and deflection/velocity/acceleration are to be sufficiently predicted.

A three-dimensional finite element model representing the entire ship hull (Figure 14.6), including the deckhouse and machinery propulsion system, needs to be developed for vibration analysis. If a global model exists from any previous tasks such as stress analysis, it needs to be conditioned for vibration analysis.

Lightship Weight Distribution

Lightship weight distribution is an important factor in any vibration analysis. Results can change dramatically if it is not properly represented. Typically, masses of all the heavy equipment are to be modeled as mass elements and are to be placed at well-supported nodes such that the total mass and center of gravity of that equipment are maintained. This distribution is to be as accurate as possible in the areas of interest. In general, the center of

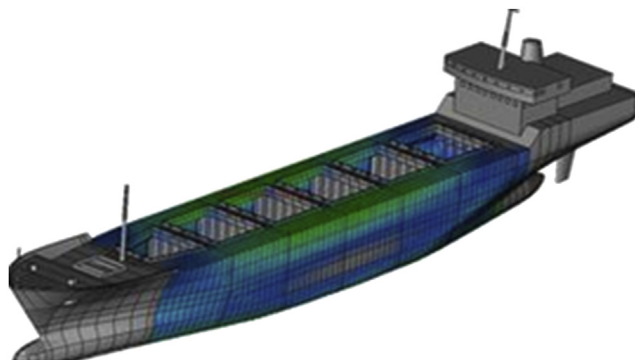


Figure 14.6

Finite element modeling.

gravity from the finite element model and the center of gravity from the T&S booklet are to be within 0.5% of the total ship length. The deckhouse superstructure weight and mass distribution, longitudinally and vertically, must also be accurately represented.

Loading Condition

The objective of the vibration analysis is to investigate the ship vibration performance at intended service conditions. Therefore, the loading conditions, such as full load condition and ballast condition, in which the ship operates at ship design speed, will be the focus of the vibration analysis. In addition, it is often desirable to investigate the sea trial condition for the purpose of calibrating calculated numerical results with measurements. Typically, considering the analysis efforts to be taken, it is recommended that vibration analysis be performed for two selective conditions, either:

- Full load condition and sea trial condition, or
- Full load condition and ballast load condition.

Depending on the loading condition, the mass of the cargo and ballast is then distributed in the structural model using mass elements. The corresponding added mass and the buoyancy springs are then calculated and added to the model.

Added Mass

The added mass can be considered through a virtual mass method using a boundary element method such as the “MFLUID” card of MSC NASTRAN. Alternatively, a three-dimensional seakeeping analysis program may be used. The analysis includes three main tasks:

- *Development of a hydrodynamic panel model:* The hydrodynamic panel model is to represent the geometry of the ship’s hull below the still-water line when using a linear seakeeping program. It is recommended that a total of about 2000 panels be used for the ship’s hull surface, including port and starboard sides. A computer program may generate the panel model using the ship’s offsets. The main particulars required for the hydrodynamic model include: ship displacement, drafts, location of center of gravity, and radii of gyration.
- *Hydrodynamic analysis:* The purpose of the analysis is to obtain the distributed added mass. In general, the natural frequency of the ship is much higher than the wave frequencies considered in the seakeeping analysis. To obtain the added mass at such high frequencies, the infinite frequency added mass option is to be used.
- *Mapping hydrodynamic results onto the finite element model:* The distributed added mass from the seakeeping analysis is represented as an added mass on each hydrodynamic panel model. An interface program can be used to map the heave added mass onto the finite element model. The user needs to check that the total added mass on the finite element model is equal to the total added mass on the hydrodynamic panel model.

Buoyancy Springs

The effect of buoyancy on hull vibration is generally regarded as small. Where it is necessary to consider the buoyancy effect, it may be modeled by adding rod elements to the wetted surface of the model. The rod elements work as springs and the total stiffness of the rod elements is to be equivalent to the ship's vertical buoyancy stiffness.

14.6.3 Free Vibration

Computation of the natural frequencies and mode shapes is to be performed by solving an eigenvalue problem. The natural frequencies (eigenvalues) and corresponding mode shapes (eigenvectors) of the three-dimensional finite element model can be obtained by solving the following equation of motion:

$$[M]\{\ddot{u}(t)\} + [C]\{\dot{u}(t)\} + [K]\{u(t)\} = \{F(t)\}$$

where

$[C]$ = damping matrix

\ddot{u} = column matrix of accelerations

\dot{u} = column matrix of velocities

u = column matrix of displacements

F = column matrix of harmonic forces

For free vibration, damping $[C]$ and forces $\{F\}$ are zero. The solution would then be from

$$[K]\{\Phi\} = \omega^2[M]\{\Phi\}$$

where

$[K]$ = symmetrical stiffness matrix

$[M]$ = diagonal mass matrix

$\{\Phi\}$ = column mode shape matrix

ω = natural frequency

This problem can be solved by normal mode analysis. An important characteristic of normal modes is that the scaling or magnitude of the eigenvectors is arbitrary. Mode shapes are fundamental characteristic shapes of the structure, and are therefore relative quantities. Examples of mode shapes of a typical liquefied natural gas carrier are shown in [Figures 14.7 and 14.8](#). The natural frequencies obtained from the analysis can then be compared to the excitation frequencies to check for resonance.

14.6.4 Forced Vibration

Frequency response analysis is a method used to compute structural response to steady-state oscillatory excitation. The three-dimensional finite element model is subject to

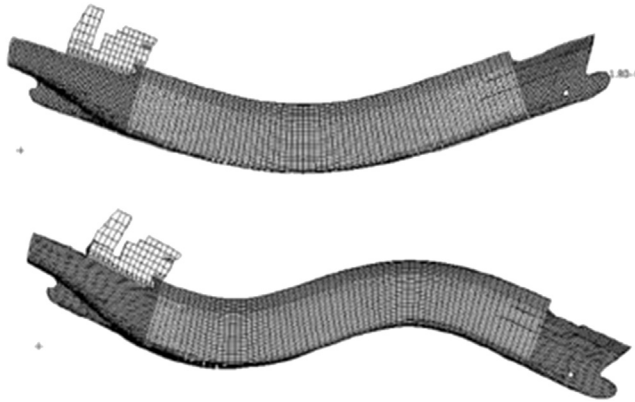


Figure 14.7
First two vertical mode shapes.

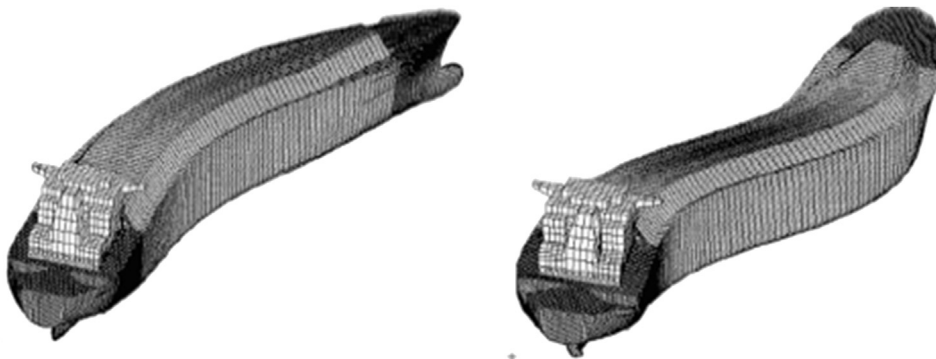


Figure 14.8
First two horizontal mode shapes.

systems of harmonic loads that represent the oscillatory excitation forces induced by propeller and main engine. Two different numerical methods can be used in frequency response analysis. A direct method solves the coupled equations of motion in terms of forcing frequency. A modal method utilizes the mode shapes of the structure to reduce and uncouple the equations of motion. The solution for a particular forcing frequency is obtained through the summation of the individual modal responses. The choice of the method depends on the model size, number of the excitation frequencies, and the frequency of excitation. If the modal method is used, all modes up to at least two to three times the highest forcing frequency are to be retained.

A frequency response is obtained by applying the cyclic propeller and engine forces and moments with varying frequencies, related to the shaft rpm, the number of blades per propeller, and the order of the main engine, to the model and solving the resulting dynamic problem given by the following equation of motion.

The structural response to this harmonic load is a steady-state response at the frequency of the load. (It is assumed that the harmonic load continues long enough so that the transient response damps out.) Therefore

$$F(t) = Fe^{i\omega t}$$
$$u(t) = ue^{i\omega t}$$

Upon substitution, the equations of motion reduce to

$$[K + i\omega C - \omega^2 M] \{u\} = \{F\}$$

It is noted that both $\{F\}$ and $\{u\}$ are complex quantities due to damping C and to the fact that the various components of propeller and engine-induced vibratory forces are not in phase with one another.

Further Reading

- Pettersen, J.W.E., Sigvaldsen, Vedeler, B., 1971. Vibration in the afterbody of ships. Transactions of the RINA. Vibration Characteristics of Two-stroke Low Speed Diesel Engines, MAN-B&W Publication.
- Jackobsen, S.B., 1991. Coupled axial and torsional vibration calculations on long-stroke diesel engines. Transactions of the SNAME.
- Carlton, J.S., Holland, C.H. Aspects of twin screw ship technology. Transactions of the LRTA (Paper No. 6, Session 1998/9).
- Carlton, J.S., Fitzsimmons, P.A., August 6 and 7, 2004. Cavitation: some full scale experience of complex structures and methods of analysis and observation. In: ATTC Conf. St John's Newfoundland.
- Carlton, J.S., April 2005. Afterbody Slamming. The Naval Architect.
- Carlton, J.S., McMorris, S.M., 2002. Passenger and crew accommodation comfort: the optimisation of the shipboard environment. In: Seatrade Med Conf. Genoa.
- American Bureau of Shipping. Guidance Notes on Ship Vibration.

Buckling/Collapse of Columns and Beam-Columns

15.1 Buckling Behavior and Ultimate Strength of Columns

This chapter does not intend to repeat the equations and concepts that may be found in existing books on buckling and ultimate strength (e.g., [Timoshenko and Gere \(1961\)](#) and [Galambos \(2000\)](#)), but instead is intended to address some unique formulations and practical engineering applications.

15.1.1 Buckling Behavior

For a column subjected to an axial force, the deflection produced by the axial force will be substantially amplified by the initial imperfections. Such a situation for a beam-column with sinusoidal imperfections is illustrated in [Figure 15.1](#).

Consider the case in which the initial shape of the axis of the column is given by the following equation.

$$w_0 = w_{0max} \sin \frac{\pi x}{l} \quad (15.1)$$

Initially, the axis of the beam-column has the form of a sine curve with a maximum value of w_{0max} in the middle. If this column is under the action of a longitudinal compressive force P , an additional deflection w_1 will be produced, and the final form of the deflection curve is

$$w = w_0 + w_1 \quad (15.2)$$

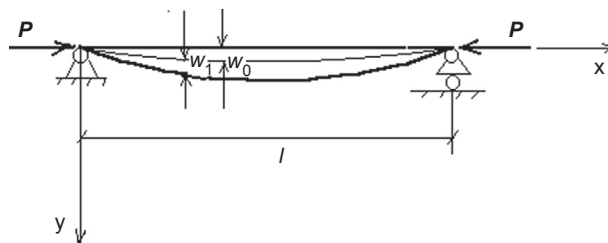


Figure 15.1

Coordinate systems and displacements of a beam-column with sinusoidal imperfections.

The bending moment at any point along the column axis is

$$M = P(w_0 + w_1) \quad (15.3)$$

Then the deflection w_1 , due to the initial deformation, is determined from the differential equation

$$EI \frac{d^2 w_1}{dx^2} = -P(w_0 + w_1) \quad (15.4)$$

Substituting Eqn (15.1) in Eqn (15.4), the following equation is obtained.

$$\frac{d^2 w_1}{dx^2} + k^2 w_1 = -k^2 w_{0max} \sin \frac{\pi x}{l} \quad (15.5)$$

where

$$k^2 = \frac{P}{EI}$$

The general solution of Eqn (15.5) is

$$w_1 = A \sin kx + B \cos kx + \frac{1}{\frac{\pi^2}{k^2 l^2} - 1} w_{0max} \sin \frac{\pi x}{l} \quad (15.6)$$

To satisfy the boundary condition ($w_1 = 0$ for $x = 0$ and $x = l$) for any value of k , $A = B = 0$. Also, by using the notation α for the ratio of the longitudinal force to its critical value

$$\alpha = \frac{P}{P_E} \quad (15.7)$$

where

$$P_E = \frac{\pi^2 EI}{l^2},$$

the following is obtained.

$$w_1 = \frac{\alpha}{1 - \alpha} w_{0max} \sin \frac{\pi x}{l} \quad (15.8)$$

The final form of the deflection curve is

$$w = w_0 + w_1 = w_{0max} \sin \frac{\pi x}{l} + \frac{\alpha}{1 - \alpha} w_{0max} \sin \frac{\pi x}{l} = \frac{w_{0max}}{1 - \alpha} \sin \frac{\pi x}{l} \quad (15.9)$$

This equation shows that the initial deflection w_{0max} at the middle of the column is magnified at the ratio $\frac{\alpha}{1 - \alpha}$ by the action of the longitudinal compressive force. When the compressive force P approaches its critical value, α approaches 1.0, and the deflection w increases infinitely.

Substituting Eqn (15.9) in Eqn (15.3), the following equation is obtained.

$$M = \frac{w_{0max} P}{1 - \alpha} \sin \frac{\pi x}{l} = \frac{w_{0max} P}{1 - \frac{P}{P_E}} \sin \frac{\pi x}{l} \quad (15.10)$$

From Eqn (15.10), the maximum bending moment at $x = \frac{l}{2}$ is obtained.

$$M_{MAX} = \frac{w_{0max} P}{1 - P/P_E} \quad (15.11)$$

The maximum stress in the cross section, where $x = \frac{l}{2}$, is

$$\sigma_{MAX} = \frac{P}{A} + \frac{M_{MAX}}{W} \quad (15.12)$$

Equation (15.12) can be rewritten as follows:

$$\sigma_{MAX} = \frac{P}{A} \left[1 + \frac{w_{0max} c}{r^2} \frac{P_E}{P_E - P} \right] \quad (15.13)$$

where

W = Section modulus

A = Area of the cross section

C = Distance from the neutral axis to the extreme fiber

r = Radius of gyration of the cross section

s = Radius of the core: $s = \frac{W}{A}$

By taking the first term of the Fourier expansion

$$\frac{P_E}{P - P_E} = 1 + \frac{P}{P_E} + \left(\frac{P}{P_E} \right)^2 + \dots$$

the following can be obtained.

$$\frac{P_E}{P - P_E} = 1 + \frac{P}{P_E} \quad (15.14)$$

Combining Eqns (15.14) and (15.13), the maximum stress is given by

$$\sigma_{MAX} = \frac{P}{A} \left[\left(1 + \frac{w_{0max}}{s} \right) + \frac{w_{0max}}{s} \frac{P}{P_E} \right] \quad (15.15)$$

15.1.2 Perry—Robertson Formula

A simple method to derive the ultimate strength of a column is to equate σ_{MAX} in Eqn (15.12) to the yield stress σ_Y

$$\frac{P_{ULT}}{A} + \frac{1}{W} \frac{w_{0max} P_{ULT}}{1 - P_{ULT}/P_E} = \sigma_Y \quad (15.16)$$

The above equation can be rewritten as

$$\sigma_{ULT}^2 - \left[\sigma_y + \left(1 + \frac{w_{0max} A}{W} \right) \sigma_E \right] \sigma_{ULT} + \sigma_E \sigma_Y = 0 \quad (15.17)$$

where

$$\sigma_E = \frac{P_E}{A} \quad \text{and} \quad \sigma_{ULT} = \frac{P_{ULT}}{A}$$

Its solution is called the Perry–Robertson formula and can be expressed as

$$\frac{\sigma_{ULT}}{\sigma_Y} = \frac{1 + \eta + \gamma - \sqrt{(1 + \eta + \gamma)^2 - 4\gamma}}{2\gamma} \quad (15.18)$$

where

$$\eta = \frac{w_{0max} A}{W} \quad \text{and} \quad \gamma = \frac{\sigma_Y}{\sigma_E}$$

In the Perry–Robertson formula, the effect of initial deflection is explicitly included. Comparison with more precise solutions, such as finite element analysis results, demonstrates that the formula is accurate when the initial deflection is within the range of fabrication tolerance. When the initial deflection is due to in-service damage, which may be up to 1% of the column length, the formula may in fact underestimate ultimate strength. The formula may be extended to account for the effect of residual stress explicitly. Perry–Robertson formula has been frequently used in European steel structure codes.

15.1.3 Johnson–Ostenfeld Formula

The effect of plasticity may be accounted for by correcting the Euler buckling stress using the Johnson–Ostenfeld approach (see Galambos, 2000), denoted by Figure 15.2

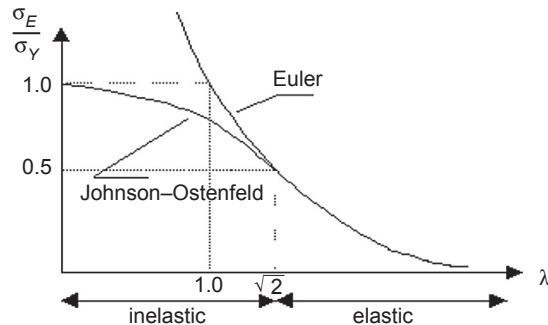


Figure 15.2
Johnson–Ostenfeld approach curve.

$$\sigma_{ULT} = \sigma_E \quad \text{for } \sigma_E/\sigma_Y \leq 0.5 \quad (15.19)$$

$$\sigma_{ULT} = \sigma_Y \left(1 - \frac{1}{4\sigma_E/\sigma_Y} \right) \quad \text{for } \sigma_E/\sigma_Y \geq 0.5 \quad (15.20)$$

The Johnson–Ostenfeld approach was recommended in the first edition of the book *Guide to Stability Design Criteria for Metal Structures* in 1960, and has since been adopted in many North American structural design codes in which a moderate amount of imperfection has been implicitly accounted for. The Johnson–Ostenfeld formula was actually an empirical equation derived from column tests in the 1950s. It has been applied to many kinds of structural components and loads. See Part 2, Chapters 16 and 17 of this book for more detail.

15.2 Buckling Behavior and Ultimate Strength of Beam-Columns

15.2.1 Beam-Column with Eccentric Load

Consider a beam-column with an eccentric distance of e_1 at each end—see [Figure 15.3](#). The equilibrium equation can then be written as

$$EI \frac{d^2w}{dx^2} + P(w + e_1) = 0 \quad (15.21)$$

The general solution of [Eqn \(15.21\)](#) is

$$w = A \sin kx + b \cos kx - e_1 \quad (15.22)$$

Using the boundary conditions

$$w = 0 \quad \text{at } x = \pm \frac{l}{2}$$

$$EI \frac{d^2w}{dx^2} = -Pe_1 \quad \text{at } x = \pm \frac{l}{2}$$

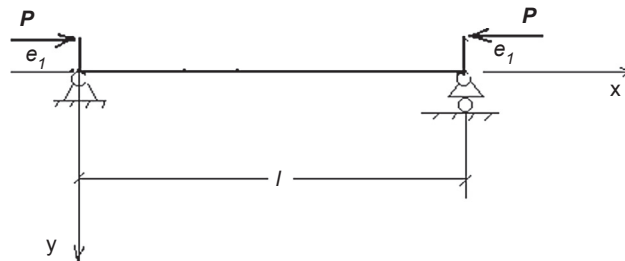


Figure 15.3
Beam-column applied eccentric load.

The integral constant can be obtained, and the solution of Eqn (15.21) is

$$w = e_1 \left(\sec \frac{kl}{2} \cos kx - 1 \right) \quad (15.23)$$

The maximum deflection at the middle of the beam-column is given by

$$w_{MAX} = e_1 \sec \frac{kl}{2} \quad (15.24)$$

The maximum moment and stress at the middle of the beam-column are given by

$$M_{MAX} = Pe_1 \frac{1}{\cos \frac{kl}{2}} \quad (15.25)$$

$$\sigma_{MAX} = \frac{P}{A} + \frac{Pw_{MAX}}{I} = \frac{P}{A} \left(1 + \frac{e_1 A}{W} \sec \frac{kl}{2} \right) \quad (15.26)$$

Equation (15.26) is called the secant formula. Taking the first two terms of the formula expansion,

$$\sec \frac{\pi}{2} \sqrt{\frac{P}{Pe}} \approx 1 + \frac{\pi^2}{8} \frac{P}{P_E} \quad (15.27)$$

and substituting Eqn (15.27) in Eqn (15.28), the following can be obtained.

$$\sigma_{MAX} = \frac{P}{A} \left[\left(1 + \frac{e_1}{s} \right) + \frac{\pi^2}{8} \frac{e_1}{s} \frac{P}{P_E} \right] \quad (15.28)$$

15.2.2 Beam-Column with Initial Deflection and an Eccentric Load

The deflection for the beam-column in Figure 15.4 can be obtained easily by superposition of Eqn (15.9) and Eqn (15.23), and the resulting total deflection is

$$w = \frac{w_{0max}}{1 - \alpha} \sin \frac{\pi x}{l} + \frac{e_1}{\cos \frac{kl}{2}} \left[\cos \left(\frac{kl}{2} - kx \right) - \cos \frac{kl}{2} \right] \quad (15.29)$$

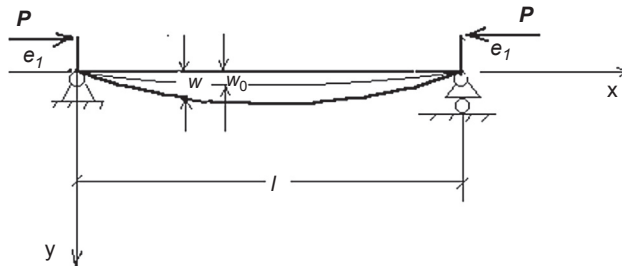


Figure 15.4

An initially curved beam-column carrying eccentrically applied loads.

The maximum deflection occurs at the center of the beam-column

$$w_{MAX} = w \Big|_{x=\frac{l}{2}} = \frac{w_{0max}}{1 - \alpha} + e_1 \left(\sec \frac{kl}{2} - 1 \right) \quad (15.30)$$

The bending moment at any section x of the beam-column is

$$\begin{aligned} M &= P(e_1 + w) \\ &= P \left[\frac{w_{0max}}{1 - \alpha} \sin \frac{\pi x}{l} + \frac{e_1}{\cos \frac{kl}{2}} \cos \left(\frac{kl}{2} - kx \right) \right] \end{aligned} \quad (15.31)$$

and the maximum moment at the center of the beam-column is

$$M_{MAX} = P \left(\frac{w_{0max}}{1 - \frac{P}{P_E}} + \frac{e_1}{\cos \frac{kl}{2}} \right) \quad (15.32)$$

From Eqn (15.15) and Eqn (15.28), the maximum stress at the center of the beam-column is

$$\sigma_{MAX} = \frac{P}{A} \left[\left(1 + \frac{w_{0max} + e_1}{s} \right) + \frac{(w_{0max} + 1.234e_1)}{s} \frac{P}{P_E} \right] \quad (15.33)$$

15.2.3 Ultimate Strength of Beam-Columns

For practical design, the linear interaction for the ultimate strength of a beam-column under combined axial force and bending is often expressed as

$$\frac{P}{P_{ULT}} + \frac{M_{MAX}}{M_{ULT}} \leq 1 \quad (15.34)$$

where P_{ULT} and M_{ULT} are the ultimate strength and ultimate bending moments of the beam-column under a single load respectively. Based on Eqn (15.34), the maximum moment in a beam-column under combined axial forces and symmetric bending moments, M_0 , is given by

$$M_{MAX} = \frac{M_0}{\cos \frac{\pi}{2} \sqrt{\frac{P}{P_E}}} \approx \frac{M_0}{1 - \frac{P}{P_E}} \quad (15.35)$$

Then, the ultimate strength interaction equation may be expressed as

$$\frac{P}{P_{ULT}} + \frac{M_0}{\left(1 - \frac{P}{P_{ULT}} \right) M_{ULT}} \leq 1 \quad (15.36)$$

Determining the exact location of the maximum bending moment for beam-columns under nonsymmetric bending moments is not a very straightforward process. Instead, M_0 is substituted by an equivalent moment, $M_{EQ} = C_M M_A$.

$$\frac{P}{P_{ULT}} + \frac{C_M M_A}{\left(1 - \frac{P}{P_E}\right) M_{ULT}} \leq 1 \quad (15.37)$$

where (Galambos, 2000)

$$C_M = 0.6 - 0.4 \frac{M_B}{M_A} \geq 0.4 \quad (15.38)$$

and where M_A and M_B are end moments.

For beam-columns under combined external pressure, compression, and bending moments, the ultimate strength interaction equation can be expressed as

$$\frac{P}{P_{UQ}} + \frac{C_M M_A}{M_{PQ}(1 - P/P_E)} = 1 \quad (15.39)$$

where the ultimate axial strength P_{UQ} and the plastic moment capacity M_{PQ} (considering the effects of hydrostatic pressure) are used to replace the parameters in Eqn (15.37) that do not account for the effect of hydrostatic pressure when calculating P_{ULT} and M_{ULT} .

15.2.4 Alternative Ultimate Strength Equation—Initial Yielding

For a beam-column with initial deflection and eccentric load as discussed in Section 20.2.2, an ultimate strength equation can be derived from an initial yielding condition

$$\sigma_{max} = \sigma_Y \quad (15.40)$$

where σ_{MAX} is given by Eqn (15.31). Hughes (1988) extended the Perry–Robertson formula to beam-columns under combined axial compression and lateral pressure, as expressed in the following:

$$\frac{\sigma_{ULT}}{\sigma_Y} = \frac{1}{2\gamma} \left[(1 + \eta + \gamma(1 - \mu)) - \sqrt{(1 + \eta + \gamma(1 - \mu))^2 - 4\gamma(1 - \mu)} \right] \quad (15.41)$$

where

$$\mu = \frac{M_{qmax}}{\sigma_Y W} \quad \text{and} \quad \eta = \frac{(w_{0max} + w_{qmax})A}{W} \quad (15.42)$$

In Eqn (15.42), the maximum moment and lateral deflection due to lateral pressure are obtained as follows:

$$M_{qmax} = \frac{ql^2}{8} \quad \text{and} \quad w_{qmax} = \frac{5ql^4}{384EI} \quad (15.43)$$

where q is the lateral pressure per unit length of the beam-column. It should be noted that the effect of the boundary condition on beam-column strength under combined compression and lateral pressure is significant, and may be accounted for by using the maximum moment and lateral deflection that are derived for the concerned boundary conditions. The general solution for elastic deflection of beam-columns under combined axial force, lateral pressure, and end moments can be found in Part 2, Chapter 16 of this book.

15.3 Plastic Design of Beam-Columns

15.3.1 Plastic Bending of Beam Cross Section

When a beam cross section is in fully plastic status due to pure bending, M_p , the plastic neutral axis shall separate the cross-sectional area equally into two parts. Assuming the distance from the plastic neutral axis to the geometric centers of the upper part and lower part of the cross section is y_U and y_L , the expression for M_p can be derived as

$$M_p = y_U \frac{A}{2} \sigma_Y + y_L \frac{A}{2} \sigma_Y = \frac{A}{2} \sigma_Y (y_U + y_L) \quad (15.44)$$

where A is sectional area and σ_y denotes yield strength of the material. If the plastic modulus Z is defined as

$$Z = M_p / \sigma_Y \quad (15.45)$$

Substituting Eqn (15.44) in Eqn (15.45) gives

$$Z = \frac{A}{2} (y_L + y_U) \quad (15.46)$$

The initial yielding moment M_Y may be defined, using the elastic sectional modulus W , as

$$M_Y = \sigma_Y W \quad (15.47)$$

It is then easy to get the ratio of the fully plastic moment and initial yielding moment as

$$f = M_P / M_Y = Z / W \quad (15.48)$$

Sectional moduli for some typical cross sections are seen below.

Rectangular Cross Section

$$Z = \frac{A}{2} (y_L + y_U) = \frac{bh^2}{4} \quad (15.49)$$

$$W = \frac{bh^2}{6} \quad (15.50)$$

$$f = \frac{Z}{W} = 1.5 \quad (15.51)$$

Tubular Cross Section ($t \ll d$)

$$I = \frac{\pi}{8}d^3t \quad (15.52)$$

$$W = \frac{\pi}{4}d^2t \quad (15.53)$$

$$f = \frac{Z}{W} = 1.27 \quad (15.54)$$

I-Profile ($t \ll h$)

$$Z = bth + \frac{sh^2}{4} \quad (15.55)$$

$$W = bth + \frac{bh^2}{6} \quad (15.56)$$

For some standard types of hot-rolled I-profiles, the ratio of the fully plastic moment and initial yielding moment lies in the range of 1.1–1.114.

15.3.2 Plastic Hinge Load

Let us consider a fully clamped beam under a laterally uniform pressure p , where the work done by the external load p may be calculated as

$$W_e = \int_0^l p dy = 2p \int_0^{l/2} \theta x dx = \frac{pl^2}{4} \theta \quad (15.57)$$

and where l is the beam length and θ denotes the rotational angle at two ends where plastic hinges occur. The work done by the plastic hinges at two ends and the center is

$$W_i = M_p \theta (1 + 2 + 1) = 4M_p \theta \quad (15.58)$$

Equating the work done by lateral pressure and internal work due to hinging,

$$M_p = \frac{pl^2}{16} \quad (15.59)$$

The collapse load $P = pl$ can be given as

$$P = \frac{16}{l} M_p \quad (15.60)$$

For a beam that is simply supported at its two ends, plastic collapse load P can be derived as

$$P = \frac{8}{l} M_p \quad (15.61)$$

In design codes, a mean value of the collapse load P for these two extreme boundary conditions is used to determine the required plastic section modulus

$$P = \frac{12}{l} M_p \quad (15.62)$$

The required section modulus Z is

$$W = \frac{Pl}{12\sigma_Y} \quad (15.63)$$

15.3.3 Plastic Interaction under Combined Axial Force and Bending

This subsection derives the plastic interaction equation for a beam-column due to the action of combined moment and axial load for the two most commonly used types of cross sections.

Rectangular Section

The rectangular section is characterized by its width b and height h . When it is in a fully plastic status, the stress in the middle will form a reduced axial load N . The stress in the upper and lower parts will contribute to the reduced plastic moment M . Assuming that the height of the middle part that forms a reduced axial load N is e , the following can be derived.

$$M = \frac{bh^2}{4} \sigma_Y - \frac{be^2}{4} \sigma_Y = \frac{bh^2}{4} \sigma_Y \left(1 - \frac{e^2}{h^2} \right) = M_P \left(1 - \frac{e^2}{h^2} \right) \quad (15.64)$$

$$N = be\sigma_Y = bh \frac{e}{h} \sigma_Y = N_P \frac{e}{h} \quad (15.65)$$

The combination of Eqns (15.64) and (15.65) gives

$$\frac{M}{M_P} + \frac{N^2}{N_P^2} = 1 \quad (15.66)$$

The above equation is the interaction formula for a rectangular cross section under combined axial load and bending.

Tubular Members

For tubular members, the interaction formula for the cross section can be given as

$$\frac{M}{M_P} = \cos\left(\frac{\pi}{2} \frac{P}{P_P}\right) \quad (15.67)$$

where

$$P_P = \sigma_Y A$$

$$M_P = 2\pi R t \sigma_Y$$

and where R is radius of the cross section.

15.4 Examples**15.4.1 Example 15.1: Elastic Buckling of Columns with Alternative Boundary Conditions****Problem:**

Derivation of the elastic buckling strength equation is based on the basic differential equation for initially straight columns

$$\frac{d^4 w}{dx^4} + k^2 \frac{d^2 w}{dx^2} = 0 \quad (15.68)$$

Solution:

The general solution of Eqn (15.68) is

$$w = A \sin kx + B \cos kx + Cx + D \quad (15.69)$$

1. Columns with Hinged Ends

The deflection and bending moments are zero at both ends

$$w = \frac{d^2 w}{dx^2} = 0 \quad \text{at } x = 0 \quad \text{and } x = l \quad (15.70)$$

Applying the boundary conditions to the general solution, the following is obtained.

$$B = C = D = 0 \quad \sin kl = 0 \quad (15.71)$$

Hence,

$$kl = n\pi, \quad n = 1 \quad (15.72)$$

Equation (15.72) yields to

$$P_E = \frac{\pi^2 EI}{l^2} \quad (15.73)$$

2. Columns with Fixed Ends

The boundary conditions are

$$w = \frac{dw}{dx} = 0 \quad \text{at} \quad x = 0 \quad \text{and} \quad x = l \quad (15.74)$$

Applying the boundary conditions to the general solution,

$$A = C = 0, \quad B = -D, \quad \sin \frac{kl}{2} = 0 \quad (15.75)$$

Hence,

$$kl = 2n\pi, \quad n = 1 \quad (15.76)$$

Equations (15.76) yields to

$$P_E = \frac{4\pi^2 EI}{l^2} \quad (15.77)$$

3. Columns with One End Fixed and the Other Free

The boundary condition at the fixed end is

$$w = \frac{dw}{dx} = 0 \quad \text{at} \quad x = 0 \quad (15.78)$$

At the free ends, the bending moment and shear force must equal zero.

$$\frac{d^2 w}{dx^2} = 0 \quad \text{at} \quad x = l \quad (15.79)$$

$$\frac{d^3 w}{dx^3} + k^2 \frac{dw}{dx} = 0 \quad \text{at} \quad x = l \quad (15.80)$$

Applying the boundary conditions to the general solution, the elastic buckling force is

$$P_E = \frac{\pi^2 EI}{4l^2} \quad (15.81)$$

4. Columns with One End Fixed and the Other Pinned

Applying the boundary conditions to the general solution, the following equation is obtained.

$$P_E = \frac{\pi^2 EI}{(0.7l)^2} \quad (15.82)$$

The results of this example are summarized in [Figure 15.5](#), showing the end-fixity coefficients and effective column length with various boundary conditions. A general buckling force equation may be obtained as

$$P_E = \frac{\pi^2 c EI}{l^2} \quad (15.83)$$

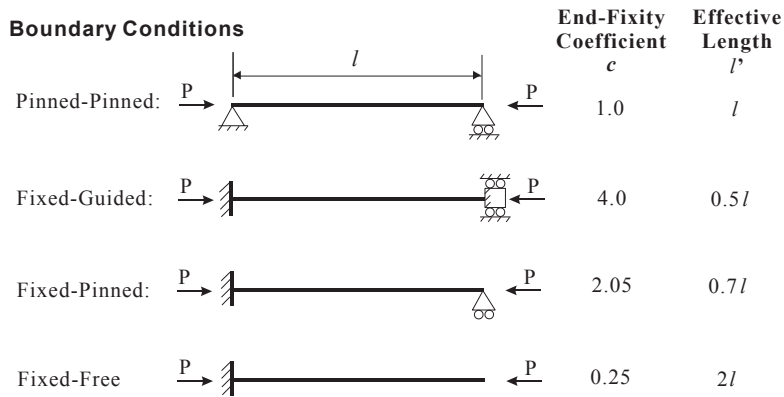


Figure 15.5

End-fixity coefficients and effective length for column buckling with various boundary conditions.

where c is the end-fixity coefficient and l' is the effective length.

$$P_E = \frac{\pi^2 EI}{l'^2} \tag{15.84}$$

15.4.2 Example 15.2: Two Types of Ultimate Strength: Buckling versus Fracture

Problem:

To compare different types of ultimate strength problems in a table: buckling vs fracture.

Solution:

Normally, ultimate strength analysis is inelastic buckling analysis for beam-columns, plates, and shells with initial imperfections. However, it should be pointed out that final

Table 15.1: Comparison of buckling strength analysis and fracture strength analysis

	Buckling Strength	Fracture Strength
Loads	Compression/torsion/shear force	Tensile loads
Imperfection	Geometrical imperfection and residual stress due to welding, impacts, etc.	Defects due to fabrication and fatigue loads
Linear solution	Elastic buckling	Linear fracture mechanics
Design criteria	Curve fitting of theoretical equations (Perry–Robertson, Johnson–Ostenfeld, etc.) to test results	Curve fitting of theoretical equations (interaction equation between ductile collapse and brittle fracture) to test results
Analysis objectives	<ol style="list-style-type: none"> 1. Determine buckling load 2. Determine allowable imperfections 3. Determine dimensions: stiffness, wall thickness, etc. 	<ol style="list-style-type: none"> 1. Determine fracture load 2. Determine allowable defect size 3. Determine dimensions: wall thickness, etc.

fracture is also a part of ultimate strength analysis. The assessment of final fracture has been mainly based on BPD6493 (or BS7910) in Europe and API 579 in the United States (see Chapter 29). In fact, there is similarity between buckling strength analysis and fracture strength analysis, as compared in [Table 15.1](#) below.

References

- Galambos, T.V., 2000. Guide to Stability Design Criteria for Metal Structures, fourth ed. John Wiley & Sons.
- Hughes, O., 1988. Ship Structural Design, A Rationally Based, Computer Aided Optimization Approach. SNAME (previously published by John Wiley & Sons, in 1983).
- Timoshenko, S.P., Gere, J., 1961. Theory of Elastic Stability. McGraw Hill.

Buckling and Local Buckling of Tubular Members

16.1 Introduction

16.1.1 General

Equations for buckling strength of tubular members may be found in several books (such as [Chen and Han, 1985](#)) and offshore design codes (such as [AISC \(1978\)](#) and [API RP 2A \(2001\)](#)). This chapter will address the interaction between the beam-column buckling mode and local (shell) buckling mode, based on [Yao et al. \(1986, 1988\)](#).

In the past 40 years, many kinds of offshore structures have been built and are in service for drilling and production in the oil and gas industry. Semisubmersible drilling units are among the most commonly used offshore structures owing to their high operation rates and good performance in rough seas. However, this type of offshore structure has no self-navigating systems and cannot escape from storms and rough sea conditions. Thus, the structure must have enough strength to withstand extreme sea conditions (i.e., the 100-year storm). Consequently, if structural members are free of damage, no buckling and/or plastic collapse may take place under ordinary rough sea conditions.

On the other hand, bracing members of drilling units are often subjected to accidental loads such as minor supply boat collisions and dropped objects from decks. Furthermore, a fatigue crack may occur after a service period. Such damage not only will cause a decrease in the load-carrying capacity of the damaged member, but also will change the internal forces in undamaged members. Consequently, under rough sea conditions, buckling and/or plastic collapse may take place in the undamaged and damaged members. This can cause a loss of integrity of the structural system. From this point of view, the ultimate strength limits and load-carrying capacity of tubular bracing members in semisubmersible drilling units should be assessed carefully.

Many studies have been performed during the last decade regarding the ultimate strength of tubular members. For example, [Chen and Han \(1985\)](#) investigated the influence of initial imperfections such as distortions and welding residual stresses on the ultimate strength of tubular members, and proposed a practical formula to evaluate ultimate strength. [Rashed \(1980\)](#) and [Ueda et al. \(1984\)](#) developed the *idealized structural unit* (element) for a tubular member, which accurately simulates its actual behavior including

overall buckling and plastification phenomena. They showed that when this model is applied, accurate results are obtained within a very short computation time.

However, these results can only be applied to tubular members with small diameter-to-thickness ratios—for example, D/t less than 30–50 for a typical bracing member in jackets and jack-ups. Local shell buckling does not need to be considered in these members. On the other hand, bracing members in semisubmersible drilling units have large D/t ratios—for example, between 70 and 130. For such tubular members, local buckling may take place before or after ultimate strength is attained, just as [Smith et al. \(1979\)](#) and [Bouwkamp \(1975\)](#) observed in their experiments. Therefore, for the assessment of the load-carrying capacity of such bracing members, both ultimate strength and strength reduction due to local buckling must be considered. However, a systematic study of this phenomenon has not been performed yet.

In this chapter, a series of experiments are first carried out using large-scale tubular test specimens that model a bracing member in an existing semisubmersible drilling unit. Axial compressive loads are applied with eccentricity. Small-scale tubular test specimens are prepared with D/t ratios between 40 and 97, and tested under the same loading conditions. Based on experimental results, an analytical model is then proposed to simulate the actual behavior of a tubular member, taking into consideration the influence of local buckling. Furthermore, by incorporating this model, the idealized structural unit is developed. The validity and usefulness of the proposed model is demonstrated by comparing the calculated results with present and previous experimental results.

16.1.2 Safety Factors for Offshore Strength Assessment

The basic safety factors in offshore structural designs are defined for two cases:

- Static loading: 1.67 for axial or bending stress. Static loads include the operational gravity loading and weight of the vessel.
- Combined static and environmental loads: 1.25 for axial or bending stress. Static loads are combined with relevant environmental loads including acceleration and heeling forces.

For members under axial tension or bending, the allowable stress is the yield stress divided by the factor of safety defined above.

16.2 Experiments

16.2.1 Test Specimens

Dimensions of a typical bracing member in an existing semisubmersible drilling unit are shown in [Table 16.1](#). The slenderness ratio is not so different from that of a bracing member in a fixed-jacket or jack-up drilling unit.

Table 16.1: Dimensions of existing bracing member and test specimen

	Length L (mm)	Outer Diameter D (mm)	Thickness T (mm)	D/t	L/d	R
Existing bracing member	27,840	1800	14.5	124	15.5	631.3
Test specimen	8000	508	6.4	78	15.7	177.4

$$r = \sqrt{I/A}, \quad I = \frac{\pi}{64} [D^4 - (D - 2t)^4], \quad A = \frac{\pi}{4} [D^2 - (D - 2t)^2]$$

Taking E and σ_y as 21,000 and 32 kgf/mm², respectively, the critical D/t is 73. If D/t is beyond the critical ratio, local buckling may occur before the plasticity of the cross section. It is known that for a D/t of 124, the existing bracing member is far above the critical value.

From this exercise, it may be concluded that local buckling takes place before the fully plastic condition is satisfied at the cross section where internal forces are most severe. Welded tubes on the market are selected as test specimens whose collapse behavior is expected to be close to that of the above-mentioned bracing member. The dimensions of the test specimens are shown in Table 16.1. Their diameter is 508 mm, and their length is taken to be 8000 mm so that their slenderness ratio will be close to that of the existing bracing member. The scale factor is 1/3.5, and this specimen is referred to as a large-scale test specimen. The D/t is 78, which is small compared with that of the already existing one. However, it is still large enough for local buckling to be a concern.

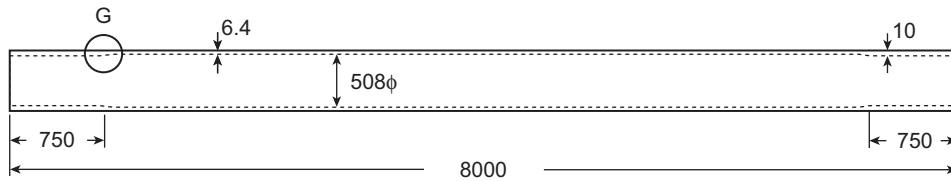
The large-scale test specimen is illustrated in Figure 16.1. The tube's wall thickness is 6.4 mm. However, within 750 mm for both ends, the thickness is increased to 10 mm in order to avoid the occurrence of local collapse near the ends.

Test specimens of alternative sizes are also tested. The inner diameter is kept as 95 mm, and the tube wall thickness varies as 1.0, 1.2, 1.6, and 2.5 mm. The D/t ratios of these test specimens are then varied between 40 and 97, and correspondence with the bracing members in the existing semisubmersible drilling unit is not considered. The thickness near both ends is not increased. The dimensions of small-scale test specimens are shown in Table 16.2, along with material properties and experimental results.

16.2.2 Material Tests

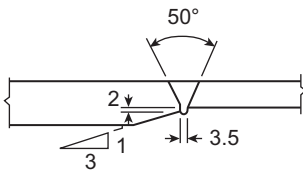
The large-scale test specimens were fabricated by welding a circular member that has been bent from a flat plate. To avoid the effect of residual stress on the measured material properties, four pieces of tensile test specimen were cut from the side opposite to the weld line. From the tensile tests, the measured Young's modulus is $E = 21,180$ kgf/mm², and the Poisson's ratio is $\nu = 0.32$. The measured yield stress (corresponding to a 0.2% offset

(a) Large-scale test specimen



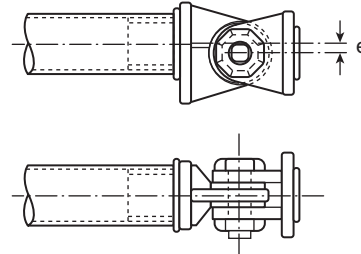
Test specimen

(b) Detail at G



Detail at G

(c) End fixture



End fixture

Figure 16.1

Large-scale test specimen and its end fixture.

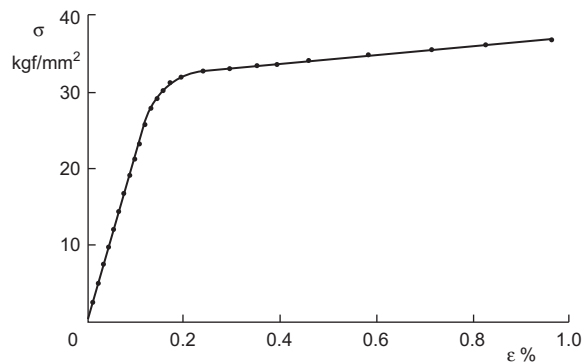
strain) is: $\sigma_Y = 34.55 \text{ kgf/mm}^2$. The nominal stress—strain relation from the material is shown in Figure 16.2. The small-scale test specimens consist of four different D/t ratios, namely series A, B, C, and D. Due to the lack of available pipes of these sizes, test specimens were fabricated by cold-forming pipe with a wall thickness of 3.2 mm. As a result of the Bauschinger effect being introduced in the cold-fabrication process, the ultimate tensile stress is much higher than the ultimate compressive stress. Tensile test specimens were fabricated by cutting from the circular pipe along the longitudinal direction. The cross section of the material test specimens was fabricated to a rectangular cross section according to the industry standard for material tensile testing. In the two sides of the central cross section, strain gauges were attached to measure the strain. The nominal stress—strain relationships for the specimens of the A, B, C, and D series are shown in Figure 16.3 as solid lines. The ductility of the material was reduced due to the cold-fabrication process. Tensile failure occurred when the strain was on the order of 6–14%.

Measured cross-sectional areas for specimens, measured Young's moduli, and yield stresses are listed in Table 16.3. Two types of yield stresses were defined: yield strength corresponding to a 0.2% offset plastic strain $\sigma_{0.2}$ and yield strength corresponding to a 0.5% total strain $\sigma_{0.5}$.

The compressive material tests were conducted using the stub pipe. The length of the test specimen was selected such that column buckling would not be a concern, and a specimen

Table 16.2: Dimensions and test results for small-scale test specimens

Specimen Number	Outer Diameter D (mm)	Wall Thickness t (mm)	Length L (mm)	Initial Deflection (mm)	Load Eccentricity e/D	Young's Modulus (kgf/mm)	0.2%Yield Stress (kgf/mm)	Ultimate Load (ton)	Buckling Mode
HA0	97.0	1.0	1430	—	0	19,645	35.25	7.51	DENT
HA2	97.0	1.0	1635	0.43	1/4	19,645	35.25	5.75	DENT
HA3	97.0	1.0	895	0.13	1/16	19,645	35.25	15.78	DENT
HA4	97.0	1.0	605	0.25	1/16	19,645	35.25	10.08	DENT
HB1	97.4	1.2	1635	0.10	1/32	19,616	37.50	15.90	DENT
HB2	97.4	1.2	1430	0.61	1/16	19,616	37.50	15.10	DENT
HB3	97.4	1.2	1430	1.02	1/8	19,616	37.50	7.95	DENT
HC1	98.2	1.6	1430	0.44	1/32	19,160	37.00	13.76	DENT
HC2	98.2	1.6	1430	0.64	1/16	19,160	37.00	11.90	DENT
HC3	98.2	1.6	1430	1.40	1/8	19,160	37.00	15.99	COS
HD1	100.0	2.5	1430	0.73	1/32	18,109	33.00	115.70	DENT
HD2	100.0	2.5	1430	0.63	1/16	18,809	33.00	17.95	DENT
HD3	100.0	2.5	1430	0.87	1/8	18,809	33.00	14.95	DENT
HD4	100.0	2.5	1635	1.44	1/4	18,809	33.00	13.46	COS
HD5	100.0	2.5	895	0.35	1/32	18,809	33.00	26.85	COS
HD6	100.0	2.5	575	0.35	1/16	18,809	33.00	30.55	COS
BA1	97.0	1.0	650	—	Bending	19,645	35.25	2.75	DENT
BB1	97.4	1.2	650	—	Bending	19,616	37.50	3.09	DENT
BB2	97.4	1.2	650	—	Bending	19,616	37.50	3.05	DENT
BC1	98.2	1.6	650	—	Bending	19,610	37.00	4.68	DENT
BC2	98.2	1.6	650	—	Bending	19,610	37.00	4.66	DENT
BD1	100.0	2.5	650	—	Bending	18,809	33.00	7.84	DENT

**Figure 16.2**

Tensile stress–strain curve for large-scale test specimens.

length of 300 mm was chosen for all test specimens. Four biaxial strain gauges were put on the central cross-sectional pieces of the test specimens. The nominal stress–strain relations are plotted in [Figure 16.3](#) and denoted by dotted lines. Because shell mode buckling occurred in the upper or lower edges, the stress–strain relationship was measured up to a strain level of 1%. The obtained yield strength is given in [Table 16.3](#).

Due to tensile expansion applied in manufacturing for specimens along the longitudinal direction, a significant Bauschinger effect was observed. There is little strain-hardening effect in the tensile side of the stress–strain relation. On the other hand, a significant strain-hardening effect was observed for the compressive side. As shown in the stress–strain curves, there is a significant difference between the material properties in the tensile side and the compressive side. This difference in material properties could be a primary reason for the difference between test results and analytical solutions for the load-deflection and load-end-shortening curves. Heat treatment should probably have been introduced to eliminate differences in material properties for the tensile and compressive sides and to reduce the Bauschinger effect. However, due to the potential for buckling of the thin-walled pipe, such a heat treatment was not applied.

16.2.3 Buckling Test Procedures

For large-scale test specimens, axial compressive loads are applied with eccentricity using large-scale model testing machines installed at Hiroshima University and weighing roughly 3000 tons. Simply supported end conditions are simulated at both ends with pinned joints. Both ends of each test specimen are attached to loading heads through cylindrical plugs, as illustrated in [Figure 16.1\(c\)](#). The eccentricity of the axial load is taken to be 1/8, 1/4, and 3/8 times that of the outer diameter. These eccentricities are obtained by changing the position of the plug relative to the loading heads. This testing machine is

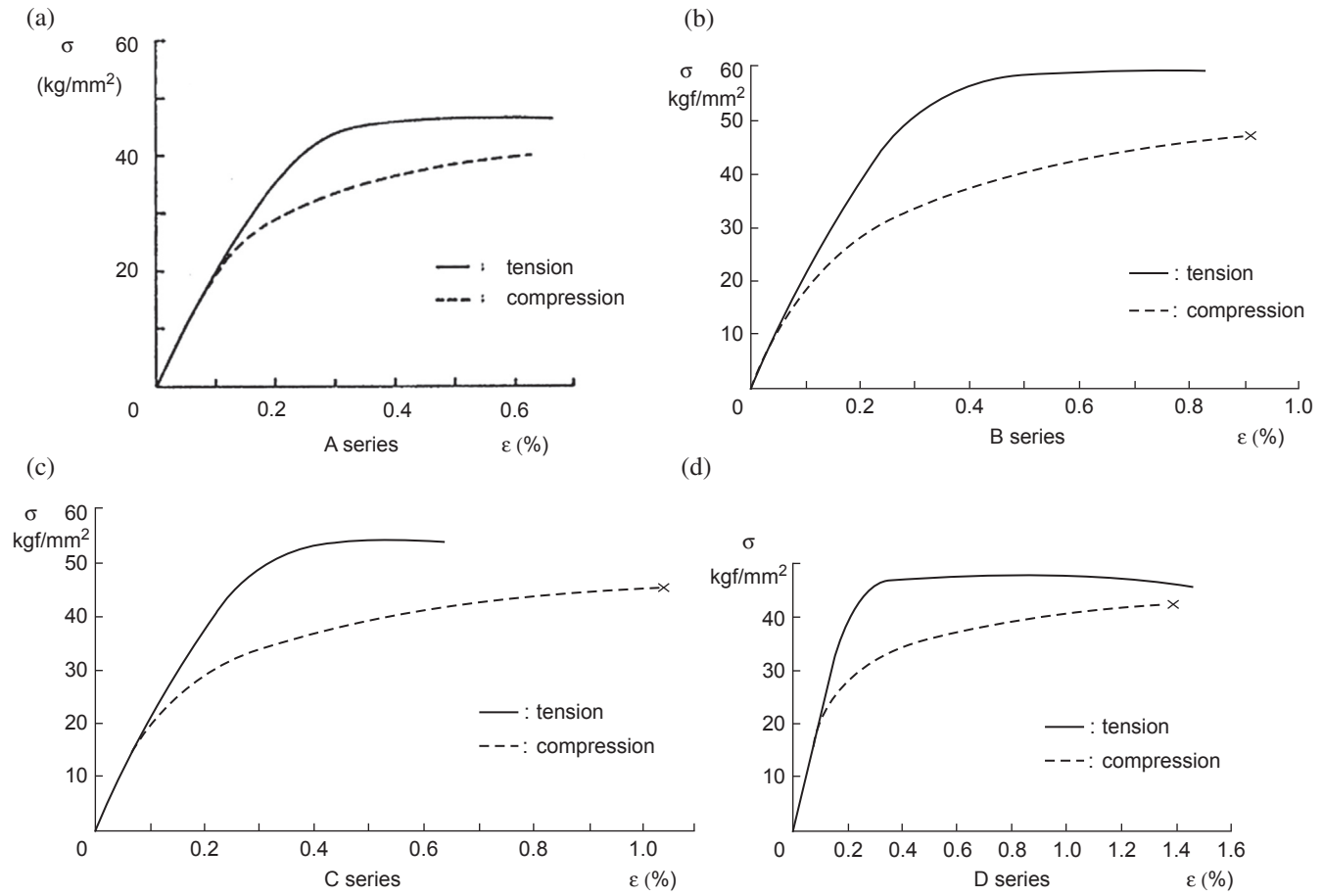


Figure 16.3
Tensile stress–strain curve for small-scale test specimens, series (a–d).

Table 16.3: Dimensions and results of material tests for small-scale test specimens

Specimen Number	Wall Thickness T (mm)	D/t ratio (—)	Specimen Cross-Sectional Area A (m ²)	Tensile Test		Compressive Test		Compressive Test	
				Yield Stress $\sigma_{0.2}$ (kgf/mm ²)	Tensile Test Yield Force $P_{0.2}$ (kgf)	Test Yield Stress $\sigma_{0.2}$ (kgf/mm ²)	Test Yield Force $P_{0.2}$ (kgf)	Test Yield Stress $\sigma_{0.5}$ (kgf/mm ²)	Test Yield Force $P_{0.5}$ (kgf)
A	1.0	97.0	301.59	45.00	13,751.55	35.25	10,631.05	40.00	12,063.60
B	1.2	81.2	362.67	58.00	21,034.86	37.50	13,600.13	44.50	16,138.82
C	1.6	61.4	485.56	54.23	26,341.63	37.00	17,965.72	42.75	20,757.69
D	2.5	40.0	765.76	46.75	357,915.28	33.00	25,270.08	38.25	29,290.32

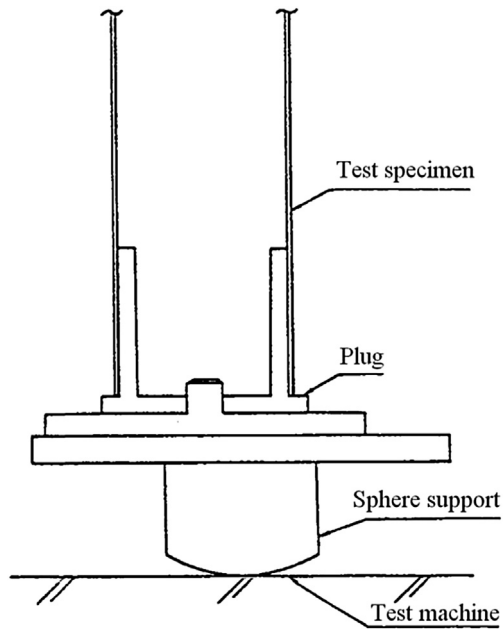


Figure 16.4

End fixtures for eccentric axial thrust of small-scale test specimens.

a horizontal type, and the test specimens are placed horizontally. Therefore, an initial deflection of 0.63 mm is produced due to the specimen's own weight.

For small-scale test specimens, two types of loads are applied, axial compressive loads with eccentricity and pure bending loads. Eccentric axial loads are applied through a plug and a spherical support as illustrated in Figure 16.4. The pure bending is applied using a four-point bending as illustrated in Figure 16.5. Rigid tubes are inserted into both ends of

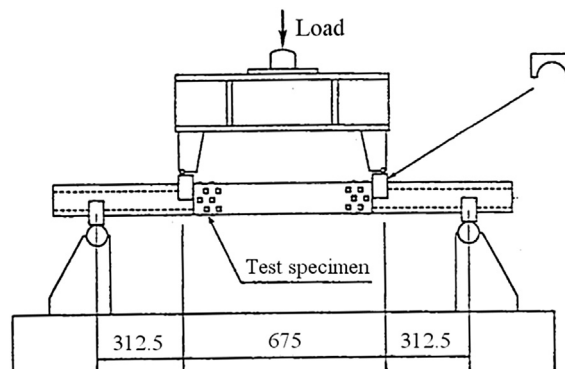


Figure 16.5

Apparatus for pure bending test of small-scale test specimen.

the specimen so that the specimen does not deform locally at the loading points. A test specimen is connected to rigid tubes with friction bolts.

Unloading and reloading are performed several times during the experiment, especially after the occurrence of local buckling. Strains in axial and circumferential directions, lateral deflections, and load-line displacements are all measured during the experiment.

16.2.4 Test Results

Eccentric Axial Compression Tests Using Large-Scale Specimens

Axial loads versus lateral deflection relationships are plotted using the solid lines shown in Figure 16.7. In all cases, no significant deformation of cross sections is observed until ultimate strength is attained. After reaching ultimate strength, load decreases as lateral deflection increases, while local buckling takes place near a midspan point, and the load-carrying capacity suddenly decreases. The local buckling mode in terms of cross-sectional deformation may be approximated by a cosine mode, illustrated in Figure 16.8(a). The wavelength of this local buckling mode is almost a half-circle in the circumferential direction and is very short in the axial direction. With a further increase in lateral deflection, local denting deformation takes place at the foot of the initial cosine-buckling wave, as shown in Figure 16.8(b).

The horizontally flattened part grows and folds toward the inside of cross section $c-c'$. At the same time, a similar phenomenon is observed at cross section $a-a'$, but with two dents, $A-B$ and $A-C$. The horizontally flattened part of cross section $c-c'$ grows until it

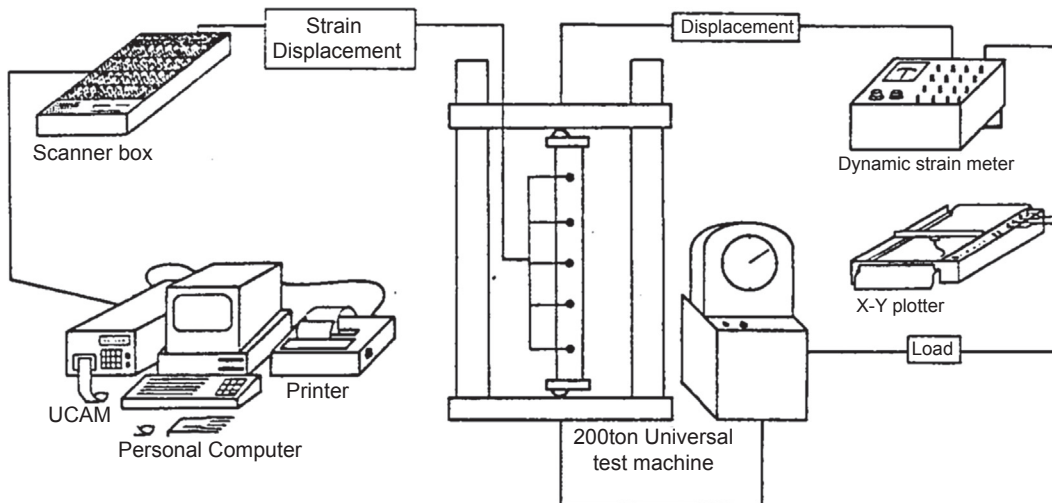
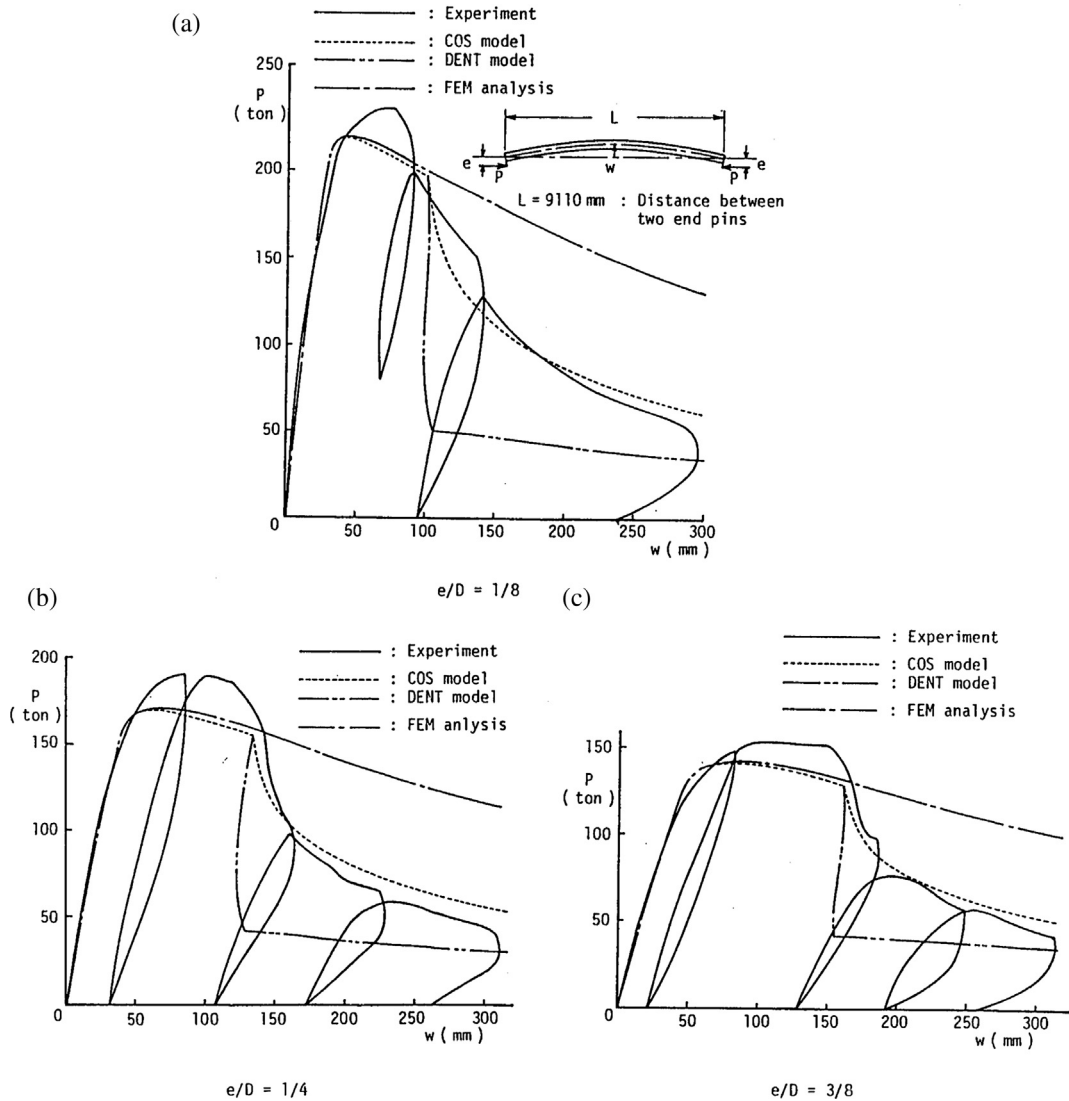


Figure 16.6
Instrumentation diagram for buckling/collapse tests.


Figure 16.7

Load—lateral deflection curves of large scale test specimens subjected to axial thrust with eccentricity.

becomes nearly equal to a quarter-circle—see $B'-C'$ in Figure 16.8(c). Then, two other dents, $A'-B'$ and $C'-D'$, begin to grow as illustrated in Figure 16.8(c). At this stage, significant deformation is observed at cross section $b-b'$. A local cosine-buckling wave occurring in the area of maximum compressive strain is followed by the formation of dents at both sides of the wave. This type of collapse mode is observed in all large-scale test specimens regardless of the magnitude of eccentricity. It should be noted that the

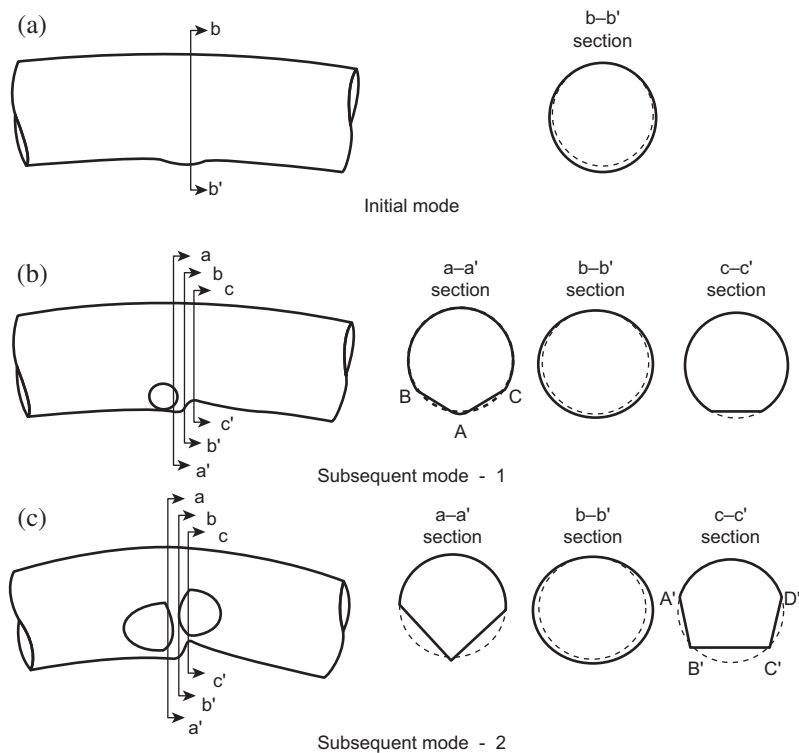


Figure 16.8
Local buckling in cosine mode.

length of a fully developed buckling wave— $B'-C'$ in [Figure 16.8\(c\)](#)—is close to that for shell buckling under pure compression.

Eccentric Axial Compression Test Using Small-Scale Specimens

Test facilities and instrumentations are illustrated in [Figure 16.6](#).

Axial loads versus end-shortening relationships are plotted in [Figure 16.9\(a–d\)](#). These figures indicate that as eccentricity increases, ultimate strength decreases and a larger displacement is produced before local buckling takes place. Unloading and reloading paths are omitted in these figures.

As length increases, the same tendency is observed.

If the length and the D/t ratio are the same, the load–displacement path, after local buckling, converges to a certain value.

In the case of large-scale test specimens, local buckling takes place in a cosine mode. However, only three small-scale test specimens have local buckling of a cosine mode.

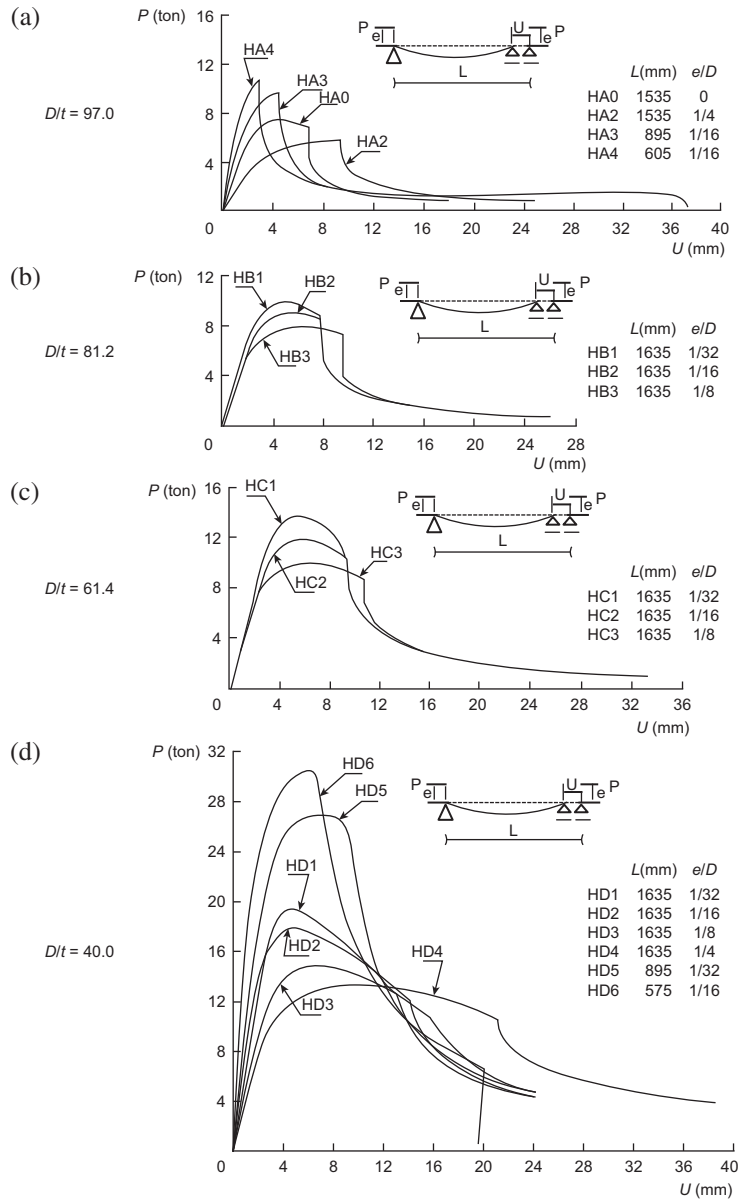


Figure 16.9

Load-end shortening curves for small-scale test specimens subjected to axial thrust with eccentricity.

In the other 13 specimens, local buckling takes place in a dent node. The local buckling of a dent type initializes dent growth as the lateral deflection increases, until it becomes about the size of a quarter-circle. Then, two dents are formed at cross section $b-b'$ adjacent to the initial dent as illustrated in Figure 16.10(b). With a further increase in

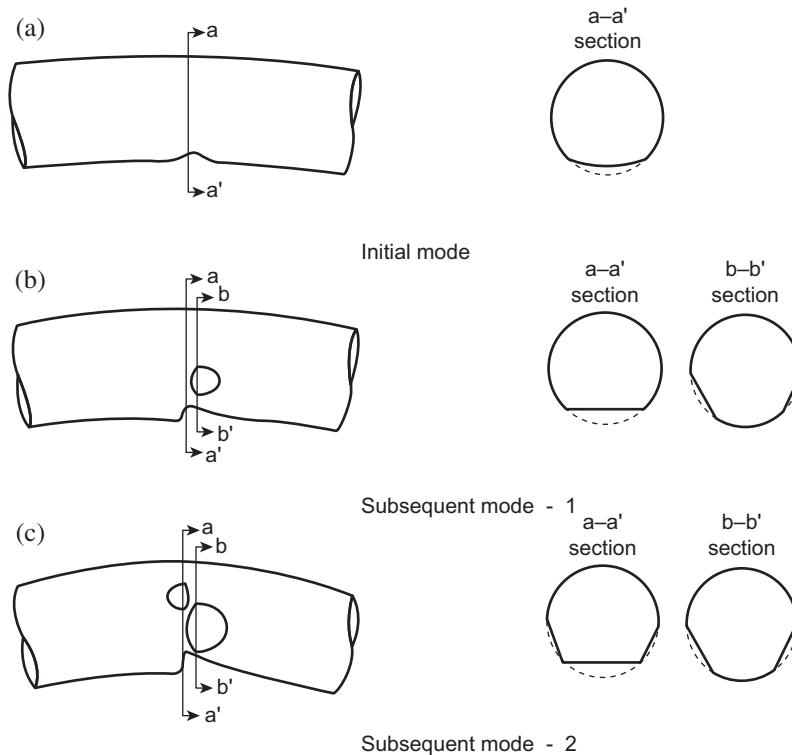


Figure 16.10
Local buckling in dent mode.

lateral deflection, two other dents begin to grow at cross section a—a' of the initial dent as shown in [Figure 16.10\(c\)](#). It is not clear which mode of local buckling would take place. However, the buckling mode depends on the diameter to thickness ratio, the combination of axial forces and bending moments at the cross section, and material properties.

Pure Bending Test for Small-Scale Specimens

Loads versus load-line displacement relationships are plotted in [Figure 16.11](#). In the case of the BD1 specimen, the breaking of the specimen occurred from a bolt-hole near the end before local buckling took place. In all specimens, cross-sectional flattening is observed as the load increases. Furthermore, deformation in a ripple pattern with two or three half-waves begins to grow near the ultimate strength. Ultimate strength seems to be attained by cross-sectional flattening and the formation of ripples. In the case of thin-walled tubes, the bottom of one wave ripple suddenly changes due to a dent near the ultimate strength, causing load-carrying capacity to decrease. Contrary to this, the ripple deformation grows after the ultimate strength is attained in the case of thick-walled specimens. Then, the ripple suddenly changes to a local dent.

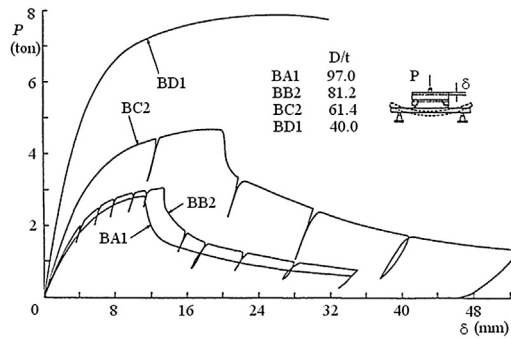


Figure 16.11

Load versus load-line curves for small-scale test specimens subjected to pure bending loads.

It is not clear whether the initiation of local buckling is due to the formation of a ripple pattern or the formation of a dent. However, much attention has to be paid to the formation of a dent, as this causes a sudden drop in the load-carrying capacity.

The formation of new dents after the initial dent has formed is almost the same as in the case of eccentric axial compression.

16.3 Theory of Analysis

16.3.1 Simplified Elastoplastic Large Deflection Analysis

In this section, an analytical model is proposed that simulates the elastoplastic large deflection behavior of a tubular member. The model takes into account the influence of local buckling. The material is assumed elastic–perfectly plastic. It is also assumed that local buckling takes place after plastification occurs.

Preanalysis of Local Buckling

A tubular member is assumed to be accompanied by the initial deflection of a sinusoidal form

$$w_0 = a_0 \sin \frac{\pi x}{l} \quad (16.1)$$

where

l = Length of a tubular member

a_0 = Magnitude of initial deflection

The equilibrium equation of a beam-column may be written as

$$EI \frac{d^4}{dx^4} (w - w_0) + P \frac{d^2 w}{dx^2} = q \quad (16.2)$$

where

$$\begin{aligned} w &= \text{Total deflection} & P &= \text{Axial force (positive in compressive)} \\ E &= \text{Young's modulus} & I &= \text{Moment of inertia of a cross section} \end{aligned}$$

The general solution of Eqn (16.2) is expressed as follows

$$w = \alpha_1 \cos kx + \alpha_2 \sin kx + \alpha_3 x + \alpha_4 + Q' \sin \pi x/l + f(q) \quad (16.3)$$

where

$$k = \sqrt{P/EI} \quad (16.4)$$

$$Q' = a_0 P_E / (P_E - P) \quad (16.5)$$

$$P_E = \pi^2 EI / l^2 \quad (16.6)$$

and $f(q)$ represents the deflection due to the lateral load q .

It is assumed that the member is subjected to axial compression, end moments, and linearly distributed lateral loads as illustrated in Figure 16.12. If both ends are simply supported, Eqn (16.3) reduces to

$$\begin{aligned} w_e = \frac{1}{P} \left[\left(M_i + \frac{q_i}{k^2} \right) \left\{ \frac{\sin k(l-x)}{\sin kl} + \frac{l-x}{l} \right\} - \left(M_j + \frac{q_j}{k^2} \right) \left(\frac{\sin kx}{\sin kl} + \frac{x}{l} \right) \right] \\ + \frac{a_0 P}{P_E - P} + \frac{1}{P} \left\{ - \left[\frac{q_j}{6} + \frac{q_i}{3} \right] lx + \frac{1}{2} q_i x^2 + \frac{1}{6l} (q_j - q_i) x^3 \right\} \end{aligned} \quad (16.7)$$

The suffix e in Eqn (16.7) implies the elastic range. Equation (16.7) give the relationship between the axial force and lateral deflection until plastification takes place. Using this deflection, the mean compressive axial strain is expressed as

$$\varepsilon = \frac{P}{EA} + \frac{1}{2l} \int_0^l \left[\left(\frac{dw_e}{dx} \right)^2 - \left(\frac{dw_0}{dx} \right)^2 \right] dx \quad (16.8)$$

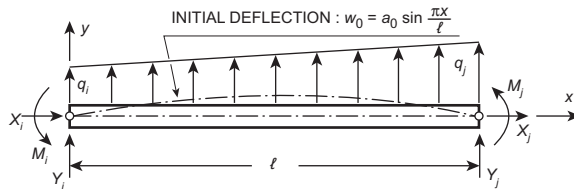


Figure 16.12
Beam-column member under external loads.

In the inelastic region, flexural rigidity is not uniform along the length of a member. For this case, the plastic component of deflection w_p is introduced. Then, the total deflection is expressed as the sum of the elastic and the plastic components.

$$w = w_e + w_p \quad (16.9)$$

Here, w_p is evaluated as the cumulative value of all increments of the plastic components of deflection, which are assumed in the following forms

$$\text{I} \quad 0 \leq x < l_1 \quad dw_p = cx/l_1 \quad (16.10)$$

$$\text{II} \quad l_1 \leq x < l_1 + l_p \quad dw_p = c(\gamma_1 x^2 + \gamma_2 x + \gamma_3) \quad (16.11)$$

$$\text{III} \quad l_1 + l_p \leq x \leq l \quad dw_p = c(l-x)/l_{11} \quad (16.12)$$

where

$$\gamma_1 = -l/2l_1 l_{11} l_p \quad (16.13)$$

$$\gamma_2 = (l_{11} l_p + ll_1)/l_1 l_{11} l_p \quad (16.14)$$

$$\gamma_3 = -l_1^2 l/2l_1 l_{11} l_p \quad (16.15)$$

The deflection modes represented by Eqns (16.10) through (16.12) are shown in Figure 16.13. The increment of this plastic deflection component produces a constant plastic curvature in the region l_p ($l_1 \leq x \leq l_1 + l_p$). The procedure used to estimate l_p will be discussed later.

The inelastic analysis is performed in an incremental form. Thus, w_p in Eqn (16.9), at the nm -th step of this analysis, is expressed as

$$w_p(n) = w_p(n-1) + dw_p(n) \quad (16.16)$$

where $w_p(n-1)$ is the cumulative value of the increments of plastic deflection until the $(n-1)$ th step and $dw_p(n)$ is the increment at the n -th step.

Two possible stress distributions may exist at a cross section after initial yielding, depending on the magnitude of the strain at the tension side of the bending;

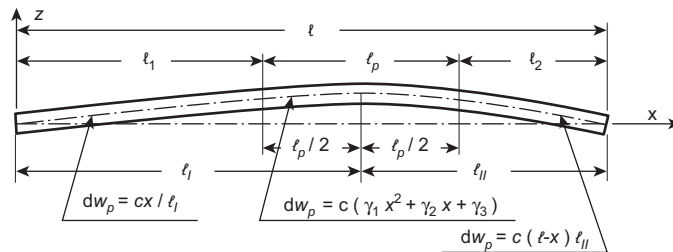


Figure 16.13
Plastic component of lateral deflection.

see Figure 16.14. For these stress distributions, the axial force and the bending moment are evaluated as

$$P = 2 \int_0^{\alpha_1} \sigma_y R t d\theta + 2 \int_{\alpha_1}^{\pi-\alpha_2} \frac{\eta + R \cos \theta}{\eta + R \cos \alpha_1} \sigma_y R t d\theta - 2 \int_{\pi-\alpha_2}^{\pi} \sigma_y R t d\theta \quad (16.17)$$

$$M = 2 \int_0^{\alpha_1} \sigma_y R^2 t \cos \theta d\theta + 2 \int_{\alpha_1}^{\pi-\alpha_2} \frac{\eta + \cos \theta}{\eta + \cos \alpha_1} \sigma_y R^2 t \cos \theta d\theta - 2 \int_{\pi-\alpha_2}^{\pi} \sigma_y R^2 t \cos \theta d\theta \quad (16.18)$$

where σ_y is the yield stress. For the Case A stress distribution, α_2 is taken as 0.

The equilibrium condition for the bending moment gives the following:

$$P(w_e + w_p + e_0) + Q = M \quad (16.19)$$

where

$$e_0 = e_i + l_1(e_i - e_j)/l, \quad e_i = M_i/P, \quad e_j = -M_j/P \quad (16.20)$$

and Q is the bending moment due to distributed lateral loads, q .

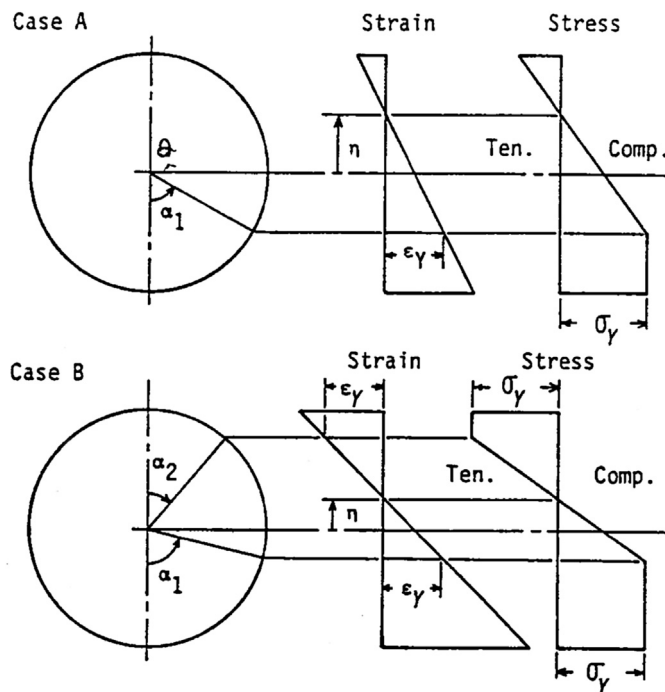


Figure 16.14
Elastoplastic stress distribution free from local buckling.

On the other hand, the curvature at a cross section may be expressed as

$$\frac{1}{\rho} = -\frac{\sigma_y}{E(\eta + R \cos \alpha_1)} = \frac{d^2}{dx^2} (w_e + w_p - w_0) \quad (16.21)$$

For the Case A stress distribution, Eqns (16.17), (16.19), and (16.21) reduce to the following using Eqns (16.7), (16.10)–(16.12)

$$P(\eta + f_1) = f_2 + c_1 \eta \quad (16.22)$$

$$P(w + e_0) = f_3 + (f_4 + f_5 \eta) / (\eta + f_1) + f_6 \quad (16.23)$$

$$c_2 / (\eta + f_1) = \kappa \quad (16.24)$$

where

$$\begin{aligned} f_1 &= R \cos \alpha_1 \\ f_2 &= 2\sigma_y R^2 t (\alpha_1 \cos \alpha_1 - \sin \alpha_1) \\ f_3 &= 2\sigma_y R^2 t \sin \alpha_1 \\ f_4 &= \sigma_y R^3 t (\pi - \alpha_1 - \sin \alpha_1 \cos \alpha_1) \end{aligned} \quad (16.25)$$

$$\begin{aligned} f_5 &= -2\sigma_y R^2 t \sin \alpha_1 \\ f_6 &= q_j \left(l_1^3 / l - ll_1 \right) / 6 - q_i \left(l_1^3 / 6l - l_1^2 / 2 + ll_1 / 3 \right) \\ c_1 &= 2\pi \sigma_y R t \end{aligned} \quad (16.26)$$

$$c_2 = l^2 \sigma_y / \pi^2 E \quad (16.27)$$

$$w = (w_e + w_p) |_{x=l_1} \quad (16.27)$$

$$\kappa = \frac{d^2 (w_e + w_p - w_0)}{dx^2} |_{x=l_1}$$

Similarly, the following equations are obtained for the Case B stress distribution.

$$P(\eta + f_1) = f_2 + h_1 + (c_2 - h_2) \eta \quad (16.28)$$

$$P(w + e_0) = f_3 + h_4 + \{f_4 - h_3 + (f_5 + h_4) \eta\} / (\eta + f_1) + f_6 \quad (16.29)$$

$$c_2 / (\eta + f_1) = \kappa \quad (16.30)$$

$$\eta = R(\cos \alpha_2 - \cos \alpha_1) / 2 \quad (16.31)$$

where

$$\begin{aligned} h_1 &= 2\sigma_y R^2 t (\sin \alpha_2 - \alpha_2 \cos \alpha_1) \\ h_2 &= 4\sigma_y R t \alpha_2 \\ h_3 &= \sigma_y R^3 t (\alpha_2 + \sin \alpha_2 \cos \alpha_2) \\ h_4 &= 2\sigma_y R^2 t \sin \alpha_2 \end{aligned} \quad (16.32)$$

Solving Eqns (16.22) through (16.24) for Case A and Eqns (16.28) through (16.31) for Case B with respect to P , η , α_1 , and α_2 , respectively, the relationship between axial load and lateral deflection can be obtained.

The mean compressive axial strain in the elastoplastic range can be given as

$$\varepsilon = \frac{P}{EA} \frac{l-2R}{l} + \frac{2R}{l} \frac{\eta\sigma_y}{E(\eta + R \cos \alpha_1)} + \frac{1}{2l} \int_0^l \left[\left(\frac{dw}{dx} \right)^2 - \left(\frac{dw_0}{dx} \right)^2 \right] dx \quad (16.33)$$

The second term on the right-hand side of Eqn (16.33) represents the plastic component of the axial strain. It is assumed that the plastic strain of $\eta\sigma_y/(\eta + R \cos \alpha_1)$ is uniformly distributed within a region $2R$.

Critical Condition for Local Buckling

According to the classical theory of elastic stability, critical buckling strain in a cylindrical shell under axial compression is given by the following (Timoshenko and Gere, 1961):

$$\varepsilon_{cr} = \frac{1}{3\sqrt{1-\nu^2}} \frac{t}{R} = 0.61 \frac{t}{R} \quad (16.34)$$

However, the critical strain for plastic shell buckling is instead given by Gerard (1962), Batterman (1965), as well as others. Reddy (1979) concluded that the critical buckling strain of a shell occurs within the limits represented below, including the pure bending case

$$0.2 \frac{t}{R} < \varepsilon_{cr} < 0.4 \frac{t}{R} \quad (16.35)$$

In general, the axial force and bending moment exist at the cross sections of tubular members. Consequently, the strain at a cross section is not uniform. This chapter proposes an empirical formula, where the critical buckling strain is in terms of the ratio of maximum bending strain to axial strain $\varepsilon_b/\varepsilon_a$, and the wall thickness to radius ratio t/R :

$$\varepsilon_{cr} = 0.155 \left\{ 0.25(\varepsilon_b/\varepsilon_a)^2 + 1.0 \right\} (t/R) \quad \text{for } \varepsilon_b/\varepsilon_a < 2.5 \quad (16.36)$$

$$\varepsilon_{cr} = 0.4t/R \quad \text{for } \varepsilon_b/\varepsilon_a \geq 2.5$$

Figure 16.15 shows the experimental critical buckling strains collected and arranged by Reddy (1979). The critical buckling strain evaluated by Eqn (16.36) falls between two lines, $0.115 t/R$ and $0.4 t/R$, depending on the magnitude of $\varepsilon_b/\varepsilon_a$.

Post-Local-Buckling Analysis

As described in Chapter 21.2, local buckling takes place in a cosine mode or a dent mode. Accordingly, two kinds of analytical models are proposed, the COS model and the DENT model.

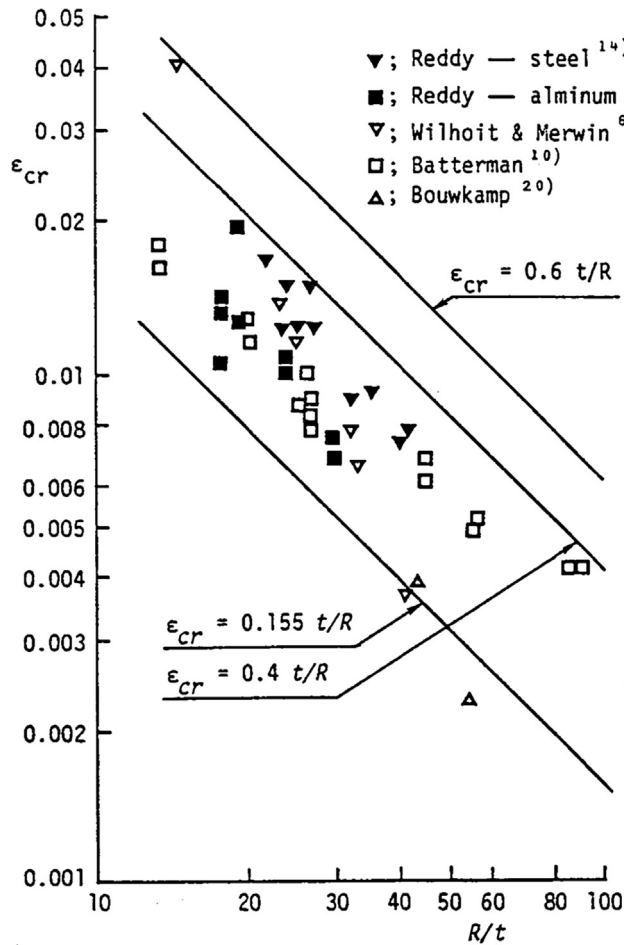


Figure 16.15
Critical buckling strain.

COS Model

Within the region where the strain in the axial direction exceeds ϵ_{cr} , local buckling deformation is assumed to take place. Its mode in the axial direction is approximated as follows (see Figure 16.16(a)):

$$w_b = (\delta/2)\{1 - \cos(2\pi x/s)\} \quad (16.37)$$

where s represents the buckling wave length in the axial direction. Here, s is taken as 0.7 times the wavelength of the elastic buckling evaluated by the classical theory of elastic stability. That is,

$$s = 0.7 \frac{\pi}{\sqrt[4]{12(1-\nu^2)}} \sqrt{Rt} = 1.21\sqrt{Rt} \quad (16.38)$$

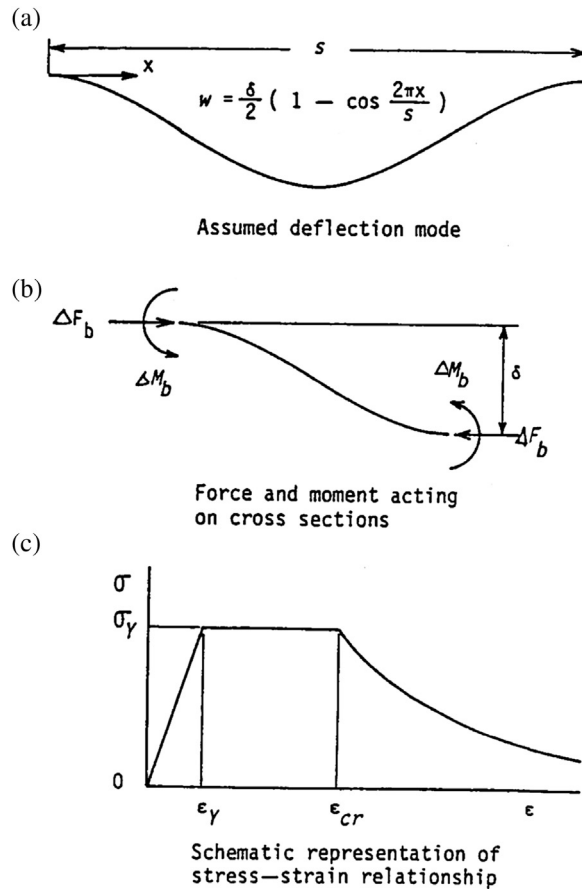


Figure 16.16

Assumed local buckling mode for the COS model.

The axial strain in a tube wall fiber where local buckling has occurred can be expressed as

$$\epsilon = \epsilon_{cr} + (1/2s) \int_0^s (dw_b/dx)^2 dx = \epsilon_{cr} + (\pi^2/4)(\delta/s)^2 \quad (16.39)$$

On the other hand, considering the equilibrium condition of a bending moment in a strip with its unit width cut out from the tube wall, the following equation is obtained (see [Figure 16.16\(b\)](#)):

$$\Delta F_b \delta - 2\Delta M_b = 0 \quad (16.40)$$

The interaction between the strips is not considered when [Eqn \(16.40\)](#) is derived.

According to the previous assumptions, local buckling takes place in the plastic region.

Consequently, ΔF_b and ΔM_b should satisfy the fully plastic interaction relationships, which are expressed as

$$\Delta M_b/M_0 = 1 - (\Delta F_b/F_0)^2 \quad (16.41)$$

where

$$\begin{aligned} F_0 &= t\sigma_r \\ M_0 &= t^2\sigma_y/4 \end{aligned} \quad (16.42)$$

Using Eqns (16.39)–(16.41), the stress–strain and local lateral deflection stress relationships can be acquired

$$\sigma/\sigma_y = \left[\sqrt{4 + \mu^2} - \mu \right] / 2 \quad (16.43)$$

$$\delta/t = (1 - \sigma/\sigma_y)^2 / (2\sigma/\sigma_y) \quad (16.44)$$

where

$$\mu = (4s/\pi t)\sqrt{\varepsilon - \varepsilon_{cr}} \quad (16.45)$$

The stress–strain relationship represented by Eqn (16.43) is schematically illustrated in Figure 16.16(c). Applying this model, the stress distributions for the tube cross section, after the occurrence of local buckling, are represented in Figure 16.17. For the Case A' stress distribution, the following relationships are derived in place of Eqns (16.22) and (16.23).

$$P(\eta + f_1) = f_2 + f_2' + (c + c_1')\eta \quad (16.46)$$

$$P(\omega + e_0) = f_3 + f_3' + (f_4 + f_5\eta)/(f_1 + \eta) + f_6 \quad (16.47)$$

where

$$f_2' = 2\sigma_y R^2 t (g_1 - \alpha) \cos \alpha_1 \quad (16.48)$$

$$f_3' = 2\sigma_y R t (g_2 - R \sin \alpha)$$

$$g_1 = \int_0^\alpha (\sigma/\sigma_y) d\theta$$

$$g_2 = \int_0^\alpha (R + \delta)(\sigma/\sigma_y) \cos \theta d\theta \quad (16.49)$$

$$c_1' = 2\sigma_y R t (g_1 - \alpha) \quad (16.50)$$

For the Case B' stress distributions, Eqns (16.28) and (16.29) are replaced by

$$P(\eta + f_1) = f_2 + f_2' + h_1 + (c + c_1' - h_2)\eta \quad (16.51)$$

$$P(\omega + e_0) = f_3 + f_3' + h_4 + \{f_4 - h_3 + (f_5 + h_4)\eta\}/(\eta + f_1) + f_6 \quad (16.52)$$

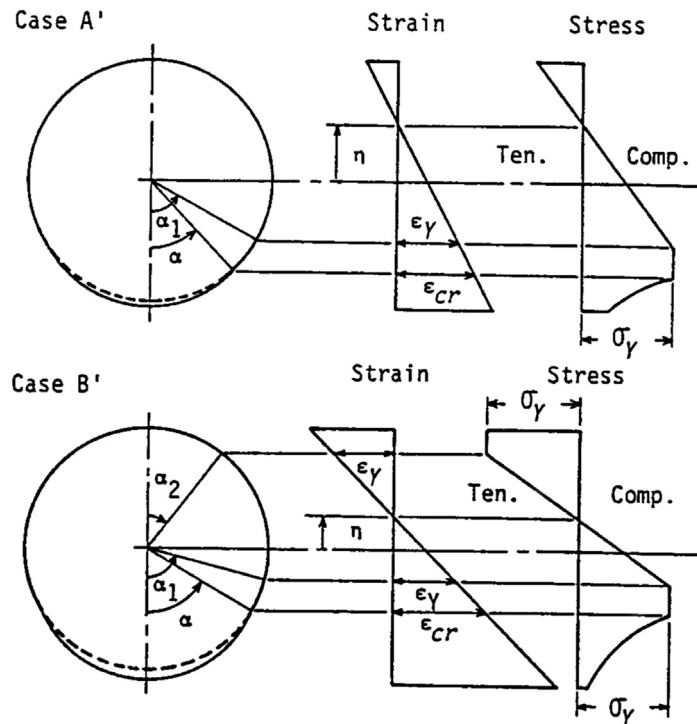


Figure 16.17

Elastoplastic stress distribution accompanied by local buckling (COS model).

DENT Model

In this model, the cross section $c-c'$ in Figure 16.8 is considered. A dent is shown in Figure 16.18, as well as the equilibrium condition of the forces and moments acting on a strip ij . The following equation is derived:

$$\Delta F_b R(\cos \theta - \cos \alpha) - 2\Delta M_b = 0 \quad (16.53)$$

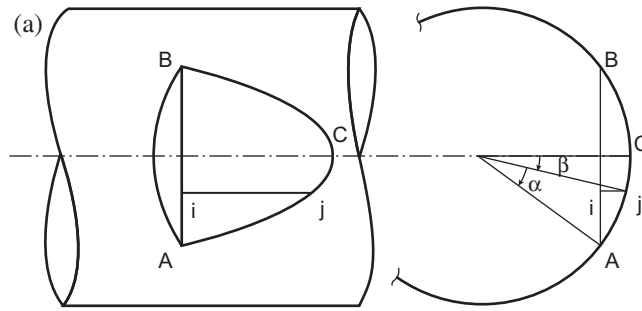
Solving Eqn (16.53), and considering the fully plastic condition expressed by Eqn (16.41), ΔF_b and ΔM_b are derived from

$$\Delta F_b = \left[-R(\cos \theta - \cos \alpha) + \sqrt{R^2(\cos \theta - \cos \alpha)^2 + t^2} \right] \sigma_y \quad (16.54)$$

$$\Delta M_b = R(\cos \theta - \cos \alpha) \Delta F_b / 2 \quad (16.55)$$

Integrating ΔF_b and ΔM_b , respectively, the force F_b and the bending moment M_b acting at the bottom of a dent are found to be

$$F_b = 2 \int_0^\alpha \Delta F_b d\theta \quad (16.56)$$



Assumed dent mode

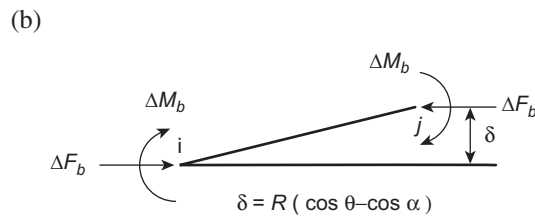

 Force and moment acting
on cross sections

Figure 16.18

Assumed buckling mode for the DENT model.

$$M_b = 2 \int_0^\alpha \Delta M_b d\theta \quad (16.57)$$

where α represents a half-dent angle and has a limiting value α_L as mentioned in Chapter 21.2. After α_L is attained, two other dents are introduced as illustrated in Figure 16.10(c). The specimen tested in this chapter, $\alpha_L = \pi/4$, coincides with the calculated results by Toi et al. (1983).

Applying this model, the stress distributions after local buckling can be represented by Figure 16.19. In this figure, the case with one dent is indicated as a Case A'' distribution, and the case with three dents is a Case B'' distribution. For a Case A'' stress distribution, Eqns (16.22) and (16.23) are replaced with

$$(P - f_1'')(\eta + f_1) = f_2 + c_1 \eta \quad (16.58)$$

$$P(\omega + e_0) = f_3 + f_3'' + (f_4 + f_5 \eta)/(\eta + f_1) + f_6 \quad (16.59)$$

where

$$f_1'' = \sum F_{bi} \quad (16.60)$$

$$f_3'' = \sum M_{bi} + \sum F_{bi} R \cos \beta_i \quad (16.61)$$

β_i is the angle of the center of the i th dent measured from the vertical centerline, as shown in Figure 16.19.

For a Case B'' stress distribution, Eqns (16.28) and (16.29) are replaced with

$$(P - f_1'')(\eta + f_1) = f_2 + h_1 + (c_1 - h_2)\eta \quad (16.62)$$

$$P(W + e_0) = f_3 + f_3'' + h_4 + \{f_4 - h_3 + (f_5 + h_4)\eta\}/(\eta + f_1) + f_6 \quad (16.63)$$

Procedure of Numerical Analysis

Until initial yielding is detected, Eqn (16.3) gives the relationship between axial compressive loads and lateral deflection. The mean compressive axial strain is evaluated by Eqn (16.8).

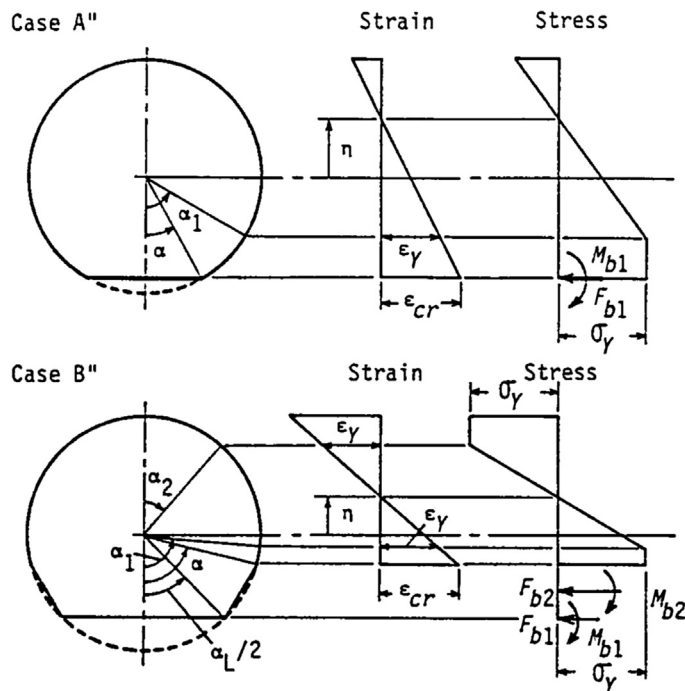


Figure 16.19

Elastoplastic stress distribution accompanied by local buckling (DENT model).

After plastification has started, the analysis is performed in an incremental manner using the plastic component of deflection shown in Figure 16.13. This deflection mode expressed by Eqns (16.10) through (16.12) gives a constant plastic curvature increment in the region l_p . If the actual plastic region length l_d in Figure 16.20(a) is taken as l_p , it reduces to prescribe excess plastic curvature, especially near the ends of the plastic region. To avoid this, a bilinear distribution of plastic curvature increments is assumed in the region l_d as indicated in Figure 16.20(b). The change of the plastic slope increment along the plastic region l_d can be expressed as

$$d\theta_p = l_d d\kappa_p / 2 \quad (16.64)$$

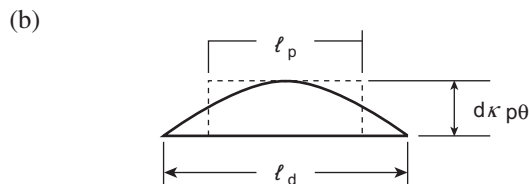
where $d\kappa_p$ is the increment of plastic curvature at the center of a plastic region.

However, if $d\kappa_p$ is assumed to be uniformly distributed along the plastic region l_d , as indicated by Eqns (16.10) through (16.12), the change of plastic slope increments along the plastic region l_d may be expressed as

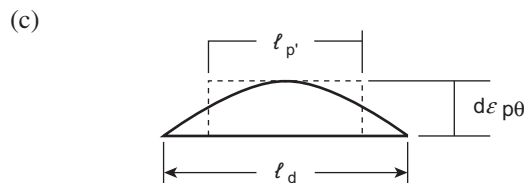
$$d\theta_p^* = l_p d\kappa_p \quad (16.65)$$



Actual plastic zone under combined thrust and bending



Distribution of increment of plastic curvature



Distribution of increment of plastic axial strain

Figure 16.20

Equivalent length of the plastic zone.

Here, l_p is determined so that $d\theta_p^* = d\theta_p$. This is equivalent to the condition that the integrated values of plastic curvature in the plastic regions are the same for both cases, which reduces to

$$l_p = l_d/2 \quad (16.66)$$

The above-mentioned procedure used to estimate l_p is only an approximation. In [Section 16.3.2](#), a more accurate procedure is described. To evaluate the actual plastic region size l_d for the calculated deflection, the stress is analyzed at 100 points along a span with equal spacing, and the bending moment at each point is evaluated. After local buckling has occurred, plastic deformation will be concentrated at the locally buckled region. For this case, l_p is considered equal to the tube's outer diameter, which may be approximately the size of the plastically deformed region after local buckling.

16.3.2 Idealized Structural Unit Analysis

Pre-ultimate-strength Analysis

Throughout the analysis of a beam-column using the ordinary idealized structural unit method, an element is regarded to be elastic until the fully plastic condition and/or the buckling criterion is satisfied. When the axial force is in tension, a relatively accurate ultimate strength may be evaluated with the former conditions along with the post-yielding calculation. However, when the axial force is in compression, the ultimate strength evaluated by the latter criterion is not so accurate, as the latter criterion is based on a semiempirical formula. In the present study, the simplified elastoplastic large deflection analysis described in [Section 16.3.1](#) is incorporated into the idealized structural unit (element) in order to accurately evaluate the ultimate strength under the influence of compressive axial forces.

The idealized structural unit method uses incremental analysis. The ordinary increment calculation is performed until initial yielding is detected. Initial yielding is checked by evaluating the bending moment along the span of an element and the deflection expressed by [Eqn \(16.9\)](#). After the yielding has been detected, the simplified method described in [Section 16.3.1](#) is introduced.

Here, it is assumed that the calculation of the $(n + 1)$ th step has ended. Therefore, the following equilibrium equation is derived, similar to [Eqn \(16.19\)](#):

$$P(w_e + w_p) + \Delta P(e_m + e_q) + M_i + Q = M \quad (16.67)$$

where

P = Axial force given by [Eqn \(16.17\)](#)

$\Delta P = P - X_i (\leq \Delta X_i)$

M_i = Bending moment at the nodal point i at the end of the n th step

Q = Bending moment due to distributed lateral load

M = Bending moment given by Eqn (16.18)

X_i = Axial force at the end of the n th step

ΔX_i = Increment of axial force during the $(n + 1)$ th step

ΔM_i = Increment of bending moment at the nodal point i during the $(n + 1)$ th step

ΔQ = Bending moment increment from the distributed lateral load during the $(n + 1)$ th step

$$e_m = \Delta M_i / \Delta X_i \quad e_q = \Delta Q / \Delta X_i \quad (16.68)$$

The variables X_i , ΔX_i , M_i , ΔM_i , Q , and ΔQ are known after the $(n + 1)$ th step has ended.

Considering the equilibrium condition of the forces in the axial direction, geometric conditions regarding the slope, and Eqn (16.77), the following equations are obtained:

Case A Stress Distribution

$$P(\eta + f_1) = f_2 + c_1 \eta \quad (16.69)$$

$$PW + \Delta P(e_m + e_q) = f_3 + (f_4 + f_5 \eta) / (\eta + f_1) + f_6 \quad (16.70)$$

$$c_2 / (\eta + f_1) = \kappa \quad (16.71)$$

Case B Stress Distribution

$$P(\eta + f_1) = f_2 + h_1 + (c_1 - h_2) \eta \quad (16.72)$$

$$PW + \Delta P(e_m + e_q) = f_3 + h_4 + \{f_4 - h_3 + (f_5 + h_4) \eta\} / (\eta + f_1) + f_6 \quad (16.73)$$

$$c_2 / (\eta + f_1) = \kappa \quad (16.74)$$

$$\eta = R(\cos \alpha_2 - \cos \alpha_1) / 2 \quad (16.75)$$

After the initial yielding, the elastoplastic analysis by the simplified method is performed using Eqns (16.69) through (16.71) or Eqns (16.72) through (16.77) at each step of the idealized structural unit analysis until the ultimate strength is attained.

Here, a more accurate method is introduced to determine the length of the plastic zone l_p . If the axial force P and bending moment M are given, the parameters η , α_1 , and α_2 , which determine axial strain ε and curvature $\phi(x)$, are obtained from Eqns (16.17) and (16.18). The increment of the curvature $d\phi(x)$ from the former step is evaluated, which allows for the length of the plastic zone to be given as

$$l_p = \int d\phi_p(x) dx / d\phi_{p0} \quad (16.76)$$

$$d\phi_p(x) = d\phi(x) - dM(x) / EI \quad (16.77)$$

where $d\phi_{p0}$ represents the maximum plastic curvature increment in the plastic region.

System Analysis

The procedure used for the system analysis, which uses the proposed idealized structural unit, can be expressed as described below:

- At each step of the incremental calculation, moment distributions are evaluated in elements where the axial force is in compression.
- Based on the moment and axial force distribution, the stress is calculated and the yielding of the element is checked.
- If yielding is detected in an element at a certain step, the initial yielding load of this element is evaluated. Then, the elastoplastic analysis is performed using Eqns (16.69) through (16.71) or Eqns (16.72) through (16.75) until ΔP becomes ΔX_i .

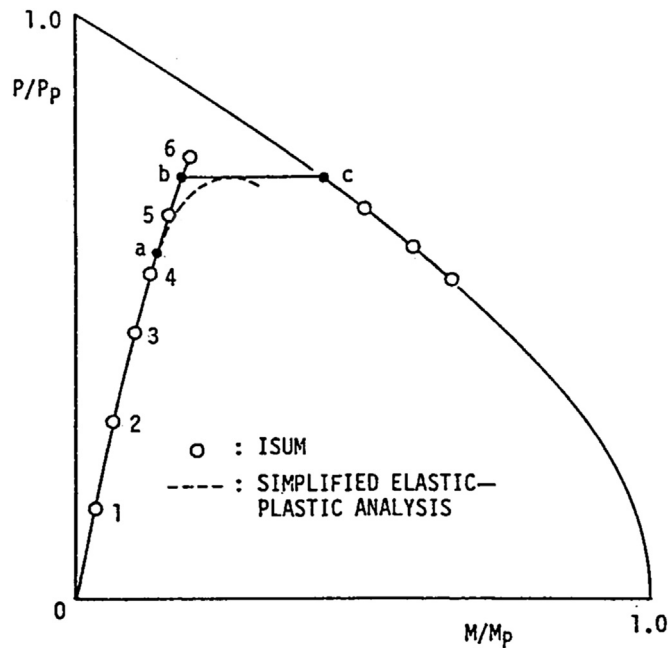
In the following steps, the same calculation is performed at each element where plastification takes place. If ΔP shows its maximum value ΔP_{max} in a certain element before it reaches ΔX_i at a certain step, then this element is regarded as having attained its ultimate strength $P_u (= X_i + \Delta P_{max})$. Then, all the increments at this step are multiplied by $\Delta P_{max}/\Delta X_i$.

For elements that have attained ultimate strength, deflection is increased by keeping axial force constant until the fully plastic condition is satisfied at the cross section where the bending moment is at maximum. Then, this element is divided into two elements, and a plastic node is inserted at the cross section.

The results of such analyses are schematically illustrated in terms of axial forces and bending moments in Figure 16.21. In the figure, “O” represents the results of the idealized structural unit method, and the dashed line represents the results of the simplified method. Until point 4, no plastification occurs. Between points 4 and 5, yielding takes place, and the analysis using simplified methods starts where the yielding occurs. No decrease is observed in this step. At the next step between points 5 and 6, the ultimate strength is attained. Then, the increment of this step is multiplied by $b5/56$. While keeping the axial force constant, the bending moment is increased up to point c, and a plastic node is introduced. After this, the plastic node method (Ueda and Yao, 1982) is applied.

Evaluation of Strain at Plastic Node

In the plastic node method (Ueda and Yao, 1982), the yield function is defined in terms of nodal forces or plastic potentials. Therefore, plastic deformation occurs in the form of plastic components of nodal displacements, and only the elastic deformation is produced in an element. Physically, these plastic components of nodal displacements are equivalent to the integrated plastic strain distribution near the nodal point. If the plastic work done by the nodal forces and plastic nodal displacements is equal to those evaluated by distributed stresses and plastic strains, the plastic nodal displacements are equivalent to the plastic


Figure 16.21

Schematic representation of internal forces.

strain field in the evaluation of the element stiffness matrix (Ueda and Fujikabo, 1986). However, there is no mathematical relationship between plastic nodal displacements and plastic strains at the nodal point. Therefore, an approximate method is needed to evaluate the plastic strain at nodal points, based on the results of the plastic node method analysis.

Here, the internal forces move along the fully plastic interaction curve after the plastic node is introduced, as indicated by a solid line in Figure 16.22. The results of the accurate elastoplastic analysis, using finite element analysis (FEA) methods, are represented by a dashed line in Figure 16.22. The chain line with one dot represents the results obtained from the simplified method.

The bending moment occurring after the ultimate strength is attained, is approximated by the equation

$$M = M_p \cos \frac{\pi}{2} \frac{P}{P_p} - \Delta M \left(\frac{P}{P_u} \right)^n \quad (16.78)$$

where

$$M_p = 4\sigma_y R^2 t \quad P_p = 2\pi\sigma_y R t \quad (16.79)$$

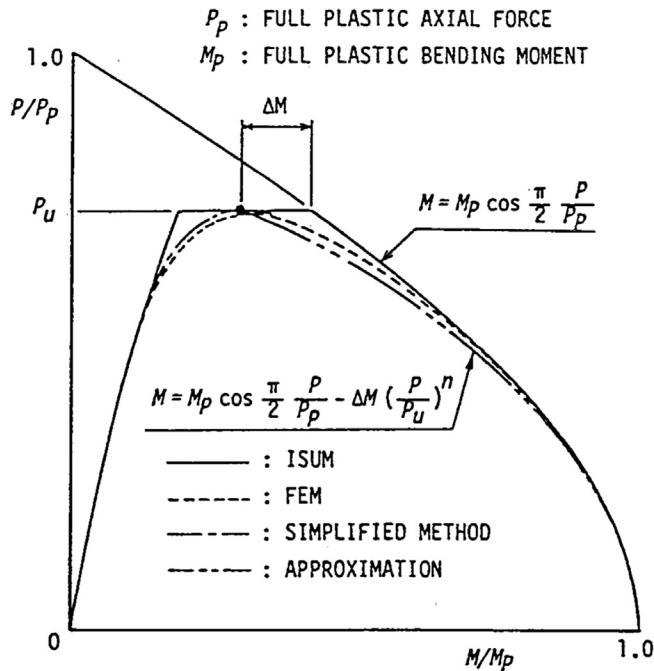


Figure 16.22

Determination of an approximate relationship between axial forces and bending moments.

and ΔM is as indicated in Figure 16.22. The relationship between the bending moment and the axial force is denoted by the chain line consisting of two dashes that can be seen in Figure 16.22.

Substituting both the axial force P and the evaluated bending moment from Eqn (16.79) into Eqns (16.17) and (16.18), respectively, the strain can be evaluated. If the maximum strain (sum of the axial strain and maximum bending strain) reaches the critical strain expressed by Eqn (16.36), the post-local-buckling analysis will begin.

Post-Local-Buckling Analysis

The fully plastic interaction relationship after local buckling takes place can be expressed as

$$\Gamma = M - M_d - M_p \cos \left[\frac{\pi}{2} \left(\frac{P}{P_p} - \frac{F_d}{P_p} \right) + \frac{\alpha}{2} \right] + \frac{1}{2} M_p \sin \alpha \quad (16.80)$$

where F_d and M_d are given below

COS model

$$F_d = 2 \int R t \sigma d\theta \quad (16.81)$$

$$M_d = 2 \int Rt \delta \sigma \cos \theta d\theta \quad (16.82)$$

DENT model

$$F_d = \sum F_{bi} \quad (16.83)$$

$$M_d = \sum M_{bi} + \sum F_{bi} R \cos \beta_i \quad (16.84)$$

In the above expressions, σ and δ are given by Eqns (16.43) and (16.44), and F_{bi} and M_{bi} are equal to F_b and M_b as previously given by Eqns (16.56) and (16.57) of the i th dent.

Here, the angle α represents the size of a locally buckled part and is a function of the axial strain e and the curvature κ of a cross section, expressed as

$$\alpha = \cos^{-1}[(\varepsilon_{cr} - e)/(\kappa R)] \quad (16.85)$$

At the same time, F_d and M_d are functions of e , and κ through α . Consequently, the fully plastic interaction relationship is rewritten in the following form:

$$\Gamma(P, M, e, \kappa) = 0 \quad (16.86)$$

As described in Section 16.3.2.3, no one-to-one correspondence exists between plastic nodal displacements and plastic strains at a nodal point. However, plastic strains may be concentrated near the cross section where local buckling occurs. Consequently, the axial strain and curvature at this cross section are approximated by

$$e = P/EA + e_{pcr} + (u_p - u_{pcr})/l_p \quad (16.87)$$

$$\kappa = M/EI + \kappa_{pcr} + (\theta_p - \theta_{pcr})/l_p \quad (16.88)$$

The length of the plastic zone is represented by l_p in the above equations, and is taken to be equal to the diameter $D(=2R)$ as in the case of a simplified method. Considering Eqns (16.87) and (16.88), the fully plastic interaction relationship reduces to

$$\Gamma(P, M, u_p, \theta_p) = 0 \quad (16.89)$$

The elastoplastic stiffness matrix, after local buckling occurs, is derived based on the fully plastic interaction relationship expressed by Eqn (16.89). The condition to maintain the plastic state is written as

$$d\Gamma = \frac{\partial \Gamma}{\partial P} dP + \frac{\partial \Gamma}{\partial M} dM + \frac{\partial \Gamma}{\partial u_p} du_p + \frac{\partial \Gamma}{\partial \theta_p} d\theta_p = 0 \quad (16.90)$$

or in the matrix form as

$$\begin{bmatrix} \phi_i^T & 0 \\ 0 & \phi_j^T \end{bmatrix} \begin{Bmatrix} dR_i \\ dR_j \end{Bmatrix} + \begin{bmatrix} \psi_i^T & 0 \\ 0 & \psi_j^T \end{bmatrix} \begin{Bmatrix} dh_{pi} \\ dh_{pj} \end{Bmatrix} = 0 \quad (16.91)$$

where $\{dR\}$ and $\{dh_p\}$ are the increments of nodal forces and plastic nodal displacements, respectively. These can be seen in [Figure 16.12](#) and the following equations

$$\begin{aligned}\phi_i &= \{\partial\Gamma/\partial X_i, \partial\Gamma/\partial Z_i, \partial\Gamma/\partial M_i\}^T \\ \phi_j &= \{\partial\Gamma/\partial X_j, \partial\Gamma/\partial Z_j, \partial\Gamma/\partial M_j\}^T\end{aligned}\quad (16.92)$$

$$\begin{aligned}\psi_i &= \{\partial\Gamma/\partial u_{pi}, \partial\Gamma/\partial w_{pi}, \partial\Gamma/\partial\theta_{pi}\}^T \\ \psi_j &= \{\partial\Gamma/\partial u_{pj}, \partial\Gamma/\partial w_{pj}, \partial\Gamma/\partial\theta_{pj}\}^R\end{aligned}\quad (16.93)$$

Here, considering Γ as a plastic potential, the increments of plastic nodal displacements are given as

$$\begin{Bmatrix} dh_{pi} \\ dh_{pj} \end{Bmatrix} = \begin{bmatrix} d\lambda_i & 0 \\ 0 & d\lambda_j \end{bmatrix} \begin{Bmatrix} \phi_i \\ \phi_j \end{Bmatrix}\quad (16.94)$$

When only nodal point j is plastic, $d\lambda_i = 0$. Contrary to this, $d\lambda_j = 0$ when only nodal point i is plastic.

On the other hand, increments of nodal forces are expressed in terms of the elastic stiffness matrix, and the elastic components of nodal displacement increments, as follows:

$$\begin{Bmatrix} dR_i \\ dR_j \end{Bmatrix} = \begin{bmatrix} K_{ii}^e & K_{ij}^e \\ K_{ji}^e & K_{jj}^e \end{bmatrix} \left(\begin{Bmatrix} dh_i \\ dh_j \end{Bmatrix} - \begin{Bmatrix} dh_{pi} \\ dh_{pj} \end{Bmatrix} \right)\quad (16.95)$$

where $\{dh\}$ represents the increments of nodal displacements.

Substituting [Eqns \(16.94\) and \(16.95\)](#) into [Eqn \(16.92\)](#), $d\lambda_i$ and $d\lambda_j$ are expressed in terms of $\{dh\}$. Substituting them into [Eqn \(16.95\)](#), the elastoplastic stiffness matrix, after local buckling, is derived as

$$\begin{Bmatrix} dR_i \\ dR_j \end{Bmatrix} = \begin{bmatrix} K_{ii}^D & K_{ij}^D \\ K_{ji}^D & K_{jj}^D \end{bmatrix} \begin{Bmatrix} dh_i \\ dh_j \end{Bmatrix}\quad (16.96)$$

For the case in which local buckling is not considered, the elastoplastic stiffness matrix is given in a more concrete form in [Ueda et al \(1969\)](#). When local buckling is considered, the terms $\phi_i^T K_{ii} \phi_i$ and $\phi_j^T K_{jj} \phi_j$ in the denominators in [Ueda and Yao \(1982\)](#) are replaced by $\phi_i^T K_{ii} \phi_i - \psi_i^T \psi_i$ and $\phi_j^T K_{jj} \phi_j - \psi_j^T \psi_j$, respectively.

16.4 Calculation Results

16.4.1 Simplified Elastoplastic Large Deflection Analysis

In order to check the validity of the proposed method of analysis, a series of calculations are performed on test specimens, as summarized in [Table 16.4](#), where a comparison is

Table 16.4: Specimen size, material properties, and results of experiment and calculation

Specimen Number	Mean Diameter D (mm)	Thickness t (mm)	Length L (mm)	Initial Deflection a (mm)	Load Eccentricity e (mm)	Young's Modulus E (kg/mm)	Yield Stress σ_y (kg/mm)	Ultimate Strength σ_u/σ_y		Ref. No.
								Measured	Calculated	
H1	501.6	6.40	8000	0.63	63.50	21,180.0	34.55	0.68	0.63	Present
H2	501.6	6.40	8000	0.63	127.00	21,180.0	34.55	0.55	0.49	Present
H3	501.6	6.40	8000	0.63	190.50	21,180.0	34.55	0.44	0.41	Present
A1	61.5	2.11	2150	0.0	0.00	20,496.3	23.25	0.84	0.76	11
A2	61.5	2.12	2150	0.0	9.84	21,210.1	23.25	0.49	0.43	11
B1	77.8	1.74	2150	0.0	0.00	20,802.2	19.88	1.00	0.94	11
B2	77.8	1.71	2150	0.0	10.11	23,351.5	20.29	0.60	0.59	11
C1	100.0	1.66	2150	0.0	0.00	20,496.3	21.52	1.10	0.95	11
C2	99.9	1.73	2150	0.0	9.99	21,006.2	28.95	0.58	0.63	11
D1	89.0	1.02	2150	0.0	0.00	22,535.7	49.46	0.75	0.83	11
D2	89.0	1.01	2150	0.0	15.13	26,002.8	47.52	0.50	0.47	11
S1	213.5	5.56	4572	0.0	0.00	20,256.1	41.69	0.84	0.82	5
S2	213.5	5.56	6096	0.0	0.00	20,256.1	41.69	0.72	0.59	5
S3	213.5	5.56	7620	0.0	0.00	20,256.1	41.69	0.54	0.41	5
S4	213.5	5.56	9144	0.0	0.00	20,256.1	41.69	0.32	0.29	5

made between calculated and measured results. Three types of analyses are performed: a simplified elastoplastic large deflection analysis combined with a COS model and a DENT model, for all specimens; and an elastoplastic large deflection analysis without considering local buckling by the FEA method. The calculated results, applying the COS model and DENT model, are plotted in the following figures along with those analyzed using the FEA method. The experimental results are plotted using solid lines.

H Series

This series is newly tested. The measured and calculated load-deflection curves are plotted in [Figure 16.7](#). First, the results from the simplified method have a good correlation with those obtained from the FEA method until the ultimate strength is attained. However, they begin to show a little difference as lateral deflection increases. This may be attributed to overestimation of the plastic region size during this stage.

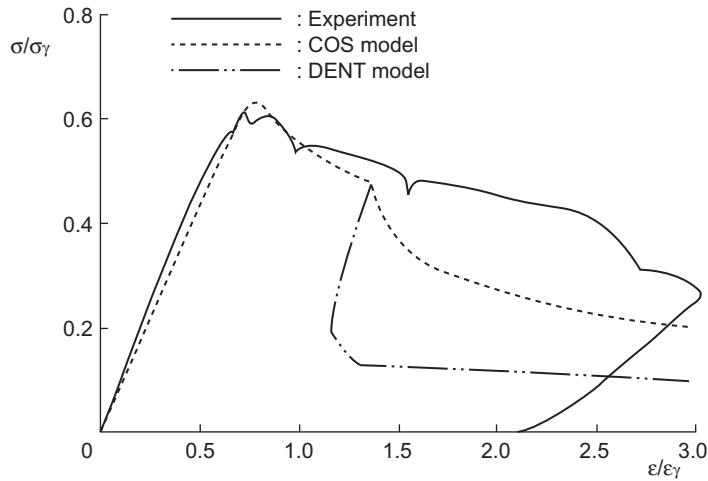
The calculated ultimate strengths are 7–10% lower than the experimental ones. This may be due to a poor simulation of the simply supported end condition and the strain-hardening effect of the material. Contrary to this, the onset points of local buckling calculated using [Eqn \(16.33\)](#) agree quite well with the measured ones. The post-local-buckling behavior is also well simulated by the COS model, but not so well by the DENT model. Such a difference between the measured and the calculated behaviors, applying the DENT model, is observed in all analyzed test specimens except for the D series. This may be due to underestimation of forces and moments acting at the bottom of a dent, and further consideration may be necessary for the DENT model.

C Series

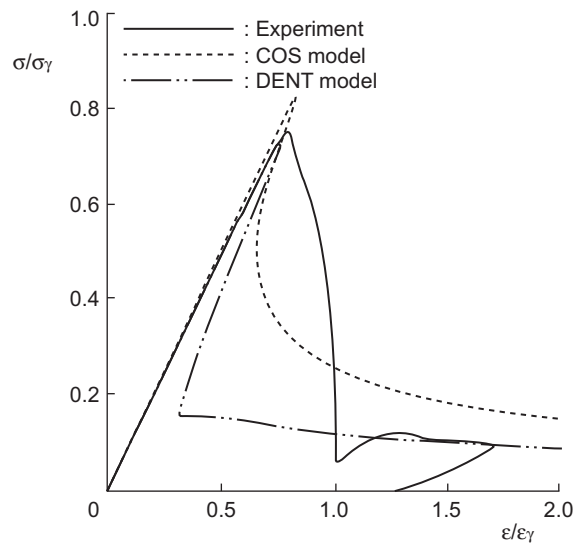
C series experiments are carried out by [Smith et al. \(1979\)](#). Specimens C1 and C2, which are not accompanied by denting damage, are analyzed. The calculated results for Specimen C2 are plotted together with the measured result in [Figure 16.23](#). Smith wrote in his paper that local buckling took place when the end-shortening strain reached 2.5 times the yield strain ϵ_y , while it occurred in the analysis when the strain reached 1.4 times ϵ_y . However, the behavior up to the onset of local buckling is well simulated by the proposed method of simplified elastoplastic large deflection analysis. On the other hand, in the case of Specimen C1, local buckling takes place just after the ultimate strength is attained, both in the experiment and in the analysis. The calculated ultimate strength is far below the measured one, as indicated in [Table 16.4](#). This may be attributed to some issues within the experiment itself, since the measured ultimate strength is 1.1 times the fully plastic strength.

D Series

This series is also tested by [Smith et al. \(1979\)](#). The analysis is performed on Specimens D1 and D2. Here, the results for Specimen D1 are plotted in [Figure 16.24](#). It may be said


Figure 16.23

Comparison of measured and calculated results (C2).


Figure 16.24

Comparison of calculated and measured results (D1).

that a good correlation is observed between the calculated and measured results in the ultimate strength and in the onset of local buckling. However, the behavior occurring just after the local buckling is somewhat different between the experiment and the analysis. This may be because the experimental behavior at this stage is a dynamic one, which is a kind of snap-through phenomenon, as Smith mentioned. As for the load-carrying capacity after the dynamic behavior, the DENT model gives a better estimate than the COS model does.

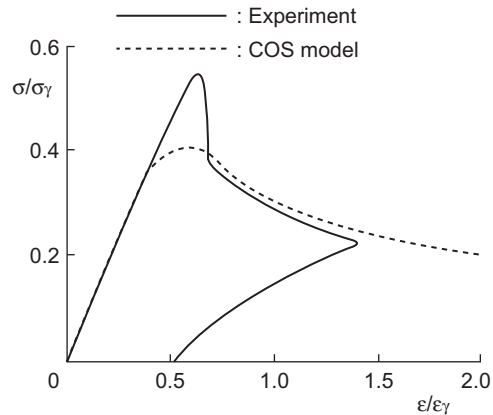


Figure 16.25
Comparison of calculated and measured results (S3).

A similar result is observed in Specimen D2. However, in this case, the predicted onset of local buckling is later than in the measured one.

S Series

This series is a part of the experiments carried out by [Bouwkamp \(1975\)](#). The calculated and measured results for Specimen S3 are shown in [Figure 16.25](#). First, the measured ultimate strength is far above the elastic Eulerian buckling strength. This must be due to a difficulty in simulating the simply supported end conditions. Consequently, instability took place just after the ultimate strength was attained, and a dynamic unloading behavior may have occurred. After this, a stable equilibrium path was obtained, which coincides well with calculated results.

The same features are observed in Specimens S1, S2, and S3. Bouwkamp wrote in his paper that local buckling took place after the ultimate strength was attained. However, no local buckling occurred for this series analysis.

A Series and B Series

A and B series by [Smith et al. \(1979\)](#) show local buckling neither in the experiments nor in the analyses. The calculated ultimate strengths show a good agreement with the measured ones, with the exception of Specimen A1.

16.4.2 Idealized Structural Unit Method Analysis

Members with Constraints against Rotation at Both Ends

An end rotation of a structural member in a structural system is constrained by other members. This effect of constraint may be equivalent to placing springs, which resist

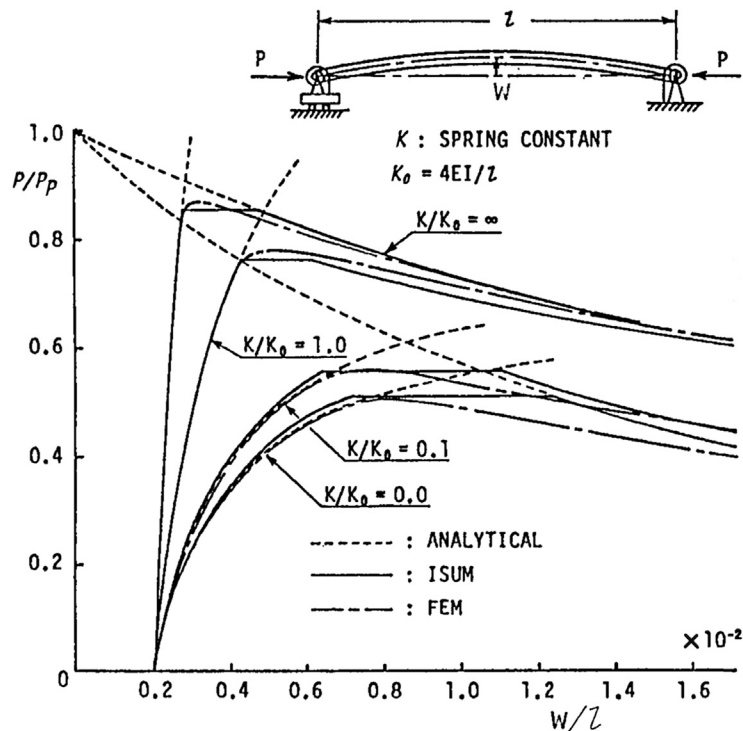


Figure 16.26

Load—lateral deflection curves of simply supported tube with end constraint against rotation.

rotation, at both ends of a member when one member is isolated from the system. For such a member with springs at both ends, a series of analyses are performed by changing the spring constant between 0 and ∞ . The wall thickness and outer diameter are taken as 20 and 2000 mm, respectively. The initial deflection of magnitude $1/500$ times the length is imposed to know the characteristics of the proposed idealized structural unit model. The yield stress of the material is chosen as 30 kgf/mm^2 , and the magnitudes of the springs at both ends are the same. Local buckling is not considered in this analysis. The calculation results for $l/\sqrt{I/A} = 100$ are shown in Figures 16.26 and 16.27. Figure 16.26 represents the load versus lateral deflection relationship, and Figure 16.27 represents the change of internal forces at a midspan point and the end. In these figures, solid lines and chain lines represent results obtained when using the present method and the FEA method, respectively. On the other hand, dashed lines represent analytical solutions, expressed as

Perfectly Elastic Solution

$$w = 2M[1/(2\cos kl/2) - 1] + a_0 P_E/(P_E - P) \quad (16.97)$$

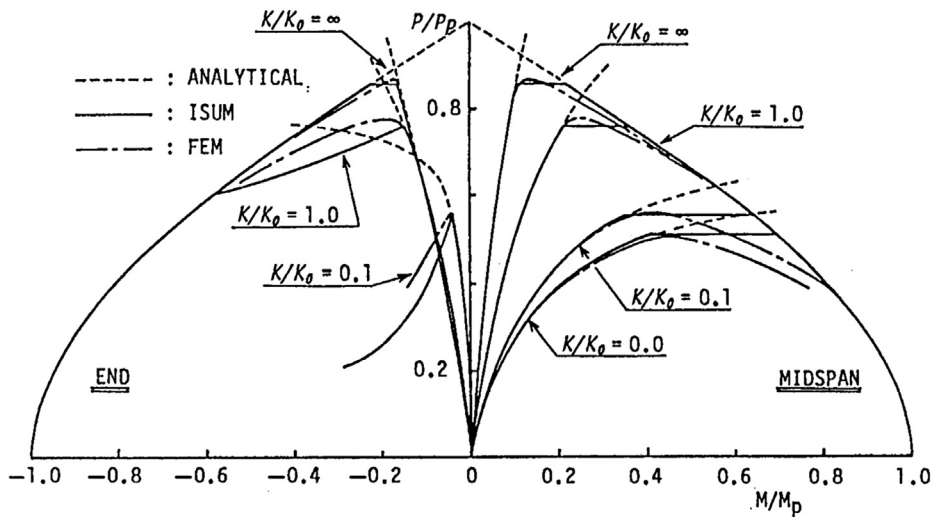


Figure 16.27
Axial force bending moment relationships.

where

$$M = -[\pi a_0 P / l (P_e - P)] \left/ \left[k(1 - \cos kl / (P \sin kl)) + \frac{1}{k} \right] \right. \quad (16.98)$$

and k represents the magnitude of springs placed at both ends, while P_E is given in Eqn (16.6).

Rigid-Plastic Solution

$$w = M_p [\cos(\pi P / 2P_p)] / P \quad \text{for } k = 0 \quad (16.99)$$

$$w = 2M_p [\cos(\pi P / 2P_p)] / P \quad \text{for } k = \infty \quad (16.100)$$

where k/k_0 is taken as 0.0, 0.1, 1.0, and ∞ where $k_0 = 4EI/l$.

The ultimate strength evaluated by the proposed method is slightly lower than the ultimate strength proposed by the FEA method when the constraint is weak, but it becomes proportionally higher as the constraint is increased. However, the proposed method gives a very accurate ultimate strength.

In the case of $K = \infty$, the axial load still increases after a plastic node is introduced at a midspan point where the ultimate strength is attained according to a simplified method. It begins to decrease after the fully plastic condition is satisfied at both ends. However, the load increment that comes after a plastic node has been introduced at a midspan point is very small. Therefore, an alternative analysis is performed, in which three plastic nodes are simultaneously introduced at a midspan and both ends when the ultimate strength is attained

by a simplified method. The curves for $K = \infty$ in Figures 16.26 and 16.27 are the results of the latter analysis. Further considerations should be made when regarding this procedure.

H Series

A series of analyses are performed on H series specimens in order to check the accuracy of post-local-buckling behavior predicted by the present method. The coefficient n in Eqn (16.78) is interchanged between 8 and 16 when using the COS model.

The load versus lateral deflection relationships, and the interaction relationships of internal forces, are plotted in Figures 16.28 and 16.29, respectively. The solid and dashed lines

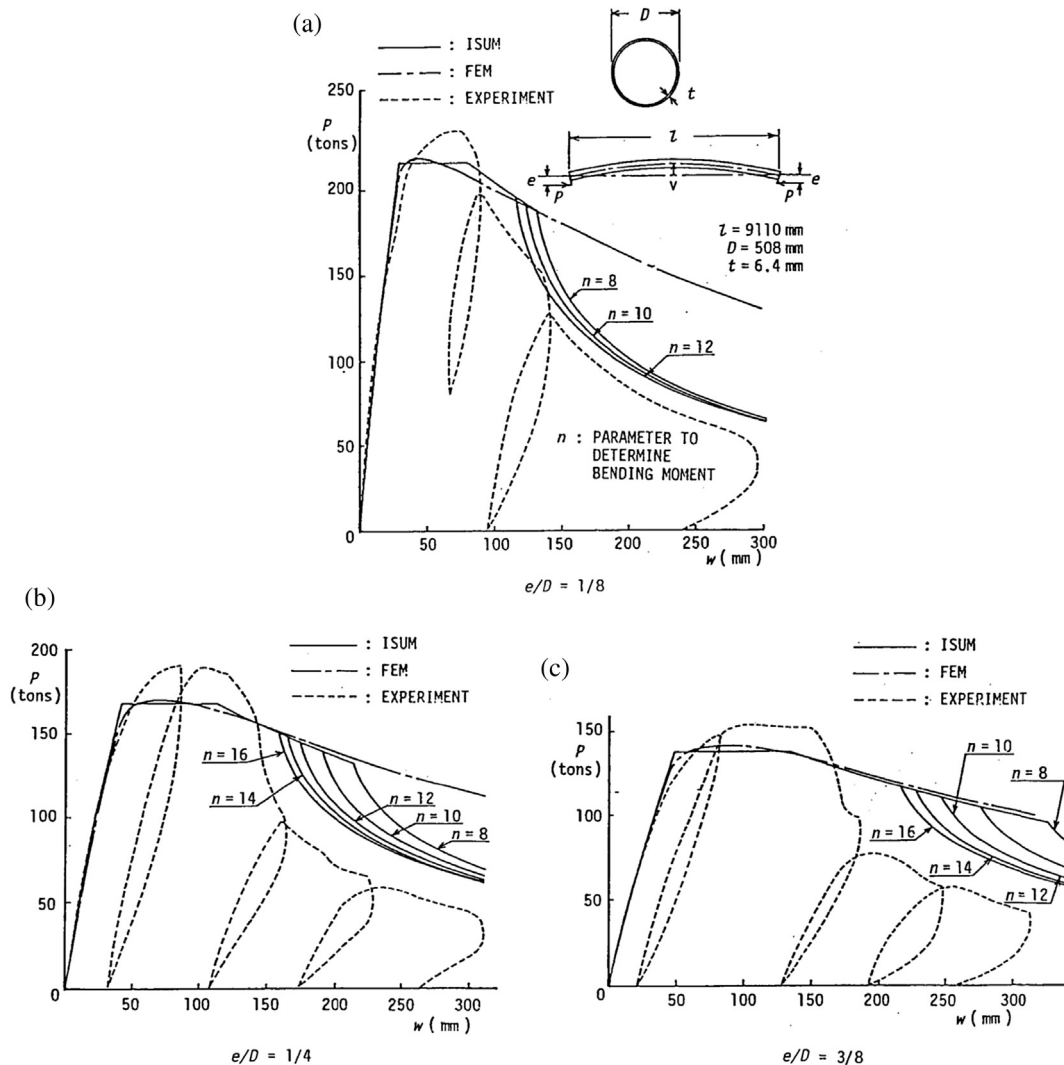


Figure 16.28
Load—lateral deflection curves of H series specimens.

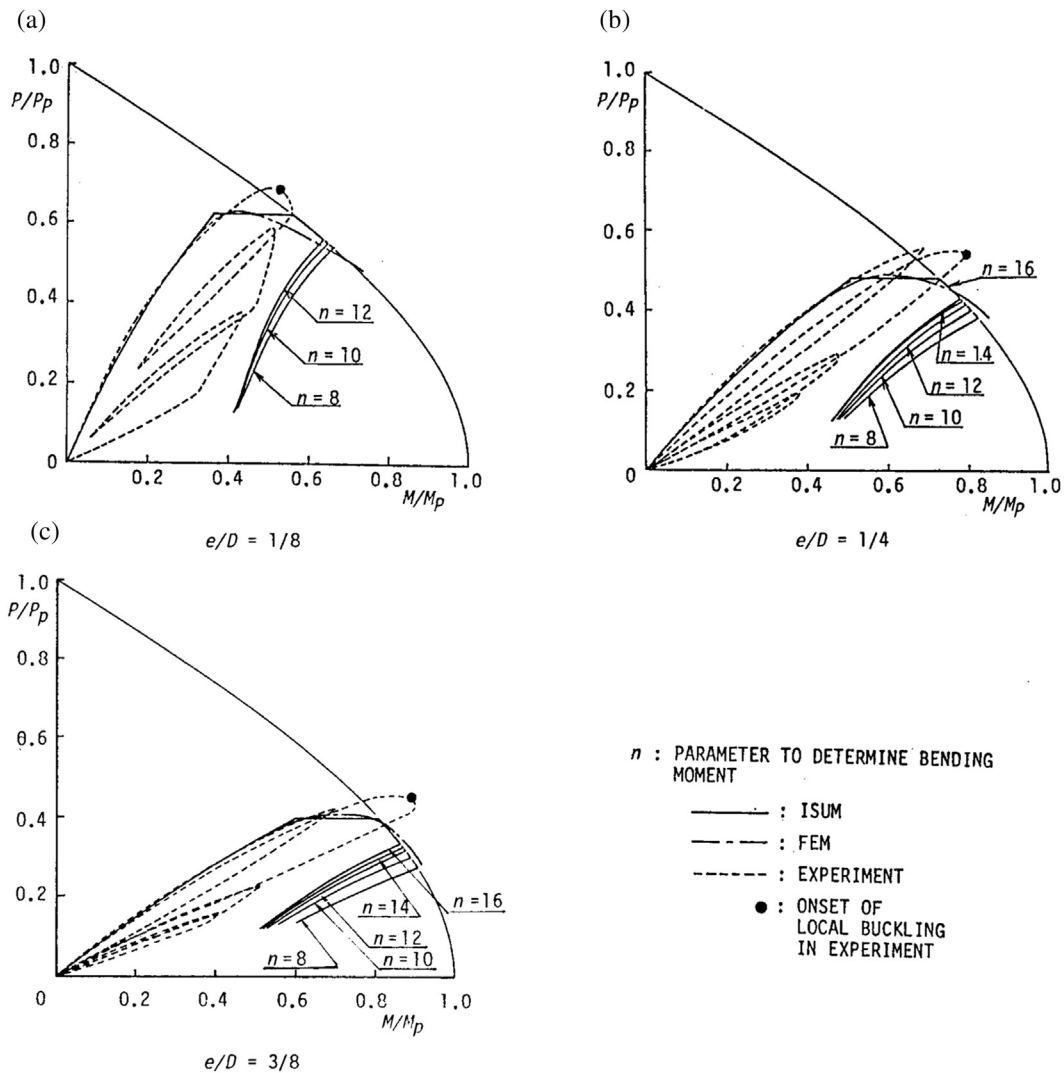


Figure 16.29

Measured and calculated relationship between axial force and bending moment.

represent results obtained from the present method and experiment, respectively, and the chain lines represent results obtained from the FEA method without considering local buckling.

Until local buckling takes place, both results obtained from the present method and the FEA method show good correlations including ultimate strength. The comparison of these results using the FEM to the results of other experiments shows small differences among them, which may be attributed to the reasons described in Section 16.4.1. However, judging from the interaction relationships shown in Figure 16.29, these differences may

alternatively be attributed to the material properties of the actual material and assumed material used for the analysis. The yield stress used in the analysis is determined based on the results of the tensile test, and may be very accurate as long as the stress is in tension. It is not completely clear, but there may be some differences in the material properties in tensile and compressive ranges.

Post-local-buckling behavior is simulated quite well, even though the calculated starting points of local buckling are a little different from the measured ones. The difference in the onset point of local buckling may be due to inaccuracies of the critical buckling strain evaluated by Eqn (16.31) and the estimated strain using Eqn (16.67). At present, the value to be employed as n remains unknown. However, it is known that larger values may give good results, as indicated in Figures 16.28 and 16.215.

The curves changing the value of n may be regarded as the results of the numerical experiment changing the onset point of local buckling. A greater reduction is observed in the load-carrying capacity (axial load), as the critical load for buckling increases.

The same analysis is performed on small-scale test specimens. Relatively good correlations are observed between the calculated and experimental results for the ultimate strength in all specimens. However, the calculated post-ultimate-strength behavior is slightly different from observed behavior. This may be attributed to a difference in the assumed stress–strain relationship used during the analysis, and the actual experiment. An elastic–perfectly plastic stress–strain relationship is assumed in the analysis. Contrary to this, the actual material showed relatively high strain hardening. In order to analyze such cases, the influence of strain hardening must be taken into account. The strain-hardening effect may be easily incorporated into the simplified analysis. Applying the plastic node method for the post-ultimate-strength analysis is a basic idea presented in Ueda and Fujikubo (1986). These ideas are currently still in progress.

If pure bending is obtained, the axial force is zero, and the proposed method does not need to be applied. In this case, the fully plastic condition will give an accurate ultimate strength. However, this method is not necessary when the axial force is in tension.

16.5 Conclusions

Local buckling of tubular members is investigated in this chapter both theoretically and experimentally. First, a series of experiments are carried out on large- and small-scale tubular specimens. Large-scale test specimens are 1/3.5 scale models of a bracing member in an already existing semisubmersible drilling unit, and their diameter to thickness ratio, D/t , is 78. The D/t ratio of small-scale specimens varies between 40 and 97. Axial compression tests with load eccentricity are carried out on both specimens, whereas pure bending tests are carried out on small-scale specimens only. These experiments have shown that after the

ultimate strength has been attained, local buckling takes place at the area of maximum compressive strain. Two types of buckling modes are observed, which are denoted as a cosine mode and a dent mode. The buckling wave of a cosine mode spreads about a half-circle in the circumferential direction, and a dent mode is about a quarter-circle in the circumferential direction. Nevertheless, both modes have a short wavelength in the axial direction.

The load-carrying capacity suddenly decreases due to the initiation of local buckling.

In the case of a cosine mode, the formation of local denting deformation follows at the foot of the initial cosine-buckling wave. Other local denting deformations are formed adjacent to the initial dent and during dent mode buckling.

A simplified method is proposed to analyze the elastoplastic behavior of a tubular member subjected to axial compression, end moments, and distributed lateral loads. Two models are proposed that simulate the post-local-buckling behavior of a tubular member based on the observed results of experiments. They are the COS and the DENT model.

Combining these models with the simplified method, a series of analyses have been performed on the newly tested specimens and on those previously reported. Analysis results are compared with experimental results, and the validity and usefulness of the proposed simplified methods of analysis are both evaluated.

The idealized structural unit model (element) is developed through the incorporation of the proposed simplified method. Using this model, the ultimate strength is automatically evaluated under axial compression. After the local buckling has started, its influence is reflected upon the fully plastic strength interaction relationship through plastic nodal displacements of the element. A few example calculations apply the newly developed element, and the calculated results are compared with those obtained using the FEA method. The validity and usefulness of this element are also demonstrated.

Remaining research for future work includes

- accurate estimates of plastic strain and curvature at a plastic node;
- accurate evaluation of critical buckling strain;
- system analysis using the proposed idealized structural unit model.

16.6 Example

16.6.1 Example 16.1: Comparison of the Idealized Structural Unit Method and Plastic Node Methods

Problem:

Describe the differences and similarities between the idealized structural unit methods and plastic node methods.

Solution:

Plastic node methods, as described in Part II, Chapter 19, are a generalization of the plastic hinge methods that have been popular for plastic analysis of beams and framed structures. The generalization makes it possible to effectively conduct analysis of plated structures and shell structures; see [Ueda and Yao \(1982\)](#). It is also possible to include the effect of strain hardening in the formulation; see [Ueda and Fujikubo \(1986\)](#). However, geometric nonlinearity is not a subject discussed in the plastic node methods.

The idealized structural unit methods ([Ueda and Rashed, 1984](#)) make use of the plastic node methods to deal with plasticity, and utilize empirical formulae (such as those in design codes) for the ultimate strength analysis of individual components. In this chapter, however, an attempt has been made to predict the ultimate strength of the components using simplified inelastic analysis instead of empirical formulae. The advantage of using the simplified inelastic analysis is its ability to account for more complex imperfections and boundary conditions not covered by empirical formulae. However, the disadvantage is its demand for computing effort and complexity, which may lead to a loss of convergence in complex engineering analyses.

References

- AISC, 1978. Specification for the Design, Fabrication and Erection of Structural Steel for Buildings, with Commentary. American Institute of Steel Construction.
- API RP 2A, 2001. Recommended Practice for Planning, Designing and Constructing Fixed Offshore Platforms – Working Stress Design (WSD), or – Load Resistance Factored Design (LRFD) (latest revision). American Petroleum Institute.
- Batterman, C.S., 1965. Plastic buckling of axially compressed cylindrical shells. *AIAA Journal* 3, 316–325.
- Bouwkamp, J.G., 1975. Buckling and Post-Suckling Strength of Circular Tubular Section. OTC. No-2204, pp. 583–592.
- Chen, W.F., Han, D.J., 1985. *Tubular Members in Offshore Structures*. Pitman Publishing Ltd.
- Gerard, G., 1962. *Introduction to Structural Stability Theory*. McGraw-Hill International Book Company, New York.
- Rashed, S.M.H., 1980. Behaviour to Ultimate Strength of Tubular Offshore Structures by the Idealized Structural Unit Method. Report SK/R 51. Division of Marine Structure, Norwegian Institute of Technology, Trondheim, Norway.
- Reddy, B.D., 1979. An experimental study of the plastic buckling of circular cylinder in pure bending. *International Journal of Solids and Structures* 15, 669–683.
- Smith, C.S., Somerville, W.L., Swan, J.W., 1979. Buckling strength and post-collapse behaviour of tubular bracing members including damage effects. BOSS 303–325.
- Toi, Y., Kawai, T., 1983. Discrete limit analysis of thin-walled structures (Part 5) – non-axisymmetric plastic buckling mode of axially compressed circular shells. *Journal of the Society of Naval Architects of Japan* Na.154, pp. 337–247 (in Japanese).
- Ueda, Y., Akamatsu, T., Ohmi, Y., 1969. Elastic-plastic analysis of framed structures using matrix method (2nd rep.). *Journal of the Society of Naval Architects of Japan* 126, 253–262 (in Japanese).
- Ueda, Y., Fujikubo, M., 1986. Plastic collocation method considering strain-hardening effects. *Journal of the Society of Naval Architects of Japan* Val.160, 306–317 (in Japanese).

- Ueda, Y., Rashed, S.M.H., 1984. The idealized structural unit method and its application to deep grider structures. *Computers & Structures* 18 (2), 277–293.
- Ueda, Y., Rashed, S.M.H., Nakacho, K., 1984. New efficient and accurate method of nonlinear analysis of offshore structures. *Proceeding of OMAE* 528–536.
- Ueda, Y., Yao, T., 1982. The plastic node method: a new method of plastic analysis. *Computer Methods in Applied Mechanics and Engineering* Val.34, 1089–1104.
- Yao, T., Fujikubo, M., Bai, Y., Nawata, T., Tamehiro, M., 1986. Local buckling of bracing members (1st report). *Journal of the Society of Naval Architects of Japan* 160.
- Yao, T., Fujikubo, M., Bai, Y., Nawata, T., Tamehiro, M., 1988. Local buckling of bracing members (2nd report). *Journal of the Society of Naval Architects of Japan* 164.

Ultimate Strength of Plates and Stiffened Plates

17.1 Introduction

17.1.1 General

Stiffened plates are frequently used as load-bearing components in marine structures. Typical example uses are the hull girder of a ship, the pontoons of a semisubmersible, and the decks of offshore platforms. The main type of framing system in hull girders consists of relatively closely spaced longitudinal stiffeners with more widely spaced heavier girders in the transverse direction. This is illustrated in [Figure 17.1](#) for a bottom/side structure. The hydrostatic load—the difference between external and internal pressure—is transferred from plates to stiffeners, which again through beam action transfer the loads to the transverse girders.

As illustrated in [Figure 17.1](#), the bottom plates, in addition to the hydrostatic pressure, will be subjected to biaxial in-plane loads. This is due to the longitudinal bending of the hull girder and the hydrostatic pressure applied on the sides.

Factors affecting the behavior of stiffened plates are, for example, stiffener slenderness and spacing, plate geometry, and material yield stress. In addition, residual stresses, initial deformations, boundary conditions, and types of loading will also affect the behavior of stiffened plates.

The potential failure modes for plates (or stiffened plates) under combined loads may be classified as:

- Buckling and collapse of plates—lateral deflection develops in the postbuckling region and ultimate strength is reached due to yielding (see [Sections 17.3 and 17.4](#))
- Collapse of stiffeners with associated plates—beam-column mode buckling in which attaching plates are accounted for as effective plates (see [Section 17.5.1](#))
- Tripping of stiffeners—tripping due to buckling of stiffeners and loss of the rotational restraint provided by the plating (see [Section 17.5.2](#))
- Grillage buckling—involves bending of transverse girders and longitudinal stiffeners (see [Section 17.6](#))

As a book for graduate courses, the objective of this chapter is to introduce buckling strength analysis. More detailed mathematical theories can be found in the books listed in

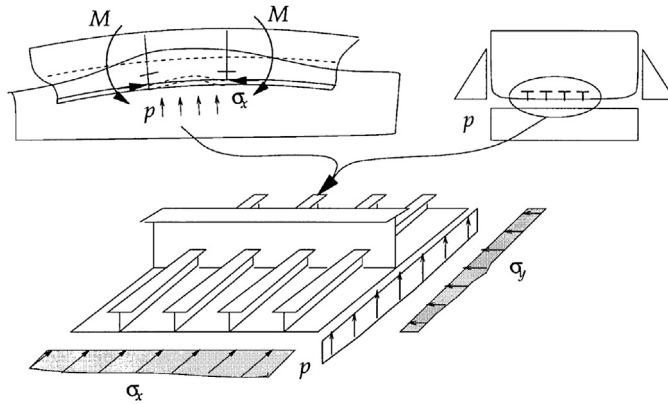


Figure 17.1

Stiffened panels in a ship bottom structure.

the reference section. Some equations from design codes are used for illustration and educational purposes only, and engineering projects should directly use the relevant codes without any deviations.

17.1.2 Solution of Differential Equation

The procedure for calculating the elastic buckling load is illustrated for an initially plane plate, subjected to an in-plane uniform compression. The equilibrium equation for a plate is given by

$$\nabla^4 w = \frac{1}{D} \left(q + N_x \frac{\partial^2 w}{\partial x^2} + 2N_{xy} \frac{\partial^2 w}{\partial x \partial y} + N_y \frac{\partial^2 w}{\partial y^2} \right) \quad (17.1)$$

where the plate stiffness is given by

$$D = \frac{Et^3}{12(1 - \nu^2)} \quad (17.2)$$

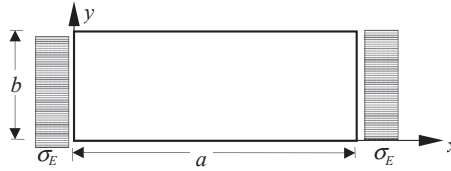
and

$$\nabla^4 = (\nabla^2)^2 = \left(\frac{\partial^2}{\partial x^2} + \frac{\partial^2}{\partial y^2} \right)^2 \quad (17.3)$$

The quantities

$$\left. \begin{aligned} N_x &= \sigma_x t \\ N_y &= \sigma_y t \\ N_{xy} &= \sigma_{xy} t \end{aligned} \right\} \quad (17.4)$$

are the membrane stress resultants.


Figure 17.2

Simply supported plate subjected to uniform compression.

For simply supported plates under pure compression (see Figure 17.2), Eqn (17.1) takes the form

$$\nabla^4 w = \frac{N_x}{D} \frac{\partial^2 w}{\partial x^2} \quad (17.5)$$

Based on the boundary conditions, the following displacement function is assumed and substituted into Eqn (17.5)

$$w = C_{mn} \sin \frac{m\pi x}{a} \sin \frac{n\pi y}{b} \quad (17.6)$$

where m and n are the number of half-waves in the x - and y -directions. The solution for elastic buckling stress is given by the expression

$$\sigma_E = \frac{\pi^2 E}{12(1-\nu^2)} \left(\frac{t}{b}\right)^2 \cdot c = \frac{\pi^2 D}{tb^2} \cdot c \quad (17.7)$$

where c is a factor depending on the plate aspect ratio a/b (see Figure 17.3).

In Figure 17.3, the buckling coefficient c has been plotted against the aspect ratio for a simply supported plate that was subjected to uniform compression. It appears that the minimum buckling stress occurs when the length is a multiple of the width. For intermediate values, the number of waves is incompatible with the plate's length, therefore raising the buckling load. In practice, however, this additional strength is not taken into account.

17.1.3 Boundary Conditions

Actual boundary conditions will differ from idealized cases. The major influence stems from conditions at unloaded edges. With reference to Figure 17.4, Plates F, B, and A can be considered restrained, constrained, and unrestrained, respectively. In the restrained case, the edges remain undistorted, while in the constrained case, lateral deflection is allowed but the edges are forced to remain straight. In the unrestrained case, the edges are completely free with respect to lateral deflection. The difference in boundary conditions between Plates B

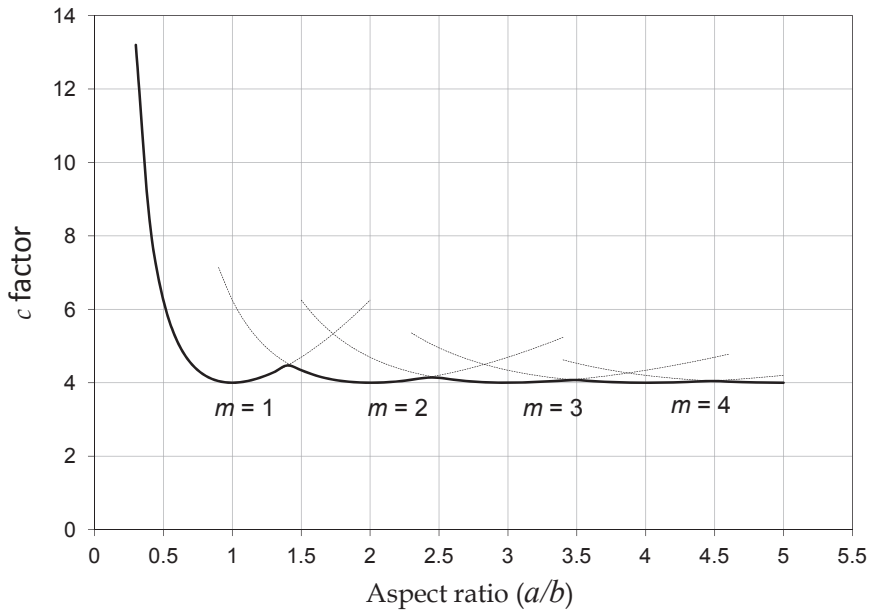


Figure 17.3
Buckling coefficient versus plate aspect ratio.

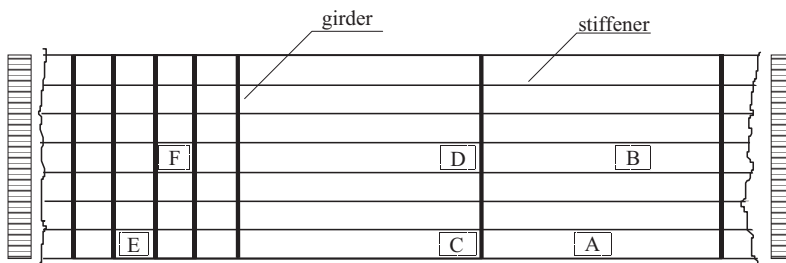


Figure 17.4
Various boundary conditions for plate elements in a stiffened panel.

and F is caused by the aspect ratio. The closeness of the transverse girders at F does not allow lateral deflection; however, it may potentially occur at the midsection of Plate B.

In general, boundary conditions of loaded edges do not have a significant influence on the ultimate strength. In this chapter, strength criteria are based on assumptions that at the ultimate load condition

- all boundary conditions may be taken as simply supported (due to yielding);
- boundary edges are kept straight by supporting structures.

These two approximations will lead to slightly pessimistic, but adequate, results.

17.1.4 Fabrication-Related Imperfections and In-service Structural Degradation

Several sources of structural deterioration affecting buckling and ultimate strength may exist in the actual structure, such as

- residual stresses due to welding;
- initial deflection due to welding and other fabrication-related processes;
- plate perforations such as manholes and cutouts;
- corrosion damage and fatigue cracks of in-service structures.

Usually, residual stresses and initial deflection are implicitly included in the strength formulations as long as they do not exceed the fabrication tolerance criteria. If other types of structural deterioration are present, it is recommended that additional strength analyses by more refined methods be performed to derive reduction factors.

The welding-induced residual stress pattern in a stiffened panel is shown in Figure 17.5. This includes a tension block in yield, located at the stiffener attachment, that is balanced by a zone of uniform compressive residual stresses in the center of the plate. The magnitude of the compressive residual stresses may be obtained from equilibrium considerations.

$$\frac{\sigma_r}{\sigma_Y} = \frac{2\eta}{\frac{b}{t} - 2\eta} \quad (17.8)$$

The value of η tends to be high for as-welded structures. However, if the member is subject to alternating in-service loads, the residual stresses will be reduced due to a shakeout by occasional tensile loads. Faulkner (1975) has suggested that the design values of η may be taken to be between 3 and 4.5.

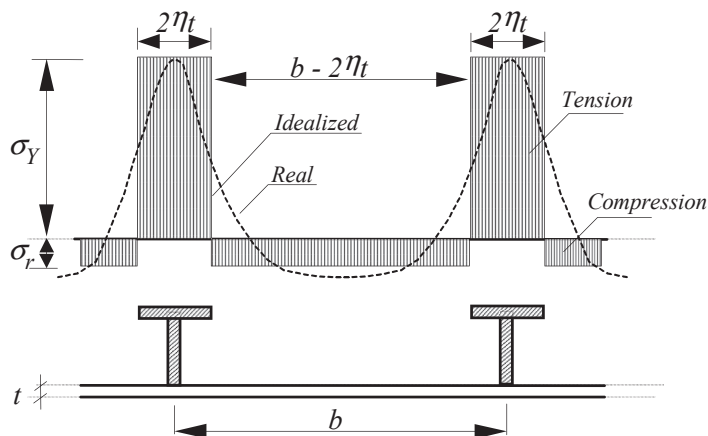


Figure 17.5
Welding residual stress in plates.

The effect of residual stresses may cause a loss of compressive plate stiffness. This is because of premature yielding in the compression zone. A reduction factor R_r may be introduced for strength analysis, as given below.

$$R_r = 1 - \frac{\sigma_r}{\sigma_Y} \frac{E_t}{E} = 1 - \frac{2\eta}{\frac{b}{t} - 2\eta} \frac{2(\beta - 1)}{\beta}, \quad 1 < \beta < 2.5 \quad (17.9)$$

where E_t is the tangent modulus of the plate.

The levels and distributions of residual stresses in plates and stiffeners are illustrated in Figure 17.5. They vary depending on the plate's material properties and on the fabrication methods used, such as rolling, welding, mechanical straightening, and heat treatment. Special high-strength steels allow large heat-affected zones with considerable residual stresses to form. High residual stresses may be a considerable factor in structural strength loss.

The welding-induced residual tensile stresses along welded edges are assumed to not exceed the plate's yield stress. For mild steels, the compressive residual stresses in any direction may be taken as 5–10% of the plate's yield stress. For high-strength steels, higher values for compressive residual stresses should be considered.

For the stiffener web, residual compressive stresses may be taken as 3–5% of the stiffener yield stress for mild steels, and a little higher for high-strength steels.

Initial structural imperfections may be induced by welding, manufacturing, heat treatment, transportation, and storage. The effects of imperfections on the ultimate strength of plates depend strongly on their shapes. In most theoretical studies, initial deflections have been assumed to have the same shape as the buckling mode, because the initial deflection has the most significant influence on the ultimate strength when its shape coincides with the buckling mode. Statistical analysis of measured plate distortions shows that the amplitude of the buckling component is about half that of the maximum distortions.

Various formulas are available for predicting the maximum distortion. However, the following relation has been frequently used

$$\frac{\delta_o}{t} = C_2 \frac{b}{t} - C_3, \quad \frac{b}{t} > 40 \quad (17.10)$$

where typically, $C_2 = 0.016$ and $C_3 = 0.36$.

The fabrication tolerance criteria are usually defined in design codes for the strength criteria defined. If the fabrication tolerance criteria are violated, imperfections will have to be repaired. Alternatively, the effects of imperfections are to be explicitly accounted for using advanced formulae or numerical/mechanical tests.

17.1.5 Correction for Plasticity

For plates with a low width-to-thickness ratio, Eqn (17.7) may theoretically predict a critical stress if an excess of the yield stress occurs, but physically it cannot. Various methods exist to account for plasticity effects. A convenient technique for modifying the elastic critical stress caused by plasticity is the ϕ -method, where the elastic–plastic buckling stress is given by

$$\sigma_{cr} = \phi \cdot \sigma_Y \quad (17.11)$$

and where ϕ is an empirical function of the structural slenderness, defined below

$$\bar{\lambda} = \sqrt{\frac{\sigma_Y}{\sigma_E}} \quad (17.12)$$

Various expressions for ϕ exist. One method for plasticity correction is to use an elliptical interaction equation (Odland, 1988):

$$\left(\frac{\sigma_{cr}}{\sigma_Y}\right)^2 + \left(\frac{\sigma_{cr}}{\sigma_E}\right)^2 = 1$$

It can be seen that

$$\begin{aligned} \sigma_{cr} &\rightarrow \sigma_Y & \text{when } \sigma_E &\rightarrow \infty \\ \sigma_{cr} &\rightarrow \sigma_E & \text{when } \sigma_E &\ll \sigma_Y \end{aligned}$$

Hence, the formula converges to the correct solution for both stocky members and slender members. Solving for σ_{cr} , the following is obtained:

$$\sigma_{cr} = \frac{\sigma_Y}{\sqrt{1 + \bar{\lambda}^4}} \Rightarrow \phi = \frac{1}{\sqrt{1 + \bar{\lambda}^4}} \quad (17.13)$$

Another well-known solution is the so-called Johnson–Ostenfeld formula, adopted by several North American design codes

$$\phi = \begin{cases} 1 - \frac{\bar{\lambda}^2}{4}, & \bar{\lambda}^2 \leq 2 \\ \frac{1}{\bar{\lambda}^2}, & \bar{\lambda}^2 \geq 2 \end{cases} \quad (17.14)$$

17.2 Combined Loads

In a limit-state design, buckling criteria and ultimate strength criteria are also termed the serviceability limit state (SLS) and ultimate limit state (ULS).

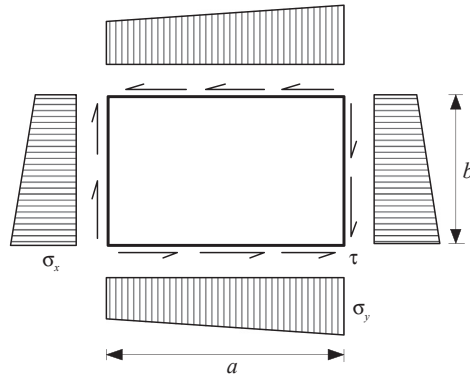


Figure 17.6
Combined loading.

17.2.1 Buckling—SLS

In the case of a combined loading as shown in Figure 17.6, the above procedure may be applied if an equivalent stress and an equivalent elastic buckling stress are defined. This is conveniently expressed by the following interaction formula

$$\left(\frac{\sigma_e}{\sigma_{Ee}}\right)^c = \left(\frac{\sigma_x}{\sigma_{Ex}}\right)^c + \left(\frac{\sigma_y}{\sigma_{Ey}}\right)^c + \left(\frac{\tau}{\tau_E}\right)^c \quad (17.15)$$

where σ_{Ex} , σ_{Ey} , and τ_E are the elastic buckling stresses when the corresponding stress component acts alone, and σ_{Ee} is the equivalent elastic buckling stress corresponding to the equivalent stress $\sigma_e = \sqrt{\sigma_x^2 + \sigma_y^2 - \sigma_x\sigma_y + 3\tau^2}$.

The equivalent reduced slenderness ratio used in the above plasticity correction can then be expressed as (DNV, CN 30.1, 1995)

$$\bar{\lambda}_e^2 = \frac{\sigma_Y}{\sigma_{Ee}} = \frac{\sigma_Y}{\sigma_e} \left[\left(\frac{\sigma_x}{\sigma_{Ex}}\right)^c + \left(\frac{\sigma_Y}{\sigma_{Ey}}\right)^c + \left(\frac{\tau}{\tau_E}\right)^c \right]^{\frac{1}{c}} \quad (17.16)$$

The exponent c depends on the plate aspect ratio. Square plates tend to be more sensitive to combined loadings than long plates are, because the two buckling modes coincide for biaxial compression. Therefore, a linear interaction is often used for square plates, and an elliptic interaction is used for long plates. DNV CN 30.1 (1995) proposes the following equation for the buckling strength of the plate under combined loads:

$$\sigma_{cr} = \frac{\sigma_Y}{\sqrt{1 + \bar{\lambda}_e^4}} \quad (17.17)$$

17.2.2 Ultimate Strength—ULS

The ultimate strength of the plate may be estimated as (DNV, CN 30.1, 1995)

$$\sigma_{ult} = \frac{\sigma_Y}{\sqrt{1 + \bar{\lambda}_e^4}}, \quad \bar{\lambda}_e \leq 1 \quad (17.18)$$

$$\sigma_{ult} = \frac{\sigma_Y}{\bar{\lambda}_e \sqrt{2}}, \quad 1.0 < \bar{\lambda}_e \leq 5.0 \quad (17.19)$$

The SLS and ULS are compared in Figure 17.7. For very slender plates, the ultimate strength is significantly larger than the buckling strength.

Balint et al. (2002) propose the following equation for the ultimate strength of plates under combined loads:

$$\left(\frac{\sigma_1}{\sigma_{L1}}\right)^A - \alpha \left(\frac{\sigma_1}{\sigma_{L1}}\right) \left(\frac{\sigma_2}{\sigma_{L2}}\right) + \left(\frac{\sigma_2}{\sigma_{L2}}\right)^2 + \left(\frac{\tau}{\tau_L}\right)^2 = 1 \quad (17.20)$$

where

σ_1 = Axial stress in direction 1

σ_2 = Axial stress in direction 2

τ = Shear stress

σ_{L1} = Limiting axial stress for σ_1

σ_{L2} = Limiting axial stress for σ_2

τ_L = Limiting shear stress.

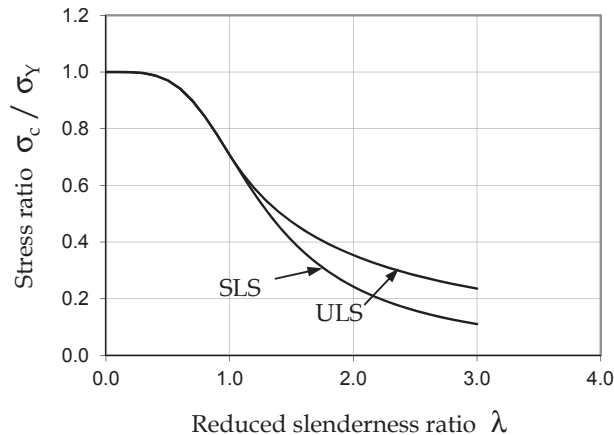


Figure 17.7
Ultimate strength versus buckling strength of plates.

Following the example of [Bais \(2001\)](#), the following strength criteria may also be applicable for ultimate strength (of plates or stiffened plates) under combined loads

$$\left(\frac{\sigma_1}{\sigma_{L1}}\right)^2 - \alpha \left(\frac{\sigma_1}{\sigma_{L1}}\right) \left(\frac{\sigma_2}{\sigma_{L2}}\right) + \left(\frac{\sigma_2}{\sigma_{L2}}\right)^2 + \left(\frac{\tau}{\tau_L}\right)^2 + \left(\frac{p}{p_L}\right)^2 = 1 \quad (17.21)$$

where

p = Lateral pressure

p_L = Limiting lateral pressure.

[Equation \(17.21\)](#) has been proposed because it approaches von Mises yield conditions for inelastic buckling cases and may lead to linear interaction for elastic buckling cases. According to [API 2V \(1987\)](#), the coefficient α may be taken as 0 when both stresses σ_1 and σ_2 are compressive, and as 1 when σ_1 , σ_2 , or both are tensile. To be accurate, the coefficient α should be derived based on finite element analysis and mechanical testing.

17.3 Buckling Strength of Plates

The Johnson—Ostenfeld formula (or [Odland, 1988](#)) may be applied for plasticity correction. To calculate elastic buckling stress under combined loads, the equations in [Section 17.2](#) may be used. The elastic buckling strength for plates under compressive stress and in-plane bending can be expressed as

$$\sigma_E = k_s \frac{\pi^2 E}{12(1 - \nu^2)} \left(\frac{t}{b}\right)^2 \quad (17.22)$$

An expression that gives good accuracy with the exact elastic buckling solution for a simply supported plate exposed to pure shear stress is given in [Timoshenko and Gear \(1961\)](#),

$$\tau_{EI} = k_s \frac{\pi^2 E}{12(1 - \nu^2)} \left(\frac{t}{b}\right)^2 \quad (17.23)$$

where

$$k_s = 4.0 \left(\frac{b}{a}\right)^2 + 5.34 \quad (17.24)$$

and

ν = Poisson's ratio.

Yield stress in shear may be estimated as $\frac{\sigma_0}{\sqrt{3}}$, where σ_0 = yield stress of the plate.

17.4 Ultimate Strength of Unstiffened Plates

17.4.1 Long Plates and Wide Plates

Slender plates can carry loads larger than what is predicted by the elastic theory if their unloaded edges are constrained to remain straight. Because of large lateral deflections, membrane stresses develop in the transverse direction, which tend to stabilize the plates. At this stage, the distribution of stresses along the unloaded edges is no longer uniform, but instead increases toward the stiffeners. According to the effective width method, the ultimate strength is obtained when the edge stress σ_e in Figure 17.8 approaches the yield stress. The following formula has been widely used for simply supported plates where the unloaded edges are constrained to remain straight (Faulkner, 1975):

$$\frac{b_e}{b} = \frac{\sigma_{xm}}{\sigma_y} = \begin{cases} \frac{2}{\beta} - \frac{1}{\beta^2} & \beta \geq 1 \\ 1 & \beta \leq 1 \end{cases} \quad (17.25)$$

where the plate slenderness ratio is given by

$$\beta = \frac{b}{t} \sqrt{\frac{\sigma_Y}{E}} \quad (17.26)$$

Equation (17.25) accounts for a reasonable degree of initial deflection in the buckling mode, but does not account for residual stresses.

The following effective width formula may be used for compressive loads acting on the long edge, $a/b \geq 1.0$, and short edge, $a/b < 1.0$ (Mansour, 1997).

$$b_e = \begin{cases} C_b & \text{for } \frac{a}{b} \geq 1.0 \\ \frac{a}{b} C_b + 0.08 \left(1 - \frac{a}{b}\right) \left(1 - \frac{1}{\beta^2}\right)^2 \leq 1.0 & \text{for } \frac{a}{b} < 1.0 \end{cases} \quad (17.27)$$

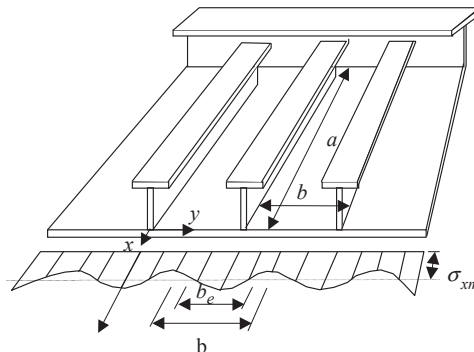


Figure 17.8
Actual stress distribution in a compressed stiffened plate.

$$C_b = \begin{cases} 1 & \text{for } \beta < 1.25 \\ \frac{2.25}{\beta} - \frac{1.25}{\beta^2} & \text{for } 1.25 \leq \beta < 3.5 \\ \sqrt{\frac{4\pi^2}{12(1-\nu^2)}} \frac{1}{\beta^2} & \text{for } \beta \geq 3.5 \end{cases} \quad (17.28)$$

17.4.2 Plates Under Lateral Pressure

The ultimate strength of plates in shear can be assumed to be the shear yield stress.

17.4.3 Shear Strength

The ultimate strength of plates in shear can be assumed to be the shear yield stress.

17.4.4 Combined Loads

The equations for plates under combined loads may be found in [Section 17.2.2](#).

17.5 Ultimate Strength of Stiffened Panels

17.5.1 Beam-Column Buckling

When a stiffened panel is subjected to a combined axial stress σ and bending moment M (induced by lateral load), the ultimate strength can be predicted using [Mansour \(1997\)](#).

$$\frac{\sigma}{\sigma_{\text{column}}} + C_M \frac{M}{\sigma_{\text{beam}}} = 1 \quad (17.29)$$

where the column buckling strength for stiffened plates, σ_{column} , can be predicted using the Johnson–Ostenfeld formula or the Perry–Robertson formula, which is based on the elastic buckling stress

$$\sigma_E = \frac{\pi^2 EI_s}{l_s^2 A_s} \quad (17.30)$$

where

E = Elasticity modulus

I_s = Moment of inertia of the stiffened plate

l_s = Stiffener length

A_s = Cross-sectional area of the stiffened plate.

While the Johnson–Ostenfeld formula for column buckling is very simple, it does not account for the effect of initial imperfection. An alternative equation is the Perry–Robertson formula (see Part II, Chapter 28 of this book). The coefficient C_M is a function of the ratio of the bending moment acting at the two ends of the beam M_A/M_B .

$$C_m = \frac{0.6 + 0.4M_A/M_B}{1 - \sigma/\sigma_E} \quad (17.31)$$

The ultimate bending moment for the stiffened plates under pure bending can be taken as a fully plastic bending moment.

17.5.2 Tripping of Stiffeners

When the web height-to-thickness ratio is large and it is combined with a flange that is inadequate to remain straight under the combined uniaxial compressive load and lateral pressure, the stiffener may twist sideways in the tripping failure mode. The tripping strength can be predicted by the Johnson–Ostenfeld formula and the elastic buckling stress equation (see Eqn (4.30) in Part I, Chapter 15, as well as by [Ma \(1994\)](#)).

17.6 Gross Buckling of Stiffened Panels (Overall Grillage Buckling)

Using the orthotropic plate theory, [Mansour \(1977\)](#) derived the following buckling equation that may be used in a number of stiffeners in each direction:

$$\sigma_E = k \frac{\pi^2 \sqrt{D_x D_y}}{h_x B^2} \quad (17.32)$$

where B is gross panel width and h_x is effective thickness. For a simply supported gross panel, k may be taken as

$$k = \frac{m^2}{\rho^2} + 2\mu + \frac{\rho^2}{m^2} \quad (17.33)$$

where m is the number of half-waves for a buckled plate, and μ and ρ are the torsion coefficient and the theoretical aspect ratio, respectively.

References

- API 2V, 1987. Bulletin on Design of Flat Plate Structures, first ed. (ANSI/API Bull 2V-1992).
 Bai, Y., 2001. Pipelines and Risers. In: Elsevier Ocean Engineering Book Series, vol. 3.
 Balint, S.W., Serrahn, C.S., Chang, B.C., 2002. Background to new edition of API bulletin 2V: design of flat plate structures. In: Proceedings of Offshore Technology Conferences, OTC 14187.

- DNV CN 30.1, 1995. Buckling Strength Analysis. Det Norske Veritas.
- Faulkner, D., 1975. A review of effective plating for use in the analysis of stiffened plating in bending and compression. *Journal of Ship Research* 19.
- Ma, M., 1994. Elastic and Inelastic Analysis of Panel Collapse by Stiffener Buckling (Ph.D. thesis). Virginia Polytechnic Institute and State University.
- Mansour, A., 1977. Gross Panel Strength under Combined Loading. Ship Structures Committee Report, SSC-270.
- Mansour, A.E., 1997. Assessment of Reliability of Ship Structures. SSC Report, SSC-398.
- Odland, J., June 1988. Improvement in Design Methodology for Stiffened and Unstiffened Cylindrical Structures. BOSS-1988. In: Moan, T. (Ed.). Tapir Publisher.
- Timoshenko, S., Gere, J.M., 1961. *Theory of Elastic Stability*. McGraw-Hill Book Company, Inc.

Ultimate Strength of Cylindrical Shells

18.1 Introduction

18.1.1 General

Cylindrical shells are *essential* structural elements in offshore structures, submarines, and airspace crafts. They are often subjected to combined compressive stress and external pressure, and therefore must be designed to meet strength requirements. A theoretical load-end-shortening curve, representing unstiffened cylindrical shells under axial compression, can be seen in Figure 18.1. For a perfect shell, the stress–strain relation is linear until bifurcation point B is reached, where buckling occurs and load-carrying capacity decreases sharply. For an imperfect shell, the stress–strain relation is nonlinear from an early stage of loading; buckling occurs at point L without showing an obvious bifurcation phenomenon.

The strength of an imperfect cylindrical shell may be significantly lower than the bifurcation load. The design of cylindrical shells is based on the modification of theoretical predictions using a knockdown factor for the imperfection effect.

18.1.2 Buckling Failure Modes

The characteristic geometric parameters of a stiffened cylindrical shell are defined in Figure 18.2.

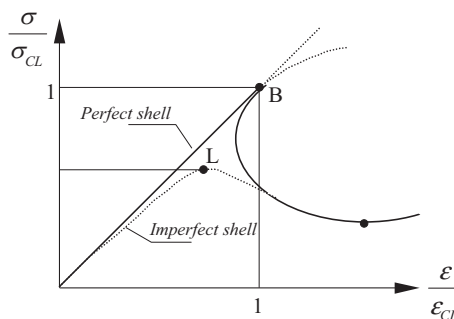


Figure 18.1
Stress–strain relations for perfect and imperfect shells.

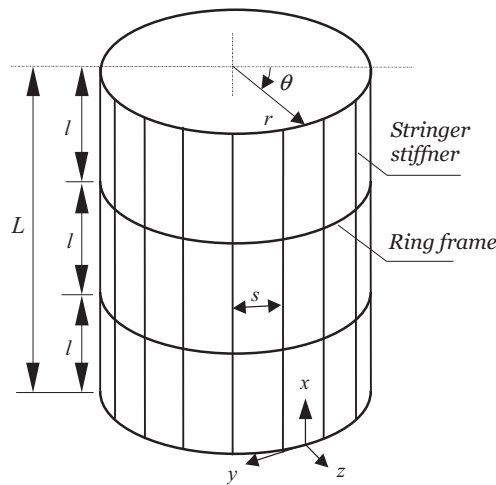


Figure 18.2

Geometric parameters of a stiffened cylindrical shell.

Boundary conditions are assumed simply supported and constrained. Design loads include:

- Compressive stress due to longitudinal force and bending moment
- External overpressure
- Combined compressive stress and external pressure

Major factors affecting the strength of cylindrical shells include:

- Residual stresses and geometric imperfections
- Dents
- Corrosion defects

The effects of residual stresses and geometric imperfections are implicitly accounted for in the criteria discussed in this chapter. However, if the fabrication tolerance is violated, or dents and significant corrosion defects are found in an in-service structure, repairs and additional strength analysis are necessary. For pressure vessels, pipelines, and risers, criteria for pressurized cylinders under combined external/internal pressure, axial force, and bending can all be seen in [Bai \(2001\)](#).

18.2 Elastic Buckling of Unstiffened Cylindrical Shells

18.2.1 Equilibrium Equations for Cylindrical Shells

[Figure 18.3](#) shows an infinitesimal element of a shell with its associated stress resultants from membrane and bending actions. Considering equilibrium in the axial, circumferential, and radial directions, the following equations are obtained.

$$r \frac{\partial N_x}{\partial x} + \frac{\partial N_{\theta x}}{\partial \theta} = 0 \quad (18.1)$$

$$r \frac{\partial N_{x\theta}}{\partial x} + \frac{\partial N_\theta}{\partial \theta} = 0 \quad (18.2)$$

$$\nabla^4 w = \frac{1}{D} \left(p + N_x \frac{\partial^2 w}{\partial x^2} + \frac{2}{r} N_{x\theta} \frac{\partial^2 w}{\partial x \partial \theta} + \frac{1}{r^2} N_\theta \frac{\partial^2 w}{\partial \theta^2} - \frac{1}{r} N_\theta \right) \quad (18.3)$$

where

$$\begin{aligned} N_x &= \sigma_x t \\ N_{x\theta} &= N_{\theta x} = \sigma_{x\theta} t \end{aligned} \quad (18.4)$$

$$N_\theta = \sigma_\theta t$$

$$\nabla^4 = (\nabla^2)^2 = \left(\frac{\partial^2}{\partial x^2} + \frac{1}{r^2} \frac{\partial^2}{\partial \theta^2} \right)^2$$

The plate stiffness, D , is given as

$$D = \frac{Et^3}{12(1-\nu^2)} \quad (18.5)$$

The pressure, p , is positively going outwards. Note the similarity between Eqn (18.3) and the corresponding expression for plate equilibrium, by substituting

$$\frac{\partial}{\partial y} = \frac{1}{r} \frac{\partial}{\partial \theta}, \quad \frac{\partial^2}{\partial y^2} = \frac{1}{r^2} \frac{\partial^2}{\partial \theta^2} \quad (18.6)$$

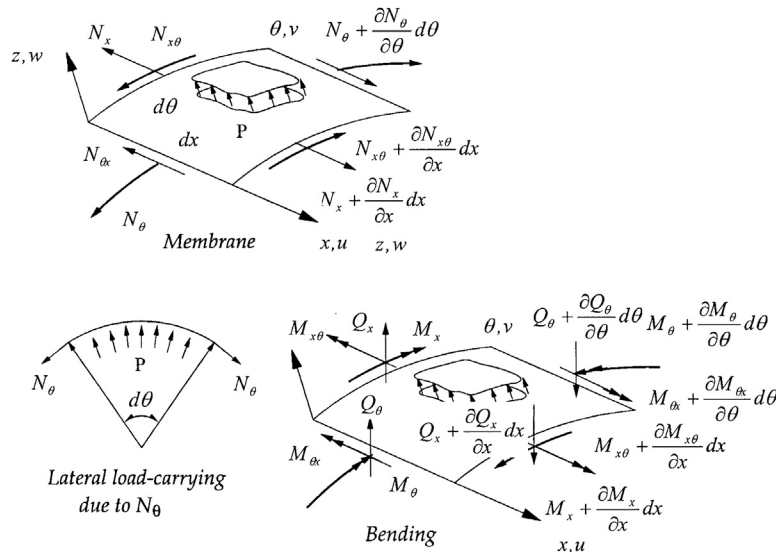


Figure 18.3
Shell stress resultant.

The only new term is N_θ/r , which represents the lateral component of the circumferential stress. Thus unlike plates, cylindrical shells can carry lateral loads by pure membrane action and no bending. This is a very efficient property, but at the same time this makes shells sensitive to buckling.

Equations (18.1) through Eqn (18.3) form a coupled set of three nonlinear equations with four variables— N_x , $N_{x\theta}$, N_θ , and w . By introducing the kinematic and constitutive relationships, as well as applying operator ∇ , Eqn (18.3) can be rewritten as

$$\nabla^8 w = \frac{\nabla^4}{D} \left(N_x \frac{\partial^2 w}{\partial x^2} + \frac{2}{r} N_{x\theta} \frac{\partial^2 w}{\partial x \partial \theta} + \frac{1}{r^2} N_\theta \frac{\partial^2 w}{\partial \theta^2} \right) - \frac{Et}{Dr^2} \frac{\partial^4 w}{\partial x^4} \quad (18.7)$$

which is also known as Donnell's equation.

18.2.2 Axial Compression

Consider a cylinder subjected to an axial compressive load, P . If the end effects are neglected, the following assumptions apply.

$$N_x = \frac{P}{2\pi r}, \quad N_{x\theta} = N_\theta = 0 \quad (18.8)$$

Introduction of these values into Eqn (18.7) gives

$$D\nabla^8 w + \frac{Et}{r^2} \frac{\partial^4 w}{\partial x^4} + \frac{P}{2\pi r} \nabla^4 \left(\frac{\partial^2 w}{\partial x^2} \right) = 0 \quad (18.9)$$

The solution to this differential equation takes the form

$$w = \delta \left(\sin \frac{m\pi x}{l} \right) \sin n\theta \quad (18.10)$$

where m is the number of half-waves in the longitudinal direction, and n is the number of entire waves in the circumferential direction, giving

$$\sigma_{xE} = \frac{\pi^2 E}{12(1-\nu^2)} \left(\frac{t}{l} \right)^2 \left[\frac{(m^2 + \bar{n}^2)^2}{m^2} + \frac{12Z^2}{\pi^4} \frac{m^2}{(m^2 + \bar{n}^2)^2} \right] \quad (18.11)$$

where Z is the Batdorf parameter,

$$Z = \frac{l^2}{rt} \sqrt{(1-\nu^2)} \quad (18.12)$$

and

$$\bar{n} = \frac{nl}{\pi r} \quad (18.13)$$

The solution to Eqn (18.11) may be expressed as

$$\sigma_{xE} = k_c \frac{\pi^2 E}{12(1-\nu^2)} \left(\frac{t}{l}\right)^2 \quad (18.14)$$

For cylinders of intermediate length, a close estimate of the smallest critical load may be obtained by analytically minimizing Eqn (18.11) with respect to the following quantity

$$\left(\frac{m^2 + \bar{n}^2}{m}\right)^2$$

The minimum is found to be

$$\left(\frac{m^2 + \bar{n}^2}{m}\right)^2 = \frac{2\sqrt{3}}{\pi^2} Z \quad (18.15)$$

which gives the following critical load,

$$\sigma_{xE} = \frac{\pi^2 E}{12(1-\nu^2)} \left(\frac{t}{l}\right)^2 \cdot \frac{4\sqrt{3}}{\pi^2} Z = 0.605 \frac{Et}{r} = \sigma_{cl} \quad (18.16)$$

This is the classical solution for an axially compressed cylinder. It should be noted that m and \bar{n} are treated as continuous variables (for diamond-shaped bulges) in the minimization process. However, they are actually discrete quantities, and the correct values can be found by trial and error.

For short cylinders, the buckling mode will be asymmetric with $m = 1$ and $n = 0$, which is plate-like buckling. The following is the obtained buckling coefficient.

$$k_c = 1 + \frac{12Z^2}{\pi^4} \quad (18.17)$$

and is valid for

$$Z < \frac{\pi^2}{2\sqrt{3}} = 2.85 \quad (18.18)$$

For long cylinders, column buckling is a potential collapse mode, and the buckling stress is expressed by

$$\sigma_E = \frac{\pi^2 EI}{Al^2} \approx \frac{\pi^2 E}{2} \left(\frac{r}{l}\right)^2 \quad (18.19)$$

18.2.3 Bending

In elastic regions, studies carried out in this field indicate that the buckling stress in bending is close to that of buckling in axial compression, for all practical purposes; see [Timoshenko and Gere \(1961\)](#). It is complicated to analyze cylinders subjected to bending because

- The initial stress distribution is no longer constant around the circumference, and
- The prebuckling deformations of cylinders are highly nonlinear due to ovalization of the cross section.

[Brazier \(1927\)](#) was the first researcher to derive elastic bending moments and cross-sectional ovalizations as functions of curvature in elasticity. He found that the maximum moment is reached when critical stress is

$$\sigma_{xE} = 0.33 \frac{Et}{r} \quad (18.20)$$

However, in plastic regions, the buckling strain for cylinders in pure bending may be substantially higher than that given by the plastic buckling theory for cylinders in pure compression. Many researchers have tried to derive mathematical solutions for inelastic cylinders in pure bending (see [Ades, 1957](#) and [Gellin, 1980](#)). Unfortunately, no one has been successful thus far.

The effects of boundary conditions may also play an important role in the buckling strength of unstiffened short shells under bending. The shorter the cylinder, the higher the buckling strength. This is because prebuckling deformation, which is low for shorter cylinders, may reduce shell buckling strength. When the length of the cylinder is long enough, the bending strength may be close to those given by [Beazier \(1927\)](#), [Ades \(1957\)](#), and [Gellin \(1980\)](#).

18.2.4 External Lateral Pressure

In the prebuckling state, the external pressure sets up compressive membrane stresses in the meridian direction. Retaining only the linear terms in [Eqn \(18.3\)](#)

$$N_{\theta} = -pr \quad (18.21)$$

Introducing [Eqn \(18.21\)](#) into [Eqn \(18.8\)](#) yields the following stability equation

$$D\nabla^8 w + \frac{Et}{r^2} \frac{\partial^4 w}{\partial x^4} + \frac{1}{r} p \nabla^4 \left(w \frac{\partial^2 w}{\partial \theta^2} \right) = 0 \quad (18.22)$$

The displacement function is of the same form as the axial compression. Introducing Eqn (18.22) yields

$$\sigma_{\theta E} = -\frac{pr}{t} = \frac{\pi^2 E}{12(1-\nu^2)} \left(\frac{t}{l}\right)^2 \left[\frac{(1+\bar{n}^2)^2}{\bar{n}^2} + \frac{12Z^2}{\pi^4 \bar{n}^2 (1+\bar{n}^2)^2} \right] \quad (18.23)$$

where one axial wave ($m = 1$) gives the lowest buckling load. The last term is interpreted to be the buckling coefficient, k_θ . The smallest value of k_θ may be determined by trial. If \bar{n} is assumed to be large ($\gg 1$), then analytically minimizing Eqn (18.23) will give

$$k_\theta = \frac{4\sqrt{6}}{3\pi} \cdot \sqrt{Z} \quad (18.24)$$

The approximate buckling coefficient valid for small and medium values of Z is now

$$k_\theta = 4\sqrt{1 + \frac{2Z}{3\pi^2}} \quad (18.25)$$

The first term is identical to the buckling coefficient of a long plane plate. When l/r approaches infinity, Eqn (18.23) reduces to

$$\sigma_{\theta E} = \frac{n^2 E}{12(1-\nu^2)} \left(\frac{t}{r}\right)^2 = 0.275E \left(\frac{t}{r}\right)^2 \quad (18.26)$$

Long cylinders fail by ovalization, for which $n = 2$, and the above equation yields the elastic buckling stress for pipelines and risers under external pressure.

18.3 Buckling of Ring-Stiffened Shells

This section discusses the ultimate strength of cylindrical shells that have been strengthened by ring frames and are subjected to axial compression, external pressure, and a combination of the two. The formulation deals with shell failure; for the stiffener design, separate consideration should be given to general stability and torsional instability; see Ellinas et al. (1984).

18.3.1 Axial Compression

The potential failure modes for ring-stiffened shells under compression include:

- Unstiffened cylinder or inter-ring shell failure (axisymmetric collapse & diamond shape collapse)
- General instability
- Ring stiffener failure
- Combinations of the above

The failure mode of general instability failure is avoided by placing requirements on stiffener geometry (such as the moment of inertia) in design codes. Design codes require that the buckling stress for general instability is at least 2.5 times that of local panel buckling.

Once general instability failure is suppressed, ring stiffener failure is unlikely to occur in ring-stiffened cylinders. However, tripping of ring stiffeners may possibly occur in conjunction with general instability, therefore weakening the strength against general instability. Therefore, geometric requirements are applied to ring stiffeners in order to avoid the interaction of tripping with general instability.

The following formulation is given for the first failure mode listed above: unstiffened cylinder failure. [Balint et al. \(2002\)](#) proposed to use the format of Batdorf for elastic buckling of perfect cylinders

$$\sigma_{crx} = k_{xL} \frac{\pi^2 E}{12(1-\nu^2)} \left(\frac{t}{L_r} \right)^2 \quad (18.27)$$

where the buckling coefficient k_{xL} is a function of geometric parameter M_{xL} ([Capanoglu and Balint, 2002](#))

$$k_{xL} = \sqrt{1 + \frac{150}{D/t} (\alpha_{xL})^2 (M_x)^4} \quad (18.28)$$

and where

$$M_x = \frac{L_r}{\sqrt{Rt}} \quad (18.29)$$

and L_r is the ring spacing. The coefficient α_{xL} may be expressed as ([Capanoglu and Balint, 2002](#))

$$\alpha_{xL} = \frac{9}{[300 + D/t]^{0.4}} \quad (18.30)$$

[Equation \(18.27\)](#) will yield the buckling stress for a flat plate when the plate curvature is small. This is an advantage over the critical buckling stress equation for long cylinders used in *API Bulletin 2U* and *API RP 2A*.

Inelastic buckling strength may be estimated using the plasticity correction factor presented in Part II, Chapter 17.

18.3.2 Hydrostatic Pressure

General

Three failure modes may possibly occur for ring-stiffened cylinders under external pressure:

- Local inter-ring shell failure
- General instability
- Ring stiffener failure

For ring-framed cylinders subject to external hydrostatic pressure, BS5500 (1976) and Faulkner et al. (1983) combined the elastic buckling stress with the Johnson–Ostenfeld plasticity correction factor previously presented in Part II, Chapter 17. It is noted that about 700 model tests, with geometries in the range of $6 \leq R/t \leq 250$ and $0.04 \leq L/R \leq 50$, lie above the so-called “guaranteed” shell collapse pressure predicted by this formulation. The bias of the mean strength for this lower bound curve is estimated to be 1.17, and in the usual design range, and the COV is estimated to be 5% (Faulkner et al., 1983).

Local Inter-ring Shell Failure

The best-known solution for the elastic buckling of the unsupported cylinder results from the von Mises equation, which is minimized with respect to the circumferential mode number and given by (see Timoshenko and Gere, 1961)

$$p_E = \frac{\frac{Et}{R}}{n^2 - 1 + \frac{1}{2} \left(\frac{\pi R}{L} \right)^2} \left\{ \frac{1}{\left[n^2 \left(\frac{L}{\pi R} \right)^2 + 1 \right]^2} + \frac{t^2}{12R^2(1 - \mu^2)} \left[n^2 - 1 + \left(\frac{\pi R}{L} \right)^2 \right]^2 \right\} \quad (18.31)$$

Windenburg and Trilling (1934) minimized the expression with respect to n , the number of complete circumferential waves or lobes. By making further approximations, Windenburg obtained the following expression for the minimum buckling pressure.

$$p_E = \frac{0.919 E(t/R)^2}{L/(Rt)^{1/2} - 0.636} \quad (18.32)$$

Equation (18.32) is invalid for very small or very large values of $L/(Rt)^{1/2}$, but in the design range its accuracy is sufficient. The analysis assumes the cylinder is pinned at nondeflecting cylindrical supports. More refined analyses are now available that, for example, consider the influence of ring frames on deformations before and during buckling. These analyses show that p_E becomes inaccurate for closely spaced frames. Nevertheless, the Von Mises expression is still widely used, as it can be represented in a relatively simple form and is in most cases only slightly conservative.

General Instability

Owing to the catastrophic postcollapse characteristics associated with this failure mode, design codes require the effective moment of inertia for ring stiffeners with associated shell plating to be sufficiently high. This is so that the ratio of general to local elastic buckling stresses is equal to 1.2 (e.g., ASME (1980), *Boiler and Pressure Vessel Code*).

Ring Stiffener Failure

Ring stiffener failure may occur as the torsional buckling or tripping of stiffeners, seriously weakening the resistance of the shell to general instability. Therefore, design

codes specify requirements for ring stiffener geometry to prevent this type of failure from occurring. Imperfections in the form of lateral deformations of ring stiffeners may have a strong detrimental effect by reducing the stiffener's resistance to torsional buckling. Similar to the tripping of stiffened plates, fabrication tolerance has been established for such imperfections.

18.3.3 Combined Axial Compression and External Pressure

The strength of a ring-stiffened cylinder under combined axial compression and external pressure can be expressed as

$$\left(\frac{\sigma}{\sigma_c}\right)^m + \left(\frac{p}{p_{hc}}\right)^n \leq 1 \quad (18.33)$$

Recommendations by various codes are found to differ greatly, ranging from the linear interaction ($m = n = 1$) recommended by [ECCS \(1981\)](#) to the circular one ($m = n = 2$) required by [DNV \(2000\)](#). The ASME Code Case N-284 suggests a combination of straight lines and parabolas that appears to agree quite well with test data. [Das et al. \(2001\)](#) suggested that the parabola ($m = 1, n = 2$) offers the best fit to available data, with values very close to those of the ASME recommendations.

18.4 Buckling of Stringer- and Ring-Stiffened Shells

18.4.1 Axial Compression

General

This section is based on simplifications of the theories from [Faulkner et al. \(1983\)](#), [Ellinas et al. \(1984\)](#), and [Das et al. \(1992, 2001\)](#). The buckling of a stringer-stiffened cylinder is usually the governing failure mode. Other failure modes such as local panel buckling, local stiffener tripping, and general instability may also occur; see [Ellinas et al. \(1984\)](#). In many practical design situations, the buckling of stringer- and ring-stiffened shells is assessed as the buckling of stiffened plates, using the formulation presented in Part II, Chapter 17.

Local Panel Buckling

Similar to Eqn (10.19) in Section 10.3, the elastic buckling strength of axially compressed cylindrical panels may be expressed as

$$\sigma_E = k_s \frac{\pi^2 E}{12(1 - \nu^2)} \left(\frac{t}{L_s}\right)^2 \quad (18.34)$$

where L_s is the distance between the adjacent stringer stiffeners. The buckling coefficient k_s is a function of the geometric parameter $M_s = L_s/\sqrt{Rt}$, and may be taken as 4 when

$M_s < 1.73$. Capanoglu and Balint (2002) proposed to use the following equation for the geometric parameter k_s ,

$$k_s = 4\alpha_{xL} \left[1 + 0.038(M_s - 2)^3 \right] \quad (18.35)$$

The plasticity correction factor φ in Section 10.1.6 may then be used to derive the inelastic buckling strength.

Stringer-Stiffened Cylinder Buckling

The elastic stress for column shell combinations can be estimated as

$$\sigma_E = \sigma_{col} + \rho_s \sigma_s$$

where ρ_s is the shell knockdown factor, which is set at 0.75.

The elastic stress for a column is

$$\sigma_{col} = \frac{\pi^2 EI'_e}{L^2(A_s + s_{ew}t)} \quad (18.36)$$

where S_{ew} is the effective width of shell plating and I'_e is the effective moment of inertia.

The elastic critical stress for an unstiffened shell is thus

$$\sigma_s = \frac{0.605 E \frac{t}{R}}{1 + \frac{A_s}{s_{ew}t}} \quad (18.37)$$

The inelastic buckling stress σ_c may be calculated using the plasticity correction factor φ from Section 10.1.6.

Local Stiffener Tripping

When the torsional stiffness of stiffeners is low, and the shell skin D/t ratio is relatively high, stiffeners can experience torsional instability at stresses lower than those required for local or orthotropic buckling. When the stiffener buckles, it loses a large portion of its effectiveness in maintaining the initial shape of the shell. This reduction in lateral support will eventually lead to overall shell failure. Much of the load carried by the stiffener will then be shifted to the shell skin. Restrictions on the geometry of the stiffeners are applied in design codes in order to avoid this failure mode. The restrictions on the geometry of the stiffeners are similar to those used for stiffened plates. The out-of-straightness of stiffeners can result in a reduction of the load-carrying capacity as an effect of initial deflection on column buckling. Therefore, fabrication tolerance is applied to stiffeners.

General Instability

General instability involves buckling of both stringer and ring stiffeners, along with the shell plating. This failure mode may have catastrophic consequences; therefore,

restrictions are applied in design codes to the second moment of inertia for ring stiffeners. Such restrictions are to assure that the buckling strength for the general instability mode is one to four times that of stringer-stiffened cylinder buckling.

18.4.2 Radial Pressure

External pressure may be applied either purely radially, known as “external lateral pressure loading,” or all around the shell (both radially and axially), known as “external hydrostatic pressure loading.” Potential failure modes include:

- Local buckling of the panels between stringer stiffeners
- Stringer buckling
- General instability
- Local stiffener tripping
- Interaction of the above failure modes

The formulation for collapse pressure p_{hc} can be found from [API Bulletin 2U \(1987\)](#) and [Das et al. \(1992, 2001\)](#).

[Balint et al. \(2002\)](#) modified the formulae in [API Bulletin 2U \(1987\)](#) and suggested the following elastic buckling equation:

$$\sigma_E = k_\theta \frac{\pi^2 E}{12(1-\nu^2)} \left(\frac{t}{L_r} \right)^2 \quad (18.38)$$

[Capanoglu and Balint \(2002\)](#) proposed to use the following equation for the geometric parameter k_θ

$$k_\theta = \alpha_{\theta L} \left[\frac{1 + (L_r/L_s)^2}{L_r/L_s} \right]^2 \left[1 + \frac{0.011M_x^2}{0.5[1 + (L_r/L_s)^2]^2} \right] \quad (18.39)$$

where the imperfection parameter $\alpha_{\theta L}$ can be taken as 0.8. The plasticity correction factor φ in Section 10.1.6 is then used to derive the inelastic buckling strength.

18.4.3 Axial Compression and Radial Pressure

A simple interaction equation for the strength of the stringer- and ringer-stiffened cylinders under a combined axial compression and external pressure can be expressed as

$$\left(\frac{\sigma}{\sigma_c} \right)^m + \left(\frac{p}{p_{hc}} \right)^n \leq 1 \quad (18.40)$$

where σ and p are the applied axial compressive stress and radial pressure, respectively. Ellinas et al. (1984) recommended that $m = n = 2$. A more refined interaction equation for the combined axial compression and radial pressure may be found in Das et al. (1992, 2001). The accuracy of the above equations, compared with mechanical tests and other design codes, is given in Das et al. (2001).

References

- Ades, C.S., 1957. Buckling strength of tubing in plastic region. *Journal of the Aeronautical Science* 24, 605–610.
- API 2U, 1987. *Bulletin on Stability Design of Cylindrical Shells*, first ed. (ANSI/API Bull 2U-1992).
- ASME, 1980. *Boiler and Pressure Vessel Code Case N-284*.
- Bai, Y., 2001. *Pipelines and Risers*, vol. 3. Elsevier Ocean Engineering Book Series.
- Balint, S.W., Capanoglu, C., Kamal, R., 2002. In: *Background to New Edition of API Bulletin 2U: Stability Design of Cylindrical Shells*, Proceedings of Offshore Technology Conferences, OTC 14188.
- Brazier, L.G., 1927. On the flexure of thin cylindrical shells and other thin sections. *Proceedings of the Royal Society, Series A* 116, 104–114.
- BS 5500, 1976. *Specification for Unfired Fusion Welded Pressure Vessels*. B.S.I. Section 3.
- Capanoglu, C., Balint, S.W., 2002. Comparative assessment of design based on revised API bulletin 2U and other recommendations. In: *Proceedings of ISOPE Conf.*
- Das, P.K., Faulkner, D., Zimmer, R.A., 1992. Selection of Robust Strength Models for Efficient Design and Ring and Stringer Stiffened Cylinders Under Combined Loads. In: *Safety and Reliability*, vol. II. OMAE.
- Das, P.K., Thavalingam, A., Hauch, S., Bai, Y., 2001. A New Look into Buckling and Ultimate Strength Criteria of Stiffened Shells for Reliability Analysis. *OMAE*, 01–2131.
- DNV, 2000. *RP-C202, Buckling Strength of Shells*. Det Norske Veritas (also in DNV CN 30.1).
- ECCS, 1981. *European Recommendations for Steel Construction*. Section 4.6. Buckling of Shells.
- Ellinas, C.P., Supple, W.J., Walker, A.C., 1984. *Buckling of Offshore Structures* (Granada).
- Faulkner, D., Chen, Y.N., de Oliveira, J.G., 1983. In: *Limit State Design Criteria for Stiffened Cylinders of Offshore Structures*, ASME 83-PVP-8, Presented in Portland, Oregon, June 1983.
- Gellen, S., 1980. The plastic buckling of long cylindrical shells under pure bending. *International Journal of Solids and Structures* 10, 394–407.
- Timoshenko, S., Gere, J.M., 1961. *Theory of Elastic Stability*. McGraw-Hill Book Company, Inc.
- Windenburg, D.F., Trilling, C., 1934. Collapse of instability of thin cylindrical shells under external pressure. *Transaction the ASME* 56, 819.

A Theory of Nonlinear Finite Element Analysis

19.1 General

A variety of situations exist in which a structure may be subjected to large dynamic loads, which can cause permanent deformation or damage to the structure. Therefore, structural dynamics and impact mechanics have an important role in the engineering design.

Earlier investigations on structural impacts have been well described by [Jones \(1989\)](#). The development of theoretical methods, for impact mechanics, has been aided by an idealization of real complex material behaviors, such as a rigid perfectly plastic material behavior. These methods are classified as rigid-plastic analysis methods. Theoretical predictions based on rigid-plastic analyses can give important information on the impact of plastic behavior in a simple form. The results are often in good agreement with the corresponding experimental results. However, it is difficult to make a more realistic modeling of the plastic deformations because they are interspersed with elastic deformation. Plastic flow causes a change in the shape and size, and the plastic regions may disappear and reappear. The structure may invoke strain hardening as well as strain-rate hardening when it is yielded due to time-dependent loadings.

General solutions for arbitrary types of structures that are subjected to arbitrary impacts can be obtained by numerical methods, such as finite element methods. Considerable progress has been made for dynamic plastic analysis, in both the theoretical aspects and the development of general-purpose computer programs. Unfortunately, there is insufficient theoretical knowledge on the effect of the strain rate on material properties, and on the consistent constitutive modeling of plasticity. Benchmark tests use a number of well-known computer programs, which require substantial computer speeds and capacities, and show that only a few programs can give reliable solutions ([Symonds and Yu, 1985](#)). In addition, such programs are not particularly well suited and convenient to use for analysis of complex structures. Therefore, there is a demand for numerical analysis procedures, which can be used to simulate the impact behavior of frame

structures with large displacements and strain hardening, as well as strain-rate hardening.

This chapter presents a simple and efficient procedure for the large displacement plastic analysis of beam-column elements. The elastic stiffness matrix is established by combining a linear stiffness matrix (Przemieniecki, 1968), a geometrical stiffness matrix (Archer, 1965), and a deformation stiffness matrix (Nedergaard and Pedersen, 1986). Furthermore, the effect of plastic deformation is taken into account in an efficient and accurate way by means of the plastic node method (Ueda and Yao, 1982; Ueda and Fujikubo, 1986; Fujikubo et al., 1991). In the plastic node method, the distributed plastic deformation of the element is concentrated to the nodes using a plastic hinge mechanism. The elastic–plastic stiffness matrices of the elements are derived without requiring numerical integration.

The objective of this chapter is to present a theoretical formulation for the modeling of strain-rate hardening effects, and show how these effects can be implemented in three-dimensional finite beam-column elements. The finite beam-column element is ideally suited for the impact analysis of frames with large displacements, strain hardening, and strain-rate hardening. The accuracy and efficiency of the element are examined by comparing the present results with those obtained from experiments by others, from rigid-plastic analyses and from existing finite element analysis results (see Part II, Chapters 19–22). For the fundamental theory of finite element analysis, refer to Przemieniecki (1968), Zienkiewicz (1977), Bathe (1986), among many others. To understand plasticity used in the section on the plastic node method, some basic books by Save and Massonnet (1972), Yagawa and Miyazaki (1985), Chen and Han (1987), and Chakrabarty (1987) may be helpful. To aid in the understanding of the plastic node method, a basic theory of plasticity is presented for finite element analysis of solids, based on the work of Yagawa and Miyazaki (1985).

Part of the formulation presented in this chapter previously appeared in Bai and Pedersen (1991) and Fujikubo et al. (1991). This new extension accounts for the effect of strain-rate hardening for dynamic analysis.

19.2 Elastic Beam-Column with Large Displacements

The element has three translational displacements u_x , u_y , and u_z and three rotational displacements θ_x , θ_y , and θ_z (see Figure 19.1).

These displacements are interpolated by using a polynomial interpolation of functions, which are associated with the Timoshenko beam theory. A generalized strain vector is subsequently established in the form

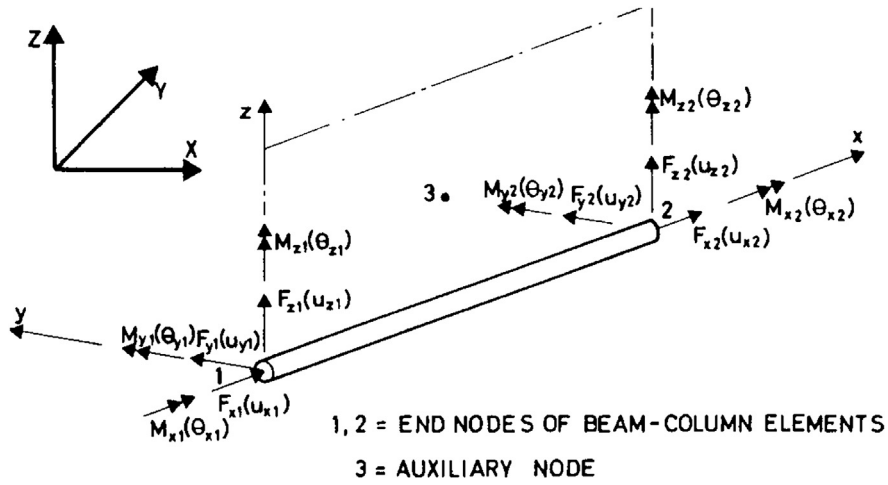


Figure 19.1

Three-dimensional beam elements with nodal forces.

$$\{\varepsilon\} = \begin{Bmatrix} e_x \\ e_y \\ e_z \\ \kappa_x \\ \kappa_y \\ \kappa_z \end{Bmatrix} = \begin{Bmatrix} u'_x + \frac{1}{2} \left[(u'_x)^2 + (u'_y)^2 + (u'_z)^2 \right] \\ u'_y - \theta_z \\ u'_y + \theta_y \\ \theta'_x \\ \theta'_y \\ \theta'_z \end{Bmatrix} \quad (19.1)$$

where $()' \equiv d/ds$ and s denote the axial coordinate of the element.

A generalized elastic stress vector $\{\sigma\}$ is expressed as

$$\begin{aligned} \{d\sigma\} &= [D_E]\{d\varepsilon\} \\ \{\sigma\} &= \{F_x \ F_y \ F_z \ M_x \ M_y \ M_z\}^T \\ [D_E] &= [EA_x \ GA_y \ GA_z \ GI_x \ GI_y \ GI_z] \end{aligned} \quad (19.2)$$

where E is the Young's modulus, G is the shear modulus, A_x denotes the area of the cross section, A_y and A_z denote the effective shear areas, I_y and I_z are moments of inertia, and I_x denotes the torsional moment of inertia.

Applying a virtual work principle results in the following equation

$$\{\delta du^e\}^T(\{f\} + \{df\}) = \int_L \{\delta d\varepsilon\}(\{\sigma\} + \{d\sigma\})ds \quad (19.3)$$

where L is the length of the element, $\{u^e\}$ is the elastic nodal displacement vector, and $\{f\}$ is the external load vector. Substituting the strains and stresses defined in Eqns (19.1) and (19.2) in Eqn (19.3), and omitting the second-order terms of the displacements, the following equation is obtained (Bai and Pedersen, 1991):

$$[k_E]\{du^e\} = \{dx\} \quad (19.4)$$

where

$$[k_E] = [k_L] + [k_G] + [k_D] \quad (19.5)$$

and

$$\{dx\} = \{f\} + \{df\} - ([k_L] + [k_G])\{u^e\} \quad (19.6)$$

The matrix $[k_L]$ is a standard linear stiffness matrix (Przemieniecki, 1968), $[k_G]$ is a geometrical stiffness matrix (Archer, 1965), and $[k_D]$ is a deformation stiffness matrix (Nedergaard and Pedersen, 1986).

19.3 The Plastic Node Method

19.3.1 History of the Plastic Node Method

The plastic node method was named by Ueda et al. (1979). It is a generalization of the plastic hinge method developed by Ueda et al. (1967) and others. Ueda and Yao (1980) published the plastic node method in an international journal, and Fujikubo (1987) published his Ph.D. thesis on this simplified plastic analysis method.

Fujikubo et al. (1991) further extended the theory of the plastic node method, in order to account for the effect of strain hardening. In the following sections, the existing theory is further extended to account for the effects of strain-rate hardening.

19.3.2 Consistency Condition and Hardening Rates for Beam Cross Sections

For a beam-column element with strain hardening and strain-rate hardening, the yield condition of its cross section is expressed as

$$f = Y(\{\sigma - \alpha\}) - \sigma_0(\bar{\varepsilon}^p, \dot{\bar{\varepsilon}}^p) = 0 \quad (19.7)$$

where Y is the yield (full plastic) function, $\{\alpha\}$ represents the translation of the yield surface due to kinematic hardening, and σ_0 is a parameter expressing the size of the

yield surface. The vector $\{\alpha\}$ has the same dimension as the generalized stress and is expressed as

$$\{\alpha\} = \{\alpha_{fx} \quad \alpha_{fy} \quad \alpha_{fz} \quad \alpha_{mx} \quad \alpha_{my} \quad \alpha_{mz}\}^T \quad (19.8)$$

Owing to isotropic hardening, the yield surface expands as the plastic deformations increase. This expansion of the yield surface is expressed by the stress parameter σ_0 , which is a function of the generalized equivalent plastic strain $\bar{\epsilon}^P$ and of the plastic strain-rate $\dot{\bar{\epsilon}}^P$. The equivalent strain $\bar{\epsilon}^P$ is evaluated as a summation of its increments, which are defined as

$$\sigma_0 d\bar{\epsilon}^P = \{\sigma - \alpha\}^T \{d\epsilon^P\} \quad (19.9)$$

where the increments of the generalized plastic strain are taken to be

$$\{d\epsilon^P\} = \{de_x^P \quad de_y^P \quad de_z^P \quad d\kappa_x^P \quad d\kappa_y^P \quad d\kappa_z^P\}^T \quad (19.10)$$

The equivalent plastic strain-rate $\dot{\bar{\epsilon}}^P$ is defined as

$$\dot{\bar{\epsilon}}^P = \frac{d\bar{\epsilon}^P}{dt} \quad (19.11)$$

where dt is an increment of time t .

The increment of the parameter σ_0 due to isotropic strain hardening and that due to strain-rate hardening are decoupled to the simplest form.

$$d\sigma_0 = dg_1(\bar{\epsilon}^P) + dg_2(\dot{\bar{\epsilon}}^P) \quad (19.12)$$

where $dg_1(\bar{\epsilon}^P)$ expresses the increment of the parameter σ_0 for a beam cross section due to isotropic strain hardening and $dg_2(\dot{\bar{\epsilon}}^P)$ denotes the increment of the parameter σ_0 due to strain-rate hardening. Similar equations were used by [Yoshimura et al. \(1987\)](#) and [Mosquera et al. \(1985a,b\)](#).

The consistency condition for a yielded cross section satisfying the yield condition, [Eqn \(19.7\)](#), is expressed as

$$df = \left\{ \frac{\partial f}{\partial \sigma} \right\}^T \{d\sigma\} - \left\{ \frac{\partial f}{\partial \alpha} \right\}^T \{d\alpha\} - \frac{dg_1}{d\bar{\epsilon}^P} d\bar{\epsilon}^P - \frac{dg_2}{d\dot{\bar{\epsilon}}^P} d\dot{\bar{\epsilon}}^P = 0 \quad (19.13)$$

Here, a kinematic hardening rate H'_{sk} and an isotropic hardening rate H'_{si} for the full plastic cross sections are introduced and are defined by

$$H'_{sk} = \{\partial f / \partial \sigma\}^T \{d\alpha\} / d\bar{\epsilon}^P \quad (19.14)$$

and

$$H'_{si} = dg_1/d\bar{\epsilon}^P \quad (19.15)$$

Similarly, a strain-rate hardening rate H'_{sr} for the full plastic cross section is defined as

$$H'_{sr} = dg_2/d\dot{\bar{\epsilon}}^P \quad (19.16)$$

With these definitions, the consistency condition Eqn (19.13) may be rewritten as

$$df = \left\{ \frac{\partial f}{\partial \sigma} \right\}^T \{d\sigma\} - (H'_{sk} + H'_{si})d\bar{\epsilon}^P - H'_{sr}d\dot{\bar{\epsilon}}^P = 0 \quad (19.17)$$

The subscript “s” in Eqns (19.14)–(19.17) indicates generalized values related to the full beam cross section. To avoid confusion, the kinematic and isotropic material-hardening rate obtained from uniaxial tests is denoted as H'_k and H'_i , respectively.

Introducing a linear interpolation for $d\bar{\epsilon}^P$, it is found that

$$d\bar{\epsilon}^P = \dot{\bar{\epsilon}}^P_{(t+dt)}\theta dt + \dot{\bar{\epsilon}}^P_{(t)}(1 - \theta)dt \quad (19.18)$$

where θ is a parameter, which will be taken as 1/2 in the numerical examples.

From Eqn (19.18), it is determined that

$$\dot{\bar{\epsilon}}^P_{(t+dt)} = \left[d\bar{\epsilon}^P - (1 - \theta)\dot{\bar{\epsilon}}^P_{(t)}dt \right] / (\theta dt) \quad (19.19)$$

Then the increment of the equivalent plastic strain-rate $d\dot{\bar{\epsilon}}^P$ may be estimated as

$$d\dot{\bar{\epsilon}}^P = \dot{\bar{\epsilon}}^P_{(t+dt)} - \dot{\bar{\epsilon}}^P_{(t)} = \left[d\bar{\epsilon}^P - \dot{\bar{\epsilon}}^P_{(t)}dt \right] / (\theta dt) \quad (19.20)$$

For simplicity, in the following equations, the subscript “t” will be omitted.

Considering Eqn (19.20), the consistency condition in Eqn (19.17) is rewritten in the following form

$$df = \{ \partial f / \partial \sigma \}^T \{ d\sigma \} - (H'_{sk} + H'_{si} + H'_{sr}/(\theta dt))d\bar{\epsilon}^P + [H'_{sr}/\theta]\dot{\bar{\epsilon}}^P = 0 \quad (19.21)$$

The hardening rates H'_{si} , H'_{sk} , and H'_{sr} in Eqn (19.21) are discussed below.

The isotropic hardening rate for the cross section is evaluated as follows. Following Ueda and Fujikubo (1986) and Fujikubo et al. (1991), the increments of the generalized stress, due to isotropic hardening, are estimated to be

$$\{d\sigma\} = [H'_{si}]\{d\epsilon^P\} \quad (19.22)$$

and the matrix $[H'_{si}]$ is obtained by first deriving a relationship between the stress increments and the plastic strain increments for points, and then integrating the stresses

over the cross section. If Von Mises yield criteria are used, and the interaction between shear stress and axial stresses is neglected, Eqn (19.23) is obtained.

$$[H'_{si}] = [H'_i A_x H'_i A_y / 3H'_i A_z / 3H'_i I_x / 3H_i I_y H'_i I_z] \quad (19.23)$$

Considering f in Eqn (19.7) to be the plastic potential and applying the flow theory of plasticity, the following equation can be obtained.

$$\{d\epsilon_P\} = cd\bar{\epsilon}_P \left\{ \frac{\partial f}{\partial \sigma} \right\} \quad (19.24)$$

where

$$c = \sigma_0 / (\{\sigma - \alpha\}^T \{\partial f / \partial \sigma\}) \quad (19.25)$$

The increment of the parameter σ_0 due to isotropic strain hardening is defined as

$$dg_1 = \{\partial f / \partial \sigma\}^T \{d\sigma\} \quad (19.26)$$

Substituting Eqns (19.22) and (19.24) into Eqn (19.26), the isotropic cross-sectional strain hardening rate, which is defined in Eqn (19.15), is given as

$$H'_{si} = c \left\{ \frac{\partial f}{\partial \sigma} \right\}^T [H'_{si}] \left\{ \frac{\partial f}{\partial \sigma} \right\} \quad (19.27)$$

The kinematic hardening rate for the cross section will be derived using a similar approach. The yield surface translation increment $\{d\alpha\}$ can be obtained using Ziegler's rule and the Mises yield criteria (Fujikubo et al., 1991).

$$\{d\alpha\} = [H'_{sk}] \{d\epsilon^P\} \quad (19.28)$$

where $[H'_{sk}]$ used in the present chapter is taken as

$$[H'_{sk}] = [H'_k A_x H'_k A_y / 3H'_k A_z / 3H'_k I_x / 3H'_k I_y H'_k I_z] \quad (19.29)$$

Substituting Eqns (19.24) and (19.28) into Eqn (19.14)

$$H'_{sk} = c \left\{ \frac{\partial f}{\partial \sigma} \right\}^T [H'_{sk}] \left\{ \frac{\partial f}{\partial \sigma} \right\} \quad (19.30)$$

Finally, the strain-rate hardening rate for the cross sections will need to be determined. The increment of the parameter σ_0 due to strain-rate hardening is estimated by the constitutive equation that expresses the relationship between g_2 and the equivalent plastic strain. For instance, the Cowper–Symonds constitutive equation is expressed as (Jones, 1989)

$$\sigma_{0x} = \sigma_y \left[1 + \left(\dot{\epsilon}_x^P / D \right)^{1/q} \right] \quad (19.31)$$

where σ_y is the yield stress and $\bar{\epsilon}_x^p$ denotes the plastic strain rate for a point. The following are often used values of D and q

Mild steel	$D = 40.4 \text{ s}^{-1}$	$q = 5$
Aluminium alloy	$D = 6500 \text{ s}^{-1}$	$q = 4$

Equation (19.31) was obtained from uniaxial stress tests. It is assumed that this equation is still a valid approximation when it is applied to multiaxially loaded beam cross sections.

Equation (19.31) becomes

$$g_2(\dot{\bar{\epsilon}}^p) = N_Y \left[1 + (\dot{\bar{\epsilon}}^p/D)^{1/q} \right] \quad (19.32)$$

where $N_Y = A_x \sigma_y$

Using Eqn (19.32), the strain-rate hardening rate defined in Eqn (19.16) may be given as

$$H'_{sr} = N_Y (\dot{\bar{\epsilon}}^p/D)^{\frac{(1-q)}{q}} / q \quad (19.33)$$

19.3.3 Plastic Displacement and Strain at Nodes

The plastic deformations of the element are concentrated at the node in a mechanism similar to that of the plastic hinge. Referring to Eqn (19.7), the yield condition at the node is expressed as

$$F_i = Y_i(\{\sigma_i - \alpha_i\}) - \sigma_{0i}(\bar{\epsilon}_i^p, \dot{\bar{\epsilon}}_i^p) = 0 \quad (19.34)$$

where subscript “i” denotes values at the node No. i. From Eqn (19.21), the consistency condition for the node i is expressed as

$$dF_i\{\phi_i\}^T\{dx\} - [H'_{sk} + H'_{si} + H'_{sr}/(\theta dt)]_i d\bar{\epsilon}_i^p + a_i = 0 \quad (19.35)$$

where

$$\{\phi_i\} = \{\partial F_i / \partial x\} \quad (19.36)$$

$$a_i = [H'_{sr}/\theta]_i \dot{\bar{\epsilon}}_i^p \quad (19.37)$$

where $\{x\}$ is the nodal force vector.

Applying the plastic flow theory, the increments of plastic nodal displacement of the element, due to plasticity at node i, are estimated as (Ueda and Yao, 1982)

$$\{du_i^p\} = d\lambda_i\{\phi_i\} \quad (19.38)$$

where $d\lambda_i$ is a measure of the magnitude of plastic deformation.

In the following paragraphs, a relationship will be established between $d\bar{\epsilon}_i^p$ and $d\lambda_i$ using a plastic work procedure (Ueda and Fujikubo, 1986; Fujikubo et al., 1991). The increment of the plastic work done at plastic node i is expressed as

$$dw_i^p = \{x\}^T \{du_i^p\} = \{x\}^T \{\phi_i\} d\lambda_i \quad (19.39)$$

The increment of the plastic work done in the actual plastic region around node i is evaluated as

$$dw_i^{p*} = \int_{L_i^p} \{\sigma\}^T \{d\epsilon^p\} ds = \int_{L_i^p} c \{\sigma\}^T \left\{ \frac{\partial f}{\partial \sigma} \right\} d\bar{\epsilon}^p ds \quad (19.40)$$

From Eqn (19.21), the increment of the equivalent plastic strain, at a coordinate s , can be expressed as a function of the value at node i in the form

$$d\bar{\epsilon}^p = g(s) d\bar{\epsilon}_i^p \quad (19.41)$$

where

$$g(s) = \frac{[H'_{sk} + H'_{si} + H'_{sr}/(\theta dt)]_i \{\partial f / \partial \sigma\}^T \{d\sigma\} + (H'_{sr}/\theta) \dot{\bar{\epsilon}}^p}{H'_{sk} + H'_{si} + H'_{sr}/(\theta dt) \{\partial f_i / \partial \sigma_i\}^T \{d\sigma_i\} + (H'_{sr}/\theta)_i \dot{\bar{\epsilon}}_i^p}$$

substituting Eqn (19.41) into Eqn (19.40), Eqn (19.42) is obtained.

$$dw_i^{p*} = d\bar{\epsilon}_i^p \int_{L_i^p} c \{\sigma\}^T \left\{ \frac{\partial f}{\partial \sigma} \right\} g(s) ds \quad (19.42)$$

Equating the plastic work increments dw_i^p in Eqn (19.39) and dw_i^{p*} in Eqn (19.42), Eqn (19.43) is determined to be

$$d\bar{\epsilon}_i^p = h_i d\lambda_i \quad (19.43)$$

where

$$h_i = \{x\}^T \{\phi_i\} \bigg/ \int_{L_i^p} c \{\sigma\}^T \left\{ \frac{\partial f}{\partial \sigma} \right\} g(s) ds \quad (19.44)$$

A simpler alternative approach for determining the strain-hardening rate at a plastic node is to establish relationships between the plastic nodal displacements and the generalized plastic strain vector at the node, in the form of

$$\{d\bar{\epsilon}_i^p\} = \{du_i^p\} / L_{di} = \{\phi_i\} d\lambda_i / L_{di} \quad (19.45)$$

where L_{di} denotes an equivalent length of the plastic region.

The increment of the equivalent plastic strain at the node can be evaluated by substituting Eqn (19.45) into Eqn (19.9) and acquiring Eqn (19.43)

$$h_i = \{\sigma_i - \alpha_i\}^T \{\phi_i\} / (L_{di} \sigma_{0i}) \quad (19.46)$$

Integration along the axial axis of the element becomes unnecessary when Eqn (19.46) is applied to calculate $d\varepsilon_i^p$ instead of Eqn (19.44). This results in an extremely simple numerical procedure. Unfortunately, the actual regions where the plastic flow occurs cause a change in shape and size and may disappear/reappear. Evidently, the equivalent length of the plastic region for each stress component should be different and considered to be a function of time. However, for simplicity, it is important to find a constant value that will provide adequate approximations. Then length L_{di} can simply be approximated as

$$L_{di} = \alpha_D H \quad (19.47)$$

or

$$L_{di} = \alpha_L L \quad (19.48)$$

where α_D and α_L are coefficients, H is the diameter for a circular cross section or a width (or height) for a rectangular cross section, etc. This approach will be used in the case where a structural member is modeled by only one element. Substitution of Eqn (19.43) into Eqn (19.35) gives

$$dF_i = \{\phi_i\}^T \{dx\} - H'_{ni} d\lambda_i + a_i = 0 \quad (19.49)$$

where

$$H'_{ni} = [H'_{sk} + H'_{si} + H'_{sr}/(\theta dt)]_i h_i \quad (19.50)$$

19.3.4 Elastic–Plastic Stiffness Equation for Elements

When both nodes 1 and 2 are plastic, the following matrix equation may be established from Eqn (19.49).

$$[\Phi]^T \{dx\} - [H'] \{d\lambda\} + \{A\} = 0 \quad (19.51)$$

where

$$\begin{aligned} [\Phi] &= [\{\phi_1\} \{\phi_2\}] \\ [H'] &= [H'_{n1} H'_{n2}] (2 \times 2 \text{ diagonal matrix}) \\ \{d\lambda\} &= \{d\lambda_1 \ d\lambda_2\}^T \end{aligned}$$

and

$$\{A\} = \{a_1 \ a_2\}^T$$

From Eqn (19.38), the increments of the plastic nodal displacement $\{du^p\}$ are given as

$$\{du^p\} = [\Phi]\{d\lambda\} \quad (19.52)$$

The increments of the total nodal displacement $\{du\}$ are expressed by the summation of the elastic and plastic components below

$$\{du\} = \{du^e\} + \{du^p\} \quad (19.53)$$

Substitution of Eqns (19.52) and (19.53) into Eqn (19.4) gives

$$[k_E](\{du\} - [\Phi]\{d\lambda\}) = \{dx\} \quad (19.54)$$

Solving Eqns (19.51) and (19.54) with respect to $\{d\lambda\}$

$$\{d\lambda\} = \left([H'] + [\Phi]^T [k_E] [\Phi] \right)^{-1} \left([\Phi]^T [k_E] \{du\} + \{A\} \right) \quad (19.55)$$

and substituting $\{d\lambda\}$ into Eqn (19.54) gives the elastic–plastic stiffness equation

$$[k_p]\{du\} = \{dx\} + \{dx\} \quad (19.56)$$

where

$$[k_p] = [k_E] - [k_E][\Phi] \left([H'] + [\Phi]^T [k_E] [\Phi] \right)^{-1} [\Phi]^T [k_E] \quad (19.57)$$

$$\{dx'\} = [k_E][\Phi] \left([H'] + [\Phi]^T [k_E] [\Phi] \right)^{-1} \{A\} \quad (19.58)$$

If the sign of $\{d\lambda_1\}$ or $\{d\lambda_2\}$ is found to be negative, unloading occurs at the plastic node and the node should then be treated as elastic. It is noted that the effects of large displacements and strain hardening as well as strain-rate hardening have been taken into account in the derived elastic–plastic stiffness equation.

19.4 Transformation Matrix

In this section, a new transformation matrix $[T_t]$ is described, which transfers element displacements that are measured in the global coordinate system XYZ to element displacements measured in the local coordinate xyz, at time t . The transformation matrix is evaluated as

$$[T_t] = [\Delta T][T_t - dt] \quad (19.59)$$

where $[T_t - da]$ is a matrix, which transfers the element displacements to the local coordinate system at time $t - dt$. $[\Delta T]$ is a matrix that transfers the element displacements

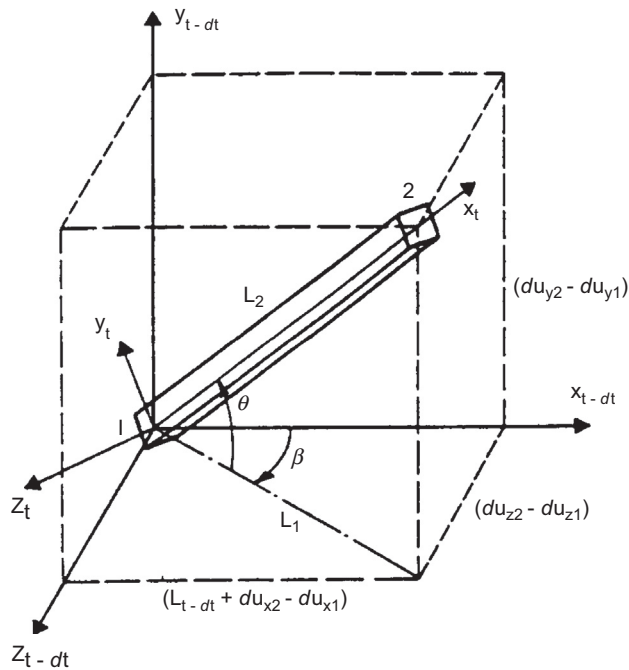


Figure 19.2
Transformation matrix.

that are measured in the local coordinate system, at time $t-dt$, to the local coordinate system at time t (Figure 19.2).

The transformation matrix $[\Delta T]$ is composed of submatrices $[tt]$, which transform the displacement vectors. The submatrix $[tt]$ is evaluated as

$$[tt] = [t_a] + [t_b] \quad (19.60)$$

where

$$[t_a] = \begin{bmatrix} 1 & 0 & 0 \\ 0 & \cos \alpha & \sin \alpha \\ 0 & -\sin \alpha & \cos \alpha \end{bmatrix} \quad (19.61)$$

$$[t_b] = \begin{bmatrix} \cos \beta \cos \theta & \sin \theta & \sin \beta \cos \theta \\ -\cos \beta \sin \theta & \cos \theta & -\sin \beta \sin \theta \\ -\sin \beta & 0 & \cos \beta \end{bmatrix}$$

By considering the increments of nodal displacement from time $t-dt$ to time t , measured in the local coordinate system at time $t-dt$, then

$$\begin{aligned} \sin \beta &= (du_{z2} - du_{z1})/L_1 \\ \cos \beta &= (L_{t-dt} + du_{x2} - du_{x1})/L_1 \\ \sin \theta &= (du_{y2} - du_{y1})/L_2 \\ \cos \theta &= L_1/L_2 \end{aligned} \tag{19.62}$$

where

$$\begin{aligned} L_1 &= \left[(L_{t-dt} + du_{x2} - du_{x1})^2 + (du_{z2} - du_{z1})^2 \right]^{\frac{1}{2}} \\ L_2 &= \left[L_1^2 + (du_{y2} - du_{y1})^2 \right]^{\frac{1}{2}} \end{aligned} \tag{19.63}$$

L_{t-dt} is the distance between nodes 1 and 2 at time $t-dt$. Furthermore, angle α is calculated as

$$\alpha = \frac{1}{2} \left[t_{b11}(d\theta_{x1} + d\theta_{x2}) + t_{b12}(d\theta_{y1} + d\theta_{y2}) + t_{b13}(d\theta_{z1} + d\theta_{z2}) \right] \tag{19.64}$$

19.5 Appendix A: Stress-Based Plasticity Constitutive Equations

19.5.1 General

This appendix is written based on a Japanese book authored by [Yagawa and Miyazaki \(1985\)](#). When the formulation presented in this chapter was made, the author had been inspired by this book and that by [Yamada et al. \(1968\)](#). The objective of this appendix is to describe the basics of plasticity that may be useful in understanding the mathematical formulations presented in the main body of this chapter.

In the uniaxial tensile test, when the stress is small, the material behavior is elastic. The proportional constant E is the Young's modulus. If the load is released, the stress will become 0, and the material will return to its original condition. On the other hand, when the stress exceeds a limit, permanent deformation may occur. The permanent deformation is called plastic deformation.

[Figure A.1](#) shows a typical stress–strain diagram of metallic materials. The material is in the elastic behavior range until it reaches the yield point A , and the stress σ and strain ε are in proportion. This proportional relationship is called Hook's law. After going over point A , the gradient of the stress–strain curve decreases, and the gradient H'_0 is called the tangent modulus. If unloading occurs at point B , the stress will decrease along with $B \rightarrow C$,

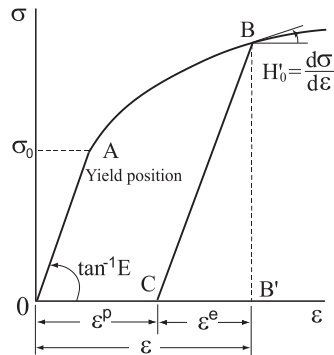


Figure A.1
Stress and strain diagram.

which is parallel to OA . The residual strain is called plastic strain, ε^p . On the other hand, the recovered strain corresponding to CB' is called elastic strain, ε^e . The total strain is the sum of the elastic strain and the plastic strain.

$$\varepsilon = \varepsilon^e + \varepsilon^p \quad (\text{A.1})$$

Figure A.2 shows the relationship between stress and plastic strain. The gradient H' in this stress–plastic strain curve is called the strain-hardening rate. Referring to Figures A.1 and A.2, the following relationship is obtained.

$$d\varepsilon = \frac{d\sigma}{H'_0} = d\varepsilon^e + d\varepsilon^p = \frac{d\sigma}{E} + \frac{d\sigma}{H'} \quad (\text{A.2})$$

where H'_0 and H' can be expressed as

$$H' = \frac{EH'_0}{E - H'_0}, \quad H'_0 = \frac{EH'}{E + H'} \quad (\text{A.3})$$

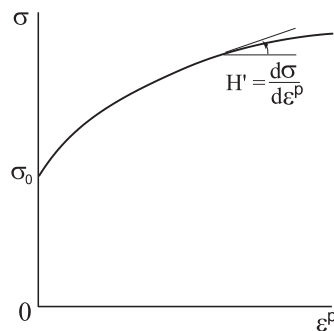


Figure A.2
Curve of strain hardening.

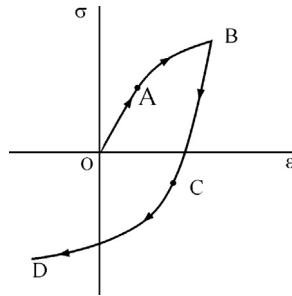


Figure A.3
Bauschinger's effect.

As shown in [Figure A.3](#), when the stress is beyond the yield point of material, plastic strain occurs; if the load is released after point *B*, and a compressive load is applied, the relationship between stress and strain will follow curve *BCD*, and the material yields at a compressive stress (point *C*) that is lower than its initial yield stress. This phenomenon is called Bauschinger's effect.

Although there is a one-to-one correspondence between stress and strain in the elastic region, as described by Hook's law, this correlation does not exist in the plastic region. This means that if the strain is above a certain level, it is dependent on the deformation history along with the stress. For an elasto-plastic solid, the incremental theory (or flow theory) is widely used to account for the deformation history. However, to simplify the calculation, the total strain theory (or deformation theory) is also used when the finite element method is not applied.

19.5.2 Relationship between Stress and Strain in the Elastic Region

The relationship between stress and strain in the elastic region can be repressed in the matrix form, as

$$\left. \begin{aligned} \{\sigma\} &= [D^e]\{\varepsilon\} \quad \text{or} \quad \{\varepsilon\} = [C^e]\{\sigma\} \\ [D^e] &= [C^e]^{-1} \end{aligned} \right\} \quad (\text{A.4})$$

where

$$\{\sigma\} = \begin{Bmatrix} \sigma_x \\ \sigma_y \\ \sigma_z \\ \tau_{xy} \\ \tau_{yz} \\ \tau_{zx} \end{Bmatrix}, \quad \{\varepsilon\} = \begin{Bmatrix} \varepsilon_x \\ \varepsilon_y \\ \varepsilon_z \\ \gamma_{xy} \\ \gamma_{yz} \\ \gamma_{zx} \end{Bmatrix} \quad (\text{A.5})$$

For an isotropic material, $[D^e]$, $[C^e]$ are formulated with the Young's modulus, E , and Poisson's ratio in the form of

$$[D^e] = \frac{E(1-\nu)}{(1+\nu)(1-2\nu)} \begin{bmatrix} 1 & \frac{\nu}{1-\nu} & \frac{\nu}{1-\nu} & 0 & 0 & 0 \\ & 1 & \frac{\nu}{1-\nu} & 0 & 0 & 0 \\ & & 1 & 0 & 0 & 0 \\ & & & \frac{1-2\nu}{2(1-\nu)} & 0 & 0 \\ & & & & \frac{1-2\nu}{2(1-\nu)} & 0 \\ & & & & & \frac{1-2\nu}{2(1-\nu)} \end{bmatrix} \quad (\text{A.6})$$

$$[C^e] = \frac{1}{E} \begin{bmatrix} 1 & -\nu & -\nu & 0 & 0 & 0 \\ & 1 & -\nu & 0 & 0 & 0 \\ & & 1 & 0 & 0 & 0 \\ & & & 2(1+\nu) & 0 & 0 \\ & & & & 2(1+\nu) & 0 \\ & & & & & 2(1+\nu) \end{bmatrix} \quad (\text{A.7})$$

In the elastic region, the relationship between the stress increment and the strain increment can be written based on Eqn (A.4).

$$\{\Delta\sigma\} = [D^e]\{\Delta\varepsilon\} \quad \text{or} \quad \{\Delta\varepsilon\} = [C^e]\{\Delta\sigma\} \quad (\text{A.8})$$

where Δ is an increment.

19.5.3 Yield Criterion

The stress condition for the initiation of plastic deformation is called yield criterion and is generally written as a yield function f .

$$f(J_1, J_2, J_3) = 0 \quad (\text{A.9})$$

where J_1, J_2, J_3 are the invariants and are expressed as

$$\left. \begin{aligned} J_1 &= \sigma_x + \sigma_y + \sigma_z \\ J_2 &= -(\sigma_x\sigma_y + \sigma_y\sigma_z + \sigma_z\sigma_x) + \tau_{xy}^2 + \tau_{yz}^2 + \tau_{zx}^2 \\ J_3 &= \sigma_x\sigma_y\sigma_z - \sigma_x\tau_{yz}^2 - \sigma_y\tau_{zx}^2 - \sigma_z\tau_{xy}^2 + 2\tau_{yz}\tau_{zx}\tau_{xy} \end{aligned} \right\} \quad (\text{A.10})$$

The geometrical surface for the yield criterion in a stress space is called the yield surface. Because the first approximation of the yield function has no relation with the hydrostatic pressure for the metallic materials, the yield criterion can be expressed as

$$f(J'_2, J'_3) = 0, \quad J'_1 = 0 \tag{A.11}$$

where J'_1, J'_2, J'_3 are called the invariants of the deviatoric stress, which are shown below.

$$\left. \begin{aligned} \sigma'_x &= \sigma_x - \sigma_m, & \sigma'_y &= \sigma_y - \sigma_m, & \sigma'_z &= \sigma_z - \sigma_m, \\ \sigma_m &= \frac{\sigma_x + \sigma_y + \sigma_z}{3}, \\ \tau'_{xy} &= \tau_{xy}, & \tau'_{yz} &= \tau_{yz}, & \tau'_{zx} &= \tau_{zx} \end{aligned} \right\} \tag{A.12}$$

The most widely used yield criterion for metallic materials is Mises's yield criterion, in which function f in Eqn (A.11) is only expressed as a function of the secondary invariant of deviatoric stress, J'_2 .

$$f = \sqrt{3J'_2} - \sigma_0 \tag{A.13}$$

where σ_0 is the yield stress for uniaxial loading. Here, J'_2 is

$$\begin{aligned} J'_2 &= -\left(\sigma'_x\sigma'_y + \sigma'_y\sigma'_z + \sigma'_z\sigma'_x\right) + \tau'^2_{xy} + \tau'^2_{yz} + \tau'^2_{zx} \\ &= \frac{1}{2}\left[\sigma'^2_x + \sigma'^2_y + \sigma'^2_z + 2\left(\tau'^2_{xy} + \tau'^2_{yz} + \tau'^2_{zx}\right)\right]^{\frac{1}{2}} \\ &= \frac{1}{6}\left[(\sigma_x - \sigma_y)^2 + (\sigma_y - \sigma_z)^2 + (\sigma_z - \sigma_x)^2 + 6\left(\tau^2_{xy} + \tau^2_{yz} + \tau^2_{zx}\right)\right] \end{aligned} \tag{A.14}$$

If the equivalent stress $\bar{\sigma}$ is defined as

$$\begin{aligned} \bar{\sigma} &= \sqrt{3J'_2} = \sqrt{\frac{3}{2}\left[\sigma'^2_x + \sigma'^2_y + \sigma'^2_z + 2\left(\tau'^2_{xy} + \tau'^2_{yz} + \tau'^2_{zx}\right)\right]^{\frac{1}{2}}} \\ &= \frac{1}{\sqrt{2}}\left[(\sigma_x - \sigma_y)^2 + (\sigma_y - \sigma_z)^2 + (\sigma_z - \sigma_x)^2 + 6\left(\tau^2_{xy} + \tau^2_{yz} + \tau^2_{zx}\right)\right]^{\frac{1}{2}} \end{aligned} \tag{A.15}$$

the yield criterion becomes

$$\bar{\sigma} = \sigma_0 \tag{A.16}$$

The multiaxial stress condition can then be corresponded to the uniaxial stress condition.

When the stress is larger than the yield criterion of the material, hardening and plastic deformation occur, and the yield function $f = 0$ must be satisfied. However, if $f < 0$, then unloading will occur and the material will be in the elastic region.

19.5.4 Plastic Strain Increment

When plastic deformation occurs, the shape of yield surface may change following the hardening rule. Here, the isotropic hardening rule and the kinematic hardening rule are described below.

Isotropic Hardening Rule

As shown in Figure A.4, in the hardening process, the size of the yield surface may increase but there is no change in the position and shape of the yield surface. Figure A.5 shows the relationship between uniaxial stress and strain. After loading along the curve OYA , and unloading to point B , continue in the reverse direction to point C , $\overline{AB} = \overline{BC}$, $\overline{BC} > \overline{OY}$. If the strain hardening is considered, the yield function in Eqn (A.13) becomes

$$f = \sqrt{3J'_2} - \sigma_0 = \bar{\sigma} - \sigma_0(\bar{\epsilon}^P) \quad (\text{A.17})$$

where $\bar{\epsilon}^P$ is the equivalent plastic strain, and may be expressed as

$$\bar{\epsilon}^P = \int d\bar{\epsilon}^P \quad (\text{A.18})$$

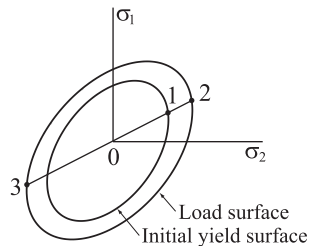


Figure A.4
Isotropic hardening rule.

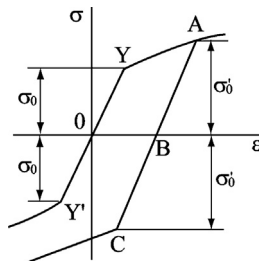


Figure A.5
Uniaxial stress and strain relation based on the isotropic hardening rule.

$d\bar{\epsilon}^p$ in the above equation may be estimated as

$$\begin{aligned}
 d\bar{\epsilon}^p &= \Delta\bar{\epsilon}^p = \sqrt{\frac{2}{3}} \left[\Delta\epsilon_x^{p2} + \Delta\epsilon_y^{p2} + \Delta\epsilon_z^{p2} + \frac{1}{2} (\Delta\gamma_{xy}^{p2} + \Delta\gamma_{yz}^{p2} + \Delta\gamma_{zx}^{p2}) \right]^{\frac{1}{2}} \\
 &= \frac{\sqrt{2}}{3} \left[(\Delta\epsilon_x^p - \Delta\epsilon_y^p)^2 + (\Delta\epsilon_y^p - \Delta\epsilon_z^p)^2 + (\Delta\epsilon_z^p - \Delta\epsilon_x^p)^2 \right. \\
 &\quad \left. + \frac{3}{2} (\Delta\gamma_{xy}^{p2} + \Delta\gamma_{yz}^{p2} + \Delta\gamma_{zx}^{p2}) \right]^{1/2}
 \end{aligned} \tag{A.19}$$

If the plastic strain increment in the uniaxial loading in the x direction is defined as $\Delta\epsilon_x^p$, and the condition below for incompressibility of plastic strain is used,

$$\Delta\epsilon_x^p + \Delta\epsilon_y^p + \Delta\epsilon_z^p = 0 \tag{A.20}$$

the following equation can be obtained.

$$\Delta\epsilon_y^p = \Delta\epsilon_z^p = -\frac{\Delta\epsilon_x^p}{2}, \quad \Delta\gamma_{xy}^p = \Delta\gamma_{yz}^p = \Delta\gamma_{zx}^p = 0 \tag{A.21}$$

Substituting Eqn (A.21) into Eqn (A.19)

$$\Delta\bar{\epsilon}^p = \Delta\epsilon_x^p \tag{A.22}$$

This means that the increment of the equivalent plastic strain is a conversion of the plastic strain increment under multiaxial stress conditions into that of the uniaxial stress condition.

The plastic strain increment may be obtained from the flow rule. If the plastic potential is defined as yield function f , the plastic strain increment is expressed as

$$\{\Delta\epsilon^p\} = \Delta\lambda \left\{ \frac{\partial f}{\partial \sigma} \right\} = \Delta\lambda \frac{3}{2\bar{\sigma}} \{\sigma'\} \tag{A.23}$$

where yield function f is expressed in Eqn (A.17). $\Delta\lambda (:>0)$ is an undetermined scalar constant, and $\{\sigma'\}$ is a vector of the deviatoric stress, as seen below,

$$\{\sigma'\} = \left\{ \begin{array}{c} \sigma'_x \\ \sigma'_y \\ \sigma'_z \\ 2\tau_{xy} \\ 2\tau_{yz} \\ 2\tau_{zx} \end{array} \right\} \tag{A.24}$$

Equation (A.24) means that the plastic strain increment is in the perpendicular direction of the yield surface, $f = 0$, as shown in Figure A.6.

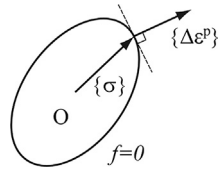


Figure A.6
Flow rule.

Kinematic Hardening Rule

In the kinematic hardening rule, although the size of the yield surface does not change due to the hardening process, the position of its center moves, as shown in [Figure A.7](#). The relationship between stress and strain for a uniaxial stress case is shown in [Figure A.8](#). From the relationship of $\overline{YY'} = \overline{AC}$, $\overline{BC} < \overline{OY}$, Bauschinger's effect may be qualitatively expressed in the following figure.

The yield function for the kinematic hardening rule is defined as

$$f = f(\{\sigma\} - \{\alpha_0\}) \quad (\text{A.25})$$

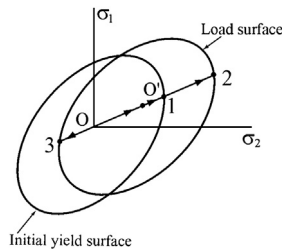


Figure A.7
Kinematic hardening rule.

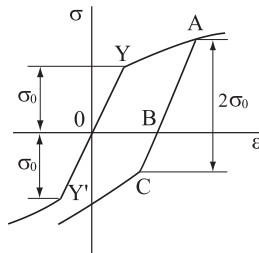


Figure A.8
Uniaxial stress and strain relation based on the kinematic hardening rule.

where $\{\alpha_0\}$ is the center of the yield surface and may be expressed as

$$\{\alpha_0\} = \begin{Bmatrix} \alpha_x \\ \alpha_y \\ \alpha_z \\ \alpha_{xy} \\ \alpha_{yz} \\ \alpha_{zx} \end{Bmatrix} \quad (\text{A.26})$$

There are two ways to determine $\{\alpha_0\}$: the Prager kinematic hardening rule and the Ziegler kinematic hardening rule.

$$\{\Delta\alpha_0\} = C\{\Delta\varepsilon^p\} \quad : \text{Prager} \quad (\text{A.27})$$

$$\{\Delta\alpha_0\} = \Delta\mu(\{\sigma\} - \{\alpha_0\}) \quad : \text{Ziegler} \quad (\text{A.28})$$

As shown in [Figure A.9](#), the Prager kinematic hardening rule moves in the direction perpendicular to the yield surface; the Ziegler kinematic hardening rule moves along the direction from the center of yield surface $\{\alpha_0\}$ to the stress point $\{\sigma\}$.

From [Eqn \(A.25\)](#), the yield condition becomes

$$f(\{\sigma_\alpha\}) = \bar{\sigma}_\alpha - \sigma_0 = 0 \quad (\text{A.29})$$

where

$$\{\sigma_\alpha\} = \{\sigma\} - \{\alpha_0\} \quad (\text{A.30})$$

$\bar{\sigma}_\alpha$ is the equivalent stress, which considers the movement of yield surface, and is expressed as

$$\begin{aligned} \bar{\sigma}_\alpha = \frac{1}{\sqrt{2}} & \left[\{(\sigma_x - \alpha_x) - (\sigma_y - \alpha_y)\}^2 + \{(\sigma_y - \alpha_y) - (\sigma_z - \alpha_z)\}^2 \right. \\ & + \{(\sigma_z - \alpha_z) - (\sigma_x - \alpha_x)\}^2 \\ & \left. + 6\{(\tau_{xy} - \alpha_{xy})^2 + (\tau_{yz} - \alpha_{yz})^2 + (\tau_{zx} - \alpha_{zx})^2\} \right]^{1/2} \end{aligned} \quad (\text{A.31})$$

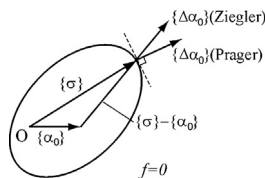


Figure A.9

Movement toward the direction of center for yield surface.

By setting the yield function f as the plastic potential, the plastic strain increment may be expressed as

$$\{\Delta \varepsilon^P\} = \Delta \lambda \left\{ \frac{\partial f}{\partial \sigma} \right\} = \Delta \lambda \frac{3}{2\bar{\sigma}_\alpha} \{\sigma'_\alpha\} \quad (\text{A.32})$$

where

$$\{\sigma'_\alpha\} = \{\sigma'\} - \{\alpha'_0\} \quad (\text{A.33})$$

19.5.5 Stress Increment—Strain Increment Relation in the Plastic Region

The total strain increment is the sum of the elastic strain increment and the plastic strain increment,

$$\{\Delta \varepsilon\} = \{\Delta \varepsilon^e\} + \{\Delta \varepsilon^P\} \quad (\text{A.34})$$

On the other hand, the relationship between the stress increment and the elastic strain increment may be expressed as

$$\{\Delta \sigma\} = [D^e] \{\Delta \varepsilon^e\} \quad (\text{A.35})$$

Substituting this equation into Eqn (A.34), the following equation is obtained.

$$\{\Delta \sigma\} = [D^e] (\{\Delta \varepsilon\} - \{\Delta \varepsilon^P\}) \quad (\text{A.36})$$

If the associated flow rule in accord with the yield function and plastic potential are used, the plastic strain increment $\{\Delta \varepsilon^P\}$ can be expressed as

$$\{\Delta \varepsilon^P\} = \Delta \lambda \left\{ \frac{\partial f}{\partial \sigma} \right\} \quad (\text{A.37})$$

In general, the yield function f is a function of stress and plastic strain, and may be written as

$$f = f(\{\sigma\}, \{\varepsilon^P\}) \quad (\text{A.38})$$

when plastic deformation occurs, the following equation can be obtained.

$$\Delta f = \left\{ \frac{\partial f}{\partial \sigma} \right\}^T \{\Delta \sigma\} + \left\{ \frac{\partial f}{\partial \varepsilon^P} \right\}^T \{\Delta \varepsilon^P\} = 0 \quad (\text{A.39})$$

Substituting Eqn (A.37) into Eqns (A.36) and (A.39), then

$$\{\Delta \sigma\} = [D^e] \left(\{\Delta \varepsilon\} - \Delta \lambda \left\{ \frac{\partial f}{\partial \sigma} \right\} \right) \quad (\text{A.40})$$

$$\left\{ \frac{\partial f}{\partial \sigma} \right\}^T \{\Delta \sigma\} + \left\{ \frac{\partial f}{\partial \varepsilon^P} \right\}^T \left\{ \frac{\partial f}{\partial \sigma} \right\} \Delta \lambda = 0 \quad (\text{A.41})$$

Eliminating $\{\Delta\sigma\}$ from Eqns (A.40) and (A.41), $\Delta\lambda$ is obtained from the following equation,

$$\Delta\lambda = \frac{\left\{\frac{\partial f}{\partial\sigma}\right\}^T [D^e]\{\Delta\varepsilon\}}{-\left\{\frac{\partial f}{\partial\varepsilon^p}\right\}^T \left\{\frac{\partial f}{\partial\sigma}\right\} + \left\{\frac{\partial f}{\partial\sigma}\right\}^T [D^e]\left\{\frac{\partial f}{\partial\sigma}\right\}} \quad (\text{A.42})$$

Substituting Eqn (A.42) into Eqn (A.40), then

$$\begin{aligned} \{\Delta\sigma\} &= \left([D^e] - \frac{[D^e]\left\{\frac{\partial f}{\partial\sigma}\right\}\left\{\frac{\partial f}{\partial\sigma}\right\}^T [D^e]}{-\left\{\frac{\partial f}{\partial\varepsilon^p}\right\}^T \left\{\frac{\partial f}{\partial\sigma}\right\} + \left\{\frac{\partial f}{\partial\sigma}\right\}^T [D^e]\left\{\frac{\partial f}{\partial\sigma}\right\}} \right) \{\Delta\varepsilon\} \\ &= ([D^e] + [D^p])\{\Delta\varepsilon\} \end{aligned} \quad (\text{A.43})$$

here $[D^p]$ is expressed as

$$[D^p] = -\frac{[D^e]\left\{\frac{\partial f}{\partial\sigma}\right\}\left\{\frac{\partial f}{\partial\sigma}\right\}^T [D^e]}{-\left\{\frac{\partial f}{\partial\varepsilon^p}\right\}^T \left\{\frac{\partial f}{\partial\sigma}\right\} + \left\{\frac{\partial f}{\partial\sigma}\right\}^T [D^e]\left\{\frac{\partial f}{\partial\sigma}\right\}} \quad (\text{A.44})$$

and this must be considered when the material is in the plastic condition.

Substituting Eqn (A.42) into Eqn (A.37), the plastic strain increment is expressed as

$$\{\Delta\varepsilon^p\} = \frac{\left\{\frac{\partial f}{\partial\sigma}\right\}\left\{\frac{\partial f}{\partial\sigma}\right\}^T [D^e]\{\Delta\varepsilon\}}{-\left\{\frac{\partial f}{\partial\varepsilon^p}\right\}^T \left\{\frac{\partial f}{\partial\sigma}\right\} + \left\{\frac{\partial f}{\partial\sigma}\right\}^T [D^e]\left\{\frac{\partial f}{\partial\sigma}\right\}} \quad (\text{A.45})$$

In the process of plastic deformation, $\Delta\lambda$ in Eqn (A.37) must have a positive value. Therefore, by checking the sign of $\Delta\lambda$ in Eqn (A.42), the unloading condition can be detected.

19.6 Appendix B: Deformation Matrix

The deformation matrix $[k_D]$ is symmetric; the nonzero terms are given as follows:

$$k_D(1,2) = k_D(7,8) = -k_D(1,8) = -k_D(2,7) = -\rho_z^2(EA/L)(\theta_{z1} + \theta_{z2})/10 \quad (\text{B.1})$$

$$k_D(1,3) = k_D(7,9) = -k_D(1,9) = -k_D(3,7) = \rho_y^2(EA/L)(\theta_{y1} + \theta_{y2})/10 \quad (\text{B.2})$$

$$k_D(1,5) = -k_D(5,7) = -\alpha_y + \rho_y^2 EA(-4\theta_{z1} + \theta_{z2})/30 \quad (\text{B.3})$$

$$k_D(1, 6) = -k_D(6, 7) = -\alpha_z + \rho_z^2 EA(-4\theta_{z1} + \theta_{z2})/30 \quad (\text{B.4})$$

$$k_D(1, 11) = -k_D(7, 11) = \alpha_y + \rho_y^2 EA(\theta_{y1} - 4\theta_{y2})/30 \quad (\text{B.5})$$

$$k_D(1, 12) = -k_D(7, 12) = -\alpha_z + \rho_z^2 EA(\theta_{z1} - 4\theta_{z2})/30 \quad (\text{B.6})$$

where

$$\eta_y = EI_y/(GA_z L^2) \quad \eta_z = EI_z/(GA_y L^2) \quad (\text{B.7})$$

$$\rho_y = 1/\left(1 + 12\eta_y\right) \quad \rho_z = 1/(1 + 12\eta_z) \quad (\text{B.8})$$

$$\alpha_y = 2\rho_y^2 EA\eta_y(1 + 6\eta_y)(\theta_{y1} - \theta_{y2}) \quad (\text{B.9})$$

$$\alpha_z = 2\rho_z^2 EA\eta_z(1 + 6\eta_z)(\theta_{z1} - \theta_{z2}) \quad (\text{B.10})$$

References

- Archer, J.S., 1965. Consistent matrix formulations for structural analysis using finite element techniques. *AIAA Journal* 3, 1910–1918.
- Bai, Y., Pedersen, P.T., 1991a. Earthquake response of offshore structures. In: Proc. of the 10th Int. Conference on Offshore Mechanics and Arctic Engineering, OMAE '91, Stavanger.
- Bai, Y., Pedersen, P.T., 1991b. Collision response of offshore structures and bridges. In: International Symposium on Marine Structures, ISMS '91, Shanghai.
- Bathe, K.J., 1986. *Finite Element Methods*. Springer.
- Chakrabarty, J., 1987. *Theory of Plasticity*. McGraw-Hill Book Company.
- Chen, W.F., Han, D.J., 1987. *Plasticity for Structural Engineers*. Springer.
- Fujikubo, M., Bai, Y., Ueda, Y., 1991. Dynamic elastic-plastic analysis of offshore framed structures by plastic node method considering strain-hardening effects. *International Journal of Offshore and Polar Engineering Conference* 1 (3), 220–227.
- Jones, N., 1989. *Structural Impacts*. Cambridge University Press.
- Mosquera, J.M., Symonds, P.S., Kolsky, H., 1985a. On elastic-plastic rigid-plastic dynamic response with strain rate sensitivity. *International Journal of Mechanical Sciences* 27, 741–749.
- Mosquera, J.M., Symonds, P.S., Kolsky, H., 1985b. Impact tests on frames and elastic-plastic solutions. *Journal of Engineering Mechanics ASCE* 111 (11), 1380–1401.
- Nedergaard, H., Pedersen, P.T., 1986. Analysis procedure for space frame with material and geometrical nonlinearities. In: Bergan, B., Wunderlich (Eds.), *Europe-US Symposium—Finite Element Methods for Nonlinear Problems*. Springer, pp. 211–230.
- Przemieniecki, J.S., 1968. *Theory of Matrix Structural Analysis*. McGraw-Hill, Inc.
- Save, M.A., Massonnet, C.E., 1972. *Plastic Analysis and Design of Plates, Shells and Disks*. North-Holland Publishing Company.
- Symonds, P.S., Yu, T.X., 1985. Counter-intuitive behavior in a problem of elastic-plastic beam dynamics. *Journal of Applied Mechanics* 52, 517–522.
- Ueda, Y., Fujikubo, M., 1986. Plastic collocation method considering strain hardening effects. *Journal of the Society of Naval Architects of Japan* 160, 306–317 (in Japanese).
- Ueda, Y., Yao, T., 1982. The plastic node method: a new method of plastic analysis. *Computer Methods in Applied Mechanics and Engineering* 34, 1089–1104.

- Yamada, Y., Yoshimura, N., Sakurai, T., 1968. Plastic stress-strain matrix and its application for the solution of elastic-plastic problems by the finite element method. *International Journal of Mechanical Sciences* 10, 343–354.
- Yagawa, G., Miyazaki, N., 1985. *Heat Induced Stress, Creep and Heat Transfer Analysis Based on the Finite Element Analysis*. Science Publisher (in Japanese).
- Yoshimura, S., Chen, K.L., Atluri, S.N., 1987. A study of two alternate tangent modulus formulations and attendant implicit algorithms for creep as well as high-strain-rate plasticity. *International Journal of Plasticity* 3, 391–413.
- Zienkiewicz, O.C., 1977. *The Finite Element Method*. McGraw-Hill Book Company.

Collapse Analysis of Ship Hulls

20.1 Introduction

In carrying out the limit-state design of ship hulls, it is necessary to estimate the ultimate longitudinal strength of hull girders. Furthermore, in order to estimate oil spills due to tanker collisions and grounding, an investigation of the global dynamic behavior, as well as the local plastic response of the individual ship hulls, is required.

The collapse strength of the ship hull is governed by buckling, yielding, tension-tearing rupture, and brittle failure of the materials. Moreover, the strength against each failure mode is influenced by initial deformations, residual stresses, corrosion damages, and fatigue cracks. The complexity of these problems requires that the collapse response of ship hulls be investigated by means of numerical procedures such as finite element methods (FEM). However, traditional FEM requires a considerable amount of computer CPU and manpower to prepare input data and to interpret output data. Consequently, their applications to hull strength and collision problems are limited. Furthermore, the accuracy of these FEM methods is not always guaranteed (Valsgård and Steen, 1991).

Since 1980, several mathematical models have been applied to longitudinal strength analysis for ship hulls. First, Caldwell (1965) introduced a plastic design method for ships. He estimated the longitudinal strength of a ship hull based on the full plastic moment of a cross section. The effect of buckling is accounted for by reducing the load-carrying capacity of compressed members. Mansour and Thayamballi (1980) considered torsional buckling of stiffeners in their analysis.

Caldwell's method was further modified by Smith (1977), who proposed that the progressive collapse of stiffened plates due to buckling and yielding can be included as stress–strain relationships of fibers of the hull cross section, while also considering postbuckling behavior. In the Smith method, the hull section is discretized into stiffened panels and corner elements. The prediction of load–shortening behavior of stiffened panels up to the post collapse region is very important. Several algorithms for the modified Smith method have been applied based on different formulas for plating effective widths and beam-columns.

The above-noted methods are simple and accurate for prismatic ship hulls subjected to pure bending. However, they are less accurate when other sectional forces and lateral

pressure are present, because plane sections of hull girders are assumed to remain plane within the model.

Chen et al. (1983) presented a general finite element approach for the collapse analysis of ship hulls. Their approach is applicable to any type of loading and any type of structure, but it is costly with respect to both computer CPU and manpower. Ueda et al. (1986) presented a finite element procedure based on the idealized structural unit method (ISUM), which has been used for the ultimate strength analysis of ship hulls by Paik (1991). This method leads to a considerable reduction in the size of the mathematical model. Furthermore, Valsgård and Pettersen (1982) and Valsgård and Steen (1991) developed a nonlinear superelement procedure, which can also model a complicated structure using only a few elements. So far the ISUM method has not been applied to dynamic response analysis because geometrical nonlinearities have been accounted for using empirical equations. It is difficult to derive empirical equations for dynamic geometrical nonlinear analysis.

With regard to collision damages to ship hulls, there is increasing international concern for oil pollution from tankers due to different degrees of collision damage. Very little research has been done on minor ship collisions, as opposed to the extensive investigations in the 1970s, which related to major collisions involving nuclear vessels. McDermott et al. (1974) and Kinkead (1980) presented simplified methods for analyzing local deformations of a ship that was struck in any minor collision. Van Mater et al. (1979) reviewed low-energy ship collision damage theories and design methodologies. Ito et al. (1984) conducted systematic large-scale static tests and presented an excellent simplified method, which was used to analyze the strength of double-hulled structures in collisions.

The purpose of this chapter is to develop a procedure in order to enable the calculation of the ultimate hull girder strength, which will be as accurate as Smith's method (1977) is for pure bending. It is based on an FEM approach, and the procedure may save just as much manpower and computer CPU as the ISUM and the superelement approach. Combining the plastic node method (PNM) with the general FEM approach for geometrically nonlinear problems, the present PNM approach may be applied to dynamic geometrical and material nonlinear analysis that is useful for both ultimate strength and impact response analysis.

Firstly, this chapter presents both an accurate and an efficient finite element procedure for the static and dynamic collapse analyses of ship hulls. This procedure accounts for geometric and material nonlinearities by combining large elastic displacement analysis theories with a plastic hinge model. A set of finite elements such as the beam-column, stiffened plate, and shear panel is developed. Second, mathematical equations for the estimation of the ultimate moment and the moment's interaction are then presented and discussed. Third, the Smith method for hull girder analysis is modified to account for the effect of corrosion defects and fatigue cracks. These equations and analysis methods are

then compared through the ultimate strength analysis of a couple of ship hull girders. Finally, practical applications to the ultimate longitudinal strength analysis of ship hulls and response analysis of tankers involved in collisions are also demonstrated.

This chapter is based on the work of Bai et al. (1993) and Sun and Bai (2001).

20.2 Hull Structural Analysis Based on the PNM

The finite element formulation for the collapse analysis of ship hulls is described in the following sections. The analysis is based on a standard beam-column analysis. This involves formulations for the collapse of plates and stiffened plates, shear panel elements, and nonlinear spring elements.

20.2.1 Beam-Column Element

Figure 20.1 shows a three-dimensional beam-column element. It is a prismatic Timoshenko beam, which has an arbitrary cross-sectional shape. An updated Lagrangian approach has been adopted for large displacement analyses. Arbitrarily large rotations but small strains are assumed. Using the virtual work principle, the following is obtained (Bai and Pedersen, 1991)

$$[k_E]\{du^e\} = \{dx\} \quad (20.1)$$

where

$$[k_E] = [k_L] + [k_G] + [k_D] \quad (20.2)$$

and $\{d_u^e\} \{dx\}$ are the increments of the elastic nodal displacements and nodal forces. The elastic stiffness matrix $[k_E]$ is composed of a linear stiffness matrix $[k_L]$, a geometric

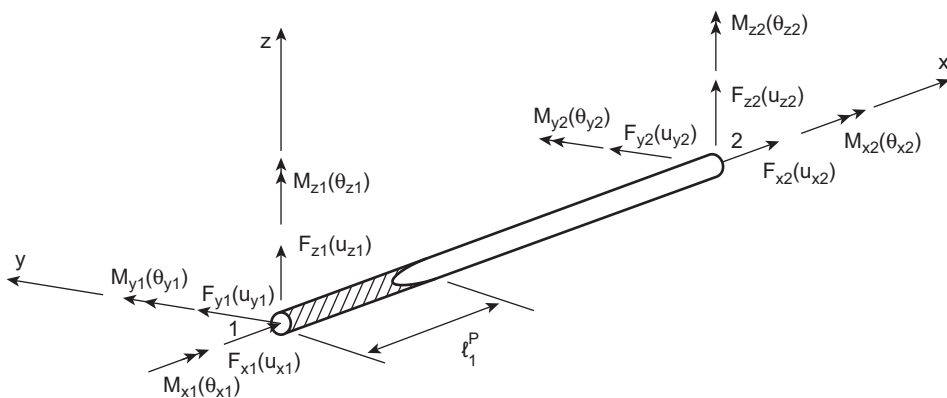


Figure 20.1
Beam-column element l_1^P and plastic region length near node 1.

stiffness matrix $[K_G]$, and a deformation stiffness matrix $[K_D]$. The deformation stiffness matrix $[K_D]$ makes it possible to model a beam-column member using a minimum number of elements, as it accounts for the coupling between axial and lateral deformations.

The elastic–plastic stiffness matrix $[K_P]$ is obtained by applying the PNM (Ueda and Yao, 1982).

$$[k_P]\{du\} = \{dx\} \quad (20.3)$$

where

$$[k_P] = [k_E] - [k_E][\Phi] \left([\Phi]^T [k_E] [\Phi] \right)^{-1} [\Phi]^T [k_E] \quad (20.4)$$

$$[\Phi] = \begin{bmatrix} \{\Phi_1\} & \{0\} \\ \{0\} & \{\Phi_2\} \end{bmatrix} \quad (20.5)$$

and $\{du\}$ denotes the increment of nodal displacements

$$\{\Phi_i\} = \begin{cases} \{0\} & \text{for elastic node} \\ \{\partial \Gamma_i / \partial x_i\} & \text{for plastic node} \end{cases} \quad (i = 1, 2) \quad (20.6)$$

where Γ_i is a fully plastic yield function and $\{x_i\}$ denotes the nodal forces at node “i.”

In order to apply the fracture mechanics criteria, the increment of plastic strain $\{d\epsilon^P\}$ at every node is evaluated as

$$\{d\epsilon^P\} = \frac{1}{l_d} \{du_P\} \quad (20.7)$$

where l_d is the equivalent length of the plastic region. The value of l_d is evaluated to be half the partial yielded region l_p , as shown in Figure 20.1.

Before the local stiffness matrix is added to the global stiffness matrix, several transformations are necessary. It may be convenient that the local axes do not coincide with the neutral axes. Furthermore, the neutral axis moves when the effective width of the plating changes during loading. Finally, the shear center may differ from the neutral axis of bending. A transformation matrix $[S]$ that accounts for this can be found in standard textbooks (Pedersen and Jensen, 1983). This matrix transforms the stiffness matrix into

$$[k^*] = [S]^T [k_P] [S] \quad (20.8)$$

where $[k_P]$ is the local stiffness matrix with respect to the neutral axes, and $[k^*]$ is the local stiffness matrix with respect to the nodal axis. This matrix is transformed to obtain the global coordinate

$$[k_{\text{glob}}] = [T]^T [k^*] [T] = [T]^T [S]^T [k_P] [S] [T] \quad (20.9)$$

where $[k_{\text{glob}}]$ is the stiffness matrix in global coordinates

$$[S] = \begin{bmatrix} [S_1] & [0] \\ [0] & [S_2] \end{bmatrix} \quad (20.10)$$

and

$$[S_i] = \begin{bmatrix} 1 & 0 & 0 & 0 & E_{zi} & -E_{yi} \\ 0 & 1 & 0 & -e_{zi} & 0 & E_{xi} \\ 0 & 0 & 1 & e_{yi} & E_{xi} & 0 \\ 0 & 0 & 0 & 1 & 0 & 0 \\ 0 & 0 & 0 & 0 & 1 & 0 \\ 0 & 0 & 0 & 0 & 0 & 1 \end{bmatrix} \quad (20.11)$$

where (e_{yi}, e_{zi}) are the coordinates of the shear center and (E_{yi}, E_{zi}) are the coordinates of the neutral axis, in the local system, to the beam end, for the node "i." This transformation for a neutral axis offset is extremely convenient when only part of the hull is being analyzed.

20.2.2 Attached Plating Element

The stiffened plate element is an extension of the beam-column in which an effective width is added to the beam. For a long plate, see Figure 20.2, the effective width is obtained by assuming that Carlsen's ultimate stress equation (Carlsen, 1977) is valid for the region up to, and beyond, the ultimate state.

$$\frac{b_e}{b} = \left(\frac{2.1}{\beta_e} - \frac{0.9}{\beta_e^2} \right) \left(1 - \frac{0.75w_{0\text{max}}}{\beta t} \right) \left(1 + \frac{\sigma_r}{\sigma_y} \right)^{-1} R_2 R_\tau \quad (20.12)$$

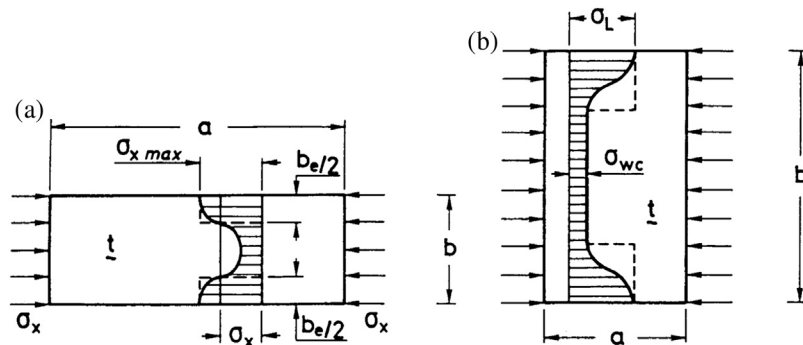


Figure 20.2

Stress distribution after buckling in long and wide plate. (a) Long plate; (b) wide plate.

where $\beta_e = \frac{b}{t} \sqrt{\frac{\sigma_x}{E}}$ and $\beta = \frac{b}{t} \sqrt{\frac{\sigma_y}{E}}$ and b and t are the plate width and thickness, respectively. The maximum initial deflection w_0 max and the residual stress σ_r can be determined by following [Faulkner's method \(1975\)](#). The reduction coefficient R_2 for the transverse stress σ_2 can be determined from

$$R_2 = \begin{cases} 1 - (\sigma_2/\sigma_{2u})^2 & \text{for compressive } \sigma_2 \\ 1 & \text{for tensile } \sigma_2 \end{cases} \quad (20.13)$$

where σ_{2u} is the ultimate stress of the plate and is subjected to an uniaxial transverse compression. The reduction coefficient R_τ for shear stress τ is determined by

$$R_\tau = \left[1 - (\tau/\tau_u)^2 \right]^{1/2} \quad (20.14)$$

where

$$\tau_u = \sigma_y / \sqrt{3} \quad (20.15)$$

To calculate the stiffness of the plate part, a reduced effective width \tilde{b}_e is introduced as

$$\tilde{b}_e = b \cdot \frac{d(b_e \sigma_x)}{d\sigma_x} \quad (20.16)$$

For a wide plate ([Figure 20.2](#)), the ultimate effective width b_{eu} is determined by following [Hughes \(1983\)](#).

$$\frac{b_{eu}}{b} = \frac{\sigma_L}{\sigma_Y} \frac{a}{b} + \left(1 - \frac{a}{b} \right) \frac{\sigma_{WC}}{\sigma_Y} \quad (20.17)$$

where the ultimate stress at two sides of the plate, σ_L , is equal to the ultimate stress of a square plate of width a , evaluated according to [Carlsen \(Eqn \(20.9\)\)](#). Finally, σ_{WC} is the ultimate strength of a wide column. According to [Smith \(1981\)](#) it may be approximated by

$$\sigma_{WC} = \frac{0.63}{1 + 3.27 \frac{W_{0max}}{\beta_L^2 t}} \quad (20.18)$$

where $\beta_L = \frac{a}{t} \sqrt{\frac{\sigma_Y}{E}}$ and W_{0max} denotes the maximum initial deflection of the wide column. In the present study, the effective width of the plate is assumed to change until it reaches the ultimate state in a manner similar to that of the effective width of a long plate

$$\frac{b_e}{b} = \begin{cases} R_2 R_\tau & \text{for } \sigma_x < \sigma_{WC} \\ \left(\frac{c_1}{\sqrt{\sigma_x}} - \frac{c_2}{\sigma_x} \right) R_2 R_\tau & \text{for } \sigma_{WC} \leq \sigma_x < \sigma_y \\ \frac{b_{eu}}{b} & \text{for } \sigma_x = \sigma_y \end{cases} \quad (20.19)$$

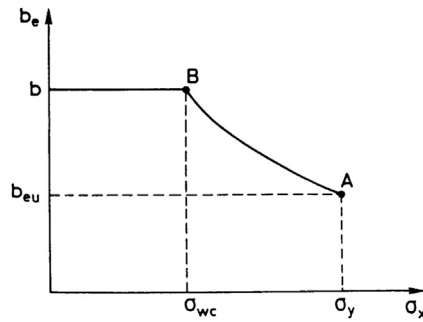


Figure 20.3
Effective width for a wide plate.

where the coefficients c_1 and c_2 can be determined from two points A and B in [Figure 20.3](#).

The contribution of the plate to the beam-column's stiffness is updated every time a load is added. The generalized ultimate plastic forces in compression, tension, and bending are calculated using the corresponding ultimate reduction factors. A yield surface in the form of a sphere is constructed based on these reduction factors. After yielding, the surface is kept constant and the nodal forces will move along the surface, following the PNM ([Ueda and Yao, 1982](#)).

20.2.3 Shear Panel Element

The shear stiffness is lost when a stiffened plate structure is modeled as a grillage. Considering this, an additional element that only has shear stiffness is used. The increment of the shear strain, $d\gamma$, in the local coordinate system is related to the increments of the nodal displacements $\{du_s\}$, which can be seen below ([Bathe, 1982](#))

$$d\gamma = [B_s]\{du_s\} \quad (20.20)$$

where $[B_s]$ denotes the strain–displacement matrix.

The tangent stress–strain relationship is taken as

$$d\tau = G_T d\gamma \quad (20.21)$$

where

$$G_T = \begin{cases} G & \text{for } \gamma \leq \gamma_y \\ 0 & \text{for } \gamma > \gamma_y \end{cases} \quad (20.22)$$

where γ_y denotes the shear strain for yielding.

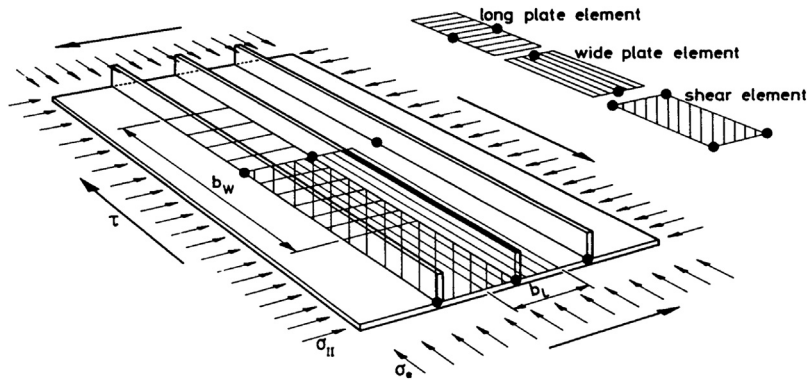


Figure 20.4
Element type.

Finally, the element stiffness matrix is obtained.

$$[k_s] = \int_V [B_s]^T G_T [B_s] dv \quad (20.23)$$

where V is the volume of the element. The local coordinate system of the element is updated and a coordinate transformation is carried out at each time step.

The element and their interactions are best understood from [Figure 20.4](#).

20.2.4 Nonlinear Spring Element

In addition to the three element types, a spring with nonlinear stiffness can also be employed. Any node may be connected, in any of the six degrees of freedom, by nonlinear springs. Stiffness, given by points on the force–displacement curve, is given as a function of displacement, and is the slope of the curve seen in [Figure 20.5](#). In addition to the points on this curve, the unloading stiffness must be defined.

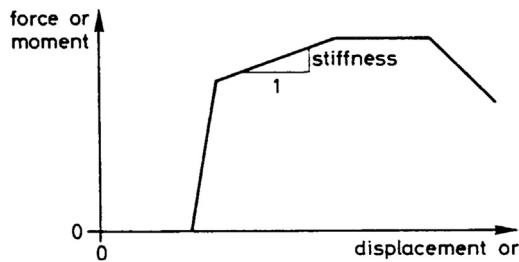


Figure 20.5
Force–displacement curve for a nonlinear spring.

20.2.5 Tension-Tearing Rupture

During a collapse, fatigue cracks and/or welding defects may initiate cleavage, ductile tearing, plastic collapse, or a combination of these events. This chapter determines the capacity of cracked members by either the crack tip opening displacement (CTOD) design curve approach (Burdekin and Dawes, 1971) or the level-3 CTOD method (Andersen, 1988).

In terms of the applied strain ε , the CTOD design curve is expressed as

$$\Phi = \frac{\delta_{cr}}{2\pi \bar{a}\sigma_y} = \begin{cases} (\varepsilon_{\max}/\varepsilon_y)^2 & \text{for } \varepsilon_{\max}/\varepsilon_y \leq 0.5 \\ \varepsilon_{\max}/\varepsilon_y & \text{for } \varepsilon_{\max}/\varepsilon_y > 0.5 \end{cases} \quad (20.24)$$

where δ_{cr} and \bar{a} are a critical CTOD and an equivalent crack length, respectively. E , σ_y , and ε_y are the Young's modulus, yield stress, and yield strain, respectively. It is noted that the applied strain ε_{\max} is evaluated by disregarding the effects of the crack.

To achieve a more accurate CTOD prediction, the level-3 CTOD method can be used

$$\frac{\delta_{cr}E}{\pi \bar{a}\sigma_y} = \left[\left(\frac{\sigma_{\max}}{\sigma_y} \right) \left\{ \frac{\sigma_{\max}^2}{2\sigma_y^2(1 + \sigma_{\max}/\sigma_y)} + \frac{E\varepsilon_{\max}}{\sigma_{\max}} \right\}^{1/2} + \frac{\sigma_r}{\sigma_y} \right]^2 \quad (20.25)$$

where σ_{\max} and ε_{\max} are the maximum stress and strain, respectively, and σ_r denotes the residual welding stress.

Failure is assumed to take place, and the cracked member is removed from the structural system when the specified equivalent strain satisfies the selected fracture mechanics criterion. The element forces are applied as unbalanced forces to the system. These fracture mechanics criteria are used for all of the elements presented in this chapter.

After collision, the area where tension-tearing rupture has taken place is considered as the "hole." These data are important for the simulation of oil spills resulting from collisions and groundings.

20.2.6 Computational Procedures

This chapter outlines the computer program SANDY and the computational procedures implemented in the program. Further information can be found within the program manuals (Bai, 1991) and in publications (Bai and Pedersen, 1991, 1993; Bendiksen, 1992).

Computer Program SANDY

The theory presented in this chapter has been implemented in the general-purpose computer program SANDY (Bai, 1991). Depending on the problem, the following solution procedures can be applied:

- Quasi-static analysis using:
 - Load increment
 - Displacement
 - Automatic loading, by using the current stiffness parameter method (Bergan and Soreide, 1978).
- Dynamic analysis (time-integration method):
 - Applying dynamic loads as time histories of both nodal and element forces
 - Modeling the problem as a structure struck by a deformable mass
 - Applying dynamic loads as initial nodal velocities
 - Earthquake response analysis.

Computational Procedure

The nonlinear calculation procedure:

- The size of the increment is determined; this is often determined in the input data.
- The increment of the load vector is assembled.

The stiffness matrix is calculated for each element. Shear elements G_t and stiffness matrices are dependent on the current load. For nonlinear spring elements, the stiffness factor is calculated as a function of the displacement and the direction of the increment. For plate elements, the effective width and the linear stiffness, plus the eccentricity, are all calculated. Subsequently, the element is treated the way any other beam-column element is treated. The two geometric matrices are calculated and added to the linear matrix. If the element is in the plastic range, the plastic stiffness matrix is calculated.

If a standard stiffened plate section is used, the program may first recalculate the yield surface, by taking the new reduction factors caused by transverse and shear stress into account. If the element is plastic, these reduction factors are kept constant; otherwise, they would influence the compatibility equations.

The transformation equation for each element is updated and the stiffness matrices are transformed and added into the global matrix.

In the first step of a dynamic simulation, the global mass matrix is calculated. The system of equations is modified according to a time-integration scheme, for example, Newmark- β method. Finally, the system of equations is solved. Here, LDL decomposition is used, along with a back substitution.

Each plastified node is checked for unloading. For nodes in nonlinear spring elements as well as for shear panel elements, unloading is detected when the load increment and the load have different signs. For all elements with unloading nodes, the stiffness is changed and the procedure is continued from point (f).

When no further unloading is detected, the increments of displacement are obtained. Then the internal forces for each element are calculated. For each elastic element, a check may be made to determine whether yielding occurs during the step. If this is the case, the increment for that element is divided into a part that is treated elastically and a part that is treated like plastic. The increment in the internal force for the element is calculated from

$$\{dx\} = factor \cdot [K_E]\{du\} + (1 - factor)[K_P]\{du\} \quad (20.26)$$

where *factor* is the elastic fraction of the increment.

Unloading is then checked again.

If either loading or unloading takes place, and no kind of iteration is carried out, the change of state gives rise to unbalanced forces, which need to be added to the load in the next step. This unbalanced force is calculated to be the difference in internal forces due to changes in the elastic–plastic state. This gives place to yielding $\{dx\} = (1 - factor) ([K_E] - [K_P])\{du\}$ and to unloading $\{df\} = ([K_P] - [K_E])\{du\}$.

Note that the global set of equations remains unchanged due to plastification in the elements. This means that the influence on the global situation from one node changing its state is disregarded.

A revision is made to determine whether any elements have torn. If this is the case, these elements are removed and their internal forces are added in as unbalanced loads during the next step.

When the step is accepted, a new increment begins at that new point (a).

20.3 Analytical Equations for Hull Girder Ultimate Strength

Buckling and collapse strength of hull girders under bending may be predicted as the fully plastic moment, the initial yield moment, and the progressive collapse moment. The last includes buckling and postbuckling strength of individual components of the hull girder. The fully plastic mode provides an upper bound of the ultimate strength, which is never attained in a hull of normal configurations. The initial yield mode assumes that buckling does not occur prior to yielding. The initial yield strength is a function of the elastic section modulus of the hull girder and yield strength of the material.

In this section an ultimate strength equation is proposed, to account for the effects of lateral pressures, biaxial loading, and shear stress using analytical solutions. The ultimate

strength equation is then compared to the sophisticated approach described in Section 20.4. The ultimate strength equation may be applied for the quantification of structural risks of aging ships with corrosion and fatigue defects (see Parts IV and I).

20.3.1 Ultimate Moment Capacity Based on Elastic Section Modulus

In the initial yield moment approach, it is assumed that the ultimate strength of the hull girder is reached when the deck (alone) has yielded. Premature buckling is assumed not to occur. In this approach, the elastic section modulus is the primary factor for measuring the longitudinal bending strength of the hull. With these assumptions, the initial yield moment can be written as

$$M_I = (SM)_e \sigma_y \quad (20.27)$$

here, $(SM)_e$ is the elastic section modulus. Owing to the use of greater slenderness ratios for stiffeners and plate panels, and high yield steels, the possibility of buckling failure has increased. The initial yield moment may not always be the lower bound to hull girder strength, since the buckling of the individual structural elements was not accounted for.

Owing to the simplicity of the initial yield moment equation, it can frequently be used in practical engineering. Vasta (1958) suggested that the ship hull would reach its ultimate strength when the compression flange in the upper deck (in the sagging condition) or the bottom plating (in the hogging condition) collapses, and that the yield stress in the initial yield moment, Eqn (20.24), may be replaced by the ultimate strength σ_u of the upper deck or the bottom plating.

Mansour and Faulkner (1973) suggested the Vasta formula can be modified to account for the shift in the neutral axis location after the buckling of the compression flange.

$$M_u = (1 + k)(SM)_e \sigma_u \quad (20.28)$$

where k is a function of the ratio of the areas for a one side shell to the compression flange. For a frigate, the calculated value of k is approximately 0.1.

Viner (1986) suggested that hull girders collapse immediately after the longitudinal on the compression flange reaches its ultimate strength, and suggested the following ultimate moment equation,

$$M_u = a(SM)_e \sigma_u \quad (20.29)$$

where a is normal in the range of 0.92–1.05 (mean 0.985).

The findings of Mansour and Faulkner (1973) and Viner (1986) are very useful because of their simplicity—ultimate moment capacity is approximately the product of the elastic section modulus and the ultimate strength of the compression flange.

Valsgård and Steen (1991) pointed out that hull sections have strength reserves beyond the onset of the collapse of the hull section strength margin, and suggested that a is 1.127 for the single-hull VLCC Energy Concentration, which collapsed in 1980.

Faulkner and Sadden (1979) made further modifications,

$$M_I = 1.15(SM)_e \sigma_y \left[-0.1 + 1.4465 \sigma_u / \sigma_y - 0.3465 (\sigma_u / \sigma_y)^2 \right] \quad (20.30)$$

where σ_U is the ultimate strength of the most critical stiffened panels.

20.3.2 Ultimate Moment Capacity Based on Fully Plastic Moment

Caldwell (1965) assumed that the ultimate collapse condition is reached when the entire cross section of the hull including the side shell has reached the yield state. The material is assumed to be elastic–perfectly plastic; for example, the strain-hardening effect is ignored. Also, the effect of buckling and the effects of axial and shear forces are neglected. With these assumptions, the fully plastic collapse moment, M_p , can be estimated as

$$M_p = (SM)_p \sigma_y \quad (20.31)$$

where M_p is the fully plastic moment, σ_y is the yield strength of the material, and $(SM)_p$ is the plastic section modulus.

Frieze and Lin (1991) derived the ultimate moment capacity as a function of normalized ultimate strength of the compression flange using the quadratic equation,

$$M_u / M_p = d_1 + d_2 \frac{\sigma_u}{\sigma_y} + d_3 \left(\frac{\sigma_u}{\sigma_y} \right)^2 \quad (20.32)$$

where

$$\begin{aligned} d_1 = -0.172, \quad d_2 = 1.548, \quad d_3 = -0.368, & \quad \text{for sagging} \\ d_1 = 0.003, \quad d_2 = 1.459, \quad d_3 = -0.461, & \quad \text{for hogging} \end{aligned}$$

Mansour (1997) reviewed the above-noted empirical moment capacity equations and compared them with test results.

Based on fully plastic moment interactions, Mansour and Thayamballi (1980) derived the following ultimate strength relation between vertical and horizontal moments,

$$m_x + km_y^2 = 1 \quad \text{if} \quad |m_y| \leq |m_x| \quad (20.33)$$

$$m_y + km_x^2 = 1 \quad \text{if} \quad |m_y| \geq |m_x| \quad (20.34)$$

where

$$m_x = \frac{M_x}{M_{xu}}, \quad m_y = \frac{M_y}{M_{yu}} \quad (20.35)$$

$$k = \frac{(A + 2A_S)^2}{16A_S(A - A_S) - 4(A_D - A_B)^2} \quad (20.36)$$

$$A = A_D + A_B + 2A_S \quad (20.37)$$

and where

M_x = bending moment in vertical direction

M_y = bending moment in horizontal direction

M_{xu} = vertical ultimate collapse bending moment

M_{yu} = horizontal ultimate collapse bending moment

A_D = cross-sectional area of the deck including stiffeners

A_B = cross-sectional area of the bottom including stiffeners

A_S = cross-sectional area of one side including stiffeners.

Mansour (1997) demonstrated that the above equations fit well with the finite element analysis results for ultimate strength of hull girders under combined vertical and horizontal moments.

20.3.3 Proposed Ultimate Strength Equations

The ultimate moment capacity, obtained from the modified Smith method, is the maximum value on the bending moment–curvature curve. It is time-consuming when reliability analysis relative to the ultimate strength failure mode is carried out, by means of the modified Smith method. Some ultimate strength equations have been proposed based on various assumptions of stress distribution over the cross section. For instance, a moment capacity equation may be derived based on the assumption that the midship section is fully plastic (elastic–perfectly plastic) for the tensile side and is in ultimate strength condition for the compressive side. This assumption gives generally good agreement with more exact predictions by correctly estimating the position of the neutral axis. Successful experience using this approach has been described in a study involving the ultimate strength of corroded pipes under a combined (internal/external) pressure, axial force, and bending. See Bai (2001).

Several other assumed stress distributions are available from Bai (2001), including a stress distribution that assumes that the middle of the hull depth is elastic, while the rest of the hull depth is plastic/ultimate strength. Xu and Cui (2000) assumed a stress distribution in which the middle one-third of the hull depth is elastic while the rest of the hull depth is plastic/ultimate strength. The present authors suggest that the ultimate moment capacity M_u can be predicted by the equation

$$M_u = \sum_i \sigma_{u_i}^c A_{ps_i} z_i + \sum_j \sigma_{u_j}^t A_{ps_j} z_j + \sum_k \sigma_k^e A_{ps_k} z_k \quad (20.38)$$

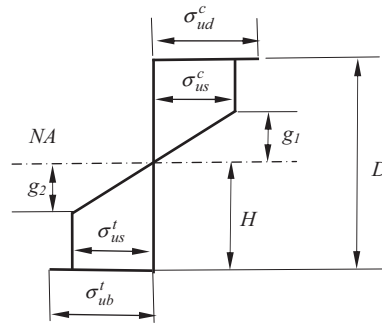


Figure 20.6

Illustration of the assumed stress distribution for hull girder collapse—deck in compression.

where A_{ps} is the area of stiffened panels/hard corners and z is the distance to the neutral axis. Figure 20.6 shows a schematic diagram of stress distribution, under sagging conditions. The stress distribution used in Eqn (20.38) does account for the ultimate strength of individual stiffened panels and hard corners; for example, it is not uniformly distributed in Figure 20.6.

In Eqn (20.38), the compressive ultimate strength region, tensile ultimate strength region, and elastic region are denoted by i, j, k , respectively. σ_u^C is the ultimate compressive strength for stiffened panels or yield stress for hard corners. σ_u^T is the ultimate tensile strength (yield stress). Elastic stress σ^e has a linear distribution around the neutral axis. Based on observations of stress distributions from more comprehensive numerical analysis, it is suggested by the present authors that the total height of the elastic region may be taken as half of the hull depth, for example, $g_1 + g_2 = D/2$. The height of the compressive region, g_1 , and the height of the tensile region, g_2 , may be estimated based on the beam theory, which assumes that the plane remains plane after bending.

Based on Eqn (20.38), the ultimate moment capacity of a hull girder can be estimated by the following steps:

- Subdivide the cross section into stiffened panels and hard corners;
- Estimate the ultimate strength of each stiffened panel using recognized formulas;
- Calculate the distance “H” from the bottom of the ship to the neutral axis, by assuming the total force from the stress integration over the cross section is zero;
- Calculate the ultimate moment capacity of the hull girder using Eqn (20.38).

In addition, it is necessary to check vertical shear strength F_u using

$$F_u = \sum \tau_{u_i} A_{p_i} \quad (20.39)$$

where A_{p_i} is the area of the panel in the shear element (plate area only) and τ_{u_i} is the characteristic ultimate shear stress in the panel. Here, i includes all panels in the longitudinal shear element.

20.4 Modified Smith Method Accounting for Corrosion and Fatigue Defects

Considering a hull girder as a beam section under bending, [Smith \(1975, 1977\)](#) proposed a simple procedure to calculate the moment–curvature relationship and ultimate strength of a hull girder. The basic assumptions of the Smith method are summarized as follows:

1. The hull cross section is subdivided into a number of subdivisions, such as stiffeners with associated plating and corner elements, which are considered to act and behave independently.
2. For each such panel the load–shortening curve is constructed. This can be accomplished by a number of methods, including experimental results, nonlinear finite element analysis, and simplified elastic–plastic buckling analysis. The Smith method can also account for the manufacturing residual imperfections including deflections and stresses of plating and columns.
3. The hull is then subjected to an incrementally increasing curvature, in which it is assumed that the cross sections that are initially plane remain plane after bending, and experience only rotation about an assumed neutral axis. The overall grillage collapse of the deck and bottom structures is avoided by using sufficiently strong transverse frames.
4. The total axial force and bending moment acting on the cross section are obtained through an integration of the stress over all of the components that make up the cross section. Through iteration, the location of the neutral axis is obtained by equating the total axial force to the longitudinal force that is zero.

This section presents a modified version of Smith’s method ([Smith, 1975, 1977](#); [Yao and Nikolov, 1991, 1992](#); [Rahman and Chow, 1996](#)) in which the effect of corrosion defects, fatigue crack, and lateral pressure are all accounted for.

As demonstrated by previous researchers, the advantages of the modified Smith method include (1) efficiency, (2) flexibility, to account for the effects of corrosion defects, fatigue cracks, etc., and (3) accuracy.

The stress–strain relationship for the elements are given below.

20.4.1 Tensile and Corner Elements

The stress–strain relationship for tensile and corner elements is assumed to be linear elastic and elastic–perfectly plastic,

$$\sigma_x = \begin{cases} \varepsilon_x E & \varepsilon \leq \varepsilon_y \\ \sigma_y & \varepsilon \geq \varepsilon_y \end{cases} \quad (20.40)$$

where E , σ_y , and ε_y are the elastic modulus, yield stress, and yield strain of the material, respectively.

20.4.2 Compressive Stiffened Panels

A stiffened panel is composed of a longitudinal stiffener with its attached plating. Following the approach of [Rahman and Chowdhury \(1996\)](#), three distinct zones in the whole range of the load–shortening behavior are considered: stable zone, no-load-shedding zone, and load-shedding zone, which can be seen in [Figure 20.7](#). The stable zone is in the preultimate strength region. The no-load-shedding zone does not require any load shedding in order to maintain equilibrium. When the strain increases, the final zone is characterized by a drop-off.

More information on compressive stiffened panels may be found from [Smith \(1975\)](#).

A stiffened panel is composed of a longitudinal stiffener with its attached plating. Following the approach of [Rahman and Chowdhury \(1996\)](#), three distinct zones, covering the entire range of the stiffened panel’s loading–shortening behavior, are considered. The ultimate strength of a stiffened panel is given by

$$\sigma_{pu} = \min(\sigma_{uf}, \sigma_{up}) \quad (20.41)$$

where σ_{uf} and σ_{up} are the ultimate beam-column failure values of the panel when lateral pressure causes compression of stiffener flange and plating, respectively. According to [Hughes \(1983\)](#), a solution may be obtained by solving the following equations for stiffener failure,

$$\sigma_y = \sigma_{uf} + \frac{M_0 y_f}{I} + \frac{\sigma_{uf} A (\delta_0 + \Delta) y_f}{I} \Phi \quad (20.42)$$

and for plate failure,

$$\sigma_y = \sigma_{up} + \frac{M_0 y_p}{I_e} + \frac{\sigma_{up} A_e (\delta_0 + \Delta + \Delta_p / \Phi) y_p}{I_e} \Phi \quad (20.43)$$

where Δ is the initial eccentricity; δ_0 and M_0 are the maximum deflection and bending moments due to lateral loads; Δ_p is the eccentricity caused by reduced stiffness of

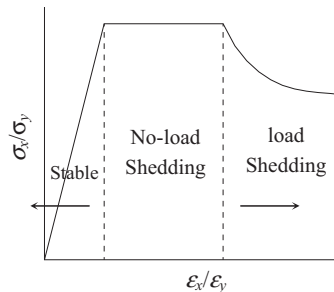


Figure 20.7

Typical stress–strain relation of a stiffened panel.

compressed plating; I and A are respectively the second moment and the sectional area of the panel, considering that b_P (panel width) is fully effective; whereas I_e and A_e are similar properties but for a transformed section replacing b_P by b_{Pe} (effective width); y_f is the distance from the panel neutral axis to the stiffener flange and y_P to the plating of the transformed section; Φ is the magnification factor for a combined loading.

20.4.3 Crack Propagation Prediction

To predict the crack propagation and fatigue life, the Paris–Erdogan equation is used,

$$\frac{da}{dN} = C \Delta K^m \quad (20.44)$$

where a is the crack size, N is the number of cycles, ΔK is the stress range intensity factor, and C and m are material parameters. The stress intensity factor is given by

$$\Delta K = \Delta \sigma Y(a) \sqrt{\pi a} \quad (20.45)$$

where $\Delta \sigma$ is the stress range and $Y(a)$ is the geometry function.

If $Y(a) = Y$ is a constant and $m \neq 2$, then integration of Eqn (20.44) gives

$$a(t) = \left[a_0^{\left(1-\frac{m}{2}\right)} + \left(1 - \frac{m}{2}\right) C (\Delta \sigma Y \sqrt{\pi})^m v_0 t \right]^{\frac{1}{1-\frac{m}{2}}} \quad (20.46)$$

where a_0 is the initial crack size, and the complete fatigue life T_f is equal to the sum of time to crack propagation T_P , and T_i is the time to crack initiation.

$$T_i = k T_P \quad (20.47)$$

where k can vary from 0.1 to 0.15. The crack size is assumed to have a normal distribution with the mean and variance (see Guedes Soares and Garbatov, 1996, 1999).

Two types of cracks are considered in the stiffened panel, one propagating away from the stiffener in a transverse direction, decreasing the width of attached plating, and the other across the web of stiffener, decreasing the web height.

20.4.4 Corrosion Rate Model

Corrosion rates depend on many factors including coating properties, cargo composition, inert gas properties, temperature of cargo, and maintenance systems and practices. For this reason, the corrosion rate model should be appropriately based on the statistics of measurement data.

Practically, the time-variant corrosion rate model may be divided into three phases. In the first one, there is no corrosion because of the protection of coatings, and the corrosion rate

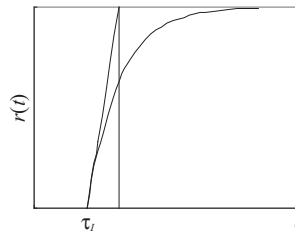


Figure 20.8

Model of corrosion rate.

is zero. The second phase is initiated when the corrosion protection is damaged and corrosion occurs, which reduces the plate thickness. The third phase corresponds to a constant corrosion rate. The present authors suggested a model such as

$$r(t) = r_s \left(1 - e^{-\frac{t-\tau_i}{\tau_t}} \right) \quad (20.48)$$

where τ_i is the coating lifetime, τ_t is the transition time, and r_s is the steady corrosion rate. [Figure 20.8](#) shows the corrosion rate model.

By integrating [Eqn \(20.36\)](#), the corrosion depth can be obtained by

$$d(t) = r_s \left[t - (\tau_i + \tau_t) + \tau_t e^{-\frac{t-\tau_i}{\tau_t}} \right] \quad (20.49)$$

where the parameters τ_i , τ_t , and r_s should be fitted to inspection results. [Figure 20.9](#) shows the corrosion depth as a time function. The coating lifetime τ_i is assumed to be fitted by a Weibull distribution,

$$f(\tau_i) = \frac{\alpha}{\beta} \left(\frac{\tau_i}{\beta} \right)^{\alpha-1} \exp \left[-\left(\frac{\tau_i}{\beta} \right)^\alpha \right] \quad (20.50)$$

and r_s , to be fitted by a normal distribution. [Figures 20.10 and 20.11](#) illustrate the corrosion depth reproduced by the present model based on the net measurement data of [Yamamoto \(1998\)](#). Some variability of the data exists along the regression curve.

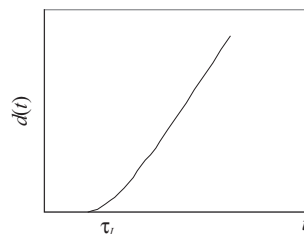


Figure 20.9

Loss of plating thickness from corrosion as time function.

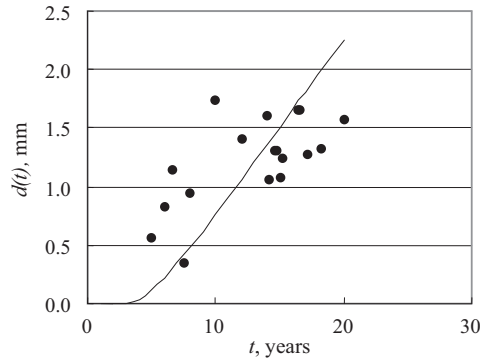


Figure 20.10

Loss of plating thickness from corrosion for inner bottom plates of bulk carriers.

The net area $A_i(t)$ of the stiffened panel, available to carry longitudinal stress, is dependent on the crack size $a_i(t)$ and the corrosion depth $d_i(t)$.

$$A_i(t) = [b_p - 2a_i(t)] [h_p - d_i(t)] + [h_s - a_i(t)t][b_s - d_i(t)] \quad (20.51)$$

where b_p and h_p are the width and thickness of the attached plating, and h_s and b_s are the web height and thickness of the stiffener.

From an engineering viewpoint, a stiffened panel is considered ineffective when the crack size exceeds the critical crack size, previously determined by the CTOD method (Ghose, 1995) or when the corrosion-induced thickness reduction exceeds 25% of the original plate thickness.

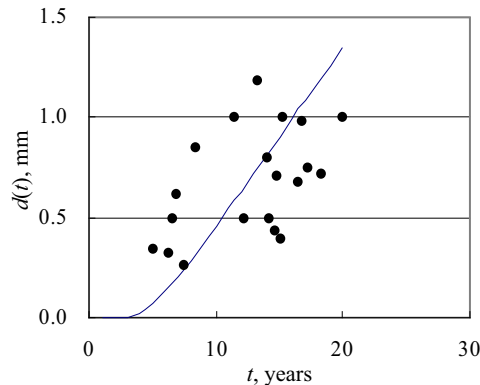


Figure 20.11

Loss of plating thickness from corrosion for side shells of bulk carriers.

20.5 Comparisons of Hull Girder Strength Equations and Smith Method

Many examples of progressive collapse analysis for box girders and ship primary hulls have been calculated to verify the efficiency and accuracy of the present modified Smith method. The examples used in the International Ship and Offshore Structures Congress (ISSC) benchmark calculations by Yao et al. (2000), which are given in Table 20.1 together with the results of the modified Smith method described in Section 20.4, and the equation described in Section 20.3.

The results from the simplified method and ultimate strength equation presented by the authors agree well with the results reported by Yao et al. (2000). Figure 20.12 shows the moment–curvature response for the five hull girders, where the positive value of M_U/M_P is hogging.

The mean moment–curvature responses of the FPSO hull girder are shown in Figure 20.13 for different service years, each considering the degradation effects of fatigue and corrosion. The number on the curve represents the service year.

From Figure 20.13 it is easy to appreciate the importance of conducting inspection and repair. When inspection and repair are not conducted, the load-carrying capacity decreases with time.

Table 20.1: Ultimate strength calculations

Ship Type	Load Condition	ISSC ^a		Modified Smith Method (MNm)	Proposed Equation (MNm)
		Mean (MNm)	Cov		
Bulk carrier	Sagging	1.52×10^4	0.07	1.53×10^4	1.53×10^4
	Hogging	1.86×10^4	0.04	1.72×10^4	1.70×10^4
Container ship	Sagging	6.51×10^3	0.14	5.84×10^3	6.25×10^3
	Hogging	7.43×10^3	0.08	6.93×10^3	6.80×10^3
DH VLCC	Sagging	2.24×10^4	0.11	1.98×10^4	2.23×10^4
	Hogging	2.91×10^4	0.04	2.76×10^4	2.68×10^4
SH VLCC	Sagging	1.72×10^4	0.02	1.46×10^{4b}	1.70×10^4
	Hogging	1.82×10^4	0.02	1.79×10^{4b}	1.81×10^4
Frigate Model	Sagging	10.39	0.07	9.61	9.73
	Hogging	12.38	0.08	12.10	12.26
FPSO	Sagging	—	—	3.58×10^3	3.61×10^3
	Hogging	—	—	5.14×10^3	4.90×10^3

^aThe results are obtained by averaging the values of all participants in ISSC VI.2 (Yao et al., 2000).

^bThe external pressure is applied consistent with the analysis by Rutherford and Caldwell (1990).

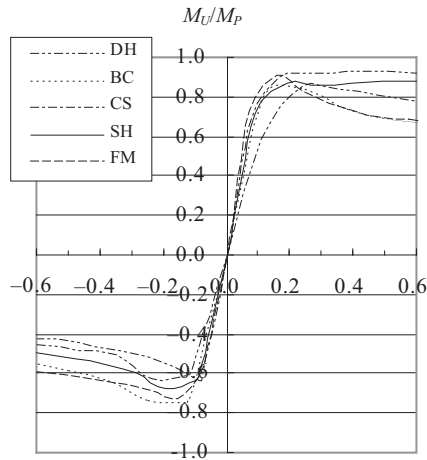


Figure 20.12

Bending moment vs curvature response for the hull girders used in ISSC benchmark.

The mean maximum values of the ultimate strength are plotted in [Figure 20.14](#) as a time function, where four cases of degradation effects are considered based on the corrosion rates in Table 2 of [Sun and Bai \(2001\)](#), that is,

- Case (1): no corrosion;
- Case (2): half-mean steady corrosion rates;
- Case (3): mean steady corrosion rates;
- Case (4): double mean steady corrosion rates.

The solid lines in [Figure 20.14](#) denote the time at which both corrosion and fatigue degradation effects are taken into account, while the dotted lines indicate when only the corrosion effect is taken into consideration. The mean maximum ultimate strength of the

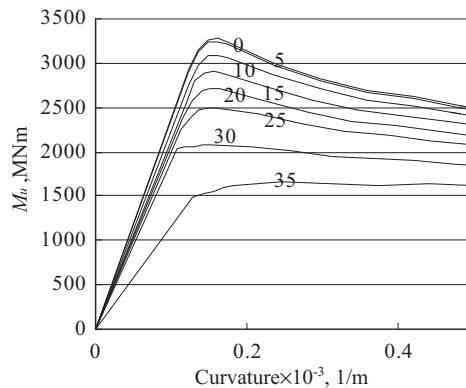


Figure 20.13

Mean moment—curvature responses.

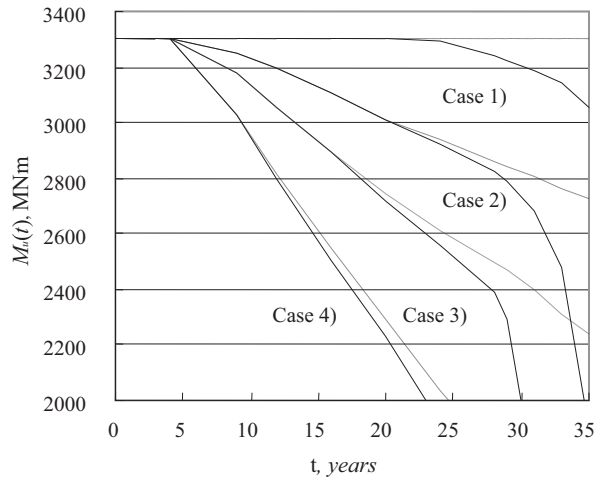


Figure 20.14

Mean ultimate strength for four cases of mean steady corrosion rates.

hull girder has been observed to reduce significantly, mainly as a result of the corrosion defects, if additional effects of fatigue are relatively small, although residual strength is dictated primarily by the corrosion rates. The degradation rates are different from those of Ghose et al. (1995), because only fatigue effects were considered.

20.6 Numerical Examples Using the Proposed PNM

In this chapter, five typical application examples of ship collapse analysis are presented. The first three examples have been chosen to validate the proposed analysis procedure. The complexity of the analyzed structures has changed from a single structural component to an entire structural system. After validating the analysis procedure, examples are presented of ultimate longitudinal strength and collision analyses of hull scale ships. This analysis is described in more detail by Bendiksen (1992).

20.6.1 Collapse of a Stiffened Plate

This procedure has been compared to a model of an experimental investigation of the ultimate load-carrying capacity of longitudinally stiffened plates (Faulkner, 1976). The plate is compressed in the longitudinal direction (see Figure 20.15) and has residual stresses from welding and an initial deflection ($w_0 = 0.12\beta^2 t$). The stiffener also has an initial deflection (of magnitude $L/1000$). The load end-shortening curve, shown in Figure 20.16, was obtained by the present method in which two elements are used. The obtained buckling load agrees with the experimental result within 2%. In conclusion, the position of the loading plane is a decisive parameter.

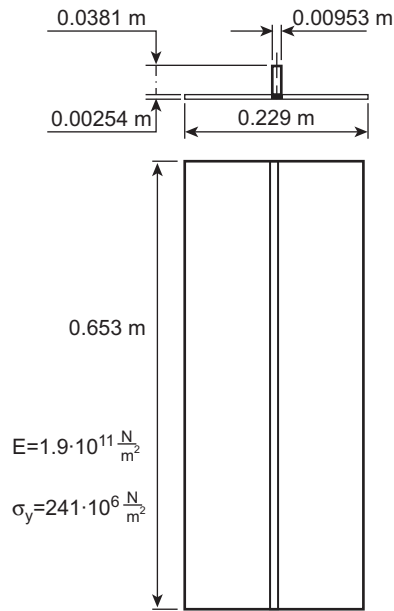


Figure 20.15
Stiffened plate.

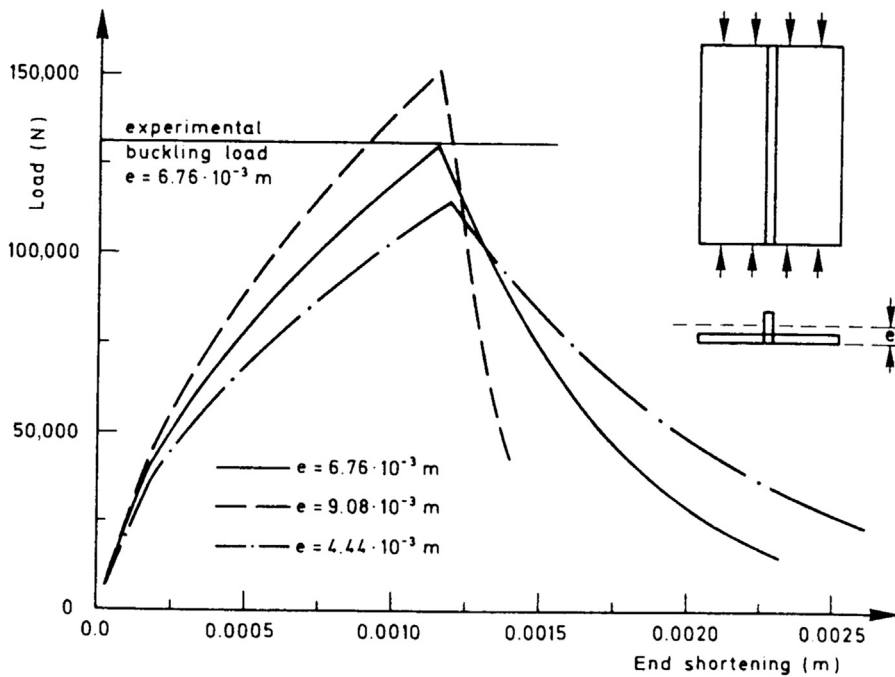


Figure 20.16
Load end-shortening curve for stiffened plates.

20.6.2 Collapse of an Upper Deck Structure

The next example, shown in Figure 20.17, is of a longitudinally and transversely stiffened plate. The plate is analyzed by means of four nodal plate elements in an ISUM procedure, done by Ueda et al. (1986). The plate has an average initial deflection of $w_0/t = 0.25$ and a welding residual stress of $\sigma_r/\sigma_y = 0.2$. The shifting of the neutral axis is not considered in this example. The result of the analysis, as shown in Figure 20.18, provides a very good agreement between the four-node ISUM procedure and the present procedure. Both were evaluated with respect to buckling loads and end-shortening loads, using only 24 nodes.

20.6.3 Collapse of Stiffened Box Girders

This procedure has been compared to experimental results that were based on the ultimate longitudinal strength of ship hull models (Nishihara, 1984). The experiments consisted of a ship hull model being exposed to a four point bending load. The present

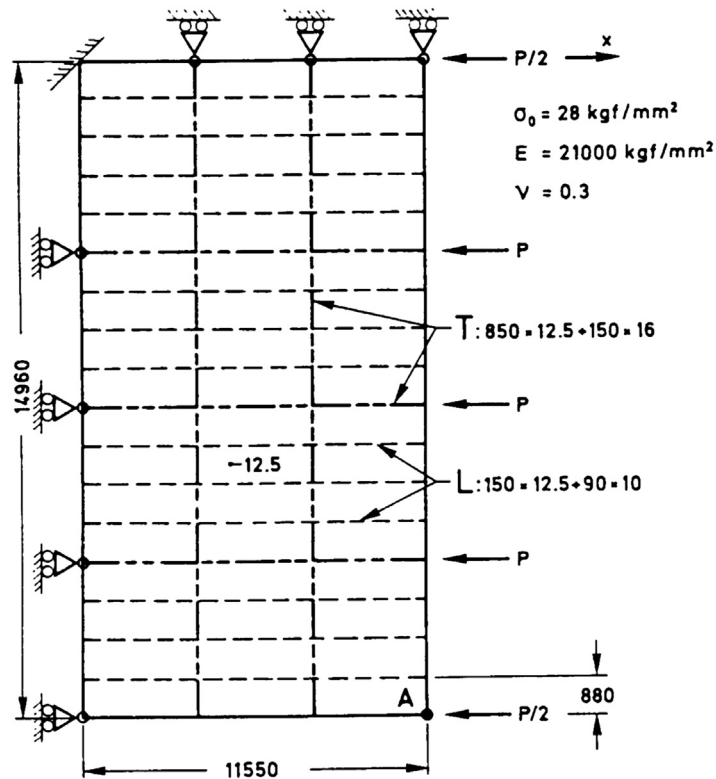


Figure 20.17

Upper deck structure in compression.

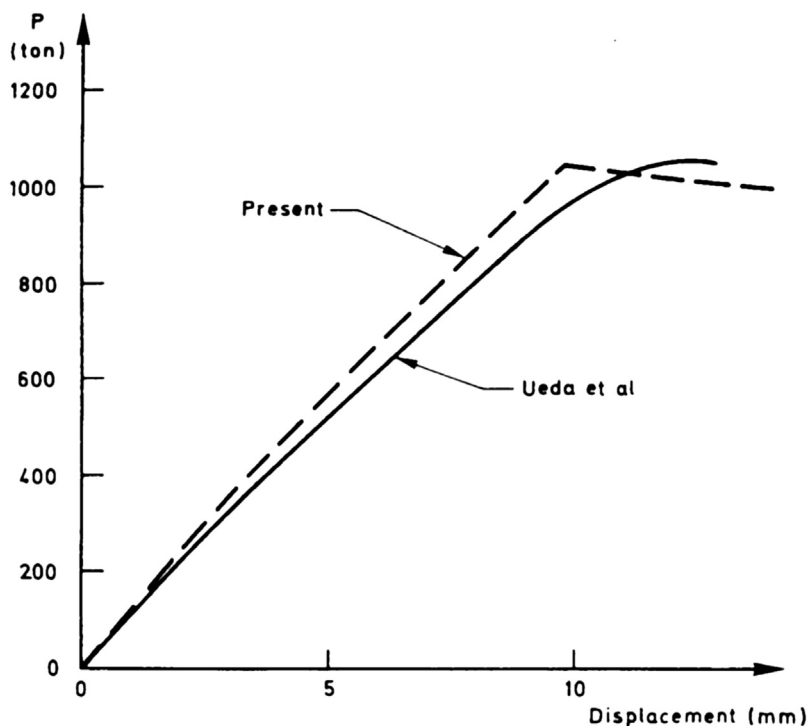


Figure 20.18
Load—displacement curves for deck structure.

numerical analysis connected a detailed model of the middle section of the hull to simple beams that model the less stressed ends of the hull. This was done using a transformation for the nodes placed outside the neutral axis, allowing for a number of longitudinal plate elements in the cross section to be connected to one node at each end of the analyzed model.

If the initial plate and overall deflections are of magnitude $0.12\beta^2 t$ and $L/1000$, respectively, and the residual stress level is $\sigma_r/\sigma_y = 0.1$, then the result for a tanker-like section (spectrum MST-3) (Figure 20.19) is compared with the experimental result in Figure 20.19. Figure 20.19 shows that the analysis is in agreement with the experiment and the initial imperfections reduce the ultimate moment by approximately 14%. Furthermore, the analytical fully plastic moment $M_p = 787$ kNm is a well-predicted value by the present method.

In Figure 20.20, the collapsed shape of the hull is indicated and the buckling of the bottom is evident. Figure 20.21 shows how the nodes are connected using the transformation matrix \underline{S} .

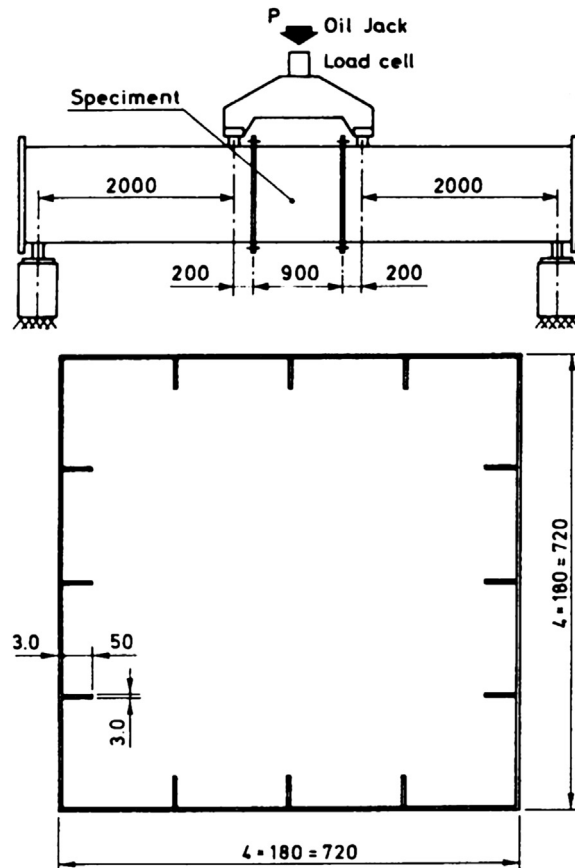


Figure 20.19

Model of a tanker measured in millimeters.

20.6.4 Ultimate Longitudinal Strength of Hull Girders

The ultimate longitudinal strength is calculated for a 60,000 dwt double hull, double bottom product tanker. Because of symmetry, only a quarter of the center tank is modeled (see Figure 20.22). The boundary conditions are specified in the planes of symmetry.

Since pure bending is applied, it is valid to assume that plane boundaries remain plane. Therefore, only one nodal point is used in the fore end of the tank. Again, this is possible with the transformation for node points out of the neutral axis. The end of the section is loaded with a vertical bending moment that is controlled by the current stiffness parameter method. It is possible to load the hull in pure bending throughout the calculation, without knowing the new position of the neutral axis for the hull. Note that in this procedure, plane sections are not restricted to remain plane, except for the end section described by

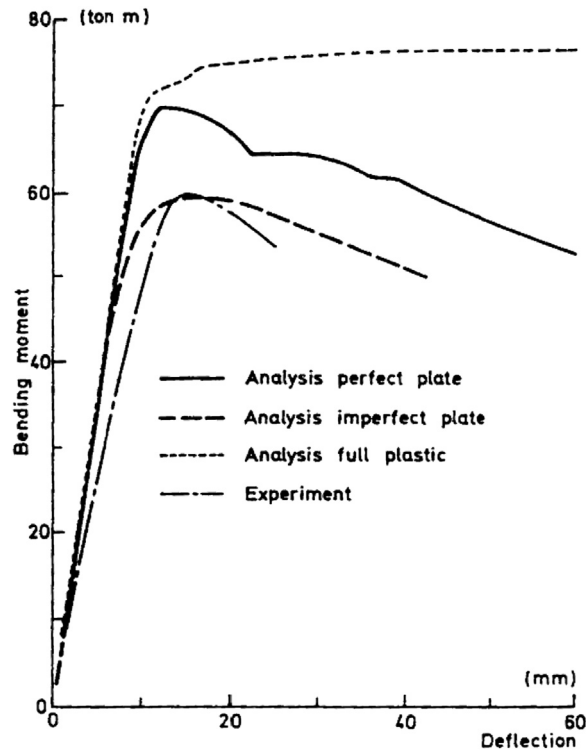


Figure 20.20

Ultimate behavior for the tanker model.

only one node. The curvature—moment relationship for the hull is shown in [Figure 20.23](#) and is compared to the full plastic moment.

The formulas relating the ultimate moment to the fully plastic moment imply that the ultimate moment under the influence of a sagging load is $0.86 M_p$ and under the influence

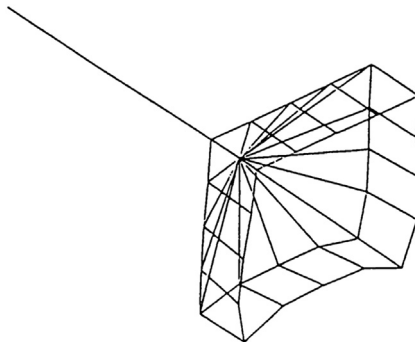


Figure 20.21

Boundary condition model for ship's midsection.

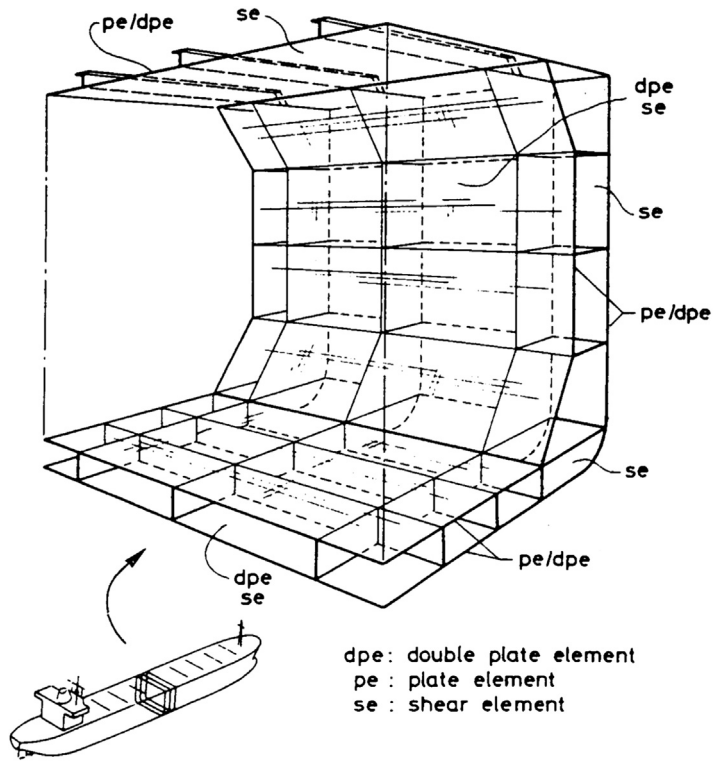


Figure 20.22

Quarter of the tank that is the extent of the detailed model.

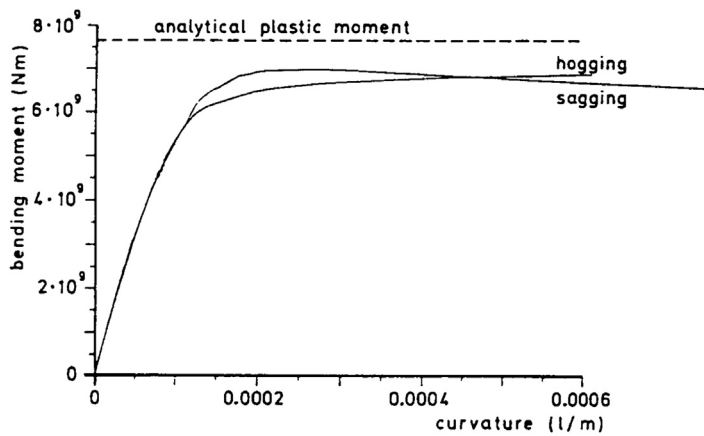


Figure 20.23

Moment and curvature relation of the ship.

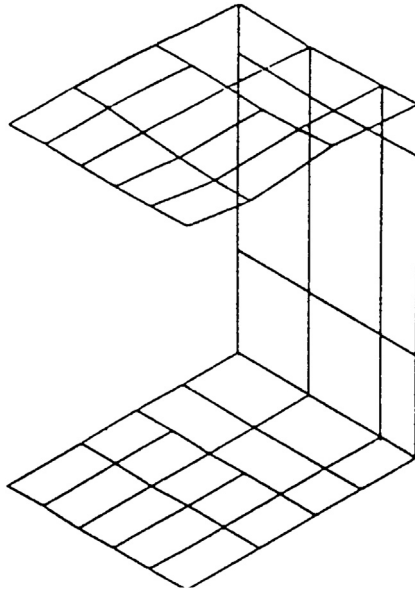


Figure 20.24

Deflected shape in sagging.

of a hogging type load is $0.89 M_p$ (Frieze and Lin, 1991). The present analysis gives results of $0.89 M_p$ and $0.88 M_p$, respectively. The failure mode in sagging causes overall buckling of the deck, as seen in Figure 20.24. The failure mode in hogging causes plate buckling combined with plasticity in the bottom and lower part of the side, and limits the load-carrying capacity.

20.6.5 Quasi-static Analysis of a Side Collision

The next example is a side collision. To be more precise, an infinitely stiff object is forced into the side of a ship hull in a quasi-static analysis. The ship hull is the same as the one used in the hull-bending example; therefore, the finite element model used in this example has minor modifications. Shear elements have been added in the deck and at the bottom.

A concentrated load is applied at the middle of the side, while the current stiffness parameter method is employed to control the load. The force—indentation curve for this example can be seen in Figure 20.25.

The results may be compared with simplified analyses (Søreide, 1981). The maximum force in the first phase can be calculated as the load that makes the longitudinal beam collapse as if it were a plastic mechanism. Assuming it is clamped when M_p is calculated for a beam breadth of 5 m, its collapse load becomes 6.65 MNm and the load at the end of phase one becomes

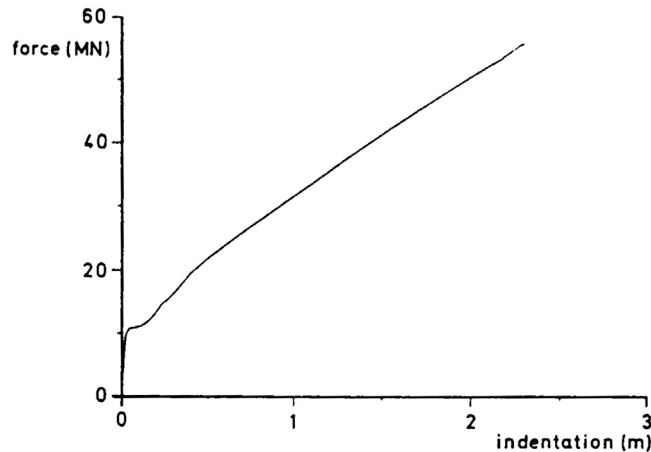


Figure 20.25

Force/indentation curve for the hull loaded quasi-static by a concentrated force.

$$P_0 = \frac{46.65 \text{ MNm}}{2.5 \text{ m}} = 10.6 \text{ MN}$$

This is extremely close to what is seen in [Figure 20.25](#).

In phase two, the membrane forces in the two side shells carry the load. Simplified calculations can be used to verify the numerical results.

In this example, tearing is assumed to take place at an equivalent strain of 5%. The calculation shows that the vertical elements near the collision point begin to tear at an indentation of 1.5 m. The calculation ends when the longitudinal elements, at the collision point and at an indentation of 2.3 m, begin to tear.

20.7 Conclusions

The progressive collapse of ship hulls, subjected to bending and collision loads, has been studied using the PNM. A new element for modeling stiffened plates has been derived. A transformation between the nodal axis and the neutral axis is used when parts of the modeled structure, in different finite element meshes, are connected. No assumptions are made about the position of the neutral axis for the hull beam when a progressive collapse is analyzed. By using this transformation, the shifting of the neutral axis in the plate elements is also taken into account.

The results obtained from this PNM method have been compared with experimental results and other numerical solutions, which have experienced problems with plate and overall buckling. The comparison appears to be in a good agreement with these simple examples.

The present PNM method has been compared with experiments that deal with the ultimate longitudinal strength of a tanker. Calculations have been performed with and without initial plate imperfections. When disregarding the plate imperfections, the ultimate load is 16% higher.

The calculation of the ultimate longitudinal strength of an existing double hull product tanker is shown. The ratio between the ultimate moment and the plastic moment was compared with an empirical prediction and the results were shown to be in agreement. The result of the analysis is not only the ultimate bending moment but also the ultimate failure mode. A failure in sagging would be the most dramatic.

Finally, the PNM method was used to derive the force–indentation curve for a double-hulled product tanker subjected to a concentrated force in the middle of the side. The force–indentation curve derived by a quasi-static analysis is in agreement with the approximate method.

This work has shown that the PNM, along with the new element, is in agreement with existing approximate methods for hull collapse loads and, moreover, provides much more information about the progressive failure. In this respect, the PNM approaches the general FEM while using a much simpler element mesh that is considered to be more efficient.

A modified Smith method was introduced that computes the ultimate value of the longitudinal bending moment at the midship section using an effective width formula for the plating. The modified Smith method accounts for the manufacturing imperfections, including initial eccentricity of stiffeners, the plating's initial residual stress, and deflection. The corrosion defect was considered as an exponential time function with a random steady corrosion rate, which is assumed to uniformly reduce the plate thickness. Crack propagation was predicted based on the Paris–Erdogen equation. Both the crack initiation time and the coating lifetime were also taken into account.

An equation for estimating the ultimate strength of hull girders was suggested. The hull girders used in the ISSC benchmark calculations by Yao et al. (2000) were used to examine the accuracy of this equation. It has been demonstrated that the equation provides quite reasonable results and may be useful in estimating the bending moment strength.

References

- Andersen, T.L., 1988. Ductile and Brittle Fracture Analysis of Surface Flows Using CTOD. *Experimental Mechanics*, pp. 188–193.
- Bai, Y., Bendiksen, E., Pedersen, P.T., 1993. Collapse analysis of ship hull. *Journal of Marine Structures* 6, 485–507.
- Bai, Y., Pedersen, P.T., 1991. Earthquake response of offshore structures. In: *Proceedings of the 10th Offshore Mechanics and Arctic Engineering Conference, OMAE'91. Part B, Stavanger*, vol. 1, pp. 571–578.

- Bai, Y., Pedersen, P.T., 1993. Elastic-plastic behaviour of offshore steel structures under impact loads. *International Journal of Impact Engineering* 13 (1), 99–115.
- Bai, Y., August 1991. SANDY - A Structural Analysis Program for Static and Dynamic Response of Nonlinear Systems. Theoretical Manual and Demonstration Problem Manual. Version 2. Department of Ocean Engineering, The Technical University of Denmark.
- Bai, Y., 2001. Pipelines and Risers. Elsevier Science Ocean Engineering Book Series.
- Bathe, L., 1982. Finite Element Procedures in Engineering Analysis. Prentice-Hall, Englewood Cliffs, NJ, 200–210.
- Bendiksen, E., 1992. Hull Girder Collapse (Ph.D. dissertation). Department of Naval Architecture and Offshore Engineering, The Technical University of Denmark.
- Bergan, P.G., Soreide, T.H., 1978. Solution of large displacement and instability problems using the current stiffness parameter. In: Bergan, P.G., et al. (Eds.), *Finite Elements in Nonlinear Mechanics*. Tapir, pp. 647–699.
- Burdekin, F.M., Dawes, M.G., May 1971. Practical use of linear elastic and yielding fracture mechanics with particular reference to pressure vessels. In: *Proceedings of the Institute of Mechanical Engineers Conference*, London.
- Caldwell, J.B., 1965. Ultimate longitudinal strength. *Transactions of Royal Institution of Naval Architects* 107, 411–430.
- Carlsen, C.A., 1977. Simplified collapse analysis of stiffened plates. *Norwegian Maritime Research* 5 (4), 20–36.
- Chen, Y.K., Kutt, L.M., Plaszczyk, C.M., Bieniek, M.P., 1983. Ultimate strength of ship structures. *Transactions of the Society of Naval Architects and Marine Engineers* 91, 149–168.
- Faulkner, D., 1975. A review of effective plating for use in the analysis of stiffened plating in bending and compression. *Journal of Ship Research* 19 (1), 1–17.
- Faulkner, D., 1976. Compression test on welded eccentrically stiffened plate panels. In: Dowling, P.J., Harding, J.E., Frieze, P.A. (Eds.), *Steel Plated Structures*. Crosby Lockwood Staples, London.
- Faulkner, D., Sadden, J.A., 1979. Toward a unified approach to ship structural safety. *Transactions of RINA* 121, 1–38.
- Frieze, P.A., Lin, Y.T., 1991. Ship longitudinal strength modeling for reliability analysis. In: *Proc. of the Marine Structural Inspection, Maintenance, and Monitoring Symposium*, p. III.C. SSC/SNAME.
- Ghose, D.J., et al., 1995. Residual Strength of Marine Structures. Ship Structure Committee. SSC-381.
- Guedes Soares, C., Garbatov, Y., 1996. Fatigue reliability of the ship hull girders. *Marine Structures* 9, 495–516.
- Guedes Soares, C., Garbatov, Y., 1999. Reliability of corrosion protected and maintained ship hulls subjected to corrosion and fatigue. *Journal of Ship Research* 43 (2), 65–78.
- Hughes, O., 1983. “Ship Structural Design”, a Rationally Based, Computer Aided, Optimization Approach. John Wiley & Sons, New York, pp. 432–436.
- Ito, H., Kondo, K., Yoshimura, N., Kawashima, M., Yamamoto, S., 1984. A simplified method to analyse the strength of double hulled structures in collision. *Journal of the Society of Naval Architects of Japan* 156, 283–296.
- Kinhead, A.N., 1980. A method for analysing cargo protection afforded by ship structures in collision and its application to an LNG carrier. *Transactions of Royal Institution of Naval Architects* 122, 299–323.
- Mansour, A., Faulkner, D., 1973. On applying the statistical approach to extreme sea loads and ship hull strength. *RINA Transactions* 115, 277–319.
- Mansour, A.E., Thayamballi, A., 1980. Ultimate Strength of a Ship’s Hull Girder Plastic and Buckling Modes. SSC Report-299. Ship Structure Committee.
- Mansour, A., 1997. Assessment of Reliability of Ship Structures. SSC-398. Ship Structures Committee.
- McDermott, J.F., Kline, R.G., Jones, E.J., Maniar, N.M., Chang, W.P., 1974. Tanker structural analysis for minor collisions. *Transactions of the Society of Naval Architects and Marine Engineers* 82, 382–416.

- Nishihara, S., 1984. Ultimate longitudinal strength modeling. *Naval Architecture and Ocean Engineering* (SNAJ Publication) 22, 200–216.
- Paik, J.K., 1990, 1991. Ultimate longitudinal strength-based safety and reliability assessment of ship's hull girder. *Journal of the Society of Naval Architects of Japan* 168, 395–407; 169, 403–416.
- Pedersen, P.T., Jensen, J.J., 1983. *Strength Analysis of Maritime Structures, Part 2 Numerical Methods*. Den Private Ingeniorfond, Copenhagen (in Danish).
- Rahman, M.K., Chowdhury, M., 1996. Estimation of ultimate longitudinal strength of ships and box girders. *Journal of Ship Research* 40, 244–257.
- Rutherford, S.E., Caldwell, J.B., 1990. Ultimate longitudinal Strength of a ship's hull. *Transactions of SNAME* 98, 441–471.
- Smith, C.S., 1975. Compressive strength of welded steel ship grillages. *Transactions of RINA* 117 (1975), 325–359.
- Smith, C.S., October 1977. Influence of local compressive failure on ultimate longitudinal strength of a ship's hull. In: *Proc. of International Symposium on Practical Design in Shipbuilding (PRADS)*. Society of Naval Architects of Japan, Tokyo, pp. 73–79.
- Smith, C.S., 1981. Imperfection effects and design tolerances in ships and offshore structures. *Transactions of Institution of Engineers and Shipbuilders in Scotland* 124 (1981), 37–46.
- Sun, H.H., Bai, Y., 2001. Time-variant reliability of FPSO hulls. *Transactions of the Society of Naval Architects and Marine Engineers* 109.
- Søreide, T.H., 1981. *Ultimate Load Analysis of Marine Structures*. Tapir, Trondheim.
- Ueda, Y., Rashed, S.M.H., Paik, J.K., 1984, 1986. Plates and stiffened plate units of the idealized structural unit method. *Journal of the Society of Naval Architects of Japan* 156, 366–377; 160, 318–336 (in Japanese).
- Ueda, Y., Yao, T., 1982. The plastic node method: a new method of plastic analysis. *Computer Methods in Applied Mechanics and Engineering* 34, 1089–1106.
- Valsgård, S., Pettersen, E., 1982. Simplified nonlinear analysis of ship/ship collisions. *Norwegian Maritime Research* 10 (3), 2–17.
- Valsgård, S., Steen, E., 1991. Ultimate hull girder strength margins in present class requirements. In: *The Marine Structural Inspection, Maintenance and Monitoring Symposium, III B-1–19*. Society of Naval Architects and Marine Engineers, Arlington, VA.
- Vasta, J., 1958. Lessons learned from full-scale structural tests. *Transactions of SNAME* 66, 165–243.
- Van Mater, P.R., Glannotti, J.G., Jones, N., Genalls, P., April 1979. *Critical Evaluation of Low Energy Ship Collision-damage Theories and Design Methodologies*, vol. 11. Ship Structure Committee, Washington. SSC Report-285.
- Viner, A.C., 1986. Development of ship strength formulation. In: *Proc. of Int. Conf. on Advanced in Marine Structures*. Elsevier, pp. 152–173.
- Xu, X.D., Cui, W., et al., 2000. An experimental and theoretical study on ultimate strength of a box girder. *Journal of Ship Mechanics* 4 (5), 36–43.
- Yao, T., Nikolov, P.I., 1991, 1992. Progressive collapse analysis of a ship's hull under longitudinal bending (1st and 2nd reports). *Journal of SNAJ* 171, 449–461; 172, 437–446.
- Yao, T., et al., 2000. Ultimate Hull girder strength. In: *VI.II. Proc.14th. ISSC Special Task Committee*, Nagasaki, Japan.
- Yamamoto, N., 1998. Reliability based criteria for measures to corrosion. In: *Proc.17th OMAE'98*. ASME, New York, USA.

Offshore Structures Under Impact Loads

21.1 General

Large plastic deformations can develop in offshore structures due to severe ship–platform collisions. Such collisions are considered to be a dynamic phenomenon that has costly consequences in terms of the material and the environment and to humans. The dynamic collision response of platforms should be analyzed at the design stage. This precaution ensures that the structure has sufficient strength to withstand an impact and therefore has a low probability of severe collision damage.

Petersen and Pedersen (1981) and Pedersen and Jensen (1991) pointed out that after a minor collision, a considerable amount of the available kinematic energy could be stored as elastic vibration energy in the affected structure. In such cases, the global dynamic load effects can be significant and the structural systems equations of motion, for the striking and the struck structures, should be established and solved. The elastic–plastic deformation modes of the structural system during a collision can be classified as (1) indentation of the striking ship, (2) local indentation of the hit member, and (3) overall deformation of the affected structure. In earlier studies, the response of the affected structure, excluding the hit member, was treated linearly. This analysis approach overlooked the possibility of analyzing and treating the plastic deformation behavior of the affected structure.

Based on Bai and Pedersen (1993), this chapter deals with the dynamic response of the steel offshore structure. A system of equations describing the local as well as the global elastic–plastic behavior of the structural system is derived. These highly nonlinear equations are then solved in the given time domain. In order to derive these equations, a nonlinear force–deformation relation that can model the local indentation of a hit tubular member is calculated. This derivation is based on a linear elastic solution, numerical results from Ueda et al. (1989), and experimental results from Smith (1983) and Ellinas and Walker (1983). Thereafter, a three-dimensional beam-column element that is used to model the global behavior of the affected structure is developed. A large displacement analysis of the beam-column elements is established by combining a linear stiffness matrix, a geometrical stiffness matrix, and a deformation stiffness matrix (Bai and Pedersen, 1991). Furthermore, the effects of plasticity and strain hardening of beam-column elements are taken into account by the plastic node method.

Some basic numerical examples are presented, in order to demonstrate the accuracy and efficiency of the developed beam-column element. Calculated results are compared with numerical results obtained from general-purpose finite element programs, reported experimental results, and a rigid-plastic analysis results. In addition, the dynamic plastic responses of two offshore platforms in typical ship–platform collision situations are analyzed.

21.2 Finite Element Formulation

21.2.1 Equations of Motion

The striking and the affected structure are considered to be one structural system connected by spring elements.

The equations of motion for the structural system are established under the following assumptions:

- The striking ship is treated as a rigid body without volume, and all the deformations in the ship are assumed to take place in a zone around an impact point.
- The deformations in the ship and the local indentation in the affected member of the offshore structure are simulated by using nonlinear spring elements in which only compression forces act. The force–deformation curves for those spring elements are functions of the strain rate.
- The deformation of the affected structure, except for the local indentation in the hit member, is taken into account by using a model of the structure, which is composed of three-dimensional beam-column elements.
- The hydrodynamic forces acting on the ship are accounted for by introducing an added mass concept. Morison’s equation is applied with the purpose of including the fluid–structure interaction to the affected structure’s analysis.

When considering the dynamic equilibrium of the structural system, the equations of motion may be written in an incremental form, such as

$$[M]\{d\ddot{u}\} + [C]\{d\dot{u}\} + [K_T]\{du\} = \{dF_d\} \quad (21.1)$$

where $\{du\}$, $\{d\dot{u}\}$, and $\{d\ddot{u}\}$ are the increments of nodal displacements, velocities, and accelerations, respectively. $[M]$ is a structural mass matrix, $[C]$ is a structural damping matrix, and $[K_T]$ denotes the structural tangent stiffness matrix. The external load vector $\{dF_d\}$ is due to the drag force term in Morison’s equation, which is evaluated using an approach described by [Bai and Pederson \(1991\)](#). The added mass term in Morison’s equation is included in the structural mass matrix $[M]$.

The equation of motion, [Eqn \(21.1\)](#), is solved by using the Newmark- β method.

21.2.2 Load–Displacement Relationship of the Hit Member

In this section, a derivation of a nonlinear spring element will be used to model the local indentation in the hit/affected member. The spring element will be used for steel platforms and the hit/affected members are therefore assumed to be circular thin-walled tubes.

The linear elastic displacement of the load point, for a pinch loaded tubular member, can be determined by

$$\delta_E = 0.1116 \left(\frac{D}{T} \right)^3 \frac{P}{EL_c} \quad (21.2)$$

where P is the force and δ_E denotes the elastic displacement, E is the Young's modulus, and T is the thickness of the tube wall. D denotes the outer diameter of the tube while L_c is the characteristic length of the contact area along the axial direction of the tube.

The characteristic length L_c is a function of the outer diameter, the length of the tube, and the shape of indenture. In order to obtain an empirical equation, linear finite shell element analysis results from [Ueda et al. \(1989\)](#) and indentation tests conducted by [Smith \(1983\)](#) are analyzed. A mean value is found to be

$$L_c = 1.9D \quad (21.3)$$

More experimental or numerical data are necessary to gain a more rational value of the characteristic length L_c .

When the load P is larger than the critical value P_0 , a permanent indentation will take place, and the critical value can be determined using a rigid-plastic analysis for a pinch loaded ring with length L_c . The result obtained is

$$P_0 = 2\sigma_y T^2 L_c / D \quad (21.4)$$

where σ_y is the yield stress of the material.

The permanent indentation δ_P can be calculated using a semiempirical equation. Through energy considerations and curve fitting of experimental data, [Ellinas and Walker \(1983\)](#) obtained

$$\delta_P = D \left(\frac{P}{37.5\sigma_y T^2} \right)^2 \quad (21.5)$$

The unloading linear deformation δ'_E can be obtained by multiplying the linear elastic solution by a coefficient α .

$$\delta'_E = 0.1116\alpha \left(\frac{D}{T} \right)^3 \frac{P}{EL_c} \quad (21.6)$$

The coefficient α will be less than or equal to 1.0, depending on the deformation at the unloading point.

Finally, the local displacement at the load point for a load larger than the P_0 is calculated as

$$\delta = \delta'_E + \delta_P \quad (21.7)$$

21.2.3 Beam-Column Element for Modeling of the Struck Structure

A finite beam-column element, as described in Chapter 26 of this section, is adopted to model the affected structure.

21.2.4 Computational Procedure

The procedure described above has been implemented into the computer program SANDY (Bai, 1991); three types of loads can be applied to the simulated model to obtain the collision analysis of the affected structure.

Impact loads are applied at the node points and/or are spatially distributed over the finite elements. The time variation of these loads is given as input data before initiating a calculation. This type of loading is used in Examples 21.1–21.3.

Dynamic loads applied as initial velocities of a colliding structure initiate the calculation with the simulation of the dynamic motion of the colliding structure. The impact loads between the structures are obtained as the result of the simulation. Once an impact force in a certain direction is detected to be in tension during the simulation, the contact is released. Therefore, the striker is assumed to move as a free body in that direction with a given constant velocity. The criterion for reestablishing a contact is that the displacement of the striker will exceed the displacement of the corresponding point on the affected structure. This type of loading is used in Examples 21.5–21.7.

Dynamic loads applied as initial velocities of the struck/affected structure are usually used only for high-speed impacts. In such cases, the time history of the applied loading is not of interest. The response of the struck/affected structure depends on the time integration of the loads (the momentum of pulse), in other words, the initial velocities of the affected structure.

For large displacement analyses, an updated Lagrangian approach is adopted. At each load step, the element stiffness matrices are reformed in the local coordinate systems and then transformed to the global coordinate system. Here, the global stiffness matrix is assembled, and the increments of nodal displacements, measured in the global coordinate system, are evaluated. Using the element transformation matrix, the increments of element displacements can be calculated, and the element displacements and forces are updated.

The new transformation matrices can then be evaluated and the updated element displacements and forces are transformed to the new local coordinate system and used in the following calculation for the next load step.

During the elastic–plastic analysis, the loading and unloading of nodes are checked carefully. Once loading takes place in a node, a Newton–Raphson iteration is carried out in order to find the exact load increments at which the element nodal forces may come to and subsequently move along the yield surface. At each time step, the structural stiffness matrix is evaluated based on the elastic–plastic status of the element nodes at the end of the previous load increment. However, as soon as the equations of motion are solved, a check is performed to analyze whether unloading of the plastic nodes takes place. If this is the case, the structural stiffness matrix is updated until no further unloading of plastic nodes is detected. Finally, the nodal displacement increments are the solution to the equations of motion after the final iteration. The nodal forces and the elastic–plastic status of elements are updated and the unloading is reevaluated. In addition, when the elastic–plastic status of a node has changed, the unbalanced forces are evaluated and transformed to the global coordinate system. The transformed unbalanced forces are added to the load increments for the next time step.

For further cross sections, there are two corners on the yield surface. The corners are at the points where there are only axial forces acting on the beam element. When the forces at an element node are at such a corner or close to a corner, then the element is treated as a truss element, which is only subjected to an axial force. For such truss elements, unloading is checked, based on the axial forces and the axial displacement increments. Once unloading is detected, the elements are treated as normal three-dimensional beam-column elements.

21.3 Collision Mechanics

21.3.1 Fundamental Principles

The analysis of collision mechanics is generally based on the solution of the differential equations of dynamic equilibrium. The collision force is a function of the relative indentation of the ship and platform. Thus, an incremental solution procedure is required.

The problem is greatly simplified if the collision duration is considerably smaller than the natural period of the governing motion. This assumption is often valid for relevant rigid body motions of floating and articulated platforms. In this case, the solution can be based on a quasi-static solution using the principles of:

- Conservation of momentum
- Conservation of energy

This way, the determination of impact kinematics and energy transfer during collisions can be decoupled from the analysis of strain energy dissipation in colliding objects.

A static solution applies for collisions lasting significantly longer than the natural period of the governing motion.

For jackets at medium water depths, the ratio between the collision duration and the natural period of vibration for leg impacts may be such that significant dynamic effects are involved. This has been investigated to a very small extent. Normally, a static analysis is considered appropriate, but possible dynamic magnifications should also be evaluated.

21.3.2 Conservation of Momentum

In the following sections, the energy to be dissipated as strain energy is determined by considering translational motions only. More accuracy may be obtained by considering more motion components (platform and vessel rotations), and therefore formulating a complex derivation. It is always conservative to use the formulas given in [Section 28.3.3](#).

The conservation of momentum for a central collision between a ship and a platform moving in the same direction is expressed by

$$m_s v_s + m_p v_p = (m_s + m_p) v_c \quad (21.8)$$

where

v_c = Common velocity after impact

v_s = Velocity of ship $v_s > v_p$

v_p = Wave induced velocity of platform

m_s = Mass of ship including added mass

m_p = Mass of platform including added mass.

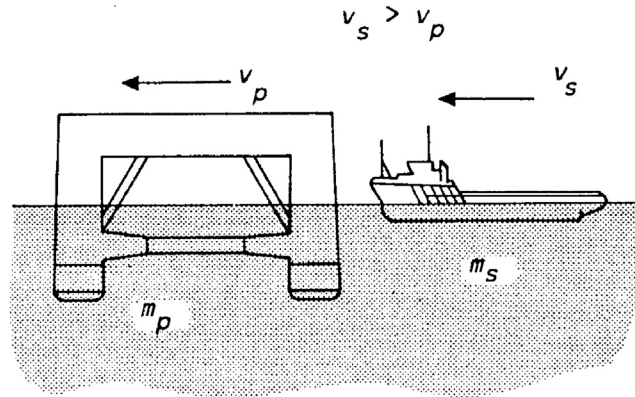
The common velocity is thus defined by ([Figure 21.1](#))

$$v_c = \frac{m_s v_s + m_p v_p}{m_s + m_p} \quad (21.9)$$

21.3.3 Conservation of Energy

In a central collision, all the kinematic energy dissipates as strain energy (elastic or plastic) in the ship (E_s) and the platform (E_p).

In the case of an eccentric collision, some of the kinematic energy will remain as rotational energy of the vessel or the platform after the collision.


Figure 21.1

Collision between supply vessel and semisubmersible platform.

The equation of conservation of energy assuming central collision is given as

$$\frac{1}{2} m_s v_s^2 + \frac{1}{2} m_p v_p^2 = \frac{1}{2} (m_s + m_p) v_c^2 + E_s + E_p \quad (21.10)$$

where

E_s = Strain energy dissipated by the ship

E_p = Strain energy dissipated by the platform.

Combining this equation with the equation for the common velocity, v_c , the following expression for the dissipated strain energy emerges.

$$E_s + E_p = \frac{1}{2} m_s v_s^2 \frac{\left(1 - \frac{v_p}{v_s}\right)^2}{\left(1 + \frac{m_s}{m_p}\right)} \quad (21.11)$$

The wave induced platform motion is often small compared to the ship velocity and can be neglected. Otherwise, the characteristic velocity should be based on a stochastic evaluation of the relative collision velocity between the ship and the platform, $(v_s - v_p)$ accounting for the phase lag between the respective motions (Table 21.1).

Table 21.1: Total strain energy dissipation

Platform Types			
Fixed	Floating	Articulated Column	Jackup ^a
$\frac{1}{2} m_s v_s^2$	$\frac{1}{2} m_s v_s^2 \frac{\left(1 - \frac{v_p}{v_s}\right)^2}{1 + \frac{m_s}{m_p}}$	$\frac{1}{2} m_s v_s^2 \frac{\left(1 - \frac{v_p}{v_s}\right)^2}{1 + \frac{m_s z^2}{J}}$	$\frac{1}{2} m_s v_s^2 \frac{1}{1 + \frac{m_s}{m_p}}$

^aIf the duration of the collision is significantly smaller than the fundamental period of vibration.

where

J = Mass moment of inertia of the column (including added mass) with respect to the effective pivot point.

Z = Distance from the effective pivot point to the point of contact.

21.4 Examples

21.4.1 Mathematical Equations for Impact Forces and Energies in Ship/Platform Collisions

Problem

A derivation of the equations for calculating maximum impact force and impact energy during a collision between a ship and fixed platform (Søreide, 1985) is calculated. The force–deformation relations for the ship and platform may be modeled as linear springs of k_s and k_p , respectively. The ship is assumed to have a weight of m (including added mass) and move at a speed of v , immediately prior to the collision. In deriving the formulation, it is further assumed that the damping effect may be ignored, and the impact mechanics may be expressed as a free vibration, mass–spring system.

Solution

The ship/platform system can be considered as a mass–spring system. The deformations in the ship and platform are denoted as x_s and x_p , respectively. Denoting total deformation as $x = x_s + x_p$, the following is derived from the force equilibrium

$$F = kx = k_s x_s = k_p x_p \quad (21.12)$$

where

$$k = \frac{k_s k_p}{k_s + k_p} = \text{equivalent spring stiffness for the system.}$$

The motion of the mass–spring system may then be expressed as

$$m \frac{d^2 x}{dt^2} + kx = 0 \quad (21.13)$$

Considering the initial conditions (mass moves at velocity v , $x = 0$ when $t = 0$), the solution to the above differential equation is

$$x = v \sqrt{\frac{m}{k}} \sin \omega t \quad (21.14)$$

where the natural frequency is

$$\omega = \sqrt{\frac{k}{m}} \text{ (rad/sec)} \quad (21.15)$$

From Eqn (21.14), the maximum impact force is obtained as

$$F_{\max} = kx_{\max} = v\sqrt{mk} \quad (21.16)$$

and impact duration (the time from the initiation of the impact to the peak impact force) is

$$T_0 = \frac{\pi}{2} \sqrt{\frac{m}{k}} \quad (21.17)$$

The impact duration T_0 is typically 1–2 s (see also Figures 21.6 and 21.7), and it is much longer than the natural frequency of the main member and structure system that were hit. Hence, ship impact is usually handled in a quasi-static way. The time history of the impact force is illustrated in Figures 21.6(e) and 21.7(b). When the impact force is at a maximum, the velocities of the motions for the ship and platform are zero and the deformation energies in the ship and platform are as follows:

$$E_s = \frac{1}{2} k_s x_s^2 = \frac{F_{\max}^2}{2k_s} \quad (21.18)$$

$$E_p = \frac{1}{2} k_p x_p^2 = \frac{F_{\max}^2}{2k_p} \quad (21.19)$$

The maximum impact force expressed in Eqn (21.16) can also be obtained by

$$E_s + E_p = \frac{1}{2} mv^2 \quad (21.20)$$

21.4.2 Basic Numerical Examples

In the following section, a number of simple numerical examples, which serve to demonstrate the accuracy and the efficiency of the developed three-dimensional beam-column elements, will be presented (Bai and Pedersen, 1993).

The first three examples are problems that can be solved assuming small displacements, but the material has kinematic strain hardening. The last example is a clamped beam struck by a mass, which involves both large displacements and strain hardening.

Example 21.1: Fixed Beam under a Central Lateral Impact Load

The dynamic elastic–plastic behavior of a rectangular beam, clamped at both ends, as shown in Figure 21.2(a), is analyzed.

The beam is subjected to a concentrated step load at the midspan, as shown in Figure 21.2(b). Symmetry allows only half of the beam to be modeled. In an analysis using the MARC FEM program, five elements of element type 5 are used and can be seen in Figure 21.2(c). The element is a two-dimensional rectangular section of a beam-column element. In the

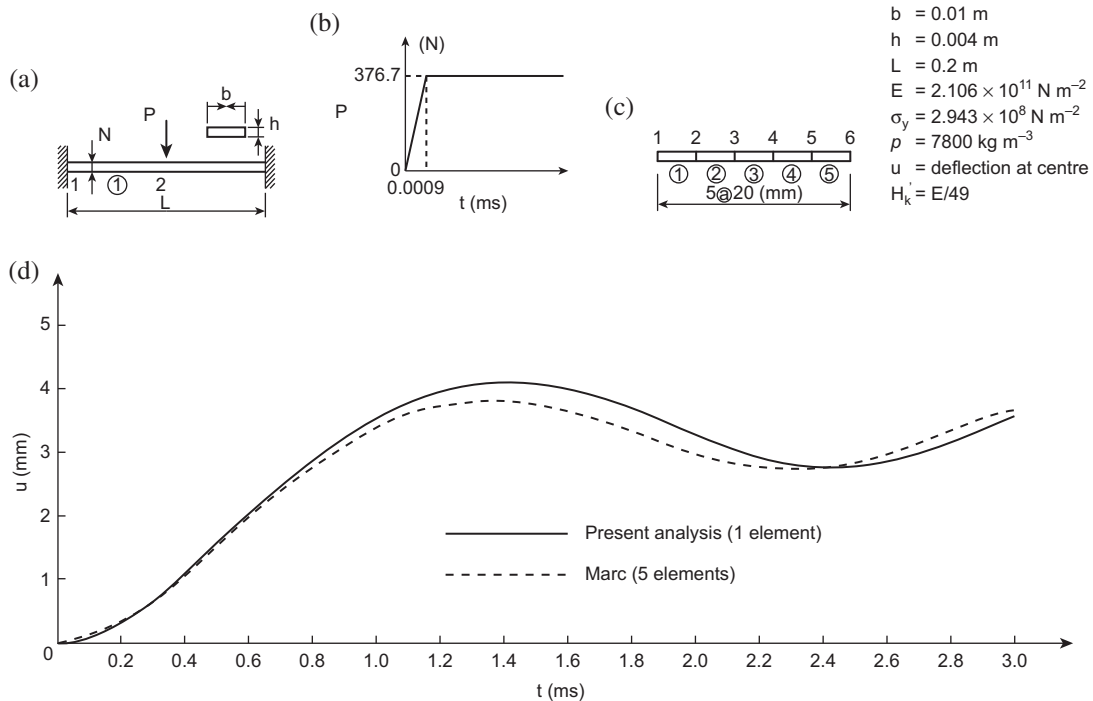


Figure 21.2

Dynamic elastic–plastic behavior of a clamped beam under central lateral impact load. (a) Calculation model. (b) Applied load–time relationship. (c) FE model in MARC analysis. (d) Time history of displacement at impact point.

evaluation of the element stiffness, three Gaussian integration points are chosen along the axial direction of the element. At each Gaussian point, the cross section is divided into 11 Simpson integration points. Only normal stresses are considered in the elastic–plastic analysis. Since this is a small displacement problem, the axial sectional force will always be zero. Therefore, the plastic yield condition used in the present analysis is taken to be

$$M_z/M_{zp} - 1 = 0 \quad (21.21)$$

where m_z is a bending moment and the subscript “ p ” indicates the fully plastic value for the corresponding force component. The time history of the displacement at the impact point is shown in Figure 21.2(d). The solid line depicts the results obtained when using only one element. It is easily observed that even the use of one element is sufficient to obtain reasonably accurate results.

Example 21.2: Rectangular Portal Frame Subjected to Impact Loads

The rectangular portal frame shown in Figure 21.3(a) is subjected to concentrated pulse loads as shown in Figure 21.3(b).

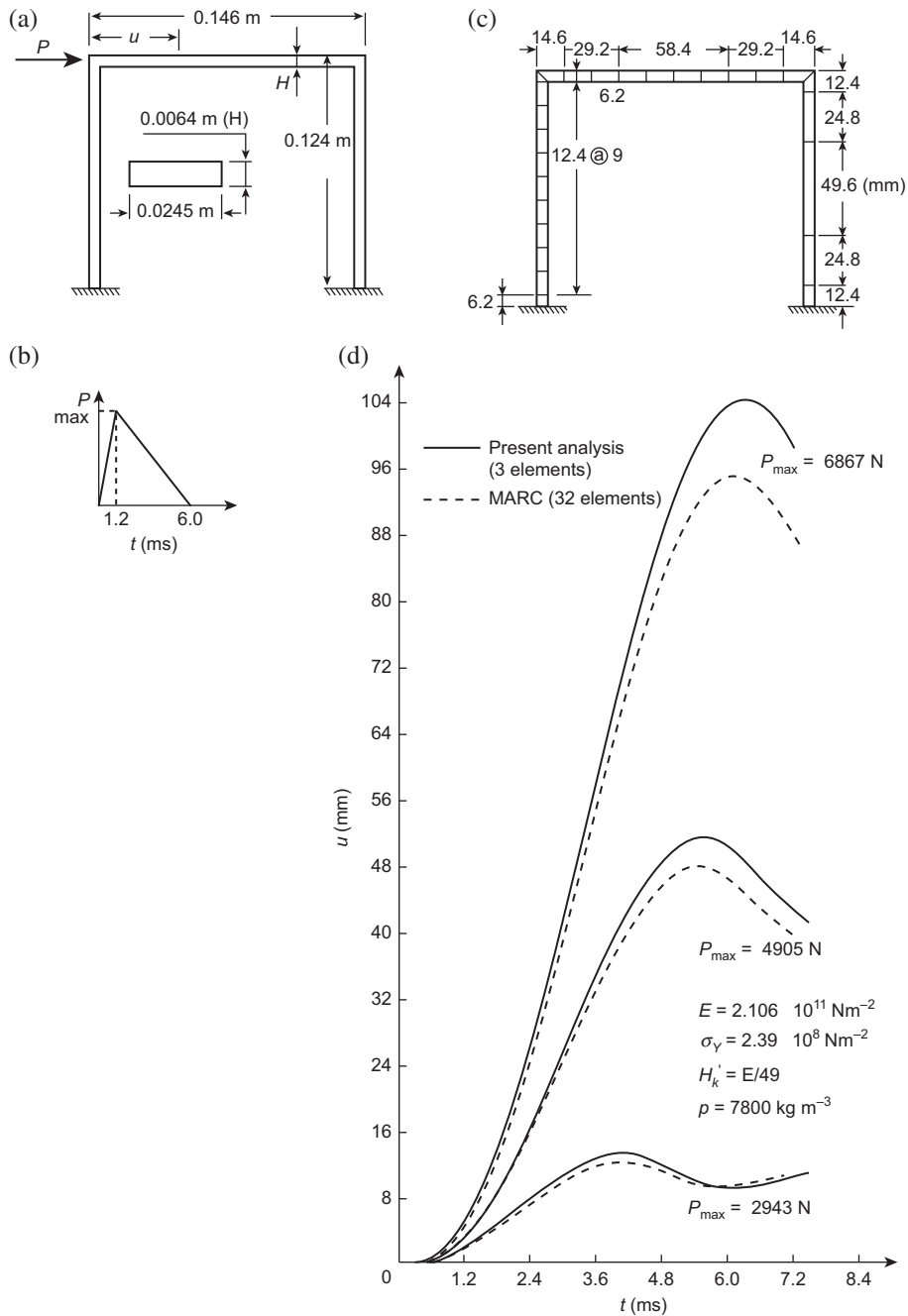


Figure 21.3

Dynamic elastic–plastic behavior of portal frame subjected to impact loads. (a) A 2D frame. (b) Applied impact load. (c) FE model in MARC analysis. (d) Time history of displacement at impact point.

In a MARC FEM analysis, the frame is modeled using 32 elements (element type 16), as shown in Figure 21.3(c). The element is a curved, two-dimensional, rectangular, cross-sectional beam-column element. Integration points for the evaluation of the element stiffness are the same as in Example 21.1. Only normal stresses due to axial forces and bending moments are considered in the plastic analysis.

The plastic yield condition used in the present analysis is taken as

$$\left(M_z/M_{zp}\right)^2 + F_x/F_{xp} - 1 = 0 \quad (21.22)$$

where f_x is an axial force.

The time history of the displacements, located at the impact points along the load direction, is plotted in Figure 21.3(d). Again, it is observed that the present method is quite accurate when using only one element for each structural member.

Example 21.3: Tubular Space Frame under Impact Load

The tubular space frame shown in Figure 21.4(a) is subjected to a step load as illustrated in Figure 21.4(b).

In a MARC FEM analysis, element type 14 is used and each structural member is discretized by 10 elements, as shown in Figure 21.4(c). The element is a three-dimensional thin-walled tubular beam-column. There are three Gaussian points, which are further divided into 16 Simpson integration points along the circumferential direction. Plasticity is taken into account at these integration points by applying the Von Mises's yield condition and taking into account, the stresses due to axial forces, two bending moments, and torsional moments. Therefore, the plastic yield condition used in the present analysis is taken to be

$$\left(M_x/M_{xp}\right)^2 + \left(M_y/M_{yp}\right)^2 + \left(M_z/M_{zp}\right)^2 + \sin\left(\frac{\pi}{2}\left(F_x/F_{xp}\right)\right) - 1 = 0 \quad (21.23)$$

where M_x is the sectional torsional moment and M_y and M_z are the bending moments.

The time history of the impact displacement is presented in Figure 21.4(d).

Example 21.4: Clamped Aluminum Alloy Beam Struck Transversely by a Mass

The clamped beam, shown in Figure 21.5(a), was studied by Yu and Jones (1989), in which they used the ABAQUS FEM program. In their analysis, eight-node isoparametric plane stress elements were used. The finite element mesh consists of 75 elements and 279 nodes. The mesh near the impact point and the supports were made finer in order to obtain more detailed information. A true stress/true strain relationship of the material is shown in Figure 21.5(b). The time variations of the maximum transverse deflection are shown in Figure 21.5(c). The experimental results conducted by Liu and Jones as

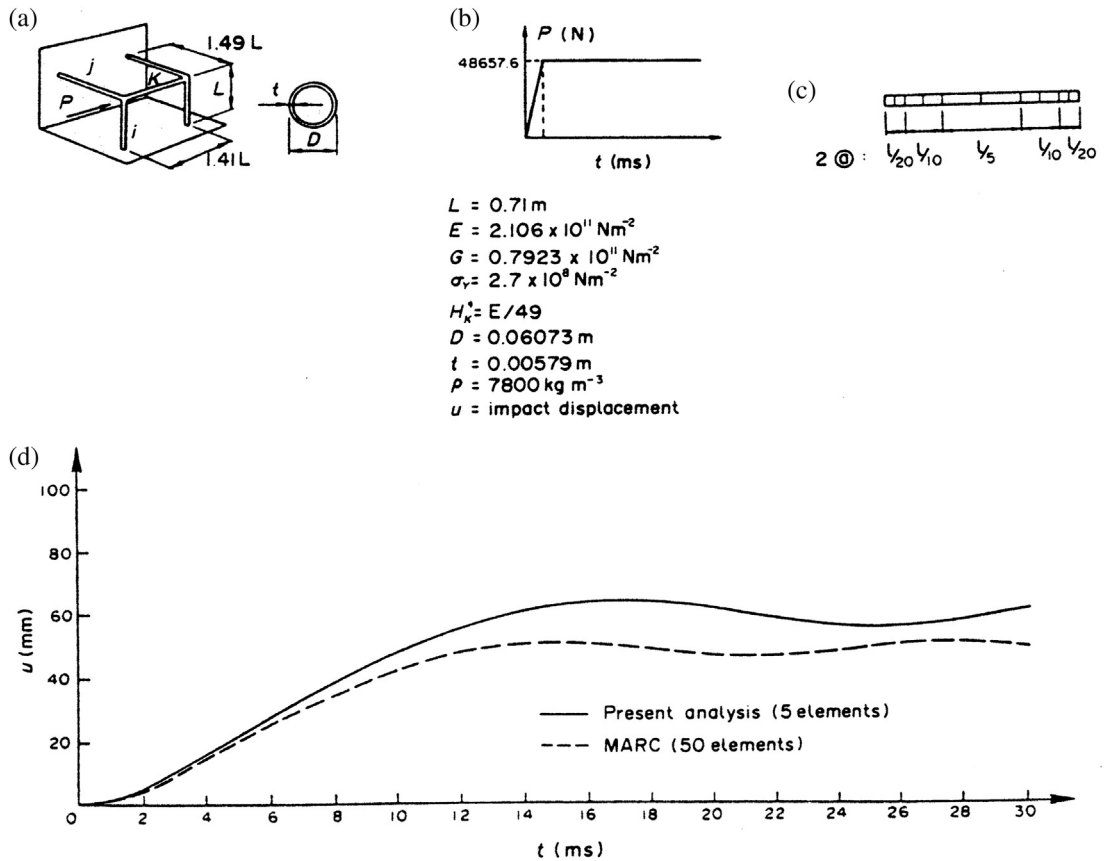


Figure 21.4

Dynamic elastic-plastic behavior of space frame under impact load. (a) Calculation model. (b) Applied load-time relationship. (c) FE model in MARC analysis. (d) Time history of displacement at impact point.

described by [Yu and Jones \(1989\)](#) are also plotted in this figure. The associated time histories of the dimensionless bending moment M_z/M_{zp} and axial force F_x/F_p are shown in [Figure 21.5\(d\) and \(e\)](#).

The plastic yield condition used in this example is the same as in Example 21.2.

The ABAQUS FEM analysis employs the true stress/true strain curve, shown in [Figure 21.5\(b\)](#). This analysis assumes that the material has linear kinematic strain hardening and each side of the beam is modeled as one element. [Figure 21.5\(c–e\)](#) shows that the structural response is sensitive to the yield stress. However, the agreement between the results predicted by both programs is good.

The examples presented in this section demonstrated that the nodal displacements and forces predicted by the actual beam-column element agree with those obtained by

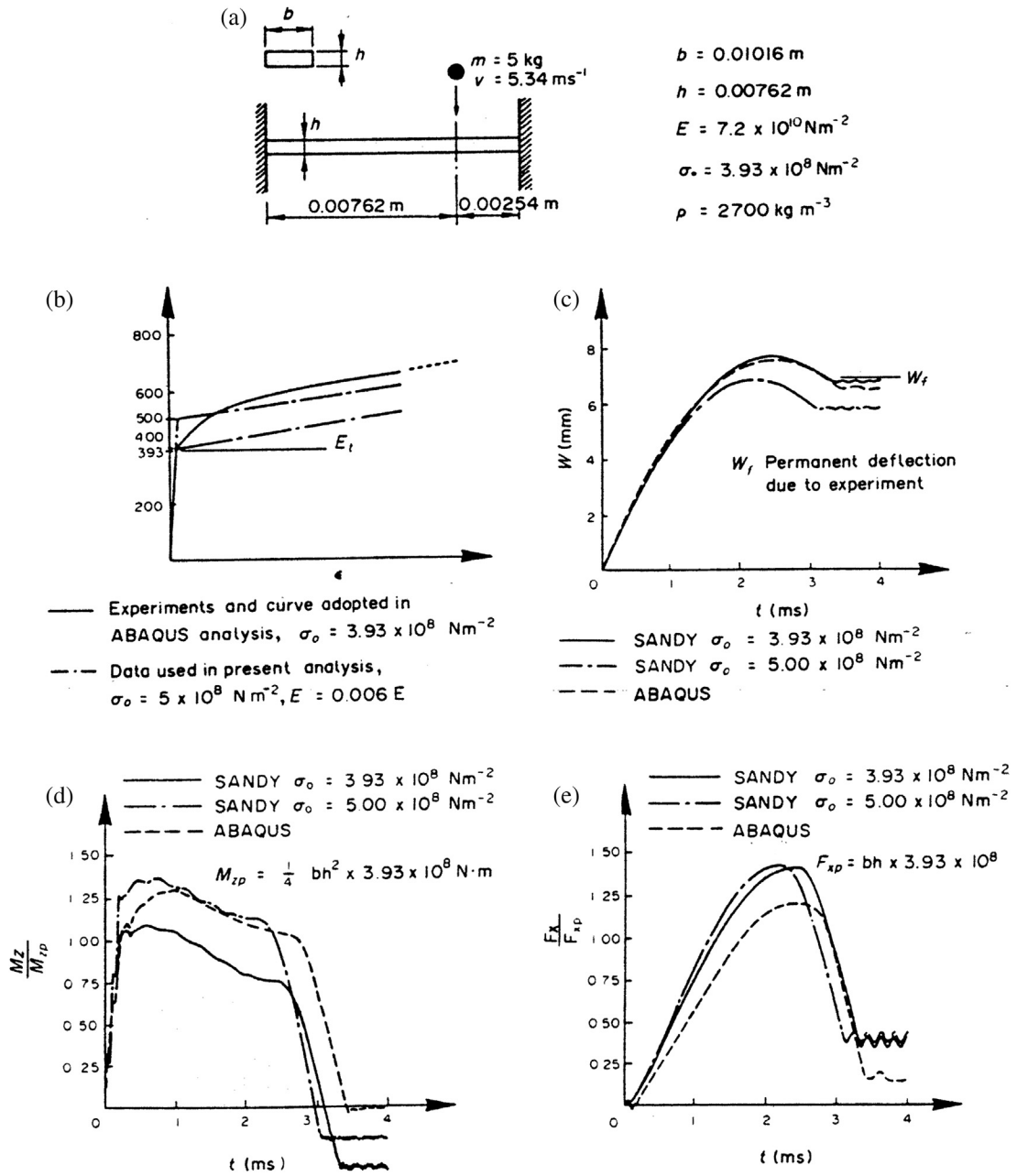


Figure 21.5

Dynamic elastic–plastic behavior of a clamped beam struck by mass. (a) A clamped beam struck by a mass. (b) True stress–true strain relationship. (c) Time histories of deflection at the impact point. (d) Time histories of bending moment at impact point. (e) Time histories of axial force at the impact point.

experiments and by general finite element program analyses. Reasonable results can be obtained by the beam-column elements, even if the structural member is discretized by an absolute minimum number of elements allowed (normally one element per member).

21.4.3 Application to Practical Collision Problems

The procedure implemented in the SANDY program can be used to simulate many different ship collision problems, such as side central collisions, bow collisions, and stern collisions against structures such as offshore platforms and ridges. The simulation results include motion (displacements), velocities/accelerations of the striking and the struck structures, indentation in the striking ship and the hit member, impact forces, member forces, base shear and overturning moments for the affected structures, kinetic energy, and elastic/plastic deformation energy of the striking and the affected structures.

In this section three typical ship collision problems are selected. These include ship—unmanned, platform, and ship—jacket platform collisions.

Example 21.5: Unmanned platform struck by a supply ship

The small unmanned platform is considered first. It can be seen in [Figure 21.6\(a\)](#), and is assumed to have been hit by a 5000-ton supply vessel. The dominant design criterion for this platform type is often ship collisions, while for traditional platforms it is normally wave loadings. The supply ship is supported to drift sideways with a speed 2.0 ms^{-1} under calm sea conditions. The added mass for the sideways ship sway motion is taken to be 0.5 times that of the ship mass. The force—indentation relationship for the ship is taken as is shown in [Figure 21.6\(b\)](#). The added mass is included following Morison's equation and the added mass and drag coefficients are taken to be 1.0. The tubes under the water surface are assumed to be filled with water. Therefore, the mass due to the entrapped water is also included. The force—indentation relationship is established using [Eqns \(21.2\) and \(21.7\)](#), and by following further approximations such as multilinear lines, which can be seen in [Figure 21.6\(c\)](#). The soil—structure interaction is taken into account using linear springs.

First, a linear analysis was carried out by means of a load vector given by the gravity loading on the structures. Then, a dynamic analysis is completed, which considers large displacements, plasticity, and hardening effects. The plastic yield condition is as follows:

$$\left(M_z/M_{zp}\right)^2 + \sin^2\left[\frac{\pi}{2}\left(F_x/F_{xp}\right)\right] - 1 = 0 \quad (21.24)$$

It is noted that the indentation in the hit tube will reduce the load carrying capacity of the tube greatly. This effect has not been taken into account in the present analysis. However, a possible procedure is suggested by [Yao et al. \(1988\)](#), which would account for the indentation effect, and would reduce the plastic yield capacity of the element nodes at the impact point.

The numerical results are shown in Figure 21.6(d–e). The effect of strain hardening in these figures is indicated; when the strain hardening is included, the structure becomes stiffer and more energy is absorbed by the ship. Therefore, the deck displacement is smaller, and the collision force and overturning moment increase.

Example 21.6: Jacket platform struck by a supply ship

The four-legged steel jacket platform, which can be seen in Figure 21.7(a), was struck by a 4590-ton supply ship. Both the platform and the ship are existent structures. The ship is supposed to surge into the platform with the velocities 0.5, 2, and 6 ms^{-1} , corresponding to the operation impact, accidental impact, and passing vessel collision, respectively.

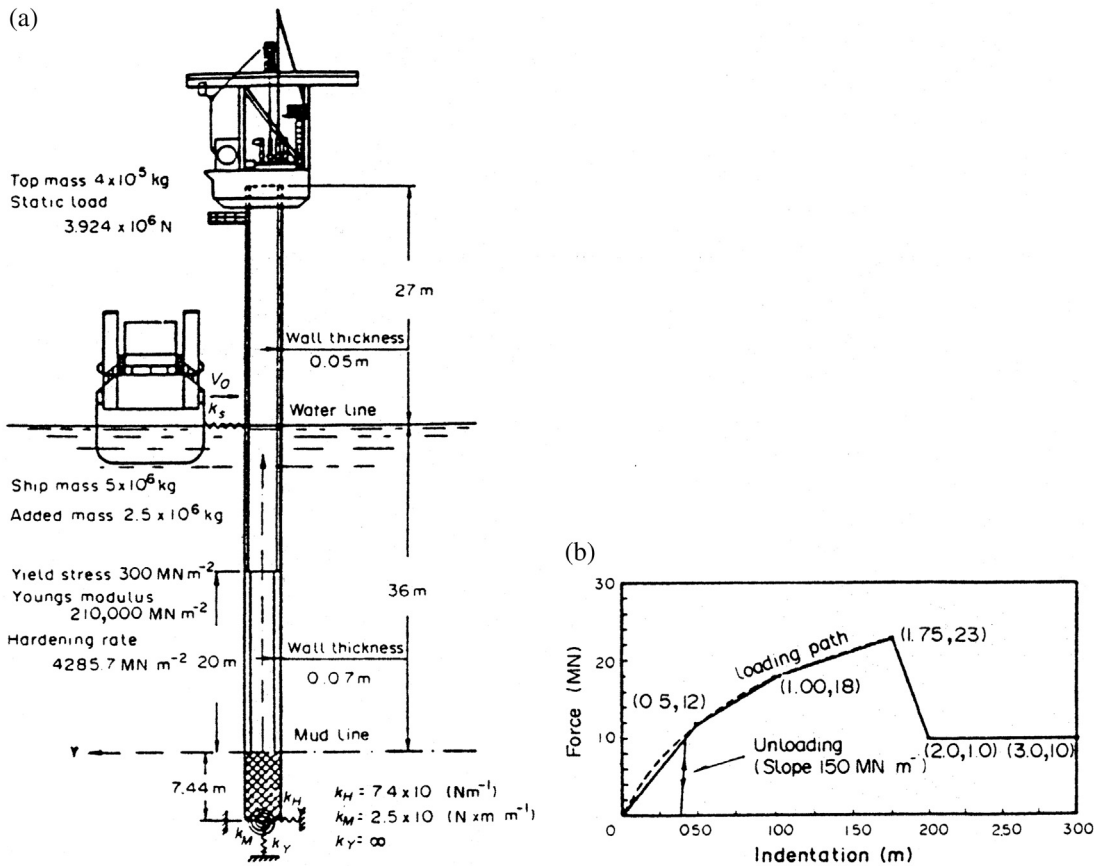


Figure 21.6

Response caused by collision between supply ship and unmanned platform. (a) Ship–platform collision. (b) Local load–indentation relationship for the ship side (continued overleaf). (c) Local force–indentation relationship for the hit tube. (d) Deck displacement time history of the platform. (e) Impact force time history. (f) Overturning moment time history of the platform.

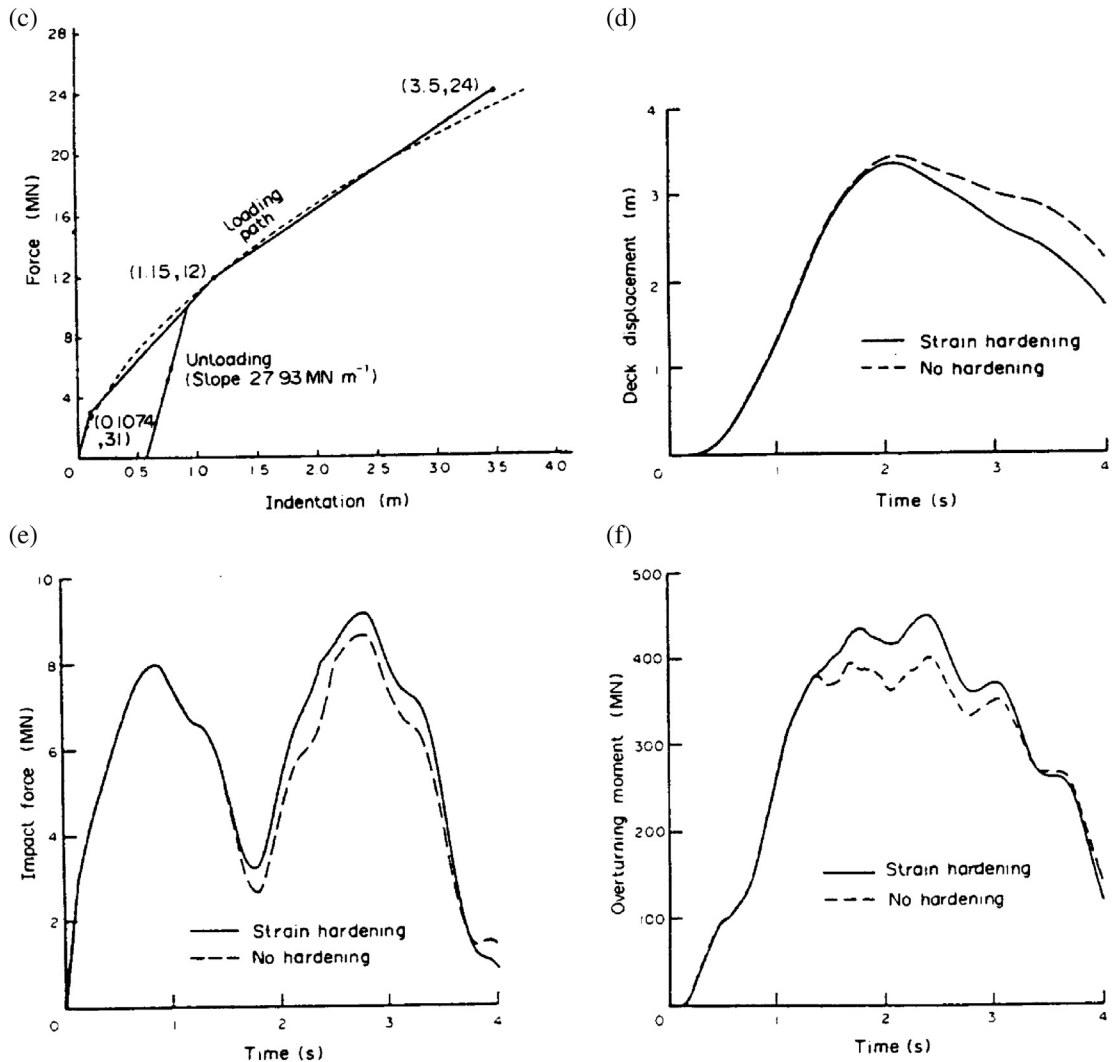


Figure 21.6
cont'd

The force-indentation relationship for the ship bow is obtained using axial crushing elements, in which a mean crushing force applied by a rigid-plastic theory has been adopted. The local indentation curve for the tubular member, which was hit, in the jacket platform is established using Eqns (21.2) and (21.7). Both indentation curves are further approximated as multilinear curves. First, linear static analysis is carried out for the gravity loading, and then a nonlinear dynamic analysis is performed, which includes fluid-structure interaction, soil-structure interaction, large displacements, and plasticity and kinematic strain-hardening effects for the affected platform.

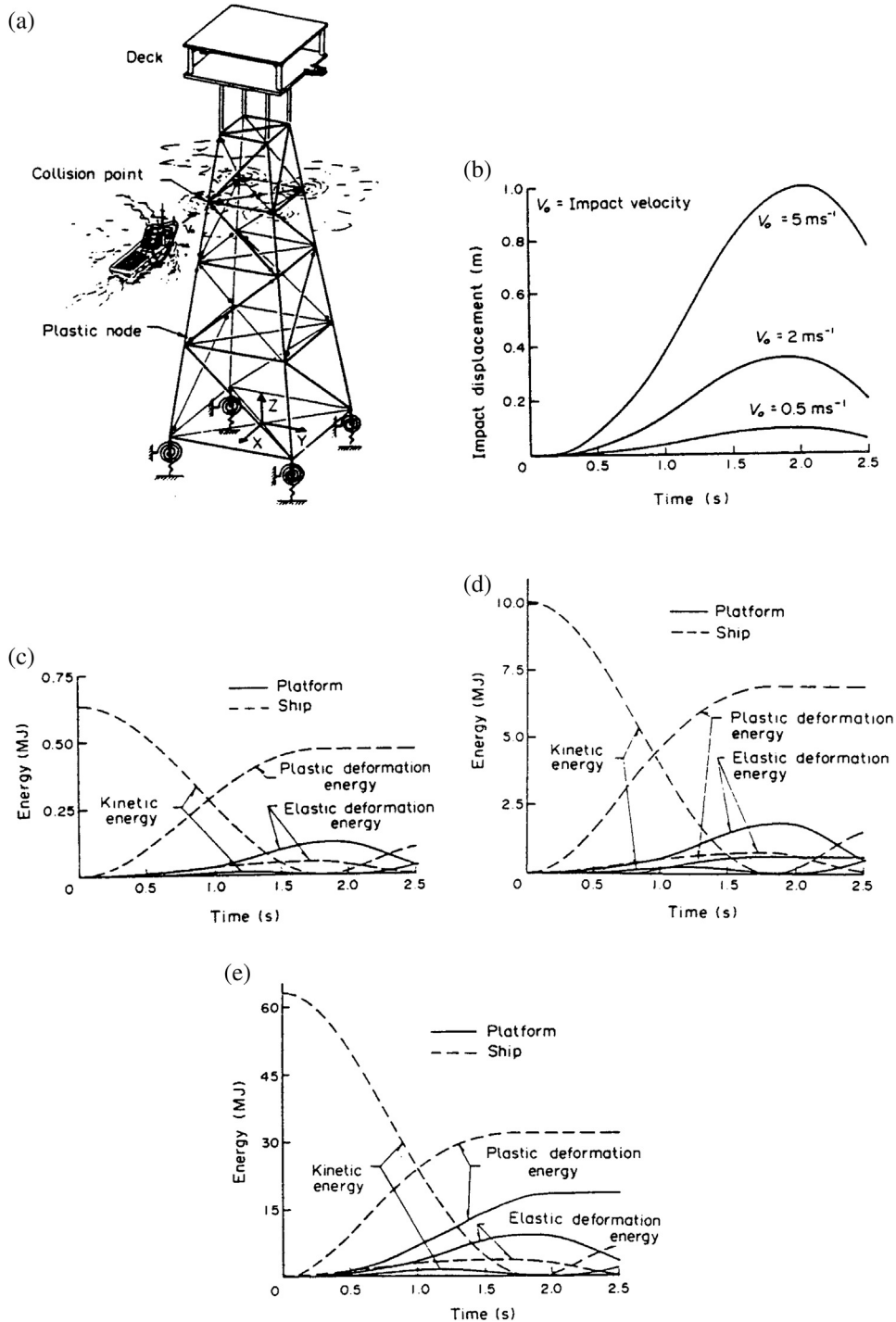


Figure 21.7

Response caused by collision between supply ship and jacket platform. (a) Jacket platform struck by supply ship, showing distribution of plastic nodes (ship velocity, $v_0 = 5 \text{ ms}^{-1}$, time, 1.45 s). (b) Impact displacement time histories of the platform. (c) Time history of energies during ship impact on jacket platform (impact velocity, $V_0 = 0.5 \text{ ms}^{-1}$). (d) Time history of energies during ship impact on jacket platform (impact velocity, $V_0 = 2 \text{ ms}^{-1}$). (e) Time history of energies during ship impact on jacket platform (impact velocity, $V_0 = 5 \text{ ms}^{-1}$).

Table 21.2: Main results of ship–jacket platform collisions

Impact Velocity (ms^{-1})	Impact Energy (MJ)	Impact Force (MN)	Dent in Ship (m)	Local Dent in Platform (m)
0.5	0.631	2.116	0.437	0
2.0	10.1	8.194	1.69	0.083
5.0	63.1	18.88	3.40	0.616

The time history of the impact deflections is shown in [Figure 21.7\(b\)](#). [Figure 21.7\(c–e\)](#) shows how the energy is shifted between the ship and the platform, and among kinetic energy, elastic deformation energy, and plastic deformation energy.

Using the present procedure, the following can be obtained: impact forces, dent in ship, and local dent depth of the hit member, provided that the impact velocity and indentation curve of the ship are known. The main results of the example are listed in [Table 21.2](#).

Finally, the distribution of the plastic nodes for an impact velocity of 5 ms^{-1} at time 1.45 s is shown in [Figure 21.7\(a\)](#).

21.5 Conclusions

A consistent procedure has been presented for collision analysis. A nonlinear force–displacement relationship has been derived for the determination of the local indentation of the hit member, and a three-dimensional beam-column element has been developed for the modeling of the damaged structure. The elastic large displacement analysis theory and the plastic node method have been combined in order to describe the effects of large deformation, plasticity, and strain hardening of the beam-column members.

The accuracy and efficiency of the beam-column elements have been examined through simple numerical examples. This was done by comparing the present results with those obtained by experiments and the finite element program analyses using the MARC and ABAQUS programs. It is shown that the present beam-column elements are able to accurately model the dynamic plastic behavior of frame structures, by using the absolute minimum number of elements per the structural member.

In addition, examples, where the dynamic elastic–plastic behaviors of offshore platforms and bridges in typical collision situations are calculated, have been presented.

All examples show that strain hardening plays an important role in the impact response of the struck or affected structure. The strain hardening results in both smaller deformations and more energy that will be absorbed by the striking structure. Therefore, the impact force is larger. Thus, a rational collision analysis should take the strain hardening effect into account.

References

- Bai, Y., 1991. SANDY-A Structural Analysis Program for Static and Dynamic Response of Nonlinear Systems. User's Manual, Version 2. Department of Ocean Engineering, The Technical University of Denmark.
- Bai, Y., Pedersen, P.T., 1991. Earthquake response of offshore structure. In: Proc. 10th Int. Conf. on Offshore Mechanics Arctic Engineering, OMAE'91, June.
- Bai, Y., Pedersen, P.T., 1993. Elastic-plastic behavior of offshore steel structures under impact loads. *International Journal of Impact Engineering* 13 (1), 99–117.
- Ellinas, C.P., Walker, A.C., 1983. Damage of offshore tubular bracing members. In: Proc. IABSE Colloquium on Ship Collision with Bridges and Offshore Structures, Copenhagen, pp. 253–261.
- Petersen, M.J., Pedersen, P.T., 1981. Collisions between ships and offshore platforms. In: Proc. 13th Annual Offshore Technology Conference, OTC 4134.
- Pedersen, P.T., Jensen, J.J., May 1991. Ship Impact Analysis for Bottom Supported Offshore Structures. In: Smith, Dow (Eds.), Second Int. Conf. on Advances in Marine Structures, Dunfermline, Scotland, May 1991. Elsevier, Amsterdam, pp. 276–297.
- Smith, C.S., 1983. Assessment of damage in offshore steel platform. In: Proc. Int. Conf. on Marine Safety, Paper 15.
- Sørøide, T.H., 1985. Ultimate Load Analysis of Marine Structures. Tapir, Trondheim, Norway.
- Ueda, Y., Murakawa, H., Xiang, D., 1989. Classification of dynamic response of a tubular beam under collision. In: Proc. 8th Int. Conf. on Offshore Mechanics and Arctic Engineering, vol. 2, pp. 645–652.
- Yao, T., Taby, J., Moan, T., 1988. Ultimate strength and post-ultimate strength behaviour of damaged tubular members in offshore structures. *Journal of Offshore Mechanics and Arctic Engineering*, ASMA 110, 254–262.
- Yu, J., Jones, N., 1989. Numerical simulation of a clamped beam under impact loading. *Computer & Structures* 32 (2), 281–293.

Offshore Structures Under Earthquake Loads

22.1 General

Bottom-supported offshore structures in seismic areas may be subjected to intensive ground shaking that causes structures to undergo large deformations well into the plastic range. Previous research in this area has mainly resulted in procedures that have sought solutions in the frequency plane (Penzien, 1976). The present chapter is devoted to time-domain solutions that allow the development of plastic deformations that can be examined in detail.

The basic dynamics of earthquake action on structures has been discussed in Clough and Penzien (1975) and Chopra (1995). There have been extensive investigations on earthquake response of building structures in the time domain (Powell, 1973).

Unfortunately, most works have been limited to plane frames. Furthermore, for offshore structures, hydrodynamic loads have to be taken into account and the geometric nonlinearities become more important than in building structures. Therefore, there is the need for a procedure to predict earthquake responses of offshore structures that includes both geometric and material nonlinearities.

Methods for analysis of frame structures including geometric nonlinearities have been based on either the finite element approach (Nedergaard and Pedersen, 1986) or the beam-column approach (Yao et al., 1986). Nedergaard and Pedersen (1986) derived a deformation stiffness matrix for beam-column elements. This matrix is a function of element deformations and incorporates coupling between axial and lateral deformations. It is used together with linear and the geometric stiffness matrices.

Material nonlinearity can be taken into account in an efficient and accurate way by use of the plastic node method (Ueda and Yao, 1982). Using ordinary finite elements, the plastic deformation of the elements is concentrated to the nodes in a mechanism similar to plastic hinges. Applying the plastic flow theory, the elastic-plastic stiffness matrices are derived without numerical integration.

In this chapter, a procedure based on the finite element and plastic node methods is proposed for earthquake response analysis of three-dimensional frames with geometric and

material nonlinearities. Using the proposed procedure, the earthquake response of a jacket platform is investigated. Part of this chapter appeared in [Bai and Terndrup Pedersen \(1991\)](#). The new extension outlines earthquake designs of fixed platforms based on American Petroleum Institute (API) RP2A.

22.2 Earthquake Design per API RP2A

[API RP2A \(1991\)](#) applies in general to all fixed platform types. Most of the recommendations, however, are typical for pile steel jacket platforms. The principles and procedures given in [API \(1991\)](#) are summarized below. The design philosophy for earthquake leads in [API \(1991\)](#) is illustrated in [Table 22.1](#).

The API's seismic design recommendations are based upon a two-level design approach that includes:

- **Strength requirements:** the platform is designed for a severe earthquake having a reasonable likelihood of not being exceeded during a platform life with a typical return period of hundreds of years, known as a strength-level earthquake (SLE).
- **Ductility requirements:** the platform is then checked for a rare earthquake having a very low probability of occurrence during a typical return period of thousands of years, known as a ductility-level earthquake (DLE).

The objective of the strength requirements is to prevent a significant interruption of normal platform operations after exposure to a relatively severe earthquake. A response spectrum method of the time history approach is normally applied.

The objective of the ductility requirements is to ensure that the platform has adequate capacity to prevent total collapse under a rare intense earthquake. Member damage such as inelastic member yielding and member buckling is allowed to occur, but the structure's foundation system should be ductile under severe earthquakes, such that it absorbs the imposed energy. The energy absorbed by the foundation is expected to mostly dissipate through the nonlinear behavior of the soil.

Table 22.1: Earthquake design philosophy, API RP2A

	Strength-Level Earthquake (SLE)	Ductility-Level Earthquake (DLE)
Philosophy	Prevent interruption of normal platform operations	Prevent loss of life and maintain well control
Design	Ground shaking that has a reasonable likelihood of not being exceeded during the platform life	Rare intense ground shaking that is unlikely to occur during the platform life
Performance	No significant structural damage, essentially elastic response	No collapse, although structural damage is allowed; inelastic response

For some typical jacket structures, both the strength and ductility required by the API are considered satisfied if the below-listed provisions are implemented in the strength design of said platforms:

- Strength requirements for SLE loads are generally documented.
- Strength requirements are documented for jacket legs, including enclosed piles, using two times the SLE loads (i.e., $2 * \text{SLE}$).
- Rare, intense earthquake ground motion is less than two times the earthquake ground motion applied for documentation of strength level requirements (i.e., $\text{DLE} < 2 * \text{SLE}$).
- Geometric and ultimate strength requirements for primary members and their connections as given by API are satisfied. These requirements are concerned with the number of legs, jacket foundation system, diagonal bracing configuration in vertical frames, horizontal members, slenderness and diameter/thickness ratio of diagonal bracing, and tubular joint capacities.

22.3 Equations and Motion

22.3.1 Equation of Motion

The equations of motion for a nonlinear offshore structure subjected to an earthquake loading can be expressed as

$$[M]\{d\ddot{U}\} + [C]\{d\dot{U}\} + [K_T]\{dU\} = -[M]\{d\ddot{U}_g\} + \{dX_e\} \quad (22.1)$$

where $\{dU\}$, $\{d\dot{U}\}$, and $\{d\ddot{U}\}$ are the increments of nodal displacement, velocity, and acceleration, respectively, relative to the ground. The structural mass matrix is represented by $[M]$, while $[C]$ is the structural damping matrix, $[K_T]$ denotes the structural tangent stiffness matrix, and $\{dX_e\}$ are increments of the hydrodynamic load. The ground acceleration vector $\{\ddot{U}_g\}$ is formed as an assembly of three-dimensional ground motions.

It can be assumed that at the time of the earthquake, there is no wind, wave, or current loading on the structure. According to the Morison equation (Sarpkaya and Isaacson, 1981), the hydrodynamic load per unit length along a tubular beam member can be evaluated as

$$\{f_M\} = -\rho C_A A \{\ddot{u}_n\} - \frac{1}{2} \rho C_D D |\{\dot{u}_n\}| \{\dot{u}_n\} \quad (22.2)$$

where ρ is the mass density of the surrounding water, D is the beam diameter, C_A is an added mass coefficient, C_D is the drag coefficient, $A = \pi D^2/4$, and $\{\dot{u}_n\}$ denotes the normal components of the absolute velocity vector. The absolute velocity vector is

$$\{\dot{u}_a\} = \{\dot{u}\} + \{\dot{u}_g\} \quad (22.3)$$

Using a standard lumping technique, Eqn (22.1) can be rewritten as

$$([M] + [M_a])\{d\ddot{U}\} + [C]\{d\dot{U}\} + [K_T]\{dU\} = -([M] + [M_a])\{d\ddot{U}_g\} + \{dF_D\} \quad (22.4)$$

where $[M_a]$ is an added mass matrix containing the added mass terms of Eqn (22.2). The increments of drag force terms from time (t) to $(t + dt)$ are evaluated as

$$\{dF_D\} = \sum [T_{t+dt}]^T \{f_D\}_{(t+dt)} - \sum [T_t]^T \{f_D\}_{(t)} \quad (22.5)$$

where \sum denotes summation along all members in the water, while $\{f_D\}$ are the results of integration of the drag force terms of Eqn (22.2) along the member. The transformation matrix is represented by $[T_t]$. The equations from motion Eqn (22.4) are solved by the Newmark- β method (Newmark, 1959).

22.3.2 Nonlinear Finite Element Model

The finite element model was given in Part II, Chapter 18.

22.3.3 Analysis Procedure

The design of offshore structures for earthquake resistance should consider the operational and safety requirements of critical piping, equipment, and other important components. These dual criteria are usually provided for by designing a structure where deformations are within acceptable levels and satisfy a set of yield or buckling criteria for the maximum expected level of the earthquake ground motion. Therefore, nonlinear dynamic analysis is necessary.

Some features of the present analytical procedure are:

- An acceleration record such as El Centro N–S is scaled by a scale factor to match the probable earthquake in the areas where the structure will be installed.
- A frame model is established by three-dimensional finite elements. Soil–structure interaction is taken into account by the use of spring elements.
- Fluid–structure interaction is induced. The contribution from the added mass is taken into account by an increase of the mass of the beam-column elements. The drag forces are treated as external loads.
- A linear static analysis is performed for a structure subjected to gravity loading. The results are used as an initial condition for the subsequent dynamic analysis.
- The structure mass matrix may consist of both masses applied directly at the nodes, and element masses that are evaluated using either a lumped-mass or a consistent-mass method.

Geometric and material nonlinearities are taken into account by use of the theory described in the preceding chapters.

Time history, maximum and minimum values of displacements, and forces are all presented as calculation results. From these results, structural integrity against earthquakes is assessed.

The procedure has been implemented in the computer program SANDY (Bai, 1990) and used in several analyses.

22.4 Numerical Examples

22.4.1 Example 22.1: Clamped Beam under Lateral Load

This example (see Figure 22.1) is chosen to show the efficiency of the present procedure. In the present analysis, only one beam-column element is used to model half of the beam. The linear and geometric stiffness matrices as well as the deformation matrix are used. The plastic yield condition used for the rectangular cross section is taken as

$$M_z/M_{zp} + (F_x/F_{xp})^2 - 1 = 0 \quad (22.6)$$

where the subscript “*p*” indicates fully plastic values for each stress component.

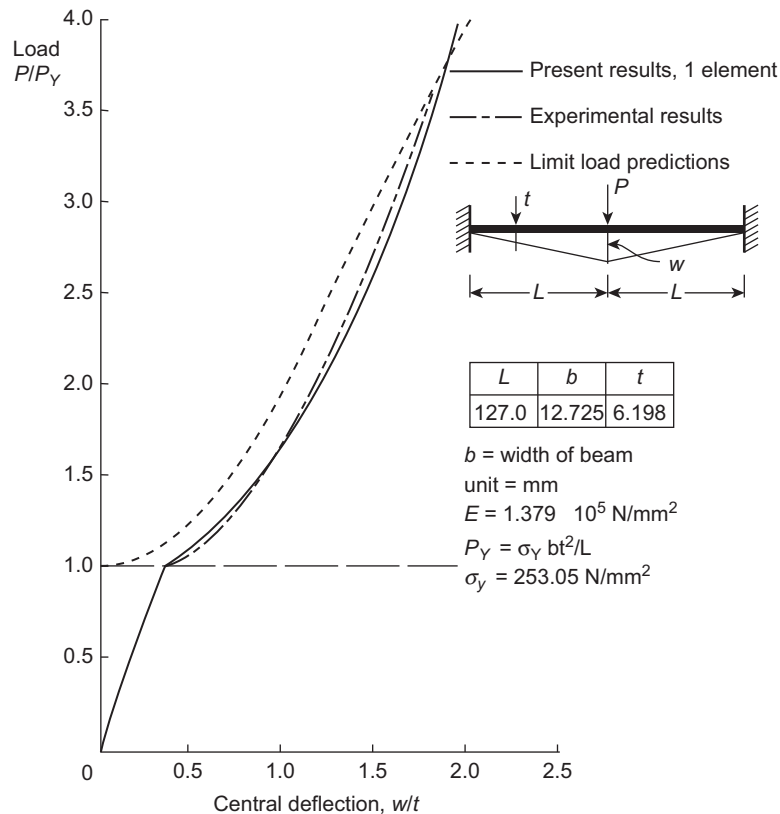


Figure 22.1

Elastic-plastic large-displacement analysis of a clamped beam under central load.

Figure 22.1 shows that the present results agree with experimental and limit load theory results (Haythornthwaite, 1957). The limit load is P_y when geometric nonlinearity is not taken into account.

22.4.2 Example 22.2: Two-Dimensional Frame Subjected to Earthquake Loading

The 10-story three-bay frame shown in Figure 22.2 has been taken from the user's guide of DRAIN-2D, which is a well-known nonlinear earthquake response analysis program for plane structures (Kannan and Powell, 1973). Using the static load shown in Figure 22.3, a linear static analysis is performed. The results are used as the initial conditions for the dynamic analysis. The frame has been analyzed for the first 7 s of the El Centro 1940 N-S record, and scaled by a factor of 1.57 to give a peak ground acceleration of 0.5 g. The mass lumped at the nodes is based on the dead load of the structure. The damping matrix is determined as $[C] = 0.3[M]$. The frame is modeled by using one element per

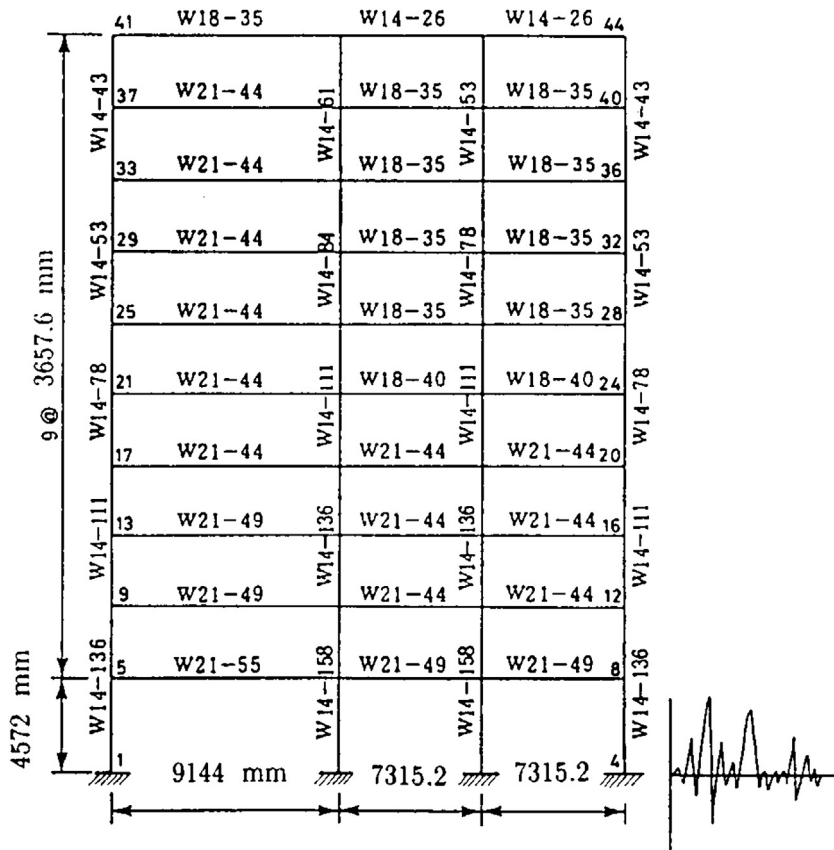


Figure 22.2
Two-dimensional frame subjected to earthquake loading.

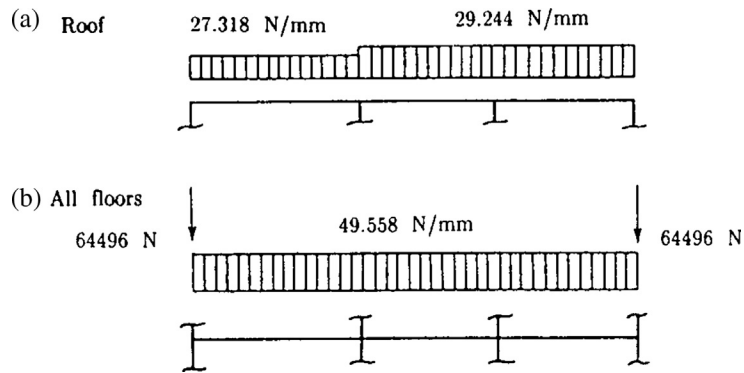


Figure 22.3

Lumped masses and static loads applied on the 2-D frame.

physical member. Horizontal nodal displacements at each floor are constrained to be identical. In the analysis, geometric nonlinearity is not taken into account. The plastic yield condition for the i steel beam is assumed as

$$M_z/M_{zp} + 1.66(F_x/F_{xp})^2 - 1 = 0 \quad (22.7)$$

Typical results are shown in [Figure 22.4](#), together with those predicted by DRAIN-2D. The two programs are also in good agreement.

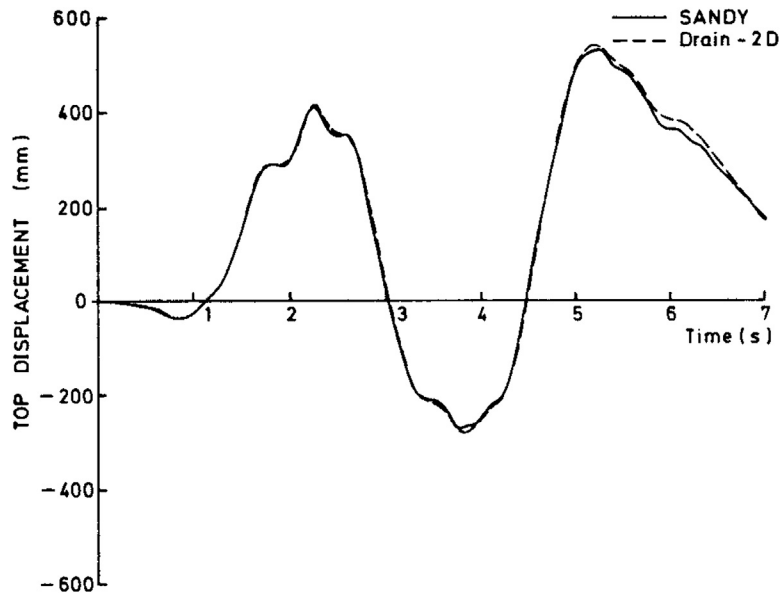


Figure 22.4

Time history of roof displacement for the 2-D frame.

22.4.3 Example 22.3: Offshore Jacket Platform Subjected to Earthquake Loading

The four-legged steel jacket platform shown in Figure 22.5 is an already existing structure. It is subjected to a horizontal earthquake loading. The applied ground acceleration time history is again the first 7 s of El Centro N–S, along with amplification factors. A linear static analysis is carried out using the dead load applied on the deck. Fluid–structure interaction, soil–structure interaction, and geometric and material nonlinearities are taken into account. Each structural member is modeled as only one beam-column element. The plastic yield condition used for thin-walled circular tubes is expressed as

$$\begin{aligned} & (M_x/M_{xp})^2 + (M_y/M_{yp})^2 + (M_z/M_{zp})^2 \\ & + \sin^2 \left\{ \frac{\pi}{2} \left[(F_x/F_{xp})^2 + (F_y/F_{yp})^2 + (F_z/F_{zp})^2 \right]^{1/2} \right\} - 1 = 0 \end{aligned} \quad (22.8)$$

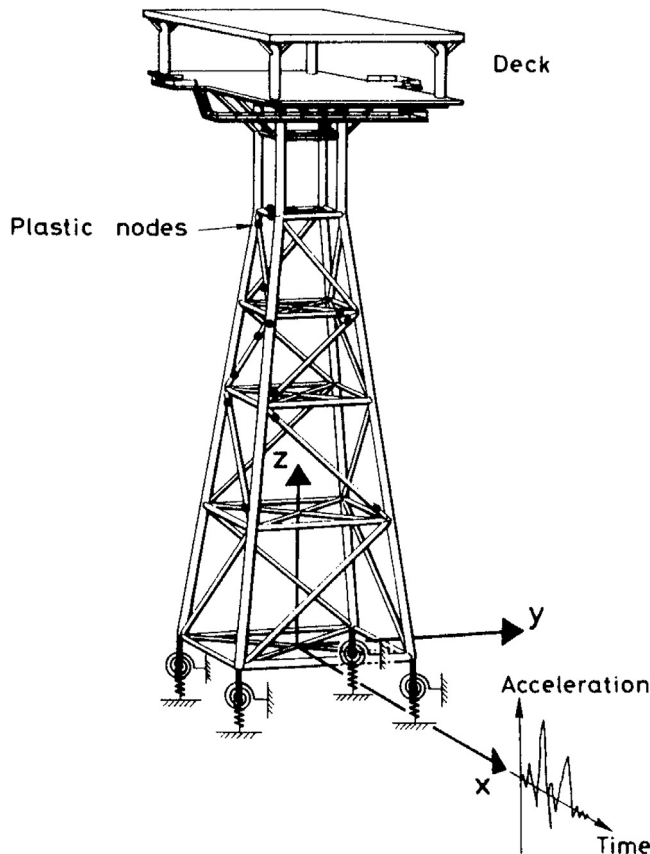


Figure 22.5

Offshore jacket platform subjected to earthquake loading showing distribution of plastic nodes (earthquake scale factor 4.5, time 3.0 s).

The effects of earthquake acceleration amplification factors are shown in [Figure 22.6](#). Plastic nodes have been observed when the amplification is greater than 2.25. The distribution of plastic nodes at time 3.00 s for a scale factor of 4.5 is shown in [Figure 22.5](#). The structure undergoes large deformations as well as plasticity when subjected to intensive ground shaking.

[Figure 22.7](#) shows time histories of the lateral displacements at the deck of the platform in the x-direction for a scale factor of 3. It is observed that in this example, the hydrodynamic damping effect associated with drag forces can be ignored.

[Figure 22.8](#) presents foundation stiffness effects on the time histories of the lateral displacements. The vibration period and maximum displacement increases greatly as soil stiffness decreases. No plastic node has been observed when soil stiffness has been scaled by a factor of 0.1. This figure also shows the importance of modeling the soil–structure interaction with reasonable accuracy. The maximum value of the lateral displacement will be very large and cause problems for the piping system and equipment on the deck.

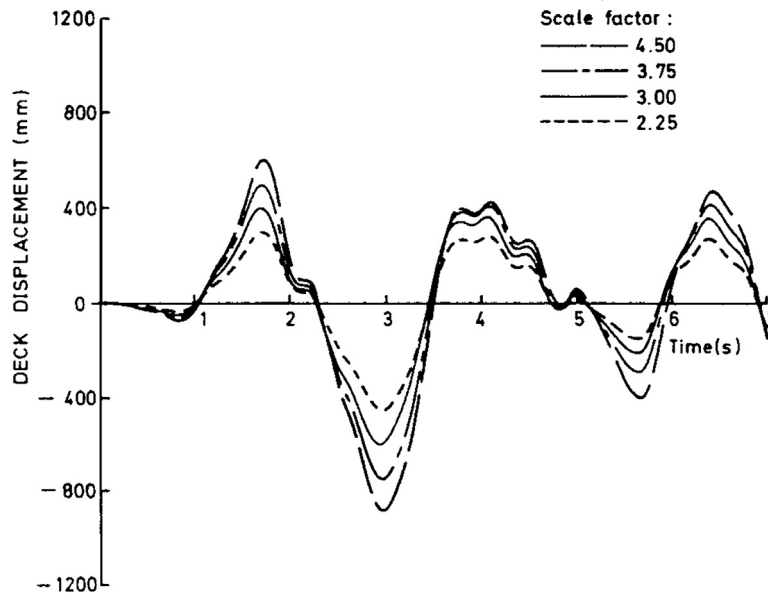


Figure 22.6
Effects of earthquake acceleration scale factors.

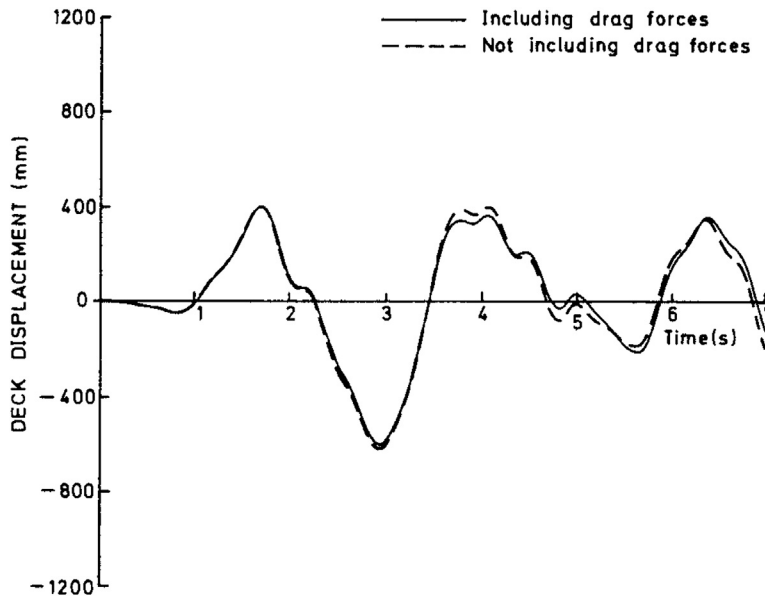


Figure 22.7

Hydrodynamic damping effect associated with drag forces (earthquake acceleration scale factor 3.0).

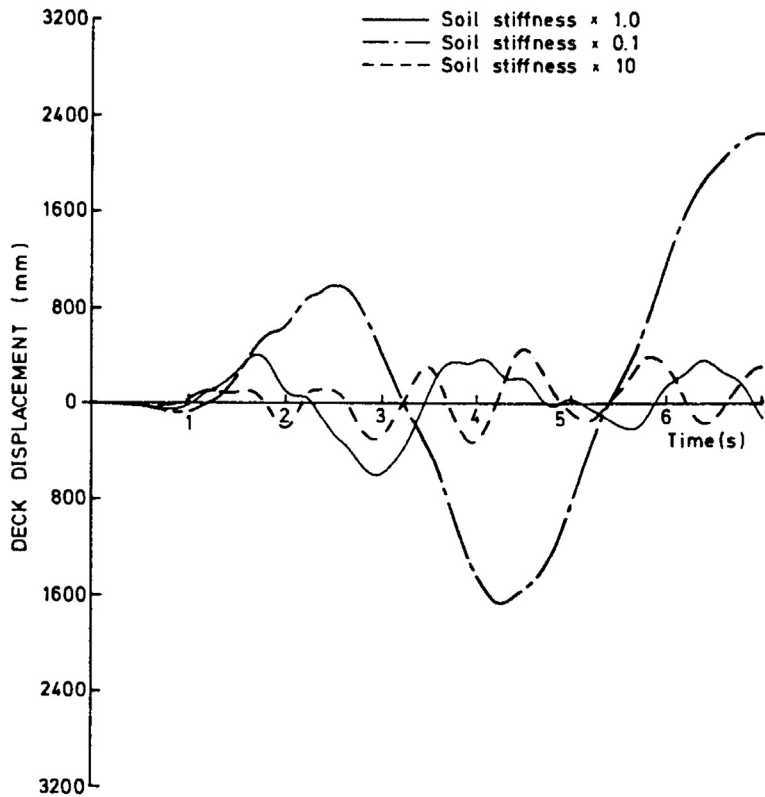


Figure 22.8

Foundation stiffness effects (earthquake acceleration scale factor 3.0).

22.5 Conclusions

A procedure for earthquake response analysis of three-dimensional frames with geometric and material nonlinearities has been presented. A deformation stiffness matrix $[k_D]$ and an internal force vector $\{r\}$ have been derived. This matrix incorporates the coupling between axial and lateral deformations of the elements. In conjunction with the plastic node method, the proposed approach enables accurate modeling of frames using only one element per physical member. Element stiffness matrices are evaluated without the numerical integration usually required by traditional finite element methods.

The numerical examples show that the procedure is efficient and accurate. In addition, the time to prepare input data is low. It can also be applied to nonlinear dynamic response analysis of offshore structures under collision loads.

From Example 22.3, the following results have been observed:

- In an analysis of a structure subjected to a strong earthquake loading, it is important to take both geometric and material nonlinearities into account.
- The hydrodynamic damping effects associated with drag forces are small.
- The foundation stiffness effects are very significant, and it is important to accurately model soil–structure interaction.

References

- API, August 1, 1991. Recommendations for Planning, Designing and Constructing Fixed Offshore Platforms. API Recommended Practice 2A (RP 2A), nineteenth ed. American Petroleum Institute.
- Bai, Y., 1990. SANDY-A Structural Analysis Program for Static and Dynamic Response of Nonlinear Systems. Theoretical Manual. User's Manual and Demonstration Problem Manual. Century Research Center Corporation, Japan.
- Bai, Y., Terndrup Pedersen, P., 1991. Earthquake response of offshore structures. In: Proc. 10th Int. Conf. on Offshore Mechanics Arctic Engineering, OMAE '91, June.
- Chopra, A.K., 1995. Dynamics of Structures, Theory and Applications to Earthquake Engineering. Prentice-Hall, Inc.
- Clough, R.W., Penzien, J., 1975. Dynamics of Structures. McGraw-Hill.
- Haythornthwaite, R.M., 1957. Beams with full end fixity. Engineering 183, 110–112.
- Kannan, A.E., Powell, G.H., 1973. DRAIN-2D – A General Purpose Computer Program for Dynamic Response of Inelastic Plane Structures. User's Guide, Report No. EERC 73-6. University of California, Berkeley.
- Nedergaard, H., Pedersen, P.T., 1986. Analysis procedure for space frames with material and geometrical nonlinearities. In: Bergan, B., Wunderlich (Eds.), Europe-us Symposium – Finite Element Methods for Nonlinear Problems. Springer, pp. 211–230.
- Newmark, N.M., 1959. A method of computation for structural dynamics. Journal of Engineering Mechanics Division, ASCE 85, 67–94.
- Penzien, J., 1976. Seismic analysis of gravity platforms including soil-structure interaction effects. In: Offshore Technology Conference (OTC), Paper No. 2674.

- Sarpkaya, T., Isaacson, M., 1981. *Mechanics of Wave Forces on Offshore Structures*. Van Nostrand Reinhold Company.
- Ueda, Y., Yao, T., 1982. The plastic node method: a new method of plastic analysis. *Computer Methods in Applied Mechanics and Engineering* 34, 1089–1104.
- Yao, T., Fujikubo, M., Bai, Y., Nawata, T., Tamemiro, M., 1986. Local buckling of bracing members in semi-submersible drilling unit (1st report). *Journal of the Society of Naval Architects of Japan* 160, 359–371 (in Japanese).

Ship Collision and Grounding

23.1 Introduction

When collision or grounding happens, a ship's hull suffers a great load in a short time. It is a nonlinear dynamic response process including material, geometric, and contact nonlinearities. Aspects that need to be examined include fatalities, cargo spills, damage stability, residual strength, and economic and social impacts. The research of ship collision and grounding includes many uncertain factors such as environmental conditions, collision or grounding properties, and strength. With decades of data, the research approach for ship collision and grounding can be divided into five methods: analytical; numerical simulation; empirical formula; experimental research; and risk analysis, which has been developed in recent years. The analytical and numerical simulation methods are older than the others. Because of a lack of accident data, the accuracy of the empirical formula method is limited. Because of similar uncertainty rates, only the local part of the ship, or the single member, can be used in the experimental research method, thus hindering scalability. The risk analysis method unites probability and statistical methods with the damage mechanism concerning the probability of and results from accidents.

Collision and grounding at sea may cause serious problems for ships, the environment, and human life. To understand the consequences of ship collision and grounding, the following aspects need to be researched:

- Oil outflow
- Damage stability
- Ship evacuation
- Residual strength
- Postaccidental loads
- Other consequences include but are not limited to fire following an accident, blocked traffic, and leakage of liquid natural gas.

To reduce the risks of ship collision and grounding accidents, ship operations need to be improved to reduce the likelihood of accidents. Specifically, the arrangement of cargo tanks, and structural crashworthiness, must be improved. Once an accident happens, emergency response and life systems play important parts.

23.1.1 Collision and Grounding Design Standards

There are no universally accepted design standards for collision and grounding. Principles are based on design objectives. Germanischer Lloyd has a class notation, COLL, that ranks collision resistance. The American Bureau of Shipping has a class notation for safehull vessels. It demonstrates the adequate residual hull girder following collision or grounding accidents. The International Association of Classification Societies has developed a series of unified requirements for bulk carriers under flooded conditions. Though flooded conditions have not been defined, some requirements are against accidents like collision and grounding.

Ship designs usually consider four accident limit states: serviceability, ultimate, fatigue, and accidental. Different loading scenarios can be created depending on the nature of different accident types ranging from fires, explosions, and blasts to collisions and groundings. Based on the different objectives to be met such as safety, environmental, and property parameters, the accidental limit state can be established.

23.2 Mechanics of Ship Collision and Grounding

Minorsky's famous formula relates absorbed energy to destroyed material volume. It has been widely used in the past 40 years. The mechanics involved in ship collision and grounding accidents are classified as internal and external. Internal mechanics calculate a ship's structural failure response. A ship's rigid-body global motion under the forces of collision, grounding, and hydrodynamic pressures is calculated using external mechanics.

23.2.1 Internal Mechanics

There are four methods for analyzing internal mechanics: simple formulae, simplified analytical, simplified finite element model (FEM), and nonlinear FEM simulation.

The simple formulae method involves the least computation among the methods. Recent studies include head-on collision by Zhang et al., grounding by Zhang, Pedersen, and Zhang, and ship-to-bridge collision by Pedersen et al.; in addition, Wang and Yi have presented many formulae. The accuracy of results for initial energy absorption is acceptable, but not suited for loads and stresses. The simplified analytical method has advanced in the last 20 years, and its applications were summarized by Wang et al. It captures the basic characteristics of structural crashworthiness without much modeling effort. Besides energy absorption, it is suited for load simulations.

Simplified FEM has been used by Paik et al. in 1999, but is not yet widely used. Nonlinear FEM simulation has been widely developed in recent years as computer technology and software capacity have improved. Nonlinear FEM simulation has become

a preferred choice over other methods. By using this method, more complex situations involving high nonlinearity, friction, and contact can be considered, and the result is quite accurate, something that other typical methods are unable to achieve. FEM packages include DYNA3D, DYTRAN, and PAMCRASH.

23.2.2 External Mechanics

The widely used method in external mechanics is simplified methodology.

Matusiak made a full six-degrees-of-freedom simulation for ship motions in ship collision and grounding accidents. For external mechanics, the problem lies in how to model the contact force between struck and striking ships. One solution is to run a nonlinear FEM analysis first in order to determine the contact force. Then, loads are applied to the ship motion analysis.

Full-scale experiments were carried out in the Netherlands. Later, 37 laboratory tests were performed to study the motions of colliding ships and interactions with water. Five parameters—collision velocity, collision angle, location, mass ratio of two ships, and bulbous bow—were studied to find their effects on motions.

23.3 Ship Collision Research

Factors related to ship collision are

1. the property of the collision: collision with a rigid body, offshore platforms, or another ship;
2. the strength of the collision: speed, displacement, bow ship, draft, and relative azimuth of the colliding ship;
3. the condition of the struck ship: displacement, draft, speed, and relative azimuth;
4. environmental conditions: wind, waves, and current;
5. the capacity of the ship's structure to bear the collision.

Generally, a collision involves two objects: either a struck ship and a colliding object, or two ships striking each other. According to the centerline and relative location of the colliding ship, as well as the velocity vector of the object, a collision can be defined as either a head-on or a side collision; structural response depends greatly on relative position.

23.3.1 Ship—Ship Collision Research

Many researchers have done significant research in this area, including Pedersen, Samuelides, Frieze, and Zhang. Based on the general theory of rigid-body collision

mechanics, Pedersen and Zhang have completed research on the external mechanics of ship collision and put forward a kind of analysis method that can calculate energy conversion and impulse changes. The method gives that the amount of the energy loss during a collision is determined by the mass of the colliding ship, collision speed, collision position, collision angle, etc.

$$\begin{aligned}\Delta E &= \frac{1}{2}(1 + C_{a1})m_1(V_r)^2 - \frac{1}{2}[(1 + C_{a1})m_1 + (1 + C_{a2})m_2] \cdot V^2 \\ &= \frac{1}{2} \cdot \frac{(1 + C_{a1})(1 + C_{a2})m_1m_2}{(1 + C_{a1})m_1 + (1 + C_{a2})m_2}(V_r)^2\end{aligned}\quad (23.1)$$

During research on the influence of the size of a ship to the distribution of the damage in a ship after collision, Pedersen and Zhang found that the damage on the side of the ship would be smaller if the struck ship were larger.

During research on the internal mechanics of ship collision, Paik et al. (1999) separated the damage mechanism of the ship bow and ship side. His method assumes that during the analysis of one collision part, the other part is rigid (Figures 23.1 and 23.2).

Wang and Ohtsuo gave a set of formulae about the failure mode of the plate, which were used to analyze ship side collision and grounding. Wang and others have done a group of tests concerning the internal mechanics of the deformation mode and energy absorption for double-hull ships during collision or grounding. Hysin and Scharrer have successfully completed a series of calculations of ship roll-on—roll-off with a simplified method, and predicted the collision force, collision depth curve, absorbed energy—collision depth curve, and size of the damage area in the ship's side.

Paik made the finite element analysis program ALPS/SCOL, which was used to calculate the side structure response of the struck ship under the collision of the rigid ship bow. The program chooses the technology of the nonlinear element, which can reduce the amount of time and modeling work.

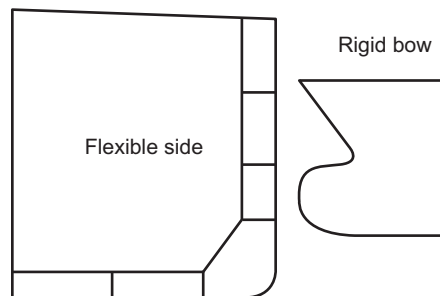


Figure 23.1

Analysis for damage of the ship's side structure.

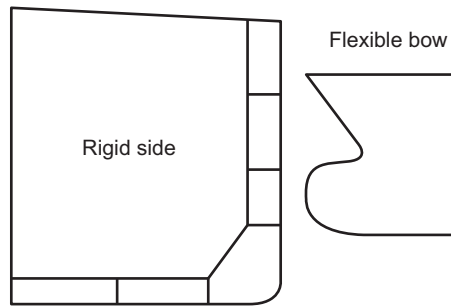


Figure 23.2
Analysis for damage of the ship's bow.

The SIMCOL program, introduced by Brown, can be used to analyze the internal and external dynamics of the collision in the time domain. The DAMAGE program introduced by Simonsen can be used to analyze the ship structure under collision, and has accounted for deformation of the ship bow since version 5.0. The DTU model program developed by Pedersen and Zhang can be used to analyze the external dynamics of the ship collision.

Figure 23.3 shows the procedure for the potential loss of property (PLP) calculation in ship–ship collision cases (Youssef et al., 2014a). PLP is defined as the product of the collision frequency and the corresponding economic consequence of each individual scenario. It can represent the asset risk associated with accidents. First, a targeted structure is identified in terms of its principal particulars and structural design characteristics. Then, FEMs for both the struck and the striking ship are established. In the models, the element type, mesh size, structural material model, failure mode, and surrounding water effects are identified. Explicit collision simulations are conducted using nonlinear FEM to calculate

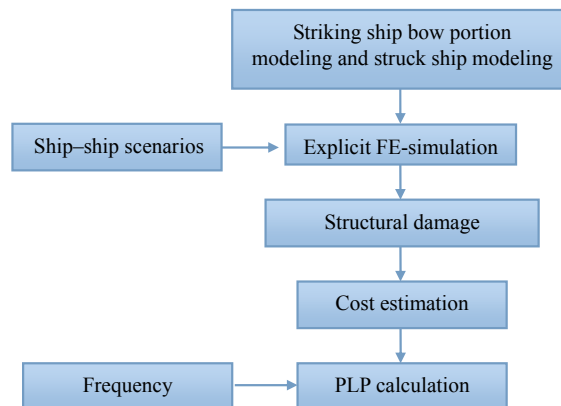


Figure 23.3
The procedure of PLP calculation.

the structural damage to the targeted ship. The amount of damaged steel is then calculated. The repair costs for the damage replacement can be estimated according to the amount of damaged steel. Once the frequency of ship–ship collision for each scenario is determined, PLP can be calculated by summing the products of the frequencies and their respective repair costs.

As it is impossible to consider every collision scenario, a sampling technique is used to select several random scenarios—not only the worst one, but also other minor collision events (Youssef et al., 2014b). Each scenario is determined by a set of parameters including the ship’s mass, colliding ship’s speed, draft, collision angle, collision location, and bow shape of the striking ship. Every parameter is a random variable with a specific probability density distribution. According to historical data or data from other sources, the probability density function (PDF) can be fitted. Based on PDFs for all of the parameters, several groups of random numbers for these parameters can be generated. Selected scenarios can then be determined using the randomly generated parameters.

In the colliding ship modeling process, all plates and stiffeners of the struck ship are modeled with piecewise linear plasticity. In order to achieve more accurate results, the colliding part of the struck ship that includes the ship’s side and some part of the bottom and deck is highlighted with a precise mesh. The other part could be a coarse mesh so that time consumption is less. Figure 23.4 is the FEM of a Suezmax-class double hull oil tanker.

In different collision scenarios, different types of striking ships are applied. According to Lützen, different bow-shaped models, containers, tankers, cargo, etc. are displayed. Figure 23.5 shows the geometric models of different striking ship bow portions that can be used in the FEM for the striking ship.

The nonlinear finite element method is used in the simulation of ship–ship collision. Both the struck ship FEM and striking ship bow portion FEM are inputs to the method. The assessment of the consequence (i.e., structural damage) of every scenario is then conducted. Figure 23.6 shows a simulation instance for one ship–ship collision scenario.



Figure 23.4

The FEM of a Suezmax-class double-hull oil tanker.



Figure 23.5
Striking ship bow geometric models.

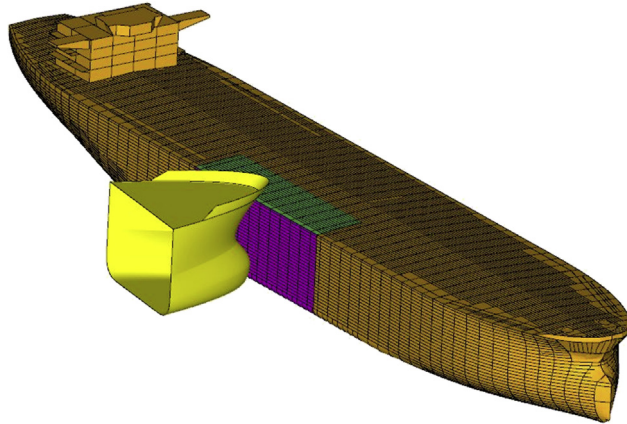


Figure 23.6
Example of a ship–ship collision finite element simulation.

The effect of the surrounding seawater is taken into consideration as a virtual added mass of the struck ship in surge, sway, and yaw (Paik and Pedersen, 1996).

After simulating and analyzing all of the selected scenarios, the structural damage of the struck ship is determined. The change in volume of the struck ship can be calculated in the analysis program. However, the results cannot be used directly as the amount of damaged steel to be replaced. In order to estimate the amount of damaged steel to be replaced, a marginal factor is introduced for each scenario.

Ship repair costs can be considered the economic consequences of damage. Ship repair cost estimates include insurance industry and expert group estimates (Ellis et al., 2012). Ship repair costs include steel repair, damaged equipment, lost cargo, etc. For example, steel repair costs are estimated from the amount of damaged steel.

The Finnish Maritime Administration (FMA) presented research (*Costs of Vessel Traffic Accidents, Finnish Maritime Administration publication, 3/2008, 2008*) that provides an estimation of costs for the most commonly encountered types of accident (i.e., collision, grounding, and contact) in Finnish waters. The FMA estimated the reparation costs for a

ship, including the amount of steel to be replaced, reparation costs of equipment, and other costs, based on indemnities paid by insurance companies.

Collision and grounding frequencies are calculated by multiplying the causation probability and the geometric probability (Fujii and Tanaka, 1971; Macduff, 1974). The causation probability is the probability of failing to avoid an accident when ships are about to collide. The geometric probability is the probability of a given number of collision candidates if no action is taken by the navigator. The causation probability can be calculated by historical accident statistics using the fault tree method or a Bayesian network approach. Pedersen's model (Pedersen, 1995) is used to calculate geometric probability. Figure 23.7 shows this model. The model considers collisions in the intersection of two waterways. Equation (23.2) is the formula for calculating the number of collision candidates.

$$N_a = \sum_{i,j} \frac{Q_i^{(1)} Q_j^{(2)}}{V_i^{(1)} V_j^{(2)}} D_{ij} V_{ij} \frac{1}{\sin \theta} \quad (23.2)$$

where V_{ij} is the relative velocity of the colliding ship; D_{ij} is the geometric collision diameter; and $Q_i^{(1)}$ and $Q_j^{(2)}$ stand for traffic flows, and $V_i^{(1)}$ and $V_j^{(2)}$ for velocities, for struck and striking ships, respectively.

The International Maritime Organization estimates PLP as the product of the accident frequency and the corresponding material damage costs. So PLP can be calculated using the equation below:

$$PLP = \sum_i F_i \times C_{rep,i} \quad (23.3)$$

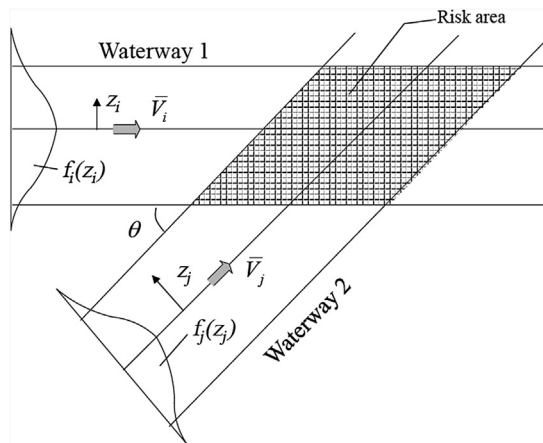


Figure 23.7

Pedersen's model for the intersection of waterways.

where F_i is the i th collision scenario and $C_{rep,i}$ is the economic consequence correlated with the i th collision scenario. So, the total PLP is the sum of the individual PLPs for each scenario.

23.4 Ship Grounding Research

Factors related to ship grounding are,

- the property of the grounding obstacles: soft or hard ground, the vertical location, shape and size of the obstacles under the free surface, and the environment;
- the condition of the grounding ship: the displacement, the draft, the speed and the bearing capacity of the ship structure to the bottom bending moment or raking damage.

The ship grounding process begins when obstacles make the bottom of the structure bend in or rake during ship navigation. Deformation along the ship depends on the resistance of the ship to bottom penetration into the seabed, and the stability of the ship. The vertical component of the collision force will introduce ship heaving and pitching. The friction of the ship bottom plate and the seabed will also consume some energy. If fracture happens, obstacles then start to rake the outer plate when the ship moves, thus introducing raking damage, and the problem will be very complex. If the ship stays on obstacles after grounding, more damage may occur depending on the length of time that passes. So, ship grounding research should be divided into three parts (initial grounding, raking, and damage after grounding) when studied.

Compared with ship collision research, less research was conducted on ship grounding in the early days (Jones, 1979). Card has done the first statistical investigation. Vaughan extended Minorky's empirical formula to the ship grounding condition and assumed that ship collision or grounding energy can be divided into two parts, surface and volume. Surface energy corresponds to tearing or cutting, and volume energy corresponds to deformation. Proportional coefficients can be derived from the tests.

Amdahl and Kavlie did grounding experiments and numerical simulation on a one-fifth-scale model of a double-hull ship structure. Paik and Lee introduced a series of reduced-scale-model experiments on wedge cutting stiffened plates. Vredveldt and Wevers introduced three grounding experiments that used a one-quarter-scale model of the oil tanker double-hull ship structure, and the experiments were used to obtain data like penetration, impact force, structural failure, and rigid body motion. Of the three experiments, one is like light grounding, while the other two are like serious grounding with cracking of the inner hull. According to experimental results, longitudinal stiffeners were not capable of bearing longitudinal penetration, because the welds connecting the stiffeners and the ship bottom plate failed before the ship contacted the metal rock. For cutting, increasing the number of transverse stiffeners or the thickness of the plate is better

than increasing the longitudinal members. Sterndorff and Pedersen did a series of grounding experiments utilizing an abandoned fishing boat on an artificial island, with a grounding speed from 2 to 5.5 m/s. In the experiment, data for the surge, heave, and pitch accelerations, as well as the deformation of the beach and ship, were tested. According to the accelerations, the rigid speed and its motion can be determined, and the interaction force of the seabed and the ship bow can be obtained by solving the motion equation.

The shapes and sizes of striking objects are considered important factors. Alsos et al. defined three types of seabed indenter according to shape: rock, reef, and shoal. Shoal grounding is still the most commonly encountered in practice, compared with rock grounding, even though it is not given a lot of attention.

23.4.1 Ship Grounding on Shoal

A theoretical model was introduced by Yao et al. for structural performance of double-bottom tankers during shoal grounding accidents. The theoretical model integrates Hong and Amdahl's simplified analytical model for girders and plating, and Yu and Hu's model for attached stiffeners. With this method, total distortion energy and grounding resistance are determined at the same time.

The three typical kinds of double-bottom structural components are longitudinal girders, transverse floors, and outer bottom plating. Hong et al. developed three simplified analytical models. Yu et al. demonstrated that stiffeners on the plates are of importance during grounding. However, the previous method for dealing with stiffeners cannot capture deformation characteristics in detail. Therefore, Yu et al. developed simplified analytical models of stiffeners on longitudinal girders, transverse floors, and outer bottom platings.

Theoretical Model for Longitudinal Girders

According to Hong and Amdahl, the distortion energy can be expressed as:

$$E_{girder} = M_{0_girder} \pi H \left(1 + 2\sqrt{1 + \tan^2 \theta} \right) \cdot \frac{1 - \tan^2 \theta}{\tan \theta} + \frac{4N_{0_girder} H^2}{\sqrt{3}} \sqrt{\frac{1}{4} + \tan^2 \theta} \quad (23.4)$$

where M_0 and N_0 are the fully plastic bending moment per unit of plate strips, and the corresponding plastic membrane force of a plate strip, respectively; and H and θ are half of the vertical crushing distance, and the crushing wave angle of the mechanism, respectively. They are calculated by

$$2H = 1.0836D + 0.0652 \quad (23.5)$$

$$2\theta = 0.94\alpha - 0.0048\alpha^2 \quad (23.6)$$

where D and α are the indentation of the indenter and the slope angle, respectively.

Theoretical Model for Floors

The distortion energy of floors is divided into two parts: central and side. They are expressed respectively as

$$E_{floor,central} = 4M_{0_floor} \left(2.58 \frac{H^2}{t} + \left(\frac{\pi}{2} \right)^2 + \pi C \right) \quad (23.7)$$

$$E_{floor,side} = \frac{14}{3} \pi M_{0_floor} b + 29.68 \frac{N_{0_floor} H^3}{b} \quad (23.8)$$

where C is the transverse half-width of the contact surface; b is calculated by

$$b = 2.85H \sqrt{\frac{H}{t_{floor}}} \quad (23.9)$$

where t is the thickness of the floor.

Theoretical Model for Outer Bottom Plating

The distortion energy of the outer bottom plating is expressed as

$$E_{plating} = 4l \left(M_{0_plating} \Delta\varphi + \frac{N_{0_plating}}{\sqrt{3}} \sqrt{u_0^2 + v_0^2} + \frac{2M_{0_plating}C}{R} \right) \quad (23.10)$$

where l is the crushing length. The first item in the equation is the plastic bending energy; the second item is the membrane stretching energy of the material between the longitudinal hinge lines; and the third item is the distortion energy of the plate that contacts the front surface of the indenter.

Theoretical Model for Stiffeners

The three types of stiffeners on the bottom during grounding are defined by their locations on (1) longitudinal girders, (2) transverse floors, and (3) outer bottom platings. Models for each type of girder are presented in Yu and Hu's study. The distortion energy of the three types of stiffeners can be calculated, with the symbols E_{gs} , E_{fs} , and E_{ps} representing the respective distortion energies. It is remarkable that the distortion energy of stiffeners on outer bottom platings involves an item that considers the grounding resistance normal to the contact surface. More details are in Yu and Hu's work.

Figure 23.8 shows the procedure of calculating the total distortion energy and grounding resistance.

The total energy is the sum of the distortion energy for all of the components calculated before. The internal forces $F_{H,plasticity}$ and $F_{V,plasticity}$ are derived from the total distortion energy:

$$E_{total} = F_{H,plasticity} + F_{V,plasticity} \cdot D \quad (23.11)$$

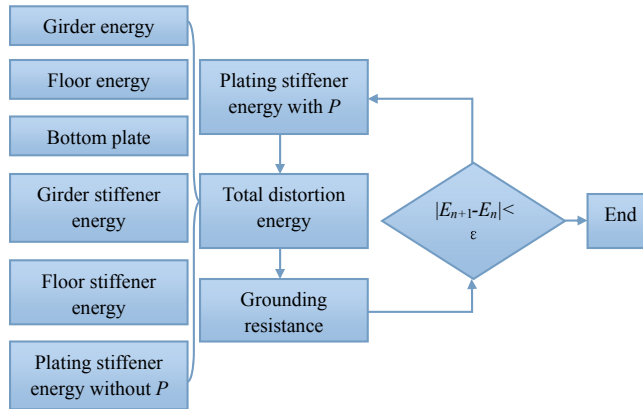


Figure 23.8

The procedure of calculation of distortion energy and grounding resistance.

$$F_{V,plasticity} = F_{H,plasticity} / \tan \alpha \quad (23.12)$$

Consider the friction in grounding, where F_H can be expressed as

$$F_H = g(\mu, \alpha) \cdot F_{H,plasticity} \quad (23.13)$$

$$g(\mu, \alpha) = 1 + \frac{\mu}{\tan \alpha} \quad (23.14)$$

According to the balance on forces, F_V and P can be derived as

$$F_V = g(\mu, \alpha) \cdot F_{H,plasticity} / \tan \alpha \quad (23.15)$$

$$P = \sqrt{F_H^2 + F_V^2} \quad (23.16)$$

where μ is the friction coefficient, and F_H and F_V are the horizontal and vertical grounding resistances, respectively. The symbol P represents the grounding resistance normal to the contact surface of the indenter.

The distortion energy is coupled with the grounding resistance, so it is an iterative process until the distortion energy converges. First, calculate the total distortion energy. When doing so, the distortion energy of stiffeners on outer bottom plating is calculated without the item involving P . Grounding resistance is then calculated. Replace the distortion energy of stiffeners on the outer bottom using the grounding resistance calculated in the above step. Repeat these steps until the convergence criterion is met.

23.5 Designs against Collision and Grounding

Based on the study of the deformation mode, energy absorption, and the relationship between collision force and penetration of the ship's side and bottom structure in ship collision and

grounding accidents, researchers are putting more effort into developing new designs against collision and grounding. The structural crashworthiness of struck ships must be improved, but reducing striking-ship stiffness is also an option. The degree of damage varies according to vessel positions, and the relative stiffness between struck and striking ships.

The ASIS research program funded by the Japanese transportation department aims at increasing the safety of oil tanker collisions and groundings. From the perspective of initiative and passivity of reducing structural damage, the new structural design methods can be classified into new ship design and soft-bow design.

The new ship design is a passive design. The aim of increasing the crashworthiness of the ship's side structure and the ability of the bottom structure against grounding can be achieved by changing the traditional side and bottom structures. The soft-bow design is an initiative design. It can reduce the damage on the side of the struck ship by reducing the stiffness of the bow structure without remarkably affecting the ship's hydrodynamic performance.

23.5.1 Buffer Bow

Having weaker striking bows can reduce the damage to a ship's side structure, whereas reinforcing the side structure is not cost-effective. This results in the buffer bow design. Transversely framed bows are more flexible than longitudinal framed bows, and the energy absorption is improved. Bows built in a blunter form can result in shallower penetration when collision happens.

Gu Yongning and Jiang Huatao presented a method named continuous deck design. It reduces the longitudinal stiffness by staggering the deck height between the transverse bulkheads in the bow area. They also presented a method that can reduce bow stiffness by using high-strength steel. Their research showed that the new type of buffer bow using continuous deck design can improve the energy absorption performance of the bow.

23.5.2 Sandwich Panels

Klanac et al. studied several conceptual crashworthy steel sandwich designs and compared them with traditional structures for ship side shells. The energy absorption of steel sandwich designs is proved to be higher than traditional ones. The EU Sandwich project studied the behavior of steel sandwich panels under local impact loading by experimental, numerical, and analytical methods. The results also proved good energy absorption capacity.

23.5.3 Innovative Double-Hull Designs

Double hull is currently the mainstream side structural design for large oil tankers. It not only meets the mandatory requirements of US OPA90 bill but also reduces environmental

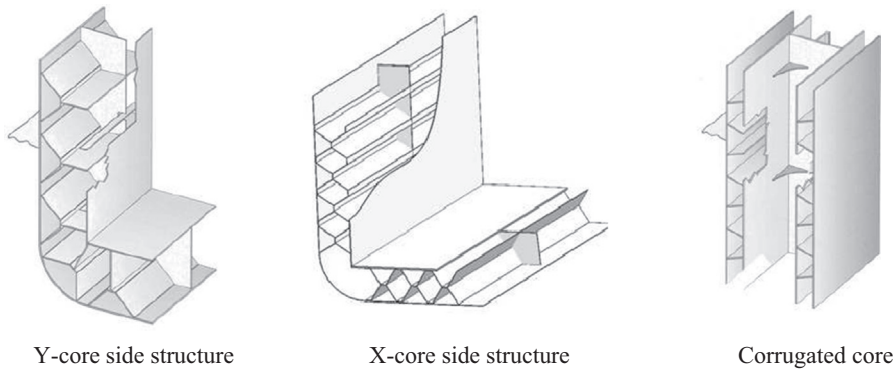


Figure 23.9
Innovative double-hull designs.

pollution caused by ship collisions, which has been proved in practice. So the various new methods of side structural design developed in recent years mainly make changes to the structure and layout of the shell plate and side stringer.

The new structural designs change components between double shells, including the side structure of “NOAHS” and “NOAH II,” the Y-core side structure using Y-stringer structure, stiffened plate structure, side structure using mixed stringer (Paik et al., 1999), etc. These new types of side structures all intend to improve the absorption effect of the impact energy of the side structure. Figure 23.9 shows some innovative double-hull designs by Schelde Naval Shipbuilding and Ship Laboratory of the Helsinki University of Technology.

Wang Zili presented a new crashworthy type of double-hull structure for LPGs and VLCCs. Brown et al. presented a method to improve the crashworthiness of the side structure by increasing the number of horizontal girders and ribs, and changing sizes.

One disadvantage of the new type of ship side structural design methods is the increase in structure weight. The effect of energy absorption from new design methods is favorable to traditional designs only with marked increases in structure weight. This disadvantage restricts the promotion of these new types of ship side structural forms. So it becomes significant to develop a ship side structural form that can remarkably improve the effect of energy absorption without increasing weight.

References

- FMA, 2008. Costs of Vessel Traffic Accidents, Finnish Maritime Administration Publication, 3/2008. Helsinki, Finland.
- Ellis, J., Lundkvist, M., Arola, T., 2012. Methods to Quantify Maritime Accidents for Risk-based Decision Making, Efficient, Safe and Sustainable Traffic at Sea (EfficienSea).

- Fujii, Y., Tanaka, K., 1971. Traffic capacity. *Journal of Navigation* 24 (04), 543–552.
- Jones, N.A., 1979. Literature Survey on the Collision and Grounding Protection of Ships. Ship Structure Committee Report No. SSC-283.
- Macduff, T., 1974. The probability of vessel collisions. *Ocean Industry* 9 (9).
- Paik, J.K., Chung, J.Y., Pedersen, P.T., Ge, W., 1999. On rational design of double hull tanker structures against collision. In: *The Society of Naval Architectures and Marine Engineers 1999 Annual Meeting Preprints*.
- Paik, J.K., Pedersen, P.T., 1996. Modelling of the internal mechanics in ship collisions. *Ocean Engineering* 23 (2), 107–142.
- Pedersen, P.T., 1995. Collision and grounding mechanics. In: *Proceedings of WEMT, 1995*, vol. 95, pp. 125–157. Seoul, 1995, 2.
- Youssef, S., Ince, S.T., Kim, Y.S., 2014a. Potential loss of property evaluation for suezmax-class double-hull oil tanker involved in ship-ship collisions. In: *International Proceedings of the ICTWS 2014 7th International Conference on Thin-walled Structures*. Korea.
- Youssef, S.A.M., Kim, Y.S., Paik, J.K., Cheng, F., Kim, M.S., 2014b. Hazard identification and probabilistic scenario selection for ship–ship collision accidents. *International Journal of Maritime Engineering* 156 (Part A1), 61–80.

Mechanism of Fatigue and Fracture

24.1 Introduction

Fatigue is the cumulative material damage caused by cyclic loadings. Many structural members must withstand numerous stress reversals during their service lives. Examples of this type of loading in marine structures include alternating stresses associated with wave-induced loading, vortex-induced vibrations, and load fluctuations due to the wind and other environmental effects. In the following sections, a basic fatigue mechanism will be reviewed. A detailed theoretical background for fatigue analysis is given by [Almar-Naess \(1985\)](#), [Gurney \(1979\)](#), [Maddox \(1992\)](#), [Suresh \(1991\)](#), and [Dover and Madhav Rao \(1996\)](#). An extensive list of recently published papers may be found from the ISSC proceedings (1988, 1991, 1994, 1997, 2000). The code of the American Welding Society ([AWS, 1985](#)) can be considered a representative code for fatigue strength design. Recent developments in ship fatigue research may be found in [Xu \(1997\)](#) and [Xu and Bea \(1997\)](#).

As part of the limit-state design criteria, Part III of this book covers the following aspects:

Chapter 24	Basic mechanism of fatigue and fracture
Chapter 25	Fatigue criteria such as S–N curves and stress concentration factors
Chapter 26	Fatigue loads and stresses determined based on deterministic methods, stochastic methods, and Weibull distributions
Chapter 27	Simplified fatigue assessment based on a Weibull distribution of a long-term stress range
Chapter 28	Spectral fatigue analysis and time-domain fatigue analysis and their applications to structural design
Chapter 29	Fracture mechanics and its applications to the assessment of crack propagation, the final fracture, and the calibration of fatigue design S–N curves
Chapter 30	Material selection and damage tolerance criteria

24.2 Fatigue Overview

Generally, the load amplitude of each cycle is not large enough to cause structural failure on its own. But failure could occur when the accumulated damage experienced by the structure reaches a critical level. The fatigue life of a structural detail is

directly linked to the fatigue process, which can be grouped into the following three stages:

- Crack initiation
- Crack propagation
- Final fracture failure

Crack initiation: This is tied to microscopic material behavior. To a certain degree, weld defects always exist both internally and on the weld surface. These weld defects may trigger growth in the cracks that usually form on the weld surface.

Crack propagation: Compared with crack initiation, the crack propagation stage is better understood, and different theories exist to model crack growth (e.g., fracture mechanics). The major parameter governing crack propagation is the stress range to which the structural detail is subjected. In addition, welding geometry and initial crack size have large impacts on the fatigue life of the structural detail. In welded structures, fatigue cracks almost always start at a weld defect, and the propagation period accounts for more than 90% of the fatigue life.

Fracture failure: Fracture failure of structural details will eventually occur when the crack size propagates to a critical size. The final fracture depends upon a couple of parameters, such as stress level, crack size, and material toughness. Similar to crack initiation, fatigue life during final fracture is a small part of total fatigue life, and is usually negligible compared with the crack propagation stage.

Fatigue can be classified as:

- High-cycle (low-stress) fatigue
- Low-cycle (high-stress) fatigue

Typically, fatigue failure is called “low-cycle fatigue” if the number of cycles to failure is less than 10^4 . The number of cycles in high-cycle fatigue is usually several million. For marine structures, the latter has become a real concern.

Methods for fatigue analysis: In general, there are two methods for fatigue analysis, namely the S–N approach (based on fatigue tests; see Chapter 25) and the fracture mechanics approach (see Chapter 21). For fatigue design purposes, the S–N curve approach is widely used and is often the most suitable. The fracture mechanics method is used to determine acceptable flaw sizes, assess fatigue crack growth, plan inspection and repair strategies, etc. For the S–N curve approach, there are three methodologies for fatigue damage calculation that depend on the methods used in determining fatigue loads (see Chapter 26):

- Simplified fatigue analysis (see Chapter 27)
- Spectral fatigue analysis (see Chapter 28)
- Time–domain fatigue analysis (see Chapter 28)

In order to study the fatigue and fracture damage mechanism, numerous experiments have been conducted to investigate material characteristics. These experiments can be divided into two categories: stress-controlled fatigue and strain-controlled fatigue.

24.3 Stress-Controlled Fatigue

Stress-controlled fatigue is generally related to high-cycle (low-stress) fatigue in which a major part of the material behaves elastically. Even though the material immediately adjacent to the notch may become plastic, both the extent of the plastic zone and the stress within it are limited. Since stress is directly proportional to strain, conventionally the fatigue strength is expressed in terms of stress.

In 1893 Wohler, who studied railroad-wheel-axle failure, was one of the earliest to investigate the effects of stress-controlled cyclic loadings on fatigue life. Several important facts were revealed from this investigation, as can be seen in the plot of the stress range versus the number of cycles to failure shown in [Figure 24.1](#). First, the number of cycles to failure increases with a decreasing stress range. Below certain stress ranges, generally an area referred to as the fatigue endurance limit, fatigue life is infinite. Second, fatigue life is reduced dramatically by the presence of a notch. These observations indicate that fatigue is a three-stage process involving initiation, propagation, and a final failure stage ([Figure 24.2](#)).

The S–N curves established by stress-controlled fatigue tests are generally expressed as

$$N = K \cdot S^{-m} \quad (24.1)$$

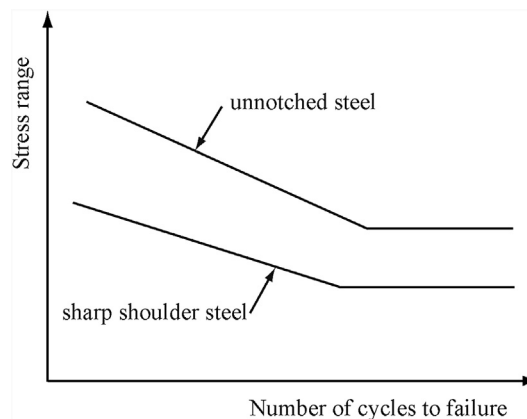


Figure 24.1

Wohler's S–N curves for Krupp axle steel.

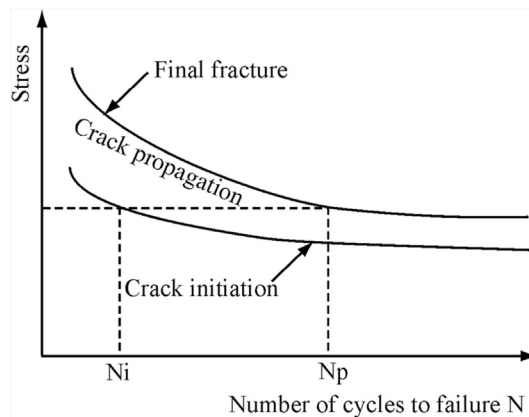


Figure 24.2

Illustration of fatigue life (initiation and propagation stages).

where

N = Number of cycles to failure

S = Stress range

m, K = Material constants that depend on the environment, test conditions, etc.

In most cases, the y-axis of S–N diagrams is stress amplitude that is half the total stress range. It should be noted that considerable scatter exists in the S–N curves. The scatter is due to factors affecting S–N curves such as:

- Wall thickness
- Corrosion
- Type and condition of the material, including a number of metallurgical variables
- Test environment, specimen surface, alignment of the test machine, etc.
- Residual stress, mean stress, or stress ratio
- Local stress peaks (notch effects)

The first two factors in the above list are explicitly accounted for in fatigue design codes.

24.4 Cumulative Damage for Variable Amplitude Loading

Much of the fatigue data discussed so far were generated from constant-amplitude and constant-frequency tests. However, these results are not realistic under actual field service conditions. Many structures are subjected to a range of load fluctuations and frequencies. In order to predict the fatigue life of a structural detail subjected to a variable load history, using constant-amplitude test data, a number of cumulative damage theories have been

proposed. For instance, the Palmgren–Miner cumulative damage law (Miner, 1945) states that

$$\sum_{i=1}^k \frac{n_i}{N_i} = 1 \quad (24.2)$$

where,

k = Number of stress range levels in the block of load spectrum

S_i = i th stress range level

n_i = Number of stress cycles applied at S_i

N_i = Fatigue life at S_i

The hypothesis of Miner was originally based on several assumptions (Fricke et al., 1997):

- Sinusoidal load cycles
- Purely alternating load
- Crack initiation as the failure mode
- No contribution to damage by load cycles below the endurance limit
- Sequence of load cycles not considered

Several modifications to the Palmgren–Miner law have been suggested and are related to the damage ratio, endurance limits, etc. The Palmgren–Miner law has been widely applied in engineering due to its simplicity.

24.5 Strain-Controlled Fatigue

The fatigue of a specimen subjected to strain-controlled loading is generally related to low-cycle high-stress fatigue. The stress associated with low-cycle fatigue will usually be high enough to cause a considerable amount of plastic deformation in the stress concentration region. Thus, the relationship between stress and strain will no longer be linear. This relationship is often characterized by a hysteresis loop (Figure 24.3) that may change from cycle to cycle. In Figure 24.3, $\Delta\epsilon_p$ is the plastic strain range and $\Delta\epsilon_t$ is the total strain range. The elastic strain range is $\Delta\epsilon_e = \Delta\epsilon_t - \Delta\epsilon_p$.

In engineering applications, much of the basic testing related to low-cycle fatigue has been carried out under constant-strain-range conditions. The test results have indicated that there is a relation between the fatigue life (N) and a strain parameter. Based on his test data, Manson and Hirschberg (1964) suggested that the relationship between the strain and the fatigue life can be expressed as

$$(\Delta\epsilon_p)^m N = \text{constant} \quad (24.3)$$

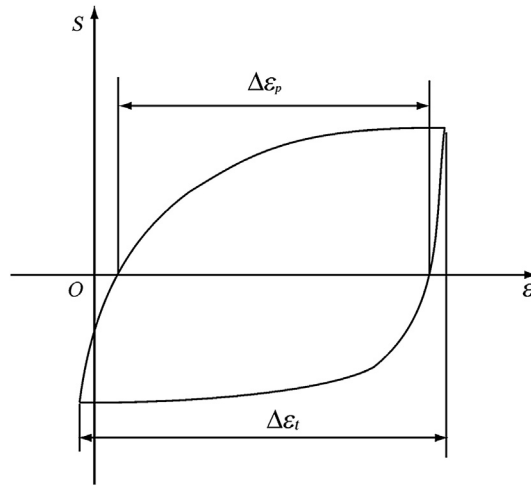


Figure 24.3
Cyclic stress–strain loop.

The above equation implies a straight-line relationship between $\log(\Delta\epsilon_p)$ and $\log N$, with a slope of $-m$. The value of the index m is a variable depending on material and environmental conditions, and is approximately 0.5.

In order to derive $\Delta\epsilon-N$ curves, it is convenient to consider elastic and plastic strains separately. The elastic strain range is often described in terms of a relationship between the stress amplitude and the number of load reversals ($S-N$ diagram).

$$\frac{\Delta\epsilon_e E}{2} = S_a = S'_f (2N_f)^b \quad (24.4)$$

where,

$$\frac{\Delta\epsilon_e}{2} = \text{Elastic strain amplitude}$$

E = Modulus of elasticity

S_a = Stress amplitude

S'_f = Fatigue strength coefficient, defined by the stress intercept at one load reversal
($2N_f = 1$)

N_f = Cycles to failure

$2N_f$ = Number of load reversals to failure

b = Fatigue strength exponent

The plastic component of strain is described by the Manson–Coffin relationship (Manson and Hirschberg, 1964; Coffin and Tavernelli, 1959)

$$\frac{\Delta\epsilon_p}{2} = \epsilon'_f (2N_f)^c \quad (24.5)$$

where,

$$\frac{\Delta \varepsilon_p}{2} = \text{Plastic strain amplitude}$$

$$\varepsilon'_f = \text{Fatigue ductility coefficient defined by the strain intercept at one load reversal} \\ (2N_f = 1)$$

$$2N_f = \text{Total strain reversals to failure}$$

$$c = \text{Fatigue ductility exponent, a material property in the range of } -0.5 \text{ to } -0.7$$

Manson suggested that the fatigue resistance of a material subjected to a given strain range can be estimated by the superposition of the elastic and plastic strain components.

Therefore, combining Eqns (24.4) and (24.5), the total strain amplitude can be given by

$$\frac{\Delta \varepsilon_T}{2} = \frac{\Delta \varepsilon_e}{2} + \frac{\Delta \varepsilon_p}{2} = \frac{S'_f}{E} (2N_f)^b + \varepsilon'_f (2N_f)^c \quad (24.6)$$

Figure 24.4 illustrates the combination of high-cycle and low-cycle fatigue. The total-strain life curve approaches the plastic-strain life curve in the low-cycle region, and approaches the stress life curve in the high-cycle region. The parameters used in Eqn (24.6) that determine strain-life curves are given by Boller and Seeger (1987) for various materials.

According to the AWS, a $\Delta \varepsilon$ - N curve is expressed below (Marshall, 1992)

$$\Delta \varepsilon = 0.055N^{-0.4} \quad \text{for} \quad \Delta \varepsilon \geq 0.002 \quad (24.7)$$

and

$$\Delta \varepsilon = 0.016N^{-0.25} \quad \text{for} \quad \Delta \varepsilon \leq 0.002 \quad (24.8)$$

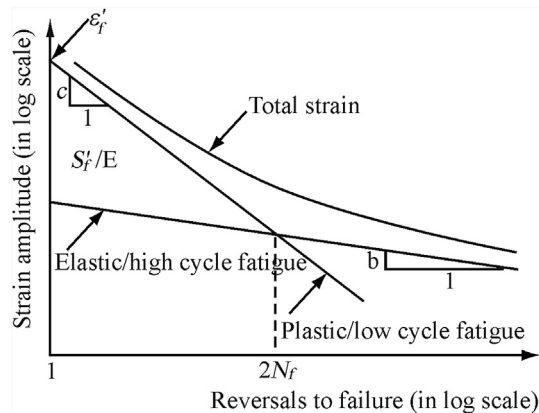


Figure 24.4

Superposition of stress (high-cycle) and strain (low-cycle) life curves.

The strain range $\Delta\varepsilon$ is the maximum strain, excluding the minimum strain near the weld, during steady cyclic bending loads.

Test data for the design of the Asgard flowlines (Bai et al., 1999) confirmed that the above AWS curves were applicable to flowlines and risers, although they were originally developed for tubular joints. Original test data for pipes under low-cycle fatigue are also given in Bai et al. (1999). A study of low-cycle fatigue conducted as part of the DEEPIPE JIP is summarized by Igland et al. (2000).

24.6 Fracture Mechanics in Fatigue Analysis

For a plate under uniform stress, the stress intensity factor K may be estimated as

$$K = \sigma\sqrt{\pi a} F \quad (24.9)$$

where a is the crack width and the geometric correction factor, and F is the product of a couple of factors such as back crack shape, front face, finite thickness, finite width, and stress gradient.

For fatigue crack growth, the zone of inelasticity is often small enough for the small-scale yielding assumption to be valid. Linear fracture mechanics can thus be applied in fatigue crack-growth analysis.

Paris and Erdogan (1963) suggested that the most relevant parameter that describes fatigue crack growth is the range of the stress intensity factor ΔK . In Figure 24.5, a schematic of the crack growth rate curve is shown. Three distinct regions are indicated: (1) the well-known threshold region, (2) the intermediate region, and (3) the failure region.

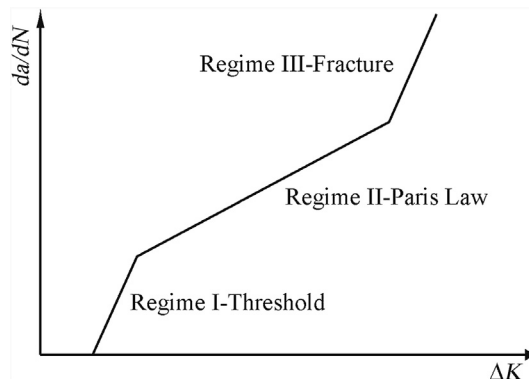


Figure 24.5

Schematic crack growth rate curve showing the relation of the crack propagation rate (da/dN) and stress intensity factors.

There is no crack growth for a sufficiently low-stress range in the threshold region. The corresponding value of the stress intensity factor is called the threshold stress intensity factor range (ΔK_{th}).

At intermediate values of K , there is an approximately linear relationship between the crack growth rate and ΔK on a log–log scale. This is generally characterized by the Paris equation

$$\frac{da}{dN} = C(\Delta K)^m \quad (24.10)$$

where

$$\Delta K = K_{\max} - K_{\min} \quad (24.11)$$

At the upper and lower limit stresses during a cyclic loading, K_{\max} and K_{\min} are the maximum and minimum values of the stress intensity factor. References on fracture assessment are, for example, Broek (1989) and Rolfe and Barsom (1999); see Part III, Chapter 29 for more details.

24.7 Examples

24.7.1 Example 24.1: Fatigue Life Cycle Calculation

Problem:

A pipe having a 30-mm-thick wall is subjected to a long-term stress distribution as shown in Figure 24.6. What is the fatigue life of this pipe that is welded from one side?

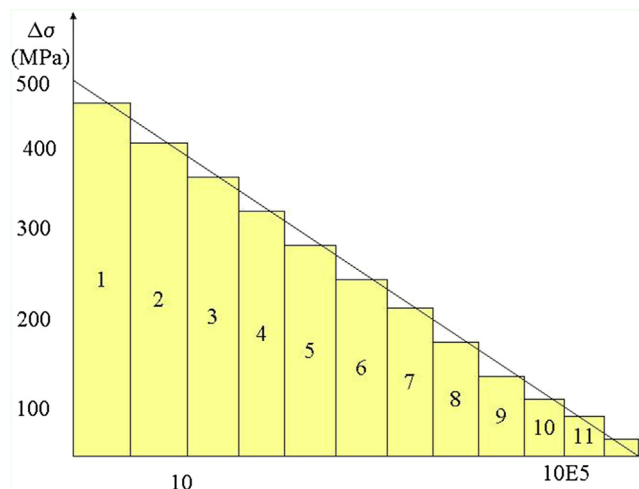


Figure 24.6
Stress cycles for fatigue life calculation.

Solution:

The welded component falls under the F2 joint classification. By including the thickness effect, the S–N curve can be formulated as

$$\log N = 11.63 - \frac{3}{4} \log \left(\frac{t}{22} \right) - 3 \log S = 11.53 - 3.0 \log S$$

According to the damage calculation tabulated below, the total damage ratio is 0.3523. The number of cycles to failure is then,

$$N = \frac{n_0}{D} = \frac{411,110}{0.3523} = 1.1669 \cdot 10^6$$

Block	n_i	S_i	N_i	n_i/N_i
1	3	450	3718	0.0008
2	7	400	4941	0.0014
3	30	350	7903	0.0038
4	70	300	12,550	0.0056
5	300	250	21,686	0.1353
6	700	210	36,588	0.0191
7	3000	170	68,969	0.0435
8	7000	130	154,230	0.0454
9	30,000	90	464,807	0.0645
10	70,000	50	2,710,753	0.0258
11	300,000	20	42,355,520	0.0071
	$n_0 = 411,110$		$D = 0.3523$	

24.7.2 Example 24.2: Fracture-Mechanics-Based Crack Growth Life Integration

Problem: Assuming that a very wide plate is subjected to a contact amplitude uniaxial cyclic loading that produces nominal varying stresses between 200 and -100 MPa, the critical stress intensity factor is $K_{CR} = 104 \text{ MPa}\sqrt{\text{m}}$. The material constants are $m = 3$ and $C = 7.1\text{E-}12 \text{ m}/(\text{MPa}\sqrt{\text{m}})^3$. What is the fatigue life if the initial crack length is less than 2.5 mm?

Solution:

Crack growth can be predicted using the Paris equation. Integration of this equation involves numerical methods unless F is independent of the crack length. In an infinite plate under uniform tension, F is constant (1.12). The compressive stress of -100 MPa may be ignored in the fracture calculation. The critical crack length at final fracture can be obtained from Eqn (24.9),

$$a_{CR} = \frac{1}{\pi} \left(\frac{K_{CR}}{F \cdot \sigma_{\max}} \right)^2 = \pi^{-1} \left(\frac{104}{1.12 \cdot 200} \right)^2 = 0.068 \text{ m}$$

Integrating the Paris equation Eqn (24.10), the constant amplitude fatigue life can be estimated as

$$N_p = \frac{\int_{a_0}^{a_{CR}} \frac{da}{a^{m/2} \cdot F^m}}{C \cdot S^m \pi^{m/2}} = \frac{0.068^{-0.5} - 0.0025^{-0.5}}{-0.5 \cdot (7.1 \cdot 10^{-12}) \cdot 200^3 \cdot \pi^{1.5} \cdot 1.12^3} = 72887 \text{ cycles}$$

References

- Almar-Naess, A., 1985. Fatigue Handbook, Offshore Steel Structures. Tapir, Norway.
- AWS, 1985. Structural Welding Code – Steel. ANSI/AWS D1–85. American Welding Society, Miami, USA (now updated to AWS D1-92-14th Edition).
- Bai, Y., Damsleth, P.A., Dretvik, S., 1999. The asgard flowlines project – limit state design experience. In: IBC Conference on Risk-Based & Limit-State Design & Operation of Pipelines, Oslo, Oct. 1999.
- Boller, C., Seeger, T., 1987. Materials Data for Cyclic Loading, Part A–E. Elsevier, Amsterdam.
- Broek, D., 1989. The Practical Use of Fracture Mechanics. Kluwer Academic Publisher.
- Coffin, L.F., Tavernelli, J.F., 1959. The cyclic straining and fatigue of metals. Transaction of the Metallurgical Society of AIME 215, 794.
- Dover, W.D., Madhav Rao, A.G., 1996. Fatigue in Offshore Structures. A.A. Balkema.
- Fricke, W., Petershagen, H., Paetzold, H., 1997. Fatigue Strength of Ship Structures, Part I: Basic Principles, Part 2: Examples. GL Technology.
- Gurney, T.R., 1979. Fatigue of Welded Structures, second ed. Cambridge University Press.
- Iglund, R.T., Saevik, S., Bai, Y., Berge, S., Collberg, L., Gotoh, K., Mainuon, P., Thaulow, C., 2000. Deepwater pipelines and flowlines. In: Proc. of OTC'2000 Conference.
- ISSC, 1988, 1991, 1994, 1997, 2000. Fatigue and fracture, Report of technical Committee III.2. In: Proceedings of the International Ship and Offshore Structures Congress.
- Maddox, S.J., 1992. Fatigue Strength of Welded Structures. Abington Publishing.
- Manson, S.S., Hirschberg, M.H., 1964. Fatigue: An Interdisciplinary Approach. Syracuse University Press, NY, p. 133.
- Marshall, P.W., 1992. Design of Welded Tubular Connections. Elsevier Press, Amsterdam.
- Miner, M.A., 1945. Cumulative damage in fatigue. Journal of Applied Mechanics, ASME 12 (3), 159–164.
- Paris, P., Erdogan, F., 1963. A critical analysis of crack propagation laws. Journal of Basic Engineering 85 (4), 528–533.
- Rolf, S.T., Barsom, J.T., 1999. Fracture and Fatigue Control in Structures, third ed. Prentice-Hall, Englewood Cliffs, NJ.
- Suresh, S., 1991. Fatigue of Materials. Cambridge Press.
- Xu, T., 1997. Fatigue of ship structural details – technical development and problems. Journal of Ship Research, SNAME 41 (4), 318–331.
- Xu, T., Bea, R.G., May 1997. Fatigue of ship critical structural details. Journal of Offshore Mechanics and Arctic Engineering, ASME 119 (2), 96–107.

Fatigue Capacity

25.1 *S–N* Curves

25.1.1 General

Part III, Chapter 24 states that the relationship between the stress range and the number of cycles to failure is a function of the type of joint, the environment, and the plate thickness. Within this chapter, the factors that affect *S–N* curves will be discussed in [Section 25.1](#), while the determination of the stress range at the critical location (hot spot) of the joint will be discussed in [Section 25.2](#). Methods for determining stress concentration factors (SCFs) will be presented in [Section 25.3](#). In Part III, tubular joints and plated connections are also termed “critical details” or simply “details.”

For fatigue analysis based on the nominal stress approach, welded joints are divided into several classes. Each class has a designated *S–N* curve. The classification of *S–N* curves depends on the geometry of the detail, the direction of the fluctuating stress relative to the detail, and the method of fabrication and inspection of the detail. The types of joints, including plate-to-plate, tube-to-plate, and tube-to-tube connections, all have alphabetical classification types, where each type relates to a particular *S–N* relationship as determined by experimental fatigue tests. Design *S–N* curves are based on mean-minus-two-standard-deviations curves for relevant experimental data. The *S–N* curves are thus associated with a 97.6% probability of survival.

For example, Norwegian and British codes reference the D curve for simple plate connections with the load transverse to the direction of the weld, and the T curve for tubular brace-to-chord connections, as shown in [Figure 25.1](#).

In the American codes (e.g., API RP2A), fatigue has been relatively less of a concern. Consequently, the number of joint classifications is less than that recommended in Europe.

Each construction detail at which fatigue cracks may potentially develop should be placed in its relevant joint class in accordance with criteria given in the codes. Fatigue cracks can develop in several locations—for example, at the weld toe in each of the parts joined, at the weld ends, and in the weld itself. Each location should be classified separately

The basic design *S–N* curve is given as

$$\log N = \log K - m \log S \quad (25.1)$$

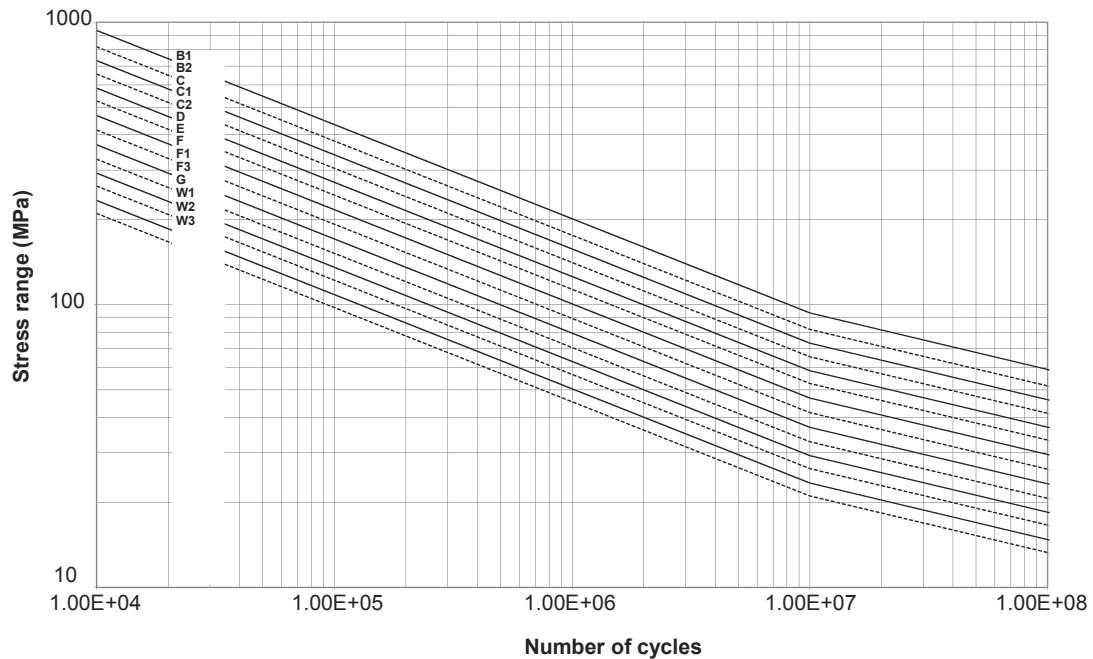


Figure 25.1

Examples of $S-N$ curves in air (NTS, 1998).

where,

S = Stress range

N = Predicted number of cycles to failure for stress range S

m = Negative inverse slope of $S-N$ curve (typically $m = 3$)

$\log K$ = Intercept of $\log N$ -axis by $S-N$ curve = $\log a - 2(\text{std})$

where a and std are constants relating to the mean $S-N$ curve and standard deviation of $\log N$, respectively.

Examples of $S-N$ curves in air are given in Figure 25.1. These $S-N$ curves have a bilinear relationship between $\log(S)$ and $\log(N)$, and the change in slope from a gradient of $1/3$ to a gradient of $1/5$ occurs at $10E7$ cycles. The lower right side of the $S-N$ curves reflects the considerably longer life associated with tests of joints at low stress ranges.

The second part of the design $S-N$ curve is given as (NTS, 1998)

$$\log N = \log C - r \log S \quad (25.2)$$

where,

r = Negative inverse slope of the second $S-N$ curve (typically $r = 5$)

$\log C$ = Intercept of $\log N$ -axis by the second $S-N$ curve

The relationship between the stress range and the number of cycles to failure indicates that a relatively small change in the estimated stress range has a significant effect on fatigue life. For example, the life of a joint will be halved by a 26% increase in stress. Estimates of stresses in joints are considered to be within 20% of mechanical tests or refined FE analyses, and within 25% for well-calibrated empirical formulae for SCFs. Thus, accurate estimates of stress ranges at the critical areas on joints are essential when determining fatigue lives. Methods for estimating stress ranges are discussed further in [Section 25.2](#).

In some design codes, there is a cutoff limit, and low fatigue damage is assumed when the stress range is below the cutoff limit.

For the sake of consistency, discussions of the fatigue criteria in this chapter will be mainly based on NORSOK ([NTS, 1998](#)). However, it is recommended that readers refer to the codes relevant to particular projects, such as IIW ([Hobbacher \(1996\)](#)); [Eurocode 3 \(1993\)](#); [IACS \(1999\)](#); [ABS \(1992\)](#); and [DNV \(2000\)](#), among others).

25.1.2 Effect of Plate Thickness

The thickness effect is due to the local geometry of the weld toe in relation to the thickness of the adjoining plates, and to the stress gradient over the thickness. It can be accounted for by

$$\log N = \log K - m \log \left(S \left(\frac{t}{t_{\text{ref}}} \right)^k \right) \quad (25.3)$$

where,

t_{ref} = Reference thickness, which in some design codes is 32 and 25 mm for tubular joints and other types of welded connections, respectively ([NTS, 1998](#))

t = Thickness through which a crack will most likely grow

k = Thickness exponent on fatigue strength in the range 0.00–0.25 depending on the code employed, S – N curves selected, etc. ([NTS, 1998](#))

In other words, the thickness effect can be accounted for by multiplying a factor of $(t/t_{\text{ref}})^k$ by the stress range. In [HSE \(1995\)](#), the values of k and the reference thickness t_{ref} are 0.25 and 22 mm, respectively. In general, the thickness correction to the design equation for the S – N curve is required when the plate thickness is thicker than the reference thickness. To some extent, the thickness correction also accounts for the size of the weld and its attachments. However, it does not account for the weld length or the length of a component that is different from the tested component.

25.1.3 Effect of Seawater and Corrosion Protection

In Figure 25.2 below, three types of $S-N$ curves are compared for tubular joints. The $S-N$ curves compared are in-air, in-seawater with cathodic protection (CP), and in-seawater under free corrosion. The relationship between in-air and in-seawater with CP varies between codes. Using NORSOK (NTS, 1998), the fatigue life at high stress ranges (when N is less than 10^6 cycles) in seawater with CP is considered 40% of that in air. However, there is no difference between $S-N$ curves at lower stress ranges (when N is in excess of 10^7 cycles).

In general, the fatigue life in seawater under free corrosion is 33% of the life in air at high stress ranges (when N is less than 10^7 cycles). There is no change in slope for the free-corrosion $S-N$ curve, and hence fatigue lives are around 10% of the equivalent lives for the in-air $S-N$ curve (when N is more than 10^7 cycles).

25.1.4 Effect of Mean Stress

Compressive mean stress has a beneficial effect on fatigue capacity. Normally, it is not required in order to account for the effect of the mean stress. However, in some special

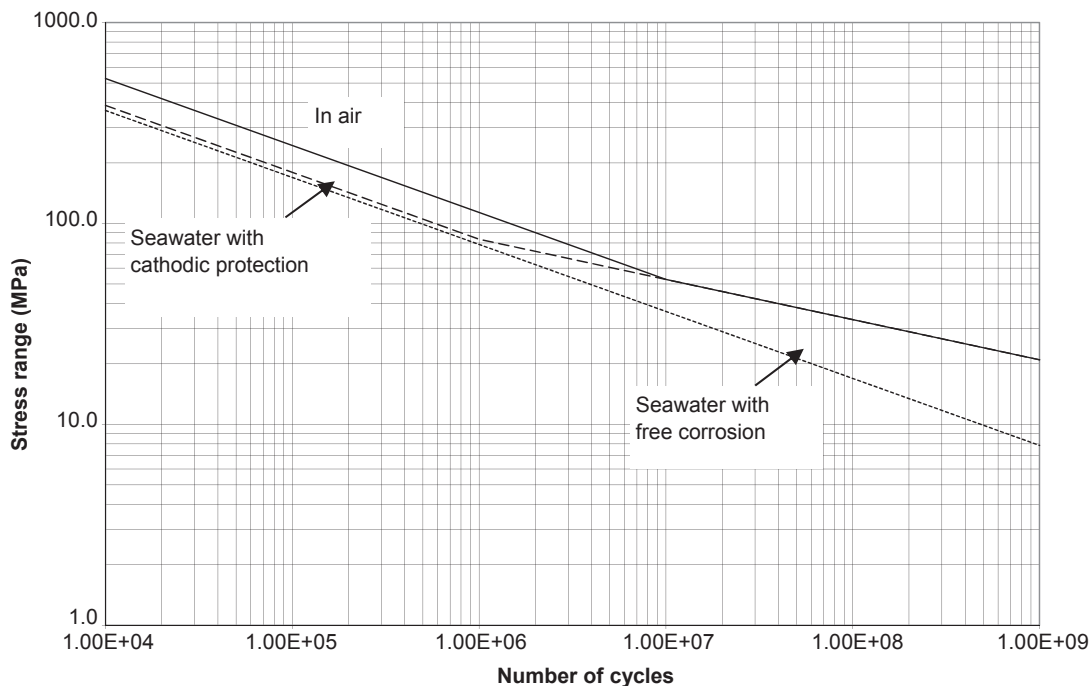


Figure 25.2

Comparison of $S-N$ curves for tubular joints (NTS, 1998).

cases, it is necessary in order to account for mean stress effect that modifies the selected $S-N$ curves—for example, for the fatigue assessment of TLP tethers and mooring lines whose nonlinear response is important. Within this text, several models are available to correct $S-N$ curves for the mean stress effect, the most popular being the so-called modified Goodman relation that can be expressed as (Almar-Naess, 1985)

$$S_{a,N} = \frac{S_a}{1 - \sigma_m/\sigma_u} \quad (25.4)$$

where $S_{a,N}$ = the stress at a given fatigue life under reversed loading (mean stress is 0), S_a is the alternative stress applied, and σ_m and σ_u are the mean stress and ultimate stress, respectively. The stress $S_{a,N}$ defined in Eqn (25.4) should be used as the stress range in the corrected $S-N$ curve.

25.1.5 Comparisons of $S-N$ Curves in Design Standards

There are various kinds of fatigue design codes in the literature; for example:

- General steel codes: BS 7608, BS 7910, Eurocode 3, NS 3472
- Offshore industry: NORSOK, UK HSE (UK DEn), API, etc.
- Ship industry: classification rules, IACS requirements
- IIW (International Institute of Welding), AWS (American Welding Society)
- Automobile industry, aerospace & aircraft industries, etc.
- Bridges industry: BS5400 (BSI, 1979), AASHTO (1989)
- ASME pressure vessels codes
- Welded aluminum codes: BS8118 (BSI, 1991), ECCS (1992)

In Europe, UK HSE (1995) replaced UK DEn (1990). The main change is that m and r become independent of the $S-N$ curves selected. A weld classification factor f (to be multiplied to the stress range) has been introduced in UK HSE (1995) so that various $S-N$ curves in UK DEn (1990) may be expressed in one $S-N$ equation. In other words, the $S-N$ curves in UK HSE (1995) are unified to a single equation by defining the stress range as

$$S = f * S_g \left(\frac{t}{t_{\text{ref}}} \right)^k \quad (25.5)$$

where S_g = stress range that includes weld macrogeometry but excludes the peak stress due to local defects that have been implicitly accounted for in the weld classification factor f .

The relationships between the weld class (B, C, D, etc.) and the weld classification factor f are B ($f = 0.64$), C ($f = 0.76$), D ($f = 1$), E ($f = 1.14$), F ($f = 1.34$), F2 ($f = 1.52$), G ($f = 1.83$), and W ($f = 2.13$).

Since 1948, Norwegian standard NS3472 has been used in the design of land and offshore steel structures in Norway. In 1998, NS3472 was revised and at the same time, NORSOK N-004 (NTS, 1998) was developed for the design of offshore steel structures. NORSOK is a Norwegian initiative taken by the industry to develop a design standard for more cost-effective offshore development. Eurocode 3 is a European standard for designing building structures. Table 25.1 lists the $S-N$ curves used in Europe for air environments.

In the United States, fatigue design is based on API RP 2A WSD and AWS D1.1. A detailed background of AWS code provisions is given by Marshall (1992) and outlined by Marshall (1993). Geyer and Stahl (1986) presented a simplified fatigue design procedure for offshore structures. The latest developments in the research on $S-N$ curves may be found from Maddox (2001).

In API RP 2A, the X' curve is used for welded connections without a profile control. Thickness correction only applies if the wall thickness is greater than 0.625 inches (16 mm). In API RP2A, the thickness correction exponent k is taken as 0.25. The X curve is used for welded connections with profile control, and the wall-thickness correction factor applies when the wall thickness is greater than 1 inch (25 mm). However, after the thickness correction, the X curve cannot be reduced to be lower than the X' curve.

Table 25.1: Comparison of European standards for fatigue $S-N$ curves for air environments (Fricke et al., 2000)

Euro Code 3 Notation (FAT)	NORSOK/NS 3472/HSE Notation	Log K For $N \leq 10E7$ ($m = 3$)	Log C For $N > 10E7$ ($r = 5$)	Stress		SCF as Derived by the Hot-Spot Stress
				Amplitude at transition (MPa)	Thickness Exponent k	
160	B1	12.913	16.856	93.57	0	
140	B2	12.739	16.566	81.87	0	
125	C	12.592	16.320	73.10	0.15	
112	C1	12.449	16.081	65.50	0.15	
100	C2	12.301	15.835	58/48	0.15	
90	D	12.164	15.606	52.63	0.25	1
80	E	12.010	15.350	46.78	0.25	1.13
71	F	11.855	15.091	41.52	0.25	1.27
63	F1	11.699	14.832	36.84	0.25	1.43
56	F3	11.546	14.576	32.75	0.25	1.61
50	G	11.398	14.330	29.24	0.25	1.80
45	W1	11.261	14.101	26.32	0.25	2.00
40	W2	11.107	13.845	23.39	0.25	2.25
36	W3	10.970	13.617	21.05	0.25	2.50
	T	Same as D	Same as D	Same as D	Same as D	Same as D

Note: For thickness correction, the reference thickness is 32 and 25 mm for welded connections for tubular joints and nontubular joints, respectively.

API $S-N$ curves are singular (not bilinear) and have an endurance limit. The endurance limits for the X and X' curves are 35 and 23 MPa, respectively. The values of K and m for the X curve are 1.15E15 and 4.38, respectively. For the X' curve, K and m are 2.50E13 and 3.74, respectively.

The classification societies define fatigue criteria in their rules and guidance/guidelines. IACS requirements for fatigue assessment were developed by unifying the requirements of the individual classification societies for ship structural assessment. Fatigue $S-N$ curves for ship structures are mainly based on the UK DEn basic $S-N$ curves and the IIW $S-N$ curves.

The IIW $S-N$ curves assume that the slope of all $S-N$ curves is $m = 3$, and the change in slope ($m-5$) occurs for $N = 5 \times 10^6$ cycles (Hobbacher, 1996). These $S-N$ curves are based on nominal stress ranges, and correspond to -noncorrosive conditions. They are given for the mean minus two standard deviations. Their fatigue class is characterized by the fatigue strength at 2×10^6 cycles (e.g., the stress ranges corresponding to 2×10^6 cycles (FAT) are 160, 140, 125, 112, 100, 90, 80, 71, 63, 56, 50, 45, 40, and 36; see Table 25.1).

BV (1998) proposed corrections of the design $S-N$ curves to account for various factors such as:

- **Influence of static and residual stresses:** Tensile residual stress in the magnitude of yield stress will reduce fatigue life, and in such cases the maximum stress is assumed to be the yield stress irrespective of the amount of actual maximum stress. Postweld treatment may improve weld geometry and fatigue capacity.
- **Influence of compressive stresses:** To account for the less damaging effects of compressive stresses while the stress range is greater than the yield stress, the calculated local stress range S_{local} can be corrected using the British Standard 5400, defining the stress range as

$$S = \sigma_Y + 0.6(S_{\text{local}} - \sigma_Y) \quad \text{for } \sigma_Y \leq S_{\text{local}} \leq 2\sigma_Y \quad (25.6)$$

$$S = 0.8S_{\text{local}} \quad \text{for } S_{\text{local}} > 2\sigma_Y \quad (25.7)$$

- **Influence of plate thickness**
- **Influence of the material:** The fatigue strength of welded joints is nearly independent of material properties such as material grades. However, for machined plates the effect of yield strength is large.
- **Influence of the environment**
- **Workmanship:** $S-N$ curves have been derived for standard workmanship and welding procedures. In some instances, the effects of imperfection and misalignment should be taken into account when determining hot-spot stresses.

While the influences of the environment and plate thickness are explicitly taken into account in most design codes, other items listed above may not be required considerations in some design codes.

25.1.6 Fatigue Strength Improvement

When the theoretically calculated fatigue life is less than the required fatigue life, methods of justifying the fatigue design include

- Improved design of structural details (e.g., to reduce stress concentration, residual stress and misalignment, and to locally increase the wall thickness)
- Improved analytical methods: Spectral fatigue analysis is usually more accurate than a simplified fatigue assessment. Time-domain analysis may be better than the spectral fatigue analysis. The selection of sea states, loading conditions, and the quality of the environmental data will influence fatigue analysis results.

From a capacity point of view, the three most important factors affecting fatigue are the stress concentration due to weld geometry, defect shape, and distribution and residual stress. Therefore, methods for improving fatigue capacity through fabrication and repair include (BV, 1998)

- Modification of the weld geometry by grinding or weld toe remelting;
- Improvement of welding procedures and workmanship;
- Introduction of compressive stresses; for example, by hammer or shot peening;
- Postweld heat treatment.

However, the most efficient methods are possible improvements of the design, such as reducing geometric SCFs (BV, 1998):

- Shape improvement of cutouts
- Softening of bracket toes
- Local increases in thickness

More detailed discussions of improvements in weld details and fatigue design are given in Part III, Chapter 30.

25.1.7 Experimental $S-N$ Curves

Most $S-N$ curves are determined in laboratories where test specimens are subjected to constant amplitudes until failure. The $S-N$ curves are derived by their mean fatigue life and the standard deviation of $\log N$. The mean $S-N$ curve shows that 50% of the specimens will fail. The basic design $S-N$ curve is given as

$$\log N = \log K_{50} - m \log S \quad (25.8)$$

where K_{50} is obtained from the mean value of $\log K_{50}$. To derive the $S-N$ curves, a large number of tests are required. However, when the coefficient m is known, 10 tests may be sufficient to accurately derive the $S-N$ curve (BV, 1998):

- Five at the stress level corresponding to $N = 10^4$
- Five at the stress level corresponding to $N = 5 \cdot 10^5$

If p is the percentage of test specimens that fall below the design $S-N$ curve, the design $S-N$ curve may be defined as

$$\log N = \log K_{50} - \lambda_p S_d - m \log S \quad (25.9)$$

where S_d is the standard deviation of $\log K_{50}$. The relationship between the value of λ_p and the failure probability is (BV, 1998)

- Fail-safe design: $p = 2.5\%$, $\lambda_p = 2$ (normally used to derive design $S-N$ curves)
- Safe-life design: $p = 0.1\%$, $\lambda_p = 3$ (for special welded specimens that represent structural details that cannot be easily inspected and repaired)

25.2 Estimation of the Stress Range

The fatigue analysis procedure is based on the ranges of cyclic principal stresses.

To determine the stress range, two approaches have been developed. The “nominal stress” approach has been applied to plated structures and the “hot-spot stress” approach has been developed for tubular joints. Note that a “notch stress” approach is also suggested by some design codes. Within recent years, attempts have been made to apply the hot-spot stress approach to plated structures.

25.2.1 Nominal Stress Approach

In the nominal stress approach, stress concentrations caused by the weld profile have been included in the $S-N$ curves.

The determination of stresses applied to fatigue analysis of structural details is generally undertaken by a global–local finite element analysis (FEA) of the pertinent stress in accordance with the chosen $S-N$ curves. In other words, the calculated stress for the considered local hot-spot area of structural details should resemble the nominal stress of the test specimens from which the $S-N$ curves were established. Unfortunately, in most cases, structural details are more complex than the nominal stresses of test specimens, both in geometry and in applied loadings. Consequently, a relationship between the $S-N$ data stress and calculated stress may not be easily established.

Another problem associated with the nominal stress approach is the classification of structural details. The primary difference between UK DEn curves and recent European

$S-N$ curves is that UK DEn curves do not have a fatigue endurance limit. The fatigue endurance limit found in the constant cyclic loading test usually does not exist for marine structural details for a variety of reasons including welding, corrosion, and the load sequence effects of random loading.

The relevant fatigue stress for fatigue design would be the tensile stress σ , for example, for the weld shown in Figure 25.3(a). For the weld shown in Figure 25.3(b), the SCF for the global geometry must be accounted for by using the relevant fatigue stress of $SCF \cdot \sigma$, where SCF is the SCF due to the hole.

If a corner detail with zero radii is modeled, the calculated stress will approach infinity as the element size is decreased to zero. The modeling of a relevant radius requires a very fine element mesh, increasing the size of the FEM. In addition, the selection of the proper radius to be used for the analysis needs to be discussed.

25.2.2 Hot-Spot Stress Approach

The nominal stress approach has two disadvantages for tubular joints. First, it is not possible to define a reasonable nominal stress due to the complex geometry and the applied loading. Second, suitable fatigue test data are often not available for large complex tubular joints. Therefore, a hot-spot stress approach has been developed in order to overcome these difficulties (Kung et al., 1975; Lalani, 1992).

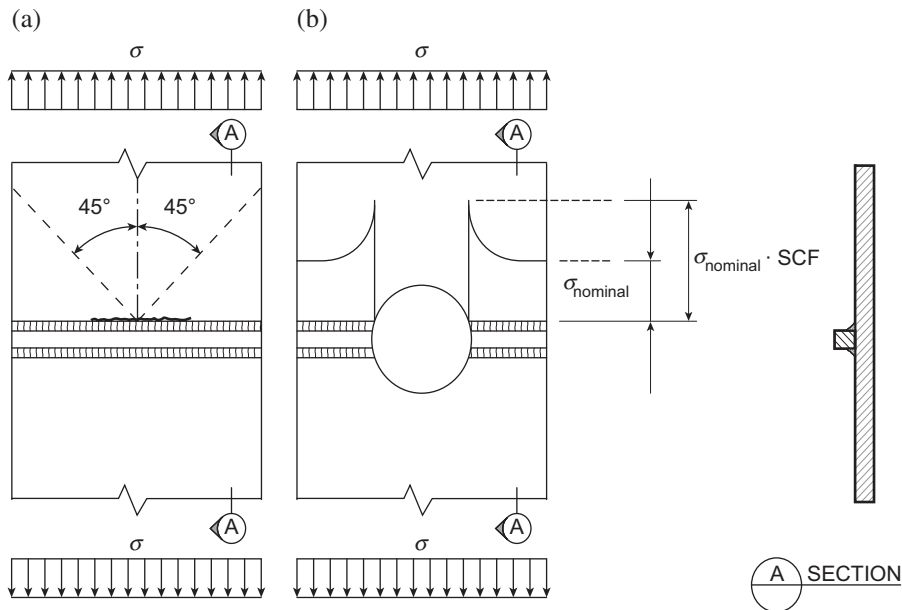


Figure 25.3

Description of stress in two plated sections (NTS, 1998).

The hot-spot stress reduces the various $S-N$ design curves of the nominal stress approach to two baseline curves. One is the curve for nonwelded structures (e.g., cutouts and plate edges), and the other is the curve for welded structures. This is accomplished by using the stress nearest to the weld, which is defined as hot-spot fatigue stress.

The hot-spot stress approach was developed based on the observation that experimentally derived $S-N$ curves are nearly parallel. This implies that all $S-N$ curves can be related to each other by some factors. For example, in UK DEn curves, the E and F curves are correlated by a factor of 1.2 or 1.3, assuming the following:

- This correlated factor represents the difference of structural configurations between different details.
- The local fatigue failure is independent of the detail type. The difference in fatigue resistance between details is due to different structural configurations.
- The structural SCF (SCF_{struct}) can represent the effects of structural configurations entirely.

The stress range at tubular joint hot spots should be combined with the $S-N$ curve T. The stress range at the hot spot of plated structures should be combined with UK $S-N$ curve D. The C curve may be used if machining of the weld surface to the base material is performed. Then, the machining must be performed such that local stress concentration due to the weld is removed.

The hot-spot stress concept assumes that the effect of the local stress factor due to the weld profile should be included in the $S-N$ curves. The stress concentration due to gross and local geometry changes should be included in the hot-spot stress. The problem with the hot-spot stress approach is that stress gradients are very high in the vicinities of weld and plate intersections. Because of high gradients, stresses computed using FEA are extremely sensitive to the finite element mesh size. This mesh sensitivity results in an inaccurate definition of the hot-spot stress during application.

In order to define the hot-spot stress, stresses from an FEA or mechanical test may be linearly extrapolated (see [Figure 25.4](#)). The dotted straight line is based on the stresses at distances $t/2$ and $3t/2$ from the weld toe (this distance may depend on the codes used).

The hot-spot stress approach is preferred in cases where.

- There is no defined nominal stress due to complicated geometry effects.
- The structural discontinuity is not comparable with any classified details.
- The fatigue test is performed together with strain gauge measurements to determine the hot-spot stress.
- The offset or angular misalignments exceed the fabrication tolerance used for the nominal stress approach.

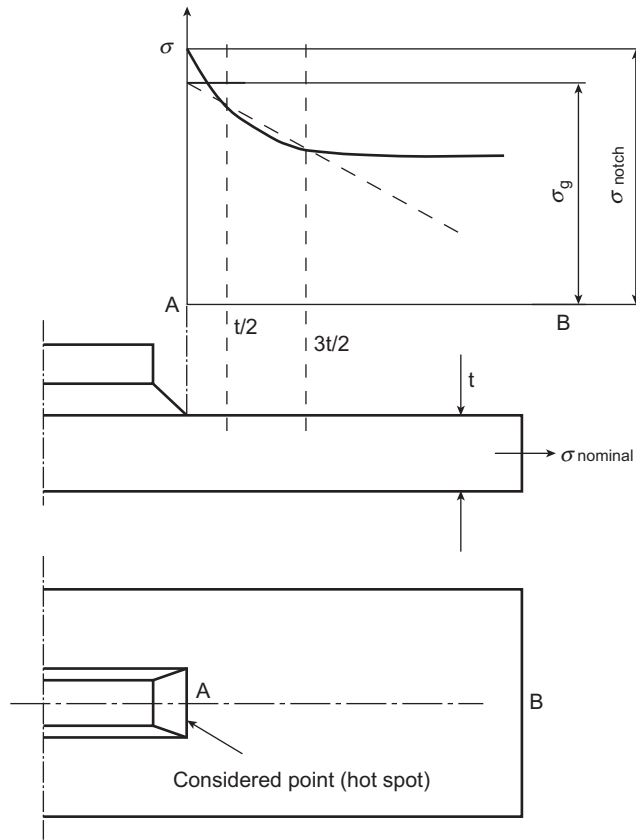


Figure 25.4

Stress distribution at an attachment and extrapolation of stresses (NTS, 1998).

25.2.3 Notch Stress Approach

The notch stress approach is based on the determination of a peak stress that accounts for the weld profile. The notch stress is therefore estimated as the product of the hot-spot stress and the SCF for a weld profile (the so-called weld concentration factor). The weld concentration factor may be estimated from diagrams, parametric equations, experimental measurements, and FEA. The presence of welds should be given due consideration in the notch stress approach.

The IIW (Hobbacher, 1996) recommended the following procedure for the calculation of notch stresses:

- An effective weld root radius of $r = 1$ mm needs to be considered.
- The method is restricted to weld joints that are expected to fail from the weld toe or the weld root.

- Flank angles of 30° for butt welds and 45° for filler welds can be considered.
- The method is limited to thicknesses larger than 5 mm.

25.3 Stress Concentration Factors

25.3.1 Definition of SCFs

The aim of the stress analysis is to calculate the stress at the weld toe (hot spot), $\sigma_{\text{hot spot}}$. The SCF due to the geometry effect is defined as

$$\text{SCF} = \frac{\sigma_{\text{hot spot}}}{\sigma_{\text{nominal}}} \quad (25.10)$$

There are three approaches in determining the SCF:

- Experimental data
- FEA
- Parametric equations based on experimental data or FEA.

The above approaches are detailed in the below subsections.

25.3.2 Determination of SCF by Experimental Measurement

Using strain measurements in fatigue tests to determine SCF is the most reliable method. However, it is important to decide exactly where to locate strain gauges to ensure that the values obtained are compatible with the chosen design $S-N$ curve. If this is not achieved, gross errors can occur.

The existing method of defining SCF for use in $S-N$ curves is based on extrapolation to the weld toe from an area of linear stress data. This includes varying proportions of the notch SCF, depending on the weld detail and the geometric stress concentration. This is due to the fundamental assumption in the hot-spot stress concept, as structural geometry effects may not be completely separated from local weld geometry effects. Size effects, weld profiles, residual stresses, and stress distributions are usually the sources of this variation. The weld profile effect in tubular joints is not primarily due to the weld shape itself; it is due to the position of the weld toe on the chord, which significantly affects the hot-spot stress at the weld toe. Therefore, a consistent stress recovery procedure should be developed in the SCF measurement.

25.3.3 Parametric Equations for SCFs

Given that a variety of SCFs need to be estimated on any given tubular joint, SCF determinations have to rely more on sets of parametric equations that account for joint geometry configurations and applied loadings.

An SCF can be defined as the ratio of the hot-spot stress range over the nominal stress range. All stress risers have to be considered when evaluating SCFs. The resulting SCF is derived as

$$\text{SCF} = \text{SCF}_g \cdot \text{SCF}_w \cdot \text{SCF}_{te} \cdot \text{SCF}_{ta} \cdot \text{SCF}_n \quad (25.11)$$

where,

SCF_g = Stress concentration factor due to gross geometry of the detail considered

SCF_w = Stress concentration factor due to weld geometry

SCF_{te} = Additional SCF due to eccentricity tolerance (normally used for plate connections only)

SCF_{ta} = Additional SCF due to angular mismatch (normally used for plate connections only)

SCF_n = Additional SCF for unsymmetrical stiffeners on laterally loaded panels, applicable when the nominal stress is derived from simple beam analysis

The best-known SCF formulae for the fatigue assessment of offshore structures are those of [Efthymiou \(1988\)](#). There are various parametric equations in the literature for the determination of SCFs. F, for instance:

- SCF equations for tubular connections: API RP2A-WSD, NORSOK N-004 ([NTS, 1998](#)) and [Efthymiou \(1988\)](#). In addition, [Smedley and Fisher \(1990\)](#) gave SCFs for ring-stiffened tubular joints under axial loads, in-plane bending, and out-of-plane bending. For rectangular hollow sections, reference is made to [Van Wingerde et al. \(1993\)](#) and [Soh and Soh \(1992\)](#).
- SCF equations for tube-to-plate connections: NORSOK N-004 and [Pilkey \(1997\)](#)
- SCF for girth welds: NORSOK N-004 ([NTS, 1998](#))

The SCF equations from the references mentioned above have been previously summarized in [DNV \(2000\)](#).

It should be noted that parametric equations are valid only for the applicability range defined in terms of geometry and loads. A general approach for the determination of SCFs is to use FEA.

25.3.4 Hot-Spot Stress Calculation Based on FEA

The aim of FEA is to calculate the geometric stress distribution in the hot-spot region so that those stresses can be used to derive SCFs. The result of the FEA of SCFs largely depends on the modeling techniques and computer program used. The use of different elements and meshes, modeling of the welds, and definition of chord length substantially influence the computed SCF ([Healy and Bultrago, 1994](#)).

By decreasing the element size, the finite element model stresses at discontinuities may approach infinity. In order to have a uniform basis for a comparison of results from different computer programs and users, it is necessary to set a lower bound for the element size and use an extrapolation procedure for the hot spot.

Stresses in FEA are normally derived at the Gaussian integration points. Depending on the element type, it may be necessary to perform several extrapolations in order to determine the stress at the weld toe. In order to preserve the information of the direction of principal stresses at the hot spot, component stresses are to be used for the extrapolation.

The analysis method should be tested against a well-known detail prior to using it in fatigue assessment. There are numerous types of elements that can be used; the SCF depends on the elements chosen. Therefore, a consistent stress recovery procedure must be calibrated when assessing data from FEA.

FEA programs such as NASTRAN, ABAQUS, and ANSYS use structural elements such as thin plate, thick plate, or shell. When modeling fabricated tubular joints, the welds may not be properly modeled by thin-plate or shell elements. Consequently, the model does not account for any notch effects due to the presence of the weld, and micro-effects due to the weld shape.

The stresses in thin-shelled plates are calculated from a membrane stress and moment at the mid-surface of the element. The total free surface stresses are determined by superposition. At a plate intersection, the peak stresses will be predicted at positions that lie inside the actual joint. Comparisons between these values and experimental measurements have indicated that thin-shell analysis overestimates the actual surface stresses or SCF present in the real structure.

Most finite elements are based on a displacement formulation. This means that displacements or deformations will be continuous throughout the mesh, but stresses will be discontinuous between elements. Thus, nodal average stresses may be recommended. However, limited comparison between these values and experimental measurements indicates that this will generally over-predict hot-spot stress or SCF, especially on the brace side.

As opposed to shell elements, a model using solid elements can include welded regions (see [Figure 25.5](#)). In these types of models, the SCFs may be derived through an extrapolation of stress components to relevant weld toes. The extrapolation direction should be normal to the weld toes. However, there is still a considerable amount of uncertainty associated with the modeling of the weld region and weld shape.

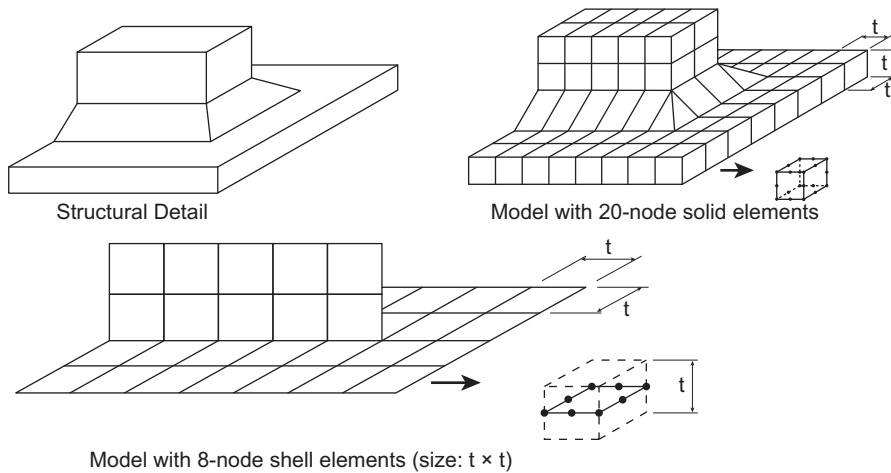


Figure 25.5
Examples of modeling (NTS, 1998).

Fricke (2002) recommended hot-spot analysis procedures for structural details of ships and FPSOs based on round-robin FE analysis. Some of his findings are

- If hot-spot stress is evaluated by linear extrapolation from stresses at $0.5t$ and $1.5t$, the fatigue strength may be assessed using a usual design $S-N$ curve based on a hot-spot stress (e.g., Hobbacher, 1996 and Maddox, 2001).
- If hot-spot stress is defined at $0.5t$ without stress extrapolation, the design $S-N$ curve should be downgraded one fatigue class.
- If the hot-spot stress is evaluated from strain measurements or refined models with improved finite elements, a stress extrapolation over reference points at distances $0.4t$ and $1.0t$, or a quadratic extrapolation, is recommended (Hobbacher, 1996).

It should be pointed out that the determination of hot-spot stress based on FEA is still a very active field. Research is ongoing, since the accuracy and efficiency of the stress determination are of high importance. Other known research work includes Niemi (1993, 1994).

25.4 Examples

25.4.1 Example 25.1: Fatigue Damage Calculation

Problem:

Two plates A and B are doubled-sided butt welded, and another plate C is welded to plate A by fillet welds, as shown in Figure 25.6. The thickness of the plate is 20 mm. The plate is subjected to cyclic loadings with a constant stress range of $S = 200$ MPa and a total

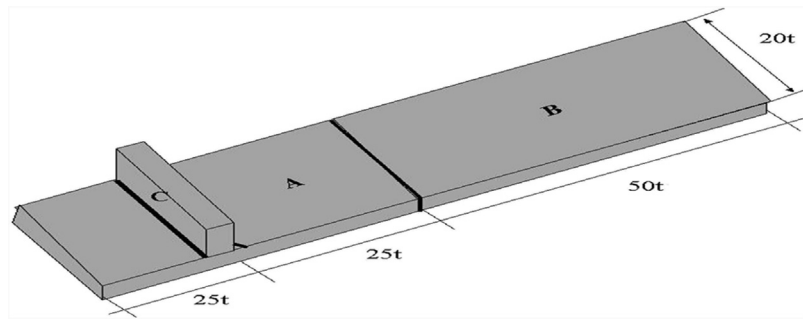


Figure 25.6
Fatigue of welded plates.

number of cycles $n_0 = 10^5$. It is assumed that the maximum misalignment of the weld is 4 mm. What is the fatigue damage at these welds?

Solution:

Misalignment introduces the bending moment in the plates. The corresponding bending stress range at the butt weld is

$$S_b = \frac{\Delta M}{W} = \frac{S \cdot t \cdot \frac{e}{2}}{\frac{t^3}{6}} = \frac{S \cdot 3e}{t}$$

The maximum stress range at the butt weld is

$$S_{\text{local}} = \left(1 + \frac{3e}{t}\right) \cdot S = \text{SCF}_{\text{global}} \cdot S = 120 \text{ MPa}$$

S – N curve C should be used for the butt weld with $m = 3.5$, $\log \bar{a} = 13.63$. This gives the following damage ratio:

$$D = \frac{\Delta \sigma_{\text{local}}^m}{\bar{a}} \cdot n_0 = \frac{120^{3.5}}{10^{13.63}} \cdot 10^5 = 0.044$$

The local stress range at the fillet weld is

$$S_{\text{local}} = 0.5 \left[S + S \left(1 + \frac{3e}{t}\right) \right] = 160 \text{ MPa}$$

Since the fillet weld is off the edge of the plate, S – N curve G should be used with $m = 3.0$, $\log \bar{a} = 11.39$; this gives the following damage ratio

$$D = \frac{\Delta \sigma_{\text{local}}^m}{\bar{a}} \cdot n_0 = \frac{160^{3.0}}{10^{11.39}} \cdot 10^5 = 1.669$$

References

- AASHTO, 1989. Standard Specification for Highway Bridges, fourteenth ed. American Association of State Highway Transportation Officials, Washington DC.
- ABS, 1992. Guide for the fatigue strength assessment of tankers. In: ABS Steel Vessel Rules. American Bureau of Shipping (latest revision).
- Almar-Naess, A., 1985. Fatigue Handbook, Offshore Steel Structures. Tapir, Norway.
- BS 5400, 1979. Steel, Concrete and Composite Bridges, Part 10, Codes of Practice for Fatigue. British Standard Institute.
- BV, 1998. Fatigue Strength of Welded Ship Structures. Bureau Veritas.
- DNV, 2000. RP-C203, Fatigue Strength Analysis of Offshore Steel Structures. Det Norske Veritas.
- ECCS, 1992. European Recommendations for Aluminum Alloy Structures: Fatigue Design. ECCS Report No. 68. European Convention for Structural Steelwork, Brussels, Belgium.
- Eurocode 3, 1993. Design of Steel Structures. European Standards.
- Efthymiou, M., 1988. Development of SCF formulae and generalized influence functions for use in fatigue analysis. In: Offshore Tubular Joints Conference OTJ, Egham, Surrey, UK.
- Fricke, W., 2002. Recommended hot-spot analysis procedures for structural details of ships and FPSOs based on round-robin FE analysis. Journal of ISOPE 12 (1), 40–47.
- Fricke, W., Berge, S., Brennan, F., Cui, W., Josefson, L., Kierkegaard, H., Kihl, D., Koval, M., Mikkola, T.P., Parmentier, G., Toyosada, M., Yoon, J.H., 2000. Fatigue and fracture. In: Committee Report of ISSC (Int. Ship and Offshore Structures Congress), Nagasaki, Japan.
- Geyer, J.F., Stahl, B., 1986. Simplified fatigue design procedure for offshore structures. In: Offshore Technology Conference, OTC Paper 5331, Houston, Texas, May 5–8.
- Healy, B.E., Bultrago, J., 1994. Extrapolation procedures for determining SCFs in mid-surface tubular joint models. In: 6th International Symposium on Tubular Joint Structures, Monash University, Melbourne, Australia.
- Hobbacher, A., 1996. Fatigue design of welded joints and components. In: International Institute of Welding (IIW), XIII-1539-96/XV-845-96, Abington Pub., Cambridge, UK.
- HSE, 1995. Offshore Installation, Guidance on Design, Construction and Certification, fourth ed. UK Health and Safety Executives. Section 21.
- IACS, July 1999. Recom. 56.1: Fatigue Assessment of Ship Structures. International Association of Classification Societies.
- Kung, J.G., Potvin, A., et al., 1975. Stress concentrations in tubular joints. Paper OTC 2205. In: Offshore Technology Conference.
- Lalani, M., 1992. Developments in tubular joint technology for offshore structures. In: Proceedings of the International Conference on Offshore and Polar Engineering, San Francisco, CA.
- Maddox, S., 2001. Recommended Design S-N Curves for Fatigue Assessment of FPSOs. ISOPE, Stavanger.
- Marshall, P.W., 1992. Design of Welded Tubular Connections. Elsevier Press, Amsterdam.
- Marshall, P.W., 1993. API provisions for SCF, SN and size-profile effects. In: Offshore Technology Conference, Houston, TX.
- Niemi, E., 1993. Stress Determination for Fatigue Analysis of Welded Components. International Institute of Welding (IIW). Technical Report IIS/IIW-1221–93.
- Niemi, E., 1994. On the Determination of Hot Spot Stress in the Vicinity of Edge Gussets. International Institute of Welding (IIW). Technical Report IIS/IIW-1555–94.
- NTS, 1998. Design of Offshore Structures, Annex C, Fatigue Strength Analysis. NOR-SOK Standard N-004.
- Pilkey, W., 1997. Petersen's Stress Concentration Factors, second ed. John Wiley and Sons, Inc.
- Smedley, P., Fisher, P., 1990. Stress concentration factors for ring-stiffened tubular joints. In: International Symposium on Tubular Structures, Delft, June 1990.
- Soh, A.K., Soh, C.K., 1992. Stress concentrations in T/Y and K spare-to-spare and square-to-round tubular joints. Journal of OMAE 114.

UK DEn, 1990. Offshore Installations: Guidance on Design, Construction, and Certification, third ed. UK Department of Energy (Now UK Health and Safety Executives).

Van Wingerde, A.M., Packer, J.A., Wardenier, J., Dutta, D., Marchall, P., 1993. Proposed revisions for fatigue design of planar welded connections made of hollow structural sections. paper 65. In: Coutie, et al. (Eds.), Tubular Structures.

Fatigue Loading and Stresses

26.1 Introduction

Marine structures are exposed to a variety of loads during their life cycles. The loads are commonly classified as:

- Functional
 - Dead loads
 - Live loads
- Environmental
 - Sea loads (waves and currents)
 - Wind loads
 - Seismic loads
- Accidental

All loads that vary in magnitude and/or direction will cause stress variations in a structure that may potentially lead to fatigue damage. Live loads and environmental loads are especially important in this respect. Environmental loads dominate, for the most part, in marine structures. Waves and currents are considered the most important sources of environmental loads that act on marine structures. Moored floating structures are also sensitive to wind loads.

Fatigue loading, a key parameter in fatigue analysis, is long-term loading during the fatigue damage process. Various studies have been conducted on the fatigue loading of marine structures in order to characterize the sea environment, the structural response, and a statistical description. The sea environment is generally characterized by the wave spectrum. Structural response is determined using hydrodynamic theory and finite element analysis.

The objective of this chapter is to present a general procedure for long-term fatigue stress described using Weibull distribution functions. Other methods of fatigue loading include the design wave and wave scatter diagram approaches. The Weibull stress distribution function has been used in the simplified fatigue assessment (see Chapter 27), while the wave scatter diagram approach is applied in frequency–domain and time–domain fatigue analyses (see Chapter 28).

Some earlier research on fatigue loads has been summarized by [Almar-Naess \(1985\)](#). Recent developments in this field may be found in [Baltrop \(1998\)](#), as well as in papers such as [Chen and Shin \(1995\)](#) and the ISSC committee reports.

26.2 Fatigue Loading for Oceangoing Ships

For oceangoing ships, two basic sea states are considered in the determination of global bending loads and local pressure: the head sea condition and the oblique sea condition. Cumulative fatigue damage should be calculated for the fully laden condition and the ballast condition, respectively. The probability for each of these conditions is defined by the classification rules according to the type of vessel (seen below) ([Table 26.1](#)):

The two basic sea states combine the various dynamic effects of the environment on hull structures. The load components for these sea states depend on the ship classification rules applied. For instance, [BV \(1998\)](#) further defines hull girder loads and local loads (pressure and internal loads) for four cases as shown in [Table 26.2](#).

Global loads include the still-water bending moment M_{SW} for the load condition considered, and the vertical wave bending moment. The vertical bending stress σ_L is further defined:

- In sagging condition for maximum internal cargo or ballast loads

$$\sigma_L = (M_{SW} + A_{\max}(M_{WV})_S) \frac{z - N}{I_V} + BM_{WH} \frac{y}{I_H} \quad (26.1)$$

- In hogging condition for minimum internal cargo or ballast loads

$$\sigma_L = (M_{SW} + A_{\min}(M_{WV})_H) \frac{z - N}{I_V} + BM_{WH} \frac{y}{I_H} \quad (26.2)$$

where,

I_V and I_H are the moments of inertia of a cross section about the horizontal and vertical neutral axes, respectively.

N and z are the vertical distances from the keel line to the neutral axis, and from the keel line to the load point, respectively.

y is the horizontal distance from the load point to the centerline.

Table 26.1: Percentage of fatigue loading conditions (IACS, 1999)

	Fully Laden Load, α (%)	Ballast, β (%)
Oil tankers, liquefied gas carriers	50	50
Bulk carriers	60	40
Container ships, cargo ships	75	25

Table 26.2: Load cases for oceangoing ships (BV, 1998)

	Head Sea Condition, α	Oblique Sea Condition, β
Static sea pressure associated with maximum and minimum inertia cargo or blast loads	Case 11 $A_{\max} = -0.45$ $A_{\min} = 0.45$ $B = 0$	Case 21 $A_{\max} = -0.30$ $A_{\min} = 0.30$ $B = 0.45$
Maximum (ship on crest of wave) and minimum (ship on trough of wave) wave-induced sea pressure associated with static internal cargo or ballast loads	Case 12 $A_{\max} = 0.625$ $A_{\min} = -0.625$ $B = 0.45$	Case 22 $A_{\max} = -0.30 \operatorname{sgn}(z-N)$ $A_{\min} = 0.30 \operatorname{sgn}(z-N)$ $B = -0.625$

$(M_{WV})_S$ and $(M_{WV})_H$ are vertical wave bending moments for sagging and hogging conditions, respectively, according to IACS requirements.

A_{\max} , A_{\min} , and B are coefficients defined in Table 26.2.

Local loads include static sea pressure and internal cargo or ballast loads. The stress ranges for fully laden load conditions are estimated as

$$S_{ij} = \left| (\sigma_{ij})_{\max} - (\sigma_{ij})_{\min} \right| \quad (26.3)$$

Similarly, the stress ranges for ballast load conditions may be estimated by

$$S'_{ij} = \left| (\sigma'_{ij})_{\max} - (\sigma'_{ij})_{\min} \right| \quad (26.4)$$

The long-term distribution of the hull girder stress range can be represented by a two-parameter Weibull distribution. When long-term analysis of ship behavior performed at sea enables the long-term distribution of hull girder bending stress to be determined, the shape parameter ξ can be determined as follows (BV, 1998):

$$\xi = 0.47 / \ln \left(\frac{\sigma_{10^{-8}}}{\sigma_{10^{-5}}} \right) \quad (26.5)$$

where $\sigma_{10^{-8}}$ and $\sigma_{10^{-5}}$ are the extreme hull girder bending stresses for a probability of exceedance of 10^{-8} and 10^{-5} , respectively.

If no direct analysis of the ship's behavior at sea is performed, a first approximation of the shape parameter ξ for oceangoing steel vessels can be taken from IACS (1999) as

$$\xi = 1.1 - 0.35 \frac{L - 100}{300} \quad \text{where } L \text{ is ship length in m} \quad (26.6)$$

26.3 Fatigue Stresses

26.3.1 General

As preparation for Chapter 27, this section presents three different approaches for the estimation of long-term fatigue stress, which will be used respectively by subsequent chapters and are based on the:

- Weibull distribution
- Deterministic approach
- Stochastic approach

26.3.2 Long-Term Fatigue Stress Based on the Weibull Distribution

The Weibull probability density function for long-term fatigue stress S can be described as

$$f(S) = \frac{\xi}{A} \left(\frac{S}{A}\right)^{\xi-1} \exp\left[-\left(\frac{S}{A}\right)^{\xi}\right] \quad (26.7)$$

where A is a scale parameter, and ξ is a shape parameter that is a function of the type of structure and its location. See [Table 26.3](#) for typical values for the shape parameter ξ .

The Weibull shape parameter is generally dependent on the load categories contributing to the occurrence of cyclic stress.

The Weibull distribution function is then

$$F(S) = \int_0^S f(S)dS = 1 - \exp\left[-\left(\frac{S}{A}\right)^{\xi}\right] \quad (26.8)$$

The stress exceedance probability may then be expressed as

$$p = 1 - \int_0^S f(S)dS = \exp\left[-\left(\frac{S}{A}\right)^{\xi}\right] \quad (26.9)$$

Table 26.3: Typical Weibull shape parameter values for simplified fatigue assessment

Typical Values for Shape Parameter ξ	
Fast cargo ships	$\xi > 1$, may be as high as 1.3 or a little more
Slower ships in equatorial waters	$\xi < 1$, and perhaps as low as 0.7
Gulf of Mexico fixed platforms	$\xi \cong 0.7$
North Sea fixed platforms	$\xi > 1$, may be as high as 1.4 if the platform is slender and dynamically active

If S_0 is the expected extreme stress occurring once in a lifetime of N_0 wave encounters (or stress reversals), Eqn (26.9) becomes

$$p(S_0) = \exp \left[- \left(\frac{S_0}{A} \right)^\xi \right] = \frac{1}{N_0} \quad (26.10)$$

From the above equation, the equation below is obtained (Almar-Naess, 1985).

$$A = S_0 (\ln N_0)^{-1/\xi} \quad (26.11)$$

The special case of $\xi = 1$ is the well-known exponential distribution in which the log(n) plot of stress exceedance is a straight line. Substituting Eqn (26.10) in Eqn (26.7)

$$p = \exp \left[- (\ln N_0) \left(\frac{S}{S_0} \right)^\xi \right] = \frac{1}{N} \quad (26.12)$$

From Eqn (26.11)

$$S = S_0 \left[\frac{\log N}{\log N_0} \right]^{1/\xi} \quad (26.13)$$

26.3.3 Long-Term Stress Distribution Based on the Deterministic Approach

This method is based on the deterministic calculation of wave forces, and it involves (Almar-Naess, 1985):

1. Selection of major wave directions
Four to eight major wave directions are selected for analysis. The selection of major wave directions must consider those that cause high stresses on key structural members. All of the waves are distributed among these major directions.
2. Establishment of long-term distributions of waves
For each wave direction selected, a long-term distribution of wave height is established by a set of regular waves that adequately describes the directional long-term wave distributions. The range of wave heights that gives the highest contribution to fatigue damage is given special attention. The most probable period may be taken as the wave period.
3. Prediction of stress ranges
For each wave identified (direction, height, period), a stress range is predicted using a deterministic method for hydrodynamic loads and structural responses.

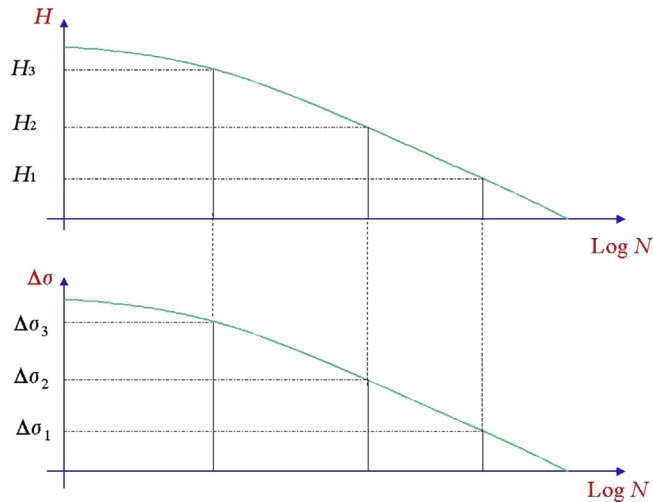


Figure 26.1
Stress distribution illustration.

4. Selection of stress distribution

The long-term stress exceedance diagram from the wave exceedance diagram is illustrated in [Figure 26.1](#), where $\Delta\sigma_i$ and H_i denote stress range and wave height, respectively.

A simplified fatigue analysis has been coded in [API 2A – WSD \(2001\)](#), assuming that the relation between the stress range S and wave height H has been obtained using the deterministic approach.

$$\Delta\sigma = CH^g \quad (26.14)$$

where C is a calibrated constant and g is a calibrated exponent. The long-term wave height distribution is represented by the sum of two Weibull distributions: one for the normal condition H_0 , and one for the hurricane condition H_1 .

$$\Delta\sigma = CH_0^g \text{ for normal condition} \quad (26.15)$$

$$\Delta\sigma = CH_1^g \text{ for hurricane condition} \quad (26.16)$$

Based on the methodology described in [Chapter 27](#), the cumulative fatigue damage can easily be derived for normal and hurricane conditions. The formulae for the cumulative fatigue damage based on the deterministic method can be found as part of the commentary on fatigue in [API RP 2A—WSD](#).

26.3.4 Long-Term Stress Distribution—Spectral Approach

The spectral approach requires a more comprehensive description of environmental data and loads, and a more detailed knowledge of these phenomena. Using the spectral approach, the dynamic effects and irregularities of waves may be more properly accounted for.

This approach involves the following steps:

- Selection of major wave directions. The same considerations are applied as in the previous discussion regarding the deterministic approach.
- For each wave direction, select a number of sea states and associated durations that adequately describe the long-term distribution of the wave.
- For each sea state, calculate the short-term distribution of stress ranges using a spectral method.

Combine the results for all sea states in order to derive the long-term distribution of the stress range. In the following, a formulation is used to further illustrate the spectral approach (DNV, 1998).

A wave scatter diagram may be used to describe the wave climate for fatigue damage assessment. The wave scatter diagram is represented by the distribution of H_s and T_z . The environmental wave spectrum $S_\eta(\omega)$ for the different sea states can be defined—for example, by applying the Pierson–Moskowitz wave spectrum (see Chapter 5).

When the relationship between the unit wave height and stresses, “the transfer function $H_\sigma(\omega|\theta)$,” is established, the stress spectrum $S_\sigma(\omega)$ is obtained.

$$S_\sigma(\omega) = |H_\sigma(\omega)|^2 \cdot S_\eta(\omega) \tag{26.17}$$

The n th spectral moment of the stress response can be described as

$$m_n = \int_0^\infty \omega^n \cdot S_\sigma(\omega) d\omega \tag{26.18}$$

A spreading function may be used to include wave spreading,

$$f(\theta) = k \cos^n(\theta) \tag{26.19}$$

where k is selected, such that $\sum_{\theta=-90^\circ}^{\theta+90^\circ} f(\theta) = 1$. Normally, $n = 2$. The spectral moment can then be expressed as

$$m_{ni} = \int_0^\infty \sum_{\theta=-90}^{\theta+90} f_S(\theta) \cdot \omega^n \cdot S_\sigma(\omega) d\omega \tag{26.20}$$

where m_{0i} is the 0th spectral moment. The average stress cycle period is thus

$$T_{02i} = \frac{1}{\nu_{0i}} = 2\pi \sqrt{\frac{m_{0i}}{m_{2i}}} \tag{26.21}$$

and the number of cycles within the sea state of period T_i is

$$n_i = \frac{T_i}{T_{02i}} \quad (26.22)$$

Nonlinear effects due to large amplitude motions and large waves can be neglected in the fatigue assessment, since the stress ranges at lower load levels contribute relatively more to cumulative fatigue damage. In cases where linearization is required, it is recommended that the linearization is performed at a load level representative for stress ranges that contribute the most to fatigue damage—that is, stresses at probability levels of exceedance between 10^{-2} and 10^{-4} . The stress range response may be assumed to be Rayleigh-distributed within each sea state as

$$F_i(S) = 1 - \exp\left(-\frac{S^2}{8m_{0i}}\right) \quad (26.23)$$

The long-term distribution of the stress range may be estimated by a weighted sum over all sea states as

$$F(S) = \sum_{i=1}^{\text{All Sea states}} r_i p_i F_i(S) \quad (26.24)$$

where p_i is the probability of occurrence of the i th sea state, and the weighted coefficient is

$$r_i = \frac{\nu_{0i}}{\sum \nu_{0i} p_i} \quad (26.25)$$

The obtained long-term distribution of the stress range can be described using a probability function—for example, Weibull distribution functions in which Weibull parameters are determined through curve fitting.

26.4 Fatigue Loading Defined Using Scatter Diagrams

26.4.1 General

A “short-term” description of the sea (or sea state) means the significant wave height and the mean wave period are assumed to be constant during the considered time period. To construct a “long-term” description of the sea, scatter diagrams are needed. The scatter diagrams are used for spectral and time–domain fatigue analyses, where waves and currents are defined using wave scatter diagrams and current scatter diagrams, respectively. The environmental criteria are defined as directional sea, swell, winds, and currents, as well as their combinations, that the structure will be subjected to throughout its life cycle.

Unless the mean stress is very large (e.g., for TLP tethers), its effects are ignored. Hence, steady current is normally not given attention, except for the effect it has on nonlinear

dynamic responses. The current scatter diagram is mainly used for the prediction of vortex-induced vibrations.

The joint frequencies of significant wave height H_s and spectral wave period T_z are defined using the wave scatter diagram. Each cell of the diagram represents a particular combination of H_s and T_z , and its probability of occurrence. The fatigue analysis involves a random sea analysis for each sea state in the scatter diagram, and then the calculated fatigue damages based on the probability of occurrence for the corresponding sea state are summed. From the motion analysis, the stress amplitude operator (RAO) is obtained for a particular reference sea state.

Long-term directionality effects are also accounted for using wave scatter diagrams in which the probability of each direction is defined. For each set of significant wave height H_s and spectral wave period T_z , the total summed probability for all directions should equal 1.0.

26.4.2 Mooring- and Riser-Induced Damping in Fatigue Sea States

Viscous damping due to drag on mooring lines and risers can significantly affect the motions of deepwater floating structures. Traditionally, the motion response of moored floating structures has been evaluated by modeling mooring lines and risers as massless springs. In this uncoupled approach, the inertia, damping, and stiffness of mooring lines and risers are not properly included in the prediction of vessel motions.

The dynamic interaction between the floating structure, mooring lines, and risers should be evaluated using a coupled analysis that provides consistent modeling of the drag-induced damping from mooring lines and risers. The coupled analysis can be based on a frequency—domain (Garrett et al., 2002) or time—domain approach. In coupled approaches, mooring lines and risers are included in the model, together with the floating structure.

In return, vessel motions impact the fatigue of TLP tethers, mooring lines, and risers. For the fatigue analysis, it is necessary to calculate vessel motions such as:

- Linear wave-induced motions and loads
- Second-order nonlinear motions

Motion-induced fatigue is a key factor when selecting the riser departure angle.

26.5 Fatigue Load Combinations

26.5.1 General

One field that is perhaps in need of more research is load combinations for fatigue design, even though earlier research has been done by Wen (1990) and Chakrabarti (1991).

In the determination of extreme loads for ultimate strength analysis, the main objective is to select the maximum anticipated load effect when the structure is subject to one of the design load sets. However, for fatigue design, it is necessary to estimate the governing design load sets and the shape of the long-term stress range distribution at any structural location.

26.5.2 Fatigue Load Combinations for Ship Structures

For ship structural design, [Munse et al. \(1983\)](#) identified the following cyclic fatigue load sources:

- Low-frequency wave-induced loads: 10^7 – 10^8 reversals during a ship's life
- High-frequency wave-induced loads: 10^6 reversals during a ship's life
- Still-water loading: 300–500 cycles
- Thermal loads: 7000 cycles

The amplitude of fatigue loads is influenced by wave statistics, changes in course, speed, and the deadweight condition. [Mansour and Thayamballi \(1993\)](#) suggested considering the following loads and their combinations:

- Fatigue loads resulting from hull girder bending
- Fatigue loads resulting from local pressure oscillations
- Cargo loading and unloading (low cycle effects)
- Still-water bending (mean level) effects

Of the loads listed above, hull girder bending and local pressure fluctuation contribute most to total fatigue damage. Depending on the location, one of these two loads will typically dominate. For instance, vertical bending moments related to stress fluctuations at the ship deck predominate, while the stress range on the side shell near the waterline is almost entirely due to local (internal/external) pressure. Structural details in the ship bottom are influenced by a combination of bending and local pressure effects.

Pressure variations near the waterline are the main cause of fatigue damage to the side shell ([Friis-Hansen and Winterstein, 1995](#)).

For spectral fatigue analysis of ships for an unrestricted service, the nominal North Atlantic wave environment is frequently used. For a site-specific assessment (of FPSO), or for a trade route known to be more severe than the North Atlantic, the more stringent wave scatter diagram should be applied. When motions and loads are frequency dependent, it is necessary to include wave-period variations.

The fatigue loading conditions for ships are fully laden and ballast. According to the classification rules (e.g., [BV, 1998](#)) for each relevant loading condition, two basic sea

states must be considered: the head sea condition and the oblique sea condition. The total cumulative damage may be estimated as

$$D = \alpha D_0 + \beta D'_0 \quad (26.26)$$

where the coefficients α and β are given in [Table 26.1](#). Cumulative damage due to fully laden and ballast load conditions is represented by D_0 and D'_0 , respectively.

$$D_0 = (D_1 + D_2) \quad (26.27)$$

$$D'_0 = (D'_1 + D'_2) \quad (26.28)$$

where,

$$D_i = \max(D_{i1}, D_{i2}), \quad i = 1, 2 \text{ for fully laden load condition} \quad (26.29)$$

$$D'_i = \max(D'_{i1}, D'_{i2}), \quad i = 1, 2 \text{ for ballast load condition} \quad (26.30)$$

where D_{11} , D_{12} or D'_{11} , D'_{12} are cumulative damage for the static sea pressure associated with maximum and minimum inertia cargo or ballast loads, respectively, and D_{21} , D_{22} or D'_{21} , D'_{22} are cumulative damage for the maximum (ship on crest of wave) and minimum (ship on trough of wave) wave-induced sea pressures associated with static internal cargo or ballast loads, respectively.

26.5.3 Fatigue Load Combinations for Offshore Structures

When defining environmental conditions for offshore structural design, it is necessary to derive combinations of the directional sea, swell, wind, and current that the offshore structure will encounter during its life. The fatigue of hull structures, mooring lines, and risers is largely dependent on sea and swell conditions, while the current may cause vortex-induced vibrations on risers, mooring lines, and TLP tethers. Directional scatter diagrams must therefore be defined for sea states, for swells, and sometimes for currents. Swells will only be properly considered (typically by adding a separate swell spectrum into the analysis and so obtaining a multi-peaked sea-plus-swell spectrum) if it is of particular importance; this is the case, for instance, in offshore West Africa and Australia ([Baltrop, 1998](#)). An alternative approach for properly accounting for swells is to use two separated scatter diagrams for the directional sea and swell, respectively. In this case, the probability of each individual bin (sea-states, cells) is properly defined, and each bin (cell) is represented by a single peak spectrum defined by significant wave height H_s and spectral wave period T_z . Swells in some instances come from a single direction without much variation. However, in general, directionality should be considered when defining scatter diagrams. The selection of sea states for combined sea, swell, current, and wind is a complex subject and requires certain engineering judgment based on an understanding of environmental data and structural dynamic response.

Other critical issues that must be accounted for are the load cases and the loading conditions. To estimate fatigue damage during operating conditions, vessel motions and RAO data should be generated under normal operating conditions. Similar statements are also often valid for the estimation of fatigue damage during transportation and installation phases. The total accumulated damage is then obtained by adding the damage for each phase of the design fatigue life and the period/probability of the respective phase. For fatigue analysis of TLP tethers, mooring lines and risers, it is necessary to define the vessel motions and the RAO at the point where tethers, mooring lines, and risers are attached to the vessel.

Francois et al. (2000) compared fatigue analysis results from classification societies and full-scale field data.

An example analysis was conducted by Nordstrom et al. (2002) to demonstrate the heading methodology and to assess its efficiency for use on an FPSO project. Their proposed heading and fatigue analysis procedure could potentially lead to a more effective fatigue design for FPSOs in noncollinear environments.

26.6 Examples

26.6.1 Example 26.1: Long-Term Stress Range Distribution—Deterministic Approach

Problem:

Determine the long-term stress range distribution of the spanned riser clamped to a jacket platform as shown in Figure 26.2 below. This example is chosen to illustrate the deterministic approach in Section 26.3.3 (Almar-Naess, 1985). It may be assumed that

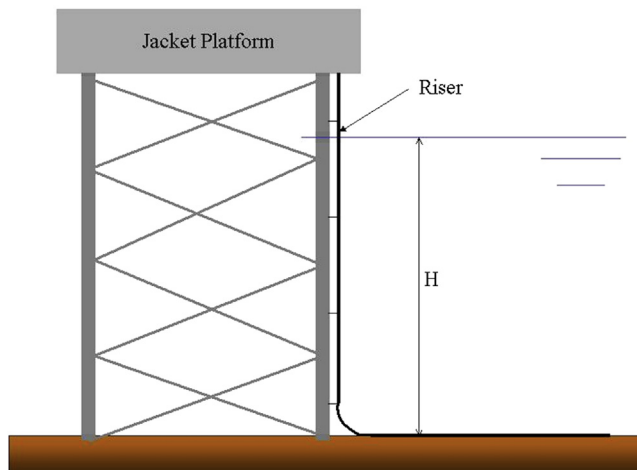


Figure 26.2

Spanned riser attached to platform.

the riser span length is $l = 10$ m, outer diameter $OD = 0.27$ m, wall thickness $WT = 0.0015$ m, moment of inertia $I = 9.8 \cdot 10^{-5} \text{ m}^4$, and the water depth is 100 m. All waves are assumed to approach from the same direction.

Solution:

The first natural period of the span, f_N , can be calculated by

$$f_N = \frac{1}{2\pi} \cdot a_N \cdot \sqrt{\frac{EI}{m \cdot l^4}} = 0.17 \text{ s}$$

where,

EI = Bending stiffness

l = Span length

m = Mass per unit length

a_N = Numerical constant, for a beam fixed at both ends, $a_N = 22$ for the first mode.

The wave force intensity is denoted as $F(x)$. The moment at the span center is given by

$$M = \int_{-25}^{-15} [x - (-20)] \cdot F(x) \cdot dx$$

The long-term distribution of individual wave heights is given by

$$P_L(H) = 1 - \exp \left[1 - \left(\frac{H}{C^* H_C} \right)^D \right]$$

where $H_c = 2.7$, $C = 0.462$, and $D = 0.928$.

The number of waves exceeding a wave height H per year is given by

$$N = N_0 [1 - P_L(H)]$$

where N_0 is the total number of waves in one year, $N_0 = 106.72$. The wave force is calculated based on Morison's equation,

$$F = \frac{1}{2} \rho C_D D \cdot v^2 + \rho C_M \frac{\pi D^2}{4} a$$

where $C_D = 1.0$, $C_M = 2.0$.

Considering the wave: $H = 11.0$ m, $T = 11.7$ s, the angular frequency is

$$\omega = \frac{2\pi}{T} = 0.537 \text{ s}^{-1}$$

Applying the linear wave theory, the wave number k is given by

$$\frac{\omega^2}{g} = k \cdot \tan h(kd)$$

where d is the water depth. Numerically solve this equation gives $k = 0.0296 \text{ m}^{-1}$.

Setting $x = 0$ at the riser center, the horizontal wave-induced water particle velocity is given by

$$v(x) = \omega \frac{H}{2} \cdot \frac{\cos h(k * (x + d))}{\sin h(k * d)} * \sin(\omega t)$$

and the horizontal wave-induced acceleration is

$$a(x) = \omega^2 \cdot \frac{H}{2} \cdot \frac{\cos h(k * (x + d))}{\sin h(k * d)} \cos(\omega t)$$

When the linear wave theory is used, the calculations can be simplified by separating the drag and inertial forces

$$M(\omega t) = M_D(\omega t) + M_I(\omega t)$$

where the moments due to drag forces and inertial forces are given by

$$M_D(\omega t) = M_{D,max} * \sin^2(\omega t) = 4596 * \sin^2(\omega t) (\text{Nm})$$

$$M_I(\omega t) = M_{I,max} * \cos(\omega t) = 1306 * \cos(\omega t) (\text{Nm})$$

Maximizing $M(\omega t)$ gives

$$\cos(\omega t) = \frac{M_{I,max}}{2 * M_{D,max}} = 0.142, \omega t = 81.8^\circ$$

The maximum moment is then given by

$$M_{max} = 4689 \text{ Nm.}$$

And the resulting stress range is,

$$S = 2\sigma_{max} = \frac{MD}{I} = 12.9 \text{ MPa}$$

The procedure above is repeated for all waves, and the analysis results are summarized in the below table for the establishment of a stress range exceedance diagram (Table 26.4).

Table 26.4: Long-term distribution of wave height and stress range

H (m)	T (s)	F_{\max} (N/m)	S (Mpa)	Log N
0		0	0	6.72
3.0	7.2	28	1.0	5.74
5.0	8.7	66	2.3	5.14
7.0	9.8	140	4.8	4.57
9.0	10.8	250	8.6	4.00
11.0	11.7	384	13.2	3.45
15.0	13.1	738	25.4	2.35
20.0	14.6	1326	46.7	1.00

Note that N is the number of cycles exceeding a given wave height, force, and stress range in one year. A stress range exceedance diagram can be plotted based on the S –Log N relationship given in the table.

26.6.2 Example 26.2: Long-Term Stress Range Distribution—Spectral Approach

Problem:

Determine the long-term stress range distribution of the spanned riser that was considered in Example 26.1, using the spectral approach. This example illustrates the spectral approach for the determination of long-term stress ranges, as described in Section 26.3.4 (Almar-Naess, 1985).

Solution:

The long-term stress range distribution is obtained from Eqn (26.21) by summing the short-term distributions for a number of sea states. The procedure for deriving short-term stress distributions using Eqn (26.20) is illustrated below. The most probable wave period for a given wave height is

$$T = \frac{2\pi}{\omega} = 0.7 + 4.2H^{0.4}$$

The transfer function may be expressed as

$$H_{\sigma}(\omega) = \frac{\sigma_{\max}(\omega)}{H/2}$$

where $\sigma_{\max}(\omega)$ is the maximum stress caused by wave frequency ω .

Again, wave height $H = 11$ m, $T = 11.7$ s, and $\omega = 0.539$ are considered. From deterministic analysis, it can be found that

$$M_{\max}(\omega = 0.539) = 4698 \text{ Nm}, \quad \sigma_{\max}(\omega = 0.539) = 6.9 \text{ MPa}$$

The transfer function may then be calculated from $\sigma_{\max}(\omega)$ and H . This calculation is repeated for a set of wave periods between 3 and 25 s in order to derive the relationship between $H_{\sigma}(\omega)$ and ω .

When the relationship between the unit wave height and the stresses, “the transfer function $H_{\sigma}(\omega|\theta)$,” is established, the stress spectrum can be given as

$$S_{\sigma}(\omega) = |H_{\sigma}(\omega)|^2 \cdot S_{\eta}(\omega)$$

The n th spectral moment of the stress response may be described for the i th sea state as

$$m_{0i} = \int_0^{\infty} S_{\sigma}(\omega) d\omega = 115.6 \text{ MPa}^2$$

$$m_{2i} = \int_0^{\infty} \omega^2 S_{\sigma}(\omega) d\omega = 35.74 (\text{MPa/s})^2$$

The average stress cycle period is thus

$$T_{02i} = 2\pi \sqrt{\frac{m_{0i}}{m_{2i}}} = 11.3 \text{ s}$$

and the number of cycles within the sea state of period T_i is

$$n_i = \frac{T_i}{T_{02i}} = \frac{3 \times 3600}{11.3} = 956$$

The stress range response may be assumed to be Rayleigh-distributed within each sea state as

$$F_i(S) = 1 - \exp\left(-\frac{S^2}{8m_{0i}}\right)$$

26.7 Concluding Remarks

In this chapter, fatigue loads for ships and offshore structures have been discussed for simplified fatigue assessment and spectral fatigue assessment.

For ship structures, the key fatigue loads are global wave loads, local pressure, and internal loads. These fatigue loads are applied to a structural response model. The fatigue loads can be applied using a simplified fatigue assessment and a spectral fatigue assessment, see [Sections 26.3](#) and [26.4](#). Areas that require future research include ([Chen and Shin, 1995](#)):

- Calculation of loads accounting for nonlinearities
- Development of a theoretical method to combine high- and low-frequency responses (e.g., ordinary wave-induced loads plus slam-induced whipping)

- Development of hull-stress monitoring systems that link a ship's service experiences with anticipated fatigue failure
- Quantification of uncertainty in load predictions, including load combinations

For offshore structures, key issues include the definition of scatter diagrams for random sea, swell, wind, and current loads for all specific sites offshore. Another key issue is the estimation of vessel motions and RAO based on the structural model, environmental conditions, and loads. Areas that require more research include:

- Collection of reliable environmental data for specific sites
- Fatigue load combinations for random sea, swell, wind, and currents
- Evaluation of vessel motion, RAO, and low-frequency motions

References

- Almar-Naess, A. (Ed.), 1985. *Fatigue Handbook - Offshore Steel Structures*. Tapir Press, Norway.
- API RP2A – WSD, 2001. *Recommended Practice for Planning, Designing and Constructing Fixed Offshore Platforms – Working Stress Design*. American Petroleum Institute.
- Baltrop, N., 1998. *Floating Structures: A Guide for Design and Analysis*, vol. 1. Oilfield Publications, Inc.
- BV, July 1998. *Fatigue Strength of Welded Ship Structures*. Bureau Veritas.
- Chakrabarti, S.K., 1991. *Strategies for Nonlinear Analysis of Marine Structures*. Report No. SSC-347. Ship Structure Committee.
- Chen, Y.N., Shin, Y.S., 1995. Consideration of loads for fatigue assessment of ship structures. In: *Proc. Symposium and Workshop on the Prevention of Fracture in Ship Structures*, Washington, DC.
- DNV, 1998. *Fatigue Assessment of Ship Structures*. Det Norske Veritas. Classification Notes No. 30.7.
- Francois, M., Mo, O., Fricke, W., Mitchell, K., Healy, B., 2000. *FPSO Integrity: Comparative Study of Fatigue Analysis Methods*. OTC 12148.
- Friis-Hansen, P., Winterstein, S.R., 1995. Fatigue damage in the side shell of ships. *Journal of Marine Structures* 8 (6), 631–655.
- Garrett, D.L., Gordon, R.B., Chappell, J.F., 2002. *Mooring and Riser Induced Damping in Fatigue Seastate*. OMAE2002–28550.
- IACS, 1999. *Fatigue Assessment of Ship Structures*. International Association of Classification Societies. Recommendation 56.1.
- Mansour, A., Thayamballi, A., 1993. *Probability-based Ship Design Loads and Load Combinations*. Report No. SSC-373. Ship Structure Committee.
- Munse, W.H., Wibur, T.W., Telalian, M.L., Nicol, K., Wilson, K., 1983. *Fatigue Characterization of Fabricated Ship Details for Design*. Report No. SSC-318. Ship Structure Committee.
- Nordstrom, C.D., Lacey, P.B., Grant, R., Hee, D.D., 2002. *Impact of FPSO Heading on Fatigue Design in Non-collinear Environments*. OMAE2002–28133.
- Wen, Y.K., 1990. *Structural Load Modeling and Combination for Performance and Safety Evaluation*. Elsevier.

Simplified Fatigue Assessment

27.1 Introduction

Fatigue assessment of structural connections (tubular joints, plated connections, pipe welds, etc.) is one of the most critical issues in the design of marine structures including ships, fixed platforms, floating structures, pipelines, risers, and mooring lines. The results of a fatigue assessment are influenced by several aspects of cost and safety:

- Quality of the connection material
- Quality of welding fabrication (welding, heat treatment, etc.)
- Frequency of inspections and repairs
- Consequences of potential fatigue failure
- Residual strength of partially damaged structural systems

There are five key methodologies for the estimation of accumulated fatigue damage:

1. Deterministic fatigue analysis
2. Simplified fatigue assessment—assuming that the stress range follows a Weibull distribution (discussed in this chapter)
3. Spectral fatigue analysis (Chapter 28)
4. Time–Domain fatigue analysis (Chapter 28)
5. Fracture mechanics—based assessment of fatigue damages (Chapter 29)

The first four methodologies estimate fatigue damages using the S–N curve, while the last is based on the fracture mechanics approach.

Fatigue criteria in the classifications rules—such as the [ABS \(2002\)](#) steel vessel rules—use a simplified fatigue assessment based on empirical values for Weibull shape parameters. The simplified fatigue assessment is also supported by [API RP 2A \(2001\)](#) for some cases.

This chapter describes a simplified procedure for fatigue assessment based on a two-parameter Weibull distribution. The Weibull shape parameter depends on the wave climate and the character of the structural response, especially the possible influence of structural dynamics. The fatigue evaluation result is very sensitive to the Weibull shape parameter. The advantage of the simplified fatigue assessment is that a closed-form expression for fatigue damage can be derived, and the Weibull shape parameter can be calibrated based on historical data of fatigue cracks.

27.2 Deterministic Fatigue Analysis

In the deterministic fatigue analysis of marine structures, “blocks” of periodic single waves with specified wave height H_i and period T_i are used, where $i = 1, 2, 3, \dots, n$. Considering the fatigue damage for a reference time period T_R , the analysis procedures are illustrated in Figure 27.1 and detailed below:

- Calculate the number of occurrences for the i th wave block: $n_i = T_R \cdot P_i / T_i$, where P_i is the probability (relative frequency) of the wave height H_i .
- Calculate the stress range $s_i(H_i)$ based on static analysis of the structural response to wave height H_i and period T_i . The stress concentration factor SCF (which is denoted as K in Figure 27.1) is obtained using parametric equations or experimental/numerical analysis. The dynamic amplification factor D represents the ratio of the dynamic stress range to the quasistatic stress range.
- Calculate the number of cycles to failure N_i for the stress range $D \cdot SCF \cdot s_i(H_i)$ based on the design S–N curve.
- Calculate the fatigue damage for each wave block: n_i / N_i .
- Calculate the cumulative fatigue damage based on Miner’s law.

$$D_{fat} = \sum_{i=1}^I \frac{n_i}{N_i} \quad (27.1)$$

27.3 Simplified Fatigue Assessment

27.3.1 Calculation of Accumulated Damage

It is assumed that the linear cumulative Palmgren–Miner law is applicable, and is written as

$$D_{fat} = \int_0^{\infty} \frac{N_0 f(S)}{N(S)} dS \quad (27.2)$$

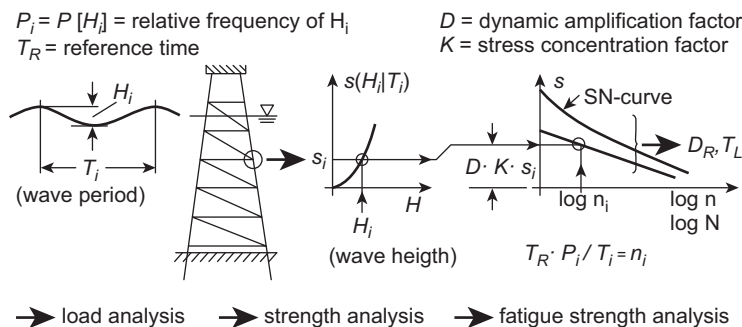


Figure 27.1

Deterministic fatigue analysis (Clausen et al., 1994).

where,

N_0 = Total number of cycles in the long-term period considered

$f(S)$ = Probability density function for the stress range (the number of cycles for the stress range S is $N_0 f(S) dS$)

As discussed in Chapter 24, S–N curves can be expressed as $N = KS^{-m}$. Substituting this equation into Eqn (27.2),

$$D_{fat} = \frac{N_0}{K} \int_0^{\infty} S^m f(S) dS \quad (27.3)$$

For marine structures, the probability density function of stress ranges can be represented by a two-parameter Weibull distribution,

$$f(S) = \frac{\xi}{A} \left(\frac{S}{A}\right)^{\xi-1} \exp\left(-\frac{S}{A}\right)^{\xi} \quad (27.4)$$

where A and ξ denote a scale parameter and a shape parameter, respectively. Combining Eqns (27.3) and (27.4),

$$D_{fat} = \frac{N_0}{K} \int_0^{\infty} S^m \frac{\xi}{A} \left(\frac{S}{A}\right)^{\xi-1} \exp\left(-\frac{S}{A}\right)^{\xi} dS \quad (27.5)$$

Introducing

$$x = \left(\frac{S}{A}\right)^{\xi} \quad (27.6)$$

presents

$$D_{fat} = \frac{N_0}{K} A^m \int_0^{\infty} x^{1+m/\xi} \exp(-x) dx \quad (27.7)$$

The gamma function is defined as,

$$\Gamma(k) = \int_0^{\infty} e^{-x} x^{k-1} dx \quad (27.8)$$

Combining Eqns (27.7) and (27.8), the long-term cumulative damage can be written as

$$D_{fat} = \frac{N_0}{K} A^m \Gamma\left(1 + \frac{m}{\xi}\right) \quad (27.9)$$

In Part III, Chapter 26, it was derived that

$$A = \left[\frac{S_0^\xi}{\ln N_0} \right]^{1/\xi} \quad (27.10)$$

Hence, the long-term cumulative damage can be written as (Almar-Naess, 1985)

$$D_{fat} = \frac{N_0}{K} \left[\frac{S_0^\xi}{\ln N_0} \right]^{m/\xi} \Gamma \left(1 + \frac{m}{\xi} \right) \quad (27.11)$$

where,

N_0 = Total number of cycles in the long-term period (e.g., service life) considered

S_0 = Expected maximum stress range in N_0 cycles, with

$P(S > S_0) = 1/N_0$ (fatigue stress range S exceeds S_0 once every N_0 cycles)

ξ = Shape parameter of the Weibull distribution for the stress cycles

K, m = Material parameters of the S–N curve

27.3.2 Weibull Stress Distribution Parameters

When the shape parameter ξ equals 1, the Weibull distribution yields to the exponential distribution. The value of ξ can be greater than or less than 1. The higher the ξ value, the more severe the cyclic loading condition. The shape parameter is a function of the cyclic loading environment in which the system exists, and how the system responds to this environment (e.g., local loading effects and dynamic loading effects). A suitable value for the shape parameter should be chosen based on the fatigue analysis of similar structures in the same site. In order to evaluate the accuracy of the selected shape parameters, the predicted fatigue damage corresponding to given shape parameters can be compared with the measured data or more refined analysis (e.g., spectral fatigue analysis). Typical values for the Weibull shape parameter ξ for some commercial ships and offshore structures are given in Table 26.3.

The spectral fatigue analysis and extensive fatigue damage data can be used to calibrate the Weibull parameters for various types of ships and offshore structures. Luyties and Stoebner (1998) presented a procedure for calibrating the API simplified fatigue design method using spectral fatigue analysis.

27.4 Simplified Fatigue Assessment for Bilinear S–N Curves

When S–N curves are expressed as bilinear curves (see Part III, Chapter 25), fatigue damage may be predicted using

$$D_{fat} = \frac{N_0}{K} \left[\frac{S_0^\xi}{\ln N_0} \right]^{m/\xi} \Gamma \left(1 + \frac{m}{\xi}, z \right) + \frac{N_0}{C} \left[\frac{S_0^\xi}{\ln N_0} \right]^{r/\xi} \Gamma_0 \left(1 + \frac{r}{\xi}, z \right) \quad (27.12)$$

where incomplete gamma functions are defined as

$$\Gamma(k, z) = \int_z^{\infty} e^{-x} x^{k-1} dx \quad (27.13)$$

$$\Gamma_0(k, z) = \int_0^z e^{-x} x^{k-1} dx \quad (27.14)$$

and

$$z = \left(\frac{S_1}{S_0} \right)^{\xi} \quad (27.15)$$

and where S_1 is the stress range at the crossing of two S–N curves (e.g., corresponding to fatigue life of 10^7).

The formula for simplified fatigue assessment based on bilinear S–N curves was derived by [Wirsching and Chen \(1987\)](#), and appeared in DNV Classification Note 30.7 for ship structures and [DNV \(2000\)](#) for steel offshore structures.

Tables of gamma functions and incomplete gamma functions are given in [BV \(1998\)](#) for convenient use in fatigue damage estimation.

27.5 Allowable Stress Range

A fatigue check format based on the simplified fatigue assessment is

$$S_0 \leq S_{o \text{ allowable}} \quad (27.16)$$

where the design stress range S_0 is the local stress range related to a given probability of occurrence during the design life. The allowable extreme stress range, $S_{o \text{ allowable}}$, is determined by solving [Eqn \(27.12\)](#) using the appropriate S–N curve, the allowable cumulative damage ratio, and knowledge about stress distribution.

For prompt fatigue assessment, allowable extreme stress ranges have usually been precalculated and listed in fatigue guidance documents as functions of the types of S–N curves, the Weibull shape parameter, and the environment.

Reference is made to [Zhao et al. \(2001\)](#) for formulations of the strength and fatigue assessment of converted FPSOs.

27.6 Design Criteria for Connections around Cutout Openings

27.6.1 General

Cracks around cutout openings (also known as slots) are seen often in many types of ship structures; see [Figure 27.2](#). Past studies ([Bea et al., 1995](#)) have concluded that

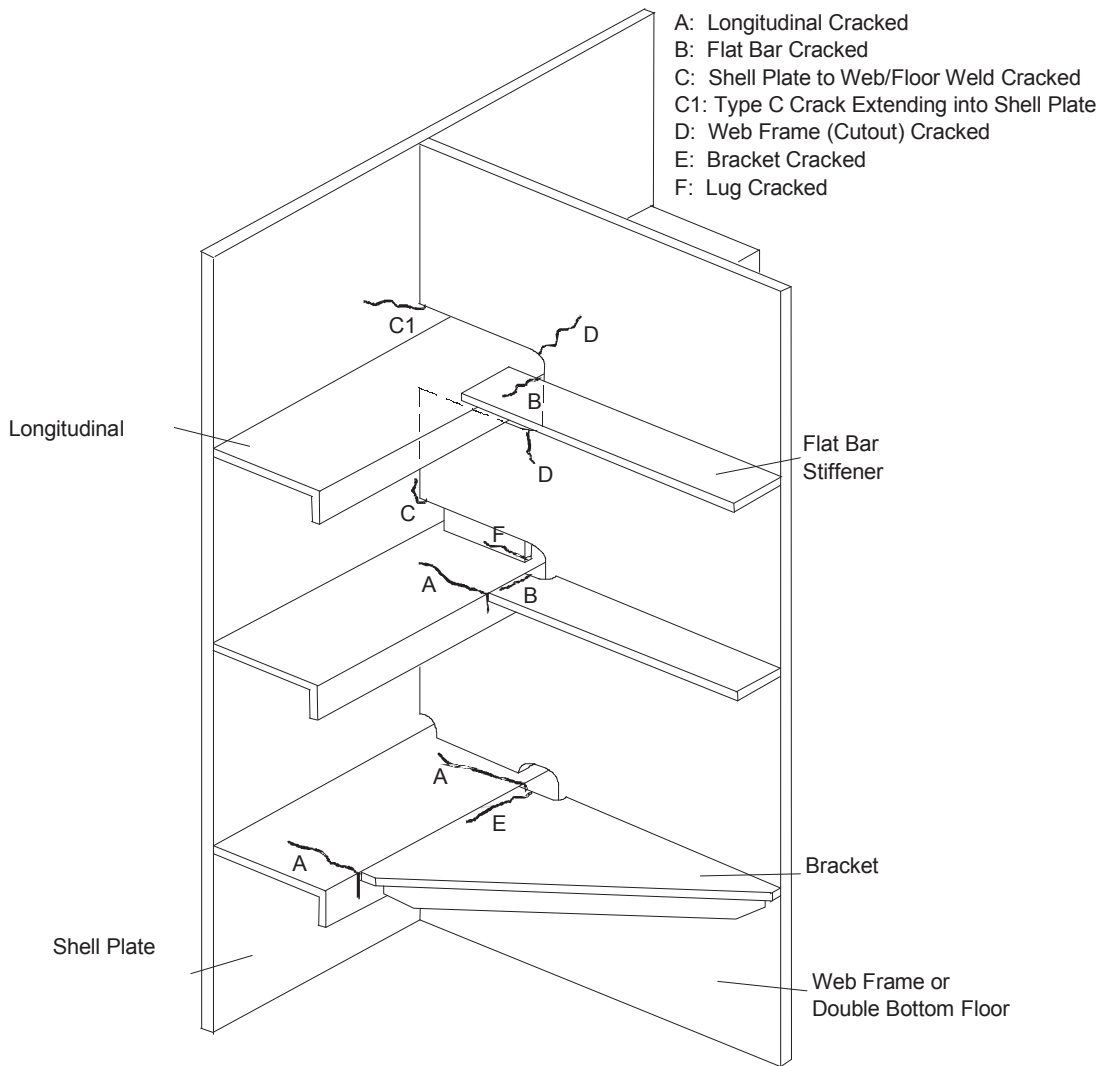


Figure 27.2
 Different types of cracks around cutout openings.

single-hull tankers experience most of these cracks in the side shell and bottom shell areas due to cyclic wave pressure. In double-hull tankers, however, the double bottom seems to be the main problem area due to very high differential pressure between laden and ballast conditions. A large number of cracks have been observed in the inner bottom structures of several double-hull tankers (Cheung and Slaughter, 1998). Many cracks occur along the flat-bar weld between frame vertical stiffeners and the inner bottom longitudinal.

Similarly, many survey reports show that cracks occur in the connections of the longitudinal-to-transverse floors inside the double bottoms and hoppers of bulk carriers (IACS, 1994).

The flat bar appears to be the weakest link in the connections. Some survey reports list hundreds of flat bar failures in a single vessel (Ma, 1998; Bea et al., 1995). This subject was investigated by Glasfeld et al. (1977), who concluded that approximately 75% of the total cracks found around slots are at flat bars.

Cracking around end connections typically follows a sequence. The first crack normally appears along the footprint of the flat bar on the flange of a longitudinal (type B crack in Figure 27.2). The extensive corrosion commonly observed at these cracks indicates that the crack growth rate is slow. As the flat-bar cracks grow slowly with time, stresses redistribute to the web frame through collar plates. Once the flat bar has cracked through, it loses its load-carrying capability completely, and the additional load transfers to the remaining one or two collar connections. If this defect is not found and rectified, a second crack will start at the radius of the cutout (type D in Figure 27.2), and a third crack will eventually occur at the fillet weld on the shell plate (type C or C1 in Figure 27.2). This crack sequence has been confirmed by many survey reports and field observations. These show that a cutout radius crack is only found when the flat bar has completely cracked through.

27.6.2 Stress Criteria for Collar Plate Design

In Ma et al. (2000), simple criteria have been developed for ship designers to perform quick checks of their designs of end connections. The criteria require that two checks be performed for each of the end connection designs. First, the calculated mean normal stress in the flat bar, σ_{fb} , should be less than an allowable value; see Eqn (27.17). Second, the calculated mean shear stress at the collar plate, τ_{dc} , should also be less than its allowable value; see Eqn (27.18).

$$\sigma_{fb} = \frac{ps(l - 0.7s)}{A_1 + 0.33c_s(A_2 + A_3)} < 140 \text{ N/mm}^2 \quad (27.17)$$

$$\tau_{dc} = \frac{ps(l - 0.7s)}{\frac{3.0}{c_s}A_1 + (A_2 + A_3)} < 70 \text{ N/mm}^2 \quad (27.18)$$

Here, p , s , and l represent the static design pressure, panel width, and panel length (see Figure 27.3), respectively. A_1 , A_2 , and A_3 are the flat-bar footprint area, direct connection area, and collar connection area (see Figure 27.4), respectively. Units are in millimeters, newtons, or their combinations.

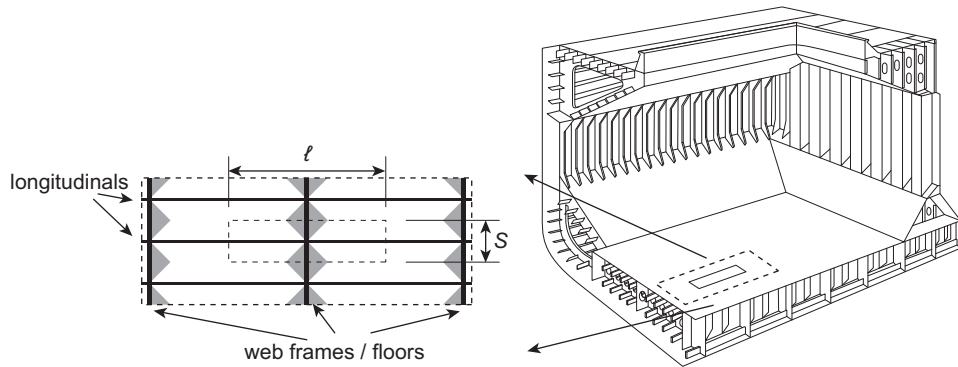


Figure 27.3

Pressure on shaded area goes into web frame/floor differently (Ma et al., 2000).

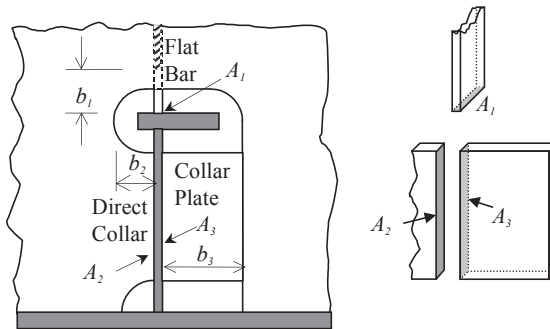


Figure 27.4

Definitions of geometry parameters (Ma et al., 2000).

The coefficient c_s can be easily determined as follows:

$c_s = 1.0$ for symmetrical longitudinal stiffeners

$c_s = 1.41$ for unsymmetrical longitudinal stiffeners with one-sided support

$c_s = 1.12$ for unsymmetrical longitudinal stiffeners with two-sided supports

27.7 Examples

27.7.1 Example 27.1: Fatigue Design of a Semisubmersible

Problem:

Calculate the maximum allowable stress range for a semisubmersible using the long-term stress range distribution

$$S = S_0 \left[1 - \frac{\log N}{\log N_0} \right]^{1/\xi}$$

with the Weibull distribution parameter $\xi = 1.1$. The total number of stress cycles $N_0 = 108$, allowable damage ratio $\eta = 0.20$, with class *F* weld ($m = 3$, $K = 10E11.8$).

Solution:

The maximum allowable stress range can be derived as

$$S_{0\text{ allowable}} = \left(\frac{\eta K}{N_0}\right)^{1/m} \cdot \frac{(\ln N_0)^{1/\xi}}{\sqrt[m]{\Gamma\left(1 + \frac{m}{\xi}\right)}} = 93.6 \text{ MPa}$$

if the maximum allowable stress range is scaled by a factor of $\eta^{1/3}$. For instance, for $\eta = 0.1$, the maximum allowable stress range becomes

$$S_{0\text{ allowable}} = 93.6 \cdot (0.1/0.2)^{1/3} = 74.2 \text{ MPa}$$

References

- ABS, 2002. Rule for Building and Classing Steel Vessels. American Bureau of Shipping.
- Almar-Naess, A., 1985. Fatigue Handbook, Offshore Steel Structures. Tapir, Norway.
- API, 2001. Recommendations for Planning, Designing and Constructing Fixed Offshore Platforms. API Recommended Practice 2A (RP 2A), twenty-first ed. American Petroleum Institute.
- Bea, R.G., Cramer, E., Schulte-Strauthaus, R., Mayoss, R., Gallion, K., Ma, K.T., Holzman, R., Demsetz, L., 1995. Ship's Maintenance Project. Conducted at University of California, Berkeley for U.S. Coast Guard/Ship Structure Committee (SSC). SSC-386.
- BV, 1998. Fatigue Strength of Welded Ship Structures. Bureau Veritas.
- Cheung, M.C., Slaughter, S.B., April 1998. Inner Bottom Design Problems in Double-Hull Tankers. Marine Technology.
- Clauss, G., Lehmann, E., Ostergaard, C., 1994. Offshore Structures, Vol. II - Strength and Safety for Structural Design. Springer-Verlag.
- DNV, 2000. RP-C203, Fatigue Strength Analysis of Offshore Steel Structures. Det Norske Veritas.
- Glasfeld, R., Jordan, D., Kerr, M., Zoller, D., 1977. Review of Ship Structural Details. Ship Structure Committee. Report SSC-226.
- IACS, 1994. Bulk Carriers – Guidelines for Surveys, Assessment and Repair of Hull Structure. International Association of Classification Societies.
- Luyties, W.H., Stoebner, A.M., 1998. The Use of API Simplified Fatigue Design Methodology for Gulf of Mexico Structures. OTC 8823.
- Ma, K.T., 1998. Tanker Inspection and a Risk-Based Approach. Proceedings of ISOPE98, International Offshore and Polar Engineering Conference, Montreal.
- Ma, K.T., Srinivasan, S., Zhang, H., Healy, B., Peng, H., 2000. Developing design criteria for connections around cutout (slot) openings. SNAME Transactions 227–248.
- Wirsching, P.H., Chen, Y.N., 1987. Fatigue design criteria for TLP tendons. Journal of Structural Engineering, ASCE 113 (7).
- Zhao, C.T., Bai, Y., Shin, Y., 2001. Extreme Response and Fatigue Damages for FPSO Structural Analysis. Proc. of ISOPE'2001.

Spectral Fatigue Analysis and Design

28.1 Introduction

28.1.1 General

Recent offshore field development based on tension leg platforms (TLPs), semisubmersibles, SPARs, FPSOs, and other types of floating structures has clearly demonstrated that operators are confident in deepwater technology and will continue the development of fields for increasing water depths. Therefore, cost-effective floating structures will continue to be developed for deepwater field development.

In simplified fatigue assessment, fatigue damage is estimated assuming that long-term stress response follows a Weibull distribution. Simplified fatigue assessment has been successfully applied to ship fatigue design in which allowable stresses are precalculated for different locations in a ship. Due to the excessive sensitivity of estimated fatigue damage to Weibull parameters, spectral fatigue assessment has become more popular for offshore structural analysis (Chen and Mavrakis, 1988).

Fatigue analysis and design includes several steps of analysis:

- Fatigue screening
- Detailed structural analysis
- Reanalysis of welding improvements
- Reanalysis of design improvements
- Reanalysis of combined design and welding improvements

This chapter describes fatigue analysis of floating structures, such as:

- Spectral fatigue analysis (SFA) including computer modeling, load conditions, structural analysis and validation, loading combinations, and fatigue damage assessment
- Time—domain fatigue analysis (TFA)
- Fatigue design of local structural details

SFA can also be applied to ship structures, provided that the wave-scatter diagram is adequately defined, because ships are designed for unrestricted services.

The frequently used codes and standards for fatigue analysis of floating structures are [API RP 2T \(1997\)](#), [API 2FPS \(2001\)](#), [AWS \(1997\)](#), [UK DEn \(1990\)](#), and guidance from classification societies.

28.1.2 Terminology

Some terms applied in fatigue analysis have specific meanings, defined as follows:

Mean zero-crossing period: the average time between successive crossings with a positive slope (upcrossings) of the zero axis in a time history

Random waves: represent the irregular surface elevations and associated water-particle kinematics of the marine environment. Random waves can be represented analytically by a summation of sinusoidal waves of different heights

Regular waves: unidirectional waves having cyclic water particle kinematics and surface elevation

Sea state: an oceanographic wave condition that can be characterized for a specified time period as a stationary random process

Significant wave height: the average height of the highest one-third of all individual waves presented in a sea state

Transfer function: defined as the ratio of a structural response quantity to wave height as a frequency function

S–N curves: empirically represent the relationships between the stress range and the number of cycles to failure

Nominal stress: the stress determined from member section properties and the resultant forces and moments at member ends; section properties must account for the existence of thickened or flared stub ends

Hot-spot stress: the stress located at the weld toe of a structural detail

28.2 Spectral Fatigue Analysis

28.2.1 Fatigue Damage Acceptance Criteria

The fatigue damage assessment is based on Miner's rule

$$D_{fat} = \sum \frac{n_i}{N_i} \leq \eta \quad (28.1)$$

where D_{fat} is the accumulated lifetime fatigue damage, η is the allowable damage ratio, and N_i is the number of cycles to failure at stress S_i as defined by the S–N curve of the form

$$N = K \cdot S^{-m} \quad (28.2)$$

28.2.2 Fatigue Damage Calculated Using the Frequency–Domain Solution

Fatigue Damage for the i th Sea State

For a narrowbanded response, the accumulated damage of a sea state may be expressed in the continuous form

$$D_{fat} = \int_0^{\infty} \frac{n(S)}{N(S)} dS \quad (28.3)$$

where $n(S)dS$ represents the number of stress ranges between S and $S + dS$. If a stationary response process of duration T_{life} is assumed, the total number of stress cycles will be

$$n(S)dS = \nu_{0i} T_{life} p(S) dS \quad (28.4)$$

where the zero-upcrossing frequency ν_{0i} is

$$\nu_{0i} = \frac{1}{2\pi} \sqrt{\frac{m_{2i}}{m_{0i}}} \quad (28.5)$$

where,

m_{0i} = Spectral zero moment of the hot-spot stress spectrum

m_{2i} = Spectral second moment of the hot-spot stress spectrum. The Rayleigh probability density function for stress range S is

$$p(S) = \frac{S}{4\sigma_i^2} \exp\left(-\frac{S^2}{8\sigma_i^2}\right) \quad (28.6)$$

where the root mean square stress σ_i is

$$\sigma_i = \sqrt{m_{0i}} \quad (28.7)$$

Then, the following is obtained.

$$D_{fat} = \nu_{0i} T_{life} \int_0^{\infty} \frac{p(S)}{N(S)} ds = \frac{\nu_{0i} T_{life}}{K} \int \frac{S^{m+1}}{4\sigma_i^2} \exp\left(-\frac{S^2}{8\sigma_i^2}\right) ds \quad (28.8)$$

Using the following notation,

$$x = \frac{S^2}{8\sigma_i^2} \quad (28.9)$$

and the gamma function

$$\Gamma\left(1 + \frac{m}{2}\right) = \int_0^{\infty} e^{-x} x^{\frac{m}{2}} dx \quad (28.10)$$

it is obtained that,

$$D_{fat} = \frac{v_{0i} T_{life}}{K} \cdot (8m_{0i})^{\frac{m}{2}} \cdot \Gamma\left(1 + \frac{m}{2}\right) \quad (28.11)$$

Fatigue Damage for All Sea States

From the damage equation for one sea state, the damage accumulated for all sea states is easily calculated by

$$D_{fat} = \sum_i^{all\ sea-states} p_i \frac{v_{0i} T_{life}}{K} \cdot (8m_{0i})^{\frac{m}{2}} \cdot \Gamma\left(1 + \frac{m}{2}\right) \quad (28.12)$$

where, p_i = Probability of occurrence of the i th sea state.

Based on Eqn (28.12), the transformation of a stress range spectrum to fatigue damage is straightforward. Applying SFA, analytical expressions can be derived as transfer functions from wave spectra to response amplitude spectra and, finally to a stress range spectrum. Using the root mean square stress σ_i , the accumulated damage equation (Eqn (28.12)) can be re-expressed as,

$$D_{fat} = \sum_i p_i \frac{v_{0i} T_{life}}{K} \cdot (2\sqrt{2}\sigma_i)^m \cdot \Gamma\left(1 + \frac{m}{2}\right) \quad (28.13)$$

When wave direction is also accounted for in defining the sea states, the probability of each sea state may be expressed as p_{ij} , where j denotes the j th direction.

$$D_{fat} = \sum_i \sum_j p_{ij} \frac{v_{0ij} T_{life}}{K} \cdot (8m_{0ij})^{\frac{m}{2}} \cdot \Gamma\left(1 + \frac{m}{2}\right) \quad (28.14)$$

When the S–N curves are defined using bilinear curves, the accumulated fatigue damage may be determined as

$$D_{fat} = \sum_i^{all\ sea-states} p_i \frac{v_{0i} T_{life}}{K} \cdot (8m_{0i})^{\frac{m}{2}} \cdot \Gamma\left(1 + \frac{m}{2}, z\right) + \sum_i^{all\ sea-states} p_i \frac{v_{0i} T_{life}}{C} \cdot (8m_{0i})^{\frac{r}{2}} \cdot \Gamma_0\left(1 + \frac{r}{2}, z\right) \quad (28.15)$$

where the incomplete gamma functions are defined as

$$\Gamma(k, z) = \int_z^{\infty} e^{-x} x^{k-1} dx \quad (28.16)$$

$$\Gamma_0(k, z) = \int_0^z e^{-x} x^{k-1} dx \quad (28.17)$$

and

$$z = \left(\frac{S_1}{2\sqrt{2}m_{0i}} \right)^2 \quad (28.18)$$

where S_1 is the stress range at the crossing of two S–N curves (e.g., corresponding to a fatigue life of 10^7).

The formulation for spectral fatigue assessment based on bilinear S–N curves appeared in DNV Classification Note 30.7 for ship structures, and [DNV \(2000\)](#) for steel offshore structures.

28.3 Time–Domain Fatigue Analysis

28.3.1 Application

- Similarities between TFA and SFA: Both procedures are based on the wave–scatter diagram.
- Differences between TFA and SFA: TFA is a deterministic analysis and includes the effects of nonlinearity. SFA is a stochastic approach based on linear analysis.

TFA is mainly applied to the following scenarios:

- Fatigue of pipelines and risers due to wave-induced forces ([Bai, 2001](#))
- Fatigue of TLP tethers ([Fylling and Larsen, 1989](#))
- Fatigue of SPAR structures due to low frequency motions ([Luo, 2001](#))

28.3.2 Analysis Methodology for Time–Domain Fatigue of Pipelines

In the following, a fatigue damage equation will be derived for the fatigue of pipelines and risers due to wave forces. The number of cycles n_i corresponding to the stress range block S_i is given by

$$n_i = P(\cdot) f_v T_{life} \quad (28.19)$$

$P(\cdot)$ is the probability of a combined wave- and-current-induced flow event. The dominating vibration frequency is represented by f_v for the considered pipe response, and T_{life} is the time of exposure to fatigue load effects. Using Miner's law and an S–N curve, [Eqn \(28.3\)](#) for fatigue damage may be evaluated for each sea state of the scatter diagram in terms of H_s , T_p , and θ_w .

$$D_{fat} = \frac{T_{life}}{K} \sum_{H_s T_p \theta_w} P(\cdot) \int_0^{\infty} \max[f_v S^m] dF_{U_c} \quad (28.20)$$

where,

$P(\cdot)$ is the joint probability of occurrence for the given sea state in terms of significant wave height H_s , wave peak period T_p , and mean wave direction.

The long-term distribution function for the current velocity is denoted by dF_{U_c} . The notation “max” denotes that the mode associated with the largest fatigue damage must be applied when several potential modes exist at a given current velocity.

In the time–domain analysis, the long-term irregular wave condition is divided into representative sea states. For each sea state, a time history of wave kinematics is generated from the wave spectrum. Hydrodynamic loads are then predicted using wave kinematics and are applied to the structures. Stress ranges are calculated through structural analysis. Fatigue damage is then calculated using Miner’s law.

In Bai (2001), the stress range is calculated in the time–domain model for each sea state with a constant value of wave-induced velocity, but for a range of current velocities from zero to a maximum value with nearly zero probability of occurrence. The calculated stress ranges are used to evaluate the integral in Eqn (28.20). For each sea state, the fatigue damage associated with each current velocity is multiplied by the probability of occurrence of the current velocity. When stress ranges for all sea states are obtained through the wave force model, the fatigue damage is calculated using Eqn (28.20). The advantage of using the time–domain fatigue for pipeline and riser assessment is that it accounts for the nonlinearity in drag forces and the structural dynamic response. The other benefit is reduced conservatism in the boundary condition for SFA. An engineering practice is used to derive the ratio of the predicted fatigue life from these two approaches for a few well-selected and performed analyses, and then it is used to apply this ratio to similar fatigue scenarios.

28.3.3 Analysis Methodology for Time–Domain Fatigue of Risers

A time–domain dynamic analysis is performed for all sea states in the wave-scatter diagram, and for each direction with a nonzero probability of occurrence. In frequency–domain fatigue analysis of risers, the touchdown point is fixed. The time–domain analysis is applied when the soil–pipe interaction needs to be accounted for in order to remove the conservatism introduced in the frequency–domain analysis. Second-order (drift) motions of the vessel can significantly affect the results of the fatigue analysis. It is difficult to include second-order motions using stress RAOs to transfer wave spectra into stress

spectra. Based on the stress time histories from the time–domain dynamic analysis, the fatigue damage may be:

- Estimated based on the moments of spectra (as those used in the frequency–domain analysis), and the stress-spectra are calculated using a fast Fourier transform algorithm.
- Calculated directly from the stress time-history using rainflow-counting techniques.

The dynamic simulation should be long enough because the dominant period of second-order motions is on the order of 100 s.

28.3.4 Analysis Methodology for Time–Domain Fatigue of Nonlinear Ship Response

[Jha and Winterstein \(1998\)](#) proposed a “nonlinear transfer function (NTF)” method for efficient prediction of the stochastic accumulation of fatigue damage due to nonlinear shiploads in random seas. Nonlinear time–domain shipload analysis may reveal asymmetry in sag and hog moments at midship. The goal of the NTF method is to derive accurate predictions using only a limited amount of nonlinear analysis based on regular waves. The analysis cost is reduced because expensive time–domain analysis over many cycles of irregular sea states is replaced by a limited number of regular wave analyses.

The NTF is the generally nonlinear transformation from wave amplitude and period to the load amplitude measure of interest (e.g., total load range for rainflow-counting). Stochastic process theory is applied to:

- Identify a minimal set of regular waves (i.e., wave heights and associated periods) to be applied based on a discretized version of the [Foristall \(1978\)](#) wave height distribution and [Longuet-Higgins \(1983\)](#) model for wave period selection.
- Assign an appropriate set of “side waves” to be spatially distributed along the ship based on probability theory.
- Determine how these results should be weighted in predicting statistics of the loads produced in random seas.

The prediction of the TFA is compared with frequency–domain stochastic fatigue analysis that assumes a linear model of ship behavior. It was revealed that the nonlinear effect is significant. The NTF method may also be applied to any offshore structures.

28.4 Structural Analysis

28.4.1 Overall Structural Analysis

Overall structural analyses are usually performed using space frame models and fine finite element analysis (FEA) models. Space frame analyses define the boundary loads for local

structural models. To get the stress transfer functions for fatigue damage assessment, these boundary loads are used to factor in the results of fine FEA unit load analysis.

This section presents aspects of modeling, load evaluation, and structural analysis applicable to overall structural analysis.

Space Frame Model

The space frame model includes all the important characteristics of stiffness, mass, damping, and loading properties of the structure and the foundation for the structural system; it consists primarily of beam elements. The accuracy of the calculated member end forces depends mainly on the modeling techniques used.

Figure 28.1 shows a space frame model for TLP hull primary structures and deck primary structures. Although not shown in this figure, tendons are included in the model as a supporting structure to provide the proper vertical stiffness. Tubular beam elements are used to model the tendons. Applied load cases are in general self-balancing and should result in zero net loadings at the tops of tendons. Thus, relatively flexible lateral springs are provided at the tops of all tendons in order to stabilize the analysis model against small net lateral loads.

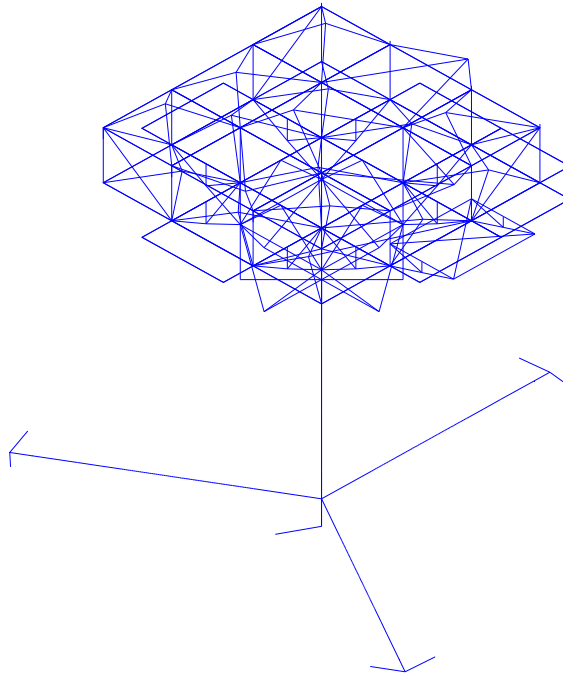


Figure 28.1
Space frame model for a TLP.

The hull's column and pontoon structures are modeled using beam-column elements. Joint and member definitions are interfaced from the global analysis model, as interfaced loads from this analysis must be consistent with the model. Member properties are determined based on member cross-sectional and material properties. Yield stresses of plate and stiffener components are input along with the maximum bracket spacing for ring stiffener frames.

Additional joints and members are included to ensure that the tendons and deck structure are structurally stable; additional load collectors are added where appropriate. Deck members are modeled using tubular or American Institute of Steel Construction (AISC) elements. Deck equipment mass locations are determined for each major deck area and specifically included in the model, so that proper inertial load magnitudes and centers of action are generated in the analysis.

Fine FEA Model

A fine FEA model may be used to analyze the hull structure or a part of the hull structure, in detail. All relevant structural components can be included in the model. In the fine FEA model, major primary structural components are fully modeled using three- and four-node plate/shell and solid elements. Some secondary structural components can be modeled as two-node beam elements.

Design Loading Conditions

To adequately cover the fatigue environment, the fatigue design loading conditions consist of cyclic environmental load components at a sufficient number of wave frequencies.

These loading conditions include:

- Hydrodynamic loads due to waves, including dynamic pressure
- Inertial loads due to motions
- Other cyclic loading

The loading components are either explicitly generated or interfaced from the global motion analysis. Load summaries are made for each design loading condition and checked for accuracy and load imbalances.

Global motion analysis serves as a basis for dynamic load development. The actual interface from global to structural analysis consists of several loading components for each analyzed wave period and direction: the real and imaginary applied unit amplitude, wave diffraction and radiation loads, the associated inertial loads, and other cyclic loadings such as tendon dynamic reactions. The successful interface of these load components depends on a consistent geometric and mass model between motion and the structural analyses, and also depends on the consistent generation of loading components in the motion analysis. Consistent modeling is obtained by interfacing the model geometry directly from the

motion analysis wherever possible. Consistent mass is obtained by interfacing with the same weight control database for both the motions and structural analyses, when available.

Load combinations are formed for each wave period and direction. These combinations consist of the applied wave load, the generated inertial load, and the associated cyclic loadings such as tendon dynamic reactions for both real and imaginary loadings of the floating structures. These combinations form the total cyclic load condition for each wave period and direction to be used in SFA.

Analysis and Validation

Hull structural analyses are performed using linear finite element methods. The reaction forces include total force and moment reactions and the analysis results are verified. Symmetrical or asymmetrical load conditions are checked to confirm symmetrical or asymmetrical analysis results.

28.4.2 Local Structural Analysis

Local structural details are included as a part of the analyses for the entire hull structure.

The analysis of structural details may be performed using finite element programs such as ABAQUS (HKS, 2002), etc. The FEA model is three-dimensional, and linear stress analysis is performed. The results from the FEA model are interfaced into the fatigue model for additional model validation and subsequent SFA of the local structural details. The entire model is plotted and revised for accuracy, both from the FEA model and after the interface to the fatigue model.

Loading conditions for FEA of local structural details should be based on the hull's structural analysis, since it includes all cyclic loadings of the structure.

The unit loading conditions are frequently applied. The resulting stresses for each unit load condition are interfaced to the fatigue model for subsequent combination into fatigue design loads.

28.5 Fatigue Analysis and Design

28.5.1 Overall Design

A spectral fatigue assessment should be carried out for each individual structural detail. It should be noted that each structural detail, each welded joint/attachment, or any other form of stress concentration is potentially a source of fatigue cracking and should be considered individually.

The United Kingdom's DEN procedure, or its modified versions, is recommended in Europe for the fatigue analysis and design of floating structures, since it is the most widely

accepted code. Design standards such as AWS (1997) are used in the United States. However, it should be noted that different design standards provide different procedures for fatigue stress determination and S–N classification, which can result in large discrepancies in predicted fatigue damage. Therefore, a consistent procedure based on one design standard should be used.

The safety factors for the fatigue design of floating structures are given by the design standards listed in Section 28.2 and are based on:

- Criticality of the joint
- Inspectability and repairability

The criticality of a joint is determined based on its structural redundancy. A joint is critical if its failure will potentially lead to the failure of the structure.

28.5.2 Stress Range Analysis

A stress range analysis is performed using fatigue software as a precursor to the fatigue damage calculation. The FEA unit load, model geometry, and element stress results are interfaced into the fatigue calculation model. Loading combinations will then be defined for each fatigue wave load based on applied boundary loads.

Geometry and element properties from the space frame model are plotted and revised for accuracy. Any detected errors are corrected in the FEA input file and the FEA is repeated.

The FEA model of the specific hot-spot region is developed based on the procedures; the finite element size requirement is defined by the design standards.

In the FEA model, the unit load results will be interfaced into the space frame model database. These unit loads are then appropriately combined based on applied boundary loads.

28.5.3 Spectral Fatigue Parameters

Wave Environment

The wave environment consists of wave-scatter diagram data and wave directional probabilities.

The scatter diagram data consist of annual probabilities of occurrence as functions of significant wave heights and peak periods at the structure installation site. For SFA, a wave spectrum (e.g., Pierson–Moskowitz) is associated with each cell of the scatter diagram.

Directional probabilities for fatigue waves are also included in the fatigue assessment. Generally, it is not very conservative to ignore any nonuniform distributions in the

directional probabilities. However, in lieu of such information, the wind directional probability can be used to account for nonuniformity in the wave-approaching direction and to provide conservatism in the fatigue damage calculation.

Stress Concentration Factors

Determination of the appropriate SCF in fatigue analysis is a complex task. It also depends on the S–N classification and stress analysis methods. The general rule of thumb is that the stress used in the fatigue analysis should resemble the fatigue stress obtained from the specimen tested when deriving the S–N curves. The fatigue stress does not mean the most accurate stress determined by the high-resolution fine mesh FEA, but instead is the pertinent stress in accordance with the chosen S–N curves. A discussion of SCF and S–N classification is given in later sections.

The SCF can be determined based on parametric equations and FEA.

S–N Curves

In the United States, [AWS \(1997\)](#) S–N curves are used to analyze structural details of floating structures. Where variations of stress are applied to conventional weld details identified in Figure 9.1 of [AWS \(1997\)](#), the associated S–N curves in Figure 9.2 or 9.3 should be used depending on the degree of criticality. Such variations of stress are applied to situations identified in [AWS \(1997\)](#), Table 10.3. The associated S–N curves are provided in AWS D1.1, Figure 10.6. For referenced S–N curves in [AWS \(1997\)](#), Figures 9.2, 9.3, and 10.6 are class curves. For such curves, the nominal stress range in the vicinity of the detail should be used.

In Europe, [UK DEn \(1990\)](#) S–N curves are used for structural details in floating structures. The S–N classification is determined based on structural configurations, applied loading, and welding quality.

As discussed earlier, the UK DEn procedure is recommended in this chapter and discussed in detail; see [Table 28.1](#).

Joint Classification

Guidelines on joint classification may be found in [UK DEn \(1990\)](#). Note that the S–N curves in [UK DEn \(1990\)](#) were previously modified by [HSE \(1995\)](#).

The [UK DEn \(1990\)](#) guidelines apply only to welded joints that are free from serious defects or discontinuities. Factors such as undercut at the toe, internal or surface breaking defects or cracks, and geometric irregularities may cause reductions in fatigue strength and should be evaluated separately.

The [UK DEn \(1990\)](#) guidelines allocate various types of welded joints into one of nine joint classes. To determine the correct classification for a particular weld detail, it is

Table 28.1: Comparison between European and US standards

Subject	Europe Standards (e.g., UK DEn, 1990)	US Standards (e.g., AWS D1.1, 1997)
S–N curves	Mean-minus-two-standard-deviation curves	Lower bound
S–N classifications	Full penetration welds—T curve Partial penetration welds—W curve One of 8 classes—B, C, D, E, F, F2, G, and W—depending on geometry, stress direction, and method of fabrication and inspection	X curve is sufficiently devalued to account for thickness/size effect Smooth weld metal merging with parent metal—X curve; otherwise, X' curve
Fatigue damage assessment	Simplified fatigue—the long-term wave height distribution can be represented by the Weibull distribution Or spectral fatigue analysis	Simplified fatigue—the long-term wave height distribution may be represented by the sum of two Weibull distributions—one for normal and the other for hurricane conditions Or spectral fatigue analysis
Cathodic protection	Cathodically protected joints in seawater equivalent to joints in air Unprotected joints in seawater require S–N curve to be reduced by a factor of 2 on life	S–N curves (X' and X) presume effective cathodic protection Fatigue provisions of AWS D1.1 apply to members and joints in atmospheric service. Does not recommend further reduction of S–N curve for free corrosion
Welding improvement	Included	Not covered Use X curve rather than X' curve

necessary to identify the weld type and the direction of the applied loading, and to consider all potential cracking locations. For most types of joints, the weld toes, weld ends, and weld roots are considered the most important locations.

The joints with the highest classifications are those stressed in a direction parallel to the weld. Fillet or butt weld joints fall into class C or B in [UK DEn \(1990\)](#) guidelines, depending on whether the manufacturing process is manual or automatic. Such joints seldom govern the fatigue strength of a welded detail, since other joints are likely to fall into lower joint classes.

The classification of transverse butt welds is more complex. They can fall into class D or E depending upon the details of the manufacturing process, position, and location, all of which may influence the weld profile. Class C may be justified if the weld's overfill is removed by grinding, or the weld is shown to be free from significant defects by using nondestructive testing. However, if access is limited and the weld must be made from one side only, a lower fatigue strength is assumed.

The [UK DEn \(1990\)](#) guidelines downgrade butt welds to class F. The guidelines also warn against the use of tack welds within short distances of the plate's edge, in which case the classification is lowered to class G.

Tack welds are a controversial topic. A number of studies have been conducted for different methods of attaching the backing to the plates prior to making the butt weld. Tacking the backing strip to the root preparation, and incorporating this into the final weld, gives a small improvement in fatigue strength over joints in which the backing strip is fillet welded to one of the plates. However, the increase is not sufficient to warrant a higher joint classification. In either case, failure may initiate at the root of the butt weld.

Currently, butt welds made onto temporary backing such as glass or ceramic backing strips are not classified and require further research. The availability of electrodes designed specifically for root runs has resulted in an improvement in the quality of single-sided welds made without backing. In recognition of this welding quality improvement, such joints can be considered as class F2 if full penetration is achieved. This classification should be used with caution, because fatigue strength in some areas may be much lower due to lack of penetration at the root.

Fatigue strength is seldom governed by butt-welded joints, because these joints in general possess superior strength over fillet-welded joints. Fillet welds fall into class F, F2, or G depending on their size, orientation, and location in relation to a free plate edge. However, recent studies have shown that fillet welds possess a fatigue strength lower than that predicted by class G if the weld is continued over the corner of the plate.

In addition to the weld toe, which is the most usual site for fatigue cracking to occur, all load-carrying fillet welds and partial-penetration butt welds must be evaluated to assess possible weld throat failure. To avoid this type of failure, it is necessary to ensure that these joints are adequately dimensioned. This may be achieved using the class W design S–N curve. One should note that the maximum shear stress range is associated with the class W design S–N curve.

Structural Details

UK DEn fatigue design and assessment guidelines provide sketches that provide assistance in the S–N classification of structural details. According to [UK DEn \(1990\)](#) guidelines, joints are subdivided into the following types:

- Metal free from welding
- Continuous welds essentially parallel to the direction of applied stress
- Transverse butt welds
- Weld attachments on the surface of a stressed member
- Load-carrying fillet and T butt welds
- Details in welded girders

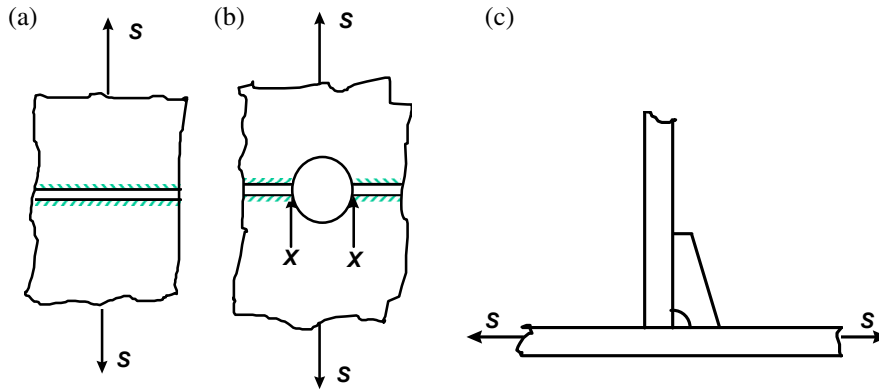


Figure 28.2

Explanation of fatigue stress when the weld is situated in the region of stress concentration resulting from the structure's gross shape.

UK DEn curves were developed based on small test specimens. In the S–N classification of structural details, users first carefully related the fatigue stress in tests with the stress of structural details under consideration. For example, the fatigue stress in the test for the weld shown in [Figure 28.2\(a\)](#) would be the tensile stress, S , on the cross section, but for the weld shown in [Figure 28.2\(b\)](#) it would be $SCF \cdot S$, where SCF is the stress concentration factor caused by the hole. This is due to the fact that at the point x , the stress near the weld is $SCF \cdot S$. However, for a small cutout in [Figure 28.2\(c\)](#), the stress concentration due to the small hole shall not be included, since microstructural effects have been included in the S–N curves.

Theoretically, structural details should be classified and considered for each loading step throughout the fatigue analysis, since different loading steps result in different applied loading directions. This approach is generally prohibitively complex. Therefore, simplified S–N classification is used, based on the rule of thumb in engineering applications.

When classifying the weld's structural details in large complex structural systems from a series of design drawings, it is important to:

- Consider each weld individually
- Consider each direction of applied stress
- Evaluate all possible cracking locations, because each may yield a different classification
- Consider any possible stress concentration effects

[Figures 28.3 and 28.4](#) show two typical examples of details found in a floating structure. In the section shown in [Figure 28.3](#), the classifications range from class C to F2 and W, depending upon the direction of the applied stress. In these examples, stresses in the three

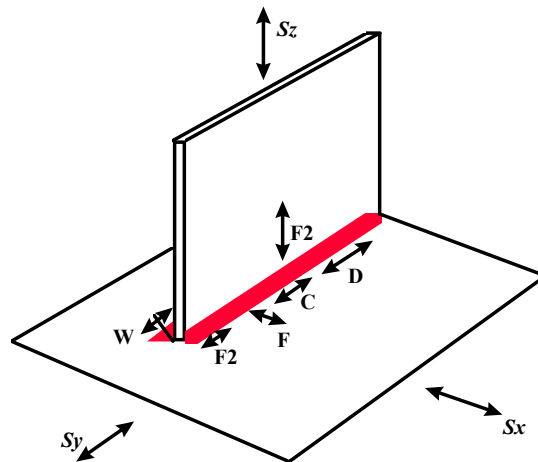


Figure 28.3

S–N classification of structural details subjected to triaxial loading.

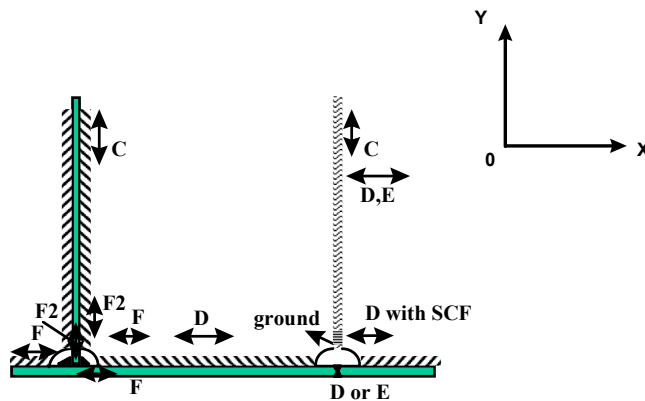


Figure 28.4

S–N classification of structural details.

principal directions S_x , S_y , and S_z are not equal. Thus, the design stress range for each class will differ. However, for simple design purposes, the maximum principal stress and F2 classification are assigned for the overall structural details.

It is particularly difficult to classify the details that have a hole, and to identify potential crack locations. Holes in a continuous longitudinal weld are covered in the UK DEn fatigue design guidelines labeled as class F without any requirement for an additional stress concentration factor. However, a web should be incorporated into this detail. The end of a web butt weld at the hole is a more severe detail that should be ground. For the ground detail, class E or D is recommended. Due to the presence of the hole, a stress

concentration factor of 2.2 or 2.4 needs to be included. If the end of the butt weld is not ground, a class F or F2 curve together with the geometric stress concentration factor (2.2–2.4) is recommended.

If any concerns remain about the use of a cope hole, it is possible to improve its fatigue strength by cutting back and grinding the weld end as shown in Figure 28.5. In such cases, the weld between the flange and web should be fully penetrated over the regions on either side of the cope hole in order to avoid failure through the weld throat (W class).

Figure 28.6 illustrates the third example of S–N classification of structural details. It is the small bracket between the pontoon and the base node in a TLP structure. Based on the [UK DEn \(1990\)](#) guidelines and published fatigue test data, the hot-spot areas can be classified as F or F2.

S–N classification of structural details in floating structures is a challenging task. During the design process, there are many structural details that cannot be classified based on [UK DEn \(1990\)](#) guidelines. In this case, other design standards such as [AWS \(1997\)](#) or published fatigue test data can be used to justify the classification.

28.5.4 Fatigue Damage Assessment

The fatigue life of structural details is calculated based on the S–N curve approach, assuming linear cumulative damage (Palmgren–Miner rule). An SFA is used where the long-term stress range distribution is defined through a short-term Rayleigh distribution within each short-term period for different wave directions. A one-slope or bilinear S–N curve can be assumed.

Fatigue lives are determined by service life and safety factors. An additional margin is desirable due to uncertainties associated with fatigue assessment procedures.

Initial Hot-Spot Screening

The objective of the initial screening is to identify fatigue critical areas based on experience and in-service data. Fatigue damage is calculated for each element in the group assuming a conservative S–N curve and upper-bound SCF for each element. The calculated damages are reviewed, and all elements with fatigue lives less than the required minimum, are analyzed in further detail in the specific hot-spot analysis.

Specific Hot-Spot Analysis

Elements that do not pass the initial hot-spot screening need to be reanalyzed using SCFs and the associated S–N curves that are more appropriate for the actual structural detail and welding procedure. The calculated damages are reviewed and, at the least, all elements with fatigue lives less than the required minimum are summarized for further

review and potential redesign and/or modification of the welding procedures, and reanalysis.

Specific Hot-Spot Design

Structural details that do not pass the specific hot-spot analysis are redesigned to improve their fatigue strength. SCFs and associated S–N curves that are appropriate for the redesigned structural details and welding procedures will be used in the fatigue reanalysis. All structural details must meet minimum fatigue requirements after their redesign and welding procedures are finalized.

Detail Improvement

It is clear that the best time to improve the fatigue strength of welded structural details is during the design stage. Two factors need to be especially considered when improving the fatigue strength of a structural detail:

- Nominal stress level
The most efficient approach to improving fatigue strength is to increase the local scantling and configure the additional load path within the structure. This approach can reduce the nominal stress level and hence the hot-spot stress for a given structural detail.
- Geometric stress concentration
Adopting a good design of detail configuration, by providing softer connections, reduces the geometric stress concentration factor originally caused by geometric discontinuity. It is the most effective technique to improve fatigue strength. However, this technique usually requires good workmanship, since a soft toe/heel is used.

28.5.5 Fatigue Analysis and Design Checklist

Each item in the following checklist should be checked prior to the completion of fatigue analysis:

- Computer model topology—the model is plotted in sufficient views to validate model connectivity.
- Loading conditions—each applied loading condition is checked for accuracy.
- Analysis and validation—analysis results are checked step by step; discrepancies between expected and obtained analysis results should be documented and explained.
- Loading combinations—each applied loading combination should be summarized and checked for accuracy.
- Environmental conditions—the wave-scatter diagram and directional probability input should be checked.

- SCFs—SCFs used in the analysis should be confirmed for validity and applicability.
- S—N curves—S—N curves used in the analysis should be confirmed for validity and applicability.

28.5.6 Drawing Verification

Design drawings corresponding to this design task should be verified according to the design results, for both correctness and acceptability. Nonconforming drawings are to be revised and/or documented depending on their acceptability in the task technical report.

28.6 Classification Society Interface

28.6.1 Submittal and Approval of Design Brief

The design brief is submitted to the classification society for review, comments, and approval. The classification society's comments are to be incorporated into the design brief, and the revised design brief will be reissued. If necessary, the analysis should be repeated to verify and validate the results and design brief revisions.

28.6.2 Submittal and Approval of Task Report

A technical task report is issued after the analysis is completed in order to document analysis and design results. This report should follow the analysis methodology documented in the design brief and discuss any variations from the design brief. The task report includes supporting information, hand calculations, and computer outputs.

The task report and supplemental calculations are submitted to the classification society for review, comment, and approval, and will be available to postdesign personnel for reference during fabrication.

28.6.3 Incorporation of Comments from Classification Society

Comments on the design brief and the task report are incorporated into the applicable revised document. The revised document is issued for recording and final approval, if required.

References

- API, 1997. Recommended Practice for Planning, Designing, and Constructing Tension Leg Platforms. API Recommended Practice 2T (RP 2T), first ed. American Petroleum Institute.
- API, 2001. API RP 2FPS, Recommended Practice for Planning, Designing and Constructing Floating Production Systems, first ed. API.
- AWS, 1997. AWS Structural Welding Code - Steel, AWS D1.1—96. American Welding Society.

- Bai, Y., 2001. Pipelines and Risers. In: Elsevier Ocean Engineering Book Series, vol. 3.
- DNV, 2000. RP-C203, Fatigue Strength Analysis of Offshore Steel Structures. Det Norske Veritas.
- Forristall, G.Z., 1978. On the statistical distribution of wave heights in a storm. *Journal of Geophysical Research* 83 (C5), 2353–2358.
- Fylling, I.J., Larsen, C.M., 1989. TLP tendon analysis. In: Demirebilek, Z. (Ed.), *Tension Leg Platforms – a State of the Art Review*.
- HKS, 2002. ABAQUS/Standard User's Manual, Version 5.6. Hibbitt, Karlsson & Sorensen, Inc.
- HSE, 1995. Offshore Installation, Guidance on Design, Construction and Certification, fourth ed. UK Health and Safety Executives. Section 21.
- Jha, A.K., Winterstein, S.R., 1998. Stochastic fatigue damages accumulated due to nonlinear ship loads. In: *Proceedings of OMAE*, Lisbon.
- Longuet-Higgins, M.S., 1983. On the joint distribution of wave periods and amplitude in a random wave field. *Proceedings of the Royal Society of London* 241–258. <http://dx.doi.org/10.1098/rspa.1983.0107>.
- Luo, Y.H., Lu, R., Wang, J., Berg, S., 2001. Time-domain analysis for critical connections of truss spar. In: *Proceedings of ISOPE*, Stavanger.
- UK DEn, 1990. Offshore Installations: Guidance on Design, Construction, and Certification, third ed. UK Department of Energy (Now UK Health and Safety Executives).

Application of Fracture Mechanics

29.1 Introduction

29.1.1 General

Applications of fracture mechanics in marine structural designs include:

- Assessment of the final fracture
- Determination of crack propagation to plan in-service inspection and the determination of the remaining life of an existing structure
- Fatigue assessment in the case of S–N based fatigue assessment is inappropriate
- Calibration of the fatigue design S–N curves

In this chapter, three levels of fracture assessment are outlined, the Paris equation is applied to predict crack propagation, and comparison is made between the S–N curve-based and the fracture mechanics-based fatigue assessments.

29.1.2 Fracture Mechanics Design Check

The fracture mechanics design check of ultimate limit state can be applied in three alternative ways, which are evaluations of

- Maximum allowable stress
- Minimum required fracture toughness
- Maximum tolerable defect size

Maximum Allowable Stress

The fracture mechanics strength criteria can be applied to the derivation of the maximum allowable stress at a given cross section. This value is obtained when the material fracture toughness and the defect size are specified. If the actual local stress exceeds the maximum allowable stress derived, a different local design should be undertaken in order to reduce the local stress level and fulfill the fracture mechanics criteria.

Minimum Required Fracture Toughness

The minimum required fracture toughness should be derived through the fracture mechanics design check when the design geometry is established and a defect tolerance

parameter is specified. The derived fracture toughness then allows designers to select a suitable material for any particular structure of concern.

Maximum Tolerable Defect Size

A maximum tolerable defect size can be derived when the geometry and the fracture toughness of the selected material are known. For statically loaded structures, the maximum tolerable defect size must satisfy the fracture mechanics criteria. For dynamically loaded structures, the maximum tolerable defect size represents the critical crack size in a fatigue failure event. It may be used to minimize the risk of unstable fracture throughout the operating life of the structure. The result also gives direct input to the calculation of the fatigue crack growth period.

The three levels of procedure applied in fracture assessment (Reemsnyder, 1997) are:

Level 1. Utilization of the crack-tip opening displacement (CTOD) design curve (explained in Section 38.2)

Level 2. The normal assessment or design safety format that makes use of the failure assessment diagram (FAD) (described in Section 39.3). No practical safety factors need to be applied here.

Level 3. Utilization of the FAD based on detailed information on the stress–strain curves of materials. Partial safety factors are applied to the defect size, stress level, etc.; see Section 39.4.

More information can be obtained from [API 579 \(2001\)](#), [Andersen \(1991\)](#), and [BSI \(1999\)](#).

29.2 Level 1: The CTOD Design Curve

29.2.1 The Empirical Equations

The CTOD design curve may be used to evaluate the resistance against fracture for a wide range of structures such as pipelines, pressure vessels, and ships, and offshore structures, buildings, and bridges. One of the most commonly used CTOD Design curves is the one developed by the British Welding Institute (BWI) that relates the CTOD to some critical event, the yield strength σ_Y , the nominal strain at a notch ϵ , and the flaw size a ([Burdekin and Dawes, 1971](#); [Dawes, 1974](#)). This design curve was initially included in the first edition of the BSI fitness to give guidance ([BSI PD 6493, 1980](#)). The [BSI \(1980\)](#) CTOD design curve can be expressed as

$$\Phi = \left(\frac{\epsilon}{\epsilon_Y} \right)^2 \quad \text{for} \quad \frac{\epsilon}{\epsilon_Y} \leq 0.5 \quad (29.1)$$

and

$$\Phi = \left(\frac{\varepsilon}{\varepsilon_Y} \right) - 0.25 \quad \text{for} \quad \frac{\varepsilon}{\varepsilon_Y} > 0.5 \quad (29.2)$$

where the nondimensionalized CTOD is Φ ,

$$\Phi = \frac{CTOD}{2\pi\varepsilon_Y a} \quad (29.3)$$

with the yield strain ε_Y

$$\varepsilon_Y = \frac{\sigma_Y}{E} \quad (29.4)$$

where a is the length of a through-crack in an infinite plate equivalent in severity to that of the crack in the element under investigation, and E is the Young's modulus.

29.2.2 The British Welding Institute CTOD Design Curve

The BSI (1980) CTOD design curve shown in Figure 29.1 was constructed relative to the wide-plate test results with a safety factor of 2 on flaw size a .

Three alternative applications for the CTOD design curve are:

- **Maximum allowable strain:** Solving Eqns (29.1) and (29.2) for $\varepsilon/\varepsilon_Y$, the maximum allowable strain for the given values of material fracture toughness CTOD and crack size a can be defined.
- **Minimum required fracture toughness:** A material with an adequate toughness CTOD can be selected for the critical region, given the maximum possible flaw size a and a strain level of $\varepsilon/\varepsilon_Y$.

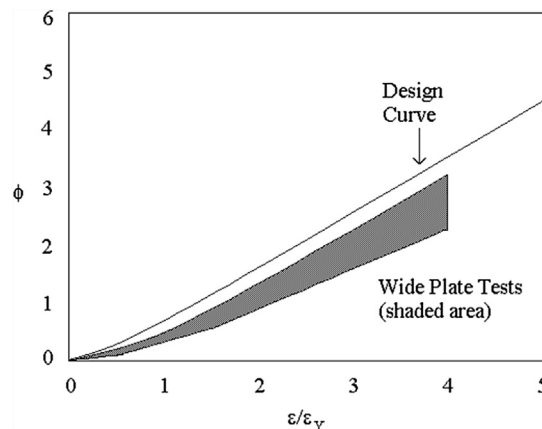


Figure 29.1

The British Welding Institute CTOD design curve.

- **Maximum allowable flaw size:** Given $\varepsilon/\varepsilon_Y$ in a critical region from the stress analysis of the structure, Φ is determined from the diagram. From this value of Φ , the maximum allowable flaw size a , in the critical region can be established, given the toughness CTOD of the material.

The TWI CTOD design curve was also adopted by the American Petroleum Institute in [API 1104 \(1994\)](#) as a basis for its fitness-for-purpose criteria.

29.3 Level 2: The Central Electricity Generating Board R6 Diagram

This level-2 assessment provides a simplified method of checking whether particular flaws present in a structure can potentially lead to fracture failure, or whether the flaws can be considered safe without having to go through more complex assessment procedures. The approach adopted in this preliminary assessment uses a variable safety factor on flaw size that averages about 2. No additional partial safety factors should be used in level-2 assessment.

Two normalized parameters are specified and given as

$$K_R = \frac{K}{K_{MAT}} \quad (29.5)$$

and

$$S_R = \frac{\sigma_N}{\sigma_{FLOW}} \quad (29.6)$$

where K_R is the fracture ratio,

K = Stress-intensity factor (a function of net section stress σ_N , crack size a , and geometry) at the fracture of the component

K_{MAT} = Linear elastic fracture toughness of the component

S_R = Collapse ratio

σ_N = Net section stress in the component at fracture

σ_{FLOW} = Flow stress defined as the average of yield stress and tensile stress in [BS 7910 \(1999\)](#)

The original FAD was developed by the United Kingdom's Central Electricity Generating Board (CEGB). This FAD is shown in [Figure 29.2](#). The CEGB approach ([Milne et al., 1986, 1988; Kanninen and Popelar, 1985](#)) addressed postyield fracture by an interpolation formula between two limiting cases: linear elastic fracture and plastic collapse. The interpolation formula called the failure assessment or R6 curve (see [Figure 29.2](#)) is given as follows

$$K_R = \frac{S_R}{\sqrt{\frac{8}{\pi^2} \ln[\sec(0.5\pi S_R)]}} \quad (29.7)$$

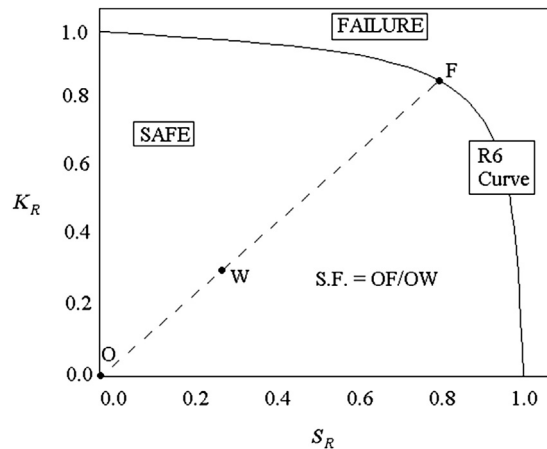


Figure 29.2
CEGB R6 curve.

The right-hand side of Eqn (29.7) is the plastic correction to the small-scale yielding prediction. The CEGB R6 curve in Figure 29.2 may be interpreted as follows: A structural component is safe if point W, describing its state, falls inside of the R6 curve. The component fails if point W is on or above the R6 curve. The utilization factor on the load is OW/OF , where point F is on the R6 curve and point O is in the origin.

29.4 Level 3: The FAD

The FAD utilized in level-3 assessment is depicted schematically in Figure 29.3:

- The collapse ratio, L_R , is the ratio of the net section stress at the fracture to the flow stress.
- The fracture ratio, K_R , is the ratio of the crack driving force (including residual stresses) to the material toughness (which could be K_{MAT} or CTOD).

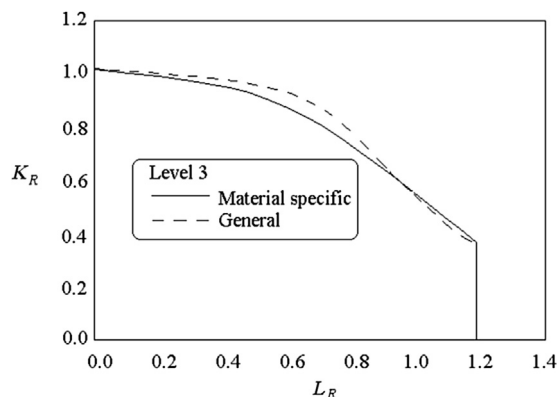


Figure 29.3
The failure assessment diagram.

The failure assessment curve defines the critical combination of service loads, material stress–strain properties, and geometries of the cracked member at which failure might be expected. Applications of the FAD to design codes include:

- CEGB R6—Revision 3
- BSI (1999) PD 6493
- Electric Power Research Institute/General Electric model
- ASME Section XI Code Case (DPFAD) for ferritic piping
- API 579 (2001)

Level 3 is the most sophisticated of the three levels, and will normally be used in the assessment of high strain-hardening materials and/or stable tearing where the level-2 approach would prove too conservative. In PD 6493 (now BS 7910), level-3 FAD consists of two alternative criteria: (1) a general FAD and (2) a material-specific FAD in which material stress–strain curves are also the input data to the FAD assessment.

CTOD is popular in the United Kingdom and other European countries, whereas the J-integral is used in the United States (e.g., by the nuclear engineering industry).

29.5 Fatigue Damage Estimation Based on Fracture Mechanics

29.5.1 Crack Growth Due to Constant Amplitude Loading

The total number of cycles to the final fracture is the sum of the number of cycles for the crack initiation phase and crack propagation phase. The number of cycles for the crack propagation phase, N_p , may be estimated using,

$$N_p = \int_{a_0}^{a_{CR}} \frac{da}{da/dN} \quad (29.8)$$

where a_0 and a_{CR} are crack depth (or length) at crack initiation and final fracture, respectively. The value of a_{CR} may be determined using methods for the assessment of final fracture, as discussed in Section 39.1 through Section 39.4. The crack propagation may be predicted using the Paris law. Substituting the Paris law into the above equation, the following is obtained,

$$N_p = \int_{a_0}^{a_{CR}} \frac{da}{C(\Delta K)^m} = \int_{a_0}^{a_{CR}} \frac{da}{C(S\sqrt{\pi a}F)^m} \quad (29.9)$$

where F is the so-called crack shape factor and S denotes the stress range. When the stress range S is of constant amplitude, the above equation can be rewritten as

$$N_p = \frac{1}{C(S\sqrt{\pi})^m} \int_{a_0}^{a_{CR}} \frac{da}{(\sqrt{a}F)^m} \quad (29.10)$$

If F does not depend on a , the above equation may lead to (Almar-Naess, 1985)

$$N_p = \frac{a_{CR}^{1-m/2} - a_0^{1-m/2}}{C(S\sqrt{\pi}F)^m(1-m/2)} \quad \text{for } m \neq 2 \quad (29.11)$$

The Paris parameters C and m can be found from Gurney (1979), IIW (1996), BS 7910 (1999), and API 579 (2001). The values of C and m depend on the material, service environment, and stress ratio. The value of C may also be determined by mechanical tests, and the chosen value is the mean value plus two standard deviations of $\log da/dN$.

The size of the initial crack a_0 needs to consider the accuracy of the nondestructive testing that is used to inspect the defects during fabrication.

29.5.2 Crack Growth due to Variable Amplitude Loading

The equations presented in Section 39.5.1 can be applied to risk-based inspections where the crack growth is predicted using the Paris law. Predicting the number of cycles for the crack propagation phase for variable amplitude loadings is complex and a computer program is needed to do the numerical integration for Eqn (29.9). The number of occurrences n_i in a block for stress range S_i for the crack depth from a_i to a_{i+1} can be estimated as (Almar-Naess, 1985),

$$n_I = \frac{1}{C(S_I\sqrt{\pi})^m} \int_{a_i}^{a_{i+1}} \frac{da}{(\sqrt{a}F)^m} \quad (29.12)$$

and the fatigue life N_i at a constant amplitude stress S_i is given by

$$N_I = \frac{1}{C(S_I\sqrt{\pi})^m} \int_{a_0}^{a_{CR}} \frac{da}{(\sqrt{a}F)^m} \quad (29.13)$$

Hence, the accumulated fatigue damage may then be estimated using Miner's law, which is

$$D = \sum_{I=1}^K \frac{n_I}{N_I} \quad (29.14)$$

Table 29.1: Comparison of fracture mechanics and S–N curve for fatigue

Fracture Mechanics	S–N Curve
Region I: Threshold region (no crack growth)	Fatigue endurance limit (infinite life)
Region II: Paris equation	S–N curve (high-cycle fatigue)
Region III: Final fracture (yielding)	Low-cycle fatigue, failure region

29.6 Comparison of Fracture Mechanics and S–N Curve Approaches for Fatigue Assessment

As compared in Table 29.1, the Paris equation can be transformed to the equation of an S–N curve. Equation (29.10) may be rewritten as

$$N_p = \frac{I}{C_I(S)^m} \quad (29.15)$$

where I is an integral. The total number of cycles N is close to N_p , because the number of cycles to the initiation of crack propagation is small. Hence, the above equation may be further written as

$$N = \frac{I}{C_I}(S)^{-m} \quad (29.16)$$

29.7 Fracture Mechanics Applied in Aerospace and Power Generation Industries

Fracture control in the aerospace industry is based on the fracture mechanics analysis of the growth of assumed preexisting cracks, of a size related to inspection detection capabilities (Harris, 1995). For space structures, the NASA (1988) requirements are applied to all payloads in the space shuttle, as well as life/mission-control items in space applications such as the space station. A fracture mechanics analysis of the component is conducted using an initial flaw size that is referred to as the nondestructive examination size. Smaller sizes can be assumed in the analysis if a better detection capability can be demonstrated for the particular examination method applied. Median material properties are used in the crack growth calculations; commercial software is available to calculate crack-growth based on fracture mechanics. The requirement is that the flaw size should be demonstrated to survive four lifetimes.

Fracture mechanics have been applied to aircraft structures because of the high-required reliability and severe weight penalties for overly conservative designs. Probabilistic methods have been applied to deal with the randomness of initial flaws and load spectra.

Provan (1987) described the military aircraft approaches known as “damage tolerance” and “fail-safe,” which are seen in Part III, Section 30.4. The purpose of damage tolerance analysis is to ensure structural safety throughout the life of a structure. The analysis evaluates the effects of accidental damage that might occur during the service life and verifies that the structure can withstand this damage until the next inspection or until the current mission is completed with a safety factor of two.

Harris (1995) also reviewed applications of fracture mechanics in the electric power generation industry for nuclear pressure vessels, steam turbine rotors, etc. The requirement for extreme reliability and the prohibitive cost of full-scale testing (as used in the aircraft industry) led to the extensive use of fracture mechanics to predict the behavior of defective components. The ASME (1989) Boiler and Pressure Vessel Code Section XI was developed for in-service nondestructive inspection intended to detect cracks before they grow and lead to failure. The code defines locations to be inspected, procedures to be used, and procedures for analyzing future behavior if a crack is found. As the code used in aerospace and aircraft industries, the ASME code also gives procedures for defining initial crack size, material (fatigue crack-growth) properties, and stress-intensity factors that are used in fracture mechanics analysis. Tables of crack sizes are also given to define the crack sizes that need not be further analyzed if the detected size is smaller. Cracks larger than these tabulated values can still be left in service if a more detailed analysis shows them not growing beyond a specified fraction of the critical crack size, during the remaining desired lifetime. The ASME (1991, 1992, 1994) provides guidelines for risk-based inspections of the most risk-prone locations, and consequently provides a greater risk reduction for a given number of inspections, or the same risk reduction for fewer inspections.

The probabilistic fracture mechanics developed in these industries have been applied and further developed by the shipping, bridge, and oil/gas industries for the design and operation of marine structures. In particular, the defect control criteria for pipeline installation, and the damage/defect tolerance criteria and inspection planning methods applied in the operation of tubular joints and pipelines have benefited from the research efforts of the aerospace and aircraft industries.

Fracture mechanics also play a major role in the analysis and control of failure in the chemical and petroleum industries, where “fitness-for-service” is employed.

29.8 Examples

29.8.1 Example 29.1: Maximum Tolerable Defect Size in Butt Weld

Problem: A butt-welded plate thickness of 150 mm, yield stress of 500 MPa. There is a surface crack with an aspect ratio $c/a = 1$. Its minimum critical CTOD is 0.00036 m.

The weld is loaded in uniaxial tension perpendicular to the crack plane, and the stress in the weldment is less than or equal to 60% of the yield stress. What is maximum allowable crack width?

Solution:

$$\frac{\varepsilon}{\varepsilon_y} = 0.60$$

$$\Phi = \frac{\delta_c}{2\pi\varepsilon_y a_{\max}} = \frac{0.00036}{2\pi \frac{500}{2.0E5} a_{\max}} = \frac{0.0259}{a_{\max}}$$

The following relation exists

$$\Phi = \frac{\varepsilon}{\varepsilon_y} - 0.25 = \frac{0.0259}{a_{\max}}$$

and therefore, the maximum half-width is $a_{\max} = 0.074$ m.

References

- Almar-Naess, A., 1985. *Fatigue Handbook, Offshore Steel Structures*. Tapir, Norway.
- API 1104, 1994. *Alternate Standards for Acceptability for Girth Welds*. Appendix A, *Standards for Welding Pipelines and Related Facilities*, eighteenth ed. American Petroleum Institute.
- API 579, 2001. *Recommended Practice for Fitness for Service*. American Petroleum Institute.
- ASME, 1989. *ASME Boiler and Pressure Vessel Code, Section XI, Rules for In-service Inspection of Nuclear Plant Components*. American Society of Mechanical Engineers.
- ASME, 1991, 1992, 1994. *Risk-based Inspection - Development of Guidelines*. Vol. 20.1 (1991): *General Guidelines*, Vol. 20.2(1992): *Light Water Reactor Nuclear Power Plant Components*, Vol. 20.3 (1994): *Fossil Fuel-Fired Electric Power Generating Station Applications*. American Society of Mechanical Engineers.
- Andersen, T.L., 1991. *Fracture Mechanics – Fundamentals and Application*. CRC Press.
- BSI, 1980. PD 6493-Guidance on Some Methods for the Derivation of Acceptance Levels for Defects in Fusion Welded Joints. BSI, London.
- BSI, 1999. BS7910-Guidance on Methods for Assessing the Acceptability of Flaws in Fusion Welded Structures. BSI.
- Burdekin, F.M., Dawes, M.G., 1971. Practical use of linear elastic and yielding fracture mechanics with particular reference to pressure vessels. In: *Practical Application of Fracture Mechanics to Pressure Vessel Technology*. The Institution of Mechanical Engineers, London, pp. 28–37.
- Dawes, M.G., 1974. Fracture control in high strength weldments. *Welding Journal* 53, 369-s–379-s.
- Gurney, T.R., 1979. *Fatigue of Welded Structures*, second ed. Cambridge University Press.
- Harris, D.O., 1995. *Fatigue and Fracture Control in the Aerospace and Power Generation Industries*. In: *Prevention of Fracture in Ship Structures*. By the Committee on Marine Structures, Marine Board, National Research Council, Washington, DC.
- IIW, 1996. *Fatigue Design of Welded Joints and Components*. Report XIII-1539–96/XV/845-96. The International Institute of Welding, Abington Publishing, Cambridge, England.
- Kanninen, M.F., Popelar, C.H., 1985. *Advanced Fracture Mechanics*. Oxford University Press, New York.
- Milne, I., Ainsworth, R.A., Dowling, A.R., Stewart, A.T., 1986. *Assessment of the Integrity of Structures Containing Defects*. R/H/R6. Revision 3. Leatherhead, Surrey, England: Central Electricity Generating Board.

- Milne, I., Ainsworth, R.A., Dowling, A.R., Stewart, A.T., 1988. Assessment of the integrity of structures containing defects. *International Journal of Pressure Vessels and Piping* 32, 3–104.
- NASA, 1988. Fracture Control Requirements for Payloads Using the National Space Transportation System, NASA NHB 8071.1. National Aeronautics and Space Administration.
- Provan, J.W., 1987. Probabilistic Fracture Mechanics and Reliability. Martinus Nijhoff Publishers, Boston, Massachusetts.
- Reemsnyder, H.S., 1997. Fatigue and Fracture of Ship Structures. In: *Prevention of Fracture in Ship Structures*. By the Committee on Marine Structures, Marine Board, National Research Council, Washington, DC.

Material Selections and Damage Tolerance Criteria

30.1 Introduction

Engineering applications of fatigue and fracture technologies will be discussed in this chapter, including:

- Material selection and fracture prevention
- Weld improvement and repair
- Damage assessment and damage tolerance criteria
- Nondestructive inspection

30.2 Material Selection and Fracture Prevention

30.2.1 Material Selection

Tensile strength is the key mechanical property for strength design for structures. The materials used are required to have satisfactory weldability and fracture toughness for the intended application environment (temperature). Fatigue and corrosion characteristics are also important material properties. In design codes, requirements for materials and welding are defined for the construction of the hull and machinery; for example, see [ABS \(2002\)](#). The material requirements in rules are defined for ordinary steel, higher-strength steel, and low-temperature materials, including:

- Process of manufacture
- Chemical composition
- Condition of the supply
- Tensile properties
- Impact properties
- Marking
- Surface finish

To certify compliance with the above material requirements, the test specimens and number of tests are defined by the rules along with the requirements for approval of welding procedures and qualification of welders.

30.2.2 Higher-Strength Steel

For ship structures, the yield strength for ordinary steel is 24 kgf/mm² (or 235 N/mm²). The higher-strength steel is HT32 (yield strength of 32 kgf/mm²) and HT36 (Yamamoto et al., 1986). The allowable stress for hull girder strength is defined for individual grades of material. The use of higher-strength steel may lead to reduction of plate wall thickness. However, corrosion resistance for higher-strength steel is equivalent to that for ordinary steel. Therefore, corrosion allowance should also be taken as 2.5–3.5 mm. Elastic buckling strength is only determined by geometric dimensions and is not influenced by yield strength. Therefore, elastic buckling strength is decreased due to the wall-thickness deduction for higher-strength steel. To avoid reductions in buckling strength, it may be necessary to reduce the spacing of stiffeners. The postyielding behavior for higher-strength steel is different from that for ordinary steel in that the ratio between the linear stress limit and the yield strength is higher for higher-strength steel. For instance, the proportional limit for the yield strength of steel between 50 and 60 kgf/mm² is 0.7–0.8, whereas the proportional limit for ordinary steel is 0.6. Hence, there is less tensile strain (at tensile failure) for higher-strength steel, and strength redundancy in the postyield region is less. In the heat-affected zone (HAZ), Charpy V-notch energy for high-strength steel may be significantly low. It may be necessary to control the heat energy in the welding process and increase the number of passes in a single-sided welding.

The weldability of steel is a measure of the ease of producing a crack-free and sound structural joint. The carbon equivalent (C_{eq}) for evaluating the weldability may be calculated from the ladle analysis in accordance with the following equation:

$$C_{eq} = C + \frac{M_n}{6} + \frac{C_r + M_0 + V}{5} + \frac{N_i + C_u}{15} \% \quad (30.1)$$

Selecting C_{eq} and its maximum value must agree with the fabricator and the steel mill because its value represents the tensile strength and weldability. The higher the C_{eq} , the higher the tensile strength, and the worse the weldability will be.

Welding procedures should be based on a steel's chemistry instead of the published maximum alloy content, since most mills run below the maximum alloy limits set by its specifications. When a mill produces a run of steel, chemical content is also recorded in a mill test report. If there is any variation in chemical content above maximum allowable limits, special welding procedures should be developed to ensure a properly welded joint.

For higher-strength steel, the fatigue resistance may not increase as much as the increase of stress in the stress concentration areas of the weld details. It is therefore necessary to reduce the stress concentration and improve the fatigue resistance for the weld details.

30.2.3 Prevention of Fracture

During the Second World War, accidents occurred due to brittle fractures in welded ships. In the United States, a thorough investigation was carried out on the temperature dependency of brittle fracture. It is now known that the toughness is higher if the Mn/C ratio is higher. With the development of fracture mechanics, it became clear that brittle fracture is due to the reduction of the fracture toughness K_{IC} in lower temperatures (below 0 °C). In order to determine fracture toughness, it is necessary to conduct accurate measurements using large test specimens. For practical purposes, the result of Charpy V-notch impact tests has been correlated with the fracture toughness K_{IC} and used in the specification for steels used in lower temperatures. In ship design rules, Charpy V-notch impact tests are not required in production for A, B, D, and E grades, and are to be tested at 0 °C, -10 °C, and -40 °C respectively. The energy average for standard Charpy test specimens is required to be higher than 27 J (or 2.8 kgf/m). As steels for hull structures, the E grades have the highest toughness, and may be used as crack arrestors to stop the propagation of brittle fracture. They are used in location for primary members that are critical for longitudinal strength. In many cases, the toughness criteria for secondary members may be relaxed.

In order to prevent fatigue cracks in welded details, allowable stress criteria have been defined in ship design rules based on simplified fatigue analysis (see Part III, Chapter 36) and an assumed design life of 20 years. The allowable stress criteria shall be satisfied in the determination of net wall thickness.

For quality control purpose, the materials are inspected when the steel is delivered from steelmakers. The inspection requirements are given in classification rules. For ships in operation, surveys are conducted by classification societies, the reduction of wall thickness due to corrosion is measured, and fatigue cracks and dent damage are given attention in the survey process. The causes of damage are investigated, and damage is repaired or weld details are modified when necessary. The damage tolerance criteria are discussed in [Section 30.4](#) of this chapter. Feedback from the process of inspection, cause investigation, repair, and modification is given to design through rule changes and the development of design guidance such as fatigue-resistant details; see [Subsection 30.3.2](#) of this chapter.

30.3 Weld Improvement and Repair

30.3.1 General

In many cases, the fatigue performance of severely loaded details can be designed to be fatigue resistant, and improved by upgrading the welded detail class to one having higher fatigue strength. In some cases, procedures that reduce the severity of the stress concentration at the weld, remove imperfections, and/or introduce local compressive

stresses can be used for improvement of fatigue life. Similarly, these fatigue improvement techniques can be applied as remedial measures to extend the fatigue life of critical weld details that have cracked.

In the following subsections, discussions are made of welding improvements through modifications of the weld toe profile and modifications of the residual stress distribution (Almar-Naess, 1985; Kirkhope et al., 1997).

30.3.2 Fatigue-Resistant Details

Fatigue strength of the weld details is based on “good” fabrication practice in terms of:

- Design that minimizes the restraint and geometric discontinuity in the design of cruciform joint misalignment, lap connection, and fillet welds.
- Welding practice for fillet weld fit-up, weld shape, and continuity
- Residual stress
- Weld toe dressing treatments

Based on classification rules, Glenn et al. (1999) cataloged fatigue resistant details in tanker structures, bulk carrier structures, container ships, and warships. These cataloged details may be used for designers as guidance, while the criteria made by Ma et al. (2000) may be used to assess the acceptability of a particular design (see Part III, Section 27.6).

30.3.3 Weld Improvement

Both contour grinding of the weld profile and local grinding of the weld toe area are recommended for modifying the weld profile and improving fatigue strength. When modifying the weld toe profile, the essential objectives are:

- Remove defects at the weld toe
- Develop a smooth transition between weld material and parent plate

Fatigue life can be increased by applying local grinding or remelting techniques to remove defects and discontinuities.

Grinding

Full-profile burr grinding, toe burr grinding, and localized disk grinding are widely used grinding methods. Considering the time required for grinding, local weld toe grinding has become one of the best grinding methods. Careful and controlled local grinding of the weld toe improves the fatigue strength of a specimen in the air by at least 30%; this is equivalent to increased fatigue life by a factor greater than 2. However, in order to obtain such a benefit, grinding should extend about 0.04 inch (1 mm) beneath the plate surface.

Controlled Erosion

An alternative weld toe modification technique uses a high-pressure water jet. Under carefully controlled conditions, the weld toe area can be eroded as if it were ground. Early research indicates that fatigue life improvements due to abrasive water jet (AWJ) erosion and toe grinding are comparable. The advantage of controlled erosion is that it does not require heat input and it can be carried out quickly.

Remelting Techniques

Remelting weld material to a shallow depth along the weld toe results in removal of inclusions and helps achieve a smooth transition between the weld and the plate material. Tungsten-inert-gas (TIG) and plasma welding are not practical techniques for routine use, but TIG and plasma dressing can be used to improve the fatigue strength of selected hot-spot areas.

TIG welding is based on a stringer-bead process. TIG dressing is performed on welds made by other processes where the toe region is melted to a shallow depth without the use of filler material. Slag particles in the remelted zone are brought to the surface, leaving the weld toe area practically defect-free. High heat input should be maintained to obtain a good profile and a low hardness. A low hardness in the HAZ may also be achieved by a second TIG application.

Plasma dressing requires remelting the weld toe using the plasma arc welding technique. It is very similar to TIG dressing, but plasma dressing uses a wider weld pool and higher heat input. This technique is relatively insensitive to the electrode position, because fatigue strength improvements using plasma dressing are better than those obtained when using TIG.

Although overall weld profiling is considered desirable for fatigue strength improvement, rules and recommendations other than API (2001) do not allow for consideration of improvements in fatigue strength due to weld profiling, unless weld profiling is accompanied by weld toe grinding. It should also be noted that the data associated with weld profiling and weld toe grinding are limited. Therefore, expert judgment should be used to quantify fatigue strength improvement due to the modification of the weld profile.

30.3.4 Modification of Residual Stress Distribution

By using the following methods, undesirable tensile residual stresses found at the weld can be modified to obtain desirable compressive stresses at the weld toe.

Stress Relief

Various fatigue tests on simple small-plate specimens indicate that improved fatigue strength can be obtained by stress relief due to postweld heat treatment. However, plate

and stiffening elements of continuous systems rarely require stress relief. It is also doubtful that a complex structural detail with built-in constraints can be effectively stress relieved.

Compressive Overstressing

Compressive overstressing is a technique in which compressive residual stresses are introduced at the weld toe. Experimental results and analytical work demonstrate the effectiveness of preoverstressing, but the procedure to be implemented does not appear to be practical for most marine structures.

Peening

Peening is a cold-working process intended to produce surface deformations with the purpose of developing residual compressive stresses. When impact loads on the material surface would cause the surface layer to expand laterally, the layer underneath prevents surface layer expansion, creating the compressive residual stresses at the surface. Typical peening methods are hammer peening, shot peening, and needle peening.

30.3.5 Discussion

Fatigue strength improvement techniques are time-consuming and costly and they should be applied selectively. Comparison of different techniques allows for assessment of their effectiveness and cost. The recommended improvement strategies depend on the characteristics of the (global and local) structure, and the preference for one technique over others is based on effectiveness, cost, and fabrication yard characteristics.

Comparisons of various approaches available that improve the fatigue strength of welded details are:

- Full-profile burr grinding is preferable to toe burr grinding or disk grinding only, because it results in higher fatigue strength even at a substantial cost penalty.
- Disk grinding requires the least time and cost. However, it produces score marks perpendicular to the principal stress direction, making this technique less effective than others.
- Using a high-pressure AWJ process for controlled erosion of the weld toe area can be as effective as grinding. Its simplicity, speed, and nonutilization of heat make controlled erosion very promising.
- A wider weld pool makes plasma dressing less sensitive to the position of the electrode relative to the weld toe, compared with TIG dressing. Therefore, the fatigue strength improvement obtained from plasma dressing is better than that obtained from TIG dressing.

- Review of grinding, remelting, and peening techniques indicate substantial scatter of fatigue strength improvements. Typically, the best fatigue strength improvements are achieved when using TIG dressing and hammer peening. Toe disk grinding is the least effective technique.

30.4 Damage Tolerance Criteria

30.4.1 General

Marine structures are subjected to various sources of cyclic loading that may cause fatigue cracks to propagate at welded details. The propagation of these cracks may eventually threaten structural strength and stability. Therefore, severe fabrication flaws and cracks detected in service are to be repaired. Similarly, corrosion defects and dent damages need to be inspected and repaired. In order to optimize the life-cycle inspection and maintenance costs, there is the need for a rational criterion to determine the acceptability of damages.

Damage tolerance is the ability for a structure to sustain anticipated loads in the presence of fatigue cracks, corrosion defects, or damage induced by accidental loads until such damage is detected through inspection or malfunctions and repaired. In this Section, focus will be devoted to fatigue cracks. Damage tolerance analysis for fatigue cracks makes use of fracture mechanics to quantitatively assess the residual strength and residual life of a cracked weld detail.

[Yee et al. \(1997\)](#) and [Reemsnyder \(1998\)](#) presented detailed guidance on the application of damage tolerance analysis for marine structures. The damage tolerance analysis consists of the following essential elements:

- The use of FADs to assess the local residual strength of a cracked structural detail
- The use of linear elastic fracture mechanic models for fatigue crack growth to predict the residual life of a cracked structural member
- The estimation of peak stress and cyclic loads over the assessment interval of interest
- Inspection to detect damage and its accuracy

Some items above will be discussed in the subsections that follow.

30.4.2 Residual Strength Assessment Using Failure Assessment Diagram

The FAD may be used to predict residual strength of a cracked member for a given set of fracture toughnesses and defect sizes; see Part III, Section 38.1.2. If the peak stress

exceeds the residual strength derived through FAD, failure may occur. For the accurate prediction of residual strength, it is important to properly:

- Assess the maximum defect size, considering damage detachability for the inspection programs
- Determine the material toughness and the applied/residual stresses
- Select an appropriate failure assessment diagram and define its net-section stress and stress intensity factor

While the residual strength represents the “capacity” of the damaged member, the “load” is the peak stress that may be applied to the cracked member over the assessment interval of interest. The calculation of stresses and crack driving forces may also significantly influence the result of the safety check for the cracked weld detail.

30.4.3 Residual Life Prediction Using Paris Law

The Paris Law may be used to calculate crack growth due to cyclic loads of constant or variable amplitudes; see Part III, Section 38.5. For the reliable prediction of crack growth, it is important to accurately:

- Predict the Paris parameters (C and m) used in the Paris equation
- Assess the initial crack size to be used in the Paris equation
- Calculate cyclic stresses and the stress intensity range

The outcome of integrating the Paris equation is the number of cycles from the time the crack is inspected to the final fracture. The damage tolerance criterion requires that this predicted fatigue life be longer than the sum of the time to the next inspection and the time required for repair or for replacement. If no damage is detected in the inspection, the minimum inspectable size for cracks shall be used as the initial crack size.

30.4.4 Discussions

A damage tolerance analysis may be conducted during the design and fabrication stage, while performing an in-service inspection or in the course of extending the design life of a structure. BS 7608 (BSI, 1993) may be used for the damage tolerance analysis. It recommends selecting the materials and reducing stress so that the crack growth rate is low and critical crack size is large. Providing readily inspectable and crack arresting details may also help.

The above discussions are made using fatigue and fracture as an example. Similar discussions may be made on corrosion defects and wear-out. In the evaluation of the tolerance criterion for corrosion defects, it is necessary to predict the

- initial corrosion defect size;
- residual strength of corroded member;

- future growth of corrosion defects using an adequate corrosion rate model;
- maximum loads that may occur for the period of interests or until the end of design life.

Dent damage caused by accidental loads will not grow, and therefore its tolerance criterion may be simply determined by comparing the residual strength with the maximum load expected for the interval of interest.

30.5 Nondestructive Inspection

[Almar-Naess \(1985\)](#) and [Marshall \(1992\)](#) outlined several methods for the inspection of cracks in weld details, such as:

- Liquid penetrant (to reveal surface flaws; requires a clean surface)
- Magnetic particles (to reveal surface flaws; does not require a clean surface)
- Eddy currents (primarily for detecting surface flaws; magnetic-field based)
- Radiography (for detecting internal cracks using x or γ radiation recorded in film)
- Ultrasonic testing (UT) (sizing internal defects using ultrasonic signals)

Radiography is most sensitive to volumetric defects, such as porosity or slag. Any detectable crack is rejected because of the difficulty of detecting and sizing crack-like defects.

Among of the above inspection methods, UT is the most reliable way of detecting and sizing internal defects. UT works very much like radar. Probes can be moved over the surface in the region to be inspected, and piezoelectric crystals generate ultrasonic signals. The waves are reflected by the surface of the examined body and any defects that might be in their way. The probe that generates the signal also detects these echoes. By measuring the time delay between the emission signal and the reception of each reflection, the source of reflection can be located and the position of defects identified. The basic features of UT are that:

- UT is more sensitive to the more serious types of defects because it depends on the signals being reflected. In decreasing order, the severities of defects are: cracks, incomplete fusion, inadequate penetration, slag, and porosity.
- UT can locate defects in three dimensions.
- UT can be conducted quickly and simply without radiation hazards.
- UT can handle complex geometry of welded connections through use of the transducer.

Over 70% of defects can be detected by UT, and the false alarm rate is less than 30%.

Where radiographic or ultrasonic inspection is required, the extent and location of inspection, and choice of inspection methods, are to be in accordance with [AWS \(1997\)](#) and [ABS \(1986\)](#), the materials and welding procedures involved, the quality control procedures employed and the results of visual inspection. In [AWS \(1997\)](#) and [ABS \(1986\)](#),

criteria are defined for determining whether inspection results (signals) are to be nonconforming, disregarded, or evaluated against defect acceptance criteria.

References

- ABS, 1986. Rules for Non-destructive Inspection of Hull Welds. American Bureau of Shipping.
- ABS, 2002. Rule Requirement for Materials and Welding. American Bureau of Shipping.
- Almar-Naess, A., 1985. Fatigue Handbook, Offshore Steel Structures. Tapir, Norway.
- AWS, 1997. AWS Structural Welding Code - Steel, AWS D1.1-96. American Welding Society.
- BSI, 1993. BS 7608-Code of Practice for Fatigue Design and Assessment of Steel Structures.
- Glenn, I.F., Paterson, R.B., Luznik, L., Dinovitzer, A., Bayley, C., 1999. Fatigue Resistant Detail Design Guide for Ship Structures. Ship Structures Committee. Report SSC-405.
- Kirkhope, K.J., Bell, R., Caron, L., Basu, R., 1997. Weld Detail Fatigue Life Improvement Techniques. Ship Structures Committee. Report SSC-400.
- Ma, K.T., Srinivasan, S., Zhang, H., Healy, B., Peng, H., 2000. Developing design criteria for connections around cutout (Slot) openings. SNAME Transactions 227-248.
- Marshall, P.W., 1992. Design of Welded Tubular Connections. Elsevier Press, Amsterdam.
- Reemsnyder, H.S., 1998. Guide to damage tolerance analysis. In: Course Notes "Fatigue and Fracture Analysis of Ship Structures". SSC.
- Yamamoto, Y., Ohtsubo, H., Sumi, Y., Fujino, M., 1986. Ship Structural Mechanics. Nariyamato Book, (in Japanese).
- Yee, R.D., Malik, L., Basu, R., Kikhope, K., 1997. Guide to Damage Tolerance Analysis of Marine Structures. Ship Structures Committee. Report SSC-402.

Basics of Structural Reliability

31.1 Introduction

Part IV describes structural reliability methods for the design of marine structures, with emphasis on their practical application—for example, in ship structures. Focuses are given to basic concepts, methodologies, and applications. Examples are given to demonstrate the application of the methodology.

Details of the structural reliability theory can be referred to—for example, [Ang and Tang \(1975, 1984\)](#), [Thoft-Christensen and Baker \(1982\)](#), [Madsen et al. \(1986\)](#), [Schneider \(1997\)](#), and [Melchers \(1999\)](#). Discussions are given on simple analytical equations that are based on lognormal assumptions. The papers on numerical approaches—for example, [Song and Moan \(1998\)](#)—are also mentioned briefly.

The following subjects are addressed in detail:

- Reliability of marine structures
- Reliability-based design and code calibration
- Fatigue reliability
- Probability- and risk-based inspection planning

31.2 Uncertainty and Uncertainty Modeling

31.2.1 General

In general, marine structural analysis deals with load effects (demand) and structural strength (capacity). In design, the dimensions of the structural members are determined based on the requirement that there is a sufficient safety margin between demand and capacity.

Uncertainties are involved in all the steps for structural analysis and in strength evaluations. These uncertainties are due to the randomness of the environment, geometric, and material properties, as well as inaccuracies in the prediction of loads, responses, and strength.

Rational design and analysis of marine structures require consideration of all the uncertainties involved in predicting load effects and structural modeling. Uncertainty analysis is the key in any reliability evaluation, such as reliability-based design or the requalification for marine structures.

The development of probabilistic analysis methods and design codes increases the importance of quantifying uncertainties. The results of the studies on uncertainty modeling can be used to assess the relative importance of the various types of uncertainties. For example, one of the conclusions drawn from a study on offshore structures was that the uncertainty in the lifetime extreme wave height is the most significant one. The error in predicting the most severe sea condition over the design lifetime is one of the major components of uncertainty.

The reliability of a structural system depends on the load and strength variables. Each variable can be calculated with different degrees of accuracy. For example, for most of the cases, the response of an offshore platform to dead loads can be evaluated with high accuracy, while wave-induced responses may not be predicted with the same confidence. Therefore, when assessing structural safety and making design decisions, the differences in the confidence levels associated with each load and strength variable must be taken into account. For example, in a reliability-based design code for offshore structures, the load factor for wave loads is larger than that for dead loads, because the modeling uncertainty associated with the former is larger.

31.2.2 Natural versus Modeling Uncertainties

Uncertainties in analysis of marine structures can be categorized into either natural (random) or modeling types. The former is due to the statistical nature of the environment and the resulting loads. The latter is due to the imperfect knowledge of various phenomena, and idealizations and simplifications in analysis models. These uncertainties introduce bias and scatter. An example of a natural uncertainty is that which is associated with the wave elevation at a given position in the ocean. An example of a modeling uncertainty is the error in calculating the stresses and strength in a structure when the applied loads are known; the error is only due to the assumptions and simplifications in the structural analysis.

Modeling uncertainties can be reduced as the mathematical models representing them become more accurate. This is not the case with random uncertainties that do not decrease as more information is gathered. Both random and modeling uncertainties must be quantified and accounted for in reliability analysis and in the development of reliability-based design codes.

Let X be the actual value of some quantity of interest and X_0 be the corresponding value specified by a design code. According to [Ang and Cornell \(1974\)](#),

$$X = B_I B_{II} X_0 \quad (31.1)$$

where $B_I = X_P/X_0$ and X_P is the theoretically predicted value for this quantity, and $B_{II} = X/X_P$. B_I is a measure of natural (random) variability, and B_{II} is a measure of modeling uncertainty.

The mean values of random variables B_I and B_{II} , and $E(B_I)$ and $E(B_{II})$, are the biases corresponding to natural and modeling uncertainties, with subscript I indicating natural uncertainty and subscript II representing modeling uncertainty. Assuming that the random and modeling uncertainties are statistically independent, and by using a linear expansion of the expression for B about the mean value of the random variables, the total uncertainty in X is quantified as

$$E(B) = E(B_I)E(B_{II}) \text{ and } COV_B = (COV_{B_I^2} + COV_{B_{II}^2})^{1/2} \quad (31.2)$$

where $B = B_I B_{II}$ and COV stands for the coefficient of variation of the quantity specified by the subscript.

Equation (31.2) is only valid for small coefficients of variation (less than 0.10). However, the above approximations are frequently used.

31.3 Basic Concepts

31.3.1 General

Structural engineering deals with load S and strength R in terms of forces, displacements, and stresses acting on the structures. Structural design codes commonly specify loads, strength, and appropriate safety factors to be used. Structural reliability theory is the evaluation of the failure probability taking into account the uncertainties in both the loads and the strength. During the last two decades, many efforts have been made on structural reliability and their application to practical structural engineering.

31.3.2 Limit State and Failure Mode

A structural component can fall into a safe or failure state. The borderline (or surface) between the safe and failure states is named as a limit state, and expressed as $g(Z) = R - S$. The following conditions describe the possible states of a structural component:

- $g(Z) < 0$ represents a failure state where loads S exceeds the strength R .
- $g(Z) > 0$ represents a safe state since strength R is larger than loads S .
- $g(Z) = 0$ represents the limit state line (or surface).

Figure 31.1 below roughly shows the concept of the limit state.

For marine structures, the limit states are defined in accordance with the different requirements, such as serviceability and ultimate strength.

31.3.3 Calculation of Structural Reliability

By quantifying the uncertainties using probabilistic methods, the structural reliability can be measured by means of failure probability.

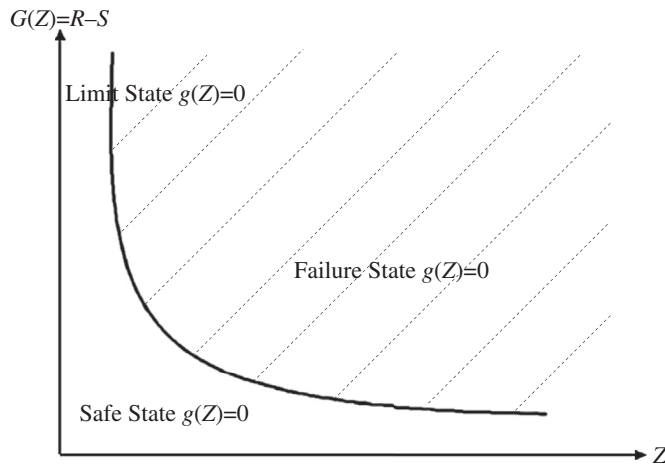


Figure 31.1
Limit state concept

For a structure described by a set of random variables Z with joint distribution $f_Z(z)$, it must be possible for each set of values of z to state whether the structure has failed. This leads to a unique division of Z space into two sets, called the safe set and the failure set respectively. These two sets are separated by the failure surface (limit state).

The structural failure probability P_f can then be calculated as

$$P_f = P(g(Z) \leq 0) = \int_{g(z) \leq 0} f_Z(z) dz \quad (31.3)$$

and the reliability R is

$$R = 1 - P_f = P(g(Z) > 0) \quad (31.4)$$

The exact numerical integration is only practical for a very limited class of simple problems. A variety of procedures representing different levels of sophistication may be used to calculate the failure probabilities, namely the safety index method, the analytical approach, and the numerical approach.

Cornell Safety Index Method

Assuming that the limit state function is given below

$$g(Z) = R - S \quad (31.5)$$

where R and S are random variables representing the strength and load, respectively; [Cornell \(1969\)](#) proposed to estimate the safety index using,

$$\beta = \frac{g(\bar{Z})}{\sigma_g} = \frac{\bar{R} - \bar{S}}{\sqrt{\sigma_R^2 + \sigma_S^2}} \quad (31.6)$$

where \bar{R} and \bar{S} are the mean values of R and S ; σ_R and σ_S are standard deviations of R and S respectively. The safety index is uniquely related to the failure probability by

$$P_f = \Phi(-\beta) \quad (31.7)$$

where Φ is the standard normal distribution function; see [Table 31.1](#).

The reliability index β is related approximately to the failure probability as

$$P_f \approx 0.475 \exp(-\beta^{1.6}) \quad (31.8)$$

or

$$P_f \approx 10^{-\beta} \quad (31.9)$$

The Hasofer–Lind Safety Index Method

An important step in the calculation of failure probability was previously made by [Hasofer and Lind \(1974\)](#). They transformed the limit state function into the so-called standard space. This transformation is shown here for the two variables R and S only.

The random variables R and S are transformed and standardized into U_1 and U_2 , respectively.

$$U_1 = \frac{R - \mu_R}{\sigma_R} \quad (31.10)$$

$$U_2 = \frac{S - \mu_S}{\sigma_S} \quad (31.11)$$

Hence, the random variables R and S can be expressed as

$$R = U_1\sigma_R + \mu_R \quad (31.12)$$

$$S = U_2\sigma_S + \mu_S \quad (31.13)$$

Thus, the new variables have a mean value of 0 and a standard deviation of 1. In the new coordinate system, the straight line is expressed as

$$g(\mathbf{Z}) = R - S = (\mu_R - \mu_S) + (U_1\sigma_R - U_2\sigma_S) \quad (31.14)$$

The distance from the design point to the origin is equal to the distance marked with β , the so-called β safety index (or β index or Hasofer–Lind index), as shown in [Figure 31.2](#).

Table 31.1: Relation between β and $\Phi(-\beta)$

Standard Normal Distribution Table										
β	0.0	0.1	0.2	0.3	0.4	0.5	0.6	0.7	0.8	0.9
$\Phi(-\beta)$	0.5	0.46017	0.42074	0.38209	0.34458	0.30854	0.27425	0.24196	0.21186	0.18406
β	1.0	1.1	1.2	1.3	1.4	1.5	1.6	1.7	1.8	1.9
$\Phi(-\beta)$	0.15866	0.13567	0.11507	0.09680	0.08076	0.06681	0.0548	0.04457	0.03593	0.02872
β	2.0	2.1	2.2	2.3	2.4	2.5	2.6	2.7	2.8	2.9
$\Phi(-\beta)$	0.02275	0.01786	0.0139	0.01072	0.0082	0.00621	0.00466	0.00347	0.002555	0.001866
β	3	3.1	3.2	3.3	3.4	3.5	3.6	3.7	3.8	3.9
$\Phi(-\beta)$	0.001499	0.000968	0.000687	0.000483	0.000337	0.000233	0.0001591	0.0001078	0.0000723	0.0000483
β	4	4.1	4.2	4.3	4.4	4.5	4.6	4.7	4.8	4.9
$\Phi(-\beta)$	3.170E-05	2.070E-05	1.330E-05	8.500E-06	5.400E-06	3.400E-06	2.100E-06	1.300E-06	8.000E-07	5.000E-07

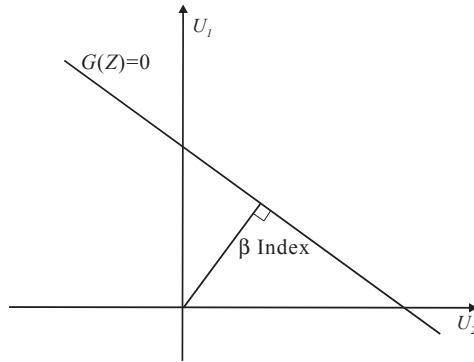


Figure 31.2
 β index method.

Example 31.1, given in [Section 31.11](#), demonstrates the β index method.

Analytical Approach

As an approximate method to compute the failure probability, the first-order reliability method (FORM) is the most widely accepted one. FORM also provides the sensitivity of the failure probability with respect to different input parameters, which is essential when optimizing the reliability of the structure in design, construction, and maintenance.

The second-order reliability method (SORM) is for approximating the limit-state surface by a second-order surface fitted at the design point. The most common approximation is the parabolic surface.

FORM and SORM usually give a proper approximation for small probabilities, but their accuracy and feasibility decrease with increasing nonlinearity for the limit state and number of nonnormal random variables. In such cases, the failure probability may be estimated by simulation methods.

Simulation Approach

Instead of using an analytical solution, the Monte Carlo simulation (MCS) is a numerical technique based on experiments on a digital computer. The failure probability is interpreted as the relative frequency. The MCS involves randomly sampling a large number of realizations for the failure function, $g(Z)$, and observing the results (i.e., whether the failure function is less than or equal to zero). If the experiment is repeated N times and failure occurs n times, the failure probability is estimated as $P_f = n/N$.

There are two main classes of the simulation methods applied for reliability analysis, (1) the zero-one indicator method and (2) the semianalytical conditional expectation method.

31.3.4 Calculation by FORM

In FORM, the failure set is approximated by first transforming the limit state surface into U space and then replacing it by its tangent hyperplane at the design point \mathbf{u}^* .

The Rosenblatt transformation is used,

$$U_i = \Phi^{-1}(F_i(Z_i|Z_1, \dots, Z_{i-1})) \quad i = 1, 2, \dots, n \quad (31.15)$$

If the random variables Z are mutually independent, the transformation is

$$U_i = \Phi^{-1}(F_i(Z_i)) \quad i = 1, 2, \dots, n \quad (31.16)$$

The limit state surface $g(\mathbf{Z}) = 0$ in Z space is transformed into a corresponding limit state surface $g(\mathbf{u}) = 0$ in U space. In the next step, the design point has to be determined in U space. This point lies on $g(\mathbf{u}) = 0$, and is the point in the failure set with the largest probability density, that is, the closest point on the failure surface to the origin of the U space. An interactive procedure is applied to find the design point \mathbf{u}^* , which is expressed as

$$\mathbf{u}^* = \beta \boldsymbol{\alpha}^* \quad (31.17)$$

in which β is the first-order reliability index, or the distance between the design point and the origin. The unit normal vector $\boldsymbol{\alpha}^*$ to the failure surface at \mathbf{u}^* are calculated by

$$\boldsymbol{\alpha}^* = -\frac{\nabla g(\mathbf{u}^*)}{|\nabla g(\mathbf{u}^*)|} \quad (31.18)$$

where $\nabla g(\mathbf{u})$ is the gradient vector. The actual limit state surface $g(\mathbf{u}) = 0$ is then approximated by its tangent hyperplane, which, at the design point \mathbf{u}^* , is

$$g(\mathbf{u}) = \beta + \boldsymbol{\alpha}^T \mathbf{u} = 0 \quad (31.19)$$

The first-order safety margin M is defined as

$$M = g(\mathbf{U}) = \beta + \boldsymbol{\alpha}^T \mathbf{U} \quad (31.20)$$

The corresponding approximation to the failure probability is

$$P_f \approx \Phi(-\beta) \quad (31.21)$$

From the above descriptions of FORM, it is seen that FORM is used to approximate the failure set through replacement of the limit state surface in u -space by its tangent hyperplane at the design point as defined by Eqn (31.19). Figure 31.3 illustrates this method.

This is the first-order approximation to the failure probability P_f , and β is the corresponding first-order approximation to the reliability index. The accuracy of the

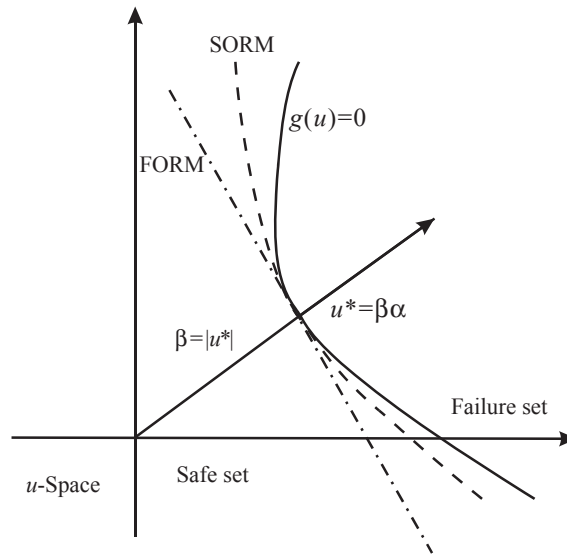


Figure 31.3
Illustration of FORM and SORM.

estimate depends upon how well the true failure surface is represented by the linear approximation, and may usually be improved by SORM, which is described in the following subsection. The problem affecting accuracy most is that FORM may not find the global design point in cases of multiple design points.

31.3.5 Calculation by SORM

In the second-order reliability method (SORM), the limit state surface is approximated by a hyperparaboloid with the same tangent hyperplane and the main curvatures at the design point. An approximation to the failure probability is then

$$\begin{aligned}
 P_{f,\text{SORM}} \approx & \Phi(-\beta) \prod_{j=1}^{n-1} (1 - \beta_{k_j})^{-1/2} + [\beta\Phi(-\beta) - \phi(\beta)] \\
 & \times \left\{ \prod_{j=1}^{n-1} (1 - \beta_{k_j})^{-1/2} - \prod_{j=1}^{n-1} (1 - (\beta + 1)_{k_j})^{-1/2} \right\} + (\beta + 1)[\beta\Phi(-\beta) - \phi(\beta)] \\
 & \times \left\{ \prod_{j=1}^{n-1} (1 - \beta_{k_j})^{-1/2} - \text{Re} \left\{ \prod_{j=1}^{n-1} (1 - (\beta + i)_{k_j})^{-1/2} \right\} \right\}
 \end{aligned} \tag{31.22}$$

where i in the third term is the imaginary unit, $\text{Re}()$ denotes the real part, and k_j ($j = 1, 2, \dots, n-1$) are the principal curvatures at the design point. The first term is the asymptotic result for $\beta \rightarrow \infty$.

Using SORM, an equivalent hyperplane can be defined as a linear approximation to the true failure surface with a reliability index

$$\beta_{\text{SORM}} = -\Phi^{-1}(P_{f,\text{SORM}}) \quad (31.23)$$

The unit normal vector α_{SORM} is in practice approximately set equal to that obtained by FORM.

In SORM, the limit state surface is approximated by a curvature fitted hyperparaboloid at the design point u^* , as sketched in Figure 31.3. Compared SORM with FORM, the estimate accuracy has been improved by a second-order approximation.

31.4 Component Reliability

The concepts introduced in Section 31.3 are mainly for the reliability evaluation at the component level, which means that the concern is on the failure probability for problems modeled by a single limit state function. Component reliability is the basis for structural reliability analysis since all marine structures are composed of components.

31.5 System Reliability Analysis

31.5.1 General

This section deals with the formulation and evaluation of the failure probability in problems where more than one limit state function must be considered (i.e., system reliability analysis).

A system is generally composed of many elements where each element may have one or more failure modes described by their individual limit state functions. Moreover, a system may have many failure modes, where each system failure mode may be due to the failure of one element only or due to the failure of several elements jointly.

Series and parallel are the two fundamental types of systems from which any other system can be built.

31.5.2 Series System Reliability

A system is called a series system if the system is in a state of failure whenever any of its elements fail. Such systems are often referred to as weakest-link systems. A typical example of this is marine pipelines or risers.

The failure probability of a series system can be formulated as the probability of the union of failure events. For a system with m failure elements defined by their safety margins M_i , the probability of failure can be formulated as

$$P_{f,\text{sys}} = P \left[\bigcup_{i=1}^m (M_i \leq 0) \right] = P \left[\bigcup_{i=1}^m (\beta_i - \alpha_i^T u) \right] \quad (31.24)$$

$$= 1 - \Phi_m(\beta, \rho)$$

where Φ_m is the m -dimensional standard normal distribution function, $\beta = [\beta_1, \beta_2, \dots]$ is the vector of reliability indices for the m failure elements, and ρ is the corresponding correlation matrix.

To demonstrate the reliability calculation of series system, an example is given in [Section 31.11](#).

31.5.3 Parallel System Reliability

A parallel system fails when all elements in the system fail. For a parallel system, all elements have to fail for system failure to occur. The failure probability can be formulated as the intersection of the element failure events

$$P_{f,\text{sys}} = P \left[\bigcap_{i=1}^m (M_i \leq 0) \right] = P \left[\bigcap_{i=1}^m (\beta_i - \alpha_i^T u) \right] \quad (31.25)$$

$$= \Phi_m(-\beta, \rho)$$

It is seen from the above two equations that the evaluation of the failure probability of series and parallel systems amounts to an evaluation of the standard multinormal integral. This is however a difficult task for problems of large dimensions.

To demonstrate the reliability calculation of a simple parallel system, an example is given in [Section 31.11](#).

31.6 Combination of Statistical Loads

31.6.1 General

In general, loads can be grouped into the following three classes, based on statistical characteristics of their form and history:

- Time-invariant loads: for example, dead loads
- Random loads: for example, wave loads
- Transient random loads: for example, earthquake loads

When two or more random loads act on a structure, the combination of statistical loads must be considered based on statistical characteristics of the individual loads.

For instance, the primary types of load combinations for ship structures are

- Hull girder loads
- Hull girder loads and local pressure
- Hull girder loads and transient loads

A simple load combination problem can be expressed—for example, a hull girder collapse—as

$$M_t(t) = M_s(t) + M_w(t) \quad (31.26)$$

where

$M_t(t)$ = total bending moment acting ship hull girder;

$M_s(t)$ = still water bending moment;

$M_w(t)$ = vertical wave bending moment.

In most current ship design rules, the peak coincidence method for the combination of still-water bending moment and vertical-wave bending moment is applied as

$$M_{t,\max}(t) = M_{s,\max}(t) + M_{w,\max}(t) \quad (31.27)$$

This is based on the very conservative assumption that the maximum values of the two bending moments occur simultaneously.

However, the combination of statistical loads is complex, and a number of methods have been derived to solve this problem. Here, only the application of Turkstra's rule (Turkstra, 1972) and the Ferry Borges—Castanheta (1971) model are presented.

31.6.2 Turkstra's Rule

The loading processes may be searched for some defined maximum in a systematic manner. A procedure proposed by Turkstra (1972) has found its way into practice. It is based on a combination model for stationary random processes. Its principle is that when one random load achieves its maximum value in time T , the transient values of other loads can be used to form the maximum load combination value. Assuming the random loads are represented by $S_i(t)$, the load combination is $S(t)$ —that is,

$$S(t) = \sum_i S_i(t) \quad (31.28)$$

Then, the maximum value of $S(t)$ can be expressed as

$$S_M = \max_{t \in T} S(t) = \max_{t \in T} \left[\max_{t \in T} S_i(t) + \sum_{j=1}^n S_j(t) \right] \quad (31.29)$$

where $\max S_i(t)$ is the maximum value of $S_i(t)$ in time T and $S_j(t)$ is the transient value of other random loads.

It should be noted that different load combinations can be performed for Eqn (31.29) to derive the maximum value.

31.6.3 Ferry Borges—Castanheta Model

The Ferry Borges—Castanheta (FBC) model (Ferry-Borges and Castanheta (1971)) represents each individual stochastic process in the form of a series of rectangular pulses as shown in Figure 31.4. The value of such a pulse represents the intensity of the load. The duration of the pulse remains constant within the series. This time interval is chosen such that the pulses can be considered as independent repetitions of the respective actions.

Time intervals of different processes are chosen, such that the longer interval is an integer multiple of the next shorter one, valid for all processes involved. This is a prerequisite for easy calculations of the maximum value distribution of the combination of the two processes, because the pulse of the shorter step process is repeated exactly n -times within the pulse duration of the longer step one.

Consider the case where three load processes X_1 , X_2 , and X_3 are acting on a marine structure. The FBC load model then considers a new variable for the maximum of X_3

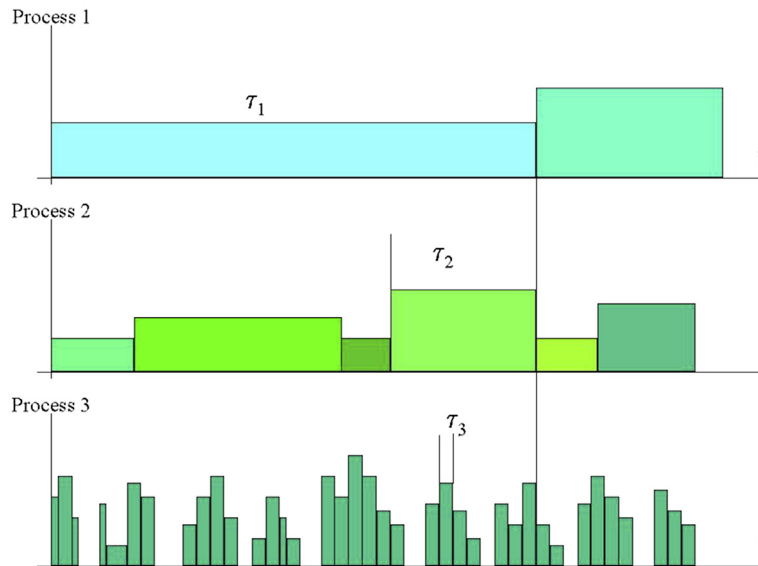


Figure 31.4
Illustration of the FBC model.

within an interval τ_2 together with X_2 . This variable, in turn, is searched for its maximum during an interval τ_1 and is then added to X_1 . From this, finally, the maximum during the lifetime T is considered as the variable representing all three processes together.

The variable Y representing the maximum combined loads of the three processes, may be written as

$$Y = \max_T \left\{ X_1 + \max_{\tau_1} \left(X_2 + \max_{\tau_2} X_3 \right) \right\} \quad (31.30)$$

Herein, the X_1 represents the load distribution. The terms $\max X_1$ represents the maximum values of the random variable X_1 within the period τ_1 or T , respectively.

31.7 Time-Variant Reliability

Marine structures can be subjected to time-varying loads (e.g., wind loads). Structural strength may also present a time-varying behavior (e.g., deterioration of component strength due to corrosion attacks). The basic variables that are related to these time-dependent values are stochastic processes. The reliability problem becomes time-variant, as defined by,

Set of basic stochastic processes:	$X(t) = \{X_1(t), X_2(t), \dots, X_n(t)\}$
Joint distribution function of $X(t)$:	$F_{X(t)}(X(t), t)$
Limit-state surface:	$g(x(t)) = 0$

The main interests in time-variant reliability problem lies in the time t of the first passage from the safe domain, $g(x(t)) > 0$, to the failure domain, $g(x(t)) \leq 0$, during the life of the structure, $t \in [0, T]$, as illustrated in Figure 31.5. T is the design life of marine structures or

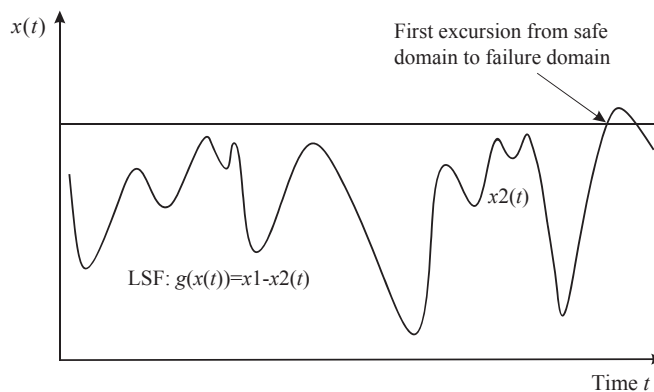


Figure 31.5
Time-variant reliability.

the reference period for reliability analysis. The time t for the first excursion $g(x(t)) \leq 0$ is called time to failure and is a random variable.

The probability of occurrence of $g(x(t)) \leq 0$ during the design life of the marine structures, T , is called first-passage probability. This probability may be considered equivalent to the failure probability $p_f(t)$ during a given period $[0, t]$, defined by (Melchers, 1999).

$$p_f(t) = 1 - P[N(t) = 0 \cap g(x(0)) > 0] \quad (31.31)$$

or

$$p_f(t) = 1 - P[N(t) = 0 | g(x(0)) > 0] \cdot P[g(x(0)) > 0] \quad (31.32)$$

where $N(t)$ is the number of outcrossings in the interval $[0, t]$. Outcrossings are the excursions from the safe domain to the failure domain.

For marine structural analysis, stochastic load processes are often replaced by time-invariant random variables to represent the lifetime loads. This also applies to cases of simultaneous random loads. The combined extreme load needs to be determined appropriately since the respective maximum values of different load processes do not necessarily occur simultaneously. This depends upon the application of methods for load combinations as described in the above subsection.

31.8 Reliability Updating

Reliability methodology can be used as a tool to reassess structural integrity. Such reassessment is required, for example, when inspection results are available or design conditions are changed. New measures of structural reliability are achieved based on new information. The information can be grouped in two classes:

- Sampling of quantities
- Observations

To demonstrate the reliability updating, a component, with load S and strength R , is taken as an example. The failure probability is

$$P_f = P[R - S \leq 0] = \int_{-\infty}^{\infty} F_R(s) f_s(s) ds \quad (31.33)$$

Assuming that the component is subject to a proof load, q^* , and that it survives the load, the strength $r \geq q^*$ is implied.

The updating of P_f can be formed as

$$\begin{aligned}
P_{f,up} &= P[R - S \leq 0 | R \geq q^*] \\
&= P[R - S \leq 0 | H \geq 0] \\
&= \frac{P[R - S \leq 0 \cap H \geq 0]}{P[H \geq 0]} = \frac{P[R - S \leq 0 \cap -H \leq 0]}{P[-H \leq 0]}
\end{aligned} \tag{31.34}$$

where $H = R - q^*$

In general, different methods are available to update the structural reliability based on new information. [Song and Moan \(1998\)](#) presented methods of reliability updated for ships and jackets, as detailed in Part IV, Chapter 36.

31.9 Target Probability

31.9.1 General

Guidelines are provided for structural designers on acceptable failure probabilities associated with each failure mode—that is, the minimum acceptable reliability index β_0 , frequently referred to as the target probability. When carrying out structural reliability analysis, an appropriate safety level should be selected based on factors such as consequence of failure, relevant design codes, and accessibility to inspection and repair. Target probability levels have to be met in the design in order to ensure that certain safety levels are achieved.

31.9.2 Target Probability

A design is safe if,

$$\beta > \beta_0 \tag{31.35}$$

where

β_0 = target safety index

β = safety index as estimated from analyses

The regulatory bodies or classification societies and/or professions agree upon a reasonable value. This may be used for novel structures where there is no prior history.

Code calibration is used to calibrate reliability levels that are implied in currently used codes. The level of risk is estimated for each provision of a successful code. Safety margins are adjusted to eliminate inconsistencies in the requirements. This method has been commonly used for the rules development.

Target probabilities are chosen to minimize total expected costs over the service life of the structure. A cost-benefit analysis approach may be used effectively to define the target

Table 31.2: Recommended Target Safety Indices for Ship Structures

Failure Mode	Commercial Ships	Naval Ships
Primary (initial yield)	5.0 (2.97E-7)	6.0 (1.0E-9)
Primary (ultimate)	3.5 (2.3E-4)	4.0 (3.2E-5)
Secondary	2.5 (6.2E-3)	3.0 (1.4E-3)
Tertiary	2.0 (2.3E-2)	2.5 (6.2E-3)

probability for a design in which failures result in only economic losses and consequences. Although this method is logical on an economic basis, a major shortcoming is its need to measure the value of human life.

The target probabilities, for a reliability-based design, are based on calibrated values of implied safety levels in the currently used design practice—as shown, for example, by [Bai et al. \(1997\)](#). The argument behind this approach is that a code represents a documentation of an accepted practice. Therefore, it can be used as a launching point for code revision and calibration. Any adjustments in the implied safety levels should be for the purpose of creating a consistency in the reliability among the resulting designs according to the reliability-based code.

31.9.3 Recommended Target Safety Indices for Ship Structures

Recommended target safety levels for the hull girder (primary), stiffened panel (secondary), and unstiffened plate (tertiary) mode of failure and the corresponding notional probabilities of failure, are summarized in [Table 31.2 \(Mansour et al., 1997\)](#). It should be pointed out that the values of the target safety index are also dependent on the methods used to calibrate the reliability levels.

31.10 Software for Reliability Calculations

The following are a few selected computer programs for the calculation of structural reliability.

PROBAN:

A probabilistic analysis tools for general structures developed by DNV that is part of the SESAM package

STRUREL:

A general structural reliability analysis software including component reliability calculation (COMREL), system reliability calculation (SYSREL), and statistical analysis of reliability data (STAREL) developed by RCP Consult GmbH in Germany

ISPUD:	Specially designed for structural reliability calculation using the MCS
CALREL:	A general structural reliability software developed by UC Berkeley. Its capabilities include (1) failure probability estimate for components; (2) failure probability estimate for systems; (3) FORM and SORM analysis; (4) direct MCS analysis; and (5) sensitivity analysis

31.11 Numerical Examples

31.11.1 Example 31.1: Safety Index Calculation of a Ship Hull

Problem:

The sketch in [Figure 31.6](#) shows the probability density functions of the load and strength of the ship hull girder in terms of applied bending moment and ultimate moment capacity of the hull, respectively. Both the load S and the strength R are assumed to follow normal probability distribution with mean values $\mu_S = 20,000$ ft-ton and $\mu_Z = 30,000$ ft-ton, respectively, and standard deviations of $\sigma_Z = 2500$ ft-ton and $\sigma_S = 3000$ ft-ton, respectively. What is the failure probability for the hull?

Solution:

The reliability index, β , can be estimated using the Cornell safety index method,

$$\beta = \frac{\mu_R - \mu_S}{\sqrt{\sigma_R^2 + \sigma_S^2}}$$

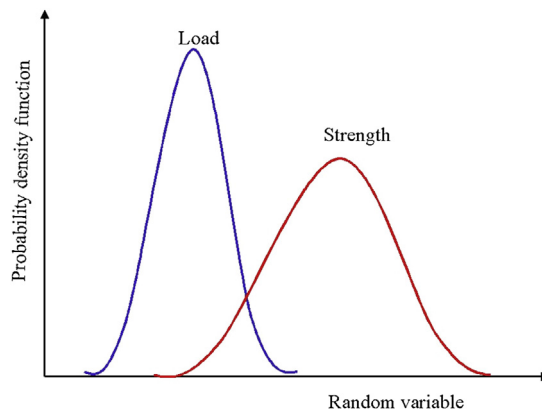


Figure 31.6
Load and strength probability density functions.

Substituting in the numerical values for μ_R , μ_S , σ_R , and σ_S ,

$$\beta = \frac{30,000 - 20,000}{\sqrt{2500^2 + 3000^2}} = 2.56$$

The corresponding failure probability is

$$P_f = 5.23 * E - 3$$

31.11.2 Example 31.2: β Safety Index Method

Problem:

Assuming the random variables R and S are corresponding to the bending moments of a ship hull girder with normal distributions. The mean value and standard deviations of R and S are $\mu_R = 150$, $\sigma_R = 20$, and $\mu_S = 90$ and $\sigma_S = 30$ respectively. What is the β index value and P_f using Hasofer–Lind method?

Solution:

The limit state function can be formed as

$$g(Z) = R - S$$

Based on Eqns (31.12) and (31.13), the random variables R and S can be expressed using variables in standard normal space:

$$R = 20 * U_1 + 150$$

$$S = 30 * U_2 + 90$$

Then, the limit state function can be re-formed as

$$G(Z) = 20U_1 - 30U_2 + 60$$

The distance of the straight line from the origin of coordinates can quickly be calculated as

$$\beta = \frac{60}{\sqrt{20^2 + (-30)^2}} = 1.664$$

Using the standard normal distribution table (Table 31.1), the probability of failure can be estimated as

$$P_f = \Phi(-\beta) = \Phi(-1.664) = 4.9\%$$

31.11.3 Example 31.3: Reliability Calculation of Series System

Problem:

Considering the simple structure shown in [Figure 31.7](#), and assuming the capacities of components 1 and 2 are $R_1 = 1.5R$ and $R_2 = R$ respectively, the acting load P and resistance R follow independent normal distributions with the following characteristics:

$$\begin{aligned}\mu_P &= 4 \text{ kN}, & \sigma_P &= 0.8 \text{ kN} \\ \mu_R &= 4 \text{ kN}, & \sigma_R &= 0.4 \text{ kN}\end{aligned}$$

What is the probability of failure for this system?

Solution:

The LSFs of components 1 and 2 can be formulated as

$$\begin{aligned}g_1(Z) &= \frac{3}{2}R - \frac{\sqrt{2}}{2}P \\ g_2(Z) &= R - \frac{\sqrt{2}}{2}P\end{aligned}$$

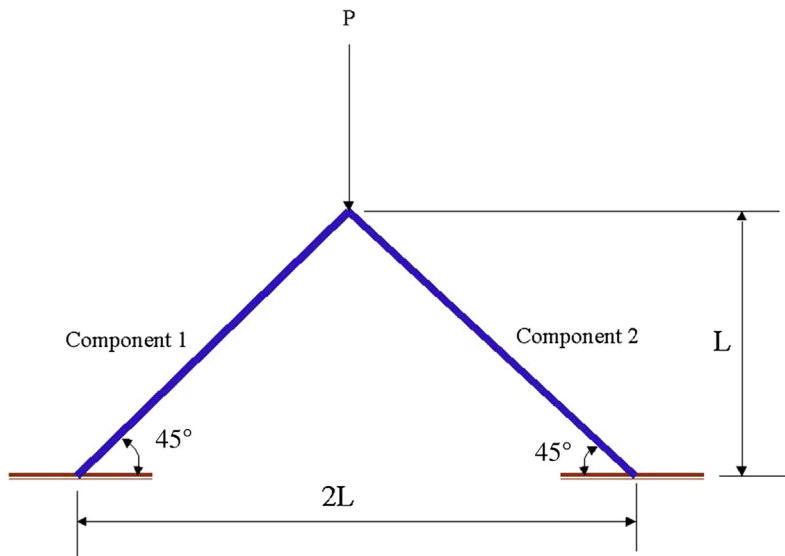


Figure 31.7
Reliability of series system.

To normalize the random variables in the above equations, the following need to be formed:

$$x_1 = \frac{R - 4}{0.4}$$

$$x_2 = \frac{P - 4}{0.8}$$

Based on the β index method described in [Section 31.3.3](#) and Example 31.2, the following can be obtained:

$$Z_1 = 0.728x_1 - 0.686x_2 + 3.846$$

$$Z_2 = 0.577x_1 - 0.816x_2 + 1.691$$

Accordingly, the reliability index of component one and two are estimated as

$$\beta_1 = 3.846$$

$$\beta_2 = 1.691$$

The corresponding probabilities of failure are obtained

$$P_{f,1} = \Phi(-\beta_1) = 0.00006$$

$$P_{f,2} = \Phi(-\beta_2) = 0.04794$$

The failure probability of the system is approximated by

$$\max P_{f,i} \leq P_{f,sys} \leq \sum P_{f,i}$$

Hence,

$$0.04794 \leq P_{f,sys} \leq 0.04800$$

Besides, the correlation coefficient of Z_1 and Z_2 is obtained as

$$\rho = \sum a_i b_i = 0.728 \times 0.577 + 0.686 \times 0.861 = 0.98$$

For this system, the correlation coefficient is nearly equal to 1. Accordingly, the failure probability of the system $P_{f,sys}$ is approximately equal to the lower bound,

$$P_{f,sys} = 0.04794$$

31.11.4 Example 31.4: Reliability Calculation of Parallel System

Problem:

Assume that a structure is composed of four parallel components, their corresponding reliability indexes are, $\beta_1 = 3.57$, $\beta_2 = 3.41$, $\beta_3 = 4.24$, and $\beta_4 = 5.48$ respectively. What are the bounds of the failure probability of the parallel system?

Solution:

The failure probability of each component can be estimated as

$$P_{f,1} = \Phi(-\beta_1) = 1.7849 \times 10^{-4}$$

$$P_{f,2} = \Phi(-\beta_2) = 3.2481 \times 10^{-4}$$

$$P_{f,3} = \Phi(-\beta_3) = 1.1176 \times 10^{-5}$$

$$P_{f,4} = \Phi(-\beta_4) = 2.1266 \times 10^{-8}$$

For a parallel system, the following bounds exist:

$$\prod P(Q_i) \leq P_{f,sys} \leq \min P(Q_i)$$

Hence, the simple bounds of this parallel system can be estimated as

$$1.3779 \times 10^{-20} \leq P_{f,sys} \leq 2.1266 \times 10^{-8}$$

and the corresponding bounds of the reliability index are obtained:

$$5.48 \leq \beta_{sys} \leq 9.23$$

It should be noted that in general the bound values given by the equation above for the parallel system are too wide.

References

- Ang, S.H., Cornell, C.A., 1974. Reliability bases of structural safety and design. *Journal of Structural Engineering*, ASCE 100 (9), 1755–1769.
- Ang, A.H.-S., Tang, W., 1975, 1984. *Probability Concepts in Engineering Planning and Design*, vols I & II. John Wiley and Sons, New York.
- Bai, Y., Xu, T., Bea, R., 1997. Reliability-Based Design and Requalification Criteria for Longitudinally Corroded Pipes. ISOPE-1997.
- Cornell, C.A., 1969. A probability-based structural code. *ACI-Journal* 66, 974–985.
- Ferry-Borges, J., Castanheta, M., 1971. *Structural Safety*. Laboratoria Nacional de Engenharia Civil, Lisbon.
- Hasofer, A.M., Lind, N.C., 1974. An exact and invariant first order reliability format. *ASCE Journal of Engineering Mechanics and Division* 111–121.
- Madsen, H.O., et al., 1986. *Methods of Structural Safety*. Prentice-Hall, Inc., Englewood Cliffs.
- Mansour, A.E., et al., 1997. Assessment of Reliability of Ship Structures. SSC-398. Ship Structures Committee.
- Melchers, R.E., 1999. *Structural Reliability Analysis and Prediction*, second ed. John Wiley & Sons Ltd.
- Moan, T., Song, R., 1998. Implication of inspection updating on system fatigue reliability of offshore structures. In: *The Proc. 17th OMAE*, Lisbon, Portugal, 1998.
- Schneider, J., 1997. Introduction to safety and reliability of structures. In: *Structural Engineering Documents*, vol. 5. International Association for Bridge and Structural Engineering (IABSE).
- Song, R., Moan, T., 1998. Fatigue reliability of large catamaran considering inspection updating. In: *Proceeding of the 8th International Offshore and Polar Engineering Conference (ISOPE'98)*, Montreal, Canada, May, 1998.
- Thoft-Christensen, P., Baker, M.J., 1982. *Structural Reliability, Theory and Its Applications*. Springer-Verlag.
- Turkstra, C.J., 1972. Theory of structural design decisions. Study No. 2. In: *Solid Mechanics Division*. University of Waterloo, Canada.

Structural Reliability Analysis Using Uncertainty Theory

32.1 Introduction

The theory of structural reliability is widely applied in many fields, such as architectural design, civil engineering, and mechanical engineering. In structural engineering, because of the required long-term security commitments that are subject to various loads, the analysis of the reliability is particularly important. The improvement of structural reliability theory was gradually strengthened and enhanced along with the continuous development of mathematical sciences, because a large number of mathematical tools were used in the study. For a long time, the concept of “reliability” has been used to evaluate the quality of engineering structures. However, due to the uncertainty of material properties and loads, and various types of errors in the structure’s construction and use from an engineering viewpoint, a structural problem can be considered “uncertain” when some lack of knowledge exists about the theoretical model that describes the structural system and its behavior, either with respect to the model itself or the value of its significant parameters. In the early twentieth century, probability theory and mathematical statistics were applied to structural reliability analysis and can be marked as period when the theory of structural reliability was created.

[Freudenthal \(1947\)](#) was among the first in the world to develop a theory of structural reliability; that is, the application of probabilistic methods to evaluate the safety of structures that are made of various materials. From the early 1940s to the 1960s, structural reliability theory advanced greatly. Although applying the probability theory to the research of structural reliability theory was fruitful, there is still an obstacle for researching and putting it into practice, because stochastic analysis requires much statistical data, but data in real life are sometimes difficult to obtain. Therefore, after [Zadeh \(1965\)](#) proposed fuzzy set theory in 1965, many scholars began to apply fuzzy theory to structural reliability analysis. Early study in this area is [Brown \(1979\)](#). In recent years, [Fabio et al. \(2004\)](#) also had analyzed the reliability of concrete structures under fuzzy theory; [Adduri and Penmetsa \(2009\)](#) studied structural reliability problems in environments where there are both fuzzy and random variables; [Marano and Quaranta \(2010\)](#) proposed a new reliability index under the possibility theory. A number of other scholars studied this issue from different perspectives ([Yao, 2001](#); [Kala, 2007](#);

Marano et al., 2008; Silva et al., 2008; Chandrashekhar and Ganguli, 2009; Graf et al., 2009; Ramezani-pour et al., 2009).

However, fuzzy theory fails to explain many subjective uncertain phenomena, such that computational results often are not consistent with real conditions. Hence in 2007, based on normality, monotonicity, and countable subadditivity, Liu (2007) proposed uncertainty theory, which is a powerful tool for interpreting subject uncertainty. In 2010, Liu (2010b) proposed uncertain reliability and uncertain risk. Zhuo Wang (2010) had studied the problems of structural reliability within the framework of uncertainty theory.

32.2 Preliminaries

Uncertainty theory based on normality, monotonicity, and countable subadditivity was founded in 2007 by Liu (2007) and refined in 2010 by Liu (2010a). In this section, some basic concepts about uncertainty theory such as uncertain measure, uncertain variable, uncertainty distribution, and uncertain reliability are given.

32.2.1 Uncertainty Theory

Definition 2.1 (Liu, 2007). Let Γ be a nonempty set. A collection \mathbf{L} of subsets of Γ is a σ -algebra. Each element Λ in the σ -algebra \mathbf{L} is called an event. If function \mathbf{M} on \mathbf{L} subjected to

1. $\mathbf{M}\{\Gamma\} = 1$
2. $\Lambda_1 \subset \Gamma_2$ whenever $\mathbf{M}\{\Gamma_1\} \leq \mathbf{M}\{\Gamma_2\}$
3. $\mathbf{M}\{\Lambda\} + \mathbf{M}\{\Lambda^C\} = 1$ for each event Λ
4. For every countable sequence of events $\{\Lambda_i\}$, we have

$$\mathbf{M}\left\{\bigcup_{i=1}^{\infty} \Lambda_i\right\} \leq \sum_{i=1}^{\infty} \mathbf{M}\{\Lambda_i\}$$

then \mathbf{M} is an uncertain measure, $(\Gamma, \mathbf{L}, \mathbf{M})$ is an uncertainty space.

In order to describe the uncertain phenomenon, Liu (2007) gave the definition of uncertain variables.

Definition 2.2 (Liu, 2007). An uncertain variable is a measurable function from an uncertainty space $(\Gamma, \mathbf{L}, \mathbf{M})$ to the set of real numbers—that is, for any Borel set B of real numbers, the set of real numbers, the set

$$\xi^{-1}(B) = \{\gamma \in \Gamma | \xi(\gamma) \in B\} \quad (32.1)$$

is an event.

Definition 2.3 (Liu, 2009). The uncertain variables $(\xi_1, \xi_2, \dots, \xi_m)$ are said to be independent if

$$M\left\{\bigcup_{i=1}^m \{\xi_i \in B_i\}\right\} = \min_{1 \leq i \leq m} M\{\xi_i \in B_i\} \quad (32.2)$$

for any Borel sets B_1, B_2, \dots, B_m of real numbers.

Since we have the definition of uncertain variables and uncertain measures, we must consider the product measure and uncertain arithmetic. In 2009, Liu (2009) proposed the product measure axiom.

Axiom 2.1 (Liu, 2009). Let Γ_k be nonempty sets on which M_k are uncertain measures, and $k = 1, 2, \dots, k$, respectively. Then the product uncertainty measure M is an uncertain measure on the product σ -algebra $L_1 \times L_2 \times \dots \times L_n$ satisfying

$$M\left\{\bigcup_{i=1}^{\infty} \Lambda_k\right\} = \min_{1 \leq k \leq n} M_k\{\Lambda_k\}$$

That is, for each event $\Lambda \in L$, we have.

In order to characterize uncertain variables, in 2007, Liu (2007) proposed the concept of uncertainty distribution. Then, in 2009, a sufficient and necessary condition for uncertainty distribution was proposed by Peng and Iwamura (unpublished).

Definition 2.4 (Liu, 2007). The uncertainty distribution Φ of an uncertain variable ξ is defined by

$$\Phi(x) = M\{\xi \leq x\}$$

for any real number x .

Theorem 2.1 (Peng and Iwamura, unpublished). A function $\Phi: R \rightarrow [0, 1]$ is an uncertainty distribution if and only if it is an increasing function, except $\Phi \equiv 0$ and $\Phi \equiv 1$.

Theorem 2.2 (Liu, 2010a). Let Φ_i be the uncertainty distributions of uncertain variables ξ_i , $i = 1, 2, \dots, m$, respectively, and Φ the joint uncertainty distribution of uncertain vector $(\xi_1, \xi_2, \dots, \xi_m)$. If $(\xi_1, \xi_2, \dots, \xi_m)$ are independent, then we have

$$\Phi(x_1, x_2, \dots, x_m) = \min_{1 \leq i \leq m} \Phi_i(x_i)$$

for any real numbers x_1, x_2, \dots, x_m .

Theorem 2.3 (Liu, 2010a). Let $(\xi_1, \xi_2, \dots, \xi_m)$ be independent uncertain variables with uncertainty distributions $\Phi_1, \Phi_2, \dots, \Phi_m$, respectively. If $f: R^n \rightarrow R$ is a strictly increasing function, then

$$\xi = f(\xi_1, \xi_2, \dots, \xi_n) \quad (32.3)$$

is an uncertain variable whose inverse uncertainty distribution is

$$\Psi^{-1}(\alpha) = f(\Phi_1^{-1}(\alpha), \Phi_2^{-1}(\alpha), \dots, \Phi_n^{-1}(\alpha)), 0 < \alpha < 1.$$

Theorem 2.4 (Liu, 2010a). Let $\xi_1, \xi_2, \dots, \xi_n$ be independent uncertain variables with uncertainty distributions $\Phi_1, \Phi_2, \dots, \Phi_n$, respectively. If $f: R^n \rightarrow R$ is a strictly decreasing function, then

$$\xi = f(\xi_1, \xi_2, \dots, \xi_n)$$

is an uncertain variable with inverse uncertainty distribution

$$\Psi^{-1}(\alpha) = f(\Phi_1^{-1}(1 - \alpha), \Phi_2^{-1}(1 - \alpha), \dots, \Phi_n^{-1}(1 - \alpha)), 0 < \alpha < 1.$$

Theorem 2.5 (Liu, 2010a). Let $\xi_1, \xi_2, \dots, \xi_n$ be independent uncertain variables with uncertainty distributions $\Phi_1, \Phi_2, \dots, \Phi_n$, respectively. If the function $f(x_1, x_2, \dots, x_n)$ is strictly increasing with respect to x_1, x_2, \dots, x_m and strictly decreasing with respect to $x_{m+1}, x_{m+2}, \dots, x_n$, then

$$\xi = f(\xi_1, \dots, \xi_m, \xi_{m+1}, \dots, \xi_n)$$

is an uncertain variable with inverse uncertainty distribution

$$\Psi^{-1}(\alpha) = f(\Phi_1^{-1}(\alpha), \dots, \Phi_m^{-1}(\alpha), \Phi_{m+1}^{-1}(1 - \alpha), \dots, \Phi_n^{-1}(1 - \alpha)).$$

32.2.2 Uncertain Reliability

In 2010, Liu (2010b) proposed uncertain reliability analysis as a tool to deal with system reliability via uncertainty theory. Reliability index is defined as the uncertain measure that the system is working.

Definition 2.5 (Liu, 2010b). Assume a system contains uncertain variables $\xi_1, \xi_2, \dots, \xi_n$, and is working if and only if $R(\xi_1, \xi_2, \dots, \xi_n) \geq 0$. Then the reliability index is

$$\text{Reliability} = M\{R(\xi_1, \xi_2, \dots, \xi_n) \geq 0\} \quad (32.4)$$

Theorem 2.6 (Liu, 2010b). Assume $\xi_1, \xi_2, \dots, \xi_n$ are independent uncertain variables with uncertainty distributions $\Phi_1, \Phi_2, \dots, \Phi_n$, respectively, and R is a strictly increasing function. If some system is working if and only if $R(\xi_1, \xi_2, \dots, \xi_n) \geq 0$, then the reliability index is

$$\text{Reliability} = \alpha \quad (32.5)$$

where α is the root

$$R(\Phi_1^{-1}(1 - \alpha), \Phi_2^{-1}(1 - \alpha), \dots, \Phi_n^{-1}(1 - \alpha)) = 0 \quad (32.6)$$

Theorem 2.7 (Liu, 2010b). Assume $\xi_1, \xi_2, \dots, \xi_n$ are independent uncertain variables with uncertainty distributions $\Phi_1, \Phi_2, \dots, \Phi_n$, respectively, and R is a strictly decreasing function. If some system is working if and only if $R(\xi_1, \xi_2, \dots, \xi_n) \geq 0$, then the reliability index is

$$\text{Reliability} = \alpha \tag{32.7}$$

where α is the root of

$$R(\Phi_1^{-1}(\alpha), \Phi_2^{-1}(\alpha), \dots, \Phi_n^{-1}(\alpha)) = 0 \tag{32.8}$$

Theorem 2.8 (Liu, 2010b). Assume $\xi_1, \xi_2, \dots, \xi_n$ are independent uncertain variables with uncertainty distributions $\Phi_1, \Phi_2, \dots, \Phi_n$, respectively, and the function $R(x_1, x_2, \dots, x_n)$ is strictly increasing with respect to x_1, x_2, \dots, x_n and strictly decreasing with respect to $x_{m+1}, x_{m+2}, \dots, x_n$. If some system is working if and only if $R(\xi_1, \xi_2, \dots, \xi_n) \geq 0$, then the reliability index is

$$\text{Reliability} = \alpha \tag{32.9}$$

where α is the root of

$$R(\Phi_1^{-1}(1 - \alpha), \Phi_m^{-1}(1 - \alpha), \Phi_{m+1}^{-1}(\alpha), \dots, \Phi_n^{-1}(\alpha)) = 0 \tag{32.10}$$

32.3 Structural Reliability

The structural reliability index is defined as the uncertain measure that the resistance is larger than the load. According to the meaning of structural reliability index, it is determined by the resistance and the load. For each rod, if it fails, then we say the structure fails. Now, some theorems of basic structural reliability index are given below (Miao, 2013).

Assume a structure contains uncertain variables $\xi_1, \xi_2, \dots, \xi_n$, and is working if and only if $R(\xi_1, \xi_2, \dots, \xi_n) \geq 0$ where R is the functional function of the structure, where $\xi_1, \xi_2, \dots, \xi_n$ are basic variables of the structure, which can be different load effects, the material parameter, the geometric parameter, etc.

Theorem 3.1. The structure is shown in Figure 32.1. The gravity of the object is an uncertain variable, and its distribution is Ψ . The resistances of each rods are $\beta_1, \beta_2, \dots, \beta_n$, and the distributions of them are $\Phi_1, \Phi_2, \dots, \Phi_n$, respectively. The resistance of the structure is ν . Then the reliability index is

$$\alpha = \alpha_1 \wedge \alpha_2 \wedge \dots \wedge \alpha_n$$

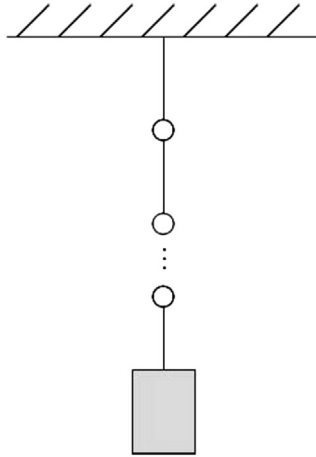


Figure 32.1
Series system.

where $\alpha_1, \alpha_2, \dots, \alpha_n$ are the roots of the equations

$$\begin{aligned}\Phi_1^{-1}(\alpha_1) &= \Psi^{-1}(1 - \alpha_1) \\ \Phi_2^{-1}(\alpha_2) &= \Psi^{-1}(1 - \alpha_2) \\ &\vdots \\ \Phi_n^{-1}(\alpha_n) &= \Psi^{-1}(1 - \alpha_n)\end{aligned}$$

Proof. The resistance of the structure β is $\beta_1 \wedge \beta_2 \wedge \dots \wedge \beta_n$, and the load of each rod is ν . So the functional function of this structure can be expressed as

$$R(\beta_1, \beta_2, \dots, \beta_n, \nu) = \beta_1 \wedge \beta_2 \wedge \dots \wedge \beta_n - \nu$$

If and only if $R \geq 0$, it works. Then the reliability index α is the root of

$$\Phi_1^{-1}(1 - \alpha) \wedge \Phi_2^{-1}(1 - \alpha) \wedge \dots \wedge \Phi_n^{-1}(1 - \alpha) = \Psi^{-1}(\alpha)$$

Let α_i be the roots of $\Phi_i^{-1}(1 - \alpha_i) = \Psi^{-1}(\alpha_i)$, for $i = 1, 2, \dots, n$, respectively. Then the reliability index of the structure must be the reliability index of one of the rods.

It means that there exists i , $1 \leq i \leq n$, subject to $\alpha = \alpha_i$, and we have $\Phi_i^{-1}(1 - \alpha) = \Psi^{-1}(\alpha)$. According to the property of the distribution functions, Φ^{-1} and Ψ^{-1} are all increasing functions. The reliability index α is the minimum of the liability index of each rod, that is $\alpha = \alpha_1 \wedge \alpha_2 \wedge \dots \wedge \alpha_n$.

Apparently, it is not enough to do analysis just using the series theorem above. We have to meet another type of structure, the parallel structure. The parallel structure is different from other parallel system. It may be applied more in the analysis of existing structures and other fields.

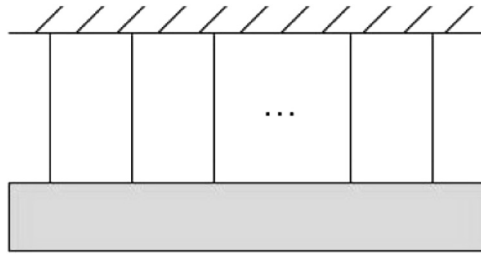


Figure 32.2
Parallel system.

Theorem 3.2. The structure is shown in Figure 32.2. And the whole rods can work under plastic stage. The gravity of the object is an uncertain variable ν , and its distribution is Ψ . The resistances of the rods are $\beta_1, \beta_2, \dots, \beta_n$, and the distributions of them are $\Psi_1, \Psi_2, \dots, \Psi_n$ respectively. The resistance of the structure is β . The reliability index α of the system is the root of the equation

$$\sum_{i=1}^n \Phi_i^{-1}(\alpha) - \Psi^{-1}(1 - \alpha) = 0$$

Proof. The material of the rods being under plastic stage means the strain and the stress are no longer linear. It leads to the stress distribution of each rod being not available by stress analysis, neither is the reliability of each rod. While one rod has been reaching the limit load, the strain of the rod will keep increasing without stress increasing. Hence the limit state of such structure means that all the rods reach the limit state together. Since the resistances of rods are $\beta_1, \beta_2, \dots, \beta_n$, the total resistance force of the system is $\beta_1 + \beta_2 + \dots + \beta_n$. It can be inferred that the function $R(\beta_1, \beta_2, \dots, \beta_n, \nu)$ of this system is

$$R = \sum_{i=1}^n \beta_i - \nu < 0$$

The system works if and only if $R \leq 0$. The reliability index α of the system can be expressed as the root of the equation

$$\sum_{i=1}^n \Phi_i^{-1}(\alpha) - \Psi^{-1}(1 - \alpha) = 0$$

32.4 Numerical Examples

The structural design is based on the limit state of the structure. The so-called structure limit state is defined as follows: If the entire structure or part of it is over a particular

state, and the structure does not meet the requirement of the design rules of a particular function, then this particular state is called the limit state (Freudenthal, 1947). In structural design, consideration should be given to all the corresponding limit state, to ensure that the structure has enough safety, durability, and suitability.

For a certain structural system, certain structural mechanics tools are enough to analyze the stress state of the structure. But in fact, even in the case of certain structural styles, the stress of the structure or the resistance is not as imagined to be a certain amount. Uncertainty needs to be taken into account and evaluated.

Example 4.1. The structure is shown in Figure 32.3. All the joints are articulated. The side length of the square grid is 5 m and the height is 2.5 m. The stiffness of each rod $EA = 10^5$ kN. The external force of the system is uncertain force ν just vertically downward, and its distribution is Φ . The resistances of rods are $\beta_1, \beta_2, \dots, \beta_9$, and their distributions are $\Psi_1, \Psi_2, \dots, \Psi_n$, respectively. The resistance of the structure is β . In order to discuss conveniently, the distributions Ψ are assumed to be linear uncertainty distributions $L(a_i, b_i), i = 1, 2, \dots, 9$; and Φ is a linear uncertainty distribution $L(a_0, b_0)$ (Table 32.1).

Such a style of structure is widely used in grid structures and reticulated shell structures as a single element.

Setup of the internal force of the lever i suffered for T_i is inferred within structural mechanics as

$$\begin{cases} T_1 = T_2 = T_3 = T_4 = -0.3537\nu, \\ T_5 = T_6 = T_7 = T_8 = 0.433\nu, \\ T_9 = \nu \end{cases}$$

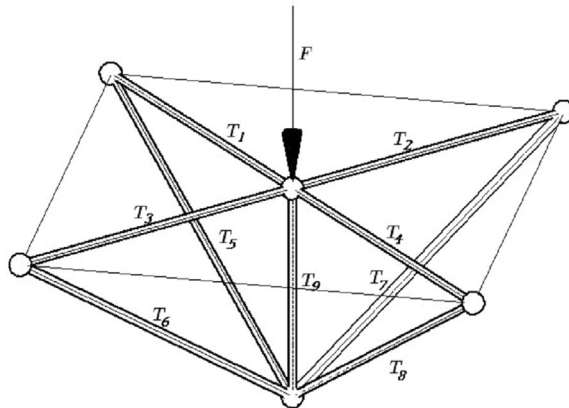


Figure 32.3

A typical element in a space structure.

Table 32.1: Data of Example 4.1

i	a_i	b_i
0	2	7
1, 2, 3, 4	2	5
5, 6, 7, 8	2	6
9	6	9

It can be expressed as $T_i = t_i \cdot \nu, i = 1, 2, \dots, 9$. The failure mode of each rod is $\beta_i - T_i \leq 0$, and the reliability of each rod is the root of the equation

$$\Psi_i^{-1}(1 - \alpha) = t_i \cdot \Phi^{-1}(\alpha_i)$$

According to Theorem 3.1, we have

$$\alpha = \alpha_1 \wedge \alpha_2 \wedge \dots \wedge \alpha_9$$

Then according to the calculated rules of linear distribution,

$$\begin{aligned} \alpha_1 &= \alpha_2 = \alpha_3 = \alpha_4 \\ &= 0 \vee \frac{b_1 - 0.354a_0}{(b_1 - a_1) + 0.354(b_0 - a_0)} \wedge 1 \\ &= 0.900, \\ \alpha_5 &= \alpha_6 = \alpha_7 = \alpha_8 \\ &= 0 \vee \frac{b_6 - 0.433a_0}{(b_6 - a_6) + 0.433(b_0 - a_0)} \wedge 1 \\ &= 0.833, \\ \alpha_9 &= 0 \vee \frac{b_9 - a_0}{(b_9 - a_9) + (b_0 - a_0)} \wedge 1 \\ &= 0.875 \end{aligned}$$

So, the reliability index of the structure in Figure 32.1 is

$$\alpha = \alpha_1 \wedge \alpha_2 \wedge \dots \wedge \alpha_9 = 0.833$$

Example 4.2. The structure is shown in Figure 32.4. Joints 1, 3, and 5 are articulated, and Joint 7 is fixed. The length of each rod is shown in the figure, and $l = 2$ m. The external force q is uncertain force ν just vertical downward, and its distribution is Φ . The bending moments of joints are M_1, M_2, \dots, M_7 . Since Joint 1 is free to rotate, $M_1 = 0$. The other distributions of the limit resistances are $\Psi_2, \Psi_3, \dots, \Psi_7$, respectively. In order to discuss conveniently, the distributions $\Psi_i (i = 2, 3, \dots, 7)$ are assumed to be linear uncertainty distributions $L(a_i, b_i), i = 2, 3, \dots, 7$; and Φ is linear uncertainty distribution $L(a_0, b_0)$ (Table 32.2).

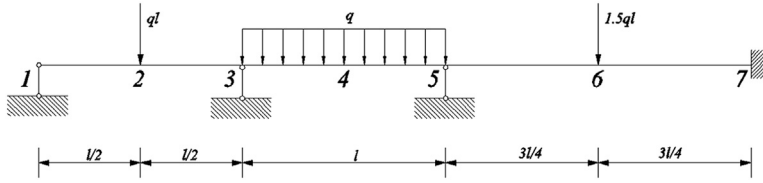


Figure 32.4
A continuous beam.

Table 32.2: Data of example 4.2

i	a_i	b_i
0	0	1
2, 3	0.5	1
4, 5	0	1
6, 7	1	2

Based on structural mechanics, it is inferred that the continuous beam under loads of the same direction can only be damaged independently in each span, instead of being damaged compositely. Hence this continuous beam has only three different limit states in each span. This example shows how the combination of series and parallel systems works. In each span, the limit state works as a parallel system, and also as a series system as a whole.

In the first span, according to the virtual work principle, we have

$$ql\Delta = M_3 \frac{\Delta}{0.5l} + 2M_2 \frac{\Delta}{0.5l}$$

Then

$$R_1 = 2M_3 + 4M_2 - ql^2 \geq 0$$

In a similar way, in the second and third spans,

$$R_2 = 4M_3 + 8M_2 + 2M_5 - ql^2 \geq 0$$

$$R_3 = \frac{8}{9}M_5 + \frac{16}{9}M_6 + \frac{8}{9}M_7 - ql^2 \geq 0$$

Then according to Theorems 3.1 and 3.2, the reliability of the span is $\alpha = \alpha_1 \wedge \alpha_2 \wedge \alpha_3$, where $\alpha_1, \alpha_2, \alpha_3$ are the roots of the equation,

$$\begin{aligned} 4\Psi_2^{-1}(1 - \alpha_1) + 2\Psi_3^{-1}(1 - \alpha_1) - \Phi^{-1}(\alpha_1) &= 0 \\ 4\Psi_3^{-1}(1 - \alpha_2) + 8\Psi_4^{-1}(1 - \alpha_2) + 2\Psi_5^{-1}(1 - \alpha_2) - \Phi^{-1}(\alpha_2) &= 0 \\ \frac{8}{9}\Psi_5^{-1}(1 - \alpha_3) + \frac{16}{9}\Psi_6^{-1}(1 - \alpha_3) + \frac{8}{9}\Psi_7^{-1}(1 - \alpha_3) - \Phi^{-1}(\alpha_3) &= 0 \end{aligned}$$

respectively. According to the operation law of uncertain variables, we have

$$\alpha_1 = \frac{6b_2 - 4a_0}{6(b_2 - a_2) + 4(b_0 - a_0)} = 0.8571$$

$$\alpha_2 = \frac{4b_3 + 8b_4 + 4b_5 - 4a_0}{4(b_3 - a_3) + 8(b_4 - a_4) + 4(b_5 - a_5) + 4(b_0 - a_0)} = 0.8889$$

Similarly, $\alpha_3 = 0.8235$.

So, the reliability of the structure in [Figure 32.4](#) is

$$\alpha = \alpha_1 \wedge \alpha_2 \wedge \alpha_3 = 0.8235$$

Then it is easily concluded that the third span is the most dangerous span.

32.5 Conclusions

The theory of structural reliability is widely applied in many fields, such as architectural design and mechanical engineering. In this chapter, the resident and load of a structure are defined as uncertain variables, and the reliability index is defined as the uncertain measure of the event that the resident is larger than the load.

References

- Adduri, P.R., Penmetsa, R.C., 2009. System reliability analysis for mixed uncertain variables. *Structural Safety* 31, 375C382.
- Brown, C., 1979. Fuzzy safety measure. *Journal of the Engineering Mechanics Division-ASCE* 105, 855–872.
- Chandrashekhar, M., Ganguli, R., 2009. Uncertainty handling in structural damage detection using fuzzy logic and probabilistic simulation. *Mechanical Systems and Signal Processing* 23, 384C404.
- Freudenthal, A., 1947. Safety of structures. *Transactions ASCE* 112, 125–180.
- Fabio, B., Franco, B., Pier, G., 2004. Fuzzy reliability analysis of concrete structures. *Computers & Structures* 82, 1033–1052.
- Graf, W., Jenkel, C., Pannier, S., Sickert, J.U., Steinigen, F., 2009. Numerical structural monitoring with the uncertainty model fuzzy randomness. *International Journal of Reliability and Safety* 3 (1–3), 218–234.
- Kala, Z., 2007. Fuzzy probabilistic analysis of steel structure focused on reliability design concept of eurocodes. *Nonlinear Analysis Modelling and Control* 12 (3), 371–382.
- Liu, B., 2007. *Uncertainty Theory*, second ed. Springer-Verlag, Berlin.
- Liu, B., 2009. Some research problems in uncertainty theory. *Journal of Uncertain Systems* 3 (1.), 3–10.
- Liu, B., 2010a. *Uncertainty Theory: A Branch of Mathematics for Modeling Human Uncertainty*. Springer-Verlag, Berlin.
- Liu, B., 2010b. Uncertain risk analysis and uncertain reliability analysis. *Journal of Uncertain Systems* 4 (3), 163–170.
- Marano, G., Quaranta, G., 2010. A new possibilistic reliability index definition. *Acta Mechanica* 210, 291–303.
- Marano, G.C., Quaranta, G., Mezzina, M., 2008. Fuzzy time-dependent reliability analysis of RC beams subject to pitting corrosion. *Journal of Materials in Civil Engineering* 20 (9), 578–587.
- Miao, Yi, August 3–9, 2013. Uncertain structural reliability analysis. In: *Proceedings of the Twelfth International Conference on Information and Management Sciences*, Kunming, China, pp. 230–234.
- Peng, Z., Iwamura, K.A. Sufficient and necessary condition of uncertainty distribution. *Journal of Interdisciplinary Mathematics*, unpublished.

- Ramezaniapour, A., Shahhosseini, V., Moodi, F., 2009. A fuzzy expert system for diagnosis assessment of reinforced concrete bridge decks. *Computers and Concrete* 6 (4), 281–303.
- Silva, Samuel da, Dias Junior, Milton, et al., 2008. Structural damage detection by fuzzy clustering. *Mechanical Systems and Signal Processing* 22, 1636C1649.
- Wang, Zhuo, August 11–19, 2010. Structural reliability analysis using uncertainty theory. In: *Proceedings of the First International Conference on Uncertainty Theory*, Urumchi, China, pp. 166–170.
- Yao, Kawamura, 2001. On structural reliability. *Journal of Temporal Design in Architecture and the Environment* 1, 1–4.
- Zadeh, L., 1965. Fuzzy set. *Information and Control* 8, 338–353.

Random Variables and Uncertainty Analysis

33.1 Introduction

Strictly speaking, all variables in engineering structures are stochastic to a certain degree. Structural reliability analysis deals with the rational treatment of random variables and uncertainties within structural engineering designs, inspections, maintenance, and decision-making.

This chapter presents the basic statistical descriptions of random variables that are the foundation for reliability analysis. Measures of uncertainties are discussed; loads and capacity of ship structures are used to illustrate the uncertainty analysis. For further reading, reference is made to [Ang and Tang \(1975\)](#), [Benjamin and Cornell \(1970\)](#), [Thoft-Christensen and Baker \(1982\)](#), [Mansour \(1997\)](#), and [Melchers \(1999\)](#).

33.2 Random Variables

33.2.1 General

Marine structures are subjected to random loads such as wave currents and wind actions. It is not possible to exactly determine, for example, the height and direction of the next single wave that will act on a structure. Neither is it possible to deterministically predict the structural responses to those actions.

Random variables may be used to describe uncertainties in the basic variables of spatial and time variation of external loads, material properties, dimensions, etc. In practice, these variables are basic in the sense that they are the most fundamental quantities used by engineers and analysts in structural analysis and design. For instance, the yield stress of steel can be considered as a basic random variable for the purpose of structural reliability analysis. It should be mentioned that it is generally impractical to obtain sufficient statistical data to model the variations in the loads and strength for structures. Reliance must be placed on the ability of the analyst to synthesize this high-level information whenever required.

33.2.2 Statistical Descriptions

A random variable X is a real function defined on a sample space. For every real number x there exists a probability $P[X \leq x]$. A realization x of the random variable X is any outcome of the random phenomenon X . In this section, random variables are denoted by capital letters and the corresponding small letters denote their realizations.

A random variable is characterized by its probability density function $p(x)$ and its cumulative distribution function $F_X(x) = P[X \leq x]$. The random variable is often described by its statistical description, namely the mean (or expected) value and variance (or standard deviation), which are defined as

The n th moment

$$\mu_n = E[X^n], \quad n = 1, 2, 3, \dots \quad (33.1)$$

The n th central moment

$$\varsigma_n = E[(X - \mu_1)^n] \quad (33.2)$$

where

$\mu_1 = \text{mean (or expected) value of } X$

$\varsigma_2 = \text{Var}[X] = \text{variance of } X$

$\sigma_X = \sqrt{\varsigma_2} = \text{standard deviation of } X$

The mean value is the center of gravity of the probability density function. The standard deviation is the measure of the dispersion around the mean value. The coefficient of variation (CoV) is an uncertainty measure for the random variable X .

The following nondimensional values of the central moments are defined as

Coefficient of variance

$$\text{CoV} = \frac{\sqrt{\varsigma_2}}{\mu_1} \quad (33.3)$$

Skewness

$$\gamma_1 = \frac{\varsigma_3}{\varsigma_2^{3/2}} \quad (33.4)$$

Kurtosis

$$\gamma_2 = \frac{\varsigma_4}{\varsigma_2^2} \quad (33.5)$$

33.2.3 Probabilistic Distributions

A random variable may be described by its cumulative distribution function. Some distribution models are of special interest in stochastic and reliability analysis of marine structures. These models include the normal distribution, the lognormal distribution, the Rayleigh distribution, and the Weibull distribution, which are detailed below. Melchers (1999) also defined other types of distribution functions such as Poisson, gamma, Beta and extreme value distribution type I, II, III.

Normal (or Gaussian) Distribution

The probability density function and its cumulative distribution function for the normal distribution are defined by

$$p(x) = \frac{1}{\sqrt{2\pi}\sigma_X} \exp\left[-\frac{1}{2}\left(\frac{x - \mu_X}{\sigma_X}\right)^2\right] \quad \text{for } -\infty \leq x \leq \infty \quad (33.6)$$

$$F_X(x) = \frac{1}{\sqrt{2\pi} \int_{-\infty}^s \exp\left(-\frac{1}{2}v^2\right) dv} \quad \text{for } -\infty \leq x \leq \infty \quad (33.7)$$

where $s = (x - \mu_X)/\sigma_X$. When $\mu_X = 0$, $\sigma_X = 1$, and the normal distribution is called the standard normal distribution.

Lognormal Distribution

The probability density function and its cumulative distribution function for the lognormal distribution are defined by

$$p(x) = \frac{1}{\sqrt{2\pi x} \sigma_{\ln X}} \exp\left[-\frac{1}{2}\left(\frac{\ln(x) - \mu_{\ln X}}{\sigma_{\ln X}}\right)^2\right] \quad \text{for } x \geq 0 \quad (33.8)$$

$$F_X(x) = \Phi\left(\frac{\ln(x) - \mu_{\ln X}}{\sigma_{\ln X}}\right) \quad \text{for } x \geq 0 \quad (33.9)$$

where the mean value and standard deviation are given by

$$\mu_X = \exp\left(\mu_{\ln X} + \frac{\sigma_{\ln X}^2}{2}\right) \quad (33.10)$$

$$\sigma_X = \sqrt{\mu_X^2 [\exp(\sigma_{\ln X}^2) - 1]} \quad (33.11)$$

Rayleigh Distribution

The Rayleigh distribution is defined by

$$p(x) = \frac{(x-u)}{\alpha^2} \exp \left[-\frac{1}{2} \left(\frac{x-u}{\alpha} \right)^2 \right] \quad \text{for } x \geq u \quad (33.12)$$

$$F_X(x) = 1 - \exp \left[-\frac{1}{2} \left(\frac{x-u}{\alpha} \right)^2 \right] \quad \text{for } x \geq u \quad (33.13)$$

where

u = location parameter

α = scale parameter

The mean value and standard deviation are given by

$$\mu_X = u + \alpha \sqrt{\frac{\pi}{2}} \quad (33.14)$$

$$\sigma_X = \alpha \sqrt{\frac{4-\pi}{2}} \quad (33.15)$$

Weibull Distribution

The Weibull distribution is defined by

$$p(x) = \frac{(x-u)^{\lambda-1}}{\alpha^\lambda} \lambda \exp \left[-\left(\frac{x-u}{\alpha} \right)^\lambda \right] \quad \text{for } x \geq u \quad (33.16)$$

$$F_X(x) = 1 - \exp \left[-\left(\frac{x-u}{\alpha} \right)^\lambda \right] \quad \text{for } x \geq u \quad (33.17)$$

where

u = location parameter

α = scale parameter

λ = shape parameter

The mean value and standard deviation for the Weibull distribution are defined by

$$\mu_X = u + \alpha \Gamma \left(1 + \frac{1}{\lambda} \right) \quad (33.18)$$

$$\sigma_X = \alpha \sqrt{\Gamma \left(1 + \frac{2}{\lambda} \right) - \Gamma^2 \left(1 + \frac{1}{\lambda} \right)} \quad (33.19)$$

33.3 Uncertainty Analysis

33.3.1 Uncertainty Classification

For the purpose of reliability analysis, the uncertainties can be classified as:

- Inherent uncertainty
- Measurement uncertainty
- Statistical uncertainty
- Model uncertainty

Inherent Uncertainty

Inherent uncertainty is also known as fundamental or physical uncertainty. It is a natural randomness of a quantity, such as the variability in wind and wave loadings. The uncertainty source cannot be reduced by more information. These uncertainties are the result of natural variability, which is inherent in physical wave, wind, or human-made processes. For instance, the variability of wave height for a sea state with a given significant wave height and period is fundamentally random. Also, the occurrence of sea states, characterized by H_s and T_s , is fundamentally random. Examples of human-made phenomena that are fundamentally random are functional loads on structures and structural resistance. Contrary to natural processes, human-made processes are influenced by human intervention, the QA/QC of human activities, and the fabricated structure itself.

Measurement Uncertainty

Measurement uncertainty is caused by imperfect instruments and sample disturbances, during any observation made using equipment. This uncertainty source can be reduced by more information.

Statistical Uncertainty

Statistical uncertainty is due to limited information such as a limited number of observations of certain quantities; obtaining more information can reduce this uncertainty.

The statistical uncertainty associated with limited data is represented by applied statistical methods. Data can be collected for the selection of an appropriate probability distribution type, and determination of numerical values for its parameters. In practice, very large samples are required in order to select the distribution type and to reliably estimate the numerical values for its parameters. Therefore, for a given set of data, the distribution parameters can themselves be considered random variables whose uncertainties are dependent on the amount of sample data and any prior knowledge.

Model Uncertainty

Model uncertainty is uncertainty due to imperfections and idealizations made in physical model formulations for load and resistance, as well as in the choices of probability distribution types for the representation of uncertainties.

With very few exceptions, it is often not possible to make highly accurate predictions about the magnitude of the typical structure responses due to loadings, even when governing input quantities are known. In other words, the structural response contains a component of uncertainty, in addition to those arising from uncertainties from the basic loading and strength variables. This additional source of uncertainty is termed model uncertainty, and occurs as a result of simplifying assumptions, unknown boundary conditions, and the unknown effects and interactions of other variables that are not included.

Model uncertainties can be assessed by comparing them with other more refined methods, or with test results and in-service experiences. Assuming that the true value X_{true} is observed in service or in a laboratory test and the predicted value is X_{pred} , the model uncertainty B is then defined by

$$B = \frac{X_{\text{true}}}{X_{\text{pred}}} \quad (33.20)$$

By making many observations and corresponding predictions, B can be characterized probabilistically. A mean value, not equal to 1.0, expresses bias in the model. The standard deviation expresses the variability of predictions by the model. In many cases, model uncertainties have large effects on structural reliability and should not be neglected.

33.3.2 Uncertainty Modeling

Variables whose uncertainties are considered important—for example, by experience or by sensitivity studies—can be represented as random variables. The corresponding probability distributions can be defined based on the statistical analysis of available observations of the individual variables. This provides information on their mean values, standard deviations, correlation with other variables, and in some cases distribution types, as presented in [Section 33.2](#) of this chapter. In some cases, correlation between variables exists—for example, between the two parameters used to describe the Weibull long-term stress distribution.

33.4 Selection of Distribution Functions

The probability distribution function for a random variable is most conveniently given in terms of a standard distribution type with some distribution parameters. Regressions, of the available observations of certain quantities will not always provide enough information to

allow for an interpretation of the distribution type for the uncertain quantity; a choice of the distribution type must be made. The results of a reliability analysis can be very sensitive to the tail of the probability distribution. Therefore, a proper choice of the distribution type is often crucial. Mean and standard deviations are normally obtained from recognized data sources.

Normal or lognormal distributions are normally used when no detailed information is available. The lognormal distribution is used to describe load variables, whereas the normal distribution is used to describe resistance variables. However, a variable that is known as never taking on negative values is normally assigned a lognormal distribution rather than a normal distribution. The following procedure may be applied in order to determine the distribution type and to estimate the associated distribution parameters:

1. Based on experience from similar types of problems, physical knowledge or analytical results, choose a set of possible distributions.
2. Estimate the parameters in these distributions by statistical analysis of available observations of the uncertainty quantities. Regressions may be based on:
 - a. Moment estimators
 - b. Least-square fit methods
 - c. Maximum-likelihood methods
 - d. Visual inspections of data plotted on probability paper
3. If there are several possible choices, the following technique can be used for the acceptance or rejection of the selected distribution functions:
 - a. Visual identification by a plot of data on probability paper or comparison of moments
 - b. Statistical tests (e.g., chi-square)
 - c. Asymptotic behavior for extreme value distributions
4. If two types of distributions give equally good fits, it is recommended, particularly for load variables, that the chosen distribution is the one that better fits possible data observations in the tail.

When distributions are chosen using the above methods, it is important that such choices, including the steps leading up to them, are satisfactorily documented.

33.5 Uncertainty in Ship Structural Design

33.5.1 General

The design of any structure by rational means involves consideration of the uncertainties that arise concerning the external actions imposed on the structure, as well as the strength and response properties of the structural elements. These different uncertainties can be taken into account by introducing probability concepts into the structural design procedure.

In the case of ship structural design, these concepts were introduced by St. Denis and Pierson when determining ship motions, structural loads, etc. due to operating in a realistic random seaway. At about the same time, other work was being carried out in the probabilistic designs of structures.

Freudenthal gave a basic application of the probabilistic approach to the safe design of engineering structures, and later he dealt specifically with marine structures. Others have considered this ship issue, including Mansour (1972), Mansour (1997), Mansour and Faulkner (1973), and Stiansen et al. (1980), where the theory of structural reliability was applied to ships. Nikolaidis and Kaplan (1991) and Nikolaidis et al. (1993) evaluated uncertainties in the stress analysis of marine structures and presented a methodology for the reliability assessment of ship structures.

Longitudinal strength analysis has been based mainly on the elastic beam theory with emphasis on the maximum expected load (bending moment) and the minimum strength that provides a factor of safety against unspecified failure. It is possible to calculate the probability of failure if the probability distributions for loads (demand) and strength (capacity) are completely and clearly defined. The objective of this section is to discuss uncertainties in loads (demand) and strength (capacity).

33.5.2 Uncertainties in Loads Acting on Ships

The principal loads acting on a ship's hull may be summarized as follows, with particular reference to longitudinal hull bending:

- Still-water bending moments due to an uneven distribution of weights and buoyancy in still water
- Quasi-static bending moments due to relatively long encountered waves
- Dynamic bending moments caused by wave impacts or high-frequency wave forces
- Thermal loads induced by uneven temperature gradients

Other loads not mentioned above are internal loads caused by liquid cargoes, machinery or propellers, collision grounding and docking loads, and aerodynamic and ice loads.

Quasi-static Wave Bending Moment

Quasi-static wave bending moments have been dealt with using the probabilistic approach, since the waves causing such bending moments can only be described statistically. A specific sea condition can be fully described by its directional spectrum, defining the component wave frequencies and directions that are present.

Uncertainties arise from:

- Variability in the directional properties of wave spectra, with only limited data available
- Combined effects of two storms, or sea and swell
- Variability of spectral shapes for a given significant height

Referring to Part I, Chapter 7, short-term response, can be calculated statistically by a linear superposition of the calculated RAO (response amplitude operator), which is the amplitude of the ship's response to a unit sinusoidal wave at a certain frequency.

Uncertainties involved in the calculation of RAOs are due to the assumed linearity of the response in relation to wave height, the inaccuracy of strip theory, and the effect of variation in weight distributions on motions. In addition, there are uncertainties in the statistics of response. The use of a simple Rayleigh distribution can result in a bias toward values that are too high in severe seas.

The operation of the ship may also contribute to the uncertainty of wave-induced bending moments, including:

- Cargo distribution and resulting drafts
- Ship headings to the sea
- Ship speed

Still-water Bending Moments

It is relatively easy to calculate still-water bending moments if the distribution of cargo and other weights is known. However, the still-water bending moments vary between voyages, and in any case, they are seldom recorded. Hence, little statistical data are available. Estimates can be made based on calculations customarily made for every new ship design.

Load Combinations

Correlation exists between the loads discussed above. For example, high dynamic loads may often occur in rough seas when large low-frequency loads are also occurring. However, high thermal effects generally correspond with calm, sunny days, where wave-induced loads are relatively mild. It is difficult to combine quasi-static and high-frequency wave-induced loads.

33.5.3 Uncertainties in Ship Structural Capacity

When considering structural failure, separate analyses are necessary for all possible failure modes such as:

- Tensile failure
- Buckling and collapse
- Brittle fracture
- Fatigue

Buckling and collapsing are both important subjects, as the strength in buckling failure modes is much lower than the tensile failure mode. Brittle fracture failure has been

controlled through improved material toughness and through the design of structural details, workmanship and use of crack stoppers, to provide a “fail-safe” design. Fatigue failure is an important subject, even though fatigue cracks do not normally threaten to result in complete failure of the hull girder.

Ultimate failure is complicated by the fact that buckling may occur progressively in different segments of the structure and the first occurrence of a buckle does not usually constitute failure. Loads may successively transfer from buckled areas to those that are still effective.

Objective uncertainties are measurable and include:

- Main dimensions of hull
- Material properties including yield strength, ultimate strength, and Young’s modulus
- Variations in material thickness and shape dimensions
- Manufacturing imperfections, including variations in fabrication tolerances, weld quality, alignment, and residual stresses in welds
- Corrosion, wear, and fatigue cracks, which involve “time-dependent strength”

It should be noted that all of the above involve physical uncertainties in the materials used or in the methods for ship construction. Uncertainties may also arise from methods of calculating structural responses, including the effect of boundary conditions, and the variability in the physical behavior of materials and structures.

The subjective uncertainties require judgment and include:

- Shear lag and other shear effects (considered negligible)
- Major discontinuities; openings, superstructures
- Torsional and distortional warping
- Poisson’s ratio effects, especially at transverse bulkheads and diaphragms
- Stress redistribution arising from changes in stiffness due to deformations, inelasticity, or both
- Gross panel compression nonlinearities; effective width, inelasticity, residual stresses, and shakeout effects (considered negligible)

Other subjective uncertainties not mentioned in the above are the residual strength after the ultimate strength of the global panel, which may significantly affect ultimate strength and its variability.

References

- Ang, A.H.-S., Tang, W., 1975, 1984. *Probability Concepts in Engineering Planning and Design*, vols. I & II. John Wiley and Sons, New York.
- Benjamin, J., Allin Cornell, C., 1970. *Probability, Statistics and Decision for Civil Engineers*. McGraw-Hill, Inc.
- Mansour, A.E., 1972. Probabilistic Design Concept in Ship Structural Safety and Reliability, vol. 80. *Trans. SNAME*, pp. 64–97.

- Mansour, A., Faulkner, D., 1973. On Applying the Statistical Approach to Extreme Sea Loads and Ship Hull Strength, vol. 115. RINA Trans., pp. 277–313.
- Mansour, A.E., 1997. Assessment of reliability of ship structures. In: SSC-398. Ship Structures Committee.
- Melchers, R.E., 1999. Structural Reliability Analysis and Prediction, second ed. John Wiley & Sons Ltd.
- Nikolaidis, E., Kaplan, P., 1991. Uncertainties in stress analysis on Marine structures. In: Ship Structure Committee Report SSC-363.
- Nikolaidis, E., Hughes, O.F., Ayyub, B.M., White, G.J., 1993. A methodology for reliability assessment of ship structures. In: Ship Structures Symposium 93. SSC/SNAME, Arlington, VA, pp. H1–H10.
- Stiansen, S.G., Mansour, A.E., Jan, H.Y., Thayamballi, A., 1980. Reliability Methods in Ship Structures. Transactions of RINA 122.
- Thoft-Christensen, P., Baker, M.J., 1982. Structural Reliability, Theory and Its Applications. Springer-Verlag.

Reliability of Ship Structures

34.1 General

Since researchers first began to apply probabilistic methods in the structural design of ships (Mansour, 1972; Mansour and Faulkner, 1973), a significant amount of achievement has been accomplished. The earliest applications of reliability methods to ship structures focused on overall hull girder reliability subjected to wave bending moments (Mansour, 1974; Stiansen and Mansour, 1980; White and Ayyub, 1985; Guedes Soares et al., 1996). Recent work in applying reliability methods to the ultimate strength of gross panels using second-moment methods (Nikolaidis et al., 1993) has shown considerable promise. Casella and Rizzuto (1998) presented a second-level reliability analysis of a double-hull oil tanker, while Frieze and Lin (1991) assessed the reliability for ship longitudinal strength. Efforts continue to look at how these methods and procedures can be used in a system analysis.

There has been a tremendous amount of effort to develop statistical models for load effects (e.g., Guedes Soares and Moan, 1985, 1988; Ochi, 1978; Sikora et al., 1983; Mansour, 1987). Recent research includes the uncertainties associated with loads and load effects (Nikolaidis and Kaplan, 1991), and on loads and load combinations (Mansour et al., 1993).

FPSOs have been used worldwide as an economic solution for the development of offshore oil and gas. Actually, many FPSOs are sited at locations with dynamic components of their loading that are less than those arising from unrestricted service conditions. The reliability of FPSO hull girders for site-specific conditions is quite different from that of oil tankers for unrestricted service conditions. Therefore, it is necessary to assess the reliability of FPSO hull girders in order to develop rational design criteria.

As oceangoing cargo ships, the most catastrophic potential event for FPSOs is the structural failure of hull girders due to extreme bending moments. During their service lives, FPSO hull girders predominantly withstand still-water and wave-induced bending moments. The former is caused by the action of self-weight, cargo, or deadweight. The latter is a result from the wave action at specific installation locations. The “environmental severity factors (ESFs)” should be introduced in order to account for site-specific conditions in the wave-induced bending moments (ABS, 2000). Because the maximum values of the still-water and wave-induced bending moments do not occur at the same instant, the stochastic combination method should be used, in order to more rationally

determine the maximum value of the combined loads—for example, [Guedes Soares \(1990\)](#), [Mansour \(1994\)](#), and [Wang et al. \(1996\)](#).

In carrying out the reliability assessment relating to the failure of progressive collapse, the limit-state function is very complex and may only be expressed implicitly. Among the methods available for solving such a problem, the response surface method is an effective and powerful tool, in which the limit-state function is approximated by a simple and explicit function at the sampling points—for example, [Bucher and Bourgound \(1990\)](#) and [Liu and Moses \(1994\)](#).

This chapter presents a methodology for the time-variant reliability assessment relating to the ultimate strength of the midsection for hull girders subjected to the structural degradations of corrosion and fatigue. It includes three aspects: (1) closed form equations for assessment of the hull girder reliability, (2) load effects and load combination, and (3) time-variant reliability. The progressive collapse analysis of hull girder strength used in the time-variant reliability is a modified version of Smith's method ([Smith, 1977](#)). The modification is to account for corrosion defects and fatigue cracks; see Part II, Chapter 13.

34.2 Closed Form Method for Hull Girder Reliability

For the vertical bending of the hull girder for seagoing conditions, the limit-state function can be expressed by the following equation

$$g(X_i) = M_u - (M_{SW} + M_{WV}) \quad (34.1)$$

where

M_u = ultimate vertical bending moment

M_{SW} = still-water bending moment for seagoing condition

M_{WV} = vertical wave bending moment for in sagging or hogging condition

Assuming that these load and resistance variables follow a normal distribution and have the same coefficient of variation (COV), the following equation based on the Cornell safety index method Eqn (23.6), can be obtained.

$$\beta = \frac{M_u - (M_{SW} + M_{WV})}{\text{COV} \cdot \sqrt{M_u^2 + M_{SW}^2 + M_{WV}^2}} \quad (34.2)$$

Moreover, taking into account the assumptions adopted for modeling of the random variables, [Eqn \(34.2\)](#) shows that the safety index for seagoing conditions is inversely proportional to the COV. For a 50% increase in the COV, the safety index is reduced by 35%.

The Cornell safety index method is also called the mean value first-order second-moment concept, where the reliability index β is defined as the mean of the limit-state function divided by its standard deviation.

The limit-state function g and the reliability index β for different failure modes include

1. For Hull Primary Failure

$$g = M_u - [M_S + k_w(M_w + k_d M_d)] \quad (34.3)$$

$$\beta = \frac{\mu_g}{\sigma_g} \quad (34.4)$$

where

$$\mu_g = \mu_{M_u} - [\mu_{M_S} + k_w(\mu_{M_w} + k_d \mu_{M_d})] \quad (34.5)$$

$$\sigma_g = \sqrt{\sigma_{M_u}^2 + \sigma_{M_S}^2 + k_w^2 \sigma_{M_d}^2 + k_w^2 k_d^2 \sigma_{M_d}^2 + 2\rho_{M_w M_d} k_w k_d \sigma_{M_w} \sigma_{M_d}} \quad (34.6)$$

where

M_u = ultimate strength

M_S = still-water bending moment

M_w = wave bending moment

M_d = dynamic bending moment

k_w = load combination factor for still-water and wave/dynamic moments

k_d = load combination factor for wave and dynamic moments

μ_i = mean of component i

σ_i = standard deviation of component i

2. For Secondary and Tertiary Failure Mode

$$g = f_u SM - [M_S + k_w(M_w + k_d M_d)] \quad (34.7)$$

$$\beta = \frac{\mu_g}{\sigma_g} \quad (34.8)$$

where,

$$\mu_g = \mu_u \mu_{SM} - [\mu_{M_S} + k_w(\mu_{M_w} + k_d \mu_{M_d})] \quad (34.9)$$

$$\sigma_g = \sqrt{(\sigma_u^2 \sigma_{SM}^2 + \sigma_u^2 \mu_{SM}^2 + \mu_u^2 \sigma_{SM}^2) + \sigma_{M_S}^2 + k_w^2 \sigma_{M_d}^2 + k_w^2 k_d^2 \sigma_{M_d}^2 + 2\rho_{M_w M_d} k_w k_d \sigma_{M_w} \sigma_{M_d}} \quad (34.10)$$

where

SM = section modulus

f_u = ultimate stress

M_S = still-water bending moment

M_w = wave bending moment

M_d = dynamic bending moment

k_w = load combination factor for still-water and wave/dynamic moments

k_d = load combination factor for wave and dynamic moments

μ_i = mean of component i

σ_i = standard deviation of component i

34.3 Load Effects and Load Combination

The following sections are based on [Sun and Bai \(2001\)](#) with a few modifications.

FPSO hull girders are predominantly subjected to combining actions of still-water and wave-induced bending moments. A still-water bending moment (SWBM) is created from the action of a ship's self-weight, cargo, deadweight, and buoyancy. Compared with that of an oceangoing cargo ship, the SWBM of an FPSO varies more frequently from one load condition to the next due to loading patterns and human actions. In the long term, this needs to be considered a stochastic process.

For an FPSO, a Poisson rectangular pulse process in a time domain is applied in order to model the SWBM. Its cumulative distribution can be fitted by a Raleigh distribution for the sagging condition and by an exponential distribution for the hogging conditions, according to [Wang et al. \(1996\)](#)—for example,

$$F_{M_s}(M_s) = 1 - \exp \left[- \ln(v_s T_0) \left(\frac{M_s}{M_{s,0}} \right)^2 \right] \quad (34.11)$$

for sagging SWBM and,

$$F_{M_s}(M_s) = 1 - \exp \left[- \ln(v_s T_0) \left(\frac{M_s}{M_{s,0}} \right) \right] \quad (34.12)$$

for hogging conditions where M_s is the SWBM of an individual load condition and v_s is the mean arrival rate of one load condition. The specified maximum SWBM in a design lifetime of $T_0 = 20$ years, $M_{s,0}$ is ([IACS, 1995](#))

$$M_{s,0} = \begin{cases} -0.065 C_w L^2 B (C_B + 0.7) & (\text{sagging}) \\ C_w L^2 B (0.1225 - 0.015 C_B) & (\text{hogging}) \end{cases} \quad (34.13)$$

where L , B , and C_B are the ship length, breadth, and block coefficient, respectively, and C_w is the wave coefficient given by

$$C_w = \begin{cases} 10.75 - ((300 - L)/100)^{3/2} & 100 < L \leq 300 \\ 10.75 & 300 < L \leq 350 \\ 10.75 - ((L - 350)/150)^{3/2} & L > 350 \end{cases} \quad (34.14)$$

The cumulative distribution function (CDF) for the largest individual SWBMs can be found for a total of $v_s T$ repetitions by using the extreme theory,

$$F_{X_s} = \exp \left[-e^{-\alpha_s(X_s - \mu_s)} \right] \quad (34.15)$$

where $X_s = M_s/M_{s,0}$ and the parameters α_s and μ_s are given by

$$\mu_s = \sqrt{\frac{\ln(v_s T)}{\ln(v_s T_0)}}, \quad \alpha_s = 2\sqrt{\ln(v_s T_0)\ln(v_s T)} \quad (\text{sagging})$$

$$\mu_s = \frac{\ln(v_s T)}{\ln(v_s T_0)}, \quad \alpha_s = \ln(v_s T_0) \quad (\text{hogging})$$

Many research efforts have been made regarding the prediction of VWBM experienced on ship hulls. Research has used both linear and nonlinear methods for unrestricted service conditions. VWBM is a naturally stochastic process and can be described by either short-term or long-term statistics. The long-term VWBM is based on weighted short-term statistics. It is generally accepted that the long-term VWBM can be modeled as a Poisson process and the peak of each individual VWBM, M_w , can be well approximated by a Weibull distribution:

$$F_{M_w}(M_w) = 1 - \exp \left[-\ln(v_w T_0) \left(\frac{M_w}{M_{w,0}} \right)^{h_w} \right] \quad (34.16)$$

where v_w is the mean arrival rate of one wave cycle and h_w is the shape parameter varying from 0.9 to 1.1. Reasonably taking 1.0 as a representative value, $M_{w,0}$ is the maximum VWBM in the reference design period of $T_0 = 20$ years,

$$M_{w,0} = \begin{cases} -0.11(\text{ESF})_s C_w L^2 B (C_B + 0.7) & (\text{sagging}) \\ 0.19(\text{ESF})_h C_w L^2 B C_B & (\text{hogging}) \end{cases} \quad (34.17)$$

where $(\text{ESF})_s$ and $(\text{ESF})_h$ are the ESFs for sagging and hogging conditions, which can be taken from 0.5 to 1.0, consistent with the specific installation site (ABS, 2000).

Similar to that of SWBM, the CDF for the largest individual VBWBMs can be found:

$$F_{X_w} = \exp \left[-e^{-\alpha_w(X_w - \mu_w)} \right] \quad (34.18)$$

where $X_w = M_w/M_{w,0}$ and the parameters α_w and μ_w are given by

$$\mu_w = \frac{\ln(v_w T)}{\ln(v_w T_0)}, \quad \alpha_w = \ln(v_w T_0)$$

Based on the *Ferry–Borges* method, the CDF of the combined bending moment is expressed as (Wang et al., 1996)

$$F_{M_t}(M_t) = \int_0^{M_t} \frac{f_{M_s}(M_t - u) du}{1 + v_w/v_s[1 - F_{M_w}(u)]} \quad (34.19)$$

The combined bending moment in a given time T is obtained from the below equation:

$$F(M_t) = 1 - 1/v_s T \quad (34.20)$$

For practical design considerations, load combination factors for SWBM and VWBM, denoted as φ_s and φ_w , are introduced.

$$M_{t,T} = M_{w,T} + \varphi_s M_{s,T} = M_{s,T} + \varphi_w M_{w,T} \quad (34.21)$$

The CDF for the largest of the individual combined bending moments can be expressed as

$$F_{\max}(M_t) = [F(M_t)]^{v_s T} \quad (34.22)$$

34.4 Procedure for Reliability Analysis of Ship Structures

34.4.1 General

Since the early 1970s, when researchers first began to look at the desirability of using probabilistic methods in the structural design of ships, vast numbers of publications have become available regarding reliability analysis of existing ships. The details of the analytical methods may vary from one paper to another. However, generally speaking, the reliability analysis of existing ships should cover the basic steps outlined below.

Step 1: Definition of the objective ship and its mission tasks

In order to carry out the reliability analysis of a ship, the basic geometry and scantlings of the ship must be known. Furthermore, the environmental conditions, including loading conditions and sea conditions the ship has been exposed over its service life, should also be defined.

Step 2: Definition of the limit-state functions

Knowledge regarding the limiting conditions, beyond which a ship will fail to perform its intended functions, will undoubtedly help in assessing more accurately the true safety margin of the ship. The equations that represent these limiting conditions are called limit-state equations; establishing these equations is a significant step within the

reliability analysis procedure. Generally speaking, there are two categories of limit-state equations: serviceability versus strength. For each category, four different levels of limit states exist. These are

1. Limit-state functions for hull girder collapse
2. Limit-state functions for stiffened panels
3. Limit-state functions for buckling of plates between stiffeners
4. Limit-state functions for fatigue of Critical Structural Details (CSD)

Step 3: Definition of the statistical characteristics of the random variables

Step 4: Selection of the reliability calculation methods

Step 5: For the given ship, calculate the probability of failure for each failure mode

When the limit-state function is complex, a response surface method may be applied to approximate the limit-state surface, using a polynomial type function. Using the response surface, a standard FORM/SORM algorithm may then be used to estimate failure probability.

34.4.2 Response Surface Method

The limit-state function at time t relating to the ultimate strength failure of an FPSO hull girder is given by

$$g(\mathbf{x}|t) = C_u M_u(t) - C_p [\phi_s M_s(t) + M_w(t)] \quad (34.23)$$

where $M_u(t)$ is the ultimate strength, $M_s(t)$ and $M_w(t)$ are the still-water and wave-induced moments, respectively; C_u and C_p represent the model errors when predicting the hull's ultimate strength and the combined total bending moment the ship experiences, respectively. The failure probability at the time T is expressed by

$$P_f(T) = \int_0^T \left[\int_{g(\mathbf{x}|t) < 0} \dots \int f_X(\mathbf{x}|t) d\mathbf{x} \right] f_T(t) dt \quad (34.24)$$

where $f_X(\mathbf{x}|t)$ is the joint probability density function and $f_T(t)$ is the probability density function of occurrence time T , which is assumed as a uniform distribution, $f_T(t) = 1/T$.

Therefore, Eqn (34.24) can be rewritten as

$$P_f(T) = \frac{1}{T} \int_0^T \left[\int_{g(\mathbf{x}|t) < 0} \dots \int f_X(\mathbf{x}|t) d\mathbf{x} \right] dt \quad (34.25)$$

By defining $P_f(t)$ as a conditional failure probability at time t ,

$$P_f(t) = \int_{g(\mathbf{x}|t) < 0} \dots \int f_X(\mathbf{x}|t) d\mathbf{x} \quad (34.26)$$

The simple form of this probability is

$$P_f(T_s) = \frac{1}{T} \int_0^T P_f(t) dt \quad (34.27)$$

The response surface method (Bucher and Bourgound, 1990) is applied when the limit-state function $g(\mathbf{x}|t)$ is expressed implicitly and has a nonlinear form, in order to overcome the expensive computational effort of integrating Eqn (34.25) into the evaluation of the failure probability.

The basic concept of the response surface method is to approximate the original complex and/or implicit limit-state function using a simple and explicit function. The accuracy of the results depends highly on how accurately the characteristics of the original limit state are represented by the approximate function. The suitability of the response surface obtained relies mainly on the proper location of so-called sampling points. Many algorithms have been proposed to select appropriate sampling points that promise to yield better surface-fitting responses. In addition, the basic function shape is also known as another major factor that influences both the accuracy of the response surface method, and the selection of the reliability evaluation method.

Many practical reliability evaluation techniques are available once the failure surface $G(\mathbf{x})$ is defined in an explicit closed form. Among those techniques, the first-order method is commonly used due to its efficiency and acceptable accuracy. An equivalent linearized limit state at the so-called design point is taken and the safety margin of the structural system is determined. The safety margin is taken as the minimum distance from the origin to the original nonlinear limit surface within the independent standard normal space.

In this study, a response surface with a polynomial type function including squared but not cross terms is adopted,

$$G(\mathbf{x}) = a + \sum_{i=1}^r b_i x_i + \sum_{i=1}^r c_i x_i^2 \quad (34.28)$$

where r is the number of basic random variables; $\mathbf{x} = (x_1, x_2, \dots, x_r)$ is the basic random vector; and a , b_i , and c_i are the unknown coefficients that can be determined using $2r + 1$ sampling points. The sampling points are selected to be located at the design point $(\bar{x}_1, \bar{x}_2, \dots, \bar{x}_r)$ and other $2r$ points $(\bar{x}_1, \dots, \bar{x}_i \pm f\sigma_i, \dots, \bar{x}_r)$, where f is a parameter determining the upper and lower bounds of the selection range. This process should be iterative to guarantee that the sampling points chosen from the new design point sufficiently include the information from the original failure surface. Once the response surface is defined, the failure probability is computed using a modified Monte Carlo simulation technique (Sun and Chen, 1997).

Table 34.1: Principal particulars of an FPSO

Description	Value
Length, between perpendiculars	194.2 m
Length, for scantling	194.2 m
Breadth, molded	32.0 m
Depth, molded, including box keel	18.0 m
Depth, molded, from base line	16.0 m
Block coefficient	0.816
Transverse web frame spacing	3.7 m

34.5 Time-Variant Reliability Assessment of FPSO Hull Girders

The time-variant reliability estimation of an FPSO hull girder subjected to degradations of corrosion and fatigue is studied and discussed within this subsection. The relevant principal particulars of the FPSO are listed in [Table 34.1](#). The midsection is shown in [Figure 34.1](#). [Table 34.2](#) summarizes the variable measurements in this assessment. The determination of the various variables is based on the previous studies of FPSOs.

34.5.1 Load Combination Factors

Since the failure mode under sagging conditions is most prominent, the results for sagging conditions are demonstrated below.

The parameter analysis of the load combination factors φ_s and φ_w for the FPSO is carried out first.

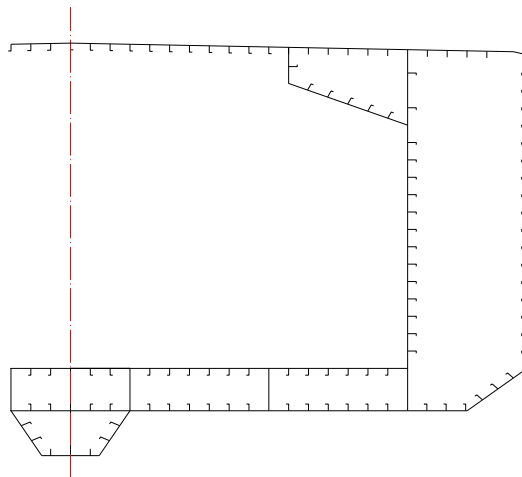


Figure 34.1
FPSO midsection.

Table 34.2: Variable measurements

Variable	Description
E	Elastic modulus, normal variable, mean = 2.06×10^5 MN/m ² , COV = 0.08
σ_y	Yielding stress, normal variable, mean = 315 MN/m ² , COV = 0.06
Δ	Stiffened panel eccentricity, normal variable, mean = 0.00555 m, COV = 0.1
W/h_p	Initial center deflection of plating, normal variable, mean = 0.5, COV = 0.1
τ_c	Transition time of corrosion, constant, $\tau_c = 3$ years
μ_c^d	Steady corrosion rate of the stiffened panels at deck, normal variable, mean = 1.4×10^{-4} m/year, COV = 0.1
μ_c^s	Steady corrosion rate of the stiffened panels at side shell and longitudinal bulkhead, normal variable, mean = 1.25×10^{-4} m/year, COV = 0.1
μ_c^{ob}	Steady corrosion rate of the stiffened panels at outer bottom, normal variable, mean = 5.4×10^{-5} m/year, COV = 0.11
μ_c^{ib}	Steady corrosion rate of the stiffened panels at inner bottom, normal variable, mean = 1.79×10^{-4} m/year, COV = 0.16
μ_c^c	Steady corrosion rate of corner elements, normal variable, mean = 5.4×10^{-5} m/year, COV = 0.10
C	Material parameter in Paris–Erdogen equation, normal variable, mean = 4.349×10^{-12} , COV = 0.206
M	Material parameter in Paris–Erdogen equation, constant, $m = 3.07$
a_0	Initial crack size, normal variable, mean = 1.0×10^{-3} m, COV = 0.18
M_s	Maximum value of still bending moment, type I extreme variable, average arrival period $(1/v_s) = 1$ day
M_w	Maximum value of wave-induced bending moment, type I extreme variable, average arrival rate $(v_w) = 10^8$ in a 20-year design life
$(ESF)_s$	Environmental severity factor for sagging condition, constant, $(ESF)_s = 0.80$
$(ESF)_h$	Environmental severity factor for hogging condition, constant, $(ESF)_h = 0.80$
C_u	Model error of predicting ultimate strength, normal variable, mean = 1, COV = 0.1
C_p	Model error of predicting combined total bending moment, normal variable, mean = 1, COV = 0.25 (sagging condition)

Figure 34.2 shows the effect of the mean arrival period ($1/v_s$) of SWBM on combination factors. The total number of 10^8 wave cycles in 20 service-years is selected, and the environmental severity factor $(ESF)_s$ is taken to be 0.80. It can be seen that load combination factors are sensitive to the mean arrival period of SWBM.

Figure 34.3 shows the dependence of load combination factors as a time function where the environmental severity factor $(ESF)_s$ is also taken to be 0.80. It is demonstrated that load combination factors gradually decrease with increases in service years.

Figure 34.4 shows the dependence of load combination factors with the ESF, where a total number of 10^8 wave cycles in 20 service-years and the SWBM mean arrival period ($1/v_s$) of 1 day are selected. It is shown that the decreasing trend of φ_s is much greater than the increasing trend of φ_w when the ESF increases. It implies that the load combination makes it so the effect of the ESF is small.

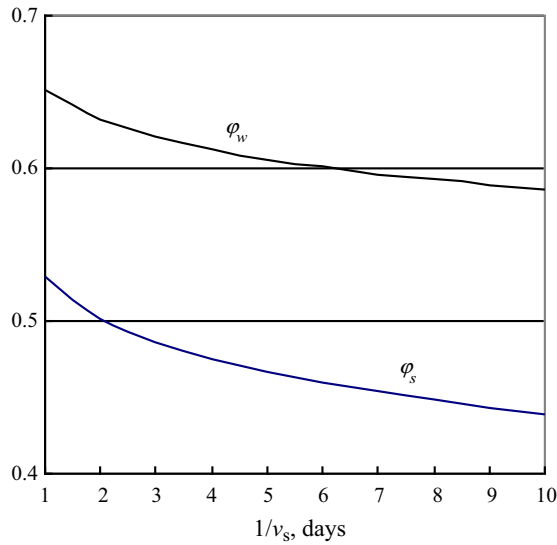


Figure 34.2
Load combination factors versus $1/\nu$.

34.5.2 Time-Variant Reliability Assessment

Figure 34.5 shows the conditional reliability as a time function that considers the four cases of degradation. Here, the conditional reliability is defined by $R(t) = 1 - P_f(t)$. For different service years and mean-steady corrosion rates, reductive ratios of the corresponding conditional reliability index compared with initial values are listed in Table 34.3.

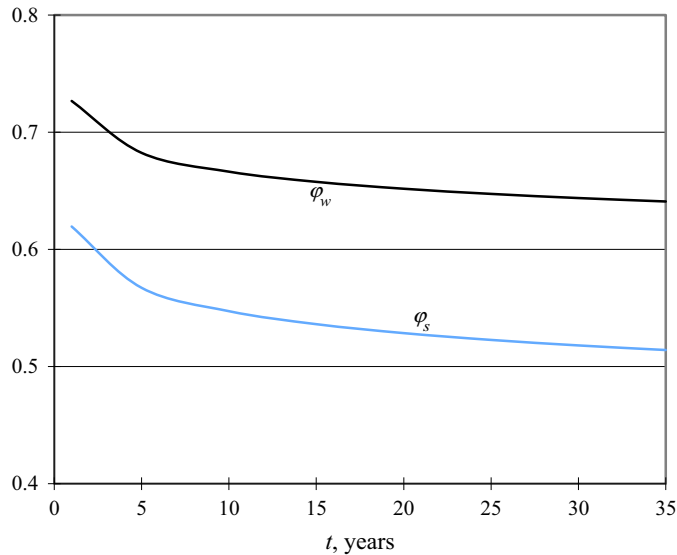


Figure 34.3
Load combination factors as a time function.

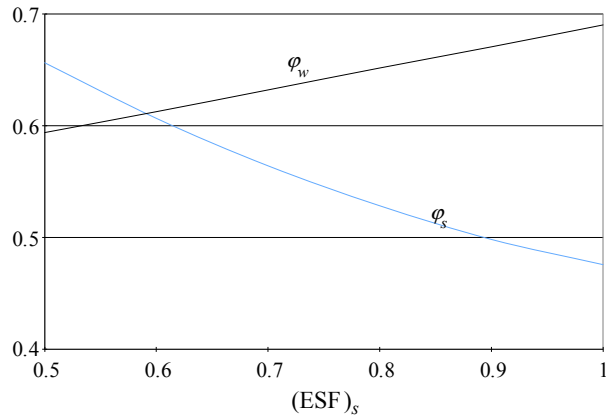


Figure 34.4
Load combination factors versus ESF

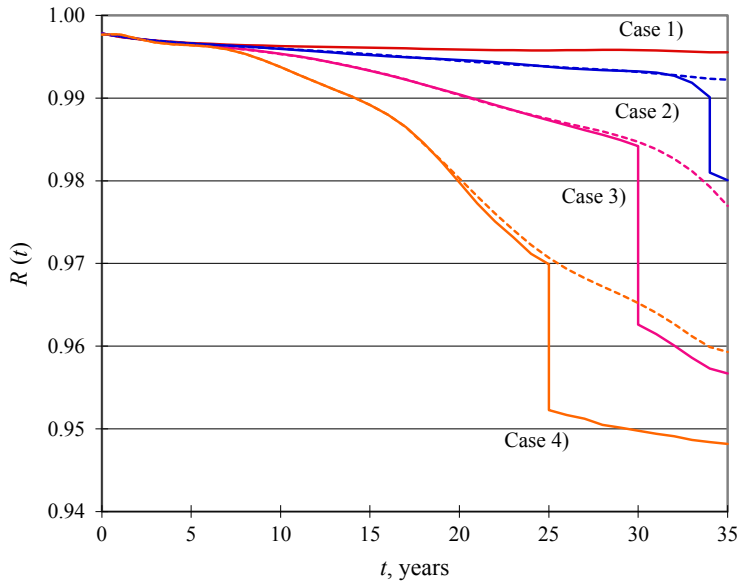


Figure 34.5
Conditional reliability with four cases of mean-steady corrosion rates.

Table 34.3: The reductive ratios of conditional reliability index

Service Year Corrosion	5	10	15	20	25	30	35
Case 1	95.17%	93.91%	93.29%	92.64%	92.37%	92.45%	91.67%
Case 2	95.10%	93.11%	91.01%	89.64%	87.88%	86.81%	72.23%
Case 3	94.76%	91.50%	86.94%	82.39%	78.60%	62.66%	60.26%
Case 4	94.87%	88.15%	81.09%	72.35%	58.86%	57.99%	57.45%

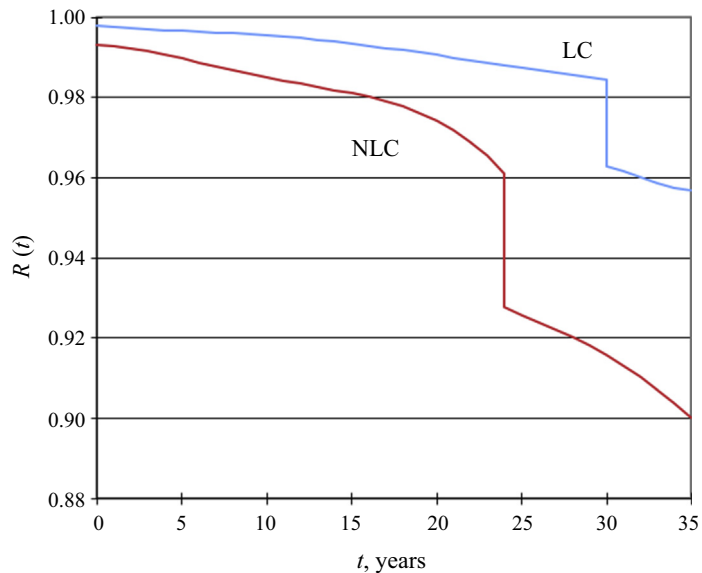


Figure 34.6

Influence of load combination on conditional reliability.

The conditional reliability of the hull girder also significantly decreased along with the mean ultimate strength. If a reductive ratio of 90% of the conditional reliability index is selected as the reliability threshold in order to maintain the hull reliability level, then inspections should be made for both Case 3 and Case 4 at about the 10th service year. The degradation effects of fatigue cracks seem to be unimportant to hull girder reliability, before they unsteadily propagate. However, during inspections, potential disasters of the hull girder reliability need to be considered. The unsteady propagation of fatigue cracks might result in catastrophic events for the FPSO.

It is quite conservative to even simply add the extreme values of SWBM and VWBM. It can be found in [Figure 34.6](#), where “LC” and “NLC” represent the load combination and no-load combination, respectively.

[Figure 34.7](#) shows the influence of “ESFs” on the conditional reliability, where the number denotes the value of ESFs. Accuracy measurements of site-specific installation conditions are very important for FPSO hull girder designs and inspections.

The transition time τ_t is another important parameter related to reliability. Its effects at various values are shown in [Figure 34.8](#), where the number on the curve denotes transition years. A relatively larger transition time will keep reliability relatively higher and postpone the unsteady propagation of fatigue cracks. This result was also obtained by [Guedes](#)

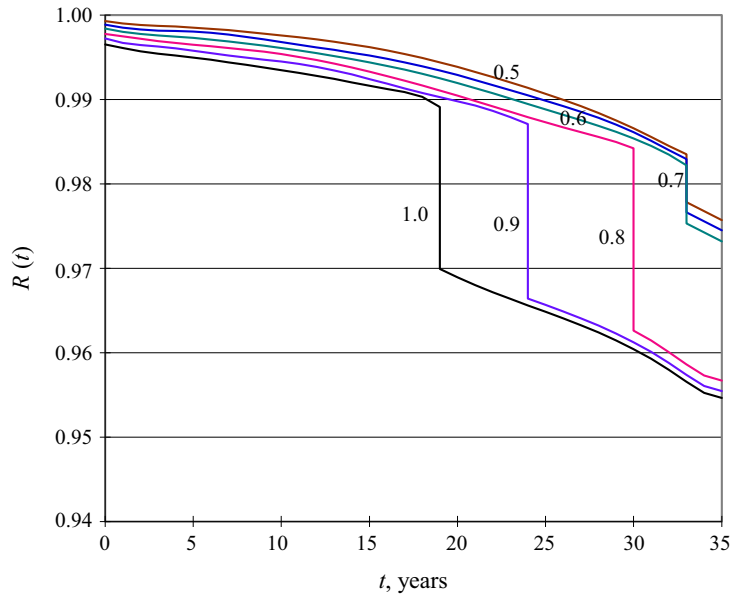


Figure 34.7
Influence of ESFs on conditional reliability.

Soares and Garbatov (1999a,1999b), who carried out the reliability analysis of maintained corrosion-protected plates.

Corrosion wastage depends on many factors including coating properties, cargo composition, inert gas properties, the temperature of the cargo, and maintenance systems and practices. Spot-checks may not be measured in the same location as prior spot-checks in normal thickness measurements. This makes any theoretical construction of a corrosion model quite difficult. In the numerical analysis, the mean steady corrosion rates were used. These rates correspond to the permissible values of corrosion wastage of oil tankers for the rules set by the classification society. The COV, for corrosion rates, typically increases with time from 10% at the 10th service year to 100% or even larger at the 20th service year. However, the contribution to the total uncertainty of hull girder ultimate strength is very limited based on the sensitivity analysis (see Figure 34.9).

Figure 34.10 shows the results of the uncertainty analysis for the ultimate strength of the hull girder. In this analysis, CRM represents the result from the response surface method. It is found that the COV, for the ultimate strength, is 10% of the upper bound of any considered corrosion case.

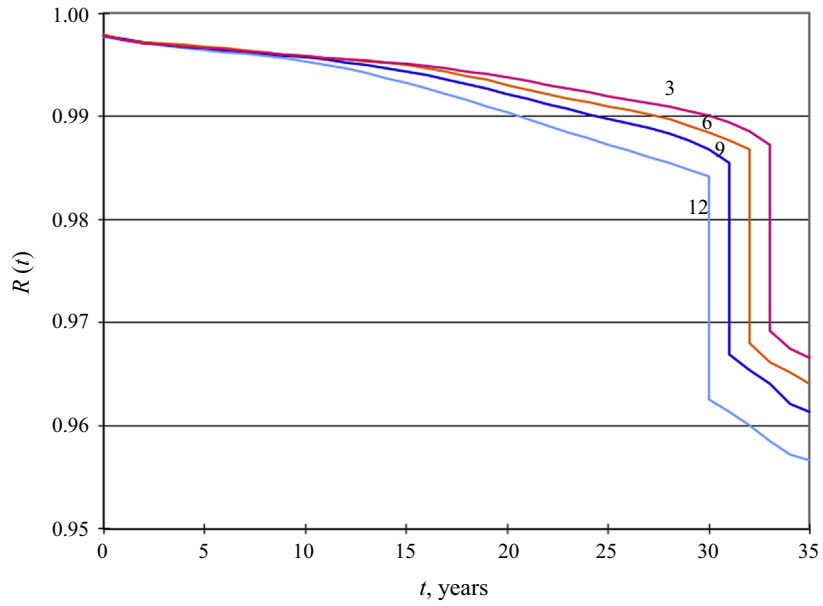


Figure 34.8
Influence of transition time on conditional reliability.

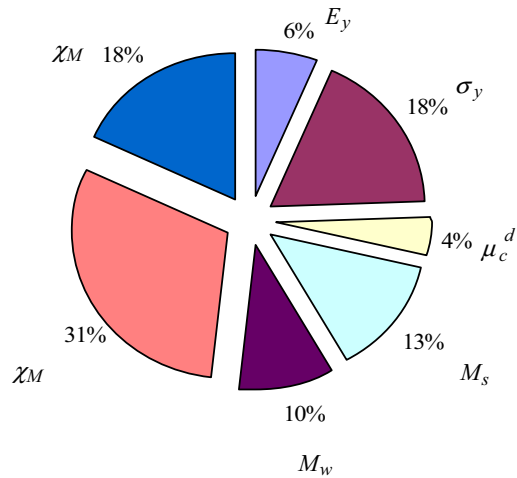


Figure 34.9
Sensitivity data at 20th service year for nominal corrosion rate.

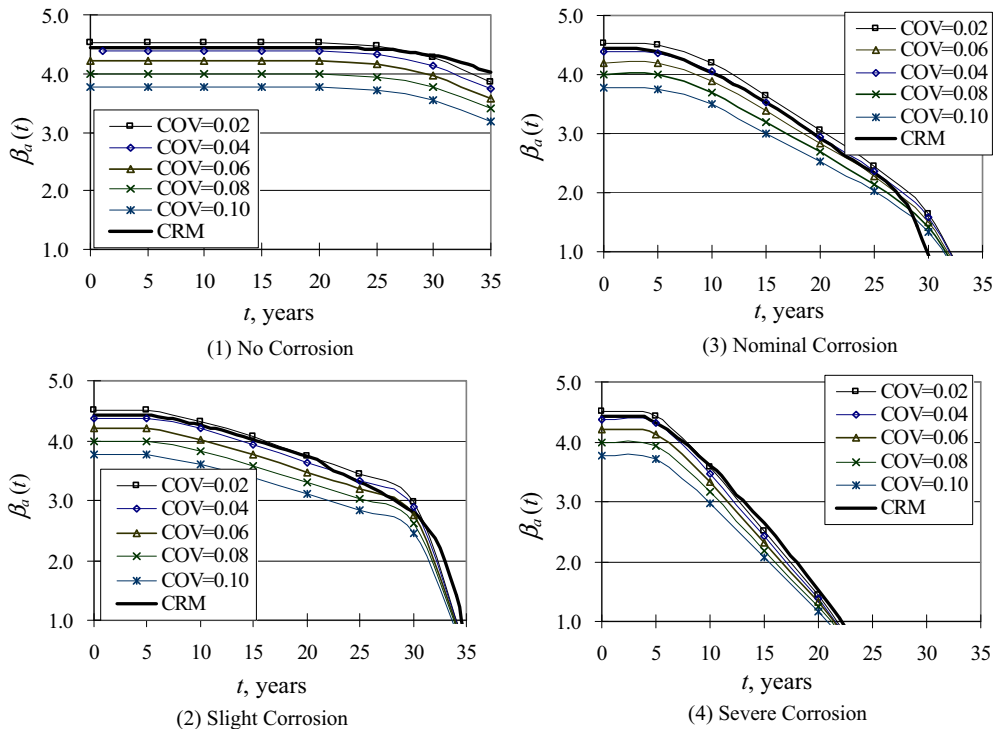


Figure 34.10
Uncertainty analysis for ultimate strength.

There are several corrosion rate models within this test. The simplest being, the model with assumed constant corrosion rate, which is entirely estimated from observations made as part of normal surveys. Due to the products of corrosion, the corrosion rate decreases with time. But other observations from oil tankers showed that in most cases the corrosion rate appears to actually increase with time and then stay constant. The reason for this appears to be related to the dynamic loading that spill off corrosion products in ocean environments. The corrosion rate model proposed in this section falls under these particular conditions. However, when more data on corrosion wastage becomes available, further work is needed in order to improve the corrosion rate model. The rational way to keep the safety level of the FPSO hull girders in present practice is to establish, a risk-based program of inspection planning, and reliability-based renewal criteria for corroded components.

34.5.3 Conclusions

A time-variant, structural reliability assessment of an FPSO hull girder, relative to the ultimate strength, requires the consideration of the following three characteristics: (1) load effects and their combination, (2) the hulls ultimate strength, and (3) methods of reliability analysis.

The ESFs are introduced to fit the wave-induced bending moments, while accounting for the site-specific conditions. The *Ferry—Borges* method is applied to combine stochastic processes of still-water and wave-induced bending moments, and to evaluate the time-variation of the maximum combined bending moment.

- The mean value, first-order, second-moment method was applied to calculate the failure probability of ship structures.
- A procedure for time-variant reliability analysis has been developed.
- An effective response surface approach is used to evaluate the failure function at sampling points. A modified Monte Carlo simulation technique is applied to evaluate the failure probability.
- The time-variant reliability and the parametric analysis for an FPSO hull girder are both quantified. It is found that the steady corrosion rate, a combination of SWBM and VWBM, the ESFs and transition time in the present corrosion model are very important when estimating the reliability of the hull girder.
- It is concluded that the load combination factors obtained from this method are dependent on the mean arrival rate of SWBM, service lifetime, and the ESFs.

References

- ABS, 2000. Guide for Building and Classing Floating Production Installations. American Bureau of Shipping.
- Bucher, C.G., Bourground, U.A., 1990. A fast and efficient response surface approach for structural reliability problems. *Structural Safety* 7, 57–66.
- Casella, G., Rizzuto, E., 1998. Second-level reliability analysis of a double-hull oil tanker. *Marine Structures* 11, 373–399.
- Frieze, P.A., Lin, Y.T., 1991. Ship longitudinal strength modeling for reliability analysis. In: Proc. of Marine Structural Inspection, Maintenance and Monitoring Symposium. SNAME, Arlington, VA.
- Guedes Soares, C., 1990. Stochastic models of loads effects for the preliminary ship hulls. *Structural Safety* 8, 353–368.
- Guedes Soares, C., Moan, T., 1985. Uncertainty analysis and code calibration of the primary load effects in ship structures. In: Proc. 4th International Conference on Structural Safety and Reliability (ICOSSAR '85), Kobe, Japan, vol. 3, pp. 501–512.
- Guedes Soares, C., Moan, T., 1988. Statistical analysis of still-water load effects in ship structures. *Transactions of the SNAME* 96, 129–156.
- Guedes Soares, C., Dogliani, M., Ostergaard, C., Parmentier, G., Terndrup Pedersen, P., 1996. Reliability based ship structural design. *Transactions of the SNAME* 104, 357–389.
- Guedes Soares, C., Garbatov, Y., 1999a. Reliability of corrosion protected and maintained ship hulls subjected to corrosion and fatigue. *Journal of Ship Research* 43 (2), 65–78.
- Guedes Soares, C., Garbatov, Y., 1999b. Reliability of maintained, corrosion protected plates subjected to nonlinear corrosion and compressive loads. *Journal of Marine Structures* 12, 425–445.
- IACS, 1995. Requirement S11, Longitudinal Strength Standards. Int. Association of Classification Societies.
- Liu, Y.W., Moses, F., 1994. A sequential response surface method and its application in the reliability analysis of aircraft structural system. *Journal of Structural Safety* 16, 36–46.
- Mansour, A.E., 1972. Probabilistic design concept in ship structural safety and reliability. *Transactions of the SNAME* 80, 64–97.

- Mansour, A., Faulkner, D., 1973. On applying the statistical approach to extreme sea loads and ship hull strength. *Transactions of the RINA* 115, 277–313.
- Mansour, A.E., 1974. Approximate probabilistic methods of calculating ship longitudinal strength. *Journal of Ship Research* 18.
- Mansour, A.E., 1987. Extreme value distributions of wave loads and their application to marine structures. In: *Marine Structural Reliability Symposium*, Arlington, VA.
- Mansour, A.E., Lin, M., Hovem, L., Thayamballi, A., 1993. Probability-Based Ship Design Procedure – a Demonstration. SSC Report, SSC-368.
- Mansour, A.E., 1994. Probability Based Ship Design Procedures: Loads and Load Combination. Ship Structure Committee, SSC-373.
- Nikolaïdis, E., Kaplan, P., 1991. Uncertainties in Stress Analysis on Marine Structures. Ship Structure Committee Report, SSC-363.
- Nikolaïdis, E., Hughes, O.F., Ayyub, B.M., White, G.J., 1993. A methodology for reliability assessment of ship structures. In: *Ship Structures Symposium 93*. SSC/SNAME, Arlington, VA, pp. H1–H10.
- Ochi, M.K., 1978. Wave statistics for the design of ships. *Transactions of SNAME* 86, 47–76.
- Sikora, J.P., Disenbacher, A., Beach, J.E., 1983. A method for estimating lifetime loads and fatigue lives for SWATH and conventional monohulls. *Naval Engineering Journal*, ASNE 95 (4), 63–85.
- Smith, C.S., 1977. Influence of local compressive failure on the ultimate longitudinal strength of a ship hull. In: *Proc. of Int. Symposium on Practical Design of Ships (PRADS '77)*, Tokyo, Japan, pp. 73–79.
- Stiansen, S.G., Mansour, A.E., 1980. Reliability methods in ship structures. *Journal of RINA* vol. 122, 381–397.
- Sun, H.H., Chen, T.Y., 1997. Buckling strength analysis of ring-stiffened circular cylindrical shells under hydrostatic pressure. In: *ISOPE-97*, Honolulu, pp. 361–366.
- Sun, H.H., Bai, Y., 2001. Time-variant reliability of FPSO hulls. *Transactions of the SNAME* 109.
- Wang, X., Jiao, G., Moan, T., 1996. Analysis of oil production ships considering load combination, ultimate strength and structural reliability. *Transaction of the SNAME* 104, 3–30.
- White, G.J., Ayyub, B.N., 1985. Reliability methods for ship structures. *Journal of Naval Engineers* 97 (4).

Reliability-Based Design and Code Calibration

35.1 General

The most important applications for the structural reliability methods are perhaps the reliability-based design and calibration of the safety factors in the design codes.

In structural design, there are always uncertainties involved in determining loads and capacities. Historically, the engineering design process has compensated for these uncertainties by the use of safety factors. However, with reliability technology, these uncertainties can be considered more quantitatively. Specifically, the use of probability-based design criteria has the promise of producing better-engineered designs. For a marine structure, implementation of a probability-based design code can produce a structure that has, relative to the structure designed by current procedures, (1) a higher level of reliability, (2) lower overall weight (which means cost savings), or (3) both.

35.2 General Design Principles

General design principles used in practice are outlined in this subsection. Reliability-based design is one of the design methodologies, but it is highlighted as a separate section in this chapter.

35.2.1 Concept of Safety Factors

Structural safety measures of different kinds are generally used and referred to without always giving a clear picture about their physical meaning. The safety factor concept is frequently applied without giving any corresponding quantitative measures related to the actual structural safety level. Traditional design practice is based on the application of some kind of deterministic safety measures. The greater the ignorance about an event, the larger the safety factor that should be applied. In principle, the safety factors of the design check of components should depend upon the consequence of failure and the type of structural model.

35.2.2 Allowable Stress Design

The allowable stress design (ASD) criterion has been used for a long time now by use of explicit design formulae, which can be expressed as

$$\sigma \leq \sigma_A \quad \text{where} \quad \sigma_A = \frac{\sigma_L}{\gamma} = \eta \sigma_L \quad (35.1)$$

where σ is the stress in the structures obtained by the linear elastic theory for the maximum loads, σ_A is the allowable stress, σ_L , typically the yield stress, γ is the safety factor, and $\eta (=1/\gamma)$ is the usage factor. In ASD methods, the design check is made at a capacity/load effect level below the first yield of a component.

Linear elastic analyses are used to describe the structure response characteristics for a given nominal design loading. The complexity of the design format depends on the failure mode considered (failure in compression, tension, buckling, etc). Design codes formulate these equations and provide the safety factors to be used. However, there are some objections to the application of ASD due to differences in the uncertainties with the various loads and resistances, and due to the over-design.

The ASD used by the American Institute for Steel Construction (AISC) is called WSD by API RP2A.

35.2.3 Load and Resistance Factored Design

Owing to statistical variability in the applied loads and component resistance, and due to certain assumptions and approximations made in the design procedure, use of a single safety factor for all load combinations cannot maintain a constant level of structural safety. Partial safety factors may generally reflect the inherent uncertainties in load effects and strength, as well as the consequence of failure and the safety philosophy.

The load and resistance factored design (LRFD) procedure was issued by the AISC in 1986. The AISC-LRFD criteria was developed under the leadership of T.V. Galambos, and a series of eight papers was published in the ASCE Journal of the Structural Division—for example, see Ravindra and Galambos (1978).

The American Petroleum Institute (API) extrapolated this technology for offshore structures with the development of API RP2A-LRFD, in 1989.

Loads acting on the structures can be divided into several types such as functional loads and environmental loads. If the concept of multiple load factors is introduced, the LRFD design criterion can be reformulated as

$$R\left(\frac{f_k}{\gamma_m}, \dots\right) \geq S(\gamma_{f_i} \Psi_i Q_k) \quad (35.2)$$

where γ_{fi} are load factors to account for uncertainties in each individual load Q_i , Ψ_i are load combination factors. The safety factor in Eqn (35.2), γ_m , reflects the uncertainty of a given component due to variations in the size, shape, local stress concentrations, metallurgical effects, residual stress, fabrication process, etc. The safety factors applied to loads, γ_f , reflect the uncertainty in estimating the magnitude of the applied loads, the conversion of these loads into stresses, etc.

If R and S are linear functions of f_k and Q_i , respectively, the above format can be written as

$$\phi R(f_k) \geq \sum_{i=1}^m \gamma_{fi} \Psi_i S(Q_{ik}) \quad (35.3)$$

where Ψ_i are load combination factors. In the API–LRFD code, resistance factor $\phi (=1/\gamma_m)$ is defined instead of material factors.

It is emphasized that the safety factors γ_m and γ_{fi} should be seen in conjunction with the definition of the characteristic values of resistance and loads, and the method used to calculate these values. Even if the characteristic values are the same in the design codes for different regions, the safety factors may be different due to the difference in uncertainties involved in the resistance and the load, differences in target safety levels and differences in environmental and soil conditions.

Comparing LRFD with WSD methods, for the LRFD method the loads and capacities are modified by factors representing their statistical uncertainties. This results in a uniform safety for a wide range of loads and load combinations and component types. Even though the LRFD format is similar to the ASD format, there exists a substantially different physical interpretation.

The design format should account for the different load conditions and relevant magnitudes of uncertainties encountered by structures. As briefly reviewed by [Efthymiou et al. \(1997\)](#), load and resistance factors in API-RP2A LRFD were derived based on calibration to the API-RP2A WSD. The objective was to derive load and resistance factors that would achieve, on average, the same calculated component reliabilities as obtained using API-RP2A WSD. To achieve this objective, reliability analyses were used to derive safety indices for components designed to API-RP2A WSD for a range of gravity and environmental load situations and were then averaged to obtain the target safety index for the LRFD code.

35.2.4 Plastic Design

Traditionally, Part 2 of the AISC specification is called “Plastic Design.” Plastic design is a special case of limit-state designs (LSDs), wherein the limit state for strength is the

achievement of the plastic moment strength M_p . Plastic moment strength is the moment strength when all fibers of the cross section are at the yield stress. The design philosophy as per AISC is applied to flexural members such as beam-columns. In recent years, plastic design became a component of LRFD.

35.2.5 Limit-State Design

Marine structures are composed of components (e.g., tubular joints, brackets, and panels) that are subject to different load conditions, including functional loads, environmental loads, and accidental loads, and may fail within different failure modes. Usually, the ultimate limit state (ULS) for a specified failure mode is expressed by a mathematical formula in which uncertainties associating with loads, strength, and models cannot be avoided.

LSD examines the structural condition at failure, comparing a reduced capacity with an amplified load effect for the safety check.

Besides, LSD covers various kinds of failure modes, such as:

- ULS
- Fatigue limit state
- Accidental limit state

The LSD criteria can be formulated in ASD format or LRFD format. The relationship between ASD and LSD has been discussed by, for example, [Song et al. \(1998\)](#) and [Bai and Song \(1997, 1998\)](#).

35.2.6 Life Cycle Cost Design

With the application of structural reliability methodology, an optimum life cycle cost (LCC) of the structural design, meeting complex combinations of economic, operational, and safety requirements can be targeted. These targets may vary in both time and geopolitical location and further, may be continuously affected by technological changes and market forces. To deal with such design targets in structural design, formal procedures of optimization are required to make decisions about materials, configurations, scantlings, etc. In the optimal design process, the key stage is the specification of optimum design targets. General types of design targets may be the cost (initial/operational), the functional efficiency, and the reliability.

By using the LCC design, it is possible to express the total cost of a design alternative in terms of mathematical expression, which can be generically described as

$$\text{TOTAL(NPV)} = \text{CAPEX(NPV)} + \text{OPEX(NPV)} + \text{RISKEX(NPV)} \quad (35.4)$$

where

CAPEX = the capital expenditure of initial investment

OPEX = operational costs

RISKEX = unplanned risk costs

NPV = net present value

One main difficulty that often arises is the identification of costs for accidental situations such as the grounding or collision of ships. In this case, safety is the primary design objective, while economics take on the role of important side constraints. One way to deal with this particular situation is the introduction of high-cost penalties for certain failure modes—for example, a high value of C_F in the following equation

$$C_T = C_I + P_F C_F = C_I + R \quad (35.5)$$

or

$$R = P_F C_F = \sum (P_{F_i} C_{F_i}) = \sum R_i \quad (35.6)$$

where P_{F_i} is the failure rate of a particular mode i , and C_{F_i} is the cost penalty associated with that failure mode.

35.3 Reliability-Based Design

35.3.1 General

The role of a safety factor in traditional deterministic design is to compensate for uncertainties affecting performance. Safety factors evolved through long-term experience. Experience, however, is not always transferable from one class of structures to another, nor can it be readily extrapolated to novel structures. Further, any single class of a traditionally designed structure typically has been found to have a large variability in actual safety levels, implying that resources could perhaps have been more optimally used. Particularly in the context of the present trend toward reliability-based designs, reliability methods are suitable to bridge such gaps in traditional designs. This is because performance uncertainty can be considered both directly and quantitatively with the reliability methodology.

Relative to the conventional factors of safety codes, a probability-based design code has the promise of producing a better-engineered structure. Specific benefits are well documented in the literature:

- A more efficiently balanced design results in weight savings and/or improvements in reliability
- Uncertainties in design are treated more rigorously

- Because of an improved perspective of the overall design process, development of probability-based design procedures can stimulate important advances in structural engineering
- The codes become a living document. They can be easily revised periodically to include new sources of information and to reflect additional statistical data on design factors.
- The partial safety factor format used herein also provides a framework for extrapolating existing design practice to new ships where experience is limited.

Experience has shown that using the probability-based design code results in significant savings in weight. Designers have commented that, relative to the conventional working stress code, the new AISC-LRFD requirements are saving anywhere from 5% to 30% of steel weight, with about 10% being typical. This may or may not be the case for ships and other marine structures.

In reliability-based marine structural designs, the effect of uncertainties in loads, the strength and condition assessments are accounted for directly. Safety measures are calculated in order to assesses the designs or decide on the design targets.

35.3.2 Application of Reliability Methods to the ASD Format

A design equation may be formulated using the ASD format as

$$R_D \geq \eta \cdot S_D \quad (35.7)$$

Alternatively, the safety factor can be referenced to the capacity of the entire structural system. Based on characterization of demands and capacities as lognormally distributed, the usage factor η in ASD can be expressed as (Bea and Craig, 1997)

$$\eta = \alpha \frac{B_S}{B_R} \exp[(\beta\sigma - 2.33\sigma_s)] \quad (35.8)$$

where

η = usage (safety) factor

α = factor that incorporates the interactive dynamic effects—transient loading and dynamic behavior of the system

B_S = median bias in the maximum demand (loading)

B_R = median bias in the capacity of the element

β = annual safety index

σ = total uncertainty in the demands and capacities

σ_s = uncertainty in the annual expected maximum loadings

The number 2.33 in Eqn (35.8) refers to the 2.33 standard deviations from the mean value, or from the 99th percentile. This is equivalent to the reference of the design loading to an

average annual return period of 100 years. In case installation conditions are defined based on a 10-year return period condition, a value of 1.28 should be used (90th percentile).

The transient/dynamic loading—nonlinear performance factor, α , is dependent on the ductility (strain—deformation—deformation capacity), residual strength (load—stress capacity beyond the yield), and hysteric (cyclic load—deformation—damping behavior) characteristics of the structure. It is also dependent on the transient/dynamic loading.

The safety index can be thought of as a type of safety factor; as β gets bigger, the system gets more reliable. The total uncertainty in the demands S and capacities R is determined from

$$\sigma = \sqrt{\sigma_S^2 + \sigma_R^2} \quad (35.9)$$

where

σ_S = uncertainty in the annual maximum demands

σ_R = uncertainty in the capacities of the elements

35.4 Reliability-Based Code Calibrations

35.4.1 General

One of the important applications of the structural reliability methods is to calibrate safety factors in the design format, in order to achieve a consistent safety level. The safety factors are determined so that the calibrated failure probability, $P_{f,i}$ for various conditions, is as close to the target reliability level P_f^T as possible. In the following, the various terms and steps involved in a reliability-based code calibration are defined and presented.

35.4.2 Code Calibration Principles

The scope of the structural design code consists of a class of design cases formed by the possible combinations of:

- Structures
- Materials
- Environmental and soil conditions
- Failure modes or limit states that the code is meant to cover.

The code objective is the target reliability index that corresponds to the safety level, which it is aimed at in the design. For simplicity, in the following, the same β_t is assumed for all limit states covered by the scope of the code. In practice, however, β_t can vary from one limit state to another, if the consequences of the associated failures are different.

The demand function expresses the frequency of occurrence of a particular point in data space—that is, of a certain combination of the structure, material, geographical location, and limit state. The demand function is used to define the weighting factor, w , for the various combinations of structures, materials, and limit states with the scope of the code. The weighting factors thus represent the relative frequency of the various design cases within the scope, and their sum is 1.0. The weighting factors are taken as those that represent the expected future demand. For this purpose, it is common to assume that the demand seen in the past is a representative for the demand in the future.

Because the code cannot be calibrated so that the design exactly meets the target reliability, a closeness measure needs to be defined. This can be expressed in term of a penalty function for a deviation from the target reliability. Several possible choices for the penalty function exist. One that penalizes the over and under-design equally on the β scale is given by

$$M = \sum_i \sum_j \sum_k \sum_l \left(w_{i,j,k,l} (\beta_{i,j,k,l} - \beta_t)^2 \right) \quad (35.10)$$

where M denotes the penalty, $w_{i,j,k,l}$ is the weighting factor for the design case identified by the index set (i,j,k,l) , and $\beta_{i,j,k,l}$ is the reliability index that is obtained for the design case by the design according to the code. This expression for the penalty function M may be interpreted as the expected squared deviation from the target reliability, over the scope of the design cases.

A prime requirement for the calibration of a common set of safety factors for the entire scope of code is that, over the scope of code, the calibrated set of safety factors must lead to designs with safety levels as close as possible to the target. The common set of safety factors is therefore determined as the set γ that minimize the penalty function M .

$$\text{Minimize}\{M\} \quad (35.11)$$

$$\text{subject to: } \beta_{ijkl} \geq \beta_{\min} \quad (35.12)$$

over the scope of the code.

In which β_{\min} is the minimum acceptable reliability index. This is achieved by means of an optimization technique, and this applies if another choice for the penalty function is made, such as one that is more heavily biased against under-design than against over-design.

35.4.3 Code Calibration Procedure

Combining the calibration principles outlined above with a practical design consideration, the following steps should, in general be considered as the proper reliability-based code calibration procedure.

- Step 1: Identify the failure modes for the considered design case
- Step 2: Define design equation
- Step 3: Form limit-state function (LSF)
- Step 4: Measure uncertainties involved in all random variables in LSF
- Step 5: Estimate failure probability
- Step 6: Determine target safety level
- Step 7: Calibrate safety factors
- Step 8: Evaluate the results

35.4.4 Simple Example of Code Calibration

To demonstrate the code calibration principles and procedure, a simple example is given below.

Problem

Assume that a strength design check for a ship's structural details in terms of resistance R and load effect S is given by

$$R_C \geq \gamma \cdot S_C$$

where the characteristic strength, R_C , is

$$R_C = 0.85 \cdot \mu_R$$

and the characteristic load effect, S_C , is

$$S_C = \mu_S$$

μ_R and μ_S are mean values. The corresponding coefficients of variation are $V_R = 0.1$ and $V_S = 0.2$. The standard deviation are given by $\sigma_R = V_R \mu_R$ and $\sigma_S = V_S \mu_S$. Assume that the design check is fulfilled, by checking the equality sign. What value should γ have so that the design check corresponds to a failure probability of 10^{-3} and 10^{-4} , respectively?

Solution

Given

$$R_C = 0.85 \mu_R$$

$$S_C = \mu_S$$

Applies the equality condition in the design check formula

$$R_C = \gamma S_C$$

$$0.85 \mu_R = \gamma \mu_S$$

$$\mu_R / \mu_S = 1.18 \gamma$$

The reliability index, β , is given by

$$\beta = \frac{\mu_R - \mu_S}{\sqrt{\sigma_R^2 + \sigma_S^2}} = \frac{\mu_R - \mu_S}{\sqrt{(V_R\mu_R)^2 + (V_S\mu_S)^2}}$$

Then,

$$\beta = \frac{\mu_R/\mu_S - 1}{\sqrt{0.01 \cdot (\mu_R/\mu_S)^2 + 0.04}} = \frac{1.18\gamma - 1}{\sqrt{0.014\gamma^2 + 0.04}}$$

To reach the failure probability of 10^{-3}

$$\begin{aligned}\Phi(-\beta) &= 10^{-3} \\ \beta &= \frac{1.18\gamma - 1}{\sqrt{0.014\gamma^2 + 0.04}} = 3.09\end{aligned}$$

Hence,

$$\gamma = 1.56$$

To reach the failure probability of 10^{-4}

$$\begin{aligned}\Phi(-\beta) &= 10^{-4} \\ \beta &= \frac{1.18\gamma - 1}{\sqrt{0.014\gamma^2 + 0.04}} = 3.72\end{aligned}$$

Hence,

$$\gamma = 1.76$$

Note that the expression for the reliability index β , assuming μ_R/μ_S follows lognormal distribution, may be defined by

$$\beta = \frac{\ln(\mu_R/\mu_S)}{\sqrt{V_R^2 + V_S^2}}$$

35.5 Numerical Example for Tubular Structure

35.5.1 Case Description

To demonstrate the calibration procedure, a detailed example is given below, which is directly adopted from [Song et al. \(1998\)](#). The case study presented in this study is of a simple T joint with its geometry and notation defined in [Figure 35.1](#).

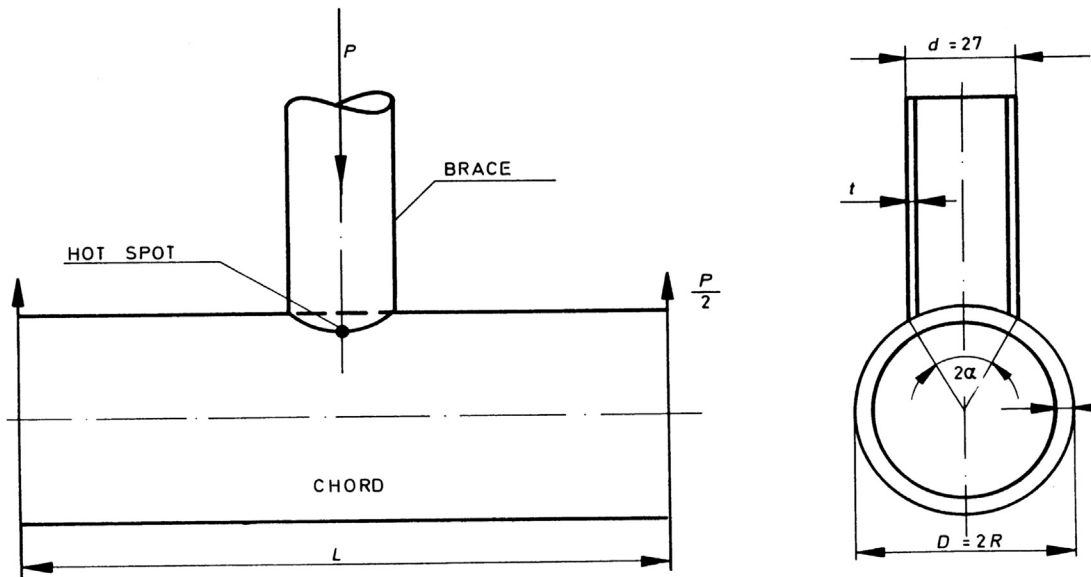


Figure 35.1
Geometric profile of a simple T joint.

35.5.2 Design Equations

A simple tubular joint of fixed offshore platforms is shown in [Figure 35.2](#), in which the terminology and geometric parameters are defined. θ is the brace angle measured from chord, g is the gap between braces, t is the brace thickness, T is the chord thickness, d is the brace diameter, and D is the chord diameter. The nondimensional geometric parameters include: diameter ratio ($\beta = d/D$), chord stiffness ($\gamma = D/2T$), wall-thickness ratio ($\tau = t/T$), chord length parameter ($\alpha = L/D$), gap parameter ($p = g/D$).

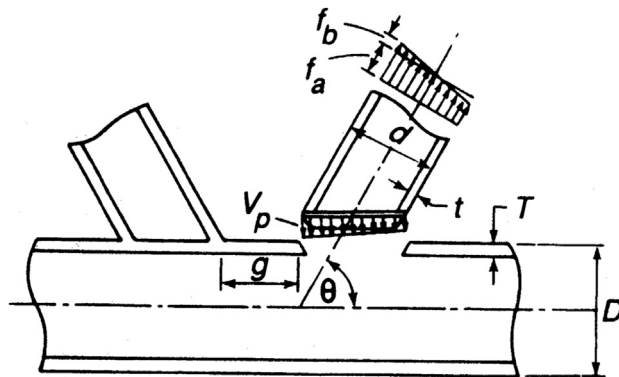


Figure 35.2
Geometric parameters for simple tubular joint connections.

According to API RP2A-LRFD, the strength check of simple joints can be performed based on joint capacity satisfying the following

$$P_D < \phi_j P_{uj} \quad (35.13)$$

$$M_D < \phi_j M_{uj} \quad (35.14)$$

where P_D is the factored axial load in the brace member, P_{uj} is the ultimate joint axial capacity, M_D is the factored bending moment in the brace member, M_{uj} is the ultimate joint bending moment capacity, and ϕ_j is the resistance factor for tubular joints.

The ultimate capacities are defined as (API, 2000)

$$P_{uj} = \frac{F_Y T^2}{\sin\theta} Q_u Q_f \quad (35.15)$$

$$M_{uj} = \frac{F_Y T^2}{\sin\theta} (0.8d) Q_u Q_f \quad (35.16)$$

where F_Y is the yield strength of the chord member at the joint, Q_f is the design factor that accounts for the presence of longitudinal factored load in the chord, and Q_u is the ultimate strength factor that varies with the joint and load type. Detailed determination of these two factors can be referred to the code (API, 2000).

35.5.3 Limit-State Function

Generally, the LSF can be expressed as follows for the convenience of the reliability-based calibration of safety factors,

$$g(Z) = g \left[(\gamma_i Q_i), (\phi_j R_j) \right] \quad (35.17)$$

where Q_i and R_j are sets of random variables of load effect and strength (resistance) respectively; γ_i and ϕ_j are partial safety factors to be calibrated for Q_i and R_j .

LSF can be formed based on failure criteria for the specified case. The failure criterion considered here for a simple tubular joint is defined as the exceedance of the static strength in compliance with the API code check. The LSF based on ultimate static strength criterion can be formulated as

$$g(Z) = \phi_j \frac{F_Y T^2}{\sin\theta} Q_u Q_f - P_D \quad (35.18)$$

$$g(Z) = \phi_j \frac{F_Y T^2}{\sin\theta} (0.8d) Q_u Q_f - M_D \quad (35.19)$$

35.5.4 Uncertainty Modeling

The main goal of the uncertainty analysis is to identify and quantify the different sources of uncertainties that are present, and to decide how to consider them for the subsequent reliability analysis. Uncertainty is measured by the probability distribution function and its statistical values.

Considering uncertainties involved in the LSF, each random variable X_i may be specified as

$$X_i = B_X \cdot X_C \quad (35.20)$$

where X_C is the characteristic value of X_i , and B_X is a normalized variable reflecting the uncertainty in X_i .

Besides the model uncertainty discussed above, other major uncertainties considered in this study include:

Yield strength uncertainty X_y : Uncertainty for yield strength, usually depends on the quality of the material used for tubular joints and manufacturing specifications. A normal distribution can be applied to measure this uncertainty with a COV = 2–5%.

Diameter uncertainty X_d : This is caused by fabrication and measurement. Due to the large enough diameter, the COV of this uncertainty is not expected to be large.

Wall-thickness uncertainty X_t : This uncertainty is due to fabrication and measurement. The uncertainty in the chord and brace thickness is considered by bias X_t following a normal distribution.

Load uncertainty X_s : This is due to the uncertainties or variability in environmental descriptions and loads calculation. For a sea state defined by a constant significant wave height and a total number of waves, Rayleigh distribution is usually applied to model the distribution of the largest wave. The COV of the foregoing distributions is a useful parameter characterizing the short-term variability, which may vary with types of storms from 7.5% to 15% (Efthymiou et al., 1997). The wave loads variability given by COV arises from the natural variability in wave height. The deficiencies in the wave theory, force coefficients, are also causing the uncertainty in wave load calculation. From full-scale measurements, it suggests that the wave load methods are not significant. Based on comparisons of some studies, the wave force model uncertainty is represented by COV = 8%. This representation is expected to be on the conservative side (Efthymiou et al., 1997). This uncertainty is included in the analysis by introducing a bias factor X_S with a COV into the LSF. Presently, a lognormal distribution is applied for this uncertainty.

Ultimate strength uncertainty X_R : The ultimate strength of offshore frame structures are primarily governed by the strength characteristics of members (braces) in compression or tension and the strength of tubular joints under axial loadings. For these critical

Table 35.1: Basic probabilistic parameter descriptions

Random Variable	Distribution	Mean	COV
Model uncertainty, X_m	Lognormal	1.16	0.138
Yield strength uncertainty, X_y	Lognormal	1.14	0.04
Diameter uncertainty, X_D	Normal	1.02	0.02
Thickness uncertainty, X_T	Normal	1.04	0.02
Load uncertainty, X_S	Lognormal	0.90	0.08
Strength uncertainty, X_R	Lognormal	1.05	0.05

components, the uncertainty in component strength is adequately represented by $COV = 10\%$, as indicated by the strength databases both in the US and Europe (Eftymiou et al., 1997). When a number of members are involved in the collapse mechanism, the uncertainty in the system strength reduces. This implies, if the method of nonlinear analysis is sufficiently accurate, the variability in system strength is less than 10% for ductile systems.

By introducing those considered uncertainties into LSF, the LSF can be re-expressed simply as

$$g(Z) = X_Y X_T^2 X_R X_m - \phi X_S \quad (35.21)$$

$$g(Z) = X_Y X_T^2 X_d X_R X_m - \phi X_S \quad (35.22)$$

The reliability analysis is based on the probabilistic data given in Table 35.1.

35.5.5 Target Safety Levels

When carrying out structural reliability analysis, appropriate safety levels should be selected based on factors like consequence of failure, relevant rules, access to inspection and repair, etc; it is termed as the target safety level. Target safety levels must be met in the design in order to ensure that certain safety levels are achieved.

Any evaluation of safety levels should be based on information regarding the safety level implied by the design codes and components with historical data on reported failures. The safety level of existing tubular joints designed according to traditional procedures may be a good reference for the target level if reliability is generally satisfactory. It is important to state that this is related to the average failure rate only, as there is expected to be a large variability in the real safety from one tubular joint to another, due to differences and shortcomings in past design practices. The target safety level should further be related to the consequences of failure modes as well as the nature of failure, and it may be found that the target reliability level should be increased or even could be decreased concerning specific failure modes.

Table 35.2: Recommended target safety level

Safety Classes	Target	Safety
Low	$P_F = 10^{-2}$	$\beta = 2.32$
Normal	$P_F = 10^{-3}$	$\beta = 3.09$
High	$P_F = 10^{-4}$	$\beta = 3.72$

A target safety level normally reflects the consequences of failure, the safety philosophy, the access to inspection and repair, and the behavior of the structural components. Safety classes are generally based mainly on the consequences and types of failure, which can be generally divided into a low, normal, and high safety class, depending on the considered platform and components (Table 35.2).

Low safety class: where failure of a component or tubular joint implies no risk to human safety and environmental damage. When certain damage is found in this class, its condition can be monitored, and no other necessary measures need to be applied.

Normal safety class: where failure implies negligible risk to human safety, minor danger to the main part of the platform, minor damages to the environment, and certain economic loss.

High safety class: where failure implies risk to the total safety of the platform so as to human safety and environmental pollution. High economic loss cannot be avoided.

35.5.6 Calibration of Safety Factors

Besides the direct use of the reliability calculation for a tubular joint design, representing a full probabilistic design, reliability methods can also be used indirectly for the design purpose based on a calibrated design check with the main goal of obtaining a uniform safety level. The main objective of reliability-based calibration of tubular joint design is to achieve the optimal set of partial safety factors based on a uniform reliability level.

Since the joints have been divided into three classes with low, normal, and high safety, different safety factors can be applied according to the safety class of the considered joints. The influence of the safety factor applied in the design on the reliability index is given in Figure 35.3. It is recommended that safety factors corresponding to low, normal, and high classes of safety are of 1.1, 0.95, and 0.86 respectively. It must be pointed out that the calibrated safety factor might be different from the practical applied safety factor. A necessary modification based on practical engineering judgment should be applied to the calibrated safety factor. The existing experience with use of safety factors for the specified tubular joints should be considered in the judgment.

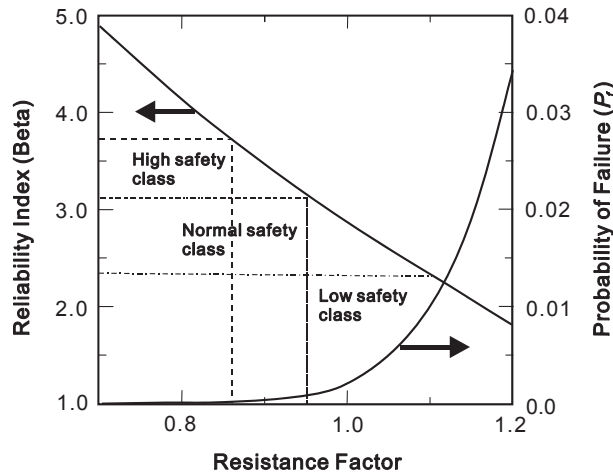


Figure 35.3

Calibration of safety factor for tubular joint design.

35.6 Numerical Example for Hull Girder Collapse of FPSOs

With a reference to Part II, Chapter 13 and Part IV, Chapter 25, this section presents a reliability-based calibration for hull girder collapse for FPSO (Sun and Bai, 2001). The bending moment criteria can be expressed as

$$\gamma_s M_s + \gamma_w \phi_w M_w \leq \phi_u M_u \quad (35.23)$$

where γ_s , γ_w , and ϕ_u are partial safety factors.

Selecting target reliability levels is a difficult task and should be based on the consequences of failure, reliability formulation, accessibility to inspection, and the possibility of repair.

Three methods have been applied (Mansour, 1997):

1. Agreeing upon a “reasonable” value in the case of novel structures without prior experience
2. Calibrating reliability levels implied in currently used design codes (commonly used for code revision)
3. Cost–benefit analysis. Target reliability is chosen to minimize total expected costs over the service life of the structure. This method is preferred but is impractical due to the data requirements of the method.

Mansour (1997) reviewed the sources of information on target reliabilities and suggested that the reliability index for the collapse strength of commercial ships be set at 3.5.

Guedes Soares et al. (1996), suggested that the tentative reliability indices against hull

Table 35.3: Variable reference measurements

Variable	Description
M_u	Ultimate strength, lognormal variable, mean = undermined, COV = 0.10
M_s	SWBM, type I extreme variable
M_w	VWBM, type I extreme variable
ϕ_w	Load reduction factor
χ_u	Model error of predicting ultimate strength, normal variable, mean = 1, COV = 0.05
χ_s	Model error of predicting SWBM, normal variable, mean = 1, COV = 0.1
χ_w	Model error of predicting VWBM, normal variable, mean = 1, COV = 0.24 (sagging condition)
β^0	Target annual reliability index in new-built state $\beta^0 = 3.7$
β^c	Target annual reliability index in corroded state $\beta^c = 3.0$

girder collapse be set at 3.7 for the “as-built” state and 3.0 for the lower limit of corroded hulls. This is based on their investigation of worldwide causalities and structural safety levels implicitly built into present-day ship design practice. The corroded state was defined as such that the section modulus was 90% of the original (“new-built”). Two methods can be used to evaluate the partial safety factors: γ_s , γ_w , and ϕ_u are given by the ratio of the design value of the variables to the corresponding nominal value. The design value is the most likely failure point as calculated by the first-order reliability method. The following relationships can be derived (Mansour, 1997)

$$\gamma_s = \frac{\chi_s^* M_s^*}{M_s^n}, \gamma_w = \frac{\chi_w^* M_w^*}{M_w^n}, \phi_u = \frac{\chi_u^* M_u^*}{M_u^n}$$

where X^* is design value and X^n is the nominal value.

For a given target reliability index β_0 , characteristics for the strength (COV) and the probability distribution of load effects, the partial safety factors, and the minimum required strength can all be determined by the first-order reliability method.

Table 35.3 is used to define guidance for the hull girder strength design.

Figures 35.4 and 35.5 show the required ultimate strength of a new-built and converted FPSO as a function of the environmental severity factor and the geometric parameter Ψ defined by the combination of principal particulars—for example,

$$\Psi = C_w L^2 B (C_B + 0.7) \quad (35.24)$$

The numerical range of Ψ is between 1.3757×10^8 and 5.2879×10^8 , which covers the length of 180–260 m, the breadth of 30–46 m, and block coefficient of 0.80–0.92 according to the principal particulars of most existing FPSOs (MacGregor et al., 2000). The symbols of A1–A5 in Figures 35.4 and 35.5 represent the values of Ψ being

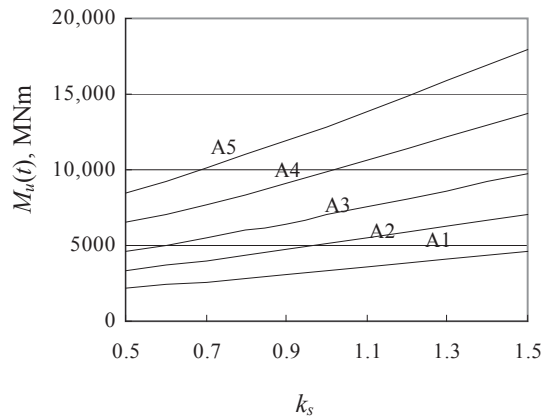


Figure 35.4

Effect of environmental severity factor and ship's principal particulars on minimum required ultimate strength for a new-built FPSO.

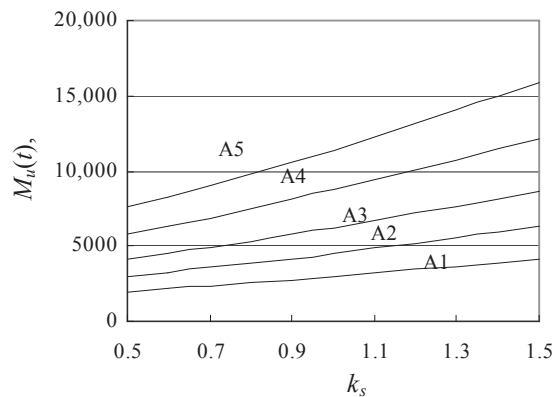
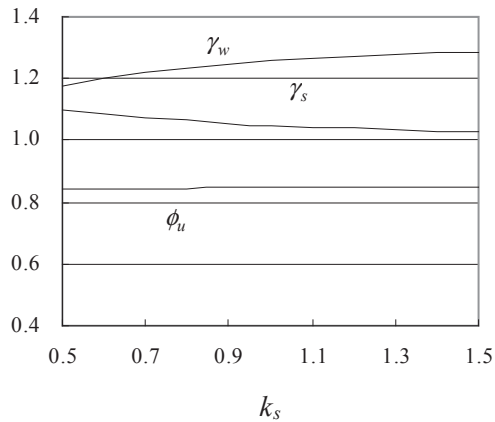


Figure 35.5

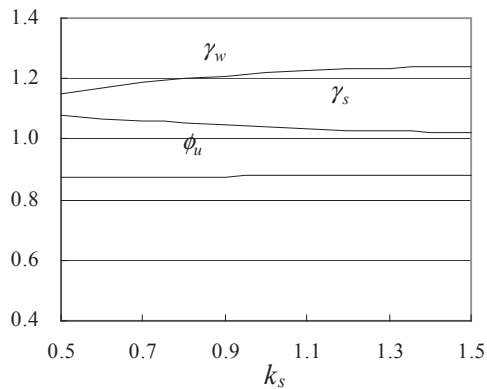
Effects of the environmental severity factor and the ship's principal particulars on minimum required ultimate strength for a converted FPSO.

1.3757×10^8 , 2.0884×10^8 , 2.8879×10^8 , 4.0504×10^8 , and 5.2879×10^8 respectively. With the increase of the environmental severity factor or the dimension parameter Ψ , the required ultimate strength increases. The required ultimate strength is approximately a bilinear function of the environmental severity factor, and of the geometric parameter Ψ .

Other results from current calculations are the partial safety factors. It is found that the resistance factor is slightly dependent on the environmental severity factor and independent of the geometric parameter Ψ . The relationships between the partial safety factors and the environmental severity factors are shown in [Figures 35.6 and 35.7](#) for new-built and converted FPSO.


Figure 35.6

Partial safety factors versus k_s for a new FPSO.


Figure 35.7

Partial safety factors versus k_s for a converted FPSO.

In accordance with the results of [Figures 35.4 and 35.5](#), the following two regressive formulas have been obtained.

For a new-built FPSO

$$M_u = -0.065(1 + 2.778k_s)C_wL^2B(C_B + 0.7) \quad (35.25)$$

For a converted FPSO

$$M_u = -0.060(1 + 2.635k_s)C_wL^2B(C_B + 0.7) \quad (35.26)$$

It should be emphasized that the above formulas cannot be interpreted in an absolute way, and the numbers cited should only be considered guidance. However, the methodology can

be applied to develop structural design criteria for new-built FPSOs and converted FPSOs, when sufficient data are available.

35.7 LRFD Example for Plates of Semisubmersible Platforms

35.7.1 Case Description

In this case, the ultimate strength f_u , which causes the collapse of a plate between stiffeners, is given by one of the following two cases.

1. For $a/b > 1.0$,

$$f_u = \begin{cases} F_y \sqrt{\frac{\pi^2}{3(1-\nu^2)B^2}} & (B \geq 3.5) \\ F_y \left(\frac{2.25}{B} - \frac{1.25}{B^2} \right) & (1.0 \leq B < 3.5) \\ F_y & (B < 1.0) \end{cases} \quad (35.27)$$

2. For $a/b < 1.0$,

$$f_u = F_y \left[\alpha C_u + 0.08(1-\alpha) \left(1 + \frac{1}{B^2} \right) \right]^2 \leq F_y \quad (35.28)$$

where F_y = yield strength (stress) of plate, a = length or span of plate, b = distance between longitudinal stiffeners, $B = \frac{b}{t} \sqrt{\frac{F_y}{E}}$, $\alpha = a/b$, t = thickness of the plate, E = the modulus of elasticity, ν = Poisson's ratio, and

$$C_u = \begin{cases} \sqrt{\frac{\pi^2}{3(1-\nu^2)B^2}} & (B \geq 3.5) \\ \frac{2.25}{B} - \frac{1.25}{B^2} & (1.0 \leq B < 3.5) \\ 1.0 & (B < 1.0) \end{cases} \quad (35.29)$$

In this case, the target reliability index is set to be from 3.0 to 4.0, and the loads acting on the plates of semisubmersible platforms can be categorized into three main types: Still-water loads, wave loads, and dynamic loads. Under this condition, the load and resistance factors for the design format can be described as

$$0.96f_u \geq 1.07f_s + k_w(1.64f_w + 1.17k_D f_D) \quad (35.30)$$

Table 35.4: Ranges of key parameters

Parameter	Ranges
β	3.0, 3.5, and 4.0
COV (f_u)	0.02 and 0.05
f_s/\bar{f}_W	0.2, 0.3, and 0.4
f_D/\bar{f}_W	0.25, 0.30, and 0.35

Table 35.5: Probabilistic characteristic of strength and loads

Random Variable	COV (Recommended)	Distribution Type	Total Bias
f_u	0.02–0.05 (0.04)	Lognormal	1.16
f_s	0.15 (0.15)	Normal	0.7
f_W	0.1–0.2 (0.15)	Type I largest	1.0
f_D	0.2–0.3 (0.25)	Type I largest	1.0

Change this format into LSF as

$$g = f_u - f_s - k_W(f_W + k_D f_D) \quad (35.31)$$

where f_u is the ultimate strength for plates under uniaxial compression, f_s = stress due to still-water bending moment, f_W = stress due to waves bending moment, f_D = stress due to dynamic bending moment, k_W = load combination factor that equals 1.0 and k_D = load combination factor that equals 0.7.

The mean values of still-water, wave, and dynamic stresses are given in the form of a ratio of f_s/\bar{f}_W as shown in Table 35.4. The table also shows the ranges of the target reliability index and the uncertainty (COV) in the strength f_u . The probabilistic characteristics for both the strength and the loads are summarized in Table 35.5.

35.7.2 Design Steps

Dimensionless Random Variables.

The ratio of different loads can be categorized by statistical results. A variable conversion is below.

$$f_u/\bar{f}_W = X_1 \quad (35.32)$$

$$f_s/\bar{f}_W = X_2 \quad (35.33)$$

$$k_W * (f_W/\bar{f}_W) = X_3 \quad (35.34)$$

$$k_W * k_D * (f_D/\bar{f}_W) = X_4 \quad (35.35)$$

Table 35.6: A set of data input

Input	X_1		X_2		X_3		X_4		β_0
1	μ	COV	μ	COV	μ	COV	μ	COV	3.0
	2.5	0.04	0.2	0.15	1.0	0.15	0.25	0.25	

According to this conversion, the LSF can be changed as

$$g = X_1 - X_2 - X_3 - X_4 \quad (35.36)$$

A case, for example, is ($\beta_0 = 3.0$)

As described in Table 35.6, a set of data is input, and the target reliability index β_0 is chosen to be 3.0.

So, using the software MATLAB,

$$\mu_{X_i} = [2.5, 0.2, 1.0, 0.25], \text{COV}_{X_i} = [0.04, 0.15, 0.15]$$

1. Assume a design point x_i^* and obtain $x_i'^*$ in the reduced coordinate using the following equation.

$$x_i'^* = \frac{x_i^* - \mu_{X_i}}{\sigma_{X_i}} \quad (35.37)$$

where, $x_i'^* = -\alpha_i^* \beta$, μ_{X_i} = mean value of the basic random variable, and σ_{X_i} = stand deviation of the basic random variable. The notation x_i^* and $x_i'^*$ are used respectively for the design point in the regular coordinates and in the reduced coordinates. The mean values of the basic random variables μ_{X_i} can be used as initial values for the design points.

2. Evaluate the equivalent normal distributions for the nonnormal basic random variables at the design point using the following equations.

$$\mu_X^N = x^* - \Phi^{-1}(F_X(x^*))\sigma_X^N \quad (35.38)$$

$$\sigma_X^N = \frac{\phi(\Phi^{-1}(F_X(x^*)))}{f_X(x^*)} \quad (35.39)$$

where, μ_X^N = mean of the equivalent normal distribution, σ_X^N = standard deviation of the equivalent normal distribution, $F_X(x^*)$ = original (nonnormal) cumulative distribution function (CDF) of x_i^* evaluated at the design point, $f_X(x^*)$ = original probability density function (PDF) of x_i^* evaluated at the design point, $\Phi(\cdot)$ = CDF of the standard normal distribution, $\phi(\cdot)$ = PDF of the standard normal distribution.

The results of means and standard deviation of the equivalent normal distribution is evaluated as: $\mu_{X_i}^N = [2.498, 0.2, 0.9746, 0.2394]$, $\sigma_{X_i}^N = [0.0981, 0.03, 0.1434, 0.0598]$.

3. Compute the directional cosines at the design point (α_i^* , $i = 1, 2, \dots, n$) using the following equations.

$$\alpha_i^* = \frac{\left(\frac{\partial g}{\partial x_i'}\right)_*}{\sqrt{\sum_{i=1}^n \left(\frac{\partial g}{\partial x_i'}\right)_*^2}} \quad (35.40)$$

where

$$\left(\frac{\partial g}{\partial x_i'}\right)_* = \left(\frac{\partial g}{\partial x_i}\right)_* \sigma_{X_i}^N \quad (35.41)$$

Calculated as $\alpha_i^* = [0.5271, -0.1612, -0.7706, -0.3213]$

4. $\alpha_i^* \mu_{X_i}^N$ and $\sigma_{X_i}^N$ are now known, and the following equation can be solved for the root β

$$g\left[\left(\mu_{X_1}^N - \alpha_{X_1}^* \sigma_{X_1}^N \beta\right), \dots, \left(\mu_{X_n}^N - \alpha_{X_n}^* \sigma_{X_n}^N \beta\right)\right] = 0 \quad (35.42)$$

Calculated as $\beta = 5.825$.

5. Using the β obtained in Step 4, a new design point can be obtained from the following equation.

$$x_i^* = \mu_{X_i}^N - \alpha_i^* \sigma_{X_i}^N \beta \quad (35.43)$$

Calculated as $x_i^* = [2.197, 0.228, 1.618, 0.351]$

6. Repeat Steps 1–5, and do the following loop calculation.
If $\beta - \beta_0 > 0.01$,

$$\mu(R^*) = \mu(R^*) - \mu(R^*)/100 \quad (35.44)$$

If $\beta - \beta_0 < 0.01$,

$$\mu(R^*) = \mu(R^*) + \mu(R^*)/100 \quad (35.45)$$

Convergence value β and μ_R are 3.00988 and 2.11296, respectively (See [Table 35.7](#)).

The mean value of the resistance and the design point can be used to compute the required mean partial design safety factors as follows:

$$\phi' = \frac{R^*}{\mu_R} \quad (35.46)$$

$$\gamma'_i = \frac{L_i^*}{\mu_{L_i}} \quad (35.47)$$

Table 35.7: Data input

Input Number	X_1		X_2		X_3		X_4		β_0
	μ	COV	μ	COV	μ	COV	μ	COV	
1	2.5	0.04	0.2	0.15	1.0	0.15	0.25	0.25	3.0
2	2.5	0.04		0.15	1.0	0.15		0.25	3.5
3	2.5	0.04		0.15	1.0	0.15		0.25	4.0
4	2.5	0.04	0.2	0.15	1.0	0.15	0.30	0.25	3.0
5	2.5	0.04		0.15	1.0	0.15		0.25	3.5
6	2.5	0.04		0.15	1.0	0.15		0.25	4.0
7	2.5	0.04	0.2	0.15	1.0	0.15	0.35	0.25	3.0
8	2.5	0.04		0.15	1.0	0.15		0.25	3.5
9	2.5	0.04		0.15	1.0	0.15		0.25	4.0
10	2.5	0.04	0.3	0.15	1.0	0.15	0.25	0.25	3.0
11	2.5	0.04		0.15	1.0	0.15		0.25	3.5
12	2.5	0.04		0.15	1.0	0.15		0.25	4.0
13	2.5	0.04	0.3	0.15	1.0	0.15	0.30	0.25	3.0
14	2.5	0.04		0.15	1.0	0.15		0.25	3.5
15	2.5	0.04		0.15	1.0	0.15		0.25	4.0
16	2.5	0.04	0.3	0.15	1.0	0.15	0.35	0.25	3.0
17	2.5	0.04		0.15	1.0	0.15		0.25	3.5
18	2.5	0.04		0.15	1.0	0.15		0.25	4.0
19	2.5	0.04	0.4	0.15	1.0	0.15	0.25	0.25	3.0
20	2.5	0.04		0.15	1.0	0.15		0.25	3.5
21	2.5	0.04		0.15	1.0	0.15		0.25	4.0
22	2.5	0.04	0.4	0.15	1.0	0.15	0.30	0.25	3.0
23	2.5	0.04		0.15	1.0	0.15		0.25	3.5
24	2.5	0.04		0.15	1.0	0.15		0.25	4.0
25	2.5	0.04	0.4	0.15	1.0	0.15	0.35	0.25	3.0
26	2.5	0.04		0.15	1.0	0.15		0.25	3.5
27	2.5	0.04		0.15	1.0	0.15		0.25	4.0

The strength factors are generally less than one, whereas the load factors are greater than one. According to this set of data, the mean load and resistance factors are as follows:

Mean strength reduction factor (ϕ_{fu}) = 0.965611.

Mean still-water load factor (γ_{fs}) = 1.03481.

Mean wave-induced load factor (γ_{fw}) = 1.64282.

Mean dynamic load factor (γ_{fd}) = 1.08861.

35.7.3 Statistical Results

The data input of LRFD for plates of semisubmersible platforms is given as the [Table 35.7](#), and according to the MATLAB software, the partial safety factors under different safety levels are obtained and the statistical results are shown in [Table 35.8](#).

Table 35.8: Data output

Output Number	ϕ_{fu}	γ_{fs}	γ_{fw}	γ_{fD}	β	$\mu(R)$
1	0.965611	1.03481	1.64282	1.08861	3.00988	2.11296
2	0.962692	1.03568	1.84032	1.09308	3.50956	2.32551
3	0.959579	1.03627	2.06441	1.09617	4.00997	2.56727
4	0.965261	1.03474	1.63128	1.12667	3.00995	2.1495
5	0.962317	1.03563	1.82818	1.13326	3.50989	2.36231
6	0.959225	1.03624	2.04926	1.13778	4.00502	2.60151
7	0.964932	1.03464	1.61543	1.17194	3.00977	2.18614
8	0.961958	1.03557	1.81118	1.18178	3.50989	2.39909
9	0.958818	1.0362	2.03363	1.18862	4.00979	2.64083
10	0.964484	1.05214	1.63511	1.08838	3.00986	2.22007
11	0.96153	1.05347	1.83225	1.09294	3.50978	2.43316
12	0.9584	1.05437	2.05583	1.09607	4.00999	2.67525
13	0.964139	1.05203	1.6236	1.12633	3.00995	2.25666
14	0.961161	1.05341	1.81992	1.13305	3.50969	2.46981
15	0.958079	1.05432	2.03847	1.13761	4.00038	2.70714
16	0.963817	1.05188	1.60775	1.17143	3.00963	2.29329
17	0.960806	1.05332	1.80294	1.18146	3.50968	2.50663
18	0.957645	1.05427	2.02502	1.18841	4.00977	2.74888
19	0.963354	1.0694	1.62548	1.08808	3.0096	2.329
20	0.960361	1.07123	1.8221	1.09276	3.50963	2.54261
21	0.957211	1.07245	2.04505	1.09595	4.00951	2.78499
22	0.963014	1.06926	1.61398	1.12589	3.00963	2.36562
23	0.960043	1.07112	1.80652	1.13269	3.50174	2.57575
24	0.956891	1.07238	2.02782	1.13743	4.00018	2.81706
25	0.981421	1.0696	1.64151	1.17358	3.00731	2.40149
26	0.959643	1.07102	1.79291	1.18106	3.50968	2.61625
27	0.956457	1.07232	2.01456	1.18815	4.00998	2.85907

According to the output data from the table, data statistics under each reliability index can be made from taking the minimum coefficient of resistance, and the maximum load factor. This value method can more effectively ensure the safety of the structure, and improve the reliability of the structure. Statistical results are shown below in [Table 35.9](#).

The resulting partial safety factors can be used, for example, to design the ultimate capacity of a plate under a combination of still-water, wave-induced, and dynamic bending moments by satisfying the following design criterion ($\beta_0 = 3.0$).

Table 35.9: Results of PSF under different safety levels

β_0	ϕ_{fu}	γ_{fs}	γ_{fw}	γ_{fD}
3.0	0.96	1.07	1.64	1.17
3.5	0.96	1.07	1.84	1.18
4.0	0.96	1.07	2.06	1.18

$$0.96f_u \geq 1.07f_s + k_w(1.64f_w + 1.17k_{DFD}) \quad (35.48)$$

Therefore, reliability-based design rules can be expressed in the designs of various hull structural elements.

References

- AISC, 1986. Load and resistance factor design. In: Manual of Steel Construction. American Institute of Steel Construction, Chicago.
- API, 1989. Recommended Practice for Planning, Designing and Constructing Fixed Offshore Platforms—Load and Resistance Factor Design. API RP2A-LRFD. American Petroleum Institute, TX.
- API, 2000. Recommended Practice for Planning, Designing and Constructing Fixed Offshore Platforms—Working Stress Design. API RP2A-WSD. American Petroleum Institute, Washington.
- Bai, Y., Song, R., 1997. Fracture assessment of dented pipes with cracks and reliability-based calibration of safety factors. *International Journal of Pressure Vessels and Piping* 74, 221–229.
- Bai, Y., Song, R., 1998. Reliability-based limit state design and requalification of pipelines. In: *Proceedings of 17th Offshore Mechanics and Arctic Engineering (OMAE'98)*, Portugal, July, 1998.
- Bea, R., Craig, M., 1997. Reliability based load and resistance factor design guidelines for offshore platforms to resist earthquakes. In: *Proc. 16th OMAE*, Yokohama, Japan.
- Efthymiou, M., Van, J.W., Tromans, P.S., Hines, I.M., May 1997. Reliability-based criteria for fixed steel offshore platforms. *Journal of OMAE* 119, 120–124.
- Guedes Soares, C., Dogliani, M., Ostergaard, C., Parmentier, G., Terndrup Pedersen, P., 1996. Reliability based ship structural design. *Transactions of the SNAME* 104, 375–389.
- MacGregor, J.R., et al., 2000. Design and construction of the FPSO vessel for the Schiehallion Field. *Transactions of the RINA* 142, 270–304.
- Mansour, A.E., 1997. Assessment of Reliability of Ship Structures. SSC-398, Report of Ship Structures Committee.
- Ravindra, M.K., Galambos, T.V., 1978. Load and resistance factor design for steel. *Journal of the Structural Division* 104, 1337–1353.
- Song, R., Tjelta, E., Bai, Y., 1998. Reliability-based calibration of safety factors for tubular joint design. In: *Proc. 8th International Offshore and Polar Engineering Conference (ISOPE'98)*, Montreal, Canada, May, 1998.
- Sun, H.H., Bai, Y., 2001. Time-variant reliability of FPSO hulls. *SNAME Transactions* 109.

Fatigue Reliability

36.1 Introduction

In conventional strength assessments, the safety of the marine structure is considered under a static maximum design load. However, marine structures are to a large extent affected by stresses that vary over time. The causes of these stresses are the forces generated by a seaway and a propulsion plant, but also can be generated by changes in the cargo loading.

The failure behavior of a structure subjected to fatigue loading, deviates significantly from that of a structure subjected only to static loading. Static loading can give rise to various forms of failure such as yielding, instability, or brittle fracture. Such failure occurs under a single extreme load. The damage caused by fatigue loading can be outlined as follows: In the crack initiation phase, microscopic fatigue cracks are formed as the result of an accumulation of alternating plastic deformations. Here local structural changes, precipitation, microstructure changes, etc. can occur. Further in the course of the damage, the fatigue crack develops out of one or more microcracks running along slip bands.

Fatigue is a typical failure mode for in-service structures. Proper prediction of fatigue behavior is of vital importance to maintain a sufficient level of reliability and integrity in structures.

High-cycle fatigue is a governing design criterion for certain welded components in marine structures with large dynamic loadings, high stress concentrations and high stress levels due to the use of high-strength steel, notably brace-to-deck connections. Fatigue may be of concern for the primary strength of ships. However, most fatigue cracks have been experienced in secondary members, such as transverse frames, especially in joints between longitudinal stiffeners and frames.

A large uncertainty is introduced in fatigue assessment, due to various assumptions and hypotheses. Additional uncertainties are due to the lack of the data, and inherent random nature exists in the analysis. This necessitates the use of statistical and reliability approaches.

The fundamentals of fatigue strength assessment for ships and other marine structures are explained, for example, in Part IV of this book and by [Almar-Næss \(1985\)](#), [Rice et al. \(1988\)](#), and [Maddox \(1991\)](#), among others.

36.2 Uncertainty in Fatigue Stress Model

36.2.1 Stress Modeling

The process of computing stresses in a component includes the following steps:

1. Defining and modeling the environment
2. Translating the environment into forces on the structure
3. Computing the response of the structure to the environmental loads
4. Computing nominal stresses in the components
5. Computing the stresses to be used for design—for example, the stress at points of stress concentration. Assumptions are made at each step, and all assumptions contain some uncertainty.

36.2.2 Stress Modeling Error

A simple way to measure the stress modeling error is to define a model uncertainty, with a random variable B ; see Part IV, Chapters 31 and 33.

$$S_a = B \cdot S \quad (36.1)$$

where

B = bias that quantifies the modeling error

S_a = actual stress

S = estimated stress

Several sources can contribute to the model uncertainty—for example, [Wirsching and Chen \(1988\)](#):

B_M = manufacturing fabrication and assembly operation

B_S = sea state description

B_F = wave force prediction

B_N = nominal member loads

B_H = estimation of the stress concentration factor (SCF) in stress analysis. Using these five bias factors, the following representation of B is obtained:

$$B = B_M \cdot B_S \cdot B_F \cdot B_N \cdot B_H \quad (36.2)$$

Assuming that each random variable is lognormally distributed, the mean and the COV of B are respectively

$$\bar{B} = \prod_i \bar{B}_i \quad (36.3)$$

where $i = M, S, F, N,$ and H , and the COV is

Table 36.1: Levels of uncertainty in stress prediction

Level	Coefficient of Variation C_B	Tolerance Level ^a
1	0.30	0.55–1.80
2	0.25	0.61–1.65
3	0.20	0.67–1.50
4	0.15	0.74–1.35

^aAssume: (1) $\tilde{B} = 1.0$; (2) B has a lognormal distribution; and (3) tolerances based on ± 2 standard deviations.

$$C_B = \sqrt{\prod_i (1 + C_i^2)} - 1 \quad (36.4)$$

Four levels of refinement for stress analysis are possible as shown in Table 36.1. Note that the intervals are not symmetric because the lognormal is not symmetric.

Some general guidelines regarding the choice of level are:

- | | |
|---------|--|
| Level 1 | Use of a safety check expression using design stress. Default values are assumed for the Weibull shape parameter and the service life. There is little confidence in the estimates of the loads. |
| Level 2 | The Weibull model for long-term stress ranges is used. Reasonable estimates of the parameters are available. |
| Level 3 | The Weibull model for long-term stress ranges is used with good estimates of the parameters obtained from tests on similar ships. The histogram and/or spectral methods with only moderate confidence of the parameters. |
| Level 4 | A comprehensive dynamic and structural analysis of the ship over its predicted service history has been performed as the basis for the input for the histogram or spectral method. |

36.3 Fatigue Reliability Models

36.3.1 Introduction

The calculation of the fatigue damage for a structural detail is based on several variables. Each of these variables is, to some extent, random. In order to account for this randomness, implicit and explicit safety factors are used. The safety factors are rather subjective measures that are calibrated based on past experiences. Information about the degree of uncertainty of different variables cannot be used effectively.

The reliability theory offers a way to include the uncertainty information in the fatigue damage calculation. It allows calculating the component reliability—that is, the probability that a detail has failed at the end of the specified lifetime. Using system reliability, it is possible to evaluate the reliability of a system of structural details.

A probabilistic approach to fatigue life prediction consists of probabilistic methods applied in combination with either the S–N approach or the fracture mechanics (FM) approach. Probabilistic analysis in combination with the S–N approach is usually carried out at the structural design stage while the probabilistic analysis of remaining life after inspection is usually based on FM techniques.

This section documents the fatigue reliability models; there are many papers on this subject—for example, [Wirsching \(1984\)](#), [White and Ayyub \(1987\)](#), [Hovde and Moan \(1994\)](#), [Xu and Bea \(1997\)](#), and [Wirsching and Mansour \(1997\)](#).

36.3.2 Fatigue Reliability—S–N Approach

Based on Part III, Chapter 27, the cumulative fatigue damage in a period with N_0 cycles can be expressed as

$$D = \frac{N_0}{K} \cdot \frac{S_0^m}{(\ln N_0)^{m/\xi}} \Gamma\left(1 + \frac{m}{\xi}\right) \quad (36.5)$$

where K and m are material parameters, and $\Gamma(\cdot)$ is the gamma function. S_0 and ξ are the maximum stress range and the Weibull shape parameter for long-term distribution of the stress range. The fatigue failure criterion is defined as

$$D \geq \Delta \quad (36.6)$$

where Δ is the Miner's sum at failure. The uncertainties in the endurance limit N_0 may be considered as a variable X_{N_0} following a lognormal distribution with COV ranging from 5% to 20%. Introducing the stress modeling parameter B , the limit-state function (LSF) can be written as

$$g_i(Z) = \Delta - \frac{N_0}{K} \cdot \frac{B^m S_0^m}{(\ln N_0)^{m/\xi}} \Gamma\left(1 + \frac{m}{\xi}\right) \quad (36.7)$$

The above LSF may be re-expressed as

$$g_i(Z) = K\Delta \cdot \frac{(\ln N_0)^{m/\xi}}{B^m S_0^m \Gamma\left(1 + \frac{m}{\xi}\right)} - N_T \quad (36.8)$$

where N_T denotes the intended service life.

36.3.3 Fatigue Reliability—FM Approach

The probabilistic FM is extended from the deterministic Paris–Erdogan's equation for the crack increment per cycle.

$$\frac{da}{dN} = C \cdot (\Delta K)^m \quad (36.9)$$

where

a = crack depth

N = number of cycles

C, m = material constants

$\Delta K = K_{\max} - K_{\min}$ range of stress intensity factor, $K = S \cdot \sqrt{\pi \cdot a} \cdot F$

S = nominal stress in the member normal to the crack

F = correction factor depending on the geometry of the member and the crack

Initial crack size: Surface defects are usually more dangerous than embedded defects because they are often located at stress concentrations, have a crack-like shape, and are oriented normal to the principal stress. The statistical distribution for such defects is necessary information. The initial crack size is assumed to be independent and treated as a random variable following an exponential distribution.

$$F_{A_0}(a_0) = 1 - \exp\left(-\frac{a_0}{\lambda_0}\right) \quad (36.10)$$

where λ_0 is the distribution parameter of initial crack size.

Crack initiation time: For lack of data about the crack initiation time, a simple model assumes that the crack initial time t_0 is some percentage of crack propagation time T_P , and may be expressed as,

$$t_0 = \delta \cdot T_P \quad (36.11)$$

where, δ is a constant, T_P is crack propagation time.

Crack propagation prediction: Considering the effect of the stress ratio, the modified Paris law can be rewritten as,

$$\frac{da}{dN} = C \left(\frac{\Delta K}{1 - R} \right)^m \quad (36.12)$$

where a is the crack size, N is the number of stress cycles, C and m are parameters depending on the material and environment, and R is the stress ratio, which depends on the stress amplitude in stochastic time history. R is set to 0 in the following analysis. The stress intensity factor range ΔK can be estimated from Newman's approximation (Newman and Raju, 1981) given by

$$\Delta K = S \varepsilon_Y Y(a, X) \sqrt{\pi a} \quad (36.13)$$

where S is the stress range and $Y(a, X)$ is a geometry function accounting for the shape of the specimen and the crack geometry, ε_Y is a randomized model uncertainty of a geometry function.

By separating variables in Eqn (36.12) and introducing Eqn (36.13),

$$\frac{da}{\varepsilon_Y^m \cdot Y(a, X)^m \cdot (\sqrt{\pi a})^m} = C(\Delta S)^m dN \quad (36.14)$$

Then, the differential equation can be expressed as

$$\int_{a_0}^{a_N} \frac{da}{\varepsilon_Y^m \cdot Y(a, X)^m \cdot (\sqrt{\pi a})^m} = C \sum_{i=1}^N (\Delta S_i)^m = N \sum_{i=1}^N \frac{1}{N} (\Delta S_i)^m = NE[(\Delta S)^m] \quad (36.15)$$

Since the stress response induced by sea loads is typically a narrow-band process, the number of stress cycles spent for crack growth N may be defined as

$$N = \nu_0(r \cdot t - t_0) \quad (36.16)$$

where ν_0 is the average zero-crossing rate of stress cycles over the lifetime of the ship, r is the fraction of service time for the ship.

The crack size at the i th ship structural detail location at time t can be derived from the above equations with $R = 0$ (Song and Moan, 1998) as

$$a_i(t) = \Psi^{-1} \left(\Psi(a_{0i}) + C_i \nu_0 (rt - t_0) \varepsilon_S^m A_i^m \Gamma \left(1 + \frac{m}{\xi} \right) \right) \quad (36.17)$$

where $\Psi(\cdot)$ is the auxiliary function, which is monotonically increasing with the crack size a , expressed as

$$\Psi(a) = \int_0^a \frac{da}{(\varepsilon_Y Y(a, X) \sqrt{\pi a})^m} \quad (36.18)$$

and

$$A_i = \frac{S_0}{(\ln N_0)^{1/\xi}} \quad (36.19)$$

which assumes that $\ln A_i$ follows a normal distribution.

Fatigue failure criterion: When the critical crack size a_c is defined, which may be considered according to serviceability, the fatigue failure criterion at cycle number N is defined as

$$a_c - a(t) < 0 \quad (36.20)$$

LSF: Based on FM, the failure criterion is written in terms of the crack size at time t . The LSF for the i th ship structural detail location can thus be written equivalently as (see, e.g., Madsen et al., 1986)

$$g_i(Z) = \int_{a_{0i}}^{a_{ci}} \frac{da}{(\epsilon_Y Y(a, X) \sqrt{\pi a})^m} - C_i v_0 (rt - t_0) \epsilon_S^m A_i^m \Gamma\left(1 + \frac{m}{\xi}\right) \quad (36.21)$$

where Z is a set of random variables of material and stress parameters, geometry functions, initial crack size, crack growth time, etc. In addition, a_{ci} is the critical crack size of the i th potential crack site, and a_{0i} is the initial crack size at the i th crack site that can be calibrated with respect to the crack growth part of the S–N curve.

Uncertainty in FM model: Uncertainties associated with the probabilistic FM model include the following:

- Initial crack size
- Long-term loading
- Material parameters
- Geometry correction factor in stress intensity factor computation
- Critical crack size

Initial crack size depends mainly on the material microstructure and fabrication process and the welding quality. Thus, a large uncertainty in initial crack size is obvious. In general, the initial crack size is treated as a random variable where the distribution is selected as exponential, as given by Eqn (36.10).

The material constants in crack growth analysis are characterized by the two parameters C and m . Due to the uncertainties observed from the experimental studies, C and m should be modeled as random variables. It is generally accepted that C is modeled as lognormally distributed, and m is normally distributed.

The geometry correction factor that is determined by the Newman–Raju equation or the hybrid method involves large uncertainties. Its uncertainty is included in ϵ_y .

The critical crack size can be selected as a random variable or fixed variable based on serviceability conditions.

36.3.4 Simplified Fatigue Reliability Model—Lognormal Format

For fatigue reliability assessment using the lognormal format, uncertainty is introduced as a bias factor in fatigue stress, while the other uncertainties associated with fatigue strength are all treated as lognormal random variables. This was first developed by Wirsching (1984) and further implemented by Wirsching and Chen (1988).

Equation (36.8) can be rewritten as

$$g_i(Z) = \frac{K\Delta}{B^m\Omega} - N_T \quad (36.22)$$

where the stress parameter is defined as follows and may be considered deterministic,

$$\Omega = S_0^m \frac{\Gamma\left(1 + \frac{m}{\xi}\right)}{(\ln N_0)^{m/\xi}} \quad (36.23)$$

There is a closed-form solution for the fatigue failure probability,

$$P_f = P[N \leq N_T] \quad (36.24)$$

Assuming the analytical form follows the lognormal format, the reliability index β can be defined as

$$\beta = \frac{\ln(\tilde{N}/N_T)}{\sigma_{\ln N}} \quad (36.25)$$

$$\tilde{N} = \frac{\tilde{K}\tilde{\Delta}}{\tilde{B}^m \Omega} \quad (36.26)$$

$$\sigma_{\ln N} = \sqrt{\ln\left[(1 + C_K^2)(1 + C_\Delta^2)(1 + C_B^2)\right]^{m^2}} \quad (36.27)$$

where C_s denotes the COV of each variable.

Uncertainty measures: For the Wirsching's S–N lognormal reliability model, it is necessary to specify the mean and COV of K , B , and Δ , which are assumed to be lognormally distributed variables.

The variables B and Δ are used to quantify modeling error associated with assumptions made in the stress analysis and description of the fatigue strength.

For random variable Δ describing the modeling error associated with the Palmgren–Miner hypothesis, the following values for $\bar{\Delta}$ and C_Δ are often used: $\bar{\Delta} = 1.0$ and $C_\Delta = 0.3$.

The random variable K is associated with uncertainty in the S–N relationship. For S–N curves established from fatigue tests, the median value is determined by the experimental tests for different S–N categories, while the COV is derived as 0.3–0.6 based on experimental data analysis.

36.4 Calibration of FM Model by S–N Approach

Both the S–N curve approach and the FM approach have been applied to calculate failure probability:

- Based on the S–N curve and Miner's rule, the LSF can be written as Eqn (36.7), where Δ is the Miner's sum at failure, and N_0 is the number of cycles over the design lifetime

that causes initiation and propagation. In addition, $\ln K$ is modeled as a normal distribution.

- Alternatively, a_0 and t_0 used in the FM-based LSF Eqn (36.21) can be combined by neglecting t_0 in the expression and substituting a_0 with $a_{0,eq}$, which is an equivalent initial crack size accommodating the crack initiation time.

Accordingly, there is correlation between these two approaches. This means that the initial crack size used in the FM model can be calibrated to the S–N approach (Song and Moan, 1998).

The numbers of stress cycles to failure can be written as

$$N = KS^{-m} = N_i + N_g = N_i + \int_{a_0}^{a_c} \frac{da}{C(\varepsilon_Y Y(a, X) \sqrt{\pi a})^m} \quad (36.28)$$

where a_0 corresponds to the crack size after N_i cycles of crack initiation.

Assuming that $N_i = \delta \cdot N$, the calibration of initial crack size a_0 can be done according to

$$N - N_i = (1 - \delta)N = \int_{a_0}^{a_c} \frac{da}{C(\varepsilon_Y Y(a, X) \sqrt{\pi a})^m} \quad (36.29)$$

The median value of the initial crack size a_0 can be calibrated by other variables from Eqn (36.29). It is generally believed that the calibrated a_0 will also depend on the crack initiation period indicated by δ . In the calibration, m may be modeled as a fixed value or a random variable of normal distribution.

In a similar way, the S–N approach can be calibrated against the FM approach. In other words, the crack size can be explicitly included in an S–N curve. No matter which approach is going to be calibrated, the principle of calibration is that the different approaches should yield consistent fatigue life.

36.5 Fatigue Reliability Application—Fatigue Safety Check

36.5.1 Target Safety Index for Fatigue

The basic design requirement is that the safety index describing the reliability of a component exceeds the minimum allowable, or target, safety index.

$$\beta \geq \beta_0 \quad (36.30)$$

The value of β_0 and the statistics on the design variables are used to derive the expression for the target damage level.

Table 36.2: Target safety index (Mansour, 1997)

	Description	Target Safety Index, β_0
Category 1	A significant fatigue crack is not considered to be dangerous to the crew, will not compromise the integrity of the ship structure, will not result in pollution; repairs should be relatively inexpensive.	1.0
Category 2	A significant fatigue crack is not considered to be immediately dangerous to the crew, will not immediately compromise the integrity of the ship, and will not result in pollution; repairs will be relatively expensive.	2.5
Category 3	A significant fatigue crack is considered to compromise the integrity of the ship and put the crew at risk and/or will result in pollution. Severe economic and political consequences will result from significant growth of the crack.	3.0

For a safety check expression, it is necessary to specify a minimum allowable safety index (or target safety index), β_0 . The target safety index for each of the categories was chosen to be compatible with the values selected for other similar applications (Table 36.2).

36.5.2 Partial Safety Factors

An alternative approach to developing probability-based design criteria for the fatigue limit state is to use partial safety factors. Equation (36.22) is expressed as

$$N = \frac{K\Delta}{B^m S_e^m} \quad (36.31)$$

Letting the cycles to failure N equal the service life, N_S , and assuming $\tilde{B} = 1.0$, Eqn (36.31) can be rewritten as

$$S_e = \left[\frac{K\Delta}{N_S} \right]^{1/m} \quad (36.32)$$

Considering S_e , Δ , and K as random variables, the following safety-check expression may be defined,

$$S_e \leq \frac{1}{\gamma_S} \left[\frac{(\gamma_\Delta \Delta_n)(\gamma_K K_n)}{N_S} \right]^{1/m} \quad (36.33)$$

where the subscript n refers to nominal or design values. Reliability methods may be applied to calibrate the partial safety factors: stress factor γ_S , damage safety factor γ_Δ , and material property safety factor γ_K . See Stahl and Banon (2002) for the latest development on this subject.

36.6 Numerical Examples

36.6.1 Example 36.1: Fatigue Reliability Based on Simple S–N Approach

Problem

Assuming that fatigue strength is described by an S–N curve, and that fatigue loads are described by a Weibull distribution, fatigue damage can be obtained by Eqn (36.7), given by

$$D = \frac{N_0}{K} \cdot \frac{S_0^m}{(\ln N_0)^{m/\xi}} \Gamma\left(1 + \frac{m}{\xi}\right)$$

If only Δ , S_0 and K are considered random variables, the failure probability may be written as

$$P_f = \int_{g(Z) \leq 0} f_x(x) dx \tag{36.34}$$

where

$$g(Z) = X_1 - k \frac{X_2^m}{X_3} \tag{36.35}$$

and k is a constant.

Assuming $m = 3$, $k = 10^6$, and X_1 , X_2 , and X_3 are independent and specified in Table 36.3, find the distribution of $g(Z)$ and calculate the failure probability directly using the simple approach.

Solution

Before using FORM, it is shown that a simple approach can be applied to calculate P_f in the case. The Eqn (36.51) can be rewritten as

$$g(Z) = \ln X_1 - m \ln X_2 + \ln X_3 - \ln k \tag{36.36}$$

Since X_1 is deterministic and equal to 1 the following simplification of Eqn (36.36) can be performed

$$g(Z) = -m \ln X_2 + \ln X_3 - \ln k \tag{36.37}$$

Table 36.3: Input data

Random Variable	Mean Value	COV	Distribution
X_1	1	0	Deterministic
X_2	200	0.2	Lognormal
X_3	$6.93 \cdot 10^{13}$	0.5	Lognormal

The random variables X_2 and X_3 are lognormally distributed, which implies that $\ln X_2$, $\ln X_3$, and $g(Z)$ are normal distributions with the following mean and COV values,

$$\begin{aligned}\sigma_{\ln X_2} &= \sqrt{\ln(1 + \text{COV}_{X_2}^2)} = 0.198 \\ \mu_{\ln X_2} &= \ln \mu_{X_2} - 0.5\sigma_{\ln X_2}^2 = 5.279 \\ \sigma_{\ln X_3} &= \sqrt{\ln(1 + \text{COV}_{X_3}^2)} = 0.472 \\ \mu_{\ln X_3} &= \ln \mu_{X_3} - 0.5\sigma_{\ln X_3}^2 = 31.758 \\ \sigma_g &= \sqrt{m^2\sigma_{\ln X_2}^2 + \sigma_{\ln X_3}^2} = 0.759 \\ \mu_g &= -m\mu_{\ln X_2} + \mu_{\ln X_3} - \ln k = 2.105\end{aligned}$$

The reliability index and the failure probability are then,

$$\begin{aligned}\beta &= \frac{\mu_g}{\sigma_g} = 2.774 \\ P_f &= \Phi(-\beta) = 2.76 \cdot 10^{-3}\end{aligned}$$

36.6.2 Example 36.2: Fatigue Reliability of Large Aluminum Catamaran

The example given here is directly from [Song and Moan \(1998\)](#), and demonstrates the application of fatigue reliability to a large aluminum catamaran. Refer to their paper for further details.

Description of the Case

The midship section of a catamaran, and local structural details in the vicinity of the welds, are shown in [Figures 36.1 and 36.2](#). Aluminum alloy 5083 is considered. The material properties are as follows: the Young's modulus $E = 68.6 \times 210^3$ MPa, yield strength $\sigma_y = 250$ MPa, density $\rho = 2700$ kg/m³. The statistical value of material parameter $\ln C$ is taken from [Table 36.4](#) assuming a COV of 0.5. The scale parameter A is determined from the implied cumulative damage criterion and is given in [Table 36.5](#). Fatigue parameters K and m are determined from the BS8118 code ([BSI, 1992](#)). Data for $R = 0$ is applied and numerical calculations are conducted based on parameters listed in [Table 36.6](#).

Note: Correlation between m and $\ln C$ is $\rho(m, \ln C) = -0.95$; a_0 is calibrated by the S-N approach; $\ln A$ is estimated based on the BS8118 code with $D = 0.1$, $K = 2.09E + 11$, $m = 3.25$.

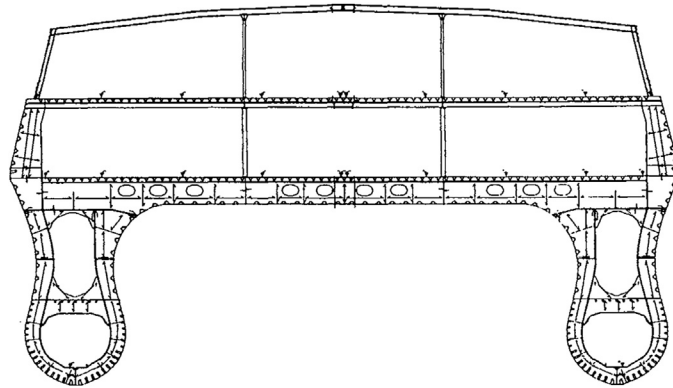


Figure 36.1
Typical midship section of a catamaran (Song and Moan, 1998).

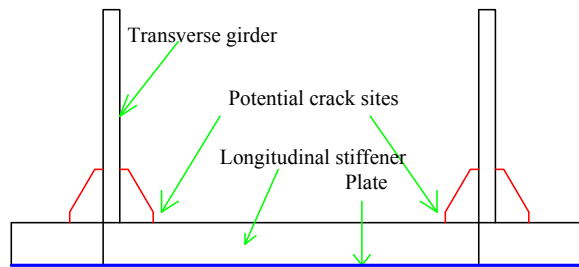


Figure 36.2
Considered structural details.

Table 36.4: Statistical value of material parameter $\ln C$ (Song and Moan, 1998)

		m (BS8118)	$\log C = a + bm$	$\ln C$
$R = 0$	$a = -6.74$	3.25	-10.12	-23.30
	$b = -1.04$	3.5	-10.38	-23.90
$R = 0.3$	$a = -7.09$	3.25	-9.8525	-22.69
	$b = -0.85$	3.5	-10.065	-23.18

Table 36.5: Stress scale parameter $\ln A$ based on BS8118 (BSI, 1992)

D	S-N Characteristic Values	Parameter A	$\ln A$
0.1	$K = 2.09E+11, m = 3.25$	0.27707E+01	0.1019E+01
	$K = 9.60E+11, m = 3.5$	0.35842E+01	0.1276E+01
0.3	$K = 2.09E+11, m = 3.25$	0.38850E+01	0.1357E+01
	$K = 9.60E+11, m = 3.5$	0.49058E+01	0.1590E+01

Table 36.6: Probabilistic parameters for fatigue analysis (Song and Moan, 1998)

Variable	Distribution	Mean	COV
Initial crack size, a_0	Exponential	0.02	1.0
Crack initial time ratio, δ	Fixed	0.10	—
Detectable crack size, a_D	Exponential	1.0	1.0
Geometry bias factor, ε_Y	Normal	1.0	0.1
Stress model error, ε_S	Lognormal	1.0	0.1
Material parameter, $\ln C$	Normal	-23.30	0.022
Stress scale parameter, $\ln A$	Normal	1.019	0.10
Crack aspect ratio, a/c	Fixed	0.5	—
Random bias of a/c , $\varepsilon_{a/c}$	Normal	1.0	0.1
Miner's sum at failure, Δ	Lognormal	1.0	0.3
S-N fatigue parameter, $\ln K$	Normal	27.065	0.019
Stress shape parameter, ξ	Fixed	0.95	—
Material parameter, m	Normal	3.25	0.06
Plate thickness, T_H	Fixed	30	—
Plate width, w_p	Fixed	100	—
Stress ratio, R	Fixed	0.0	—
Stress cycles per year, ν_0	Fixed	2.5E+6	—
Fraction of a ship at sea, r	Fixed	0.765	—

Results and assessment

Calibration of FM model: S-N curves have been developed based on laboratory tests; there are larger uncertainties in the material parameters that are used in FM predictions. It is therefore useful to calibrate the FM material parameters against SN curves. Several analyses were performed with different FM models. Figure 36.3 gives the results of this calibration to achieve a consistent fatigue life based on FM and S-N approaches respectively. It is seen that if an identical parameter $m = 3.25$ is used for FM and S-N, the calibrated results are a_0 -EXP(0.02), m -N(3.25,0.06) and $\rho(m, \ln C) = -0.95$, or a_0 -EXP(0.007) and fixed $m = 3.25$. If fixed $m = 3.5$ is used for FM and S-N, the calibrated results are a_0 -EXP(0.007), or a_0 -EXP(0.015), m -N(3.5,0.06), and $\rho(m, \ln C) = -0.95$. However, different m values can be applied for different models. If fixed $m = 3.5$ is used for the S-N approach and $m = 3.25$ is used for FM model, then the calibrated a_0 follows EXP(0.02). It is seen clearly that different calibrated a_0 are available based on the assumptions made. If the crack initiation time ratio $\delta = 0.1$, this will increase a_0 by about 20% compared with the case with $\delta = 0$. If more cycles of N are assumed spent in crack initiation, the calibrated a_0 is expected to be greater.

Basic parameter studies: Figure 36.3 shows the sensitivity of the reliability at $t = 4$ years, with no inspection based on FORM analysis.

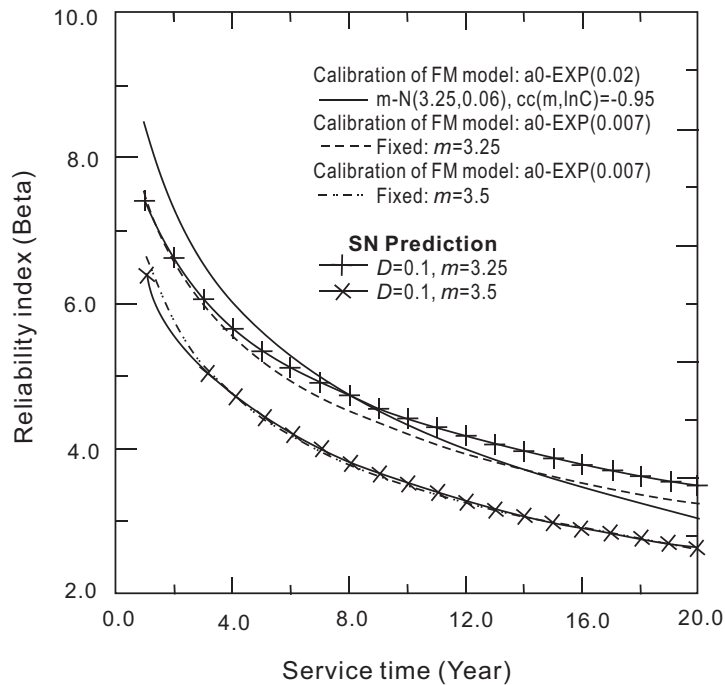


Figure 36.3

Calibration of FM model to S–N approach for sites with cumulative damage equal to $D = 0.1$. cc, correlation coefficient (Song and Moan, 1998).

Effect of S–N fatigue parameters: The determination of the fatigue parameters K , m of the S–N formulation depends strongly on how the considered structural details are classified. It is assumed that the implied accumulated damage D equals to 0.1 and 0.3, respectively, corresponding parameters K and m are given in Table 36.6, COV of $\ln C$ and $\ln A$ are set to 0.5 and 0.1 respectively.

Effect of the Weibull shape parameter: Based on preliminary investigations of the long-term distribution, it is assumed that B is 0.95 in this case study. A parametric study is performed with the results shown in Figure 36.4. It is seen that the shape parameter B is quite influential on the fatigue reliability. Generally, the shape parameter B is in the range of 0.8–1.0 for ships. Instead of modeling B as a fixed value, it may be modeled as a stochastic variable. From the results shown in Figure 36.5, it is seen that if $1/B$ is modeled as a normal distribution with $\mu = 1.0526$ and COV = 0.1, the β will decrease compared with the results of the fixed B . If it is assumed that $\rho(1/B, \ln A) = -0.8$, the effect of B is almost as the same as when B is modeled as fixed.

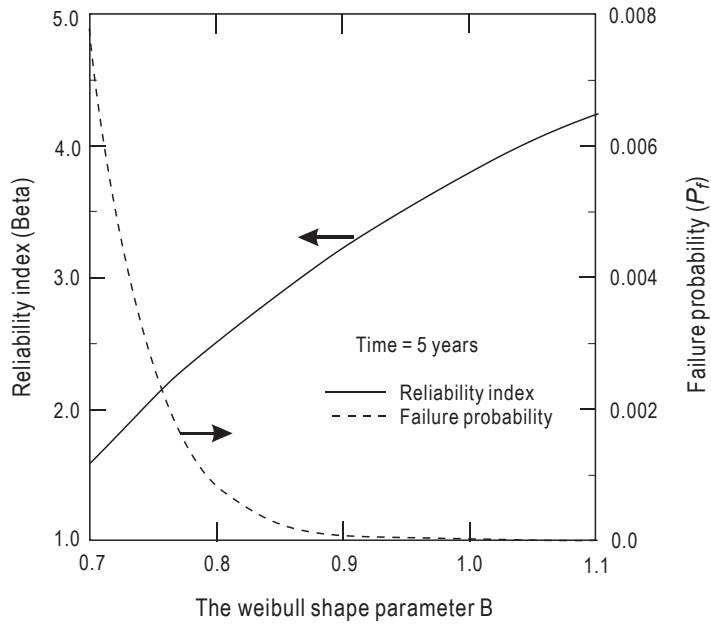


Figure 36.4

Effect of shape parameter B on β and P_F of a component (Song and Moan, 1998).

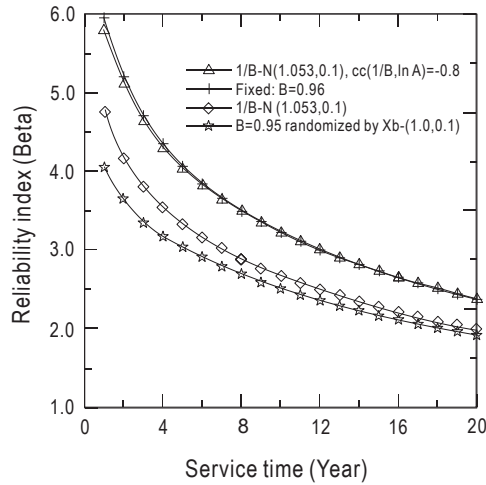


Figure 36.5

Effect of different models of shape parameter B on β of a component. cc, correlation coefficient (Song and Moan, 1998).

References

- Almar-Næss, A. (Ed.), 1985. *Fatigue Handbook - Offshore Steel Structures*. Tapir Press, Norway.
- BSI, 1992. *British Standards 8118, Code of Practice for the Structural Use of Aluminum*. British Standards Institution, London.
- Hovde, G.O., Moan, T., 1994. Fatigue reliability of TLP tether systems. In: *Proc. 13th OMAE*.
- Maddox, S., 1991. *Fatigue Strength of Welded Structures*. Abington Publishing, Cambridge, UK.
- Madsen, H.O., et al., 1986. *Methods of Structural Safety*. Prentice-Hall, Inc., Englewood Cliffs.
- Mansour, A.E., et al., 1997. Assessment of Reliability of Ship Structures, SSC-398. Ship Structures Committee.
- Newman Jr., J.C., Raju, I.S., 1981. An empirical stress-intensity factor equation for the surface crack. *Engineering Fracture Mechanics* 15, 185–192.
- Rice, R.C., et al., 1988. *Fatigue Design Handbook*. Society of Automotive Engineers Inc., Warrendale, USA.
- Song, R., Moan, T., 1998. Fatigue reliability of large catamaran considering inspection updating. In: *Proceeding of the 8th International Offshore and Polar Engineering Conference (ISOPE'98)*. Montreal, Canada.
- Stahl, B., Banon, H., 2002. Fatigue Safety Factors for Deepwater Risers. OMAE2002–28405.
- White, G.J., Ayyub, B.N., 1987. Reliability based fatigue design for ship structures. *Journal of Naval Engineers* 99 (3), 135–149.
- Wirsching, P.H., 1984. Fatigue reliability of offshore structures. *Journal of Structural Engineering* 110, 2340–2356.
- Wirsching, P.H., Chen, Y.N., 1988. Considerations of probability-based fatigue design criteria for marine structures. *Journal of Marine Structures* 1, 23–45.
- Wirsching, P.H., Mansour, A.E., 1997. Reliability in fatigue and fracture analysis of ship structures. In: Reemsnyder, H (Ed.), *Proc. Symposium and Workshop on the Prevention of Fracture in Ship Structures*. Washington, DC.
- Xu, T., Bea, R., 1997. *Marine Infrastructure Rejuvenation Engineering-Fatigue and Fracture of Critical Structural Details (CSD)*. JIP report. Marine Technology & Management Group, University of California at Berkeley.

Probability- and Risk-Based Inspection Planning

37.1 Introduction

In-service inspections of marine structures are carried out in order to assure structural integrity. To optimize in-service inspections, it is necessary to deal with uncertainties in design, fabrication, and damage detection, and the adequacy of examining only a limited number of critical elements. Many efforts have been devoted to reliability updating through inspection and repair; see [Moan \(1993, 1997\)](#) and [Xu and Bea \(1997\)](#). [Song and Moan \(1998\)](#) have studied inspection updating based on system considerations. Uses of probability-based inspection in other engineering fields are given by, for example, [Yazdan and Albrecht \(1990\)](#).

Risk assessment can be used as a valuable tool to assign priorities among inspection and maintenance activities. A throughout discussion of risk assessment is given in Part V of this book. This chapter covers:

- Concepts of risk-based inspection
- Reliability-updating theory for probability-based inspection
- Risk-based inspection examples
- Risk-based optimum inspection

37.2 Concepts for Risk-Based Inspection Planning

In general, the dimensions of risk can be considered in the following three main categories:

- Personnel risk
 - Fatality risk
 - Impairment risk
- Environmental risk
- Asset risk
 - Material (structural) damage risk
 - Production delay risk

Risk is defined as,

$$R = f(P_f, C) \quad (37.1)$$

where P_f is the failure probability; C is the consequence of the failure.

A more general expression of the risk for practical calculation is given by

$$R = \sum (P_{f_i} \cdot C_i) \quad (37.2)$$

The risk-based inspection can be planned by minimizing the risk:

$$\min\{R\} \quad (37.3)$$

The development of a system-level risk-based inspection process includes the prioritization of systems, subsystems, and elements using risk measures, and definitions of an inspection strategy (i.e., the frequency, method, and scope/sample size) for performing inspections. The process also includes the decisions about maintenance and repair following inspections. Finally, there is a strategy for updating the inspection strategy for a given system, subsystem, or component/element, using the results of the inspection that are performed.

[Figure 37.1](#) illustrates the overall risk-based inspection process, which is made up of the following four steps:

- Definition of the system that is being considered for inspection.
- Use of a qualitative risk assessment that utilizes expert judgment and experience in identifying failure modes, causes, and consequences for initial rankings of systems and elements under inspection.
- Application of quantitative risk analysis methods, primarily using enhanced failure modes, effects, and criticality analysis; treating uncertainties, as necessary, to focus the inspection efforts on systems and components/elements associated with the highest calculated safety, economic, or environmental risk.
- Development of the inspection program for the components, using decision analysis to include economic considerations, beginning with an initial inspection strategy and ending with an update of that strategy, based on the findings and experience from the inspection that is performed.

Several feedback loops are shown in [Figure 37.1](#) to represent a living process for the definition of the system, the ranking of components/elements, and the inspection strategy for each component/element. A key objective is to develop a risk-based inspection process that is first established and then kept up to date by incorporating new information from each subsequent inspection.

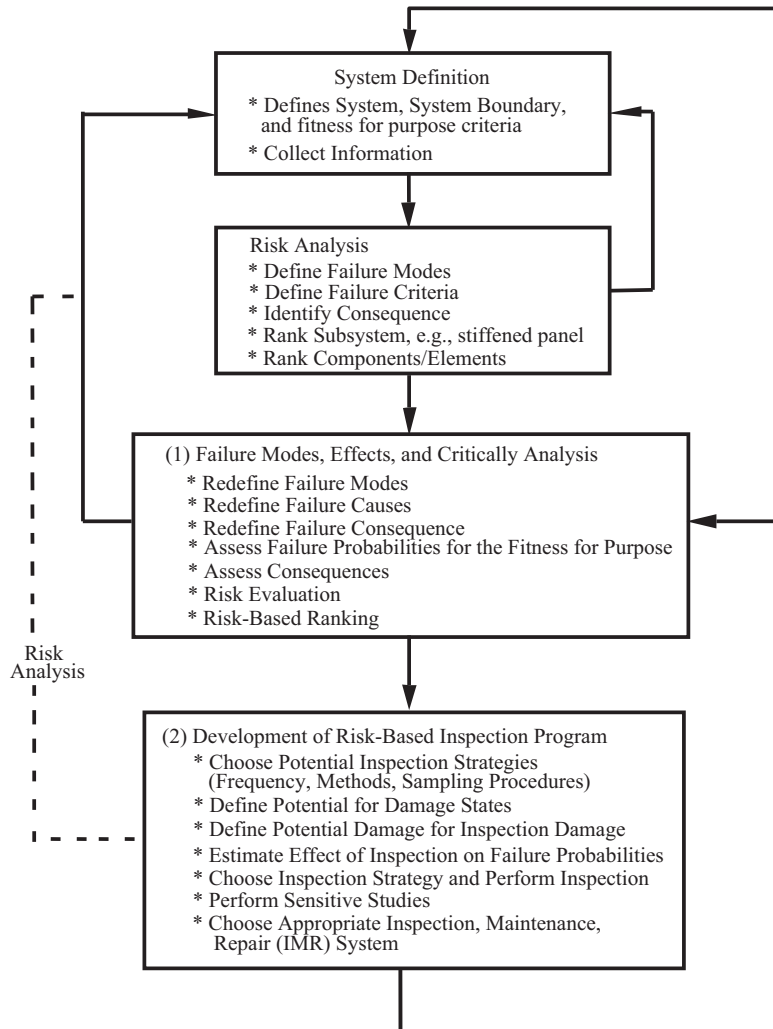


Figure 37.1
Risk-based inspection process (Xu et al., 2001).

37.3 Reliability-Updating Theory for Probability-Based Inspection Planning

37.3.1 General

Bayesian models are often applied to reliability updating for probability-based inspection planning. This section presents two major approaches that have been developed in the past 30 years.

Updating through inspection events to update the probability of events such as fatigue failure directly (Yang, 1976; Itagaki et al., 1983; Moan, 1993, 1997). Yang (1976) and Itagaki et al. (1983) proposed a simplified Bayesian method that only considers crack initiation, propagation, and detection as random variables and independent components in a series system.

Updating through variables to recalculate the failure probability using the updated probability distributions for defect size, etc. (Shinozuka and Deodatis, 1989). The change in the reliability index is caused by changes in random variables. The distribution of a variable can be updated based on inspection events. When the variables are updated, the failure probability can easily be calculated. However, if several variables are updated based on the same inspection event, the increased correlation between the updated variables needs to be accounted for.

The approach for updating through inspection events will be further explained in the next subsection.

37.3.2 Inspection Planning for Fatigue Damage

Fatigue failure is defined by the fatigue crack growth reaching critical size (e.g., the wall thickness of the pipe). Based on fracture mechanics, the criterion is written in terms of the crack size at time t . By integrating Paris law, the limit-state function can be written as (see Part IV, Chapter 36 of this book and Madsen et al., 1986).

$$g(Z) = \int_{a_0}^{a_c} \frac{da}{(\varepsilon_Y Y(a, X) \sqrt{\pi a})^m} - C \nu_0 t \varepsilon_S^m A^m \Gamma\left(1 + \frac{m}{\xi}\right) \quad (37.4)$$

where $Y(a, X)$ is the finite geometric correction factor, ε_S is the stress modeling error, ε_Y is randomized modification factor of a geometry function, ν_0 is the average zero-crossing rate of stress cycles over a lifetime, and $\Gamma(\cdot)$ is the gamma function.

Basically, the two most common inspection results are considered here, namely: no crack detected, and crack detected and measured (and repaired); see Madsen et al. (1986).

No Crack Detection

This means that no crack exists or the existing crack is too small to be detected. This inspection event margin, for the i th detail, can be expressed as

$$\begin{aligned} I_{no,i}(t_I) &= a_D - a_i(t_I) \\ &= \Psi(a_D) - \Psi(a_{0i}) - C_i \nu_0 t_I \varepsilon_S^m A_i^m \Gamma\left(1 + \frac{m}{\xi}\right) > 0 \end{aligned} \quad (37.5)$$

in which $a(t_i)$ is the crack size predicted at inspection time t_i , and a_D is the detectable crack size.

The detectable crack size a_D is related to a specified inspection method and modeled as a stochastic variable reflecting the actual probability of detection (POD) curve. Among several formulations of POD available, the commonly used exponential distribution is selected in this case.

$$P_D(a_D) = 1 - \exp\left(-\frac{a_D}{\lambda}\right) \quad (37.6)$$

where λ is the mean detectable crack size.

Crack Detected and Measured

If a crack is detected and measured for a weld detail i , this inspection event can be written as

$$\begin{aligned} I_{yes,i}(t_I) &= a_m - a_i(t_I) \\ &= \Psi(a_m) - \Psi(a_0) - C_i v_0 t_I e_S^m A_i^m \Gamma\left(1 + \frac{m}{\xi}\right) = 0 \end{aligned} \quad (37.7)$$

where a_m is the measured crack size at time t_I and regarded as a random variable due to uncertainties involved in sizing. $\Psi(a)$ is a function reflecting the damage accumulation from zero to crack size a , and is defined as (Paris and Erdogan, 1963; Newman and Raju, 1981)

$$\Psi(a) = \int_0^a \frac{da}{(\epsilon_Y Y(a, X) \sqrt{\pi a})^m}$$

Repair Events

The inspection itself does not increase the reliability of the structure, but it makes it possible to take necessary corrective actions—for example, repair—if a crack is detected. After repair, it is assumed that the material parameters and initial crack size follow the previous models but are statistically independent. This repair event based on cracks detected and measured is the same as given by Eqn (37.7)—that is, $I_R = I_{yes}$. After repair, the failure event also needs to be modified as discussed below.

Reliability Updating through Repair

If a crack is detected, measured, and repaired, statistical properties of the material are expected to be of the same magnitude but statistically independent. Weld defects, a_R , after (underwater) repair, depend on repair and postrepair treatment methods

(grind, a_{Rg} or weld, a_{Rw}). Here it is assumed to follow the same model as a_0 . The new safety margin after repair, $M_R(t)$, becomes

$$M_R(t) = \int_{a_R}^{a_c} \frac{da}{(\varepsilon_Y Y(a, X) \sqrt{\pi a})^{m_R}} - C_R \nu_0 (t - t_R) \varepsilon_S^{m_R} A^{m_R} \Gamma\left(1 + \frac{m_R}{\xi}\right) \quad (37.8)$$

where t_R is the repair time. Parameters a_R , C_R , and m_R are assumed to follow the previous models but are statistically independent.

Updated failure probability for repaired structural details is written as

$$P_{F,up} = P[M_R(t) \leq 0 | I_R(t_R) = 0] \quad t > t_R \quad (37.9)$$

It should be mentioned that an alternative way to consider the repair effect is to update the random variables in Eqn (37.8), based on inspection events. Then, the reliability can be estimated through repair safety margins by introducing the initial crack size a_R , depending upon the repair methods applied.

37.4 Risk-Based Inspection Examples

The methodology presented in Part IV Section 25.5 could be extended to risk-based inspection planning (Sun and Bai, 2001). As an example, the risk is defined as:

$$\text{Risk} = (\text{Consequence of failure}) \times (\text{Likelihood of failure})$$

Where the consequence of failure can be measured by:

- C1: Loss of hull, cargo, and life, which is the most serious consequence
- C2: Minor oil spills, serviceability loss, and salvage
- C3: Unscheduled repair and serviceability reduction.

The likelihood of failure may be divided into three categories:

- L1: Rapid corrosion rate
- L2: Nominal corrosion rate
- L3: Slow corrosion rate.

In the present analysis, it is assumed that all components with corrosion wastage larger than the critical size with a certain POD will be replaced, and after, their state will be recovered to its original form.

The inspections can be made once a year (Annual Survey), every 2.5 years (intermediate survey), and every 5 years (special survey) based on the survey strategy by the classification

societies. The four levels of POD for the thickness measurement are considered—that is, 60%, 80%, 90%, and 95% under the inspection condition that POD is 99.9% when the thickness of the corroded component reaches 75% of its original thickness.

The tentative reliability indices against hull girder collapse (one of most serious consequences of failure) are set at 3.7 for the “new-built” state and 3.0 for the lower limit of corroded hulls.

Figure 37.2 shows the time-variant reliability with the risk of C1 and L1 combined.

It can be seen that the thickness measurement and renewal for the components with POD of less than 80% need to be carried out in each Annual Survey after the 10th service year, in order to meet the annual reliability index over the lowest limit of safety levels.

Figure 37.3 demonstrates the time-variant reliability with the risk of C1 and L2 combined.

It can be seen from the above figure that thickness measurements and renewal for the components with POD of less than 80% should be carried out in order to guarantee the annual reliability index over the lowest limit of the safety level during the first 20 service-years. They may be done in special survey No. 3 during the first 20 service years, but should be implemented in the annual survey if the FPSO is required to be kept in service for over 20 service-years.

Figure 37.4 shows the time-variant reliability with the risk of C1 and L3 combined. From this figure, it is found that the annual reliability index is always greater than the lower limit of the safety level and the thickness measurement may not be necessary during the first 20 service-years, but the thickness measurement and the renewal for the components with POD of less than 80% in the intermediate survey, should be carried out if the FPSO is required to be kept in service for over 20 service-years.

From the above example, it is concluded that the inspection planning is dependent on the consequences of failure (lower limit of safety level), corrosion rate, ship age, and POD. The requirements of inspection are gradually more demanding, with the increase of the consequence of failure (lower limit of safety level), corrosion rate, and ship age, as well as with the decrease of POD. The latter usually makes thickness gauging and judgment more difficult.

37.5 Risk-Based “Optimum” Inspection

This subsection is based on Xu et al. (2001). Experiences with in-service inspections for ships and offshore structures have adequately demonstrated that there are two categories for damage:

- Those that could have been or were anticipated (natural, predictable)
- Those that could not have been anticipated (human-caused, unpredictable)

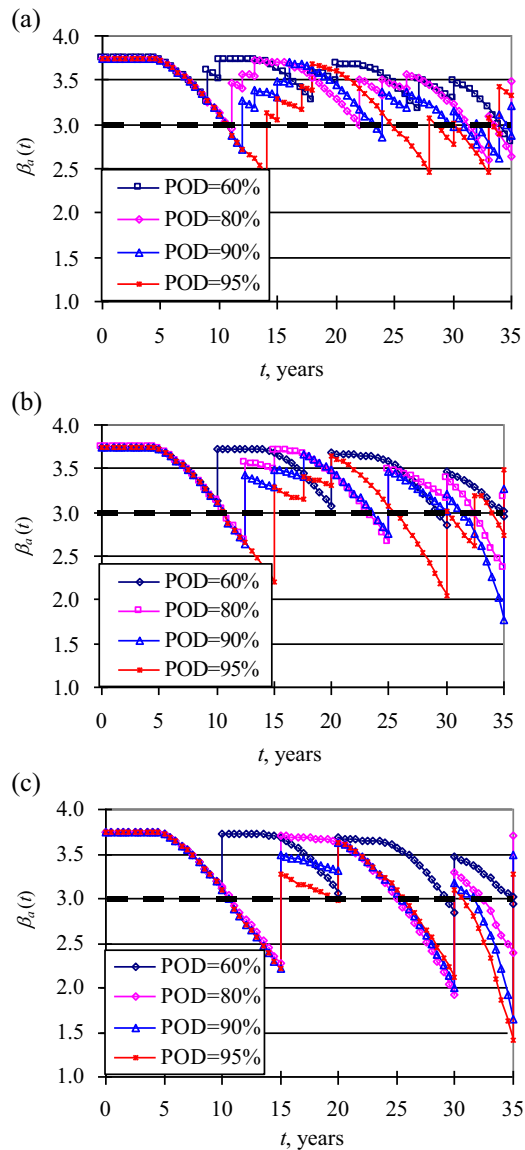


Figure 37.2

Time-variant reliability with risk of C1 and L1 combination. (a) Annual survey, (b) Intermediate survey, (c) Special survey.

A substantial amount (if not a majority) of damage falls into the second category—unpredictable and due to the “erroneous” actions and inactions of people.

Quantitative inspection analyses (e.g., probability- or risk-based inspection methods and programs) can help address the first category of defects by providing insights of when, where, and how to inspect and repair. However, such an analysis cannot be relied upon to

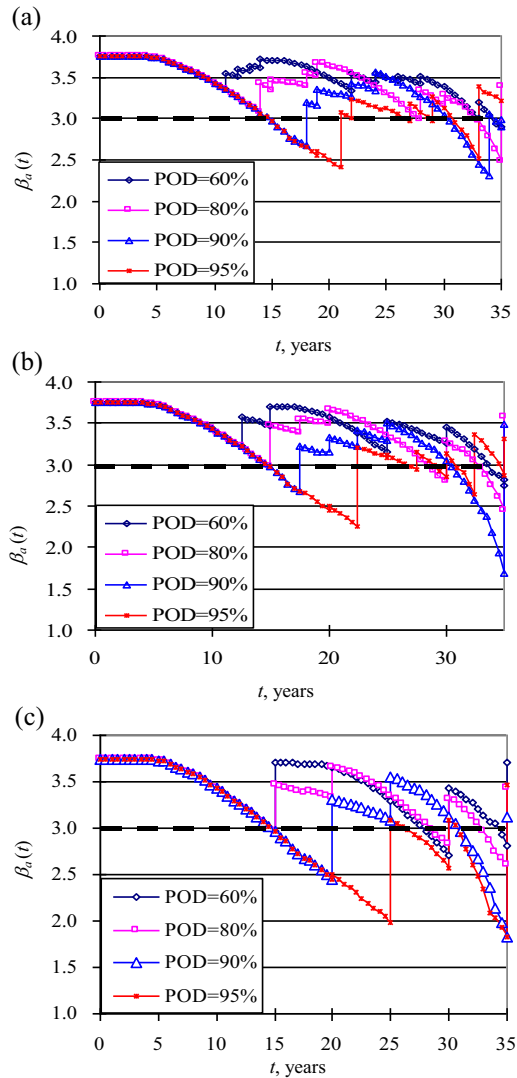


Figure 37.3

Time-variant reliability with risk of C1 and L2 combination. (a) Annual survey, (b) Intermediate survey, (c) Special survey.

provide information that addresses the second category of defects. Expert observation and deduction (diagnostic) techniques must be used to address the second category of defects.

Such recognition techniques lead to the development of the “optimum” inspection method (Xu et al., 2001). The overall objective of the “optimum” inspection method is to develop an effective and efficient safety and quality control system in the life-cycle management of the structural systems.

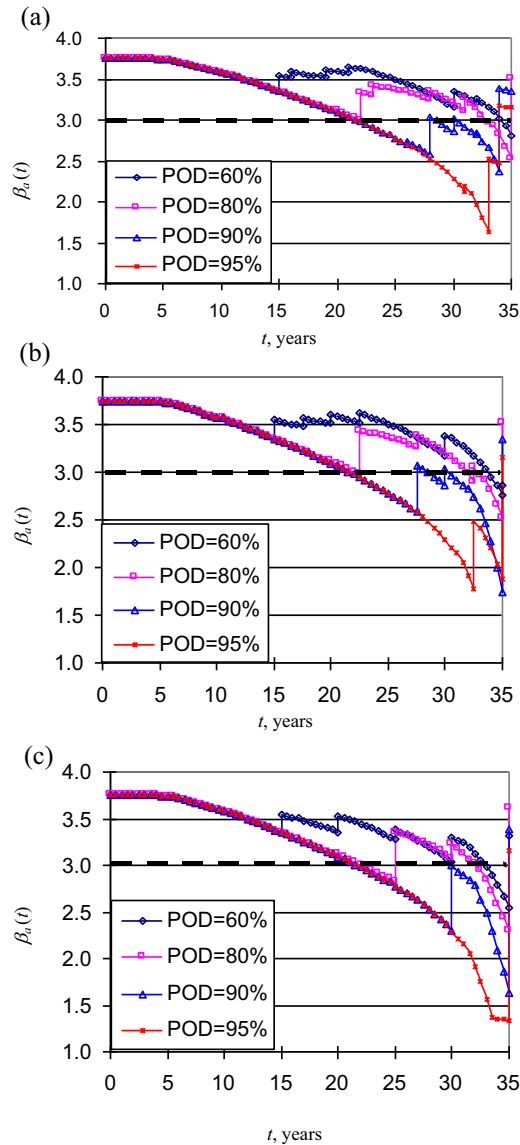


Figure 37.4

Time-variant reliability with risk of C1 and L3 combination. (a) Annual survey, (b) Intermediate survey, (c) Special survey.

37.5.1 Inspection Performance

Inspection performance is influenced by the vessel, inspector, and environment.

Vessel factors can be divided into two categories: design factors and condition/maintenance factors. Design factors, including structural layout, size, and coating, are fixed at the initial

design or at the redesign that may accompany repair. Condition/maintenance factors reflect the change in a vessel as it ages, including the operation history and characteristics of individual damages/defects (crack, corrosion, bucking), its size, and its location.

The person (inspector) who carries out an inspection can greatly influence the inspection performance. Performance varies not only from inspector to inspector, but also from inspection to inspection with the same inspector based on his/her mental and physical condition. Factors associated with the inspector include experience, training, fatigue, and motivation.

The environment in which the inspection is carried out has a major influence on performance. Environmental factors can be divided into two categories: external factors that cannot be modified by inspection procedures, and procedure factors that can be modified. External factors include weather and the location of the vessel—that is, whether the inspection is performed while underway, in port, or in dry dock. Procedural factors reflect the condition during the inspection (lighting, cleanliness, temperature, ventilation), the way in which the inspection is conducted (access method, inspection method, crew support, time available), and the overall specification for inspection (inspection type).

37.5.2 Inspection Strategies

Inspections, data recording, data archiving (storage), and data analysis should all be a part of a comprehensive and optimum inspection system. Records and thorough understanding of the information contained in the records are an essential aspect of inspection programs.

Inspection is one part of the “system” that is intended to help disclose the presence of “anticipated” and “unanticipated” defects and damage. Development of inspection programs should address:

- Elements to be inspected (where and how many?)
- Defects, degradation, and damages to be detected (what?)
- Methods to be used to inspect, record, archive, and report results (how?)
- Timing and scheduling (when?)
- Organization, selection, training, verification, conflict resolution, and responsibilities (who?)
- Objectives (why?)
- Where and how many?

The definition of the elements to be inspected is based on two principal aspects:

- Consequences of defects and damage
- Likelihood of defects and damage

The consequence evaluation essentially focuses on defining those elements and components that have a major influence on the quality and safety of an FPSO. Evaluation of the potential consequences should be based on historical data (experience) and analysis, in order to define the elements that are critical in maintaining the integrity of an FPSO. The likelihood evaluation focuses on defining those elements that have high likelihoods of being damaged. Experience and analyses are complementary means of identifying the following elements.

What?

A substantial amount (if not the majority) of the damage is unpredictable due to the unanticipated “erroneous” actions and inactions of people.

Current experience also indicates that the majority of damage that is associated with accidents (collisions, dropped objects) is discovered after the incident occurs. About 60% of damages due to fatigue and corrosion is detected during routine inspections. However, the balance of 40% is discovered accidentally or during nonroutine inspections.

How?

The methods to be used in FPSO inspections are visual. In one form or another, these methods are primarily focused on getting an inspector close enough to the surface to be inspected so that he/she can visually determine if there are significant defects or damages. However, ultrasonic gauging, magnetic particles, radiographic, and other nondestructive methods, are sometimes necessary for structures.

When?

There are no general answers to the timing of inspections, and is dependent on:

- The initial and long-term durability characteristics of the FPSO structure
- The margins that the operator wants in place over minimums so that there is sufficient time to plan and implement effective repairs
- The quality of the inspections and repairs
- The basis for maintenance—“on demand” (repair when it “breaks or leaks” or “programmed” (repair or replace on standard time basis).

Who?

Experience has adequately demonstrated that the single most important part of the inspection system is the inspector. The skills, knowledge, motivation, and integrity of the inspector are critically important. Equally important are the organizational influences exerted on the inspector, the procedures, and processes that he/she is required to follow, the environments in which he/she must work, and the support hardware/systems that are

provided to perform his/her work. Thus, the inspector is significantly influenced by the (1) organization, (2) procedure, (3) hardware (facilities), and (4) environment.

Much has been learned about how to improve the effectiveness and efficiency of the inspector. It is important that the inspector be recognized as a part of the system as new inspection systems are designed.

Why?

The inspection should have objectives at several levels. First, it should provide the general information and knowledge about the in-service structures for fitness for the purpose of evaluation. Second, it should detect the damage/defects so effective and efficient maintenance and repair programs can be implemented to correct these damages/defects (quality control and assurance). Third, it is a safety control tool to prevent the failure or loss of the in-service structures during the inspection interval (safety control and assurance).

The inspection strategies (when, where, how, who) for different level objectives should be different. The first level inspection should select typical elements/components to provide general information about the in-service structures for fitness for the purpose of evaluation. Less detailed inspections are frequently associated with long-term maintenance and repair programs. The second-level (quality control) inspection should focus on the critical components/elements in order to detect as many damage/defects as possible; it is associated with the short-term maintenance and repair program. The third-level inspection (safety control) is used to prevent the most critical damage/defects or errors to ensure a safe operation during the inspection interval. It is the most detailed and difficult inspection, which identifies safety-related predictable or unpredictable damages/defects and errors. Every inspection practice for a specific fleet should be a combination of these three different inspection strategies.

The value of the inspection for objectives of different levels should also be different. The value of the first-level inspection is about the decision on whether the existing structure can fulfill the purpose for extended service. The importance of the second-level inspection is the decision of whether the maintenance and repair program should change. The value of the third-level inspection is about the decision of whether to take intermediate actions. Value analysis (value of information) can help in making these decisions.

“Optimum” Inspection Method

The “optimum” inspection method can be proactive (focused on prevention) or it can be reactive (focused on correction). It should have four functions:

- Assess the general conditions of the in-service offshore structures
- To confirm what is thought; to address the intrinsic damages/defects that can be prediction-based results from technical analyses

- To disclose what is not known before inspection; to address damage/defects that cannot be predicted based on technical analyses
- To control the predictable and unpredictable damages
- To develop a high-quality maintenance and repair program.

The “optimum” inspection program should begin with the design of the structure (conception), proceed through the life of the structure, and conclude with its scrapping (life cycle). The optimum inspection program should include not only the hull structure, but also the structure’s equipment and personnel. The optimum inspections should become the means to assess the general conditions of the whole structure. The optimum inspections are also the means to detect unpredictable flaws and damages of the structural elements, and permit appropriate measures to be taken to preserve the safety and integrity of the structure. The optimum inspections are also the means to assure that all is going as expected, that the structural elements are performing as expected, and that corrosion protection and mitigation (e.g., patching pits and renewing locally excessively corroded plates) are both maintained.

The “optimum” inspection method starts from the survey for the intrinsic damage that is common for the class of structures. Based on experience, the inspection for the intrinsic damage can be conducted in a rational way. The existing risk-based inspection method discussed in earlier sections, is the framework for the intrinsic damages/defects for the structural system. The probability-based inspection method can be applied to specific elements/components based on the results of the risk-based inspection. For the extrinsic damage of each individual structure, the knowledge-based diagnosis method should be developed. The systematic knowledge-based diagnosis process is a potential means to identify the extrinsic damages.

Knowledge systems routinely do diagnostic reasoning using three methods: model-based diagnosis, heuristic classification, and case-based reasoning. The system used uses a combination of these methods.

Model-based diagnosis is used to identify the details of a large class of possible problems, heuristic classification is used to identify the presence of a set of idiosyncratic problems, and case-based reasoning is used to compare observations with previously identified cases.

An “optimum” inspection method can include:

- Developing a standard task checklist to ensure that relevant data and tasks are not lost because of distractions or workloads.
- Performing global surveys to develop situation awareness for potential expected and unexpected damages and defects.
- Inspecting the high likelihood of damages or defect “parts” and high consequence parts. If something “suspicious” is found, the inspection is intensified by model-based diagnosis, heuristic classification, and case-based reasoning until root causes (not symptoms) are determined.

- Periodic inspections, decreasing the time between inspections as the rate of degradation or likelihood of defects and damage increase.
- Inspecting after accidents or “early warning” signals are detected.
- Implement the long-term and short-term maintenance and repair strategies based on the inspection results.
- Update the IMMR (Inspection, Maintenance, Monitoring, and Repair) plan based on the survey results and the results from maintenance and repair.
- Performing inspections that are independent from the circumstances that cause potential defects and damage.
- Using qualified and experienced inspectors that have sufficient resources and incentives to perform quality inspections.

Prior to the commencement of any general survey, a standard checklist and procedure should be established from the Structural Life-Cycle Information Management System, in order to carry out an effective evaluation of the structure’s general conditions:

- Structural drawing
- Operating history and conditions
- Previous damage/defects inspection results
- Condition and extent of protective coatings
- Classification status, including any outstanding conditions of class
- Previous repair and maintenance work
- Previous information on unpredictable damage or defects
- Expert judgments and comments
- Relevant information from similar structures.

With this information and previous inspection guidelines regarding critical elements/subsystems in the structural systems that are considered to be sites of potential damage/defects based on historical data, analyses results, and experts’ judgments; it is possible to target the appropriate inspection strategies for the potential areas within the structure for a general survey and the initial scope of the inspection. After completing the initial inspection to determine the general condition of the system, the inspector can develop situation awareness to identify some potential unpredictable critical damage/defect sites. Further knowledge-based diagnosis should be conducted for these suspicious areas. The knowledge-based diagnosis is conducted along with detailed inspections.

Inspection Data System

Little thought has been given to the efficient gathering of data and information, even less thought has been given to what is done with this data and information when it is obtained, and far less thought has been given to the archiving, analysis, and reporting of the data. The interfaces in the data gathering, archiving, analysis, and reporting activities have

received very little systematic thought. Current work has not been able to identify a single coherent and optimum inspection data system.

Advances in information technology have resulted in better ways to use information for the management of safe and efficient ships and offshore structures. The integration of stand-alone systems, combined with improved information recording, organization, and communication, offer substantial benefits for the life-cycle management of ships and offshore structures. A life-cycle structural information management system (SMIS) is intended to facilitate the life-cycle management. This includes areas from design and construction as well as operations including inspection, maintenance, monitoring, and repair (IMMR). The inspection data system is a component of the IMMUR module in SMIS.

The general objectives of an inspection data system are:

- Collect inspection data
- Store the data
- Provide means for logic inspection data management
- Allow for the organization of the inspection data in a form suitable for fitness or purpose analyses, and failure analyses
- Analyze the data
- Show trends of the information such as damage/defects associated with structural integrity
- Communicate and report the data.

Once a structure is ready for service, a series of inspections are scheduled according to the inspection programs. The objective and scope of the internal tank inspections are defined. The access methods and data recording methods are chosen, and the inspections are performed. The inspection results including the corrosion gauging, cracking, status of coating, and the corrosion protection systems, as well as other structure/equipment defects are updated into the corresponding database. Using the inspected data, maintenance and repair strategies can be developed and the repairs can finally be carried out.

References

- Itagaki, H., Akita, Y., Nitta, A., November 1983. Application of subjective reliability analysis to the evaluation of inspection procedures on ship structures. In: Proc. Int. Symp. on the Role of Design, Inspection and Redundancy in Marine Structural Reliability. National Academic Press.
- Madsen, H.O., et al., 1986. Methods of Structural Safety. Prentice-Hall, Inc, Englewood Cliffs.
- Moan, T., 1993. Reliability and risk analysis for design and operations planning of offshore structures. In: Proc of the 6th Intl. Conf. on Struct. Safety and Reliability, ICOSSAR'93.
- Moan, T., 1997. Current trends in the safety of offshore structures, keynote lecture. In: Proc. 7th ISOPE, vol. VI. Honolulu, USA.
- Newman, J.C., Raju, I.S., 1981. An empirical stress intensity factor equation for surface crack. Engineering Fracture Mechanics 15, 185–192.

- Paris, P.C., Erdogan, F., 1963. A critical analysis of crack propagation laws. *Journal of Fluids Engineering*. ASME 85, 528–533.
- Shinozuka, M., Deodatis, O., 1989. Reliability of Marine Structures under Bayesian Inspection.
- Song, R., Moan, T., 1998. Fatigue reliability of large catamaran considering inspection updating. In: *Proceeding of the 8th International Offshore and Polar Engineering Conference (ISOPE'98)*, Montreal, Canada, May.
- Sun, H., Bai, Y., 2001. Time-variant reliability of FPSO hulls. *SNAME Transactions* 109.
- Xu, T., Bai, Y., Wang, M., Bea, R.G., May 2001. Risk Based Optimum Inspection of FPSO Hulls. OTC12949.
- Xu, T., Bea, R., 1997. Marine Infrastructure Rejuvenation Engineering-fatigue and Fracture of Critical Structural Details (CSD). JIP report. Marine Technology & Management Group, University of California at Berkeley.
- Yang, J.N., 1976. Inspection optimization for aircraft structures based on reliability analysis. *Journal of Aircraft*, AIAA Journal 14 (9), 1225–1234.
- Yazdan, N., Albrecht, P., 1990. Probabilistic fracture mechanics application to highway bridges. *Engineering Fracture Mechanics* 37, 969–985.

Risk Assessment Methodology

38.1 Introduction

38.1.1 Health, Safety and Environment Protection

In recent years, the management of health, safety and environmental protection (HSE) has become an important subject for the design and construction of marine structures. The objective of any design project is to engineer safe, robust, and operable structural systems at a minimum life cycle cost. The HSE target is to have an injury/illness free workplace during the design and construction process (Toellner, 2001). In addition, attention has been given to ergonomics and noise control for health protection (ASTM, 1988, 1995). Some other important subjects in HSE are, for instance, emergency response, evacuation, escape and rescue, fire protection and medical response. From the viewpoint of the environmental protection, the leakage of hydrocarbon from pipelines and risers, tankers and facilities need to meet the required standards. On many deepwater offshore projects, an environmental impact assessment is conducted. Air emission and discharges of waste are controlled.

Risk assessment is a tool for the management of safety, health and environmental protection.

38.1.2 Overview of Risk Assessment

Risk assessment is more frequently applied in managing safety, environmental and business risk. The purpose of this chapter is to discuss the basic procedures for the risk assessment, as shown in the flowchart in Figure 38.1 (NTS, 1998). Furthermore, this chapter explains risk concepts and risk acceptance criteria. More information may be found from NORSOK standard NTS (1998), Arendt et al. (1989), Aven (1992, 1994), Guedes Soares (1998).

Risk assessment was initially developed by the nuclear engineering community as a “probabilistic safety assessment” (NRC, 1983). It has also been applied by the chemical industry as a “quantitative risk assessment (QRA)” for risk management of chemical processes and chemical transportation (CCPS, 1989, 1995; Arendt et al., 1989). In recent years, it has been accepted by the marine and offshore industry; see Vinnem (1999) and CMPT (1999). In general, applications to engineering systems are discussed in Wilcox and Ayyub (2002). An extensive list of the recently published papers on marine risk assessment may be found in ISSC (2000).

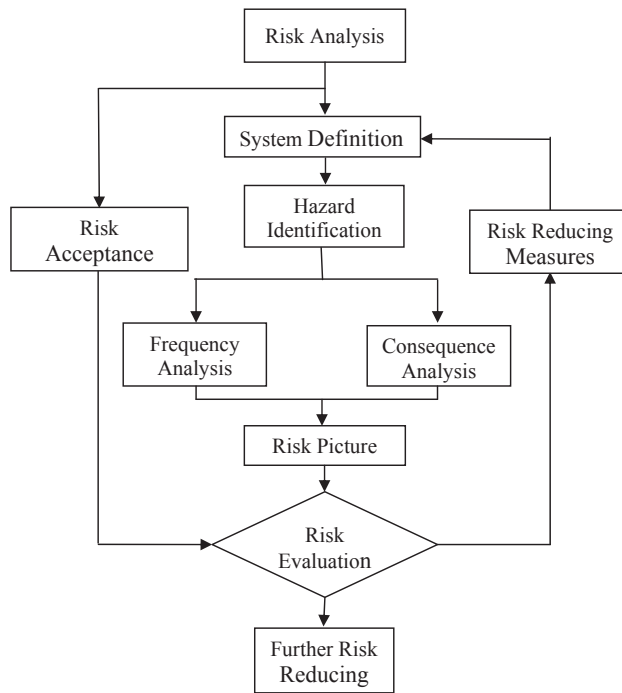


Figure 38.1

Risk estimation, analysis, and evaluation.

As shown in [Figure 38.1](#), the main steps of a risk assessment are:

- Planning of risk analysis
- System description
- Hazard identification
- Analysis of causes and frequency of initiating events
- Consequence and escalation analysis
- Identification of possible risk reducing measures

Each of the above steps is further explained below.

The risk assessment provides a qualitative/quantitative measure of risk. Through hazard identification, it is possible to separate critical hazards from uncritical ones. The process of risk reducing measures may control risk through a cost-effective design and procedure improvements.

38.1.3 Planning of Risk Analysis

Risk analyses are carried out as an integrated part of the design and construction project, so that these analyses form part of the decision-making basis for the design of safe, technical sound, cost-effective, and environmental friendly facilities.

Risk analyses are also conducted in connection with major facility modifications, such as change of installation sites and/or decommissioning/disposal of installations, and in connection with major changes to the organization and manning level.

The purpose and scope of work for the risk analysis should be clearly defined in accordance with the needs of the activity. The risk acceptance criteria need to be defined prior to the initiation of the risk analysis. It is helpful to involve operational personnel in the project execution. For the activity related to the design and construction of ships, mobile offshore drilling units and floating production installations, applicable regulations, classification rules, and industry standards/specifications, may all be useful.

When a quantitative risk analysis is carried out, the data basis should be appropriately selected. A sufficiently extensive data basis is a must in order to draw reliable conclusions. In some situations, comparative risk studies may lead to more meaningful conclusions.

To quantify accident frequency or causes, it is particularly important to establish a reliable data basis. The data basis should be consistent with relevant phases and operations. The analysis model shall comply with the requirements to input data and assumptions, etc. The quality and depth of the frequency, escalation and consequence modeling determine how detailed conclusions may be made for the systems involved in the analysis. The level of accuracy in the results may not be more extensive than what is justifiable, based on the data and models that are used for the quantification of the frequency and the consequence. For instance, risk may not be expressed on a continuous scale when the estimation of frequencies and/or consequences are based on categories.

38.1.4 System Description

The next step in a risk assessment is a detailed study of the system used, including a general description of the system's structure and operation, functional relationship between the elements of the system, and any other system constraints. The description of the system includes the technical system, period of time, personnel groups, the external environment, and the assets to which the risk assessment relates, as well as the capabilities of the system in relation to its ability to tolerate failures and its vulnerability to accidental effects.

38.1.5 Hazard Identification

Hazard identification establishes the foundation on which subsequent frequency and consequence estimates are made. The hazard identification yields a list of accidental situations that could result in a variety of potential consequences. The potential hazards are identified in order to avoid ignorance of the potential hazardous accidents in the risk assessment. Identification of hazards also includes a ranking of the significance of each hazard in relation to the total risk. For the subsequent analysis, hazards are roughly

classified into critical hazards and noncritical hazards. The criteria used in the screening of the hazards should be stated. The evaluations made for the classification of the noncritical hazards should be documented.

There are several approaches for hazard identification, and selecting a successful technique depends on the knowledge and information available. Possible data and tools for the hazard identification are a literature review, checklists and accident statistics, hazard and operability studies, and failure mode and effect analysis (FMEA). A safety audit, brainstorming, and experiences from previous projects may also be useful. It is also important to involve operational personnel.

38.1.6 Analysis of Causes and Frequency of Initiating Events

Analysis of possible causes of the initiating events gives the best basis for identifying measures that may prevent the occurrence of these events and thus prevent any accidents. Frequency assessment methods include:

- Historical data
- Fault tree analysis
- Event tree analysis
- FMEA
- Human reliability analysis

It is important to include contributions from both humans and operational factors.

In many cases, frequency may be estimated through a direct comparison with experience, or extrapolation from historical data. However, in most risk assessments, the frequencies are very low and therefore must be synthesized, which involves:

- Appropriate probabilistic mathematics
- Development of basic failure data, taken from available industry data
- Determination of the combinations of failures and circumstances that can cause accidents

38.1.7 Consequence and Escalation Analysis

This term is used in a wide sense, including the estimation of accidental loads and consequence modeling, the modeling of an escalation, and the estimation of responses to accidental loads. The distinction between cause analysis and consequence analysis may vary somewhat according to the purpose and the nature of the analysis. The most relevant methods for the escalation analysis include:

- Event tree analysis
- Fault tree analysis
- Simulation/probabilistic analysis.

The consequence analysis involves the following:

- To characterize the release of material or energy due to the hazards being identified, through the use of experiments and analysis models that have been developed for consequence analysis.
- To measure/estimate the release/propagation of the material/energy in the environment on the target of interest.
- To quantify the safety, health, environmental and economical impacts on the target of interests, in terms of the number of fatalities and injuries, amount of materials released to the environment, and the dollar values lost.

Like frequency estimates, there are large uncertainties in the consequence estimates due to differences in time-dependent meteorological conditions, basic uncertainties in physical and chemical properties, and model uncertainties.

In any case, examining the uncertainties and sensitivities of the results to the changes in assumptions and boundary conditions, may provide great perspective. It is necessary to put one-third to one-half of the total effort of a risk assessment into the consequence evaluation, depending on the number of different accident scenarios and accidental sequences that are being considered.

38.1.8 Risk Estimation

A general expression of risk “ R ” is:

$$R = \sum f(p, C) \quad (38.1)$$

where p and C denote frequency and consequence of accidents respectively. The risks due to all possible events can be summed up for all situations considered in the analysis. The results of the uncertainty analysis can be presented as a range defined by the upper and lower confidence bounds and the best estimates. It should also be kept in mind that potential severe accidents usually generate greater concern than smaller accidents, even though the risk (product of frequency and consequence) may be equivalent.

The estimated frequencies and consequences are integrated into a presentation format on an absolute basis compared with a specific acceptance criterion, or on a relative basis to avoid arguments regarding the adequacy of the absolute numbers.

When evaluating risk estimates, it is recommended to calculate the importance of various components, from human errors and accident scenarios to the total risk. It may be useful to calculate the total risk estimate sensitivity to changes in assumptions, frequencies, or consequences. Through these exercises, the major risk contributors may be identified, and on which risk reducing measures can then be taken.

38.1.9 Risk Reducing Measures

Risk reducing measures include frequency reducing and consequence reducing activities, and their combinations. The measures may be of a technical, operational, and/or organizational nature. Choosing the types of measures is normally based on a broad evaluation, where risk aspects are considered. Emphasis should be put on an integrated evaluation of the total effects that any risk reducing measures may have on the risk. If alternative measures are proposed, possible coupling between risk reducing measures should be communicated explicitly to the decision-makers. Priority is given to the measures that reduce the frequency for a hazardous situation, when choosing which measures are initiated and developed into an accident event. In order to reduce any consequences, measures should be taken into account for the design of load bearing structures and passive fire protection, etc. Layout arrangements are suitable for the operations and minimize the exposure of personnel to accidental loads.

When selecting risk reducing measures, consideration is given to their reliability and the possibility of documenting and verifying the estimated extent of risk reduction. Consequence reducing measures (especially passive measures such as passive fire protection) will often have a higher reliability than frequency reducing measures, especially for the operating conditions.

The possibility of implementing certain risk reducing measures is dependent on factors such as available technology, the current phase in the activity, and the results of cost–benefit analysis. The choice of risk reducing measures can therefore be explained in relation to such aspects.

38.1.10 Emergency Preparedness

Emergency preparedness is also a part of the risk assessment. The goal of emergency preparedness is to be prepared to take the most appropriate action to minimize effects and to transfer personnel to a safer place in the event that a hazard becomes a reality (NTS, 1998; Wang, 2002). In the United Kingdom, it is not legal to operate an offshore installation without an accepted operational safety case, which is a written submission prepared by the operator for the installation.

38.1.11 Time-Variant Risk

Risk, $R(t)$, is a function of time, and may be denoted as the production of the time-variant probability, $p(t)$ and time-variant consequence, $C(t)$

$$R(t) = \sum \{p(t) \times C(t)\} \quad (38.2)$$

The time rate of change of risk may be written as

$$\frac{dR(t)}{dt} = \sum \left\{ \frac{dp(t)}{dt} \times C(t) + p(t) \times \frac{dC(t)}{dt} \right\} \quad (38.3)$$

The above equation shows that the most significant measures taken to reduce risk are, to reduce the probability of the largest consequence events, and to reduce the consequence of the highest probability events. In incremental form, the effect of risk reducing measures may be expressed as

$$dR(t) = \sum \{ dp(t) \times C(t) + p(t) \times dC(t) \} \quad (38.4)$$

A negative value of $dR(t)$ would mean the overall risk level has been reduced, due to reduced probability, reduced consequence, or a combination of both.

38.2 Risk Estimation

38.2.1 Risk to Personnel

The risk to personnel is often expressed as a fatality risk, or sometimes as a risk in relation to personnel injury. An estimate of the personnel injured in accidents is often required as input for an emergency preparedness analysis.

Individual Risks

The most common measure of the fatality risk is the risk to individuals. PLL (Potential Loss of Life) is calculated according to Eqn (38.5) below

$$PLL = \sum_N \sum_J f_{nj} \times c_{nj} \quad (38.5)$$

where

- f_{nj} = Annual frequency of accident scenario n with personnel consequence j
- c_{nj} = Annual number of fatalities for scenario n with personnel consequence j
- N = Total number of accident scenarios in all event trees
- J = Total number of personnel consequence types, usually immediate, escape, evacuation and rescue effects

FAR (Fatal Accident Rate) and AIR (Average Individual Risk) express the IR (Individual Risk). The FAR value expresses the number of fatalities per 100 million exposed hours for a defined group of personnel. The AIR value indicates the fatality risk per each exposed person onboard. Both FAR or AIR can be based on the total offshore hours (8760 h per year), as shown below.

$$FAR = \frac{PLL \times 10^8}{Exposed\ hours} = \frac{PLL \times 10^8}{POB_{ev} \times 8760} \quad (38.6)$$

$$AIR = \frac{PLL}{Exposed\ Individuals} = \frac{PLL}{POB_{ev} \times \frac{8760}{H}} \quad (38.7)$$

where,

POB_{ev} = Average annual number of manning levels

H = Annual number of offshore hours per individual

Society Risks and f - N Curves

Society has shown that it is concerned with the effects on society that may occur from an accident. Therefore, some measure of risk to society (i.e., the total effect of accidents on society) is required. This is the group risk's (GR's) main goal. Group risk is often expressed in terms of an " f - N " curve (f = frequency, N = number—i.e., measurement of consequence), as shown in Figure 38.2 below.

The f - N curve expresses the acceptable risk level, according to a curve where the frequency is dependent on the extent of consequences, such as the number of fatalities per accident. The calculation of values for the f - N curve is cumulative—that is, a particular frequency relates to " N or more" fatalities.

38.2.2 Risk to Environment

The assessment of environmental risk includes, an establishment of a release duration distribution, a simulation of an oil spill for relevant scenarios, an estimation of the effects

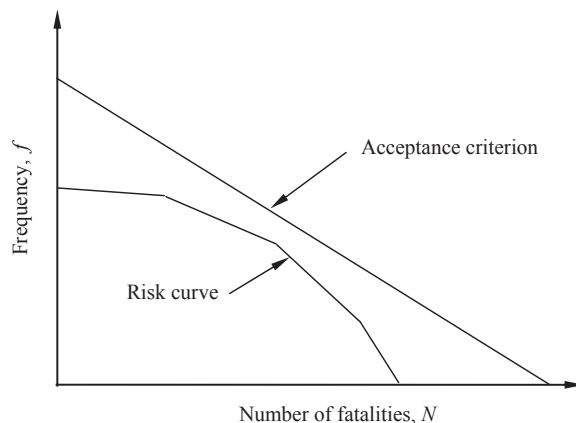


Figure 38.2
 f - N curve.

on environmental resources and the restoration time. The overall principles used to estimate environmental risk are (NTS, 1998):

- Valued ecological components (VECs) are identified
- Assessment is focused on “most vulnerable resources”
- Damage frequency is assessed for each VEC
- Restoration time is used to measure environmental damage

The environmental damage may have the following categories, based on the restoration time:

- Minor—environmental damage with recovery between 1 and 12 months
- Moderate—environmental damage with recovery between 1 and 3 years
- Significant—environmental damage with recovery between 3 and 10 years
- Serious—environmental damage with recovery in excess of 10 years

38.2.3 Risk to Assets (Material Damage and Production Loss/Delay)

The risk to assets is usually referred to as material damage and production loss/delay. The material damage can be categorized as, the local, one module, several modules, or total loss. The production delay is categorized by the delay time: 1–7 days, 1 week–3 months, 3 months–1 year, above 1 year, etc.

In order to estimate the risk for asset damage and production delay, the distribution for duration of accidental events is established, and a response is calculated in the form of equipment and structures.

38.3 Risk Acceptance Criteria

38.3.1 General

How safe is safe enough? Risk acceptance criterion defines the overall risk level that is considered acceptable, with respect to a defined activity period. The criteria are a reference for the evaluation of the need for risk reducing measures, and therefore need to be defined prior to initiating the risk analysis. Additionally, the risk acceptance criteria must reflect the safety objectives and the distinctive characteristics of the activity.

The risk acceptance criteria may be defined in either qualitative or quantitative terms, depending on the expression for risk. The basis for their definition includes:

- Governmental legislation applicable to the safety in the activity
- Recognized industry standards for the activity
- Knowledge of accidental events and their effects
- Experience from now and past activities

According to the purpose and the level of detail for the risk analysis, the acceptance criteria may be:

- High-level criteria for quantitative studies
- Risk matrices and the ALARP principle
- Risk comparison criteria

Fischhoff et al. (1981) identified and characterized various methods for the selection of risk acceptance criteria. They indicated that values, beliefs, and other factors all influence the selection of risk acceptance criteria. The complexity of defining risk acceptance criteria should be explicitly recognized, due to the uncertainty of their definition, lack of relevant facts, conflicting social values, and disagreements between technical experts and the public. The selection of risk acceptance criteria is subject to a rigorous critique, in terms of philosophical presuppositions, technical feasibility, political acceptability, and the validity of underlying assumptions made about human factors.

38.3.2 Risk Matrices

The arrangement of accident frequency and the corresponding consequences in a matrix (see Figure 38.3) may be a suitable expression of risk where many accidental events are involved or where single value calculations are difficult. The matrix is separated into three regions, including:

- Unacceptable risk
- Acceptable risk

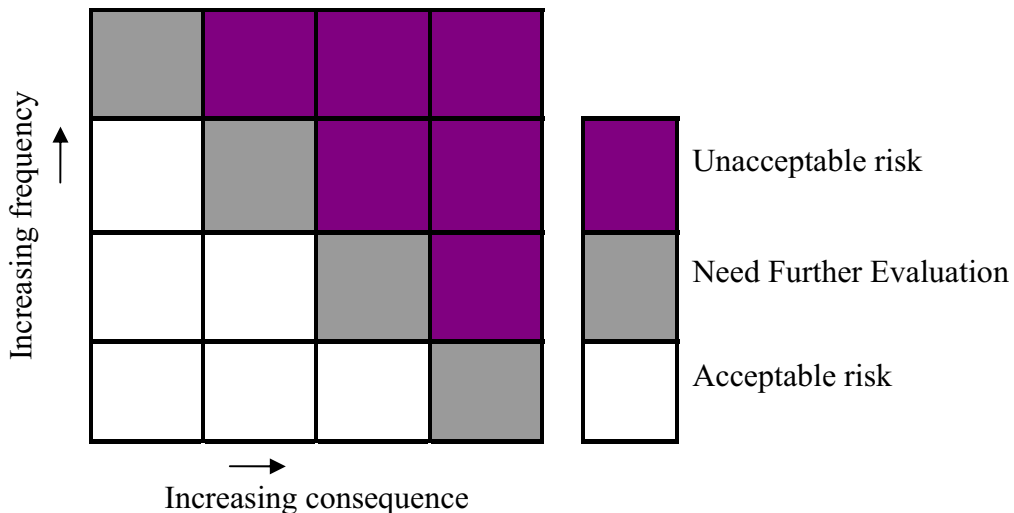


Figure 38.3
Risk matrix.

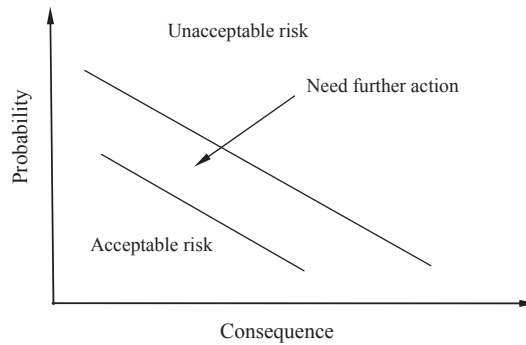


Figure 38.4

Risk matrix in terms of continuous variables.

- A region between acceptable and unacceptable risk, where evaluations have to be carried out in order to determine whether further risk reduction is required or whether more detailed studies should be conducted.

The limits of acceptability are set by defining regions in the matrix, which represent unacceptable and acceptable risk. The risk matrix may be used for qualitative and quantitative studies. If frequency is classified in broader categories such as rare and frequent, and consequences are classified as small, medium, and catastrophic, the results from a qualitative study can be shown in the risk matrix. The definition of the categories is particularly important in the case of qualitative use.

The categories and the boxes in the risk matrix can be replaced by continuous variables, implying a full quantification. An illustration of this is shown in [Figure 38.4](#).

The following are examples of situations where the use of a risk matrix is natural:

- Evaluation of personnel risk for different solutions such as integrated versus separate quarters.
- Evaluation of risk in relation to operations such as exploration drilling.
- Evaluation of risk in relation to a particular system such as mechanical pipe handling.
- Evaluation of environmental risk.

38.3.3 The ALARP Principle

The ALARP (“as low as reasonably practicable”; see [Figure 38.5](#)) principle is sometimes used in the oil and gas industry ([UK HSE, 1992](#)). The use of the ALARP principle may be interpreted as, satisfying a requirement to keep the risk level “as low as possible” provided that the ALARP evaluations are extensively documented. In the ALARP region (between “lower tolerable limit” and “upper tolerable limit”), the risk is tolerable, only if risk

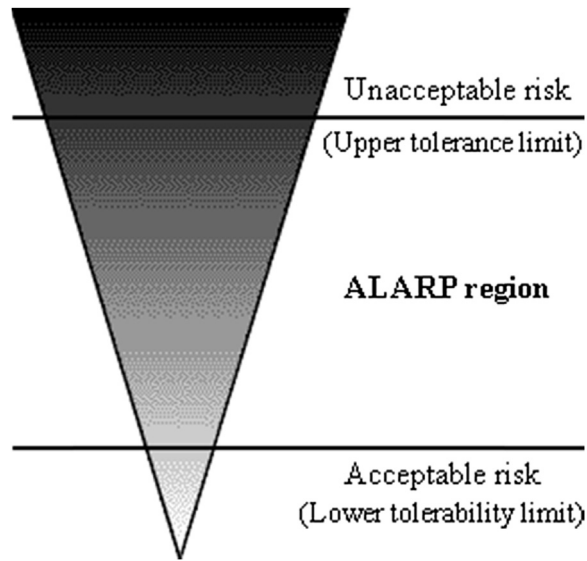


Figure 38.5
The ALARP principle.

reduction is impracticable or if its cost is grossly disproportionate to the improvement gained. The common way to determine what is practicable is to use cost–benefit evaluations as a basis for the decision on whether certain risk reducing measures should be implemented. A risk may not be justified in any ordinary circumstance, if it is higher than the “upper tolerable limit.” The “upper tolerable limit” is usually defined, whereas the “lower tolerable limit” may sometimes be left undefined. This will not prohibit effective use of the approach, as it implies that ALARP evaluations of risk reducing measures will always be required. The ALARP principle used for risk acceptance is applicable to risks regarding personnel, the environment, and assets. [Trbojevic \(2002\)](#) illustrated the use of the ALARP principle for a design.

38.3.4 Comparison Criteria

This type of criteria is suitable for more limited studies that aim at comparing certain concepts or solutions for a particular purpose with established or accepted practices. The criteria are suitable in relation to operations that are often repeated such as drilling and well interventions, heavy lift operations, and diving. The use of the comparison criteria requires that the basis of the comparison be expressed precisely.

The formulation of the acceptance criterion in this context may be that the new solution cannot represent any increase in risk, in relation to current practices.

Examples of comparison criteria are:

- Alternative design (or use of new technology) for a fire water system can be at least as safe as conventional technology
- The risk level for the environment cannot be higher than with the existing solution
- Alternative solutions can be at least as cost-effective as the established practice

This type of risk acceptance criteria is also suitable for risk regarding personnel, the environment, and assets.

38.4 Using Risk Assessment to Determine Performance Standard

38.4.1 General

LR (1999) published guidelines for classification, using risk assessment techniques to determine performance criteria. The risk assessment methodology used in LR (1999) is similar to that described in Section 381 through Section 383 of this chapter. LR (1999) guidelines include the following:

- A “critical element” is a part of the installation, or a system, subsystem, or component that is essential to the safety and integrity of the installation, all in relation to identified hazards.
- “Performance standards” are statements that can be expressed in qualitative or quantitative terms. They state the performance required of a critical element, in order to manage the identified hazards, and ensure the safety and integrity of the installation.
- “Verification” is the confirmation of the design, manufacturing, construction, installation, and commissioning of critical elements in order to demonstrate that they meet the required performance standards. The verification may be used for new construction and in-service installations.
- “Inspection and maintenance plan” is the owner/operator’s program of scheduled inspection and maintenance activities that ensure the required performance standards continue to be met in service, as well as to maintain the safety and integrity of the installation against any identified hazards.

38.4.2 Risk-Based Fatigue Criteria for Critical Weld Details

An example application is used for the determination of the fatigue acceptance criteria for critical weld details, and for the development of corresponding inspection and maintenance plan, as laid out below:

- Critical elements (weld details) are identified in relation to the fatigue failure through screen analysis, based on simplified fatigue assessment. The consequence of failure may also be accounted for in relation to a reduction in safety and integrity of the installation.

- In the design phase, performance standards (fatigue acceptance criteria) may be established in quantitative terms in order to ensure that it will not experience the fatigue failure that threatens the safety and integrity of the installation.
- A verification process is applied for new construction projects, in order to confirm that the selected critical elements (weld details) meet the predefined performance criteria (fatigue acceptance criteria).
- For an in-service installation, a program is established to schedule and plan inspection and maintenance activities that ensure the required fatigue criteria are met. Verification is conducted to confirm that the identified critical weld details continue to meet the predefined fatigue criteria.

38.4.3 Risk-Based Compliance Process for Engineering Systems

Owing to the difficulty of developing prescriptive requirements for all possible system designs, governmental regulations and industry design codes provide provisions for the design equivalency of an alternate design, to the existing requirements. [Wilcox and Ayyub \(2002\)](#) proposed a risk-based compliance approval process, to deal with new concepts and special classes of engineering designs, by establishing safety equivalency to current standards and existing accepted designs. Risk is used as an overall performance measure to assist in the decision-making for a system design. The risk-based compliance approval methodology aids in identifying critical factors. The process may also be suitable for assessing conventional engineering systems and performing safety calibrations. The risk acceptance criteria may be established through the calibration of existing codes and safety goals. Testing and monitoring programs, improve the understanding of system performance, they help control risk, and improve quality in manufacturing and operational phases.

References

- Arendt, J.S., Lorenzo, D.K., Lusby, A.F., 1989. Evaluating Process Safety in the Chemical Industry—A Manager's Guide to Quantitative Risk Assessment. Chemical Manufactures Association.
- ASTM, 1988, 1995. ASTM F1166–95a: Standard Practice for Human Engineering Design for Marine Systems, Equipment and Facilities. American Society of Testing and Materials.
- Aven, T., 1994. On safety management in the petroleum activities on the Norwegian continental shelf. *Journal of Reliability Engineering and System Safety* 45, 285–291.
- Aven, T., 1992. *Reliability and Risk Analysis*. Elsevier, England.
- CCPS, 1989. *Guidelines for Chemical Process Quantitative Risk Analysis*. Center for Chemical Process Safety, American Institute of Chemical Engineers.
- CCPS, 1995. *Chemical Transportation Risk Analysis*. Center for Chemical Process Safety, American Institute of Chemical Engineers.
- CMPT, 1999. *A Guide to Quantitative Risk Assessment of Offshore Installations*.
- Fischhoff, B., Lichtenstein, S., Slovic, P., Berby, S.L., Keeney, R., 1981. *Acceptable Risk*. Cambridge University Press.

- Guedes Soares, C., 1998. Risk and Reliability in Marine Technology. A.A. Balkema, Rotterdam, The Netherlands.
- ISSC, 2000. Risk assessment. In: Proceedings of the International Ship and Offshore Structures Congress, Nagasaki, Japan.
- LR, 1999. Guidelines for Classification Using Risk Assessment Techniques to Determine Performance Criteria. Part 1A of the LR Rules and Regulations for the Classification of a Floating Offshore Installation at a Fixed Location, Lloyd's Register.
- NRC, January 1983. PRA Procedures Guide—A Guide to the Performance of Probabilistic Risk Assessment for Nuclear Power Plants. NUREG/CR-2300. Nuclear Regulatory Commission.
- NTS, March 1998. Risk and Emergency Preparedness Analysis. NORSOK Z-013. Norwegian Technology Standards.
- Toeliner, J., 2001. Safety Partnerships with Contractors: A Hoover/Diana Project Success Story. OTC 13080.
- Trbojevic, V.M., 2002. ALARP principle in design. In: Proceedings of OMAE Conference.
- UK HSE, 1992. Safety Case Regulations. Health and Safety Executives, HMSO.
- Vinnem, J.E., 1999. Quantified Risk Assessment—Principles, Modelling and Applications of QRA Studies. Kluwer Academic Publishers.
- Wang, J., 2002. A brief review of marine and offshore safety assessment. SNAME Journal of Marine Technology 39 (2), 77–85.
- Wilcox, R., Ayyub, B.M., 2002. A risk-based compliance process for engineering systems. In: SNAME Annual Conference Proceedings and Transactions.

Risk-Based Decision-Making

Most participants in the maritime and other industries are continually faced with difficult decisions. It is a simple fact that the hazards of greatest concern today are more difficult to observe and evaluate than were the major hazards of the past. Five factors, and likely more, contribute to the growing difficulty in making “good” decisions. These factors include: complexity (of the choices and environment in which made), multiple (and often conflicting) objectives, different perspectives of those involved, sensitivity of decisions to changes (in information, conditions, etc.), and finally the uncertainty of key variables in the decision process. The latter is an important but often-neglected point, and worthy of additional discussion (Duane Boniface).

Uncertainties (or variabilities) pervade every aspect of the maritime industry from design, through construction and operation, until the final scrapping of a ship, platform, or facility. Variabilities in material properties, construction techniques, and operations are an everyday fact of life in any technical field. Table 39.1 lists and describes the three categories of uncertainties that are encountered. These uncertainties are the primary cause of the risks associated with the maritime industry. The effects of these uncertainties are felt by all involved in the marine system. The field of risk-based decision-making (RBDM), sometimes called risk analysis or risk management, was developed in order to deal with these uncertainties. RBDM allows the uncertainties to be characterized, and integrated into such activities as planning, crisis prevention, and management. RBDM methods form a process by which decisions can be made regarding safety, durability, serviceability, and compatibility.

Table 39.1: Types of uncertainties

Category	Description	Examples
I—Inherent	Natural randomness of a quantity	Structural strength and loading
II—Model	Randomness due to imperfections in imitations of the real world by mathematical models	Assumptions such as holding gravitational acceleration constant
III—Human and organizational error	Variability due to effects of human involvement	Differences in skill and performance levels between individuals and organizations

RBDM processes have been the subject of a great deal of interest in industry recently, with their ability to encode and incorporate the uncertainties inherent in today's highly complex and variable times. RBDM provides a process to ensure that optimal decisions consistent with the goals and perceptions of those involved are reached. This process ensures that all available information is considered and used as appropriate to the decision at hand. This process should include not only information held by the US Coast Guard (USCG), but also information that can be obtained from other stakeholders. "Optimal" decisions are not necessarily those that achieve the best outcome, which is a result of chance as much as decision-making skill, but rather those that are most appropriate for the information, values, and goals of the particular situation. On average and over time, these decisions should provide the best outcomes. The use of a risk-based system allows consistent decisions to be made that are also consistent with the stated values of the organization. Finally, use of the formal assessment processes minimizes the number and degree of surprises encountered, due to the thorough study of the problem.

There are many benefits from using risk-based methods. First and foremost among these is the ability to optimize a system (hardware, procedures, regulations, personnel, etc.) for a given application and set of conditions. "Traditional" management techniques will tend to overstrengthen some aspects of the system and insufficiently address others. RBDM, on the other hand, allows the manager to address uncertainties associated with the process and identify areas that may be over- or underdesigned. Furthermore, analysis of safety levels of new and unique situations can be made and compared with those deemed "safe," which cannot be done using other methods. With these increased insights into the strengths and weaknesses of a given structure or system comes the ability to prioritize attention on those areas that have the lowest safety levels.

The RBDM process outlined later in these Guidelines does not replace a decision maker. Its sole purpose is to support the decision maker as a source of information, supplying not only the optimal solution, but also insight regarding the situation, including uncertainties involved, objectives, trade-offs, and the various value judgments and assessments of the stakeholders involved.

To use RBDM methods, you must start with a review of the fundamentals of probability and statistics. Following this, the basic principles of RBDM will be discussed. These precepts will be expanded upon in the following sections.

39.1 Basic Probability Concepts

The concept of probability (and therefore, risk) is interpreted from three very different viewpoints. These three interpretations are shown in [Table 39.2](#) below. While all three can and should be used to support decision-making, the third interpretation (subjective) is

Table 39.2: Probability interpretations

Probability Interpretation	Description
Classical	The probability of an event is the ratio of the number of outcomes with the attributes of the event to the total number of equally likely and different ways.
Frequency	The probability of an event is given by the limit of its relative frequency as the number of samples becomes large.
Subjective	The probability of an event is a measure of the degree of belief that one holds for that event.

perhaps the most valuable to the maritime manager. Rarely does he/she have the luxury of obtaining a large number of tests (as required for the frequency method), nor are exact probabilities known for most events (as required for the classical method). All three interpretations follow the same rules and axioms, and can therefore be used together to allow the strengths of each to be used.

One of the first concepts that must be understood before undertaking RBDM is that most fundamental notion: “What is risk?” Given the relatively recent development of the field of risk analysis and risk management, there has not been time to reach a consensus on the exact definition of this term. Here, we will define risk as the exposure to the chance of loss, or the combination of the probability of a hazard occurring and the significance of the consequence of the hazard occurring. Mathematically, this is can be interpreted as shown in Equation 1-1.

Risk of a specific hazard = Probability of that hazard * Consequence of that hazard if it were to occur.

Hazards are potential undesirable events in a given system along with their associated consequences, and are characterized in terms of those consequences (dollars spent, lives lost, etc.). Risk, on the other hand, is a somewhat more nebulous quantity, as it incorporates the likelihood of experiencing that hazard. In attempting to prevent and mitigate hazards within maritime systems, we define and rank their associated risks.

Risks can be characterized in terms of probability (the likelihood of some event occurring), consequences (monetary and nonmonetary “costs” of an event), and sensitivity to countermeasures (susceptibility to risk management measures), as shown in [Figure 39.1](#).

Risk characteristics can be rated either qualitatively (e.g., low, medium, or high) or quantitatively (e.g., dollar amounts or numerical probabilities). Quantitative ranking systems are the easier to utilize, if risk characteristics can be naturally derived from available data. Qualitative ranking systems are useful in comparing dissimilar risks or risks for which reliable data are not available.

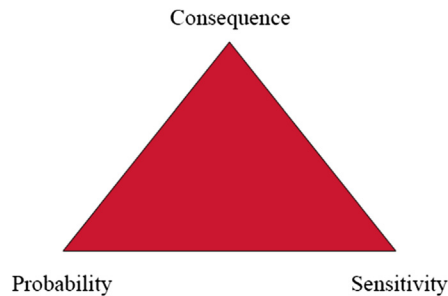


Figure 39.1
Risk characteristics.

Risk characterization typically takes place in the risk assessment process (as shown and described below), although it can be continued in the risk management phase as well. These processes will now be briefly described.

39.2 The RBDM Process

RBDM comprises five major components as shown in [Figure 39.2](#). This is an iterative, never-ending process. While this may seem to be troublesome given the limited resources available to a manager, it should be noted that, after experience with the process and philosophy of RBDM, this will become almost second nature. It is our goal that the use of RBDM as a formal program be short-lived. Instead, it should be deformalized and incorporated into everyday management activities.

The first step in this decision-making process is the identification and delineation of a set of goals for the group. This step, as with every step, should be a group effort, ratified by group consensus. Not shown here, but a critical step in the process is the involvement of stakeholders in identifying and resolving problem areas. With increased group involvement come many benefits, such as greater acceptance of goals (with the resultant increase in



Figure 39.2
RBDM process.

motivation) and better understanding of goals (with the increased ability to effectively support goal-related activities). Goal selection, while a very important step, is covered in other guidelines and directives, and will not be covered here. In this guideline, geared toward helping marine safety units in supporting and achieving local business plan goals, the assumption is that group goals have already been established and validated. What remains is the development of the rest of the process, whereby assessments and plans are made for the achievement of those goals, as well as the development of a feedback loop, which provides for the continual improvement of the goals. These stages are briefly described here in order to provide a basic understanding of the overall process. They will be described individually in greater detail in later enclosures, to provide you with adequate information and guidance for utilizing the process.

39.2.1 Risk Assessment

Risk assessment is the process of identifying potential hazards in the system and ranking them (and/or their components) in terms of risk characteristics as defined previously. As such, it attempts to provide answers to the following questions:

- What can go wrong?
- What is the likelihood that it will go wrong?
- What are the consequences?

39.2.2 Risk Management

Once a screened and prioritized list of risks has been developed, a risk management action plan can be developed. As risk countermeasures will vary widely for different situations, no comprehensive list of potential management actions is possible. Generally, risk management attempts to provide answers to the following questions:

- What can be done?
- What options are available and what are their associated trade-offs?
- What are the effects of current decisions on future options?

39.2.3 Impact Assessment

In order to provide input for future risk assessments and goal setting and selection, an assessment of the effects of the countermeasures used must be conducted. As with all the data collection and analysis in this process, both subjective and objective means should be used to identify and rank the changes in risk resulting from risk management activities. For objective data, sources such as governmental and industry databases should be investigated for relevant and accurate data.

39.2.4 Risk Communication

As shown in Figure 39.2, effective risk communication is a two-way process that must take place throughout the RBDM process. It starts in the assessment process with the incorporation of subjective and objective stakeholder input. This not only provides a more complete set of information for the analysis, but also heightens awareness and goes a long way toward ensuring “buy-in” to assessment results and subsequent management activities. After the screened and prioritized list of risks has been developed, it must then be communicated to stakeholders. Urgent items should be forwarded up the chain of command for informational and action/decision purposes. Once stakeholders have had time to review and discuss assessment results, communication would continue by way of them providing input for determining appropriate management actions. Finally, reports on the results shall be made to stakeholders and up the chain of command. Senior commands would review these in order to obtain the information needed for their own risk assessment and management activities.

What has been presented here is but a brief summary of RBDM. A great deal more information is available in the literature of the field. This Guideline is not intended to replace or repeat the numerous references available. Instead, the goal here is to present a decision-making methodology and the major principles contained and used therein.

39.3 A Step-by-step Example of the RBDM Process in the Field

Figure 39.3 summarizes the key RBDM steps in this application. The tables following the figure illustrate the steps applied by the unit for this decision-making process.

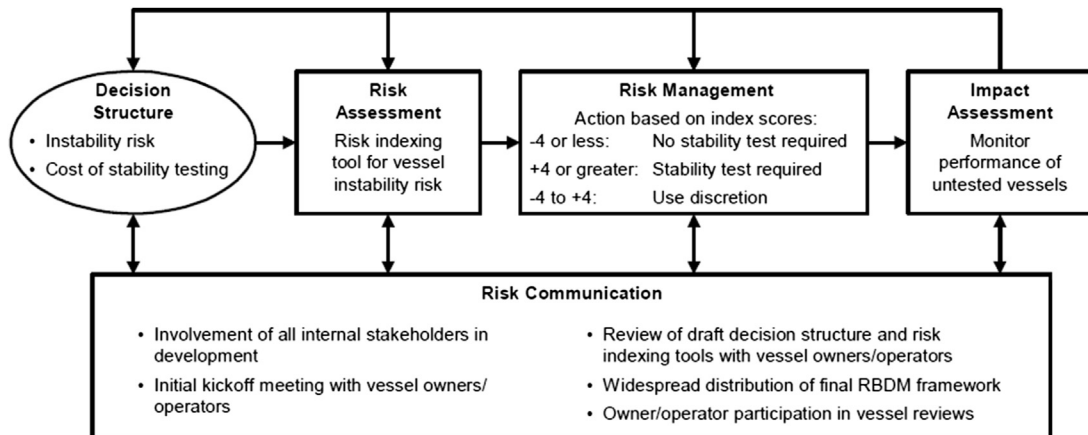


Figure 39.3
RBDM process for stability testing application.

Step 1: Establish the Decision Structure

Step 1a: Define the Decision

Description:

Specifically describe what decision(s) must be made. Major categories of decisions include (1) accepting or rejecting a proposed facility or operation, (2) determining who and what to inspect, and (3) determining how to best improve a facility or operation.

Example result:

The officer-in-Charge, Marine Inspections (OCMI) can require stability evaluations of new and existing vessels if stability is in question. The unit defined the decision as follows: “For which vessels is a stability evaluation warranted because the potential benefit of detecting an unknown stability deficiency would outweigh the vessel owner’s cost of conducting the evaluation?”

Step 1b: Determine Who Needs to Be Involved in the Decision

Description:

Identify and solicit involvement from key stakeholders who (1) should be involved in making the decision or (2) will be affected by actions resulting from the decision-making process.

Example result:

The unit decided that the OCMI, the inspection department, and the USCG Marine Safety Center were the key stakeholders involved in making the decision. They also chose to involve a marine engineering consultant on vessel stability. The RBDM team also knew that the potentially affected vessel owners/operators were stakeholders and should be involved through special outreach efforts.

Step 1c: Identify the Options Available to the Decision Maker

Description:

Describe the choices available to the decision maker. This will help focus efforts only on issues likely to influence the choice among credible alternatives.

Example result:

The unit decided that the following options were available to the decision maker:

- Require simplified stability tests for all vessels.
- Require simplified stability tests only where indicated by regulations.
- Require simplified stability tests only for “high-risk” vessels or as specifically required by regulations.

Step 1d: Identify Factors That Will Influence the Decision (Including Risk Factors)

Description:

Few decisions are based on only one factor. Most require consideration of costs, schedules, risks, etc., at the same time. The stakeholders must identify the relevant decision factors.

Example result:

The unit identified the following decision factors:

- Vessel instability risk based on Route
 - operations;
 - design;
 - modifications;
 - vessel history;
 - cost of conducting simplified stability tests (including actual testing and loss of service time).

The unit did note a few special cases that warranted prescriptive decisions:

- Never require a stability test for a powered catamaran.

- Never require a stability test for a vessel with a true sister ship (whose stability is already established).
- Always require a stability test for a vessel on an exposed route.
- Always require a stability test if a vessel has had a >2% aggregate weight change.

Step 1e: Gather Information About the Factors That Influence Stakeholders

Description:
Perform specific analyses (e.g., risk assessments and cost studies) to measure against the decision factors.

Example result:
The unit understood the approximate cost of simplified stability tests and the associated loss of service time for vessels. The team chose not to evaluate this factor further.
Instead, the unit focused on measuring relative risks of vessel instability among new and existing vessels in the unit's zone. The unit decided to use a risk assessment process (as described in step 2) to measure the relative risks.

Step 2: Perform the Risk Assessment

Step 2a: Establish the Risk-Related Questions That Need Answers

Description:
Decide what questions, if answered, would provide the risk insights needed by the decision maker.

Example result:
The unit decided that the basic risk-related question was as follows: "What combination of vessel and operational characteristics poses significant vessel instability risks that might require a simplified stability test?"

Step 2b: Determine the Risk-Related Information Needed to Answer the Questions

Description:
Describe the information necessary to answer each question posed in the previous step. For each information item, specify the following:

- Information type needed
- Precision required
- Certainty required
- Analysis resources (staff hours, costs, etc.) available.

Example result:
Information type needed:
A risk index number is needed for measuring the risk of an unknown instability for a given vessel and operational condition.
Precision required:
The index number does not have to be highly precise (e.g., integer values), but the risk factors considered must be defined very specifically.
Certainty required:
The RBDM team needs to have high confidence that high index scores reflect high risk and low index scores reflect low risk, recognizing that some intermediate scores may represent a gray area where the risk is unclear.
Analysis resources available:
Application of the risk-scoring process to a particular vessel must be very efficient (e.g., requiring only a few minutes to apply) and must not require a risk analysis expert. However, the unit was willing to spend a couple of days developing a risk analysis job aid.

Step 2c: Select the Risk Analysis Tool(s)

Description:

Select the risk analysis tool(s) that will most efficiently develop the required risk-related information.

Example result:

Based on the decision-making situation and the type of information needed, the unit decided to create a simple **relative ranking/risk indexing tool**. The team also used **event tree analysis** to help ensure that the right risk factors were built into the index tool. The team determined that the following actions should be taken for certain risk index values:

- -4 or less: No stability test required
- +4 or greater: Stability test required
- -4 to +4: Use discretion in deciding.

Step 2d: Establish the Scope for the Analysis Tool(s)

Description:

Set any appropriate physical or analytical boundaries for the analysis.

Example result:

The unit focused only on vessels for which stability tests were not specifically required by regulations. The unit’s analysis considered only the risk factors that the team explicitly built into the risk index tool (i.e., no other brainstorming was performed).

In addition, the unit did not apply the tool to powered catamarans, vessels with true sister ships, or vessels on exposed routes because the decisions for these vessels would not be affected by the risk scores (as mentioned previously).

Step 2e: Generate Risk-Based Information Using Analysis Tools

Description:

Apply the selected risk analysis tool(s). This may require the use of more than one analysis tool and may involve some iterative analysis (i.e., starting with a general low-detail analysis and progressing toward a more specific high-detail analysis).

Example result:

First, the unit applied the risk index tool to a number of test case vessels to ensure that the tool was “tuned” properly. The unit compared the resulting risk priorities to its own subjective priorities assigned from experience. Based on these tests, the unit made some revisions to the index tool. This reality check helped validate the tool before it was used in actual RBDM applications for vessels.

Then, the unit began applying the risk indexing tool for specific vessels needing stability test determinations.

The unit uses the results to help make risk management decisions for each vessel. Vessel owners/operators (or their representatives) are directly involved with unit personnel in this process.

Step 3: Apply the Results to Risk Management Decision-Making

Step 3a: Assess Possible Risk Management Options

Description:

Determine how the risks can be managed most effectively. This decision may include (1) accepting/

Example result:

For each vessel, the unit looks for simple vessel configuration or operational changes that might make stability testing unnecessary, especially when a

rejecting the risk or (2) finding specific ways to reduce the risk.

preliminary analysis indicates that testing may be required (or if the decision is unclear). Once improvement options have been fully considered, the team uses the final risk index value to help make a decision about stability testing.

Step 3b: Use Risk-Based Information in Decision-Making

Description:

Use the risk-related information within the overall decision framework to make an informed, rational decision. This final decision-making step often involves significant communication with a broad set of stakeholders.

Example result:

For vessels with extreme risk index scores (above +4 or below -4), the index score drives the decision as described previously. For intermediate scores, stakeholders discuss how severely the cost of the stability test and the interruption in service time would affect the owner/operator. The OCMI ultimately determines whether a stability test will be required.

Step 4: Monitor Effectiveness Through Impact Assessment

Description:

Track the effectiveness of actions taken to manage risks. The goal is to verify that the organization is getting the expected results from its risk management decisions. If not, a new decision-making process must be considered.

Example result:

The unit is monitoring the long-term results of decisions made using this RBDM process. If (1) stability issues arise that were not predicted by the index tool, or (2) other exclusions from the use of the tool become evident, the unit will revisit the RBDM process and make appropriate improvements.

All Steps: Facilitate Risk Communication

Description:

Encourage two-way, open communication among all stakeholders so that they will:

- Provide guidance on key issues to consider
- Provide relevant information needed for assessments
- Provide buy-in for final decisions.

Example result:

The unit directly involved important stakeholders within the USCG in the process. Vessel owners/operators were involved at various stages of the RBDM process through the following:

- An initial kickoff meeting to gather ideas, discuss issues, and solicit other input
- A review meeting to present a draft of the USCG's RBDM framework and index tools and to solicit comments
- Widespread distribution of the final RBDM framework and index tools before actual use
- Owner/operator participation in individual vessel reviews.

References

- Duane Boniface, L.T., U.S. Coast Guard. Risk-Based Decision Making Guidelines.
- Macesker, B., Myers, J.J., Guthrie, V.H., Walker, D.A. Quick-Reference Guide to Risk-Based Decision Making (RBDM): A Step-by-step Example of the RBDM Process in the Field.

Risk Assessment Applied to Offshore Structures

40.1 Introduction

Use of offshore risk assessment started in the late 1970s, based on the methodologies and data from the nuclear power generation industry. Following the Alexander L. Kielland accident in 1981 that resulted in the total loss of the platform and 123 fatalities, the Norwegian Petroleum Directorate issued guidelines that required quantitative risk assessment be carried out for all new offshore installations during the conceptual design phase (NPD, 1992). Another significant step was the Safety Case Legislation in the United Kingdom in 1992, following the Piper Alpha accident that resulted in total loss of the platform and 165 fatalities in 1988 (UK HSE, 1992, 1995).

There are several types of offshore risks:

- Structural and marine events
- Collisions
- Fires
- Dropped objects
- Blowouts
- Riser/pipeline leaks and process leaks
- Transport accidents

Risk due to structural failure is discussed in Part IV. Risks associated with blowouts, riser/pipeline hydrocarbon leaks, process leaks, transport accidents, etc. are discussed by CCPS (1995) and CMPT (1999). Reference is made to specialized books (e.g., Vinnem, 1999) that cover the basic methodologies for risk evaluation, such as:

- Hazard modeling and cause analysis
- Fault tree analysis and event tree analysis
- Failure mode and effect analysis

In the following sections, risks associated with collision, explosion, fire, and dropped objects will be discussed, including:

- Overview
- Frequency analysis

- Loads and consequence analysis
- Risk reduction

40.2 Collision Risk

Ship/platform collision is one of the main risk contributors in offshore exploration and production activities. The most frequently occurring collisions are the impacts between offshore supply vessels and platforms. In most situations, this type of collision only causes minor damage to platforms.

40.2.1 Colliding Vessel Categories

The first step in evaluating the collision risk is to specify the different types of vessels that may collide with an offshore platform. Collision hazards due to field-related supply vessels are characterized as high frequency and low consequence. The passing vessels may lose their power and drift, resulting in collisions with the platforms. In the North Sea, merchant vessels represent the greatest hazard since they are often large and thus have considerable impact energy in a collision with platforms. Further, in some areas the merchant traffic can be very busy. [Table 40.1](#) summarizes the colliding vessel categories, based on information in [Vinnem \(1999\)](#). In the following sections, only the external passing vessel collision is evaluated.

40.2.2 Collision Frequency

Based on the collision risk model proposed by [Haugen \(1991\)](#), the passing vessel collisions can be subdivided into two groups:

- Powered collisions: Vessels are steaming toward the platform while the navigator might not be aware of the situation.
- Drifting collisions: Vessels are out of control and drift toward the platform under the influence of environmental conditions.

Table 40.1: Colliding vessel categories

External Traffic		Field-Related Traffic	
Merchant	Merchant ship	Offshore	Standby vessel
Naval	Surface ship	(to/from field itself)	Supply vessel
	Submarine		Working vessel
Fishing	Trawler		Offshore tanker
Offshore	Standby vessel	Floating units	Storage vessel
(to/from another field)	Supply vessel		Flotel/Barge
	Offshore tanker		Drilling unit
	Tug		Crane/Diving vessel

The overall collision frequency can therefore be expressed as

$$P_{CP} = P_{CPP} + P_{CPD} \quad (40.1)$$

where

P_{CP} = Frequency of passing vessel collision

P_{CPP} = Frequency of powered passing vessel collision

P_{CPD} = Frequency of collision due to a passing vessel in drift

The frequencies of powered and drifting vessel collisions are generally dependent on the location of ship routes relative to the platform. This information can be obtained by assessing a database of ship routes or by performing a localized survey for the area.

Powered Ship Collision

A powered ship collision may occur when the following three conditions are met:

- The ship is on a collision course to the platform.
- The navigator is not aware of the situation early enough before the ship reaches the platform.
- The ship and the platform both fail to normalize the situation.

The basic mathematical expression for powered ship collision frequency can be written as

$$P_{CPP} = N \cdot P_{CC} \cdot P_{FSIR} \cdot P_{FPIR} \quad (40.2)$$

where

N = Annual number of passing vessels

P_{CC} = Probability of passing vessel on a collision course

P_{FSIR} = Failure probability of ship-initiated recovery

P_{FPIR} = Failure probability of platform-initiated recovery

The probability of being on a collision course, P_{CC} , is a geometric factor. It is based on the composition and position of the traffic flow. For a vessel that does not take preplanning to avoid a site, it may be assumed that the vessel will be normally distributed about the route center. The fraction of vessels on a collision course can be found based on the route details and the collision diameter presented by the platform. For a vessel that has taken deliberate steps to avoid a platform or to use it for position fixing, re-modeling is needed to modify the traffic distribution. Generally, a skewed distribution can be observed instead of a normal distribution.

The ship-initiated recovery from a collision course is divided into two cases: early recovery and late recovery. Early recovery is a normal operation under sound command. The ship is recovered from a collision course in the early recovery zone. Late recovery occurs under the condition that early recovery fails. This reflects recognition of an emergency and quick

response recovery. The failure frequency of ship-initiated recovery can be calculated by fault trees involving a number of factors such as a watch-keeping failure mode, visibility, the vessel type and size categories, a traffic-planning group, and a vessel flag.

The platform-initiated recovery is to alert the ship, by platform or standby vessel, in time to prevent a collision. The failure probability of platform-initiated recovery is highly dependent on the reason for the failure of the ship-initiated recovery; it can be estimated by event trees based on whether the following actions are taken in time:

- Identification of the vessel as a possible threat
- Attempt to inform the vessel on radio/VHF
- Standby vessel reaches position alongside the coming vessel
- Correct avoidance action by the vessel

Drifting Vessel Collisions

A drifting vessel collision will occur if the following conditions are all satisfied.

- The vessel loses propulsion
- The vessel drifts toward the platform
- The vessel fails to recover from its collision course due to either failure of external assistance or failure of its own recovery measures

Based on information for the rate of propulsion failure, vessel sizes, types, and flags, the likelihood of a vessel drifting can be estimated. The likely positions of vessels when in drift can be determined by using the route pattern. The metocean data for the location can then be used to determine the probability of the vessel drifting toward the platform.

External assistance includes, for example, towing the drifting vessel away—its failure probability depends on factors such as the relative size of the vessel and the location of the towing tug. Collision avoidance by a vessel's own measures depends on the probability of a drifting vessel regaining power (e.g., by restarting engines), or avoiding collision by steering with the rudder.

The above discussions have been based on research for collisions between ships and fixed platforms (Haugen, 1991, Vinnem, 1999). For new types of floating structures like floating production storage and offloading units (FPSOs), additional considerations are necessary (e.g., collisions during offloading operations).

Chen and Moan (2002) suggested that the collision probability of the FPSO-tanker offloading operation, is the product of the probability of a tanker's uncontrolled forward movement (in the initiating stage), and the probability of a recovery failure, initiated from a tanker and FPSO conditioned on the tanker's uncontrolled forward movement (in the recovery stage). The probability of uncontrolled forward movement in the initiating stage is predicted as the

sum of the probability of a tanker's *powered* forward movement and the probability of a tanker's *drifting* forward movement. The drift forward movement is a low probability and low consequence event. The probabilistic model for tanker powered forward movement involves complex human–machine interactions, human factors, and their interactions.

40.2.3 Collision Consequence

A number of factors can influence the collision consequences:

- Mass and velocity of colliding vessel
- Collision geometry
- Criteria that were applied for the structural design of the platform
- Platform topology
- Fender and reinforcement on platform

The most critical factors in the above list are the vessel mass and velocity that determines the impact energy level. Further, the collision geometry is also an important factor, since it will influence the energy distribution between the vessel and the platform. The following distinctions of collision geometry are made for a jacket structure:

- *Impact on the vertical column or bracing:* Vessel hitting a column or bracing will result in a high proportion of energy being absorbed by the platform, and thus leading to large plastic deformations.
- *Glancing bow:* Considerable amount of kinetic energy may be retained on the vessel after collision if the hit is a glancing bow, possibly resulting from last minute evasive actions.
- *Rotation of vessel:* Kinetic energy may be transferred to the vessel rotation, thus only a limited amount of energy is absorbed by the platform.
- *Contact spot on vessel:* The contact spots on the vessel are important. If a “hard spot” is hit on the vessel (e.g., heavily framed curvatures such as bulb or stern), high puncture loads may be generated.

The collision response and consequence for the platform can be predicated on nonlinear finite element analysis (Bai and Perderson, 1993); see Part II, Chapter 20 of this book.

40.2.4 Collision Risk Reduction

When considering risk reduction measures, the type of vessel representing the greatest risk to the platform needs to be analyzed. For the passing vessel collision, the risk reduction measures are:

- Improving the information distribution for the platform's site—this measure can increase the probability of the platform being located, and subsequently ships may preplan their voyage to avoid collision.

- Warning to the incoming ships as early as possible if they come along a collision course—calling the vessel on VHF/radio and actively using a standby vessel to intercept the incoming vessel are also effective risk reduction measures.

Collision consequence reduction measures include the use of rubber fenders and protection nets on the platform, which are standard design practice.

40.3 Explosion Risk

A gas explosion is a process with a rapid increase of pressure caused by the combustion of premixed fuel and air. Gas explosions can occur inside the process equipment or pipes, in buildings or modules, in open process areas or in unconfined areas. The design of topside structures to resist explosions and fires requires special considerations such as (Burgan and Hamdan, 2002):

- Characteristics of the explosion such as overpressure and gas velocities
- The response of the structure including high strain rate material property design data that can be used in explosion-resistant design
- Performance requirements of the structure such as strength, deformation limits, and load shedding
- Elevated temperature material property design data for use in fire engineering
- Analysis techniques for fire and explosion design
- Design methods based on codified rules and advanced techniques such as risk-based methods
- The explosion load may be categorized by its maximum overpressure. For instance,
 - If the overpressure is smaller than 0.2 bar, it is typically an “insignificant” explosion
 - If the overpressure is larger than 2 bar, it is considered a severe explosion.

In the Piper Alpha accident, an explosion due to ignited gas leakage set off an uncontrolled fire, which in the end led to the total loss of the platform. In the last few years, large-scale tests were conducted to study explosion modeling. The test results revealed that the blast loads due to explosion had been significantly underestimated previously, and these loads cannot be predesigned in many cases. Therefore, the explosion risk picture may be even more severe than previously thought.

40.3.1 Explosion Frequency

If the gas cloud formed by the gas leak is outside the flammable concentration range, or the ignition source is lacking, no explosion will occur. Subsequently the gas cloud will dilute and disappear. Thus, three factors may influence the explosion occurrence—that is,

gas leak sources, ventilation/dispersion, and ignition sources. The overall explosion frequency can be expressed as:

$$P_{EP} = P_{Leak} \cdot P_{GC} \cdot P_{Ignition} \quad (40.3)$$

where

P_{EP} = Frequency of explosion

P_{Leak} = Probability of gas leakage

P_{GC} = Probability of gas concentration

$P_{Ignition}$ = Probability of ignition

Gas leak sources are important for the gas dispersion. Generally, the following aspects need to be considered:

- Location of the leak source, in a three-dimensional space
- Gas composition and characteristics (i.e., temperature and specific weight)
- Leak rate
- Direction of flow from the leak source
- Unrestricted gas jet or diffuse gas leak

The ventilation conditions also have considerable influence on the dispersion of a gas leak and the resulting gas cloud. Most platforms have natural ventilation, implying that the dispersion of a gas leak will be strongly dependent on the wind speed and direction.

The actual location of the ignition point may vary considerably, depending on the type of ignition source. The ignition sources are generally identified by one of the following three types:

- *Rotating equipment*: Major equipment units, with a discrete distribution related to the location of each unit
- *Electrical equipment*: A high number of possible sources, may be described as a continuous distribution
- *Hot work*: Usually possible in most locations, such as welding; may be described as a continuous distribution over the area

The frequency of explosion events may be estimated using an event tree analysis. For example, given a medium gas leak, a number of conditions may be considered to determine the possible explosion events. Then the calculation of event frequencies in the event tree will establish the explosion frequencies for all explosion cases. This simple event tree assumes that all ignitions of the gas leak lead to explosions. A more detailed event tree will differentiate, more explicitly, between ignition causing an explosion or just causing a fire.

40.3.2 Explosion Load Assessment

Since the 1990s, gas explosions have been subjected to extensive research and load characteristics including (Burgan and Hamdan, 2002):

- Experimental studies at scales representative of offshore scenarios
- Computer simulation models
- Formal explosion model evaluation protocols, either phenomenological or based on computational fluid dynamics (CFD)

In order to determine the explosion loads (blast loads), an exceedance function needs to be established for each structural element. This exceedance function can be defined as “The annual frequency of exceeding a specified overpressure load as a function of the overpressure level,” based on analysis of uncertainties and probability distributions for variables such as:

- Location and direction of the leak source
- Flow rate of the leak
- Wind direction and speed
- Ignition source and strength

Distribution for the location and the direction of the leak are usually based on geometric considerations. Distributions for the flow rates can be derived using hole size distributions that are usually available from the leak statistics. Wind data can be obtained from the environmental criteria. These variations will generate input scenarios to dispersion simulations—for example, by CFD. Nonrelevant dispersion scenarios need to be eliminated later. Then explosion simulations (e.g., by CFD) can be carried out to determine the blast loads. When blast loads for all the cases have been simulated, the blast load distribution can be generated from a combination of simulated blast loads and scenario frequencies.

40.3.3 Explosion Consequence

Determining explosion loads on a structure, and estimating responses, involves the following calculations:

- Hydrocarbon release
- Explosion overpressure loads as a function of time
- Structural response to the time dependent overpressure loads
- Secondary blast effects such as missiles and flying objects

The consequence of an explosion is also dependent on the space and environment in which the gas cloud is contained. Therefore, it is natural to classify explosions into the following three categories (Vinnem, 1999):

- *Confined Explosion (internal explosion)* occurs within tanks, process equipment, pipes, and closed rooms, etc. For this kind of explosion, the combustion process does not need to be fast in order to cause serious pressure build-up.

- *Partly Confined Explosion* occurs inside partially opened buildings. Typical cases are compressor rooms and offshore modules. The explosion pressure can only be relieved through the vent areas, or if the surrounding enclosure fails.
- *Unconfined Explosion* occurs in open areas such as process plants. A truly unconfined, unobstructed gas cloud ignited by a weak ignition source may produce low overpressures. In a process plant, there are local areas, which are partly confined and obstructed. These areas are causing high explosion pressures. However, if an unconfined gas cloud detonates, the explosion pressure will be as high as 20 bars, independent of confinement and obstructions.

Depending on the amount of the explosion loads, the types of damage on structures include:

- Direct catastrophic failure
- Considerable damage that may be further extended by the subsequent fire
- Little or no damage to structures, but causing critical failure of safety systems and thereby preventing control of the fire
- Damage to passive fire protection, thereby reducing the survivability of structural members
- Damage to process equipment, thereby causing immediate escalation of the accident

The damages to the structures can be predicted using simplified analysis (such as a single-degree-of-freedom model for dynamics) and can be simulated using nonlinear finite element analysis, based on a methodology that is similar to the collision analysis discussed in Part II, Chapter 20 of this book. The explosion consequence is also dependent on the overpressure loading duration in relation to the natural period of the structure being subjected to the explosion loads.

- Impulsive loads with duration that is shorter than the natural period of the structure
- Dynamic loads with duration that is comparable to the natural period of the structure
- Quasi-static loads that are applied slowly

The overpressure time history should be properly modeled in the explosion consequence analysis as it may significantly affect the results.

The acceptance criteria (performance requirements) include strength criteria for structural failure and deformation criteria for operating critical equipment.

40.3.4 Explosion Risk Reduction

To reduce the risk of explosion, the first priority is to reduce the frequency of its occurrence. This may be achieved by the following three measures (Vinnem, 1999):

Prevent Gas Leakage

The most effective action for the prevention of gas leakage is to reduce the number of sources for potential leakage (e.g., the number of flanges). This can easily be

accomplished for a new platform. However, it is generally more difficult for existing platforms. The number of gas leaks may also be reduced by:

- Improving the maintenance quality in the process area
- Selecting high-quality material for gaskets
- Following up the minor leakage to identify trends and unwanted tendencies

Prevent Ignitable Concentrations

The next step to reduce the explosion risk is to prevent the formation of any ignitable atmospheres (e.g., through extensive natural ventilation). In the design phase, good natural ventilation is normally provided. During operation, ventilation may have been purposely reduced (e.g., by temporary equipment being installed or left in the openings, or to improve the working environment). It is therefore a difficult trade-off between the increased natural ventilation and the deteriorated working conditions. Mechanical ventilation systems may be effective for small gas leaks. However, for massive gas releases, the forced ventilation is generally insufficient.

Prevent Ignition

The next option is to prevent an explosive atmosphere from being ignited. Several actions are possible in regards to this option. The first action is to reduce the extent of hot work activities. This has been applied successfully on many installations where it has been proven that a variety of tasks may be done in a “cold” manner. The second action is to improve the maintenance of “ex-proof” equipment. Attention should also be given to so-called “continuous sources,”—that is, potential ignition sources that are constantly active, such as a lighted flare.

The following measures are effective to reduce explosion consequences.

Prevent High Turbulence

Turbulence is caused by the interaction of the flow with obstacles such as cable trays and pipe racks. The turbulence may increase the burning rate dramatically, due to the wrinkling of the flame front by large eddies and the turbulent transport of heat and mass at the reaction front. A number of basic design rules may help prevent the high turbulence—for example, optimization of the equipment arrangement, avoidance of multiple equipment pieces, and optimization of the location of pipe racks relative to likely ignition sources.

Prevent High Blockage

Small-sized objects may have the largest effect on module congestion, and in turn can lead to high overpressure. The mitigation measures are therefore used to: (1) remove temporary installations, containers, small obstacles, and weather cladding; (2) arrange vessels in a way that minimizes blockage of the most likely path of the flame front.

Avoid Human Activities from Explosion Potential

The location of control rooms, transportation, and accommodation facilities need to be far away from modules with explosion potentials.

Install Fire and Blast Barriers

Escalations caused by explosions can be limited by fire and blast barriers, which are located between modules and areas. However, the barriers themselves may cause problems for keeping ventilation and may potentially introduce more blocks. The construction/repair of such barriers may involve extensive hot work. This measure is therefore more effective in the early design stage.

Active Deluge on Gas Leakage

Leakage may be deluged out without causing any explosions or fires. Deluge may be particularly effective in preventing so-called runaway flame accelerations. It may also lead to a reduction of the peak overpressure.

The most critical aspect in the use of deluge is that it must be triggered prior to ignition (e.g., on the detection of a gas leak). Modeling the ignition has shown that the most likely time interval between release and ignition is 2–3 min. Thus, deluge activation has to be within the first half minute, in order to be effective.

Improve Resistance of Equipment and Structures

The last possibility of reducing an explosion consequence is to improve the resistance of equipment and structures to blast loads. However, it is not cost-effective to design structures for the worst-case explosion; this approach is quite expensive.

40.4 Fire Risk

In the offshore risk assessment, usually two types of fire risk are considered: the topside fire and the fire on the sea. The following sections mainly deal with the topside fire. Furthermore, the smoke effect analysis and the structural response under the fire are normally integrated into the fire risk assessment.

The distinction between what is classified a “fire” and what is called an “explosion” is relatively subjective. A small explosion initiated the total loss of the fixed platform “Piper Alpha,” but the damage was primarily due to fire.

40.4.1 Fire Frequency

Fire frequency analysis is very similar to the explosion frequency analysis. The overall fire frequency is expressed by

$$P_{FP} = P_{Leak} \cdot P_{GC} \cdot P_{Ignition} \quad (40.4)$$

where

P_{FP} = Frequency of fire

P_{Leak} = Probability of gas leakage

P_{GC} = Probability of gas concentration

$P_{Ignition}$ = Probability of ignition

The flammable gas/air concentration range determines whether it is an explosion or a fire for a given ignition. Further, fire scenarios are mainly caused from the following sources: blowout, riser failure, pipeline failure, process equipment failure, and dropped objects. The uncontrolled hydrocarbon flow (blowout or riser failure) is considered the main fire risk contributor to the structures. Further, dropped objects may contribute to fire only when they lead to the rupture of hydrocarbon containing equipment. Under certain conditions, structural failure or collision impact may also lead to fires. Their final consequences are largely dependent on the escalating sequences.

40.4.2 Fire Load and Consequence Assessment

A brief overview of some important aspects in the fire consequence analysis is made below.

Fire Types and Characteristics

Despite the fact that a fire originates from combustion reactions, the process of a fire may largely depend on factors that are not directly involved in combustion. Fires are therefore usually separated into the following types:

- Ventilation controlled fires in enclosed units (closed or partly closed)
- Fuel controlled fire in enclosures
- Pool fires in open areas or in modulus
- Jet fires
- Fires in running liquids
- Fireballs
- Gas fires (premixed, diffuse)

Other types of fire may occur in electrical equipment, in the accommodations, or on the sea. These “nonhydrocarbon” fires are not included here.

Burgan and Hamdan (2002) formed a list of research publications on fire and explosion load characteristics, structural response analysis and performance requirements. The fire loads may be converted into thermal loads (time–temperature curves) that act on the structural members. Some time–temperature curves are available in the literature in a

Table 40.2: Fire load characteristics

Jet Fire	Diffuse Gas	Pool Fire	Fire on Sea
Hole size	Release rate	Pool size	Spreading
Release velocity	Duration of leak	Wind direction	Wind direction
Direction	Air supply	Duration of fire vs leak	Wind speed
Duration of leak		Air supply	Pool breakup
Air supply			

form suitable for use in designs. The temperature–time history for a given structural member is affected by the applied heat load, the shape of the member (for heat transfer), and the use of any passive fire protection materials.

Table 40.2 summarizes the main characteristics that need to be determined for these fire types.

Fire Response Analysis Procedures

The assessment of fire responses of structures includes the following calculations:

- Releases of hydrocarbons (combustion, radiation, and convection)
- Fire loads
- Structural time–temperature distribution
- Structural response to temperature distribution

Each of these calculations can be conducted using simplified methods or nonlinear finite element simulations. Simplified calculations can be performed in the form of hand calculations or computer spreadsheets. The weakness of the simplified calculations is its inability to account for the redistribution of structural internal forces during the fire. However, the simplified calculations are normally more conservative and may be calibrated against experimental results.

Smoke Effect Analysis

Smoke does not affect structural elements, but it is one of the major hazards to personnel in fires, especially in oil fires. The smoke effects are, for example:

- Reduced visibility
- Pain and injury to the personnel due to the temperature of the smoke
- Incapacitation or death due to toxic or irritating components in the smoke

Knowledge of smoke production, smoke flow, and impact of smoke on people and the facilities is available in literature, laboratory tests, and experience of real fires, such as the fire on the Piper Alpha platform. By proper CFD codes, the smoke effects analysis for a fire scenario can be performed, and the results can be compared with the threshold values in the above three areas.

Structural Response to Fire

Simplified methods for structural response to fire have been derived based on results from fire tests and fire engineering codified methods. The sophisticated computer models are based on finite element methods that calculate the temperature increase in a structural member based on a given temperature exposure curve; the thermal properties of the materials that are also temperature dependent.

The consequences of fire include:

- “Minor damage” and “significant damage” do not reflect much damage to the main and secondary structures (support structure, main deck structure, and module structure), but rather to tertiary structures and to their equipment.
- Higher consequences—that is, “severe damage” and “total loss”—will conversely involve considerable damage to the main and secondary structures.

The performance requirements are applied for the protection of the primary structure and safety critical structures and systems. They are defined as strength (for structural failure) and deformation limits (to ensure that the support to safety critical structures, and the performance of blast/fire wall are not compromised).

40.4.3 Fire Risk Reduction

Fire risk reduction measures can be considered in the following four aspects (see [Vinnem, 1999](#) for more detail):

Leak Prevention

Adopt welded connections
Flange types with reduced leak
Probability

Leak Detection

Gas detection
Fire detection
Emergency shutdown
system
Blowdown system

Ignition Prevention

Hot work procedures
Explosion-protected equipment
Maintenance of electrical
equipment

Escalation Prevention

Installation layout
Segregation of areas
Active fire protection (deluge
water system, CO₂ system, etc.)
Passive fire protection (H-60,
H-30 segregation, etc.)

40.4.4 Guidance on Fire and Explosion Design

A probabilistic approach has been proposed in the new NORSOK guidance documents ([Pappas, 2001](#)) and in a new engineering handbook published by Corrocean ([Czujko, 2001](#)). [Walker et al. \(2002\)](#) presented a guidance document based on the risk matrix

approach described in API RP 2A (21st edition). The API risk classification method has been applied to fire and explosion engineering. Methods are proposed to enable the derivation of a dimensioning explosion overpressure that may be applied to a static or dynamic analysis, in order to assess the structure against the ductility level explosion. Two levels of explosion loadings are suggested for explosion assessment by analogy with earthquake assessment.

For the “Ductility Level” explosion, a performance standard, such as the one below, is typical: “In the case of an explosion event at least one escape route must be available after the event for all survivors. For a manned platform, a temporary refuge of safe mustering area must be available to protect those not in the immediate vicinity of an explosion.” (NO Reference- Needs a reference).

For the “Design Level” explosion, it is required that the primary structure remains elastic, with the essential safety systems remaining functional. The explosion overpressure is the cumulative overpressure distribution for the installation, showing the probability that a given overpressure will not be exceeded. The explosion overpressure may then be expressed as a function of the return period (years).

40.5 Dropped Objects

The hazards of dropped objects are mainly caused from falling crane loads. In addition, various cases of crane boom fall or entire crane fall have been documented. The risk figure, for the crane accidents in the North Sea, shows that several fatalities have occurred when an entire crane toppled overboard. The equipment was damaged due to falling objects. The subsea wellheads were damaged because of BOPs (Blow out Preventers) falling during exploration drilling.

40.5.1 Frequency of Dropped Object Impact

The frequency of dropped objects is defined as (Vinnem, 1999)

$$P_{DOI} = \sum_I N_i \cdot P_{Di} \cdot \sum_J P_{Hij} P_{Fij} \tag{40.5}$$

where

P_{DOI} = Occurrence probability of dropped object impact

N_i = Annual number of lifts per load category i

P_{Di} = Probability of load dropped from crane for load category i

P_{Hij} = Probability of equipment j being hit by falling load in category i , given that the load is dropped

P_{Fij} = Probability of failure of equipment j given impact by load in category i

Table 40.3: Typical crane load distribution (based on Vinnem, 1999)

Load Categories	Load Distributions (%)	
	Simultaneous Drilling and Production	Normal Production
Heavy or multiple drill collars	22.2	0
Other heavy (>8 tons)	0.3	0.7
Medium-heavy (2–8 tons)	27.1	33.6
Light (<2 tons)	50.5	65.7
Number of lifts per year	20,884	8768

Annual Lift Number and Load Distribution

Table 40.3 presents two representative load distributions for simultaneous drilling and production, and for normal production. Typical numbers of crane operations per crane, during 1 year on an installation, are also given.

Probability of Dropped Load

The probability of dropped loads during operations depends on the characteristics of the load and the environmental conditions. Typically, only one average frequency is estimated—that is, an average drop frequency per-lift or per-crane-year.

A typical frequency of dropped loads is in the order of $10E-5$ to $10E-4$ loads dropped per crane per year. For critical lifting operations, particular emphasis is placed on adhering to strict procedures. The dropped load frequency for this so-called “procedure lift” is typically 30–70% lower than the value for a “normal” crane operation.

Probability of Hitting Objects

A dropped crane load may hit three types of objects. Each of them with the worst-case consequences presented below.

The probability of hitting is usually based on geometric considerations reflecting the areas over which the lifting is performed. Lifting over the process area is usually prohibited by operational procedures unless special restrictions are implemented. If a load is dropped under such circumstances, it can be a critical event. The probability of topside equipment being hit can be expressed as

$$P_{H\ ij} = \frac{A_{l\ ij}}{A_{tot-i}} \cdot f_{crit} \quad (40.6)$$

where

$A_{l\ ij}$ = Area of equipment j over which loads in category i may occasionally be lifted

A_{tot-i} = Total area of hydrocarbon equipment over which load category i may be lifted

f_{crit} = Ratio of critical area to total area over which lifting is performed

The probability of hitting structural components or subsea equipment can be determined in similar equations based on areas over which the lifting is performed.

40.5.2 Drop Object Impact Load Assessment

In principal, two cases need to be considered regarding the falling objects from the crane:

- Loads that are dropped on the equipment, structures, deck, or other locations that are above the sea surface.
- Loads that are dropped into the sea and possibly hit structures in the water, or subsea equipment on the sea bottom.

The first case has only one phase—that is, the fall through air. The second case has three phases, falling through the air, impact with the sea surface, and the fall through the water. Idealized calculations that determine the impact velocities in these three phases are briefly presented below. The drift caused by the currents may also be taken into account when calculating the most probable landing point on the seabed.

Fall through the Air

A falling object will accelerate toward the sea surface in accordance with the force of gravity. The impact velocity V_1 is determined by

$$V_1 = \sqrt{2gh} \tag{40.7}$$

where

h = Height from which the drop occurs

g = Gravity acceleration

Impact with Water

A falling object may hit the sea surface and proceed through the water with the velocity V_2 as determined by Eqn (40.8). The integral represents the loss of momentum during the impact with the water surface.

$$V_2 = V_1 - \int_0^t \frac{P(t)}{M} dt \tag{40.8}$$

where

M = Object mass

$P(t)$ = Impact force

Fall through Water

After the impact, the object will accelerate from V_2 toward its terminal velocity V_t in the water.

$$V_t = \sqrt{\frac{2(W - O)}{C_d \cdot A \cdot \rho}} \quad (40.9)$$

where

W = Gravity force (in air)

O = Buoyancy force

ρ = Density of sea water

A = Cross-section area

C_d = Shape coefficient of the object depending on the Reynolds number

It is also known that an object tends to oscillate sideways during the fall through water. These oscillating movements are determined by the impact angle with the water surface and the external shape of the object. Bar-shaped objects with large surface areas will oscillate more than massive and spherical objects. An oscillating object will have a lower terminal velocity than a nonoscillating object.

40.5.3 Consequence of Dropped Object Impact

The consequences of an impact are dependent on how a falling load actually hits the equipment (topside or subsea) or the structural components—that is, velocity of the falling mass, hitting spot, impact angle, impact time, and contact area. Calculations are often made for ideal situations. It is often natural to distinguish falling loads between long cylindrical objects and bulky objects, because they have a different drop rate, trajectory/velocity in water, and effect on the structure/equipment. Some consequences of dropped object impacts are summarized in [Table 40.4](#) below.

Topside equipment such as pressure vessels and separators, are obviously vulnerable to the dropped object's impact. Subsea production systems and pipelines are also very

Table 40.4: Consequences of hitting objects

Topside equipment	May cause loss of integrity of hydrocarbon containing equipment and possibly lead to a process fire
Structural components above or in the water	May cause structural failure or loss of stability or buoyancy
Subsea equipment	May cause loss of containment of production (hydrocarbon containing) equipment, possibly lead to a significant oil spill

sensitive to dropped objects. Some calculations have indicated that a falling load with a mass of 2 tons can easily damage an actuator on the subsea production system. The same loads applied to a pipeline may cause pipeline damage and leakage. For structural components, the following component parts are often considered: (a) Topside structure, (b) Module support beams, (c) Supporting structure, and (d) Buoyancy compartments.

40.6 Case Study—Risk Assessment of Floating Production Systems

40.6.1 General

A risk assessment may be conducted as part of the offshore field development and includes the following:

- All critical elements are appropriately selected and the corresponding performance standards are adequately defined for the life cycle of the Floating Production Systems (FPS) in terms of its functionality, availability, structural integrity, survivability, dependency, and influence on the other critical elements. It is demonstrated that the critical elements fit for purpose and meet the performance standards.
- Risk acceptance criteria are defined prior to the execution of the risk assessment, and provide a level of safety is equivalent to that defined in the prescriptive rules and codes.
- All hazards with a potential to cause a major incident have been identified, their risks are evaluated and measures have been taken (or will be taken) to reduce the risk to the level that complies with the risk acceptance criteria.

Types of risks for FPS depend on the type of vessel used and the geographical region where it is sited. FPSOs used in the North Sea are mainly new vessels with turret systems. The offloading tankers come to empty the storage tanks (approximately) once per week. Offloading tankers may represent a collision hazard to the FPSO with medium frequency and potentially high consequences. So far, FPSOs in the West African offshore region are mainly based on spread mooring systems and a single-point mooring for oil exports. FPSOs used in other geographical regions are mainly based on converted tankers.

In the following, an FPSO for the Gulf of Mexico illustrates the methods of risk assessment. The methods illustrated in this section can also be applied to other types of floating production systems such as TLPs, SPARs, and semisubmersibles.

A risk assessment of FPSOs may include an evaluation of the following systems:

Process Systems

Process systems include:

- Process plant with three-stage separation, gas compression for export and gas turbine-driven power generation on deck

- Piping, pressure vessels in production and storage facilities
- Cargo tanks and crude pumping systems, offloading systems and its operation

Process risk is mainly initiated by a hydrocarbon containment loss, which might escalate to explosions and/or fire accidents. The risk assessment for process systems can be conducted using a conventional offshore QRA approach (Wolford et al., 2001).

- Development of isolatable sections
- Summarize the loss of containment frequency by using a parts count approach
- Identifying spatial interactions that could lead to escalation

Leak frequencies may be derived primarily from generic databases that are available to offshore industries. Emergency detection and process control response to a loss of containment needs to be accounted for.

API RP 14J (1993) has been used by the industry for the design and hazards analysis for facilities on offshore production installations. This RP mainly deals with the prevention of fire risk due to hydrocarbon ignition. Methodologies for hazard analysis are recommended. The API methodologies can be applied to assess explosion risk as well. Guidance is given for everything from risk management to platform equipment arrangement, hazard mitigation, and personnel evacuation. Detailed checklists are given in the appendix regarding the facility layout (and emergency response/medical, escape and rescue), process equipment, safety and electrical systems, fire and gas leakage protection, and mechanical systems, etc.

Marine Systems

The marine systems may include:

- Cargo tanks, crude pump room, boilers and engine room, power generation/supply systems, ballast system and wing tanks, etc.
- Escape and evacuation system and equipment

The risk assessment of marine systems is similar to that for process systems. The exception is, the scope of the marine system's risk is broader than the hydrocarbon containment loss. The majority of the marine system's risk is fire due to fuel leakage and electrical systems. However, there is a lack of FPSO fire initiator frequency data for the appropriate quantification of fire risk.

Structural Systems

The structural systems may include:

- Hull structures, especially the moon pool area that accommodates the turret if there is one
- Position mooring systems, such as moorings and anchors, and/or dynamic position systems

- Risers and flow lines
- Topside structures
- Helideck and helicopters operation
- Flare system

The structural system's risk is covered in Part IV of this book.

40.6.2 Hazard Identification

In an FPSO risk assessment, the primary objective of the hazard identification is to identify and register the hazardous events that may escalate into accidental events. The hazard identification task may be relatively coarse and subjective in the conceptual design phase, and become more specific in the detail design phase. A partial list of the typical hazards is given below.

- Explosions/fires in cargo and ballast tanks
 - The explosion and fire in cargo ballast tanks may result in hull structural failure and cause oil spills.
- Explosions/fires in engine room and/or pump room
 - The explosions/fires in engine room and/or pump room may cause loss/delay of production, and escalate to cargo tanks.
- Collisions from shuttle tanker or other vessels
 - Shuttle tankers, supply vessels, and pass-by vessels may collide into the FPSO due to failure of position mooring systems, errors in navigation or offloading operation, power failure, etc.
- Dropped objects
 - Dropped objects may cause damage to structures leading to loss of buoyancy and cause damages to equipment and subsea flow lines leading to hydrocarbon leaks and personnel injuries/fatalities.
- Extreme weather
 - The weather conditions may be more severe than that considered in the design. Waves whose height is lower than the 100 year return design wave height, but with more vibration sensitive wave periods, may cause larger vessel motions and green water impacts.
- Green water
 - Green water can induce impacts loads on the forecastle, topsides along the deck edges of the vessel, and may cause damage/impair of evacuation tunnels.
- Structural failure such as corrosion defects and fatigue cracks
 - Fatigue may be induced by wave loads and due to poor design of structural details. Corrosion defects may be found in cargo tanks, piping, and pressure vessels.

- Rupture in risers, flow lines, and leaks in offloading hose
 - Failure of risers, flow lines, and offloading hoses may be caused by corrosion, fatigue, and accidental loads.
- Failure of station-keeping capacity
 - A partial failure of the station-keeping system may lead to damages to risers resulting in gas leakage and fires. Loss of station-keeping capacity may lead to collisions and grounding (in shallow-water).

40.6.3 Risk Acceptance Criteria

A risk matrix approach defined in Part V, Chapter 38 can be used as the risk acceptance criterion, which consists of the failure frequency and consequences.

The failure frequency may be classed as high, medium, low, and remote:

- High—an accident that occurred at least once in the past year and is expected to occur again to the system (e.g., frequency >0.1)
- Medium—an accident that might occur at least once in the life cycle of the system, and if the accident were to occur, no one would be surprised (e.g., $0.01 < \text{frequency} < 0.1$)
- Low—an accident is considered unlikely to occur. However, similar accidents have occurred once or twice in the industry worldwide (e.g., $0.0001 < \text{frequency} < 0.01$)
- Remote—an accident is credible, but not expected to occur in the life cycle of the system (e.g., frequency < 0.0001)

The consequences of failure may depend on the type of risks considered (e.g., personnel, economic, and environmental risks):

- Catastrophic—fatality or disability injury; major loss of the FPSO or long-term loss of its production; serious oil and gas release resulting in long-term damage to the environment
- Critical—severe injury; major damage to the FPSO or its production; significant oil and gas release
- Significant—nonsevere injury; some damage to the equipment and systems and minor loss of production; oil/gas release requiring regulatory notification
- Minor—no injury; minimum component failure and no loss of production; recordable event but no regulatory involvement

The physical phenomena considered in consequence modeling includes:

- Release modeling, multiphase, near-field flow regime, and internal-pressure time history
- Thermal radiation effects to humans and equipment from jet fires and pool fires
- Explosion over-pressure that impacts human and equipment
- Evacuation of personnel on board

40.6.4 Risk Estimation and Reducing Measures

If risks are unacceptably high, measures are to be taken to eliminate/reduce the risks. Examples of the approaches to reduce risks are:

- Modify the design to eliminate the hazard
- Reduce the frequency of occurrence of an initiating event
- Reduce the frequency of the events that may cause an initiating event to become an accidental event of unacceptable consequences
- Reduce the exposure of personnel and equipment to the hazard
- Implement strict operational procedures, safety procedures, and emergency response program

More specifically, major risk estimation and reducing measures include the following:

Process Leakage

Process systems are often the main contributor to personnel risk. The gas compression has the highest leakage frequency followed by the fuel gas system and the gas dehydration system. Most of the leakage is small (e.g., less than a 10-mm-equivalent hole size). Process leaks can lead to explosions and fires. Pollution from process leaks is limited by the process shutdown and isolation system, unless an explosion with subsequent fire escalates to the cargo tanks and threatens the overall integrity of the vessel. The process leak may be reduced by: relocating process control center to within the accommodation, installing a protected escape route from bow to stern, installing additional gas detectors in the process area.

Offloading and Shuttle Tanker Risk

There are two types of oil offloading systems, namely tandem assisted offloading and single-point mooring. The former is used with turret moored FPSO and the later is applied with spread moored FPSO. The main hazards associated with tandem assisted offloading are collisions between shuttle tankers and FPSOs, and oil spillage from hose ruptures. Loading hose ruptures can occur during the connection of the transfer hose and the offloading phases, from fatigue loadings, excessive tension/pressure, or from extreme fishtailing. Fatigue cracks can develop in offloading risers for harsh environments. Failure of single-point mooring systems may lead to failure of the transfer risers if the transfer risers are structurally supported by a single-point mooring system.

Example approaches that reduce risks:

- Improving the ability to detect the failure and to activate the shutdown system
- Monitoring traffic and mooring hawsers, and deck watches
- Improving personnel training and preparedness to face accidental situations (Karsan et al., 1999)

- Isolating oil offloading risers (hoses) from the buoy of the single-point mooring system from structural redundancy point of view
- Use of standby vessels that can perform a variety of operations from providing emergency towing to assist with the mooring and hose lifting operations (Daughdrill and Clark, 2002)
- Designing offloading systems with adequate redundancy

Daughdrill and Clark (2002) outlined several published guides for offloading:

- “Offshore loading safety guideline with special relevance to harsh weather zones” by Oil Companies International Marine Forum (OCIMF) in 1999,
- “Ship to ship transfer guide (petroleum), 3rd Edition” by OCIMF in 1997,
- “The training and experience of key DP personnel,” by International Marine Contractors Association (IMCA) in 1996,
- “Risk minimization guidelines for shuttle tanker operations worldwide at offshore locations” by INTERTANKO (International Association of Independent Tanker Owner) in 2000.

To predict the relative motion (surging and yawing) and probability of collisions between FPSOs and shuttle tankers in tandem offloading operations, Chen et al. (2002) presented a simulation-based approach based on the time—domain simulation code SIMO. The collisions are modeled in two stages: the initiating stage and the recovery stage. The initiating stage is the situations where something could possibly go wrong to cause an uncontrolled forward movement of a tanker, while the recovery stage is the initiation by the tankers to avoid collision after the occurrence of the initiating stage. In the probabilistic model for the initiation stage, Chen et al. (2002) integrated technical events, human actions and their interactions. The SIMO simulation models are calibrated for a typical North Sea FPSO and a DP shuttle tanker. The extreme values for the simulated relative distance and heading between the FPSO and the tanker are analyzed by fitting with statistical models. Chen et al. (2002) estimated the frequencies of both excessive surging and yawing to be on the order of $10E-3$ per year. Sensitivities to various technical and operating factors are studied, and measures are identified to minimize the probability of collision.

Marine System Risk

Only cargo tank systems for oil storage are considered herein. The cargo tanks are provided with inert gas systems and crude oil washing systems. Explosions and fires may occur in cargo tanks, although there is a lack of incident data for the frequency quantification. A cargo tank explosion may cause structural damage and damage to the process plant. This would more than likely result in a hydrocarbon leak from the process system and a possible subsequent fire in the process area. Immediate fatalities are mainly

due to the effect of the explosion in the process area. Smoke may be a treat to personnel safety. The potential risk reduction measures are:

- Improving procedures for tank intervention
- Improving reliability of the inert gas system
- Installing thrusters to allow the vessel to change heading (to avoid fire engulfing the accommodation)
- Improving the fire/blast protection of the front wall of the accommodation (Nesje et al., 1999)

Collision Risk

The wing tanks of the vessel ballasted with water provide a dual barrier against the puncturing of the cargo tanks. Measures for collision avoidance and consequence reduction include radar surveillance, having a standby vessel, developing hazard management plans and installation of thrusters to reduce the target for a drifting vessel on course to a collision. Protection of risers, offloading lines and fluid transfer lines are all designed to meet the energy absorption requirements.

MacDonald et al. (1999) provided an overview of ship/FPSO collision risks and presented methodologies for quantifying the frequencies and consequences of these events. Measures that have the potential to reduce the risk of ship collisions are highlighted focusing on the scenarios most likely to result in pollution, loss of life and asset and production loss/delay.

Explosion Risk

In the detailed design phase, explosion risk is estimated and effort is made to minimize explosion overpressures. Hydrocarbon lines and riser/fluid transfer lines are appropriately routed, such that possible leakage on the main decks is minimized.

Fire Risk

Jet fires and pool fires represent risks for equipment. The design fire duration is determined considering the ability of personnel to escape to a safe location and the reduction of the pollution of hydrocarbon to the environment.

Dropped Object Risk

The design criterion for equipment protection depends on the size and location of the lifts and the frequency of their operations. Normally a dropped object study is conducted as part of the detailed design, in which credible dropped weight and the loads acting on the equipment are calculated, and the structural response and the failure frequency are estimated.

40.6.5 Comparative Risk Analysis

Risk assessment can also be applied in a comparative risk analysis that compares a particular design with other designs that have been accepted to have adequate levels of safety. For instance, [Gilbert et al. \(2001\)](#) presented a study comparing the risks of FPSOs never used in the Gulf of Mexico with risks for deepwater FPS (TLP and SPAR) already existing there, and a shallow-water jacket serving as a hub and host to deepwater platforms. The whole production systems were considered, from the wells through the transport of the product to shore. Three risk measures were assessed and analyzed for each system in a 20-year production life: the total number of the human fatality risk, the total volume of oil spilled as a measure of the chronic environmental risk, and the maximum volume spilled in a single incident. It was concluded that there are no significant differences in the fatality risks and the environmental risks between the four types of systems studied. This study has been very useful for the regulatory agency and offshore industry in regards to accepting the use of FPSOs in the Gulf of Mexico.

40.6.6 Risk-Based Inspection

Three fundamental questions need to be answered when planning a risk-based inspection ([Xu et al., 2001](#)).

- What should be inspected?
- How much effort should be made on individual components or details?
- When the inspection should be conducted?

The key step in inspection planning is the ranking of the components for inspection. A rating system should be created including the analysis of frequency and consequences and the detection of defects through inspection. The frequency analysis can be based on databases for failure frequency, or for analytical methods, or a combination of both the databases and analysis.

The consequence of failure considered in the inspection of the FPSO structures include the following:

Structures Including Vessel Hull and Topside Structures

- Catastrophic—loss of stability and structural integrity or leading to downtime of more than 1 year
- Critical—loss of structural integrity that requires excessive dry dock repairs or down time of between 6 months and 1 year
- Severe—moderate structural damage that requires minor dry dock repairs or downtime of between 1 and 6 months
- Minor—minor damage that requires a quick onboard repair or a down time of less than 1 month

Mooring Systems and the Thruster System that Assists the Station-Keeping System

- Catastrophic—resulting in a big loss of asset or downtime of more than 1 year
- Critical—resulting in major collision and grounding with downtime of between 6 months and 1 year
- Severe—leading to minor collision and downtime between 1 and 6 months
- Minor—leading to repair or replacement of one line at site and two or more lines damaged

Import/Export Systems Such as Risers, Flow Lines, and Offloading Systems

- Catastrophic—resulting in major oil spill or fire due to the leakage of oil and gas
- Critical—leading to moderate oil spill and downtime of more than 6 months
- Severe—ruptures in the pipe require repair, replacement, and downtime of 1–6 months
- Minor—repair or replacement of the riser, flow line and offloading systems that cause a shutdown of less than 1 month

For generic methodologies for risk-based inspections, reference is made to API RP 580 (API, 2002). This newly developed RP contains the following sections:

- Introduction to risk-based inspection
- Screen and boundary identification
- Data and information collection for RBI assessment
- Identifying deterioration mechanisms and failure modes
- Assessing likelihood of failure
- Assessing consequences of failures
- Assessing risk
- Risk management with inspection activities
- Other risk mitigation activities
- Reassessment and updating RBI assessment
- Roles, responsibilities, training, and qualification
- RBI documentation and record keeping

The formulation for probability and risk-based inspection has been covered in Part IV, Chapter 37. The effectiveness of the inspection depends on the degradation mechanism and rate, inspection scope/frequency and detection capability, as well as the usefulness of the mitigation.

For FPSO, the biggest benefit from the use of risk-based inspection is perhaps the reduced loss of production.

40.7 Environmental Impact Assessment

In many situations, an environmental impact assessment must be conducted prior to the execution of an offshore field development. The results of the environmental impact

assessment can be used to minimize the environmental impact from development and operation of the oil/gas field. The scope of an environmental impact assessment may depend on the geographical regions and the characteristics of the field, and may, for example, include the following:

- Investigate the distribution, population size, and biology of key species of fish, birds, and mammals
- Evaluate food webs and trophic interactions, energy transfer in the ecosystem
- Assess environmental toxins in sediments, benthic organisms, and fish
- Develop oil spill modeling
- Establish databases with relevant environmental data

From an environmental protection point of view, the following items need to be considered (Gudmestad et al., 1999):

- Discharge from drilling operations such as mud and cuttings
- Produced water handling
- Ballast water storage tanks
- Selection of chemicals considering environmental data for toxicity, degradability, and potential for bioaccumulation
- Loading operations to reduce possibility for oil spills during loading
- Tanker oil transport to avoid oil spills
- Oil spill contingency plan (in situ burning, bioremediation, etc.)
- Waste handling
- Emission to air of CO₂, NO_x, and SO_x

References

- API RP 14J, 1993. API Recommended Practice for Design and Hazard Analysis for Offshore Production Facilities. American Petroleum Institute.
- API RP 580, 2002. Risk-based Inspection. American Petroleum Institute.
- Bai, Y., Pedersen, P.T., 1993. Elastic-plastic behavior of offshore steel structures under earthquake impact loads. *International Journal of Impact Engineering* 13 (1), 99–115.
- Burgan, B.A., Hamdan, F.H., 2002. Response of topside structures to fires and explosions: design considerations. In: *Offshore Technology Conference*. OTC 14141.
- CCPS, 1995. *Chemical Transportation Risk Analysis*. Center for Chemical Process Safety, American Institute of Chemical Engineers.
- Chen, H., Moan, T., 2002. Collision risk analysis of FPSO-tanker offloading operation. In: *21st Int. Conference on Offshore Mechanics and Arctic Engineering (OMAE)*. OMAE2002–28103.
- Chen, H., Moan, T., Haver, S., Larsen, K., 2002. Prediction of relative motion and probability of contact between fpso and shuttle tanker in tandem offloading operation. In: *21st Int. Conference on Offshore Mechanics and Arctic Engineering (OMAE)*. OMAE2002–28101.
- CMPT, 1999. *A Guide to Quantitative Risk Assessment of Offshore Installations*.
- Czujko, J., 2001. Design of Offshore Facilities to Resist Gas Explosion Hazard, *Engineering Handbook*. Corrocean.

- Daughdrill, W.H., Clark, T.A., 2002. Consideration in reducing risks in FPSO and shuttle vessel lighting operations. In: Offshore Technology Conference. OTC 14000.
- Gilbert, R.B., Ward, E.G., Wolford, A.J., 2001. A comparative risk analysis of FPSOs with other deepwater production systems in the Gulf of Mexico. In: Offshore Technology Conference. OTC 13173.
- Gudmestad, O.T., et al., 1999. Basics of Offshore Petroleum Engineering and Development of Marine Facilities with Emphasis on Arctic Offshore, ISBN 5-7246-0100-1.
- Haugen, S., 1991. Probabilistic Evaluation of Frequency of Collision between Ships and Offshore Platforms. Dr.ing Thesis. Division of Marine Structures, NTNU. MTA-report 1991:80.
- Karsan, D.I., Aggarwal, R.K., Nesje, J.D., Bhattacharjee, S., Arney, C.E., Haire, B.M., Ballesio, J.E., 1999. Risk Assessment of Tanker Based Floating Production Storage and Offloading (FPSO) System in Deepwater Gulf of Mexico. OTC 11000.
- MacDonald, A., Cain, M., Aggarwal, R.K., Vivalda, C., Lie, O.E., 1999. Collision Risks Associated with FPSOs in Deep Water Gulf of Mexico. OTC 10999.
- Nesje, J.D., Aggarwal, R.K., Petrauskas, C., Vennem, J.E., Keolanul, G.L., Hoffman, J., McDonnell, R., 1999. Risk Assessment Technology and its Application to Tanker Based Floating Production Storage and Offloading (FPSO) Systems. OTC 19998.
- NPD, 1992. Regulations Relating to Implementation and Use of Risk Analysis in the Petroleum Activities. Norwegian Petroleum Directorate, Stavanger, Norway.
- Pappas, J., 2001. The NORSOK procedure on probabilistic explosion simulation. Paper 5.5.1. In: ERA Conference, "Major Hazards Offshore", London, 27–28 November 2001.
- UK HSE, 1992. Safety Case Regulation. United Kingdom Health and Safety Executives.
- UK HSE, 1995. Prevention of Fire and Explosion, and Emergency Response Regulation. United Kingdom Health and Safety Executives.
- Vinnem, J.E., 1999. Quantified Risk Assessment – Principles, Modelling and Applications of QRA Studies. Kluwer Academic Publishers.
- Walker, S., Corr, B., Tam, V., O'Connor, P., Bucknell, J., 2002. New guidance on fire and explosion engineering. In: 21st Int. Conf. on Offshore Mechanics and Arctic Engineering (OMAE). OMAE2002–28623.
- Wolford, A.J., Lin, J.C., Liming, J.K., Lidstone, A., Sheppard, R.E., 2001. Integrated Risk Based Design of FPSO Topside, Structural and Marine Systems. OTC 12948.
- Xu, T., Bai, Y., Wang, M., Bea, R., 2001. Risk Based 'Optimum' Inspection for FPSO Hulls. OTC 12352.

Formal Safety Assessment Applied to Shipping Industry

41.1 Introduction

Shipping is a traditional industry in which safety has been an issue for hundreds of years. Meanwhile, accidents have often led to the recognition of the need for measures to be taken that can control the risks at sea. For example, the Titanic disaster in 1912, in which 1430 lives were lost, led to the first International Conference on Safety of Life at Sea (SOLAS). SOLAS is based around the international standards and regulations preventing such casualties. The capsizing of the liner Andrea Doria prompted the United States delegation to attend the 1960 International Safety Conference; they introduced the concept that ship safety should be measured as the extent of damage a ship could survive. A growing public concern over the devastating consequences of marine pollution, due to several oil tanker accidents, prompted the organization of the MARPOL conventions during the 1970s. The Exxon Valdez disaster in 1990 resulted in the use of double hull tankers mandated by IMO. These incidents indicate the continuous necessity for introducing modern risk assessment techniques in the commercial shipping industry.

The nuclear industry developed probabilistic safety assessments in the 1960s. In the 1970s, the chemical industry used quantitative risk assessment (QRA). Owing to the industries self-regulation, in the 1980s the offshore industry applied QRA in Norway after the Alexander accident, and then in the United Kingdom after the Piper-Alpha accident.

In 1993, a particular type of risk management framework in the ship safety regime was proposed by the United Kingdom to IMO; it was referred to as the Formal Safety Assessment (FSA). The FSA has been taken as a priority item in the IMO Maritime Safety Committee's agenda since then. IMO used the FSA process to issue FSA interim guidelines in 1997 (IMO, 1997) and again in 2001. As a tool designed to assist maritime regulators, FSA is not intended for application to individual ships, but for use in a generic way for general shipping. The main elements introduced by FSA are a formalized procedure, an audible process, communicated safety objectives, and priorities based on cost effectiveness. These have made the FSA a more rational risk assessment approach for the regulatory purposes within the shipping industry.

It should be recognized that the FSA is applied to safety issues common to a specific ship type (e.g., a bulk carrier or a high-speed craft) or a particular hazard (e.g., collision, grounding, fire, etc.). A safety case approach used in the UK offshore industry is applied to a particular offshore installation.

A comprehensive summary of the recently published work on marine risk assessment was given by [Yoshida et al. \(2000\)](#) in the ISSC report for the Specialist Committee V1 “Risk Assessment.”

The following sections in this chapter deal with the FSA. The major functional components of FSA are outlined, and followed by a detailed description of each component. A case study in the FSA regime is then briefly presented for illustrative purposes. The inclusion of human and organizational factors (HOF) within the FSA is also discussed, as well as the challenges, limitations, and concerns regarding the FSA application.

41.2 Overview of FSA

As a risk-based methodology, in some aspects FSA is similar to the Safety Case regime used for the UK Continental Shelf. A safety case should be applied to a particular offshore installation. However, the FSA is applied as a whole to shipping or to safety issues common to a ship type, such as tankers or high-speed passenger vessels. This type of application is due to a number of reasons, for example, the unique features of the shipping industry: there is no single regulator, no single culture, and no uniformed education and qualification system that exists in the maritime industry worldwide. The FSA is a tool for rule making at IMO to make the decision process more rational and to provide a proactive approach that comprises technical and operational aspects. IMO interim FSA Guidelines state “FSA can be used as a tool to help in the evaluation of new safety regulations when comparing between existing and possibly improved regulations, with a view to achieving a balance between the various technical and operational issues, including the human element, and between safety and costs.” The FSA may be used to develop “performance-based” rules stating safety objectives and functional requirements and rational “prescriptive standards” based on the performance-based rules.

The main characteristics of the FSA are presented as:

- A systematic approach considering the ships as socio-technical systems. The system may consist of hardware, environment, human organizations, operations, and procedures.
- Hazards are identified proactively through the hazard identification process. A large number of different hazard identification approaches may be put into use.
- Risks associated with various hazards are described and analyzed. The risk is a composite of the likelihood and consequences of the potential undesirable events arising from a

hazard. The risk analysis covers a certain time span, that is, the operational life, and may involve various quantitative or qualitative tools to perform likelihood and consequence calculations.

- Once a risk is quantified, it is then necessary to determine if the risk is acceptable, based on the predefined acceptance criteria. When the risk is acceptable, a cost/benefit analysis may be followed to compare the costs for preventive/protective measures with the benefits.
- The above-noted basic elements are integrated into a risk model, where the objective is to recommend the most cost-effective, preventive, and mitigating measures for risk management.

The functional components in a FSA are shown in Figure 41.1. As a risk-based approach it may look quite similar to the offshore QRA procedures. However, the

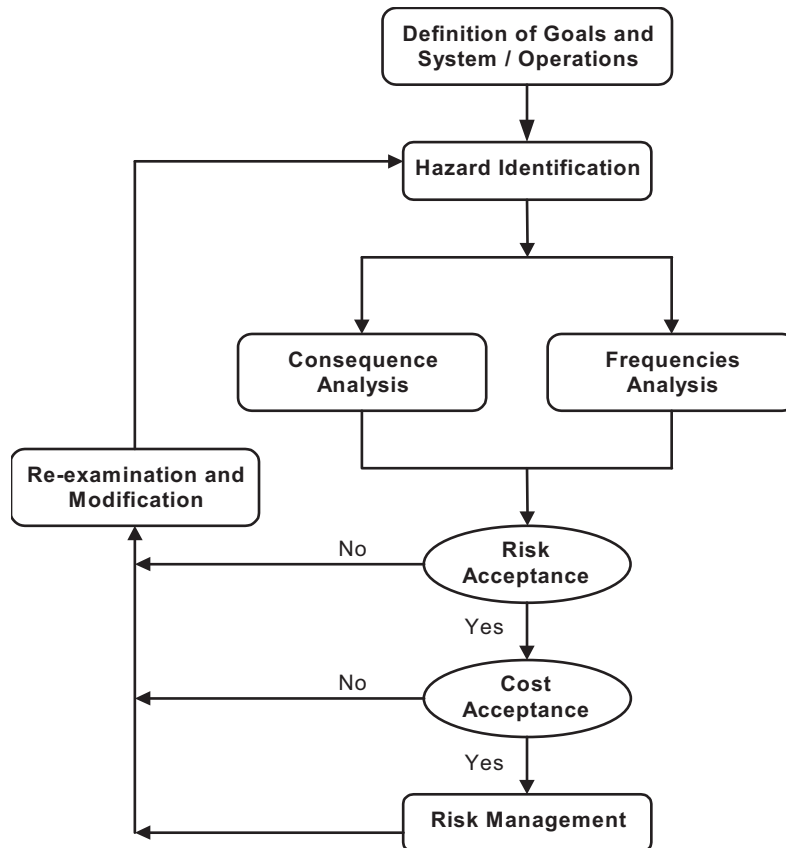


Figure 41.1
Functional components in the Formal Safety Assessment.

actual content of each step, as well as the methods and tools used, may be different from offshore applications. This is described in more detail in [Section 41.3](#).

The types of risks to be considered include:

- Risk to human safety
- Risk to the environment
- Risk to property.

41.3 Functional Components of the FSA

41.3.1 System Definition

A detailed system description is essential for risk assessment. Such descriptions usually consist of a hierarchical structure, including all hardware, people, procedures, and environments, all of which are described in a “top-down” manner. The hardware that comprises a generic ship is the most basic layer in the system definition. The interface between hardware and human operators, that is, the so-called man–machine interface, forms the second layer. The external environment could be considered as the third layer. The hardware, the individuals and organization, and the external environment, which may vary during the ship’s life cycle, all influence the overall safety. Therefore, in the following sections the ship’s hardware, the stakeholders (interested parties), and the ship’s life cycle are all discussed.

The Ship Hardware

The ship hardware can be roughly divided into two categories: structure and machinery.

The ship structure has been traditionally divided into three subcategories: hull girder, internal structure, and superstructure. Structural elements play various roles in maintaining the integrity of the ship. Structural failure may lead to cracking, localized flooding, or even ship breaking in extreme cases. Considerable progress has been made in the past few decades to analyze the capacity of complex ship structures using modern FEM tools (see Part II, Chapter 19). However, uncertainties concerning construction errors and defects and uncertainties in the load prediction still exist.

The ship machinery consists of many subsystems, that is, power generation system, propulsion system, steering and maneuvering system, navigation and communication system, cargo–fuel–ballast handling, mooring and anchoring, monitoring, and emergency response system. The integrity of these systems is vital to the operation of the ship. Improper operation or accidental system failure can directly trigger accidents, which may lead to the loss of cargo, human life, and/or severe environmental pollution.

The Stakeholders

A generic ship may involve the following stakeholders: crew, ship owner/charter, classification society, builder, cargo and cargo owner, passengers, the insurer, the port, and coastal states. Various stakeholders may have different views of safety, as well as the cost/benefits derived from the changes of the shipping safety. The interaction among these parties is complex, and will significantly influence the safety of shipping.

The Ship Life Cycle

A ship may be originated by the owner's decision to build a new ship, with characteristic dimensions that satisfy functional requirements. The second stage is the design stage. Specifications for the structures and machinery of the ship are determined. The third stage is the building stage. It consists of construction, launching, and outfitting the ship by yard. The fourth stage consists of normal operations. A typical new ship can be in service for 30 or more years, and FSA will emphasize on the normal operation. During the ship's service life, it will have four principal activities: open ocean navigation, waterway navigation, port operation, and dry-dock operation, described below in detail.

- **Open Ocean Navigation:** The largest percentage of time in the whole life of any large ship is spent in transit on open sea.
- **Waterway Navigation:** This is usually the second most frequent activity in a ship's life cycle. As a large ship approaches (or leaves) a harbor, it is common for the ship to pick up a pilot who has greater familiarity with all aspects of the waterway leading into the harbor.
- **Port Operations:** The port is where cargo or passengers are loaded or discharged. Many accidents have occurred in ports relating to the transfer of cargo. Different ships may involve different types of operation, and therefore different durations.
- **Dry-Dock Operations:** Ships dry-dock at regular intervals for the purpose of inspection, repair, and maintenance. The dry-docking can involve inspections by an agent of the classification society, and inspections by the owner.
- The last stage is the scrapping stage. Ships may be finally scrapped in a repair yard at the end of their life.

41.3.2 Hazard Identification

In the FSA regime, a hazard is broadly defined as a situation with the potential to cause harm to human life, the environment, and property. Hazards become a problem when they develop into accidents, generally this occurs through a sequence of events. There are two features for ship hazards as described below.

A ship hazard characteristic is that it is more difficult to achieve ideal levels of separation from the onboard hazards, since command and control facilities, living/working areas, fuel, propulsion, power generation plants, and emergency systems are within the ship.

Another characteristic of ship hazards is that at different phases of the operation, the ship could experience different kinds of hazards.

Hazard identification is performed by selected professionals and the purpose of hazard identification is to identify all conceivable and relevant hazards. Typically a team of 6–10 experts, including naval architects, structural engineers, machinery engineers, surveyors, human factor engineers, marine officers, and meeting moderators, provide the necessary expertise for the topic under study. The hazards are identified using historical incident databases and expertise of the team. Several analysis methods are available, including FMEA, HAZOP, etc. The identified scenarios are ranked in order by their risk levels. Prioritizing the hazards may later be subjected to more detailed analysis.

For a generic ship and its associated subsystems, the following important hazard categories are identified. Each of these categories is complex, resulting from a large number of different factors. After hazard identification, hazard ranking may be performed to prioritize the hazards, based on rough estimates of the risk associated with each identified hazard.

- Collision and grounding
- Fire
- Explosion
- Loss of structural integrity
- Loss of power
- Hazardous material
- Loading errors
- Extreme environmental conditions.

Collision and Grounding

Collision occurs when a ship strikes another ship or another object. It is a high consequence hazard for oceangoing ships. Grounding occurs when the ship bottom is penetrated by the sea bottom or by underwater rocks. Collision and grounding are low probability, high consequence events, especially in the case of tankers [Amrozowicz et al. \(1997\)](#). The assessment of grounding and collision risks includes:

- Frequency of occurrence of grounding and collision accidents
- Consequence in terms of structural damages, oil outflow, and environmental/economical impact due to the oil spill.

[Wennick \(1992\)](#) investigated the frequency of occurrence of collision and grounding in channel and port navigation using the “statistical method” and the “causal method.”

The statistical method uses historical incident records to estimate accident frequencies, while the casual method establishes the relationship between the contributing factors and the occurrence of the accidents. Although the casual method may be used to study the impact of changes in the physical plan on the risk of collision and grounding, it still must be calibrated with the statistical method.

[Sirkar et al. \(1997\)](#) proposed a risk assessment approach that accounts for the consequence of collisions and groundings. Their model for tanker environmental risk includes the calculation of accident probability, the oil outflow analysis using probabilistic methods, and an estimation of consequences using a spill response simulation. Like offshore environmental risk analysis, the volume of the oil spill is not the best measure of the environmental risk. Instead, the effect of oil spill should be used (see Part V, Section 38.1.7). In [Sirkar et al. \(1997\)](#), the probability of damage and oil outflow analysis is based on a simplified probabilistic oil outflow methodology. They proposed a method for calculating probability distributions for the damage extent and location, by simulating structural response in groundings and collisions for a large number of accident scenarios using the Monte Carlo approach. In the Monte Carlo simulations, the input variables include the accident scenarios (e.g., vessel characteristics, grounding types), and the initial distributions defined based on historical data and expert judgment.

The principal underlying cause in this category is lack of information, for example, an imprecise knowledge of one's own position at a given time, uncharted obstacles, inaccurate position, and speed of nearby vessels will all pose threats, noted above. Severe weather, human error, often in the form of miscommunication or an otherwise occupied pilot, and inappropriate speed all play an important role in causing consequential damages.

Fire

Fire is a ship hazard of higher consequence. It is estimated that more than a third of all shipboard deaths during the period 1987–1992 were due to fire accidents ([Hessler, 1995](#)). To protect from the fire effects, detection and alarm systems notify the crew to take appropriate firefighting actions and alert the passengers to evacuate from the dangerous area. Early detection of fire is vital. Once a fire has started, it is difficult to extinguish and it can easily escalate. Sometimes it may be difficult to reach a fire site due to the confined nature of quarters on board ships, limited access to the burning area, and other factors such as toxic smoke. Inadequate training of the crew in firefighting procedures may also pose a problem.

To reduce fire growth and spread, material and product performance testing are used to set limits on the heat release, on the thermal properties of structural boundaries, and on the use of restricted combustible materials. These testing requirements provide containment of

the fire in the origin area and minimize the impact of the fire on the means of escape or to the access for fire fighting. The system design to facilitate passenger evacuation can play an important role for timely passenger evacuation and firefighting.

Fires that start in the engine room are often linked to a leak in the fuel line, lubricating oil, or hydraulic fluid, with subsequent ignition. Electrical short circuits are another cause. Regions such as the galley, laundry rooms, and recreational and storage areas contain many combustible materials such as cooking oils, sugars, and flour. The crew may sometimes fail to recognize these commonplace hazards. NK (1994) issued guidance to protect engine room fires based on a series of risk assessment studies. Emi et al. (1997) summarized the engine room fire causality data. About 0.1% of ships were damaged by an engine room fire, and the same amount was due to fires in hull compartments. Seventy-five percent of engine room fires occurred when ships were underway, in which 50% of the ships became uncontrollable.

Explosion

A number of explosions that occurred in the past were initiated on crude carriers in ballast tanks after the cargo had been unloaded. Crude oil contains many volatile constituents that can create a highly explosive mixture in air. Inert gas protection techniques such as pumping pure nitrogen or carbon dioxide in the tanks as they are being emptied, or shortly after, to remove the oxygen, has offered greater protection than before. Communication and strict adherence to protocols are vital duties, which will avoid explosions during venting operations.

Human error resulting in inadequate precautions is another factor; a number of explosion accidents actually originated from mistakes or violations in the operational procedure, for example, smoke, illegal shortcut in procedure, etc.

Loss of Structural Integrity

Loss of structural integrity is a traditional concern for classification societies. Hull failure may result from faulty designs, construction, maintenance, or operation-related factors. Furthermore, the introduction of new technologies and new ship types may constantly lead to new problems.

The maintenance of aging ships may not be perfect. It is impossible to inspect some areas of the ship and register the condition of all the structural members since their condition can never be known with certainty. Cyclic loading due to waves causes the structural components to fatigue over time. The degree to which fatigue degrades the load-bearing capacity of the vessel cannot be estimated accurately. Corrosion is also a likely problem. All the above-noted possibilities may lead to the loss of the ship's structural integrity.

Loss of Power

The loss of engine power at sea is potentially very dangerous. Without power, steering the ship becomes impossible since the rudder becomes ineffective with no propeller race or forward speed. The vessel may then collide with another vessel or obstacle, or drift under the wind, waves, currents, and subsequently the ground. In heavy seas, the vessel can possibly broach and founder with no way of pointing into or running with the waves.

Power failure may result from a mechanical failure of the engine, generator breakdown, a boiler or crankcase explosion, engine room fire, etc. One known initiator of power loss is contamination of the fuel supply by water. Seawater passing through damaged fuel tank ventilators caused BRAER (crude oil tanker) to lose power and drift aground off Scotland where its cargo was then spilled.

Hazardous Material

The risks, associated with cargo such as crude oil or liquefied natural gas, are fairly obvious. However, the danger of materials such as powdered aluminum and certain types of flour may not be readily apparent. The international community has set regulations on known hazardous substances. For instance, containers carrying hazardous substances require a bold diamond-shaped label marking them “Dangerous and Hazardous” and displaying a code that indicates the contents precisely.

There is a possibility of mishandling containers during port operations, causing breaking or leakage. If a leak occurs inside a container for whatever reason, it may stay unnoticed for a while. Undetected release of toxic substances may pose a threat to the crew and cleanup on board, especially while at sea where cleanup can be difficult.

[Romer et al. \(1993\)](#) presented a risk assessment of marine transport of dangerous goods based on historical data that consist of 151 accidents in the period of 1986–1991. Their paper gave frequencies for various kinds of accidents and FN curves and frequencies, as well as the size of spills.

Loading Errors

Improperly loaded cargo may adversely affect the ship’s stability, as well as put undue strain on the hull and subsequently increase the failure probability at sea. In rare cases, a vessel can sink due to improper loading.

Vessels such as ore carriers are susceptible to payload shifts during periods of rough seas. While for container ships, container lashings can become loosened or broken, causing containers to shift or move freely. This will not only jeopardize ship stability but also pose a threat to personnel, machinery, or the hull. There is also an economic intention to fill the

vessel to its maximum capacity, especially for a short period of time. However, some overloaded fishing vessels have foundered because of this.

Extreme Environmental Conditions

Many ships were lost at sea during extreme weather. The ocean is a hazardous environment for both people and ships.

The crew is likely to lose their lives overboard if they go on deck during a sea storm. Secured components may also break and cause damage to equipment. This has happened for a BRAER tanker, where pipes stored on the deck broke free and damaged the vents serving the diesel fuel tank. This led to the diesel fuel being contaminated with seawater and finally, the vessel lost power. The vessel then drifted ashore under a prevailing current, leading to a significant oil spill. The heavy weather may also lead to a tired and seasick crew; this therefore increases the likelihood of operational errors. Rough seas may pose other hazards as well, for example, loss of visibility, position, or communications, which potentially increase the risk of grounding and colliding.

41.3.3 Frequency Analysis of Ship Accidents

The risk associated with an event is a function of two quantities: the likelihood of the event and the consequence from that event. Therefore, frequency analysis forms an essential part in the risk estimation. [CCPS \(1995\)](#) listed oceangoing vessel failure modes (e.g., collision, grounding, fire and explosion, and material/equipment failure), discussed parameters influencing accident rates and hazards release probabilities, and suggested procedures for failure (release) frequency calculations.

For ship accidents, sometimes, sufficient historical data are available for critical events. One of the best sources of data is the US Coast Guard's vessel casualty file for US waterways, the Marine Casualty Information Reporting Systems ([USCG, 1992](#)). The frequency can then be derived simply from the past data. However in most cases, a frequency analysis may not be so straightforward and it must examine the contributing factors that lead to the actual accident. In this process, it is necessary to break the compound event into individual events and put them together in a logic sequence to model how the hazards are developing into accidents via different failure paths.

After a synthesis of individual events, according to certain scenarios, the occurrence probability of the accident may be quantified by using the fault-tree technique and the event-tree technique. Normally, the fault tree is used to explore the causes of a critical event, whereas the possible outcome of the event is traced down by using the event tree. The frequency of initiating events may be drawn from historical data, for example, failure rates, mean time between repairs, or accident and incident frequencies, and then be modified based on expert judgment according to the actual system. Sometimes data for

similar accidents from other industries may be applied if they are sufficiently relevant. In all, obtaining adequate data to avoid ship hazards can be a problem and sometimes the lack of data can make the quantitative risk analysis rather difficult, if not totally impossible.

41.3.4 Consequence of Ship Accidents

The consequence is conditional depending on the probability of the accident. The general consequences from ship accidents are measured in the following terms:

- Loss of human life
- Loss of cargo
- Damage to ship or other ships
- Damage to the environment.

A unique feature for shipping is that different ship stakeholders may see, feel, and judge, the above-noted consequences, differently.

Loss of Human Life

When quantifying the consequence of loss of lives, analysts may ask a sensitive question of how much the loss of a human life will cost, for the purpose of making risk comparisons. Historically, the only way loss of human life can be compensated for, after an accident, is through monetary means. There are well-defined procedures for such compensations. Such monetary values should not be regarded as what a human life is “worth”; rather they indicate what the benefit is to a stakeholder if a life has been saved.

Typically, there is a difference made between the loss of life for ship operating personnel and passengers, since the former are supposed to know the increased risk level they are taking while the latter are not. As a result, the potential consequence of loss of a passenger ship may be very large.

Random losses of human life, in small numbers per accident, may appear to be accepted by society, but this is not the case for massive losses. The latter type of accidents will inevitably come under public scrutiny and investigation, and may end up with some new regulations. The consequences in this respect are then far beyond the monetary terms.

Loss of Cargo

Loss of cargo occurs in many marine accidents. Usually the shipper obtains insurance for the transport of cargo, and in case of a loss, the insurer will directly compensate the shipper. Reimbursement of the value of the cargo is normally the extent of the consequences. In some cases, where the time to deliver the cargo is critical, reimbursement of the value of cargo may not compensate the shipper for the total

consequences of the loss. The intangible part of the loss is difficult to assess and may vary from case to case.

Damage to Ship or Other Ships

The consequences of loss or damage to the ship also involve tangible and intangible components. If any of the ships involved are not totally lost, then the tangible costs are simply those that are incurred in getting the ships to a repair yard and completing the repairs. If the ship alone is lost entirely, then the tangible cost is simply the replacement cost for the ship.

There are many intangible consequences involved in the loss or damage of a ship and these can be more significant than the tangible cost. These are primarily business consequences due to the loss of the operation of the ship or loss of the entire ship.

Damage to the Environment

There are many ways in which a ship can damage the environment, the most obvious being the unintentional spillage of oil as a result of an accident. This can happen as a result of many types of accidents including grounding, collision, fires, and explosions. The effects that oil will have on the environment depend on the amount of oil released, the ecological fragility of the local area, the wind, waves, and currents at the time of the accident and during the attempted cleanup, etc.

From the Amoco Cadiz, Exxon Valdez, and Braer accidents, it is seen that the associated costs can be very high, even tens or hundreds of times larger than the value of the ship and cargo together.

41.3.5 Risk Evaluation

Risk estimation can identify the areas with high risk, the main contributors to risk specific hazards. The total risk to human safety, business, and the environment can then be estimated.

The first thing relating to the risk evaluation is the predefined acceptable (target) risk levels for human safety, business, and the environment. Then, the obtained risk values can be evaluated according to the target levels. Unacceptable risks will lead to a modification of the system and a need to again perform the previous steps involved in risk assessment. The determination of the target levels may be difficult; therefore, they may initially be based on values obtained from the risk analyses of existing ships.

The well-known ALARP principle is also applicable to the FSA. It requires that risks be reduced as low as reasonably practicable. To apply ALARP, the bounds of risk tolerability need to be defined. If the risk is broadly acceptable, no specific actions are

required. However if the risk is between certain levels, they will ordinarily be tolerated if they are reduced to as low as reasonably practicable; that is, the cost to reduce the risk further is grossly disproportionate to the benefit gained. This will involve cost–benefit analysis.

41.3.6 Risk Control and Cost–Benefit Analysis

There are two methods for controlling risk, namely:

- Preventive approach: to reduce the frequency of an initiating event
- Mitigating option: to reduce the severity of the failure.

The actions for controlling risk include applications of engineering and the implementation of procedures. The practical risk control approaches should be investigated and their ability to reduce risk must be documented. The effects of risk control actions can be determined by repeating the risk analyses and comparing these results to the original results. The benefits are the avoidance of accidents and these can be measured by evaluating the avoidance of harm to people, damage to property, environment, and other costs. To achieve a balance, the benefits of a risk control measure must be considered and compared to the cost of its implementation. This is done through a cost–benefit analysis.

In a cost–benefit analysis the costs associated with the risk control option or package of options are estimated considering both public cost (enforcement, inspection, etc.) and commercial sector cost (e.g., capital cost, compliance cost, etc.). A similar exercise is undertaken to estimate benefits, which for ships can include reduced environmental cleanup costs, increased vessel life, the value of saved lives, etc. The net present value of each option or option package is calculated by subtracting the benefits from the costs. Sensitivity analysis may be conducted around key assumptions to estimate the level of confidence that can be attached to the computed net value of each option package. Risk control options can be ranked based on their cost-effectiveness. The final step in a FSA is the “decision-making,” which gives recommendations for safety improvement. The selection of risk control options for the decision-making is based on the cost-effectiveness and the principles of ALARP (as low as reasonably practicable). Intolerable risk must be controlled regardless of costs. “Reasonable” means that the costs are in grossly disproportionate to the benefits.

41.4 HOF in the FSA

IMO (1997) recommends a balanced approach between human and technical factors reflecting their contributions to the safety of the overall system considered. IACS (1999) proposed Draft Guidance on Human Reliability Analysis (HRA) within FSA. The HRA

guidance was developed to assist the incorporation of HRA in the FSA process. It provides references and summaries of various HRA techniques.

The majority of ship incidents and accidents appear to have a human factor component, for example, error in loading, error in operating machinery, etc. It is therefore necessary to integrate the HOF into the FSA. To this end, it is essential to include an HOF expert and operational experience in the FSA team.

The consideration of an HOF can be done in one of two ways. The first and probably the less difficult way is to treat human behavior at a phenomenological level, to determine the probability of an improper human decision (behavior) to be made with respect to each one of the critical aspects of the operation. The second and more difficult way involves the underlying causes of the improper human decision. The following example is used to illustrate the first approach.

In a shipboard fire, many of the initiation probabilities may be a direct result of humans, like smoking. Humans may also affect the progress of the fire, by fighting it manually or using fire suppression equipment. Such influences can be incorporated in the FSA. For example, the effects of humans on fire initiation may be implicitly included in the actual historical data. Differences in crew training and safety discipline may be accounted for by using different probabilities assigned to the event tree in the risk analysis. Human errors of commission or omission can also be similarly incorporated. However, it is generally very difficult to accurately quantify the effects of different HOF.

41.5 An Example Application to the Ship's Fuel System

The above-noted FSA method can be applied to the ship's fuel system to identify appropriate risk control measures that reduce the potential for fire and failure or to mitigate the consequence.

A possible approach starts with the description of a generic ship fuel system. This consists of defining the essential features of the components fitted to all fuel systems and the fuel processing plant, and includes both high and low pressure areas.

Casualty data arising from failures of fuel systems would then need to be collected and categorized into relevant hazard categories (fire, hardware failure, etc.). Any of the existing worldwide databases for reliability data associated with marine parts, for example, rotating and reciprocating fuel pumps, piping, and connections may be used. Hazard and Operability Studies (HAZOP) can be employed to identify areas in the generic fuel systems that are most prone to failure. A fault tree could then be constructed to structure the information and assess the failure frequency. The event tree is then used to model the possible consequences.

The output of the above exercise would be a prioritized list of issues contributing to the frequency of occurrence of each accident category, combined with the severity of the consequences. A cost benefit analysis of an engine room fire or downtime, weighted against the benefits provided by increased reliability, would provide supplemental information for the decision-making.

41.6 Concerns Regarding the Use of FSA in Shipping

The FSA is a tool for supporting the development of rational regulations (such as IMO), enabling focusing on important issues, and justifying that a modification or development of a regulation is reasonable. It offers a better insight into hazard identifications and scenario developments. Indeed the FSA is a more systematic approach for managing risk.

Although many elements of the approach described in previous sections are well established in other contexts, their applications to the shipping industry in a generic way are relatively new and unproven. Trial applications are being undertaken, with the intention of accumulating relevant results and experience. The development of suitable mechanisms and procedures, in which the FSA process can be applied by the IMO committees in future decisions, is also being considered.

Useful risk estimation data include incident statistics, equipment reliability, structural reliability, human reliability, and fleet (exposure) data. The cost data are related to the estimation of investment costs, operating costs, inspection and maintenance costs, and the cost for cleanup, pollution, etc. In many cases, data are insufficient to do an appropriate estimation of risk.

As with all risk assessments, the results obtained are dependent on data and also on judgment in interpreting the data and anticipating industry trends, the impact of changes in technology, the potential for future accidents, etc. The results of an FSA study are therefore dependent on both the availability of relevant data and the qualified analysts that can undertake rational judgments. The quality of an FSA is as good as the data provided, expertise used, and mathematical models applied. There are many challenges in collecting and interpreting risk data. In many cases, it is found that the data have not been recorded, or not in the way that enables FSA. Mathematical modeling and computer simulations may be the alternatives to the data. An expert's opinion may be a necessary substitute or complement of statistical data. In undertaking such an effort, one may find that those with long experience and good background in relevant specialties may lack familiarity with expressing their judgments in probabilistic terms. The subjectivity of FSA based on incomplete information is a great concern. A study of required and existing databases pertinent to marine risk analysis is needed and a plan for a systematic collection of additional data needs to be developed and implemented.

References

- Amrozowicz, M.D., Brown, A., Golay, M., 1997. A Probabilistic Analysis of Tanker Groundings. ISOPE, Honolulu, USA.
- CCPS, 1995. Chemical Transportation Risk Analysis. Center for Chemical Process Safety, American Institute of Chemical Engineers.
- Emi, H., et al., 1997. Class NK Technical Bulletin.
- Hessler, B., May 1995. Training Ship's Crew for Effective Fire Fighting and Emergency Incident Command. The Institute of Marine Engineers.
- IACS, 1999. Draft Guidance on Human Reliability Analysis (HRA) within the Formal Safety Assessment. IMO. MSC 71/Wp.15/Add.1.
- IMO, 1997. MSC/Circ. 829 & MEPC/Circ. 335, Interim Guidelines on the Application of Formal Safety Assessment (FSA) to the IMO Rule-Making Process. International Maritime Organization.
- NK, 1994. Engine Room Fire, Guidance to Fire Prevention. Nippon Kaiji Kyokai (Class NK).
- Romer, H., Brockhoff, L., Haastrup, P., Styhr Petersen, H.J., 1993. Marine transport of dangerous goods, risk assessment based on historical accident data. *Journal of Loss Prevention in the Process Industries* 6 (4).
- Sirkar, J., Ameer, P., Brown, A., Goss, P., Michel, K., Nicastro, F., Willis, W., 1997. A Framework for Assessing the Environmental Performance of Tankers in Accidental Groundings and Collisions. *Transactions of SNAME*.
- USCG, 1992. The Marine Casualty Information Reporting Systems (CASMAIN), 1981–1991. The U.S. Coast Guard.
- Wennick, C.J., 1992. Collision and grounding risk analysis for ships navigating in confined waters. *Journal of Navigation* 45 (1), 80–91.
- Yoshida, K., et al., 2000. Risk Assessment. In: *Proceedings of ISSC-2000*, Nagasaki, Japan.

Economic Risk Assessment for Field Development

42.1 Introduction

42.1.1 Field Development Phases

An offshore field development project generally consists of four main phases, that is, exploration, development, operation, and decommission. An illustration of the development phases (mainly the first three), along with the main activities, duration, and the detailed cost for each phase, is shown in below (Figure 42.1).

The exploration phase starts after the field license is awarded. If an oil and gas field is discovered based on the results from exploration drilling, the concept screening and feasibility studies of the field will be carried out. Technically feasible and commercial

TIME	EXPLORATION	DEVELOPMENT	OPERATION
GRANTING OF PERMIT			
1			
2	Geology & Geophysics		
3			
4	Exploration & Appraisal well		
5			
6		Reservoir Engineering & Simulations	
7		Develop Transport Installations	
8			
9		Geophysics	
10		Drilling produ. Wells	Production build up
11			
12			Reservoir Engineering (continued)
13			Maximum Production
14			
15			
16			
17			
18			
19			
20			
21			
22			
23			
24			
25			
26			
...			
DECOMMISSION			
Share of Technical Cost	10–20%	40–60%	20–50%

Figure 42.1
Field development phases.

optimum solutions are identified. The exploration phase concludes with the authority approval of the Plan for Development and Operation (PDO).

The development phase starts with the conceptual engineering, which is based on the recommendations of the PDO. The final field development concept is then fixed, along with the operational philosophy, safety, environmental programs, etc. Subsequently, the whole project is executed systematically: engineering, procurement, construction, and installation. Meanwhile, production wells are being drilled if predrilling is recommended.

The operation phase typically has a period of 20 years. The production will initially increase and reach its maximum, and then it gradually declines. Meanwhile, reservoir engineering will continue to maximize the production based on updated reservoir information. The decommission phase is at the end of the field life. The platform is abandoned and removed from the site.

42.1.2 Background of Economic Evaluation

An economic evaluation is carried out throughout the life cycle of a field development project. Net present value (NPV) and internal rate of return (IRR) are the two most basic decision criteria. Recently, life cycle cost (LCC) criterion has been frequently used in decision making, and it is actually derived based on NPV.

Before and during the exploration, economic evaluation is mainly applied to assess whether or not the required investment in this project is profitable enough. An exploration decision is like a major gamble: a large field may be discovered or, at the other extreme, no oil or gas may be found at all. However, the costs incurred in individual explorations are relatively low compared to the total cost of field development if the exploration is successful. The economic evaluation is repeated at each stage during the exploration, and the results could culminate in a final decision to invest in developing the discovery. Classic economic evaluation methods by using NPV or IRR are preferred in this phase. The definitions of NPV and IRR are provided in Appendix A.

Once the project is approved and is ahead in the development and operation phases, the LCC approach is preferable. In the LCC model, all of the relevant economic implications of a decision, and the effects on the operating company, may be considered. For example, by using the LCC model, the total cost of a production facility could be expressed by the sum of the following cost elements (NORSOK O-CR-0002):

- Capital costs (CAPEX)
- Operating cost (OPEX), which covers operation and maintenance
- Cost of deferred production.

The initial capital expenditure of the facility is not the only criterion for decision making. Instead, the optimum design concept is chosen as the one that provides the minimum LCC.

42.1.3 Quantitative Economic Risk Assessment

The economic risks involved in the field development projects vary, and may include (1) technical risks (which may ultimately have their economic impact), (2) commercial risks (associated mainly with cost and income variables), (3) potential natural disaster, and so on. Uncertainties may include (1) reservoir information such as production profiles, recoverable oil and gas, (2) cost parameters such as cost of fabrication, transportation, installation, and cost of operation, maintenance, (3) financial variables such as interest rate and oil price. A systematic economic risk assessment is, therefore, needed to assess the impact of risks and uncertainties associated with the whole field development project, and to subsequently provide the necessary support for decision making.

By adopting probabilistic analysis tools, an economic risk assessment could treat the existing uncertainties and assess risks in a quantitative manner. Accordingly, probabilities of failure events, as well as the importance and sensitivity measures for each uncertainty, could be provided. Compared to simple “best case” and “worst case” estimates in traditional deterministic economic evaluations, these results could provide better support for decision making and help reduce the overall uncertainties involved in a field development project.

A quantitative economic risk assessment methodology is presented in this chapter. It is a generalization of various published economic risk studies, for example, by [Skjong et al. \(1988\)](#), [Bitner-Gregersen et al. \(1992\)](#), [Cui et al. \(1998\)](#), [Odland \(1999\)](#), and [Bai et al. \(1999\)](#). Five major steps are proposed.

- Identify the field development phase that is to be studied, previously discussed in [Section 42.1.1](#).
- Identify which decision should be made during the development phase, for example, starting exploration, comparing early production concepts, evaluating different final development concepts, and operation and maintenance strategies.
- Define the decision criteria and subsequently set up the limit-state functions, for example, by setting a certain target NPV or IRR value, or the minimum LCC.
- Model economic risk by obtaining statistical data for each parameter in the limit-state functions and calculating the failure probability. Both simulation and analytical reliability methods may be used. Parameters in limit-state functions can be classified as cost and income variables. They can be expressed in terms of statistic distributions or deterministic values.
- Perform sensitivity studies and propose economic risk reductions and uncertainty reducing measures, in order to improve the decision-making process.

42.2 Decision Criteria and Limit-State Functions

42.2.1 Decision and Decision Criteria

Various decisions and decision criteria are involved in different phases of an offshore field development project. Below are three major examples, which occur in exploration, development, and operation phases, respectively.

A. Should the Field be Developed Now?

Will the development project be at least as profitable as alternative investment opportunities? Will a development based on existing technology be acceptable in relation to the utilization of resources, for example, oil recovery factor, gas utilization, safety, and environment? Is the timing right in regard to the infrastructure? The IRR or NPV may be suitable in this context.

B. Given That the Field is Under Development, How Should It Be Developed?

Different field development concepts may be feasible. Both the value of production, the CAPEX and the OPEX, and the phasing of income and costs should be considered in a realistic and balanced way. The NPV may be the most suitable criterion in this context.

C. How Should the Project be Carried Out?

For day-to-day execution of the project, including the selection of equipment and services from contractors, it is necessary to use criteria that can be easily related to the consequences of such decisions. LCC may be a suitable criterion in this context.

42.2.2 Limit-State Functions

The limit-state functions in a probabilistic analysis are defined based on NPV or IRR. LCC criterion could virtually be traced down to NPV criterion.

If a specified IRR in this project is achieved, the limit-state function can be formulated as

$$G(\mathbf{X}) = \sum_{n=6}^{30} \frac{I_n(\mathbf{X})}{(1 + irr)^{n-1}} - \sum_{n=1}^{30} \frac{C_n(\mathbf{X})}{(1 + irr)^{n-1}} \quad (42.1)$$

The total period of 30 years is considered in Eqn (42.1). I_n denotes the income generated in the n th year and C_n is the cost in the n th year. Both I_n and C_n are functions of input variables (basic variables) expressed in the equation by \mathbf{X} . A negative value of the function $G(\mathbf{X})$ implies that the IRR is less than the irr .

The limit-state function for the decision criteria, based on the NPV, is similarly

$$G(\mathbf{X}) = \sum_{n=6}^{30} \frac{I_n(\mathbf{X})}{(1 + irr)^{n-1}} - \sum_{n=1}^{30} \frac{C_n(\mathbf{X})}{(1 + irr)^{n-1}} - npv \quad (42.2)$$

In this case, the function $G(\mathbf{X})$ is negative, if the NPV is less than the value npv for a corporate rate of return irr .

42.3 Economic Risk Modeling

The cost variables are related to the cost of design, construction, installation, and operation (including maintenance). The income variables, however, are related to the reservoir size and characteristics, oil and gas prices, currency fluctuations, inflation and interest changes, and taxation rules. Modeling the uncertainties associated with income and cost variables is therefore the core of economic risk modeling.

A typical North Sea oil and gas field project in the development and operation phase is chosen as a representative case to illustrate the economic risk modeling. These are adapted from [Bitner-Gregersen et al. \(1992\)](#). These data are listed only for the illustrative purpose, and should be updated specifically for each project considered. The field is assumed to be in production for 25 years, after a 5 year construction and installation period. The decision criteria are based on the IRR or NPV, and limit-state functions are subsequently defined in the form of [Eqns 42.1](#) and [42.2](#). Modeling of cost variables, income variables, and their uncertainties are described in the following subsections.

42.3.1 Cost Variable Modeling

An overview of the costs during development and operation phases are presented below ([Odland, 1999](#)):

- Facility Costs
 - Topsides
 - Substructure
 - Well/riser system
 - Export/import system
 - Project management and insurance
- Drilling Costs
 - Platform wells
 - Predrilling

- Operation and Maintenance Costs
 - Personnel and catering
 - Well maintenance
 - Logistics
 - Land organization and insurance

Costs of Facilities and Drilling

The costs associated with facilities mainly occur in the platform design, construction, and installation phases. Each cost center has a base value B_i and several influencing cost variables. For example, the cost of template material is a product of the template weight and the cost of template material per unit weight. In order to establish the uncertainties in the cost variables, the analysts are to assess factors and multiply the best estimates to give the 10%, 25%, 50%, 75%, and 90% fractile of the variables. The lognormal distribution is thus used for all cost variables and the distribution parameters are then determined by a least-square fit of the distribution to the data points.

Some cost variables enter more than one cost center. As an example, it is likely that if the amount of material exceeds the base estimate, then the number of man-hours spent to weld the material will also exceed the base estimate. The correlation should be accounted for properly. The correlation coefficients may be given based on an understanding of the interplay between different cost variables and experience in the form of existing data. All costs are distributed over time as a result of a scheduling program.

Costs of Operation and Maintenance

Additional costs occur for production, processing, and transportation during the production phase as discussed earlier. These costs are divided into each product, for example, oil, gas, and liquefied natural gas (LNG).

42.3.2 Income Variable Modeling

The income variables are grouped into three categories:

- Reservoir size and production profiles
- Oil and gas prices
- Taxes, inflation, and interest rates.

Reservoir Size and Production Profile

At the time the decision is made to start the construction of a platform, large uncertainties are present with respect to the total recoverable volume, the time it takes to reach full production, and the production profile. The uncertainty varies depending on the geological properties, the amount of geophysical exploration, and the number of test wells. In order

to model the production rate as it evolves in time, an analytical expression (Skjong, 1988) for the production rate is adopted

$$V(t) = \frac{V_{tot} b^{ab+1}}{\Gamma(ab+1)} t^{ab} \exp(-bt) \quad (42.3)$$

where $V(t)$ is the production rate at time t , V_{tot} is the total recoverable volume, a and b are parameters describing the production profile, and Γ is the Gamma function. By letting V_{tot} be a random variable, the uncertainty in the recoverable volume can be modeled. By letting a and b be random variables, the uncertainties involved in how early the maximum production rate can be reached and the production profile can be modeled.

Prices of Oil, Gas, and LNG

The uncertainties in the price of oil, gas, and LNG for a long period of time (5–30 years) are obviously very large. A simplified model is applied here. The mean value of the oil price 5 years from now is assumed to be 23 USD per barrel, and it is assumed to change with inflation for the total period. Applying a lognormal distribution with a 20% coefficient of variation randomizes the price each year. Therefore, there is a 10% probability that the price of oil will be less than 17.5 USD per barrel and a 10% probability the price of oil will be more than 29.4 USD per barrel.

It is likely that the oil price in 1 year is highly correlated to the price in the next year, and the correlation becomes less for the years further into the future. This is modeled by a correlation of 0.7 between values in two successive years.

Taxes, Inflation, and Interest Rates

The tax on the net profit is assumed to be 50.8%, plus an additional tax for oil companies of 30–85% of the net profit. The tax on assets is 0.5% and the depreciation period is 6 years, starting from the year the investment is made. Results are given for both consolidated and unconsolidated situations. For the consolidated case, a tax deduction that cannot be used due to a negative profit is used by the company elsewhere and credited to the project.

The inflation rate is assumed constant at 6%. The financing of the project is planned with 50% equity capital and 50% loans. The interest rate on the loan is assumed constant at 10%. The financing model can easily be made more realistic, for example, with loans in different currencies, and with different uncertain developments in the exchange rates.

42.3.3 Failure Probability Calculation

After formulating the limit-state function based on IRR or NPV criteria, the probability of getting a negative value in the limit-state function can be computed by Monte Carlo

simulations or by applying analytical reliability methods (FORM and SORM). The simulation methods represent basic calculation techniques that are often used to verify the results obtained by analytical methods.

The probability, P_E , of a desirable or undesirable event, based on a limit-state function (or performance function) $G(X)$, is defined in Eqn (42.4). The sign of the limit-state function is selected in such a way that a negative value corresponds to not achieving the desired goal.

$$P_E = P(G(X) \leq 0) \quad (42.4)$$

Corresponding to the event probability, the reliability index β_R is defined as

$$\beta_R = -\Phi^{-1}(P_E) \quad (42.5)$$

where Φ is the standardized normal distribution function. The probabilistic analysis procedure can also treat situations where several criteria must be fulfilled simultaneously.

42.4 Results Evaluation

42.4.1 Importance and Omission Factors

The importance factor, α_i , indicates the fraction of the total uncertainty arising from uncertainty in a variable. For the FORM analysis, the reliability index is increased by a factor $1/\sqrt{1 - \alpha_i^2}$ (called the omission factor), if the uncertainty in variable i is ignored and the variable is replaced by its mean value (50% fractile) as a deterministic variable. These important measures provide useful guidance in a process of choosing for which variables to collect further data, in order to reduce the overall uncertainty.

The importance of the different sources of uncertainty may be obtained from the FORM method. The total uncertainty of the project has three major contributions: Facilities (design, construction, and installation) and drilling (34.2%), Reservoir size and production profile (41.8%), and Oil price (20.3%). It is of particular interest to note the importance of the time it takes to reach the maximum oil production. This clearly indicates that the economic result of the project is dependent on good engineering, planning, and quality control. It is also observed that within the assumed model, the project result is not dominated by uncertainties in the oil price.

The use of the omission factors is illustrated by studying the well predrilling cost. Assume a fixed price contract (a deterministic value) for predrilling, which corresponds to 50% of its original distribution. This changes the reliability index β by a factor $1/\sqrt{1 - \alpha_{30}^2}$. For the consolidated IRR analysis with an IRR = 11.3% (10% fractile, worst case), the reliability index is changed from 1.28 to 1.34. The corresponding failure probability is

then 9%. This means that with a fixed price contract for predrilling, the probability of not achieving an IRR of 11.3% is reduced from 10% to 9%.

42.4.2 Sensitivity Factors

During the decision making, the following question is often asked: “What is the effect of changing this parameter?” Such a question can be answered by using sensitivity measures, which give the change in event probability (through change in reliability index) to an increment $\Delta\theta$ in any input parameter θ , whether it is a statistical distribution parameter or a deterministic parameter.

It has been shown that the time to reach the maximum oil production is very important to the final project result. The consolidated IRR analysis is used to demonstrate the use of sensitivity factors for this variable. The analysis is for an IRR = 11.3% corresponding to a 10% fractile. From FORM analysis, the change in the reliability index, due to a change in the mean time for it to reach the maximum production rate from 2.5 years to 1.5 years, is

$$\beta_{new} = \beta_{old} + \left(\frac{d\beta}{d\mu_{62}} \right) \Delta\mu_{62} = 1.28 + (-0.15)(-1.0) = 1.43 \quad (42.6)$$

The corresponding failure probability is 0.076; that is, the probability of not achieving an IRR of 11.3% is reduced from 10% to 7.6%.

The effect of reducing the uncertainty in the time to reach maximum production can also be studied. If the standard deviation can be reduced from 1.5 years to 0.5 year, the change in the reliability index is

$$\beta_{new} = \beta_{old} + \left(\frac{d\beta}{d\sigma_{62}} \right) \Delta\sigma_{62} = 1.28 + (-0.044)(-1.0) = 1.32 \quad (42.7)$$

The corresponding failure probability is 0.093, that is, the probability of not achieving an IRR of 11.3% is reduced from 10% to 9.3%.

42.4.3 Contingency Factors

In the FORM and SORM analyses, the “design point” X^* is obtained, which gives the most likely values of the input parameters if the performance function is not fulfilled

$$X_i^* = F_{X_i}^{-1}(\Phi(\beta_R a_i)) \quad (42.8)$$

where $F_{X_i}()$ is the distribution function for X_i and a_i is an output for the coordinates of the design point. The contingency measures (factors) for different variables are the ratios between the design point value and the mean value (or another base value selected beforehand).

The contingency factors depend on the probability level, that is, the confidence in achieving the desired event. In traditional deterministic analysis, base values are multiplied by contingency factors to check whether or not the required performance is achieved, but the selection of contingency factors was not done in a rigorous manner. The probabilistic analysis, however, can provide a consistent calibration of contingency factors for any desired confidence level.

References

- Bai, Y., Sørheim, M., Nødland, S., Damsleth, P.A., 1999. LCC Modelling as a Decision Making Tool in Pipeline Design. OMAE, 99.
- Bitner-Gregersen, E.M., Lereim, J., Monnier, I., Skjong, R., August 1992. Economic risk analysis of offshore projects. *Journal of Offshore Mechanics and Arctic Engineering* 114. August.
- Cui, W., Mansour, A.E., Elsayed, T., Wirsching, W., 1998. In: Oosterveld, M.W.C., Tan, S.G. (Eds.), “Reliability Based Quality and Cost Optimisation of Unstiffened Plates in Ship Structures”, Proc. of PRADS '98. Elsevier Science B.V.
- Gudemstad, O.T., et al., 1999. Basics of Offshore Petroleum Engineering and Development of Marine Facilities with Emphasis on Arctic Offshore, ISBN 5-7246-0100-1.
- Odland, J., 1999. “Lecture Note for 81063 – Development of Offshore Oil and Gas Fields, (Part 6: Cost, Economics and Decision Criteria)”, Dept. of Marine Structures. Norwegian University of Science and Technology.
- Park, C.S., Sharp-Bette, G.P., 1990. *Advanced Engineering Economics*. John Wileys & Son, Inc.
- Skjong, R., Lereim, J., Madsen, H.O., 1988. Economic risk analysis of offshore field development project. In: Proceedings of the 9th International Cost Engineering Congress, Norway.

Appendix A: Net Present Value and Internal Rate of Return

For more information on engineering economics, reference is made to [Park and Sharp-Bette \(1990\)](#) on general items and [Gudemstad et al. \(1999\)](#) on offshore field development applications. A profitability criterion, which is frequently used in decision making for offshore field development projects, is the net present value (NPV) where cash inflows and outflows are compared at the same point in time (today). Internal rate of return (IRR) is also used. An investment project is profitable if its IRR exceeds the required discount rate that is cost of capital.

Notation.

n = Time, measured in discrete compounding periods

I = Market interest rate, or opportunity interest rate

C_0 = Initial investment at time 0, a positive amount

C_n = Expense at the end of period n , $C_n \geq 0$

I_n = Revenue at end of period n , $I_n \geq 0$

N = Project life

F_n = Net cash flow at the end of period n ($F_n = I_n - C_n$; if $I_n \geq C_n$, then $F_n \geq 0$; if $I_n < C_n$, then $F_n < 0$)

Net Present Value

Consider a project that will generate cash receipts of I_n at the end of each period n . The present value of cash receipts over the project life, I , is expressed by

$$I = \sum_{n=0}^N \frac{I_n}{(1+i)^n} \quad (\text{A.1})$$

Assume that the cash expenses (including the initial investment C_0 associated with the project) at the end of each period are C_n . The present value expression of cash expenses, C , is

$$C = \sum_{n=0}^N \frac{C_n}{(1+i)^n} \quad (\text{A.2})$$

Then the NPV of the project [denoted by $\text{NPV}(i)$] is defined by the difference between I and C , that is,

$$\text{NPV}(i) = \sum_{n=0}^N \frac{I_n - C_n}{(1+i)^n} = \sum_{n=0}^N \frac{F_n}{(1+i)^n} \quad (\text{A.3})$$

A positive NPV for a project represents a positive surplus, and the project should be accepted if sufficient funds are available. A project with a negative NPV should be rejected, because investing in other projects at the market interest rate i or outside the market would be better.

Internal Rate of Return

The IRR is another time-discounted measure of investments similar to the NPV criterion. The IRR of a project is defined as the rate of interest that equates the NPV of the entire series of cash flows to zero. The project's IRR is mathematically defined by

$$\text{NPV}(irr) = \sum_{n=0}^N \frac{F_n}{(1+irr)^n} = 0 \quad (\text{A.4})$$

Note that Eqn (A.4) is a polynomial function of irr . A direct solution for such a function is not generally possible except for projects with a life of four periods or fewer. Therefore, two approximation techniques are generally used, one using iterative procedures (a trial-and-error approach) and the other using Newton's approximation to the solution of a polynomial.

Human Reliability Assessment

43.1 Introduction

Human reliability analysis plays an important role in the total reliability analysis of a man–machine system. Accidents such as Bhopal, Three Mile Island, Chernobyl, and Piper Alpha disasters are examples of human failures and show how catastrophic the consequences can be. According to studies made by Moore (1994), approximately 65% of all catastrophic marine-related accidents are the result of compounded human and organizational errors during operation. In a risk assessment, there is therefore a distinct need for properly assessing the risks from human error and finding ways to reduce system vulnerability to these human impacts. These can be achieved via human reliability assessment (HRA). The HRA may be applied in many fields, for example, in design, fabrication, installation, and operation.

Early research on human factors was done by the nuclear power industry and was summarized by Swain (1989). His work was used to further improve human performance in the chemical industry (Lorenzo, 1990). Lorenzo (1990) illustrated examples of error likely situations, suggesting strategies for improving human performance and developing human reliability analysis techniques. An extensive list of past publications may be found within these two books.

For the offshore industry, Bea (1994, 1995) studied the role of human error in design, construction, and reliability of marine structures. For more information on this subject, readers may refer to recent publications (Bea, 2001, 2002). Human and organizational factors are also considered an important part of the formal safety assessment introduced by IMO (1997) and IACS (1999) for the shipping industry (see Part 6, Chapter 42).

This chapter deals with general principles for HRA (Kirwan, 1994), and specific applications to the offshore industry (Bea, 2001, 2002). The HRA has three principal steps: human error identification (identify what errors can occur), human error quantification (decide how likely the errors are to occur), and human error reduction (reduce the error likelihood) (see Figure 43.1).

In the following sections, an overview of the HRA process is given first. Then each major step is discussed with emphasis on how to identify, assess, and reduce human error.

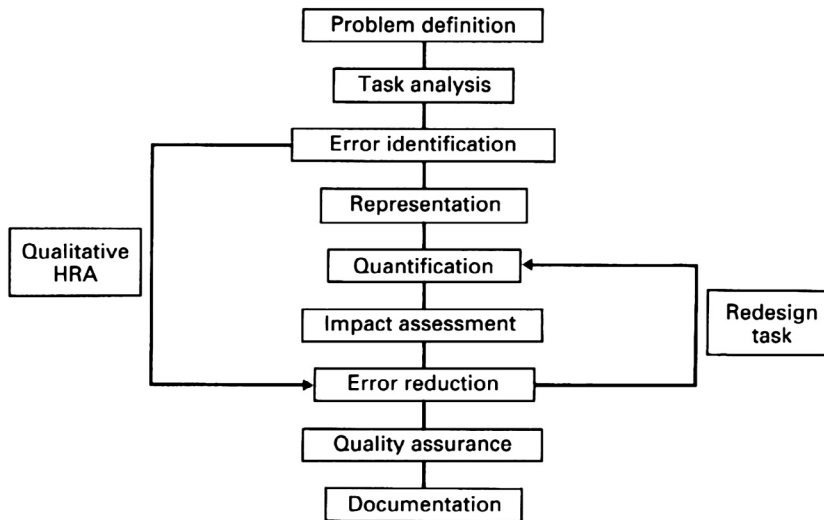


Figure 43.1

The HRA process (Kirwan, 1994).

43.2 Human Error Identification

43.2.1 Problem Definition

The essence of the HRA problem definition is to set the scope of the analysis, decide what types of human interaction should be dealt with, and find out the existing constraints of which the HRA must work.

Five common types of human interactions may appear in HRA studies. The most usual type involves the human response to a system demand, usually arising as a result of some system failure. This type of human interaction has been the focus of many risk studies, as these events are often where the system most clearly relies on human reliability to reach a safe state. The remaining four types that the HRA analysts may also consider are: (1) maintenance and testing errors; (2) human error-related initiators; (3) response failures; and (4) final recovery actions and mitigating strategies.

The resources available, in terms of funds, expertise, prior studies, and software, will constrain the HRA. Another major constraint, which interacts with the resources, is the project life-cycle stage. The earlier the life-cycle stage, the more difficult the task- and human-error identification phases will be since much of the required detail concerning operator tasks and equipment will not be available.

43.2.2 Task Analysis

Task analysis is a fundamental approach describing and analyzing how the operator interacts with a system itself and with other personnel in that system (Kirwan and Ainsworth, 1992). HRA must first have a definition of how a task should be carried out, and this requires a task analysis. The task analysis defines a model by:

- What should happen during a correct performance,
- Which is then applied to the HRA techniques as a basis for identifying what errors can occur at various steps in the task execution,
- How likely such errors are to occur, and
- Whether or not the task is adequately safe (quantitatively or qualitatively).

The task analysis in HRA mainly consists of two stages: data collection and task representation. Once data have been collected and verified, the task must be formally described and represented, to illustrate what should happen in a correct performance.

43.2.3 Human Error Identification

In Reason (1990), human error can be put into three classes:

- Slips and lapses—for example, pressing the wrong button, or forgetting a step in a long procedure. These are the most predictable errors and are usually characterized by inaccurate performances. The characteristic of this error class is that the intention is correct, but the execution is wrong.
- Mistakes—for example, misunderstanding by the operator of what is happening. The characteristic is that the intention is incorrect, which leads to erroneous actions.
- Violations—these errors involve some types of deviation from rules or procedures and consequently contain a risk-taking element. There are generally three basic types. The first is the routine violation, for example, taking an “illegal” shortcut during a procedure or corner-cutting an operation. The second is the situational violation, which appears as the only way to carry out a task practically under such situations, for example, staff shortages. The third is the extreme violation, for example, someone tries to test how far the system can be pushed in a normal operation, or disable safety interlocks, etc.

It should be noted that a brand of errors, which has yet to be properly classified, is the errors that affect an organization, and that do so at a higher level. These management-related errors, which can have a severe effect on safety levels, are the main reasons for ongoing research.

The following is a list of some well-known approaches for human error identification (Kirwan and Ainsworth, 1992).

Human HAZOP	Human error hazard and operability study (Kletz, 1974)
SRK MODEL	Skill-, rule-, and knowledge-based approaches (Rasmussen et al., 1981)
THERP	Technique for human error rate prediction (Swain and Guttman, 1983)
SHERPA	Systematic human error reduction and prediction approach (Embrey et al., 1986)
GEMS	Generic error modeling system (Reason, 1997, 1990)
HRMS	Human reliability management system (Kirwan, 1990)

However, no single technique addresses the full potential of human error on one system. Instead, there are only tools, which deal with particular types or subsets of potential human error. It is noteworthy that slips and lapses may have been identified adequately by the above-noted HEI techniques, while other areas of human involvement (particularly mistakes and violations, etc.) may not. There is clearly a need for new methods, which attempt to deal with cognitive errors especially, as well as completing validations and tests of these methods.

43.2.4 Representation

Representations should integrate the identified human contributions to the risk along side other relevant contributions (hardware, software, and environmental) in a logical and quantifiable format. Representations allow the overall risk level of the system to be accurately assessed, and enable the HRA analyst to see the relative human contributions seen in Section 43.3.2.

There are two basic issues that need to be considered in representation. The first issue is the format of the representation; usually two formats are applied, that is, the fault tree and the event tree. The second issue is about the level of decomposition in representation, that is, when to stop breaking down human errors into more detailed causes.

43.3 Human Error Analysis

43.3.1 Human Error Quantification

Once the potential human errors have been represented, the next step is to quantify the likelihood of the human errors involved. The human error probability (HEP) is defined as

$$HEP = \frac{\text{Number of errors occurred}}{\text{Number of opportunities for error to occur}}$$

In reality, there are very few recorded HEP data, due to the difficulty in estimating the number of opportunities for error in the realistically complex tasks and the unwillingness to publish data on poor performance.

Human error quantification techniques therefore rely on expert judgment or on a combination of data and psychologically based models, which evaluate the effects of

major influences on human performance. The major techniques in the field of human error quantification are listed below (Kirwan, 1994).

APJ	Absolute probability judgment (Seaver and Stillwell, 1983)
THERP	Technique used for human error rate prediction (Swain and Guttman, 1983)
SLIM—MAUD	Likelihood of success index method using multiattributed utility decomposition (Embrey et al., 1984)
HEART	Human error assessment and reduction technique (Williams, 1986)

Human error dependence is also an important issue when representing human errors and quantifying their frequencies. For example, the response to the first alarm and the response to the second alarm, it is obvious that if the same operator is involved in both actions, then the errors associated with each of these events are unlikely to be independent. Dependence at this level may be dealt with by the use of conditional probabilities.

43.3.2 Impact Assessment

Once the HEPs have been quantified and assigned to the various events in the fault trees, the overall system risk level can be evaluated mathematically, that is, the top-event (accidental) frequencies will be calculated. It is also at this point that the relative contributions of individual human errors, as well as the contribution from human error as a whole, to accident frequencies are determined. This can be done, for example, by the fault-tree—cut-set analysis.

Then, the calculated accident frequencies will be compared against predefined accident criteria. If the frequencies are violating the criteria, the individual events (human, hardware, software, or environmental—or any combination) that make a significant impact on the accident frequencies must be identified. It is these high-impact events that must be targeted for reducing risk. The risk levels must then be recalculated accordingly until the required levels of acceptable risk are achieved, or until the risk levels are as low as reasonably possible (ALARP principle). In practice, this is an iterative process.

43.4 Human Error Reduction

43.4.1 Error Reduction

Human error reduction will be implemented if the impact of human error on the system's risk level is significant, or it may be desirable to improve the system's safety level even if the target risk criteria have been met. There are a number of methods of error reduction (Kirwan, 1994).

- Consequence reduction
- Error pathway blocking
- Error recovery enhancement.

In practice, HRA analysts often give serious consideration to an error—recovery—enhancement process, since this technique is easy to implement, for example, by slight modifications to procedures, or team training. It is also advisable even in cases where risk levels are satisfactory.

43.4.2 Documentation and Quality Assurance

In this final stage of HRA, assumptions made, methods used, and results obtained are to be documented. All of the assumptions made by the HRA team shall be made clear to the project team who will run the system. In addition, the assessment should ideally be seen by the operators as a document whose use will extend over the whole lifetime of the system itself, rather than as a document that is simply put in the archives once its immediate purpose has been served.

The quality assurance (QA) in an HRA includes the assurance that a quality HRA has been carried out (i.e., the objectives have been achieved within the scope of the project and without errors), and the assurance that human-error reduction measures remain effective and the error-reduction potential is realized.

43.5 Ergonomics Applied to Design of Marine Systems

In recent years, attention has been given to ergonomics and noise control in equipment design, as for the workplace, attention has been given to minimizing design-induced human errors and maximizing productivity by reducing human fatigue and discomfort. [ASTM \(1988, 1995\)](#) issued “Standard Practice for Human Engineering Design for Marine Systems, Equipment and Facilities” in 1988 and updated it in 1995. The ASTM standard has been used by the oil and gas industries when designing offshore structures.

[ABS \(1998\)](#) issued “Guidance Notes on the Application of Ergonomics to Marine Systems,” which covers the following topics:

- Alarms, displays, control actuators, and their integration
- Valve mounting heights and orientations
- Labeling for panels, piping/electrical systems, component/hazard identifications
- Stairs, vertical ladders, walkways, and platforms
- Accommodation spaces, ventilation, temperature, humidity, noise, illumination, and noise
- The application of ergonomics in design.

The Guidance Notes suggest four steps for the application of ergonomics in design, including:

- Step 1 is to define what the tasks required for a human to operate the equipment/system being designed are. For instance, is the human required to stand or sit to perform the

operation? Must the human take the visual information being displayed and communicate with others to finish the task?

- Step 2 is to identify who the users for the equipment/system are, and to account for the difference in height and other physical dimensions between sex, race, and origin. Normally the design is made for the 5th percentile to 95th percentile persons.
- Step 3 is to determine the environmental factors, such as temperature and noise.
- Step 4 is to determine the worst case, operating scenario, for example, extreme temperature and noise.

The target of this four step process is to design the right shape, size, arrangement, layout, labeling, color, etc., so that the human operator may safely and effectively conduct the task defined in step 1.

43.6 QA and Quality Control

QA consists of the practices and procedures that are designed to help ensure that an acceptable degree of quality is maintained. Quality control (QC) is associated with the implementation and verification of the QA practices and procedures.

As a general reference on quality, reference is made to [Bergman and Kjefsjo \(1994\)](#). This book discusses the importance of quality for survival in business, and control of quality in the design and production phases, to meet customer expectations. It concludes with discussions on how leadership may influence the process and improve quality continuously.

[Bea et al. \(1997\)](#) gave a comprehensive discussion on QA/QC strategies, and their applications in jacket structures and operating safety for offshore structures and in-service inspections and repairs. They also outline the international safety management (ISM) code, for their proposed safety and quality information systems.

QA/QC procedures include those:

- Put in place before the activity (prevention)
- During the activity (self-checking, checking by team colleagues, and verification by activity supervisors)
- After the activity (inspection)
- After the manufacturing (testing)
- After the marine structure has been put in service (detection).

As will be discussed in the next section, QA/QC procedures are an important part of the process for reducing human errors.

43.7 Human and Organizational Factors in Offshore Structures

43.7.1 General

Bea (2001, 2002) defined an offshore structure system as six major interactive components and identified the associated malfunction:

- Operating teams: people who have direct contact with the design, construction, operation, maintenance, and decommissioning of the system. The single leading factor in operation malfunctions is communication. Other malfunctions include intentional infringements, ignorance, unsuitable or untrained for the activities, excessively fatigued/stressed, or mistakes.
- Organizations: groups that influence how the operating personnel conduct their operations and provide resources for the conduct of these operations. The organizational malfunctions include ineffective communication, inappropriate goals, and incentives, etc.
- Procedures and software: formal and informal, written and unwritten practices that are to be followed in performing operations. Inaccurate and incorrect procedures, software and their documentation may all cause human errors.
- Hardware/equipment: structures and equipment on which and with which the operations are performed. Poorly designed structures and equipment are difficult to construct, operate, and maintain and may lead to human error.
- Environments: wind, temperature, lighting, ventilation, noise, motion, and sociological factors (e.g., values, beliefs, morays) all may have significant effects on the performance characteristics of the operating teams and organization.
- Interfaces: among the foregoing.

The offshore structure system is measured in two types of criteria:

- Quality: which is a combination of serviceability, safety, durability, and compatibility.
- Reliability: the likelihood of obtaining acceptable quality from the design phase to decommissioning.

The quality management system consists of three basic components:

- Quality management procedures: documentation that specifies the requirements and procedures for quality management.
- Assessors: the people from the system (operators, managers, engineers, regulators) and counselors who have extensive experience with the system and operations.
- Evaluation: the quality assessment team assigned grades (normal, best, worst, etc.) for each of the component factors as well as recommendations for improvement.

The quality management system may be implemented to reduce the likelihood and consequence of the malfunctions and increase the detection and correction of

malfunctions. The system risk analysis may be conducted to characterize the human and organizational factors and their effects on the performance of a system using a couple of tools such as

- HazOp (hazard operability) and FMEA (failure mode and effects analysis), etc.
- Probabilistic risk analysis
- Quantitative risk assessment
- Structural reliability assessment.

43.7.2 Reducing Human and Organizational Errors in Design

To ensure the quality in the design of offshore structures, there are three approaches for risk management:

- Proactive: reduce the incidence of malfunctions
- Reactive: increase detection and correction of malfunctions
- Interactive: reduce the occurrence and effects of malfunction.

Several approaches may be applied to reduce human errors:

- Organizational changes: (1) avoiding compromise of the quality and reliability assurance while the management is seeking greater productivity and efficiency. (2) Preventing loss of corporate memory due to corporate downsizing because it has been a cause in many cases of structural failure. (3) Establishing policies that positively improve human performance (e.g., reward people for self-improvement and accomplishments). (4) Developing a safety culture.
- Improving performance of operating teams: (1) Training people to avoid mistakes and incorrect communications that may cause failures. (2) Taking QA/QC measures to prevent errors, detect errors, and correct them. Self-checks, independent checks, and third-party checks may be useful for QA/QC.
- Hardware/equipment change: (1) Providing equipment compatible with fundamental human capabilities (e.g., labels that can be read from a reasonable distance). (2) Eliminating opportunities for human errors (e.g., controls and displays can be simplified to minimize potential confusion and to provide clearer information).
- Procedure improvement and software verification: (1) Ensuring current and accurate procedures are used. (2) Eliminating errors embedded in the procedures and guidelines. (3) Avoiding use of the guidelines out of their validity envelopes. (3) Applying a third-party verification of the software.
- Environmental change: Providing an environment (comfortable temperature, adequate lighting, and limited noise) compatible with the physical requirements of the human conducting the operation.

References

- ABS, January 1998. Guidance Notes on the Application of Ergonomics to Marine Systems. American Bureau of Shipping.
- ASTM, 1988, 1995. ASTM F1166–95a: Standard Practice for Human Engineering Design for Marine Systems, Equipment and Facilities. American Society of Testing and Materials.
- Bea, R.G., 1994. The Role of Human Error in Design, Construction and Reliability of Marine Structures. Ship Structures Committee, SSC-378.
- Bea, R.G., 1995. Quality, Reliability, Human and Organization Factors in Design of Marine Structures. OMAE.
- Bea, R.G., et al., 1997. Quality Assurance for Marine Structures”, Report of Specialist Panel V.1. The International Congress of Ship and Offshore Structures.
- Bea, R.G., 2001. Human factors and risk management of offshore structures. In: Proceedings of the International PEP-IMP Symposium on Risk and Reliability Assessment for Offshore Structures”, Mexico City, December 3–4, 2001.
- Bea, R.G., 2002. Human & Organizational Factors in Design and Operation of Deepwater Structures. OTC, 14293.
- Bergman, B., Klefsjo, V., 1994. Quality – from Customer Needs to Customer Satisfaction. Studentlitteratur, ISBN 91-44-46331-6.
- Embrey, D.E., Carroll, J.E., et al., 1986. The INPO Human Performance Evaluation System: A review and proposals for further development. Proceedings of a conference organized by INPO and EOF, Lyons, France.
- Embrey, D.E., Humphreys, P., et al., 1984. SLIM-MAUD: An approach to assessing human error probabilities using structured expert judgment. NUREG/CR-3518. Prepared for the US NRC.
- IACS, 1999. Draft Guidance on Human Reliability Analysis (HRA) Within the Formal Safety Assessment. IMO MSC, 71/Wp.15/Add.1.
- IMO, 1997. MSC/Circ. 829 & MEPC/Circ. 335, Interim Guidelines on the Application of Formal Safety Assessment (FSA) to the IMO Rule-Making Process. International Maritime Organization.
- Kirwan, B., Ainsworth, L.K., 1992. A Guide to Task Analysis. Taylor & Francis, UK.
- Kirwan, B., 1990. A resources flexible approach to human reliability assessment for PRA. Safety and Reliability Symposium 1990. Elsevier Applied Sciences 114–135.
- Kirwan, B., 1994. A Guide to Practical Human Reliability Assessment. Taylor & Francis, UK.
- Kletz, T., 1974. HAZOP and HAZAN – Notes on the Identification and Assessment of Hazards. Institute of Chemical Engineers.
- Lorenzo, D.K., 1990. A Manager’s Guide to Reducing Human Errors – Improving Human Performance in the Chemical Industry. Chemical Manufacturers Association.
- Moore, W.H., January 1994. The grounding of Exxon Valdez: an examination of the human and organizational factors. Marine Technology 31 (1), 41–51.
- Rasmussen, J., Pedersen, O.M., Carnino, A., Griffon, M., Mancini, C., Gagnolet, P., 1981. Classification System for Reporting Events Involving Human Malfunctions. Riso National Laboratories, Denmark. Report Riso-M-2240, DK-4000.
- Reason, J., 1990. Human Error. Cambridge University Press, UK.
- Reason, J., 1997. Managing the Risks of Organizational Accidents. Ashgate, UK.
- Seaver, D.A., Stillwell, W.G., 1983. Procedures for using expert judgement to estimate human error probabilities in nuclear power plant operations. NUREG/CR-2743, Washington, DC 20555.
- Swain, A.D., 1989. Comparative Evaluation of Methods for Human Reliability Analysis, ISBN 3-923875-21-5. GRS-71.
- Swain, A.D., Guttman, H.E., 1983. A Handbook of Human Reliability Analysis with Emphasis on Nuclear Power Plant Applications. US Nuclear Regulatory Commission (USNRC), Washington DC-20555. Nureg/CR-1278, with Addendum #1 to Nureg/CR-1278 in Sept. 1985 by Swain, A.D.
- Williams, J.C., 1986. A proposed method for assessing and reducing human error. Proceedings of the 9th Advance in Reliability Technology Symposium, University of Bradford pp. B3/R/1–B3/R/13.

Risk-Centered Maintenance

44.1 Introduction

44.1.1 General

Offshore maintenance covers engineering tasks for various offshore facilities and equipment, from the seabed to the topside. The tasks include routine maintenance, inspection and repair of these facilities, and modifications/enhancements to both the plant and the equipment.

The maintenance of offshore facilities presents many unique difficulties, which are not usually encountered during inland applications. This is mainly due to factors such as:

- Statutory requirements for safety are very restrictive.
- Improper maintenance often results in substantial losses in terms of safety, environmental protection, production, material damage, and reputation.
- Maintenance costs are relatively high due to the high costs of manpower, offshore storage, transportation between onshore and offshore, etc.
- It is more difficult to perform a maintenance task in the splash zone and in the subsea.
- Maintenance activities are often restricted by seasons (e.g., adverse weather conditions).
- Offshore logistics can be a big issue during an actual maintenance task in order for the task to be resolved and then carried out.

Therefore, operators for offshore installations usually establish proper maintenance programs to ensure that the production programs are met in terms of safety, reliability, availability, quality, and quantity of the supplies.

Scheduled (proactive) maintenance includes two major classifications:

- *Preventive maintenance*: Maintenance task frequencies are determined from a known relationship between time (number of cycles, usage, age, etc.) and reliability (survival probability with respect to wear-out, corrosion, fatigue, etc.).
- *Predictive maintenance*: Condition-based maintenance tasks are scheduled based on the achievement of certain routinely measured conditions. The P-F interval is defined as the distance from the point where potential failure is found, to the point where failure actually occurs (Moubray, 1992). Condition-based maintenance tasks must be conducted at intervals that are less than the P-F interval.

This chapter describes the application of risk analysis to the maintenance of facilities on offshore installations. It mainly consists of preliminary risk analysis (PRA) and reliability-centered maintenance (RCM). The basic concept, principles, and applications of PRA and RCM are introduced for the development of an effective preventive maintenance (PM) program for offshore facilities. PRA and RCM are methods that have been used for the development and optimization of maintenance strategies in a structured and systematic way. They have been widely used in the past years in many different industries such as in nuclear power plants, aircraft, and in the offshore industry.

44.1.2 Application

This chapter is considered to be a guide for the development and optimization of maintenance strategies. The roles of PRA and RCM in the maintenance process are illustrated in [Figure 44.1 \(Rausand and Vatn, 1997\)](#). As shown in the figure, PRA analyses shall be performed for screening and rating maintainable items.

The RCM analysis is then carried out on items where PM is recommended. This means that the RCM process should focus on maintenance significant items (MSIs), while the remaining items can be assigned with maintenance tasks, by means of more traditional methods. However, all planned maintenance tasks will ultimately be integrated in a common maintenance planning and control system.

44.1.3 RCM History

RCM was first formulated for the commercial aircraft industry in the late 1960s ([Jones, 1995](#); [Rausand and Vatn, 1997](#)). It started as a result of using the reliability methods of two US airlines to analyze the data they collected. For instance, they plotted the probability of failure of components against age. To their surprise, it was found that only about 10% of the whole range of units became less reliable with advancing age. This was not because the intervals were not short enough, or inspections were not sufficiently thorough, rather, it was contrary to expectations; for many items, the frequency of failures did not increase with operating age. Consequently, a maintenance policy based exclusively on some maximum operating age would have little or no effect on the failure rate, no matter what the age limit was. This forced them to rethink the basis for PM, which at that time consisted of time-based overhauls with a considerable cost.

The Federal Aviation Agency (FAA), which is responsible for regulating airline activities in the USA, was frustrated because it was not possible for airlines to control the failure rates of certain engines by any feasible changes in the PM policy. As a result, in 1960, a task force was formed, consisting of representatives from both the FAA and the airlines, to investigate the capabilities of PM.

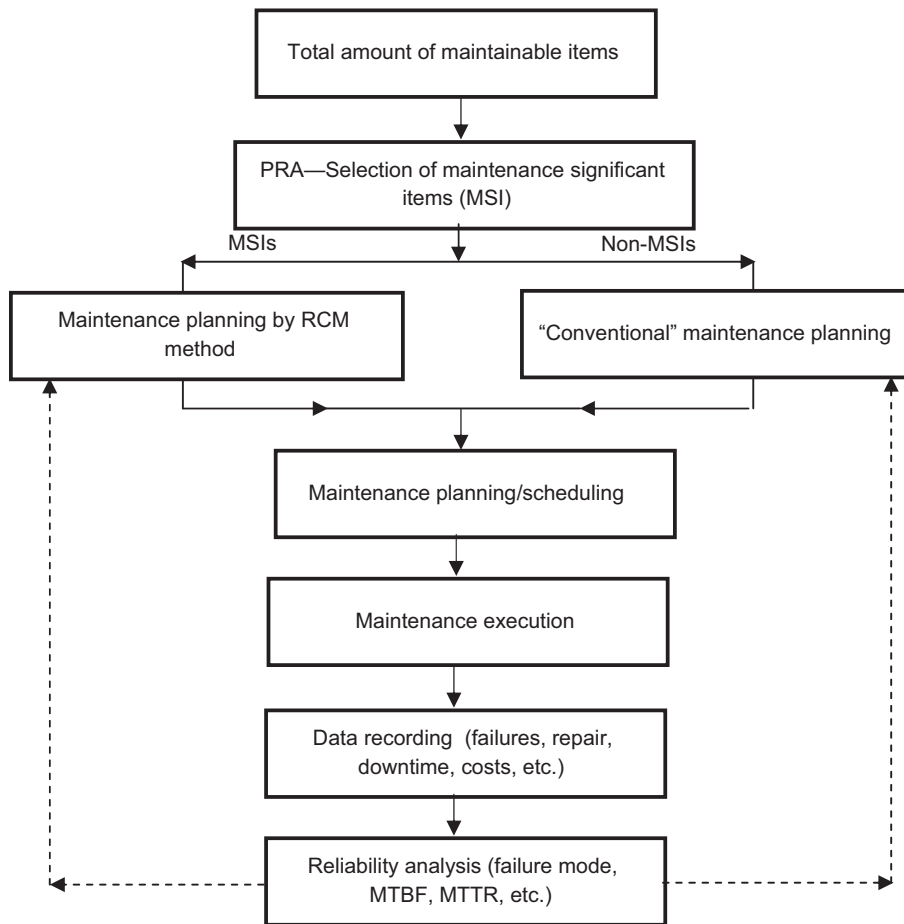


Figure 44.1

The roles of PRA and RCM in maintenance processes.

The task resulted in the FAA/Industry Reliability Program, which was issued in November 1961. The program was directed specifically at propulsion engine reliability. Further work during the 1960s, for the development of PM programs for new aircrafts, showed that more efficient programs could be developed through the use of a logical decision processes. This work was performed by a Maintenance Steering Group ([MSG-1, 1968](#)), which consisted of representatives from the aircraft manufacturers, airline companies, and the FAA.

This group developed the first version of the RCM, and it was issued as a handbook in 1968. This new maintenance philosophy was designated MSG-1, and was used as a basis for the development of the PM program for the Boeing 747 (jumbo jet). In due time, the RCM concept was further developed for use by the aircraft industry. Two revisions were made, an MSG-2 document issued in 1970 and an MSG-3 in 1980.

After the initial use of the wide-bodied aircraft (Boeing 747, DC 10, L1011 Tristar), the method was adapted and used by the European aircraft industry (Concorde, Airbus A300) and the latest type of aircraft from the USA (e.g., Boeing 757, 767).

In the early 1970s, the US Navy started to apply the RCM methodology to both new and in-service aircrafts. Shortly thereafter, the Naval Systems Command applied the RCM to surface ships, and in 1980, the RCM became the required method for defining PM programs for all new naval surface ships. The Canadian Navy then followed the same steps. The US Army and the Air Force also adopted the RCM approach.

In 1983, a pilot study, done by the Electric Power Research Institute (EPRI), was initiated to test the reliability of this method for nuclear power plants. They evaluated whether a maintenance method, which has been successfully applied in aircrafts and ships, may also be suitable for nuclear power plants. From a system point of view, all are highly redundant, complex, and have high reliability. They are all regulated by governmental agencies (the airlines are monitored by the FAA, the military has Congress, and the nuclear power plants are controlled by the Nuclear Regulatory Commission). EPRI (1985) documented that RCM applications for nuclear power plants are promising. Several labor and material intensive maintenance tasks that were performed at specified time intervals before applying the RCM were now performed, but only when the equipment had degraded to certain measurable conditions. Savings were achieved through reduced maintenance costs and enhanced reliability.

RCM applications to the maritime industry, solar receiving plants, and coal mining are discussed in Jones (1995).

44.2 Preliminary Risk Analysis

44.2.1 Purpose

The purpose of a PRA process can be summarized as follows:

- Screen operating units within a plant that are used to identify areas of higher risk.
- Assign a risk level to each equipment item based on a consistent methodology.

44.2.2 PRA Procedure

The application of PRA in offshore installations is a qualitative approach. It uses the same concepts, for the consequence and frequency, as the quantitative analysis described in the previous chapters, except that it requires less detail and can be conducted fairly quickly. While the results are not as precise as those of the quantitative analysis, it provides a basis for rationalizing maintenance efforts based on potential risks associated with each item.

Table 44.1: Classification of failure consequences

Consequence Categories	Consequences to Health, Safety, or Environment
I—Catastrophic	May cause deaths, or severe impact on the environment
II—Critical	May cause severe injury, severe occupational illness, or major impact on the environment
III—Marginal	May cause minor injury, minor occupational illness, or minor impact on the environment
IV—Negligible	Will not result in a significant injury, occupational illness, or provide a significant impact on the environment

Table 44.2: Classification of failure probabilities

Frequency Categories	Nominal Range of Frequency per Year
A—Often	$>10^{-1}$
B—Likely	$10^{-1}-10^{-2}$
C—Unlikely	$10^{-2}-10^{-3}$
D—Incredible	$<10^{-4}$

The analysis first categorizes the failure consequences within the area, and then the failure frequency. Tables 44.1 and 44.2 illustrate examples of relevant definitions.

After the categories for the consequences and frequencies have been defined, they are combined in a risk matrix to produce a risk rating, as shown in Figure 44.2.

The probability category is determined by evaluating factors that may affect the occurrence of failures. Each factor can be weighed and their combination will result in the probability. The factors that may affect probability are:

- Potential damage mechanisms
- Current equipment conditions
- Nature of the process
- Equipment design basis
- Appropriateness of basic services like lube, cleaning, and inspection.

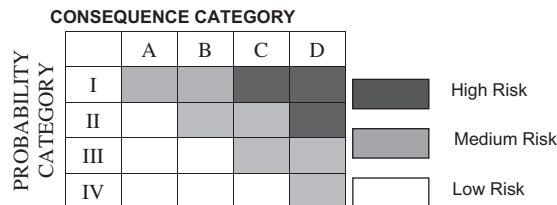


Figure 44.2
Qualitative risk matrix.

The consequence category may be determined by considering the factors that may influence the magnitude of a hazard, such as:

- Inherent tendency that a failure may occur
- Operating conditions
- Possibility of escalation from minor to serious conditions
- Engineered safeguards in place
- Degree of exposure to damage

When the resulted categories of failure consequence and frequency are plotted on the risk matrix, they give an indication of the level of risk for the unit being evaluated.

The PRA process will result in assigning each unit with a risk rating: high, medium, or low. The risk rating is often called criticality. The relevant PRA process is also called criticality analysis. The resulting risk rating may be used to group maintenance items into three categories:

- Items with a risk rating of high or medium: The items with medium risk ratings shall be further analyzed by the RCM process, in order to reduce the risk as low as reasonably practicable, which shall be detailed in the following sections.
- Items with a low risk rating: These items fall in the acceptable risk region. They may therefore be maintained using traditional maintenance methods or even “breakdown” maintenance strategies.
- Items with a high risk rating belong to the unacceptable risk region: These items shall be subject to further detailed analysis regarding design, engineering, risk, and/or maintenance. The possible decisions include change of design/engineering, adding protection measures and redundancy, and development of various PM measures such as condition monitoring, inspection, etc.

44.3 RCM Process

44.3.1 Introduction

According to the EPRI, RCM is:

“A systematic consideration of system functions, how functions can fail, and a priority-based consideration of safety and economics that identifies applicable and effective PM tasks.”

RCM is defined as a process for determining what must be done to ensure that any equipment/facility continues to do whatever its users expect it to do.

Therefore, the main focus of the RCM is the system functions, and not on the system hardware.

44.3.2 RCM Analysis Procedures

Before the actual RCM analysis is initiated, an RCM project team shall be established. The team shall include at least one person from the maintenance function and one from the operation function, in addition to an RCM specialist who serves as the facilitator for the RCM process.

The RCM team shall define the objectives and the scope of work. Requirements, policies, and acceptance criteria shall be clarified with respect to health, safety, and the environment (NPD, 1991). The RCM analysis typically focuses on improving the PM strategy. It is, however, possible to extend the analysis to cover topics like corrective maintenance strategy, spare parts, etc. The RCM team will need to clearly define the scope of the analysis. An RCM analysis process may be carried out as a sequence of activities. The six steps are described below (Rausand and Vatn, 1997; Jones, 1995):

Step 1: System Selection and Definition

The first question in the RCM analysis is “Which systems shall be analyzed by the RCM process?” This question is normally answered before the RCM analysis project is approved because clear reasons are needed to justify the initiation of the RCM analysis. The reasons can be, for example, some systems have failed too often and/or have resulted in serious consequences in terms of safety, environmental protection, and production.

The system is divided into subsystems that do not overlap each other. The level of technical hierarchy may be defined as:

- Plant: A logical grouping of systems that function together to provide an output by processing various inputs of raw materials and feedstock, for example, an offshore oil and gas production platform may be considered a plant.
- System: A logical grouping of subsystems/main equipment that will perform a series of main functions, which are required by the plant. Examples of the systems are water injection and gas compression systems on an oil and gas production platform.
- Subsystem/main equipment: A logical grouping of equipment/units that mainly perform one function, for example, one water injection package and one gas compressor.
- Equipment/instrument: A grouping or collection of components that can perform at least one significant function as stand-alone items, for example, pumps, valves, and pressure indicators.
- Component: The lowest level at which equipment can be disassembled without damage or destruction to the items involved, for example, an impeller in a pump, or a bearing in a gas compressor.

It is very important that the RCM team decides on which level the analysis shall be carried out in the initial phase of the RCM process. There are some constraints for this

issue, for example, the project's time schedule, the availability of information regarding failures, the maintenance efforts and costs, available experience, and know-hows on the systems involved. In an ideal situation, RCM analysis should be performed from the system level down to the component level. The analysis of functions and functional failures should be applied to all the levels above the component level. The failure modes and reasons should be applied to the component level.

Step 2: Functional Failure Analysis

Functional failures are the different ways a subsystem can fail to perform its functions. The tasks of functional failure analysis are:

- To identify and describe the required functions for systems, subsystems, and equipment
- To describe input interfaces required for the system to operate
- To identify the ways in which the system might fail to function

A system may have different functions that can be categorized in different ways, for example:

- Based on importance:
 - Main (essential) functions: These are the functions required to fulfill the main design service. An essential function is often reflected in the name of the item. An essential function of a pump is, for example, to pump fluid.
 - Auxiliary functions: These are the functions that are required to support the essential functions. They are usually less obvious than the essential functions but may, in certain cases, be as important as the essential functions. An auxiliary function of a pump is to contain the fluid.
- Based on functionality:
 - Protective functions: Which, for example, provide protection for safety and the environment.
 - Information functions: Which comprise condition monitoring, various gauges, alarms, etc.
 - Interface functions: Which apply to the interfaces between the item in question and other items.

Note that the classification of these functions should only be used as a checklist to ensure that all relevant functions are revealed. A system may generally have several operational modes, and several functions for each operating mode. The essential functions are often obvious and easy to establish, while other functions may be rather difficult to reveal.

The identified system functions may then be represented by functional diagrams of various types. The most common diagram is the so-called functional block diagram. A simple functional block diagram of a pump is shown in [Figure 44.3](#).

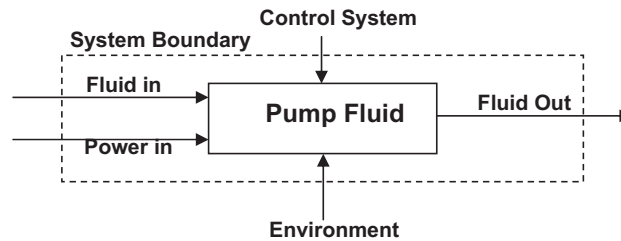


Figure 44.3
Functional block diagram for a pump.

As shown in [Figure 44.3](#), a functional diagram includes all inputs (control signals and power supplies) and outputs. It is generally not required to establish functional block diagrams for all system functions. The diagrams are often considered as efficient tools to illustrate the input/output interfaces of a system boundary.

The last task of the functional failure analysis is to identify and describe how the system functions may fail. In most of the RCM references, functional failures may be classified in three groups:

- Total loss of function: In this case, a function is not achieved at all, or the quality of the function is too far beyond what is considered acceptable.
- Partial loss of function: This group may be very broad, and may range from the nuisance category to almost a total loss of function.
- Erroneous function: This means that the item performs an action that was not intended; often it performs the opposite of the intended function.

Step 3: Failure Modes and Effects Analysis (FMEA)

The dominant failure modes are developed from failure modes and effect analysis. The FMEA identified specific conditions that need to be prevented by preemptive maintenance. After having defined system functions and functional failures, the next logical step is to identify failure modes, which may cause each identified functional failure. For example, a functional failure analysis identified that a booster pump was designed to increase water from 5 bar at the inlet to 25 bar at the outlet. Sometimes it is unable to deliver water to 25 bar. Therefore, it has a functional failure—partial loss of function. In the FMECA step, the tasks are to find out what may cause this functional failure, and what maintenance methods may be cost-effective enough to prevent failure.

A variety of FMECA forms are used in the RCM analysis. An example of the FMECA forms is shown in [Figure 44.4](#). The various columns in the form are discussed below:

MSI: the item number (tag number).

Operational mode: for example, running or standby.

System: _____ Performed by: _____
 Ref. Drawing No: _____ Date: _____

Description of unit		Failure Mode	Failure Effects								Criticality	Failure Cause	Failure Mechanism	Failure Characteristic	Maintenance Methods	Recommended Interval	
MSI	Operation Mode		Function	Failure Severity				Failure Likelihood									
				S	E	P	C	S	E	P							C

Figure 44.4
 Example of an FMECA form.

Function: for example, a function of a standby water supply pump is to start pumping water upon demand.

Failure mode: the manner by which a failure is observed and is defined as nonfulfillment for one of the equipment functions.

Failure severity: described in terms of the “worst case” impacts on safety, environmental protection, production loss/delay, and other economic costs. The severity classes may be defined using an approach that is similar to the consequence categories for qualitative risk analysis.

Failure likelihood: defined as the “worst case” probability of failure. In this stage, qualitative classes are appropriate. The relevant likelihood classes can be defined using a procedure that is similar to the probability categories for qualitative risk analysis.

Criticality: can be derived by combining the relevant failure severity and likelihood. The procedure is similar to that of determining risk levels of systems, subsystems, and equipment. However, the difference is that criticality considers failure modes.

The information described so far should be considered for all failure modes. A screening process is now appropriate, giving only critical failure modes.

For the critical failure modes the following fields are required:

Failure cause: For each failure mode there may be more than one failure cause. Note that all components should be considered at this step. A “fail to close” failure of a safety valve may, for example, be caused by a broken spring in the actuator.

Failure mechanism: Examples of failure mechanisms are fatigue, corrosion, and wear.

Failure characteristic: Failure propagation may be categorized as:

- Gradual failure: The progress of failure propagation can be measured by inspection or condition monitoring techniques.
- Aging failure: The failure propagation is age dependent, that is, a wear-out process.
- Sudden failure: Random failure that may not be detected by condition monitoring measures.

Maintenance method: May hopefully be found by the logic decision applied in Step 5. This field shall be completed in Step 5.

Recommended task interval: The identified maintenance action should recommend an estimated time interval, which shall be performed in Step 5.

Step 4: Selection of Maintenance Methods

Decision logic is designed and used to guide the RCM team through a question-and-answer process. The input to the decision logic is the dominant failure mode identified in Step 1. The design of decision logic is based on the principle that PM measures should be specified whenever they exist and are cost-effective against a critical failure.

There are generally three reasons for applying a PM task:

- To detect failures at an early stage, in order to have more time to plan and execute PMs
- To prevent equipment failures that have serious consequences
- To discover hidden failures

Only the critical failure modes shall be subjected to PM. The selection of appropriate maintenance methods is dependent on the following factors:

- Failure causes and mechanisms
- Failure characteristics
- Detection techniques

The basic maintenance methods may be classified by the following:

- Scheduled on-condition task
- Scheduled overhaul
- Scheduled replacement
- Scheduled function test
- Run to failure

Scheduled on-condition task is the scheduled inspection or condition monitoring of an item at regular intervals in order to find potential failures and can be applied when the following conditions are met:

- Potential failure condition can be clearly defined

- Potential failures can be detected by a condition monitoring technique
- There is a reasonable consistent time interval for failure detection and prevention

Scheduled overhaul can be applied to an item at or before a certain specified age limit. An overhaul task may be applicable to an item when the following criteria are met:

- There is an identifiable age after which the item's failure rate increases rapidly
- Failure resistance of the item can be restored by overhaul

Scheduled replacement is a scheduled elimination of an item or its parts at or before a certain age limit. A schedule replacement program can be applied under the following circumstances:

- There exists an identifiable age after which the item's failure rate increases rapidly
- Failure resistance of the item can be restored by replacing the item or its parts

Scheduled function test (SFT) is a scheduled inspection of a hidden failure, which is normally an on-demand failure. An SFT may be performed on an item under the following conditions:

- A functional failure is not evident to the operating crew during normal duty
- No other type of preventive tasks is as cost-effective

Run to failure is a deliberate decision allowing an item to run to failure. The main reason for the run to failure may be that no other preventive tasks are possible or as cost-effective.

The criteria given to use the preceding tasks serve only as guidelines for selecting a suitable preventive task. An example of the RCM decision logic is illustrated in [Figure 44.5](#). Note that this is a simplified version of the decision logic. Such decision logic cannot cover all situations. For example, a hidden function with aging failures may be prevented by a combination of scheduled replacements and function tests.

Step 5: Determination of Maintenance Task Intervals

After selecting the PM methods for each critical failure mode, the next step is to determine the time interval for each selected maintenance task.

The shorter the activity interval, the higher the maintenance cost. On the other hand, the longer the activity interval the higher risk of failure to occur. The optimal interval should mathematically be set at the minimum of the sum of the failure risks and maintenance costs. This is typically the task of a benefit–cost analysis.

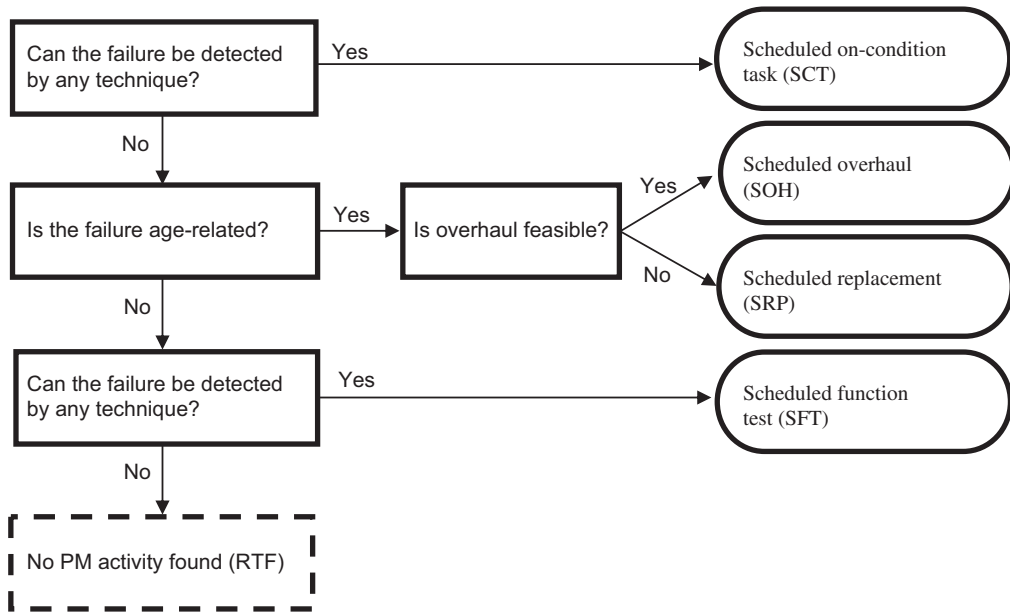


Figure 44.5
RCM decision logic.

The maintenance cost is more or less easy to estimate. Unfortunately, the benefit of a maintenance task is difficult to assess, as it depends on the following parameters:

- Risk: Failure consequence and likelihood, possibly causing an impact on:
 - Safety
 - Environment
 - Production and/or services
 - Material damage
 - Reputation
- Risk reduction by the maintenance task, which depends on:
 - Failure causes
 - Failure mechanism and distribution
 - Characteristics of the maintenance task such as SCT (Scheduled on-condition task), SOH (Scheduled overhaul), SRP (Scheduled replacement), or SFT (Scheduled function test)

The optimization of maintenance task intervals usually requires a quantitative analysis. The detailed description of the optimization process is not within the scope of this book.

Step 6: Implementation of Maintenance Tasks

Implementation is not a direct task of RCM analysis. However, in most cases, the results of the RCM analysis shall be implemented. A necessary basis for the implementation is

that the organizational and technical functions fully understand and support the results of the RCM analysis.

The maintenance actions recommended by RCM analysis are usually failure oriented. In practice, maintenance work orders are normally issued on equipment packages or modules. Therefore, the maintenance actions resulting from the RCM analysis should be grouped into maintenance program packages with a description of where, when, and what to do.

The necessary resources and skills are then allocated to implement the maintenance tasks.

A more comprehensive discussion of RCM may be found in [Moubray \(1992\)](#), including the RCM decision diagram, implementing RCM recommendations, applying the RCM process, and measuring RCM achievements. The implementation process includes:

- All the RCM recommended maintenance tasks are approved by the managers with the overall responsibility for the equipment/facility.
- All routine task descriptions are upgraded in detailed task instructions clearly and concisely.
- Routine task descriptions are incorporated into work packages.
- The work packages are implemented in systems that ensure the work is done.

44.3.3 Risk-Centered Maintenance (Risk-CM)

RCM began in the US commercial aviation industry to maintain highly redundant aircraft. Criticality class in an RCM is categorized with respect to safety, operation/production, economics, and hidden failure. The difference between Risk-CM and RCM is that the criticality class in the RCM is replaced with a direct evaluation of risks in Risk-CM ([Jones, 1995](#)). The direct risk evaluation gives a more complete description of the hazards than the coarser assessment (criticality class). This Risk-CM involves independent estimation of the frequency and consequence for each failure mode, providing the ranking mechanism, based on the risk concept. When risks are calculated for individual failure modes, it is possible to rank the priority for maintenance tasks, based on the risks. Qualitative risk assessment may be fairly adequate for Risk-CM, as comparative risks are sufficient for priority ranking. It is not required to estimate absolute risks accurately, but consistency between the risk evaluations is rather important. There are, however, two difficulties in applying the Risk-CM: (1) the risk concept is still not fully accepted by the industry in some areas and (2) there is indeed a lack of data for the adequate evaluation of risks, in particular for some new applications on which little industry experience exists.

Operational Risk Assessment

Operational risk assessment is performed in process critical equipment and facilities. Its objective is to focus the maintenance resources (money and labor) on the plants that have the highest risk. Operational risk assessments start with data gathering

and evaluations. The data used for an operation risk assessment is usually collected during the equipment/facility operations. There are three major contributors to the operational risk, namely:

- *Equipment*: There is no doubt that the equipment is a major contributor to the operational risk. Equipment is operated by humans, in order to produce products. Maintenance activities are performed on all equipment.
- *Production*: Loss production (including scheduled maintenance and turnaround) and product quality below standards are an operational risk. Production loss may be due to equipment failure, lack of raw material supplies, shortage in packaging, or shipping and storage.
- *Human*: Humans are the key contributors to operational risk. People often cause system failure and make up costs when equipment fails, and production is reduced, for example, in terms of labor costs.

Human Contribution to Risk

People are an integral part of plant operation and maintenance, and take on the main responsibilities. There are two types of human errors (Jones, 1995):

- *Active errors*: Results in instantly observable effects.
- *Latent errors*: Have consequences that are not realized for a relatively long period of time until they combine with other factors that result in accidents.

Machine operation used to have more hands-on activities. As computers have led to the promotion of people to a higher level, the information people receive is now on computer displays in the control room. Latent failures are generally major players in these situations.

Fatigue and other human factors, such as drinking and driving, make a great contribution to risks. Fatigue-induced risks become larger when control responsibilities are concentrated on a few people.

44.3.4 RCM Process—Continuous Improvement of Maintenance Strategy

It can be seen from the preceding section that the RCM process is a systematic process used to make decisions about the maintenance strategy. It is a powerful tool for developing the initial maintenance strategy by rationalizing maintenance efforts. It should also be used for continuous improvement of the existing maintenance strategy. In fact, the full benefit of the RCM is achieved when the operation and maintenance experience is fed back into the analysis process.

The process of updating the RCM analysis results is important due to the following facts:

- An RCM analysis is usually based on many assumptions due to lack of reliable data.
- The operation conditions and equipment status are changing over time.
- Real reliability data, knowledge, and know-how are growing with time.

The maintenance strategy should be updated continuously using RCM processes. The continuous improvement may follow the steps presented below:

- Assign criticality to equipment, components, and failures based on historical data, for example, failure consequences, maintenance costs, etc.
- Compare the updated criticality with that developed from the early RCM study and update or replace the assumptions with the historical reliability data
- Perform cost–benefit analyses to identify where the modification of the existing maintenance strategy may increase in reliability and reduce in cost
- Modify the existing maintenance strategy to increase the cost-effectiveness of the maintenance strategy.

44.4 RCM Application to a Shell and Tube Heat Exchanger on Floating Production, Storage, and Offloading

44.4.1 Introduction of Shell and Tube Heat Exchangers

A shell and tube heat exchanger is a class of heat exchanger design. It is the most common type of heat exchanger in oil and gas processing on Floating Production, Storage, and Offloading (FPSO), and is suited for higher-pressure applications. As its name implies, this type of heat exchanger consists of a shell (a large pressure vessel) with a bundle of tubes inside it. One fluid runs through the tubes and another fluid flows over the tubes (through the shell) to transfer heat between the two fluids. The set of tubes is called a tube bundle, and may be composed of several types of tubes: plain, longitudinally finned, etc.

Figure 44.6 shows a typical shell and tube heat exchanger, and Figure 44.7 shows the schematic diagram of a shell and tube heat exchanger.

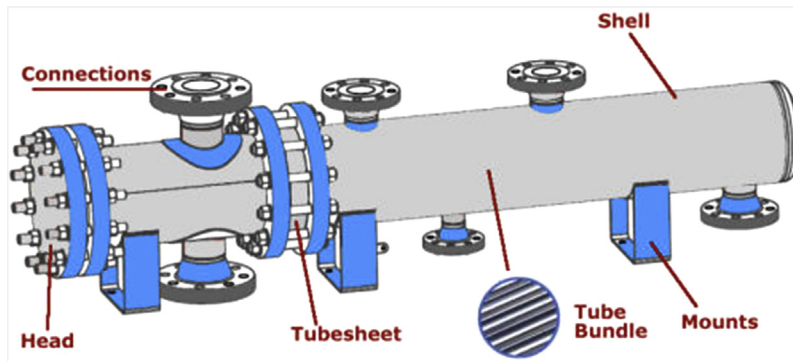


Figure 44.6

A typical shell and tube heat exchanger.

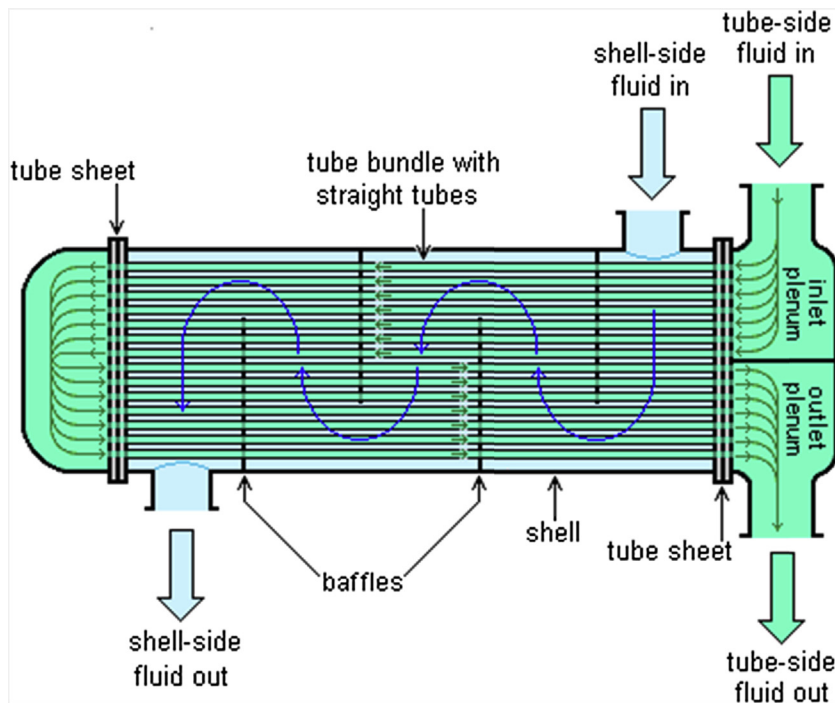


Figure 44.7
Schematic diagram of a shell and tube heat exchanger.

44.4.2 RCM Process

Heat Exchangers Inventory Description

The boundary definition is shown in [Figure 44.8](#) and corresponding subdivision in maintainable items in [Table 44.3](#).

Inlet, outlet, pressure relief, and drain valves are specifically excluded. The only valves are calibration valves and instrument valves that form a pressure boundary (e.g., block valves, control valves, calibration valves, local indicators/gauges).

Risk Criteria

[Tables 44.4–44.9](#) are the selected risk criteria for the heat exchanger.

Risk Analysis

FEMCA Analysis

OREDA is the most used databank for offshore installations. The data include failure modes, failure descriptors, failed subunits and maintainable items and detection methods. The failure typical modes of a heat exchanger are listed as the following:

- AIR Abnormal reading
- ELP External leakage—process medium

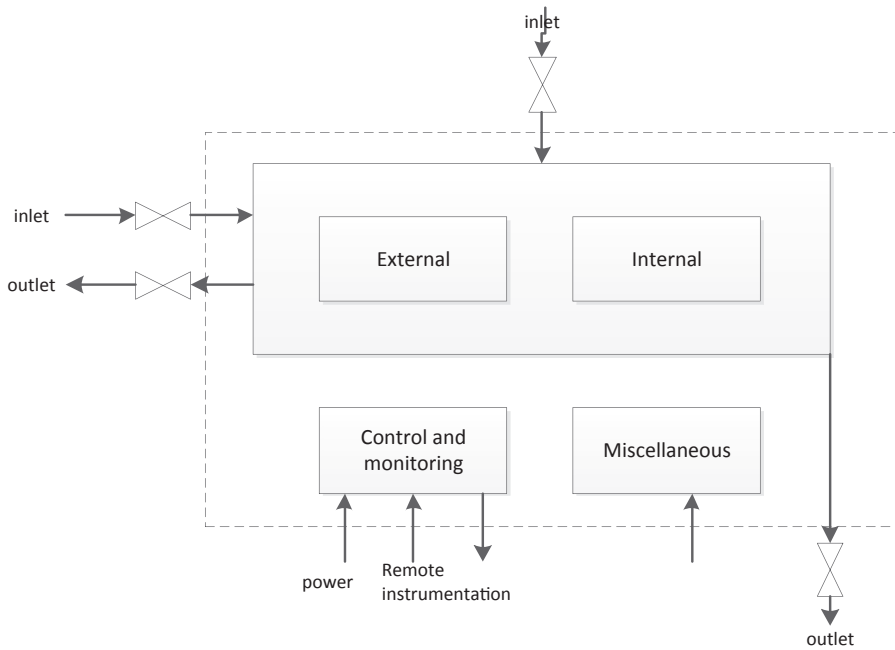


Figure 44.8
Boundary definition of heat exchangers.

Table 44.3: Heat exchanger subdivisions in maintainable items

Heat Exchangers			
External	Internal	Control and Monitoring	Miscellaneous
Support	Body/shell	Actuating device	Fan w/motor
Body/shell	Instruments	Cabling and junction boxes	
Valves and piping	Plates	Control unit	
Instruments	Seals (gaskets)	Instruments	
	Tubes	Monitoring	
		Internal power supply	
		Valves	

- ELU External leakage—utility medium
- IHT Insufficient heat transfer
- INL Internal leakage
- SER Minor in-service problems
- OTH Other
- PDE Parameter deviation
- PLU Plugged/choked
- STD Structural deficiency
- UNK Unknown

Table 44.4: Consequence level of the safety risk

Consequence Level	Definition
A—Insignificant	Will not result in a significant injury, occupational illness
B—Minor injury	May cause minor injury, minor occupational illness
C—Major injury	May cause severe injury, severe occupational illness
D—Single fatality	May cause one death
E—Multiple fatalities	May cause more than one death

Table 44.5: Consequence level of the environment risk

Consequence Level	Definition
A—Insignificant	The accident influence will be in the system, but can't cause economic consequence
B—Minor	The accident influence will be out of the equipment, but in the system, and can cause only slight economic consequence
C—Local	The accident influence will be out of the system, but can be settled down by the enterprise
D—Major	The accident can be settled down with the help of local governments
E—Significant	The accident must be dealt with through the cooperation of central governments, local governments, and international organizations

Table 44.6: Consequence level of the operation risk

Consequence Level	Definition
A—Insignificant	$\leq 3,000,000$ RMB (2 h)
B—Minor	3,000,000—6,000,000 RMB (2—4 h)
C—Local	6,000,000—12,000,000 RMB (4—8 h)
D—Major	12,000,000—35,000,000 RMB (8—24 h)
E—Significant	$\geq 35,000,000$ RMB (>24 h)

Table 44.7: Consequence level of the subsequent cost risk

Consequence Level	Definition
A—Insignificant	$\leq 10,000$ RMB
B—Minor	10—100K RMB
C—Local	100—500K RMB
D—Major	500—1000K RMB
E—Significant	$\geq 1000K$ RMB

Table 44.8: Probability level of the failure mode

Probability of Failure Level	Failure Mode Probability
5—Common occurrence	>0.8
4—Sometimes occurrence	0.1 ~ 0.8
3—Chance	0.02 ~ 0.1
2—Infrequency	0.002 ~ 0.02
1—Rare	<0.002

Table 44.9: Risk matrix

Probability of Failure		Consequences of Failure				
5	>0.8	Medium	Medium	Medium	High	High
4	0.8–0.1	Low	Medium	Medium	Medium	High
3	0.1–0.02	Low	Low	Medium	Medium	Medium
2	0.02–0.002	Low	Low	Low	Medium	Medium
1	<0.002	Low	Low	Low	Low	Medium
		A	B	C	D	E

In this chapter, one failure mode (ELP) of the external subunit of the heat exchanger was implemented to introduce the method. The process of the FEMCA is as follows:

Function

Transport the process medium and isolate it with the environment.

Functional Failure

Functional failure: External leakage—process medium

Failure probability: B

Severity class: A

Risk: medium

Failure Effect

Failure effect: Fire or explosion and then leading to casualties and interruption of the production.

FEC (failure effect and cause): The logic tree analysis is as [Figure 44.9](#) and the analysis result is 1: evident safety and environmental effect.

Failure Reason

Fatigue or corrosion of the body shell or piping.

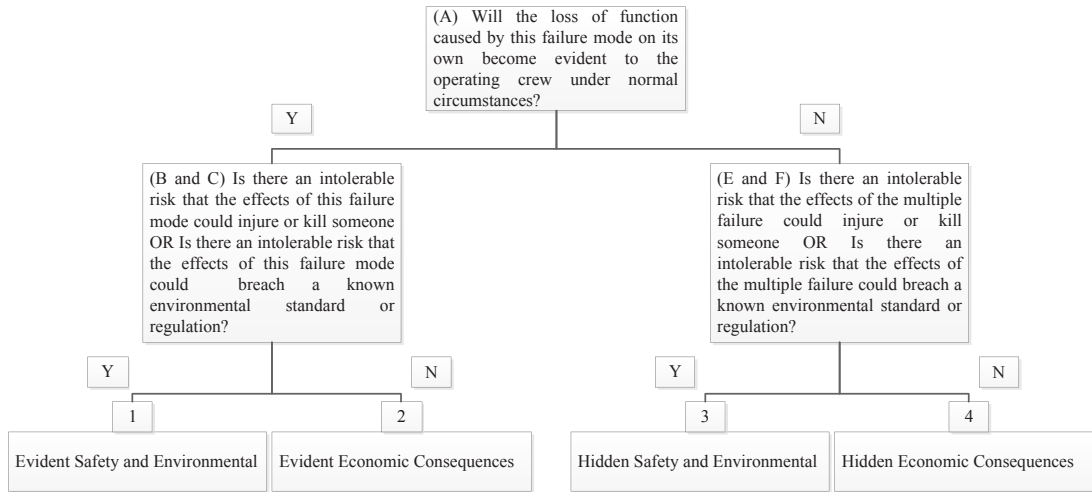


Figure 44.9
Logic tree.

Table 44.10: Task logic tree

Is a lubrication or servicing task applicable and effective?	Yes
Is an inspection or functional check to detect degradation of function applicable and effective?	Yes
Is a restoration task to reduce failure rate applicable and effective?	No
Is a discard task to avoid failures or to reduce the failure rate applicable and effective?	No

Maintenance Strategy

According to the FEMCA analysis, a series of maintenance strategies was scheduled as the following:

Task Logic Tree

Table 44.10 lists the task logic tree analysis result.

Corrective Tasks

Corrective maintenance consists of the action(s) taken to restore a failed component to operational status. Corrective maintenance is performed at unpredictable intervals because a component’s failure time is not known a priori. Table 44.11 lists the corrective task.

Scheduled Tasks

Scheduled maintenance contains three kinds of maintenances: PM, inspection, and on-condition maintenance.

Table 44.11: Corrective task

#	Task Description	Condition	Type	Interval	Crew	Duration
1	Repairing the leaking crack		Corrective		Fatigue or corrosion of the body shell or piping_Crew	1.000000 day

Table 44.12: Scheduled tasks

#	Task Description	Condition	Type	Interval	Crew	Duration
1	Applying the protective coating		S	3 years	Fatigue or corrosion of the body shell or Piping_Crew	1.000000 h
2	Crack inspection		IN	1 year	Fatigue or corrosion of the body shell or piping_Crew_2	1.000000 h

Note: S, service task (preventive task); IN, inspection task.

PM is the practice of repairing or replacing components or subsystems before they fail in order to promote continuous system operation or to avoid dangerous or inconvenient failures. The schedule for PM is based on observation of past system behavior, component wear-out mechanisms, and knowledge of which components are vital to continued system operation. In addition, cost is always a factor in the scheduling of PM. In many circumstances, it is financially more sensible to replace parts or components at predetermined intervals rather than to wait for a failure that may result in a costly disruption in operations.

Inspections are used in order to uncover hidden failures (also called “dormant failures”). They are also used as part of on-condition tasks to detect impending failures so that PM can be performed.

On-condition maintenance relies on the capability to detect failures before they happen so that PM can be initiated. If, during an inspection, maintenance personnel can find evidence that the equipment is approaching the end of its life, then it may be possible to delay the failure, prevent it from happening or replace the equipment at the earliest convenience rather than allowing the failure to occur and possibly cause severe consequences.

Table 44.12 lists the scheduled tasks of the external subunit of the heat exchanger.

References

- EPRI, October 1985. Application of Reliability-Centered Maintenance to Component Cooling Water System at Turkey Point Units 3 and 4. EPRI. NP-4271.
- Jones, R.B., 1995. Risk-Based Management — A Risk Centered Approach. Gulf Publishing Company, Houston.
- Moubray, J., 1992. Reliability Centered Maintenance. Industrial Press, Inc.

MSG1, July 1968. 747 Maintenance Steering Group Handbook: Maintenance Evaluation and Program Development (MSG-1). Air Transport Association.

NPD, 1991. Regulations Concerning Implementation and Use of Risk Analysis in the Petroleum Activities. Norwegian Petroleum Directorate.

Rausand, M., Vatn, J., 1997. Reliability Centered Maintenance. NTNU.

Structural Reassessment of Offshore Structures

45.1 Introduction

Crack and corrosion are two kinds of common damage frequently occurring in marine structures, and therefore it is important to analyze their effect on the residual ultimate strength of offshore structures. The investigation is not only related to the investment in the development of marine oil and gas resources and the use safety and applicability, but also has a positive effect on the improvement of the theory of structural reliability and life reassessment methods. Reevaluation of structural reliability and longevity is difficult and challenging. In recent decades, studies have been done at global level. But the results are not enough to satisfy the request of real projects now and in the future because the problem itself is so complicated.

This chapter summarizes several methods for reassessment of offshore structures. The factors include crack defects and corrosion.

45.2 Corrosion Model and Crack Defects Analysis

45.2.1 Corrosion Model

Before assessing the degradation of the ultimate strength of offshore structures, a proper corrosion model should be found to predict the corrosion thickness of the structure member. In the present study, a nonlinear corrosion model was considered for the offshore structures (Qin et al., 2003).

The corrosion protection system (CPS) was considered in the present corrosion model. In the model, the process of the CPS failure is a gradual process, and the corrosion starts before the total failure of the CPS. In addition, by taking into consideration the corrosion thickness and microorganism growth, the corrosion rate increases progressively and will reach the highest value, which will then decrease gradually. Therefore, for a CPS, there are two parameters (T_{st}, T_d), which can be used to describe its efficiency. T_{st} is the start time of the corrosion, and T_d is the lifetime of the CPS, and both can be acquired from tests.

Therefore, the whole corrosion progress is divided into three parts:

1. No corrosion, $t \in [0, T_{st}]$
2. Corrosion acceleration, $t \in [T_{st}, T_A]$
3. Corrosion rate slowing down, $t \in [T_A, T_L]$

Of which T_L is the assessing time for the platform, and T_A is the max corrosion rate time, and to simplify $T_A = T_d$.

A Weibull formulation was used to describe the corrosion rate:

$$r(t) = \begin{cases} 0 & 0 \leq t \leq T_{st} \\ d \frac{\beta}{\eta} \left(\frac{t - T_{st}}{\eta} \right)^{\beta-1} \exp \left\{ - \left(\frac{t - T_{st}}{\eta} \right)^{\beta} \right\} & T_{st} \leq t \leq T_L \end{cases} \quad (45.1)$$

The corrosion thickness can be described as:

$$d(t) = \begin{cases} 0 & 0 \leq t \leq T_{st} \\ d \left\{ 1 - \exp \left\{ - \left(\frac{t - T_{st}}{\eta} \right)^{\beta} \right\} \right\} & T_{st} \leq t \leq T_L \end{cases} \quad (45.2)$$

where d , β , η , and T_{st} are four parameters that need to be determined. Parameters should be chosen properly according to the experiment.

45.2.2 Crack Defects Analysis

Crack Failure Modes

Crack is a type of common damage in marine structures. There are many reasons causing this damage, such as local stress intensity in structure discontinuity, local corrosion, fatigue loading on continuous members, and so on. After offshore structures are damaged by cracks, they will have a lower ultimate strength and even present catastrophic results especially when they come across extraordinary waves or extreme loading conditions. Once cracks occur in the offshore structures, they should be found early and mended quickly. However, replacing the cracked structural member incurs very high costs and it is very difficult to carry out during the ship voyage. So we should know the crack effect on marine structure ultimate strength and evaluate the structure safety.

A wide variety of structure failure modes by crack defects make the evaluation difficult. Therefore, before investigating the influence of the crack defects to the ultimate strength of the structure, we should learn the different types of crack defects. According to fracture mechanics, there are two ways to distinguish crack defects: those classified by stress and failure mode, and those classified by the position and the shape of the crack defects.

Classified by Stress and Failure Mode

Because of the different stresses, the crack can be basically divided into three categories: the edge-opened crack, the sliding mode crack, and the tearing mode crack.

In general, they are also, respectively, called mode I crack, mode II crack, and mode III crack, as shown in Figure 45.1.

1. Edge-opened crack (mode I crack): A tensile stress normal to the plane of the crack, thus causing crack tip opening displacement where the crack surfaces move directly apart (Figure 45.1(a)).
2. Sliding mode crack (mode II crack): A shear stress acting parallel to the plane of the crack and perpendicular to the crack front, thus causing in-plane displacement where the crack surfaces slide over one another in a direction perpendicular to the leading edge of the crack (Figure 45.1(b)).
3. Tearing mode crack (mode III crack): A shear stress acting parallel to the plane of the crack and parallel to the crack front, thus causing out-of-plane displacement where the crack surfaces move relative to one another and parallel to the leading edge of the crack (Figure 45.1(c)).

In practice, crack propagation is not limited to the three basic modes and cracks often propagate under so-called mixed modes, which are a combination of the above-mentioned modes, such as I/II, I/III, II/III, and so on.

In practice, however, crack propagation under the mode I crack is the most dangerous. Under mode I, it is easier for crack propagation to trigger a brittle fracture, so it has been studied extensively. When mixed modes are encountered, it would be safer and easier to treat them as a mode I crack. Usually the offshore structures are suffering tension and compression stress under extreme conditions, which easily tends to cause crack propagation and structural failure. So, in this work, we shall focus on the mode I crack.

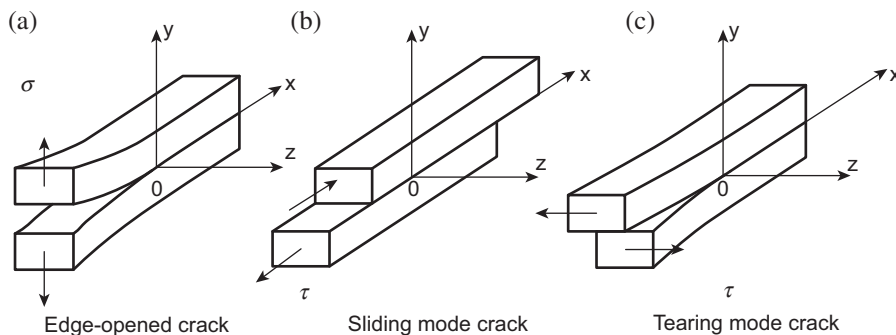


Figure 45.1

Crack defects classified by the stress and failure mode.

Classified by the Position of the Crack

Generally, there are three kinds of crack defects within structures: through crack, surface crack, and embedded crack (Figure 45.2).

1. Through crack: Usually the crack would penetrate over half the thickness of the structure member. It is often simplified as an ideal crack, that is, the curvature radius in the top of the crack tends to be zero. This simplification is easier to consider. The through crack can be linear, a curve, or any other shape.
2. Surface crack: This is where the surface of the structure member or the depth of the crack is relatively smaller than the thickness of the structure member. In general, a surface crack is usually simplified as a semi-elliptical surface crack.
3. Embedded crack: This appears in the inner part of the structure and is often simplified as the elliptical plate crack or the cone crack.

Classified by the Shape of the Crack

According to the real shape of the crack, a crack can be divided into a roundness crack, ellipse crack, surface semicircle crack, surface semielliptical surface, straight through crack, and so on.

The Effect on the Strength of the Material Due to the Crack

As we all know, engineering structures with crack defects bear stress concentrations when they are subjected to loads. And the shapelier the crack is, the more the stress concentration would be, which in practice would lead to a smaller breaking strength.

As you can see, the “infinite” sheet under one direction uniform tensile stress. There exists an elliptical cut in the sheet, where the major axis equals $2a$ and the minor equals $2b$.

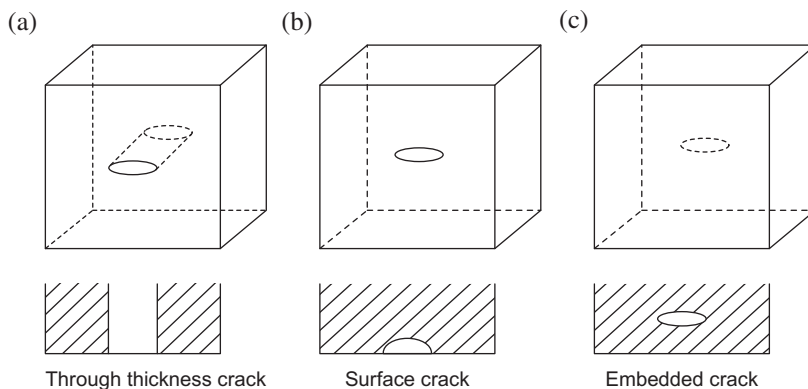


Figure 45.2

Crack defects classified by the position of the crack.

Thus, the maximum tensile stress occurs in the end of the major axis and equals:

$$(\sigma_y)_{\max} = \sigma \left(1 + \frac{2a}{b} \right) \quad (45.3)$$

While the curvature radius is $\rho = b^2/a$, the maximum tensile stress can also be:

$$(\sigma_y)_{\max} = \sigma \left(1 + 2\sqrt{\frac{a}{\rho}} \right) \quad (45.4)$$

For a circular cut, $a = \rho$, then $(\sigma_y)_{\max}/\sigma = 3$, that is, the maximum stress when there exists stress concentration is three times bigger than when there is no stress concentration.

45.3 The Residual Ultimate Strength of Hull Structural Components

Structural components are prone to corrosion damage, especially when exposed to sea conditions. This section investigates the effects of local corrosion and crack defects applied to plates and stiffened panels typically found in ship-like structures.

A significant feature of ship structural design is to describe the structural behavior of ship hull girders and to accurately predict their maximum load-carrying capacity. On the other hand, the overall failure of ship structures (which is basically an assembly of unstiffened and stiffened plate components) is certainly affected and governed by the plastic collapse of its structural elements. Therefore, from the ultimate limit state design point of view, a primary task is to predict the ultimate strength of such foregoing structural members in order to assess the safety and economical design of ship structures. In this regard, it is only necessary to consider the corrosion and crack defects that are involved in the service life.

45.3.1 Effects of Crack Defects on Plates and Stiffened Panels

This section presents the numerical study method about the ultimate compressive strength characteristics of cracked steel unstiffened and stiffened plate components used in a thin-walled structure such as ship hull girders. It also gives some study results by [Abbas Bayatfar et al. \(2014\)](#) regarding the influence of crack location and crack length on the ultimate strength characteristic of the structural element under monotonic longitudinal axial compression.

Numerical Analysis Method

The commercial finite element code [ANSYS \(2009\)](#) can be used for the numerical study of the effects of crack defects on plates and stiffened panels.

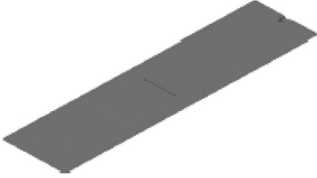
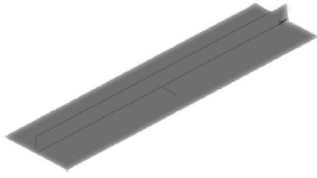
When doing analysis, the following presumptions can be followed:

1. Cracks are through-thickness, having no contact between their faces and no allowance for propagation. The size of the gap between the crack faces can be taken equal to 3 mm.
2. The cracks modeled can be assumed to be straight originally and also remain straight during loading, while their length is also considered to be fixed.
3. Flat-bar profile is the stiffener type and materials are in the category of high strength steel alloys ([Ship Structure Committee Report, 1997](#)). The material can be considered to behave in an elastic–plastic hardening manner.

Among the elements included in the ANSYS library, the SHELL181 element is suitable in order to discretize the cracked plate models. It is a four-node element with six degrees of freedom at each node: translations in the X , Y , and Z directions, and rotations about the X -, Y -, and Z -axes. This element is well suited for linear, large rotation, and/or large strain non-linear applications ([ANSYS, 2009](#)).

Cracked unstiffened or stiffened plate models can be assumed to be extracted out of a continuous plated structure such as a deck or a ship hull girder. Proper boundary and loading conditions should be imposed along the boundaries so that they can simulate real behavior as accurately as possible. Simply supported straight boundaries can be adopted for longitudinal edges of unstiffened cracked plate models. Generally, uniform compressive displacement is applied on the simply supported straight loading edge, while its opposite simply supported edge is restrained against in-plane movement. [Table 45.1](#)

Table 45.1: Example models for analysis ([Ship Structure Committee Report, 1997](#))

Description	Figure
<p>The unstiffened plate in which the crack is transversally (Y-axis direction) located in the center of the plate</p>	
<p>The stiffened plate in which the crack is transversally located in the center of the plate</p>	

lists two example models for plate and stiffened plate structures. The axial compressive capacity is usually studied through displacement control.

Crack Length and Location Influence

In order to examine the effect of crack length on the ultimate strength characteristics, [Abbas Bayatfar et al. \(2014\)](#) have studied many cases, and the crack location has been kept constant while its length alters for each of the case studies; the results are explained below.

Unstiffened Plate with a Transverse Crack Located in the Center (UTC)

Values of the ultimate strength for the model “UTC” having different crack lengths are given in [Table 45.2](#) from which it can be understood that in comparison with the reference model, increasing the crack length above 40% of the plate breadth leads to further reduction in the ultimate strength.

Unstiffened Plate with a Transversely Oriented Mid-Length Edge Crack (UT1E)

The study shows that the increase of the crack length affects the average stress—average strain curve almost from the beginning. Tangent stiffness, buckling strength, ultimate strength, and reserve strength are all decreased with the increase in the crack length.

Table 45.2: Influence of crack location on the values of the ultimate strength in case of unstiffened plates

	Case	Ultimate Strength (MPa)	Difference (%)
	REF	282.2	—
10%	UTC	282.2	0
	UT1E	270	−4.5
	UT2E	280.1	−0.7
20%	UTC	282.2	0
	UT1E	251.1	−12.4
	UT2E	256.8	−9.9
30%	UTC	281.8	−0.1
	UT1E	230.5	−22.4
	UT2E	223	−26.5
40%	UTC	278.2	−1.4
	UT1E-L250	198.3	−42.3
	UT1E-L500 (UT1E)	209.1	−35
	UT1E-L750	198	−42.5
	UT1E-L1000	209.1	−35
	UT1E-L1250	197.9	−42.6
	UT2E	203.9	−38.4
50%	UTC	245.2	−15.1
	UT1E	200	−41.1
	UT2E	182.6	−54.5

Unstiffened Plate with Two Transversely Oriented Mid-Length Edge Cracks (UT2E)

The study shows that the increase of the crack length affects the average stress–average strain curve almost from the beginning. Apparently tangent stiffness, buckling strength, ultimate strength, and reserve strength are all decreased with the increase in the crack length. In comparison with the reference model, increasing the crack length above 10% of the plate breadth leads to a larger reduction of the ultimate strength.

Stiffened Plate with a Transverse Crack Located in the Center of the Plate (STC)

The study shows that with the increase of the crack length, the average stress–average strain curves are changed for a stress level above $\sigma = \sigma_Y = 0.15$. The longer the crack, the more reduced the stiffness and ultimate strength of the model.

Values of the ultimate strength for the model “STC” having different crack lengths are given in Table 45.3 from which it can be understood that in comparison with the reference model, increasing the crack length above 20% of the plate breadth leads to a larger reduction in the ultimate strength.

Stiffened Plate with Two Cracks Located in the Plate and the Stiffener Web (STCW)

The study shows that with the increase of the length of the crack in the stiffener web, the average stress–average strain curves are slightly changed for a stress level above $\sigma = \sigma_Y = 0.3$. The longer the crack, the more reduced the stiffness and ultimate strength of the model.

Values of the ultimate strength for the model “STCW” having different crack lengths are given in Table 45.3 from which it can be understood that in comparison with the reference model, increasing the crack length does not lead to a considerable reduction in the ultimate strength.

Abbas Bayatfar et al. have also studied the effect of crack location on the ultimate strength characteristics, and for each crack length kept constant (e.g., 10%), the location of crack is changed (i.e., UTC, UT1E, and UT2E), the results can also be seen in Table 45.2.

Table 45.3: Values of the ultimate strength for the models “STC” and “STCW” having different crack lengths in comparison with the ultimate strength of the model “REF”

Model	STC						STCW				
	REF	10%	20%	30%	40%	50%	10%	20%	30%	40%	50%
Ultimate strength (MPa)	238.1	236.4	231.9	225	216.2	205.5	230.9	230.1	229.9	230.4	231.7
Difference (%)	—	−0.7	−2.7	−5.8	−10.1	−15.9	−3.1	−3.5	−3.6	−3.3	−2.8

Conclusion

According to the study of Abbas Bayatfar et al., it can be found that the most critical types of crack are those that are transversally located along the longitudinal (unloaded) edges of the plate. In this regard, the observations indicate that the reduction in ultimate strength in the case of two transversely oriented mid-length edge cracks is less than that for single edge crack as long as the total length of crack is shorter than 30% of the plate breadth. Also in the case of a transversely oriented edge crack in which the crack moves along the unloaded edge, the ultimate strength is further reduced for a crack located at the crest or the trough of plating half-wave than for cases with a crack located at zero amplitude of plating half-wave. Such findings can be taken into consideration from a structural strength assessment point of view throughout the fabrication process and also for the duration of repair and maintenance.

45.3.2 Effects of Localized Corrosion on Plates and Stiffened Panels

Numerical modeling and analysis methods of square plates and stiffened panels are introduced in this section. Failure modes for square plates and stiffened panels, the most common structural elements found on ships, are also reviewed herein.

The effect of various corrosion patterns on these two types of ship structural components, which has been studied by [Timothy et al. \(2004\)](#), is then introduced and compared to existing solutions and experimental data where available.

Numerical Modeling and Analysis Method of Square Plates and Stiffened Panels

The commercial finite element code ANSYS can be used for the numerical study of the effects of localized corrosion on plates and stiffened panels.

The plating on a stiffened panel is usually designed to fail locally prior to the overall failure of a stiffened panel. Thus, the post-ultimate load-carrying capacity of plating is an important factor in assessing the overall ultimate strength of a stiffened panel.

When modeling a square plate structure, shell elements with six degrees of freedom are suitable. Two loading conditions are usually considered: uniaxial loading condition and biaxial loading condition. When assessing the ultimate strength of the plate, all edges should be restrained in the out-of-plane direction. To prevent rigid body motion, minimum boundary conditions can be applied in the X and Y directions. The bottom corners can be restrained from motion in the X or Y direction, whereas the middle node of the upper and lower plate edges can be restrained from motion in the X or Y direction according to the load condition. A small imperfection is needed by the finite element software to induce instability. Rotational restraints need not to be applied.

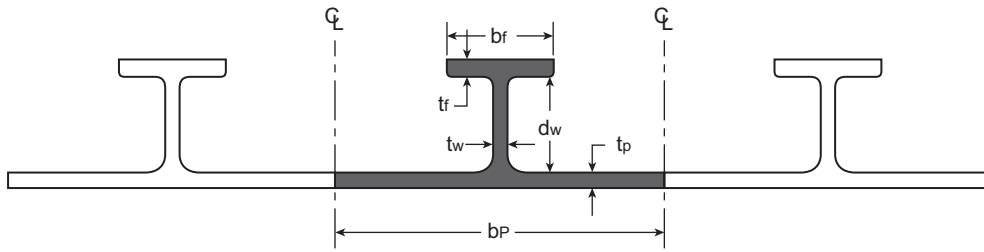


Figure 45.3
Stiffened panel diagram.

When modeling of the corrosion effect, the corrosion can be considered as the loss of the plate volume. As the corrosion area on the face of the plate decreases, the corrosion depth must increase to keep a constant volume loss.

Figure 45.3 shows an example stiffened panel.

The stiffened panel can be simply supported at both ends with symmetric boundary conditions applied to the sides (Bayatfar et al., 2014). For the nonlinear collapse analysis, an incremental axial load can be applied to the neutral axis node at the end of the panel.

The model imperfections in the form of transverse barreling of the plate and longitudinal bowing of the stiffener can be given as shown in Figure 45.4. The plating of the single stiffened panel with transverse imperfections can be applied in the form of a 1/4 sine wave on each side of the stiffener with a maximum amplitude of δ_p . The longitudinal imperfection can be applied in the form of 1/2 sine wave with a maximum amplitude of δ_s . These imperfections can be taken from the Ship Structure Committee Report (1997).

Residual stresses have a very significant impact on the non-linear mechanical behavior of stiffened panels. When geometric imperfections and corrosion damage exist, this idealized stress distribution often fails to satisfy the equilibrium condition exactly for the overall stiffened panel. To solve this difficulty, a numerical procedure based on linear thermal

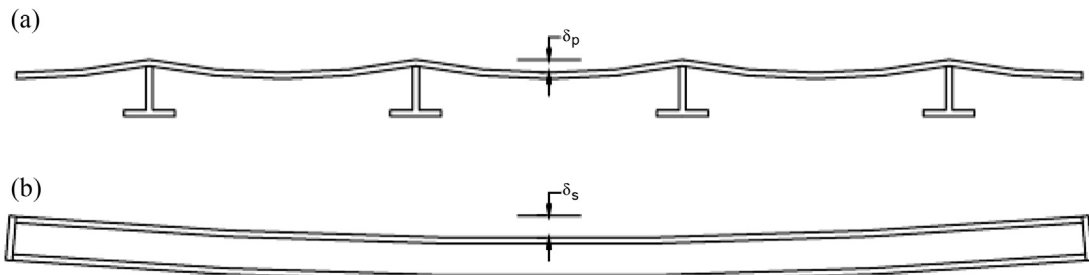


Figure 45.4

Imperfection: (a) transverse barreling of the plate and (b) longitudinal bowing of the stiffener.

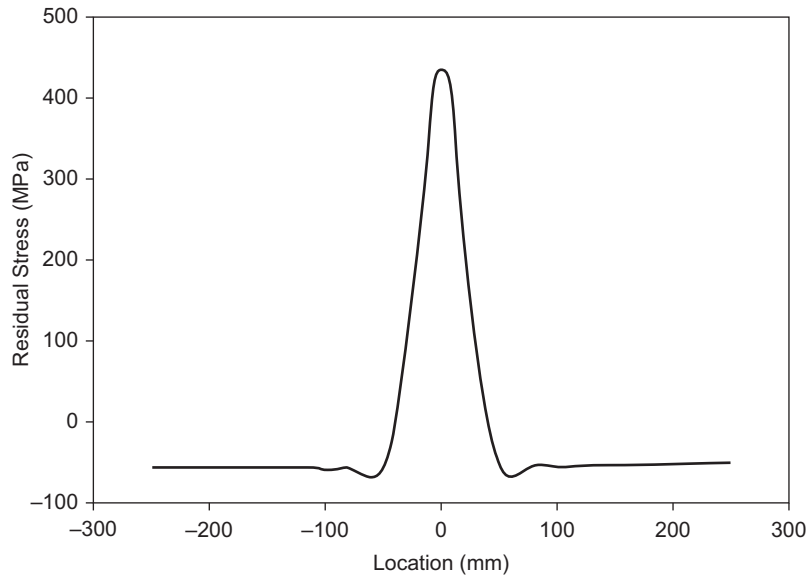


Figure 45.5
Residual stress distribution (SSC-399) (Timothy et al., 2004).

stress analysis can be used and a typical residual stress profile generated by using this method is shown in Figure 45.5. A small percentage of the first buckling mode shape can be applied in addition to the measured imperfections and residual stresses. A study by Hu et al. (1998) found that this added modification improves the numerical stability of the problem.

The symmetric imperfection pattern of the plate about the web, and the symmetric imperfections of the stiffener about the center, leads to the consideration of corrosion in only one of the four sections shown in Figure 45.6(a). Based on the patterns of buckling shape, initial imperfections, and residual stresses, this one quadrant can be further divided into four subsections in the longitudinal direction and three subsections in the transverse direction. The number 3 longitudinal (Figure 45.6(b)) strip covers the area of tensile residual stresses. It should be noted that in the analyses, corrosion should be applied to both sides of the plating.

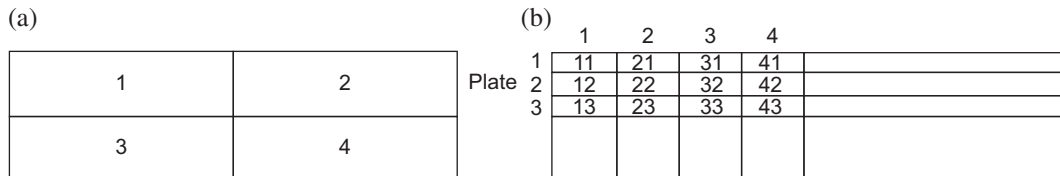


Figure 45.6
Corrosion mapping for single location damage.

Effects of Localized Corrosion on Plates

Timothy et al. (2004) have studied the effects of localized corrosion on plates with the introduced numerical method. In their study, the square plate has dimensions of $1\text{ m} \times 1\text{ m} \times 10\text{ mm}$. Steel with a Young's modulus of 207 GPa, no strain hardening, a Poisson's ratio of 0.3, a density of 7.85 mg/m^3 , a yield stress of 350 MPa, and an ultimate stress of 450 MPa was used for the model. Local corrosion loss of 10% of the plate volume was applied to the central region of the plate over square areas of varying size. The results are as follows.

When decreasing the corrosion area, the elastic buckling capacity decreases, but the ultimate capacity shows an increasing trend, particularly for the 20% area case, as shown in Figure 45.7. As the plate becomes thinner with decreased corrosion area, more out-of-plane plate displacement occurs because of elastic buckling. This higher out-of-plane displacement relative to the thickness of the plate may cause geometric nonlinearity to become more influential, which may increase the ultimate load.

Effects of Localized Corrosion on Stiffened Panels

Timothy et al. have studied the effects of localized corrosion on stiffened panels with the introduced numerical method. In their study, the initial model used was taken from Timothy et al. (2004) with overall length of 2 m and dimensions given in Table 45.4. The steel had a Young's modulus of 207 GPa and Poisson's ratio of 0.3.

The corrosion effects were considered as introduced in Figure 45.6.

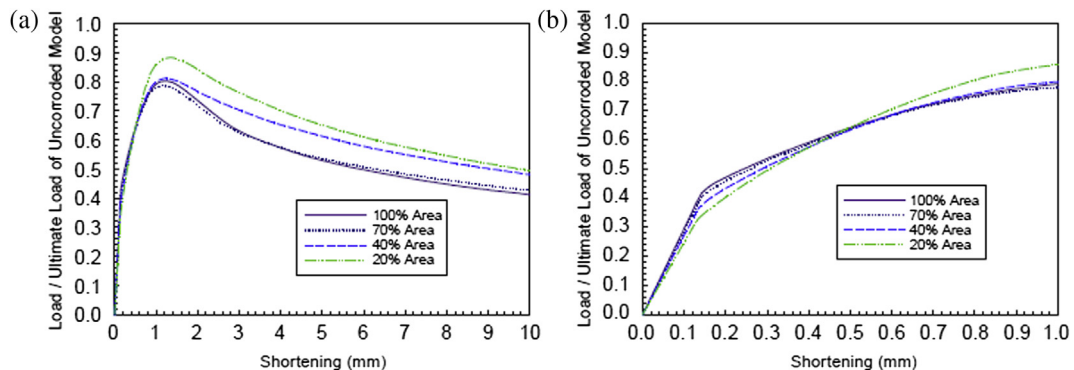


Figure 45.7

Load-shortening curves for a square plate with 10% volume loss: (a) full curve and (b) close-up of buckling.

Table 45.4: Stiffened panel dimensions

	Width (mm)	Thickness (mm)	Yield stress (MPa)
Plate	500 (b_p)	10 (t_p)	425
Web	136 (d_w)	6 (t_w)	411
Flange	103 (b_f)	8 (t_f)	395

The results of their study are given as follows.

50% Volume Loss at Location P11

Applying a corrosion loss of 10% by volume of the initial plate thickness over local locations had little effect on the load–displacement curves. Corrosion at higher levels (50% and 75% volumes) caused local buckling at the corroded region, which affected the global collapse mode of the stiffened panel. The numerical results for a corroded stiffened panel with 50% volume loss at location P11 are given in Figure 45.8. The initial buckling at the corroded side occurred in the same direction as the plate imperfection, whereas the buckling shape on the opposite side of the stiffener web was opposite to the imperfection direction. This full sine wave shape in the transverse direction of the panel was the same form as the second classical column buckling mode with a central support (the stiffener in this case).

Corrosion Location P21, P31, and P41

The next location, P21, behaved similarly to P11. After initial buckling, high stress occurred locally at the corrosion location but the main yielded area occurred on the opposite side of the web (Figure 45.9) as it locally deformed in the opposite direction of the buckling mode.

Corrosion locations P31 and P41 have the same behavior as P21 except that the initial buckling at these locations occurs in the direction from the plate to the flange.

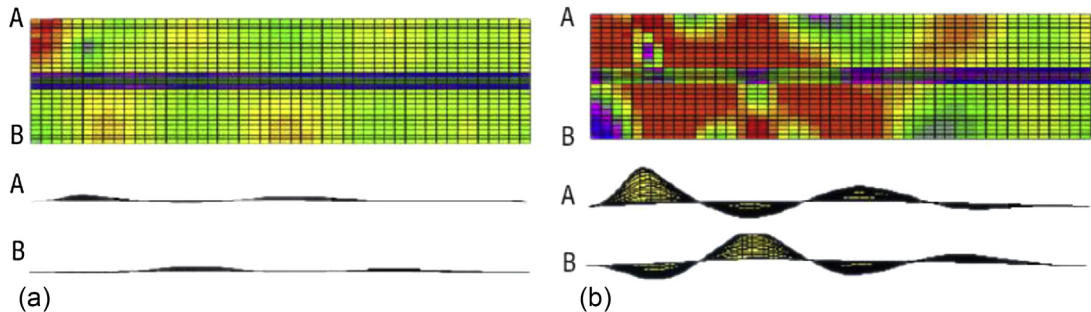


Figure 45.8

Stress and displacement distribution for plate with 50% corrosion on location P11 (a) at first yield (local) and (b) at ultimate loading.

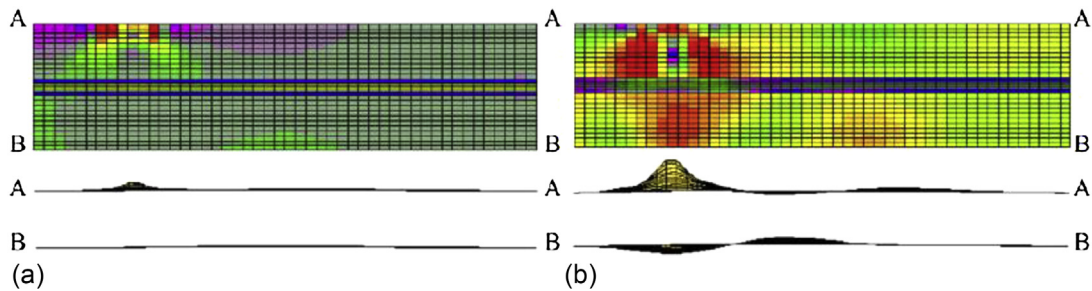


Figure 45.9

Stress and displacement distribution for plate with 75% corrosion on location P21 (a) at first yield (local) and (b) yielding (global pattern).

This response is opposite to that of the original imperfect model. Local buckling at these locations (P31 and P41) causes the global deformation pattern to be inverted.

Corrosion Locations P22, P32, and P42

Corrosion locations P22, P32, and P42 exhibited a similar pattern to that of P21, P31, and P41, mainly because all of these locations lie in the region that is initially in compression due to residual stresses.

Corrosion Locations P23, P33, and P43

Corrosion locations P23, P33, and P43 produced a pattern different from those previously discussed because they lie in the region that is initially in tension from residual stresses. Corrosion at these locations causes yielding and promotion of the global failure pattern, but local buckling does not seem to occur. Once ultimate loading is reached, load is transferred to the tensile strip, which has less ability to resist load since it is corroded. The post-ultimate load-shortening curve is thus more dramatically affected. It should also be noted that corrosion changes the distribution of residual stresses. As indicated in [Figure 45.10](#), the maximum tensile stresses are both at yield in corroded and noncorroded regions, but the compressive residual stresses are lower in the corroded region compared to noncorroded. This is because corrosion reduces material in the tensile stress region, which causes reduction of the compression residual due to the equilibrium condition.

45.4 The Residual Ultimate Strength of Hull Structures with Crack and Corrosion Damage

This section introduces the analysis method of ultimate strength of the hull structures with crack and corrosion damage. The research results of some researchers are also given in this section.

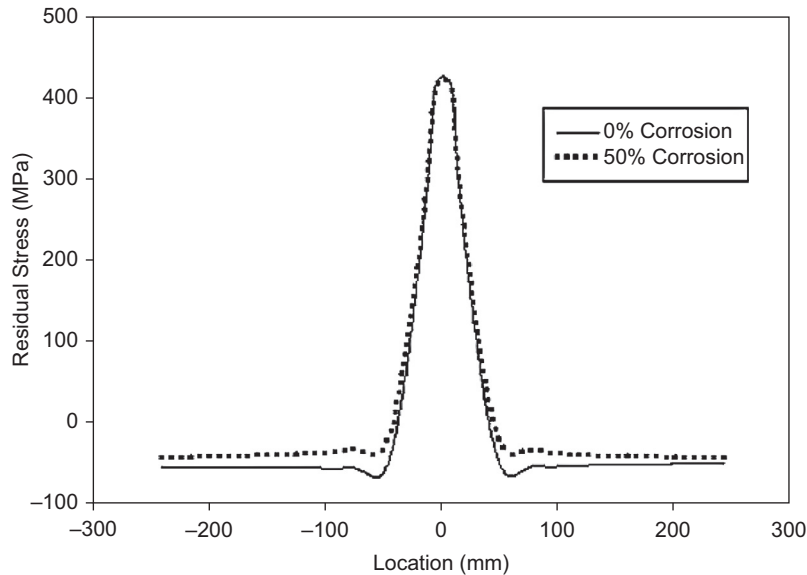


Figure 45.10

Comparison of residual stresses with and without corrosion on plate region 33.

45.4.1 Analysis Method of Ultimate Strength

The nonlinear finite element method (NFEM) is a powerful tool to solve the problems of complex engineering structures. But using NFEM to analyze hull ultimate strength will need plenty of time to fabricate models and do calculations. The most effective method to avoid this problem is to reduce the number of freedom during calculation process, that is to say, decrease the matrix order of finite element stiffness. One method is to use a large structure element called idealized structure element (ISUM). The cross-section of ship will be divided into a series of separate structure elements, which are considered to act independently and fail in their own damage modes. In order to assure the effectiveness of this method, the structure element should be reasonably divided and its damage mode should be accurately defined.

BV Mars 2000 provides a type of ISUM to analyze the ultimate strength of hull girders between two adjacent frames (Bureau Veritas, 2011). The cross-section will be divided into two kinds of structure element: stiffener attaching plating element and hard corner element. The former will present a buckling or yielding damage mode when in compression; however, it will present only an elastic–plastic damage mode when in tension. The latter, constituting plating crossing, collapses mainly according to elastic–plastic failure mode.

The International Ship and Offshore Structures Congress (ISSC) container ship's yielding stress of steel in a strengthened deck is 352.8 MPa and other parts are 313.6 MPa

Table 45.5: Ultimate strength of the ISSC container ship

Items	Chen	Cho	Masaoka	Rigo	Soares	Yao	ISUM	NFEM
I_y (m ⁴)	250.94	226.7	235.6	254.3	238.73	238.21	233.71	—
Z_G (m)	8.86	8.84	8.54	8.10	8.51	8.63	8.81	—
SM_{btm} (m ³)	28.32	25.64	27.59	31.40	28.05	27.60	26.53	—
SM_{dk} (m ³)	19.57	17.66	17.93	18.73	18.13	18.25	18.16	—
M_{UH} ($\times 10^3$ MNm)	6.82	7.05	8.06	8.00	7.75	6.90	7.51	7.44
M_{US} ($\times 10^3$ MNm)	5.54	5.29	7.79	6.93	6.68	6.84	6.89	7.46

Notes: I_y , moment of inertia with respect to horizontal neutral axis; Z_G , location of neutral axis above keel; SM_{btm} , bottom modulus; SM_{dk} , deck modulus; M_{UH} , hogging ultimate strength; M_{US} , sagging ultimate strength.

(ISSC, 2000). According to the research made by Gao Da-wei et al. (2012), the results of ultimate strength calculated by ISUM and NFEM are compared in Table 45.5, including results of seven other analysis methods, which proves that the NFEM methods can predict accurately the hull vertical ultimate strength.

45.4.2 Modeling

Gao Da-wei et al. (2012) have done some research on the focusing area. In their study, the main dimensions of three sample ships are shown in Table 45.6. ISSC is a container ship given by the ISSC committee; the 3100TEU container ship is in active service; however, the 9600TEU container ship is assumed based on the same type of vessels and conforms to the China Classification Society (CCS) rules and regulations (CCS, 2006). IACS (2000) summarized common crack types, damage cause, and repair recommendations in container carriers. Seven types of representative crack were chosen in their study to analyze their effect on ultimate strength, all of which are assumed to be located at strengthened members.

The sample ships are modeled by the NFEM method.

45.4.3 Residual Ultimate Strength with Crack Damage

In the Gao Da-wei et al. (2012) study, appropriate presumptions were made about crack types and crack length to simplify the analysis. The transverse crack has a biggest

Table 45.6: Main dimensions of three sample ships

Items	ISSC	3100TEU	9600TEU
L_{pp} (m)	230	214.2	320
B (m)	32.2	32	45.6
D (m)	21.68	18.8	27.2

Table 45.7: Length and location of cracks

Crack	Length c (mm)			Distance between Crack Center and Initial Neutral Axis R (mm)		
	ISSC	3100TEU	9600TEU	ISSC	3100TEU	9600TEU
Crack-1	—	425	550	—	11,972	17,147
Crack-2	—	775	850	—	11,859.5	17,072
Crack-3	600	700	800	12,720	9797	14,947
Crack-4a	840	1050	1118	12,020	8872	13,950
Crack-4b	1680	2100	2236	12,030	8922	14,029
Crack-4c	4140	4000	5116	10,800	7972	12,589
Crack-5a	840	1050	1118	12,020	8872	13,950
Crack-5b	1680	2100	2236	12,030	8922	14,029
Crack-5c	4140	4000	5116	10,800	7972	12,589
Crack-6a	880	729	896	-8810	-8828	-12,053
Crack-6b	2640	1458	2686	-8810	-8828	-12,053
Crack-6c	5280	4026	5206	-8810	-8828	-12,053
Crack-7a	880	729	896	-7010	-7048	-9953
Crack-7b	2740	1458	2686	-7010	-7048	-9953
Crack-7c	5280	4026	5206	-7010	-7048	-9953

effect on reducing ultimate strength. The seven types of crack in their study were assumed to be transverse and located at the middle of the frame. The cracks with 10 mm width were through steel plates. The crack length c and distance from crack center to initial horizontal neutral axis R in the vessel cross-section are shown in Table 45.7.

In order to compare the ultimate strength of damaged vessels and intact vessels, residual ultimate strength index RIF is defined as:

$$RIF = M_{Damage}/M_{Intact} \text{ or } RIF = SM_{Damage}/SM_{Intact} \quad (45.5)$$

where M_{Damage} = ultimate strength of damaged ships; M_{Intact} = ultimate strength of intact ships; SM_{Damage} = section modulus of damaged ships; SM_{Intact} = section modulus of intact ships.

Figure 45.11 shows the residual ultimate strength of the ISSC container ship when the cracks are above neutral axis. Crack-4 locates at outer side shell, but crack-5 locates at inner side shell. However, they almost have the same effect on reducing ultimate strength when they reach the same length. Figure 45.12 shows the reduction of bottom modulus, which can be used conservatively to evaluate the change of ultimate strength when the crack locates below neutral axis.

The residual ultimate strength and cross-section modulus of the ISSC container ship are shown in Table 45.8. When the crack locates above the neutral axis, the residual ultimate

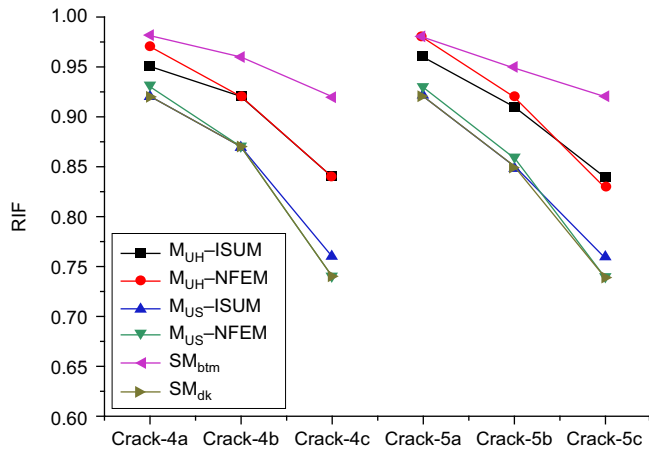


Figure 45.11

Residual ultimate strength of the ISSC container ship when cracks occur above neutral axis.

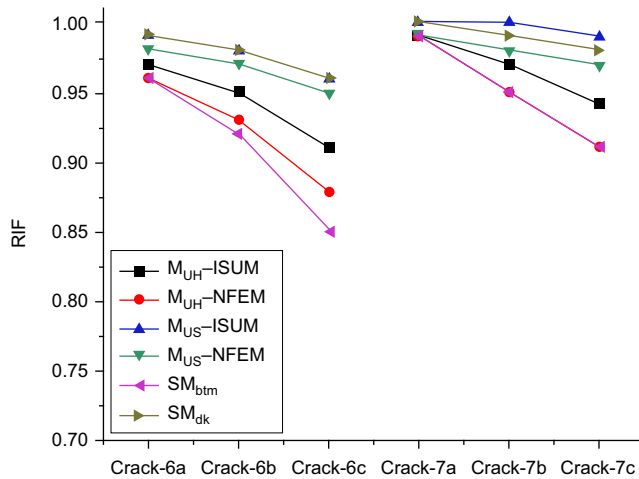


Figure 45.12

Residual ultimate strength of the ISSC container ship when cracks occur below neutral axis.

strength of the ISSC container ship is plotted in Figure 45.13 with the horizontal axis $2c(R/D)^2/D$. Using the least squares method, the residual ultimate strength curve is fitted as Eqn (45.2). The parameters in Eqn (45.6) are shown in Table 45.9:

$$RIF = a_1 \frac{2c}{D} \left(\frac{R}{D} \right)^2 + a_0 \quad (45.6)$$

where RIF is residual ultimate strength index; c is crack length; R is distance from crack center to initial neutral axis; D is depth of ship; a_0 and a_1 are the undetermined parameters.

Table 45.8: Residual ultimate strength of the ISSC container ship

Crack	M_{UH}		M_{US}		SM_{btm}	SM_{DK}
	ISUM	NFEM	ISUM	NFEM		
Crack-3	0.98	0.97	0.98	0.96	0.99	0.96
Crack-4a	0.95	0.97	0.92	0.93	0.98	0.92
Crack-4b	0.92	0.92	0.87	0.87	0.96	0.87
Crack-4c	0.84	0.84	0.76	0.74	0.92	0.74
Crack-5a	0.96	0.98	0.92	0.93	0.98	0.92
Crack-5b	0.91	0.92	0.85	0.86	0.95	0.85
Crack-5c	0.84	0.83	0.76	0.74	0.92	0.74
Crack-6a	0.97	0.96	0.99	0.98	0.96	0.99
Crack-6b	0.95	0.93	0.98	0.97	0.92	0.98
Crack-6c	0.91	0.88	0.96	0.95	0.85	0.96
Crack-7a	0.99	0.99	1.00	0.99	0.99	1.00
Crack-7b	0.97	0.95	1.00	0.98	0.95	0.99
Crack-7c	0.94	0.91	0.99	0.97	0.91	0.98

Note: M_{UH} , $(M_{UH})_{Damage}/(M_{UH})_{Intact}$; M_{US} , $(M_{US})_{Damage}/(M_{US})_{Intact}$; SM_{btm} , $(SM_{btm})_{Damage}/(SM_{btm})_{Intact}$; SM_{dk} , $(SM_{dk})_{Damage}/(SM_{dk})_{Intact}$.

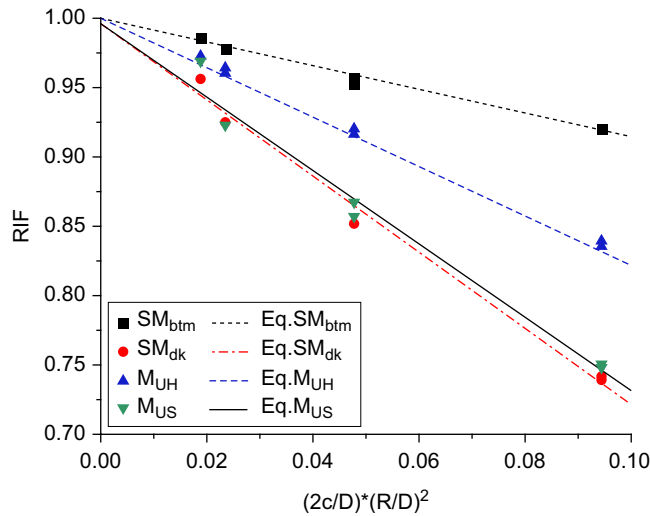


Figure 45.13

Residual ultimate strength of the ISSC container ship when cracks occur above the neutral axis.

Table 45.9: Simple equations for predicting residual strength of container ships

	Crack above Neutral Axis				Crack below Neutral Axis			
	M_{UH}		M_{US}		M_{UH}		M_{US}	
	a_1	a_0	a_1	a_0	a_1	a_0	a_1	a_0
ISSC	-1.76	1.00	-2.65	1.00	-2.13	1.00	-0.71	1.00
3100TEU	-0.89	1.00	-2.17	0.99	-2.23	1.01	-0.72	1.00
9600TEU	-1.87	1.01	-2.82	1.00	-1.50	1.00	-0.49	1.00
Mean	-1.51	1.00	-2.54	1.00	-1.95	1.00	-0.64	1.00
S.D.	0.54	0.00	0.34	0.00	0.39	0.00	0.13	0.00
COV	-0.36	0.00	-0.13	0.00	-0.20	0.00	-0.20	0.00

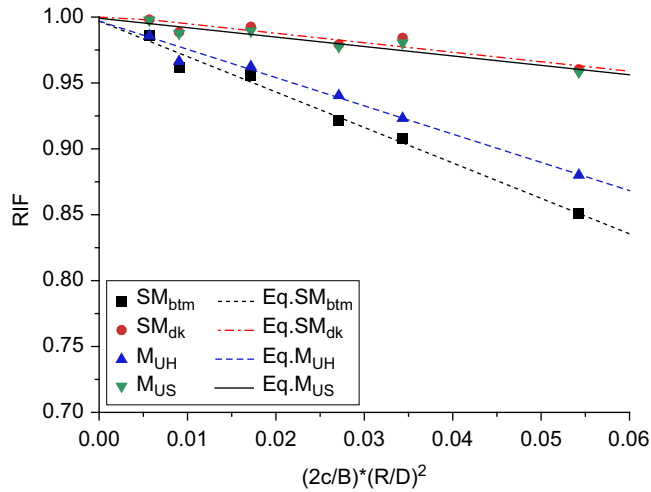


Figure 45.14

Residual ultimate strength of the ISSC container ship when cracks occur below the neutral axis.

When the crack locates below the neutral axis, the residual ultimate strength of the ISSC container ship is plotted in Figure 45.14 with the horizontal axis $2c(R/D)^2/B$. Using the least squares method, the residual ultimate strength curve is fitted as Eqn (45.7).

The parameters in the equation are shown in Table 45.9:

$$RIF = a_1 \frac{2c}{B} \left(\frac{R}{D} \right)^2 + a_0 \quad (45.7)$$

where B is breadth of ship; a_0 and a_1 are the undetermined parameters.

Using the same method, the RIF of the 3100TEU and 9600TEU container ships was analyzed and the results of a_0 and a_1 are shown in Table 45.9. The COV of the three container ships is not very big and especially the COV of the items that are heavily affected by crack damage, such as deck modulus with cracks above neutral axis and bottom modulus with cracks below neutral axis, which are much smaller. So the main dimension of the container ship has little effect and Eqns (45.6) and (45.7) can be used to predict residual ultimate strength of the container ship with crack damage.

46.4.4 Residual Ultimate Strength with Corrosion Damage

In the Gao Da-wei et al. (2012) study, in order to analyze the effect of corrosion on residual ultimate strength of container ships, the corrosion conditions ruled by the ABS, CCS, and DNV classification societies were deemed the most serious. The residual ultimate strength

and section modulus are shown in Figures 45.15 and 45.16. The corrosion has the biggest effect on reducing hogging ultimate strength, followed by bottom modulus, then sagging ultimate strength; deck modulus has the smallest reduction. So, purely from the view of corrosion, the hogging condition in aged vessels is the most dangerous.

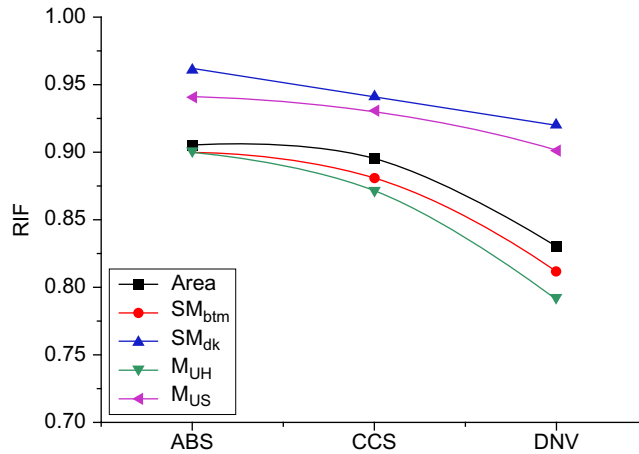


Figure 45.15

Residual ultimate strength of the 3100TEU container ship after corrosion damage.

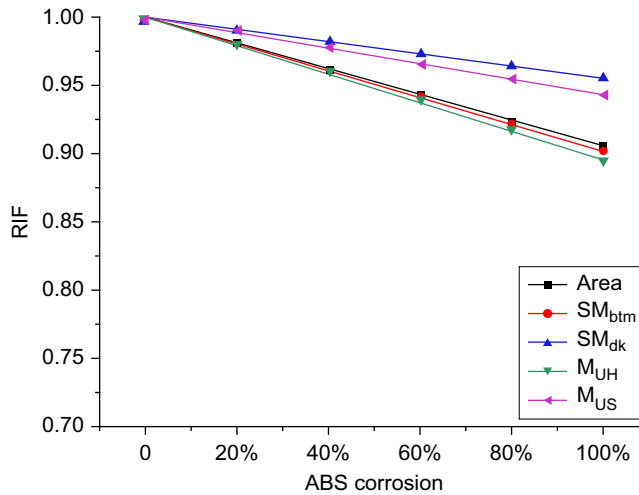


Figure 45.16

Residual ultimate strength of the 3100TEU container ship with various levels of ABS corrosion.

References

- ANSYS, 2009. User's Manual (Version 12.1). Swanson Analysis Systems Inc., Houston.
- Bayatfar, A., et al., 2014. Residual ultimate strength of cracked steel unstiffened and stiffened plates under longitudinal compression. *Thin-Walled Structures* 84, 378–392.
- Bureau Veritas (BV), November 14, 2011. Mars 2000. Users Guide – BV release.
- CCS, 2006. Rules and Regulations for the Construction and Classification of Sea-going Steel Ships.
- Gao Da-wei, et al., 2012. Residual ultimate strength of hull structures with crack and corrosion damage. *Engineering Failure Analysis* 25, 316–328.
- Hu, S.Z., Chen, Q., Pegg, N., Zimmerman, T.J.E., 1998. Ultimate collapse of tests of stiffened-plate ship structural units. *Marine Structures* 10, 587–610.
- IACS, 2000. International Association of Classification Societies Ltd.
- ISSC, 2000. In: . Proceedings of the 14th International Ship and Offshore Structures Congress. Japan.
- Qin, S.P., Cui, W.C., Shen, K., 2003. A non-linear corrosion model for time variant reliability analysis of ship structures. *Journal of Ship Mechanics* 7, 94–103.
- Ship Structure Committee Report, 1997. Strength and Stability Testing of Stiffened Plate Panels. SSC-339, USA.
- Timothy, E., et al., 2004. A computational investigation of the effects of localized corrosion on plates and stiffened panels. *Marine Structures* 17, 385–402.

Time-Dependent Reliability Assessment of Offshore Jacket Platforms

46.1 Introduction

It has been about half a century since the utilization of offshore oil. Since the first steel jacket platform was introduced in the Gulf of Mexico in 1947, it has been instated in most offshore areas across the world. Platform failures due to economical environmental and human effects have led to significant consequences. Therefore, the safety of the newly designed and the old platforms should be more thoroughly assessed.

The reliability assessment method that has been developed is considered to be suited for safety assessments of platforms. In the traditional reliability assessment method, the resistance of the structure was considered as a constant during the design reference time. In actuality, as time passes the resistance of the structure decreases. The factors leading to resistance degradation of the jacket platforms are corrosion, fatigue, fractures, etc. Therefore, a reliability assessment method that considers degradation over time is highly desirable.

The reliability assessment considering the resistance changing with time is very complicated. Studies were done in 1975 about the reliability analysis of the structures under cumulative damage (Kameda and Koike, 1975). Studies performed in 1987 showed that the reliability analysis of the structure took into account that the resistance and the load effect both changed over time (Geidl and Saunders, 1987). Studies conducted in 1993 used the Monte Carlo method on the system reliability of the time-dependent structure (Mori and Ellingwood, 1993b). The reliability of the deterioration structure with the threshold crossing theory was studied in 1995 (Li, 1995).

Much research about the time-dependent reliability analysis method has been reported in the civil engineering area. To assess safety of the aging nuclear facilities, Ellingwood et al. (Braverman et al., 2004; Ciampoli and Ellingwood, 2002; Ellingwood and Mori, 1997; Mori and Ellingwood, 1993a; Naus et al., 1996; Takahashi and Ellingwood, 2005; Zheng and Ellingwood, 1998) have done a lot of original research on the time-dependent reliability analysis method of the structure. Stewart et al. (Stewart and Rosowsky, 1998; Stewart and Suo, 2009) studied the concrete beam corrossions and established the time-dependent reliability model.

Some research has also been done on ships and offshore structures, for example, Guedes Soares et al. (Guedes Soares and Dogliani, 2000; Guedes Soares and Garbatov, 1999; Guedes Soares and Ivanov, 1989; Ivanov, 2009; Mohd et al., 2014).

In 1997, P.H. Wirsching et al. conducted studies on the reliability with respect to ultimate strength of a corroding ship hull. In 2003, J.K. Paik et al. studied a time-dependent corrosion wastage model for bulk carrier structures. In 2003, Hai-Hong Sun and Yong Bai studied the time-variant reliability assessment of floating production storage and offloading hull girders. In 2010, Tuan-Hai Chen and Guo-Ming Chen studied the time-dependent reliability of aging platforms in ice zones.

Even though some research has been done, there still remain challenges in the application of time-dependent reliability analysis of structures. The research that has been conducted was focused mainly on ships but not as much on offshore platforms.

In this study, the time-dependent reliability assessment of offshore jacket platforms was performed and a proper time-dependent reliability model for jacket platforms was developed. The base shear capacity was chosen as the resistance of the jacket platform. A method of analyzing the initial resistance was presented. The corrosion wastage over time was considered for the degradation of the resistance. Loads considered were typhoon, including wind, wave, and current loads. The method for the probability model of the typhoon load effect was derived. The time variant reliability method was demonstrated in an application to an example platform.

46.2 The Time-Dependent Reliability Model for the Jacket Platform

The random process of a limit state function for a structure can be expressed as Eqn (46.1):

$$Z(t) = g[R(t), S(t)] = R(t) - S(t) \quad (46.1)$$

where $R(t)$ is the random process of the resistance of the structure, and $S(t)$ is the load effect random process of the structure.

The reliability of a structure is the probability that the structure completes the required functions under the designed time. Therefore, during the design reference time of the structure, the reliability of the structure can be expressed as Eqn (46.2):

$$P_s(T) = P\{Z(t) > 0, t \in [0, T]\} = P\{R(t) > S(t), t \in [0, T]\} \quad (46.2)$$

During the design reference time of the structure, the failure probability of the structure can be expressed by the complementary event of the structure reliable event in Eqn (46.3):

$$P_f(T) = 1 - P_s(T) = P\{R(t) < S(t), t \in [0, T]\} \quad (46.3)$$

Equation (46.3) means that the structure during the design reference time will fail as long as the resistance is less than the load effect in t_i .

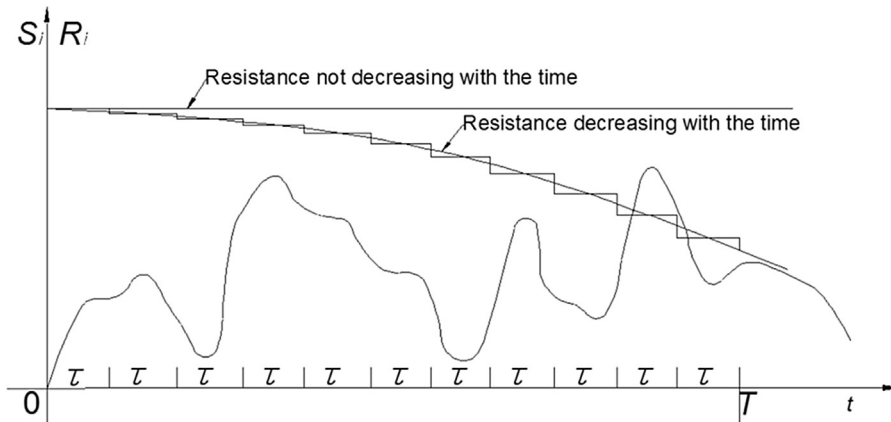


Figure 46.1

A schematic of the time-dependent reliability analysis method.

For the jacket platform, the base shear failure is a major structural mode, and has been studied in many published papers. The resistance of the jacket platform will decrease as time passes due to corrosion, fatigue, fractures, etc. For the load effect of the platform, different kinds of load combinations need to be considered during the assessment. In this study, the combination of wind, wave, and current loads was considered. The analysis methods of the resistance and load effect of the platform are given in [Sections 46.3 and 46.4](#).

According to [Eqn \(46.3\)](#), the failure probability of the structure during the design reference time can be expressed as [Eqn \(46.4\)](#):

$$P_f = P\{R(t) - S(t) < 0, t \in [0, T]\} = P\{\min[R(t) - S(t)] < 0, t \in [0, T]\} \quad (46.4)$$

If the degradation of the resistance is not considered, it can be set as $R(t) = R$, then [Eqn \(46.4\)](#) can be expressed as [Eqn \(46.5\)](#):

$$P_f(T) = P\{R - \max S(t) < 0, t \in [0, T]\} = P\{R - S_T < 0\} \quad (46.5)$$

$S_T = \max S(t), t \in [0, T]$ is the maximum random variable of $S(t)$ in the design reference time. [Equation \(46.6\)](#) can be used as the limit function of [Eqn \(46.5\)](#) to calculate the reliability:

$$Z = g(R, S_T) = R - S_T \quad (46.6)$$

To analyze the probability distribution function of S_T , the design reference time is divided into N equal segments, and then $\tau = T/N$ for every segment ([Figure 46.1](#)). Through analysis, the probability distribution function $F_{S_i}(x)$ of the max load effect S_i for τ can be determined. If it is assumed that every S_i is independent, according to the theory of extreme value statistics, the probability distribution function of S_T in the design reference time can be expressed as [Eqn \(46.7\)](#):

$$F_{S_T}(x) = [F_{S_i}(x)]^N \quad (46.7)$$

If S_i obeys the extreme value type I distribution, its probability distribution function can be expressed as Eqn (46.8):

$$F_{S_\tau}(x) = \exp\{-\exp[-\alpha(x-u)]\} \quad (46.8)$$

Then, S_T will also obey the extreme value type I distribution, and the parameter α and u can be changed to:

$$\begin{aligned} \alpha_T &= \alpha \\ u_T &= u + \frac{\ln N}{\alpha_T} \end{aligned} \quad (46.9)$$

The above equations consider that the resistance of the structure will not change with time. If R is a time variant variable, the method above will not be appropriate. The following sections will present the reliability assessment method of the structure with resistance changing with time.

According to Eqn (46.4), both $R(t)$ and $S(t)$ are divided into N equal segments in the reference design time (Figure 46.1), and the failure probability of the structure can be expressed as:

$$\begin{aligned} P_f(T) &= P\{\min[R(t_i) - S(t_i)] < 0, t_i = i\tau, i = 1, 2, \dots, N\} \\ &= P\left\{\bigcup_{i=1}^N [R(t_i) - S(t_i) < 0], t_i = i\tau\right\} \\ &= P\left\{\bigcup_{i=1}^N [R_i - S_i < 0]\right\} \end{aligned} \quad (46.10)$$

where $R(t_i)$ is the resistance value of the i -th time segment, $S(t_i)$ is the extreme load value in the i -th time segment, and τ is the duration of every time segment.

Equation (46.10) is used to solve the reliability of the N parts series systems. Assuming that every S_i is independent, Eqn (46.10) can be expressed as Eqn (46.11).

$$\begin{aligned} P_f(T) &= 1 - P\left\{\prod_{i=1}^N [R_i - S_i \geq 0]\right\} \\ &= 1 - P\left\{\prod_{i=1}^N [S_i \leq R_i]\right\} \\ &= 1 - P\left\{\prod_{i=1}^N [S_i \leq r_i | R_1 = r_1, R_2 = r_2, \dots, R_N = r_N]\right\} \times P[R_1 = r_1, R_2 = r_2, \dots, R_N = r_N] \\ &= 1 - \int_0^{+\infty} \int_0^{+\infty} \dots \int_0^{+\infty} \prod_{i=1}^N F_{S_\tau}(r_i) \cdot f_{R_1, R_2, \dots, R_N}(r_1, r_2, \dots, r_N) dr_1 dr_2 \dots dr_N \end{aligned} \quad (46.11)$$

where $f_{R_1, R_2, \dots, R_N}(r_1, r_2, \dots, r_N)$ is the joint probability density function of R_1, R_2, \dots, R_N , $F_{S_i}(\cdot)$, which is the probability distribution function of S_i .

A new random variable is defined here: S' . Its probability density function is $f_{S'}(s')$, and its probability distribution function is $F_{S'}(s')$, Eqn (46.11) can then be expressed as Eqn (46.12):

$$\begin{aligned}
 P_f(T) &= 1 - \int_0^{+\infty} \int_0^{+\infty} \dots \int_0^{+\infty} \int_0^{s' < F_{S'}^{-1} \left[\prod_{i=1}^N F_{S_\tau}(r_i) \right]} F_{S_\tau}(r_i) \cdot f_{R_1, R_2, \dots, R_N}(r_1, r_2, \dots, r_N) ds' dr_1 dr_2 \dots dr_N \\
 &= 1 - P \left\{ S' - F_{S'}^{-1} \left[\prod_{i=1}^N F_{S_\tau}(r_i) \right] < 0 \right\} \\
 &= P[g(R_1, R_2, \dots, R_N, S') < 0]
 \end{aligned} \tag{46.12}$$

where $F_{S'}^{-1}(\cdot)$ is the inverse function of $F_{S'}(\cdot)$, and Eqn (46.13) is:

$$g(R_1, R_2, \dots, R_N, S') = F_{S'}^{-1} \left[\prod_{i=1}^N F_{S_\tau}(R_i) \right] - S' = F_{S'}^{-1} \left[\prod_{i=1}^N F_{S_\tau}(R_0 \cdot \varphi_i) \right] - S' \tag{46.13}$$

where R_0 is the initial resistance, φ is the degradation rule of the resistance, which is obtained through analysis, and φ_i is the value corresponding to the specific time.

When the random variable S' is introduced, the high dimensional integral expressed by Eqn (46.11) can be expressed by Eqn (46.13) and then the conventional reliability method can be used to solve this function.

The reliability result of Eqn (46.13) has no relationship with the probability distribution type of S' , then the probability distribution type can be assumed as a normal distribution, and Eqn (46.13) can be solved using the Monte Carlo method.

When analyzing the reliability of the offshore structure, if the load effect S_T can be considered to obey the extreme value type I distribution, it can be assumed:

$$g(R_1, R_2, \dots, R_N, S') = F_{S_T}^{-1} \left\{ \prod_{i=1}^N [F_{S_\tau}(R_i)]^{1/N} \right\} - S_T \tag{46.14}$$

where:

$$S = F_{S_T}^{-1} \left\{ \prod_{i=1}^N [F_{S_\tau}(R_i)]^{1/N} \right\} \tag{46.15}$$

$$F_{S_T}(S) = \prod_{i=1}^N [F_{S_\tau}(R_i)]^{1/N} \tag{46.16}$$

The probability distribution function of the extreme value type I can be used to express Eqn (46.16) as the following equation:

$$F_{S_T}(S) = \exp\{-\exp[-\alpha_T(S - u_T)]\} = \exp\left\{-\frac{1}{N}\sum_{i=1}^N \exp[-\alpha_T(R_i - u_T)]\right\} \quad (46.17)$$

Then:

$$S = -\frac{1}{\alpha_T} \ln\left[\frac{1}{N}\sum_{i=1}^N \exp(-\alpha_T R_i)\right] \quad (46.18)$$

If Eqn (46.18) is put into Eqn (46.14), then the reliability analysis function Eqn (46.19) can be found showing that the resistance decreases with time and S_T obeys the extreme value type I distribution.

$$\begin{aligned} g(R_1, R_2, \dots, R_N, S') &= -\frac{1}{\alpha_T} \ln\left[\frac{1}{N}\sum_{i=1}^N \exp(-\alpha_T R_i)\right] - S_T \\ &= -\frac{1}{\alpha_T} \ln\left[\frac{1}{N}\sum_{i=1}^N \exp(-\alpha_T R_0 \cdot \varphi_i)\right] - S_T \end{aligned} \quad (46.19)$$

Equation (46.19) can be analyzed using the FOSM (first order second moment) method.

46.3 Probability Model for Resistance of the Jacket Platform

The ultimate strength of the global structure is an important part of the reliability assessment of a jacket platform. In this study, the resistance of the jacket platform was represented by the global ultimate strength, which was represented by the base shear capacity while other failure modes were ignored. Base shear capacity can be calculated through the finite element method. The base shear capacity of the primary jacket platform structure will decrease as times goes on for various reasons such as corrosion, fatigue, etc.

In the present study, the effects of corrosion on the structural base shear capacity were taken into account to assess the reliability of the jacket platform. Figure 46.2 gives the process of reliability analysis of the jacket platform considering corrosion.

46.3.1 Base Shear Capacity

In this study, the ANSYS multiphysics module was used to represent the finite element (FE) model of the jacket platform. Several element types (pipe20, pipe59, beam4, and shell43) were used to model different types of structural members. The base shear capacity of the jacket platform is defined as the base shear force of the jacket platform when the displacement of the platform structure at the sea level equals 1% of the water depth.

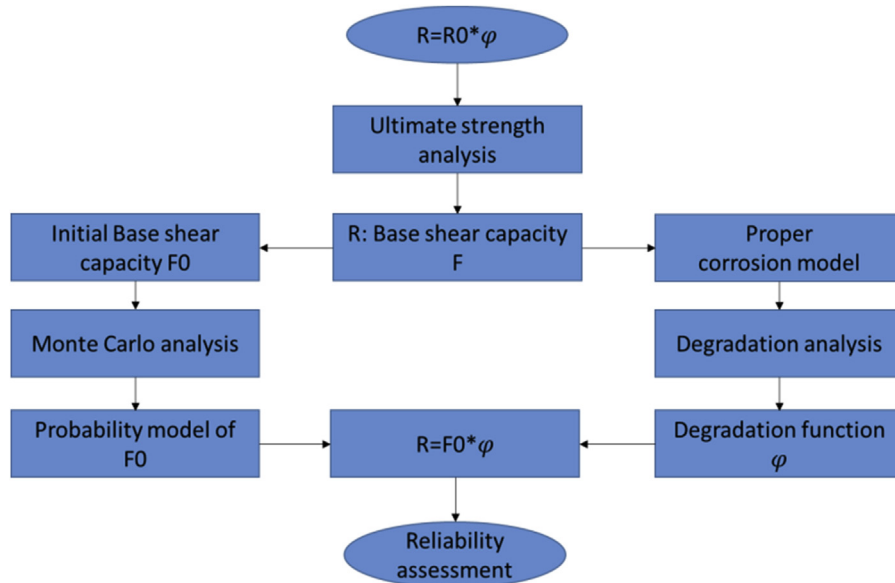


Figure 46.2

The process of reliability analysis of the jacket platform considering corrosion.

46.3.2 Probability Model of the Initial Base Shear Capacity

The platform base shear capacity is a function of many parameters, including diameters and thicknesses of different members, modulus of elasticity, strengths of different materials, etc. All these parameters are random variables, so the platform base shear capacity will be also a random variable and have its probability model. For large amounts of existing parameters, this function is not easily found. Therefore, to get the probability model of the platform base shear capacity, other ways should be used.

The PDS module of the ANSYS software can realize the analysis of the probability model of the platform base shear capacity. The process of the PDS analysis is a Monte Carlo process. For the analysis process of the jacket platform, the FE model of the platform can first be established so that the front part can be used to get the base shear capacity and then the data file should be saved. Then we can enter the PDS module, set the probability characteristics (distribution type and distribution parameters) of the input parameters, appoint the output parameter, choose the analysis method, and find the solution. Finally, the probability characteristics of the platform base shear capacity can be acquired from the output report of the PDS module. [Figure 46.3](#) gives the analysis process. In the PDS module, many kinds of probability distribution can be chosen for the input parameter and two sampling methods (directly sampling and Latin hypercube sampling) can be chosen for the Monte Carlo analysis.

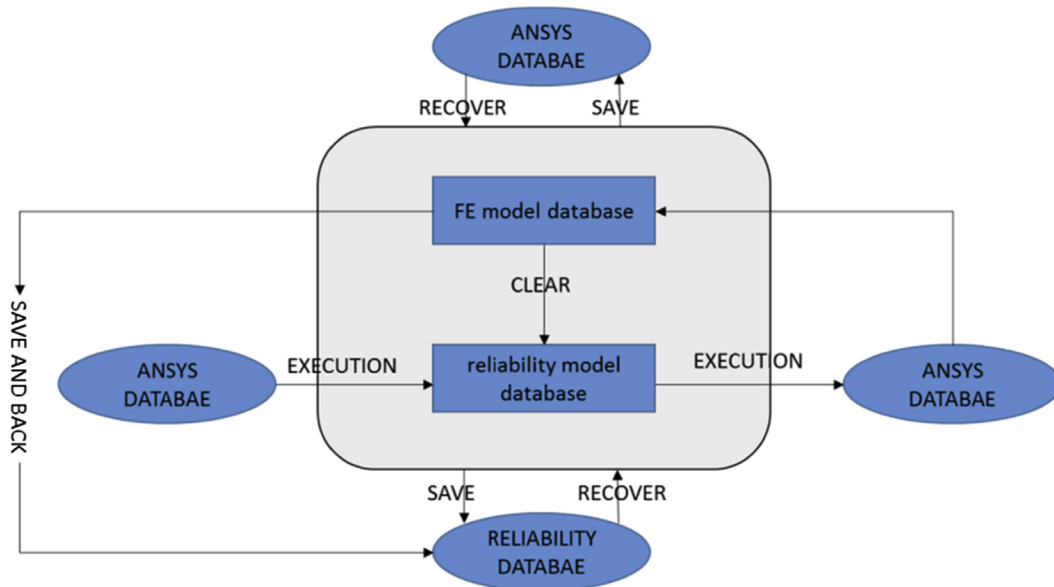


Figure 46.3
ANSYS PDS analysis process.

46.3.3 Degradation of the Base Shear Capacity under Corrosion Effect

In this study, only uniform corrosion was considered, which will result in thickness reduction.

Corrosion Model

In the present study, a nonlinear corrosion model was considered for the platform.

The corrosion protection system (CPS) was considered in the present corrosion model. In the model, the process of the CPS failure is a gradual process, and the corrosion starts before the total failure of the CPS. In addition, by taking into consideration the corrosion thickness and microorganism growth, the corrosion rate increases progressively until it reaches the highest value and then it will decrease gradually. Therefore, for a CPS, there are two parameters (T_{st}, T_{cl}), which can be used to describe its efficiency. T_{st} is the start time of the corrosion, and T_{cl} is the lifetime of the CPS, and both can be acquired from the test. Therefore, the whole corrosion progress is divided into three parts:

1. No corrosion, $t \in [0, T_{st}]$.
2. Corrosion acceleration, $t \in [T_{st}, T_A]$.
3. Corrosion rate slowing down, $t \in [T_A, T_L]$.

where T_L is the assessing time for the platform, and T_A is the time to max corrosion rate, and to simplify, $T_A = T_{cl}$.

The Weibull formulation was used to describe the corrosion rate:

$$r(t) = \begin{cases} 0 & 0 \leq t < T_{ST} \\ d \frac{\beta}{\eta} \left(\frac{t - T_{ST}}{\eta} \right)^{\beta-1} \exp \left[- \left(\frac{t - T_{ST}}{\eta} \right)^{\beta} \right] & T_{ST} \leq t \leq T_L \end{cases} \quad (46.20)$$

The corrosion wastage can be described as:

$$d(t) = \begin{cases} 0 & 0 \leq t < T_{ST} \\ d \left\{ 1 - \exp \left[- \left(\frac{t - T_{ST}}{\eta} \right)^{\beta} \right] \right\} & T_{ST} \leq t \leq T_L \end{cases} \quad (46.21)$$

where d , β , η , T_{st} are the four parameters that need to be determined. Figures 46.4–46.7 are the parameter analyses for the corrosion model, and different scales of the parameter show different shapes of the corrosion rate model.

Figure 46.4 shows effects of d on the corrosion rate. It can be found that larger d means larger corrosion rate every year. In actuality, d represents the final corrosion thickness of the structure.

Figure 46.5 shows effects of T_{st} on the corrosion rate. It shows that T_{st} only has an effect at the starting point of the corrosion, and larger T_{st} means that the corrosion will start later.

Figure 46.6 shows effects of β on the corrosion rate. When $\beta \leq 1$, the corrosion rate will start with a large value and then go down to zero year by year, but this does not meet the

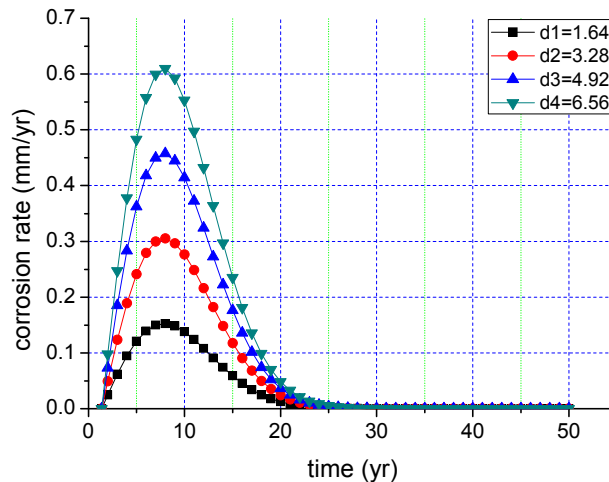


Figure 46.4

The effect of d on the corrosion rate ($T_{st} = 1.38$, $\beta = 1.99$, $\eta = 9.19$).

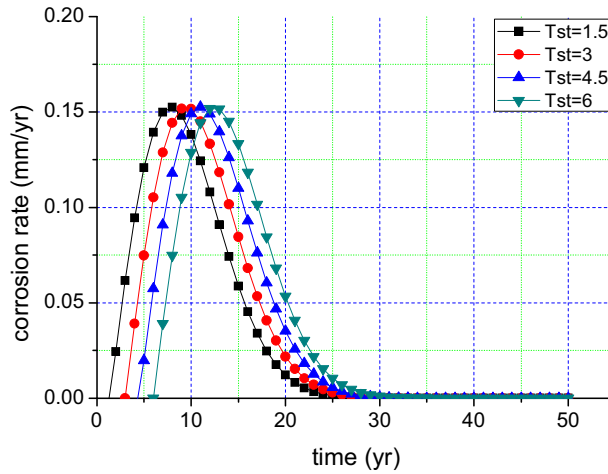


Figure 46.5

The effect of T_{st} on the corrosion rate ($d = 1.64$, $\eta = 9.19$, $\beta = 1.99$).

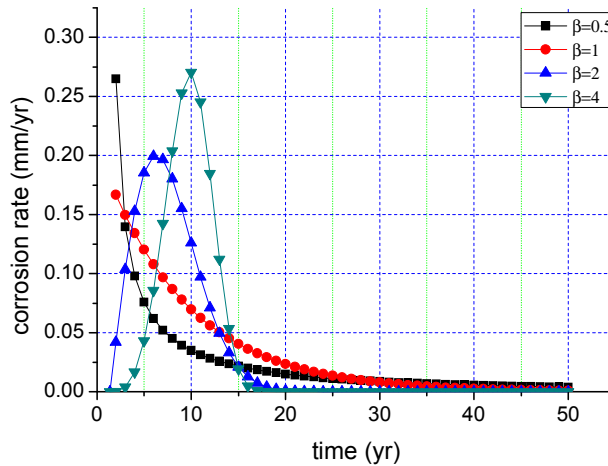


Figure 46.6

The effect of β on the corrosion rate ($d = 1.64$, $T_{st} = 1.38$, $\eta = 9.19$).

actual condition, so β should be larger than 1. When $\beta > 1$, the larger β is, the corrosion will happen in fewer years, and the corrosion rate in the early years is smaller.

Figure 46.7 shows effects of η on the corrosion rate. It shows smaller η means that corrosion happens in fewer years and that the corrosion rate in these years will be larger, and the corrosion rate in the early years is rapid.

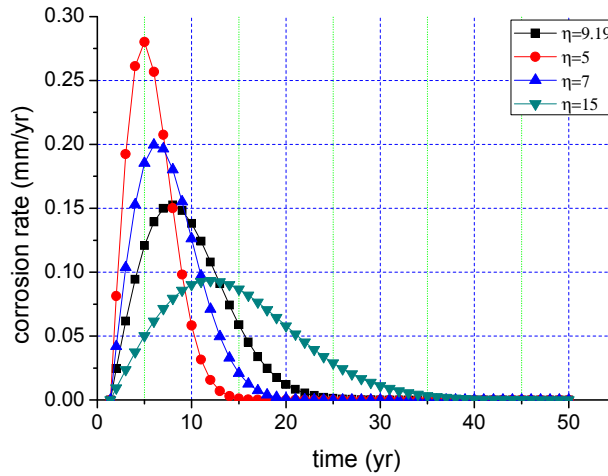


Figure 46.7

The effect of η on the corrosion rate ($d = 1.64$, $T_{st} = 1.38$, $\beta = 1.99$).

A group of parameters was chosen for the corrosion model in this study. The corrosion wastage equation is as follows:

$$d(t) = \begin{cases} 0 & 0 \leq t < 1.38 \\ 1.64 \left\{ 1 - \exp \left[- \left(\frac{t - 1.38}{9.19} \right)^{1.99} \right] \right\} & 1.38 \leq t \leq T_L \end{cases} \quad (46.22)$$

Figure 46.8 gives a brief showing of the corrosion model.

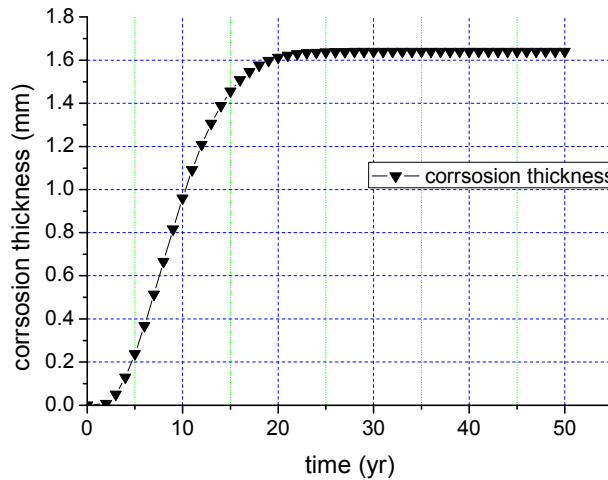


Figure 46.8

Corrosion wastage of the chosen corrosion model.

Corrosion Effect on the Base Shear Capacity

Generally, corrosion rates of different areas of the platform are different. For a typical jacket platform, the corrosion zone can be divided into three parts: atmospheric zone, splash zone, and full immersion zone. Usually, the order of the corrosion rate, from largest to smallest, is the splash zone, full immersion zone, then atmospheric zone. The atmospheric zone mainly affects the upper module, and the other two zones affect the jacket module, which is more important to the safety of the whole platform. Figure 46.9 shows the different corrosion zones of the platform.

For accurate assessment, all the corrosion zones should be assessed separately. To simplify this study and to analyze the method, only the jacket part corrosions were considered and the corrosion rates were set to be same in the splash zone and the immersion zone. According to the proper corrosion model, the diameter and thickness of every member of the jacket had a reduction every year, and according to the reduction member, every year's base shear capacity was calculated through the FE method. An equation was then chosen to describe the degradation rule of the platform base shear capacity.

46.4 Probability Model for Load Effect of the Jacket Platform

Environment loads are site dependent, for example, the ice load is considered if a platform is located in the Bohai Sea of China, but does not need to be considered in the South China Sea. Therefore, the load condition should be chosen properly according to the working area. In this study, typhoon load in the South China Sea was considered.

46.4.1 Parameter Probability Models of Typhoon Load

Typhoons are common in the South China Sea. According to [Chen and Chen \(2010\)](#), the extreme values of the wind, wave, and current parameters for typhoons in the South China Sea can be fitted by three Weibull extreme distribution parameters.

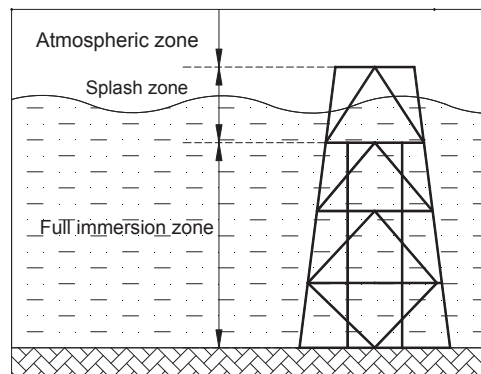


Figure 46.9

Different corrosion zones of the platform.

The wind parameter is represented by $v_{10\min}$ (the average speed in 10 min in the interest area), and the distribution function is:

$$F(v_{10\min}) = 1 - \exp \left[- \left(\frac{v_{10\min} - 28.4}{10.311} \right)^{2.625} \right] \quad (46.23)$$

The wave parameter is represented by h_s (the significant wave height), and the distribution function is:

$$F(h_s) = 1 - \exp \left[- \left(\frac{h_s - 7.6}{2.723} \right)^{2.067} \right] \quad (46.24)$$

The current parameter is represented by v_{\max} (the maximum current speed), and the distribution function is:

$$F(v_{\max}) = 1 - \exp \left[- \left(\frac{v_{\max} - 1.44}{0.374} \right)^{1.812} \right] \quad (46.25)$$

46.4.2 Load Effect of the Jacket Platform under Typhoon Load

As discussed, the load effect is the base shear force caused by the typhoon load. The separate load affects (base shear capacity) can be expressed as functions of wave, current, and wind as the following.

$$F = A \cdot H + B \cdot H^2 \quad (46.26)$$

where F is the wave load effect, H is the wave height, and A and B are the fitting factors.

$$F = C \cdot V_c^2 \quad (46.27)$$

where F is the current load effect, V_c is the current speed, and C is the fitting factor.

$$F = A_w \cdot V_{wind}^2 \quad (46.28)$$

where F is the wind load effect, V_{wind} is the wind speed, and A_w is the associated with the windward area (if the unit of the windward area is m^2 , $A_w = \text{area} \cdot 0.001$, and the unit of F is MN).

The wave and current loads mainly affect the immersion zone structure of the platform, and will show a mutual effect on the base shear force. Therefore, it is better to take the two parameters into consideration simultaneously, and the fitting function of wave and current load is as follows:

$$F = A + B \cdot H + C \cdot V_c + D \cdot H \cdot V_c + E \cdot H^2 + F \cdot V_c^2 \quad (46.29)$$

where F is the base shear force; H is the wave height; V_c is the current speed; and A , B , C , D , E , and F are the fitting factors.

As the wind load mainly affects the upper structure of the platform, the wind load effect can be analyzed separately.

According to the above analysis, the load effect fitting function can be as follows:

$$F = A + B \cdot H + C \cdot V_c + D \cdot H \cdot V_c + E \cdot H^2 + F \cdot V_c^2 + A_w \cdot V_{wind}^2 \quad (46.30)$$

Generally, eight directions of typhoon load effects should be considered to find the most dangerous load conditions. In this study, for simplicity, only one typical direction was chosen to do the analysis. The ANSYS multiphysics module was used to conduct the typhoon load analysis under different load parameters.

46.4.3 The Probability Model of the Load Effect

In this study, the Monte Carlo method was used to analyze the probability of the load effect. The process can be as the following steps:

- Select the parameters of the wind, wave, and current, and get a group of random variables;
- Put the random values into the load effect function, and gather a group of values;
- Use the statistical method to analyze the load effect values found by step 2, and find the probability model of the load effect.

46.5 Time-Dependent Reliability Assessment

46.5.1 The Example Platform

Figure 46.10 shows the example platform. Table 46.1 lists the geometric parameters of the example platform. Table 46.2 lists the material parameters of the example platform.

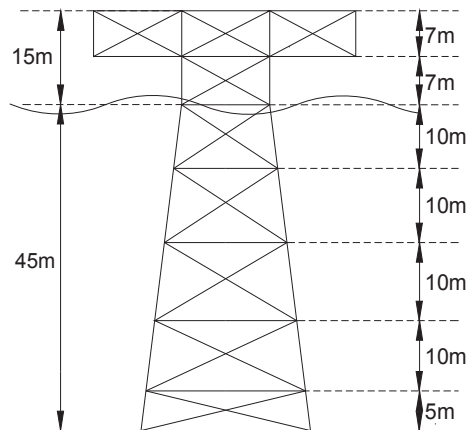


Figure 46.10
The example platform.

Table 46.1: Geometric parameters of the example platform (m)

Number	Name	Diameter	Thickness	
1	Main tubular of the jacket	1.2	0.016	
2	Main tubular of the deck, lateral bracing of the jacket	0.78	0.012	
3	Diagonal bracing of the jacket	0.508	0.01	
4	Beam of the deck	Area	Section length	Section width
		0.4 * 0.4	0.4	0.4
5	Plate of the deck	Thickness	Length	Width
		0.025	30	20

Table 46.2: Material parameters of the example platform

Modulus of Elasticity	Poisson's Ratio	Steel Density	Steel Yield Strength
2.0E5 MPa	0.3	7850 kg/m ³	235 Mpa

46.5.2 Probability Model for Resistance of the Jacket Platform

FE Model and the Base Shear Capacity of the Example Jacket Platform

Figure 46.11 shows the FE model of the considered platform. According to the theory introduced in Section 46.3.1, pipe 59 and pipe 20 elements were used to model the tubular members, beam 4 elements were used to model the deck beam members, and shell 43 was used to model the deck plates. In order to save the analysis time, the pipe and soil relationship was not considered. When analyzing the base shear capacity, nodes at the platform base were coupled and one of these nodes was fixed. Incremental displacement loads were given to nodes at the sea level. When the sea level nodes displacement equaled 0.5 m (about 1% of the water depth), the reaction force of the fixed node was chosen to represent the base shear capacity (Figure 46.12).

Probability Model of the Initial Base Shear Capacity

Eleven parameters of the platform structure were chosen as random variables, and probability models of these parameters are listed in Table 46.3 (the distribution type and COV of these parameters are based on assumptions).

Statistical parameters of the analysis results are listed in Table 46.4, and the probability density function of the initial base shear capacity is given as Eqn (46.30).

$$f(x) = \frac{1}{1.028 \cdot \sqrt{2\pi}} \cdot \exp \left[-\frac{(x - 8.692)^2}{2 \times 1.028^2} \right] \quad (46.31)$$

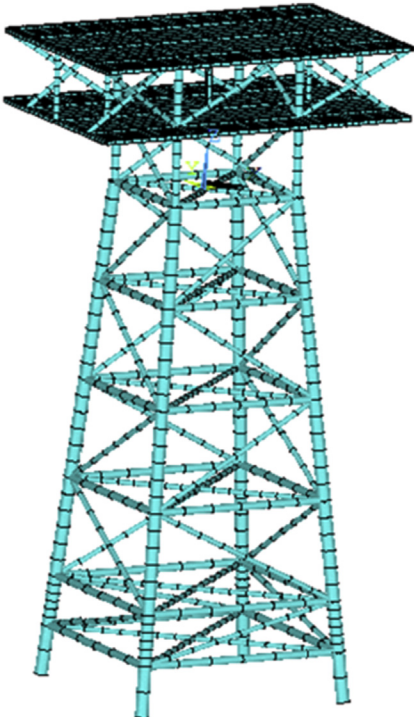


Figure 46.11
The FE model of the example platform.

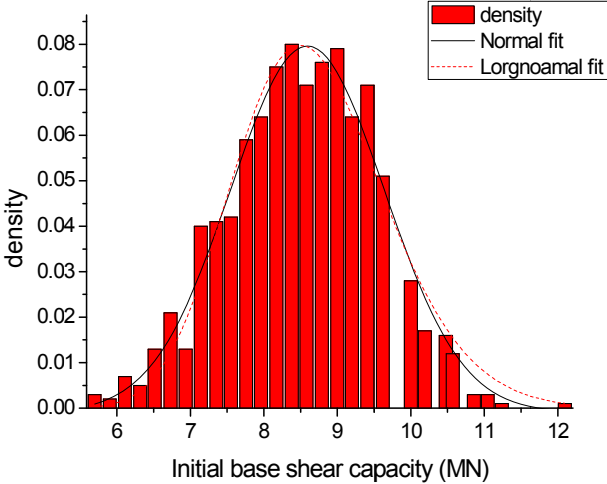


Figure 46.12
Statistical results of the initial base shear capacity.

Table 46.3: Probability models of the selected parameters

No.	Name	Distribution Type	μ	COV
1	Diameter1	Normal	1.2 m	0.02
2	Thickness1	Normal	0.016 m	0.02
3	Diameter2	Normal	0.78 m	0.02
4	Thickness2	Normal	0.012 m	0.02
5	Diameter3	Normal	0.508 m	0.02
6	Thickness3	Normal	0.01 m	0.02
7	Thickness4	Normal	0.4 m	0.02
8	Thickness5	Normal	2.5E-2 m	0.02
9	E	Normal	2.0E5 Mpa	0.08
10	Density	Uniform	MIN 3925 kg/m ³	MAX 11775 kg/m ³
11	Buckling strength	Lognormal	235 Mpa	0.15

Table 46.4: Statistical analysis parameters of the initial base shear capacity (MN)

Name	Mean	Standard Deviation	Min	Max
F0	8.692	1.028	5.697	12.095

Degradation of the Base Shear Capacity under Corrosion Effect

According to the chosen corrosion model in [Section Corrosion Model](#), the degradation of the base shear capacity of the example platform was studied. [Figure 46.13](#) shows the results. F_i represents the actual base shear capacity at year i , and F_0 represents the initial base shear capacity of the platform. F_i/F_0 shows the degradation of the base shear capacity.

The corrosion starts between the second year, so a piecewise function is used to fit the data and the fitting results make a good approximation (R -square = 0.99,999). The fitting equation is as follows:

$$\varphi = \begin{cases} 1 & 0 \leq t < 1.38 \\ 1 - 0.105 \left\{ 1 - \exp \left[- \left(\frac{t - 1.38}{9.19} \right)^{1.99} \right] \right\} & 1.38 \leq t \leq 50 \end{cases} \quad (46.32)$$

46.5.3 Probability Model for Load Effect of the Jacket Platform

According to the method mentioned in [Section 46.4.2](#), the load effect of the platform under the coaction of wave and current was studied. Six parameters were chosen separately for the wave and current conditions, and according to these data, 36 values of

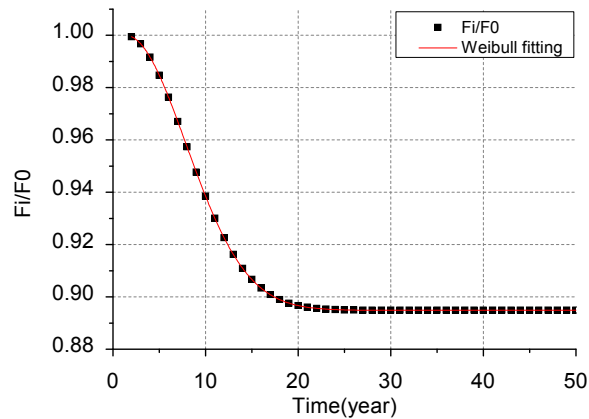


Figure 46.13

Degradation function of the base shear capacity.

the base shear forces of the platform were calculated utilizing the platform model. These data are listed in [Table 46.5](#).

According to the data in [Table 46.5](#), the surface fitting method was used to obtain the load effect function for the coaction of wave and current loads. [Equation \(46.28\)](#) mentioned in [Section 46.4.2](#) was used for the fitting. [Figure 46.14](#) plots the data in [Table 46.5](#), and [Figure 46.15](#) shows the fitting surface of the load effect equation. [Table 46.6](#) lists coefficient values of the fitting equation.

After obtaining the load effect equation of the wave and current loads, the load effect equation of wind was considered. The windward area of the considered platform is 139 m^2 ($A_w = 0.139$), and the load effect equation of the wind is $F = 0.139 \cdot V_{wind}^2$.

Then, the total load effect of the typhoon load is as follows:

$$F = 1.6142 - 0.3186H - 0.424V_c + 0.0248H^2 + 0.1476V_c^2 + 0.0975H \cdot V_c + 0.139V_w^2 \quad (46.33)$$

Table 46.5: Parameter values of the wave and current, and the corresponding load effect values (base shear force (MN))

Wave Height, m (Period)	Current Speed (m/s)					
	1.23	1.81	2.01	2.20	2.33	2.43
7.6 (9.6 s)	1.229	1.683	1.861	2.041	2.171	2.274
10.2 (11.0 s)	1.889	2.470	2.695	2.919	3.078	3.204
11.1 (11.6 s)	2.179	2.813	3.056	3.297	3.468	3.603
12.1 (12.3 s)	2.546	3.242	3.5.5	3.766	3.951	4.096
12.7 (12.8 s)	2.798	3.532	3.810	4.085	4.279	4.431
13.3 (13.2 s)	3.057	3.832	4.121	4.407	4.609	4.769

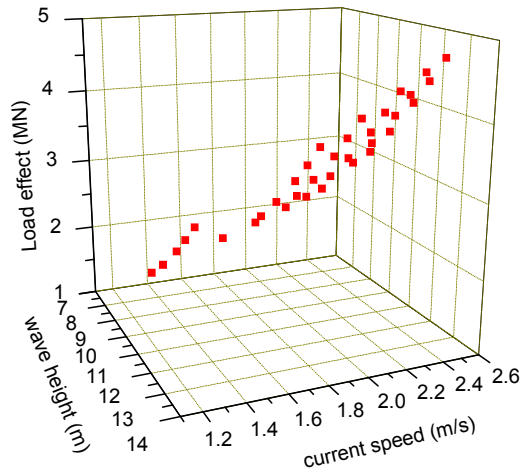


Figure 46.14

Load effect data of the platform under wave and current conditions.

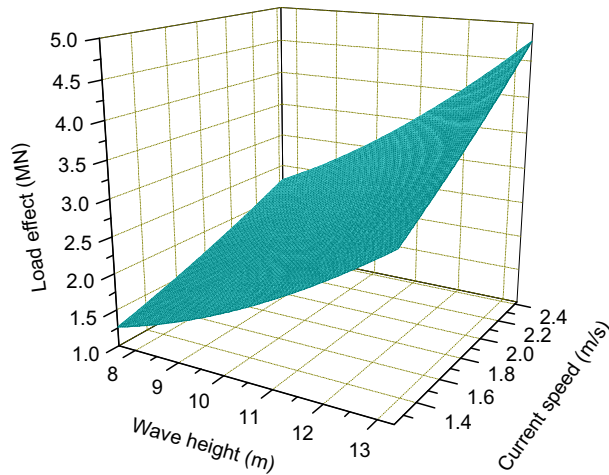


Figure 46.15

Load effect fitting surface of the platform under wave and current conditions.

Table 46.6: Fitting equation of the load effect for wave and current load (unit: MN)

Equation	$F = z_0 + a \cdot x + b \cdot y + c \cdot x^2 + d \cdot y^2 + f \cdot xy$					
Adj. R-square	0.99996					
Name	z_0	a	b	c	d	f
Value	1.6142	-0.3186	-0.4240	0.0248	0.1476	0.0975

Note: x is the wave height, and y is the current speed.

where H is the wave height, V_c is the current speed, V_w is the wind speed, and the unit of F is MN.

According to the probability model (Eqns (46.22–46.24)) of the wave, current, and wind, the probability model of typhoon load effect was studied through the Monte Carlo method mentioned in Section 46.4.3. Figure 46.16 shows the comparison of different probability models fitted for the load effect, and it shows that the generalized extreme value model is the most appropriate model for the load effect of typhoons.

The probability distribution function of the load effect is as follows:

$$F(x) = \exp \left\{ - \left[1 - 0.0267671 \left(\frac{x - 3.65582}{0.412429} \right) \right]^{1/0.0267671} \right\} \quad (46.34)$$

46.5.4 Time-Dependent Reliability Assessment Results of the Platform

According to probability models of the resistance and the load effect given in Sections 46.5.2 and 46.5.3, the time-dependent reliability analysis method introduced in Section 46.2 was used to do the analysis of the platform. The reliability of the platform that did not consider the resistance degradation was also analyzed to do the comparison, and different design reference times (25, 50, 75, 100 years) were also studied. Table 46.7 lists the analysis results, and Figure 46.17 gives a direct view of the comparison.

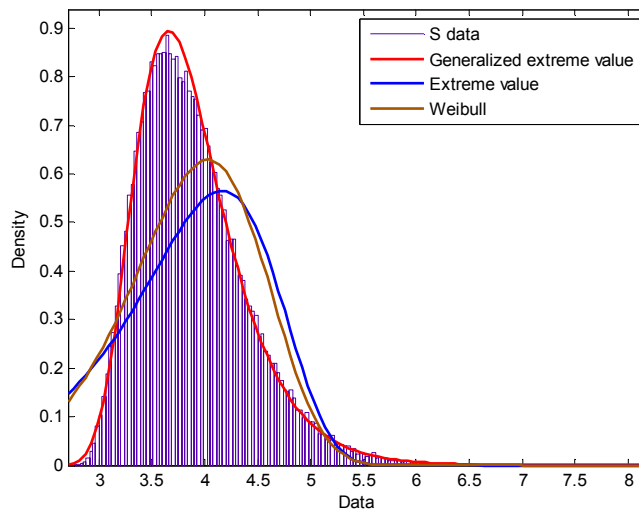


Figure 46.16
Different probability models fitting for the load effect.

Table 46.7: Analysis results of the considering platform

R0 = 8.692 MPa	25 years		50 years		75 years		100 years	
	β	P_f	β	P_f	β	P_f	β	P_f
Time-dependent reliability	2.5865	4.80e-3	2.2937	1.09e-2	2.1503	1.58e-2	2.0484	2.03e-2
Traditional reliability	2.9725	1.50e-3	2.8049	2.50e-3	2.6843	3.60e-3	2.6028	4.60e-3

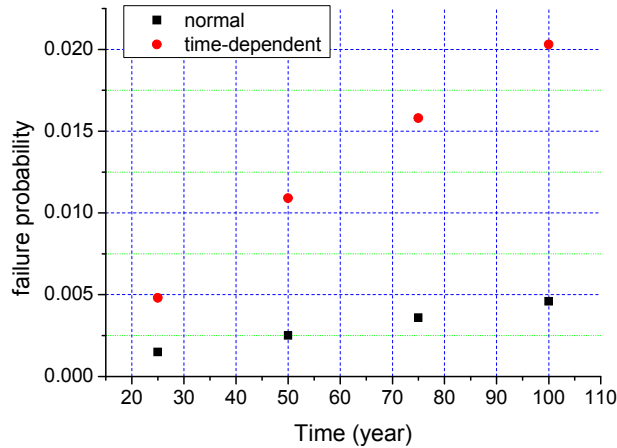


Figure 46.17

Failure probability comparison of the two conditions for different design reference times.

According to Table 46.7 and Figure 46.17, the failure probability of using the time-dependent reliability analysis method, which considered the resistance degradation, is much larger than that of using the traditional reliability method, which does not consider the resistance degradation.

46.6 Conclusion

Compared to the traditional reliability method, the time-dependent reliability analysis method is better suited for safety assessments of the jacket platform.

A time-dependent reliability assessment of a jacket platform was presented with three aspects: (1) the time-dependent reliability analysis model; (2) the ultimate limit capacity of the platform and its probability model; and (3) the load effect of the platform and its probability model.

A time-dependent reliability assessment model was presented. In the model, the resistance and the load effect of the structure were divided into N segments separately in the assessing period, and through the progress of mathematical transformation, the problem of time-dependent reliability analysis was changed to the traditional reliability analysis.

The base shear capacity due to corrosion was considered. A method of analyzing the probability model of the initial base shear capacity based on the ANSYS PDS method was also presented.

The load effect of the platform under typhoon load was studied. A method of analyzing the probability model of the typhoon load effect based on the FE method and the Monte Carlo method was presented.

The time-dependent reliability assessment of the example platform shows a specific assessment progress of the method with results that represent the time-dependent reliability analysis method being more severe than that of the traditional reliability analysis method.

References

- Braverman, J., Miller, C., Hofmayer, C., Ellingwood, B., Naus, D., Chang, T., 2004. Degradation assessment of structures and passive components at nuclear power plants. *Nuclear Engineering and Design* 228, 283–304.
- Chen, T., Chen, G., 2010. Time-dependent reliability of ageing platforms in ice zone. *Proceedings of the Proceedings of the 20th International Offshore and Polar Engineering Conference*.
- Ciampoli, M., Ellingwood, B., 2002. Probabilistic methods for assessing current and future performance of concrete structures in nuclear power plants. *Materials and Structures* 35, 3–14.
- Ellingwood, B.R., Mori, Y., 1997. Reliability-based service life assessment of concrete structures in nuclear power plants: optimum inspection and repair. *Nuclear Engineering and Design* 175, 247–258.
- Geidl, V., Saunders, S., 1987. Calculation of reliability for time-varying loads and resistances. *Structural Safety* 4, 285–292.
- Guedes Soares, C., Dogliani, M., 2000. Probabilistic modelling of time-varying still-water load effects in tankers. *Marine Structures* 13, 129–143.
- Guedes Soares, C., Garbatov, Y., 1999. Reliability of corrosion protected and maintained ship hulls subjected to corrosion and fatigue. *Journal of Ship Research* 43, 65–78.
- Guedes Soares, C., Ivanov, L., 1989. Time-dependent reliability of the primary ship structure. *Reliability Engineering & System Safety* 26, 59–71.
- Ivanov, L.D., 2009. Challenges and possible solutions of the time-variant reliability of ship's hull girder. *Ships and Offshore Structures* 4, 215–228.
- Kameda, H., Koike, T., 1975. Reliability theory of deteriorating structures. *Journal of the Structural Division* 101.
- Li, C., 1995. A case study on the reliability analysis of deteriorating structures. In: *Proceedings of the ICE-Structures and Buildings* 110, 269–277.
- Mohd, M.H., Kim, D.K., Kim, D.W., Paik, J.K., 2014. A time-variant corrosion wastage model for subsea gas pipelines. *Ships and Offshore Structures* 9, 161–176.
- Mori, Y., Ellingwood, B.R., 1993a. Reliability-based service-life assessment of aging concrete structures. *Journal of Structural Engineering* 119, 1600–1621.
- Mori, Y., Ellingwood, B.R., 1993b. Time-dependent system reliability analysis by adaptive importance sampling. *Structural Safety* 12, 59–73.
- Naus, D., Oland, C., Ellingwood, B., Graves III, H., Norris, W., 1996. Aging management of containment structures in nuclear power plants. *Nuclear Engineering and Design* 166, 367–379.
- Paik, J.K., Lee, J.M., Park, Y.I., Hwang, J.S., Kim, C.W., 2003. Time-variant ultimate longitudinal strength of corroded bulk carriers. *Marine Structures* 16, 567–600.

- Stewart, M.G., Rosowsky, D.V., 1998. Time-dependent reliability of deteriorating reinforced concrete bridge decks. *Structural Safety* 20, 91–109.
- Stewart, M.G., Suo, Q., 2009. Extent of spatially variable corrosion damage as an indicator of strength and time-dependent reliability of RC beams. *Engineering Structures* 31, 198–207.
- Sun, H.-H., Bai, Y., 2003. Time-variant reliability assessment of FPSO hull girders. *Marine Structures* 16, 219–253.
- Takahashi, T., Ellingwood, B.R., 2005. Reliability-based assessment of roofs in Japan subjected to extreme snows: incorporation of site-specific data. *Engineering Structures* 27, 89–95.
- Wirsching, P.H., Ferencic, J., Thayamballi, A., 1997. Reliability with respect to ultimate strength of a corroding ship hull. *Marine Structures* 10, 501–518.
- Zheng, R., Ellingwood, B.R., 1998. Role of non-destructive evaluation in time-dependent reliability analysis. *Structural Safety* 20, 325–339.

Reassessment of Jacket Structure

47.1 General

A number of offshore platforms operating in the years were built with the outdated criteria and these platforms have a higher probability to be weaker to the higher wave height or faster current speed of the updated environmental factors and criteria. Corrosion will still occur even if new facilities are added on the topside of the platform. This will change the function of the structure. If at least one of these situations takes place, the reassessment of the structures should be conducted for maintenance.

Reassessment of the jacket structure was conducted in the last few decades, for example, reassessment of jacket structure subjected to shakedown by [Hellan et al., 1991](#); subjected to wave in deck forces by [Hansen and Gudmestad, 2001](#); considered integrity and life extension by [Efthymiou and van de Graaf \(2011\)](#).

Corrosion effect is also one of the environmental effects which could do serious damage to ships and offshore structures. Researches about the corrosion effect on the ships were already conducted by some of the researchers mentioned earlier, but little information was found which considers the corrosion effect on the jacket structure. Because of these reasons, the reassessment of the jacket structure subjected by corrosion effect was conducted and analyses to verify which part has more corrosion influence on the jacket structure with the assumption that corrosion rate is divided into three parts.

Reassessment of a jacket structure subjected to corrosion damages was analyzed. The corrosion rate which was assumed by [Soares and Garbatov \(1999\)](#) was used and the method of the considering corrosion time and rate treated by [Sun and Bai \(2003\)](#) was used during the analyses.

Basic information such as structural, metocean, foundation, and corrosion was described in the first section. The effect of the corrosion damage on the jacket structure during the 25 years was considered in the second section. In order to estimate which part of corrosion has more effect on the ultimate strength of the jacket structure, assumed coefficients were used for the corrosion depth in the last section.

47.2 Modeling

47.2.1 Structural Model

A platform used in Dalane (1993) is the foundation to create the model in this chapter. The platform has four legs, four piles, and is a fixed steel jacket platform. Only the weight of the topside of the platform was applied as a 100 MN load on the joint (each joint subjected to 25 MN on the $-Z$ axis). The platform was operated in 70 m water depth and has -70 m mudline elevation.

The program SACS was used for modeling and conducting analysis on the jacket structure and the jacket structure was modeled as tubular beam elements. The piles were not solved out in the above picture, but they were also applied during the step of analyses. The platform is a four-floor structure and each floor has a diamond brace, and K-braces are placed between floors (Figure 47.1).

47.2.2 Metocean Data

The metocean data, which were assumed as 100-year data, were applied during the analyses shown in the Table 47.1.

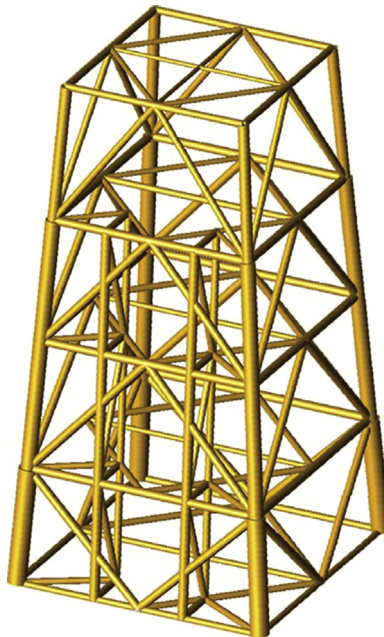


Figure 47.1
Jacket structure model.

Table 47.1: Metocean data

Wave height	29 m
Wave period	17.5 s
Current	SWL: 1.25 m/s 25 m: 0.65 m/s 70 m: 0.35 m/s
Drag, CD	0.86
Inertia, CM	2.00

Stokes fifth wave theory was used during the analysis, and constant option was selected for current stretching option. The environmental loads using above metocean data are applied as shown in Figure 47.2.

47.2.3 Foundation Model

The foundation model consisted of nonlinear beam column elements with the soil being modeled with nonlinear p-y, t-z, and Q-z to simulate its nonlinear behavior. The criteria of the foundations came from API-RP2A (2000) recommended approach.

The foundation data were used in this study. Total leg length is assumed to be 20 m. There are two kinds of leg segments, the first segment is 15 m long and the second

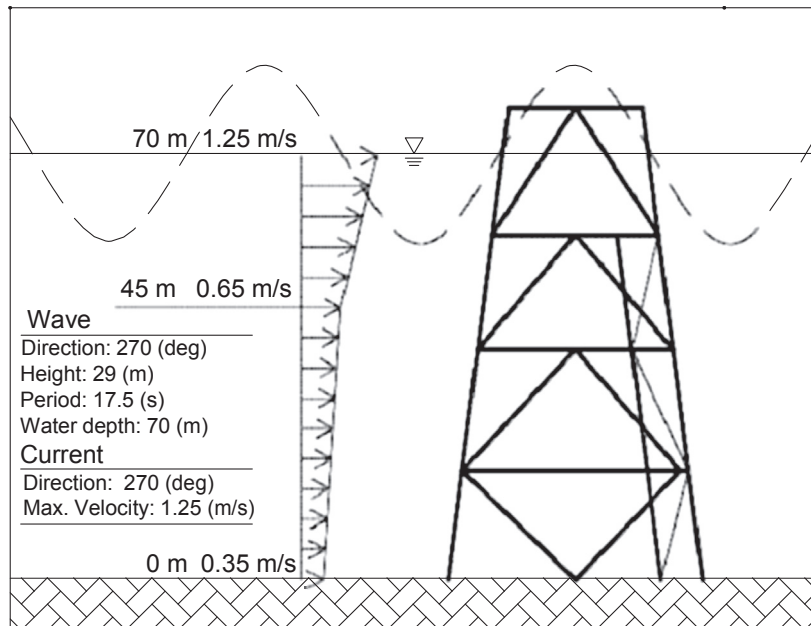


Figure 47.2
Environmental loads plot.

segment is 5 m long. The first segment has thicker thickness and higher yield stress than the second segment. The length of the pile has a relatively large influence for the ultimate strength (the longer pile is applied, the ultimate strength of jacket structure is increasing), but not for the result of this study. If the length of pile becomes longer, the calculation of ultimate strength is less accurate and unstable.

47.2.4 Corrosion Rate Model

There are two types of corrosion damage, “general corrosion” and “localized corrosion.” The general (also called uniform) corrosion is the most commonly used type of corrosion. It uniformly reduces the member wall thickness. Localized corrosion causes degradation in local regions.

Corrosion rates depend on many factors including coating properties, composition, inert gas properties, temperature of area, and maintenance systems. For this reason, the corrosion rate model should be appropriately based on the statistics of measurement data.

The time-variant corrosion rate model may be divided into three phases. The first one has no corrosion because of the protection of coatings, and corrosion rate is zero. The second phase is initiated when the corrosion protection is damaged and corrosion occurs, which reduces the tubular member elements thickness. The third phase corresponds to a constant corrosion rate. A model is suggested it to be

$$r(t) = r_s[1 - \exp(-(t - \tau_i/\tau_t))] \quad (47.1)$$

where τ_i is the coating lifetime, τ_t is the transition time, and r_s is the steady corrosion rate. Figure 47.3 shows the corrosion rate model.

By integrating Eqn (47.1), the corrosion depth can be determined to be

$$d(t) = r_s[t - (\tau_i + \tau_t) + \tau_t \exp(-(t - \tau_i/\tau_t))] \quad (47.2)$$

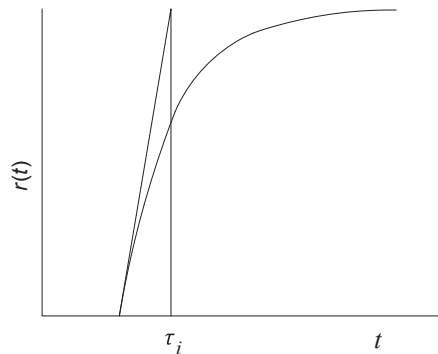


Figure 47.3
Model of corrosion rate.

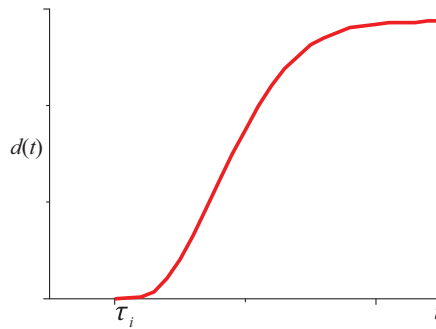


Figure 47.4
Loss of plate thickness from corrosion.

where the parameters τ_i , τ_t , and r_s should be fitted to inspection results. Figure 47.4 shows the corrosion depth as a time function. The coating lifetime, τ_i , can be assumed to be fitted by a Weibull distribution:

$$f(\tau_i) = \frac{\alpha}{\beta} \left(\frac{\tau_i}{\beta} \right)^{\alpha-1} \exp \left[- \left(\frac{\tau_i}{\beta} \right)^\alpha \right] \quad (47.3)$$

and r_s to be fitted by a normal distribution.

Figures 47.5 and 47.6 illustrate the corrosion depth reproduced by the present model based on the data from Paik et al. (1998) and assumed corrosion data are shown in Table 47.2. The corrosion damage was applied from year 0 because the durability of coating τ_i was assumed as 0 years. The increasing corrosion depth is accelerating as the time passes in

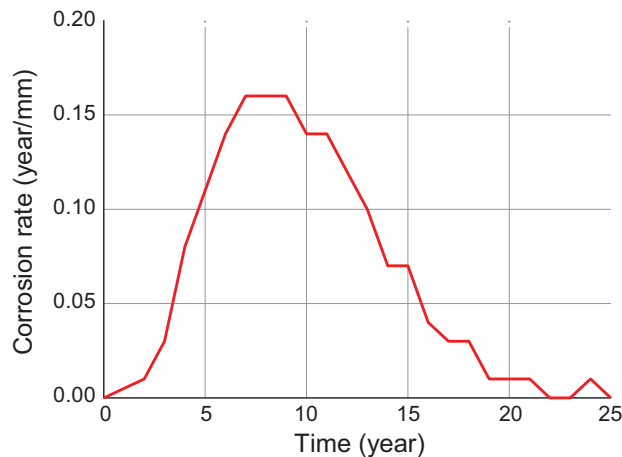


Figure 47.5
Corrosion rate model (Paik et al., 1998).

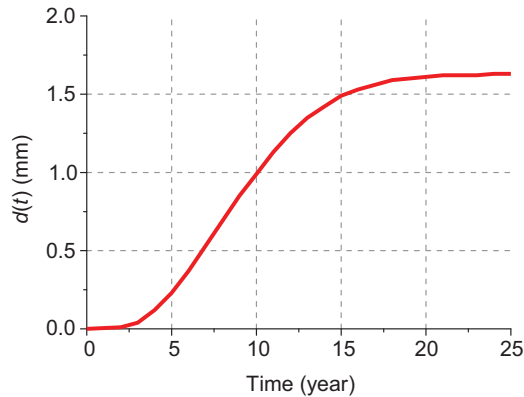


Figure 47.6

Loss of tubular member elements thickness from corrosion.

Table 47.2: Assumed corrosion data based on Paik's statistics

Time (year)	$d(t)$ (mm)	Time (year)	$d(t)$ (mm)
0	0	14	1.42
2	0.01	15	1.49
3	0.04	16	1.53
4	0.12	17	1.56
5	0.23	18	1.59
6	0.37	19	1.60
7	0.53	20	1.61
8	0.69	21	1.62
9	0.85	22	1.62
10	0.99	23	1.62
11	1.13	24	1.63
12	1.25	25	1.63
13	1.35		

the beginning. On the other hand, the increasing corrosion depth is decelerating as the time passes in the end since the corrosion lump at steel surface can interrupt the activation of corrosion progression.

47.3 Pushover Analysis

The pushover analyses also called collapse analysis were performed by using the program SACS. The SACS required three files, model input file, collapse input file, and pile soil interaction input file (pile soil interaction input file is optional) during the analyses. The analyses were performed in two steps. First, platform topside and dead weights were

applied. Second, the environmental loads were applied progressively until the failures of platforms occurred.

47.3.1 Ultimate Strength Analysis

Ultimate strength is defined when displacement reaches 1% of the height of the jacket structure or failure occurs in the member elements. It was set in the SACS program that the analysis will stop when any displacement of element on the structure reaches 1% of the height of jacket structure and the ultimate strength is decided at that time. Even though the setting for calculating the ultimate strength in the program is determined by the displacement of the elements, the first failure of the structure also occurs around the same time. The first failure on the several times analyses usually occurred on the bottom part of the structure like [Figure 47.7](#).

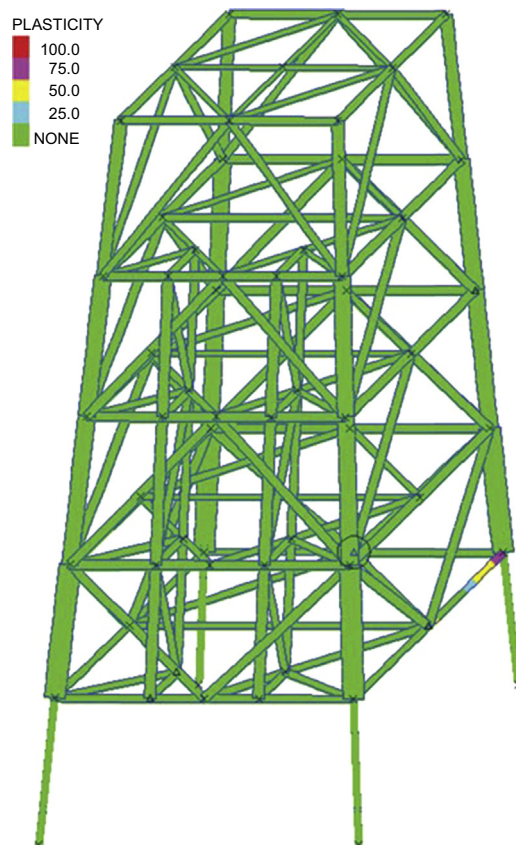


Figure 47.7
First failure of the jacket structure.

47.3.2 Reserve Strength Ratio

The platform capacity was quantified in terms of reserve strength ratio (RSR). RSR is defined as the ratio of the platform's ultimate lateral load carrying capacity to its 100-year environmental loading.

$$RSR = \frac{R_{ult}}{F_{wave(100)} + F_{current(100)} \left(+ F_{deck(100)} + F_{wind} \right)} \quad (47.4)$$

where R_{ult} is response at ultimate strength, $F_{wave(100)}$ and $F_{current(100)}$ are 100-year wave force and current force on jacket structure, respectively. If there was a topside on the structure and wind force, F_{wind} and $F_{deck(100)}$ (which is wave force on the deck) should be also considered. The RSR calculated by SACS is represented in Figure 47.8. The x -axis on the graph represents the maximum displacement along the RSR on the y -axis.

47.3.3 Incremental Wave Theory

The incremental wave approach used in SACS has the ability to evaluate the platform's behavior in the most accurate method. The structural model should be subjected individually to incremental wave heights to conduct incremental wave analysis. Nonlinear static analysis is carried out, and the structural demand parameters, such as base shear, overturning moment, and displacements, are obtained accordingly. A particular wave height at which the structure is not able to undergo the wave loading may take place and the incremental analysis should be terminated. Figure 47.8 which has the specific curve reflecting the required structural response at different wave intensity levels also represents RSR versus the jacket structure largest displacement.

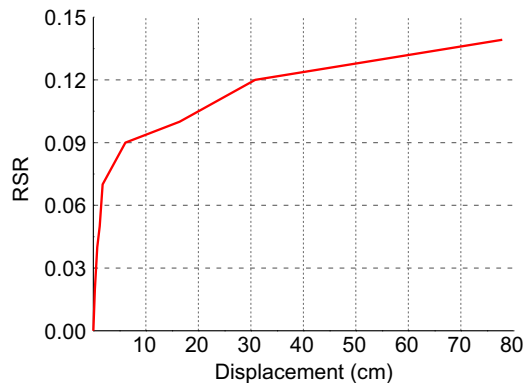


Figure 47.8
Reserve strength ratio of the jacket structure.

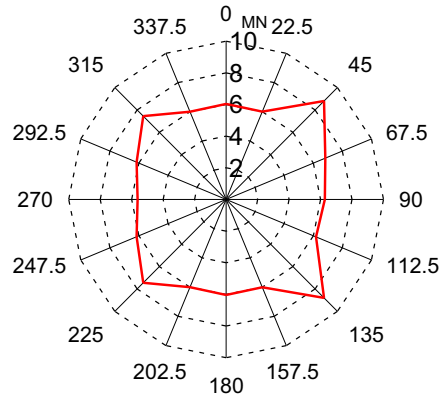


Figure 47.9
Ultimate strength along the directions.

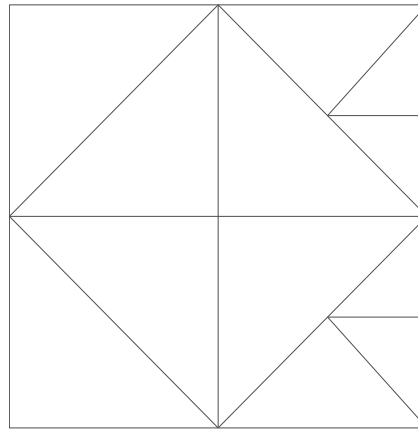


Figure 47.10
Top view of the jacket structure.

The ultimate strength analyses with the above data were conducted in several degrees to decide the direction of the metocean data. The results of the pushover analyses to find where the minimum ultimate occurred are shown in [Figure 47.9](#).

From the top view of the jacket structure ([Figure 47.10](#)), the structure is symmetric structure base on the 90° – 270° direction. Maximum ultimate strength occurred at 45° and minimum ultimate strength occurred at 270° . According to the result, 270° was selected to apply the maximum ultimate situation on the platform.

47.4 Corrosion Effect on the Jacket Structure

Several of the ultimate strength analyses using 270° were conducted along the corrosion depth data and whole structures member elements had been damaged by corrosion because

the “general corrosion” was assumed. The corrosion damages were replaced by decreasing diameter and thickness of tubular member elements. The Paik’s corrosion rate model in Figures 47.5 and 47.6 was applied for the jacket structure.

The corrosion rates of the jacket structure could be divided into three parts, atmospheric zone, splash zone, and full immersion zone (Figure 47.11). The topside of the platform is usually classified into atmospheric zone, but the topside was replaced as joints weight, therefore the atmospheric zone was not considered in this research. In the splash zone, the corrosion damage is the most serious because factors which disturb corrosion are continuously removed by wave and wind. The structure member groups that are rarely exposed to the air or fully immersed in sea water are included in full immersion zone. The corrosion damage in the full immersion zone is smaller than in splash zone. The corrosion damage decreases in full immersion zone the deeper the structure is.

In order to consider the splash zone and full immersion zone, they were multiplied by the corrosion depth $d(t)$ by each coefficient C_F and C_S , full immersion zone and splash zone, respectively. C_F and C_S are assumed coefficients which were multiplied by the corrosion depth $d(t)$, because it was considered that the corrosion rate on the jacket structure was larger than on the ship. In addition, corrosion rates may have different values along different places of the structure, but same corrosion rules are applied throughout the whole thing. Because of these reasons, the coefficients C_F and C_S were assumed to consider the difference effects. Except the thickness of the jacket structure member elements, any other variables were not changed such as wave height, period, and current velocity. How much of the corrosion effect has influenced on the jacket structure was known by using RSR/RSR_0 .

$$RSR_0 = \frac{R_{ult}^0}{F_{wave(100)} + F_{current(100)}} \quad (47.5)$$

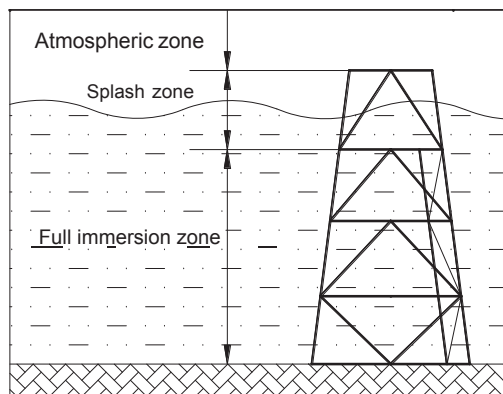
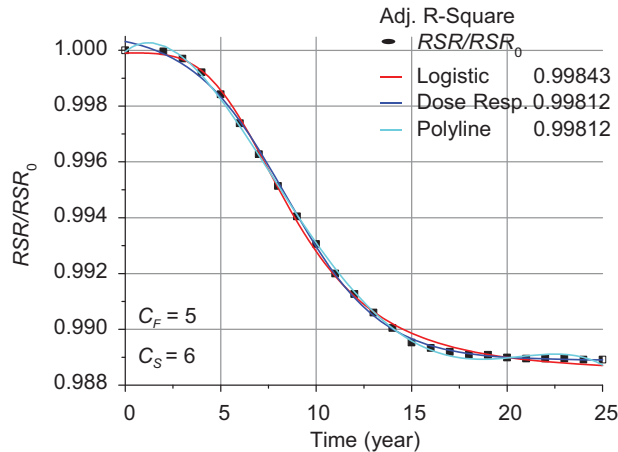


Figure 47.11

Three parts of corrosion rates for the jacket structure.


Figure 47.12

Relation between RSR/RSR_0 and time variant.

RSR_0 is RSR in 0 year, R_{ult}^0 is ultimate strength at 0 year. The result of the analyses which was calculating RSR/RSR_0 is shown in Figure 47.12.

It could be determined from the result that the effect from corrosion was accelerating at the beginning of the time. Effect from corrosion was decelerating toward the end of the test. The following relations between RSR/RSR_0 and time were established by using regression analysis:

Logistic Model R-Square : 0.99861

$$RSR/RSR_0 = \frac{0.0113}{1 + (t/8.7)^{3.64}} + 0.989 \quad (47.6)$$

Dose-Response Model R-Square : 0.99853

$$RSR/RSR_0 = 0.989 + \frac{0.012}{1 + 10^{-0.176(8.37-t)}} \quad (47.7)$$

Polyline Model R-Square : 0.99794

$$RSR/RSR_0 = 1 + (5.24E - 4)t - (2.39E - 4)t^2 + (1.44E - 5)t^3 - (2.54E - 7)t^4 \quad (47.8)$$

where t is time. The more the coefficient of determination (R-Square) is near 1, the more the equation has higher accuracy. All relation equations have over 99% accuracy. Equation (47.8) (from logistic model) is the most recommended among others.

47.5 Comparing Corrosion Effect

It is hard to tell which zone damages the jacket structure the most from the above result. In order to verify which zone had more influence of corrosion effect on the structure,

several analyses were conducted again with changing coefficient. Analyses to find them were conducted in two sections. In the first section, C_F was changing from 1 to 5 and C_S just had a value of 6. Through the first section analysis, it is possible to know about change rate of RSR/RSR_0 in the full immersion zone. In the second section, C_S was changing from 4 to 8 and C_F had fixed to 3 and change rates of RSR/RSR_0 in the splash zone could be calculated in this section. Figures 47.13 and 47.14 are the result of the analyses.

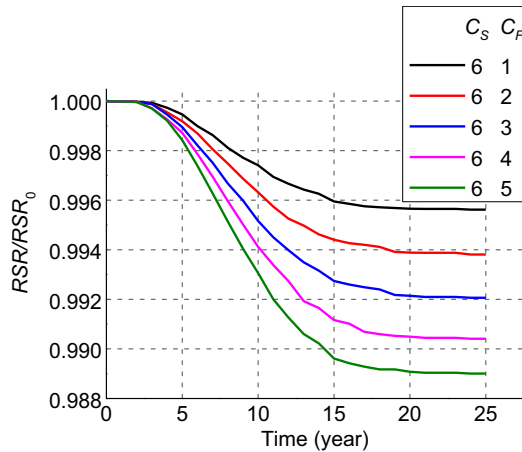


Figure 47.13
Fixed C_S and changing C_F .

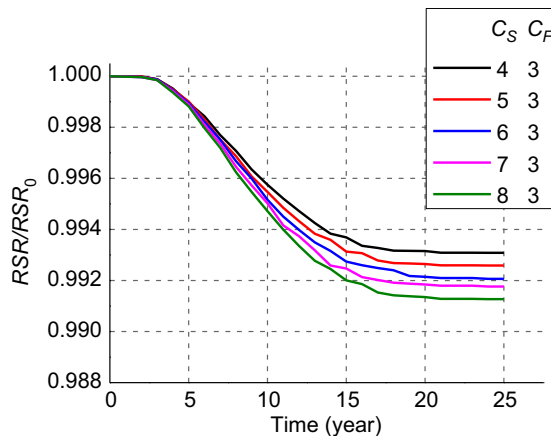


Figure 47.14
Fixed C_F and changing C_S .

The more the coefficient is increasing, the more the RSR/RSR_0 is decreasing in both analyses section. The following equations were used as the change rate to compare the corrosion effect.

$$R_{ij} = \frac{R_i - R_j}{R_i} \quad (47.9)$$

$$Q_{ij} = \frac{Q_k - Q_l}{Q_k} \quad (47.10)$$

where R_i ($i = 1, 2, 3, 4$) and Q_k ($k = 4, 5, 6, 7$) are change rates of RSR/RSR_0 when C_F is 1, 2, 3, 4 in the first section and when C_S is 4, 5, 6, 7 in the second section. R_j ($j = 2, 3, 4, 5$) and Q_l ($l = 5, 6, 7, 8$) are change rates of RSR/RSR_0 when C_F is 2, 3, 4, 5 in the first section and when C_S is 5, 6, 7, 8 in the second section, respectively.

The change rates of RSR/RSR_0 , R_{ij} , and Q_{kl} were calculated in each zone (Figures 47.15 and 47.16). It is possible to compare the corrosion effects in between the full immersion zone and the splash zone by dividing the change rate in the full immersion zone by the change rate in the splash zone.

$$\text{Comparing Ratio} = \frac{R_{ij}}{Q_{kl}} \quad (47.11)$$

The analyses result is presented in Figure 47.17. All data from the analyses are converged around 3.5. It means that the corrosion effect on the full immersion zone is 3.5 times larger damage than on the splash zone even though the splash zone has bigger corrosion rate than the full immersion zone.

The jacket structure analyzed for comparing corrosion effect was in 70 m sea level. It means the ultimate strength influenced by corrosion decreases the deeper the structure is.

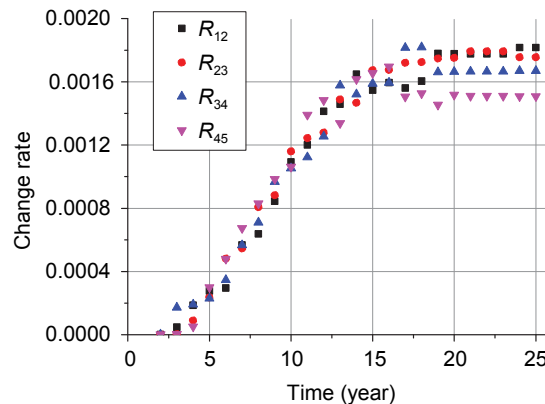


Figure 47.15
Change rate of RSR in the first section.

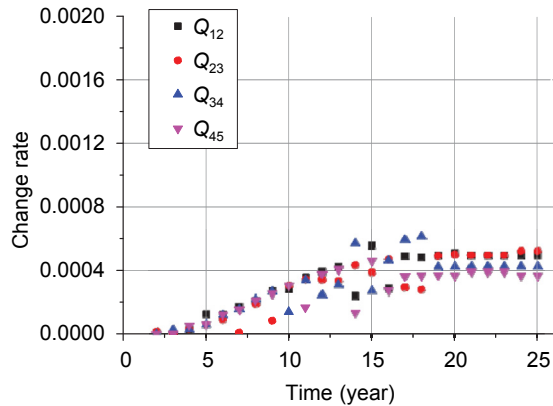


Figure 47.16
Change rate of RSR in the second section.

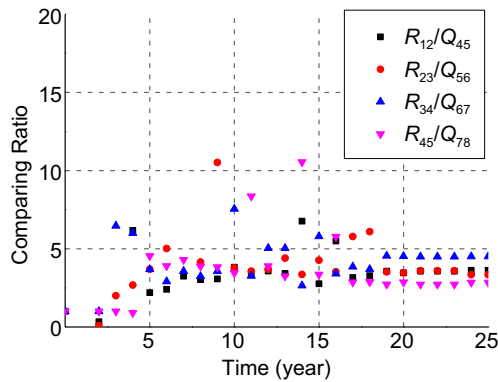


Figure 47.17
Comparing ratio of RSR between splash zone and full immersion zone.

47.6 Conclusion

A method has been proposed on the jacket structure to relate time and RSR/RSR_0 as three equations during a 25-year period. The jacket structure could be divided into three parts: atmospheric zone, splash zone, and full immersion zone. The relation equations based on the following three regression models: logistic, dose response, and polyline were derived.

It was proven in the analyses to define which zone has more influence on the jacket structure that the full immersion zone has 3.5 times more corrosion than the splash zone although the splash zone has larger coefficient than the full immersion zone. The reason of this is that the full immersion zone includes more elements of the structure than the splash zone.

Following comments could be recommended from the results:

- make the thickness of coating for the jacket structure member element in the full immersion zone thicker
- make the changing period for anode shorter or use the anode that has a larger capacity in the full immersion zone rather than in the splash zone
- it is possible to guess how the corrosion effect influenced the elements included in full immersion zone just by estimating corrosion damage of elements in the splash zone

Further work is needed to establish more reliable relations between time and corrosion effects on the jacket structure which is including local corrosion on the topside and jacket structure. It may be more complicated because the topside has more facilities and complex structure. These aspects will be addressed further within the new analyses for the whole offshore corrosion effect.

References

- API RP 2A, 2000. WSD Recommended Practice for Planning, Designing and Constructing Fixed Offshore Platforms-Working Stress Design. American Petroleum Institute.
- Dalane, J.I., 1993. System Reliability in Design and Maintenance of Fixed Offshore Structures. Department of Marine Structures the Norwegian Institute of Technology the University of Trondheim, Norway, pp. 8.1–8.34.
- Efthymiou, M., van de Graaf, J.W., 2011. Reliability and (re)assessment of fixed steel structures. In: Proceedings of the ASME 2011 30th International Conference on Ocean, Offshore and Arctic Engineering, OMAE2011–50253.
- Hellan, O., Skallerud, B., Amdahl, J., Moan, T., 1991. Reassessment of Offshore Steel Structures: Shakedown and Cyclic Nonlinear FEM Analyses. SINTEF Structural Engineering, ISOPE-91-173-03.
- Hansen, K., Gudmestad, O.T., 2001. Reassessment of jacket type of platforms subject to wave-in deck forces: current practice and future development. In: Proceedings of the Eleventh International Offshore and Polar Engineering Conference.
- Paik, J.K., Kim, S.K., Lee, S.K., 1998. Probabilistic corrosion rate estimation model for longitudinal strength members of bulk carriers. *Ocean Engineering* 25 (10), 837–860.
- Soares, C.G., Garbatov, Y., 1999. Reliability of maintained, corrosion protected plates subjected to non-linear corrosion and compressive loads. *Marine Structures* 12, 425–445.
- Sun, H.-H., Bai, Y., 2003. Time-variant reliability assessment of FPSO hull girders. *Marine Structures* 16, 219–253.

Risk and Reliability Applications to FPSO

48.1 General

In this chapter, the risk and reliability applications to FPSO (floating, production storage and offloading) will be introduced. There are three parts in terms of risk-based assessment, risk-based classification, risk-based inspection, and risk-based survey.

The risk-based classification is the verification of design and construction against the requirements set by the classification society, a society that classifies major tasks and installations. In this chapter, the issues related to such verification are described.

On a regular basis, the risk-based inspection has two kinds of inspections. One is conducted by the classification society and is part of the survey for maintenance of class. This only covers the systems classed. The other is conducted by either the owner or the operator and is part of their quality (safety and productivity) assurance program. Depending on the extent of the class coverage, it may cover an area not identical to that covered by the classification society's inspection. The last part describes the risk-based survey. The current practice of surveys has three categories: annual survey, intermediate survey, and special survey. They are practiced at intervals of 1 year, 2–3 years, and 5 years, respectively. The ABS (American Bureau of Shipping) Rules for Building and Classing Steel Vessel define the requirements and procedures for each of the three types of surveys. The surveys are also conducted during construction to ensure that the requirements defined in design are appropriately implemented in the construction.

There are two different viewpoints, one is from the classification society and another is from the operators/owners. The main purpose of the inspections done by the classification society is to check if the installation still satisfies the class requirements, while the inspections done by the operator are mainly for their safety management program designed to ensure safety and productivity. More details in terms of risk-based classification, inspection, and survey will be mentioned in the following sections.

48.2 Risk-Based Classification

48.2.1 Applicability of Risk-Based Classification

It is possible for a risk-based approach to be applied either for a whole FPSO, or for individual systems or subsystems. If the risk-based approach is applied to part of an FPSO then the following is required:

- Relevant assessment should consider all hazards and associated scenarios including the remote hazards outside the bounds of the systems under consideration.
- The remainder of the FPSO should comply with the applicable parts of the prescriptive criteria provided in the relevant ABS rules or guides.

There are a few requirements to be satisfied, such as availability of relevant databases, design phases, overall verification scheme requirements, and preference of the owner and designer; both qualitative and quantitative risk-based approaches can be applied.

48.2.2 Owner/Operator's Responsibilities

During the risk-based approach, there are also responsibilities for the owner or operator. The primary responsibility is the safety and integrity of his FPSO unit and it is the responsibility for the owner to develop a verification scheme in which all the major aspects of risk-based verification should be clearly defined. As a minimum requirement, the owner/operator is fully responsible for the following:

- All critical elements are appropriately selected and the corresponding performance standards are properly developed for the life cycle of the installation in terms of functionality, availability, structural integrity, survivability, and dependency with other critical elements and possible interactions.
- Risk acceptance criteria are appropriately determined to provide a level of safety equal to or higher than what could have been achieved if the prescriptive criteria had been applied.
- All hazards with a potential to cause a major incident have been identified, their risks are evaluated, and the measures have been and will be taken to reduce the risk at least to a level that complies with the risk acceptance criteria.
- The results of risk assessment should comply with all the applicable requirements of flag and coastal states.

More detailed risk assessment, including the methodology, risk acceptance criteria, tools and database used, hazards identified, and risk reducing measures are subjected to the Bureau's approval. Where the results of a risk assessment identify a need to depart from the prescriptive rules, the owner should detail these parameters and they should be submitted to the Bureau for approval.

48.2.3 Classifications' Responsibilities

The design reviews should be verified by the Bureau, and surveys during construction and installation that the critical elements are suitable and effective for their intended purpose, that is, should meet their reviewed and approved performance standards. These verifications and reviews cover design, construction, installation, and hook-up.

The Bureau will verify the risk acceptance criteria using historic data, good engineering practice, and sound technologies to confirm the safety and integrity of the FPSO. If the risk assessment and its results are approved by the Bureau, the Bureau will support the owner in his application for acceptance for both flag state and coastal states.

48.2.4 Submittals and Requirements for Design Verification

There are differences between the requirements and relevant submittals for a risk-based verification scheme during the design process. Minimum requirements and submittals are given below for the four major design phases and the installation hook-up phase:

- Conceptual design review
- Front end engineering and design review
- Final design review
- Review of installation, hook-up and commissioning

48.3 Risk-Based Inspection

Risk-based inspection is usually conducted by both the classification society and the owner/operator because each one has a different set of inspection procedures. The main purpose of inspection conducted by the classification society is to survey for the maintenance of a class; therefore, inspection only covers the systems classed.

In this book the inspections are categorized into a few groups:

- Structures including vessel hull and top side structures
- Mooring systems and the thruster system that assists the station-keeping system
- Import/export systems (risers and/or flow-lines and off-loading systems)
- Production facilities and marine systems

In this book, the rules from ABS were used to introduce the risk-based inspection.

48.3.1 Strengths and Weaknesses of Risk-Based Inspection (Advantages of Risk-Based Inspection)

The following three questions may be asked to address for planning and execution of a good inspection program:

- What should be inspected?
- How much effort should be made on individual components or details?
- When should the inspection be conducted?

There are two major features about the conventional inspection: fixed interval and experience dependent. Even though the rules of the risk-based inspection are already defined, the requirements or procedures from every owner or operator could be different in their separate ways. But, there is a common feature between them; they both depend on the experience of the inspector who conducts the inspection.

There are a few drawbacks of the conventional approach. First, controlling the risk level for the fixed interval inspection approach is difficult. For instance, some components may fail between two adjacent inspections, which may result in great risks to the installation. On the other hand, it is also possible for an unnecessary inspection to be conducted. In this case, both unnecessary downtime and wasting of inspector's time will increase, and it is also wasting cost and time of the operation. Similar inspection efforts are needed regardless of critical or uncritical components/details (Figure 48.1). When the risk is higher production cost, it needs a relatively long period of downtime. It could be a burden to the owner and/or operator. But, if

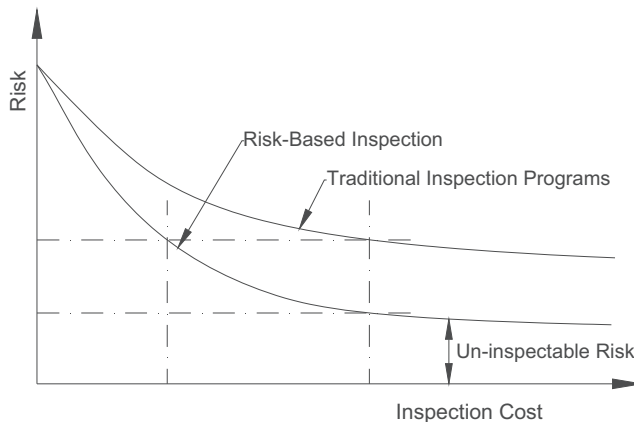


Figure 48.1

Risk level and inspection cost for two inspection approaches.

the risk-based inspection is properly used, it is possible to overcome the above drawbacks. Generally, a risk-based inspection is able to:

- Provide better capability to define, measure, and update the risks so that the management can better manage the safety, environmental, and production-interruption risks
- Allow better planning and execution of an inspection program by basing it on a risk and reliability approach
- Systematically reduce the probability of failures and production downtime.

48.3.2 Elements and Procedures of Risk-Based Inspection

The flow chart in [Figure 48.2](#) expresses the main procedure of the risk-based inspections. Inspections are the process of collecting information, screening and distinguish ranking risk, and updating information. Whole procedures are repeated following [Figure 48.2](#).

In the procedure of the risk-based inspection, the most important part is the prioritization of the components. The tasks consist of two major parts: screening and distinguish ranking of the risks for those components. At the end of the tasks, it is possible to know the answers to questions about what to inspect and what the degree of inspection should be. Both qualitative and quantitative approaches can be used for the risk screening and distinguish ranking.

The procedure of engineering analysis is also one of the important parts. This analysis is based on the data collected during the inspection. A basis for updating the condition of the components or the structural details is related with the result of the analysis. By applying reliability techniques and fracture mechanics, the degrees and rate of degradation can be determined. Such information will be inputted into the facility/structural database for planning the future inspection.

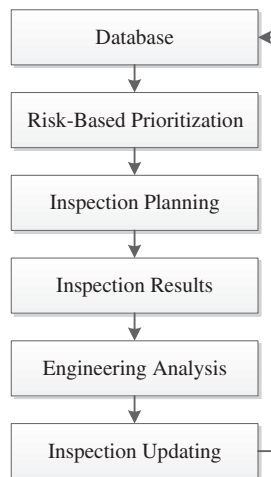


Figure 48.2

Flow chart of risk-based inspection.

48.3.3 Methodology of Risk-Based Inspection

What, where, and when are the main questions that should be answered from the analysis of the risk-based inspection approach. Generally, the component with a higher risk probability should be inspected first and the risk of a component or a structural detail is the product of the failure probability and its consequence. Thus, determining the probability of failure and the corresponding consequence are the main tasks.

It is possible to apply both qualitative and quantitative approaches to possible risk-based inspection. Each has its own strengths and weakness. There are no big differences between the two approaches in terms of function, but there are differences about their complexity level. The quantitative approach provides the specific risk value, while the qualitative approach provides the broad risk assessment data. It means that the quantitative approach not only needs more information to analyze, but also needs more detailed results. The qualitative approach provides more broad risk analysis for the facilities and subsystems; it also needs much less information than the quantitative approach.

Qualitative Approach

The qualitative approach is a relatively simple method for rating the degree of risk. The steps are usually the following:

1. Information collection
2. Consequences and likelihood analysis
3. Risk rating using the risk matrix
4. Prioritization of the subsystems/components for inspection

The ranking of the components for inspection is the one of the key steps. A rating system should be created for installation. Both the consequence analysis and the likelihood analysis should be defined by the system. [Table 48.1](#) gives an example of the consequence of category for the frequency analysis.

Table 48.1: Consequences of facility failure

Category	Consequence of Category
Catastrophic	<ol style="list-style-type: none"> 1. Loss of facilities integrity that leads to a significant influence on production 2. Systems damage that leads to a downtime that lasts for more than 1 year
Critical	<ol style="list-style-type: none"> 1. Loss of facilities integrity that requires excessive repairs 2. Systems damage that leads to a downtime for more than 6 months but less than 1 year
Severe	<ol style="list-style-type: none"> 1. Moderate facilities damage that require minor repairs 2. Systems fail to function, which leads to a downtime of 2–6 months
Minor	<ol style="list-style-type: none"> 1. Minor damage that requires a quick repair 2. Any damage or malfunction that leads to a downtime of less than 2 months

Table 48.2: Typical format of a risk matrix

Frequency	Risk Matrix			
High	M	H	H	H
Moderate	L	M	H	H
Low	L	L	M	H
Remote	L	L	L	M
Consequence	Minor	Severe	Critical	Catastrophic

H, High risk; M, Moderate risk; L, Low risk.

The frequency of each event can be determined from the relevant database or by using the reliability method. The definition of the frequency for individual events or consequences depends on the systems in question. The typical format of a risk matrix could be the only reference for this (Table 48.2).

In a high frequency, an accident has occurred to the system at least once in the past and may be expected to occur again. The typical range of frequency for this category of accidents is: frequency $>10^{-1}$.

In a medium frequency, an accident might occur in the life cycle of the system. The typical frequency range is: $10^{-2} < \text{frequency} < 10^{-1}$.

In a low frequency, an accident is considered unlikely to occur. However, similar incidents have happened once or twice in the industry worldwide. This category of accidents has a frequency range of $10^{-4} < \text{frequency} < 10^{-2}$.

In a remote frequency, an accident is credible, but not expected to occur in the life cycle of the system and it has frequency $<10^{-4}$ range.

The qualitative approach is generally used at a high level of screening and distinguish ranking of the subsystems or group of equipment. This approach is encouraged in cases where either information is relatively insufficient from the quantitative approach or the risk level is relatively low. In the prioritization procedure for the components or details to be inspected, the qualitative approach is used first to perform a high level of prioritization; then the quantitative approach is applied to the high priority components or details for more detailed analysis.

Quantitative Approach

The quantitative approach should be used for cases where a high risk is detected, for example, to the risk analysis for the high priority components or details for the inspection. It is also essentially parallel to the qualitative approach with all the items quantified, for example, both consequence and probability are given as numbers. The consequence should

be defined in dollar value so that priority and frequency of inspection can be quantitatively determined.

Consequence Analysis

A rating system should be created for the FPSO in question. Table 48.1 gives the rating system for the consequence of facilities damage for the use of the qualitative approach. The rating system with all the quantified items should be created for use in the quantitative approach. Creation of such a system depends greatly on past experience and the input from industry as well as government agencies. The best sources and tools for development of such system may be achieved by using a database for this purpose. Many tasks should be finished before such a database becomes usable.

The consequence should be quantified in terms of dollar value when considering the prioritization and planning of risk-based inspection. This analysis is the most cost efficient method and is directly applicable in the inspection planning phase.

Analysis of Failure Probability

A similar technique called consequence analysis can be used for the analysis of the failure probability of individual components. Thus, the rating system should be defined based on the past experience with consideration of original structural design, its reliability, the operational plan, and the owner's or operator's maintenance scheme.

Past experiences from the database can be used for a reliable and successful analysis of failure probability. Even though the history of FPSO is relatively short, a moderately sized database for the FPSO is accumulated. The damage information due to the planning mistakes in inspection is believed to be very rare. Therefore, it is also possible to use reliability analysis as an alternative approach.

Operational experience and other input from the owners or operators and other sources should be incorporated to gain the information related to frequency analysis. Both the first-hand operational experience and the experience and information obtained from the owner's inspection activities as well as execution of the owner's safety insurance program should be included. In these terms, the integration of the owner's or operator's inspection program with the Bureau's inspection program is of great importance.

Methods for Determining Inspection Frequency

Inspection of fatigue cracks is used as an example to illustrate the method for determining inspection frequency. Two rational methods are used to define inspection plans: the target reliability method and the fracture-mechanics-based approach.

In the target reliability method, the reliability level of the systems can be updated based on the information of the last survey and analysis using fracture mechanics. Once the annual

probability of failure exceeds the target value within a 1-year period from the time of the last survey, a survey is required to be conducted. This approach can be graphically demonstrated by the diagram in Figure 48.3. The target annual failure probability can be determined by an optimal approach as shown in Figure 48.4. Basically, this approach is to find the most cost-effective value for the target annual failure probability.

The fracture-mechanics-based approach is based on the crack growth analysis and relevant data. Figure 48.5 describes a typical crack curve. A crack with the existing technology can be detected at its minimal detectable level, shown as C in Figure 48.5.

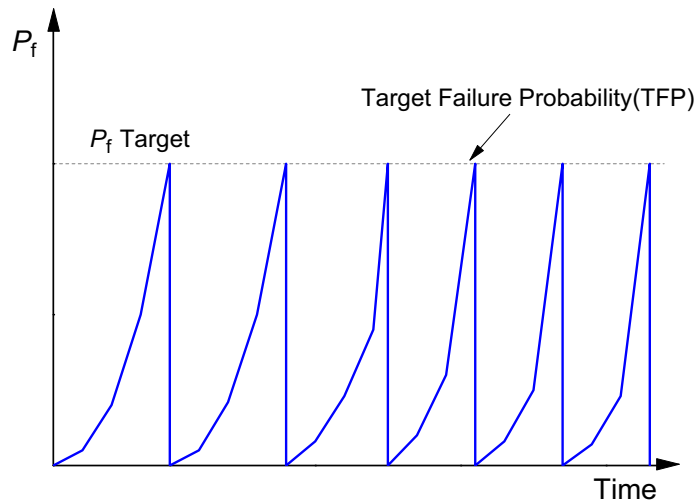


Figure 48.3
Survey planning using target reliability method.

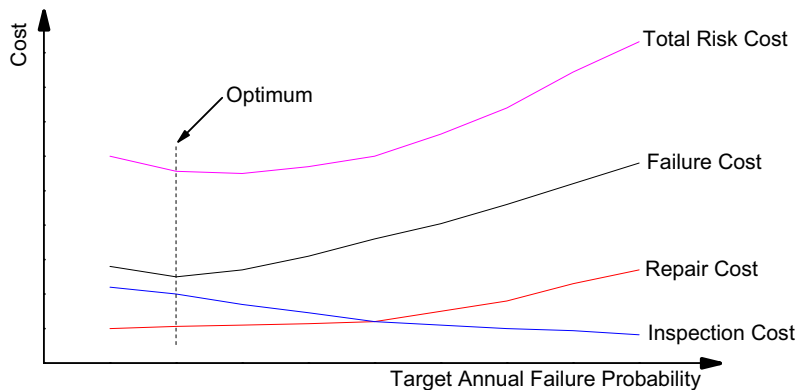


Figure 48.4
Optimal approach for planning of inspection frequency.

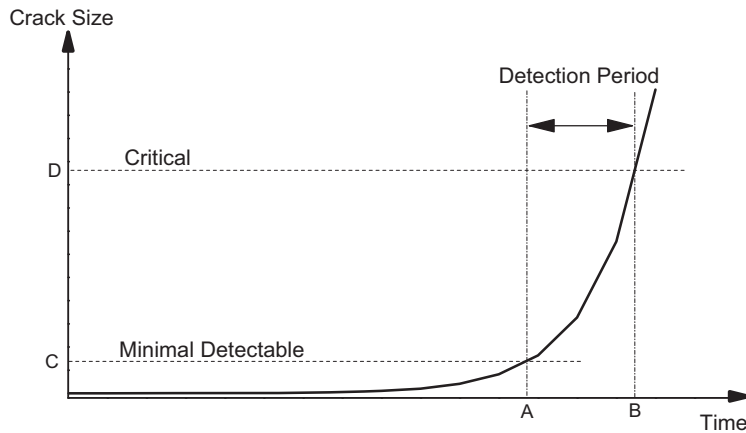


Figure 48.5

Fracture-mechanics approach for inspection frequency planning.

The crack should be repaired before it reaches the critical level shown as D in Figure 48.5. The time corresponding to these two levels of the crack are denoted as A and B, respectively, in Figure 48.5. Thus, at least one inspection should be conducted with the time interval between A and B. This provides a basis for determining inspection frequency, such as the inspection interval should not be longer than the time interval between A and B. In other words, the time interval between A and B sets an upper bound on the inspection interval.

The crack growth curve can also be used in the prioritization of inspection focus so as to help answer the question of where and what to inspect. In addition to fatigue cracks, there is also corrosion in the steel including plates and other members. Wear in the mooring lines, winches, and fairleads should be considered with equal importance. Corrosion and wearing curves should be established to form a basis for the inspection planning.

There are advantages and disadvantages for both the target reliability method and the fracture-mechanics-based approach. The target reliability method provides an overall optimal approach for inspection frequency planning, but with great difficulty in execution. The fracture-mechanics-based approach focuses on details of condition of fatigue cracks but without incorporation of cost optimization.

It is possible to consider the new and better method by combining the two methods. Planning tools from the target reliability method and a checking mechanism from the fracture-mechanics-based approach can be used in the combined method. In other words, the inspection interval can be determined using target reliability method; this interval should be checked against the one found from the fracture-mechanics-based approach.

Reliability Updating Based on Inspection Information

The inspection information can be updated using the Bayesian rule, which can be defined by the following equation:

$$p(A, B) = p(B|A)p(A) \quad (48.1)$$

where $p(A, B)$ is the joint probability of events A and B , $p(B|A)$ is the conditional probability of B under the given condition A , and $p(A)$ is the marginal probability of event A .

To improve the estimation of the probability for event A , existing observed data D can be used in combination with the information on event A :

$$p(A|D) = \frac{p(D|A)p(A)}{p(D)} \quad (48.2)$$

The updates should be applied to all the information on the components/structural details to be inspected. As an example, the approaches and the items in need of an update with regard to fatigue damage are listed below:

- Updating through inspection events
- Updating through variables, such as crack initiation, propagation, and detection
- Updating through regression analysis and adjustment
- Updating event margins, which includes four conditions: no crack detected, crack detected, repairing event, and modification to the structure

48.4 Risk-Based Survey

48.4.1 Current Practice of Surveys

The current survey practices are usually conducted in three categories, that is, annual survey, intermediate survey, and special survey, at intervals of 1 year, 2–3 years, and 5 years, respectively. The current survey practices are even based on a prescriptive approach. There are two main phases used in the overall surveys:

- The surveys during construction of new-build vessels or during conversion of tanker-converted vessels. The surveys in this phase also include those conducted during installations and hook-ups.
- The surveys for maintenance of class of a vessel.

FPSO Surveys (Construction and Installation Surveys)

The surveys of FPSO are to ensure the requirements defined in design are appropriately implemented in FPSO. The surveys are also conducted to ensure the installation and hook-up of the vessel and its mooring, riser, and flow-line systems, which are to ensure the

standards and requirements, are met. This phase of surveys is usually considered as part of the verification program, which covers design, fabrication, installation, etc. Although these surveys are not considered as part of the surveys for maintenance of class, they provide surveyors or the Bureau in general with important information such as the initial data on the installation and its equipment.

The Surveys for Maintenance of Class

Detailed requirements and procedures can be found in this document, but only some very important features of these surveys are cited here. Annual surveys are conducted within 3 months before or after each anniversary date of the crediting of the previous special periodical survey or the original construction date. The annual survey covers only those components that can be seen. Intermediate surveys are made either at the second or third annual survey or between these surveys. Special surveys are conducted within 5 years after the date of build or after the crediting date of the previous special survey. The surveys may be commenced at the fourth annual survey and be completed by the fifth anniversary date.

Special surveys are the area where more technical work is required. For the shipping industry, the ships are required to be dry docked for the special survey every 5 years. For FPSO, it is difficult to be surveyed according to the requirement because the cost is too high to do so. The difficulties are mainly from the high cost of production and the particular feature of the current FPSO.

48.4.2 The Main Drawbacks of the Current Survey Practice

Common characteristics of these surveys can be briefly described as follows:

- Each type of survey is conducted at a fixed interval, which is 1 year, 2–3 years, and 5 years for annual, intermediate, and special surveys, respectively.
- The extent of the survey is also well defined in the Steel Vessel Rules such that the extent of each survey is fixed.
- Degree of focus on the components relies greatly on the experience of the surveyor who conducts the survey. This is a typical experience-based practice.
- There is very little done by integrating Class Society Surveys with the Owner Safety Management Program implemented in all major offshore installations.

Deciding both the interval and extent of the surveys is usually based on the experience on ships or arbitrarily because there is no rigorous engineering analysis. Therefore there are drawbacks to this approach. If the FPSO is well designed and operating in benign conditions, the fixed interval could be too short to conduct a survey and unnecessary inspections are carried out. On the other hand, if the inspection interval is too long, failure may occur before the next survey is conducted.

The extent of the survey could be too large, and it may also make unnecessary inspections for the areas where no failure will occur. The overlarge range of a survey may lead to insufficient inspection for some critical areas, and it may also make some areas fail before the next survey.

It is obvious that the risk for overlong intervals and insufficient inspections on some important components could be higher. On the other hand, too short intervals can also impose some unnecessary cost to the owner or operator of the FPSO. For instance, if the downtime occurs during the day for the middle FPSO with a production rate of 100,000 barrels per day, a huge loss of about US \$80–10 million will be incurred for an oil price assumed in the range of US \$80–100 per barrel. A lot of inspection cost while considering an operation life of 20 years can be saved just by improving the survey strategy.

48.4.3 Risk-Based Survey for Maintenance of Class

Survey planning and execution are also included in the risk-based survey. The major work is the inspection discussed previously. It is obvious that both the classification society and the operator of the FPSO conduct inspections, but different focuses are applied to each of them. The inspection done by the classification society mainly focuses on checking whether the FPSO still satisfies the class requirements, but the inspection done by the operator is mainly about their safety management program, which can ensure safety and productivity.

The Survey Process and Its Integration with the Owner's Inspection Program

More and more owners and/or operators of FPSO adopt the risk-based inspection approach for their offshore structures. An integration of inspection program executed by operators and the survey program carried out by classification society become a necessary part of both programs to increase system efficiency. In addition, there are lots of things that should be done for a perfectly integrated program. [Figure 48.6](#) shows the sequence of the main survey program conducted by a classification society and the inspection program performed by the operator. The important thing is the relationship between these two programs, which can be considered as one type of integration of the classification society survey program with the owner's/operator's inspection program.

Procedures of Risk-Based Survey

The risk-based survey consists of the following major procedures:

1. Review of the owner's/operator's inspection and maintenance plan, which includes:
 - a. Critical elements and their performance standards for the operational phase
 - b. Execution process of the owner's/operator's inspection and maintenance plan

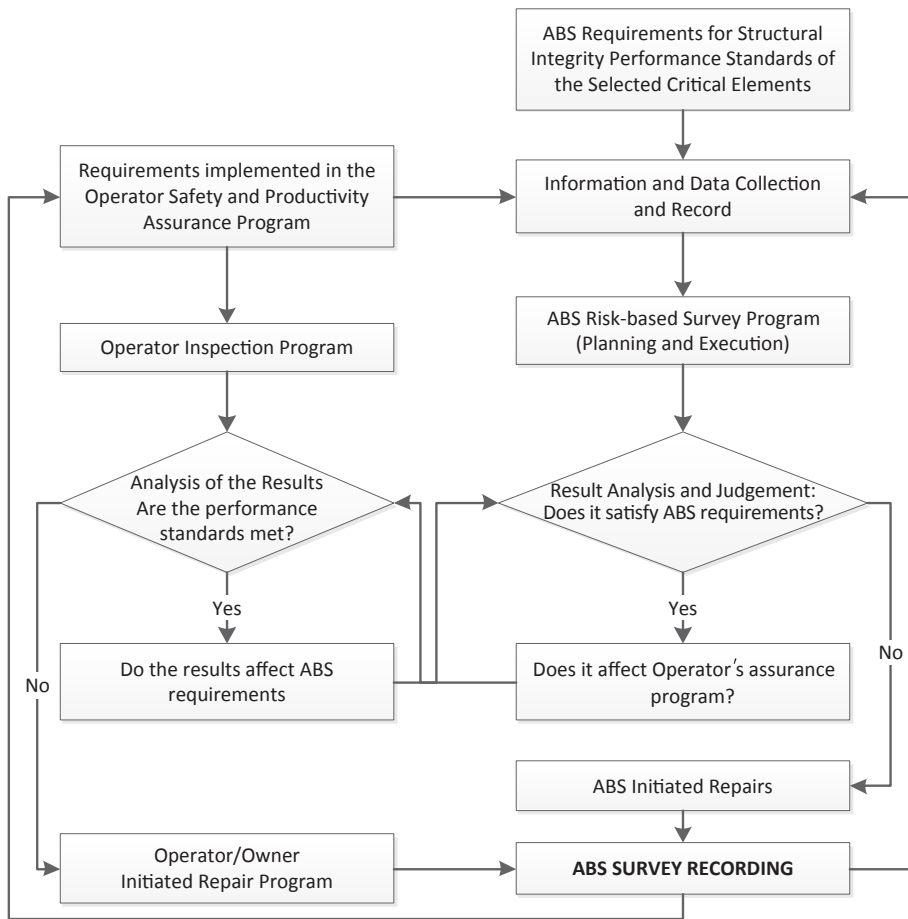


Figure 48.6

Integration of ABS survey program with operator's inspection program. The column on the right-hand side represents the key procedures for the ABS survey program. The column on the left-hand side is for the operator's inspection program.

- c. Inspection schedule and extents
 - d. Methods of inspection, measuring, testing, and recording
 - e. Software to be used for inspection and relevant analysis
 - f. Record of owner's/operator's inspection, maintenance, repairing, and modification of the FPSO
2. Review of the Owner's/Operator's operational procedures and management plan, which includes:
 - a. Operational management systems
 - b. Operational procedures
 - c. Operation manuals

3. Development of an ABS survey plan based on the information gained from the above review. The following issues will be considered in the process of the survey plan development:
 - a. Check if all the critical elements have been identified in the owner's/operator's inspection program
 - b. Examine the performance standards developed by the owner/operator to make sure the minimum requirements on safety and integrity of the FPSO are met
 - c. Modify the list of critical elements and their performance standards to include those ABS think are necessary to be accounted for
 - d. Use the sound technologies developed by ABS
 - e. Integrate the ABS survey program with the owner's/operator's by following the interaction process defined in [Figure 48.6](#)
4. Performance of the surveys
5. Analysis and recording of the survey results
6. Report of the survey results and recommendation of necessary maintenance to the owner/operator

Owner's/Operator's Responsibilities

For the initial phase to materialize the integration of the Bureau's survey program with the owner's/operator's inspection program, all the items listed in the above section should be submitted to the Bureau for review and approval. Because of their importance, the documents containing the following issues must be completed and be submitted to the Bureau for review and approval at their earliest availability:

- Owner's/operator's proposed maintenance and inspection plans including details of frequency and extent of activities
- The basis and methodology employed in the risk-based approaches
- The means by which the techniques are used to establish, update, and modify maintenance and inspection plans
- The critical elements and their performance standards for the operational phase
- Methods of inspection, measuring, testing, and recording
- Software to be used for inspection and relevant analysis
- Record of findings of each inspection, the relevant repairing and maintenance as well as any modification to the FPSO
- Operation manuals

In the owner's/operator's inspection plan, the requirements given in the last section should be met for the operational phase. The critical elements should be identified, and their performance standards should be developed with consideration of the particular features of the operational phase.

The risk assessment is site specific. For the FPSO used for a marginal field, it may be moved from one site to another. Once the FPSO is moved, the risk assessment should be reviewed by the owner/operator and resubmitted to the Bureau for approval.

The information on the items listed above should be updated after each inspection and is required to be submitted to the Bureau for review and record.

Responsibility of the Bureau

The bureau will do the following in the integrated survey/inspection program:

- Review and comment/approval of the submittals listed in the above risk-based survey
- Develop a survey plan and the detailed procedures of the survey
- Integrate the Bureau survey program with the owner's/operator's inspection program by working closely with the owner/operator
- Develop the execution plan and procedures for the survey program
- Recommend to the owner/operator any necessary maintenance of the FPSO
- Generate a status report for the classed FPSO

Further Reading

American Bureau of Shipping, 2000a. Rules for Building and Classing Steel Vessels, 2000. Part 7 (Operations and Maintenance).

American Bureau of Shipping, 2000b. Guide for Building and Classing Floating Production Installation.

API Recommended Practice 2FPX, 2000. Design Guide for Floating Production Systems.

API Recommended Practice 580, 1999. Risk Based Inspection.

Bai, Y., Xu, T., Bea, R., 1997. Reliability-based design & requalification criteria for longitudinally corroded pipelines. In: ISOPE'97.

Ma, K., Orisamolu, I.R., Bea, R., Huang, R.T., 1997. Towards optimal inspection strategies for fatigue and corrosion damage. In: SNAME Annual Meeting, Technical Session, Ottawa, Canada.

Oil Companies International Marine Forum 2012. Guidelines for the Inspection and Maintenance of Double Hull Tanker Structures.

Spouge, J., 1999. A Guide to Quantitative Risk Assessment for Offshore Installations. CMPT Publication 99/100.

Vinnem, J.E., 1999. Offshore Risk Assessment. Kluwer Academic Publishers.

Explosion and Fire Response Analysis for FPSO

49.1 Introduction

Hydrocarbon explosions and fires have been identified as major potential hazards in offshore installations. Extreme explosions and heat will pose serious consequences for safety, assets, and the surrounding environment. A number of explosion and fire accidents in offshore installations have occurred in recent decades such as the Piper Alpha accident (the accident that occurred on board the offshore platform Piper Alpha in July 1988 killed 167 people and cost billions of dollars in property damage; [Figure 49.1](#)) and the Deepwater Horizon accident, which occurred on April 20, 2010, killed 11 workers, and resulted in the largest oil spill in the United States ([Figure 49.2](#)).

Before the Piper Alpha accident, research into fire and explosion was only through experience and statistical analysis. Experts mainly focused on the lack of fire-fighting procedures and recommendations for its improvement. With the development of modern



Figure 49.1
The Piper Alpha accident.



Figure 49.2

The Deepwater Horizon accident.

methods of quantitative analysis, more and more studies are done using modern computer technology. A lot of effort now has been put into the prediction and controlling of explosions and fires in offshore installations. Risk-based approaches, rather than traditional prescriptive approaches, have begun to be more extensively applied in offshore designs.

49.2 Accident Causation Analysis

Analyzing the cause of accidents is an important part of risk management. Usually, the accident risk that exists in the system will be found and its characteristics will be discovered and identified by inspecting and analyzing the system.

According to the characteristics of hazardous energy, the source of the first hazard is defined as hazardous substances, which could be released accidentally into the system; the source of secondary hazard is referred to as all kinds of unsafe factors that exhaust measures to keep energy stable, such as loading and unloading, storage of goods, and hot work. The first kind of hazard is energy, which can cause the accidents and determine the severity of accident consequences. The source of the secondary hazard is a necessary condition to decide whether the accident occurs and affects the feasibility of the accident.

The cause of an offshore oil platform accident is shown in [Figure 49.3](#). Based on this theory, the main cause of fire and explosion accidents is shown in [Figure 49.4](#). As a matter of fact, most of the reasons for fire accidents is their relationship with human factors. The International Maritime Organization (IMO) found that almost 80% of marine accidents occurred because of human error. The results further illustrate human action is an important factor affecting the safety of the whole system.

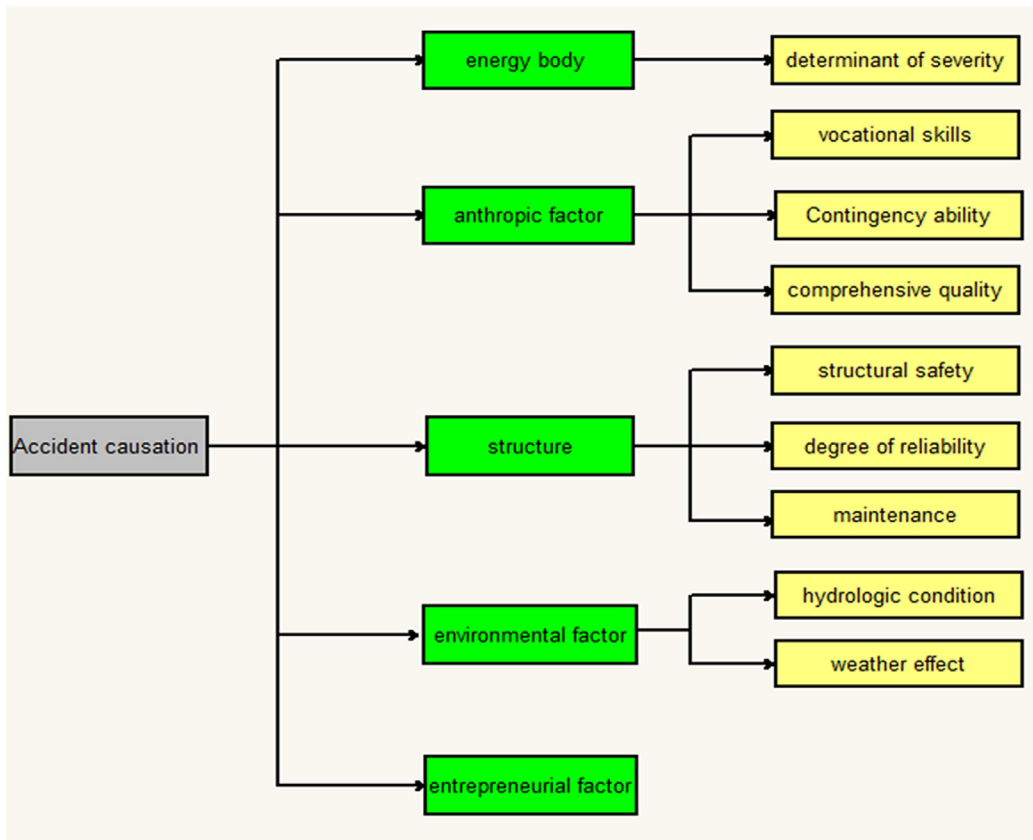


Figure 49.3
The cause analysis of marine accidents.

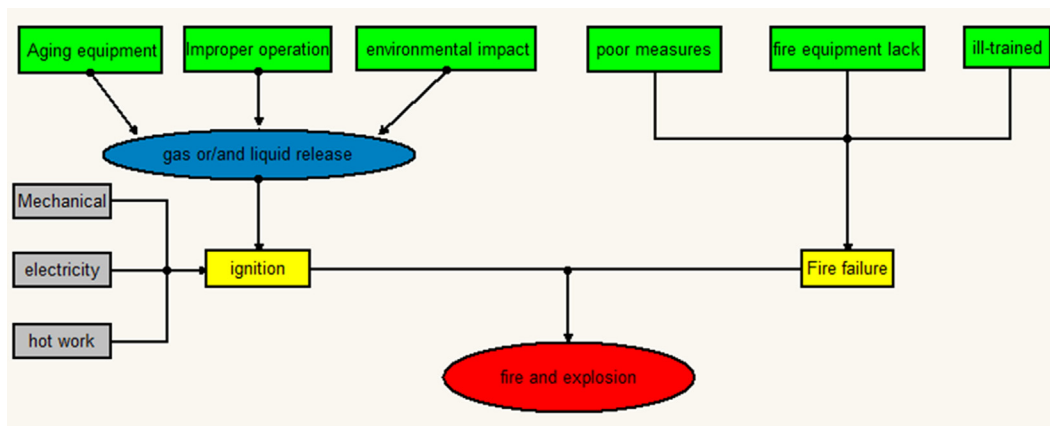


Figure 49.4
The main cause analysis of fire and explosion.

49.2.1 Formal Safety Assessment

Formal safety assessment (FSA) is a kind of integration and systematic analysis method. Its purpose is to make all aspects of the specification, design, operation, and inspection effective and to improve safety at sea comprehensively and reasonably. This includes the protection of life and health, the marine environment, and property. A summary of this method is available as follow.

Phase I, Identification of dangerous sources: Its purpose is to evaluate the system to identify all the possible dangers and find out the cause and consequences of the possible accidents, then make a list in order of the degree of dangers to further analyze major risks and put forward a corresponding control scheme.

Phase II, Risk assessment and management: In this phase the procedures are used to evaluate the risk of all kinds of danger: find the distribution of risk and the overall level of risk, focus on the high risk area and the main factors affecting the level of risk, and sort the risk in an acceptable level.

Phase III, Risk restraining project: The effective measures are put forward to reduce risk on the basis of hazard identification and risk assessment.

Phase IV, Cost and benefit evaluation: Calculate the costs of each risk control measure and the benefit from reduced risk degree.

Phase V, Suggestions and decision: Select the optimal risk control measure.

49.3 Phase I: Identification of Dangerous Sources

There are many methods to identify the dangerous sources. For example, the expert investigation method (EIM), preliminary hazard analysis (PHA), fault tree analysis (FTA), event tree analysis (ETA), failure mode and effect analysis, and hazard and operability.

1. Expert investigation method

The main task of the investigation is to find all kinds of potential dangers and measure the consequences. Many dangers are difficult to confirm with statistical methods and causal reasoning in a short period of time in marine structure engineering. For example, there are relatively few available statistical data for the fire and explosion accidents on the floating production storage and offloading (FPSO). It is obvious that EIM is prevalent to identify the danger sources. The two most commonly used methods are brainstorming and Delphi.

a. Brainstorming

Brainstorming can also be called playing imagination. It includes two stages:

Stage 1: The organizer reviews the criterion of imagination and the purpose of the meeting, and then team members express their opinions fully and put forward a series of ideas.

Stage 2: The ideas are then analyzed comprehensively. It can neither be despised nor accepted blindly.

This method can be used for selecting risk identification and risk controlling measures.

b. Delphi

The Delphi method is a typical method of risk identification task directed by the famous American consultancy the Rand Corporation. This method is widely used in the decision-making process.

2. Preliminary hazard analysis

PHA is a qualitative analysis method to evaluate the internal risk factors and the degree of risk in the system. It can be the previous step to the FTA.

3. Fault tree analysis

FTA is one of the most important analysis methods of risk and security systems engineering. FTA is a longitudinal analysis method, a graphic deductive method from the top to the basic events. It can be used for qualitative evaluation and calculating the degree of system failure probability. One top event should be designated. The top event is the accident that is not expected to happen. During this period, construction of the fault tree is core.

4. Event tree analysis

ETA is a kind of inductive method. Contrary to FTA, ETA starts with the basic event, the probability of unexpected events can be roughly calculated, and finally, the top event will be found. Usually ETA can be combined with FTA, and work together to complete the analysis.

5. Failure mode and effects analysis

Each element is investigated to detect potential various failure modes in the subsystems or components. Then precautionary measures will be put forward.

49.3.1 The Structure Function of Fault Tree

1. Basic conception

Assuming FTA is made up of n different kinds of independent events, a binary random x_i variable equal to the state of the i th bottom events e_i is defined to be:

$$x_i = \begin{cases} 1 & e_i - \text{occur} \\ 0 & e_i - \text{not - occur} \end{cases} \quad i = 1, 2, \dots, n \quad (49.1)$$

Binary random variable ϕ expresses the status of the top event T :

$$\phi = \begin{cases} 1 & T - \text{occur} \\ 0 & T - \text{not - occur} \end{cases} \quad (49.2)$$

The state variables of the top event are completely determined by the bottom event state variable values, as the top event state is completely determined by the status of the basic events. Define ϕ to be the function of $X = (x_1, x_2, \dots, x_n)$, and assume the equation is as follows:

$$\phi = \phi(x) \quad (49.3)$$

$\phi(x)$ is called the structure function of the fault tree.

2. Correlation function

a. Correlation of the bottom event: If x_i satisfies Eqn (49.4):

$$\phi(1_i, x) \neq \phi(0_i, x) \quad (49.4)$$

then it can be said that the bottom event e_i has an effect on the structure function.

b. The correlation function: If the structure function $\phi(x)$ meets the following properties, then $\phi(x)$ is called the correlation function.

- Each variable value x_i ($i = 1, 2, \dots, n$) has an effect on the structure function.
- $\phi(x)$ is correlated in terms of x_i ($i = 1, 2, \dots, n$) and is not diminishing.

In the logic operation, the structure function of the fault tree composed by logic gates always accords with (b). The structure function is called correlation function if it coincides with property (a).

Coherent structure function has the following properties:

- $\phi(0) = 0$;
- $\phi(1) = 1$;
- Given state vectors X and Y , if $X \geq Y$, namely $x_i \geq y_i$, then $\phi(x) \geq \phi(y)$;
- Suppose $\phi(x)$ is a structure function composed with n independent events, then the equation is set up as follow:

$$\bigcap_{i=1}^n x_i \leq \phi(x) \leq \bigcup_{i=1}^n x_i \quad (49.5)$$

c. Indicates that the fault tree concerning the state of the system is between the same kind of units in the series system and parallel system composed of the same unit.

Transform the equation as follows:

$$\phi(x) = x_i \phi(1_i, x) + (1 - x_i) \phi(0_i, x) \quad (49.6)$$

In terms of the fault tree composed of n independent events, its structure function can be expanded n times. So the basic form of the equation is as follows:

$$\phi(x) = \sum Y \prod_{i=1}^n x_i^{y_i} (1 - x_i)^{1-y_i} \phi(y) \quad (49.7)$$

where x_i is 1 or 0, and $\sum Y$ indicates summation of the state vector valued Y.

Figure 49.5 is as an example of a fault tree that explains Eqn (49.5); there are five bottom events, $Y = (y_1, y_2, y_3, y_4, y_5)$.

All $32(2^5)$ possible states of the fault tree are presented in Table 49.1; once $\phi(y)$ is calculated, $\phi(x)$ is obtained. From Eqn (49.7), the following equation is found:

$$\begin{aligned} \phi(x) = & (1 - x_1)(1 - x_2)x_3x_4(1 - x_5) + (1 - x_1)(1 - x_2)x_3x_4x_5 + (1 - x_1)x_2(1 - x_3)x_4x_5 \\ & + \dots + x_1x_2x_3x_4(1 - x_5) + x_1x_2x_3x_4x_5 \end{aligned} \tag{49.8}$$

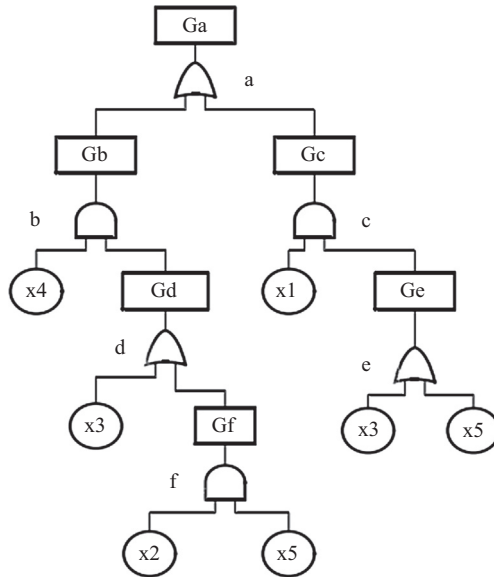
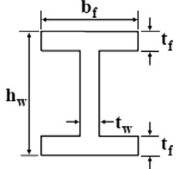


Figure 49.5
A typical example of a fault tree.

Table 49.1: Dimensions and geometric properties of the frames

	Symbol	Main Frame	Secondary Frame
	h_w (mm)	700	300
	t_w (mm)	13	10
	b_f (mm)	300	300
	t_f (mm)	24	15

49.4 Phase II: Risk Assessment and Management

Fires and explosions are continuous threats on offshore oil and gas installations. The dominant fire and explosion events are associated with hydrocarbon leaks from flanges, valves, equipment seals, nozzles, etc. Fires and explosions both result from combustion associated with hydrocarbon gas leaks. Figure 49.6 shows a sample calculation of the frequency of leaks using ETA. The methods mentioned above are often unable to identify frequency of gas leaks and ignition probability properly. More refined methods for their calculation are thus required on the basis of simulations. The EFEF JIP (explosion and fire engineering of FPSO units) has developed more refined methods to calculate the frequency of fires and explosions.

Jeom Kee Paik is the leader of the ongoing 27th Joint Industry Project on the Explosion and Fire Engineering of FPSO Units (EFEF JIP). The aim of the EFEF JIP is to develop state-of-the-art technologies for the quantitative assessment and management of the risk of hydrocarbon explosions and fires in offshore installations.

A framework for the quantitative assessment and management of the risks associated with fires and gas explosion requires the identification of both the frequency and consequences of these incidents.

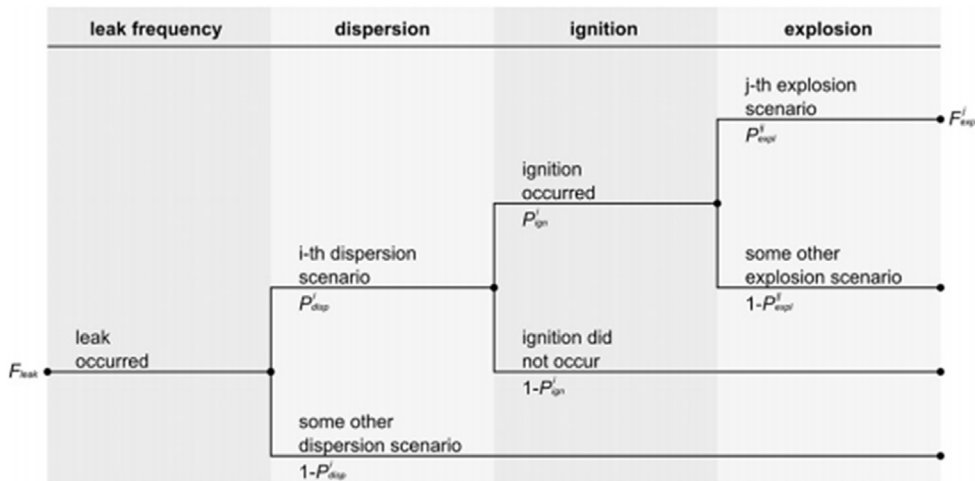


Figure 49.6

Explosion event tree analysis for a leak event.

49.4.1 Procedure for Fire Risk Assessment and Management

Figure 49.7 presents the EFEF JIP procedure for the fire risk assessment and management of offshore installations.

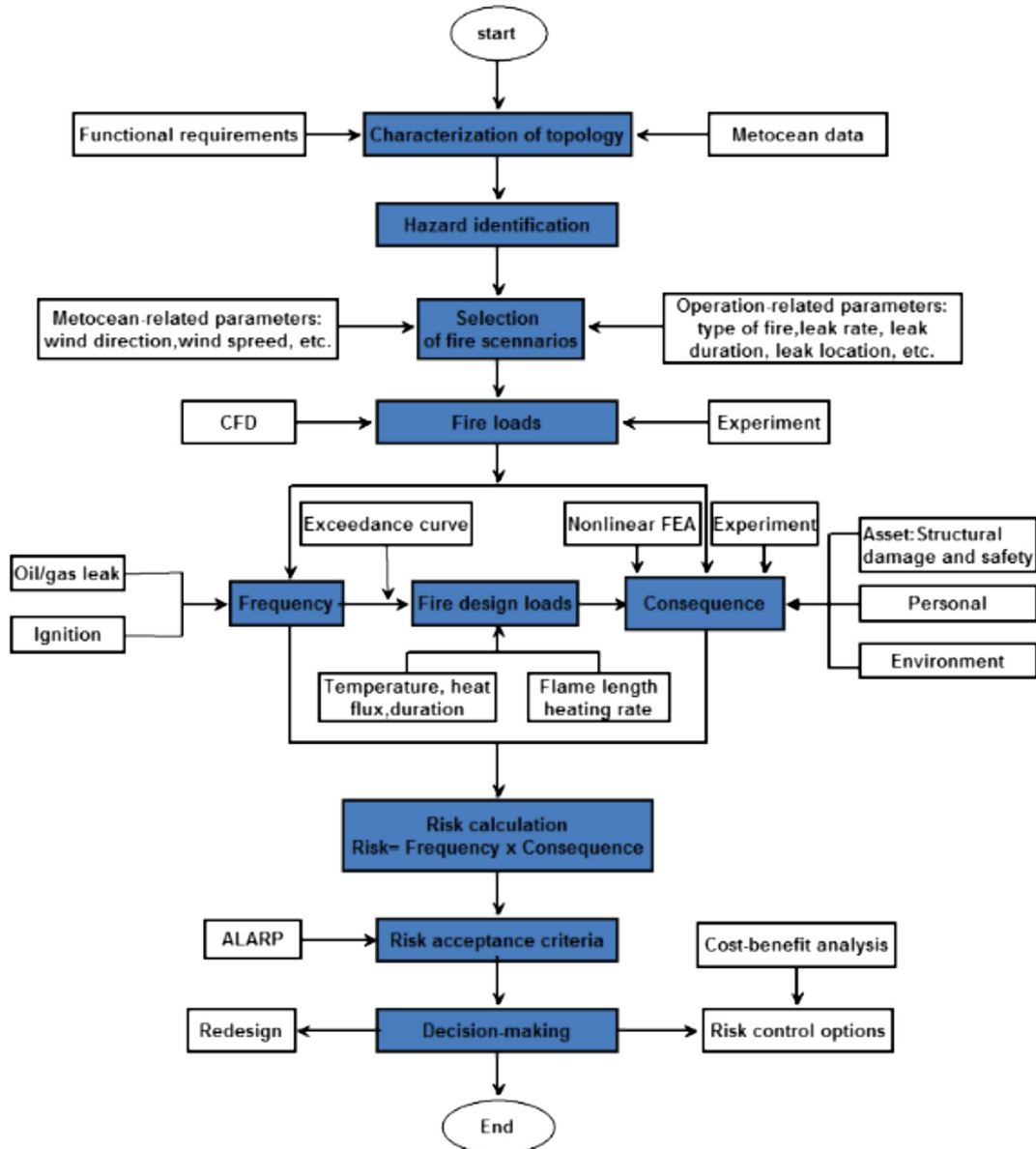


Figure 49.7

EFEF JIP procedure for the fire risk assessment and management of offshore installations.

Risk is defined as a product of frequency and consequence. Thus, the main purpose is to accurately calculate the frequency and consequences of specific events within the framework of risk assessment and management.

To estimate the risk level of a structure, the identification of danger source and action effects of fire are vital. Each of the fire scenarios can be simulated by computational fluid dynamics (CFD). This establishes and characterizes the fire load profiles based on time and space in terms of temperature and heat amount. The CFD modeling techniques employed are significantly essential to the accuracy of these CFD simulations. There are eight random variables to formulate fire scenarios via sampling techniques:

- Wind direction (X1)
- Wind speed (X2)
- Leak rate (X3)
- Leak duration (X4)
- Leak direction (X5)
- Leak position in the x direction (X6)
- Leak position in the y direction (X7)
- Leak position in the z direction (X8)

The design fire loads can be decided by the fire load profile with respect to time, temperature, and heat dose and converted to software using finite element analysis, that is, ANSYS, ABAQUS, to realize the non-linear structural response. The properties of the fire resistance of steel are the main factors affecting the structural integrity of fire. A noncontinuous segment plot based on the definition of Eurocode ([Franssen and Real, 2010](#)) is shown in [Figure 49.8](#). When it is at 400 °C the mechanical properties of steel significantly decrease. On the other hand, the heat from fire flows into steel, which is a good conductor compared to other materials. Thus, fire can lead to the collapse of steel structures.

The frequency of fire is the likelihood of accidents, leaks, and ignitions. The frequency of leaks and ignitions can be obtained by ETA. Finally, the risk is calculated. If the calculated risk level is greater than the acceptable risk level, then the system must be redesigned, or such other control measures must be taken such as a fire wall, passive fire protection, or deluge/water spray. Acceptable risk level is normally defined in terms of the probability of damage exceeding the main safety functions or probability of accident escalation.

49.4.2 Procedure for Explosion Risk Assessment and Management

In general, the response assessment methods include three main levels of analysis: screening check, strength level analysis (SLA), and ductility level analysis (DLA).

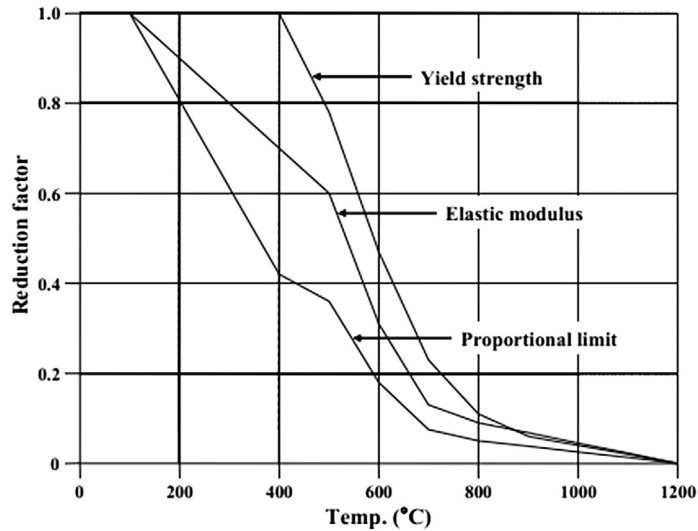


Figure 49.8

Mechanical properties of steel with temperature as the plot of Eurocode's definition.

The screening check checks for the safety and reliability of the whole structure. The SLA is used to estimate the failure of most topside components during early detailed engineering as a linear elastic analysis. However, the demand for the DLA from ship owners has increased recently rather than the preference for the SLA for most of the topside modules of FPSO/FLNG (floating liquefied natural gas) offshore facilities. [Figure 49.9](#) presents the practical approach widely used in the offshore industry based on API RP 2FB.

Kim et al. (2014) present the DLA methodology for the topside modules under blast loads in terms of the offshore industry calculation method.

Explosions create pressure waves and the energy releases take place in a very short period creating a shock front in which a peak pressure occurs. Following this, the overpressure drops very rapidly and reaches a negative phase. The typical simplified pressure–time curve is shown in [Figure 49.10](#).

In Kim et al. study, a two-time step process was applied to simulate the dynamic response for blast load by using ABAQUS software. The first step is a static analysis for self-weight stabilization, and the next step is a dynamic analysis for actual structural response under the blast loading.

The purpose of the DLA method is to verify the nonlinear dynamic structural behavior under the dynamic load (blast loading). A certain amount of resonance may occur in the vibrating response of the topside structures due to both the maximum positive and

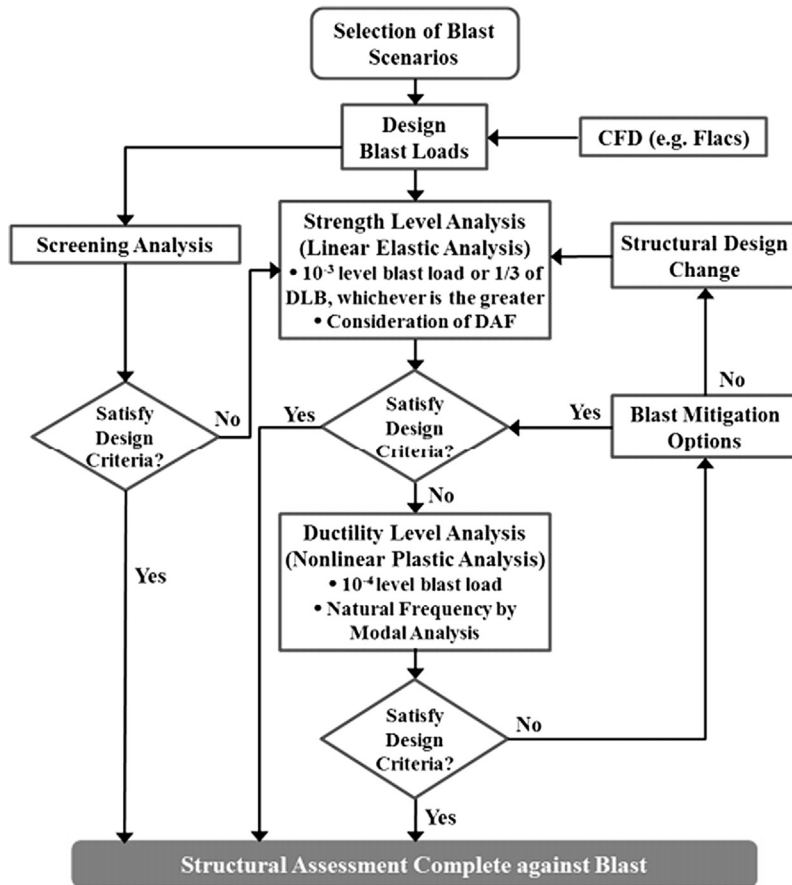


Figure 49.9

Flow chart of structural assessment against blast.

negative deflections and forces with accelerations of each structural component. It is therefore of importance to evaluate the appropriate vibration mode shape, depending on the specific relation between the natural frequency of the structure itself and triangular impulsive loads with the blast duration. Obviously, the natural frequency is of major importance to the dynamic analysis and it can be found by modal analysis.

The strain and stress of all members can be obtained during the dynamic analysis. To ensure the structure is safe all of the members should not exceed the correct plastic strain.

Once the DLA cannot satisfy the criteria of assessment, some blast mitigation should be carried out. There are two methods to minimize the damage for explosion accidents. One is to decrease the frequency of accidents in gas release, formation, and ignition of an explosive cloud. The other is to reduce the consequence by installing a safety system.

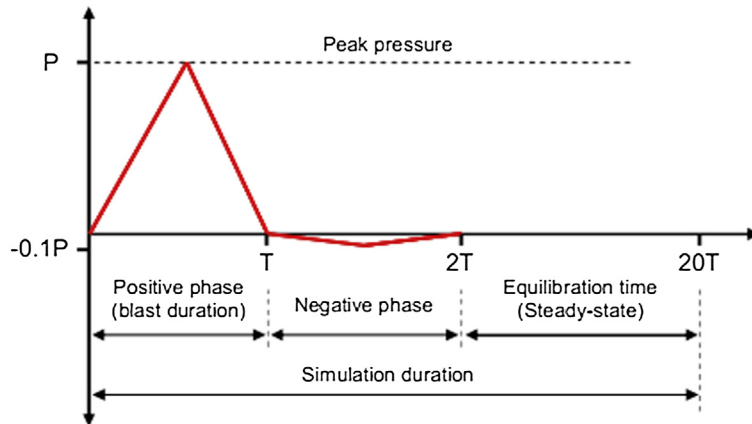


Figure 49.10
Simplified pressure–time curve.

Corrugated and flat-plate type blast walls are generally used for the purposes of reducing the explosion consequences.

49.5 Phase III: Risk Restraining Project

In terms of fire prevention and control of offshore platforms, strict precautions should be formulated to avoid fire and explosion caused by hydrocarbon combustion. The specific measures are described below.

1. Improve the layout

The platform's location should avoid an earthquake-prone belt and lightning-vulnerable areas, and fuel storage areas should be set in a well-ventilated downwind position and kept at a maximum distance from sources of ignition. In the process of building a layout for the firing of containers and work over well completion and temporary facilities, special measures should be raised.

A reasonable arrangement of a firewall will help prevent flames from spreading and provide a heat insulation barrier. Meanwhile, the firewall should avoid adverse effects of large amounts of hydrocarbon steam and combustible gas gathering.

2. Team management

For most instances of accidents, human error is the main factor. Workers manage the main body and object management, education of staff, and safety training. The education process, stricter accordance with operating instructions, and not overloading operations should be strengthened in offshore productions. Strengthening the platform patrol inspection work will guarantee a better flow of work.

3. Management of equipment

Offshore equipment suffers from perennial water and wind erosion. Therefore, strengthening the maintenance of equipment is necessary. There is a special process that forbids hot maintenance.

It is necessary to periodically blow down parts of the equipment to prevent fires and explosions caused by high pressure. Natural ventilation components shall be equipped with a spark and fire detector to prevent sparks.

4. Strengthen the inspection and maintenance of lightning protection and electric bonding facilities

Offshore platforms are flammable and explosive areas. Oil and gas production operation should be stopped during a thunderstorm. In order to avoid fire accidents caused by static electricity, certain electrostatic protection devices are necessary. Electrostatic discharge facilities should be in good condition and connection parts fixed firmly.

Operators should dress according to the rules and not wear chemical fiber clothes. A human body electrostatic touch release facility should be set up before workers take up their quarters.

5. Strengthen the inspection and maintenance of electrical facilities

Electrical safety is a comprehensive technology, requiring both engineering and organization. It includes insulation protection, barrier protection, safety distance protection, grounding lightning protection, leakage protection, automatic control equipment, etc. Offshore equipment ages quickly and erodes due to long exposure, so it is important to strengthen the maintenance inspection daily so as to prevent electrical components aging and short circuiting.

6. Hot surface protection

Structure surfaces with abnormally high temperatures should not come in contact with liquid hydrocarbon, oil, and flammable gases.

7. Security system and fire control facilities

A platform security system should be put in place to detect abnormal occurrences and prevent accidental fires. A combustible gas detector should be installed to detect the concentration of combustible gases. When the concentration reaches the explosion limit, it should provide a warning and truncate the source of the fire.

In order to prevent the spread of fire, a fixed or semifixed type of foam fire extinguisher is needed. Finally, increase the staff's education of extinguishing equipment use and their ability to make an immediate response.

49.6 Examples of Explosion Response of FPSO

49.6.1 Introduction

FPSO has become the mainstream of the development of offshore oil gas production field because of the advantages of transferable and reusable. Research into the safety and reliability of FPSO is of great significance.

The authors conducted a quantitative risk assessment of combustible gas under explosion hazards. We made a simulation of the leakage and explosion process of combustible gas in FPSO by FLACS CFD and made an analysis of the explosion load characteristics. Then we imported data of the simulation into the ANSYS/LS-DYNA computations to make an analysis of structural response of the offshore platform.

The contribution of this study is demonstrated with an applied example using a hypothetical topside structure of an FPSO that is exposed to hydrocarbon explosions. We then presented a procedure for the non-linear structural response analysis of offshore installations with a focus on explosions.

49.6.2 Gas Dispersion CFD Simulations

The FLACS code, which is a three-dimensional transient finite volume CFD program, is used to simulate gas dispersion and explosion events. The commercial version of the FLACS code provides the results at a limited number of monitoring points and/or panels.

To demonstrate the applicability of the FLACS code in the simulations of gas dispersion, an example of an explosion analysis in an offshore module is considered. [Figure 49.11](#) shows the layout and principal dimensions of this hypothetical topside module of the FPSO.

The gas dispersion simulation is performed to characterize the gas cloud size, which is affected by various factors including leak rates, duration times, positions, and wind conditions.

Gas Dispersion Scenario

Gas dispersion is as follows:

- Leak rate: 4 kg/s
- Leak location: (6,6.75,2)
- Start time: 0 s
- Leak duration: 40 s
- Temperature: 20 °C
- Gas composition: methane 91%, ethane 7%, propane 2%
- Wind speed: 3 m/s
- Wind direction: +X

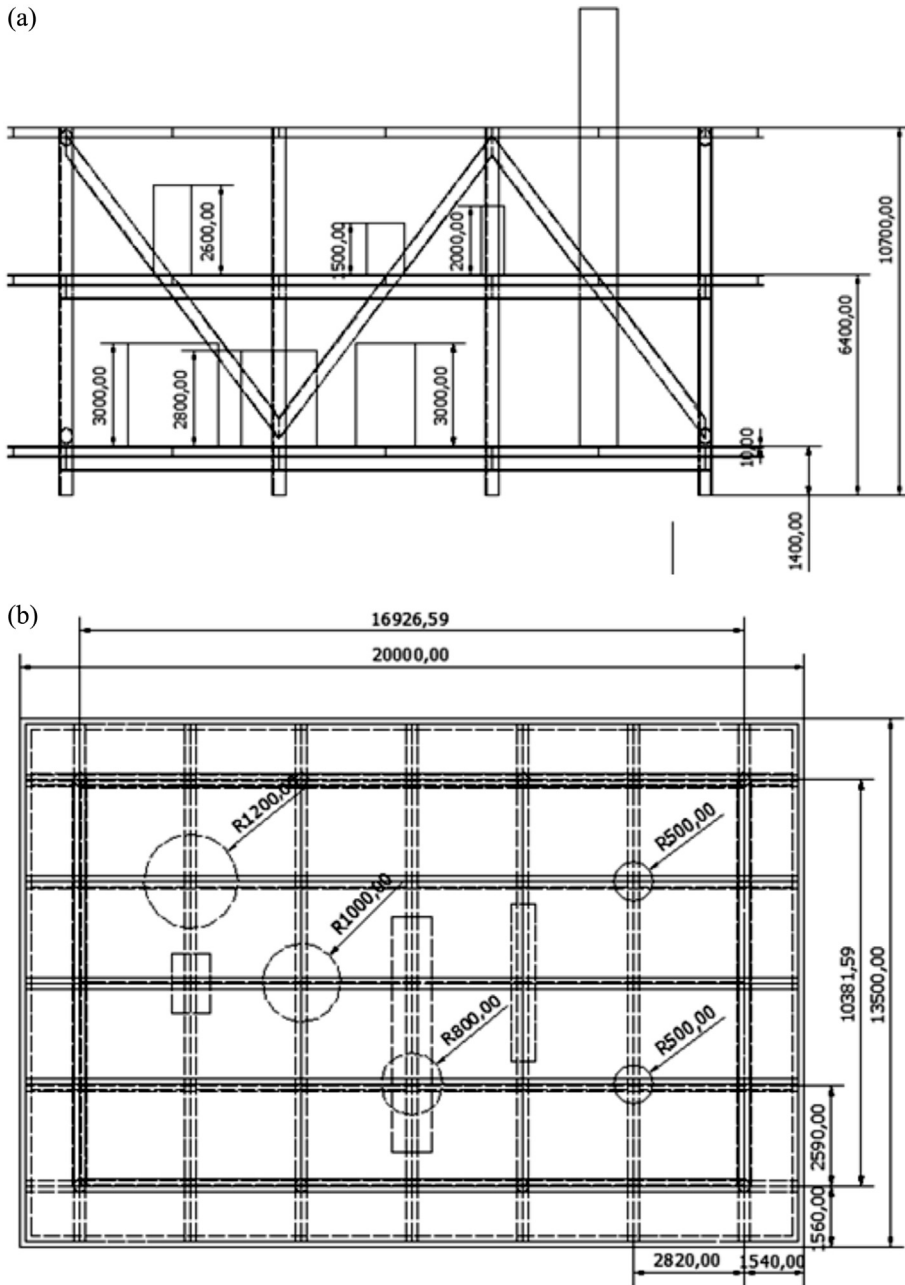


Figure 49.11

Layout and principal dimensions of the hypothetical FPSO topside module, (a) side view, (b) ichnography.

The Spatial Distribution of Gas Concentration

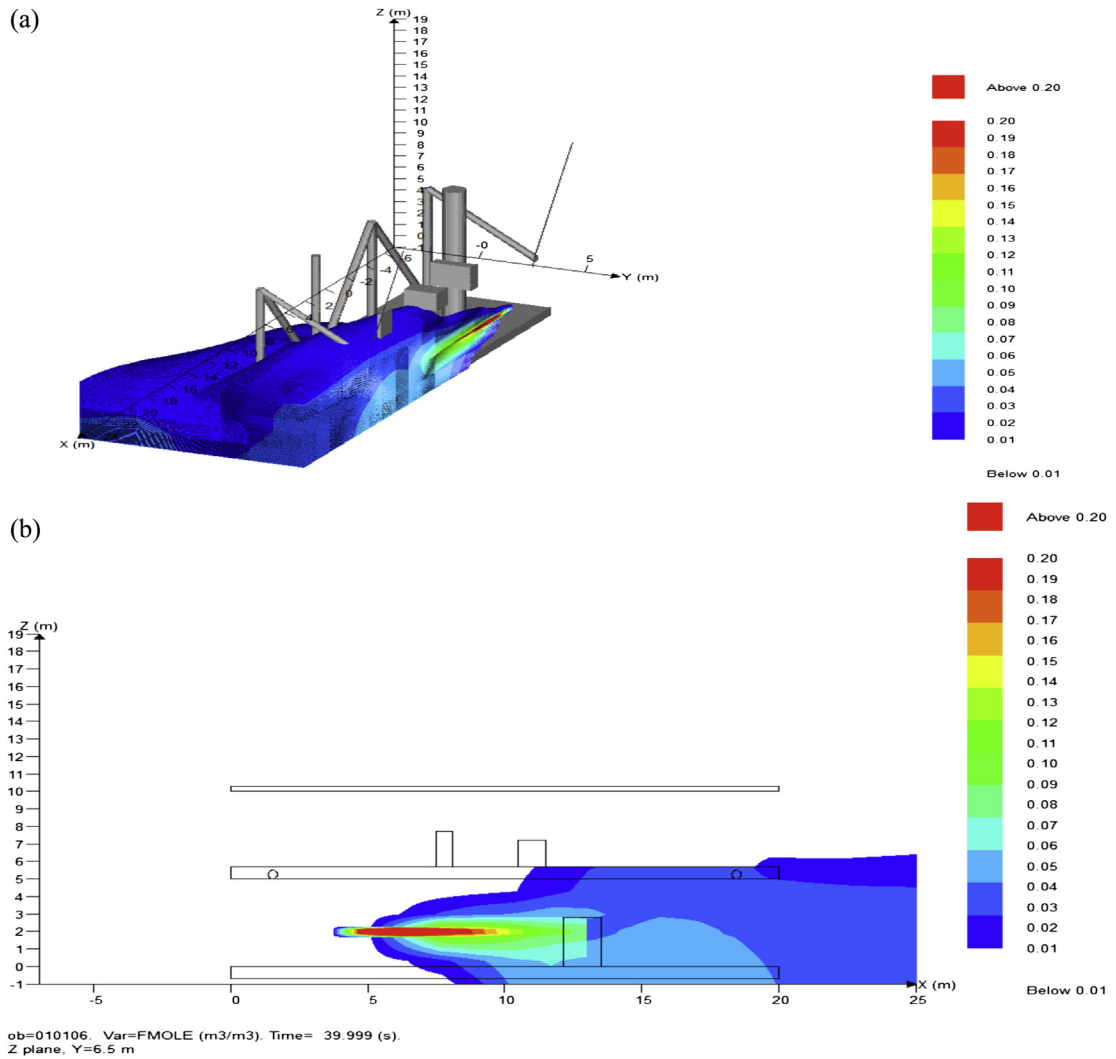


Figure 49.12

The spatial distribution of gas concentration at $t = 40$ s, (a) 3d view, (b) $y = 6.5$ m.

Actual Gas Cloud and Equivalent Gas Cloud

The cloud shown in Figure 49.12 is the actual gas cloud. The equivalent gas cloud volume is defined when the equivalent ratio defined in Eqn (49.9) equals 1.

$$ER = \frac{(m_{fuel}/m_{oxygen})_{actual}}{(m_{fuel}/m_{oxygen})_{stoichiometric}} \quad (49.9)$$

where m_{fuel} and m_{oxygen} are mass of gas and oxygen in actual or stoichiometric conditions, respectively.

Effect of Leak Rates

In the simulation process of flammable gas leakage, we set the speed as 1, 2, 3, and 4 kg/s, respectively. The volume of actual gas cloud and equivalent is showed in [Figure 49.13](#).

49.6.3 Gas Explosion CFD Simulation

A flammable gas explosion is influenced by many factors, such as leak rates, leak location, combustion source location, and so on.

Gas Explosion Scenario

The gas dispersion is as follows:

- Leak rate: 4 kg/s
- Leak location: (6,6.75,2)
- Start time: 0 s
- Leak duration: 40 s
- Temperature: 20 °C
- Gas composition: methane 91%, ethane 7%, propane 2%
- Wind speed: 3 m/s
- Wind direction: +X
- Combustion source location: (8,6.75,3)
- Ignition time: 40 s

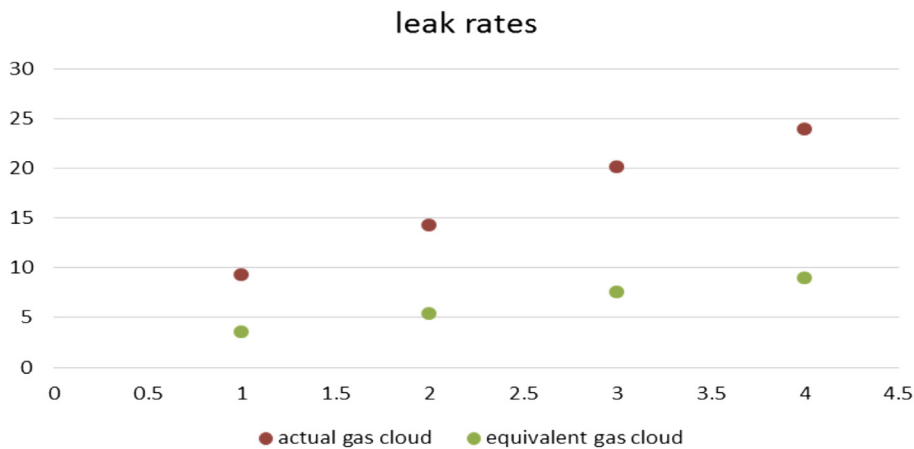


Figure 49.13
The effect of leak rates.

Figure 49.14 shows the allocation of 128 monitoring points to read overpressures (P) and combustion product mass fraction (Prod) on the positions of interest.

Figure 49.15 shows the distribution of combustion product mass fraction (Prod) at 40 s and Figure 49.16 shows overpressures (P) at monitor point 28.

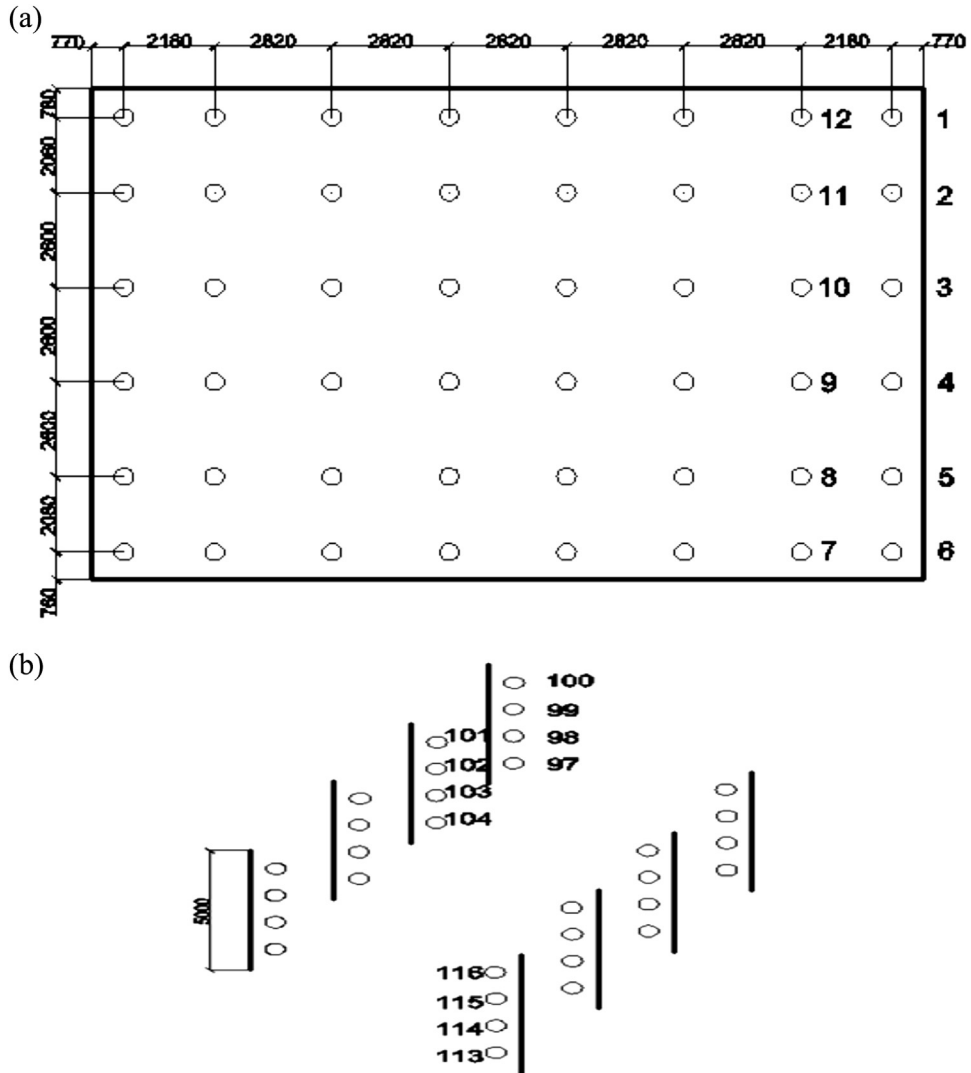


Figure 49.14

The allocation of 128 monitoring points, (a) monitoring points on mezzanine deck and process deck, (b) monitoring points on main column.

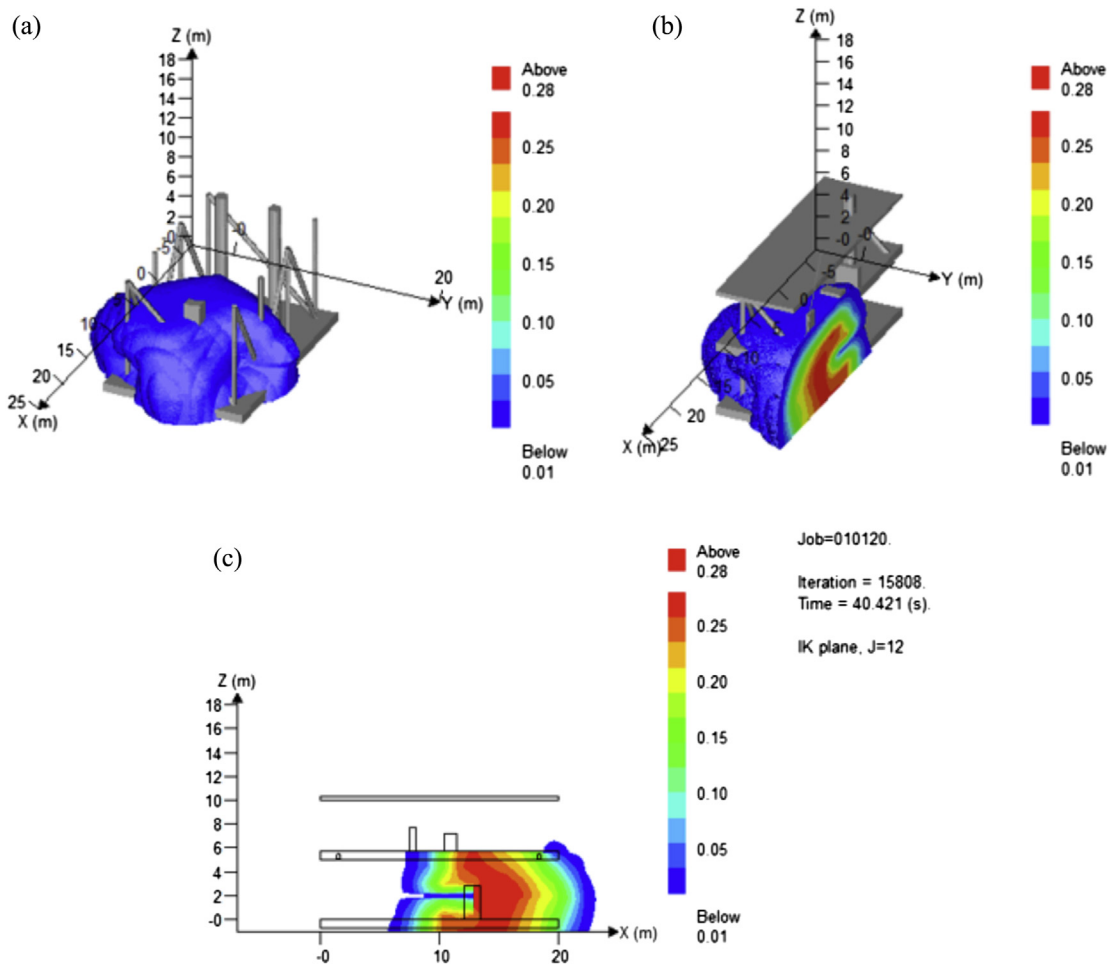


Figure 49.15

The distribution of combustion product mass fraction (Prod) at 40 s, (a) three dimensional space, (b) $y = 6.5$ m 3d profile, (c) $y = 6.5$ m 2d profile.

49.6.4 Nonlinear Structural Response Analysis

The structural response analysis is undertaken for a situation in which the topside structures are subjected to explosion loads.

Structure Model

Figure 49.17 shows the model of a target structure with SHELL163 elements. The structures are made of mild steel and the material property is presumed to be plastic

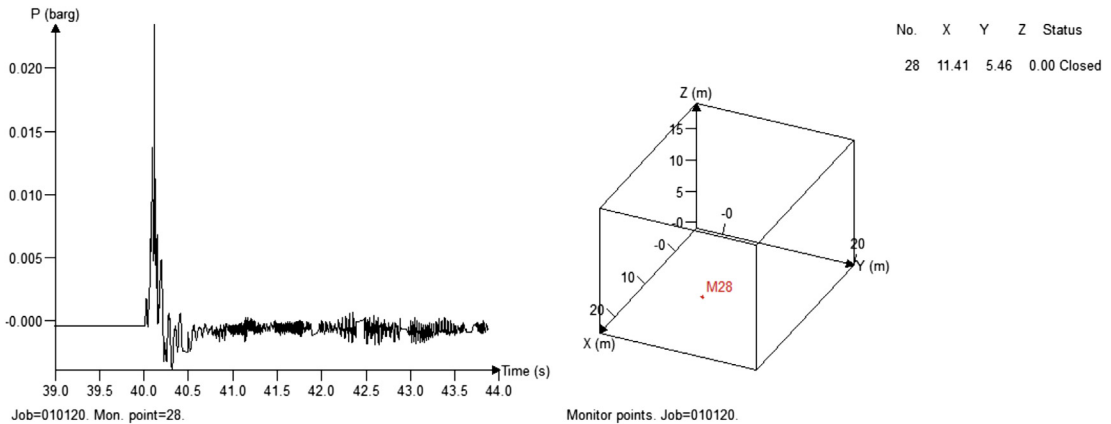


Figure 49.16

The overpressure at monitor point 28.

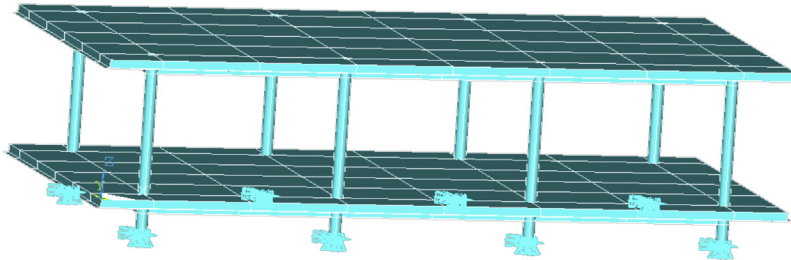


Figure 49.17

LS-DYNA structure model.

kinematic. The ends of all eight columns are set to be fixed and all other boundaries are in a free condition.

The Distribution of Structure Stress, Displacement, and Strain

Each monitoring of the overpressure curve is loaded into the structure, and we get the following platform structure displacement and stress distribution. [Figure 49.18](#), [Figure 49.19](#), and [Figure 49.20](#) show the von Mises stress distribution, displacement distribution, and strain distribution, respectively, at 0.12 s.

The Distribution of Displacement on Main Columns

We select the four elements on the column as shown in the [Figure 49.21](#) and the overpressure–time curve is showed in [Figure 49.22](#).

The results show that the overpressures on the upper and bottom of the main column are higher compared with the overpressures on the middle.

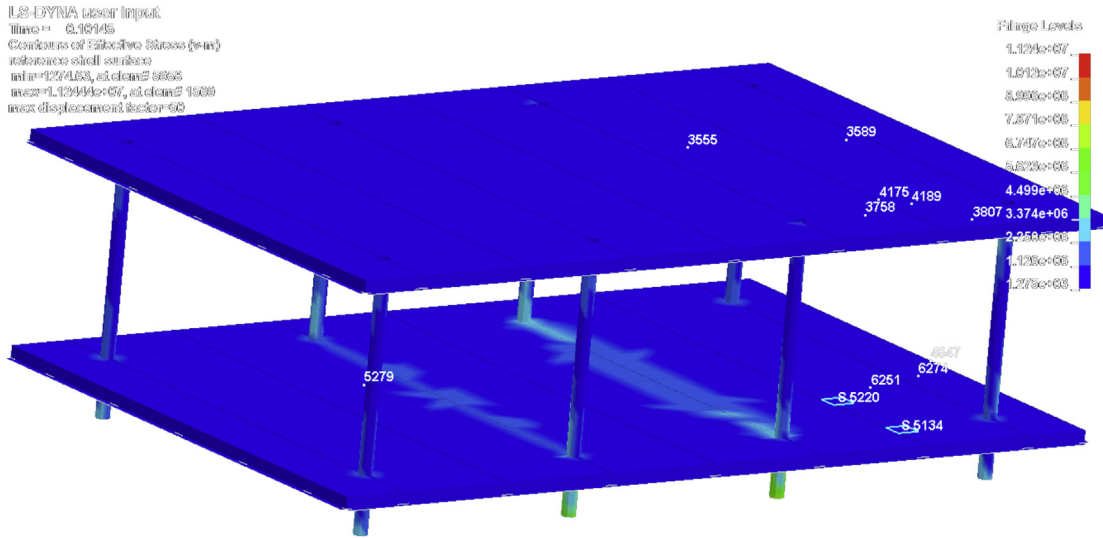


Figure 49.18
 The von Mises stress distribution at 0.12 s.

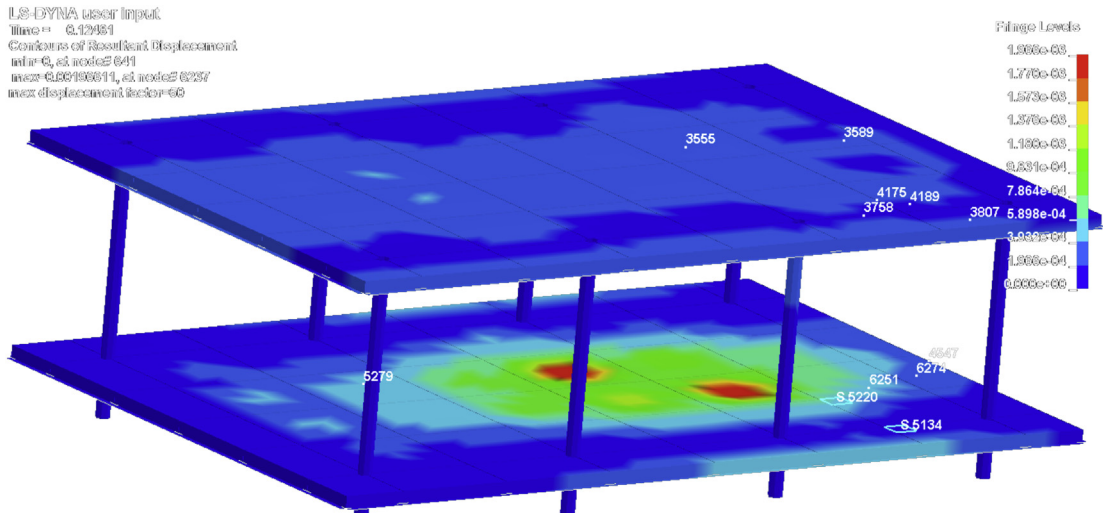
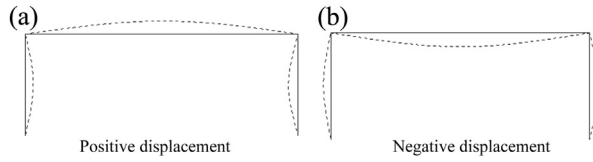


Figure 49.19
 The displacement stress distribution at 0.12 s.

The Displacements on the Midpoint of the Main Girder

For the whole deformation of the upper structure, it is vital to examine the deformation of the main girder. The displacements on the midpoint of main girder can effectively reflect the deflection of the frame.



LS-DYNA user input

time= 6.814729
 Contours of Hoop Strain-Contour Str Max/min
 min=5.62003e-06, at elem# 296
 max=6.29067e-06, at elem# 1356
 max displacement factor=60



Figure 49.20
 The strain distribution at 0.12 s.

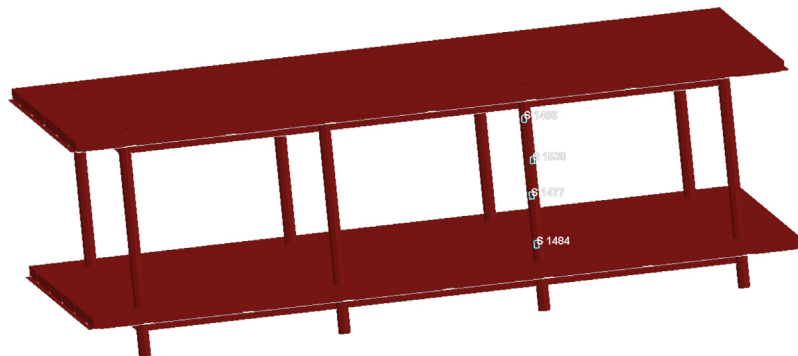


Figure 49.21
 The location of four elements.

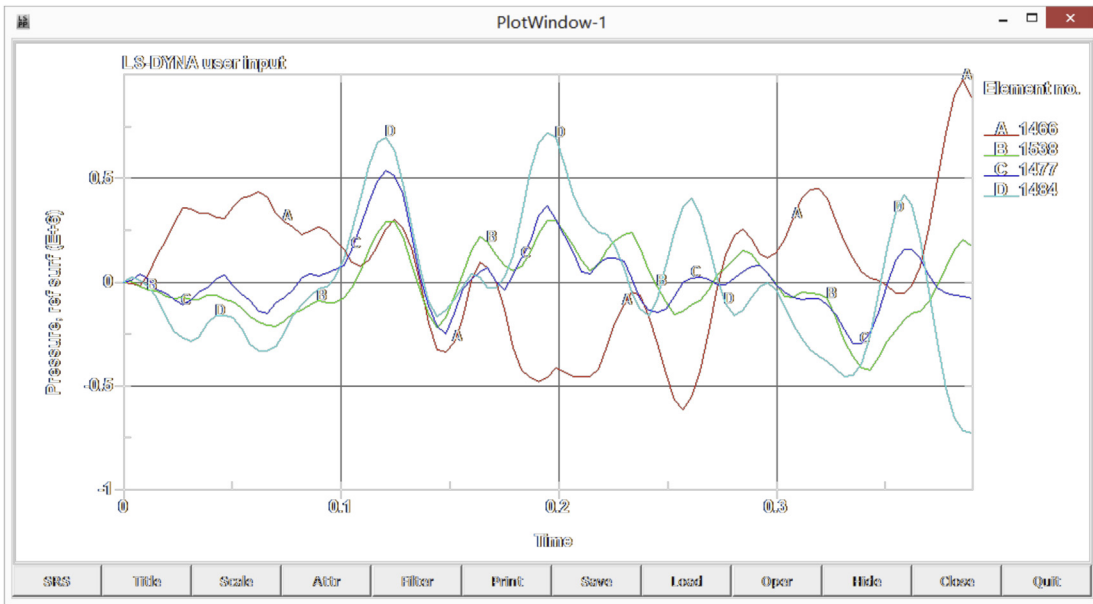


Figure 49.22
Overpressure—time curve.

The Deflection of the Frame

The location of the four midpoints of the main girder is shown in Figure 49.23 and the displacement—time curve is shown in Figure 49.24.

The displacement of the C point has the closest distance from the explosion sources reaching a maximum at $t = 0.39$ s with a value equal to 0.41 mm. The displacement of the C point is about 1.7 times the displacement of the D point.

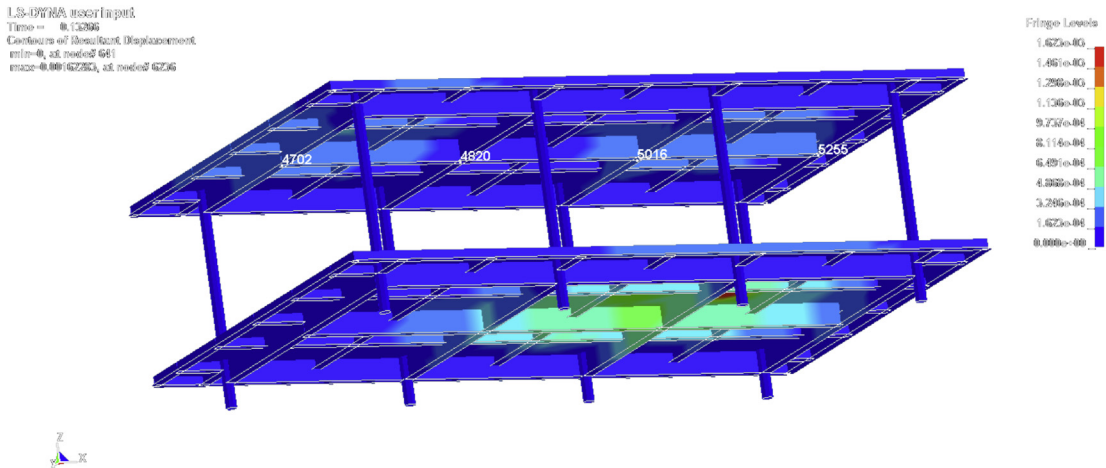


Figure 49.23
The location of the four midpoints of the main girder.

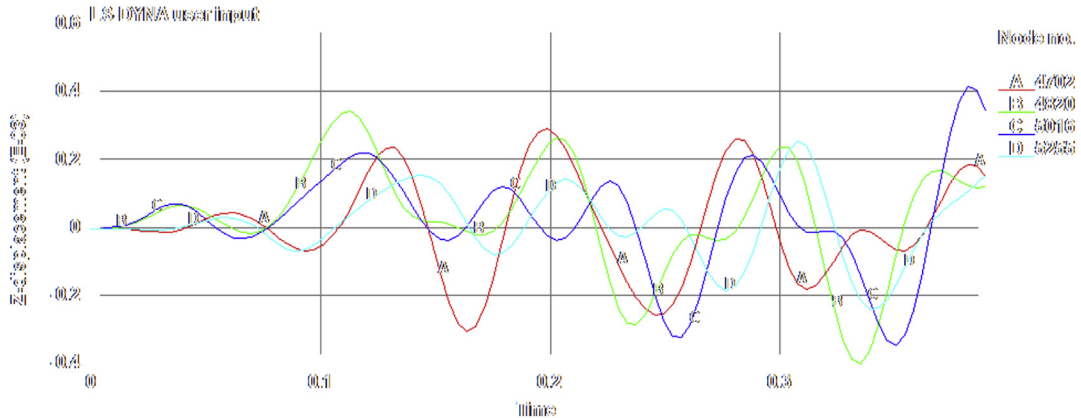


Figure 49.24
The displacement—time curve.

49.7 Example of Fire Response of FPSO

49.7.1 Fire CFD Simulation

Fire Scenario

The object of the fire CFD simulation is to simulate the gas cloud dispersion, gas cloud temperature, and heat fluxes that are time and space dependent. The fire load is correlated to the elevated temperatures obtained from the fire CFD simulation.

One of the commonly adopted tools for fire CFD simulations is the fire dynamic simulation (FDS), which is a fire dynamic simulator, a CFD model of fire-driven fluid flow. FDS solves numerically a form of the Navier—Stokes equations appropriate for low-speed, thermally driven flow with an emphasis on smoke and heat transport from fires.

The fire example we simulate here is a pool fire, which is caused by combustible liquid burning on the surface. The following fire scenario was selected in the fire CFD simulation:

- Density of heat flow = 24,000 kW/m²
- Leak area = 1.5 × 1.5 m
- Leak direction = +Z
- Leak position in the X direction = 10.75 m
- Leak position in the Y direction = 6.5 m

FDS Structure Model

Figure 49.25 shows the layout and principal dimensions of a hypothetical topside module of the FPSO. All decks are supported by strong I-girders. But here in FDS, the decks are

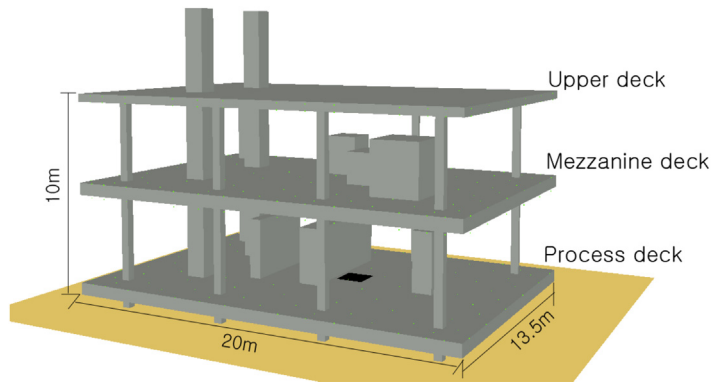


Figure 49.25

Layout and principal dimensions of the hypothetical topside module of the FPSO.

simplified as plates with different thicknesses. The process deck and mezzanine deck are 700 mm thick and the upper deck is 300 mm thick. The columns are also simplified as square columns because no round surface can be built in FDS. [Figure 49.26](#) and [Tables 49.1 and 49.2](#) present the geometric topology of the deck beams and columns.

Using FDS, monitoring points should be reasonably assigned. Each frame has a monitoring point in the middle. Part of the points can be seen in [Figure 49.27](#).

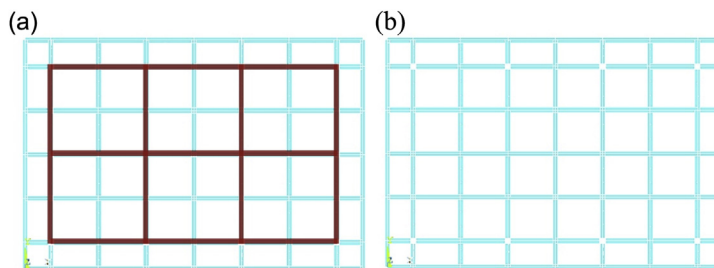
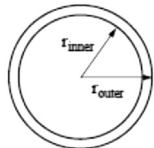


Figure 49.26

Topology of decks (red lines (dark grey in print versions) indicate main frames and dotted lines indicate secondary frames), (a) process and mezzanine deck, (b) upper deck.

Table 49.2: Dimensions and geometric properties of the columns

	Symbol	Column
	r_{inner} (mm)	160
	r_{outer} (mm)	178

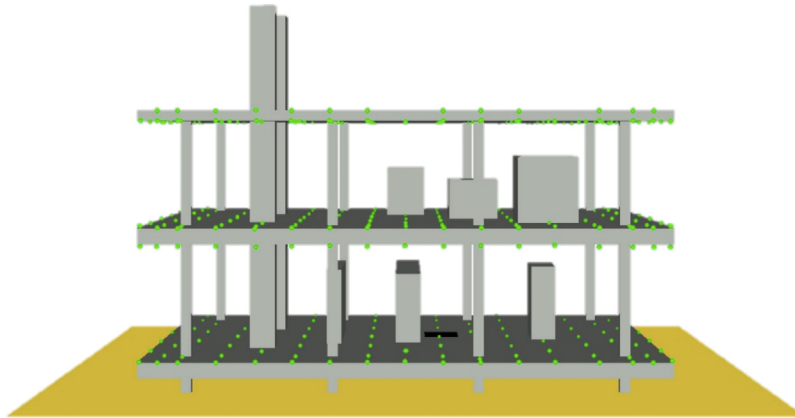


Figure 49.27
Monitoring points.

FDS Results

Smokeview is a separate visualization program that is used to display the results of an FDS.

[Figure 49.28](#) displays the heat flux at time 3.6 and 600 s.

[Figure 49.29](#) displays the temperature distribution at cross-section $Y = 7.6$ m at time 10 and 600 s.

[Figure 49.30](#) displays the temperature distribution at cross-section $X = 9.8$ m at times 10 and 600 s.

[Figure 49.31](#) displays the temperature distribution at cross-section $Z = 5.7$ m at times 10 and 600 s.

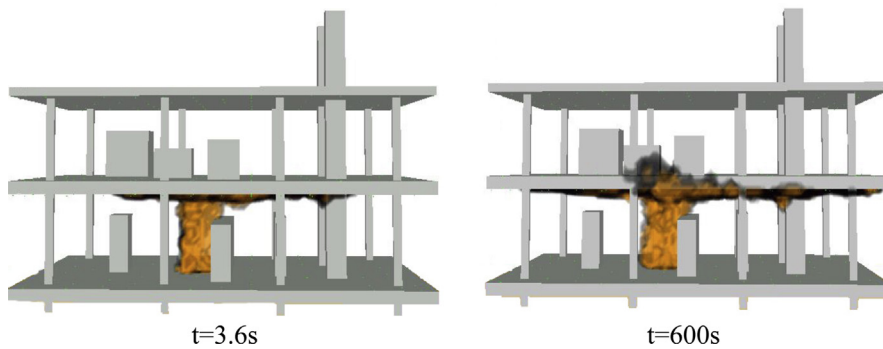


Figure 49.28
Heat flux at different simulating times.

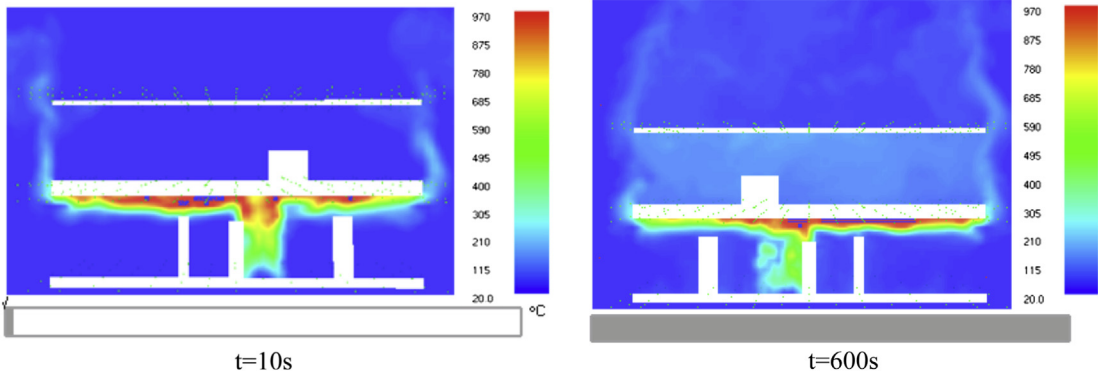


Figure 49.29
Temperature distribution at cross-section $Y = 7.6$ m at different times.

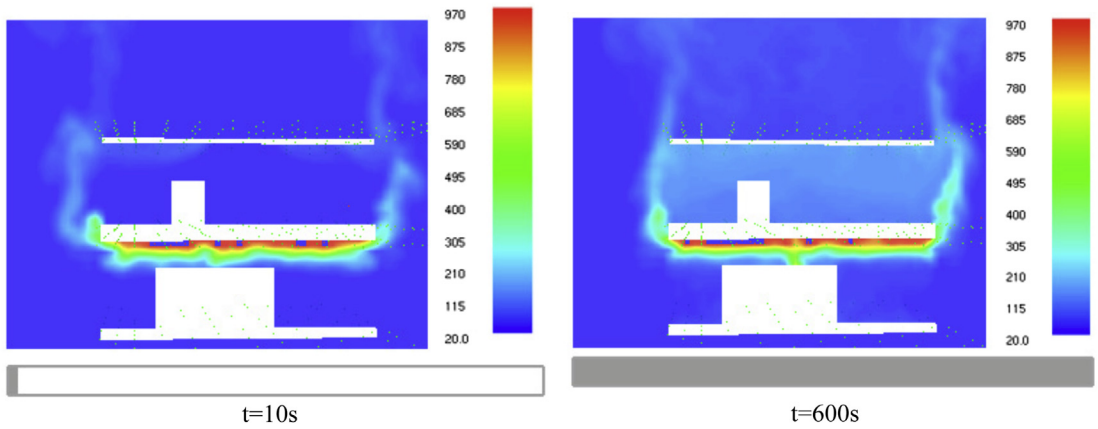


Figure 49.30
Temperature distribution at cross-section $X = 9.8$ m at different times.

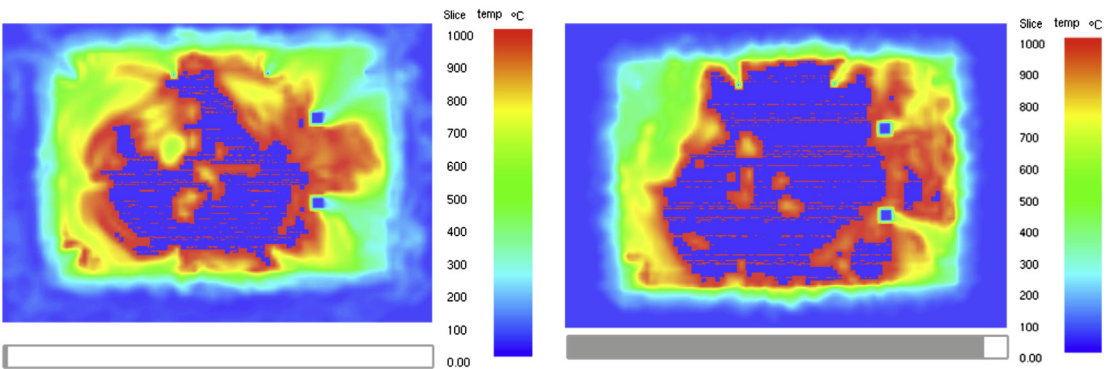


Figure 49.31
Temperature distribution at cross-section $Z = 5.7$ m at different times.

49.7.2 ANASYS Analysis

Temperature Simulation

The result of the ANASYS temperature simulation using SHELL131 is shown in Figure 49.32. The maximum temperature is 590.55 °C. The mezzanine deck is influenced mostly while the process deck remains almost the same when there is no fire.

Structure Analysis

Take Q235 steel as an example. The elasticity modulus and yield stress of Q235 change with temperature in Table 49.3.

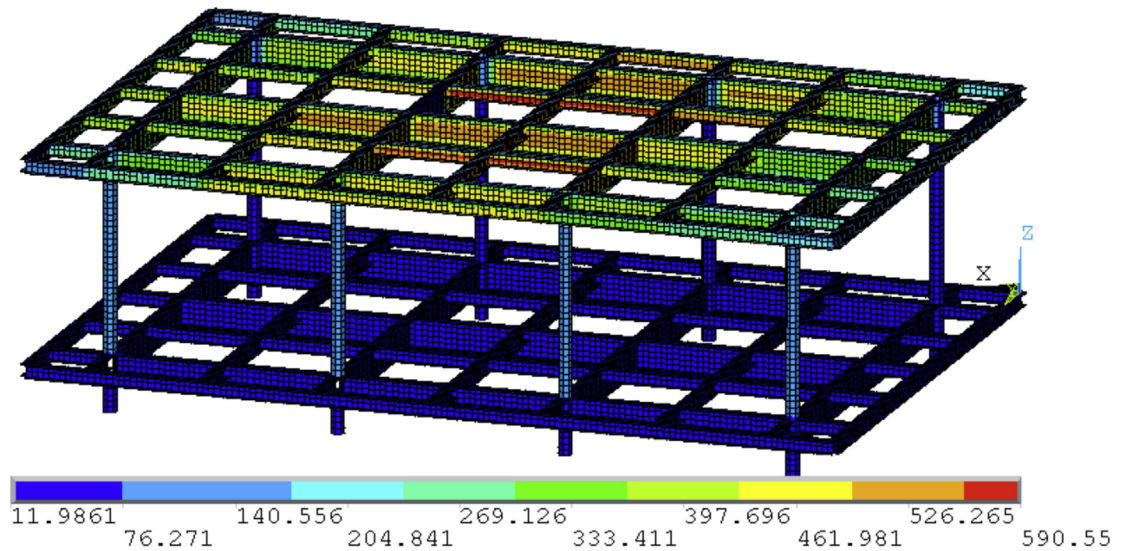


Figure 49.32

Temperature simulation in ANASYS.

Table 49.3: The elasticity modulus and yield stress of Q235

Temp (°C)	Elasticity Modulus		Yield Stress		Ton-module
	T Temp/ε = 16 °C	T Temp (MPa)	T Temp/ε = 16 °C	T Temp (MPa)	T Temp (MPa)
16	1.000	206,000	1.000	235	707
100	1.000	206,000	1.000	235	707
200	0.959	197,554	0.823	193	1800
300	0.900	185,400	0.629	148	1831
400	0.831	171,186	0.498	117	994
500	0.621	127,926	0.402	94	478
600	0.171	35,226	0.204	48	158

Add the temperature load to the structure and uniform pressure to one of the main frames. Figure 49.33 shows all loads and restrictions on structure.

Results

Structure deflection in the Z direction is shown in Figure 49.34. The biggest deflection is 358 mm.

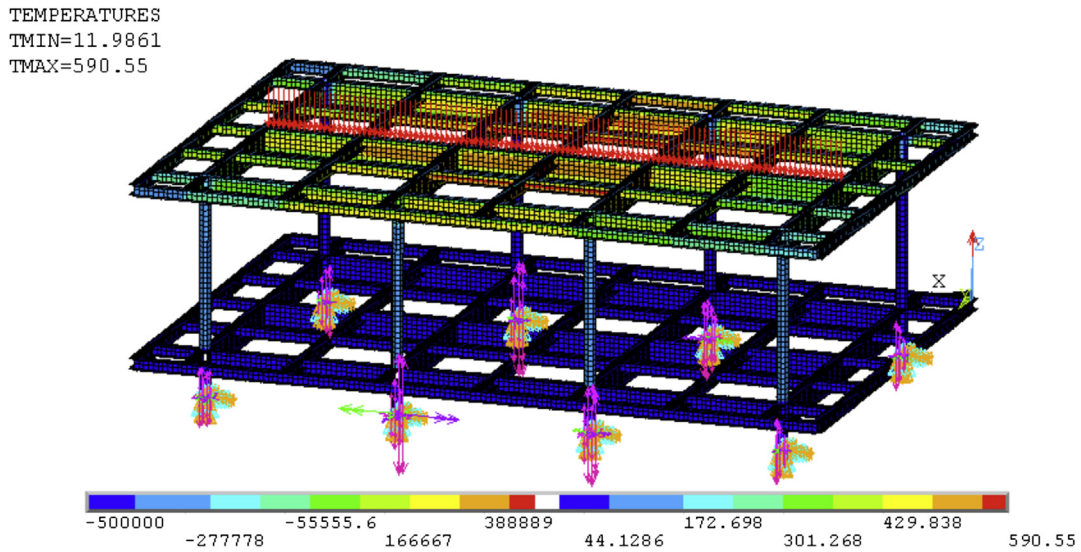


Figure 49.33
 All loads and restrictions on structure.

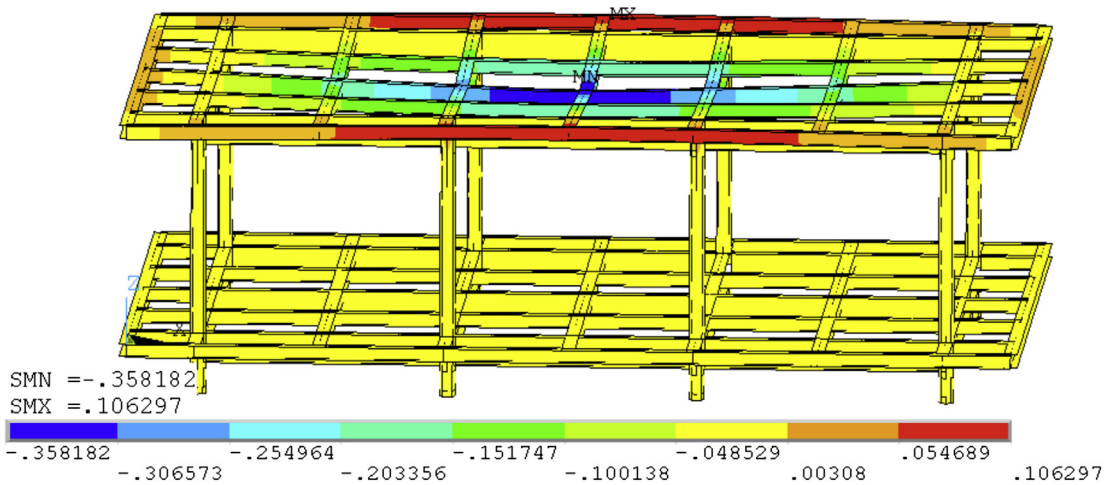


Figure 49.34
 Structure deflection in the Z direction.

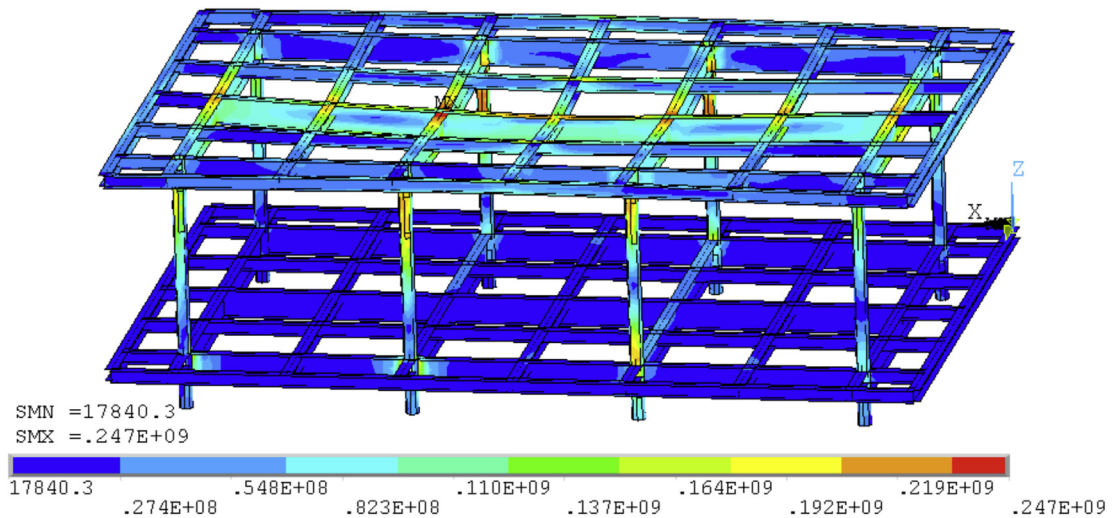


Figure 49.35
von Mises stress distribution.

The von Mises stress distribution is shown in [Figure 49.35](#). The biggest stress is 247 MPa. It takes place in the red area in [Figure 49.35](#).

References

- Bishop, S.R., et al., 1993. Nonlinear dynamics of Flashover in compartment fires. *Fire Saf. J.* 23, 11–45.
- Bossche, A., 1991. Computer-aided fault tree synthesis I. *Reliability Eng. Syst. Saf.* 33, 217–241.
- Cai, K.Y., 1996. System failure and fuzzy methodology: an introductory overview. *Fuzzy Sets Syst.* 83, 113–133.
- Cullen, L., 1990. *The Public Inquiry into the Piper Alpha Disaster*. Health and Safety Executive, HMSO, London.
- Czujko, J., 2001. *Design of Offshore Facilities to Resist Gas Explosion Hazard: Engineering Handbook*. CorrOcean, Oslo.
- Czujko, J., Paik, J.K., 2010. *Explosion and Fire Engineering of FPSOs (Phase II): Definition of Gas Explosion Design Loads*. Final Report No. EFEF JIP-04–R1. Research Institute of Ship and Offshore Structural Design Innovation, Pusan National University, Busan, Korea.
- Franssen, J.M., Real, P.V., 2010. *Fire Design of Steel Structures*. ECCS Eurocode Design Manuals. Ernst & Sohn. Germany, Berlin.
- Gee, P.H., 2000. The evolution of offshore legislation. *Trans. ImarE* 112 (1), 3–10.
- HSE, 2005. *Accident Statistics for Floating Offshore Units on the UK Continental Shelf (1980–2003)*. HMSO RR 353. Health and Safety Executive, London.
- Kim, T., 2014. *The Nonlinear Dynamic Structural Response Analysis of the FPSO Topside Module under Blast Loads*, ICTWS 2014, Busan, Korea.
- Msc/Cir.829, MEPC/Circ 335 Interim Guidelines for the Application of Formal Safety Assessment (FSA) to the IMO Rule-making Process, November 17, 1997.
- Nolan, D.P., 1996. *Handbook of Fire and Explosion Protection Engineering Principles for Oil, Gas, Chemical, and Related Facilities*. Noyes Publications, Park Ridge, NJ.

- Paik, J.K. A New Procedure for the Nonlinear Structural Response Analysis of Offshore Installations in Fires.
- Paik, J.K., Czujko, J., 2009. Explosion and Fire Engineering and Gas Explosion of FPSOs (Phase I): Hydrocarbon Releases on FPSOs—Review of HSE’s Accident Database. Final Report No. EFEF JIP-02. Research Institute of Ship and Offshore Structural Design Innovation, Pusan National University, Busan, Korea.
- Paik, J.K., Czujko, J., 2010. Explosion and Fire Engineering of FPSOs (Phase II): Definition Offire and Gas Explosion Design Loads. Final Report No. EFEF-03—R2. Research Institute of Ship and Offshore Structural Design Innovation, Pusan National University, Busan, Korea.
- Riding, J.F., 1997. Formal safety assessment (FSA): putting risk into marine regulations. *Trans. ImarE* 109 (2), 185–192.
- Spouge, J., 1999. *A Guide to Quantitative Risk Assessment for Offshore Installations*. Aberdeen: The Centre for Marine and Petroleum Technology, UK.
- Thomas, P.H., Bullen, M.L., Quintiere, J.G., McCaffrey, B., 1980. Flashover and instabilities in fire behavior. *Combustion Flame* 38, 159–171.
- Vinnem, J.E., 2007. *Offshore Risk Assessment: Principles, Modeling and Applications of QRA Studies*, second ed. Springer, London.
- Wang, J., 2006. Maritime risk assessment and its current status. *Qual. Reliability Eng. Int.* 22, 3–19.

Asset Integrity Management (AIM) for FPSO

50.1 Introduction

Asset integrity manage (AIM) is a complete and systematic management process, which uses the method of overall optimization to manage the entire life cycle of assets, in order to achieve the requirements of reliability, safety, environmental protection and economy, and sustainable development. To achieve this goal, the risk management method is the effective way. In other words, risk-based management (RBM) is the core technology of AIM.

With the advantages of strong adaptability, large storage capacity, short cycle of building, and quick return of investment, floating production storage and offloading (FPSO) has been widely used in offshore oil and gas development throughout the world and has become a mainstream offshore oil and gas production facility. In the process of design, construction, installation, debugging and operation, and complexity, FPSO has problems of uncertainty and variability, which will cause safety, environmental, and economic concerns in its operation. So in order to ensure the petroleum and chemical industry enterprise is operating safely and reliably, and to maximize economic returns, and even social benefit maximization, broad experience has shown that AIM, which is based on the analysis of risk, can achieve this goal.

50.2 Basic Theory for RBM

Based on a large number of experimental data and analysis of statistics, we have produced [Figure 50.1](#), showing the recent oil chemical accident statistics. The figure shows that 41% of accidents are generated by mechanical failure, so mechanical integrity plays an important role in the smooth running of equipment over a long period of time.

Data show that 10–20% of the equipment assumes a risk of 80–90%. Based on the above facts, RBM distinguishes between equipment according to the result of risk assessment. For high risk equipment, staff perform specific maintenance and protection, and for low risk equipment, staff perform proper maintenance and protection. In this way, inspection

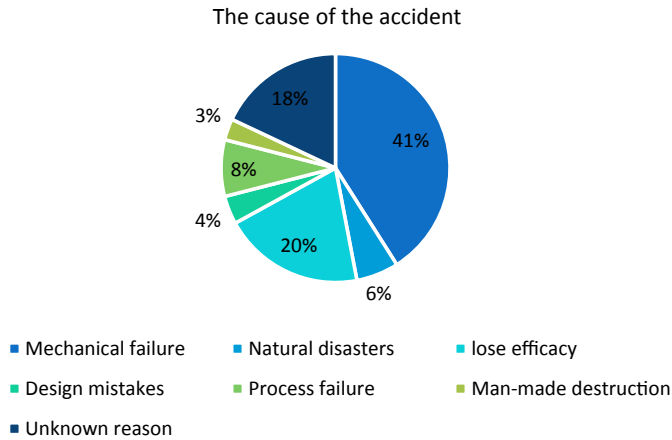


Figure 50.1
The cause of the accident.

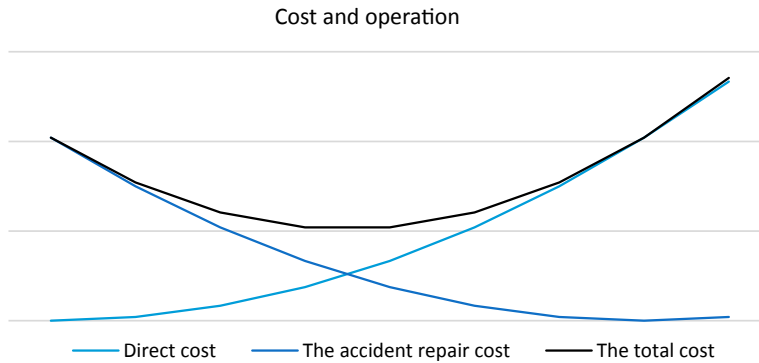


Figure 50.2
Cost and operation.

and maintenance resources are reasonably distributed, which can reduce the overall inspection and maintenance costs and improve the effectiveness of resource utilization.

As is shown in [Figure 50.2](#), we can ensure the safety of equipment and achieve the target of minimizing the cost at the same time, with the appropriate maintenance work. This is the meaning of AIM based on risk analysis of FPSO.

RBM consists of three parts: risk-based inspection (RBI), safety integrity level assessment (SIL), and reliability-centered maintenance (RCM). Considering the similarity among the three parts, this chapter focuses on RBI and makes a brief introduction to SIL and RCM.

50.3 Risk-Based Inspection

50.3.1 Introduction

RBI is a means to design and optimize an inspection scheme based on the performance of a risk assessment process using historical database, analytical methods, and experience and engineering judgment. RBI planning is a method for establishing an inspection strategy based on probabilistic risk analysis, where the inspection effort is focused on those elements with a potential to reduce the risk. Inspection planning based on the RBI approach uses safety, economic, and environmental risk of failure as a rationale, and cost-efficient decision framework for determining when, what, where, and how to inspect.

The probabilistic risk analysis techniques started in the nuclear industry in the 1970s; the American Society of Mechanical Engineers published the first RBI principles overview document in 1991. The American Petroleum Institute, Det Norske Veritas, and the American Bureau of Shipping developed RBI methodology and software in the middle of the 1990s. RBI provides an excellent tool to evaluate the consequences and likelihood of component failure from specific degradation mechanisms and develops inspection approaches that will effectively reduce the associated risk of failure. However, RBI is still a developing technology. Various RBI methodologies are available in the marketplace; each has its own merits and weaknesses. The objective of RBI is to aid the development of optimized inspection, monitoring, and testing plans for meeting specified system acceptance criteria.

A commonly used three-step RBI process is as follows:

- Define a risk and establish its acceptance criteria, such as how to define a risk, how frequently this damage-caused failure is going to occur, what consequences this damage-caused failure may result in, how to judge whether this risk is acceptable or not.
- Assess the risk, such as what method is to be used to assess the risk, how is risk to be assessed, at what level will the risk be categorized, whether the risk level is acceptable or not.
- Establish inspection plan, such as when to perform the next inspection based on the risk assessment result, how to perform, and where to look.

In an actual case, defect assessment may be performed prior to the RBI process, which provides input data such as what damage may cause a risk, where to look for the damage, how to identify the damage, etc., to the entire RBI process. In the RBI process, “high risk” areas and major failure modes are identified and analyzed. These data lead us to target inspection and maintenance resources at these areas of the structure or system where they can have the greatest effect in reducing risk, the occurrence of probability and consequences of unplanned failures, and to reduce the cost of unproductive inspections.

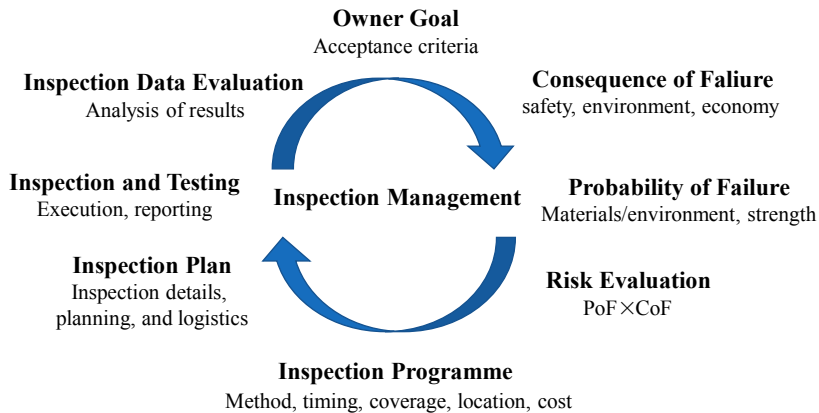


Figure 50.3
RBI management processes.

The RBI progress should be considered as a complement of risk-based integrity management processes. The final object of inspection is to assist FPSO's rectification and integrity maintenance. Once the risk level of the FPSO is identified as unacceptable an inspection or risk reduction activity is initiated, and then the update of the database for risk analysis and the optimized inspection scheme is done as shown in [Figure 50.3](#).

50.3.2 The Main Research Contents

The main research contents include the following:

- Equipment and structures of FPSO
- System classification method for equipment and structures
- Failure mechanism
- The failure consequences
- Failure probability
- The risk assessment method and risk classification method
- Test plan based on risk rating

50.3.3 Modeling the Risk

General

The implementation of an RBI procedure starts with the determination of the relevant failure modes that should be regarded. After identification of the relevant failure modes, the risk of failure can be assessed by estimating the corresponding probability and consequence in relation to a level that is acceptable, and then the inspection and repair used to ensure the level of risk remains below that acceptance limit. The risk is the

combination of the probability of some event occurring during a time period of interest and the consequences associated with the event. In the RBI analysis process, risk matrices are used to calculate the risk of associated component, in which the risk is defined as the product of the probability of failure (PoF) and the consequence of failure (CoF):

$$\text{Risk} = \text{PoF} \times \text{CoF}$$

The risk can be represented in a matrix with the columns and rows as probability and consequence, respectively. Three different risk assessment methods are commonly used in the RBI process, which are qualitative, quantitative, and semiquantitative methods.

Qualitative RBI: Qualitative methods are based on few essential data and lead to a rough estimation of the failure probability. The qualitative rankings (PoF and CoF rankings) are usually the result of using an engineering judgment-based approach to the assessment, in which a numerical value is not calculated, but a descriptive ranking is given, such as low, medium, or high. The advantages of using a qualitative approach are finishing the assessment quickly at a low initial cost, little requirements for detailed information, and the results easily presented and understood.

Quantitative RBI: Quantitative methods are model-based approaches in which quantitative values are expressed and displayed in qualitative terms by assigning bands for PoF and CoF, and assigning risk values to risk ranks to compare with the risk criteria. A much more wide database is supposed to be well prepared for the quantitative analysis, and the PoF value may be evaluated by using a numerically precise structural reliability method and CoF by well-published consequence modeling.

Semiquantitative RBI: Semiquantitative methods use more information and calculations, which results in a more accurate failure probability. The quantitative methods consider fully probabilistic approaches and lead to an accurate determination of the existing failure probability. However, in engineering practices, the data required for the fully quantitative approach are typically not available. Therefore, the semiquantitative approaches are widely used in RBI. A key to any successful risk analysis is choosing the right method or combination of methods for the problem.

Estimation of Risk

The risk associated with a failure from a given degradation mechanism is estimated as the combination of the PoF and the CoF. The risk can be presented as a matrix of CoF and PoF categories. To achieve adequate resolution of detail, a 5×5 risk matrix shown in [Table 50.1](#) is recommended. The matrix has PoF on the vertical axis and CoF on the horizontal.

In the table, the risk matrix shows three risk levels: low risk, medium risk, and high risk, and the risk increases from low level at the left-bottom corner to high level at the right-top corner.

Table 50.1: Risk matrix

Probability category	$>10^{-2}$	Very high	5	High risk				
	$10^{-3}-10^{-2}$	High	4					
	$10^{-4}-10^{-3}$	Medium	3	Medium				
	$10^{-5}-10^{-4}$	Low	2					
	$<10^{-5}$	Very low	1	Low risk				
			A					
			Very low	Low	Medium	High	Very high	
			Consequence category					

Normally, low risk is acceptable, and action such as general visual inspection needs to be taken to ensure that risk remains within this region. Medium risk is also acceptable and action such as nondestructive testing, functional tests, and other condition monitoring activities should be taken to measure the extent of degradation and ensure risks do not rise into the high risk region. High risk is unacceptable and action must be taken to reduce probability, consequence, or both to ensure that risk lies within the acceptable region.

50.3.4 RBI Process

General

The basic RBI process may be divided into the following four steps:

- Data gathering
- Screening assessment
- Detailed assessment
- Risk evaluation and optimized inspection plan

The RBI assessment starts from the collections of information for screening and other steps of the process. The first step of the RBI assessment process is the screening assessment. It is performed to focus the risk assessment on the critical failure causes identified from a wide range of possible failure causes for the various components of an FPSO system.

Data Gathering

This step includes two parts:

- Design data and maintenance record of all process piping and static equipment
- Chemical composition and operation condition

This step mainly includes the following data:

- Piping and instrumentation diagram (PID)
- Process flow diagram (PFD)
- Utility flow diagram (UFD)
- Layout
- Material balance
- Piping list
- Equipment list
- Material design
- Coating
- Insulation
- System description
- Material selection
- Effect and cause
- ESD block diagram
- Production data
- Inspection, failure, and replacing record

Screening Assessment

In the screening step, each FPSO system is addressed for all damage causes. In this step, both PoF and CoF values are identified as “insignificant” or “potential.” The initial assessment is initiated based on the screening results only when both the PoF and CoF values for the respective failure causes are evaluated as “potential.” Some general advice of further actions on the results of screening assessment are given in [Table 50.2](#) as an example of a screening matrix.

- When the PoF is “insignificant,” the inspection has no effect on further reducing the risk; if the CoF is also “insignificant,” then the recommended action is minimal surveillance.
- If the PoF is “insignificant,” but the CoF is “potential,” then preventive maintenance and/or monitoring should be considered to address the risk.
- When the PoF is “potential,” but the CoF is “insignificant,” then the inspection can be used to reduce risk, but is unlikely to be cost-effective. A likely cost-effective solution is often to carry out corrective maintenance in case of failure.

Table 50.2: Risk categories

Probability of Failure (PoF)	Risk Categories	
High	Corrective maintenance	Initial assessment initiated
Low	Minimum surveillance	Preventive maintenance and/or monitoring
Consequence of failure (CoF)	Low	High

- Where both the PoF and CoF are “potential,” the inspection can be effective in reducing the risk level. The introduction of a measurer for reducing the CoF should further be evaluated.

Detailed Assessment

Table 50.3 shows an example of a risk ranking matrix. In the detailed assessment, the PoF and CoF are analyzed at a high degree. The PoF and CoF rankings are numerically depicted. A much wider database is requested to be well prepared for the quantitative analysis, and the PoF value may be evaluated by using the structural reliability method and the CoF by numerically precise, well-published consequence modeling.

The detailed assessment is performed on a component level, defining the different sections of the FPSO.

The detailed assessment may involve the following steps:

- Segmenting the target FPSO
- Identifying the component damage causes and degradation mechanisms
- Assessing PoF for each degradation mechanisms
- Assessing CoF with consideration of safety, economy, and environmental effects
- Determining risk level for each FPSO segment and degradation mechanisms
- Ranking pipeline segments according to critical risk level or acceptance criteria
- Developing inspection plan/alternative remedial actions

Risk Evaluation and Optimized Inspection Plan

According to the results of risk analysis, and on the basis of the failure modes and failure mechanism for each device and structure, we can develop a plan of the corresponding detection, test the choice of work type, and make sure of the time interval of detection.

50.4 Safety Integrity Level Assessment

50.4.1 Introduction

SIL is according to absolute risk criteria, which is based on venture analysis for each safety system. The aim of SIL is to meet safety integrity requirements of electrical/

Table 50.3: Risk ranking matrix

5	Very high	M	H	H	VH	VH
4	High	L	M	H	H	VH
3	Medium	L	L	M	H	H
2	Low	VL	L	L	M	H
1	Very low	VL	VL	L	L	M
	PoF/CoF	A	B	C	D	E

electronic/programmable electronic systems, which are related to safety systems. Therefore, it is necessary to divide the reliability level of safety systems for units, systems, and equipment, and then to make the plan of procurement, maintenance, operation, and monitoring. SIL, which is discrete, ranks from 1 to 4.

50.4.2 The Main Research Contents

The main research contents include the following:

- Materials and data and the data processing method
- Assessment method (the method to evaluate personnel security, environmental disruption, and financial loss)
- Proof technique of SIL
- Method of test cycle

50.4.3 Research Method

Data Collection and Processing

Basic information includes the following:

- PID
- PFD
- Description of the process
- Design principle and specification of F&G and ESD
- Machine account of instrument and valve
- The layout of equipment
- Detailed list of electrical/electronic/programmable electronic systems
- Cause and effect diagram
- Internal heat detector layout
- HAZOP report

Determine the Level

This step focus on the personnel safety, environmental disruption, and financial loss risk assessment of each aspect is according to [Tables 50.4–50.6](#).

Determine the Level Verification and Test Cycle of SIL

This is a method to verify whether existing configuration of a safety instrumentation system can reach the required level of SIL requirements.

When existing configuration meets the requirements, we should determine the corresponding test cycle.

Table 50.4: Parametric description—personnel safety

Risk Parameter	Code	Rank	Note
Consequence (C)	C _A	Many injuries	Applies only to personnel safety evaluation
	C _B	Many people seriously injured	
	C _C	1–2 people were killed	
	C _D	Catastrophic consequences, killing large numbers of people	
Exposed time and frequency rate in a dangerous area (F)	F _A	Rarely in the hazard area, the ratio of the time of personnel exposed in the risk area to normal working hours is less than 10%	
	F _B	Often in the hazard area	
Possibility to avoid the adverse events (P)	P _A	Under certain conditions (alarm, long enough to escape)	This parameter considers whether there is equipment independent of the safety instrument system events to warn personnel of any dangers; at the same time there is enough time and space so that people can escape from the hazardous events
	P _B	Almost impossible (no escape alarm)	
The frequency of the incident (W)	W1	The probability of events is very low (once every 10 years (or above))	Estimate the frequency of the incident, without considering safety instrumentation system protection cases
	W2	The probability of events is medium (1–10 years at a time)	
	W3	The probability of events is high (occurs within 1 year)	

When existing configuration does not meet the requirements, we need to put forward suggestions for improvement and determine the test cycle according to the suggestions for improvement.

After determining the level verification and test cycle of SIL for each SIF, we need to make a quantitative calculation for the existing configuration of the safety instrumentation system.

50.5 Reliability-Centered Maintenance

50.5.1 Introduction

RCM is built on the basis of a risk and reliability method by using systematic methods and principles. By analyzing the screening, staff could perform research on FEMA for the equipment, and quantitatively determine the risk, failure cause, and the fundamental

Table 50.5: Parametric description—environmental disruption

Risk Parameter	Code	Rank	Note
Consequence (C)	C _A	A small amount of crude oil leak to the ship, and can clean up quickly	Applies only to personnel safety evaluation
	C _B	A large amount of crude oil leak to the ship	
	C _C	A small amount of crude oil leak to sea	
	C _D	A large amount of crude oil leak to sea	
Possibility to avoid the adverse events (P)	P _A	Under certain conditions (alarm, long enough to escape)	This parameter considers whether there is equipment independent of the safety instrument system events to warn personnel of any dangers; at the same time there is enough time and space so that people can escape from the hazardous events
	P _B	Almost impossible (no escape alarm)	
The frequency of the incident (W)	W1	The probability of events is very low (once every 10 years (or above))	Estimate the frequency of the incident, without considering safety instrumentation system protection cases
	W2	The probability of events is medium (1–10 years at a time)	
	W3	The probability of events is high (occurs within 1 year)	

Table 50.6: Parametric description—financial loss

Risk Parameter	Code	Rank	Note
Consequence (C)	C _A	<6,000,000 RMB	
	C _B	6,000,000–12,000,000 RMB	
	C _C	12,000,000–35,000,000 RMB	
	C _D	>35,000,000 RMB	
The frequency of the incident (W)	W1	The probability of events is very low (once every 10 years (or above))	Estimate the frequency of the incident, without considering safety instrumentation system protection cases
	W2	The probability of events is medium (1–10 years at a time)	
	W3	The probability of events is high (occurs within 1 year)	

reason of the equipment for each failure mode. In this way staff could recognize the inherent or potential danger in a device and its possible consequences, and come up with a maintenance strategy to reduce risk.

50.5.2 The Main Research Contents

The main research contents include the following:

- Device type applied to RCM method
- RCM screening method research
- Failure mode analysis and risk analysis method
- Specified and optimization method of equipment maintenance strategy

50.5.3 Research Method

Data Gathering

This part mainly includes the following data:

- Asset registration form (technical level and/or ERP classification)
- Safety case, performance standard
- PID, PFD
- Maintenance procedure (if necessary)
- Service manual.
- Working procedure (if necessary)
- Running program (if necessary)
- Accident, failure of history
- Expected operating costs
- The cost per hour—maintenance/contractor
- Requirements for avoiding potential leakage/environmental pollution
- Requirements for operational/shutdown/availability

Initial Screening

Low risk, moderate risk, and high risk of equipment would be divided through the initial screening, and the corresponding maintenance plan would be developed. The next step is the detailed risk assessment of RCM.

Detailed Risk Assessment

Detailed risk assessment of RCM aims at personnel safety, environmental disruption, and financial loss. The specific evaluation results will be presented in the form of a risk matrix.

Establish and Optimize the Maintenance Strategy

The following are several aspects to carry out the research:

- Make strategies for all high (very high) risk equipment
- Verify failure cause and fundamental reason for failure mode
- Formulate appropriate maintenance strategy and maintenance work
- Work optimization

Maintenance strategy optimization breaks through from the following aspects: functional assets, maintenance tasks, and reasons to improve maintenance.

50.6 Engineering Projects

50.6.1 Introduction

In order to have a better understanding of AIM for FPSO, we would like to introduce an example of an engineering project related to RBM.

The example project aims to systematically assess the risks of the device to an upper module of FPSO and determine the corresponding inspection management strategy depending on the risk to equipment and the potential failure/damage mechanism, to control the occurrence of failure/damage, prevent corrosion damage of unexpected accidents, and improve the security and reliability of the equipment.

Analysis in this engineering project could be divided into two steps: screening analysis and detailed assessment.

50.6.2 Screening Analysis

The results of screening analysis are as shown in [Table 50.7](#) and [Figure 50.4](#).

The table shows that a total of 89 sets of equipment, among them 28 sets of equipment in high risk, need further detailed assessment.

Table 50.7: The risk classification of the equipment after screening analysis

Risk Categories	Number of Devices (%)
Initial assessment	28 (31.5%)
Preventive maintenance and/or monitoring	23 (25.8%)
Corrective maintenance	5 (5.6%)
Minimum surveillance	33 (37.1%)
Total	89 (100%)

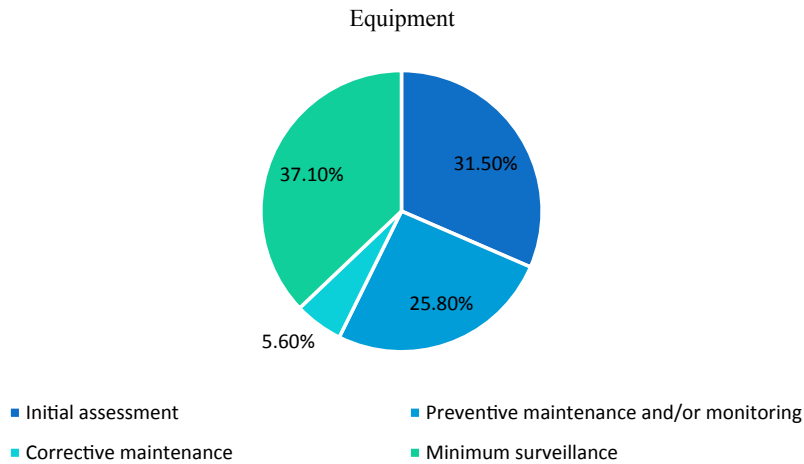


Figure 50.4

The risk classification of the equipment after screening analysis.

High Risk Projects

The results show that of a total of 89 sets of equipment, 28 sets of equipment (31.5%) are high risk and need detailed assessment.

High risk projects are caused by internal and external corrosion such as CO₂ and microbial corrosion, corrosion under the thermal insulation layer, and corrosion under the upholder caused by damage to pipeline system coating.

Low Risk Projects

The remaining 61 sets of equipment (68.5%) are in low risk and can be exempted from inspection. However, the equipment needs maintenance.

- Preventive maintenance
Twenty-three devices (25.8%) are high CoF and low PoF, and are in need of preventive maintenance. The equipment needs to do a visual inspection to protect the corrosion coating of the outer wall and avoid other accidental damage. We need to carry on the daily maintenance to maintain a low failure rate.
- Corrective maintenance
Five sets of equipment (5.6%) are low CoF and high PoF, and are in need of corrective maintenance. A high PoF of the equipment makes it easy to fail, but we only need to plan for replacement and repair during its failure. However, repetitive failure will also bring inconvenience to its operation and thus we suggest a change of design and material, and to take other measures to prevent corrosion.

Table 50.8: The risk classification of the equipment after detailed analysis

Risk Categories	Equipment	
	Economy (%)	Safety (%)
Very high	0 (0.0%)	0 (0.0%)
High	1 (3.6%)	0 (0.0%)
Medium	10 (35.7%)	0 (0.0%)
Low	17 (60.7%)	5 (17.9%)
Very low	0 (0.0%)	23 (82.1%)
<i>Total</i>	28 (100%)	28 (100%)

- Minimum surveillance
 Thirty-three sets of equipment (37.1%) are low CoF and PoF, and need minimum supervision. The equipment only needs a visual inspection to confirm the RBI analysis conditions, such as the protection of the corrosion coating of the outer wall.

50.6.3 Detailed Assessment

The results of detailed analysis are shown in Table 50.8 and Figures 50.5 and 50.6.

According to certain economic/safety risk acceptance criteria, we calculate the number of devices that have reached the risk limit. The results show that three sets of equipment out of a total of 28 sets of detailed assessment are beyond economic, safe, acceptable limits.

Figure 50.7 shows the different classification of the equipment. All equipment beyond acceptable risk limits needs to take measures to reduce risk.

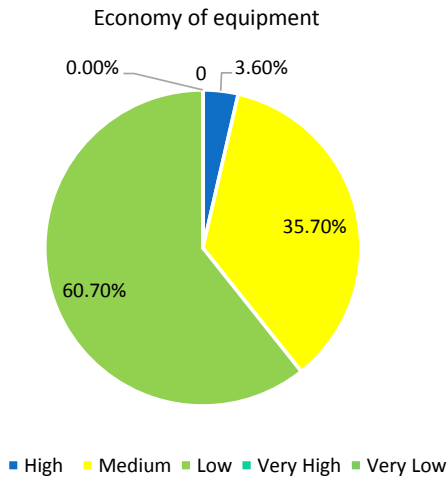


Figure 50.5

The economy risk classification of the equipment after detailed analysis.

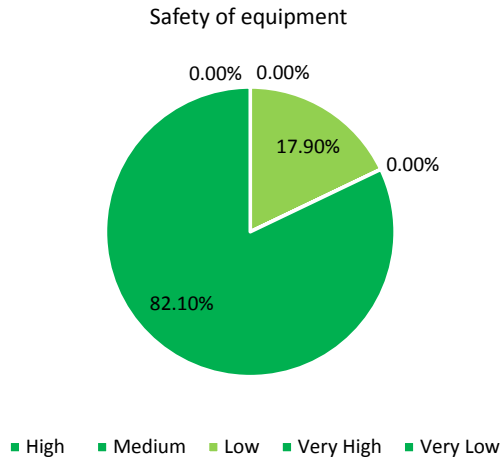


Figure 50.6

The safety risk classification of the equipment after detailed analysis.

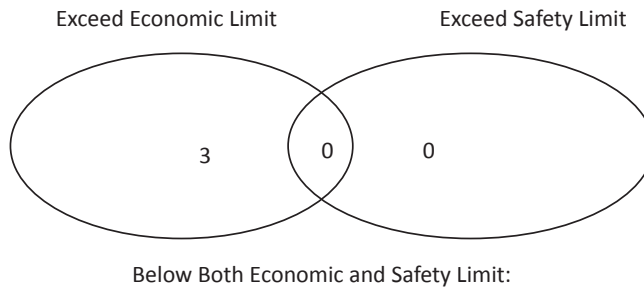


Figure 50.7

The number of devices beyond/not beyond the risk limit.

50.6.4 Risk Mitigation Plan

Most cases of risk to equipment beyond acceptable limits is due to its containing high content of CO₂ and water, which causes its corrosion rate to be higher and therefore the possibility of a higher failure rate. As a result we should make an inspection to confirm the status of the FPSO.

50.6.5 Summary

- The upper module technology and utility system has a total of 89 devices, including 28 devices that are analyzed in detail.
- Three sets of equipment in a total of 28 sets of detailed assessment are beyond economic, safe, acceptable limits. The number of equipment in medium and high risk is 11.

- The main risk of upper modules on the example FPSO is equipment damage caused by the corrosion leakage and production delays caused by economic risk. The risk of personnel safety is relatively small and the economic risks are the most important.
- The RBI method and work relies heavily on its basic data and the corresponding data-base, thus the integrity and accuracy of the data are very important.
- The control of water content and water quality is very important; it is suggested to monitor the content of CO₂ and water.

Further Reading

- ABS, 2003. Guide for Surveys Using Risk-based Inspection for the Offshore Industry. American Bureau of Shipping, Houston.
- API, 2009. Risk-based Inspection. API-RP-580, second ed. American Petroleum Institute, Washington, DC.
- ASME, 1991. Risk-based Inspection-development of Guidelines: General Document. American Society of Mechanical Engineers, New York.
- Bai, Y., 2003. Marine Structural Design. Elsevier.
- Bai, Y., Bai, Q., 2014. Subsea Pipeline Integrity and Risk Management. Gulf Professional Publishing, Houston.
- Chang, R., 2003. With maintenance management system to improve efficiency. Monthly Journal of CTCI 290, 14–23.
- DNV, August 4, 2008. FPSO Aim Project - Technology Report.
- Lassagne, M., Pang, D., Vieira, R., 2001. Prescriptive and risk-based approaches to regulation: the case of FPSOs in Deepwater Gulf of Mexico. In: Offshore Technology Conference, Houston Texas.
- Ma, G., Sun, L., 2012. The design and implement of FPSO assets management system. Procedia Environmental Sciences 12, 484–490.
- Tronstad, L., SPE, Statoil Hydro, 2009. The use of risk analysis in design: safety aspects related to the design and operation of a FPSO. In: SPE Americas E&P Environmental and Safety Conference, San Antonio, Texas.
- Yu, J., Liu, Z., Jing, Y., 2004. FPSO Assets Management. Changsha Press, Changsha (in Chinese).

Index

Note: Page numbers followed by “f” and “t” indicate figures and tables respectively.

A

- 2D frames. *See* Two-dimensional frames (2D frames)
 - A series experiments, 330
 - ABAQUS FEM program, 438–439
 - Abrasive water jet erosion (AWJ erosion), 573
 - ABS. *See* American Bureau of Shipping (ABS)
 - Accident causation analysis, 908
 - fire and explosion, 909f
 - FSA, 910
 - marine accidents, 909f
 - Accidental limit state (ALS), 245
 - Accidental loads, 509
 - Accidental loads design, 8–9
 - Actual gas cloud, 923–924
 - Added mass, 270
 - Aerospace, 564–565
 - After-body slamming, 267
 - Aging failure, 813
 - AIM. *See* Asset integrity manage (AIM)
 - AIR. *See* Average Individual Risk (AIR)
 - AISC. *See* American Institute for Steel Construction (AISC)
 - ALARP principle. *See* As low as reasonably practicable principle (ALARP principle)
 - Allowable stress design (ASD), 4, 646
 - reliability methods to, 650–651
 - ALPS/SCOL program, 462
 - ALS. *See* Accidental limit state (ALS)
 - American Bureau of Shipping (ABS), 198, 941
 - American Institute for Steel Construction (AISC), 646
 - American Petroleum Institute (API), 447–448, 646, 941
 - American Society of Mechanical Engineers (ASME), 941
 - Analysis models, 203
 - Analysis procedures, 204
 - Analytical approach, 587
 - ANASYS analysis, 935–937
 - ANSYS Multiphysics module, 856
 - API. *See* American Petroleum Institute (API)
 - Aramid fibers, 27–28
 - Arctic areas, 229
 - Arctic offshore technology development
 - Arctic offshore technology program, 237–239
 - environmental and climatic change, 237–238
 - materials for arctic, 238–239
 - three areas of focus, 237
 - concrete durability in, 242
 - historical background, 229–232
 - ice forces on fixed structures, 240–242
 - industrial development in cold regions, 233–235
 - mechanical resistance to slip movement in level ice, 239–240
 - research incentive, 232
- Arctic ships, 233–234
 - As low as reasonably possible principle. *See* As low as reasonably practicable principle (ALARP principle)
 - As low as reasonably practicable principle (ALARP principle), 217, 719–720, 720f, 776–777, 797
 - ASD. *See* Allowable stress design (ASD)
 - ASIS research program, 471
 - ASME. *See* American Society of Mechanical Engineers (ASME)
 - Asset integrity manage (AIM), 939
 - Average Individual Risk (AIR), 715–716
 - AWJ erosion. *See* Abrasive water jet erosion (AWJ erosion)
 - Axial capacity, 192–194
 - Axial compression, 356–357, 359–360

B

- B series experiments, 330
- Ballast water treatment, 44–47
- Base shear capacity, 856
- degradation under corrosion effect, 858–862
- probability model

- Base shear capacity (*Continued*)
 for jacket platform resistance, 865–867
 of initial, 857
- Basic scantling, 158
- Bauschinger effect, 298, 381
- Bayesian models, 691
- Beam-column(s)
 buckling, 350–351
 behavior and ultimate strength, 281–285
 element, 395–397
 for struck structure modeling, 430
 plastic design, 285–288
- Beam-like vibration, 259
- Bending, 358
- Bilinear S–N curves, 530–531
- Bottom-supported offshore structures, 447
- Boundary conditions, 176–177
- Boundary element methods.
See Panel methods
- Bow flare slamming, 86
- Brainstorming, 910–911
- Bretschneider spectrum, 77–78
- British Welding Institute (TWI), 558–559
 CTOD design, 559–560, 559f
- Brittle fracture avoidance, 246–247
- Buckling
 check, 178
 coefficient, 341
 failure modes, 353–354
 and local buckling of tubular members, 293
 buckling test procedures, 298–302
 calculation results, 326–335
 material tests, 295–298
 safety factors for offshore strength assessment, 294
 test results, 302–307
 test specimens, 294–295
 theory of analysis, 307–326
 of platings, 166–169
 of profiles, 169–170
 of ring-stiffened shells, 359–362
 axial compression, 359–360
 combined axial compression and external pressure, 362
 hydrostatic pressure, 360–362
 strength of plates, 348
 of stringer-and ring-stiffened shells, 362–365
 axial compression, 362, 364–365
 radial pressure, 364–365
 test procedures, 298–302
 ultimate strength, 290–291
- Buckling behavior and ultimate strength
 of beam-columns, 281–285
 with eccentric load, 281–282
 with initial deflection and eccentric load, 282–283
 initial yielding, 284–285
 ultimate strength, 283–284
 of columns, 277–281
 Johnson–Ostenfeld formula, 280–281
 Perry–Robertson formula, 279–280
- Buffer bow, 471
- Bulk loading, 52
- Bulkheads, 166
- Buoyancy springs, 271
- Bureau Veritas (BV), 198
- C**
- C series experiments, 328
- C-glass, 27
- CA. *See* Certification/Classification Authority (CA)
- CAD. *See* Computer aided design (CAD)
- CAE. *See* Computer aided engineering (CAE)
- Caldwell’s method, 393
- Calibration, 5–6
- CAM. *See* Computer aided manufacturing (CAM)
- Capacity checks, 64–66
 general principles, 64–65
 hull girder moment capacity checks, 65
 hull girder shear capacity check, 66
- CAPEX. *See* Capital expenditure (CAPEX)
- Capital costs, 782
- Capital expenditure (CAPEX), 36
- Carbon fibers, 28
- Cargo cycle, 51–53
 bulk loading, 52
 cool down, 52
 discharge, 53
 gas free, 53
 gas up, 52
 inert, 52
 voyage, 52–53
- Cargo hold and ballast tank model, 173–174
- Cathodic protection (CP), 492
- CB. *See* Center of buoyancy (CB)
- CCS. *See* China Classification Society (CCS)
- CDF. *See* Cumulative distribution function (CDF)
- CEGB. *See* Central Electricity Generating Board (CEGB)
- CEM. *See* Coastal Engineering Manual (CEM)
- Center of buoyancy (CB), 154
- Center of gravity (CG), 154
- Central Electricity Generating Board (CEGB), 560
- Certification/Classification Authority (CA), 198–199
- CFD. *See* Computational fluid dynamics (CFD)
- CG. *See* Center of gravity (CG)
- China Classification Society (CCS), 844
- Clamped aluminum alloy beam struck transversely by mass, 438–441
- Clamped beam under lateral load, 451–452
- Classification responsibilities, 893

- rules, 90, 171
 society, 891, 893, 903
 interface, 555
 Closed form method for hull girder reliability, 628–630
 Cnoidal wave theory, 122
 Coastal Engineering Manual (CEM), 15–16
 Code calibration
 principles, 651–652
 procedure, 652–653
 Codes and Standards, 199–200
 Coefficient of variation (CoV), 616, 628
 CoF. *See* Consequence of failure (CoF)
 Collapse analysis, 393, 880–881
 analytical equations for hull girder ultimate strength, 403–407
 comparisons of Hull Girder strength equations and Smith method, 413–415
 hull structural analysis, 395–403
 incremental wave theory, 882–883
 modified Smith method, 408–412
 RSR, 882
 ultimate strength analysis, 881
 Collision, 770–771. *See also* Explosion risk; Finite element formulation; Fire risk
 consequence, 739
 frequency, 736–739
 mechanics
 conservation of energy, 432–434
 conservation of momentum, 432
 fundamental principles, 431–432
 risk, 736, 759
 colliding vessel categories, 736, 736t
 reduction, 739–740
 Column-stabilized structure, 224
 Combined loads, 345–348
 SLS, 346
 ULS, 347–348
 Combined System Number One (CS1), 59
 Comparative risk analysis, 760
 Compliance matrix for lamina, 33
 Component reliability, 11, 590
 Compressive overstressing, 574
 Compressive stiffened panels, 409–410
 Compressive stress, 353
 Computational fluid dynamics (CFD), 95, 107–108, 742, 916
 fire CFD simulation, 931–933
 gas dispersion CFD simulations, 921–924
 gas explosion CFD simulation, 924–925
 Computational procedure, 401–403, 430–431
 Computational wind engineering (CWE), 110–113
 Computer aided design (CAD), 4
 Computer aided engineering (CAE), 4
 Computer aided manufacturing (CAM), 4
 Confined explosion, 742
 Consequence analysis, 898
 Consequence of failure (CoF), 942–943
 Conservation of energy, 432–434
 Conservation of momentum, 432
 Containment systems, 53–59
 membrane type, 56–59
 self-supporting type, 54–56
 IHI, 56
 moss tanks, 54–56
 Contingency factors, 789–790
 Continuous sources, 744
 Cool down, 52
 Core preparation, 187
 Cornell safety index method, 584–585, 628
 Correlation function, 912
 Corroded state, 660–661
 Corrosion
 allowance, 158
 damage, 842
 modeling, 844
 residual ultimate strength with, 848–849
 ultimate strength analysis method, 843–844
 defects, 575
 effect, 875
 base shear capacity degradation under, 858–862
 comparing, 885–887
 on jacket structure, 883–885
 model, 829–830, 858–861
 rate model, 410–412, 878–880
 thickness, 830
 Corrosion protection system (CPS), 829, 858
 COS model, 313–316, 314f, 316f, 324–325
 Cost variable modeling, 785–786
 Cost–benefit analysis, 777
 CoV. *See* Coefficient of variation (CoV)
 Cowper–Symonds constitutive equation, 373–374
 CP. *See* Cathodic protection (CP)
 CPS. *See* Corrosion protection system (CPS)
 Crack, 830
 around cutout openings, 531–532, 532f
 damage, 842
 modeling, 844
 residual ultimate strength with, 844–848
 ultimate strength analysis method, 843–844
 defects
 analysis, 830–833
 effects, 833–837
 detection, 692–693
 failure modes, 830–832
 growth
 due to constant amplitude loading, 562–563
 due to variable amplitude loading, 563

- Crack (*Continued*)
 initiation, 478
 length and location, 835–836
 measurement, 693
 propagation, 478
 prediction, 410, 675
- Crack tip opening displacement (CTOD), 401, 412
- Crack-tip opening displacement design (CTOD design), 558
 empirical equations, 558–559
 TWI, 559–560, 559f
- Critical Structural Details (CSD), 633
- CS1. *See* Combined System Number One (CS1)
- CSD. *See* Critical Structural Details (CSD)
- CTOD. *See* Crack tip opening displacement (CTOD)
- CTOD design. *See* Crack-tip opening displacement design (CTOD design)
- Cumulative distribution function (CDF), 631, 666
- Current, 121
- CWE. *See* Computational wind engineering (CWE)
- Cyclic stress–strain loop, 482f
- Cylindrical shells, ultimate strength of, 353
 buckling
 failure modes, 353–354
 of ring-stiffened shells, 359–362
 of stringer-and ring-stiffened shells, 362–365
 elastic buckling of unstiffened cylindrical shells, 354–359
- D**
- D series experiments, 328–330
- DAFs. *See* Dynamic amplification factors (DAFs)
- DAMAGE program, 463
- Damage tolerance, 575
 analysis, 576
 dent damage, 577
 residual life prediction using Paris Law, 576
 residual strength assessment, 575–576
- Damping forces, 128
- Data collection and processing, 947
- Data gathering, 944–945, 950
- Daubechies formulations, 264–265
- Dead loads, 212, 509
- Decision and decision criteria, 784
- Decommission, 781–782
- Deepwater foundation, 188–194
 for mooring, 188
 pipe piles, 192–194
 Spudcan footings, 189–192
 suction caisson, 188–189
- Deformation matrix, 389–390
- Delphi method, 911
- DENT model, 316–318
- Design basis, 201–203
 in-service inspection and repair, 203
 materials and welding, 202
 operational design criteria, 203
 reassessment, 203
 rules, regulations and codes, 202
 stability and
 compartmentalization, 202
 temporary phases, 202
 unit description and main dimensions, 201
- Design brief, 203–204
- Design codes, 197–198
- Design factors, 656
- “Design Level” explosion, 749
- Design loads, 171–173
- Design point, 634
- Det Norske Veritas (DNV), 198, 941
- Detailed assessment, 946, 953
- Deterministic approach, 513–514, 520–522
- Deterministic fatigue analysis, 528, 528f
- Diameter uncertainty, 657
- Discharge, 53
- Distortion energy, 468
- Distribution functions selection, 620–621
- DLA. *See* Ductility level analysis (DLA); Dynamic loading approach (DLA)
- DLE. *See* Ductility-level earthquake (DLE)
- DLP. *See* Dominant Load Parameters (DLP)
- DNV. *See* Det Norske Veritas (DNV)
- Dominant Load Parameters (DLP), 221
- Donnell’s equation, 356
- Dormant failures, 824
- Downhole equipment, 184
- Drag/inertia parameter method, 143–144
- Drifting collisions, 736
- Drifting vessel collisions, 738–739
- Drill rig, 184
- Drilling costs, 785
- Dropped object(s), 749
 consequences, 752–753
 frequency of impact, 749–751
 impact load assessment, 751–752
 risk, 759
- Dry-dock operations, 769
- Ductility, 246–247
- Ductility level analysis (DLA), 916–917
- “Ductility Level” explosion, 749
- Ductility-level earthquake (DLE), 448
- DWT. *See* Deadweight tonnage (DWT)
- Dynamic amplification factors (DAFs), 142
- Dynamic elastic–plastic behavior, 435, 436f–437f, 439f–440f
- Dynamic loading approach (DLA), 221
- Dynamic loads, 171–172, 430
- Dynamic wind analysis, 105–107

E

- E-glass, 27
- Earthquake design per API
RP2A, 448–449, 448t
- Eccentric axial compression tests
using large-scale specimens,
302–304
using small-scale specimens,
304–306
- Economic evaluation, 782–783
- Economic risk modeling, 785
cost variable modeling,
785–786
failure probability calculation,
787–788
income variable modeling,
786–787
- Edge-opened crack, 831
- EEDI. *See* Energy efficiency
design index (EEDI)
- EFEF JIP. *See* Joint Industry
Project on Explosion and
Fire Engineering of
Floating (EFEF JIP)
- Effectiveness cost, 574
- EIM. *See* Expert investigation
method (EIM)
- Elastic beam-column with large
displacements, 368–370
- Elastic buckling
of columns with alternative
boundary conditions,
288–290
of unstiffened cylindrical shells,
354–359
axial compression, 356–357
bending, 358
equilibrium equations for
cylindrical shells,
354–356
external lateral pressure,
358–359
- Elastic compressive buckling
stress, 166–169
- Elastic strain, 379–380
- Elastic-plastic large-displacement
analysis, 451f
- Elastic-plastic analysis, 431
- Elastic-plastic stiffness equation
for elements, 376–377
- Electric Power Research Institute
(EPRI), 806
- Embedded crack, 832
- Emissions, 39–44
effect of design variables on
EEDI, 40–42
influence of hull steel weight on
EEDI, 43–44
influence of speed on EEDI, 43
regulations on air pollution, 40
regulations on greenhouse gases,
40
- Energy efficiency design index
(EEDI), 39
- Engineering projects, 951
detailed assessment, 953
risk mitigation plan, 954
screening analysis, 951–953
- Engineering systems, risk-based
compliance process for,
722
- Environmental impact
assessment, 761–762
- Environmental loads, 125, 509
- Environmental severity factors
(ESFs), 627–628, 636
- EPRI. *See* Electric Power
Research Institute (EPRI)
- Equations of motion, 428,
449–450
- Equivalent gas cloud, 923–924
- Equivalent stress, 383
- Ergonomics, 798–799
- Erosion, controlled, 573
- Error reduction, 797–798
- Escalation analysis, 712–713
- ESFs. *See* Environmental severity
factors (ESFs)
- ETA. *See* Event tree analysis
(ETA)
- Event, 604
- Event tree analysis (ETA),
910–911, 914f
- Expert investigation method
(EIM), 910–911
- Explosion, 745, 772
- Explosion and fire response
analysis
accident causation analysis,
908–910
dangerous sources identification,
910–911
EIM, 910–911
structure function of fault
tree, 911–914
- Deepwater Horizon accident,
908f
- examples of explosion response
of FPSO, 921
ANASYS analysis, 935–937
fire CFD simulation, 931–933
gas dispersion CFD
simulations, 921–924
gas explosion CFD
simulation, 924–925
nonlinear structural response
analysis, 926–930
hydrocarbon, 907
Piper Alpha, 907–908, 907f
risk assessment and
management, 914
procedure for, 915–916
procedure for explosion,
916–919
risk restraining project,
919–920
- Explosion risk, 740, 759.
See also Collision—risk;
Fire risk
explosion consequence,
742–743
explosion frequency, 740–741
explosion load assessment, 742
explosion risk reduction,
743–745
- External hydrostatic pressure
loading, 364
- External lateral pressure,
358–359
- External pressure, 90–91
- Extreme values, 133–147
long-term extreme approach,
139–141
prediction of maximum extreme
for non-Gaussian process,
141–147
short-term extreme approach,
135–139
- Exxon Valdez disaster,
765

F

- FAA. *See* Federal Aviation Agency (FAA)
- Fabrication
 fabrication yard characteristics, 574
 fabrication-related imperfections, 343–344
 tolerance, 344, 354
- Facility costs, 785
- FAD. *See* Failure assessment diagram (FAD)
- Failure
 cause, 812
 likelihood, 812
 mechanism, 812
 modes, 362
 probability
 analysis, 898
 calculation, 787–788
 propagation, 813
 severity, 812
- Failure assessment diagram (FAD), 558, 560
 residual strength assessment using, 575–576
- Failure mode and effect analysis (FMEA), 712, 801, 811, 910–911
- FAR. *See* Fatal Accident Rate (FAR)
- Fatal Accident Rate (FAR), 715–716
- Fatigue, 477–479, 671, 851, 853. *See also* Simplified fatigue assessment
 check, 179–180
 cumulative damage for variable amplitude loading, 480–481
 design, 257–258
 durability, 257–258
 endurance limit, 479
 failure, 676, 692
 fatigue-based design, 181
 fatigue-resistant details, 572
 fracture mechanics
 in fatigue analysis, 484–485
 fracture-mechanics-based crack growth life integration, 486–487
 life cycle calculation, 485–486
 model, 176
 safety check
 partial safety factors, 680
 target safety index for fatigue, 679–680
 strain-controlled, 481–484
 stress-controlled, 479–480
- Fatigue analysis, 255–257, 478, 546–547. *See also* Spectral fatigue analysis (SFA); Time-domain fatigue analysis (TFA)
 checklist, 554–555
 drawing verification, 555
 fatigue damage assessment, 553–554
 spectral fatigue parameters, 547–553
 stress range analysis, 547
- Fatigue capacity. *See also* Simplified fatigue assessment
 fatigue damage calculation, 504–505
 SCF, 501–504
 S–N curves, 489–497
 stress range estimation, 497–501
- Fatigue damage, 537
 assessment, 553
 detail improvement, 554
 initial hot-spot screening, 553
 specific hot-spot analysis, 553
 specific hot-spot design, 554
 estimation
 crack growth due to constant amplitude loading, 562–563
 crack growth due to variable amplitude loading, 563
 evaluation, 179–180
- Fatigue limit state (FLS), 245, 253–255. *See also* Ultimate limit state (ULS)
 fatigue analysis, 255–257
 fatigue design, 257–258
- Fatigue loading, 509. *See also* Simplified fatigue assessment
 load combinations, 517–520
 for offshore structures, 519–520
 for ship structures, 518–519
 for oceangoing ships, 510–511
 using scatter diagrams, 516–517
 mooring-and riser-induced damping, 517
- Fatigue reliability
 failure behavior, 671
 fatigue safety check, 679–680
- FM calibration by S–N approach, 678–679
- models, 673
 FM approach, 674–677
 lognormal format, 677–678
 S–N approach, 674
 numerical examples, 681–685
 uncertainty in fatigue stress model
 stress modeling, 672
 stress modeling error, 672–673
- Fatigue stresses, 512. *See also* Simplified fatigue assessment
 long-term, 512–513
 long-term stress distribution deterministic approach, 513–514, 520–522
 spectral approach, 514–516, 523–524
- Fault tree analysis (FTA), 910–911
 example, 913f
 structure function, 911–914
- FBC model. *See* Ferry Borges–Castanheta model (FBC model)
- FEA. *See* Finite element analysis (FEA)
- Federal Aviation Agency (FAA), 804
- FEM. *See* Finite element model (FEM)
- Ferry Borges–Castanheta model (FBC model), 593–594

- Ferry–Borges method, 632
- Fiber reinforcements, 26–28
 aramid fibers, 27–28
 carbon fibers, 28
 glass fibers, 27
- Fiber-reinforced plastics (FRP), 19
- Field development
 decision and decision criteria, 784
 economic evaluation, 782–783
 limit-state functions, 784–785
 phases, 781–782, 781f
 quantitative economic risk assessment, 783
 results evaluation
 contingency factors, 789–790
 importance factors, 788–789
 omission factors, 788–789
 sensitivity factors, 789
- Finite element analysis (FEA), 245, 323, 497, 503, 543–544
 fine FEA model, 545
- Finite element formulation.
See also Collision mechanics
 beam-column element for struck structure modeling, 430
 computational procedure, 430–431
 equations of motion, 428
 load–displacement relationship of hit member, 429–430
- Finite element methods.
See Finite element model (FEM)
- Finite element model (FEM), 3, 171, 173, 199, 269–271, 393, 460, 856
 added mass, 270
 ALPS/SCOL program, 462
 buoyancy springs, 271
 lightship weight distribution, 269–270
 loading condition, 270
 of Suezmax-class double-hull oil tanker, 464f
- Finnish Maritime Administration (FMA), 465–466
- Fire, 771–772
 CFD simulation, 931–933
 response analysis procedures, 747
- Fire risk, 745, 759. *See also* Collision—risk; Explosion risk
 fire and explosion design, 748–749
 fire frequency, 745–746
 fire load and consequence assessment, 746–748
 fire risk reduction, 748
- First-order potential forces, 126
- First-order reliability method (FORM), 587
 calculation by, 588–589
- FLACS code, 921
- FLNG. *See* Floating liquefied natural gas (FLNG)
- Floating liquefied natural gas (FLNG), 916–917
- Floating production storage and offloading (FPSO), 86–87, 217–224, 738, 891, 910–911, 914, 939.
See also Reliability-centered maintenance (RCM)
 analysis models, 218–219
 modeling
 for compartmentalization and stability, 221–222
 for fatigue analysis, 222–224
 for ultimate strength analysis, 219–221
 structural design, 217–218
 surveys, 901–902
- Floating structure dynamics, 127–128
- Floors, theoretical model for, 469
- FLS. *See* Fatigue limit state (FLS)
- FM. *See* Fracture mechanics (FM)
- FMA. *See* Finnish Maritime Administration (FMA)
- FMEA. *See* Failure mode and effect analysis (FMEA)
- Forced vibration, 271–273
- Force–indentation relationship, 442–443
- FORM. *See* First-order reliability method (FORM)
- Formal safety assessment (FSA), 765, 910
 functional components, 767, 767f
 consequence of ship accidents, 775–776
 cost–benefit analysis, 777
 hazard identification, 769–774
 risk control, 777
 risk evaluation, 776–777
 ship accidents frequency analysis, 774–775
 system definition, 768–769
 HOF in FSA, 777–778
- Foundation model, 877–878
- Fourier techniques, 264
- FPSO. *See* Floating production storage and offloading (FPSO)
- Fracture
 failure, 478
 prevention, 571
 ultimate strength, 290–291
- Fracture mechanics (FM), 571
 application, 557
 in aerospace and power generation industries, 564–565
 CEGB R6 Diagram, 560–561
 comparison with S–N curve approaches, 564
 CTOD design curve, 558–560
 design check, 557–558
 FAD, 561–562, 561f
 fatigue damage estimation, 562–563
 maximum tolerable defect size in butt weld, 565–566
 in fatigue analysis, 484–485
 fracture-mechanics-based approach, 899–900
 crack growth life integration, 486–487
 predictions, 684
 techniques, 674–677
 calibration by S–N approach, 678–679

- Frame and girder model, 174
 Free vibration, 271
 Frequency response analysis, 271–272
 Frequency response function (FRF), 129
 FRF. *See* Frequency response function (FRF)
 Frøya wind speed profile, 98
 FRP. *See* Fiber-reinforced plastics (FRP)
 FSA. *See* Formal safety assessment (FSA)
 FTA. *See* Fault tree analysis (FTA)
 Full immersion zone, 884, 887
 Functional block diagram, 810
 Functional failure analysis, 810
 Functional loads, 509
 Fundamental uncertainty.
 See Inherent uncertainty
 Fuzzy theory, 603–604
- G**
- Gamma function, 529
 Gas
 dispersion CFD simulations, 921–924
 explosion CFD simulation, 924–925
 free, 53
 gas up, 52
 leakage prevention, 743–744
 prices, 787
 Gaussian distribution.
 See Normal distribution
 Gaussian probability density function, 74, 74f
 Gaz Transport & Technigaz (GTT), 53
 General corrosion, 878
 General instability, 361, 363–364
 Geometric imperfections, 354
 Geometric nonlinearities, 447, 450
 Geometric probability, 466
 GHG. *See* Greenhouse gas (GHG)
 Girders, 164–165
- Glass-fiber reinforced plastics (GRP), 19
 Global analysis, 173
 Global FE model, 68
 Global loads, 510–511
 Global motion analysis, 545–546
 Government requirements, 198
 GR. *See* Group risk (GR)
 Gradual failure, 813
 Green ship, 39
 ballast water treatment, 44–47
 emissions, 39–44
 effect of design variables on EEDI, 40–42
 influence of hull steel weight on EEDI, 43–44
 influence of speed on EEDI, 43
 regulations on air pollution, 40
 regulations on greenhouse gases, 40
 underwater coatings, 47
 Green water on deck, 85–87
 Green-water loads, 73
 Greenhouse gas (GHG), 39
 Grinding, 572
 Gross buckling of stiffened panels, 351
 Grounding, 770–771
 Group risk (GR), 716
 GRP. *See* Glass-fiber reinforced plastics (GRP)
 GT96, 57–58
 GTT. *See* Gaz Transport & Technigaz (GTT)
 Gumbel fitting, 144–146
- H**
- H series experiments, 328, 333–335
 Hasofer–Lind safety index method, 585–587
 HAZ. *See* Heat-affected zone (HAZ)
 Hazard and operability studies (HAZOP), 778, 910–911
 Hazard identification, 711–712, 769–774
 Hazard operability (HazOp), 801
- Hazardous material, 773
 HAZOP. *See* Hazard and operability studies (HAZOP)
 HazOp. *See* Hazard operability (HazOp)
 HD compressors. *See* High duty compressors (HD compressors)
 Health, safety and environmental protection (HSE), 709
 Heat-affected zone (HAZ), 570
 HEP. *See* Human error probability (HEP)
 High duty compressors (HD compressors), 52
 High risk projects, 952
 High-frequency response, 127–128
 Hitting objects
 consequences, 752t
 probability, 750–751
 HOF. *See* Human and organizational factors (HOF)
 Hook's law, 379–380
 Hot-spot stress approach, 498–499, 538
 HRA. *See* Human reliability assessment (HRA)
 HSE. *See* Health, safety and environmental protection (HSE); UK Health and Safety Executive (HSE)
 Hull girder ultimate strength, analytical equations for, 403–407
 ultimate moment capacity based on
 elastic section modulus, 404–405
 fully plastic moment, 405–406
 ultimate strength equations, 406–407
 Hull girder(s), 635
 collapse of FPSOs, 660–664
 FPSO midsection, 635f
 load combination factors, 635–636

- loads, 89–90
moment capacity checks, 65
reliability, closed form method
for, 628–630
shear capacity check, 66
strength, 159–161
longitudinal stress,
160–161
shear stress, 161
time-variant reliability
assessment, 637–642
variable measurements, 636t
- Hull primary failure, 629
- Hull structural analysis, 395–403
attached plating element,
397–399
beam-column element,
395–397
computational procedures,
401–403
nonlinear spring element, 400
on plastic node method,
395–403
shear panel element, 399–400
tension tearing rupture, 401
- Hull vibration damping,
262–263
- Human and organizational factors
(HOF), 778
in FSA, 777–778
- Human error
analysis
human error quantification,
796–797
impact assessment, 797
identification, 794–796
problem definition, 794
representation, 796
task analysis, 795
reduction
documentation and quality
assurance, 798
error reduction, 797–798
- Human error probability (HEP),
796
- Human factors, 15
- Human life loss, 775
- Human reliability analysis.
See Human reliability
assessment (HRA)
- Human reliability assessment
(HRA), 777–778, 793.
See also Offshore
structures
ergonomics, 798–799
process, 794f
QA, 799
QC, 799
- Hurricanes, 100
- Hydrocarbon explosions and
fires, 907
- Hydrodynamic analysis software,
129
- Hydrodynamic coefficients, 172
- Hydrostatic pressure, 360–362
- I**
- Idealized structural unit analysis
calculation results,
330–335
members with constraints
against rotation at both
ends, 330–333
theory of analysis, 307–326
evaluation of strain at plastic
node, 322–324
post-local-buckling analysis,
324–326
pre-ultimate-strength analysis,
320–321
system analysis, 322
- Idealized structural unit method
(ISUM), 394, 843
- IIW. *See* International Institute of
Welding (IIW)
- IMCA. *See* International Marine
Contractors Association
(IMCA)
- IMMR. *See* Inspection,
maintenance, monitoring,
and repair (IMMR)
- IMO. *See* International Maritime
Organization (IMO)
- Impact assessment, 729, 797
- Impact loads, 430
fixed beam under central lateral,
435–436
rectangular portal frame
subjected to, 436–438
tubular space frame under, 438
- Impact mechanics, 367
- Importance factors, 788–789
- Impulsive response, 128
- IMR. *See* Inspection,
maintenance, and repair
(IMR)
- In-service structural degradation,
343–344
- Income variable modeling,
786–787
- Incremental wave theory,
882–883
- Individual risk (IR), 715–716
- Inert, 52
- “Inertia” response, 143
- Inflation rates, 787
- Inherent uncertainty, 619
- Innovative double-hull designs,
471–472, 472f
- Inspection
data system, 703–704
strategies, 699–704
- Inspection, maintenance, and
repair (IMR), 253
- Inspection, maintenance,
monitoring, and repair
(IMMR), 703–704
- Instantaneous wind pressure, 106
- Integral equation methods.
See Panel methods
- Interest rates, 787
- Internal rate of return (IRR), 782,
790–791
- Internal tank pressure, 91
- International Institute of Welding
(IIW), 10
- International Marine Contractors
Association (IMCA), 758
- International Maritime
Organization (IMO), 39,
466–467, 908
- International safety management
(ISM), 799
- International Ship and Offshore
Structures Congress
(ISSC), 413, 843–844
- IR. *See* Individual risk (IR)
- IRR. *See* Internal rate of return
(IRR)
- Irregular waves, 122

- ISM. *See* International safety management (ISM)
- Isotropic hardening rule, 384–385
- ISSC. *See* International Ship and Offshore Structures Congress (ISSC)
- ISUM. *See* Idealized structural unit method (ISUM)
- J**
- Jacket platform
- probability model for load effect, 862, 864
 - Typhoon load, 863–864
 - Typhoon load parameter probability models, 862–863
 - probability model for load effect, 867–870
 - probability model for resistance, 856, 865–867
 - base shear capacity, 856
 - base shear capacity degradation, 858–862
 - probability model of initial base shear capacity, 857
 - struck by supply ship, 442–445
 - time-dependent reliability model for, 852–856
- Jacket structure, 214–217
- analysis models, 214–215
 - existing platforms assessment, 216
 - fire, blast, and accidental loading, 216–217
 - modeling, 876f
 - corrosion rate model, 878–880
 - for fatigue analysis, 216
 - foundation model, 877–878
 - metocean data, 876–877
 - structural model, 876
 - reassessment, 875
 - comparing corrosion effect, 885–887
 - corrosion effect on jacket structure, 883–885
 - jacket structure first failure, 881f
 - pushover analysis, 880–883
 - ultimate strength analysis, modeling for, 215–216
- Johnson–Ostenfeld formula, 280–281
- Joint classification, 548–550
- Joint Industry Project on Explosion and Fire Engineering of Floating (EFEF JIP), 914–915, 915f
- Joint North Sea Wave Project spectrum (JONSWAP spectrum), 76–77
- K**
- Kinematic hardening rule, 386–388
- Kurtosis, 616
- L**
- Laboratory equipment, 184–186
- Lamina, 29, 30f
- Large aluminum catamaran fatigue reliability, 682–685
- Large eddy simulation (LES), 115–116
- Large-scale test specimen, 295
- Lateral buckling mode, 169
- LCC. *See* Life cycle cost (LCC)
- LES. *See* Large eddy simulation (LES)
- Life cycle cost (LCC), 648–649, 782
- Lightship weight distribution, 269–270
- Limit state, 609–610
- Limit-state designs (LSDs), 4–6, 647–648
 - of offshore structures, 245–246
 - FLS design, 253–258
 - ULS design, 246–253
- Limit-state function (LSF), 653, 656, 674, 784–785
- Linear airy wave theory, 121
- Liquefied natural gas carrier (LNG carrier), 49, 49f, 786–787
 - cargo cycle, 51–53
 - containment systems, 53–59
 - development, 50–51
 - fatigue design, 66–70
 - phase, 67–70
 - preliminary design phase, 66–67
 - structural design, 59–66
- Live loads, 509
- Lloyds Register of Shipping (LR), 199
- LNG carrier. *See* Liquefied natural gas carrier (LNG carrier)
- Load and resistance factored design (LRFD), 4, 646–647
 - example for semisubmersible platforms plates, 664–670
- Load components, 89
 - stochastic method, 68
- Load uncertainty, 657
- Load-shedding zone, 409
- Load–displacement relationship of hit member, 429–430
- Loading errors, 773–774
- Local inter-ring shell failure, 361
- Local loads, 511
- Local panel buckling, 362–363
- Local stiffener tripping, 363
- Local structural analysis, 546
- Local structural models, 173
- Localized corrosion, 878
- Lognormal distribution, 617
- Lognormal format, 677–678
- Long plates, 349–350
- Long term sea state, 122–123
- Long-term extreme approach, 139–141
- Long-term fatigue stress, 512–513
- Long-term stress distribution
 - deterministic approach, 513–514, 520–522
 - spectral approach, 514–516, 523–524

- Longitudinal girders, theoretical model for, 468
- Longitudinal stresses, 63, 160–161
- Low risk projects, 952–953
- LR. *See* Lloyds Register of Shipping (LR)
- LRFD. *See* Load and resistance factored design (LRFD)
- LSDs. *See* Limit-state designs (LSDs)
- LSF. *See* Limit-state function (LSF)
- M**
- Maintenance significant items (MSI), 804
- Man–machine interface, 768
- Manson–Coffin relationship, 482–483
- MARC FEM analysis, 438
- Marine aviation vehicles, 23–25
- Marine composite materials and structure, 19, 20t, 25–29 application, 19–25 marine aviation vehicles and off-shore structure, 23–25 ocean environment, 20–22 shipbuilding industry, 22–23 challenges, 35–36 fiber reinforcements, 26–28 material property, 29–35 orthotropic properties, 31–34 orthotropic properties in plane stress, 34–35 resin systems, 28–29
- Marine Environment Protection Committee (MEPC), 40
- Marine growth prevention system (MGPS), 47
- Marine structures, 3, 615
- Marine systems, 754 risk, 758–759
- Maritime industry, 725
- Marsden areas, 76
- Mass–spring system, 434
- Material damage and production loss/delay, 717
- Material nonlinearity, 447, 450
- Material selection, 569. *See also* Damage tolerance fracture prevention, 571 higher-strength steel, 570 weld improvement and repair, 571–575
- Maximum allowable flaw size, 560 strain, 559 stress, 557
- Maximum continuous rating (MCR), 41
- “Maximum hogging” load condition, 61–62
- “Maximum sagging” load condition, 62
- Maximum tolerable defect size, 558
- Maximum wave height (H_{max}), 81
- MCR. *See* Maximum continuous rating (MCR)
- MCS. *See* Monte Carlo simulation (MCS)
- Mean stress effect, 492–493
- Mean value first-order second-moment concept. *See* Cornell safety index method
- Mean wave period, 81
- Mean zero-crossing period, 538
- Measurement uncertainty, 619
- MEPC. *See* Marine Environment Protection Committee (MEPC)
- Metocean data, 876–877
- MGPS. *See* Marine growth prevention system (MGPS)
- Miner’s rule, 538
- Minimum required fracture toughness, 557, 559
- Minimum required plate thickness, 165
- Mises’s yield criterion, 383
- Mixed modes, 831
- MMS. *See* US Mineral Management Service (MMS)
- Mobile offshore drilling units (MODU), 199
- Mode I crack. *See* Edge-opened crack
- Mode II crack. *See* Sliding mode crack
- Mode III crack. *See* Tearing mode crack
- Model uncertainty, 620
- Modeling uncertainties, natural uncertainties vs., 582–583
- Modified Smith method accounting for corrosion and fatigue defects, 408–412 compressive stiffened panels, 409–410 corrosion rate model, 410–412 crack propagation prediction, 410 tensile and corner elements, 408
- MODU. *See* Mobile offshore drilling units (MODU)
- Monte Carlo method, 864
- Monte Carlo simulation (MCS), 587
- Mooring, 188
- Morison equation, 125
- Moss tanks, 54–56
- Most probable maximum extreme (MPME), 142
- Most probable maximum value (MPM value), 141
- MPM value. *See* Most probable maximum value (MPM value)
- MPME. *See* Most probable maximum extreme (MPME)
- MSI. *See* Maintenance significant items (MSI)
- N**
- Natural uncertainties, modeling uncertainties vs., 582–583
- Nearshore geotechnical investigations, 187–188
- Net present value (NPV), 782, 790–791

- NFEM. *See* Nonlinear finite element method (NFEM)
- Nitrogen oxides (NO_x), 40
- No-load-shedding zone, 409
- Nominal stress, 538
- Nominal stress approach, 497–498
- Nondestructive examination size, 564
- Nondestructive inspection, 577–578
- Nonlinear finite element analysis theory, 367–368
- deformation matrix, 389–390
- elastic beam-column with large displacements, 368–370
- plastic node method, 370–377
- stress-based plasticity
- constitutive equations, 379–389
- transformation matrix, 377–379
- Nonlinear finite element method (NFEM), 843
- Nonlinear spring element, 400
- Nonlinear structural response analysis, 926–930
- Normal distribution, 617
- NORSOK, 492, 494
- NORSOK N-004, 248
- Northern Sea Route (NSR), 229–230
- Norwegian Petroleum Directorate (NPD), 198
- Notch stress approach, 500–501
- NO_x. *See* Nitrogen oxides (NO_x)
- NPD. *See* Norwegian Petroleum Directorate (NPD)
- NPV. *See* Net present value (NPV)
- NSR. *See* Northern Sea Route (NSR)
- Nuclear industry, 765
- Numerical analysis method, 318–320, 833–835
- O**
- Ocean environment, 20–22
- Ocean waves and wave statistics, 73–81
- basic elements of probability and random processes, 73–75
- moments of spectral density function, 79–80
- ocean wave spectra, 76–79
- statistical determination of wave heights and periods, 80–81
- statistical representation of sea surface, 76
- Ochi six-parameter spectrum, 78
- OCIMF. *See* Oil Companies International Marine Forum (OCIMF)
- Off-shore structures, 23–25, 234–235
- under earthquake loads, 447–448
- analysis procedure, 450–451
- clamped beam under lateral, 451–452
- earthquake design per API RP2A, 448–449, 448t
- equation of motion, 449–450
- offshore jacket platform, 454–455
- two-dimensional frame, 452–453, 452f
- human and organizational factors in, 800
- quality management system, 800
- reducing human and organizational errors, 801
- under impact loads, 427–428
- application to practical collision problems, 441–445
- collision mechanics, 431–434
- finite element formulation, 427–428
- mathematical equations for impact forces and energies, 434–435
- numerical examples, 435–441
- loads and dynamic response for, 119
- environmental criteria, 119–121
- environmental loads, 125
- extreme values, 133–147
- floating structure dynamics, 127–128
- irregular waves, 122
- regular waves, 121–122
- sea loads on large-volume structures, 126–127
- sea loads on slender structures, 125–126
- structural response analysis, 128–133
- wave scatter diagram, 122–125, 124t
- structural reassessment
- corrosion model, 829–830
- crack and corrosion, 829
- crack defects analysis, 830–833
- residual ultimate strength of hull structural components, 833–849
- Offloading systems, 757–758
- Offshore jacket platforms, 852
- subjected to earthquake loading, 454–455
- Offshore platforms, 875
- Offshore risk assessment, 735
- collision risk, 736–740
- dropped objects, 749–753
- environmental impact assessment, 761–762
- explosion risk, 740–745
- fire risk, 745–749
- risk assessment of floating production systems, 753–761
- types, 735
- Offshore soil geotechnics, 181
- deepwater foundation, 188–194
- subsea soil investigation, 181–188
- Offshore strength assessment, safety factors for, 294
- Offshore structural analysis, 197
- CA, 198–199
- Codes and Standards, 199–200
- design codes, 197–198

- design loads and load
 application, 212–214
 government requirements, 198
 project planning, 201–204
 structural modeling, 214–226
 FPSO, 217–224
 jacket structures, 214–217
 TLP, Spar, and
 Semisubmersible, 224–226
 technical documents, 200–201
 use of finite element analysis,
 204–212
 basic ideas, 204–205
 computation based on, 205
 marine applications, 205–206
 stiffness matrix, 206–212
- Oil Companies International
 Marine Forum (OCIMF),
 758
- Oil prices, 787
- Omission factors, 788–789
- Onboard laboratory test,
 186–187
- Onshore laboratory tests, 187
- Open sea navigation, 769
- Operating costs (OPEX), 36, 782
- Operation and maintenance costs,
 786
- Operational risk assessment,
 816–817
- OPEX. *See* Operating costs
 (OPEX)
- Optimum inspection method,
 701–703
- Organization factors, 15
- Orthotropic properties, 31–34
 in plane stress, 34–35
- Outer bottom plating, theoretical
 model for, 469
- Owner's/operator's
 responsibilities, 892,
 905–906
- P**
- Palmgren–Miner law, 528–529
 cumulative damage law,
 480–481
- Panel methods, 126
- Parallel system reliability, 591,
 601–602
- Parallel systems, 11–12
- Paris Law, residual life prediction
 using, 576
- Part-ship FE models, 68
- Partial safety factors, 680
- PCPT. *See* Piezocone penetration
 test (PCPT)
- PDO. *See* Plan for Development
 and Operation (PDO)
- Pedersen's model, 466, 466f
- Peening, 574
- Perfectly elastic solution,
 331–332
- Performance standard
 determination, 721
 risk-based compliance process
 for engineering systems,
 722
 risk-based fatigue criteria for
 critical weld details,
 721–722
- Perry–Robertson formula,
 279–280, 350
- PEV. *See* Probable extreme value
 (PEV)
- PFD. *See* Process flow diagram
 (PFD)
- PHA. *See* Preliminary hazard
 analysis (PHA)
- Physical uncertainty. *See* Inherent
 uncertainty
- PID. *See* Piping and
 instrumentation diagram
 (PID)
- Pierson–Moskowitz spectra
 (P–M spectra), 77
- Piezocone penetration test
 (PCPT), 183–184
- Piper Alpha, 907–908
 accident, 907f
- Piping and instrumentation
 diagram (PID), 945
- Plan for Development and
 Operation (PDO), 781
- Plastic deformation, 379, 427,
 481
- Plastic design, 647–648
 plastic bending of beam cross
 section, 285–286
 plastic hinge load, 286–287
- plastic interaction under
 combined axial force and
 bending, 287–288
- Plastic node method (PNM),
 370–377, 394, 447, 455
- consistency condition and
 hardening rates, 370–374
- elastic–plastic stiffness equation
 for elements, 376–377
- history, 370
- numerical examples, 415
 collapse of stiffened box
 girders, 417–418
 collapse of stiffened plate,
 415
 collapse of upper deck
 structure, 417
 quasi-static analysis of side
 collision, 422–423
 ultimate longitudinal strength
 of hull girders, 419–422
- plastic displacement and strain
 at nodes, 374–376
- Plastic strain, 379–380
 increment, 384–388
 isotropic hardening rule,
 384–385
 kinematic hardening rule,
 386–388
- Plasticity, correction for, 345
- Plate aspect ratio, 341, 346
- Plate thickness effect, 491
- Plated structures, 247–248
- Plates and stiffened panels
 effects of crack defects,
 833–837
 effects of localized corrosion,
 837–842
- Playing imagination.
See Brainstorming
- Pleasure boats industry, 22
- PLL. *See* Potential loss of life
 (PLL)
- PLP. *See* Potential loss of
 property (PLP)
- PM. *See* Preventive maintenance
 (PM)
- P–M spectra. *See* Pierson–
 Moskowitz spectra
 (P–M spectra)

- PNM. *See* Plastic node method (PNM)
- POD. *See* Probability of detection (POD)
- PoF. *See* Probability of failure (PoF)
- Poisson ratio, 32
- Port operations, 769
- Post-local-buckling analysis, 312–318
COS model, 313–316
DENT model, 316–318
- Post-local-buckling analysis, 324–326
- Postprocessing, 177–178, 205
- Potential loss of life (PLL), 715
- Potential loss of property (PLP), 463–464
- Power generation industries, 564–565
- Power loss, 773
- Powered collisions, 736
- Powered ship collision, 737–738
- PRA. *See* Preliminary risk analysis (PRA)
- Practical collision problems, application to, 441–445
- Pre-ultimate-strength analysis, 320–321
- Predictive maintenance, 803
- Preliminary hazard analysis (PHA), 910–911
- Preliminary risk analysis (PRA), 804
procedure, 806–808
purpose, 806
qualitative risk matrix, 807f
- Preventive maintenance (PM), 803–804
- Probabilistic distributions, 617–618
- Probability density function, 73–74, 617
- Probability of detection (POD), 693
- Probability of failure (PoF), 942–943
- Probability-based inspection, 689
reliability-updating theory for, 691–694
- Probable extreme value (PEV), 135
- Procedure lift, 750
- Process flow diagram (PFD), 945
- Process leakage, 757
- Process systems, 753–754
- Project planning, 201–204
design basis, 201–203
design brief, 203–204
- Propeller radiated signatures, 263–265
- Pure bending test for small-scale specimens, 306–307
- Pushover analysis. *See* Collapse analysis
- Q**
- Q-Flex, 50
- Q-Max, 50
- QA. *See* Quality assurance (QA)
- QC. *See* Quality control (QC)
- QRA. *See* Quantitative risk assessment (QRA)
- Qualitative approach, 896–897
- Quality assurance (QA), 257, 798–799
- Quality control (QC), 799
- Quantitative approach, 897
- Quantitative economic risk assessment, 783
- Quantitative risk assessment (QRA), 709, 765
- Quasi-static wave bending moment, 622–623
- R**
- Radial pressure, 364
- Radiography, 577
- Random process distribution, 74
- Random variables, 615
marine structures, 615
probabilistic distributions, 617–618
statistical descriptions, 616
- Random waves, 538
- RAO. *See* Response amplitude operator (RAO)
- Rational analysis procedure, 171
- Rational stress analysis, 171
- Rayleigh distribution, 618
- RBDM. *See* Risk-based decision-making (RBDM)
- RBI. *See* Risk-based inspection (RBI)
- RBM. *See* Risk-based management (RBM)
- RCM. *See* Reliability-centered maintenance (RCM)
- Reduction factor, 344
- Regular waves, 121–122, 538
- Reliability calculations, software for, 597–598
- Reliability updating, 595–596
- Reliability-based code
calibrations, 651
example, 653–654
principles, 651–652
procedure, 652–653
uncertainty modeling, 657–658
- Reliability-based design, 645
to ASD format, 650–651
design principles, 645–649
LRFD example for
semisubmersible platforms
plates, 664–670
numerical example
for hull girder collapse of FPSOs, 660–664
for tubular structure, 654–659
safety factor, 649
- Reliability-centered maintenance (RCM), 804, 940, 948–950
analysis procedures, 809–816
application, 804
application to shell and tube heat exchanger on FPSO, 818–824
for commercial aircraft industry, 804
decision logic, 815f
to EPRI, 808
FAA/Industry Reliability Program, 805
FMECA form, 812f
functional block diagram, 810, 811f
main research contents, 950
maintenance strategy improvement, 816–817

- offshore maintenance, 803
- pilot study, 806
- PRA, 806–808
- PRA and RCM in maintenance processes, 805f
- research method, 950–951
- risk-CM, 816–817
- scheduled maintenance, 803
- Reliability-updating theory
 - inspection planning for fatigue damage, 692–694
 - for probability-based inspection planning, 691
- Remelting techniques, 573
- Repair events, 693
- Reserve strength ratio (RSR), 882
- Residual life prediction using Paris Law, 576
- Residual stress, 354
 - distribution modification, 573–574
- Residual ultimate strength of hull structural components, 833
 - with corrosion damage, 848–849
 - with crack and corrosion damage, 842
 - modeling, 844
 - ultimate strength analysis method, 843–844
 - with crack damage, 844–848
 - effects of crack defects, 833–837
 - effects of localized corrosion, 837–842
- Resin systems, 28–29
- Response amplitude operator (RAO), 126, 129–133, 623
- Response surface method, 633–634
- Reynolds number (Re), 102
- Rigid-plastic solution, 332
- Ring stiffener failure, 361–362
- Risk, 690
 - acceptance criteria, 717
 - ALARP-principle, 719–720, 720f
 - comparison criteria, 720–721
 - risk matrices, 718–719
 - communication, 730
 - control, 777
 - estimation, 713
 - risk to assets, 717
 - risk to environment, 716–717
 - risk to personnel, 715–716
 - evaluation, 776–777
 - management, 729
 - mitigation plan, 954
 - reducing measures, 714
 - and reliability applications to FPSO, 891
 - risk-based classification, 891–893
 - risk-based inspection, 893–901
 - risk-based survey, 901–906
 - restraining project, 919–920
 - risk-based approach, 87
- Risk assessment, 689, 729
 - application, 14
 - of floating production systems, 753
 - comparative risk analysis, 760
 - hazard identification, 755–756
 - marine systems, 754
 - process systems, 753–754
 - risk acceptance criteria, 756
 - risk estimation and reducing measures, 757–759
 - risk-based inspection, 760–761
 - human and organization factors, 15
 - and management, 914
 - procedure for, 915–916
 - procedure for explosion, 916–919
- methodology
 - analysis of causes, 712
 - consequence and escalation analysis, 712–713
 - emergency preparedness, 714
 - frequency of initiating events, 712
 - hazard identification, 711–712
 - HSE, 709
 - NORSOK standard, 709
 - performance standard
 - determination, 721–722
 - planning of risk analysis, 710–711
 - risk acceptance criteria, 717–721
 - risk estimation, 713
 - risk estimation, 715–717
 - risk estimation, analysis, and evaluation, 710f
 - risk reducing measures, 714
 - system description, 711
 - time-variant risk, 714–715
- risk-based inspection, 14–15
- Risk-based classification, 891
 - applicability, 892
 - classifications responsibilities, 893
 - owner/operator's responsibilities, 892
 - submittals and requirements for design verification, 893
- Risk-based decision-making (RBDM), 725
 - probability concepts, 726–728
 - process, 728, 728f
 - impact assessment, 729
 - risk assessment, 729
 - risk communication, 730
 - risk management, 729
 - for stability testing application, 730f
 - step-by-step example, 730
 - uncertainties, 725, 725t
- Risk-based fatigue criteria for critical weld details, 721–722
- Risk-based inspection (RBI), 14–15, 760–761, 893, 940–941
 - elements and procedures, 895
 - examples, 694–695
 - flow chart, 895f
 - management processes, 942f
 - methodology, 896–901
 - modeling risk, 942–944
 - planning, 689–690, 691f
 - process, 944–946

- Risk-based inspection (RBI)
(*Continued*)
research contents, 942
risk categories, 945t
risk-based optimum inspection, 695–704
strengths and weaknesses, 894–895
three-step process, 941
- Risk-based management (RBM), 939
theory for, 939–940
- Risk-based optimum inspection, 695
inspection performance, 698–699
inspection strategies, 699–704
quantitative inspection analyses, 696–697
time-variant reliability, 696f–697f
- Risk-based survey
current practice of surveys, 901–902
drawbacks, 902–903
integration of ABS survey program, 904f
for maintenance of class, 903–906
- Risk-centered maintenance (Risk-CM), 816–817
- Root-mean-square wave height (H_{rms}), 81
- RSR. *See* Reserve strength ratio (RSR)
- S**
- S series experiments, 330
- S-glass, 27
- Safe life designs, 258
- Safety factors, 645, 649
calibration, 659
- Safety index
method, 599
ship hull calculation, 598–599
- Safety integrity level assessment (SIL), 940, 946–947
main research contents, 947
parametric description—
environmental disruption, 949t
parametric description—financial loss, 949t
parametric description—
personnel safety, 948t
research method, 947–948
- Safety of life at sea (SOLAS), 765
- Sampling points, 634
- Sandwich panels, 471
- SANDY computer program, 402
- Scantling of Ship's Hulls by rules, 153
corrosion allowance, 158
initial scantling criteria
buckling of platings, 166–169
buckling of profiles, 169–170
local bending of beams, 162–165
local bending strength of plates, 165
for local strength, 162–170
for longitudinal strength, 158–161
structure design of bulkheads, decks, and bottom, 166
for transverse strength, 161–162
stability and strength of ships, 154–158
- SCF. *See* Stress concentration factor (SCF)
- Scheduled function test (SFT), 814
- Scheduled on-condition task, 813–814
- Scheduled replacement, 814
- Screening
analysis, 951–953
assessment, 945–946
- Sea loads, 509
on large-volume structures, 126–127
on slender structures, 125–126
- Sea state, 122, 538
fatigue damage for, 540–541
- Seabed corer equipment, 183
- Second-order potential forces, 126
- Second-order reliability method (SORM), 587, 589–590
calculation by, 589–590
- Secondary failure mode, 629
- Seismic loads, 509
- Self-supporting prismatic type B tank (SPB tank), 56
- Semisubmersible, 224–226
- Semisubmersible platforms
plates, LRFD example for
case description, 664–665
design steps, 665–668
statistical results, 668–670
- Sensitivity factors, 789
- Series system reliability, 590–591, 600–601
- Series systems, 11–12
- Serviceability limit state (SLS), 245, 345
- SFA. *See* Spectral fatigue analysis (SFA)
- SFT. *See* Scheduled function test (SFT)
- Shear panel element, 399–400
- Shear stresses, 64, 161
- Shell and tube heat exchanger, 818f
application on FPSO, 818
class of heat exchanger design, 818
RCM process, 819–824
- Shells, 248–253
- Ship accidents
consequence of, 775–776
frequency analysis, 774–775
- Ship collision, 459–460
design standards, 460
designs against, 470–472
external mechanics, 461
internal mechanics, 460–461
research, 461–467
- Ship grounding, 459–460
design standards, 460
designs against, 470–472
internal mechanics, 460–461
research, 467–470
on shoal, 468–470
- Ship hardware, 768
- Ship hull scantling design, 171
design loads, 171–173
fatigue damage evaluation, 179–180
strength analysis using finite element methods, 173–178

- Ship life cycle, 769
- Ship Motion, 173
- Ship response to random sea, 81–83
- slamming and green water on deck, 85–87
 - structural response, 84–85
 - wave-induced forces, 83–84
- Ship structures
- closed form method for hull girder reliability, 628–630
 - FPSOs, 627
 - hull girders time-variant reliability assessment, 635–643
 - load effects and load combination, 630–632
 - procedure for reliability analysis, 632–633
 - response surface method, 633–634
 - reliability, 627
 - uncertainty in, 621–624
- Ship vibration
- basic beam theory of, 260–261
 - steady-state ship vibration, beam theory of, 261–262
- Ship's fuel system, application to, 778–779
- Shipbuilding industry, 22–23
- commercial applications, 23
 - military applications, 23
 - pleasure boats industry, 22
 - recreational applications, 23
- Shipping industry, 765
- application to ship's fuel system, 778–779
 - in FSA, 765
 - characteristics of, 766–767
 - functional components, 767–777, 767f
 - HOF in, 777–778
 - risk-based methodology, 766
 - uses, 779
- Ship–ship collision research, 461–467, 465f
- Short-term extreme approach, 135–139
- Short-term sea state, 122
- Short-term/long-term response, 173
- Significant wave height (H_S), 80, 538
- SIL. *See* Safety integrity level assessment (SIL)
- Simplified elastoplastic large deflection analysis, 307–320
- calculation results, 326–330
 - theory of analysis, 307–326
 - critical condition for local buckling, 312
 - post-local-buckling analysis, 312–318
 - preanalysis of local buckling, 307–312
 - procedure of numerical analysis, 318–320
- Simplified fatigue assessment, 537. *See also* Fatigue capacity; Fatigue loading; Fatigue stresses; Spectral fatigue analysis (SFA)
- accumulated damage
 - calculation, 528–530
 - allowable stress range, 531
 - for bilinear S–N curves, 530–531
 - design criteria for connections
 - around cutout openings, 531–534
 - fatigue design of semisubmersible, 534–535
 - stress criteria for collar plate design, 533–534
 - Weibull stress distribution parameters, 530
- Simulation approach, 587
- Sink-source methods. *See* Panel methods
- Skewness, 616
- SLA. *See* Strength level analysis (SLA)
- Slamming, 85–87
- SLE. *See* Strength-level earthquake (SLE)
- Slender plates, 349
- Sliding mode crack, 831
- Slots. *See* Cracks around cutout openings
- Slowly varying response, 127
- SLS. *See* Serviceability limit state (SLS)
- SMIS. *See* Structural information management system (SMIS)
- Smoke effect analysis, 747
- S–N curves, 479–480, 479f, 489–491, 529, 538, 548
- in air, 490f
 - comparisons in design standards, 493–496, 494t
 - experimental, 496–497
 - fatigue strength improvement, 496
 - mean stress effect, 492–493
 - plate thickness effect, 491
 - seawater and corrosion
 - protection effect, 492
 - S–N approach, 674
 - fatigue reliability based on, 681–682
 - FM calibration by, 678–679
- Society risks, 716
- Soil–structure interaction, 441
- SOLAS. *See* Safety of life at sea (SOLAS)
- SORM. *See* Second-order reliability method (SORM)
- SO_x. *See* Sulfur oxides (SO_x)
- Space frame model, 544–545, 544f
- Spar, 224–226
- SPB tank. *See* Self-supporting prismatic type B tank (SPB tank)
- Spectral approach, 514–516, 523–524
- Spectral density function moments, 79–80
- Spectral fatigue analysis (SFA), 537. *See also* Fatigue analysis; Simplified fatigue assessment; Time-domain fatigue analysis (TFA)

- Spectral fatigue analysis (SFA)
(*Continued*)
fatigue damage
 acceptance criteria, 538
 calculation using frequency-domain solution, 539–541
- Spectral fatigue assessment, 537
- Spectral fatigue parameters
 European and US standards comparison, 549t
 joint classification, 548–550
 S–N curves, 548
 stress concentration factors, 548
 structural details, 550–553
 wave environment, 547–548
- Spectral method, 257
- Splash zone, 884, 887
- Spudcan footings, 189–192
- Square-root-of-sum-of-squares method (SRSS method), 106–107
- SRSS method. *See* Square-root-of-sum-of-squares method (SRSS method)
- Stable zone, 409
- Stakeholders, 769
- Standard normal distribution, 617
- Standing wave theory, 122
- Static loads, 171–172
- Static sea pressure, 212
- Statistical descriptions, 616
- Statistical loads combination, 591
 FBC model, 593–594
 Turkstra's rule, 592–593
- Statistical uncertainty, 619
- STC. *See* Stiffened Plate with Transverse Crack Located in Center of Plate (STC)
- STCW. *See* Stiffened Plate with Two Cracks Located in Plate and Stiffener Web (STCW)
- Steady-state ship vibration, beam theory of, 261–262
- Steel, higher-strength, 570
- Stiffened Plate with Transverse Crack Located in Center of Plate (STC), 836
- Stiffened Plate with Two Cracks Located in Plate and Stiffener Web (STCW), 836
- Stiffened plates, 339
 boundary conditions, 341–342
 correction for plasticity, 345
 fabrication-related imperfections, 343–344
 in-service structural degradation, 343–344
 solution of differential equation, 340–341
- Stiffeners, 163–164
- Stiffeners, theoretical model for, 469–470
- Stiffness matrix
 for 2D beam elements, 206–208
 for 3D beam elements, 208–212
- Still-water bending moment (SWBM), 623, 630
- Stokes finite amplitude wave theory, 121
- Strain-controlled fatigue, 481–484
- Strain-hardening effect, 298
 rate, 380
- Stream function wave theory, 122
- Strength analysis using FEM, 173–178
 boundary conditions, 176–177
 modeling, 173–176
 cargo hold and ballast tank model, 173–174
 fatigue model, 176
 frame and girder model, 174
 global analysis, 173
 local structural models, 173
 stress concentration area, 174–175
 postprocessing, 177–178
 types of elements, 177
- Strength and fatigue analysis, 6–11
 accidental loads design, 8–9
 fatigue design, 9–11
 ultimate strength criteria, 6–8
- Strength level analysis (SLA), 916–917
- Strength-level earthquake (SLE), 448
- Stress, 29–30
 concentration area, 174–175
 modeling, 672
 error, 672–673
 relief, 573–574
- Stress concentration factor (SCF), 69, 204, 501, 548, 672
 determination by experimental measurement, 501
 hot-spot stress calculation based on FEA, 502–504
 parametric equations, 501–502
- Stress range
 analysis, 547
 estimation, 497
 hot-spot stress approach, 498–499
 nominal stress approach, 497–498
 notch stress approach, 500–501
- Stress-based plasticity
 constitutive equations, 379–389
 plastic strain increment, 384–388
 relationship between stress and strain in elastic region, 381–382
 stress increment–strain increment relation in plastic region, 388–389
 yield criterion, 382–383
- Stress-controlled fatigue, 479–480
- Stress–strain curves, 298
- Stringer-stiffened cylinder buckling, 363
- Strip theory, 82–83
- Structural analysis, 543–546
 analysis and validation, 546
 design loading conditions, 545–546
 fine FEA model, 545
 local structural analysis, 546
 space frame model, 544–545, 544f

- Structural design principles, 3–6
- Structural dynamics, 367
- Structural evaluation, 204
- Structural information
management system
(SMIS), 704
- Structural integrity loss, 772
- Structural model, 876
- Structural reliability, 581.
See also Uncertainty—
theory
- analysis, 590–591
index, 607
numerical examples, 609–613
parallel system, 609f
reliability index, 609
series system, 608f
theory of structural reliability,
603
- applications, 11–12
reliability-based calibration of
design factor, 12–13
requalification of existing
structures, 13
- calculation, 583–587
by FORM, 588–589
by SORM, 589–590
- component reliability, 590
- failure mode, 583
- limit state, 583
- numerical examples, 598–602
- reliability updating, 595–596
- software for reliability
calculations, 597–598
- statistical loads combination,
591–594
- structural engineering, 583
- target probability, 596–597
- theory, 581
- time-variant reliability,
594–595
- uncertainty and uncertainty
modeling, 581–583
- Structural response analysis,
128–133
RAO, 129–133
structural analysis, 128–129
- Structural systems, 754–755
- Structure analysis, 935–936
- Structure limit state, 609–610
- Subsea soil investigation,
181–188
equipment requirements,
182–186
subsea survey equipment
interfaces, 186–188
- Suction caisson, 188–189
- Sudden failure, 813
- Sulfur oxides (SO_x), 40
- Surface crack, 832
- SWBM. *See* Still-water bending
moment (SWBM)
- System, 590
analysis, 322
- T**
- Tangent modulus, 379–380
- Target probability, 596–597
- Target safety
index for fatigue, 679–680
levels, 658–659
- Task analysis, 795
- Taxes, 787
- Tearing mode crack, 831
- Temperature simulation, 935
- Tensile and corner elements, 408
- Tensile strength, 569
- Tension leg platforms (TLP),
105–106, 197, 224–226,
537
- Tension tearing rupture, 401
- Tertiary failure mode, 629
- Test specimens, 294–295
- TFA. *See* Time-domain fatigue
analysis (TFA)
- TGZ Mark III, 58–59
- Three-dimensional beam-column
element, 427
- Through crack, 832
- TIG. *See* Tungsten-inert-gas
(TIG)
- Time-dependent reliability
assessment. *See also*
Jacket platform
example platform, 864
offshore jacket platforms, 852
reliability assessment method,
851
results of platform,
870–871
- Time-domain fatigue analysis
(TFA), 537. *See also*
Fatigue analysis; Spectral
fatigue analysis (SFA)
- application, 541
- methodology
for nonlinear ship response,
543
for pipelines, 541–542
for risers, 542–543
- Time-domain solutions, 447
- Time-variant reliability, 594–595
assessment of FPSO hull
girders, 635–643
- Time-variant risk, 714–715
- TLP. *See* Tension leg platforms
(TLP)
- Torsional buckling mode, 170
- Transfer function, 538
- Transformation matrix, 377–379
- Transverse strength, 162, 220
- Transverse stresses, 63
- Triplex, 58
- Tripping of stiffeners, 351
- Tube bundle, 818
- Tubular structure
case description, 654
design equations, 655–656
LSF, 656
safety factors calibration, 659
target safety levels, 658–659
tubular joint connections, 655f
- Tungsten-inert-gas (TIG), 573
- Turbulence, 99, 744
- Turkstra's rule, 592–593
- TWI. *See* British Welding
Institute (TWI)
- Two-dimensional frames (2D
frames), 161–162
subjected to earthquake loading,
452–453, 452f
- Typhoon load, 863–864
parameter probability models,
862–863
- U**
- UFD. *See* Utility flow diagram
(UFD)
- UK Health and Safety Executive
(HSE), 198

- ULS. *See* Ultimate limit state (ULS)
- Ultimate limit state (ULS), 245–253, 345, 648.
See also Fatigue limit state (FLS)
- ductility and brittle fracture avoidance, 246–247
- LNG carrier, 59–66
capacity checks, 64–66
combination of stresses, 62–64
design principles, 59–60
design wave, 60–61
global load conditions, 61–62
plated structures, 247–248
shell structures, 248–253
- Ultimate strength
analysis, 843–844, 881
criteria, 6–8
equations, 406–407
of stiffened panels
 beam-column buckling, 350–351
 tripping of stiffeners, 351
uncertainty, 657–658
of unstiffened plates
 combined loads, 350
 long plates and wide plates, 349–350
 plates under lateral pressure, 350
 shear strength, 350
- Ultrasonic testing (UT), 577
- Uncertainty, 581. *See also* Structural reliability—analysis
analysis
 classification, 619–620
 in loads acting on ships, 622–623
 modeling, 620
 in ship structural capacity, 623–624
 in ship structural design, 621
 in fatigue stress model, 672–673
 and modeling, 581
 modeling, 657–658
- natural *vs.* modeling
 uncertainties, 582–583
 theory, 604
 uncertain reliability, 606–607
 uncertainty distribution, 605
- Unconfined explosion, 743
- Underwater coatings, 47
- Unidirectional layer, 31, 31f
- Uniform corrosion. *See* General corrosion
- Unmanned platform struck by supply ship, 441–442
- Unstiffened Plate with Transverse Crack Located in Center (UTC), 835
- Unstiffened Plate with Transversely Oriented Mid-Length Edge Crack (UT1E), 835
- Unstiffened Plate with Two Transversely Oriented Mid-Length Edge Cracks (UT2E), 836
- US Coast Guard (USCG), 726
- US Mineral Management Service (MMS), 198
- USCG. *See* US Coast Guard (USCG)
- UT. *See* Ultrasonic testing (UT)
- UT1E. *See* Unstiffened Plate with Transversely Oriented Mid-Length Edge Crack (UT1E)
- UT2E. *See* Unstiffened Plate with Two Transversely Oriented Mid-Length Edge Cracks (UT2E)
- UTC. *See* Unstiffened Plate with Transverse Crack Located in Center (UTC)
- Utility flow diagram (UFD), 945
- V**
- Valued ecological components (VECs), 717
- Variable amplitude loading, cumulative damage for, 480–481
- Variable loads, 212
- VECs. *See* Valued ecological components (VECs)
- Vibration analysis, 267–273
 finite element modeling, 269–271
 forced vibration, 271–273
 free vibration, 271
 procedure outline of ship vibration analysis, 268–269
- Vibration and noise control, 263–267
 after-body slamming, 267
 propeller radiated signatures, 263–265
 vortex shedding mechanisms, 265–266
- VIV. *See* Vortex-induced vibration (VIV)
- Vortex shedding mechanisms, 265–266
- Vortex-induced vibration (VIV), 126
- Voyage, 52–53
- W**
- Wall-thickness uncertainty, 657
- Waterway navigation, 769
- Wave loads for ship design, 73, 88–91
 design loads per classification rules, 88–91
 design value of ship response, 88
 ocean waves and wave statistics, 73–81
 ship response to random sea, 81–87
- Wave-frequency response, 127
- Wave-induced forces, 83–84
- Wave-induced loads, 212–213
- Wave(s), 120–121
 and currents, 509, 516
 environment, 547–548
 heading, 129
 scatter diagram, 122–125, 124t
- Weakest link systems, 11–12, 590
- Web and flange buckling, 170

- Weibull distribution, 512, 618, 631
- Weibull fitting, 144
- Weibull formulation, 830, 859
- Weibull parameters, 10
- Weibull probability density function, 512
- Weibull shape parameters, 527
- Weibull stress distribution function, 509 parameters, 530
- Weld improvement, 572–573 fatigue strength improvement techniques, 574 fatigue-resistant details, 572 improving fatigue strength, 574–575 and repair, 571–572 residual stress distribution modification, 573–574
- Welding-induced residual stress pattern, 343
- Wide plates, 349–350
- Wind, 120 conditions, 96–97 hurricanes, 100 turbulence, 99 wind profile, 97–99 wind spectra, 99–100 data, 95–96
- Wind loads, 100–101, 213–214, 509 computational fluid dynamics, 107–108 dynamic wind analysis, 105–107 for offshore structures, 95 classification rules for design, 95–108 research of wind loads on ships and platforms, 108–116 on platforms, 113–116 on ships, 108–113 wind forces, 102–105 wind pressure, 101–102 wind tunnel tests, 107
- Winterstein/Jensen method, 146–147
- Working stress design (WSD). *See* Allowable stress design
- Y**
- Yield criterion, 322–323, 382–383, 388
- Yield strength uncertainty, 657
- Yield surface, 383
- Yielding check, 178